Hans-Jürgen Biersack
Leonard M. Freeman
Editors

Clinical Nuclear Medicine

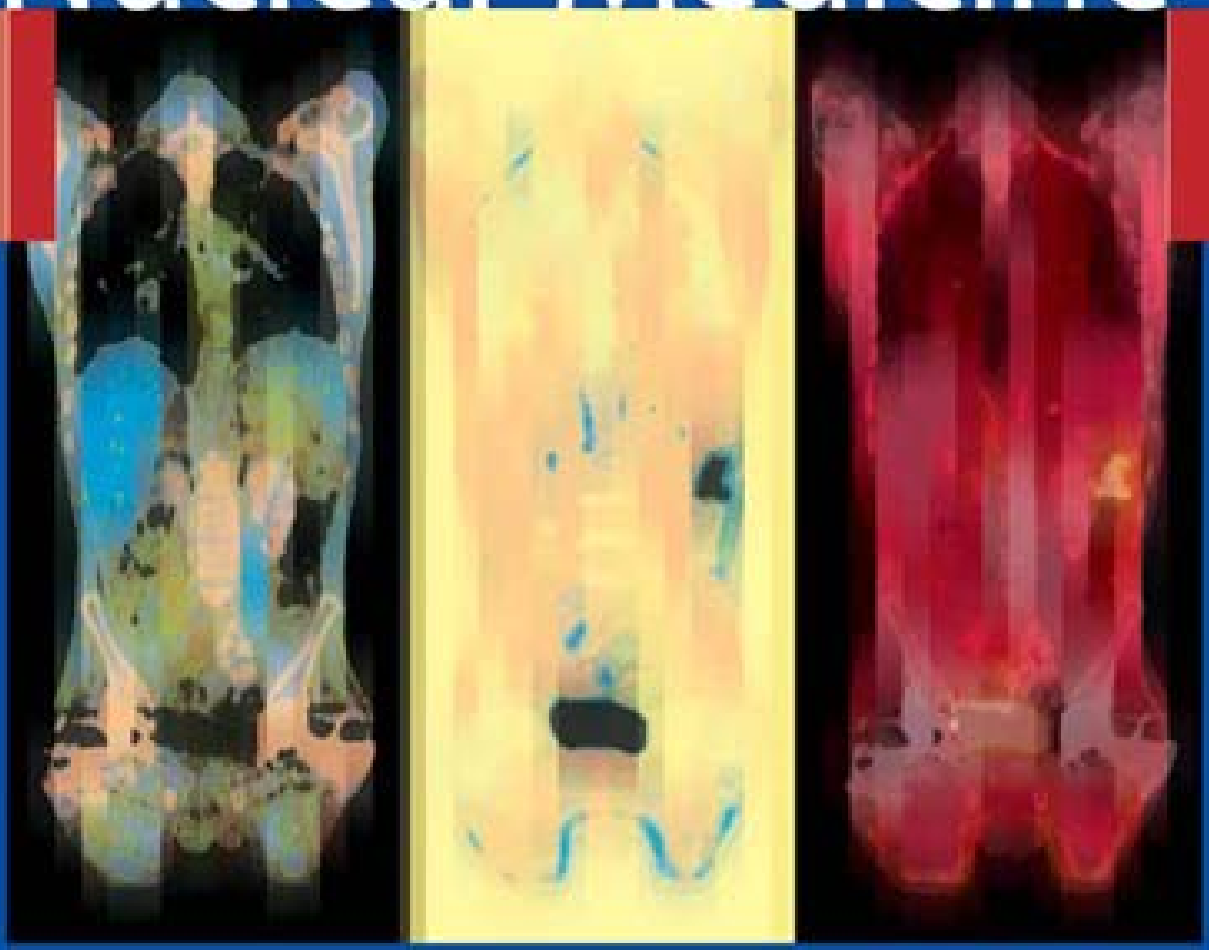

Springer

Hans-Jürgen Biersack · Leonard M. Freeman (Eds.)
Lionel S. Zuckier · Frank Grünwald (Associate Eds.)

Clinical Nuclear Medicine

With 310 Figures in 1,232 Parts and 91 Tables

Springer

Hans-Jürgen Biersack, M.D.
Professor and Chairman
Department of Nuclear Medicine
University Hospital Bonn
Sigmund-Freud-Straße 15
D-53127 Bonn
Germany

Leonard M. Freeman, M.D.
Professor of Nuclear Medicine and Radiology
Albert Einstein College of Medicine
Director, Dept. of Nuclear Medicine
Montefiore Medical Centre/Moses Division
111 East 210th Street
Bronx, NY 10467
USA

ISBN 978-3-540-28025-5 Springer-Verlag Berlin Heidelberg New York

Library of Congress Control Number: 2007928441

Printed in Germany

Editor: Dr. Ute Heilmann
Desk Editor: Dörthe Mennecke-Bühler
Copy-editing: WS Editorial Ltd, Shrewsbury, UK
Production Editor: Joachim W. Schmidt

Cover design: eStudio Calamar, Spain

Typesetting: FotoSatz Pfeifer GmbH, D-82166 Gräfelfing
Printed on acid-free paper – 24/3150 – 5 4 3 2 1 0

Preface

The modern era of radionuclide imaging and therapy is well into its seventh decade. During this era, many national and international textbooks have been published in an attempt to educate not only the practitioners of our medical discipline, but also referring physicians and medical students. Some of the more recent large multicultural texts, such as those by Ell and Ghambir, Sandler et al. and Henkin et al., provide us with very comprehensive reference sources while some of the smaller texts totally written by two or three individuals, e.g. Mettler & Guiberteau and Ziessman, O'Malley & Thrall, have achieved popularity with radiology residents and other physicians in training.

The concept of *Clinical Nuclear Medicine* arose 3 years ago from a conversation between the editors, who have been close friends for many years. We have always felt that our relationship epitomizes one of the major strengths of nuclear medicine, which is the very close ties and spirit of educational cooperation that exist between international colleagues. We all share the same aim of doing whatever we can to optimize patient care whether it be by introducing new pharmaceuticals and instruments or by developing new techniques or approaches to performing our broad spectrum of clinical procedures. Nuclear medicine physicians have almost uniformly been willing to share their expertise at national and international meetings. The international nuclear medicine community, unlike many other larger specialty areas, has remained relatively small.

It was within this spirit that *Clinical Nuclear Medicine* was born. As will become immediately evident, the chapters are almost equally split between American and European authors. Additionally, one of the chapters was contributed by one of our colleagues from Taiwan. A unique feature of this text is the incorporation of PET into each organ system or disease specific chapter rather than presenting it as a separate chapter. A considerable amount of time was spent selecting and assembling the stellar cast of authors, who have graciously contributed their time, effort and, indeed, great talent to make this text the readable, concise text that we believe it represents. We hope that you, our readers, agree. We are most grateful to our many colleagues and friends who share our vision.

Hans-Jürgen Biersack, MD
Leonard M. Freeman, MD

Contents

Nuclear Medicine Diagnosis

Nuclear Medicine Therapy

List of Contributors

Alessandra Alessi, MD
PET Unit
Nuclear Medicine Division
Fondazione IRCCS „Istituto Nazionale Tumori“
Via Venezian 1
20133 Milan
Italy

Serge Askienazy, MD, PhD
Laboratoires Cyclopharma
Biopôle Clermont-Limagne
63360 Saint Beauzire
France

Marika Bajc, MD
Department of Nuclear Medicine
University Hospital
22185 Lund
Sweden

Richard P. Baum, Prof. Dr. med.
Department of Nuclear Medicine/PET Center
Zentralklinik Bad Berka
Robert-Koch-Allee 9
99437 Bad Berka
Germany

Hans-Jürgen Biersack, Prof. Dr. med.
Klinik und Poliklinik für Nuklearmedizin
Rheinische Friedrich-Wilhelms-Universität
Sigmund-Freud-Straße 25
53127 Bonn
Germany

Chantal P. Bleeker-Rovers, MD
Centre for Infectious Diseases
Nijmegen University
Nijmegen, The Netherlands;
Department of Internal Medicine
Radboud University Nijmegen Medical Centre
Nijmegen
The Netherlands

Emilio Bombardieri, MD
Nuclear Medicine Division
Fondazione IRCCS „Istituto Nazionale Tumori“
Via Venezian 1
20133 Milan
Italy

Patrick Bourguet, MD, PhD
Medicine Nucléaire
Université de Rennes
Centre Eugène Marquis
Rue de la Bataille des Flandres-Dunkerque
BP 6279
35062 Rennes Cedex
France

Jan Bucerius, Dr. med.
Klinik und Poliklinik für Nuklearmedizin
Universitätsklinikum Bonn
Sigmund-Freud-Straße 25
53127 Bonn
Germany

Manuel D. Cerqueira, MD
Department of Molecular and Functional Imaging
Cleveland Clinic Foundation
9500 Euclid Ave., GB-3
Cleveland, OH 44195
USA

Cheng-Keng Chuang, MD, PhD
Department of Urology
Chang Gung Medical Center
199 Tung Hwa North Road
Taipei
Taiwan

Concetta de Cicco, MD
Nuclear Medicine Division
European Institute of Oncology
Via Ripamonti 435
20141 Milan
Italy

Susan E.M. Clarke, MSc, FRCP, FRCR
Department of Nuclear Medicine
Guy's & St. Thomas' NHS Foundation Trust
St. Thomas' Street
London, SE1 9RT
UK

Morton Coleman, MD
Division of Hematology/Oncology
Weill Medical College of Cornell University
and The New York Presbyterian Hospital
New York, NY 10021
USA

Gary Cook, MSc, MD, FRCP, FRCR
Department of Nuclear Medicine and PET
Royal Marsden Hospital
Sutton
Surrey, SM2 5PT
UK

Frans H.M. Corstens, MD, FRCP
Nijmegen University Centre for Infectious Diseases
Nijmegen
The Netherlands;
Department of Nuclear Medicine/Department
of Internal Medicine
Radboud University Nijmegen Medical Centre
PO Box 9101
6500 HB Nijmegen
The Netherlands

Flavio Crippa, MD
PET Unit
Nuclear Medicine Division
Fondazione IRCCS „Istituto Nazionale Tumori"
Via Venezian 1
20133 Milan
Italy

Jan-Paul Esser, MD
Department of Nuclear Medicine
Erasmus Medical Center
's-Gravendijkwal 230
3015 GD Rotterdam
The Netherlands

Maria João Vidigal Ferreira, MD
Coimbra University Hospital
Coimbra University School of Medicine
Coimbra
Portugal

Ignac Fogelman, BSc, MD, FRCP
Department of Nuclear Medicine
Guy's & St. Thomas' Hospital NHS Foundation Trust
St. Thomas' Street
London, SE1 9RT
UK

Leonard M. Freeman, MD
Albert Einstein College of Medicine
Department of Nuclear Medicine
Montefiore Medical Center/Moses Division
111 East 210th Street
Bronx, NY 10467
USA

Etienne Garin, MD, PhD
Centre Eugène Marquis
Rue de la Bataille Flandres-Dunkerque
CS 44229
35042 Rennes Cedex
France

Stanley J. Goldsmith, MD
Division of Nuclear Medicine
Weill Medical College of Cornell University and
The New York Presbyterian Hospital
New York, NY 10021
USA

Juan P. Oliva González, Prof. Dr.
Instituto Nacional De Oncología
y Radiobiología
Dpto. Medicina Nuclear
Calle 29 y E. Vedado
Vedado CP 10400
Ciudad Habana
Cuba

Gopinath Gnanasegaran, MBBS, MSc, MD
Department of Nuclear Medicine
Guy's & St. Thomas' Hospital NHS Foundation Trust
St. Thomas' Street
London, SE1 9RT
UK

Michael M. Graham, PhD, MD
Department of Radiology
Division of Nuclear Medicine
3863 JPP
University of Iowa
200 Hawkins Drive
Iowa City, IA 52242
USA

Frank Grünwald, Prof. Dr. med.
Klinik für Nuklearmedizin
Zentrum der Radiologie
Klinikum der J.-W.-Goethe-Universität
Theodor-Stern-Kai 7; Haus 21D
60590 Frankfurt/Main
Germany

Stefan Guhlke, PhD
Department of Nuclear Medicine
University of Bonn
Sigmund-Freud-Str. 25
53127 Bonn
Germany

Sherman L. Heller, PhD
Department of Nuclear Medicine
Montefiore Medical Center
111 East 210th Street
Bronx, NY 10467
USA

Masonori Ichise, MD
Department of Nuclear Medicine Division
Brigham & Women's Hospital
75 Francis Street
Boston, MA 02115
USA

Isabel Igerc, OA Dr.
Department of Nuclear Medicine and Endocrinology
PET Center Klagenfurt
LKH Klagenfurt
St. Veiterstraße 47
9020 Klagenfurt
Austria

Marion de Jong, PhD
Department of Nuclear Medicine
Erasmus Medical Center
's-Gravendijkwal 230
3015 GD Rotterdam
The Netherlands

Björn Jonson
Department for Clinical Physiology
University Hospital Lund
22185 Lund
Sweden

Susanne Kohlfürst, Ass. Dr.
Department of Nuclear Medicine and Endocrinology
PET Center Klagenfurt
LKH Klagenfurt
St. Veiterstraße 47
9020 Klagenfurt
Austria

Lale Kostakoglu, MD
Department of Radiology
Division of Nuclear Medicine
Mount Sinai Medical Center
One Gustave Levy Place
Box 1141
New York, NY 10029
USA

Eric P. Krenning, MD, PhD
Department of Nuclear Medicine
Erasmus Medical Center
's-Gravendijkwal 230
3015 GD Rotterdam
The Netherlands

Joachim Kropp, Prof. Dr.
Klinik für Nuklearmedizin
Carl-Thiem-Klinikum
Carl-Thiem-Straße 111
03048 Cottbus
Germany

Dik J. Kwekkeboom, MD, PhD
Department of Nuclear Medicine
Erasmus Medical Center
's-Gravendijkwal 230
3015 GD Rotterdam
The Netherlands

Chyong-Huey Lai, MD
Department of Obstetrics and Gynecology
Chang Gung Memorial Hospital
Linkou Medical Center
5 Fu-Shin St.
Kueishan
Taoyuan 333
Taiwan

Daniel S. Levine, MB, ChB, MRCP, FRCR
Department of Radiology
British Columbia Children's Hospital
Vancouver, British Columbia
Canada

Peter Lind, Prim. Assoc. Prof. Dr.
Department of Nuclear Medicine and Endocrinology
PET/CT Center
General Hospital Klagenfurt
St. Veiterstraße 47
9020 Klagenfurt
Austria

Yusuf Menda, MD
Department of Radiology
Division of Nuclear Medicine
University of Iowa
200 Hawkins Drive
Iowa City, IA 52242
USA

Christian Menzel, Prof. Dr. med.
Klinik für Nuklearmedizin
Zentrum der Radiologie
Klinikum der J.-W.-Goethe-Universität
Theodor-Stern-Kai 7
Haus 21D
60590 Frankfurt/Main
Germany

Gynter Mödder, Prof. Dr. med.
Praxis für Nuklearmedizin
Max-Planck-Str. 27a
50858 Köln
Germany

Helen R. Nadel, MD
Department of Nuclear Medicine
British Columbia Childrens' Hospital
4480 Oak Street
Vancouver, BC, V6H 3VA
Canada

Giovanni Paganelli, MD
European Institute of Oncology
Via Ripamonti, 435
20141 Milan
Italy

Holger Palmedo, Prof. Dr. med.
Klinik und Poliklinik für Nuklearmedizin
Universitätsklinikum Bonn
Sigmund-Freud-Straße 25
53127 Bonn
Germany

László Pávics, MD
Department of Nuclear Medicine
Albert Szent-Györgyi Medical University
Korányi fasor 8
6720 Szeged
Hungary

Vikas Prasad, Dr., DRM, DNB
Department of Nuclear Medicine/PET Center
Zentralklinik Bad Berka
Robert-Koch-Allee 9
99437 Bad Berka
Germany

Laura Ravasi, MD
Nuclear Medicine Division
European Institute of Oncology
Via Ripamonti 435
20141 Milan
Italy

Edward B. Silberstein, MD
Nuclear Medicine
University of Cincinnati Medical Center
234 Goodman Street
PO Box 67 05 77
Cincinnati, OH 45267-0577
USA

Hans C. Steinert, Prof. Dr. med.
Klinik und Poliklinik für Nuklearmedizin
Medizinische Radiologie
Universitätsspital Zürich
Rämistraße 100
8091 Zürich
Switzerland

Andrew T. Taylor, MD
Division of Nuclear Medicine
Emory University Hospital
1364 Clifton Road NE
Atlanta, GA 30350
USA

Jaap J.M. Teunissen, MD
Department of Nuclear Medicine
Erasmus Medical Center
's-Gravendijkwal 230
3015 GD Rotterdam
The Netherlands

Giuseppe Trifirò, MD
Nuclear Medicine Division
European Institute of Oncology
Via Ripamonti 435
20141 Milan
Italy

Roelf Valkema, MD, PhD
Department of Nuclear Medicine
Erasmus Medical Center
's-Gravendijkwal 230
3015 GD Rotterdam
The Netherlands

Shankar Vallabhajosula, PhD
Division of Nuclear Medicine
NY Weill Cornell Medical Center
525 East 68th Street
New York, NY 10021
USA

Ronald Van Heertum, MD
Department of Radiology
NY Presbyterian Medical Center
177 Fort Washington Ave.
New York, NY 10032
USA

A.M. Verbruggen, PhD
Laboratory of Radiopharmacy
Katholieke Universiteit Leuven
Herestraat 49
3000 Leuven
Belgium

Maria João Vidigal Ferreira, MD
Coimbra University Hospital
Coimbra University School of Medicine
Coimbra
Portugal

Carlo Villano, MD
PET Unit
Nuclear Medicine Division
Fondazione IRCCS „Istituto Nazionale Tumori“
Via Venezian 1
20133 Milan
Italy

Fidel J. Vos, MD
Centre for Infectious Diseases
Nijmegen University
Nijmegen
The Netherlands; Department of Internal Medicine
Radboud University Nijmegen Medical Centre
Nijmegen
The Netherlands

Michaela Welsch, Dr. med.
Department of Nuclear Medicine
University of Frankfurt/Main
Theodor-Stern-Kai 7
60590 Frankfurt
Germany

Tzu-Chen Yen, MD
Department of Nuclear Medicine
Chang Gung Medical Center
199, Tung Hwa North Road
Taipei
Taiwan

Pat Zanzonico, PhD
Division of Nuclear Medicine
Memorial Sloan Kettering Cancer Center
1275 York Ave.
New York, NY 10021
USA

Harvey Ziessman, MD
Division of Nuclear Medicine
The Russell H. Morgan Department of Radiology and Radiological Sciences
Johns Hopkins Medicine
Johns Hopkins Outpatient Center
601 N. Caroline Street JHOC 3231
Baltimore, MD 21287-0817
USA

Lionel S. Zuckier, MD
Department of Radiology
New Jersey Medical School
University of Medicine and Dentistry of New Jersey
Room H-141
150 Bergen Street
Newark, NJ 07103-2406
USA

Physics, Instrumentation, and Radiation Protection

1

P. Zanzonico, S. Heller

1.1 Introduction

The underlying principles of nuclear medicine imaging involve the use of unsealed sources of radioactivity which are administered in the form of radiopharmaceuticals; the ionizing radiations which accompany the decay of the administered radioactivity can be detected and measured with specially designed instruments (e.g., survey meters, gamma cameras). In order to appreciate the scientific and technical basis of nuclear medicine imaging, this chapter reviews atomic and nuclear structure, radioactivity and radioactive decay, and interactions of radiation with matter. This is followed by a discussion of techniques for detection and measurement of radiation, design and operating principles of detection and imaging instruments, instrument quality control, and radiation protection.

1.2 Basic Physics

1.2.1 Atomic and Nuclear Structure

Matter is, of course, composed of atoms, which represent the smallest indivisible sub-unit of an element which retains the characteristic physical and chemical properties of that element. Atoms are composed of a nucleus surrounded by orbital electrons, with the atomic structure maintained by electrostatic forces of attraction between the positively charged nucleus and the negatively charged electrons. Nuclei are composed of positively charged protons and electrically neutral neutrons, which are collectively referred to as nucleons. Orbital electrons are negatively charged; in an electrically neutral, or uncharged, atom, the number of negative orbital electrons equals the number of positive nuclear protons, the charge on these respective particles being equal in magnitude. The properties of these fundamental building blocks of matter – electrons, protons, and neutrons – are summarized in Table 1.1. In addition, positively charged electrons (referred to as "positrons") do not normally exist in nature but can be generated during certain modes of radioactive decay and only exist for very short periods of time (described below).

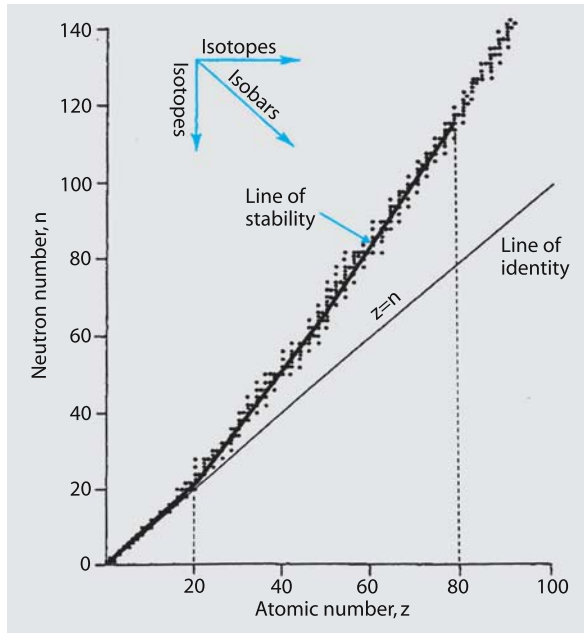

Fig. 1.1. The chart of the nuclides, a scattergram of neutron number, *N*, versus atomic number, *Z*, for all nuclides. Note that isotopes, isobars, and isotopes lie along vertical, diagonal, and horizontal lines, respectively. Note further that structurally stable and therefore non-radioactive nuclei lie along the so-called "line of stability," which runs through the center of this scattergram. The line of stability is bi-phasic, corresponding to the line of identity, $N = Z$, for small nuclei ($Z \leq \sim 20$) and to a steeper line, $N = 1.5Z$, for larger nuclei ($\sim 20 \leq Z \leq \sim 80$), and ends at $Z \approx 80$

Nuclei are structurally characterized by three parameters: atomic number, Z – the number of protons; the neutron number, N – the number of neutrons; and the mass number, $A = Z + N$, the number of nucleons (i.e., neutrons and protons). The atomic number, Z, thus indicates the positive charge of the nucleus and indicates the chemical identity of the element. For example, an atomic number of "6" defines the atom as car-

Table 1.1. Properties of the fundamental particles of matter

Particle	Symbol[a]	Mass		Rest mass energy (E_o)[b]		Charge	
		Universal mass units (u)[c]	Grams (g)	keV[d]	MeV[d]	Elementary charge	Coulombs (C)
Electron	e						
Negatron	e^-	5.486×10^{-4}	9.110×10^{-28}	511	0.511	−1	-1.602×10^{-19}
Positron	e^+	5.486×10^{-4}	9.110×10^{-28}	511	0.511	+1	$+1.602\times10^{-19}$
Proton	p/p^+	1.007	1.673×10^{-24}	938,000	938	+1	$+1.602\times10^{-19}$
Neutron	n/n^o	1.009	1.675×10^{-24}	939,000	939	0	0

[a] In representing particles, the charge is often not explicitly indicated. In the case of electrons, the symbol e (without the charge indicated) is generally interpreted as identifying a negatron

[b] From Einstein's Special Theory of Relativity, the rest mass energy E_o of a particle of mass m is given by the equation, $E_o = mc^2$, where c is the speed of light in vacuum, 3×10^8 m/s

[c] In atomic and nuclear physics, energies are commonly expressed as universal mass units (u), 1/12 of the mass of a carbon-12 atom, 1.66054×10^{-27} kg

[d] In atomic and nuclear physics, energies are commonly expressed as multiples of an electron-volt (eV), the kinetic energy of an electron after passing through a potential difference of 1 volt (V). An MeV, or mega-electron-volt, equals 1 million eV and a keV, or kilo-electron-volt, equals 1 thousand eV

Table 1.2. The electromagnetic (EM) spectrum

	Energy, E			Frequency, ν		Wavelength, λ	
	eV	keV	MeV	Hz[a]	MHz[a]	m	nm
Radio, TV	10^{-8}	10^{-11}	10^{-14}	10^6	1	10^2	10^{11}
Microwave	10^{-4}	10^{-7}	10^{-10}	10^{10}	10^4	10^{-2}	10^7
Infrared	0.1	10^{-4}	10^{-7}	10^{13}	10^7	10^{-5}	10^4
Visible	1	10^{-3}	10^{-6}	10^{14}	10^8	10^{-6}	10^3
Ultraviolet	10	10^{-2}	10^{-5}	10^{15}	10^9	10^{-7}	10^2
X- and γ-rays	10^3	1	10^{-2}	10^{18}	10^{12}	10^{-11}	10^{-2}

[a] Frequencies are typically expressed in units of hertz (Hz), equal to 1 cycle/s (or 1/s). The unit of MHz, or megahertz, equals 1 million Hz and is commonly used to express frequencies of EM radiations

bon. In shorthand, carbon can be represented by just using the chemical symbol and the atomic number, or ^{12}C. Based on these structural parameters, different nuclear "families" have been identified: "isotopes" (e.g. $^{10}_5B^5$ and $^{11}_6B^5$) are nuclei having the same atomic number, Z, and thus are nuclei of the same element; "isobars" (e.g. $^{11}_6C^5$ and $^{11}_6B^5$) have the same mass number, A; and "isotones" (e.g. $^{11}_5C^6$ and $^{10}_5B^5$) have the same neutron number, N. A useful graphical representation of the atomic nuclei is shown in Fig. 1.1, plotting the neutron number, N, versus the atomic number, Z. For relatively small nuclei ($Z < 20$), the nuclei are clustered around the line of identity (i.e., the line $N = Z$); for larger nuclei, they cluster about a steeper line (i.e., the line $N = 1.5Z$).

In the parlance of modern physics, atoms and nuclei are "quantum" systems: the values specifying the positions and energies of particles comprising atoms and nuclei are discrete. Thus, orbital electrons are found only in orbits, or shells at discrete distances from the nucleus, as shown diagrammatically in the Bohr (or "planetary") model of the atom (Fig. 1.2). Nucleons (i.e., protons and neutrons) are likewise arranged in discrete energy levels, or shells within the nucleus. The electron's binding energy, which holds the electron in its orbit, decreases, and its potential energy increases with increasing distance from the nucleus.

Atoms are of the order of 10^{-10} m in diameter and nuclei only one-thousandth of that, 10^{-13} m, in diameter. Nuclear volumes are therefore only ~1 billionth of atomic volumes. The atom and therefore matter in general is thus almost entirely empty space! Nucleon masses, on the other hand, are more than 1,000 times the mass of electrons (Table 1.1) and therefore virtually all (> 99 %) of the "mass" of the atom and of matter generally is found in the nucleus.

In so-called "ground-state" atoms, orbital electrons occupy the shells (i.e., energy levels) closest to the nucleus, that is, the lowest-energy levels. Likewise in ground-state nuclei, nucleons occupy the lowest-energy shells. At this time vacancies may be created producing a non-ground state, or "excited," atoms and nuclei. In such instances, electrons or nucleons will spontaneously move to fill these vacant lower-energy shells. In the process energy is released from the atom in the form of electromagnetic radiation (Table 1.2). This photon energy is equal to the difference between the initial and final potential energies of the electron or nucleon (Fig. 1.3a). In an atom, electron transitions from an outer shell to an inner shell result in the emission of

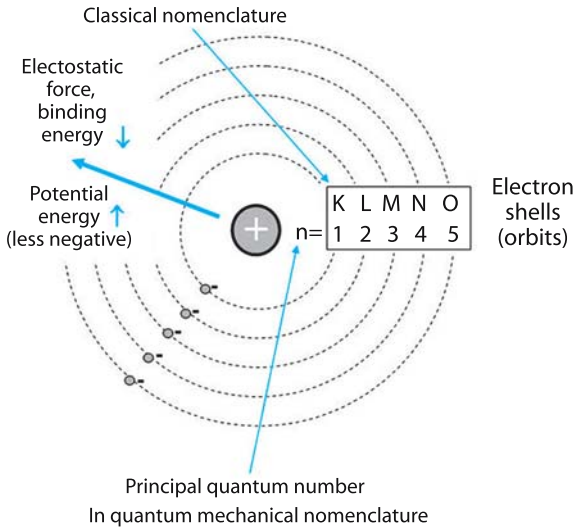

Fig. 1.2. In the Bohr (or planetary) model, the atom is depicted as a miniature solar system, with a positively charged nucleus at the center and negatively charged orbital electrons at discrete (or quantized) radial distances away. Each electron's radial distance from the nucleus, and therefore its shell (or orbit) and its potential energy, are indicated by its principal quantum n [beginning with the value 1 for the innermost, or lowest (most-negative) potential energy, shell and ascending in numerical order for further, higher-potential energy shells]. An alternative designation of the respective electron shells begins with the letter K for the innermost shell, ascending in alphabetical order for the further shells. Although not shown, each shell is composed of more closely spaced sub-shells and ultimately orbitals (designated, in order of increasing potential energy, as s, p, d, and f). There may be up to two electrons – one with spin "up" and the other with spin "down" (corresponding to spin quantum numbers +1/2 and –1/2, respectively) – per orbital. A shell with principal quantum number n may contain up to n^2 orbital and therefore up to $2n^2$ electrons

high-energy X-ray photons. The kinetic energy of the emitted X-ray is described in terms of electron volts, or eV; an eV is the increase in kinetic energy as an electron is accelerated through a potential of 1 V. Likewise, in a nucleus, nucleon transitions result in the emission of photons, or gamma (γ) rays. These photons have energies on the order of keV (10^3 eV) and MeV (10^6 eV). The energy of these photons is "characteristic" and defines the atom from which they originated. The defining difference between X- and γ-rays is related to where they originate – X-rays from the orbital electrons and γ-rays from within the nucleus.

Excited atoms and nuclei do not always result in the emission, respectively, of X- and γ-rays. In the case of excited atoms, the energy released as an orbital electron transitions from an outer to an inner shell may instead be transferred to another orbital electron within the same atom, ejecting the latter electron. The electron thus ejected is termed an "Auger electron" (Fig. 1.3b). The "fluorescent yield (ω_K)" is the probability that a shell-to-shell electron transition will yield characteristic X-rays rather than Auger electrons. This ratio increases with increasing atomic number and reaches a value of ~1 (i.e., all X-ray and no Auger-electron emission) by an atomic number of ~50. In the case of unstable nuclei, the energy released as a nucleon transition from a higher- to a lower-energy shell likewise may instead be transferred to an orbital electron within the same atom, ejecting that electron from the atom. This process is called "internal conversion" and the ejected electron is termed a "conversion electron" (Fig. 1.3c).

Some nuclei may exist in different energy states (e.g., ground and excited states) and are referred to as "isomers"; the transition from an excited state to its ground state is termed an "isomeric transition." Typically, excited nuclear states are very short-lived (of the order of 10^{-12} s or less). Certain excited nuclear states, however,

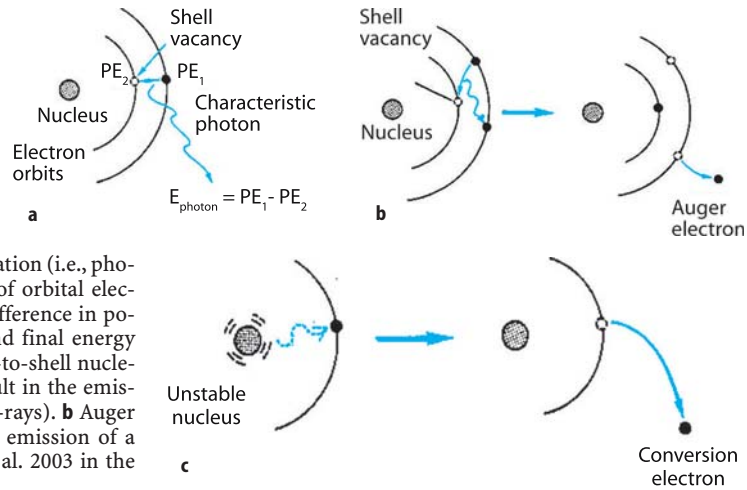

Fig. 1.3. a Emission of characteristic atomic radiation (i.e., photon) resulting from a shell-to-shell transition of orbital electrons. The photon energy, E_{photon}, equals the difference in potential energies of the electron in its initial and final energy levels, PE_1 and PE_2. Analogous processes, shell-to-shell nucleon transitions, occur in atomic nuclei and result in the emission of characteristic nuclear radiations (i.e., γ-rays). **b** Auger electron emission. **c** Internal conversion, with emission of a conversion electron. (Adapted from Cherry et al. 2003 in the "Further Reading" list)

are unusually long-lived (with lifetimes of the order of seconds to hours) and are referred to as "metastable" (or "almost-stable") states. Metastable nuclei are indicated by the letter "m" immediately following their mass number A; thus, ^{99m}Tc is a metastable excited state of ^{99}Tc and ^{99m}Tc and ^{99}Tc are isomers of technetium-99.

1.2.2 Radioactivity

1.2.2.1 Nuclear Instability

Radioactivity is a property of atomic nuclei and may be defined as the spontaneous transformation of a structurally unstable nucleus to a structurally more stable nucleus, with the emission of energy in the form of ionizing radiation. Two features largely determine the structural stability of a nucleus, the size (i.e., atomic number, Z) and the neutron-to-proton (N-to-Z) ratio. All large nuclei (i.e., $Z \geq$~80) are structurally unstable and therefore radioactive. For nuclei with an atomic number $Z \leq$~80, structural stability depends on the neutron-to-proton (N-to-Z) ratio. For small nuclei (i.e., $Z \leq$~20), stability is achieved for nuclei having an equal number of neutrons and protons, that is, an N-to-Z ratio of 1. For larger nuclei (i.e., ~20 $\leq Z \leq$ ~80), stability is achieved for nuclei having three neutrons for every two protons or an N-to-Z ratio of 1.5.

1.2.2.2 Modes of Radioactive Decay

The position of a nuclide on the chart of the nuclides determines its mode of radioactive decay. Nuclei of elements with ($Z \geq$~80) lie *above* the line of stability and are unstable; they become more stable by generating and emitting an alpha (α) particle.

An α-particle, consisting of two neutrons and two protons, is structurally identical to a helium-4 nucleus, $_2^4$He^2 and α decay reduces nuclear mass by 4. α-particles are emitted from an unstable nucleus and are monoenergetic, having a kinetic energy that is specific to the nuclei (typically of the order of 5 MeV).

For small nuclei ($Z \leq$~80) lying to the *left* of the line of stability, their N-to-Z ratio is unstably high – that is, they have an excess of neutrons and become more stable by converting a neutron to a proton and a beta (β) particle, referred to as beta-minus (β–) decay:

$$^A_N\mathrm{X}^Z \rightarrow {}^A_{N-1}\mathrm{Y}^{Z+1} + {}^0_0\beta^{-1} + \bar{\nu}. \quad (1.1)$$

A β^--particle is structurally identical to an electron, e^-, and β^- decay reduces the unstably high N-to-Z ratio to a more stable value, (N–1)/(Z+1). The emission of a β^--particle is always accompanied by the emission of a charge-less and mass-less particle know as an anti-neutrino, $\bar{\nu}$.

For small nuclei ($Z \leq$~80) lying on the opposite side – to the *right* – of the line of stability, their N-to-Z ratio is unstably low – that is, they have a deficiency of neutrons – and become more stable by converting a proton to a neutron and generating a beta-plus (β+), or positron, particle, referred to as positron decay:

$$^A_N\mathrm{Y}^Z \rightarrow {}^A_{N+1}\mathrm{Y}^{Z-1} + {}^0_0\beta^{+1} + \nu. \quad (1.2)$$

A β^+-particle is also referred to as a positron and has the same mass as a negative electron. For these nuclei with an unstable, low N-to-Z ratio, there is, in addition, an alternative mode of decay called electron capture (EC), in which an intra-nuclear proton literally captures (i.e., combines with) an orbital electron and is thereby converted to a neutron:

$$^A_N\mathrm{X}^Z + {}^0_0\mathrm{e}^{-1} \rightarrow {}^A_{N+1}\mathrm{Y}^{Z-1} + \nu. \quad (1.3)$$

Importantly, β^+ decay is only possible if the "transition energy, Q", the difference between the total mass plus nuclear binding energies between the two nuclei, exceeds an energy threshold of 1.022 MeV (= 1,022 keV). If the transition energy of the decay is less than 1.022 MeV, then *only* electron capture can occur. If, however, $Q >$ 1.022 MeV, then both β^+ decay and electron capture can occur. Both β^+ decay and electron capture increase an unstably low N-to-Z ratio to a more stable value, (N+1)/(Z–1), and are accompanied by the emission of a charge-less and mass-less neutrino, ν.

In beta (either β^- or β^+) decay and electron capture, the mass number, A, does not change. Therefore, beta decay and electron capture are known as "isobaric transitions." In beta decay of a particular radionuclide, the electrons or positrons are emitted over a range of kinetic energies from zero to a radionuclide-specific maximum energy known as the "end-point energy, $(E_\beta)_{max}$." A useful rule-of-thumb is that, for a particular radionuclide, the average β-ray energy, $\bar{E}_\beta$, is approximately one-third of the end-point energy.

Radioactive decay generally yields nuclei in excited (higher-energy) states, with dissipation of excess energy either by the emission of γ-rays or by internal conversion and emission of the resulting conversion electrons. The electron shell vacancies which result from internal conversion (or from electron capture), in turn, lead to electrons entering these inner shells and the emission of characteristic X-rays and Auger electrons. Thus, radioactive decay typically results in a complex cascade of events, beginning with the transformation of one nuclide to another and culminating in the emission of γ-rays, X-rays, and/or electrons.

1.2.2.3 Mathematics of Radioactive Decay

The physical quantity activity, "A", specifies the amount of radioactivity and is the number of radioactive disin-

tegrations (or decays) which occur per unit time. Activity is commonly expressed in disintegrations per second (dps) or disintegrations per minute (dpm):

The conventional unit of activity is the curie (Ci), which represents 3.7×10^{10} dps. (This somewhat odd value is the number of dps in 1 g of radium.) Relative to the amounts of radioactivity used clinically, 1 Ci is a very large activity. Accordingly, sub-multiples of the curie are often used: 1 millicurie (mCi), 3.7×10^{7} dps, is one-thousandth of 1 Ci and 1 microcurie (μCi), 3.7×10^{4} dps, is one-millionth of 1 Ci. The newer, System Internationale (SI) unit of activity is the "becquerel (Bq)," which corresponds to 1 dps. In contrast to 1 Ci, 1 Bq is a very small activity, and so multiples of the becquerel are often used clinically: 1 kilobecquerel (kBq), 1×10^{3} dps, is one thousand Bq and 1 megabecquerel (MBq), 1×10^{6} dps, is one million Bq. Note that 1 μCi = 37 kBq and 1 mCi = 37 MBq.

The mathematics of radioactive decay are well characterized and allow accurate and precise calculation of activities as a function of time. Radioactive nuclei decay (and become stable nuclides) in an exponential manner as a function of time, that is, for a given radionuclide the *fraction* of such nuclei decaying per unit time is constant and referred to as the physical decay constant λ, which is the fraction of radioactive nuclei decaying per unit time (e.g., 0.1 s^{-1} or 10 % decaying per second). The practical form of the exponential law of radioactivity is written as:

$$N(t) = N(0)e^{-\lambda t} \quad (1.4)$$

or

$$A(t) = A(0)e^{-\lambda t} \quad (1.5)$$

where $N(t)$ = the number of radioactive nuclei remaining at the time t
$N(0)$ = the number of radioactive nuclei at time 0
$A(t)$ = the activity remaining at time t
$A(0)$ = the activity at time 0

The quantity $e^{-\lambda t}$ is the so-called "decay factor," the fraction of activity remaining at time t. The appearance of the exponential law of radioactive decay (Eq. 1.4) on various types of graphs is presented in Fig. 1.4. Note, in particular, that such an exponential function appears as a straight line when plotted on a semi-log graph (Fig. 1.4c).

In addition to the physical decay constant, λ, there are other quantities which express the rate of decay of a given radionuclide: the half-life, $T_{1/2}$, which is the time interval for the number of disintegrations/s (decay rate) to drop by 50 % and the mean life, τ, is the time interval for one-half of a given number of radioactive nuclei to decay. The mean life is used in dosimetry calculations of radiation doses from internally administered radionuclides. The decay constant, λ, half-life, $T_{1/2}$, and mean life, τ, are mathematically related as follows:

$$\lambda = 0.693/T_{1/2} \quad (1.6)$$

or

$$T_{1/2} = 0.693/\lambda \quad (1.7)$$

$$\tau = 1.44\ T_{1/2} \quad (1.8)$$

Combining Eqs. 5 and 6 yields the more common form of the decay equation:

$$A(t) = A(0)e^{-.693t/(T\text{-}1/2)} \quad (1.9)$$

Note that when $t = T_{1/2}$ this equation correctly predicts that $A(t) = 0.5\ A(0)$.

Radionuclides often decay not to a stable (i.e., non-radioactive) nuclide but rather to another radionuclide. The resulting radionuclide, of course, will itself subsequently undergo radioactive decay. Such sequences of parent (p), daughter (d), grand-daughter (g), etc., radionuclides are known as radioactive "families" and are the basis of radionuclide generators. The most important radionuclide generator is $^{99}Mo/^{99m}Tc$,

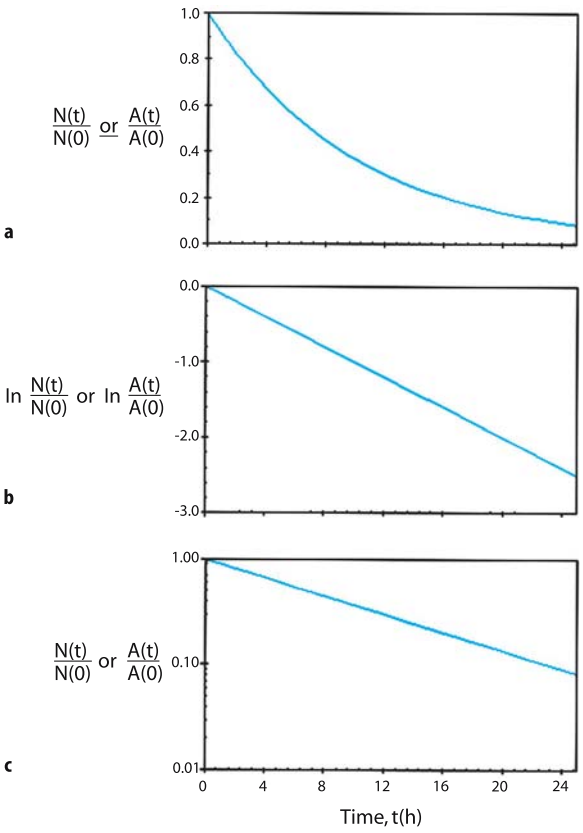

Fig. 1.4. Graphs of the exponential law of radioactive decay (Eqs. 1.4, 1.5): the fraction of the number of radioactive nuclei $[N(t)/N(0)]$ or of activity $[A(t)/A(0)]$ versus time (in hours), t, for a decay constant $\lambda = 0.1$/h. **a** Plotted on a linear-linear graph. **b** Plot of the log transform of the exponential law of radioactive decay, that is, the natural logarithm of $N(t)/N(0)$ or of $A(t)/A(0)$ plotted on a linear-linear graph. It appears as a straight line with a slope of λ and a y-intercept of 0. **c** When $N(t)/N(0)$ or $A(t)/A(0)$ is plotted on a semi-logarithmic ("semi-log") graph, it again appears as a straight line

which is a parent-daughter radionuclide pair in a container that permits separation and removal of the daughter activity. The daughter activity is continuously replenished by the decaying parent. Since the parent half-life (66 h) is significantly longer than that of the daughter (6 h), the generator can be used for more than 1 week.

1.2.3 Interactions of Radiation with Matter

1.2.3.1 Elastic and Inelastic Interactions

Radiation interacts with matter by either elastic or inelastic interactions. In an elastic interaction, the incident radiation is scattered in a different direction but does not lose energy. In contrast, in an inelastic interaction, energy is lost. Photons (X- and γ-rays) are emitted as a result of radioactive decay and are referred to as ionizing radiation; such radiations are sufficiently energetic that they can ionize atoms of a stopping medium, ejecting an electron, and producing an ion pair consisting of a free negative electron and a positive ion.

1.2.3.2 Photon (X- and γ-ray) Interactions

Ionizing radiations (i.e., X- and γ-rays) undergo inelastic interactions by one of several mechanisms: the photoelectric effect, Compton scatter, pair production, and photodisintegration. Pair production, in which an X- or γ-ray interacts with an atomic nucleus and produces a positron-electron pair, has an energy threshold (to account for the combined rest mass energies of the positron and electron created) of 1.022 MeV. Photodisintegration, in which an X- or γ-ray interacts with and fragments the nucleus, has an even higher energy threshold of at least several MeV. Pair production and photodisintegration are therefore not energetically possible for the range of relatively low-energy X- and γ-rays encountered in nuclear medicine and will not be considered further. In the photoelectric effect (Fig. 1.5a), the X- or γ-ray energy is completely transferred to an orbital electron in an atom of the stopping medium, some of the energy used to eject the electron from the atom and the remainder providing kinetic energy to the electron. Usually an inner shell electron is ejected from the atom and the inner shell vacancy is filled with an outer shell electron, the energy difference released as an X-ray. In Compton scatter (Fig. 1.5b), only a portion of the incident photon's energy is transferred to an orbital electron, which is likewise ejected from the atom. The scattered photon's energy is therefore less than that of the incident photon and it travels in a different direction. The *relative* probability of the photoelectric effect increases as the incident photon energy, E_γ, decreases and the effective atomic number, Z_{eff}, of the

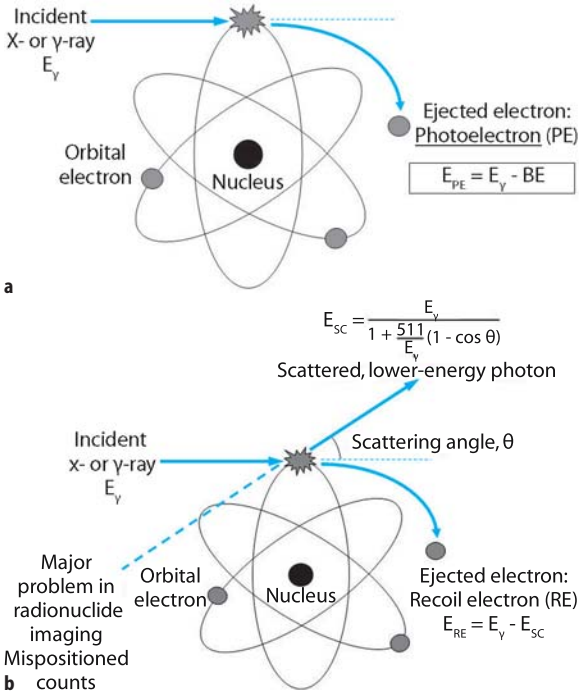

Fig. 1.5. Interactions of X- and γ-rays in matter in the energy range encountered in nuclear medicine. **a** In the photoelectric effect, the energy, E_{PE}, of the ejected electron, termed the photoelectron (PE), is E_γ–BE where E_γ is the energy of the incident photon and BE is the binding energy of that electron in the atom. Note that the incident photon disappears completely. **b** In Compton scatter, the photon does not disappear but is scattered with a lower energy (in keV), E_{SC}; E_{SC} is a function of the energy (in keV) of the incident photon, E_γ, and the scattering angle, θ, as indicated by the equation shown. The energy of the recoil electron (RE), E_{RE}, is therefore E_γ–E_{SC}. Compton scatter generally involves outer-shell orbital electrons with binding energies, BEs, negligibly small compared to typical values of E_γ and E_{SC}; the binding energy, BE, is therefore ignored in calculating the energy of the recoil electron. (Adapted from Zanzonico 2002 in the "Further Reading" list)

stopping medium increases (i.e., proportional to E^3/Z^3). Conversely, the *relative* probability of Compton scatter increases slightly as E_γ increases and Z_{eff} decreases. For X- and γ-ray energies typically encountered in nuclear medicine, the predominant mode of interaction in soft tissue (low Z) is Compton scatter and in scintillation detectors (such as thallium-doped sodium iodide, NaI(Tl)) (high Z) the photoelectric effect.

The mathematics of X- and γ-ray attenuation follows an exponential relationship and is similar in form to the mathematics of radioactive decay. For an attenuating medium of thickness x this relationship is:

$$I(x) = I(0)e^{-\mu x} \quad (1.10)$$

where μ = the linear attenuation coefficient
= the fraction of photons attenuated per unit thickness of stopping material (e.g., in cm^{-1}).

$I(x)$ = the photon intensity transmitted through a thickness x of stopping material, and
$I(0)$ = the incident photon intensity.

The linear attenuation coefficient, μ, is a property of both the photon energy and the stopping material: μ increases (i.e., photons become less penetrating) for low photon energy and low mass density.

In addition to the linear attenuation coefficient, μ, other quantities express the attenuation of X- and γ-rays in an attenuating material: the half-value layer, HVL (or half-value thickness, HVT), which is the thickness required to reduce the photon intensity by one-half; and the mean free path, MFP, is the thickness a photon travels, on average, before interacting. The linear attenuation coefficient, μ, half-value layer, HVL, and mean free path, MFP, are mathematically related as follows:

or: $\mu = 0.693/\text{HVL}$ (1.11)
$\text{HVL} = 0.693/\mu$ (1.12)
$\text{MFP} = 1.44\ \text{HVL}$ (1.14)

Combining Eqs. 10 and 11 yields the most common form of the attenuation equation:

$$I(x) = I(0)e^{-0.693/\text{HVL}} \quad (1.14$$

Note that when the absorber thickness, x, is equal the HVL, the equation correctly predicts that 50 % of the incoming radiation is stopped by the absorber. Another convenient term used when dealing with larger amounts of attenuation is the tenth value layer (TVL) or (Tenth Value Thickness), referring to a thickness which permits only 10 % of the incident radiation to penetrate a medium. The TVL is related to the HVL by TVL = 3.32 HVL.

1.2.3.3 Particulate-Radiation Interactions

Particulate radiations (i.e., β-rays, Auger and conversion electrons) interact with matter by one of two mechanisms: collisional interactions and radioactive interactions. Collisional interactions are somewhat analogous to Compton scatter: an incident β-ray or electron "collides" with and transfers sufficient energy to an orbital electron to eject it from the atom and, in the process, is scattered with a lower energy. In radioactive interactions, on the other hand, the β-ray or electron penetrates the electron "cloud" and reaches and interacts with the atomic nucleus. However, because of the large mass disparity (of the order of a thousand-fold) between electrons and nucleons, the energy lost by the incident β-ray or electron in this interaction appears as X-rays, or *Bremsstrahlung* (German for "brake radiation"), rather than as kinetic energy of the nucleus. *Bremsstrahlung* exhibits a broad energy spectrum, with X-ray energies ranging from zero to a maximum value equal to the energy of the incident particle. For the range of β-ray and electron energies (up to approximately several hundred keV) typically encountered in nuclear medicine, the predominant type of interaction in soft tissue (which has a relatively low Z_{eff}) is overwhelmingly collisional interactions, with less than 1 % of the interactions attributable to radioactive interactions.

There is a large disparity in penetrabilities of photon versus particulate radiations. The X- and γ-rays typically encountered in nuclear medicine have energies of the order of several hundred keV and thus a significant proportion of such radiations can penetrate soft-tissue thicknesses of the order of 10 cm or more. As a result, X- and γ-ray-emitting radionuclides in vivo can be detected and imaged. In contrast, β-rays and electrons are non-penetrating radiations and β-ray and electrons typically encountered in nuclear medicine have ranges in soft tissue of the order of only 1 mm or less. Thus, β-ray- and electron-emitting radionuclides in vivo cannot be detected and imaged non-invasively. In addition, since all their energy is deposited locally, particulate radiation produces a much higher local radiation burden, which makes these radionuclides well suited for radionuclide therapy.

1.3 Radiation Detection and Measurement

1.3.1 Statistical Considerations

Radioactive decay is a random process and therefore random fluctuations will occur in the measured counts or count rates arising from decay of radioactivity. Such random fluctuations complicate the accurate detection, measurement, and imaging of radioactivity. If a detector were used to repeatedly measure the counts or count rates from a given activity, slightly different values would be obtained from measurement to measurement. If an average of N counts is obtained, the standard deviation, σ, of the number of counts is:

$$\sigma = \sqrt{,N} \quad (1.15)$$

and the percent standard deviation (or "noise"), %σ, is:

$$\%\sigma = \frac{100\%}{\sqrt{N}} \quad (1.16)$$

As an example, if a sample count were 100, the %σ = 10 %. Using the laws of a normal distribution we can interpret this as: if we counted a radioactive sample many times, two-thirds of the time the count would be within 10 % of the true value. If, on the other hand, we counted for a longer time and measured 1,000 counts, the %σ = 3.3 %; two-thirds of the time the count would be within 3.3 % of the true value. Measuring for longer

times and obtaining more counts thus produces less random variation in the measurement and the measured value is closer to the true value. This principle applies to the counting of radioactive samples or to planar imaging of radioactivity [i.e., to the counts per unit picture element (or pixel) in a planar image]. In other words, the more counts in an image, the better the statistical accuracy of the image.

1.3.2 Radiation Detector Performance

Radiation detectors may be quantitatively characterized by many different performance parameters. Among the most important of these, however, are sensitivity (or efficiency), energy resolution, and, for devices which localize (image) as well as count radiation, spatial resolution and uniformity.

Sensitivity (or efficiency) is the detected count rate per unit activity. Because the count rate detected from a given activity is highly dependent on the source-detector geometry and intervening absorbing media, characterization of sensitivity can be ambiguous. There are two methods for evaluating sensitivity: geometric sensitivity and intrinsic sensitivity. Geometric sensitivity is the fraction of emitted radiations which intersect, or strike, the detector, that is, the fraction of the total solid angle subtended by the detector. It is therefore directly proportional to the radiation-sensitive detector area and, for a point source, inversely proportional to the square of the source-detector distance. Intrinsic sensitivity is the fraction of radiations intersecting the detector which is stopped within the detector. Intrinsic sensitivity is directly related to the detector thickness, effective atomic number, and mass density and decreases with increasing photon energy, since higher-energy photons are more penetrating and are more likely to pass through a detector without interacting.

Characteristic X-rays and γ-rays are emitted from radioactively decaying atoms with well-defined discrete energies. Due to photon scatter from intervening material (i.e., a patient) and even in the absence of scatter, output electrical pulses from absorption of these radiations will appear to originate from a range of energies. This reflects a limitation of the detector. For this reason, many radiation detectors employ some sort of energy-selective counting: an energy range, or window, is selected such that radiations are counted only if their detected energies lie within that range. Commonly (at least for scintillation detectors such as gamma cameras; see below), a so-called "'20%' photopeak energy window," E_γ ±10% (e.g., 126–154 keV for the 140-keV γ-ray of ^{99m}Tc) is employed, where E_γ is the primary (referred to as the photopeak) energy of the radiation. For such energy-selective counting, overall sensitivity appears to increase as the photopeak energy window is

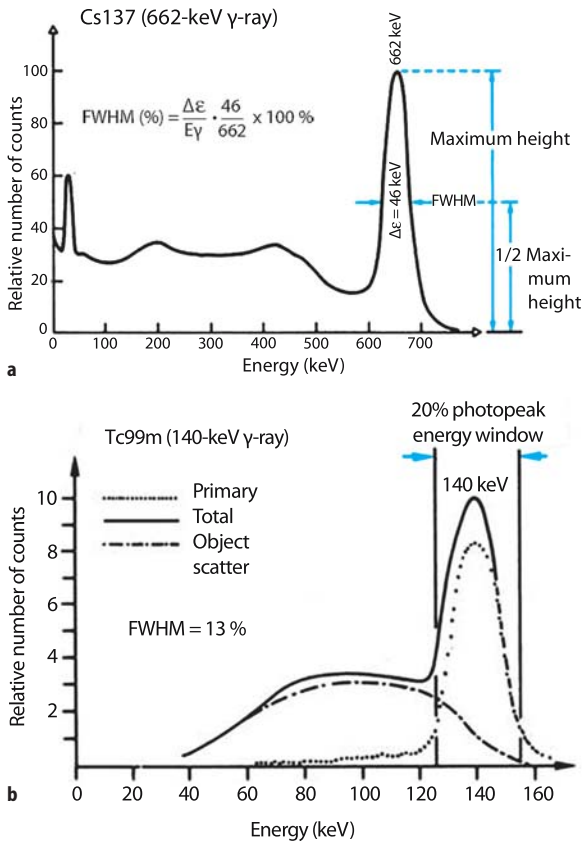

Fig. 1.6. a Energy spectrum for the 662-keV γ-rays emitted by ^{137}Cs, illustrating the definition of energy resolution as the % full-width half-maximum (FWHM) of the photopeak energy, E_γ. **b** Energy spectrum for the 140-keV γ-rays emitted by ^{99m}Tc, illustrating the contributions of primary (unscattered) and scattered radiation counts. In **a** and **b**, the energy spectra were obtained with a thallium-doped sodium iodide [NaI(Tl)] scintillation detector (see text). (Adapted from Cherry et al. 2003 in the "Further Reading" list)

widened. However, this results in acceptance of more scattered as well as primary (i.e., unscattered) radiations. *Energy resolution* quantifies the ability of a detector to separate, or discriminate, radiations of different energies. As illustrated in Fig. 1.6a, energy resolution is generally specified as the full-width at half-maximum height (FWHM = ΔE) expressed as a percentage of the photopeak energy (E_γ) of the bell-shaped photopeak,

$$\text{FWHM (\%)} = \frac{\Delta E}{E_\gamma} 100\%.$$

The importance of energy resolution lies in scatter rejection, particularly for imaging detectors. Radiation loses energy when scattered in the patient and the lower-energy scattered – and therefore mispositioned – radiations may therefore be discriminated from the primary radiations. However, the finite energy resolution of radiation detectors (i.e., the width of the photopeak in the energy spectrum) means that there will be overlap of scattered

and primary radiations, as illustrated in Fig. 1.6b. For systems with superior energy resolution (i.e., the FWHM (%) decreases and the photopeak becomes narrower), the separation of primary and scattered radiations permits scattered radiation to be eliminated while accepting more counts corresponding to primary radiation.

For detectors such as gamma cameras where radiation is localized (imaged) as well as detected and counted, *spatial resolution* is a critical performance parameter. It reflects the ability of the detector to accurately determine the location of a source or, similarly, the ability to visualize two closely spaced point sources. This is usually measured by imaging a point source and examining the spread of the image on the detector. The detector's spatial resolution can then be expressed as the full-width at half-maximum height (FWHM) of this point (or line) spread function. Spatial resolution generally worsens with increasing source-to-detector distance. There is a trade-off between sensitivity and resolution: they are inversely related: sensitivity is reduced as spatial resolution improves and spatial resolution is degraded as sensitivity increases.

Uniformity is likewise a critical parameter of gamma cameras and other imaging devices. In principle, a uniform source of radioactivity (i.e., usually a large disk with ^{57}Co uniformly imbedded in plastic) should yield a uniform image [i.e., an image in which the counts per unit picture element (or pixel) is constant over the entire image]. In practice, this is never achieved – even if one discounts the effects of count statistics (noise) – because of inevitable point-to-point variations in sensitivity of an imaging detector. Uniformity (actually, the deviation from uniformity) may be expressed by a quantity known as the "integral uniformity" (IU):

$$\mathrm{IU} = \frac{\text{Maximal counts per pixel} - \text{Minimum counts per pixel}}{\text{Maximal counts per pixel} + \text{Minimum counts per pixel}} \times 100\% \qquad (1.17)$$

To reliably estimate the IU, a very-high-count image (e.g., a 15-million count image for a gamma camera) of a uniform source minimizes the quantitative effect of count statistics (noise). Acceptable uniformity is < 3.5 %. A second more important parameter widely used to characterize uniformity (specifically, gamma camera uniformity) is the so-called "differential uniformity" (DU), the maximum value of the expression on the right side of Eq. 1.17 determined for every five-pixel segment in every row and column of a uniform-source image.

1.3.3 Basic Design and Operating Principles of Radiation Detectors

Radiation detectors are generally characterized as either scintillation or ionization detectors (Fig. 1.7). In scintillation detectors, visible light is produced as radiation exits atoms of a crystal and converted to an electronic signal, or pulse, and amplified by the photomultiplier tube (PMT). In ionization detectors, free electrons, produced as radiation ionizes a stopping material, are collected to produce an electronic signal.

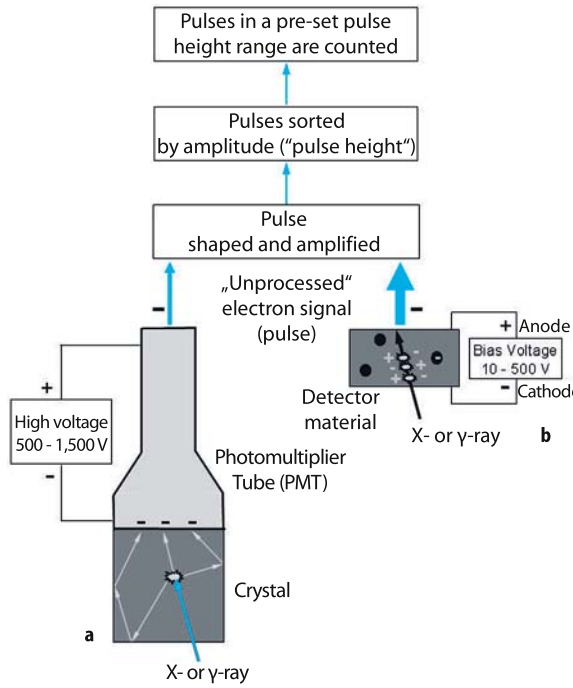

Fig. 1.7. The basic design and operating principle of **a** scintillation and **b** ionization detectors

1.3.4 Ionization Detectors

Detector materials in the most common ionization detectors are gaseous and such detectors are therefore often known as "gas-filled detectors." See design of gas detectors in Fig. 1.7. The two most important gas ionization detectors for nuclear medicine are dose calibrators and Geiger counters. The principal difference among such detectors is the magnitude of the bias voltage between the anode and cathode, as indicated in Fig. 1.8 and Table 1.3. At a bias voltage of 300 V, all of the electrons produced directly by ionization of the detector material by an incident radiation X- or gamma-ray are collected at the anode and produce a fixed detector signal per gamma-ray. In the 300- to 600-V range the overall signal is equivalent to the primary number of electrons and is therefore proportional to the energy of the incident radiation. Dose calibrators operate in this range and are used to assay radiopharmaceutical activities before injecting patients. The relatively low sensitivity of such devices is not a major disadvantage, as ra-

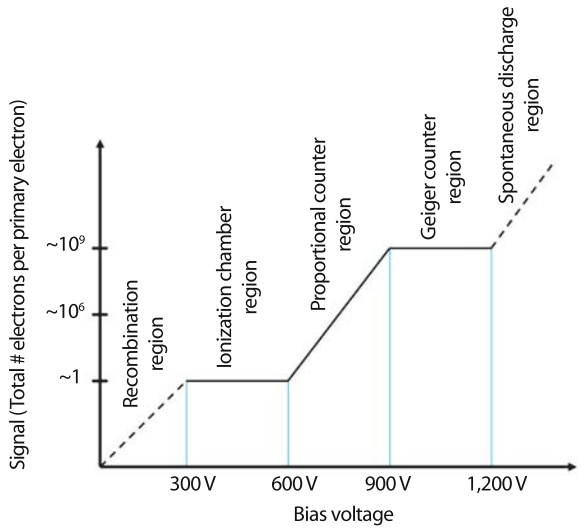

Fig. 1.8. The signal (expressed as the amplification factor, that is, the total number of electrons per primary electron produced in the detector material) as a function of the bias voltage for gas-filled ionization detectors. The principal difference among such detectors is the magnitude of the bias voltage between the anode and cathode. The amplification factors and the voltages shown are approximate

Table 1.3. Properties of gas-filled ionization detectors

	Ionization detector	Proportional counter	Geiger counter
Bias-voltage operating range	300 – 600 V	600 – 900 V	900, 1,200 V
Response stable with respect to voltage?[a]	Yes	No	Yes
Sensitivity[b]	Low	Intermediate	High
Capable of energy discrimination?	Yes	Yes	No
Applications	Dose calibrator	Research	Survey meter

[a] Stability with respect to the bias voltage corresponds to a constant signal over the respective detector's operating voltage range. In contrast to ionization detectors and Geiger counters, proportional counters are unstable with respect to the bias voltage and thus require specialized, highly stable voltage sources for constancy of response

[b] The sensitivity of a detector is related to its amplification factor (see Fig. 1.7)

[c] If the total number of electrons comprising the signal is proportional to the number of electrons directly produced by the incident radiation and therefore proportional to its energy, as in ionization detectors and proportional counters, radiations of different energies can be discriminated (i.e., separated) on the basis of the signal amplitude

diopharmaceutical activities are typically rather large (i.e., in the μCi to mCi range). Energy discrimination is usually achieved by the use of precalibrated amplifiers, one for each radionuclide. Ionization chambers operating at bias voltages in the 900- to 1,200-V range are "Geiger counters" (or "Geiger-Müller" or "GM"). In contrast to ionization chambers the Geiger counter output signal is independent of the number of primary electrons and the energy of the incident radiation. The output is referred to as an "all-or-nothing" response, meaning that if an incoming photon has sufficient energy the Geiger counter will register the count. Geiger counters, because of their high sensitivity and stability with respect to voltage (allowing the use of a portable power supply such as an ordinary battery), are well suited and widely used as survey meters for ambient radiation levels and radioactive contamination. For survey meters, sensitivity, and not energy discrimination, is critical.

1.3.5 Scintillation Detectors

In scintillation detectors (Fig. 9a), radiation interacts with and deposits energy in a scintillator, most commonly a crystalline solid such as thallium-doped sodium iodide [NaI(Tl)]. The radiation energy thus deposited is converted to visible light. Because the light is emitted isotropically (i.e., in all directions), the inner surface of the light-tight crystal housing is coated with a reflective material so that light emitted toward the sides and front of the crystal are reflected back toward a PMT (Fig. 1.9b) (gamma cameras have 37 – 105 PMTs per detector); this maximizes the amount of light collected and therefore the overall sensitivity of the detector. In addition, this insures that the amount of light detected is proportional to the energy of the absorbed photon. Interposed between the back of the crystal and the entrance window of the PMT is the light pipe, nowadays simply a thin layer of transparent optical gel. The light pipe optically couples the crystal to the PMT and thus maximizes the transmission (>90%) of the light signal from the crystal into the PMT.

The operation of the photomultiplier tube is as follows: Coated on the inner surface of the PMT is the photocathode. When struck by the light from the crystal, the photocathode, which is at ground (i.e., 0 V), emits electrons. Immediately beyond the photocathode is the focusing grid, maintained at a relatively low positive voltage of the order of 10 V. Electrons pass through the focusing grid; they are attracted by a relatively large positive voltage, ~300 V, on the first of a series of small metallic elements called dynodes. The resulting high-speed impact of each electron results in the ejection from the dynode surface of an average of three electrons. The electrons thus ejected are then attracted by the even larger positive voltage, ~400 V, on the second dynode. The impact of these electrons into the second

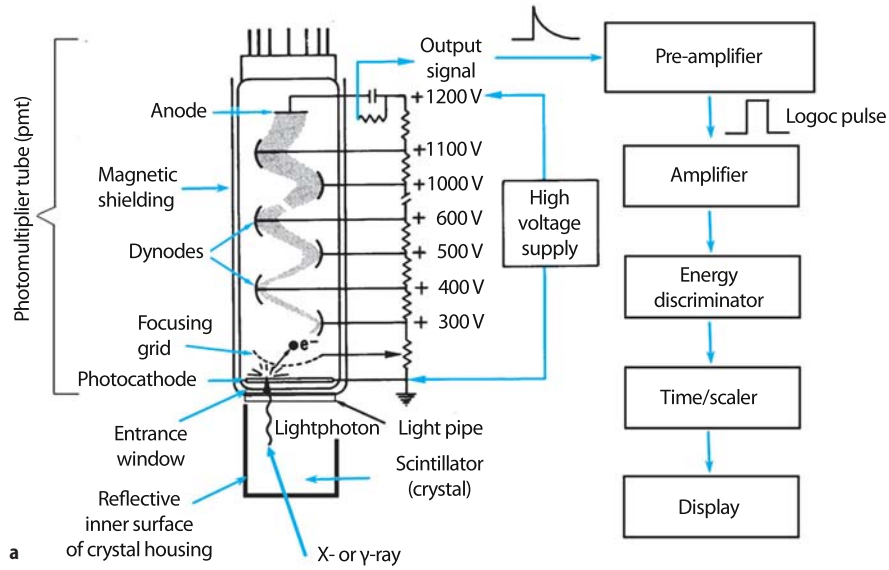

Fig. 1.9. a The basic design and operating principle of PMTs and scintillation detectors. **b** Photographs of PMTs. The PMTs circled are typical of those used in gamma cameras

dynode surface ejects an additional three electrons for each incident electron. Typically, a PMT has 10–12 such dynodes (or stages) each ~100 V more positive than the preceding dynode resulting in an overall electron amplification factor of 3^{10} to 3^{12} for the entire PMT. At the last anode an output signal is generated. The irregularly shaped PMT output signal is then shaped by a pre-amplifier and further amplified into a logic pulse that can be electronically manipulated. The resulting electrical pulses, whose amplitudes (or "heights") are proportional to the number of electrons produced at the PMT photocathode, are therefore also proportional to the energy of the incident radiation. These pulses can then be sorted according to their respective heights by an energy discriminator (also known as a pulse height analyzer) and those pulses with a pulse height (i.e., energy) within the preset photopeak energy window (Fig. 1.9a) are counted by the timer/scaler.

In addition to their widespread use in gamma cameras and SPECT and PET scanners, scintillation detectors are used in well counters, intraoperative probes, and organ ("thyroid") uptake probes.

1.4 Nuclear Medicine Instrumentation

1.4.1 Intraoperative Probes

Intraoperative probes (Fig. 1.10), small, handheld counting devices, are now widely used in the management of cancer: most commonly, to more expeditiously identify and localize sentinel lymph nodes and thereby reduce the need for more extensive surgery; in addition, to identify and localize visually occult disease at surgery following systemic administration of a radiolabeled antibody or other tumor-avid radiotracer. [Although intraoperative probes have been used almost

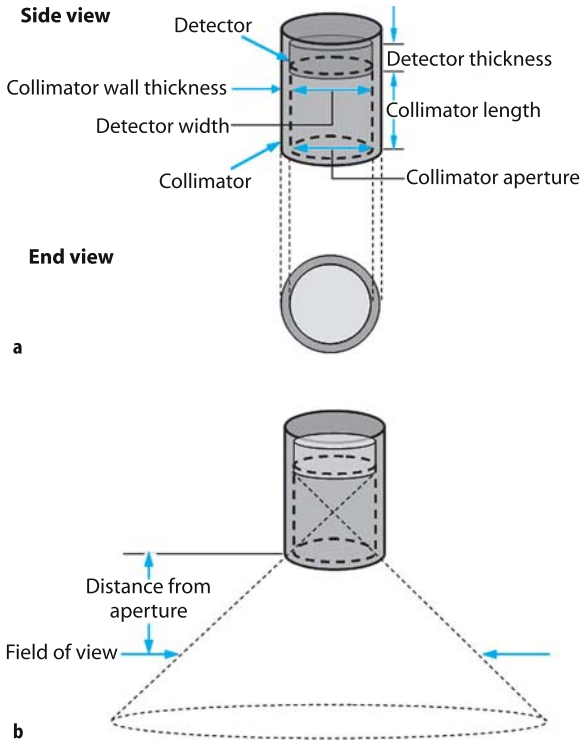

Fig. 1.10. a Basic design of a gamma probe collimator. The collimator may be thought of as an extension of the detector shielding in the forward direction, that is, beyond the detector face in the desired counting direction. A collimator may be characterized by its aperture (generally, but not necessarily, equal to the width of the detector), its length, and its wall thickness. **b** The probe's FOV, that is, the area of tissue from which unscattered X- or γ-rays may reach the detector, increases with increasing distance from the collimator aperture. The volume of tissue from which unscattered X- or γ-rays may reach the detector is thus a three-dimensional cone diverging outward from the collimator (the *dotted line*). (Adapted from Zanzonico 2002 in the "Further Reading" list)

exclusively for counting X- and γ-rays, beta (electron and positron) probes constructed with plastic scintillators have also been developed. As well, small field-of-view intraoperative gamma cameras, with up to 12.5 cm field of view, have recently become available to simplify and improve the accuracy for localization of sentinel nodes and tumors.] Intraoperative gamma probes are available with either scintillation or semiconductor (ionization) detectors. Scintillation detector-based probes have the advantages of relatively low cost and high sensitivity (mainly because of their greater thickness, ~10 mm, versus only ~1 mm in ionization detectors), especially for medium- to high-energy photons. Disadvantages include bulkiness and relatively poor energy resolution and scatter rejection relative to semi-conductor based probes. In some scintillation-detector intraoperative probes, the light signal from the crystal is guided to a remote PMT through a flexible fiberoptic cable, allowing the probe assembly to be made relatively light and compact and more like a surgical instrument, but the significant loss of light in the long cable makes it more difficult to separate scatter from direct gamma rays. On the other hand, semiconductor-based probes are compact and have excellent energy resolution and scatter rejection. To minimize an internal signal problem which degrades the energy resolution, semiconductor detectors are made relatively thin (only ~1 mm), but at the cost of lower intrinsic sensitivity. The main disadvantage of semiconductor detectors remains their limited thickness and resulting lower sensitivity, especially for medium- to-high-energy X- and γ-rays. Nonetheless, while scintillation detectors can be made thicker and therefore more sensitive, semiconductor detectors produce more electrons per X- and γ-ray stopped and therefore have superior energy resolution. To date, the few clinical studies directly comparing scintillation and semiconductor intraoperative probes have not provided a clear choice between the two types of probes.

1.4.2 Organ Uptake Probes

Historically, organ uptake probes have been used almost exclusively for measuring thyroid uptakes and are thus generally known as "thyroid" uptake probes. Thyroid uptake (i.e., the decay-corrected percent of administered activity in the thyroid) can be measured following oral administration of radioiodide (5 – 10 μCi of ^{131}I in liquid or capsule form or 100 – 200 μCi of ^{123}I in capsule form) or, less commonly, ^{99m}Tc-pertechnetate (2 – 10 mCi). The uptake probe is a radionuclide counting system consisting of a wide-aperture, diverging collimator, a NaI(Tl) crystal (typically ~5 cm thick by ~5 cm in diameter), a photomultiplier tube, a pre-amplifier, an amplifier, an energy discriminator (i.e., an energy window), and a gantry (stand). Commercially available thyroid uptake probes are generally supplied as integrated, computerized systems with automated data acquisition and processing capabilities, yielding results directly in terms of percent uptake. Each measurement of thyroid uptake generally includes the following: ambient (i.e., "room") background, a "thigh" background (measured over the patient's thigh and designed to account for the count contribution of extrathyroidal neck activity), thyroid (i.e., neck) activity, and a standard (counted in a Lucite neck phantom simulating the thyroid/neck anatomy) activity. By including measurement of a standard activity with each uptake determination, precise corrections for radioactive decay and day-to-day variation in system sensitivity are automatic. (Alternatively, one may measure the administered activity itself in a phantom immediately prior to patient administration and then correct for radioactive decay when comparing with subsequent thy-

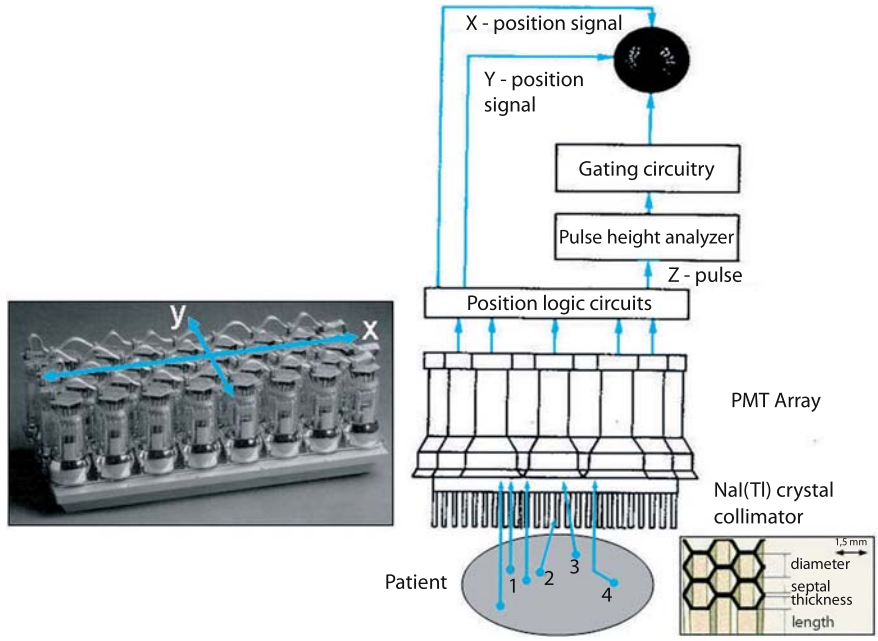

Fig. 1.11. Basic design of a gamma camera, consisting of a multi-hole collimator, a thin large-area NaI(Tl) crystal, a two-dimensional array of PMTs and associated electronics (high-voltage power supply, pre-amplifier, and amplifier), position logic circuitry, energy discriminator, and image display. Note that there are actually two position logic circuits – for the determination separately of the *x*- and *y*-positions of the scintillation within the crystal. Note further that the output signal from each PMT is actually split into three parts, one (the z pulse) for the determination of the energy of the incident radiation as well as one each for the determination of its *x*- and *y*-positions. The *left inset* shows a photograph of the two-dimensional PMT array backing the crystal in a typical rectangular field-of-view gamma camera. The *right inset* shows a drawing of a portion of a parallel-hole collimator, identifying the dimensions – aperture diameter, septal thickness, and septal length – of such a collimator. The "desirable" events (*arrows* labeled "*1*") are unscattered (i.e., photopeak) photons traveling in a direction parallel or nearly parallel to the axes of the apertures and thus yielding correctly positioned counts in the gamma camera image. "Undesirable" events include: scattered as well as unscattered photons traveling in a direction oblique to the axes of the apertures (*2*) and thus eliminated by attenuation by one or more collimator septa; septal penetration (*3*), that is, unscattered photons traveling in a direction oblique to the axes of the apertures yet passing through the septa and yielding mis-positioned counts; scatter (*4*), that is, photons undergoing Compton scatter within the patient and either eliminated by energy discrimination or not eliminated and yielding mis-positioned counts (Fig. 1.6b). (Adapted from Cherry et al. 2003 in the "Further Reading" list)

roid uptake measurements.) The standard consists of a solution containing a known amount of activity. The thyroid uptake is then calculated by subtracting room and thigh background counts from the thyroid measured activity and comparing to the phantom activity (which would represent 100 % uptake).

Thyroid uptake measurements can also be performed from planar scintigraphic images of the neck and of a standard (i.e., phantom) acquired with a gamma camera fitted with a parallel-hole collimator.

1.4.3 Gamma Cameras

Developed in the late 1950s by Hal Anger, the gamma camera (Fig. 1.11), also known as the scintillation or Anger camera, has become the predominant imaging device in nuclear medicine – mainly because its large detector area allows simultaneous and therefore rapid data acquisition over a large area of the body. Gamma camera crystals vary in thickness from 1/4" (yielding the best spatial resolution but lowest sensitivity) to 1" (yielding the highest sensitivity but coarsest resolution and mostly used for imaging the 511-keV photons of ^{18}F), with 3/8"-thick crystals providing the optimum balance between sensitivity and resolution and remaining the most widely used for general gamma camera imaging. About 95 % of the 140-keV photons from ^{99}Tc are absorbed in a 3/8" crystal. Gamma camera NaI(Tl) crystals are nowadays most commonly rectangular in shape and ~50×60 cm in area.

The gamma camera collimator, almost always composed of lead, "directionalizes" the incoming radiation: any radiation traveling at an oblique angle to the axes of the holes (apertures) will strike the lead walls (septa) between the holes and not reach the crystal, thereby allowing only radiation traveling perpendicular to the crystal surface to pass through the apertures and contribute counts to the resulting image. Of course, a certain fraction of photons striking the septa will nonetheless pass through them and reach the crystal (about 5 %); this phenomenon, which degrades image quality, is known as septal penetration. Almost all collimators are parallel hole collimators, in which the apertures and septa are parallel to one another. In addition, single-aperture pinhole collimators, most commonly used for thyroid imaging because of their pronounced magnifying effect, are available as well. Pin-hole collima-

tors, however, suffer from geometric distortion, that is, image magnification varies with both distance and lateral distance from the center of field.

Gamma camera collimators are "rated" with respect to photon energy and resolution/sensitivity. Low-energy, or "technetium," collimators, referred to as "low energy all purpose" collimators (LEAP) or "low energy high resolution" collimators (LEHR), are designed to image radionuclides emitting X- and γ-rays less than 200 keV in energy, including, most notably, ^{99m}Tc (photopeak energy: 140 keV) as well as ^{201}Tl (68 – 80 keV), ^{123}I (159 keV), and ^{57}Co (124 keV). Medium-energy, or "gallium," collimators are designed for radionuclides emitting X- and γ-rays 200 – 300 keV in energy, including ^{67}Ga (93, 185, and 300 keV) as well as ^{111}In (172 and 247 keV). High-energy, or "iodine," collimators are designed to image radionuclides emitting X- and γ-rays greater than 300 keV in energy, including ^{131}I (364 keV). Today, many departments no longer have a high energy collimator and use a medium energy collimator for imaging ^{131}I, accepting the increased septal penetration but achieving a better image quality and improved sensitivity, which is important when imaging the low ^{131}I activity in patient studies. In progressing from low- to medium- to high-energy collimation, the collimators are made longer and the septa thicker in order to interpose more lead between the patient and the crystal and to thereby maintain septal penetration (i.e., the percent of counts in an image attributable to photons that penetrate septa) at or below an acceptably low level, typically set at 5%. This, in turn, reduces the overall fraction of emitted X- and γ-rays reaching the crystal. To compensate, at least in part, for the resulting lower sensitivity, the apertures are typically made wider in progressing from low- to medium- to high-energy collimators. This, however, degrades spatial resolution. Overall, therefore, gamma camera images are progressively poorer in quality for radionuclides emitting low- versus medium- versus high-energy X- and γ-rays because of a combination of increased septal penetration with increasing photon energy, lower sensitivity because of the longer collimation, and coarser resolution because of the wider apertures. For each energy rating, collimators may also be rated as "general-purpose" (or "all-purpose"), "high-resolution," or "high-sensitivity." High-resolution collimators have narrower apertures (and therefore lower sensitivity) and high-sensitivity collimators have wider apertures (and therefore coarser resolution), respectively, than general-purpose collimators. Finally, in instances where a radionuclide emits each of a number of photons in significant amounts, it is the highest-energy photon which dictates the collimator to be used. For example, a medium-energy collimator must still be used to image ^{67}Ga (photon energies: 93, 185, and 300 keV) even if only the two lower-energy (i.e., the 93- and 185-keV) photons are used for imaging. (For some older systems, only two, rather than three, photon energies can be imaged simultaneously.)

Once the incident radiation passes through the collimator aperture, it strikes and may produce a scintillation within the crystal. The resulting light signal is spread out among the PMTs in a two-dimensional array on the back of the crystal, the intensity varying inversely with the distance between the scintillation and the respective PMT: the further the PMT is from the scintillation, the less light it receives and the smaller its output pulse. This inverse linear relationship is the basis of the Anger position logic circuitry for determining the precise position of a scintillation within the crystal. In the older gamma cameras, the *x*- and *y*-coordinates were calculated by analog circuitry, that is, using matrices of resistors. In newer models, this is done by digitizing the output signal from each PMT with an analog-to-digital converter (ADC) and using digital electronics.

1.4.4 Tomographic Scanners

1.4.4.1 Introduction

A "tomogram" is literally a picture of a slice. Tomography may be characterized as either transmission or emission tomography depending on the origin of the radiation. In transmission tomography, X-rays are transmitted through the patient; in emission tomography, X- or γ-rays are emitted from within the patient. Emission tomography can be further characterized on the basis of the nature of the emitted radiation. Single photons, such as gamma-rays associated with isomeric transition and X-rays associated with electron capture or internal conversion, form the basis of single-photon emission computed tomography (SPECT). The two 511-keV annihilation photons simultaneously emitted following positron-electron annihilation and associated with positron emission form the basis of positron emission tomography (PET).

In computed tomography, the basic paradigm includes acquisition of images from multiple angles around a patient (multiple projections), correction of the acquired data for non-uniformity, and mathematical reconstruction of thin (several-millimeter thick) transverse tissue-section images. In both SPECT and PET, the reconstructed transverse-section images are essentially contiguous, with no inter-section gaps, and therefore the reconstructed three-dimensional array of volume elements, or voxels, may be rearranged at any angle relative to the longitudinal axis of the patient and thus yield coronal, sagittal, or oblique images. The principal advantage of tomography thus lies in its improved image contrast: by eliminating the count contri-

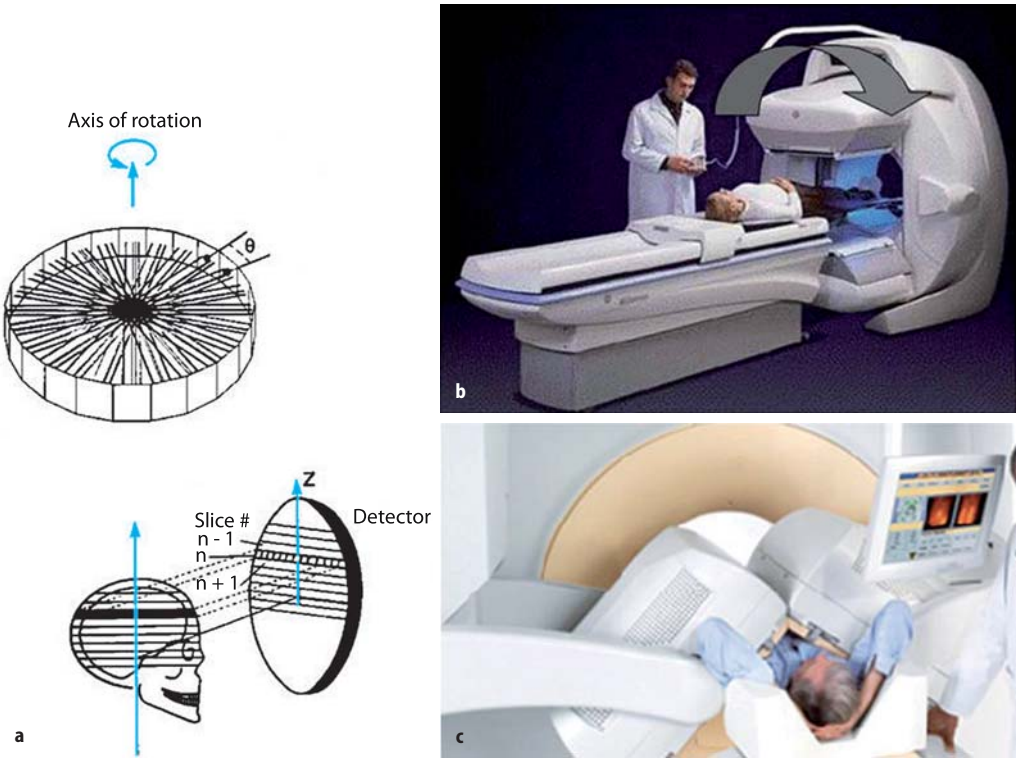

Fig. 1.12. a The basic data-acquisition paradigm in rotating gamma-camera SPECT. Photographs of modern dual-detector gamma cameras, with **b** the two detectors in opposed positions, as routinely used for a 360° rotation and general (non-cardiac) SPECT and **c** the two detectors perpendicular to each other, as routinely used for a 180° rotation and cardiac SPECT (from approximately right anterior oblique to left posterior oblique). The obvious advantage of such two-detector systems is that two projection images can be acquired simultaneously and the acquisition time therefore halved. (Adapted from Zanzonico 1995 in the "Further Reading" list)

bution from activities in tissues above and below the section of interest, the target (e.g., tumor)-to-background count ratio may dramatically improve.

1.4.4.2 SPECT Data Acquisition

Although there are many possible combinations of detector number, geometry, and motion that can acquire the necessary projection data, rotating gamma camera-based SPECT systems occasionally use one or three detectors but most commonly use two detectors. The raw data are acquired as a series of discrete planar images at multiple angles about the longitudinal axis of the patient (Fig. 1.12). The number of counts recorded in each projection-image pixel represents the ray sum, or line integral, of the sampling line perpendicular to and extending from the detector through the patient. The following are typical user-defined parameters: a 64×64 acquisition matrix with 180° rotation is routine for cardiac SPECT whereas a 128×128 acquisition matrix with a 360° rotation is common for non-cardiac SPECT.

1.4.4.3 PET Data Acquisition

PET is based on the annihilation coincidence detection (ACD) of the two co-linear (approximately 180° apart) 511-keV γ-rays resulting from the mutual annihilation of a positron and an electron (Fig. 1.13). Each time an annihilation photon is absorbed by a detector is referred to as a "single" event and the total count rate of individual annihilation photons is called the "singles count rate." When both photons from an annihilation are absorbed simultaneously (in coincidence) in two opposing detectors, this triggers the coincidence circuit and a "true coincidence event" ("true") is generated. The singles count rate in PET is typically much higher than the trues count rate. The volume between the opposed coincidence detectors absorbing the two annihilation photons (the shaded area in Fig. 1.13a) is referred to as a "line of response (LOR)." LORs are thus defined electronically, and an important advantage of ACD is that a collimator is not required. As a result, the sensitivity of PET is two to three orders of magnitude higher than that of gamma camera imaging. As shown in Fig. 1.13b, modern PET scanners employ a series of rings of discrete, small-area

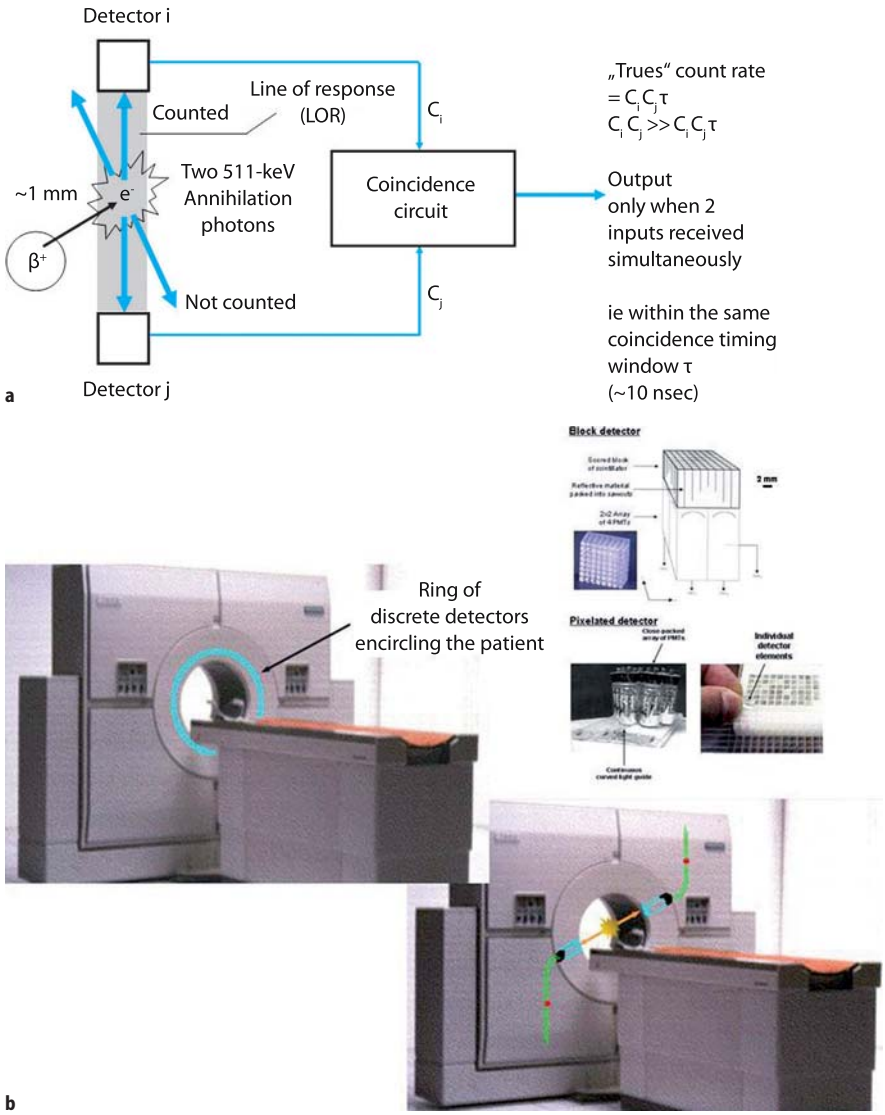

Fig. 1.13. a Annihilation coincidence detection (ACD) of the two opposed 511-keV γ-rays resulting from positron decay and positron-negatron annihilation. Note that the true coincidence (or "trues") count rate, given by the product of the singles count rates, C_i and C_j, and the coincidence timing window, τ, is much less than C_i and C_j – the coincidence timing window, τ, is short (< 10 ns) to minimize the number of random coincidence events (Fig. 1.14), and most of the annihilation photons therefore do not produce coincidence events. **b** A photograph of a modern PET, illustrating one of a number of rings of discrete detectors encircling the patient (*left-hand panel*) and ACD of an annihilation photon by a pair of these detectors. In the *insert* are shown a block detector (*top*) and pixelated detectors (*bottom*) currently used in PET scanners. The block detector consists of a cubic piece of scintillator scored to variable depths into a two-dimensional array of detector elements, typically backed by a 2×2 array of position-sensitive PMTs. Pixelated detectors consist of individual scintillator detector elements backed by a continuous light guide and a close-packed array of PMTs. For both the block and pixelated detectors, the individual detectors elements are typically ~2×2 mm in area. (Adapted from Zanzonico 2004 in the "Further Reading" list)

detectors (i.e., scored block detectors or pixelated detectors) encircling the patient and typically spanning a distance of 10 – 20 cm in the patient's longitudinal direction. Thus, a whole-body PET scan will typically require data acquisition at six to seven discrete bed positions and subsequently merge or "knit", the discrete images into a single whole-body image.

PET scintillation detectors typically have a rather coarse (up to 30%) energy resolution (compared to 8 – 9% for traditional gamma cameras) and therefore photons within a broad energy range (e.g., 250 – 650 keV) can be counted as valid annihilation γ-rays. Therefore, significant numbers of Compton-scattered annihilation γ-rays may be recorded as mis-positioned coincidence events. Since one or both may have been scattered, this creates a mispositioned event. Further, a true coincidence event is defined as a pair of annihilation photons counted by the coincidence detectors within a finite time interval called the "coincidence timing window τ," typically 6 – 12 ns – mainly due to the finite time required for scintillation detectors to detect and register a radiation event. The coincidence window is needed to reject the significant fraction of singles events. However, two random events occurring within the coincidence window will be detected as a true event. In addition, the high number of events/s that can be detected in a system with no collimator means that two unrelated singles events may also be detected within the 6- to 12-ns window as a true event. The various events associated with ACD of positron-emitting radionuclides, including trues, randoms, scatter, and spurious coincidences or singles, are illustrated in Fig. 1.14.

PET ring scanners originally employed lead or tungsten walls, or septa, positioned between and extending

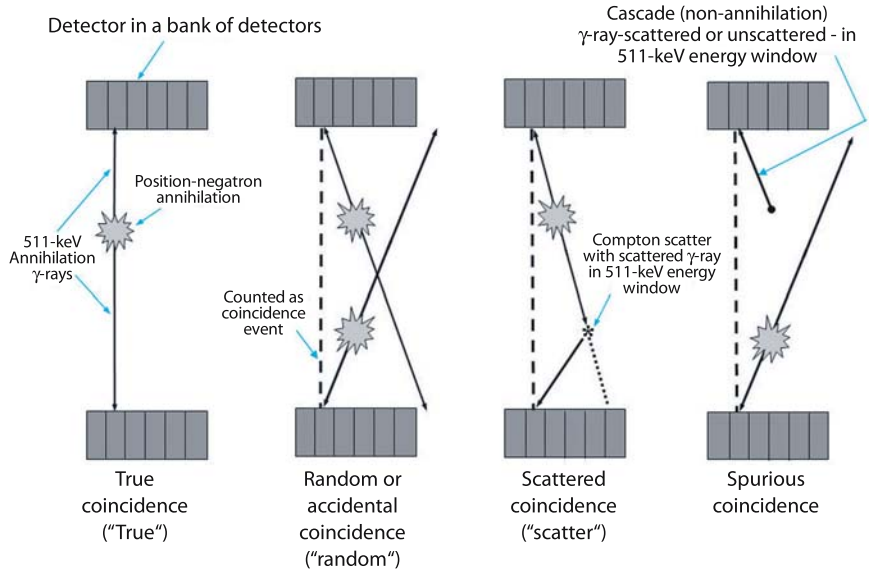

Fig. 1.14. The various events associated with ACD of positron-emitting radionuclides, illustrated for two opposed banks of coincidence detectors and assuming only one opposed pair of detectors are in coincidence. A true coincidence ("true") is counted only when each of the two 511-keV annihilation γ-rays for a single positron-negatron annihilation are not scattered and are detected within the timing window τ of the two coincidence detectors. A random or accidental coincidence ("random") is an inappropriately detected and positioned coincidence (the *dashed line*) which arises from two separate annihilations, with one γ-ray from each of the two annihilations detected within the timing window τ of the coincidence-detector pair. A scattered coincidence ("scatter") is a mispositioned coincidence (the *dashed line*) resulting from a single annihilation, with one of the γ-rays undergoing a small-angle Compton scatter but retaining sufficient energy to fall within the 511-keV energy window. A spurious coincidence is an inappropriately detected and positioned coincidence (the *dashed line*) which arises from an annihilation and a cascade γ-ray, scattered or unscattered but having sufficient energy to fall within the 511-keV energy window. Spurious coincidences occur only for radionuclides which emit both positrons and high-energy prompt cascade γ-rays, that is, γ-rays with energies (either scattered or unscattered) lying within the 511-keV energy window. (Adapted from Cherry et al. 2003 in the "Further Reading" list)

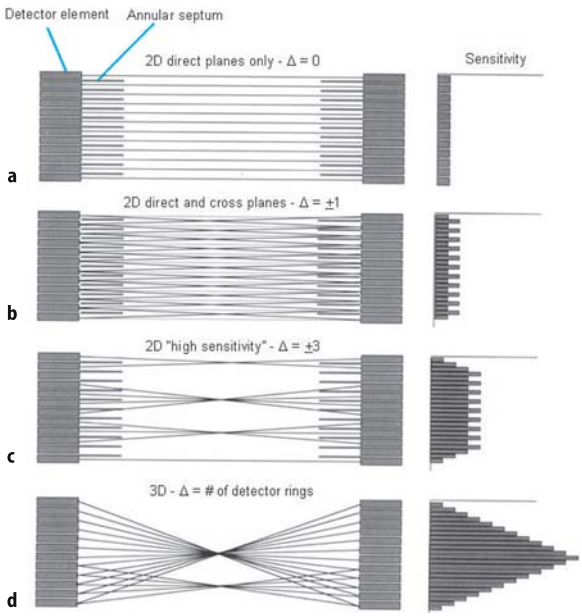

Fig. 1.15. Two-dimensional (2D) and three-dimensional (3D) PET data acquisition schemes (axial cross-sectional views of a multi-ring scanner) and the corresponding axial sensitivity profiles. **a–c** 2D data acquisition with a ring difference Δ of 0 (direct planes only), 1, and 3, respectively. **d** 3D (septa-less) data acquisition. The sensitivity profiles show the non-uniformity of response as a function of position along the axial FOV. (Adapted from Bendriem and Townsend 1998)

radially inward from the detector elements (Fig. 1.15a–c). The Advance PET scanner (General Electric Medical Systems), for example, employs tungsten septa 1 mm thick and 12 cm long. In this approach, known as two-dimensional (2D) PET, these inter-ring annular septa define plane-by-plane LORs and largely eliminate out-of-plane annihilation γ-rays. By eliminating most of the contribution from out-of-plane randoms and scatter, image quality is improved, especially for large-volume sources (i.e., as in whole-body PET). However, 2D PET also eliminates most of the trues and thus considerably reduces sensitivity. Typically, both "direct" and "cross" image planes are reconstructed from LORs within the same detector ring [corresponding to a so-called "ring difference (Δ)" of 0] and between two adjacent detector rings (ring difference of ±1), respectively. In the EXACT HR+ 2D (Siemens-CTI) PET scanner, for example, 32 detector rings span an axial FOV of 15.5 cm, yielding a total of 63 contiguous image planes comprising 32 direct and 31 cross planes. The cross-planes lie halfway between the direct planes defined by the detector elements and, conceptually, can be assigned to a "virtual" ring of detectors lying midway between two adjacent detector rings. Because the cross-plane images result from two LORs and the direct-plane images from only one, the cross-plane image sensitivity is about twice that of the direct-plane images (Fig. 1.15a–c). In an uncorrected PET study of a uniform volume source, this

results in alternating lower-count and higher-count transverse section images. In the newer 2D PET systems, LORs among as many as three adjacent rings, corresponding to a ring difference of ±2, are used to improve sensitivity. Increasing the ring difference does, however, degrade spatial resolution somewhat. Removing the septa altogether and including coincidence events from all of the LORs among all the detectors significantly increases PET detector sensitivity (Fig. 1.15d) – a system with ~10,000 detector elements has approximately 100 million LORs. This is known as three-dimensional (3D) PET, and is widely used among state-of-the-art PET scanners. Sensitivity is increased approximately fivefold in 3D relative to 2D PET – but with a considerable increase in the randoms and scatter count rates. Clinically, the scatter-to-true count rate ratios range from 0.2 (2D) to 0.5 (3D) in brain and from 0.4 (2D) to 2 (3D) in the whole body. To compensate for the increase in scatter count rates, new detector materials (such as GSO and LSO) were developed with better energy resolution (permitting a narrower energy window for improved scatter rejection) and accurate scatter-correction algorithms were developed for 3D PET. These detectors also respond much faster to an absorbed event allowing shorter coincidence timing windows to minimize the increased randoms count rates and dead-time count-rate losses. Data processing time for 3D PET is about an order of magnitude longer than for 2D PET. Axial sensitivity is also affected by removing the inter-ring septa: in contrast to the relatively uniform axial sensitivity for 2D PET, the axial sensitivity profile for a 3D PET scanner is triangular and peaks at the center of the FOV (Fig. 1.15d). To yield uniform sensitivity for whole-body images whole-body 3D PET studies require considerable overlap of adjacent bed-position acquisitions – optimally, one-half of the axial FOVs. In PET in general and 3D PET in particular, due to the lack of lead septa, it is important that the ends of the detector assembly are adequately shielded to minimize the contribution of counts from activity outside the axial FOV. This can be important since about 30 % of the injected activity may be in the brain.

To date, only four detector materials – all inorganic scintillators – have been widely used in PET scanners: thallium-doped sodium iodide [NaI(Tl), NaI:Tl], bismuth germanate (BGO, $Bi_4Ge_3O_{12}$), cerium-doped lutetium oxyorthosilicate (LSO(Ce) or simply LSO, Lu_2SiO_5:Ce), and cerium-doped gadolinium oxyorthosilicate (GSO(Ce) or simply GSO, Gd_2SiO_5:Ce). The most important practical features of scintillation detectors include: high mass density (ϱ) and effective atomic number (Z_{eff}) – to maximize the photon stopping power (i.e., intrinsic efficiency) of the detector; high light (scintillation) output – to maximize the signal and thus minimize statistical uncertainty in the energy of the detected signal; and speed of the output light pulse– to permit minimizing the coincidence timing window (τ) and random events, without sacrificing a significant portion of the signal. Higher-ϱ and -Z_{eff} atomic materials, such as BGO, LSO, and GSO, have emerged as the detectors of choice for PET because of their greater stopping power for 511-keV annihilation γ-rays. The MFP for 511-keV γ-rays is at least twice as long in NaI(Tl) as in BGO, GSO, or LSO. Among the latter three materials, GSO and LSO have a faster light output – nearly tenfold faster – than BGO, with LSO having a much greater light output – approximately threefold greater than either BGO or GSO. GSO has somewhat better energy resolution, and scatter rejection capability, than either BGO or LSO. A notable disadvantage of LSO is the presence of a naturally occurring long-lived radioisotope of lutetium, lutetium-177. Lutetium-177 has an isotopic abundance of 2.6 % and a half-life of $\sim 4\times10^{10}$ years and emits two prompt γ-rays (88 % abundance) of 201 and 306 keV in energy; the summed energy of 507 keV falls well within the 511-keV energy windows commonly used in PET scanners. The presence of lutetium-177 results in a measured background count rate of 240 cps/cm^3 of LSO and singles and trues count rates of 100,000 and 10,000 cps, respectively, for clinical LSO PET scanners. Although the former has a negligible effect on typical emission scan, the latter would significantly increase the statistical uncertainty (noise) in single-photon transmission scans (e.g., with cesium-137) used for attenuation correction.

For 2D scanners, the so-called noise-equivalent count rate (NECR), a widely used practical measure of PET scanner sensitivity, increases linearly with activity and there is no optimal count rate or activity. For 3D scanners, on the other hand, the trues and scatter count rates are proportional to the activity while the randoms count rate is proportional to the square of the activity. Thus, there exists a well-defined optimum activity in the FOV for 3D scanners above which the random count rate begins to significantly affect image quality. The faster the detectors, and therefore the shorter the coincidence window τ can be made, the lower the randoms count rate for a given activity. Consequently, the NECR occurs at a higher administered activity and its maximum value is increased. A "fast" 3D LSO scanner ($\tau \approx 6$ ns) has a maximum NECR severalfold higher than that of a "slower" 3D BGO scanner ($\tau \approx 12$ ns). A fast 3D scanner allows the use of higher administered activities and yields high "usable" count rates, short scan durations, and increased patient throughput. At clinical activities [e.g., 185 – 370 MBq (5 – 10 mCi) of fluorine-18], however, even "slow" 3D scanners have substantially higher sensitivities and NECRs than 2D scanners.

1.4.4.4 Data Processing and Tomographic Image Reconstruction

Normalization. Even optimally performing SPECT or PET scanners exhibit some non-uniformity of response. Among the thousands of pixels in a SPECT projection image and the thousands of detector elements (and therefore LORs) in a PET scanner, slight variations in detector thickness, light emission properties, electronics performance, etc., result in slightly different measured count rates for the same activity. In principle, such non-uniform response can be corrected by acquiring data from a uniform flux of X- or γ-rays and normalizing to the *mean* count rate from all the pixels in SPECT or LORs in PET. This "normalization" table or "uniformity map" corrects for the nonuniform count rate of the individual pixels or LORs to thereby yield a pixel-by-pixel or LOR-by-LOR uniformity correction. For planar gamma camera imaging as well as SPECT, such a correction table may be acquired using either a uniform flood source placed on the detector or a point source placed sufficiently far (typically ~2 m) from the uncollimated detector to approximate a uniform photon flux (see below). For PET, it may be acquired using a positron-emitting rod source (e.g., germanium-68) spanning the entire axial FOV and rotating it around the periphery of the FOV, exposing the detector pairs to a uniform photon flux per revolution. Alternatively, a uniform cylinder of a positron-emitting radionuclide can be scanned and the data thus acquired analytically corrected for attenuation; for a well-defined geometry such as a uniform cylindrical source, this correction is straightforward. However, for 3D PET, the contribution of, and correction for, scatter with such a large-volume source are non-trivial. For both planar imaging as well as SPECT and PET, acquisition of the data required for uniformity correction is somewhat problematic in practice because of statistical considerations: tens of millions (SPECT) to hundreds of millions (PET) of counts must be acquired to avoid possible "noise"-related artifacts in the uniformity correction table.

Deadtime Correction. Scintillation detectors have a finite deadtime and associated count losses. The deadtime is the length of time required for a counting system to record an event, during which additional events cannot be recorded. As a result, the measured count rate is lower than the actual count rate. Such count losses are significant, however, only at "high" count rates and are generally minimal at clinical administered activities. Nonetheless, a real-time correction for deadtime count losses is routinely applied in PET (though not in SPECT) to the measured count rates, most commonly by scaling up the measured count rate based on an empirically derived mathematical relationship between measured and true count rates.

Center-of-Rotation Misalignment Correction (SPECT). In rotating-gamma camera SPECT, the location of the projection of the center of rotation (COR) on the projection image matrix must be constant. If the mechanical and electronic CORs are aligned, the pixel location of the projection of the COR onto the projection image matrix will be the same for all projection images and, for all such images, the counts in each pixel will then be projected across the appropriate row of pixels in the tomographic image matrix. If, however, the mechanical and electronic CORs are not aligned, the pixel location of the COR will vary among the projection images and the counts in each projection-image pixel will be projected across different locations in the tomographic image matrix and blurred images will result (Fig. 1.16a). In today's SPECT systems, COR misalignment may be easily measured and corrections created and automatically applied using the system's software (Fig. 1.16b).

Randoms Correction (PET). In PET, randoms increase the detected coincidence count rate by introducing mis-positioned events and thus reduce image contrast and distort the relationship between image intensity and activity concentration. The standard approach to randoms correction, the "delayed window" method, is based on the fact that the random-coincidence γ-rays are temporally uncorrelated (i.e., not simultaneously emitted). Briefly, once singles in the coincidence timing window (typically 6 – 12 ns) are detected, the number of singles in a timing window equal in duration to, but much later (> 50 ns later) than, the coincidence timing window are determined. The number of events in the delayed timing window provides an estimate of the number of randoms in the coincidence timing window. Real-time subtraction of the delayed-window counts from the coincidence-window counts for each LOR thus corrects for randoms.

Scatter Correction. Scatter results in generally diffuse background counts in reconstructed images, reducing contrast and distorting the relationship between image intensity and activity concentration. In PET in general and 2D PET in particular, scatter correction is rather straightforward. Once the randoms correction has been applied, the peripheral "tails" in the projection-image count profiles, presumably due exclusively to scatter, are fitted to a mathematical function and then subtracted (deconvolved) from the measured profile to yield scatter-corrected profiles for tomographic image reconstruction. While this approach works reasonably well for 2D PET and small source volumes (e.g., the brain) in 3D PET, it is generally not adequate for 3D PET. Scatter corrections for 3D PET include: dual energy window-based approaches; convolution/deconvolution-based approaches (analogous to

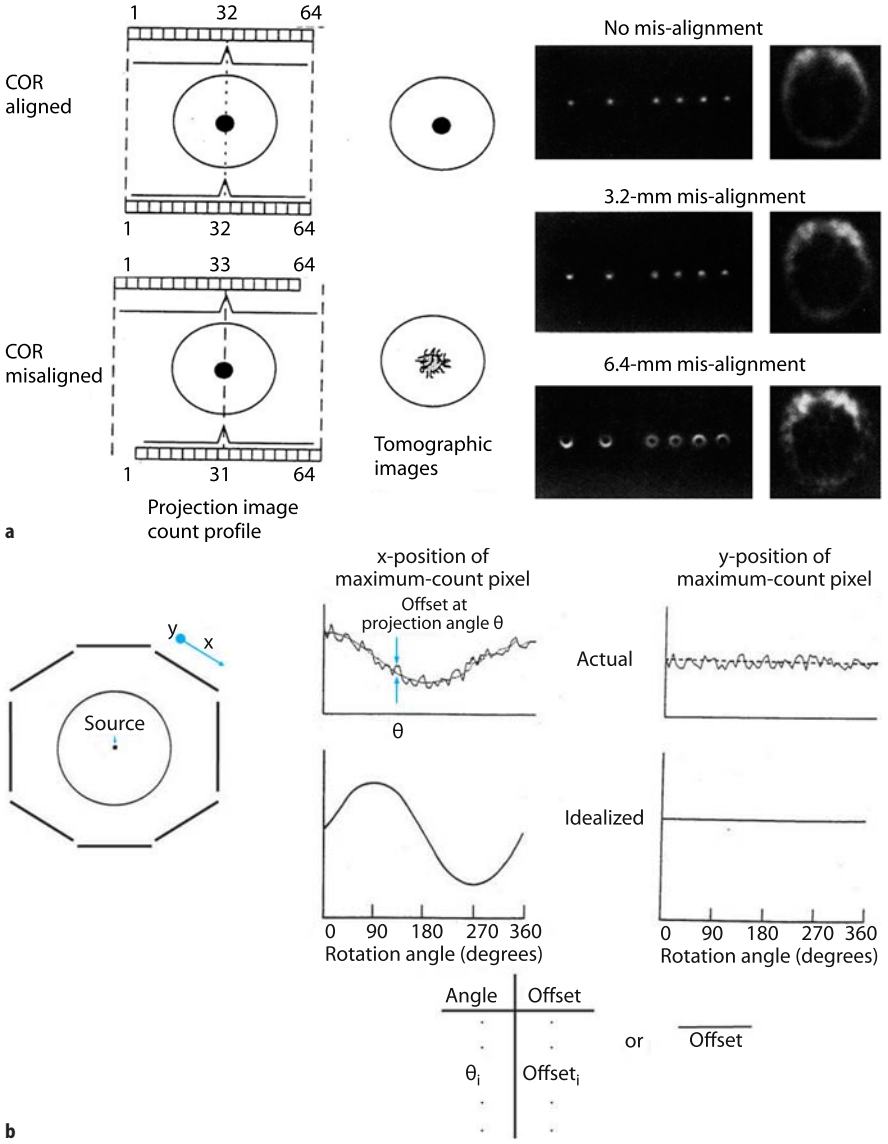

Fig. 1.16. a Center-of-rotation (COR) misalignment and resulting image-blurring artifacts in rotating-gamma camera SPECT. The degree of blurring is related to the magnitude of the spatial misalignment of the mechanical and electronic CORs. A misalignment as small as 3.2 mm (or 1/2 a pixel for a 64×64-image matrix) can produce perceptible blurring in SPECT images, with the blurring substantially worse for a misalignment of 6.4 mm (1 pixel). **b** COR misalignment can be measured and corrected based on acquiring a 360° circular SPECT study of a ^{99m}Tc point source and constructing graphs of the *x*- and *y*-positions (perpendicular and parallel to the axis of rotation, respectively) of the position of the maximum-count pixel in each projection image versus angular position. The *x*- and *y*-position-versus-angle graphs should be a sinusoidal curve and a straight line, respectively. The angle-by-angle deviation between the *x*-position on the best-fit sine curve and the *x*-position of the actual maximum-count pixel thus yields a correction table indicating the offset by which each projection image must be shifted at each angular position to align the CORs. Alternatively, the average of the offsets may be used at each angular position. (Adapted from Zanzonico 1995 in the "Further Reading" list)

the correction in 2D PET); direct estimation of scatter distribution (by Monte Carlo simulation of the imaging system); and iterative reconstruction-based scatter compensation approaches (also employing Monte Carlo simulation). The Monte Carlo simulation and subtraction of scatter have been implemented in commercial PET scanners.

Scatter corrections in SPECT are not yet as well developed or as reliable. Perhaps the most widely used approach is the "dual-window" method in which a "scatter" energy window [equal in width (in keV) to the photopeak energy window] is created and two separate images, a scatter and a photopeak image, simultaneously acquired. The scatter image is then multiplied by a fractional weighting factor, to estimate the pixel-by-pixel scatter counts appearing in the photopeak image, and the weighted scatter image is then subtracted from the photopeak image.

Attenuation Correction. Attenuation correction is generally the largest correction in tomographic imaging. In contrast to SPECT, one of the most attractive features of PET is the relative ease of applying accurate and precise corrections for attenuation, based on the fact that attenuation depends only on the total thickness of the attenuation medium. For a positron-emitting source and a volume of thickness L, the attenuation factor is $e^{-\mu L}$ and the attenuation correction factor $e^{\mu L}$ regardless of the position of the source. Accordingly, if a rod source of a positron emitter such as germanium-68 is extended along the axial FOV and rotated around the periphery of the FOV first with and then without

the patient in the imaging position – the transmission and the blank scans, respectively – the attenuation correction factor (*ACF*) can be derived from the ratio of the counts in these respective scans:

$$ACF_{ij} = e^{\mu L}ij \tag{1.18}$$

$$ACF_{ij} = \frac{[(C)_{Blank}]_{ij}}{[(C)_{Trans}]_{ij}} \tag{1.19}$$

where ACF_{ij} = the attenuation correction factor between coincident detectors i and j, L_{ij} = the thickness of the volume between coincident detectors i and j, and $[(C)_{Blank}]_{ij}$ and $[(C)_{Trans}]_{ij}$ = the external-source counts between detectors i and j in the blank and transmission scans, respectively. In practice, a blank scan is acquired only once a day. The transmission scan can be acquired before the patient has been injected with the radiopharmaceutical, after the patient has been injected with the radiopharmaceutical but before or after the emission scan, or after the patient has been injected with the radiopharmaceutical and at the same time as the emission scan. Pre-injection transmission scanning avoids any interferences between the emission and transmission data but requires that the patient remain on the imaging table before, during, and after injection of the radiotracer. It is the least efficient operationally and is rarely used in practice. Post-injection transmission scanning minimizes the effects of patient motion, relying on the much higher external-source count rates for reliable subtraction of the emission counts from the transmission counts. It is probably the most commonly used approach in "PET-only" scanners. Simultaneous emission/transmission scanning is obviously the most efficient (fastest) approach but may result in excessively high randoms and scatter counter rates in the emission data. The GE Advance employs post-injection transmission scanning using two germanium-68 rod sources each with 370 MBq (10 mCi) and a 4- to 6-min transmission scan per bed position. With the recent introduction of PET-CT scanners, attenuation correction may now be performed using CT rather than transmission sources. A CT image is basically a two-dimensional map of attenuation coefficients at the CT X-ray energy (~80 keV). For attenuation correction of the PET emission data, however, these must be appropriately scaled to the 511-keV energy of the annihilation γ-rays. The mass-attenuation coefficients (μ_m) for CT X-rays (~80 keV) and for 511-keV annihilation γ-rays are 0.182 and 0.096 cm^2/g, 0.209 and 0.093 cm^2/g, and 0.167 and 0.087 cm^2/g in soft tissue, bone, and lung, respectively. The corresponding μ_m ratios are therefore 1.90, 2.26, and 1.92, respectively. Thus, ACFs derived from CT images cannot be scaled to those for 511-keV annihilation γ-rays simply using a global factor. Accordingly, CT-based attenuation correction in PET has been implemented using a combination of segmentation – to delineate soft tissue, bone, and lung compartments – and variable scaling – to account for the different μ_m ratios in these respective tissues.

Like scatter corrections, attenuation corrections in SPECT are not yet as well developed or as reliable as those in PET. For many years, if attempted at all, SPECT attenuation correction factors were calculated (as in Chang's first-order correction and the Sorenson method) based on the assumptions – neither of which is generally true – that the body is a uniform medium with a single, well-defined value of μ and that the body's contour is known. More recently, manufacturers have incorporated long-lived radioactive sources (such as gadolinium-153) into SPECT scanners to perform attenuation correction. As part of the SPECT procedure, a shutter opens at each projection-image angle and exposes a highly collimated line source and a transmission image is acquired. The transmission images thus acquired are reconstructed into an ACF map for correction of the SPECT study. The recent introduction of SPECT-CT scanners will likely result in more practical and more accurate attenuation correction in SPECT.

Image Reconstruction. In SPECT and in 2D PET, the emission data are the one-dimensional projections [sets of parallel line-integrals (ray sums)] of the direct planes at the azimuthal, or projection, angles θ relative to the axis of the scanner. The full set of 2D projection data are usually represented as a two-dimensional matrix in polar coordinates (distance x_r, *angle* ϕ) known as a "sinogram" (or "histogram") in which each row represents the projected intensity across a single direct plane and each column the projected intensity at the same distance x_r across the projection at successive azimuthal angles θ (Fig. 1.17a). In 3D PET, the projections are two-dimensional (x_r, y_r) *parallel line-integrals with azimuthal angle* ϕ *and* oblique, or polar, angle θ. The full set of 3D projection data are then represented as a *set* of sinograms, with one sinogram per polar angle ϕ. In each sinogram, each row represents the projected intensity across a single oblique plane (at polar angle θ) and each column the projected intensity at the same position across the projection at successive azimuthal angles ϕ (Fig. 1.17b).

Analytic methods for reconstruction of 3D data characteristically suffer from incomplete sampling of the 3D volume as a result of the finite axial FOV of PET scanners. The three-dimensional re-projection (3DRP) algorithm, an extension of the standard 2D FBP algorithm (see below), has been the most widely used 3D reconstruction algorithm and has been implemented on commercial 3D scanners. In 3DRP, unsampled data are estimated by reconstruction and then 3D forward-projection of an initial image set obtained by reconstruction of the directly measured data. Such 3D reconstruction algorithms remain computer-intensive and

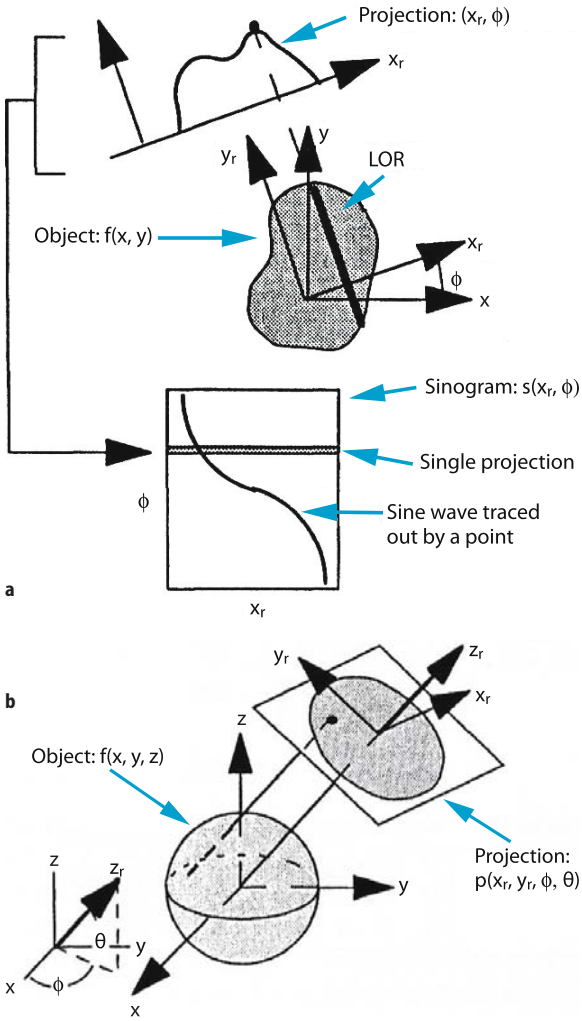

Fig. 1.17. a In 2D PET, the emission data are the one-dimensional projections (sets of parallel line-integrals) of the direct planes at the azimuthal angles ϕ relative to the axis of the scanner. In the sinogram, *each row* represents the projected intensity across a single direct plane and *each column* the projected intensity at the same distance x_r across the projection at successive azimuthal angles ϕ. **b** In 3D PET, the projections are two-dimensional (x_r, y_r) *parallel line-integrals with azimuthal angle* ϕ and oblique angle θ. The 3D projection data are represented as a set of sinograms, with one sinogram per polar angle θ, each row representing the projected intensity across a single polar angle θ and each column the projected intensity at the same position *xr* across the projection at successive azimuthal angles ϕ. (Adapted from Bendriem and Townsend 1998)

rather slow by clinical standards, however. In addition, 3D PET emission data files are very large – typically more than two orders of magnitude larger than 2D data sets. It is preferable, therefore, to reduce 3D data sets to a more manageable size for image reconstruction – by re-binning of the 3D set of oblique sinograms into a smaller number of direct 2D sinograms. The simplest method is "single-slice re-binning (SSRB)," wherein true oblique LORs are assigned to the direct plane midway between the two detector elements actually in coincidence. SSRB distorts off-axis activity and thus is accurate only for activity distributions close to the detector axis, as in brain or small-animal imaging. A second method is multi-slice re-binning (MSRB), which is fast but is susceptible to "noise"-related artifacts. The current method of choice is Fourier re-binning (FORE), based on the 2D Fourier transform of the oblique sinograms. In contrast to SSRB and MSRB, however, FORE cannot be performed in real-time and thus requires the full 3D data set.

After 2D re-binning of 3D data, 2D reconstruction algorithms can used for 3D PET as well as 2D PET and SPECT data. Note that processing of the emission data after the real-time deadtime and randoms corrections and before image reconstruction – namely, normalization, scatter correction, and then attenuation correction – is normally performed in sinogram space. One of the most widely used algorithms for reconstruction of tomographic images from 2D data (or 3D data re-binned into 2D projections) – in SPECT as well as PET – remains filtered back-projection (FBP). The basic procedure is as follows: each projection is Fourier transformed from real to frequency space; the projection is filtered in frequency space using a ramp filter; the filtered projection is inverse Fourier transformed from frequency back to real space; and the filtered projection data in real space are uniformly distributed, or back-projected, over the reconstructed image matrix. The resulting reconstructed image is inexact, however, because the ramp filter results in the inclusion of spatial frequencies beyond the maximum frequency imageable by the scanner (i.e., the Nyquist frequency, ν_N) – producing aliasing artifacts (such as the "starburst" pattern emanating from discrete, high-activity foci) – and amplifies statistical uncertainty (noise or mottle). To compensate for these effects, low-pass, or apodizing, filters (known as Hanning, Butterworth, etc.) are used in place of the ramp filter to eliminate those spatial frequencies above a cut-off frequency, ν_c, set equal to ν_N or some fraction thereof. Although the resulting reconstructed images have somewhat degraded spatial resolution, they are far less "noisy" (mottled).

In contrast to so-called "transform" reconstruction methods such as FBP, iterative algorithms attempt to progressively refine estimates of the activity distribution, rather than directly calculating the distribution, by maximizing or minimizing some "target function." The solution is said to "converge" when the difference of the target function between successive estimates (iterations) of the activity distribution is less than some pre-specified value. Importantly, iterative reconstruction algorithms allow incorporation of realistic modeling of the data acquisition process (including effects of attenuation and of scatter), modeling of statistical

noise, and inclusion of pertinent a priori information (e.g., only non-negative count values). The maximum-likelihood expectation maximization (MLEM) algorithm is based on maximizing the logarithm of a Poisson-likelihood target function. The MLEM algorithm suppresses statistical noise, but large numbers of iterations typically are required for convergence and therefore processing times are long. To accelerate this slow convergence, the ordered-subset expectation maximization (OSEM) algorithm groups the projection data into subsets composed of projections uniformly distributed around the source volume. The OSEM algorithm, which is a modified version of the MLEM algorithm in that the target is still a maximization of the log-likelihood function, converges more rapidly than MLEM and is now the most widely used iterative reconstruction method in PET as well as SPECT. The row-action maximization-likelihood (RAMLA) algorithm, related to the OSEM algorithm, has been implemented for direct reconstruction of 3D PET data in the C-PET and Allegro (Philips ADAC). The so-called 3D-RAMLA algorithm, which eliminates 2D re-binning of the 3D data, employs partially overlapping, spherically symmetric volume elements called "blobs" in place of voxels. Reconstruction times are fairly long by clinical standards but the results have been excellent.

Quantitation. Once the PET emission data have been corrected for deadtime, randoms, system response (by normalization), scatter, and attenuation, the count rate per voxel in the reconstructed tomographic images is proportional to the local activity concentration. [In principle, SPECT images can be made quantitative in an analogous manner. In practice, however, the pertinent corrections (especially scatter and attentuation corrections) are not as reliable in SPECT as in PET, as previously noted.] To make the images quantitative, then, the count rate per voxel (cps), $\dot{C}_{ijk}$, in voxel ijk should be divided by the measured system calibration factor [(μCi/cc)/(cps/voxel)], CF, to yield the activity concentration:

$$[A]_{ijk} = \frac{\dot{C}_{ijk}}{CF} \tag{1.20}$$

where $[A]_{ijk}$ = the activity concentration (μCi/cc) in voxel ijk. The calibration factor CF can be derived by scanning a calibrated standard, that is, a water-filled or water (tissue)-equivalent volume source with all linear dimensions at least twice that of the system spatial resolution (FWHM) and with a uniform, well-defined activity concentration at the time of the scan. The requirement for water equivalence is to ensure that effects such as scatter and attenuation are comparable in both the patient and the standard. And the requirement for linear dimensions at least twice that of the system spatial resolution is to ensure that the effects of partial volume averaging and associated underestimation of local count rates are negligible. Typically, a more clinically relevant expression of local activity concentration is in terms of the decay-corrected fraction or percent of the administered activity per cubic centimeter (cc) or, more commonly, in terms of the standard uptake value (SUV):

$$\text{SUV} \equiv \frac{\text{μCi/cc of tissue}}{\text{μCi injected/gm body mass}} \tag{1.21}$$

1.4.5 Gamma Camera Performance and Quality Control

Quality control (QC), a critical component of analytical procedures and instrumentation in general and medical devices in particular, is an established set of ongoing measurements and analyses designed to ensure that the performance of a procedure or instrument is within a pre-defined acceptable range. An extensive series of parameters have been developed over the years to characterize gamma camera, SPECT scanner, and PET scanner performance, and detailed data acquisition and analysis protocols have been promulgated by the National Electrical Manufacturers Association (NEMA), the American Association of Physicists in Medicine (AAPM), and others for this purpose. In practice, however, less extensive and less rigorous procedures have proven adequate for day-to-day QC.

To understand gamma camera performance and routine QC, several pertinent terms – intrinsic versus extrinsic (or system) performance and the useful versus the central field of view – must be understood. Intrinsic performance refers to gamma camera performance without a collimator in place while extrinsic (or system) performance refers to that of the entire gamma system, including collimation. The useful field of view (UFOV) of a gamma camera is essentially the entire detector (i.e., crystal) area while the central field of view (CFOV) corresponds to the inner, or central, 3/4 of the crystal area. The periphery of the gamma camera detector suffers from artifacts (e.g., edge packing) and poorer image quality in general, in part because light reflected from the mirror-like inner surface of the detector housing makes it appear that a disproportionate amount of light is emanating from this peripheral area. Accordingly, the periphery of the crystal is masked (or shielded), often by lead built into the edges of the collimator housing. Thus, the CFOV is the portion of the detector actually used in clinical imaging.

The performance parameters most commonly evaluated as part of a routine gamma camera QC program include uniformity, spatial resolution, and energy resolution (see above). Uniformity (the so-called "daily flood") should be evaluated each day either intrinsically or extrinsically (Fig. 1.18). Either ^{99m}Tc (intrinsic) or

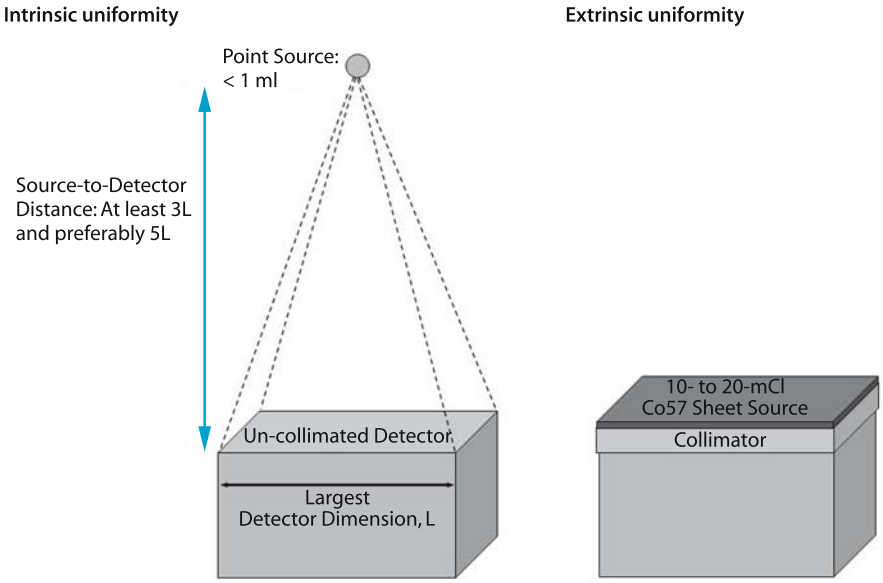

Fig. 1.18. Gamma camera uniformity may be evaluated either intrinsically or extrinsically. Intrinsically, a "point" source (<1 ml in volume and containing ~500 mCi) of ^{99m}Tc (at least for daily evaluation of uniformity) is placed at least three and preferably five crystal dimensions from and centered over the uncollimated detector to approximate a uniform photon flux. If necessary, the activity should be adjusted to yield a measured count rate no greater than 25,000 cps (to avoid deadtime counting losses and count rate-related image degradation). Extrinsically, a uniform flood, or sheet, source (typically 10–20 mCi) of ^{57}Co (for daily evaluation of uniformity) is placed directly on the collimated detector. ^{57}Co, known as "mock ^{99m}Tc," has a half-life of 270 days and emits a 122-keV γ-ray and is thus a convenient, long-lived alternative to ^{99m}Tc. Such ^{57}Co sheet sources are available commercially. A total of 10–15 million counts should be acquired and uniformity evaluated quantitatively (e.g., in terms of the integral and differential uniformities; Eq. 1.17)

^{57}Co (extrinsic) is used on a daily basis. Periodically (e.g., monthly), however, intrinsic uniformity for other radionuclides used clinically (e.g., ^{67}Ga, ^{111}In, and ^{131}I) should also be evaluated. Integral uniformities (Eq. 1.17), or IUs, up to 5% are acceptable, although nowadays IUs of 3% or better are routinely obtained. If the uniformity for any radionuclide is out of tolerance (i.e., >5%), that radionuclide's uniformity (or sensitivity) correction table should be updated. The necessary data may be acquired using the same set-up as for the daily uniformity test, except that a much larger number of counts (60–100 million) must be acquired. In today's gamma cameras, uniformity correction tables may be easily updated and the corrections created, processed, stored, and automatically applied using the system's integrated software. In addition to an outdated uniformily correction table, there are other causes of gamma camera uniformity (Fig. 1.19 and 1.20): mis-tuning (detuning), un-coupling of a PMT; a cracked crystal; or corruption or switching off of one or more of the camera's correction tables (i.e., its energy, uniformity, and/or linearity correction tables).

Spatial resolution, in practice, is generally assessed using some sort of resolution phantom (or mask), the four-quadrant bar-phantom perhaps being the one most widely used (Fig. 1.21). This should be done at least weekly. Gamma camera energy resolution per se is not generally evaluated on a routine basis. However, the energy spectrum for each radionuclide used clinically should be checked at least once a day to verify that the photopeak(s) is (are) centered in the photopeak energy window(s) currently set (Fig. 1.6b). Ideally, the energy spectrum should be checked for each patient.

In addition to the foregoing QC procedures for gamma camera imaging generally, rotating-gamma camera SPECT requires QC as well. Among the components of a routine SPECT QC program are periodic assessment of COR alignment (Fig. 1.16), tomographic uniformity, and, for lack of a better term, overall system performance. As described above and in Fig. 1.16, proper alignment of the mechanical and electronic CORs is critical in rotating-gamma camera SPECT and should be checked and, if necessary, the COR misalignment correction updated at least weekly. Tomographic uniformity may be evaluated by imaging a uniform cylinder source (at least 20 cm in diameter) and visually inspecting the resulting images for the absence of rings, or "bulls eye," attributable to system non-uniformity. Overall system performance may be evaluated using any number of commercially available fillable phantoms containing non-radioactive ("cold") inserts of different sizes and visually inspecting the resulting images to determine the size of the smallest insert that is visible. Typically, such a phantom will include a uniform portion that is used to simultaneously evaluate tomographic uniformity. PET tomographic uniformity and overall system performance may also be evaluated using such phantoms.

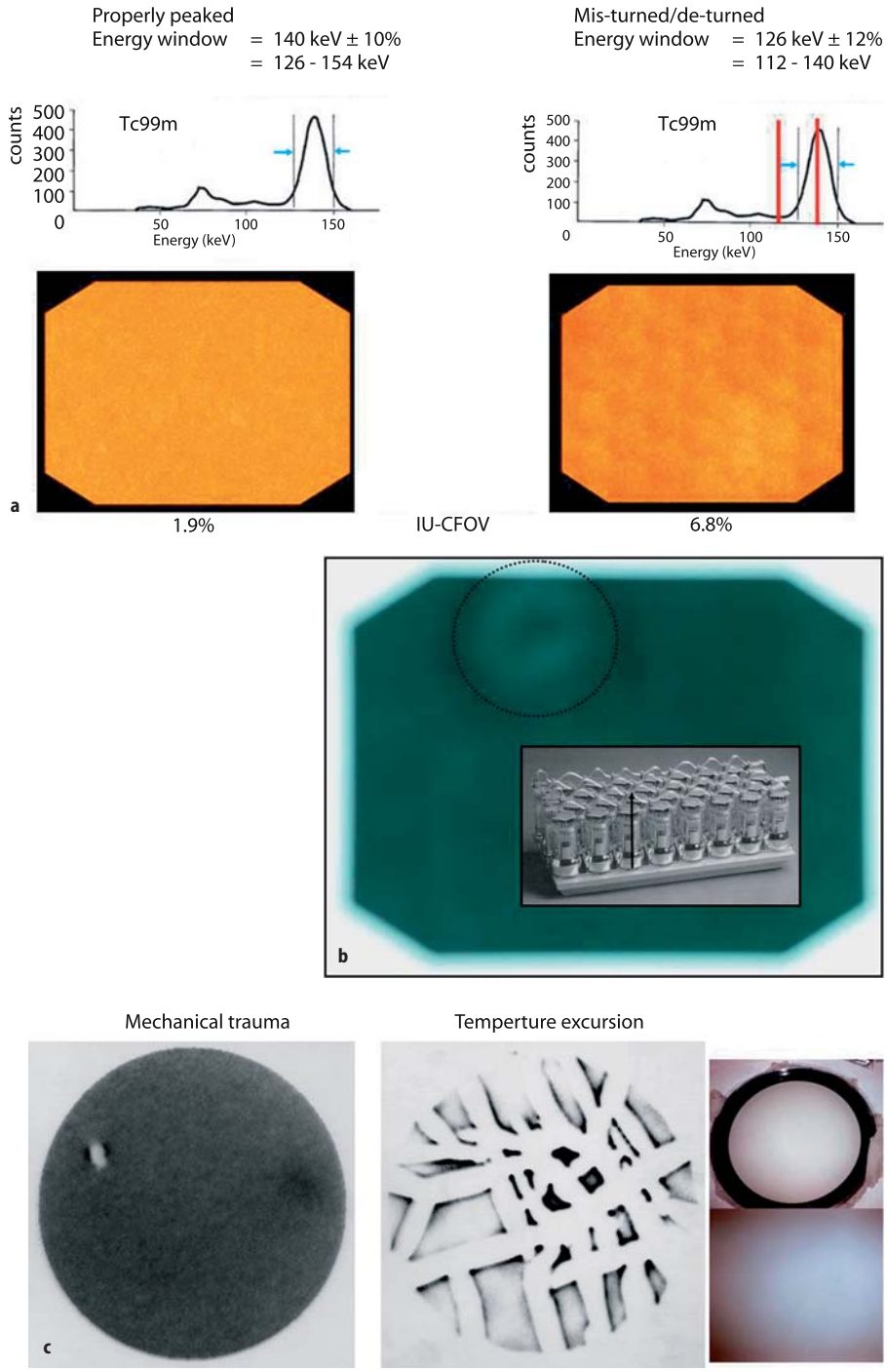

Fig. 1.19. Sources of gamma camera non-uniformity. **a** Mis-tuning (or de-tuning), meaning that the radionuclide's photopeak does not coincide with the camera's photopeak energy window, perhaps because the photopeak energy window (as shown) and/or the PMTs' high voltages are not set correctly. **b** Un-coupling of a PMT from the crystal, resulting in loss of all or part of the light signal in the resulting air gap between the PMT entrance window and the crystal. **c** Cracked crystal, either due to mechanical trauma (an impact) or a temperature incursion (i.e., a temperature increase *or* decrease at a rate faster than ~5 °C per hour causing the crystal to expand or contract, respectively, to the point of cracking). Note that it is the *rate* of the temperature change which is critical. The photographs *on the right* show the cracked crystal which produced the "temperature-excursion" image. Even though the cracks are grossly imperceptible, the artifacts produced are very dramatic. **d** Corrupted, deleted, or switched-off software correction tables. Even perfectly functioning gamma cameras have some non-uniformity due to: point-to-point variations in the energy spectra; greater sensitivity at and lower sensitivity between the PMTs; and residual non-uniformity due to ill-defined factors such as variations in crystal thickness. The associated non-uniformities are measured and used to create energy, linearity, and uniformity (or sensitivity) correction tables, respectively. Note that the linearity correction table has the biggest impact on uniformity: if corrupted, deleted, or switched-off, the PMT pattern becomes grossly apparent and the IU approaches 20 %. Fortunately, in contrast to the uniformity correction table and, to a lesser extent, the energy correction table, the linearity correction table rarely needs to be updated once a gamma camera is installed; if it becomes necessary, it is almost always done by field service personnel, not the end-user

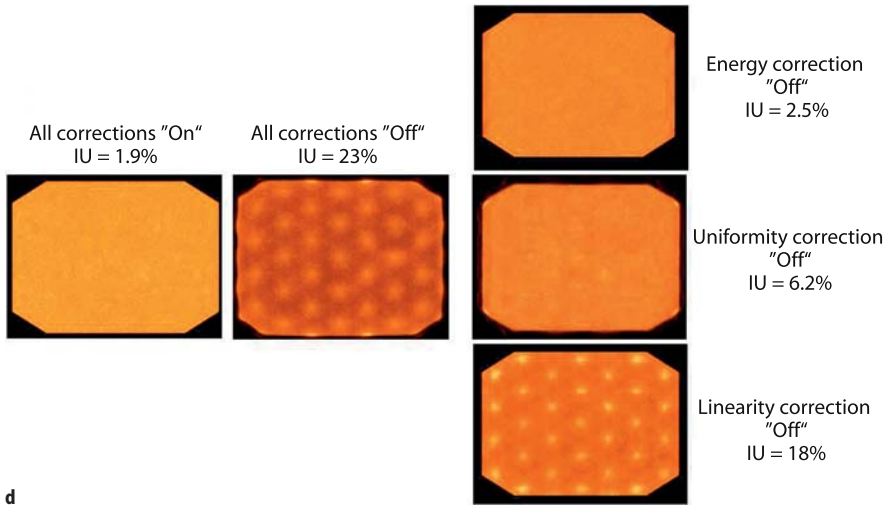

d

Fig. 1.19.(*Cont.*)

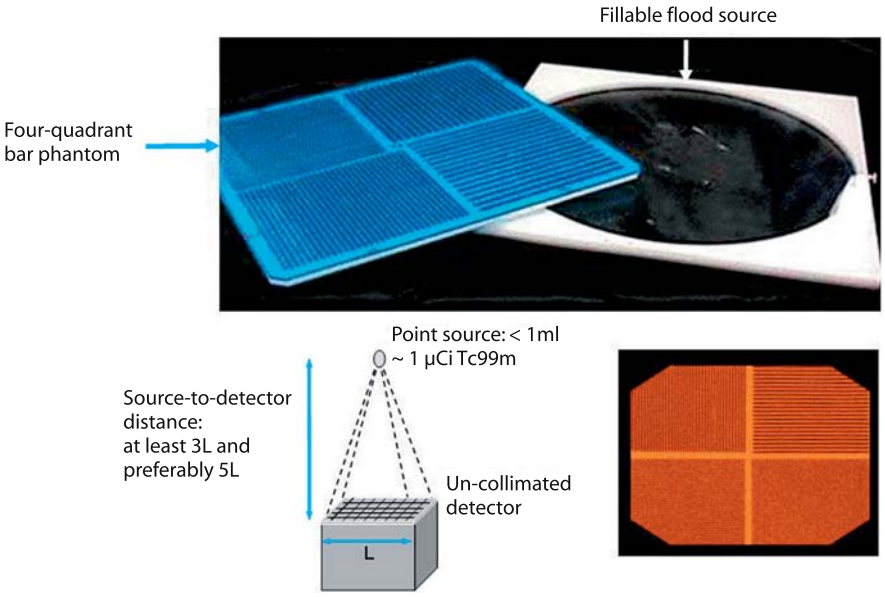

Fig. 1.20. In practice, intrinsic gamma camera resolution is often evaluated using a four-quadrant bar phantom, consisting of radiopaque lead bars and intervening radiolucent plastic strips 2, 2.5, 3, and 4 mm in width. A "point" source (<1 ml in volume and containing ~1 µCi) of ^{99m}Tc is placed at least three and preferably five crystal dimensions from and centered over the uncollimated detector, with the phantom placed directly over the detector. A 5- to 10-million-count "transmission" image is then acquired and visually inspected. The lead bars in at least the two coarsest quadrants (i.e., with the 3- and 4-mm-wide bars) should be visually resolvable. [A fillable sheet source, which may be filled with different radionuclides and used to evaluate extrinsic uniformity (see Fig. 1.19) is also shown in the photograph]

1.4.6 Multi-modality Devices and Other Developments

The major manufacturers of nuclear medicine instrumentation now market multi-modality scanners, combining high-performance state-of-the-art PET and CT scanners and, more recently, SPECT and CT scanners in a single device. These instruments provide near-perfect registration of images of in vivo function (PET or SPECT) and anatomy (CT). PET-CT scanners are already having a major impact on clinical practice, particularly in oncology, and are currently far outselling "PET-only" systems 2 to 1. Although generally encased in a single seamless housing, the PET or SPECT and CT gantries in such devices are separate; the respective FOVs are separated by a distance of the order of 1 m and the PET or SPECT and CT scans are performed sequentially. In one such device, the Gemini (Philips-ADAC), the PET and CT gantries are actually in separate housings with a sizable space between them; this not only provides access to patients but also may minimize anxiety among claustrophobic subjects. Moreover, in the Gemini the distance between the PET and CT gantries may be varied. With the incorporation of 16 and 64-slice spiral CT scanners, applications in cardiology as well as oncology are growing rapidly.

Time-of-flight (TOF) PET is based on the measurement of the difference between the detection times of

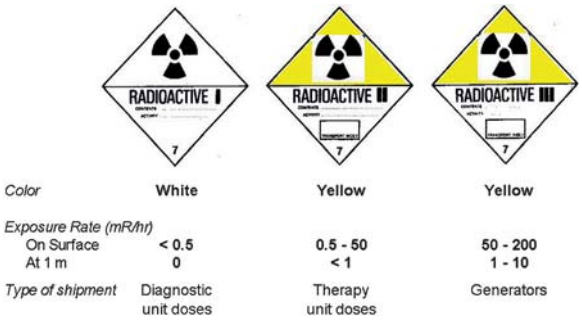

Fig. 1.21. US DOT labels required for shipment of radioactive packages. The particular label required is dictated by the package's "transport index (TI)," defined as its exposure rate in mR/h measured at a distance of 1 m from the package surface: TI = 0 (i.e., a measured exposure rate at 1 m equal to the background exposure rate) – "White I"; TI < 1 "Yellow II"; TI = 1 to 10 – "Yellow III"

the two positron-negatron annihilation photons arising from the decay of a positron, allowing spatial localization of the annihilation event along the LOR with a spatial resolution of ~100 mm assuming a coincidence time resolution (τ) of ~1 ns. Though a considerably coarser resolution than that of the conventional PET scanner (~5 mm), this approximate localization reduces the random coincidence rate and improves the signal-to-noise ratio (SNR), especially for large objects. For the TOF scanners developed in the 1980s, the SNR gain was offset by the low stopping power of the scintillation crystals [barium fluoride (BaF_2) and cesium fluoride (CsF)] used at the time and TOF PET was largely abandoned. Today, however, faster electronics and crystals such as LSO and GSO have made TOF PET feasible, and at least one manufacturer (Philips) has developed a commercial TOF scanner.

1.5 Radiation Safety

1.5.1 Regulatory Jurisdiction and Licensure

The use of radioactivity, particularly in medicine, is highly regulated, and extensive institutional as well as regulatory policies and procedures have been promulgated to ensure its save and compliant use. In the United States, the use of radioactivity is primarily regulated by a federal agency, the Nuclear Regulatory Commission (NRC), pursuant to Title 10, Part 35 of the Code of Federal Regulations (10CFR35). As stated in 10CFR35, "This part contains the requirements and provisions for the medical use of byproduct material and for issuance of specific licenses authorizing the medical use of this material. These requirements and provisions provide for the radiation safety of workers, the general public, patients, and human research subjects." However, in well over half of the states – the so-called "Agreement States," the NRC has agreed to delegate its regulatory authority to the state; in Agreement States, therefore, the use of radioactivity is directly regulated by a state agency rather than the NRC. In addition, the Food and Drug Administration (FDA), the United States Department of Transportation (US DOT), and other federal agencies maintain regulatory authority over certain aspects of the medical use of radioactivity. In any medical or other facility in which radioactive materials are used, the Radiation Safety Officer (RSO), in conjunction with a Radiation Committee and individual users, is charged with ensuring that all such materials are used in a manner which is safe and compliant with all applicable regulations.

Among the regulatory activities of the NRC and their Agreement-State counterparts are the licensing of physicians to possess radioactive materials for medical use and stipulation of the training-and-experience requirements for such licensure. For a diagnostic nuclear medicine practitioner, this includes 200 h of didactic training in the pertinent basic science (including radiation physics, radiobiology, and mathematics), 500 h of supervised training in practical radiation science, and 500 h of supervised training in clinical practice (including reading and interpreting studies). For licensure to also perform therapeutic nuclear medicine procedures, additional training and experience are required, including direct participation in the diagnosis and iodine-131 treatment of at least ten cases of hyperthyroidism and at least three cases of thyroid cancer. Physicians who are "board-eligible" for certification by the American Board of Nuclear Medicine (ABNM) and the American Board of Radiology (ABR) (special competency in nuclear medicine) will have satisfied these requirements.

1.5.2 Quantities and Units

Perhaps the most widely used and biologically meaningful quantity for expressing radiation dose, the absorbed dose, D, is defined as follows:

$$D \equiv \frac{d\bar{E}}{dm} \tag{1.22}$$

where $d\bar{E}$ is the mean energy imparted by ionizing radiation to a mass dm of matter. The SI unit is the gray (1 Gy = 1 J/kg) and the conventional unit the rad (1 rad = 100 erg/g); 1 Gy equals 100 rad and 1 rad equals 1 cGy (or 10 mGy).

Importantly, for the same absorbed dose, the frequency and/or severity of biological effects are generally less for sparsely ionizing (i.e., low-quality) than for densely ionizing (i.e., high-quality) radiations. Radia-

tion quality is characterized by the linear energy transfer, LET:

$$\mathrm{LET} \equiv \frac{\mathrm{DE}}{\mathrm{dl}} \tag{1.23}$$

where *dE* is the energy lost by a charged particle (or the secondary charged particle produced by the primary radiation) in traversing a distance *dl* in matter. The SI unit is the J/m and the conventional unit the keV/μ; 1 J/m equals 6.25×10^{9} keV/μ and 1 keV/μ equals 1.60×10^{-10} J/m. LET is of the order of 1 keV/μ for X-, γ-, and β-rays, 10 keV/μ for n and p, and 100 keV/μ for α-rays.

The influence of LET on the frequency and/or severity of biological effects is quantified by the relative biological effectiveness, RBE:

$$\mathrm{RBE(A)} \equiv \frac{\mathrm{D_{reference}}}{\mathrm{D_A}} \tag{1.24}$$

where $D_{\mathrm{reference}}$ is the absorbed dose of reference radiation (typically a widely available sparsely ionizing radiation such as cobalt-60 γ-rays) required to produce a specific biological effect and D_A is the absorbed dose of radiation *A* required to produce the same frequency and/or severity of the same specific biological effect with all pertinent parameters maintained as identical as possible. The RBE is a ratio of absorbed doses and thus is a dimensionless quantity. While its actual value for a given radiation depends on the specific biological effect, the conditions of the irradiation, etc., RBE is typically ~1 for X-, γ-, and β-rays, 5–10 for n and p, and 10–20 for α-rays. A simplified version of the RBE, the radiation weighting factor, w_R, was devised for purposes of radiation protection. The equivalent dose, H_T, in tissue or organ T, is related to the radiation weighting factors, w_R, and the mean absorbed doses, $D_{T,R}$, to tissue or organ T due to radiations R:

$$\mathrm{H_T} \equiv \sum_{\mathrm{R}} \mathrm{W_R\, D_{T,R}} \tag{1.25}$$

where w_R is assigned a value of 1 for X-, γ-, and β-rays, 2 for p, 5–20 for n, and 20 for α-rays. The radiation weighting factor, w_R, and the equivalent dose, H_T, are similar to the older quantities of quality factor, *Q*, and dose equivalent, *H*, respectively.

The effective dose (*E*) is intended to provide a single-value estimate of the overall stochastic risk (i.e., the total risk of cancer and genetic defects) of a given irradiation whether received by the whole body, part of the body, or only one or several individual organs:

$$\mathrm{E} \equiv \sum_{\mathrm{T}} \mathrm{W_T\, H_T} \tag{1.26}$$

$$\mathrm{E} \equiv \sum_{\mathrm{T}} \sum_{\mathrm{R}} {}^{\mathrm{W}}\mathrm{T}\ {}^{\mathrm{W}}\mathrm{R}\ {}^{\mathrm{D}}\mathrm{T,R} \tag{1.27}$$

where w_T is the weighting factor for tissue or organ T, a dimensionless quantity representing the fraction contributed by tissue or organ T to the *total* stochastic risk (i.e., $w_T = 0.01$ for bone and skin; 0.05 for bladder, breast, esophagus, liver, thyroid, and remainder of body; 0.12 for bone marrow, colon, lung, and stomach; and 0.20 for gonads). The effective dose is similar in concept to the effective dose equivalent, H_E (introduced previously by the ICRP and the NCRP), representing a single-value estimate of the net "harm" from any "low-dose" (e.g., diagnostic nuclear medicine or occupational) exposure. The effective dose and the effective dose equivalent do not apply to, and should not be used for, "high-dose" (e.g., therapeutic nuclear medicine) exposures. For both equivalent dose and the effective dose, the SI unit is the sievert (1 Sv = 1 J/kg) and the conventional unit the rem (1 rem = 100 erg/g); 1 Sv equals 100 rem and 1 rem equals 1 cSv (or 10 mSv).

1.5.3 Sources of Radiation Exposure and Dose Limits

Human beings are constantly and universally exposed to background radiation – from cosmic radiation from outer space, naturally occurring radionuclides in our environment and our own bodies, and other sources (Table 1.4). In the United States, the total exposure (actually, effective dose equivalent) averages 3.6 mSv, or

Table 1.4. Average annual radiation dose (expressed as dose equivalent and effective dose equivalent) to the US population, 1987. (Source: National Council on Radiation Protection and Measurements)

Source	Dose equivalent[a]		Effective dose equivalent	
	mSv	mrem	mSv	%
Natural				
Natural radon[b]	24	2.400	2.0	55
Cosmic	0.27	27	0.27	8.0
Terrestrial	0.28	28	0.28	8.0
Internal	0.39	39	0.39	11
Total natural	–	–	3.0	82
Artificial				
Medical				
X-ray diagnosis	0.39	39	0.39	11
Nuclear medicine	0.14	14	0.14	4.0
Consumer products	0.10	10	0.10	3.0
Other				
Occupational	0.009	0.9	<0.01	<0.3
Nuclear fuel cycle	<0.01	<1.0	<0.01	<0.03
Fallout	<0.01	<1.0	<0.01	<0.03
Miscellaneous[c]	<0.01	<1.0	<0.01	<0.03
Total artificial	–	–	0.63	18
Total natural and artificial	–	–	3.6	100

[a] To soft tissues
[b] Dose equivalent to bronchi from radon daughter products. The assumed weighting factor for the effective dose equivalent relative to whole-body exposure is 0.08
[c] Department of Energy facilities, smelters, transportation, etc.

360 mrem, per year. Most of this exposure, ~80 %, is natural background radiation, and about two-thirds of that is from radon. Radon results from the decay of uranium, a ubiquitous natural component of the earth's crust, and subsequently decays to plutonium. Both radon and plutonium are trans-uranic elements and thus undergo α-decay, with the emission of densely ionizing, high-LET α-rays (radiation weighting factor, $w_R = 20$). Radon is a gas and so is inhaled with the ambient air. If it decays to plutonium, a solid, while still within the lungs, the solid plutonium particle will not be exhaled but will be deposited on the surface of the pulmonary epithelium. When the plutonium subsequently undergoes α-decay in situ, a high dose equivalent (24 mSv = 2,400 mrem) is delivered to the lung and a large contribution to the effective dose equivalent (2.0 mSv = 200 mrem) results. Only ~20 % of the background radiation (0.6 Sv, or 60 mrem, per year) is from man-made sources, and almost all of this is due to medical exposures; note that this 60 mrem-per-year effective dose equivalent represents an average among all members of the US population, including those who have and those who have not had an actual medical exposure. Other specific exposures, both medical and non-medical, are presented in Table 1.5. Diagnostic medical exposures range from 4 mrem for a chest X-ray at the low end to 830 mrem for a chest CT at the high end, with nuclear medicine exposures (e.g., that from a ^{99m}Tc bone scan) generally in the middle of this range. The miscellaneous non-medical exposures range from 6 mrem for a trans-Atlantic commercial airline flight to 400 mrem per year from natural background radiation in Denver, CO. The foregoing dose estimates provide some perspective on radiation exposures: effective dose equivalents of several hundred to a thousand millirem, comparable to those received by diagnostic nuclear medicine patients and personnel, appear not to be associated with any grossly demonstrable adverse health effects.

10CFR35 stipulates radiation protection standards for occupationally exposed individuals (such as nuclear medicine technologists and physicians) as well as for non-occupationally exposed individuals. These standards are based on the assumption – the no-threshold hypothesis – that any radiation dose above natural background may create some additional risk of damage – hereditary defects, potential life-span shortening, and, in particular, cancer. Thus, it is prudent to design a radiation safety program that maintains radiation doses to workers and the public not just below the regulatory limit but as low as reasonably achievable (ALARA). The annual maximum permissible doses (MPDs) for radiation workers are currently as follows: effective dose equivalent, 50 mSv = 5 rem; dose equivalent to any one tissue or organ except the eye, 500 mSv = 50 rem; and dose equivalent to eye, 150 mSv = 15 rem.

Table 1.5. Radiation doses in perspective: effective dose equivalents for selected medical and non-medical exposures

	Effective dose equivalent (mrem)
Medical exposures	
Chest X-ray	4
Sentinel node procedure (breast)	32
Mammogram	40
Brain CT	180
^{99m}Tc bone scan	360
Intravenous urography	460
Barium enema	500
Abdominal CT	720
Chest CT	830
Non-medical exposures	
Trans-Atlantic airline flight[a]	6
Annual dose to nuclear medicine technologists – US average	180
Annual natural background radiation – US average	360
Annual natural background radiation – Denver, CO[a]	400

[a] The additional dose in Denver, CO, and the dose in a trans-Atlantic airline flight are due to increased cosmic radiations at these higher altitudes

The respective MPDs to non-occupationally exposed individuals are one-tenth of the corresponding MPD for occupationally exposed individuals, including an effective-dose-equivalent limit of 5 mSv, or 0.5 rem, per year. For the general public at large, as opposed to specific non-occupationally exposed individuals (such as a secretary in a nuclear medicine facility), the MPD is an effective dose equivalent of 1 mSv, or 0.1 rem. Finally, for a declared pregnant worker (i.e., an occupationally exposed individual who has informed her employer of her pregnancy), the MPD over the total duration of her pregnancy is the same as that of a non-occupationally exposed individual, 5 mSv = 0.5 rem.

1.5.4 Personnel Dosimetry

For occupationally exposed individuals, personnel monitors provide estimates of external exposure. Personnel monitors typically achieve an accuracy of ±30 % and a precision of ±10 % over an exposure range of 10 mR (the lowest detectable exposure) to 2,000 R with constancy (i.e., constant signal per unit exposure) over a wide X- and γ-ray energy range. Until recently, commercially supplied and processed "film badges" consisted of plastic holders containing a small piece of X-ray film in a light-tight seal. The optical density, or opacity ("blackening"), of film is directly related to its exposure. Thermoluminescent dosimeters (TLDs) have now largely replaced film in personnel monitors. TLDs

are composed of crystalline solids (most commonly, lithium fluoride, LiF), which can be formed into small disks or rods. When TLDs absorb radiation energy and are subsequently heated to sufficiently high temperatures, they emit visible light in an amount directly related to the radiation energy absorbed. "TLD readers" consist of a light-tight oven in which the TLD is heated, a PMT to detect and measure the light emitted by the TLD, and associated electronics. Prior to use (i.e., exposure to radiation), each lot of film or TLDs must be calibrated to yield a lot-specific "calibration factor" (i.e., optical density or light emitted, respectively, per unit radiation dose). Unlike film, TLDs are re-usable and, after being read out but before being re-used, must be super-heated (or annealed) to stimulate the emission of spurious (non-radiogenic) light. Among the desirable characteristics of TLDs are sensitivity (to exposures as low as ~10 mR), linear, energy-independent response, and insensitivity to heat, light, and humidity as well as re-usability. Incidental heating after radiation exposure but prior to readout may dissipate the light signal and thus yield a spuriously low signal.

Personnel dosimeters typically have a metallically filtered area (to provide an estimate of the "deep" dose) and an unfiltered area (to estimate the shallow, or "skin," dose). Both film and TLDs are "integrating" detectors and thus yield the total dose up to the time the film is developed or the TLD is read. Personnel dosimeters are generally changed monthly. Most radiation workers wear a single dosimeter, typically on the trunk of the body. Certain cohorts of workers such as radiopharmacists may wear additional dosimeters (e.g., ring and eye glass dosimeters).

1.5.5 Receipt, Transport, Storage, and Inventory of Radioactive Materials

Radioactive packages should be examined and opened on disposable pads wearing disposable gloves. Packages should be inspected immediately upon receipt for any sign of damage such as breakage, moisture, or discoloration of the outer packing. As soon as possible after receipt, packages should be monitored for external radiation levels using a survey monitor and possible surface contamination determined by wipe testing (see below). If the measured exposure rate is not consistent with the package label or if it appears that the package is damaged, the RSO or designee shall be contacted immediately. Once a package is opened, the inner container should be inspected for any breakage or leakage and wipe tested for contamination. The inner container label and the packing slip should be cross-checked to verify the vendor, the identity and physical and chemical forms of the radionuclide, the activity present and date and time of calibration. Any deviations should be reported to the shipper and resolved. The packing material and empty package should also be monitored for radioactive contamination using a survey meter before disposal. If radioactively contaminated, these materials should be treated as radioactive waste. If free of contamination, the radiation/radioactivity labels should be removed or obliterated before appropriate disposal as non-radioactive waste.

Radioactive packages cannot be transported in the same manner as non-radioactive packages and must be shipped by UD DOT-authorized "dangerous-goods" carriers. A completed "dangerous-goods" manifest, listing the names and addresses of the shipper and the consignee, the radionuclide and its activity and chemical and physical forms, a 24-h emergency contact telephone number, and the transport index (see below), must accompany the shipment. In addition, US DOT-authorized "radioactive shipment" labels must be completed and affixed to at least two surfaces of the radioactive package (Fig. 1.21).

All vials or other vessels that contain radioactive materials should be labeled appropriately with "Caution Radioactive Material" warnings and provide the identity of the radionuclide, physical and chemical forms of the radionuclide, activity, date and time of calibration. Such items should be stored in shielded (lead) containers and the containers stored in shielded cabinets or drawers or behind lead shielding. For certain radiopharmaceuticals that must be stored at low temperatures, a refrigerator may be lined with lead or a refrigerator may be located in an appropriately shielded area. Radioactive materials should be stored in secure, controlled areas, such as a radiopharmacy, posted with "Caution Radioactive Material" warning signs. If personnel inside these areas could receive a dose rate of 0.05 mSv/h (5 mrem/h) or more, the door should be posted with a "Caution Radiation Area" sign. Items such as food, beverages, and medications shall not be stored in the same area as radioactive materials. A running inventory of radioactive materials must be maintained. This inventory should include: the identity of the radionuclide, physical and chemical forms of the radionuclide, activity, date and time of calibration and of receipt activities dispensed and the dates and times of dispensing and the patient or other purpose for which it was dispensed; the activity, date and time, and method of disposal.

1.5.6 Radiation Surveys

Radiation surveys should be performed using a survey meter (such as a Geiger counter) calibrated in absolute exposure rate or absorbed dose rate units (mR/h or mrad/h, respectively). Because of the limited penetration of β-rays and other particulate radiations, the abil-

ity of each type of survey meter to detect these radiations should be clearly understood. The use of beta shields or caps may allow for measurements in fields of mixed radiations. Survey meters should include a "battery check" function. Some models may include a low-activity "check source" to provide a check on operation of the instrument immediately prior to use. These devices shall be calibrated at least annually and records of the calibrations shall be maintained.

Removable radioactive contamination can be deposited on skin or enter the body and irradiate an individual internally. Therefore, assay of removable radioactive contamination on all potentially contaminated surfaces and on sealed radioactive sources must be performed at regular intervals and whenever contamination is suspected. Non-removable radioactive contamination, i.e., fixed contamination, contributes only to external exposure and its contribution is reflected in the radiation surveys. Assay of removable radioactive contamination is typically performed using a "wipe test." In such a test, a representative area of approximately 100 cm^2 of a potentially contaminated surface is wiped with a dry piece of paper and the wipe is counted in a counting system. The resulting gross count rates are converted to net count rates by subtracting a background, or blank, count rate and the net count rates converted to activity using the counting system's measured calibration factors.

In controlled, or restricted, areas, surveys should be performed daily and wipe tests weekly. In other (uncontrolled or unrestricted) areas, surveys should be performed weekly and wipe tests monthly.

1.5.7 Waste Disposal

Nuclear medicine generates low-level radioactive waste, mostly in the form of dry waste (such as empty vials, syringes, intravenous tubing, disposable gloves, absorbent pads, paper toweling, gauze, contaminated disposable eating utensils, and partially decayed sources). Regulations concerning disposal of radioactive or radioactively contaminated waste are stringent: no waste which is detectably radioactive (i.e., yields a count rate significantly greater than the background count rate when assayed with a high-sensitivity survey meter) may be disposed of as non-radioactive waste. Depending on a facility's volume of radioactive waste and its capacity for waste storage, disposal may be accomplished by one or more of the following methods: return to vendor, decay-in-storage, transfer to a radioactive waste facility (commercial disposal), and, for liquid waste, dilution and dispersal.

Radioactively contaminated dry waste that will decay to background levels within a reasonably short period of time (i.e., up to several months) should be stored for decay. Such storage locations should be in a low-occupancy, secure and posted area of the facility and adequately shielded as required. Prior to disposal or recycling of decayed radioactive waste, such materials should be monitored with a suitable survey meter to verify that radioactivity is undetectable, and all "radioactive-material" labeling should be removed or obliterated prior to disposal or recycling. Radioactive or radioactively contaminated waste should be segregated by physical half-life to facilitate final disposal. Many hospitals have installed high-sensitivity counting systems to monitor *all* waste exiting the facility and, if necessary, divert at that point radioactively contaminated waste for decay-in-storage. Low-level, non-infectious liquid radioactive waste as well as excreta (including excreta collected in urine bags and bedpans) from nuclear medicine patients generally may be disposed of by dilution or dispersal, that is, disposal down a waste drain or toilet. The facility's radiation safety officer must assure that liquid radioactive waste discharged into the sewer does not exceed regulatory limits. Radioactivity and radioactively contaminated waste too long-lived to be practically held for decay-in-storage [such as carbon-14 ($T_{1/2}$ = 5,730 years) and tritium ($T_{1/2}$ = 12.3 years)] must be disposed of commercially (for eventual encasement, transport to, and long-term burial at one of only several low-level radioactive waste sites nationwide). Commercial disposal is extremely expensive, but, fortunately, is rarely required in nuclear medicine.

1.5.8 Radionuclide Therapy and the "New" Release Criteria

Historically, the NRC and Agreement States required radionuclide therapy patients to remain hospitalized until the retained activity in the patient was less than 1,110 MBq (30 mCi) or the dose rate at 1 m from the patient was less than 0.05 mSv/h (5 mrem/h). In 1997, however, the NRC amended its regulations concerning radionuclide therapy patients through the issuance of new rules that appeared in the Federal Register on January 29. The new NRC regulations, revised 10CFR 35.75 effective May 1997, allow for the release from medical confinement of patients if the expected total effective dose equivalent (TEDE) to individuals exposed to the patient is not likely to exceed 5 mSv (500 mrem). Guidance on determining when patients may be released based on the new criteria, when written instructions on post-release radiation precautions must be provided, and when records related to the release of the patient must be maintained are provided in NRC Regulatory Guide 8.39. A licensee may release from his or her control any patient administered (diagnostic or therapeutic) radiopharmaceuticals or therapeutically implanted with sealed radioactive sources if the TEDE to any indi-

vidual from exposure to the patient after release is not likely to exceed 5 mSv (500 mrem). Compliance with this dose limit may be demonstrated using either: (a) a default table in Regulatory Guide 8.39 for activity (e.g., <33 mCi of iodine-131 retained by the patient) or dose rate (e.g., <7 mrem/h at 1 m from an iodine-131-containing patient) or (b) patient-specific kinetic data using effective half-times or residence times and dose rate measurements and a patient-specific projected dose calculation. The use of method (b) will generally result in patients being released with substantially higher activities – up to several hundred mCi – than would method (a). Importantly, in basing release on patient-specific information [method (b)], the NRC regulations allow for representative kinetic data such as effective half-times or residence times for a particular population of patients (e.g., hyperthyroid patients) to be applied to an individual patient in that population, thus obviating the need in certain cases for measurement of kinetic data on an individual patient basis. The revised NRC regulations require that the licensee provide written instructions to the released patient regarding radiation precautions. Post-release radiation safety instructions to the patient should address maintenance of distance from other persons, separate sleeping arrangements, minimization of time in public places including public transportation facilities such as buses, trains, and planes, and measures to reduce environmental contamination. In the case of nursing mothers, recommendations on discontinuation of breast-feeding should be included as well. Information on the duration of post-release radiation precautions must also be provided. The revised NRC regulations impose, under some circumstances, certain record-keeping requirements. If patient release is based on method (a), records are not required. However, if release is based on method (b), a record of the basis for release including patient-specific factors and dose-calculation equations must be prepared and maintained for 3 years from the date of release.

1.5.9 Record-Keeping

Written and/or computerized records, maintained for periods established by regulatory agencies and/or the facility, are required. The required records and other documentation include the: radioactive materials receipt, inventory, distribution, and disposal, including radiopharmaceutical prescriptions; radiation survey data, including measurements of ambient radiation levels and surface radioactive contamination, and annotated facility diagrams indicating the sites of such measurements; monitoring records for all occupationally exposed personnel, including any bioassay data; written policies and procedures for the clinical and the radiation-safety program; description of the radiation-safety training program; the Radiation Safety Committee membership and minutes; and reports of any unusual, radiologically significant occurrences.

1.5.10 "Sensitive" Patient Populations

The administration of radioactive materials, even in diagnostic amounts, to certain "sensitive" populations – pregnant women, nursing mothers, and prospective parents – remains a matter of concern in nuclear medicine.

Pregnant Women. Increasingly accurate anatomic models of the fetus and pregnant woman have been developed, including models of the pregnant female at the beginning of pregnancy (representing the embryo as a small unit density sphere located at the uterus) and at the end of the first and third trimesters. Radiopharmaceutical kinetic data in utero and therefore fetal dose estimates are quite limited, however. Published fetal absorbed dose estimates are generally of the order of or less than 0.1 cGy (0.1 rad) per 37 mBq (1 mCi) administered to the mother. A particularly worrisome issue, however, is radioiodine administration to pregnant women. The fetal thyroid begins concentrating iodine at the 12th to 15th week of gestation. At 16 – 24 weeks, ^{131}I-iodide delivers a very large absorbed dose of 1,500 – 6,000 cGy/37 MBq (rad/mCi) to the fetal thyroid and an absorbed dose of 3 – 5 cGy/37 MBq (rad/mCi) to the fetal total body, depending on maternal thyroid uptake. For a hyperthyroid therapy administration of 185 MBq (5 mCi), 7,500 – 30,000 cGy (rad) would therefore be delivered to the fetal thyroid and 15 – 25 rad to the fetal total body. Not surprisingly, with radiogenic destruction of the fetal thyroid and thyroid hormone deficiency in utero, fetal hypothyroidism and congenital cretinism have been shown to result following radioiodine therapy of hyperthyroidism or thyroid cancer in pregnant women. It is therefore critical to avoid radioiodine administration to the pregnant patient, even in diagnostic amounts.

Nursing Mothers. Diagnostic radiopharmaceuticals administered to lactating women can achieve rather high concentrations in breast milk and potentially deliver significant radiation doses to nursing infants. For example, the cumulative breast milk activity ranged from 0.03 % to 27 % of ^{131}I-iodide administered to six women for thyroid uptake studies. Using a variety of dosimetric criteria [e.g., an effective dose equivalent to the nursing infant of 0.1 cSv (0.1 rem)], a number of authors have recommended different interruption periods prior to resuming breast-feeding following administration of radiopharmaceuticals. While there is no absolute consensus, the following are representative

of the published recommendations: 24 h following any administration of ^{99m}Tc or ^{18}F, 2 – 4 weeks following administration of ^{67}Ga-gallium citrate, and permanently for the current nursing infant following any administration of ^{131}I-iodide.

Prospective Parents. No evidence of significant germ cell damage (indicated by an increased risk of birth defects among subsequently conceived offspring) has been observed among A-bomb survivors (average gonadal absorbed dose: > 30 cGy) and exposed human cohorts and no such damage is expected, therefore, among diagnostic nuclear medicine patients. Nonetheless, demonstrable gonadal damage, specifically, *transiently* impaired fertility, may occasionally occur among thyroid cancer patients treated with much larger amounts (> 100 mCi) of ^{131}I followed by full recovery of fertility. While it is difficult to rationally formulate guidelines on the basis of the limited human data available, it is perhaps prudent that patients forego starting a family for at least several months following such high-dose radioiodine therapy.

1.5.11 Concluding Remarks

Based on the preponderance of negative ("no-effect") results from radiation epidemiology studies in the dose range of the order of 1 rem, in diagnostic nuclear medicine the activities used and the associated radiation doses are generally so low that there is no practical possibility of any short- or long-term demonstrable harm to patients, staff, and other individuals. However, because of the large relative increase in the risk of childhood cancer following even low-level exposures in utero, radiation (including nuclear medicine) procedures in pregnant women must be based on an informed and *documented* decision regarding medical necessity, This, and *not* the possibility of inducing fetal death or congenital abnormalities, is why females of child-bearing age are routinely queried about the possibility of being pregnant prior to undergoing a radiological or nuclear medicine procedure.

Further Reading

Bendriem B, Townsend DW (eds) (1998) The theory and practice of 3D PET. Kluwer Academic, Dordrecht

Cherry SR, Sorenson JA, Phelps ME (2003) Physics in nuclear medicine, 3rd edn. Saunders, Philadelphia, PA, pp 325 – 359

Zanzonico PB (1995) Technical requirements for SPECT: Equipment and quality control. In: Kramer EL, Sanger JJ (eds) Clinical applications in SPECT. Raven Press, New York, pp 7 – 41

Zanzonico P (2000) Internal radionuclide radiation dosimetry: A review of basic concepts and recent developments. J Nucl Med 41:297 – 308

Zanzonio P (2002) The intraoperative probe: design, operation, and safety. In: Cody HS III (ed) Sentinel node biopsy. Martin Dunitz, London

Zanzonico P (2004) Positron emission tomography: A review of basic principles, scanner design and performance, and current systems. Semin Nucl Med 34:87 – 111

Zanzonico P, Heller S (2000) The intraoperative gamma probe: Basic principles and choices available. Semin Nucl Med 30:33 – 48

Zanzonico P, Siegel J, St Germain J (2000) A generalized algorithm for determining the time of release and the duration of post-release radiation precautions following radionuclide therapy. Health Phys 6:648 – 659

2 Radiochemistry and Radiopharmacy

S. Guhlke, A.M. Verbruggen, S. Vallabhajosula

2.1 Radiochemistry and Radiopharmacy of SPECT Tracers and for Internal Radiotherapy

S. Guhlke, A.M. Verbruggen

2.1.1 Production of Radionuclides for SPECT and Radiotherapy

2.1.1.1 Introduction

In modern pharmaceutical development and medicine, radioactivity has an increasing impact in the field of diagnostic applications (in vitro and in vivo) as well as in therapeutic applications (Qaim and Coenen 2005; Stöcklin et al. 1995). Regarding these different forms of applications, radionuclides must be used with respect to their modes of decay. For single photon emission computed tomography (SPECT), radionuclides with a short (hours to several days) half-life and accompanying gamma emission in the range of 70 – 250 keV are the most useful. In addition, emission of only one photon per decay is of advantage, but not a must. The gamma emission has to be strong enough to easily penetrate the body barrier and also has to be well detectable by the common SPECT camera systems. Such radionuclides are commonly found among those with the decay mode of electron capture (EC) or internal conversion (IC).

Radionuclides intended for use in internal radiotherapy have naturally different demands (Volkert et al. 1991; Tolmachev et al. 2004). Coupled to targeting molecules or in some special cases just in simple ionic forms (such as iodide for therapy of thyroid cancers or some bone-seeking nuclides), the aim is to deposit a high dose on the targeted organ while the dose to healthy tissues should be as low as possible. Radionuclides used here are $\beta^{(-)}$, alpha or Auger electron emitters. Gamma emissions may or may not accompany these decay modes but usually do not contribute significantly to the therapeutic effectiveness of such radiopharmaceuticals. However, if the gamma emission is in the useful range for camera detection, it may allow for scintigraphic imaging and dose calculations.

The production of radionuclides for use in nuclear medicine requires an exact knowledge of nuclear data, production technologies (accelerators or nuclear reactors) and radiochemical purification technologies in order to meet the high purity demands of medical applications. In many cases, for one particular isotope there is more than one principal production route. Therefore the actual route of production will depend on the availability of a suitable production device, the yield and the achievable purity of the nuclide (Kocher 1983; Manual 2003).

2.1.1.2 Production Modes

According to their production modes, radionuclides used for SPECT and in radiotherapy can be differentiated into three groups:

- Reactor nuclides
- Cyclotron nuclides
- Generator nuclides

Reactor Nuclides

The spallation of [^{235}U]uranium in a nuclear reactor serves as the neutron source. Thermal neutrons will react with stable isotopes deposited inside a reaction chamber in defined areas of the nuclear reactor. Neutrons will penetrate through the target and react with the target material using the (n,γ) nuclear reaction to produce neutron-rich isotopes. This will preferably lead to β^--emitters with a mass of one unit higher than the stable target isotope. Isotopes produced like this are of relatively low specific activity as the produced isotope is of the same element as the target. Thus the produced isotope cannot be chemically separated from the target isotope.

In different regions of the nuclear reactor where fast neutrons dominate, a different nuclear reaction – the (n,p) reaction – may occur. In this case, the mass of the produced isotope will not change. However, by eliminating a proton from the target isotope a change in the element (one unit lower) will occur. In this case a chemical separation of the product from the target matrix is

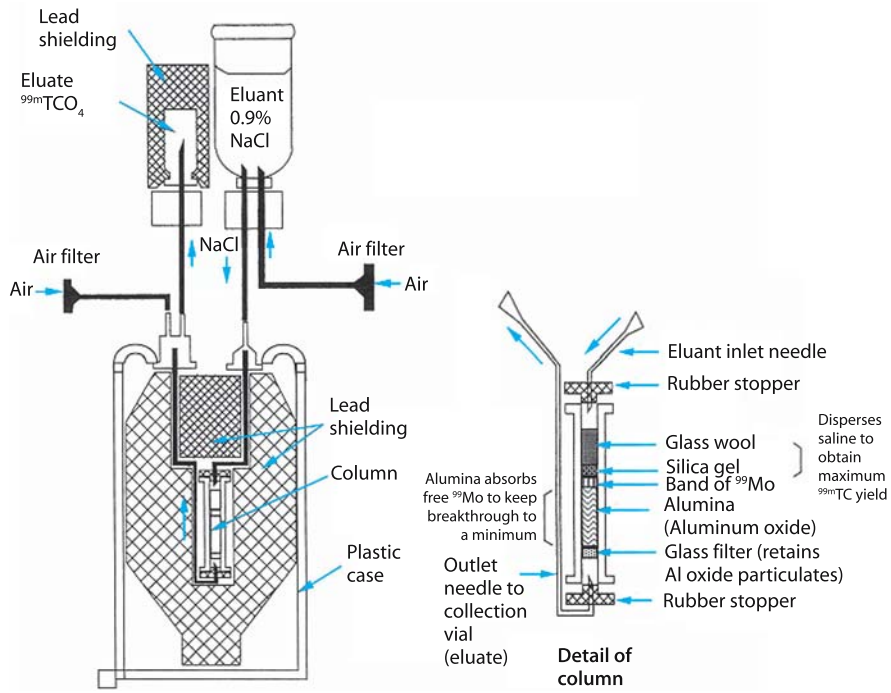

Fig. 2.1. Cross section of a $^{99}Mo/^{99m}Tc$ generator

possible. In this way high specific activity nuclides, either completely carrier free (c.f.) or at least no-carrier-added (n.c.a), can be obtained.

Cyclotron Nuclides

Because acceleratable particles are of a charged nature, typical cyclotron produced isotopes are neutron deficient. They are produced by irradiation of stable target compounds with charged particles like protons (p), deuterons (d) or helium nuclei (α). Because of the neutron deficient nature of the produced isotopes, they tend to stabilize by electron capture (EC) or by positron emission (β^+). These decay modes are particularly useful for nuclear medicine purposes as EC usually is not accompanied by β^--emission and they are thus useful diagnostic isotopes. Positron emitting isotopes are also typically produced using cyclotrons. As they are extensively used in positron emission tomography (PET), their production is discussed in detail below in Sect. 2.2, "Radiopharmaceuticals for PET."

Generator Nuclides

This production mode for isotopes is especially useful for nuclear medicine because of the demand for short lived isotopes, which is very important in order to minimize the radiation dose to a patient but also largely because of logistic considerations. The loss of activity of short lived isotopes during transport may not allow the use of a particular isotope at all or at least will contribute to higher cost. Radionuclide generator systems make use of a "mother-daughter" nuclide system and a suitable separation technique, allowing quantitative separation of the daughter from the mother nuclide. All kinds of physicochemical separation methods (e.g., distillation, precipitation, liquid/liquid extraction, liquid/solid extraction, sublimation) may be used; however, in particular chromatographic separation techniques are most useful and most if not all commercially available generator systems are based on chromatographic systems. As an example, a cross section of a typical $^{99}Mo/^{99m}Tc$-generator is given in Fig. 2.1. The eluant (phys. saline) is driven by vacuum generated through an evacuated eluate vial through the chromatography column, which is loaded with molybdenum-99. Typically the molybdenum-99 is bound strongly to the aluminum oxide matrix. The radioactive daughter nuclide ^{99m}Tc will be formed in the chemical form of pertechnetate ($^{99m}TcO_4^-$), which is weakly bound and thus easily eluted. After an elution, the ^{99m}Tc activity will regrow (transient equilibrium) to close to its maximum value within about 24 h (Fig. 2.2). After 5 days the nominal Mo activity will be around one-fifth of the initial activity and usually Mo/Tc generators will be replaced on a weekly schedule.

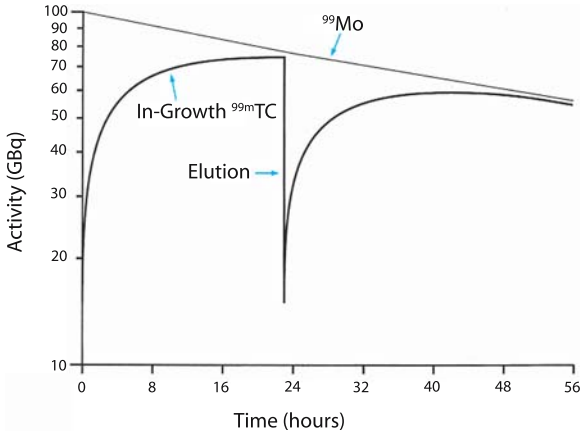

Fig. 2.2. Elution profile of a $^{99}Mo/^{99m}Tc$ generator

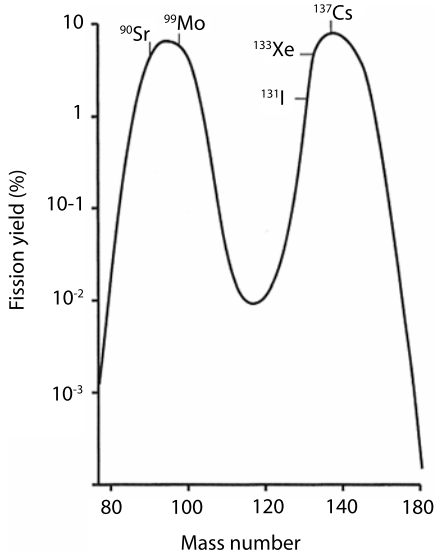

Fig. 2.3. Yield of fission products from U-235 as a function of mass number

2.1.1.3 "Diagnostic" Radionuclides for SPECT Applications

The nuclides used most often for SPECT applications are summarized in Table 2.1. Even though nuclear medicine diagnostic scans using PET or PET/CT have gained increasing importance over the last decade, about 70% of all diagnostic scans are performed using technetium-99m (^{99m}Tc)-labeled radiopharmaceuticals.

Technetium-99m

Technetium-99m decays with a half-life of 6.0 h by isomeric transition to ^{99g}Tc, thereby emitting a single photon with an energy of 141 keV. This energy almost ideally meets the sensitivity maximum of SPECT camera systems. In addition, the rich complex chemistry of technetium allows incorporation of the radioisotope into a wide variety of ligands stabilizing the radionuclide at different oxidation states. Thus hundreds of radiopharmaceuticals labeled with ^{99m}Tc have been developed and some have gained significant market success. However, the main reason for the special role of technetium in SPECT is probably the cost effectiveness and the on-demand availability of the isotope through the $^{99}Mo/^{99m}Tc$-generator system. As this generator has gained enormous importance for nuclear medicine in recent decades, nuclide production routes will be discussed here in more detail: For the production of the mother nuclide molybdenum-99 [(^{99}Mo); ($T_{1/2}$ = 66.0 h)], there are two major routes of production: one, through the $^{98}Mo(n,\gamma)^{99}Mo$ reaction, which occurs on neutron irradiation of ^{98}Mo, and a second, through the fission of uranium-235 [^{235}U(n,fission)^{99}Mo]. The preferred production mode is through uranium-235 mainly for two reasons: The mass distribution as a result of uranium fission follows an M-shaped curve (Fig. 2.3) with ^{99}Mo being close to the first maximum, thus leading to a high yield of ^{99}Mo. The second reason is that fission produced ^{99}Mo is almost carrier free and thus of the highest specific activity. Therefore it requires a much smaller amount of Al_2O_3 generator matrix compared to the approximately 100 times lower specific activity of ^{99}Mo, which can be obtained by the irradiation of stable ^{98}Mo. At the same time the much higher ratio of Al_2O_3 matrix over the ^{99}Mo load reduces the risk of ^{99}Mo breakthrough, leading to a higher radionuclidic purity of the pertechnetate-99m eluate.

Nuclide	$T_{1/2}$	Decay mode (% abundance)	Production mode	Photon emission (keV) (% abundance)
^{67}Ga	3.26 d	EC (100)	$^{68}Zn(p,2n)$	93 (36%); 185 (20%); 300 (16%); 394 (4.5%)
^{99}Mo ↓ Gen.	2.75 d	β^--(100)	$^{235}U(n,f)$ $^{98}Mo(n,\gamma)$	740 (12%); 181 (6%)
^{99m}Tc	6.0 h	IT (100)		141 (87%)
^{111}In	2.83 d	EC (100)	$^{112}Cd(p,2n)$	247 (94%); 173 (91%)
^{123}I	13.1 h	EC (100)	See Table 2.2	159 (83%); 528 (1.4%)
^{201}Tl	73.1 h	EC (100)	$^{201}Tl(p,3n)^{201}Pb$ $^{201}Pb(EC)^{201}Tl$	167 (10%); 69–80 (several X-rays)

Table 2.1. Selected radionuclides for SPECT and their decay and production modes

Table 2.2. Production routes for iodine-123

Target	Nuclear reaction	Intermediates and decays	Product	Remarks
^{127}I	(p,5n)	^{123}Xe (EC or β^+) ($T_{1/2}$ = 2.08 h)	^{123}I	0.25 % ^{125}I contaminant
^{123}Te	(p,n)	None	^{123}I	^{124}I; ^{125}I contaminants
^{124}Te	(p,2n)	None	^{123}I	^{124}I; ^{125}I contaminants
^{124}Xe	(p,2n) ~70 %	^{123}Cs (β^+), ^{123}Xe (EC or β^+) ($T_{1/2}$ = 5.9 min) ($T_{1/2}$ = 2.08 h)	^{123}I	Very pure Xe-124 very expensive
^{124}Xe	(p,pn) ~25 %	^{123}Xe (EC or β^+) ($T_{1/2}$ = 2.08 h)	^{123}I	
^{124}Xe	(p,2p) ~10 %	None	^{123}I	

Iodine-123

Because of the attractive nuclear and chemical properties of iodine, the radioisotope iodine-123 (half-life 13.2 h) is in strong demand in nuclear medicine and is often used to label radiopharmaceuticals for diagnostic imaging. There are two general categories of nuclear reactions for the production of iodine-123. The first and most widely utilized class is the reaction which yields iodine-123 directly through proton bombardment of tellurium targets in a cyclotron and the subsequent separation of iodine-123 from the irradiated target. Either a (p,n) reaction on ^{123}Te or a (p,2n) reaction on ^{124}Te may be used (Table 2.2). These reactions give optimum product yields using protons of less than 50 MeV and are generally favored by industrial scale producers and others producing on a low scale with commercially available compact cyclotrons. For the nuclear reaction, ^{124}Te(p,2n)^{123}I targets of isotopically enriched tellurium-124, either as elemental Te, or in the dioxide form (TeO_2), are employed. However, the I-123 product made by tellurium targets is not ideal for medical applications. Because of associated nuclear reactions in the target, it is unavoidably contaminated by other radioiodines, mainly iodine-124 (half-life 4.2 days) and to a lesser extent by iodine-125 (half-life 60 days). The concentration of these long-lived contaminants increases with time relative to the shorter-lived iodine-123.

The second general class of nuclear reactions used for iodine-123 production are indirect mechanisms: Here the iodine-123 production routes make use of the intermediate precursor xenon-123 (half-life 2.1 h). The chemically inert and gaseous xenon-123 rather than the iodine-123 by itself is separated from the irradiated target and then allowed to decay to iodine-123. The indirect reaction routes have the decisive advantage of higher product purity over the direct routes.

One very important indirect route to generating xenon-123 is the ^{127}I(p,5n)^{123}Xe reaction. Other xenon isotopes such as Xe-124, Xe-125 and Xe-126 are also produced and separated together with xenon-123. However, Xe-123/124 is stable and blocks the formation of iodine-124 and iodine-126 as contaminants. Xenon-125, however, leads to an iodine-125 contaminant level normally of about 0.2 % at the time of the final iodine-123 product preparation. Iodine-125 is a less undesirable contaminant than iodine-124 or iodine-126 since it does not emit photon radiation of energy sufficient to degrade diagnostic images. It does, however, contribute to a patient radiation dose to about the same extent as iodine-124. Nevertheless, iodine-123 preparations via the indirect nuclear reaction route are regarded as medically much superior to direct reaction preparations.

The purest iodine-123 is produced again indirectly via xenon-123 by a rather sophisticated production route employing very expensive, highly enriched xenon-124 as target material.

Three possible nuclear reactions (see Table 2.3), (p,n), (p,pn) and (p,2p), contribute in a ratio of about (7:2.5:1) to the formation of iodine-123. Cesium-123 is formed by the reaction ^{124}Xe(p,2n)^{123}Cs, which decays further by β+ or EC, with a very short half-life of 5.9 min to xenon-123. The nuclear reaction ^{124}Xe(p,pn)^{123}Xe leads directly to the intermediate xenon-123 and to a lesser extent (< 10 %) even the direct formation of iodine-123 via the ^{124}Xe(p,2p)^{123}I reaction is also occurring. Hence, the majority of iodine-123 is formed through xenon-123, which is removed from the target cryogenically and subsequently evacuated into a separate vial. Here the final product iodine-123 is simply formed through the decay of xenon-123 and rinsed from the vial in highest purity.

Indium-111

Another important SPECT isotope is indium-111 ($T_{1/2}$ = 2.8 days), mainly produced with cyclotrons by proton irradiation of cadmium precursors. The most important radiopharmaceutical is octreoscan. The octapeptide octreotide is labeled with In-111 through the chelating moiety diethylenetriaminepentaacetic acid (DTPA), which is coupled to the peptide's N-terminus. Because of its physical half-life of 2.8 days, In-111 is also especially useful for labeling of biomolecules with relatively slow in-vivo kinetics, and thus is often ap-

Table 2.3. Production routes for indium-111

Target	Nuclear reaction	Natural abundance of isotope (%)	Yield of ^{111}In (μCi/μAh)	Contaminants and remarks
^{112}Cd	(p,2n)	24.07	1035	In-114m; In-110m; In-109 Total at 48 h after EOB approx. 1 %
^{110}Cd	(d,n)	12.39	117	In-114m; In-110m; In-109 Total at 48 h after EOB approx. 6 %
^{109}Ag	(α,n)	48.65	2	In-110m; In-109 Total at 48 h after EOB approx. 6 %
^{109}Ag	(^{3}He,n)	48.65	55	In-110m; In-109 Total at 48 h after EOB approx. 6 %

Table 2.4. Selected radioisotopes for internal therapy

Nuclide	$T_{1/2}$	E_{max} (MeV) and type of decay	Production process	Accompanied γ-emission (keV)
β$^-$-emitters				
^{32}P	14.3 d	1.7 (β$^-$)	^{32}S(n,p)	–
^{89}Sr	50.5 d	1.5 (β$^-$)	^{89}Y(n,p)	–
^{90}Y	2.7 d	2.3 (β$^-$)	^{90}Sr→^{90}Y generator ^{235}U(n,f)	–
^{131}I	8.0 d	0.6 (β$^-$)	^{130}Te(n,γ, β$^-$) ^{235}U(n,f)	364 (81 %); 637 (7 %)
^{153}Sm	1.9 d	0.8 (β$^-$)	^{152}Sm(n,γ)	103 (29 %)
^{177}Lu	6.7 d	0.5 (β$^-$)	^{176}Lu(n,γ)	208 (11 %); 113 (6 %)
^{186}Re	3.7 d	1.1 (β$^-$)	^{187}Re(n,γ)	137 (9 %)
^{188}Re	17.0 h	2.0 (β$^-$)	^{186}W(n,γ), ^{187}W(n,γ) ^{188}W→^{188}Re generator	155 (15 %)
α-emitters				
^{211}At	7.2 h	5.9 (α)	^{209}Bi(α,n)	–
^{212}Bi	1.0 h	7.8(α)	^{224}Ra/^{212}Pb→^{212}Bi generator	727 (12 %)
^{225}Ac	10.0 h	5.8(α)	^{229}Th(α)^{225}Ra(β)^{225}Ac ^{226}Ra(p,n)	
Auger electron emitters				
^{67}Ga	3.2 d	Auger electrons	^{68}Zn(p,2n)	93 (36 %); 185 (20 %); 300 (16 %); 394 (4.5 %)
^{125}I	60.0 d	Auger electrons	^{124}Xe(n,γ,EC)	35 (6.5 %)
^{193m}Pt	4.3 d	Auger electrons	^{192}Os(α,3n) ^{192}Pt(n,γ)	–

plied in research trials of radiolabeled antibodies. The main production routes for this nuclide are summarized in Table 2.3. They either make use of the enriched cadmium isotopes Cd-112 or Cd-110 or the silver isotope Ag-109 as targets. The use of silver targets has the distinct advantage of not producing the long-lived In-114m ($T_{1/2}$ = 49.5 days) while the use, e.g., of enriched cadmium-112 has the advantage of leading to much higher yields. Hence, the production route using enriched Cd-112 targets is a good compromise between nuclear reaction efficiency and a relatively low content of longer lived contaminants and this is the preferred route.

2.1.1.4 Therapy Nuclides

For internal radiotherapy, nuclides emitting α- or β$^-$-particles or Auger electrons are of much interest as unsealed sources in the treatment of cancer. With the aim of therapy, it is extremely important to carefully consider the choice of radionuclides with respect to the in-vivo localization and the pharmacokinetic properties of the cancer targeting agent. The decay data of some selected nuclides and their production routes are summarized in Table 2.4.

Some of the β$^-$-emitting radioisotopes can be used in ionic form without any radiolabeling chemistry, such as phosphorus-32 and strontium-89, which are used as bone targeting agents in palliative therapies. The most important therapeutic nuclide is still iodine-131, which is also used in the ionic form of iodide in the treatment of thyroid cancers. In most other cases oxidation to the +1 oxidation state is needed to label aromatic or vinylic organic compounds. The trivalent ions yttrium-90, samarium-153 and lutetium-177 are most often directly labeled to strong chelating agents such as DTPA or DOTA linked to cancer targeting biomole-

cules, while the rhenium isotopes 186 and 188 which are produced in the chemical form of perrhenate require reduction to lower oxidation states before they can be labeled to a wide variety of chelating agents. In recent years Re-188 has gained a lot of attention because of its chemical similarity to technetium and the on-demand availability through the W-188/Re-188 generator system. Therapy trials employing α-emitting nuclides are rare compared to the use of β^--emitting isotopes. The high linear energy transfer (LET) of alpha radiation is very effective in damaging DNA strands and thus leads to cell death even if only a few particles enter the cell. At the same time this might be a disadvantage as cells which are only neighboring those with uptake of alpha-isotope might easily survive, such as is the case with antibodies which often cannot penetrate easily into a tumor mass and only bind to the cell surface without being internalized or even transported to the cell nucleus. Bismuth-212 is conveniently available through a radium-224 generator system, while astatine-211 requires an accelerator near the site of use. The production of pure actinium-225 from nuclear waste is very sophisticated although its nuclear properties are very attractive.

Because of the short range of Auger electrons in physiological medium, similarly to alpha emitters, these emitters also require the radiolabeled compound very close to or even within the cell nucleus, where they produce high radiotoxicity. Before replacement by suitable technetium labeled compounds, Ga-67 was used for a long time in SPECT imaging of inflammation. Today gallium-67 is gaining more interest as a therapeutic isotope especially with the use of the generator nuclide gallium-68 for PET studies.

Iodine-125 is widely available and often used for in-vitro studies. However, the rather long half-life of 60 days limits its widespread use because of radiation protection considerations. It has been employed in the therapy of prostate cancer in the form of radiolabeled seeds which are placed directly into the lesions. Platinum-193m is also being considered because it is one of the highest Auger-electron-producing isotopes of all.

2.1.2 Radiopharmaceutical Chemistry of SPECT Tracers

Radiopharmaceuticals used in SPECT imaging can be divided into two groups – those which are designed for diagnostic imaging of diseases of peripheral organs and those which are designed for imaging of diseases of the central nerve system (CNS). Because of the necessity of crossing the blood-brain barrier (BBB), the majority of CNS ligands are labeled with iodine-123, in order to avoid major alterations of the unlabeled lead structures, which would occur by introduction of chelating moieties which are used to bind radiometallic nuclides such as technetium-99m and indium-111. The majority of SPECT tracers for imaging peripheral diseases are labeled with Tc-99m as structural alterations are better tolerated than with CNS ligands. Thus the key advantages of Tc-99m, such as its physical decay characteristics, on demand availability, kit preparations of the radiopharmaceutical and lower cost, overshadow the possible use of In-111 or I-123-labeled tracers.

2.1.2.1 Technetium-99m

Radiopharmaceuticals labeled with Tc-99m play an important role in widespread applications of nuclear medicine. When ^{99m}Tc-radiopharmaceuticals began to emerge in nuclear medicine, major efforts were directed towards the development of radiopharmaceuticals for bone imaging and for the excretory functions of the liver and kidneys. Later, significant developments in technetium chemistry provided ^{99m}Tc-labeled radiopharmaceuticals for assessing regional cerebral and myocardial blood flow. More recently, efforts have been directed towards the design of ^{99m}Tc-labeled compounds, which even allow the measurement of receptor densities or transporter functions. A number of direct labeling techniques as well as indirect routes through bifunctional chelating agents even provide ^{99m}Tc-labeled proteins and peptides with high binding affinity and high in vivo stability. The latest major breakthrough was the introduction of organometallic technetium carbonyl complexes as a new class of ^{99m}Tc-radiopharmaceutical design. In the following the main aspects of the radiopharmaceutical chemistry of Tc-99m will be described and illustrated by selected examples of radiopharmaceuticals or partial structures thereof.

The transitional metal technetium (element 43) is located in the 7th group of the periodic chart between the elements manganese and rhenium. All technetium isotopes are radioactive and therefore this element is naturally not present in the earth's crust. It has to be prepared technically by man (this fact led to the name "technetium"), and this fact of course delayed the chemical development of technetium until the respective technology was available. As with manganese and rhenium, oxidation states between +7 and –1 are possible and complexes at all of these oxidation states are known. However, their stability greatly differs and therefore in radiopharmaceuticals the oxidation states +V and +I are dominant.

The basis for all technetium labeled radiopharmaceuticals is the pertechnetate anion ($[^{99m}Tc]TcO_4^-$), which is eluted from a commercial Tc-99m generator. The pertechnetate ion [oxidation state (+7)] is quite stable and rather inert to any complex chemistry.

In order to form Tc-99m-labeled organic molecules it is therefore necessary to reduce the pertechnetate an-

ion to a lower oxidation state reactive towards chelating structures.

A variety of reducing agents might be used; however, stannous(II) ions are used in most cases especially in commercial kit preparations. Before going into organic technetium complexes, it should be mentioned that inorganic complexes of Tc-99m are also used as radiopharmaceuticals.

2.1.2.1.1 Inorganic Technetium-99m Compounds

[^{99m}Tc]TcO_4^- ([^{99m}Tc]-pertechnetate)

The most prominent inorganic technetium complex for use in nuclear medicine is the pertechnetate ion itself. Because of the similar size of iodide and pertechnetate ions, it can be used as a substitute for iodide in the diagnosis of thyroid disorders. Pertechnetate is accepted by the Na^+/I^--symporter and therefore transported actively into the thyroid (Cho et al. 2000). Of course it will not participate like iodide in the thyroid hormone metabolism. However, the determination of the local iodide uptake (substituted by pertechnetate) is for most diagnostic purposes sufficient. In addition, the radiation burden on the patient is much lower than using [^{123}I]iodide.

[^{99m}Tc]Tc_2S_7 ([^{99m}Tc]Sulfur Colloid)

The physiological mechanism behind static liver scintigraphy using ^{99m}Tc-sulfur colloid is the rapid clearance by the reticuloendothelial system from the blood. Uptake of the radioactive colloid by organs of the reticuloendothelial system is dependent on both their relative blood flow rates and the functional capacity of the phagocytic cells (Jovanovic et al. 1981).

The preparation of the sulfur colloid is usually achieved by thiosulfate in acidic media as a source of sulfide ions which also serve as reductant.

^{99m}Tc on Carbon as Aerosol ([^{99m}Tc]-Technegas)

The conversion of [^{99m}Tc]Tc-pertechnetate at 2,500 °C in the presence of crucible graphite leads to ^{99m}Tc on carbon as aerosol. The particles have nm size. The aerosol is used for lung perfusion studies and requires the use of a special "Technegas generator" for the aerosol formation (Suga 2002).

2.1.2.1.2 Organic Technetium-99m Complexes

General Remarks for the Formation of Tc-99m Complexes

As a transition metal, technetium binds easily (at lower oxidation states) to complexing and chelating agents. Chelating agents have several heteroatoms geometrically arranged in such a way to form after binding into the ^{99m}Tc core 5- or 6-membered rings. Optimal heteroatoms for binding of technetium are:

- Nitrogen (in amines, amides, imines, oximes and N in aromatic rings)
- Sulfur (in thiols and thioethers)
- Phosphorus (in phosphines)
- Oxygen (in carboxylates, phenols, alcohols, enols and phosphonates)

The oxidation state in the final complex is usually not dependent on the used reducing agent but more on the nature of the binding ligand and in some cases also on the pH. An example of pH dependent complex formation is [^{99m}Tc]DMSA, which forms in slightly acidic media the complex Tc(III)-DMSA used in kidney and renal scintigraphy, while in slightly basic media the Tc(V)-DMSA complex is formed, which is used in tumor scintigraphy for medullary thyroid carcinoma and for visualization of bone metastases (Blower et al. 2000) (Fig. 2.4).

For the preparation of ^{99m}Tc complexes it is possible to form complexes directly at room temperature (or by heating) in the presence of a reducing agent, if the ligand is in metal binding form. An example of this is the direct labeling of ethylenedicysteinate (Fig. 2.5).

Different from direct labeling is the so-called exchange labeling procedure (Fig. 2.6) as exemplified by the radiopharmaceutical ^{99m}Tc-MAG_3, which is used as a functional kidney imaging agent (Fritzberg et al. 1986). If the ligand is present in protected form or if complex formation proceeds slowly, a weak chelating agent (such as tartrate or gluconate) must be present to prevent formation of colloidal TcO_2. However, direct labeling in the case of MAG_3 is also possible at elevated pH, even at room temperature, and a commercial kit using the direct approach is also available.

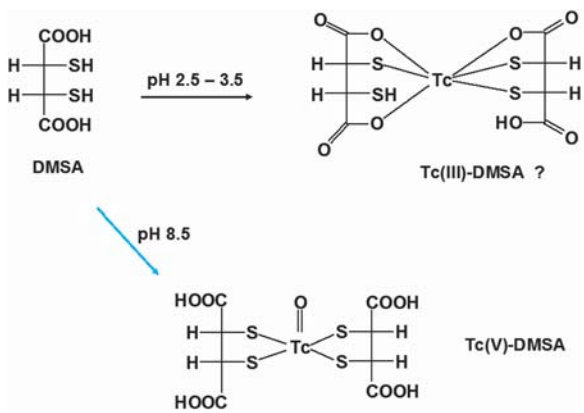

Fig. 2.4. pH determines valence of reduced Tc and nature of formed complex in the case of [^{99m}Tc]DMSA (the structure of Tc(III)-DMSA is a proposed structure)

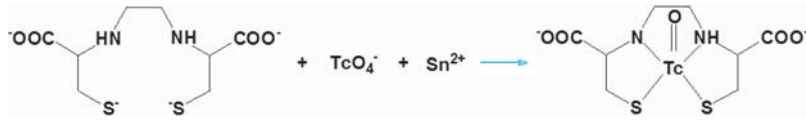

Fig. 2.5. Direct labeling can be performed if ligand is present in metal binding form

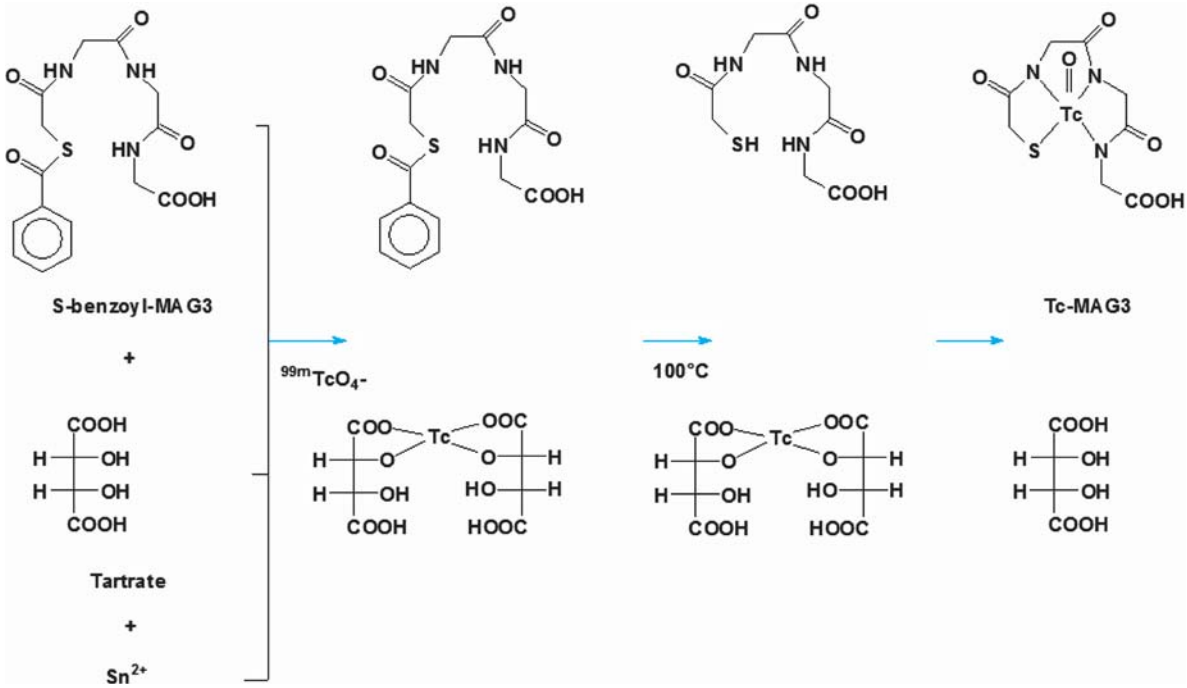

Fig. 2.6. Exchange labeling with ^{99m}Tc exemplified by ^{99m}Tc-MAG3

The labeling of the radiopharmaceutical ^{99m}Tc-ECD (Vallabhajosula et al. 1989), which is the diethylester of ethylendicysteinate shown in Fig. 2.2, is also performed by exchange labeling using mannitol as exchange ligand. Tc-ECD (Neurolite) is used for brain imaging purposes as the lipophilic diester is able to cross the blood-brain barrier. In the following the different types of Tc ligands will be discussed under their complex chemical aspects with examples of radiopharmaceuticals falling in the classes of tetra-, di- or monoligands.

2.1.2.1.3 Tetraligands

Tetraligands are very common among ^{99m}Tc-labeled radiopharmaceuticals and were already shown in the examples illustrated in Figs. 2.4 – 2.6. Most often are found combinations of N, S and O heteroatoms involved in the complex formations like N_2S_2, N_3S, N_3O or N_4. Table 2.5 gives a number of selected examples of more often used tetraligand complexes and some prominent radiopharmaceuticals labeled by this class of ligands.

2.1.2.1.4 Triligands

Triligands are by far less common than tetraligands among Tc-99m-labeled compounds. However, Tc-99m-labeled derivatives of iminodiacetic acid (IDA) are in use for hepatobiliary functional imaging (Chervu et al. 1982). A couple of minutes after intravenous injection of the tracer the liver is visualized followed by spleen and subsequently in the intestines. Hepatocytes are responsible for the uptake of IDA derivatives followed by active transport into the spleen. IDA derivatives are neither metabolized nor conjugated in the liver; however, differences between certain derivatives determine the hepatobiliary excretion rate and the competition with bilirubin for receptors on the hepatocytes.

Technetium-99m-labeled IDA derivates (Fig. 2.7) are anionic complexes of oxidation state (+III), with carboxyl and imino groups serving as tridentate ligand to the Tc core. In order to saturate the coordination sphere, two IDA molecules form dimeric complexes.

Table 2.5. Some characteristic examples of tetraligand Tc complexes

Type of ligand	Name	Characteristic structure	Substructure found for example in the radiopharmaceutical
N_2S_2	Bis(aminothiol) (BAT)	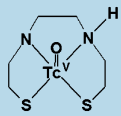	[^{99m}Tc]TRODAT-1 (Kung et al. 1997)
N_2S_2	Diamide dithiol (DADT)	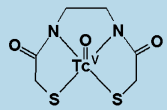	(Hui et al. 1991)
N_2S_2	Monoamide-monothiol (MAMA)	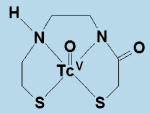	ECD (Bicisate) (Vallabhajosula et al. 1989)
N_3S	Triamidethiol	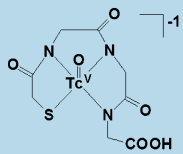	MAG_3 (Fritzberg et al. 1986)
N_3O	Hydroxytriamide	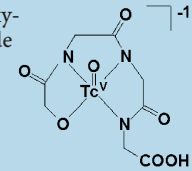	(Vanbilloen et al. 1997)
N_4	Tetraamine	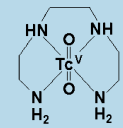	^{99m}Tc-Demotate (octreotide analog) (Nikolopoulou et al. 2006)
N_4	Bisamino oxime	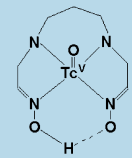	HMPAO. The complex is unstable and therefore stabilized by various methods (Neirinckx et al. 1987; Weisner et al. 1993; Kao et al. 1999)
N_4	Aminotriamide (tetrapeptide)	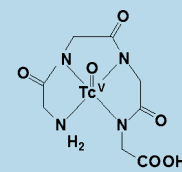	^{99m}Tc-Tetrapeptides (Vanbilloen et al. 1996)

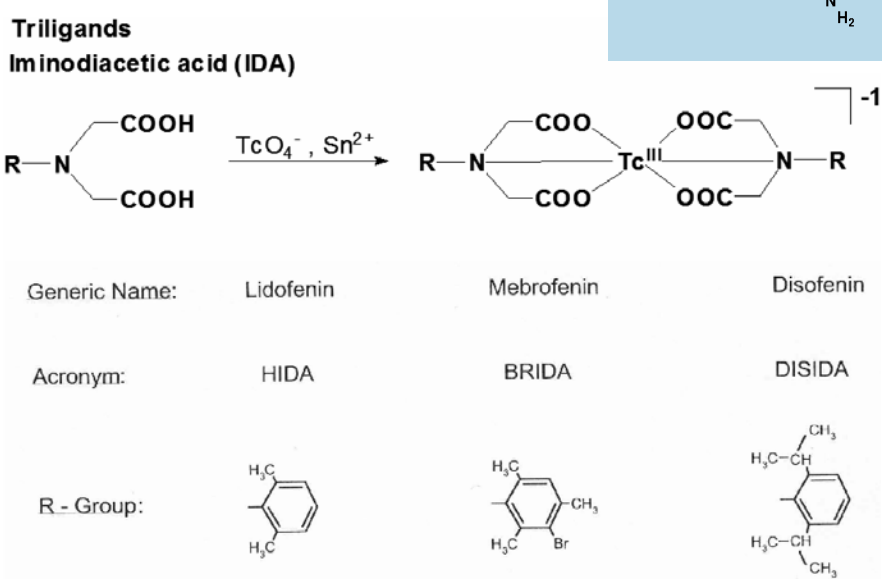

Fig. 2.7. Iminodiacetic acid deriva tives for functional hepatobiliary SPECT imaging

2.1.2.1.5 Diligands

Diligands are again more frequently found in SPECT radiopharmaceuticals. As with IDA derivatives, dimeric complexes are needed in order to saturate the coordination sphere of the Tc-99m core. ^{99m}Tc(V)-DMSA (shown in Fig. 2.4) as well as frequently used transfer complexes like tartrate (shown in Fig. 2.6) are complexes of this type. The radiopharmaceutical tetrofosmin (Higley et al. 1993) also falls into this category. It is used for SPECT imaging of myocardial perfusion and the structure is depicted in Fig. 2.8. As the complex is lipophilic and carries a positive charge (like potassium cations), the uptake in the mitochondria is thought to be mediated by passive diffusion and by the Na^+/H^+-antiporter system.

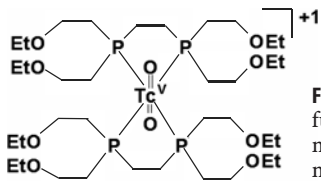

Fig. 2.8. The myocardial perfusion agent ^{99m}Tc-tetrofosmin as an example of a dimeric diligand complex

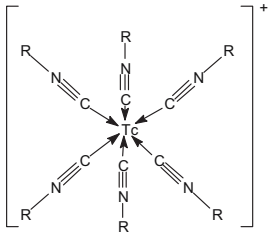

Fig. 2.9. The myocardial perfusion agent ^{99m}Tc-sestamibi as an example of a hexameric monoligand complex

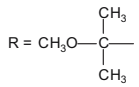

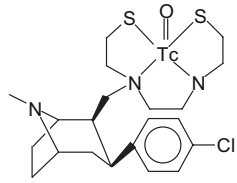

Fig. 2.10. Structure of [^{99m}Tc]TRODAT-1

[^{99m}Tc]-TRODAT-1

2.1.2.1.6 Monoligands

Monoligands play an important role especially in more recent attempts to develop Tc-99m-labeled SPECT tracers. The most prominent example among commercially successful tracers is the Tc-99m-MIBI complex, of which the structure can be seen in Fig. 2.9. This radiopharmaceutical is used under the trade name Myoview (Taillefer et al. 1988) in myocardial perfusion imaging and the uptake mechanism – being a positively charged lipophilic complex – is the same as discussed for tetrofosmin above.

Six isonitrile molecules bind to one Tc(I) atom. As isonitrile is volatile and stenchy, a copper adduct is used as precursor in the commercial labeling kit. Therefore an exchange labeling with heating is required.

2.1.2.1.7 Recent Progress in Technetium Chemistry and Newer Compounds

Since 1992, no Tc-99m-labeled radiopharmaceuticals have been approved for general use in nuclear medicine. The main reasons are the high approval costs (Nunn 2006) combined with the special difficulties for radioactive pharmaceuticals such as logistic issues and a relatively small market. Nevertheless, there have been a number of new and very interesting developments regarding new approaches to Tc-labeled compounds. The most prominent developments are:

Technetium-99m-TRODAT-1

Technetium-99m-TRODAT-1 is a conjugate of a cocaine derivative with a ^{99m}Tc(V)oxo-diaminodithiol complex (Fig. 2.10) developed by Kung and coworkers (Meegalla et al. 1996) in 1995. Its usefulness for the diagnosis of Parkinson's disease was established in clinical studies which have proven the affinity for the dopamine transporter. Using the respective stable Re-complex (Re-TRODAT-1) as surrogate, in vitro binding constants to the dopamine transporter were found to have a K_i value of 14 nM. This interesting ^{99m}Tc-labeled compound was the first and so far only useful Tc compound for receptor studies in the brain.

Technetium-99m-Depreotide

Technetium-99m-depreotide (NeoTect) (Pearson et al. 1996) has been developed by researchers at Diatide by the rational and ingenious design of a peptide that contains both a domain binding with high affinity to somatostatin receptors, which predominantly are subtypes 2, 3 and 5, and a second structural moiety able to bind Tc (Fig. 2.11). It has a high sensitivity and specificity for lung cancer lesion detection and has received FDA approval for this indication. However, PET with ^{18}F-FDG has a similar sensitivity and specificity for lesion identification in this disease, yields images with superior resolution and is currently by far the more widely used. It is therefore doubtful whether ^{99m}Tc-depreotide will continue to be commercially available.

For ^{99m}Tc-labeling of mainly peptides and proteins, the use of **hydrazinonicotinamide** (**Hynic**) as a bifunctional chelating agent has proven successful. Thrombus binding peptides, chemotactic peptides, somatostatin derivatives and annexin have been labeled by using this method. The labeling proceeds well even at very low concentrations. The binding to Tc proceeds via the hydrazine group, which acts as a monodentate ligand. The nicotinic nitrogen is not essential but supports the labeling efficiency. The complex formation requires the use of a coligand such as tricine or ethylenediamine diacetic acid (EDDA) (Fig. 2.12). Because of the presence of stereoisomers, it is difficult to determine the exact nature of the formed complexes. Clinically promising results have been obtained with ^{99m}Tc-Hynic annexin V (Ohtsuki et al. 1999) and ^{99m}Tc-Hynic-labeled somatostatin analogs (Decristoforo and Mather 1999; Bangard et al. 2000), which seem to be superior to the commercially available and fully approved ^{111}In-labeled octreotide.

The most exciting development in the field of ^{99m}Tc chemistry during the last 15 years is probably the development of a convenient method to label biomolecules with a **Tc-tricarbonyl** core by Alberto and coworkers (Alberto et al. 1998). The $Tc(CO)_3(H_2O)_3$ precursor can be prepared using CO gas and sodium borohydride as reducing agent. Using the commercially available Isolink labeling kit, which contains potassium boranocarbonate ($Na_2[H_3BCO_2]$) as both reducing agent and source of CO, the precursor formation proceeds even more easily, reproducibly and safely. The water mole-

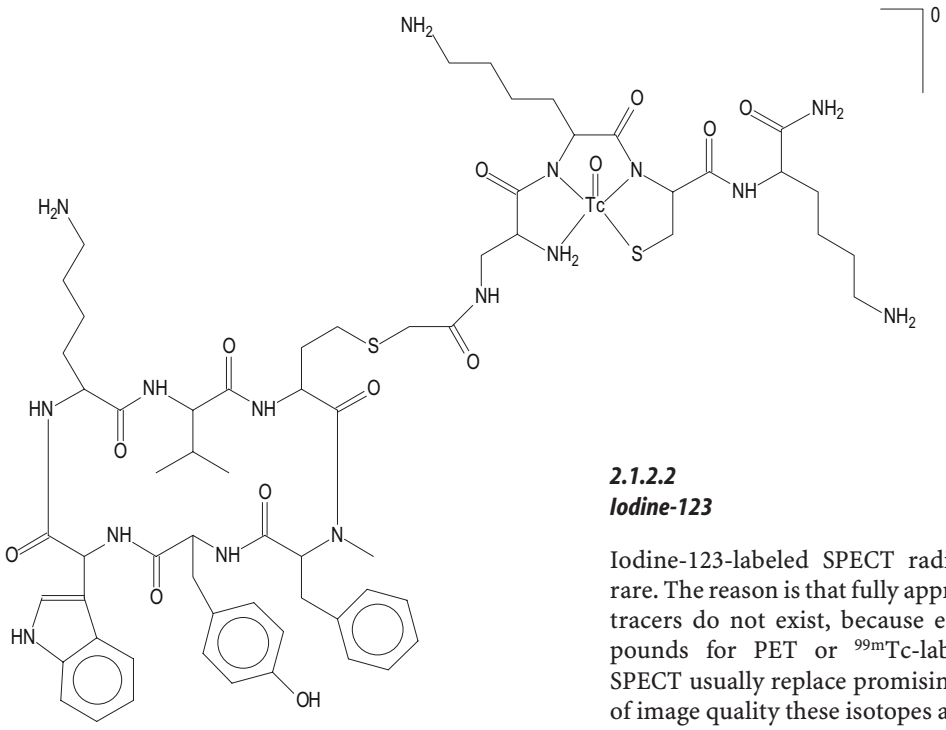

Fig. 2.11. Structure of the somatostatin analog ^{99m}Tc-depreotide

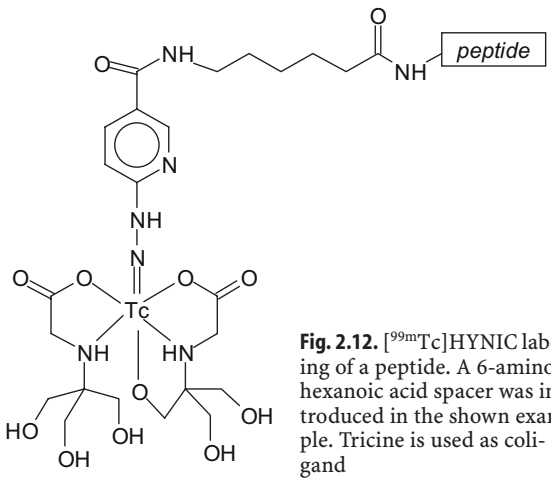

Fig. 2.12. [^{99m}Tc]HYNIC labeling of a peptide. A 6-aminohexanoic acid spacer was introduced in the shown example. Tricine is used as coligand

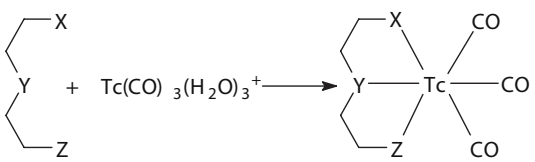

Fig. 2.13. Reaction of $Tc(CO)_3(H_2O)_3$ with a tridentate donor ligand (X, Y, Z = N, O, S or P)

cules of this precursor are substitution labile and are prone to ligand exchange with a wide variety of donor ligands (Fig. 2.13). By variation of the donor ligands, the final ^{99m}Tc-tricarbonyl-labeled biomolecule can be neutral, anionic or cationic.

2.1.2.2 Iodine-123

Iodine-123-labeled SPECT radiopharmaceuticals are rare. The reason is that fully approved iodinated SPECT tracers do not exist, because either ^{18}F-labeled compounds for PET or ^{99m}Tc-labeled compounds for SPECT usually replace promising candidates. In terms of image quality these isotopes are simply better suited than I-123 and there is no crucial advantage left for using iodine-123. Thus the main area for iodine isotopes is not SPECT with I-123 or PET (where I-124 could be principally used) but the use of I-131 in therapeutic radiopharmaceuticals. Therefore the main labeling chemistry regarding radioiodination of biologically active compounds will be described in the radiotherapy chapter.

Nevertheless, I-123 is still widely used in the development of new tracers. In the past 10 years, significant progress has been made on the development of new brain-imaging agents for single-photon emission computed tomography. Most of the new radiopharmaceuticals are designed to bind specific neurotransmitter receptor or transporter sites in the central nervous system.

Results from imaging of **benzodiazepine (γ-aminobutyric acid) receptors** by [^{123}I]iomazenil (Fig. 2.14) are useful in identifying epileptic seizure foci and changes of this receptor in psychiatric disorders (Innis et al. 1991).

Imaging of **dopamine D_2 receptors** is possible with a ^{123}I-labeled analog for SPECT, namely [^{123}I]IBZM

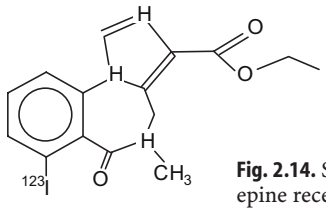

Fig. 2.14. Structure of the benzodiazepine receptor agent ^{123}I-iomazenil

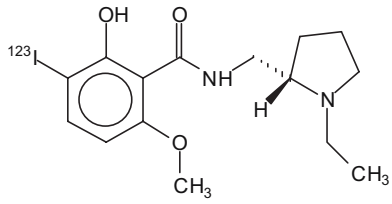

Fig. 2.15. Structure of the dopaminergic tracer ^{123}I-IBZM

(Fig. 2.15) [(*S*)-*N*-[(1-ethyl-2-pyrrolidinyl)]methyl-2-hydroxy-3-iodo-6-methoxybenzamide] (Kung et al. 1989). Biodistribution studies demonstrated that the agent is concentrated in the basal ganglia although some non-specific binding was noted in cerebral cortex and cerebellum. If receptor density or blockade is being quantified, it is necessary to correct for this non-specific binding.

Imaging of the **dopamine transporter (DAT)** with [^{123}I]CIT (2-beta-carboxymethoxy-3-beta(4-iodophenyl)tropane) and [^{123}I]FE-β-CIT or [^{123}I]FP-β-CIT (fluorethyl or fluoropropyl analogs of β-CIT) (Fig. 2.16) have proven to be a simple but powerful tool for differential diagnosis of Parkinson's and other neurodegenerative diseases (Kuikka et al. 1995).

The in vivo investigation of brain **serotonergic 5-HT receptors** has been pursued for several years. There is evidence suggesting a role for the 5-HT system, in particular 5-HT$_2$ receptors in the regulation of a wide range of central mechanisms. Abnormalities in 5-HT$_2$ receptors have been proposed in several neuropsychiatric conditions including major depression, Alzheimer-type dementia, drug abuse and schizophrenia.

For SPECT studies, ^{123}I-5-I-R91150 ([^{123}I]-4-amino-*N*-[1-[3-(4-fluorophenoxy)-propyl]-4-methyl-4-piperidinyl]-5-iodo-2-methoxybenzamide) has been synthesized by Baeken et al. (1998) by electrophilic substitution on the 5-position of the methoxybenzamide group of R91150 (Fig. 2.17). It is a 5-HT$_2$ antagonist with high affinity and selectivity for the 5-HT$_{2A}$ receptor (the main subtype of 5-HT$_2$ receptors in the brain). The in vitro binding constant (K_i) for 5-HT$_2$ receptors is 0.2 nM, whereas the selectivity to other neurotransmitter receptors (5-HTx, α_1, α_2, D_1 and D_2) is at least a factor of 50. The results obtained with this tracer agent up to now indicate that this radioligand might be very useful for in vivo 5-HT$_{2A}$ receptor mapping.

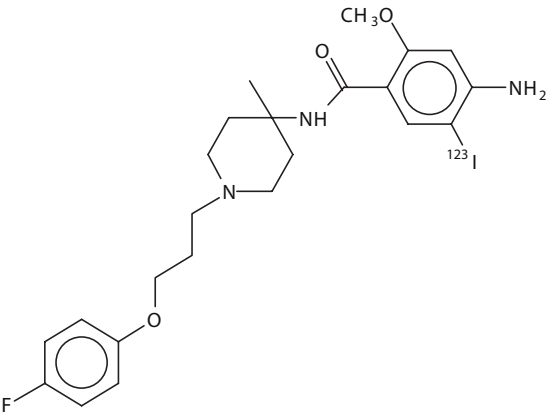

Fig. 2.17. Structure of the 5-HT$_2$ receptor tracer ^{123}I-5-I-R91150

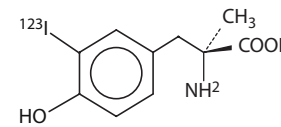

Fig. 2.18. Structure of the radiolabeled amino acids L-[3-^{123}I]iodo-α-methyltyrosine

Despite these interesting brain imaging agents, iodine-123-labeled tracers are also quite frequently found in studies on **amino acid metabolism**. The "old-timer," *L*-3-^{123}I-iodo-α-methyltyrosine (^{123}I-IMT) (Fig. 2.18) is still one of the most useful tracers for imaging of brain tumors. There is evidence suggesting that IMT is accumulated in the brain via a specific facilitating *L*-amino acid transport system. The carrier system for large neutral amino acids which also transports non-iodinated α-methyltyrosine is likely to be involved. In analogy to many other labeled amino acids, IMT is not incorporated into proteins (Langen et al. 1990) and its uptake only reflects amino acid transport (Shikano et al. 2003).

In contrast to amino acid metabolism, **amyloid imaging** is a relatively new field for SPECT tracer development. Alzheimer's disease (AD) is characterized by the presence of abundant senile plaques composed of amyloid-β (Aβ) peptides and neurofibrillary tangles formed by filaments of highly phosphorylated tau proteins. In vivo assessment of the beta-sheet proteins deposited in amyloid plaques using a radiolabeled imaging agent with high affinity for Aβ would allow localization and quantification of senile plaques in a non-invasive way and possibly in an early stage of the disease.

Fig. 2.16. Structures of the dopamine reuptake tracer agents β-CIT (**a**) and its analogs β-CIT-FE (**b**) and β-CIT-FP (**c**) (I = ^{123}I; FE = fluoroethyl-; FP = fluoropropyl)

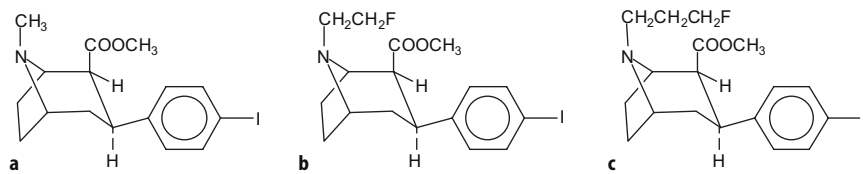

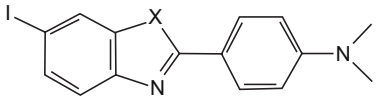

Fig. 2.19. Structure of iodinated amyloid binding agents as potential tracers for imaging Alzheimer's disease: TZDM (X = S) and IBOX (X = O) (I = ^{123}I)

Several derivatives of Congo red (this compound is used for fluorescent staining of senile plaques in postmortem brain sections of AD patients) and chrysamine G labeled with radioiodine have been developed and evaluated as potential Aβ aggregate specific imaging agents. Many of these compounds showed high in vitro binding affinity for amyloid fibrils, but their penetration through the blood-brain barrier and as a consequence their uptake in brain was very limited.

More recently, more promising radioactive compounds with smaller molecular size and increased lipophilicity, derived from the amyloid binding dye thioflavin T, have been reported. As thioflavin T contains a positively charged quaternary amine which likely will limit brain uptake, benzothiazoles which are uncharged at physiological pH were designed and tested for their amyloid-β binding properties and in vivo brain uptake.

Zhuang and coworkers (Zhuang et al. 2001) developed a series of radioiodinated benzothiazoles, of which TZDM and especially IBOX (Fig. 2.19) show the most promising properties.

2.1.2.3 Indium-111

The situation for indium-111-labeled SPECT tracers is similar to that of iodinated tracers. The radionuclidic properties are not as good as for ^{99m}Tc and thus agents that prove useful for SPECT imaging might sooner or later be replaced by respective ^{99m}Tc-labeled tracers. Therefore it is not a surprise that in recent years no fully approved In-111-labeled compounds were introduced for use in nuclear medicine.

Nevertheless one example of a successful radiopharmaceutical labeled with In-111 is octreoscan: It is a derivative of the somatostatin analog octreotide, a cyclic octapeptide containing the physiologically active four-amino acid sequence (Phe-D-Trp-Lys-Thr). In order to enable labeling of octreotide with ^{111}In, a DTPA molecule has been conjugated to the α-NH_2 group of the N-terminal D-Phe residue (Krenning et al. 1992). The generic name of this conjugate is pentetreotide (Fig. 2.20).

Because pentetreotide only binds with high affinity to the somatostatin receptor subtype SSTR2, with moderate affinity to SSTR3 and SSTR5 and not to SSTR1 and SSTR4, research has continued to develop other somatostatin analogs, which bind also with high affinity to the other receptor subtypes. Lanreotide is an octapeptide which binds to SSTR2 through SSTR5 with high affinity and to SSTR1 with low affinity. This peptide is modified with DOTA (also shown in Fig. 2.20) and labeled with ^{111}In in a similar way to octreotide. The high-affinity binding of lanreotide to sstr3 and sstr4 enables certain tumors to be visualized such as intestinal adenocarcinomas which are not visualized by ^{111}In-pentetreotide scintigraphy (Virgolini et al. 1998).

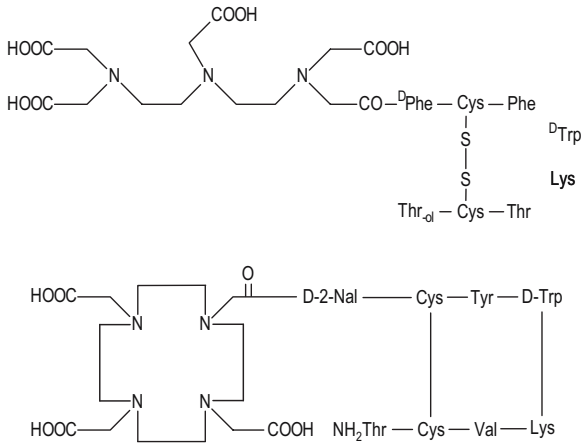

Fig. 2.20. Structures of ligands for somatostatin receptor scintigraphy with SPECT: pentetreotide (*upper*) and DOTA lanreotide (*lower*) (βNal = β-naphthylalanine)

2.1.3 Radiopharmaceuticals for Internal Radiotherapy

2.1.3.1 Introduction

In the early years of using radioisotopes in nuclear medicine there was always a focus on their application as therapeutic agents, supported by the success of using iodine-131 in the treatment of thyroid carcinomas. With the availability of more therapeutic radionuclides and the rapid progress of treatment modalities, it can be expected that non-invasive treatment with radioisotopes will gain in importance.

In comparison to diagnostic radiopharmaceuticals, the requirements for radiotherapeutics are basically different. In order to achieve a maximum therapeutic effect in the targeted tissue, the radioisotopes used in therapy include α, β^- or Auger electron emitters with a physical half-life in the range of several hours to about 10 days (Table 2.6), while a small amount of accompanying γ-emission (~10% of disintegrations; γ-energy ~150 keV) is advantageous to determine the radioactivity distribution in the body and for dosimetry purposes. The choice of the radionuclide depends on the site of targeting at the cellular level and the ef-

Table 2.6. Nuclear properties of selected therapeutic radionuclides

Type of emission	Energy range (MeV)	Range (µm) LET (keV/µm) Cell diameter	Examples[a] (half-life)
Auger electrons	10^{-5}–10^{-2}	0.01 – 1.0 4 – 26 «1	^{125}I (60.5 d), ^{123}I (13.3 h), ^{77}Br (57 h), ^{67}Ga (78.3 h), ^{111}In (3 d), ^{193m}Pt (4.3 d), ^{195m}Pt (4 d)
α-particle	2 – 10	10 – 500 µm 80 ≤10	^{211}At (7.2 h), ^{225}Ac (10 d), ^{212}Bi (61 min), ^{213}Bi (46 min)
β^--particle	0.05 – 2.5	50 – 15,000 0.2 ≤1,000	^{33}P (25.4 d), ^{177}Lu (6.7 d), ^{67}Cu (61.9 h), ^{131}I (8 d), ^{153}Sm (46.8 h), ^{186}Re (3.8 d), ^{165}Dy (2.3 h), Sr^{89} (50.5 d), ^{32}P (14.3 d), ^{166}Ho (28.8 h), ^{188}Re (17 h), ^{90}Y (64.1 h)

[a] α- and β^--emitters with increasing particle energy

fective range of the particle emission. Thus therapeutic radiopharmaceuticals labeled with Auger electron emitters should be able to target the cell nucleus and those labeled with α-emitters should be at least internalized into the cell, while compounds labeled with β^--emitters may be allowed for targeting the cell surface or for just getting into close proximity to the targeted tissue.

In addition, the higher the linear energy transfer (LET) of the emitter, the higher will be the effect on the targeted tissue per decay. Hence, the resulting therapeutic effect will be mainly determined by the physical decay and the applied dose of the used nuclide and the biodistribution and kinetics of the targeting vehicle. Radiotherapy (causal or palliative) is mainly focussed on molecular recognition sites of the targeted tissue. The uptake (and the corresponding effect) mechanisms of therapeutic radiopharmaceuticals are the same as with diagnostic tracers and often by interaction with specific receptors or antigens (peptides, antibodies). In other cases, metabolic processes of the targeted (tumor) tissue or enzyme interaction may cause the uptake. Therefore compounds developed or in use with the aim of radiotherapy are found throughout the whole molecular spectrum, from simple ionic species, such as ^{131}I-iodide, up to very complex structures of high molecular weight antibodies such as radiolabeled anti-CD20 antibodies.

2.1.3.2 Radiochemistry Using Therapy Nuclides

One crucial parameter for a medically useful radionuclide is the specific activity (GBq/µg) which can be achieved using specific production routes. High specific activities are usually necessary in order to obtain the highest possible uptake in the targeted tissue. This is especially important for radiopharmaceuticals with uptake mediated by low capacity targets such as receptors or antigens, which are expressed for example by cancer cells. In addition, the effect of therapeutic radiopharmaceuticals should be generated by the applied radioactivity and not by the administered mass of the nuclide carrying biomolecule.

With simple applications, for example with ^{131}I-iodide in the therapy of thyroid carcinomas or with ^{89}Sr-strontium cations in the palliative therapy of bone metastases, there is strictly speaking no labeling chemistry involved. The engagement of chemistry is reduced just to stabilize the oxidation state of the ion and to find a suitable drug formulation. In such cases there are usually ready to use pharmaceuticals for direct patient administration available.

The labeling of more complex radiotherapy agents, however, is often performed at the site of administration, usually shortly before patient administration; this practice helps to ensure a high radiochemical purity of the drug, as the strong radiation emission of therapy nuclides often leads to relatively rapid destruction of organic compounds due to radiolysis effects, which do not allow longer storage or transportation times. Because of the radiation risks, the labeling chemistry must be rather simple and compatible with the physical half-life of the isotope. Commercially available kit preparations allow radiolabeling with a limited number of chemical steps and easy handling, thereby leading to reproducible injectable solutions of high purity.

Among the nuclides suitable for radiotherapy, mainly heavy metals (^{90}Y, ^{153}Sm, ^{177}Lu, $^{186/188}$Re, $^{212/213}$Bi, ^{225}Ac) or heavy halogens (^{131}I, ^{211}At) are found. For radiolabeling purposes with heavy metal nuclides almost exclusively complexing agents are employed. The structure and physicochemical properties of these complexing agents and their conjugation to the targeting molecule play (despite the targeting molecule itself) a crucial role with respect to tumor uptake and tumor retention. In addition, uptake, retention

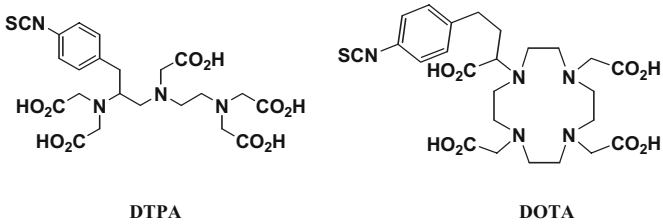

Fig. 2.21. Amine reactive DTPA and DOTA derivatives as bifunctional chelating agents for radiolabeling of biomolecules with 3-valent radiotherapeutic isotopes

and clearance in normal healthy tissues, which should receive as small a radiation dose as possible, will be affected as well. A special focus in the design and optimization of radiotherapy agents will also be on the impact of the chelating moiety with respect to specificity and binding constants of the targeting molecule (Volkert and Hoffman 1999; Ginj and Maecke 2004).

2.1.3.3 Yttrium-90, Bismuth-212/213 and Lanthanides (e.g., Samarium-153, Lutetium-177)

The stability of the chelates of the trivalent metals (Y, Bi, lanthanides) has to be ensured at highest dilutions and of course in-vivo conditions. Even thermodynamically stable complexes might dissociate in vivo if the kinetic stability is insufficient. Another problem might arise through transchelation events during the comparatively long term stay in blood or tissues. In-vivo dissociated ^{90}Y-complexes or lanthanide complexes would accumulate in bone and contribute to a high radiation dose to the bone marrow.

Among the high number of chelating substances, a few have proven to have exceptionally high thermodynamic and kinetic stability and thus are found to be well suited for their application in therapeutic radiopharmaceuticals. The two most prominent examples (Fig. 2.21) are polyaminocarboxylic acids (2-(p-isothiocyanate-benzyl)-diethylene-triamine-pentaacetic acid; a DTPA derivative) and macrocyclic ligands such as (α-[2–4-isothiocyanatophenyl)ethyl]-1,4,7,10 tetraacetic acid; a DOTA derivative). Active ester or isothiocyanate functionalized derivatives of DTPA and DOTA are well established for conjugation with biomolecules.

2.1.3.4 Rhenium-186/188

Strategies for labeling of radiotherapy agents by the nuclides Re-186 or Re-188 are typically based on the development of Tc-99m-labeled diagnostic radiopharmaceuticals (Jeong and Chung 2003).

As a transitional element of the group VII-B, rhenium complexes (as well as technetium complexes) are known in all possible oxidation states from –1 to +7. For nuclear medicine applications, complexes in the oxidation state +5 are well suited and have recently become more important also in the oxidation state +1. For radiolabeling organic molecules, direct and indirect approaches are well known: The direct approach is preferred if the molecule to be labeled (precursor) consists of suitable heteroatoms in complex formation promoting geometry. This is relatively often the case with disulfide bridge containing peptides or proteins (antibodies), which after being reduced to free thiols show strong coordination to rhenium(V) intermediates (usually generated by reduction of perrhenate with Sn(II) ions in the presence of weak chelators such as citrate, gluconate, etc.). Additional oxygen or nitrogen heteroatoms of the peptide or protein will finalize the substitution of the remaining coordination sites.

Other examples for direct labeling are found in bisphosphonates [e.g., hydroxyethylidene bisphosphonate (HEDP)]. Here the phosphorus and oxygen atoms coordinate the rhenium(V) core.

In the case of indirect labeling approaches, a number of well working bifunctional chelating agents (Bfc's) are well described in the literature (Volkert and Hoffman 1999; Jeong and Chung 2003; Schibli and Schubiger 2002) and are widely employed. Two typical examples of this kind of agent, mercaptoacetyltriglycine (MAG_3; N_3S ligand) and a dihydroxymethylene-phosphine-thia derivative (P_2S_2 ligand), are shown in Fig. 2.22.

Exceptionally stable rhenium complexes in the oxidation state +1 are claimed in the literature (Schibli and Schubiger 2002), and therefore may be best suited for radiotherapeutic agents. Figure 2.23 shows the tricarbonyl-Re(I) aqua ion. In this ion Re(I)CO bonds are stable against substitution while the Re(I)-OH_2 bonds are weak and can be substituted by a wide variety of ligands. Biomolecules containing for example nitrogen, sulfur or oxygen atoms in suitable conformation can easily displace the water ligands and lead to the respective Re(I)-carbonyl labeled compound.

2.1.3.5 Iodine-131 and Astatine-211

In contrast to the metallic therapy isotopes discussed above, the halogens iodine and astatine are used for la-

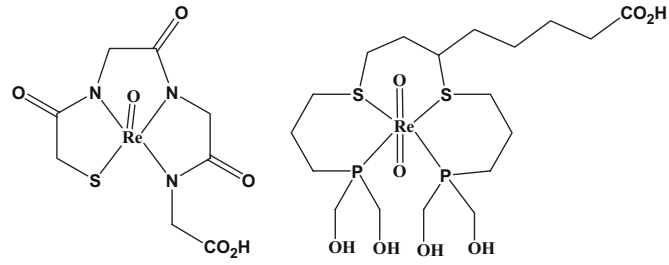

Fig. 2.22. N_3S and P_2S_2 ligands for complexation of rhenium (+V). The carboxylic acid moieties can be used for coupling to biomolecules

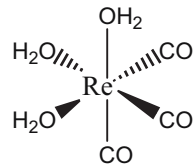

Fig. 2.23. The tricarbonyl-Re(I) aqua ion. The Re(I)-CO bonds are substitution labile – the Re(I)-OH_2 bonds are substitution stable

beling biomolecules with formation of covalent bonds. This makes the portion of alteration introduced by the radionuclide relative to the unlabeled molecule less when radiometal labeling is compared to radiohalogen labeling.

Hence, smaller molecules with lower molecular weight may preferably be labeled using halogens instead of the bulky chelating moieties needed to introduce a radiometal (Adam and Wilbur 2005). In the following the most important routes and methods for iodination and astatination will be briefly discussed:

2.1.3.6 Direct Electrophilic Substitution

The majority of radiolabeling techniques using the direct electrophilic substitution approach were initially developed for protein labeling and later broadened to label generally aromatic compounds. As is well known from the chemistry of thyroid hormones, tyrosine moieties react very well by formation of mono- or diiodotyrosine. In similar manner, tyrosine as part of the amino acid sequence in peptides or proteins will be the by far preferred site of radiolabeling in this class of substances. Iodine is commercially delivered as iodide anion (oxidation state –1). In order to perform this kind of radiolabeling, iodide is oxidized by common reagents such as chloramine-T or Iodogen (a water insoluble chloramine derivative) to form a reactive, electrophilic species in the oxidation state +1, which simply substitutes an activated proton from the aromatic ring of tyrosine in the ortho position to the phenole group. The method is simple, and usually high yields even at very low precursor concentrations are obtained. A disadvantage of this technique is the low selectivity if more than one tyrosine moiety is present and also the sometimes low stability in-vivo.

2.1.3.7 Iododemetallation

Many organometallic compounds react with iodide at very mild oxidative conditions to form the corresponding iodinated compounds by replacing the substitution label metal atom. Most often tributyl-tin precursors are used to perform this iodo-demetallation reaction. An important difference from the direct electrophilic substitution discussed above is that non-activated or even deactivated aromatic compounds can be labeled with good to excellent yields. In addition, due to the lack of activating groups the labeled compounds usually show a much higher metabolic stability when compared to the activated aromatic compounds (phenol, aniline, tyrosine, etc.). This labeling strategy is therefore also used with prosthetic group labeling (see below). The disadvantage is the often difficult synthesis of organometallic precursors.

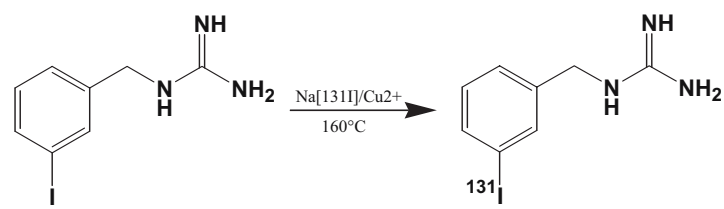

Fig. 2.24. Copper catalyzed iodine-131 labeling of MIBG by direct nucleophilic substitution (isotope exchange)

2.1.3.8 Direct Nucleophilic Substitution

The most simple and straightforward method for iodination is the direct nucleophilic substitution using iodide as nucleophile in the oxidation state –1 as it is commercially delivered. An example of this is the exchange of stable iodine bound to the precursor by radioactive iodine (isotope exchange). This can be achieved by simply heating the components in a suitable solvent such as acetone or water. The consequence, however, is a product of low specific activity and therefore only in very selected cases is it useful for nuclear medicine, for example with the clinically important [^{131}I]meta-iodobenzylguanidine ([^{131}I]MIBG) (Fig. 2.24). Higher specific activities can be obtained using bromo-precursors; however, high reaction temperatures are needed even if copper catalysts are used to assist the nucleophilic displacement reaction (Wafelman et al. 1994).

2.1.3.9 Prosthetic Groups

Many organic molecules do not exhibit structural elements that would allow radiohalogenation by the direct routes via electrophilic or nucleophilic substitution. In such cases labeling via prosthetic groups is often a suitable alternative. Prosthetic groups are bifunctional reagents – one functionality allows for high yield radiohalogenation, the other functionality allows for conjugation to the biomolecule. This strategy became known by the name "Bolten-Hunter method." Bolton-Hunter developed *N*-succinimidyl-3(4-hydroxyphenyl)propanoate with the intention of labeling proteins without exposure to oxidizing agents. This method was further developed with respect to the metabolic stability of radiohalogenated antibodies (Wilbur 1992). An interesting relatively new approach employs *residualizing prosthetic groups*. The design of these molecules focusses on the approach that once the labeled compound is internalized into the cell, the respective metabolites will be trapped and thus lead to a higher uptake compared to the biomolecules labeled by conventional prosthetic groups (Thorpe et al. 1993).

Astatine-211

For labeling of radiotherapy agents with astatine-211, techniques analogous to the radioiodination methods are used (Zalutsky and Pozzi 2004). However, the more labile carbon-astatine bond will not allow the use of the direct electrophilic substitution methods on activated aromatic compounds, as their in-vivo stability is too low to allow for radiotherapy. Much better results have been obtained employing demetallation techniques on deactivated compounds or by using the respective prosthetic group approaches. The most promising prosthetic groups for astatine-211 labeling are para- or meta-astatobenzoic acid-succinimidyl esters (Fig. 2.25). Recent approaches to increasing the in-vivo stability suggest the use of boron-cage molecules to introduce the astatine-211 label.

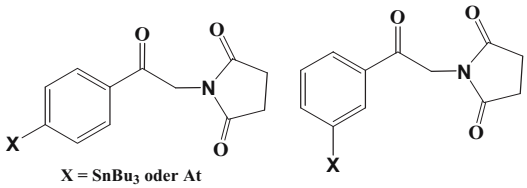

Fig. 2.25. Para- and meta-astatobenzoic acid as prosthetic groups for metabolically stable astatination of biomolecules

2.2 Radiopharmaceuticals for PET

S. Vallabhajosula

2.2.1 Introduction

The British physicist Paul A.M. Dirac combined quantum theory with special relativity in order to develop a theory of the electron which predicted the existence of positively charged electrons (antimatter), or positrons (Dirac 1928). Subsequently, Carl Anderson in 1932 discovered positrons in the stream of secondary particles that result from collisions between cosmic rays and atomic nuclei in the atmosphere (Anderson 1932). The discovery of the artificial production of positrons and radioactivity, however, was first announced by Frederic Joliot and Irene Curie in 1934. They demonstrated that when the nucleus of aluminum was bombarded with alpha particles, ^{30}P radionuclide was produced which quickly decayed to ^{30}Si with the emission of a positron (Joliot and Curie 1934).

$$^{27}_{13}Al(\alpha,n)^{30}_{15}P \rightarrow {}^{30}_{14}Si + \beta^{+}$$

Ernest Lawrence in Berkeley, California, invented the cyclotron in 1931 to accelerate the charged particles to very high energies (Lawrence and Livingston 1931). Following the discovery of Joliot and Curie, the Berkeley group produced a number of positron emitting radionuclides such as ^{11}C, ^{13}N, ^{15}O, and ^{18}F and paved the way for subsequent development of tracer studies using positron emitters.

In the early 1970s Michael Phelps and his colleagues at the Washington University in St. Louis built the first PET camera for clinical studies and demonstrated the

Table 2.7. Radionuclides for PET and SPECT: half-life and specific activity (SA)[a]

Radionuclides for PET			Radionuclides for SPECT		
Nuclide	Half-life (min)	SA (Ci/μmol)	Nuclide	Half-life (min)	SA (Ci/μmol)
^{82}Rb	1.20	150,400			
^{15}O	2.07	91,730			
^{122}I	3.62	51,912			
^{62}Cu	9.76	19,310			
^{13}N	10.0	18,900			
^{11}C	20.4	9,220			
^{94m}Tc	52.0	3,614	^{99m}Tc	360	522
^{68}Ga	68.3	2,766			
^{77}Br	96.0	1,960			
^{18}F	110	1,710			
^{66}Ga	567	331	^{67}Ga	4320	40
^{64}Cu	768	245			
^{86}Y	884	213	^{111}In	4020	47
^{124}I	6048	31	^{123}I	780	237

[a] Maximum theoretical specific activity (SA)

potential clinical utility of positron tracers such as [^{11}C]glucose, [^{13}N]ammonia and [^{15}O]water (Nutt 2002). Following the development of FDG synthesis by the Al Wolf group at Brookhaven National Laboratory, the first FDG-PET imaging studies were performed at UCLA in 1977 (Ido et al. 1978; Phelps et al. 1979). In the last 30 years, several hundred positron emitting radiotracers have been developed for PET.

2.2.1.1 Radionuclides for PET

A number of radionuclides that have been used for both PET and SPECT studies are listed in Table 2.7. The list of positron emitting radionuclides is large and consists specifically of the organic positron emitters such as ^{11}C, ^{13}N, ^{15}O and ^{18}F. The physical half-life of most of these positron emitters is relatively short (<2 h) and as a result the theoretical specific activity (SA) is very high. The SA of metallic positron emitters (^{64}Cu, ^{66}Ga, ^{86}Y) is also significantly higher than the corresponding radionuclides (^{111}In and ^{67}Ga) decaying by electron capture that are used for SPECT. Among halogens, however, the positron emitter ^{124}I has a longer half-life and lower specific activity compared to that of ^{123}I, which is used to develop radiopharmaceuticals for SPECT.

Positron Range

The basic principle of PET imaging technique is based on the coincident detection of annihilation photons produced by the interaction of positron with an electron. Since the energy of annihilation photons (511 keV) is the same for all positron emitters, the development of radiopharmaceuticals for PET is primarily based on selecting an appropriate radionuclide for a specific biochemical process. But, one of the factors limiting the ultimate spatial resolution attainable by PET is the "positron range" in vivo. As shown in Table 2.8, positron emitters differ in the energy of emitted positrons and as a result the distance traveled in vivo (positron range) is proportional to the kinetic energy of positron. For example, ^{18}F has low energy positrons (0.69 MeV) with a very short range (2.4 mm) compared to ^{82}Rb, which has high energy positrons (3.4 MeV) and a longer range (16.5 mm).

In the last 2 decades, the development of radiopharmaceuticals for SPECT was based on ^{99m}Tc, ^{123}I, and ^{111}In. While these radionuclides have appropriate gamma photons (<200 keV) for Anger cameras, their chemistry is not ideally suited for developing radio-

Table 2.8. Radionuclides for PET: positron energy and range

Nuclide	Half-life (min)	Decay	β^+ Energy (MeV)		Range in water (mm)	
		% β^+	Max.	Mean	Max.	Mean
^{18}F	109.74	96.7	0.6335	0.2498	2.4	0.6
^{64}Cu	762	17.87	0.6529	0.2781	2.9	0.64[a]
^{11}C	20.48	99.77	0.9601	0.3856	4.1	1.1
^{13}N	9.97	99.8	1.1985	0.4918	5.1	1.5
^{15}O	2.037	99.9	1.7319	0.7352	7.3	2.5
^{75}Br	96.0	75.5	1.74	0.750	7.2	2.6[a]
^{68}Ga	68.0	87.7	1.8991	0.836	8.2	2.9
^{124}I	6048	11.0	1.5323	0.6859	6.3	2.3[a]
		12.0	2.1350	0.9736	8.7	3.5
^{62}Cu	9.74	97.59	2.927	1.316	11.9	5.0[a]
^{82}Rb	1.25	83.3	3.56	1.524	14.1	5.9
		11.7	2.5795	1.157	10.5	4.3
^{86}Y	884	12.4	1.2535	0.55	5.2	1.8[a]
		5.6	1.578	0.696	6.5	2.9
^{66}Ga	564	49.3	4.153	1.9041	16.7	7.4[a]

[a] For these radionuclides the range was estimated based on published values (Bailey et al. 2005) for other nuclides in this table

Table 2.9. FDA approved PET radiopharmaceuticals

Radiotracer	Target	Clinical application
^{82}Rb chloride	Transported into myocardium as K^+ analog through Na^+/K^+ pump	Myocardial perfusion
[^{13}N]NH_4^+	Transported into myocardium as K^+ analog and trapped as glutamate	Myocardial perfusion
[^{18}F]Fluoride	Incorporated into the hydroxyapatite crystals in bone	Bone imaging
[^{18}F]Fluorodeoxyglucose	Substrate for *hexokinase* in glucose metabolism	Glucose metabolism of tumor, heart and brain

pharmaceuticals for molecular imaging of biochemical processes.

However, since gamma photons originate from the nucleus, the advantage of SPECT nuclides is that the lower limit for spatial resolution is not dependent on the choice of radionuclide, but is only dependent on the detector technology. Gamma cameras based on multi-crystal solid state scintillation detectors may provide higher sensitivity and better resolution (<5 mm) compared to the conventional gamma cameras (Patton et al. 2006).

2.2.2 PET Radiopharmaceuticals: Mechanisms of Cellular Uptake and Localization

Most diseases are characterized by specific alteration in chemical homeostasis resulting in specific biochemical abnormalities. Compared to SPECT, the PET technique has the unique advantage of developing radiopharmaceuticals based on a wide variety of positron-emitting radionuclides. Since the chemistry of positron emitting radionuclides is favorable to labeling biochemicals and drug molecules, a number of radiopharmaceuticals have been developed as diagnostic radiotracers or molecular imaging probes to detect and quantitate the function of an organ or a unique biochemical process in a specific tissue. However, at present, there are only four PET radiopharmaceuticals that were approved by the FDA for routine clinical imaging studies (Table 2.9).

PET radiopharmaceuticals can be generally classified based on their ability to image a specific biochemical process or based on their unique mechanism of localization in a specific organ/tissue of interest (Table 2.10). It is an absolute requirement that these imaging probes be designed in such a way that the study can be performed without disturbing the biochemical process under investigation.

Table 2.10. PET radiopharmaceuticals: mechanisms of uptake and localization

Biochemical process	Radiotracer	Mechanism of uptake or localization
Blood flow/perfusion	[^{15}O]Water	Freely diffusible across membranes
	[^{13}N]Ammonia	Passive diffusion and conversion to glutamine
	^{38}K and ^{82}Rb	Active transport via Na^+/K^+ pump
	^{62}Cu-PTSM	Diffusion and enzymatic reductive decomposition
Metabolism	[^{18}F]FDG	Facilitated diffusion via glucose transporters. Substrate for *hexokinase* in glucose metabolism
	[^{18}F]FTHA	Substrate for *thiokinase* in fatty acid metabolism. Trapping proportional to the rate of β-oxidation
	[^{11}C]Choline	Substrates for *choline kinase* in choline metabolism
	[^{18}F]Fluorocholine	
DNA synthesis	[^{11}C]Thymidine	Substrates for *thymidine kinase (TK)* in DNA synthesis
	[^{18}F]FLT	
Amino acid transport and protein synthesis	[^{11}C]L-methionine	Transport into the cells involves amino acid carrier protein. Intracellular trapping involves protein synthesis or transmethylation
	[^{18}F]FMT [^{18}F]FCCA	
Receptor binding	^{66}Ga or ^{68}GA-DOTATOC	Specific binding to somatostatin receptor (subtype II)
	[^{18}F]FES	Specific binding to estrogen receptors in breast cancer
β-Amyloid plaques	[^{18}F]FDDNP	Binding to β-amyloid plaques and NFTs
	[^{11}C]PIB	Binding to β-amyloid plaques
Hypoxia	[^{18}F]FMISO	Intracellular reduction and binding
	^{62}Cu-ATSM	Redox trapping mechanism, reduction of Cu(II) to Cu(I)
Gene expression	[^{18}F]Oligonucleotide	In vivo hybridization with mRNA
	[^{18}F]FHBG	Substrate to herpes virus *thymidine kinase*

2.2.2.1 Tissue/Organ Perfusion

Blood flow is the amount or volume of blood supplied to an organ (brain, myocardium) or a specific tissue (tumor) during a specific time interval. It is generally expressed as ml/min. Perfusion is defined as blood flow per unit of mass of tissue and has units as ml/min/g. An ideal flow radiotracer accumulates in a tissue or clears from a tissue proportionally linear to the blood flow. Such a linear relationship between blood flow and uptake or clearance of the tracer should be constant and independent of the pathophysiological changes and metabolism of that tissue. [^{15}O]Water meets most closely the criteria of an ideal tracer for measuring blood flow or tissue perfusion. It is freely diffusible and the first-pass extraction approaches unity and is independent of tissue blood flow and metabolic state. It is the most common radiotracer used for cerebral (Raichle et al. 1983) and myocardial (Bergmann 1984) blood flow studies as well. Several other radiotracers have been specifically developed for myocardial blood flow studies.

[^{13}N]NH_3 (ammonia) following intravenous administration, exists in blood predominantly as NH_4^+ ion, which crosses capillary and cell membranes via passive diffusion. It is effectively trapped in the myocardium following interaction with glutamine to form glutamate (Schelbert et al. 1981). The ammonium ion can substitute for K^+ ion on red blood cells and may, therefore, be actively transported into myocardium (Post and Jolly 1957) and also taken up by myocardium. The first pass extraction and retention of ammonia is 60 – 83 %.

The cation $^{82}Rb^+$ is transported into the myocardium as a K^+ analog and the first pass extraction is slightly less than that of ammonia. [^{13}N]NH_3 and ^{82}Rb are officially approved by the FDA for myocardial perfusion studies. A lipophilic, neutral copper (II) complex known as ^{62}Cu-PTSM has been developed as flow tracer for myocardium and tumor tissue. Following diffusion across cell membrane, reduction by sulfhydryl groups, and non-specific binding to intracellular macromolecules, ^{62}Cu is trapped within the cell (Green et al. 1990).

[^{11}C]Acetate has also been used for measuring the relative distribution of myocardial blood flow. Following diffusion into myocardial cells, it is converted to acetyl-CoA in cytosol and then oxidized (metabolized) in the mitochondria by the tricarboxylic acid (TCA) cycle to carbon dioxide and water. The initial uptake in the myocardium serves as a measure of blood flow, while the subsequent clearance may reflect oxidative metabolism (Sciacca et al. 2001).

2.2.2.2 Metabolism

Positron-emitting radiotracers have been developed to image metabolism of several biochemicals. The development of an imaging probe involves incorporation of ^{11}C or ^{18}F atom in the molecule of interest (substrate or an analog of the substrate). The enzyme-mediated metabolic transformation of the radiolabeled substrate and subsequent accumulation within the tissue provide a measure of the metabolic rate of the substrate. Since uptake of the probe is based on targeting these specific enzymes (such as *hexokinase*, *thymidine kinase*, etc.), the localization of the radiotracer in the tissue also reflects the level of enzyme expression in the tissue.

Glucose Metabolism

The most important molecule to provide energy for various biochemical reactions in the body is adenosine triphosphate (ATP), which is generated in mitochondria following metabolism of glucose in mitochondria. In brain, glucose metabolism generates all the ATP, while in myocardium, fatty acid metabolism is the major source for the generation of ATP. Accelerated glucose metabolism even when the oxygen supply is diminished has been observed in cancer tissue. Glucose is generally transported into the cell by facilitated diffusion through specific glucose transporters on the cell membrane. In the cytosol, glucose is converted or phosphorylated by the enzyme *hexokinase* to glucose 6-phosphate, which subsequently is metabolized to carbon dioxide and water.

In 1950s it was shown that the hydroxyl group on carbon 2 of glucose molecule is not necessary for phosphorylation by hexokinase. The deoxyglucose (DG) enters the cell and is converted to deoxyglucose 6-phosphate, which, however, does not undergo further metabolism and is trapped in the cell (Sols and Crane 1954). Therefore, the design of the 2-deoxy-2-fluorodeoxyglucose (FDG) molecule is based on labeling carbon-2 atom in DG with ^{18}F (Ido et al. 1978). Incidentally the C-F bond, which is more stable than the C-H bond, is chemically unrecognizable by *hexokinase*. As a result, FDG 6-phosphate is also trapped in the cell. In tumor cells, the increased glycolysis and increased uptake of FDG is also associated with increased levels of glucose transporter Glut 1 (insulin independent) and intracellular hexokinase expression (Brown and Wahl 1993).

Fatty Acid Metabolism

The ATP production in myocardium is based a number of substrates (free fatty acids, glucose, lactate, and ketone bodies) depending on the relative availability of

substrates, oxygen and hormonal (catecholamines, insulin, glucagons) levels. When plasma glucose levels increase, myocardium shifts to glucose metabolism and, as a result, FDG can be used to assess myocardial metabolism.

In fasting state, when insulin levels are low, FFA levels are high and as much as 70 – 80 % of ATP production is based on oxidation of FFAs. The enzyme *thiokinase* in cytosol converts FFAs to acetyl-CoA, which subsequently undergo β-oxidation in mitochondria and are broken into 2-carbon fragments that are metabolized in the TCA cycle. ^{11}C-labeled, 16 carbon FFA chain palmitate (1-[^{11}C]-palmitate) is converted to ^{11}C-acyl-CoA in cytosol. Part of this enters the mitochondria and TCA cycle for oxidation while the remaining portion is incorporated into the triglycerides and phospholipid pool in cytosol. Since the metabolism of palmitate is complex, recently ^{18}F-labeled FFA analog, known as 14(*R,S*)-[^{18}F]-fluoro-6-thia-heptadecanoic acid (FTHA), was developed which shows metabolic trapping in the myocardium with minimal back-diffusion of the tracer into blood (DeGrado et al. 2000).

Choline Metabolism

All cells utilize choline as a precursor for the biosynthesis of phospholipids, which are essential components of all membranes. Within the cell, choline can be phosphorylated, oxidized or acetylated. The phosphorylation of choline is catalyzed by the enzyme *choline kinase* (Clary et al. 1987). Phosphorylcholine is an intracellular storage pool of choline and is further incorporated into phosphatidylcholine (lecithin), a major phospholipid of all membranes.

Carcinogenesis is characterized by enhanced cell proliferation. It has been suggested that malignant transformation of cells is associated with the induction of *choline kinase* activity resulting in increased levels of phosphorylcholine. Furthermore, it is also known that rapidly proliferating tumors contain large amounts of phospholipids, particularly phosphatidylcholine. In 1997 – 98 [^{11}C]choline (CH) was introduced as a potential tracer to image brain and prostate cancer. One of the major problems of [^{11}C]choline is the metabolism in blood where it is converted to a major metabolite [^{11}C]betaine. In order to decrease metabolism in blood, [^{18}F]fluoromethylcholine or [^{18}F]fluorocholine were developed (Hara 2001).

2.2.2.3 DNA Synthesis

Increased mitotic rate, cell proliferation and lack of differentiation were regarded as the main factors responsible for accelerated growth of malignant tissue. Most benign tumors grow slowly over a period of years, but most malignant tumors grow rapidly, sometimes at an erratic pace. The number of cells in the S-phase of cell cycle is also higher compared to normal cells. As a result, there is an increased requirement of substrates (nucleotides) for DNA synthesis. Intracellularly, thymidine is phosphorylated by *thymidine kinase* (*TK*) to thymidine phosphate, which subsequently gets incorporated into DNA. Measurement of nucleotide incorporation into DNA in tumor tissue in vitro using [^{3}H]thymidine (thymidine labeling index) is a measure of tumor proliferation. [^{11}C]Thymidine has been developed as a PET tracer to image tumors and measure proliferation rate. Due to rapid metabolism of this tracer in blood, however, the tumor uptake of [^{11}C]thymidine is not optimal for imaging studies and quantitation is difficult. Metabolically stable thymidine analogs, which are substrates for the enzyme *TK* have been recently developed (Shields 1996; Grierson and Shields 2000). ^{18}F-labeled 3'-fluoro-3'-deoxythymidine ([^{18}F]FLT) is transported into the cell similar to thymidine and is phosphorylated to [^{18}F]FLT-5'-phosphate by *TK* and finally gets incorporated into DNA and metabolically trapped in the tumor cell. ^{18}F-labeled uridine analog, [^{18}F]fluorouridine, also shows accumulation by proliferating cells, but the tracer is incorporated both in DNA and RNA. Based on this molecule, however, another ^{11}C tracer known as 2'-fluoro-5-^{11}C-methyl-1-β-D-arabinofuranosyluracil ([^{11}C]FMAU) was developed, which similarly to thymidine is also phosphorylated and incorporated into DNA (Conti et al. 1995).

2.2.2.4 Amino Acid Transport and Protein Synthesis

The tumor growth and development is characterized by an increase in the rate of protein synthesis. Since amino acids are the building blocks for protein synthesis, radiolabeled amino acids can be used as imaging probes (Jaget et al. 2001). However, in addition to formation of proteins, amino acids also undergo metabolism such as transamination and decarboxylation. Therefore, the exact position where the ^{11}C or ^{18}F atom is incorporated in the molecule is crucial for the measurement of protein synthesis. [Carboxyl-^{11}C]-L-leucine and [^{11}C]-L-methionine have been investigated. In methionine, ^{11}C can be introduced into the carboxyl group or into methyl group attached to S atom. ^{11}C-*S*-methyl-L-methionine can be prepared easily, but may involve transmethylation in addition to protein synthesis. But recent studies have demonstrated potential diagnostic utility for imaging brain tumors. A number of ^{18}F-labeled tracers have been developed based on phenyl alanine and tyrosine amino acids. Among them, O-(2-[^{18}F]fluoroethyl)-L-tyrosine and L-3-[^{18}F]fluoro-α-methyltyrosine (**FMT**) have shown significant diagnostic potential to image brain tumors (Inoue et al.

1998). Recent clinical studies have shown potential clinical utility of a synthetic, non-metabolizable amino acid analog, known as 1-amino-3-[^{18}F]fluorocyclobutane-1-carboxylic acid (FCCA) (Shoup et al. 1999). With most of the radiolabeled amino acids, however, the cellular uptake and retention appear to be mainly influenced by the amino acid transport process rather than the protein synthesis.

2.2.2.5 Receptor Binding

A number of hormones and neurotransmitters bind to specific binding sites or receptors on the cell membrane (such as somatostatin receptors and dopamine receptors) or within the cell (such as estrogen receptors) in order to initiate specific actions. To measure the receptor expression as a function of disease status, radiolabeled receptor ligands (such as peptides and drug molecules) have been developed as PET imaging probes. The binding of these probes to a target site (receptor) is highly specific and depends on the affinity (K_D) of the probe to the receptor and the number of total receptors (B_{max}) available for binding. Since the number of receptor sites is very limited and low in concentration (typically, nanomoles), high specific activity (1 – 10 Ci/μmol) radiotracers are essential to measure the receptor expression. In addition, these radiotracers may have either low or high affinity to the receptors and are generally trapped in the target tissue following specific binding (reversible or irreversible) of the radiotracer to the receptors. Since agonists are quickly metabolized (or inactivated) following binding to receptors, imaging probes are generally developed using receptor binding antagonists (or receptor blockers). A number of receptor-mediated positron emitting radiopharmaceuticals have been developed in the last 2 decades.

Somatostatin Receptors

Somatostatin (SST), a 14-amino acid cyclic peptide, is secreted throughout the body and has multiple physiological functions including inhibition of secretion of growth hormone, glucagon, insulin, gastrin and other hormones secreted by the pituitary and gastrointestinal tract. The diverse biological effects of SST are mediated through a family of G protein coupled receptors, of which five subtypes have been identified. Human SST receptors (SSTR) have been identified on most of the neuroendocrine tumors, small cell lung cancers and medullary thyroid carcinoma, and express high densities of SSTRs (Reubi et al. 1992). The expression of SSTR subtypes in human tumor tissues, however, seems to vary among different tumor types (Virgolini et al. 1997). Octreotide and its analogs (DOTATOC, DOTANOC) have been labeled with positron emitting radiometals such as ^{66}Ga, ^{68}Ga and ^{86}Y and the potential clinical utility of these tracers to image SSTR positive tumors has been documented (Henze et al. 2001; Maecke et al. 2005).

Estrogen Receptors

In breast cancer, the stimulatory effect of estrogen and progesterone is mediated through nuclear estrogen receptors and progesterone receptors. A number of steroidal and non-steroidal estrogens have been labeled with positron emitting halogens (Mintum et al. 1988). The most promising imaging agent for measuring estrogen receptor status in vivo is 16α-[^{18}F]fluoro-17β-estradiol (FES) (Hostetler et al. 1999).

2.2.2.6 Neurotransmitter Systems

Neurons in the human brain communicate with each other by releasing chemical messengers called neurotransmitters, which can be either excitatory or inhibitory in their postsynaptic effect. The major neurotransmitters in brain are acetylcholine, dopamine, norepinephrine, serotonin (5-HT), and histamine. In addition, certain amino acids such as glutamate, aspartate, glycine, γ-aminobutyric acid or GABA and peptides such as enkephalin, endorphin, substance P and bombesin also act as neurotransmitters in brain. Each neutransmitter system has three steps in the utility cycle: (1) neutrotransmitters are first synthesized and packaged into vesicles in the presynaptic neuron; (2) they are released from the presynaptic cell into the synaptic cleft and bind to specific receptors on postsynaptic neurons; (3) from the synaptic cleft, they are rapidly removed (into the presynaptic cell through specific transporters) and are degraded.

A number of positron-emitting radiotracers have been developed to image neurotransmitter synthesis, neuroreceptor binding on postsynaptic neuron and specific transporters on the presynaptic neuron (Table 2.11). The rationale of the design and development of PET radiotracers for neuroreceptor systems in general can be explained based on the dopamine system paradigm described below.

Dopamine System

Dopamine plays a major role in the regulation of movement, motivation, and cognition. It is synthesized in the dopaminergic neurons in the substantia nigra, ventral tegmental area and retrorubral area of the mesencephalon. It is stored within the vesicles and released into the synapse in response to an action potential and binds to specific dopamine receptors (D_1–D_5) that are

Table 2.11. PET radiotracers for neurotransmitter systems

Neurotransmitter	Radiotracer	Mechanism of uptake and localization
Dopamine	[^{18}F]-M-tyrosine	Precursor to measure dopamine synthesis
	[^{18}F]FDOPA	Analog of L-DOPA, substrate for AAAD
	[^{11}C]Cocaine	Bind selectively to dopamine transporters
	[^{11}C]WIN35,428	
	[^{18}F]FECNT	
	[^{18}F]FP-CIT	
	α-(+)-[^{11}C]dihydro-tetrabenazine	Binds to vesicular amine transporters (VMAT) in presynaptic terminals
	[^{11}C]NMSP	High affinity irreversible D_2 receptor binding
	[^{11}C]Raclopride	Moderate affinity reversible D_2 receptor binding
	[^{18}F]Fallypride	High affinity reversible D_2 receptor binding
	[^{11}C]Chlorgyline	Suicide inactivators of *monoamine oxidase (MAO)*
	[^{11}C]-L-Deprenyl	
	[^{11}C]SCH23390	D_1 receptor antagonist
	(+)-[^{11}C]NNC-112	High affinity D_1 receptor antagonist
Serotonin	[^{11}C]5-HTP	Precursor for serotonin synthesis
	[^{11}C]WAY 100635	$5HT_{1A}$ receptor antagonist
	p-[18F]MPPF	
	[^{18}F]Altanserin	$5HT_{2A}$ receptor antagonist
	[^{18}F]Setoperone	
	[^{11}C]MDL-100907	
	(+)-[^{11}C]McN-5652	Binds to serotonin transporter
	[^{11}C]DSAB	
	[^{11}C]Citalopram	
Opiate system	[^{11}C]Carfentanil	High affinity μ opiate receptor agonist
	[^{11}C]Diprenorphine	Non-subtype (mixed) opiate receptor agonist
	[^{18}F]Cyclofoxy	High affinity μ and κ opiate receptor antagonist
Benzodiazepine (BDZ) system	[^{11}C]Flumazenil	Central BDZ receptor ($GABA_A$) antagonist
	[^{11}C]Iomezanil	
	[^{11}C]PK11195	Peripheral BDZ receptor antagonist. Binds to activated microglia and macrophages
Cholinergic system	[^{11}C]Dexetimide	Muscarinic cholinergic receptor antagonist
	[^{18}F]FP-TZTP	Potent muscarinic M_2 cholinergic receptor agonist
Adrenergic system	[^{11}C]Hydroxyephedrine	Transported into sympathetic presynaptic terminals in myocardium
	[^{18}F]Fluorometaraminol	
	[^{18}F]Fluorodopamine	

present on both postsynaptic and presynaptic sites. In Parkinson's disease, there is a significant loss of presynaptic nigrostriatal nerve terminals in the striatum due to the degeneration of dopamine producing neurons in the substantia nigra in the brain stem. As a result, there is a significant decrease in dopamine terminal density (Hughes 1997). The synaptic concentration of dopamine is regulated primarily by reuptake. Dopamine is removed or degraded by the enzymes *monoamine oxidase (MAO)* and *catechol O-methyl transferase (COMT)*.

Dopamine Metabolism Since dopamine does not cross the BBB, it is synthesized from the precursor, the amino acid tyrosine. The first step is the conversion of tyrosine to dihydroxyphenylalanine (DOPA). Subsequently, DOPA decarboxylase or aromatic amino acid decarboxylase (AAAD) converts L-DOPA to dopamine. Since L-DOPA is transported into the brain via the large neutral amino acid carrier, [^{18}F]6-fluoro-DOPA (FDOPA) was developed to examine transport of dopamine precursor from plasma and its decarboxylation by AAAD to fluorodopamine (Firnau et al. 1987). [^{18}F]Fluoro-meta-tyrosine can also be used to image dopamine synthesis (DeJesus et al. 1997).

Dopamine Transporters Dopamine transporters are exclusively localized on dopamine terminals in the striatum. Dopamine is removed into presynaptic terminals by these transporters. Drug molecules that bind specifically to dopamine transporters compete with dopamine and increase intrasynaptic dopamine concentration. Radiotracers that bind selectively to dopamine transporters provide an indirect measure of dopamine terminal density. Since cocaine binds selectively to dopamine transporters, several ^{11}C- and ^{18}F-labeled tropane analogs such as [^{11}C]WIN-35,428, [^{18}F]CFT and [^{18}F]FP-CIT were developed to image dopamine transporters (Volkow et al. 1998).

In order to prevent dopamine from degradation by *MAO*, vesicular monoamine transporters (VMAT) present on vesicles in the presynaptic nerve terminals remove dopamine from the cytosol into vesicles. Therefore, VMAT like dopamine transporters are a potential target to measure dopamine terminal density. A selective tracer for VMAT known as (+)-α-[^{11}C]dihydrotetrabenazine (DTBZ) was also developed to image dopamine terminal density or dopamine neuronal degeneration in the striatum (Kilbourn 1997).

Dopamine Receptors Among the dopamine receptors in the striatum, D_2 and D_1 receptors are relatively high in abundance with lower concentrations occurring in the extrastriatal regions. Striatal D_2-receptor density in schizophrenia has been extensively studied, because these receptors are therapeutic targets. In ad-

dition, a number of PET clinical studies have measured the D_2 receptor subtype, because of its involvement in psychiatric states, motor disorders and drug abuse. Several radiotracers have been developed based on receptor antagonists such as neuroleptics. ^{11}C- or ^{18}F-labeled *N*-methylspiroperidol (NMSP) is a high affinity irreversible radiotracer (Wong et al. 1986), while [^{11}C]raclopride is a reversible ligand with moderate affinity (Farde et al. 1985). High affinity reversible radiotracers such as [^{18}F]fallypride and [^{11}C]FLB-457 have also been developed. Since reversible ligands have the potential to compete with synaptic dopamine, these tracers may be more optimal for the measurement of quantitative parameters such as K_d, B_{max} and the binding potential (Laruelle 2000).

MAO Inhibitors Several MAO inhibitor drugs (increased dopamine terminal density) are used in the treatment of depression and Parkinson's disease. PET imaging studies of MAO expression in human brain were studied using labeled suicide enzyme inactivators, [^{11}C]clorgyline and [^{11}C]-L-deprenyl (Fowler et al. 1987). These studies demonstrated a significant decrease of MAO levels in smokers, suggesting a neurochemical link, which implies that smokers may have a decreased risk of Parkinson's disease.

2.2.2.7 β-Amyloid Plaques

One of the common features in the brain of patients with familial or sporadic Alzheimer's disease is the presence of abundant intraneuronal neurofibrils (NFTs), extracellular plaques rich in β-amyloid (APs), and neuronal loss (Trojanowski et al. 1995). NFTs are aggregates of the hyperphosphorylated tau protein. In contrast, the major components of APs are deposits of a 39- to 43-amino-acid-long β-amyloid peptide generated from a larger β-amyloid precursor protein.

Probes such as Congo red and chrysamine G known to bind to APs do not appreciably cross the BBB. Therefore, a new generation of radiolabeled highly hydrophobic naphthalene derivatives has been developed for imaging APs in vivo (Barrio et al. 1997). The investigators at UCLA developed 2-(1-{6-[(2-[^{18}F]fluoroethyl)(methyl) amino]-2-naphthyl}ethylidene) malononitrile (FDDNP) as a molecular imaging probe using PET, for the localization of NFTs and APs in the brain of living patients with AD. This tracer has the ability to easily diffuse into the brain and bind to both β-APs and NFTs with various degrees of specificity (Shogi-Jadid et al. 2002).

Modification of the amyloid binding histological dye, thioflavin-T, led to the finding that neutral benzothiazoles bound to amyloid with high affinity and crossed the blood-brain barrier very well (Mathis et al. 2003). The compound *N*-methyl-[^{11}C]2-(4'-methylamino-phenyl)-6-hydroxybenzothiazole was given the name "Pittsburgh compound B," or simply PIB. The exact form of the amyloid target of PIB binding has not yet been identified with certainty. In vitro studies suggest that PIB binds to aggregated, fibrillar Aβ deposits such as those found in the cortex and striatum, but not to the amorphous Aβ deposits such as those that predominate in the cerebellum. In a preliminary human study PIB retention correlated inversely with cerebral glucose metabolism determined with FDG (Klunk et al. 2004).

2.2.2.8 Hypoxia

With increasing tumor size, there is a reduced ability of the local vasculature to supply sufficient oxygen to rapidly dividing tumor cells (Vaupel et al. 1992). The resulting hypoxia may inhibit new cell division or even lead to cell death, but it may also lead to adaptive responses that will help cells survive and progress. The presence of hypoxia in tumors has long been established as a key factor in tumor progression and in the resistance of tumors to therapy. Well-oxygenated cells are more sensitive to the cytotoxic effects of ionizing radiation compared to poorly oxygenated cells.

Nitroimidazoles can be used as probes to detect hypoxia. The most extensively studied PET agent in the clinical setting of hypoxia is [^{18}F]fluoromisonidazole (FMISO) (Koh et al. 1992). Several other analogs such as [^{18}F]fluoroerythronitro-imidazole (FETNIM) (Gronroos et al. 2001) and 1-(5-[^{18}F]fluoro-5-deoxy-α-D-arabinofuranosyl)-2-nitroimidazole (FAZA) (Parliament et al. 1992) have been developed with more favorable pharmacokinetics. Nitroimidazoles enter cells by passive diffusion and undergo a single electron reduction to form a potentially reactive species. When oxygen is abundant, the molecule is immediately reoxidized and this futile shuttling takes place for some time, before the molecule diffuses out of the cell. Under hypoxic conditions, further reduction of the nitroimidazole molecule occurs that forms covalent bonds to intracellular macromolecules, in a process of metabolic trapping within the hypoxic cell.

Several other radiolabeled PET markers of hypoxia have been developed. Cu(II)-diacetyl-*bis*(*N*4-methylthiosemicarbazone) (Cu-ATSM) has efficient uptake and washout kinetics due to its high membrane permeability and fast tumor uptake (Lewis and Welch 2001). Preliminary clinical studies with ^{60}Cu-ATSM and ^{62}Cu-ATSM have shown it to be a selective marker for hypoxia in human cancers and predicted response to therapy.

2.2.2.9 Gene Expression

Gene therapy holds significant promise in the treatment of human diseases. The main principle of gene therapy is based on achieving a controlled and effective target-specific expression of endogenous genes or transgenes (externally transferred genes into cells) in order to cure or to slow down the progression of a disease. The in vivo method of gene therapy is based on delivering the gene to a specific organ or tissue using a viral or non-viral vector that can be introduced into the patient by inhalation, intravenous or even local administration. In the ex-vivo method, the cells from a tissue (to be treated) are removed from the patient, transfected with the therapeutic gene ex-vivo and then the transgenes reintroduced into the patient.

One of the common approaches of gene therapy in cancer treatment is suicide gene therapy, in which the genes (like non-mammalian enzymatic genes) make the tumor cells more susceptible to a subsequently introduced prodrug that can be converted to highly toxic active drug. The two most common suicide gene systems are herpes simplex virus type I *thymidine kinase* (HSV1-*tk*) (Moolten 1986) and *cytosine deaminase* (CD) (Haberkorn et al. 1996). HSV1-*tk* is capable of phosphorylating pyrimidine and purine nucleoside derivatives that can be trapped intracellularly (Alrabiah and Sacks 1996). Following treatment, pro-drugs like acyclovir, gancyclovir and pencyclovir are phosphorylated and get incorporated into host DNA in place of thymidine triphosphate. As a result, cellular replication is blocked, leading to a decrease in tumor growth. Similarly, CD, a bacterial gene, converts 5-fluorocytosine into a toxic chemical, 5-fluorouracil (5-FU), which substitutes for uracil in the cellular RNA and prevents translation or protein synthesis (Haberkorn et al. 1996).

Gene Imaging

The very first stage in gene expression involves transcription of genes into messenger RNA (mRNA), which is responsible for translation of genes into specific proteins (enzymes and receptors) in the cytosol. PET and SPECT imaging techniques are very important to identify the specific targeting of therapeutic genes, locate the magnitude of gene expression and to finally monitor the response to gene therapy. Two different strategies can be used to image gene expression (Gambhir et al. 1999) as outlined below.

Direct Gene Imaging In this approach, the endogenous gene expression (mRNA) or transgene expression (therapeutic protein) can be the target for developing radiolabeled probes. Specific sequence of mRNA can be targeted for imaging using a radiolabeled antisense oligonucleotide (RASON) probe such as ^{18}F-labeled oligonucleotide containing a complementary sequence of mRNA to be imaged. In order to target a specific therapeutic protein, radiolabeled substrates for that protein can be used. But this approach is not necessarily practical since each and every mRNA would require a specific radiolabeled oligonucleotide.

Indirect Gene Imaging The indirect approach involves coupling the therapeutic gene to a "reporter gene (RG)" and then targeting the reporter gene expression using a PET or SPECT "reporter probe (RP)" (Gambhir et al. 1999). The therapy gene and the RG with a common promoter are administered into a patient using a virus (such as adenovirus) vector, which transfers both the therapy gene and RG to the target tumor cell. Subsequently, a radiolabeled RP is used to image the expression of RP gene which indirectly would provide information about the expression of therapeutic gene. This RG-RP approach can use a gene for the production of a specific enzyme or an intracellular and/or cell-surface receptor in the target cell. When HSV1-*tk* gene is used as RG, the protein generated is the HSV1-*tk* enzyme. Among the pyrimidine analogs, the best radioiodinated (^{123}I, ^{124}I or ^{131}I) substrate for this enzyme is 5-iodo-2'-fluoro-2'-deoxy-1-β-D-arabinofuranosyl-5-iodouracil (FIAU) (Tjuvajev et al. 1998). The best RP among the acycloguanosine derivatives is 9-(4-[^{18}F]fluoro-3-hydroxy-methylbutyl) guanine (FHBG) (Alauddin and Conti 1998). Compared to FIAU, FHBG is a poor substrate for endogenous mammalian thymidine kinase. A mutant HSV1-*tk* RG was also developed which generates HSV1-sr39*tk* enzyme that showed better imaging sensitivity with [^{18}F]fluoroganciclovir (FGCV) and [^{18}F]fluoropenciclovir (FPCV) (Gambhir et al. 2000).

Based on the RG-RP approach, a number of other PET probes have been developed to image the expression of genes responsible for dopamine receptors, sodium/iodide symporter (NIS) and somatostatin receptors.

2.2.3 Production of Positron Emitting Radionuclides

Nuclear transformation or the transformation of one element into another was first demonstrated by Ernest Rutherford in 1919. Following bombardment with alpha particles, natural nitrogen atoms (^{14}N) were transformed into an isotope of oxygen (^{17}O) with the emission of protons. As mentioned earlier, the artificial production of radioisotopes and positron emitting radionuclide was discovered by Frederic and Joliot in 1934.

Table 2.12. Cyclotrons for the production of positron-emitting radionuclides

Company	Model	Particle beam Type	Energy (MeV)	Current (μA)	Number of targets
CTI[a]	RDS-111	H^+	11	50	4
CTI[a]	RDS-112	H^+	11	50	2×8[b]
IBA	Cyclone 10/5	$H^+/^2H^+$	10/5	60/35	8
IBA	Cyclone 18/9	$H^+/^2H^+$	18/9	80/35	8
GE[a]	MINItrace	H^+	9.6	50	4
GE	PETtrace	$H^+/^2H^+$	16.5/8.5	75/60	6
EBCO	TR 13/19	$H^+/^2H^+$	13, 19/9	150	2×4[c]

[a] Self shielding for cyclotrons is standard
[b] Two beam ports, each with an 8-target carousel
[c] Two beam ports, each with a 4-target carousel

2.2.3.1 Cyclotrons

Since a high energy beam of positively charged particles is required to produce proton rich radionuclides, accelerators have been developed to generate a well defined, high energy beam of charged particles with high beam intensity. A cyclotron is a cyclic accelerator, in which the charged particles move in a circular path (Fig. 2.26). The cyclotron or the medical cyclotron is the most widely used particle accelerator to produce high energy protons and deuterons for the production of positron emitting radionuclides. The technical features of several commercial cyclotrons are summarized in Table 2.12.

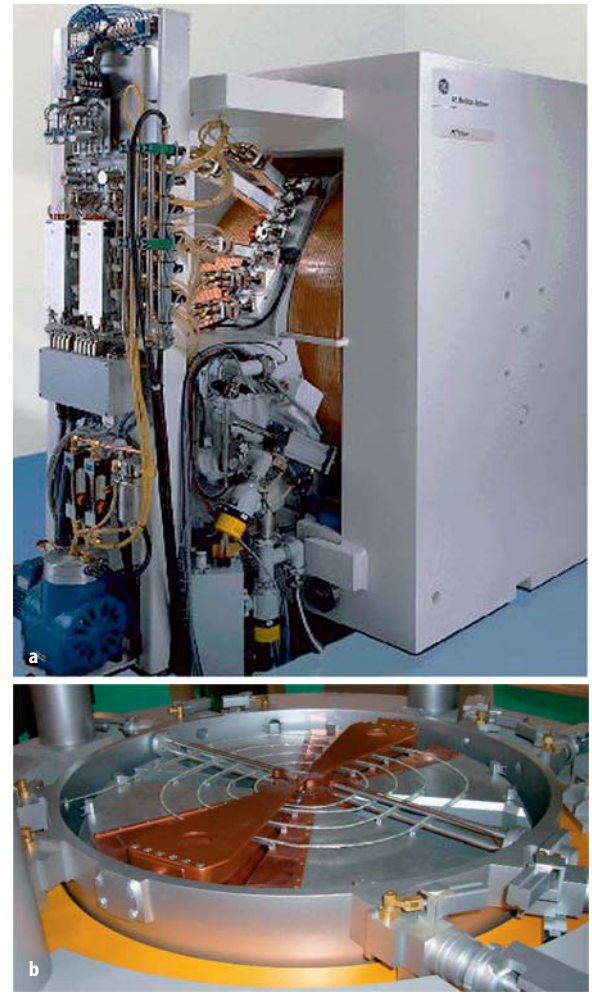

Fig. 2.26. Negative ion cyclotron (GE PETtrace). The *bottom figure* shows a model of the vacuum chamber (CTI systems) showing the copper electrodes (dees) in which is a negatively charged proton beam making circular orbits

Basic Principles of a Negative Ion Cyclotron

Traditionally, the cyclotrons were designed to accelerate positive ions (H^+ and $^2H^+$). The first cyclotron designed to accelerate negative ions, hydrogen or deuterium atoms with two electrons in the K-shell (H^- and $^2H^-$) was built in 1966. Since the 1980s all the commercial medical cyclotrons have been basically negative ion cyclotrons. One of most important advantages of the negative ion cyclotron is the elimination of a complex beam extraction system. As a result, negative ion cyclotrons provide the opportunity to extract beams with different energies, allowing simultaneous bombardment of two different targets (Satyamurthy et al. 1999; Ruth 2003).

The cyclotron consists of three major components: an electromagnet with a field strength of 1.5 – 2.0 tesla, a pair of semicircular hollow copper electrodes, called "**dees**" located between the poles of the magnet, and an ion source (Penning ion gauge) capable of generating high intensity negative ions. The entire structure of the cyclotron is kept under high vacuum (up to 10^{-7} torr). Following ionization of the hydrogen gas in an ion source, the ions (protons or deuterons) are injected into the center of the gap between the dees. When a 20 – 30 MHz radiofrequency alternating potential of 30 – 100 kV generated with an oscillator is applied to the dees, the negative ions will accelerate towards a dee that is at a positive potential. Since the magnetic field is perpendicular to the plane of the dees and particle motion, the negative ions will trace a circular path. Since the electrical potential on the dees is alternatively positive and negative, the ions will gain energy at each crossing of the gap between the dees, as they move in a spiral outward from the center. Lawrence (Lawrence and Livingston 1931) described the basic operational equations as follows;

The magnetic force operating on the ion is a centripetal force (Bev), which is exactly balanced by the centrifugal effect (mv^2/r).

$$Bev = \frac{mv^2}{r} \; and \; r = \frac{mv}{Be}$$

Radio isotope	Nuclear reaction	Target Body	Material	(ml)	Yield (mCi/μA)	Product chemical
^{18}F	$^{18}O(p,n)^{18}F$	Ag, Ti	$[^{18}O]H_2O$	0.3–3.0	110	$^{18}F^-$
^{18}F	$^{20}Ne(d,\alpha)^{18}F$	Al, Ni	Ne gas + 0.1–0.2 % F_2 gas		51	$^{18}F_2$
^{11}C	$^{14}N(p,\alpha)^{11}C$	Al	N_2 gas + < 1 % O_2 gas		40	$^{11}CO_2$
^{13}N	$^{16}O(p,\alpha)^{13}N$	Al	H_2O		7	$^{13}NH_4^+$
^{15}O	$^{14}N(d,n)^{15}O$	Al	N_2 gas		50	
^{15}O	$^{15}N(p,n)^{15}O$	Al	N_2 gas		47	
^{64}Cu	$^{64}Ni(p,n)^{64}Cu$		Ni metal		73	
^{124}I	$^{124}Te(d,2n)^{124}I$		Al oxide and Te oxide solid solution matrix		73	^{124}I as iodide

Table 2.13. Nuclear reactions for the production of positron emitting radionuclides

In the above equations, *B* is the magnetic field strength while *m*, *e*, *v* and *r* represent the mass, charge and velocity of the ion respectively. Finally, *r* represents the radius of the ion's orbit. For a given cyclotron, the maximum kinetic energy that an ion can attain can be estimated if *B* and *r* are kept constant.

$$E = \frac{B^2 r^2}{2}\left(\frac{e^2}{m}\right)$$

Beam Extraction Once the desired kinetic energy of the accelerating particles is achieved, the positively charged ions (H^+ and $2H^+$) are extracted from the cyclotron by passing the negative ion beam through an ultrathin foil of carbon (graphite), which strips the electrons. The positively charged beam will rotate in the opposite direction, which can then be directed to bombard an appropriate target for the production of a positron-emitting radioisotope. The typical intensities (beam current) and the energies of proton and deuteron beams generated in commercial cyclotrons are shown in Table 2.12. The beam current is generally expressed in units of microampere (μA). For example, a 1-μA proton beam current is equal to 6.25×10^{12} protons or deuterons/s.

2.2.3.2 Nuclear Reactions

In a nuclear reaction, when the atoms of a stable element (target) are bombarded by a subatomic particle (projectile), the nucleus of the stable atom absorbs the subatomic particle. The resultant compound nucleus is very unstable and decomposes very quickly, emitting radiation (photons and/or particles) and an unstable radioisotope (Table 2.13). When positively charged particles such as proton (H^+), deuteron ($^2H^+$) or α particle ($^4He^{2+}$) are used as the bombarding particles, neutron deficient radioisotopes are produced, which will decay by positron emission or electron capture. The "*Q* value" is the difference in the energy levels of the reactants and products. The probability for a specific nuclear reaction is given by "cross section" (σ) expressed as the effective area. The unit of cross section is called a "barn" (b) in units of cm^2/nucleus ($1\ b = 10^{-24}\ cm^2$). The positively charged bombarding particle must have kinetic energy sufficient to overcome the coulomb barrier and the negative *Q* value (kinetic energy of products is less than that of the reactants). The higher the atomic number (*Z*) of the target atoms, the higher the kinetic energy (*E*) of the charged particle needed for a higher nuclear cross section (Schlyer 2003). A graphical relationship between σ and *E* for a specific nuclear reaction is known as "**excitation function**." Figure 2.27 shows the excitation function for ^{18}F production (Hess et al. 2001).

The amount of radioactivity (dps) produced by irradiation of a target material with a charged particle beam can be described by the following equation:

$$A(dps) = I\, n\, \sigma\, (1 - e^{-\lambda t})$$

In the above equation,

- *I* is the beam current or the number of bombarding particles/cm^2

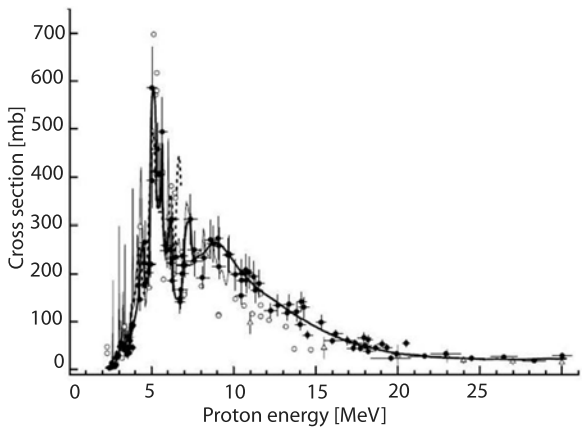

Fig. 2.27. Excitation function of the $^{18}O(p,n)^{18}F$ reaction. Results from several investigators were plotted and the *solid line* represents data from the Julich group (Hess et al. 2001)

- n is the number of target atoms g
- σ is the nuclear cross section
- λ is the decay constant of the product radionuclide and
- t is the time of irradiation in seconds.

Saturation Yield

The amount of radioactivity (mCi) produced in a nuclear reaction is generally corrected to the end of bombardment (EOB). The saturation yield (mCi/μA) is the theoretical maximum rate of production of a radioisotope for given beam energy conditions and can be calculated using the following equation:

$$Saturation\ yield\ (mCi/\mu A) = \frac{A_0}{I(1 - e^{\lambda t})}$$

where A_0 is the activity (mCi) at EOB, I is the beam current and $1-e^{-\lambda t}$ is the saturation factor for the radioisotope.

Specific Activity

It is generally defined as the amount of radioactivity per unit mass of an element, molecule, or compound, which implies that the mass represents the combined mass of radioactive species and the non-radioactive (stable or cold) counterpart. The unit of specific activity (SA) can be expressed as mCi/mg, Ci/mmol, or GBq/μmol. When dealing with chemical or molecular reactions, the standard way to express SA is mCi/μmol. Since one mole represents 6.02×10^{23} atoms or molecules (Avogadro's number), one micromole consists of 6.02×10^{17} atoms or molecules.

For example, when ^{11}C radionuclide is produced in a cyclotron as $[^{11}C]CO_2$ gas, ^{11}C carbon atoms are always contaminated with natural carbon (^{12}C) and it is very difficult to obtain pure $[^{11}C]CO_2$ only. Therefore, if the SA of $[^{11}C]CO_2$ produced in a cyclotron target is 1.0 Ci/μmol, it implies that 1.0 Ci of radioactivity is present in a total mass of 1 μmol of carbon dioxide gas or a total of 6.02×10^{17} molecules (3.4×10^{14} molecules are present as $[^{11}C]CO_2$). That means, for every molecule of $[^{11}C]CO_2$, there are about 1,700 molecules of cold, non-radioactive CO_2. The theoretical maximum specific activity (Table 2.8) is never really achieved in routine production of positron-emitting radionuclides. However, the SA concept is very important in dealing with PET radiopharmaceuticals, especially in the preparation of radiolabeled receptor binding radiopharmaceuticals.

Carrier Free It means that the radioactive species is not contaminated with non-radioactive counterpart. In the production of radionuclides in a cyclotron, the target element is converted into a different element (with a higher atomic number). As a result, cyclotron produced radionuclides are supposed to be carrier free (CF). But in reality, it is very difficult to eliminate the contamination of natural carbon, fluorine or other trace metals during the synthesis procedure. A more appropriate concept is "**no carrier added" (NCA)**, since a carrier (a stable, non-radioactive species) is not intentionally added. To facilitate chemical and biochemical reactions, carrier may be added intentionally during radioisotope production. Such preparations should specifically be reported as **carrier added (CA)**.

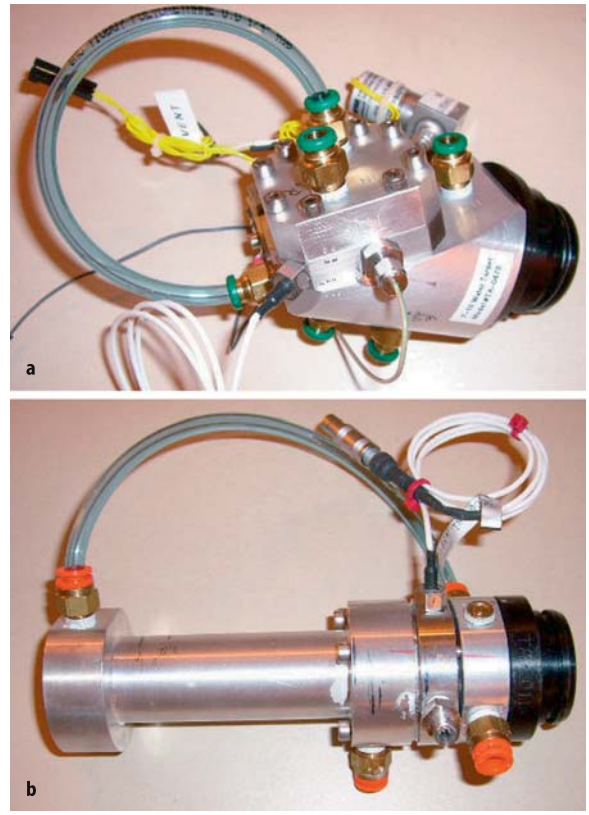

Fig. 2.28. Aluminum targets for EBCO cyclotron. An ^{18}O water target (*top*) for the production of ^{18}F as fluoride and ^{14}N gas target (*bottom*) for the production of ^{11}C as carbon dioxide

2.2.3.3 Nuclear Reactions for the Production of Positron-Emitters

The target designed for the production of a positron-emitter consists of a target body suitable for the bombardment of a specific target material (gas, liquid or solid) that undergoes nuclear transformation. Typical gas targets are made up of aluminum, while the liquid targets are made up of aluminum, silver and titanium. A generic cyclotron target (Fig. 2.28) consists of a sealed metal tube with a window of thin metal foil at one end to allow the particle beam to pass through

and irradiate the target material. In order to dissipate the excess heat generated during irradiation, the target body is generally surrounded by a cooling water jacket, while helium gas is circulated through the foils separating the target material and the vacuum isolation foil through which the beam enters the target.

Positron-Emitting Radiohalogens

Among the halogens, ^{18}F is the most important radioisotope for PET. Among the other halogens, ^{75}Br and ^{124}I may have potential clinical utility and can also be made using medical cyclotrons.

Production of ^{18}F Basically there are two kinds of targets used to produce two different chemical forms of fluorine. A liquid target for the production of ^{18}F as nucleophilic fluoride ion ($^{18}F^-$) and a gas target for the production of ^{18}F as electrophilic fluorine gas ($[^{18}F]F_2$).

The most common nuclear reaction used to produce ^{18}F as fluoride ion is based on proton bombardment of ^{18}O atoms using highly enriched [^{18}O]water as the target material (Ruth and Wolf 1979; Schlyer 2003). A typical target body is made of aluminum to hold 0.3 – 3.0 ml of target water. Several curies of ^{18}F can easily be made in 1 – 2 h using 10 – 19 MeV protons at 20 – 35 μA. While the theoretical SA of ^{18}F is 1,700 Ci/μmol, the NCA ^{18}F produced is generally < 10 Ci/μmol.

The most common nuclear reaction to produce [^{18}F]fluorine gas is based on deuteron bombardment of ^{20}Ne atoms using natural neon gas (Schlyer 2003). A passivated nickel target (NiF) is loaded with neon gas with 0.1 % of natural fluorine gas. Following bombardment for 1 – 2 h with 8 – 9 MeV deuterons, < 1.0 Ci of $[^{18}F]F_2$ is generated with very low SA (10 – 20 mCi/μmol). A "double shoot" method was developed to produce [^{18}F]fluorine gas based on proton bombardment of ^{18}O atoms using [^{18}O]oxygen gas loaded into a gas target (Nickels et al. 1983). After irradiation, ^{18}F species stick to the walls of the target. ^{18}O target gas is removed from the target and loaded with argon gas mixed with cold 1 % fluorine gas. A second short irradiation for < 10 min will generate $[^{18}F]F_2$ gas. This method is very useful to make electrophilic ^{18}F using cyclotrons generating proton beams only. Since $[^{18}F]F_2$ is always diluted with carrier (cold) fluorine gas, the SA of electrophilic [^{18}F]fluorine is very low and not optimal for synthesizing high specific activity ^{18}F-labeled radiopharmaceuticals.

Production of ^{75}B and ^{76}Br Both these radionuclides are generally made using proton (17 MeV) bombardment of ^{76}Se atoms using [^{76}Se]selenium enriched (96 %) Cu_2Se as the target material (Schlyer 2003). Subsequently ^{76}Br is separated from the solid target by thermal diffusion. The longer half-life (16.2 h) is favorable for synthesis of radiopharmaceuticals and commercialization. However, ^{76}Br has a complex decay scheme and high energy positrons which may provide unfavorable radiation dosimetry to the patient.

^{75}Br with a relatively shorter half-life (97 min) may be more optimal for developing PET radiopharmaceuticals. One of the common nuclear reactions is ^{76}Se(p,2n)^{75}Br. But the optimal energy of proton should have 18 – 28 MeV and ^{75}Br is separated from solid target by the dry distillation method and trapped using platinum wool.

Production of ^{124}I Since radioiodination of proteins, peptides and small molecules is relatively easy, ^{124}I has significant potential for developing radiopharmaceuticals for PET. However, the relatively longer half-life and complicated decay schemes with a number of high energy positrons make this radionuclide suboptimal since the radiation dosimetry to the patient can be relatively high.

A method using the proton bombardment of enriched ^{124}Te atoms using low energy protons (15 MeV) was recently developed (Sheh et al. 2000). The solid target material consists of a solid solution matrix containing aluminum oxide and enriched ^{124}Te oxide. [^{124}I]iodide is recovered from the target using dry distillation. The volatile radioiodine is trapped on a thin Pyrex glass tube coated with a small amount of sodium hydroxide.

Organic Positron-Emitters

The greatest advantage of PET is the potential to image and study the biochemical processes in vivo without altering or affecting in any way the homeostasis. Low atomic number elements such as carbon, nitrogen, oxygen and phosphorus are naturally stable. The development of cyclotrons in the 1930s created an opportunity to produce positron emitting radioisotopes of carbon (^{11}C), nitrogen (^{13}N) and oxygen (^{15}O). Since the 1950s radioisotopes of organic interest have played a significant role in the development of biochemistry and pharmacology. Since the half-lives of these radionuclides are relatively short, they were not exploited to their full potential to develop radiopharmaceuticals for routine clinical PET imaging studies. However, with the availability of several hundred medical commercial cyclotrons, PET radiopharmaceuticals for routine clinical use may be developed incorporating the organic positron-emitters.

Production of ^{11}C The most common nuclear reaction used to produce ^{11}C is the proton bombardment of

^{14}N atoms by using natural nitrogen as the target gas (Schlyer 2003). Since nitrogen gas is relatively inert, it does not interfere with carbon chemistry and can easily be eliminated. By mixing trace amounts (< 1 %) of oxygen or hydrogen with the target nitrogen gas, the chemical forms of ^{11}C produced in the target can be either $[^{11}C]CO_2$ or $[^{11}C]CH_4$ (methane). The gas target body is basically made up of an aluminum cylinder (or cone shaped) and should be able to handle gas (10 – 100 cc) pressures of 300 – 800 psi. Beam currents of 20 – 40 μA are typically used. It is very important to prepare or polish the inside of the aluminum target to significantly reduce the contamination of natural carbon. Since the natural nitrogen gas is also contaminated with CO_2 gas, it is essential to use extremely high purity (99.99999 %) target gases. $[^{11}C]CO_2$ can be produced in most cyclotron targets with a SA of 5 – 20 Ci/μmol at EOB. Even higher SA can be achieved by producing $[^{11}C]CH_4$ in the target directly.

Production of ^{13}N Since the half-life of ^{13}N is very short (9.98 min), it is very difficult to synthesize ^{13}N-labeled radiotracers for routine clinical PET studies. In the 1970s $[^{13}N]$ammonia (NH_3 or NH_4^+ ion) was shown to be clinically useful as a myocardial perfusion imaging agent. Therefore, the production of ^{13}N involves the generation of $[^{13}N]NH_3$ directly in the target itself.

The most common nuclear reaction for the production of ^{13}N is the proton (10 – 15 MeV) bombardment of natural, stable ^{16}O atoms using oxygen gas target or liquid (water) target (Schlyer 2003). When ^{13}N is produced in the target, it reacts with water, forming nitrate and nitrite ions. Addition of a reducing agent such as titanium chloride to the target water will generate $[^{13}N]NH_3$. With a pressurized target, aqueous ethanol can be used in the target and ethanol acts as a hydroxyl free radical scavenger to improve the production of $[^{11}N]NH_3$.

Production of ^{15}O The most common nuclear reaction used for the production of ^{15}O as $[^{15}O]O_2$ gas is deuteron bombardment of ^{14}N atoms using natural nitrogen as the target gas containing 0.2 – 0.5 % oxygen. In order to use low energy protons (10 – 11 MeV), the target must be highly enriched ^{15}N gas (Schlyer 2003). The target body is generally made of aluminum. To produce ^{15}O as $[^{15}O]CO_2$, the target nitrogen gas is mixed with 2 – 2.5 % carbon dioxide. To produce $[^{15}O]$water, outside the target, a stream of nitrogen gas continuously flows through the target to a hot cell containing the water synthesis module, in which ^{15}O combines with H_2 gas in the presence of palladium-aluminum catalyst at higher temperatures (300 – 400 °C) to produce water.

Positron-Emitting Radiometals (Ga, Y and Cu)

The development of SPECT radiopharmaceuticals such as ^{111}In-octreotide and ^{99m}Tc-TRODAT has clearly demonstrated the potential diagnostic value of radiolabeled peptides, small molecules and even antibody fragments targeted specifically to bind to receptors and antigens on cells. A number of positron emitting radionuclides belonging to Group III elements (Ga, In and Y) can be made in many of the medical cyclotrons. In addition, several radionuclide generator systems are available, yielding positron-emitting daughter radiometals of significant clinical interest.

^{66}Ga is a medium half-life radionuclide emitting very high energy (4.1 MeV) positrons. It can be produced via the $^{66}Zn(p,n)^{66}Ga$ nuclear reaction (Schlyer 2003). Subsequently, ^{66}Ga can easily be separated from zinc by cation exchange or solvent extraction techniques.

Yttrium-86 is also a medium half-life radionuclide emitting high energy (3.15 MeV) positrons. It has the potential clinical utility to study the biodistribution and to estimate the radiation dosimetry of labeled peptides and antibody molecules. Prior to therapy with ^{90}Y-labeled radiopharmaceuticals, ^{86}Y-labeled PET study may be necessary for documenting tumor targeting. It can be produced via the $^{86}Sr(p,n)^{86}Y$ nuclear reaction using isotopically enriched ^{86}Sr foil or strontium carbonate pellet. Subsequently, ^{86}Y can be separated by dissolving the target in an acidic solution, followed by precipitation and purification by ion exchange chromatography.

Copper has several positron emitting radioisotopes such as ^{61}Cu, ^{62}Cu and ^{64}Cu. Specifically, the low energy positrons of ^{64}Cu (similar to that of ^{18}F) may provide high resolution images. In addition, the relatively longer half-life of 12.7 h and favorable chemistry may be appropriate for developing commercial PET radiopharmaceuticals based on peptides and proteins. It can be produced via the $^{64}Ni(p,n)^{64}Cu$ nuclear reaction using enriched nickel solid target foils (Schlyler 2003). Subsequently, ^{64}Cu is separated by dissolving the target in an acidic solution, followed by ion exchange chromatography. Using similar techniques, ^{61}Cu can also be produced via the $^{61}Ni(p,n)^{61}Cu$ nuclear reaction using enriched nickel solid target foils.

2.2.3.4 Generator Produced Positron Emitters

The radionuclide generator is a device to separate a daughter radionuclide from a parent radionuclide, which is relatively longer lived compared to the daughter radionuclide. Three important generator systems are available to produce positron-emitting radionuclides of clinical interest.

$^{82}Sr \rightarrow {}^{82}Rb$ Generator (Cardiogen)

Rubidium chloride was the first PET radiopharmaceutical approved by the FDA in 1989 for the assessment of regional myocardial perfusion. Cardiogen generator is manufactured and supplied by Bracco Diagnostics. ^{82}Sr ($T_{1/2}$ = 25.6 days) is a neutron deficient radionuclide and decays by electron capture. It is produced using a high energy cyclotron. ^{82}Sr (90 – 150 mCi) is loaded on a stannic oxide column and the daughter ^{82}Rb ($T_{1/2}$ = 75 s) is eluted from the column with sterile saline solution using an infusion pump calibrated to administer a specific unit dose to a patient.

$^{62}Zn \rightarrow {}^{62}Cu$ Generator

Several ^{62}Cu radiotracers are under development and clinical evaluation for assessing perfusion and hypoxia. ^{62}Zn ($T_{1/2}$ = 9.13 h) is a neutron deficient radionuclide and decays by electron capture. It is produced using a high energy cyclotron. An acidic solution of ^{62}Zn can be loaded on an ion exchange column and the daughter ^{62}Rb ($T_{1/2}$ = 9.76 min) can be eluted from the generator for the preparation of radiotracers.

$^{68}Ge \rightarrow {}^{68}Ga$ Generator

In many PET facilities, ^{68}Ga is routinely used for transmission scans using ^{68}Ge rod source (5 – 10 mCi). The half-life of ^{68}Ga is quite appropriate for developing radiopharmaceuticals based on peptides, proteins and antibodies. The parent, ^{68}Ge, is a long lived ($T_{1/2}$ = 278 days) neutron deficient radionuclide, generally produced by high energy cyclotrons. ^{68}Ge is loaded on a tin oxide column and the daughter ^{68}Ga is eluted as chloride using hydrochloric acid (1.0 N) solution.

2.2.4 Radiochemistry of PET Radiopharmaceuticals

Synthesis of positron-emitting radiopharmaceuticals is a major challenge since the half-lives of positron-emitters are relatively short. The exposure to high levels of radiation during synthesis makes it necessary to perform the labeling procedures in a "hot cell." As a result, remote control techniques and fully automated computer controlled synthesis procedures have been developed in the last 2 decades. So the development of PET radiopharmaceuticals is a concerted effort of organic chemists, radiochemists, radiopharmacists, physicists, engineers and computer scientists. Described below are the basic principles of radiolabeling with specific examples of radiopharmaceuticals of clinical interest. The development of PET radiopharmaceuticals basically involves five major steps:

1. Synthesis of appropriate radiolabeled precursors
2. Synthesis of organic precursors ready for radiolabeling
3. Development of radiolabeling and purification methods and procedures
4. Development of automated synthesis modules
5. Design of quality control procedures applicable for PET radiopharmaceuticals

2.2.4.1 Organic Precursors for PET

It is ideal to introduce the radiolabeled isotope in the last step to avoid loss of radioactivity (due to decay) during the multi-step synthesis of a PET radiopharmaceutical. The molecules to be labeled may have a number of functional groups (such as OH, COOH, NH_2), which may react and interfere with the labeling of radioisotope in a specific position in a molecule. Therefore, in order to facilitate regioselective labeling of substrates, organic precursors have to be synthesized first with protective groups attached to functional groups. It is very important that the protective groups are very stable during the labeling procedure and can be removed (functional groups de-protected) rapidly and easily under conditions favorable to maintain the stability of the radiolabeled molecule. Examples of precursors developed for the synthesis of [^{18}F]FDG, [^{18}F]FLT, [^{18}F]FDOPA and [^{11}C]raclopride are shown in Fig. 2.29. In the case of FDG, the precursor mannose triflate was

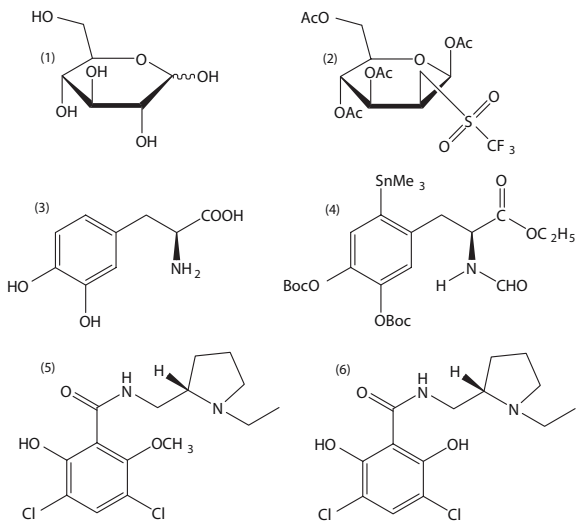

Fig. 2.29. Organic precursors for the synthesis of PET radiopharmaceuticals. For FDG synthesis, glucose (*1*) was converted to mannose triflate (*2*). For FDOPA synthesis, L-DOPA (*3*) was converted to trimethylstannyl L-DOPA (*4*). For these two precursors, the functional groups (OH, COOH and NH_2) were protected to prevent fluorination. For the synthesis of raclopride (*5*), the precursor is simply a desmethyl raclopride analog (*6*)

developed, in which the 4 hydroxyl groups of deoxyglucose are protected by converting them to acetate (Ac) groups. Also, in order to facilitate ^{18}F labeling, a leaving group, trifluoromethane sulfonate (Triflate), is added to the carbon in the 2-position to facilitate nucleophilic displacement. In the synthesis of [^{11}C]raclopride, the precursor is *O*-desmethyl raclopride. This molecule has no protective groups. It is almost the same molecule as raclopride, except for one methyl (CH_3) group. In the last 2 – 3 decades, hundreds of precursors have been developed to help synthesize PET radiopharmaceuticals rapidly. ABX Advanced Biochemical Compounds GmbH in Germany is a major supplier of precursors for PET.

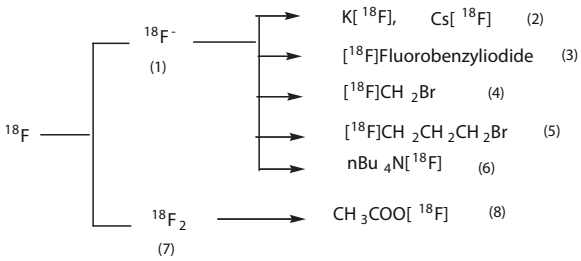

Fig. 2.30. ^{18}F precursors for the synthesis of ^{18}F radiopharmaceuticals. Starting from ^{18}F as fluoride (*1*), precursors such as alkali metal halides (*2*), fluorobromoalkanes (*4, 5*), tetrabutyl ... (*6*) have been developed. Acetyl hypofluorite (*8*) is the most common precursor developed from $^{18}F_2$ gas (*7*)

2.2.4.2 Fluorine-18 Radiochemistry

Among the halogens, the chemistries of radioiodine and radiobromine are quite similar in many ways and have already been discussed. The chemistry of ^{18}F is quite unique and with the success of FDG, a number of ^{18}F-labeled PET radiopharmaceuticals are under development.

^{18}F-Labeled Precursors

Fluorine is the most electronegative of all the elements and can react with many organic and inorganic chemicals. Being a powerful oxidizing agent, it may bind to quartz and glassware. It can react as an electrophile (positively charged) or a neutrophile (negatively charged) chemical species. Electrophilic reactions involve CA or low SA [^{18}F]F_2 gas, while nucleophilic reactions involve NCA or high SA [$^{18}F^-$] ion. In addition to these two primary ^{18}F precursors, several other secondary precursors have been developed to radiolabel a number of organic molecules (Fig. 2.30). Among them, [^{18}F]CH_3COOF (acetyl hypofluorite), metal fluorides (such as K^{18}F, Cs^{18}F), and tetra-*n*-butyl ammonium fluoride (n$Bu_4N^{18}F$) are the most widely used ^{18}F precursors in fluorination reactions (Kilbourn 1990).

Electrophilic Fluorination Reactions

The [^{18}F]F_2 precursor has only one of the atoms as ^{18}F while the other is stable ^{19}F atom. Therefore the labeling yields are always < 50 %. In 1976, FDG was first synthesized using [^{18}F]F_2. The other reactive precursor is [^{18}F]acetyl hypofluorite. With these precursors, direct electrophilic fluorinations are not regioselective and the ^{18}F atom can attack any of the C-C double bonds in the molecule. Therefore, these precursors are used only in rare situations where nucleophilic reactions are not appropriate. However, regioselective electrophilic fluorodemetallation reactions were developed to take advantage of reactive electrophiles in the preparation of ^{18}F PET tracers. In order to synthesize relatively high SA ^{18}F radiotracers based on electrophilic reactions, a multi-step method was also developed to generate high SA [^{18}F]F_2 by using [^{18}F]fluoride ion (Nickels et al. 1984). The reactive $^{18}F^-$ is first converted to [^{18}F]methyl fluoride and purified by gas chromatography. Subsequently, when methyl fluoride is passed through a discharge chamber (operating at 20 – 30 kV and 280 μA), small amounts of high SA [^{18}F]F_2 can be generated and collected using very small amounts of carrier (< 0.2 μmol) fluorine gas.

Synthesis of 6-[^{18}F]fluoro-L-DOPA (FDOPA). FDOPA is still synthesized in many PET centers using [^{18}F]F_2 gas (Fig. 2.31). Also, a fully automated synthesis module (Table 2.14) is now available for the synthesis of FDOPA. The organic precursor is an aryl substituted trialkyl tin derivative (Namavari et al. 1992; Dolle et al. 1998), in which the trimethylstannyl group ($Sn(CH_3)_3$) is replaced by the ^{18}F atom during labeling using trifluorochloro-methane or freon (CF_3Cl) as the solvent. The alkyl (tertiary butyl and ethyl) groups in the precursor protect the carboxyl groups. Finally, following acidic removal (deprotection) of the protective groups using hydrogen bromide (HBr), FDOPA can be produced with decay corrected yields of 20 – 30 %.

Similarly, the synthesis of [^{18}F]fluoro-meta-tyrosine (FMT) (VanBrocklin et al. 1998) and [^{18}F]β-CFT (Happaranta 1996) has also been accomplished using fluorodemetallation reactions. In general, electrophilic fluorination reactions produce low SA (< 30 mCi/μmol) PET radiopharmaceuticals.

Nucleophilic Fluorination Reactions

The most successful approach for preparing high SA ^{18}F radiotracers is based on nucleophilic fluorination reactions since [^{18}F]fluoride can be produced in high SA (2 – 10 Ci/μmol). Synthesis of ^{18}F-radiopharmaceuticals using fluoride ion utilizes two general categories or

Table 2.14. Automated synthesis modules

Radiotracer/precursor	Synthesis module	Manufacturer	Comments
[^{18}F]FDG	TRACERlab MX_{FDG}	GE	Disposable cartridge
	TRACERlab FX_{FDG}	GE	Multiple use
	Metatrace FDG	CTIPETNET	Infinite run capability
	FDG-plus synthesizer	Bioscan	Disposable casette
	Synthera	IBA molecular	
[^{18}F]FDOPA	TRACERLab FX_{FDOPA}	GE	FDOPA from [^{18}F]F_2
[^{11}C]CH_3I (MeI)	TRACERlab FX_c	GE	Gas phase MeI + methylation
	Microlab	GE	Gas phase MeI
	MeI-Plus	Bioscan	Liquid phase MeI
^{18}F-tracers	TRACERlab FX_{F-E}	GE	Electrophilic fluorination by use of [^{18}F]F_2
^{18}F-tracers	TRACERlab FX_{F-N}	GE	Nucleophilic fluorination by use of [^{18}F]F^- (fluoride)
^{18}F-tracers	Synthera	IBA molecular	Modular multi-purpose synthesizer
^{11}C and ^{18}F-tracers	AutoLoop	Bioscan	General purpose unit for synthesis of radiotracers

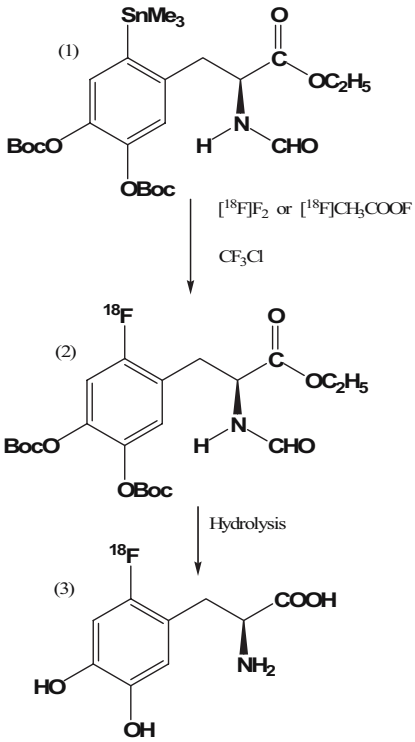

Fig. 2.31. Synthesis of 6-[^{18}F]fluoro-L-DOPA (FDOPA): The precursor, trimethylstannyl L-DOPA (*1*) in trifluorochloromethane solvent, is fluorinated using fluorine gas or acetyl hypofluorite. Subsequently, the protective groups of the fluorinated intermediate (*2*) are removed by hydrolysis to yield FDOPA (*3*)

types of chemical reactions (Kilbourn 1990): (1) aliphatic nucleophilic substitution, also known as substitution nucleophilic bimolecular (S_N2); and (2) aromatic nucleophilic substitution (S_NAr).

In S_N2 reactions, the fluoride ion attacks and binds to the carbon atom of the substrate at 180° opposite to a leaving group such as a weak base (iodide, bromide, triflate, tosylate, nosylate, mesylate, etc.). These reactions generally take place in basic or neutral conditions in the presence of an appropriate aprotic solvent (such as acetonitrile) in which the reactants show good solubility. [^{18}F]fluoride ion is generally complexed with a metal or positively charged ion. When alkali metal halides ($K^{18}F$, $Cs^{18}F$, $Rb^{18}F$) are used, it is essential to have the metal coordinated by cryptands and polyaminoethers (such as Kryptofix 2.2.2) so that the relatively free fluoride can show very good reactivity. Instead of alkali metal halides, a variety of tetraalkylammonium [^{18}F]fluorides have also been used. Sometimes, [^{18}F]fluoride ion is first converted to another reactive species such as alkyl halides ([^{18}F]fluorobromoethane, [^{18}F]fluorobromopropane) and benzylic halides (Kilbourn 1990).

Synthesis of ^{18}F Radiotracers Based on S_N2 and S_NAr Reactions. In many of these nucleophilic reactions, preparation of the reactive [^{18}F]fluoride species involves Kryptofix as a phase transfer catalyst and drying with acetonitrile to produce anhydrous [^{18}F]fluoride ion. In order to introduce ^{18}F atom using [^{18}F]fluoride, the molecule of interest must have an alkyl alcohol group, which can be activated by forming a corresponding alkyl sulfonate ester derivative such as triflate, tosylate, etc. Using this approach, several organic precursors have been synthesized. A number of radiotracers of clinical interest such as 2-deoxy-2-[^{18}F]fluoro-D-glucose (FDG) (Hamacher 1986), [^{18}F]3'-deoxy-3'-fluorothymidne (FLT) (Grierson and Shields 2000; Martin et al. 2002; Yun et al. 2003), 9-(4-[^{18}F]fluoro-3-hydroxymethylbutyl)-guanine (FHBG) (54), 1-amino-3-[^{18}F]fluorocyclobutane-1-carboxylic acid (FCBCA) (Shoup et al. 1999a) and [^{18}F]fallypride (Mukherjee et al. 1999), 16α-[18F]fluoroestradiol (Lim et al. 1996) can

all be prepared using commercially available precursors.

S_NAr nucleophilic reactions were designed to incorporate ^{18}F atom directly into the aromatic ring as well as into prosthetic groups containing aromatic ring of a molecule. In these reactions, the leaving group is activated by the electron-withdrawing groups ortho and/or para to the leaving group. The precursors for the synthesis of ^{18}F-altanserin (Tan et al. 1999) and [^{18}F]MPPF (Le Bars et al. 1998) have been designed to have a leaving nitro group (NO_2) situated para to a carbonyl group, which activates the leaving group to be substituted by reactive [^{18}F]fluoride ion.

In the preparation of certain radiotracers, the ^{18}F-labeled alkyl halides are prepared first using aliphatic nucleophilic reaction and then the [^{18}F]alkyl halide (also known as "synthon") is subsequently used to prepare the radiotracer of interest (Block et al. 1997). For example, [^{18}F]fluorobromomethane was reacted with *N,N*-dimethylamino-ethanol (precursor) to synthesize [^{18}F]fluoromethylcholine (FCH) (DeGrado et al. 2001; Iwata et al. 2002). Similarly, 1-[^{18}]fluoro-3-bromopropane is used to synthesize [^{18}F]β-CFT-FP (Kamarainen et al. 2000).

Synthesis of [^{18}F]FDG. The original synthesis developed by the Brookhaven group in 1976 was based on electrophilic reaction. Most of the current synthesis procedures use a modification of a nucleophilic procedure developed in 1986 (Hamacher et al. 1986). In the last 2 decades, the synthesis of FDG has been the most established procedure and hundreds of PET centers all over the world use automated synthesis modules (GE, Nuclear Interface, CTI, IBA, Bioscan) for the production and distribution of FDG. Almost all these modules involve the following basic steps:

1. Following production of ^{18}F in the cyclotron, the target water ([^{18}O]H_2O) containing several Ci of [^{18}F]fluoride ion is trapped on a small column of anion exchange resin (Waters Accel plus QMA cartridge) and the target water is collected in a vial for future use.
2. The [^{18}F]fluoride ion is eluted into a reaction vial using a solution of potassium carbonate (K_2CO_3), Kryptofix 222 in aqueous acetonitrile. Some procedures substitute Kryptofix either with tetramethyl ammonium carbonate or with tetrabutyl ammonium bicarbonate or hydroxide.
3. The residual water is removed by repeated azeotropic distillations using anhydrous acetonitrile and a stream of nitrogen.
4. The organic precursor, mannose triflate (10 – 25 mg) in acetonitrile, is added to the anhydrous fluoride ion and the mixture is heated at 80 – 90 °C for 3 – 5 min.
5. In order to generate FDG from [^{18}F]acetyl protected FDG (intermediate complex) hydrolysis of acetyl groups (deprotection) is done using an acidic (HCl) solution by heating the mixture at 130 °C for 10 – 15 min. In recent techniques, the acetylated FDG intermediate is loaded on a solid support (C_{18} Sep-Pak cartridge) and hydrolysis is performed in a very short time under basic conditions at room temperature using KOH or NaOH solution.
6. The purification procedures involve passing the intermediate mixtures or the final FDG solution through C_{18} Sep-Pak and alumina cartridges and washing with water to eliminate Kryptofix and organic solvent contamination.
7. The purified FDG is finally obtained from the cartridge by eluting with physiological saline and sterilized by passing through a 0.2 μm membrane filter and collecting it in a sterile vial.
8. Almost all the automated FDG synthesis modules provide FDG with a radiochemical yield of 40 – 70 % and a radiochemical purity of > 90 % in 30 – 45 min of total synthesis time.

The radiolabeling procedures involved in the preparation of ^{18}F-labeled PET radiopharmaceuticals of clinical interest such as FDG, FLT, and FCH are shown in Figs. 2.32 – 2-34.

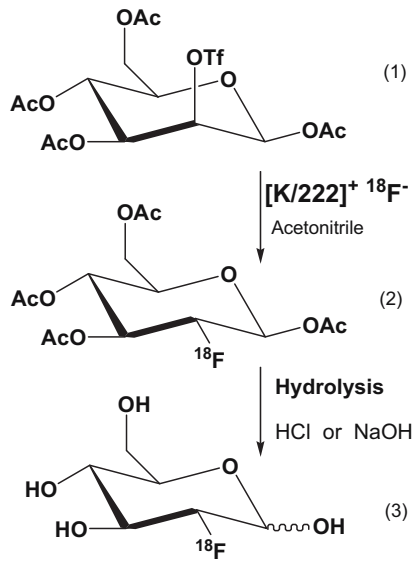

Fig. 2.32. Synthesis of 2-deoxy-2-[^{18}F]fluoro-D-glucose (FDG): Following evaporation and drying, K[^{18}F] and Kryptofix complex is incubated at 80 °C with the precursor, mannose triflate (*1*), in acetonitrile. Subsequently, FDG (*3*) is obtained following acid or base hydrolysis of the fluorinated intermediate (*2*)

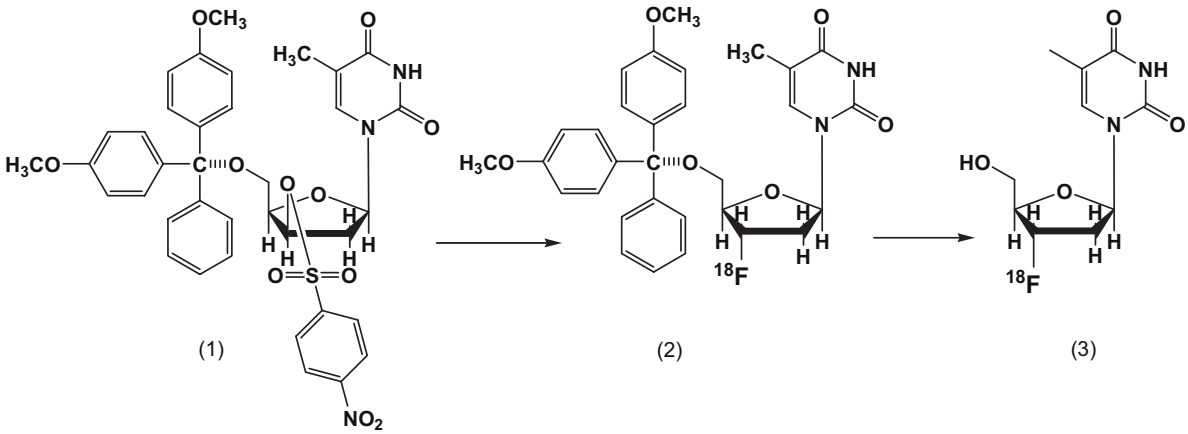

Fig. 2.33. Synthesis of 3'-deoxy-3'-[^{18}F]fluorothymidine (FLT): Following evaporation and drying, K[^{18}F] and Kryptofix complex is incubated at 80 °C with the precursor, 5'-*O*-dimethoxytrityl-3'-*O*-nosyl-thymidine (*1*) acetonitrile. Subsequently, FLT (*3*) is obtained following acid hydrolysis of the fluorinated intermediate (*2*) and HPLC purification

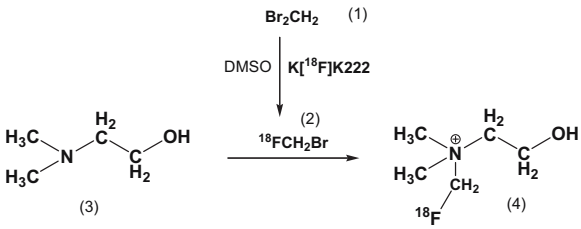

Fig. 2.34. Synthesis of [^{18}F]fluoromethylcholine (FCH): The first step in the synthesis of FCH is the preparation of [^{18}F]fluorobromomethane (FBM) (*2*) from dibromomethane (*1*) and [^{18}F]fluoride. Subsequently, FCH is synthesized by the addition of [^{18}F]CH_3 group to dimethylaminoethanol (*3*) using FBM

2.2.4.3 Carbon-11 Radiochemistry

One of the major advantages of ^{11}C as a radiolabel is the fact that it can be substituted for the stable carbon atom in an organic molecule without changing the biochemical and biophysical properties of that molecule. Also the short half-life of ^{11}C provides favorable radiation dosimetry to perform multiple studies in the same subject under different conditions. The short half-life of ^{11}C may be disadvantageous for commercial production of radiotracers, but has significant potential for developing very high SA molecular imaging probes designed to study drug interactions associated with very small concentrations of neuroreceptors.

^{11}C-Labeled Precursors

In a cyclotron target, ^{11}C radioactivity can be produced either as [$^{11}CO_2$] gas or [^{11}C]CH_4 gas. Subsequently, these gases can be converted into active precursors such as methyl iodide (Langstrom et al. 1976) and methyl triflate (Jewett 1991) either manually or using automated synthesis modules. The active ^{11}C precursors are then used to synthesize ^{11}C-labeled radiopharmaceuticals by attaching ^{11}C atom (as an alkyl group) to another carbon atom or to a nucleophilic group containing O, N or S atoms.

[^{11}C]CH_3I is the most common precursor used to make ^{11}C radiotracers. Two methods are used for the synthesis of [^{11}C]CH_3I. In a "liquid-phase" synthesis, [^{11}C]CO_2 is first reduced (using lithium aluminum hydroxide, $LiAlH_4$) to [^{11}C]CH_3OH (methanol), which then reacts with hydroiodic acid (HI) to generate methyliodide. In a "gas-phase" synthesis, [$^{11}CH_4$] gas (either from the target directly or produced from [$^{11}CO_2$]) reacts with iodine vapors generating methyl iodide. Generally, the radiochemical purity and SA of [^{11}C]CH_3I depend on the synthesis procedure and the automated module employed (Makiko et al. 2005; Kothari et al. 2005). The gas-phase method generates a higher SA of [^{11}C]CH_3I and may be appropriate for receptor binding radiotracers. [^{11}C]CH_3I gas is the most common precursor used for the synthesis of radiotracers based on alkylation reactions. It can also be used to prepare a number of secondary ^{11}C-labeled precursors (Antoni and Langstrom 2005) as shown in Fig. 2.35.

Synthesis of ^{11}C Radiopharmaceuticals

A number of ^{11}C-labeled radiopharmaceuticals of significant clinical interest have been developed (Tables 2.10, 2.11). Most ^{11}C alkylation reactions involve simple methylation using an organic desmethyl precursor, also known as nor compound (a molecule of interest without a methyl group on a specific C, N, O or S atom). Radiotracers such as [^{11}C]raclopride (Farde 1985; Langer et al. 1999), [^{11}C]PK11195 (Banati et al. 1999; Hashimoto et al. 1989), [^{11}C]flumazenil (Nagren et al. 1998), and [^{11}C]carfentanil (Dannals 1985) are prepared using the desmethyl precursors. Certain methylations, as in the case of [^{11}C]methionine, may involve

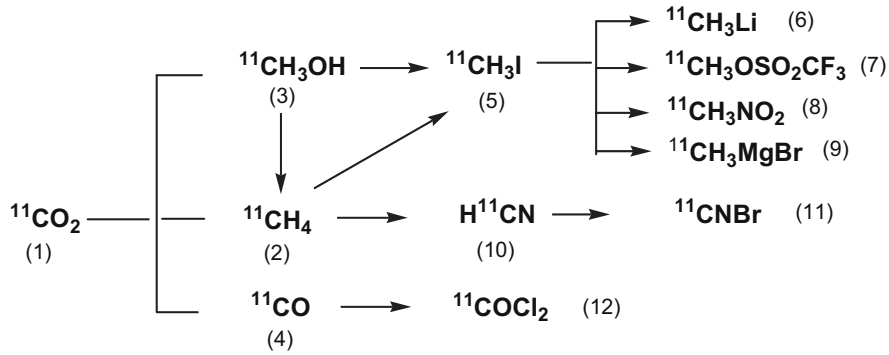

Fig. 2.35. ^{11}C precursors for the synthesis of ^{11}C-labeled radiopharmaceuticals. The most common precursor made from carbon dioxide (*1*) or methane (*2*) is methyl iodide (*5*). Subsequently, using methyl iodide other precursors such as methyl lithium (*6*), methyl triflate (*7*), nitromethane (*8*), methyl magnesium bromide or Grignard's reagent (*9*), hydrogen cyanide (*10*), and cyanogens bromide (*11*) can be made. The most common precursor made from carbon monoxide (*4*) is phosgene (*12*)

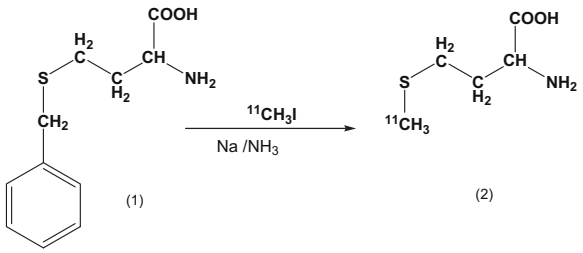

Fig. 2.36. Synthesis of L-[*S*-methyl-^{11}C]methionine (*2*). The precursor, *S*-benzyl-L-homocysteine (*1*), is alkylated with methyl iodide to produce the desired product (*2*)

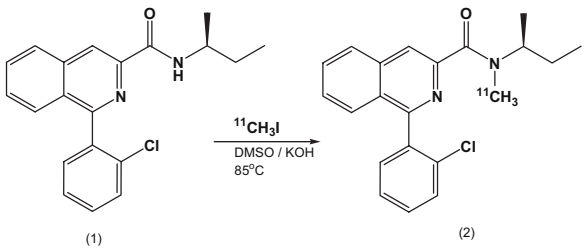

Fig. 2.37. Synthesis of [*N*-methyl-^{11}C]PIB (*3*). Following alkylation of the precursor, 2-(4'-aminophenyl)-6-methoxymethoxybenzothiazole (*1*) with methyl iodide and subsequent hydrolysis of the intermediate (*2*) yields the desired product (*3*)

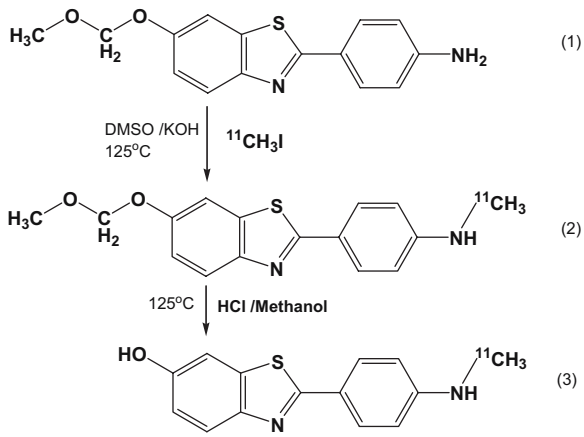

Fig. 2.38. Synthesis of R-[*N*-methyl-^{11}C]PK11195 (*2*). The precursor desmethyl-R-PK11195 (*1*) is methylated using methyl iodide

alkyl substitution of a leaving group on a nucleophilic atom in a molecule (Langstrom et al. 1976; Schmitz et al. 1995). If a molecule of interest has several reactive groups, precursors must have protective groups that can be easily de-protected by hydrolysis following methylation to produce the radiotracer such as [^{11}C]PIB (Mathis et al. 2003).

Preparation of certain ^{11}C radiopharmaceuticals can be very complicated and may involve many steps in the synthesis followed by purification procedures. ^{11}C-labeled amino acids can be prepared using enzyme catalyzed reactions especially to prepare the desired enantiomer with biological activity rather than a racemic mixture. For example, in the synthesis of [^{11}C]5-hydroxy-L-tryptophan (5-HTP) (Bjurling et al. 1989), [^{11}C]-L-alanine is synthesized first, by reacting [^{11}C]CH_3I with *N*-(diphenyl methylene)glycine tertiary butyl ester. Subsequently, [^{11}C]-L-alanine is converted to pyruvic acid using enzymes GPT, DAO and GPT. The interaction of labeled alanine with 5-hydroxy indole in the presence of tryptophanase would finally produce [^{11}C]5-HTP.

The synthesis of [^{11}C]methionine, [^{11}C]PK11195, [^{11}C]PIB and [^{11}C]5-HTP is shown in Figs. 2.36 – 2.39. All these four tracers have significant clinical potential for diagnostic imaging studies.

2.2.4.4 Radiochemistry of Metallic Radionuclides

In order to develop PET radiopharmaceuticals, positron emitting radiometals offer significantly greater potential compared with ^{18}F and ^{11}C nuclides. The experience gained from the research and development of SPECT radiopharmaceuticals based on ^{67}Ga and ^{111}In would provide the necessary knowledge to choose the appropriate molecular targets for PET radiopharma-

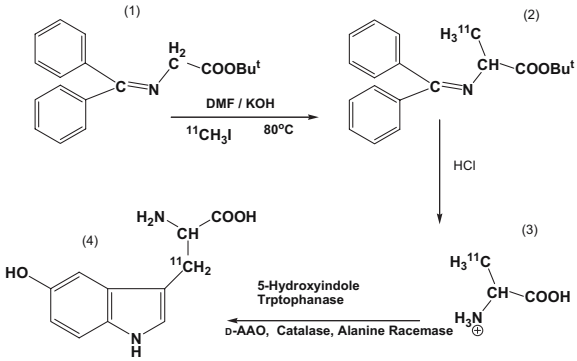

Fig. 2.39. Synthesis of [^{11}C]5-hydroxytryptophan (5-HTP) (*4*). In the first step, [^{11}C]alanine (*3*) is prepared by alkylation of the precursor, *N*-(diphenylmethylene)glycine-*t*-butyl ester (*1*), and subsequent acid hydrolysis of the intermediate (*2*). 5-HTP is then prepared by enzymatic reaction involving [^{11}C]alanine and 5-hydroxyindole

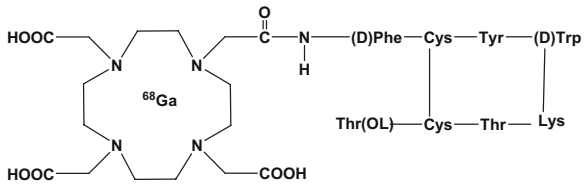

Fig. 2.41. ^{68}Ga-DOTATOC: The chelating agent DOTA is conjugated to the octreotide analog, Tyr^3-octreotide

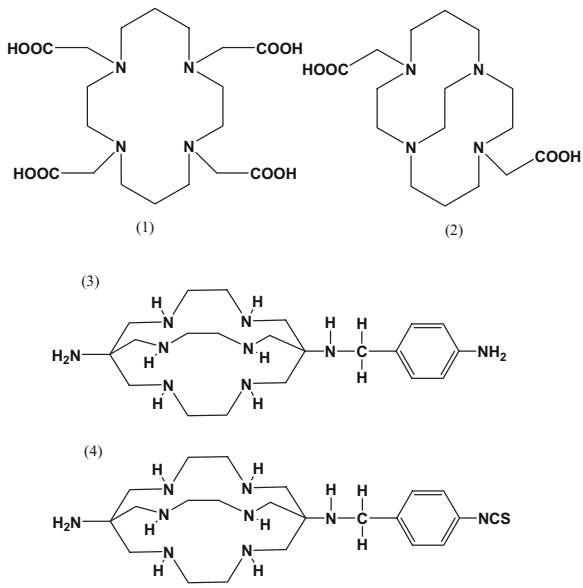

Fig. 2.42. Chelating agents to prepare copper labeled peptides and antibodies. TETA (*1*), ethylene "crossbridged" cyclam derivative, H_2CB-2ETA (*2*) and hexa-aza-cryptand ligands, SarAr (*3*) and SarArNCS (*4*)

ceuticals based on metals. As shown in Table 2.7, the nuclides with suitable half-lives, ^{64}Cu (12.6 h), ^{66}Ga (9.45 h) and ^{86}Y (14.74 h), are more appropriate for developing radiopharmaceuticals that can be transported across the country. However, the two nuclides with short half-lives, ^{68}Ga (68.3 min) and ^{62}Cu (9.76 min), can be produced on demand from generator systems without the need for an on-site cyclotron. Of all these nuclides, ^{64}Cu may be the most promising positron emitting radiometal since it has the ideal β^+ energy (0.656 MeV) and optimum half-life.

Chemistry of Gallium and Yttrium

Both Ga and Y exist predominantly in the +3 oxidation state and for insoluble hydroxides under physiological conditions. They both form strong and stable complexes with bifunctional chelating agents such as DTPA and DOTA, but yttrium forms much more stable complexes when coordinated in a macrocyclic ring configuration with chelating agents such as DOTA. An 8-amino-acid cyclic peptide, octreotide, can be labeled with ^{66}Ga or ^{68}Ga using DTPA as the chelating agent, similar to ^{111}In-octreotide. But in vitro studies demonstrated decreased stability due to transchelation of Ga species. In contrast, DOTA conjugated octreotide analog, DOTATOC, forms much more stable complexes with ^{66}Ga/^{68}Ga (Henze et al. 2001; Hofmann et al. 2001, Maecke et al. 2005) and ^{86}Y nuclides (Foerster et al. 2001). Since ^{68}Ga is generator produced (Isotope Products Laboratories, Valencia, CA) and the parent ^{68}Ge has a long half-life (275 days), ^{68}Ga-DOTATOC (Fig. 2.40) and ^{68}Ga-DOTANOC may be the preferred radiopharmaceuticals (Hofmann et al. 2001; Maecke et al. 2005). In addition, the β^+ abundance and energy of ^{68}Ga (1.9 MeV) is much more optimal for PET imaging compared to that of either ^{66}Ga (4.15 MeV) or ^{86}Y (3.15 MeV).

Chemistry of Copper

Copper is a transition metal and its chemistry is dominated by two oxidation states, I and II. In the Cu(II) oxidation state, the metal binds strongly with nitrogen and sulfur containing molecules by forming coordination complexes.

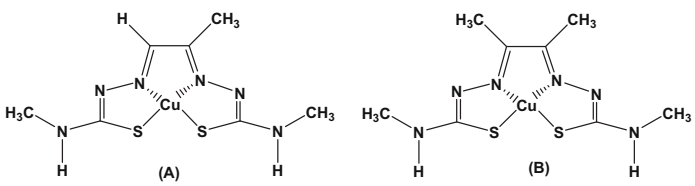

Fig. 2.40. Copper labeled bis(thiosemicarbazone) complexes: Cu-PTSM (*A*) and Cu-ATSM (*B*)

Fig. 2.43. Automated synthesis modules: **a** TRACERLab MX_{FDG}; **b** Bioscan FDG; **c** Synthera; **d** TRACERLab FX_{FDG}; **e** MEI-Plus; **f** TRACERLab FXc

Based on Cu(II)-bis(thiosemicarbazone), two PET radiopharmaceuticals (Fig. 2.41) were developed: $^{62/64}$Cu-pyruvaldehyde-bis(N^4-methylthiosemicarbazone (Cu-PTSM) and $^{62/64}$Cu-diacetyl-bis(N^4-methylthiosemicarbazone) (Cu-ATSM) (Mathias et al. 1990; Lewis and Welch 2001). Cu-PTSM was designed as a tracer to measure blood flow, while Cu-ATSM has preferential uptake in hypoxic tissue. These agents are very lipophilic and rapidly diffuse into the cells. Subsequently, the intracellular enzymes reduce the complex to the Cu(I) oxidation state, which will bind to macromolecules within the cell.

In order to bind radionuclides of copper to peptides and antibody molecules, macrocyclic chelators such as

TETA (1, 4, 8, 11-tetraazacyclotetradecane-1, 4, 8, 11-tetraacetic acid) have been developed (Blower et al. 1996; Anderson et al. 2001). But Cu(II)-TETA complexes were not optimal as imaging agents since they are not stable in vivo (Bass et al. 2000). Recently, a new class of bicyclic tetraazamacrocycles, the ethylene "crossbridged" cyclam derivatives (CB-2ETA), were developed which form highly kinetically stable complexes with Cu(II) and which are less susceptible to transchelation in vivo (Boswell et al. 2004). Similarly, another series of TETA analogs known as hexa-azacryptand ligands, SarAr and SarArNCS were also reported to form strong and stable Cu(II) complexes (Di Bartolo et al. 2001). Over the next 3 – 5 years, a new generation of PET radiopharmaceuticals of peptides and proteins will be developed using these new TETA analogs and positron emitting radionuclides of copper.

2.2.4.5 Automated Synthesis Modules

Computer controlled automation of the synthesis of PET radiopharmaceuticals is desirable for routine commercial production and to reduce radiation exposure for personnel involved in the production of these PET drugs. A number of automated synthesis modules (ASM) for routine production of radiolabeled precursors (such $^{11}CH_3I$) or radiopharmaceuticals ready for clinical studies (such as FDG, FDOPA, raclopride) are commercially available (Table 2.14, Fig. 2.43). ASMs are based on the principle of unit operations, in which a complex synthetic procedure is reduced to a series of simple operations (or reactions) such as evaporation, fluorination, chromatography, hydrolysis, purification and sterilization, etc. These operations are controlled by PCs with software programs that are user friendly and flexible to change the various reaction conditions. Some of these ASMs such as TracerLab FX are based on using sterile disposable kits with ready to use reagent vials for each batch production. At this time several commercial ASMs are used routinely for the synthesis of radiochemically pure, sterile and pyrogen free FDG for clinical studies. In future, such ASMs may be available for the production of FLT, FCH and other PET radiopharmaceuticals.

For the development of ^{11}C PET radiopharmaceuticals, ASMs capable of generating [^{11}C]methyl iodide or triflate are critical for reliable synthesis of radiotracers. Several commercial modules (Table 2.14) are under extensive testing and evaluation.

References

Adam MJ, Wilbur DS (2005) Radiohalogens for imaging and therapy. Chem Soc Rev 34:153 – 63

Alauddin MM, Conti PS (1998) Synthesis and preliminary evaluation of 9-(4-[^{18}F]-fluoro-3-hydroxymethylbutyl)guanine ([^{18}F]FHBG): a new potential imaging agent for viral infection and gene therapy using PET. Nucl Med Biol 25: 175 – 180

Alberto R, Schibli R, Egli A, Schubiger AP, Abram U, Kaden TA (1998) A novel organometallic aqua complex of technetium for the labeling of biomolecules: synthesis of $[^{99m}Tc(OH_2)_3(CO)_3]^+$ from $[^{99m}TcO_4]^-$ in aqueous solution and its reaction with a bifunctional ligand. J Am Chem Soc 120(31):7987 – 7988

Alrabiah FA, Sacks SL (1996) New anti-herpes virus agents: their targets and therapeutic potential. Drugs 52:17 – 32

Anderson C (1933) The positive electron. Phys Rev 43(6): 491 – 494

Anderson CJ, Dehdashti F, Cutler PD, et al. (2001) Copper-64-TETA-octreotide as a PET imaging agent for patients with neuroendocrine tumors. J Nucl Med 42:213 – 221

Antoni G, Langstrom B (2005) Progress in ^{11}C radiochemistry. In: Bailey DL, Townsend DW, Valk PE, Maisey MN (eds) Positron emission tomography – basic sciences. Springer-Verlag, London, pp 223 – 236

Bailey DL, Karp JS, Surti S (2005) Physics and instrumentation in PET. In: Bailey DL, Townsend DW, Valk PE, Maisey MN (eds) Positron emission tomography – basic sciences. Springer-Verlag, London, pp 223 – 236

Banati RB, Goerres GW, Myers R, et al. (1999) [^{11}C]*(R)*-PK11195 positron emission tomography imaging of activated microglia in vivo in Rasmussen's encephalitis. Neurology 53:2199 – 2203

Bangard M, Behe M, Guhlke S, Otte R, Bender H, Maecke HR, Biersack HJ (2000) Detection of somatostatin receptor-positive tumours using the new 99mTc-tricine-HYNIC-D-Phe1-Tyr3-octreotide: first results in patients and comparison with 111In-DTPA-D-Phe1-octreotide. Eur J Nucl Med 27(6): 628 – 37

Barrio JR, Huang S-C, Cole G, et al. (1997) PET imaging of tangles and plaques in Alzheimer's disease with a highly hydrophobic probe. J Label Compd Radiopharm 42:S194–S195

Bass LA, Wang M, Welch MJ, Anderson CJ (2000) In vivo transchelation of copper-64 from TETA-octreotide to superoxide dismutase in rat liver. Bioconjugate Chem 11:527 – 532

Baeken C, D'haenen H, Flamen P, Mertens J, Terriere D, Chavatte K, Boumon R, Bossuyt A (1998) 123I-5-I-R91150, a new single-photon emission tomography ligand for 5-HT2A receptors: influence of age and gender in healthy subjects. Eur J Nucl Med 25(12):1617 – 22

Bergmann SR, Fox KA, Rand AL, et al. (1984) Quantification of regional myocardial blood flow in vivo with [^{15}O]water. Circulation 70:724 – 733

Bjurling P, Watanabe Y, Tokushige M, et al. (1989) Synthesis of β-^{11}C-labeled L-tryptophan and 5-hydroxy-L-tryptophan using a multi-enzymatic reaction route. J Chem Soc Perkin Trans 1:1331 – 1334

Block D, Coenen HH, Stocklin G, et al. (1987) The NCA nucleophilic ^{18}F-fluorination of I,N-disubstituted alkanes as fluoralkylation agents. J Label Compd Radiopharm 24:1029 – 42

Blower PJ, Lewis JS, Zweit J (1996) Copper radionuclides and radiopharmaceuticals in nuclear medicine. Nucl Med Biol 23(8):957 – 980

Blower PJ, Kettle AG, O'Doherty MJ, Coakley AJ, Knapp FF, Jr (2000) 99mTc(V)DMSA quantitatively predicts 188Re(V)-DMSA distribution in patients with prostate cancer metastatic to bone. Eur J Nucl Med 27(9):1405 – 9

Boswell CA, Sun X, Niu W, et al. (2004) Comparative in vivo stability of copper-64 labeled cross-bridged and conventional tetraazamacrocyclic complexes. J Med Chem 47:1465 – 1474
Brown RS, Wahl RL (1993) Over expression of glut-1 glucose transporter in human breast cancer: an immunohistochemical study. Cancer 72:2979 – 2985
Chervu LR, Nunn AD, Loberg MD (1982) Radiopharmaceuticals for hepatobiliary imaging. Semin Nucl Med 12(1):5 – 17. Review
Cho JY, Leveille R, Kao R, Rousset B, Parlow AF, Burak WE, Jr (2000) Mazzaferri EL, Jhiang SM (2000) Hormonal regulation of radioiodide uptake activity and Na+/I- symporter expression in mammary glands. J Clin Endocrinol Metab 85(8):2936 – 43
Clary GL, Tsai C-F, Guynn RW, et al. (1987) Substrate specificity of choline kinase. Arch Biochem Biophys 254:214 – 221
Conti PS, Alauddin MM, Fissekiss JR, et al. (1995) Synthesis of 2'-fluoro-5-^{11}C-methyl-1-β-D-arabinofuranosyluracil ([^{11}C]FMAU): a potential nucleoside analog for in vivo study of cellular proliferation with PET. Nucl Med Biol 22:783 – 789
Dannals RF, Ravert HT, Frost JJ, et al. (1985) Radiosynthesis of an opiate receptor binding radiotracer: [^{11}C]carfentanyl. Int J Appl Radiat Isot 36:303 – 306
Decristoforo C, Mather SJ (1999) Preparation, 99mTc-labeling, and in vitro characterization of HYNIC and N3S modified RC-160 and [Tyr3]octreotide. Bioconjug Chem 10(3):431 – 8
DeGrado TR, Wang S, Holden JE, et al. (2000) Synthesis and preliminary evaluation of ^{18}F labeled 4-thiapalmitate as a PET tracer for myocardial fatty acid oxidation. Nucl Med Biol 27:221 – 231
DeGrado TR, Baldwin SW, Wang S, et al. (2001) Synthesis and evaluation of ^{18}F-labeled choline analogs as oncologic PET tracers. J Nucl Med 42:1805 – 1814
DeJesus OT, Endres CJ, Shelton SE, et al. (1997) Evaluation of fluorinated M-tyrosine analogs as PET imaging agents of dopamine nerve terminals: comparison with 6-fluorodopa. J Nucl Med 38:630 – 636
Dirac PAM (1928) The quantum theory of the electron. Proc R Soc (Lond) A 117:610 – 612
Di Bartolo NM, Sargeson AM, Donlevy TM, Smith SV (2001) Synthesis of a new cage ligand, SarAr, and its complexation with selected transition metal ions for potential use in radioimaging. J Chem Soc Dalton Trans 15:2303 – 2309
Dolle F, Demphel S, Hinnen F, et al. (1998) 6-[^{18}F]Fluoro-L-DOPA by radiofluorodestannylation: A short and simple synthesis of a new labeling precursor. J Label Compd Radiopharm 41:105 – 114
Farde L, Ehrin E, Eriksson L, et al. (1985) Substituted benzamides as ligands for visualization of dopamine receptor binding in the human brain by positron emission tomography. Proc Natl Acad Sci USA 82:3863 – 3867
Firnau G, Sood S, Chirakal R, et al. (1987) Cerebral metabolism of 6-[^{18}F]fluoro-L-3,4-dihydroxy-phenylalanine in the primate. J Neurochem 48:1077 – 1082
Forster GJ, Englebach M, Brockmann J, et al. (2001) Preliminary data on biodistribution and dosimetry for therapy planning of somatostatin receptor positive tumors: comparison of ^{86}Y-DOTATOC and ^{111}In-DTPA-octreotide. Eur J Nucl Med 28:1743 – 1750
Fowler JS, MacGregor RR, Wolf AP, et al. (1987) Mapping human brain monoamine oxidase A and B with ^{11}C-suicide inactivators and positron emission tomography. Science 235:481 – 485
Fowler JS, Volkow ND, Wang G-J, et al. (1996) Inhibition of monoamine oxidase B in the brains of smokers. Nature 379:733 – 736
Fritzberg AR, Kasina S, Eshima D, Johnson DL (1986) Synthesis and biological evaluation of technetium-99m MAG3 as a hippuran replacement. J Nucl Med 27(1):111 – 6
Gambhir SS, Barrio JR, Herschman HR, et al. (1999) Imaging gene expression: principles and assays. J Nucl Cardiol 6:219 – 233
Gambhir SS, Bauer E, Black ME, et al. (2000) A mutant herpes simplex virus type 1 thymidine kinase reporter gene shows improved sensitivity for imaging reporter gene expression with PET. Proc Ntl Acad Sci USA 97:2785 – 2790
Ginj M, Maecke HR (2004) Radiometallo-labeled peptides in tumor diagnosis and therapy. Met Ions Biol Syst 42:109 – 42
Green MA, Mathias CJ, Welch MJ, et al. (1990) Copper-62 labeled PTSM: synthesis and evaluation as a PET tracer for cerebral and myocardial perfusion. J Nucl Med 31:1989 – 1996
Grierson JR, Shields AF (2000) Radiosynthesis of 3'-deoxy-3'-[^{18}F]fluoro-thymidine:[^{18}F]FLT for imaging of cellular proliferation in vivo. Nucl Med Biol 27:143 – 156
Gronroos T, Eskola O, Lehtio K, et al. (2001) Pharmacokinetics of [^{18}F]FETNIM: a potential marker for PET. J Nucl Med 42:1397 – 1404
Haberkorn U, Oberdorfer F, Gebert J, et al. (1996) Monitoring of gene therapy with cytosine deaminase: in vitro studies using ^{3}H-5-fluorocytosine. J Nucl Med 37:87 – 94
Hamacher K, Coenen H, Stocklin G (1986) Efficient stereospecific synthesis of no-carrier added 2-[^{18}F]fluoro-2-deoxy-D-glucose using amino-polyether supported nucleophilic substitution. J Nucl Med 27:235 – 238
Happaranta M, Bergman J, Laakso A, et al. (1996) [^{18}F]CFT ([^{18}F]WIN,35428), a new radioligand to study the dopamine transporter with PET biodistribution in rats. Synapse 23:321 – 327
Hara T (2001) ^{18}F-Fluorocholine: a new oncologic PET tracer (invited commentary). J Nucl Med 42:1815 – 1817
Hashimoto KI, Inoue O, Suzuki K, et al. (1989) Synthesis and evaluation of ^{11}C-PK11195 for in vivo study of peripheral-type benzodiazepine receptors using positron emission tomography. Ann Nucl Med 3:63 – 71
Henze M, Schuhmacher J, Hipp P, et al. (2001) PET imaging of somatostatin receptors. J Nucl Med 42:1053 – 1056
Hess E, Takacs S, Scholten B, et al. (2001) Excitation function of the ^{18}O(p,n)^{18}F nuclear reaction from threshold up to 30 MeV. Radiochim Acta 89:357 – 362
Higley B, Smith FW, Smith T, Gemmell HG, Das Gupta P, Gvozdanovic DV, Graham D, Hinge D, Davidson J, Lahiri A (1993) Technetium-99m-1,2-bis[bis(2-ethoxyethyl) phosphino]ethane: human biodistribution, dosimetry and safety of a new myocardial perfusion imaging agent. J Nucl Med 34(1):30 – 8
Hofmann M, Maecke H, Borner R, et al. (2001) Biokinetics and imaging with the somatostatin receptor PET ligand. Eur J Nucl Med 28(12):1751 – 1757
Hostetler ED, Jonson SD, Welch MJ, et al. (1999) Synthesis of 2-[^{18}F]fluoro-estradiol, a potential diagnostic imaging agent for breast cancer: strategies to achieve nucleophilic substitution of an electron rich aromatic ring with [^{18}F]F^{-}. J Organ Chem 64:178 – 185
Hughes AJ (1997) Clinicopathological aspects of aspects of Parkinson's disease. Eur Neurol 38[Suppl 2]:13 – 20
Ido T, Wan CN, Casella JS, et al. (1978) Labeled 2-deoxy-D-glucose analogs: ^{18}F labeled 2-deoxy-2-fluoro-D-glucose, 2-deoxy-2-fluoro-D-mannose and ^{14}C-2-deoxy-2-fluoro-D-glucose. J Label Compd Radiopharmacol 14:175 – 183
Innis R, Zoghbi S, Johnson E, Woods S, al-Tikriti M, Baldwin R, Seibyl J, Malison R, Zubal G, Charney D (1991) SPECT imaging of the benzodiazepine receptor in non-human primate brain with [123I]Ro 16 – 0154. Eur J Pharmacol 193(2):249 – 52
Inoue TJ, Tomiyoshi K, Higuchi T, et al. (1998) Biodistribution studies on L-[^{18}F]fluoro-α-methyl tyrosine: a potential tumor-detecting agent. J Nucl Med 39:663 – 667
Iwata R, Pascali C, Bogni A, et al. (2002) [^{18}F]Fluoromethyl trif-

late, a novel and reactive [^{18}F]fluoromethylating agent: preparation and application to the on-column preparation of [^{18}F]fluorocholine. Appl Radiat Isotop 57:347 – 352
Jager PL, Vaalburg W, Pruim J, et al. (2001) Radiolabeled amino acids: basic aspects and clinical applications in oncology. J Nucl Med 42:432 – 445
Jeong JM, Chung JK (2003) Therapy with ^{188}Re-labeled radiopharmaceuticals: an overview of promising results from initial clinical trials. Cancer Biother Radiopharm 18:707 – 17
Jewett DM (1991) A simple synthesis of [^{11}C]methyl triflate. Appl Radiat Isot 43:1383 – 1385
Joliot F, Curie I (1934) Artificial production of a new kind of radio-element. Nature 133:201 – 202
Jovanovic V, Konstantinovska D, Milivojevic K, Bzenic J (1981) Determination of radiochemical purity and pharmacokinetic parameters of 99mTc-sulphur colloid and 99mTc-tin colloid. Nuklearmedizin 20:279 – 82
Kamarainen E-L, Kyllonen T, Airaksinen A, et al. (2000) Preparation of [^{18}F]CFT-FP and [^{11}C]CFT-FP, selective radioligands for visualization of the dopamine transporter using positron emission tomography (PET). J Label Compd Radiopharm 43:1235 – 1244
Kilbourn MR (1997) In vivo tracers for vesicular neurotransmitter transporters. Nucl Med Biol 24:615 – 619
Kilbourn MR (1990) Fluorine-I8 labeling of radiopharmaceuticals. National Academy of Sciences, National Academy Press, Nuclear Science Series no. NAS-NS-3203
Klunk WE, Engler H, Nordberg A, et al. (2004) Imaging brain amyloid in Alzheimer's disease with Pittsburgh compound-B. Ann Neurol 55:306 – 319
Kocher D (1983) Radioactive decay data tables. Medical Physics 10:1 – 921
Koh WJ, Rasey JS, Evans ML, et al. (1992) Imaging of hypoxia in human tumors with [^{18}F]fluoromisonidazole. Int J Radiat Oncol Biol Phys 22:199 – 212
Kothari PJ, Suehiro S, Vallabhajosula S (2005) Evaluation of commercial automated [^{11}C]methyl iodide (MeI-Plus) synthesis module. J Label Compd Radiopharm 48:S226
Krenning EP, Bakker WH, Kooij PP, Breeman WA, Oei HY, de Jong M, Reubi JC, Visser TJ, Bruns C, Kwekkeboom DJ (1992) Somatostatin receptor scintigraphy with indium-111-DTPA-D-Phe-1-octreotide in man: metabolism, dosimetry and comparison with iodine-123-Tyr-3-octreotide. J Nucl Med 33(5):652 – 8
Kuikka JT, Bergstrom KA, Ahonen A, Hiltunen J, Haukka J, Lansimies E, Wang S, Neumeyer JL (1995) Comparison of iodine-123 labelled 2 beta-carbomethoxy-3 beta-(4-iodophenyl)tropane and 2 beta-carbomethoxy-3 beta-(4-iodophenyl)-N-(3-fluoropropyl)nortropane for imaging of the dopamine transporter in the living human brain. Eur J Nucl Med 22(4):356 – 60
Kung HF, Pan S, Kung MP, Billings J, Kasliwal R, Reilley J, Alavi A (1989) In vitro and in vivo evaluation of [123I]IBZM: a potential CNS D-2 dopamine receptor imaging agent. J Nucl Med 30(1):88 – 92
Langen KJ, Coenen HH, Roosen N, Kling P, Muzik O, Herzog H, Kuwert T, Stocklin G, Feinendegen LE (1990) SPECT studies of brain tumors with L-3-[123I] iodo-alpha-methyl tyrosine: comparison with PET, 124IMT and first clinical results. J Nucl Med 31(3):281 – 6
Langer O, Dolle F, Halldin C, et al. (1999) A general method for the synthesis of raclopride, FLB 457 and epidepride and corresponding desmethyl-precursors. J Label Compd Radiopharm 42:5366 – 5368
Langstrom B, Lundqvist H (1976) The preparation of [^{11}C]methyl iodide and its use in the synthesis of [methyl-^{11}C]-L-methionine. Int J Appl Radiat Isot 27:357 – 363
Laruelle M (2000) Imaging synaptic neurotransmission with in vivo binding competition techniques: a critical review. J Cereb Blood Flow Metabol 20:423 – 451
Lawrence EO, Livingston MS (1931) The production of high speed protons with the use of high voltages. Phys Rev 38:834
Le Bars D, et al. (1998) High-yield radiosynthesis and preliminary in vivo evaluation of p-[^{18}F]MPPF, a fluoro analog of WAY-100635. J Nucl Med Biol 25(4):343 – 350
Lewis JS, Welch MJ (2001) PET imaging of hypoxia. Q J Nucl Med 45:183 – 188
Lim JL, Zheng L, Berridge MS, Tewson TJ (1996) The use of 3-methoxymethyl-16α, 17β-epiestriol-O-cyclic sulfone as the precursor in the synthesis of [^{18}F]-16alpha-fluoroestradiol. Nucl Med Biol 23:911 – 915
Maecke HR, Hofmann M, Haberkorn U (2005) ^{68}Ga-labeled peptides in tumor imaging. J Nucl Med 46:172S–178S
Makiko S, Kothari PJ, Vallabhajosula S (2005) Quality control studies of [^{11}C]methyl iodide produced in liquid and gas phase synthesis modules. J Label Compd Radiopharm 48:S213
Manual for reactor produced radioisotopes (2003) IAEA-TEC-DOC-1340, pp 1 – 251
Martin SJ, Eisenbarth U, Wagner-Utermann U, et al. (2002) A new precursor for the radiosynthesis of [^{18}F]FLT. Nucl Med Biol 29:263 – 273
Mathis CA, Wang Y, Holt DP, et al. (2003) Synthesis and evaluation of ^{11}C-labeled 6-substituted 2-aryl benzothiazoles as amyloid imaging agents. J Med Chem 46:2740 –2754
Meegalla S, Plossl K, Kung MP, Chumpradit S, Stevenson DA, Frederick D, Kung HF (1996) Tc-99m-labeled tropanes as dopamine transporter imaging agents. Bioconjug Chem 7(4):421 – 9
Mintum MA, Welch MJ, Siegel BA, et al. (1988) Breast cancer: PET imaging of estrogen receptors. Radiology 169:45 – 48
Moolten FL (1986) Tumor chemosensitivity conferred by inserted herpes thymidine kinase genes: paradigm for prospective cancer control strategy. Cancer Res 46:5276 – 5281
Mukherjee J, Kang ZY, Brown T, et al. (1999) Preliminary assessment of extrastriatal dopamine D2 receptor binding in the rodent and nonhuman primate brains using the high affinity radioligand, ^{18}F-Fallypride. Nucl Med Biol 26:519 – 527
Nagren K, Halldin C (1998) Methylation of amide and thiol functions with [^{11}C]methyl triflate, as exemplified by [^{11}C]NMSP, [^{11}C]flumazenil and [^{11}C]methionine. J Label Compd Radiopharm 41:831 – 841
Namavari M, Bishop A, Satyamurthy N, et al. (1992) Regioselective radiofluorodestannylation with [^{18}F]F_2 and [^{18}F]CH_3COOF. A high yield synthesis of 6-[^{18}F]Fluoro-L-DOPA. Int J Rad Appl Instrum 43:989 – 96
Nickels RJ, Hichwa RD, Daube ME, et al. (1983) An ^{18}O target for the high yield production of ^{18}F fluoride. Int J Appl Rad Isotop 34:625 – 629
Nickels RJ, Daube ME, Ruth TJ (1984) An oxygen target for the production of [^{18}F]F_2. Appl Radiat Isot 35:117 – 112
Nunn AD (2006) The cost of developing imaging agents for routine clinical use. Invest Radiol 41(3):206 – 12. Review
Nutt R (2002) The history of positron emission tomography (PET). Mol Imag Biol 4:11 – 26
Ohtsuki K, Akashi K, Aoka Y, Blankenberg FG, Kopiwoda S, Tait JF, Strauss HW (1999) Technetium-99m HYNIC-annexin V: a potential radiopharmaceutical for the in-vivo detection of apoptosis. Eur J Nucl Med 26(10):1251 – 8
Parliament MB, Chapman JD, Urtasun RC, et al. (1992) Non-invasive assessment of human tumor hypoxia with ^{123}I-iodoazomycin arabinoside: preliminary report of a clinical study. Br J Cancer 65:90 – 95
Patton J, Sandler M, Berman D, et al. (2006) D.SPECT: A new solid state camera for high speed molecular imaging. J Nucl Med 47:(5)189P

Pearson DA, Lister-James J, McBride WJ, Wilson DM, Martel LJ, Civitello ER, Taylor JE, Moyer BR, Dean RT (1996) Somatostatin receptor-binding peptides labeled with technetium-99m: chemistry and initial biological studies. J Med Chem 39(7):1361 – 71

Phelps ME, Huang SC, Hoffman EJ, et al. (1979) Tomographic measurement of local cerebral glucose metabolic rate in humans with [^{18}F]2-fluoro-2-deoxy-D-glucose: validation of method. Ann Neurol 6:371 – 388

Post RL, Jolly PC (1957) The linkage of sodium, potassium and ammonium active transport across the human erythrocyte membrane. Biochim Biophy Acta 25:118 – 128

Qaim SM, Coenen HH (2005) Reactors and cyclotrons. Pharmaceutical production of relevant radionuclides. Pharm Unserer Zeit 34(6):460 – 466

Raichle ME, Martin WRW, Herscovitch P, Mintum MA, Markham J (1973) Brain blood flow measured with intravenous H215O. II. Implementation and validation. J Nucl Med 24:790 – 798

Reubi JC, Laissue J, Krenning EP, Lamberts SWJ (1992) Somatostatin receptors in human cancer: incidence, characteristics, functional correlates and clinical implication. J Steroid Biochem Mol Biol 43:27 – 35

Ruth TJ, Wolf AP (1979) Absolute cross section for the production of ^{18}F via the ^{18}O(p,n)^{18}F reaction. Radiochimica Acta 26:21 – 24

Ruth TJ (2003) Accelerators available for isotope production. In: Welch MJ, Redvanley CS (eds) Handbook of radiopharmaceuticals, radiochemistry and applications. John Wiley & Sons, New York, pp 71 – 86

Satyamurthy N, Phelps ME, Barrio JR (1999) Electronic generators for the production of positron emitter labeled radiopharmaceuticals: Where would PET be without them? Clin Positron Imag 2:233 – 253

Schibli R, Schubiger PA (2002) Current use and future potential of organometallic radiopharmaceuticals. Eur J Nucl Med Mol Imaging 29:1529 – 42

Schlyer DJ (2003) Production of radionuclides in accelerators. In: Welch MJ, Redvanley CS (eds) Handbook of radiopharmaceuticals, radiochemistry and applications. John Wiley & Sons, New York, pp 1 – 70

Schmitz F, Plenevaux A, Del-Fiore G, et al. (1995) Fast routine production of L-[^{11}C-methyl]-methionine with Al_2O_3/KF. Appl Radiat Isot 46:893 – 897

Sciacca RR, Akinboboye O, Chou RL, et al. (2001) Measurement of myocardial blood flow with PET using 1-^{11}C acetate. J Nucl Med 42:63 – 70

Sheh Y, Koziorowski J, Balatoni J, et al. (2000) Low energy cyclotron production and chemical separation of no-carrier added iodine-124 from a reusable enriched tellurium-124 dioxide/aluminum oxide solid solution target. Radiochimica Acta 88:169 – 173

Schelbert HR, Phelps ME, Huang SC, et al. (1981) N-13 ammonia as an indicator of myocardial blood flow. Circulation 63:1259 – 1272

Shields AF, Lim K, Grierson J, et al. (1996) Development of labeled thymidine analogs for imaging tumor proliferation. Nucl Med Biol 23:17 – 22

Shikano N, Kanai Y, Kawai K, Ishikawa N, Endou H (2003) Characterization of 3-[125I]iodo-alpha-methyl-L-tyrosine transport via human L-type amino acid transporter 1. Nucl Med Biol 30(1):31 – 7

Shogi-Jadid K, Small GW, Agdeppa ED, et al. (2002) Localization of neurofibrillary tangles and beta-amyloid plaques in the brains of living patients with Alzheimer disease. Am J Geriatr Psychiatry 10:24 – 35

Shoup TM, Olson JMH, Votaw J, et al. (1999) Synthesis and evaluation of [^{18}F] 1-amino-3-fluorocyclobutane-l-carboxylic acid to image brain tumors. J Nucl Med 40: 331 – 338

Sols A, Crane RA (1954) Substrate specificity of brain hexokinase. J Bio Chem 210:581 – 595

Stöcklin G, Qaim SM, Rösch F (1995) The impact of radioactivity on medicine. Radiochimica Acta 70/71:249 – 272

Suga K (2002) Technical and analytical advances in pulmonary ventilation SPECT with xenon-133 gas and Tc-99m-Technegas. Ann Nucl Med 16(5):303 – 10

Taillefer R, Laflamme L, Dupras G, Picard M, Phaneuf DC, Leveille J (1988) Myocardial perfusion imaging with 99mTc-methoxy-isobutyl-isonitrile (MIBI): comparison of short and long time intervals between rest and stress injections. Preliminary results. Eur J Nucl Med 13(10):515 – 22

Tan PZ, Baldwin RM, Tao FU, et al. (1999) Rapid synthesis of F-18 and H-2 dual-labeled Altanserin. A metabolically resistant PET ligand for 5-HT1A receptors. J Label Compd Radiopharm 42:457 – 467

Thorpe S, Baynes J, Chroneos Z (1993) The design and application of residualizing labels for studies of protein catabolism. FASEB J 7:399 – 405

Tjuvajev JG, Arvil N, Oku T, et al. (1998) Imaging herpes virus thymidine kinase gene transfer and expression by positron emission tomography. Cancer Res 58:4333 – 4341

Tolmachev V, Carlsson J, Lundquist H (2004)A limiting factor for the progress of radionuclide-based diagnostics and therapy – availability of suitable radionuclides. Acta Oncol 43(3):264 – 275

Trojanowski JQ, Shin R-W, Schmidt ML, et al. (1995) Relationship between plaques, tangles, and dystrophic processes in Alzheimer's disease. Neurobiol Aging 16:335 – 340

Vallabhajosula S, Zimmerman RE, Picard M, Stritzke P, Mena I, Hellman RS, Tikofsky RS, Stabin MG, Morgan RA, Goldsmith SJ (1989) Technetium-99m ECD: a new brain imaging agent: in vivo kinetics and biodistribution studies in normal human subjects. J Nucl Med 30(5):599 – 604

VanBrocklin HF, Henry F, Blagoev, et al. (2004) A new precursor for the preparation of 6-[^{18}F]fluoro-L-m-tyrosine (FMT): Efficient synthesis and comparison of radiolabeling. Appl Radiat Isot 61(6):1289 – 1294

Vaupel P, Schlenger K, Hoeckel M (1992) Blood flow and tissue oxygenation of human tumors: an update. Adv Exp Med Biol 317:139 – 151

Virgolini I, Pangerl T, Bischof C, et al. (1997) Somatostatin receptor subtype expression in human tissues: a prediction for diagnosis and treatment of cancer? Eur J Clin Invest 27:645 – 647

Virgolini I, Szilvasi I, Kurtaran A, Angelberger P, Raderer M, Havlik E, Vorbeck F, Bischof C, Leimer M, Dorner G, Kletter K, Niederle B, Scheithauer W, Smith-Jones P (1998) Indium-111-DOTA-lanreotide: biodistribution, safety and radiation absorbed dose in tumor patients. J Nucl Med 39(11): 1928 – 36

Volkert WA, Goeckeler WF, Ehrhardt GJ, Ketring AR (1991) Therapeutic radionuclides: production and decay property considerations. J Nucl Med 32:174 – 185

Volkert WA, Hoffman TJ (1999) Therapeutic radiopharmaceuticals. Chem Rev 99:2269 – 9

Volkow ND, Fowler JS, Ding YS, et al. (1998) PET radioligands for dopamine transporters and studies in human and nonhuman primates. Adv Pharmacol 42:211 – 214

Wafelman AR, Konings MC, Hoefnagel CA, et al. (1994) Synthesis, radiolabelling and stability of radioiodinated m-iodobenzylguanidine, a review. Appl Radiat Isot 45:997 – 1107

Wilbur DS (1992) Radiohalogenation of proteins: an overview of radionuclides, labeling methods, and reagents for conjugate labeling. Bioconjug Chem 3:433 – 70

Yun M, Oh SJ, Ha H-J, et al. (2003) High radiochemical yield

synthesis of 3'-deoxy-3'-[^{18}F]fluorothymidine using (5'-O-dimethoxytirtyl-2'-deoxy-3'-onosyl-D-threo-pentofuranosyl)thymine and its 3-N-BOC protected analogue as a labeling precursor. Nucl Med Biol 30:151 – 157

Wong DF, Wagner HN, Tune LE, et al. (1986) Positron emission tomography reveals elevated D2 dopamine receptors in drug-naïve schizophrenics. Science 234:1558 – 1563

Zalutsky MR, Pozzi OR (2004) Radioimmunotherapy with alpha-particle emitting radionuclides. Q J Nucl Med Mol Imaging 48:289 – 96

Zhuang ZP, Kung MP, Hou C, Plossl K, Skovronsky D, Gur TL, Trojanowski JQ, Lee VM, Kung HF (2001) IBOX(2-(4'-dimethylaminophenyl)-6-iodobenzoxazole): a ligand for imaging amyloid plaques in the brain. Nucl Med Biol 28(8):887 – 94

Brain

3

R.L. Van Heertum, M. Ichise

3.1 SPECT and PET Brain Imaging in the Evaluation of Cerebrovascular Disease

Over the last 5 – 10 years, the role of brain single photon emission computed tomography (SPECT) and positron emission tomography (PET) in the assessment of cerebrovascular disease (CVD) has changed dramatically. These changes have largely occurred as a result of continuing advances in computed tomography (CT) and more importantly magnetic resonance imaging (MRI) and functional magnetic resonance (fMR) imaging technology. In addition, there has been a declining interest in the use of SPECT and PET imaging for CVD in the United States although interest remains much stronger in Europe, Japan and other select areas in Asia. Part of the decline in the US relates to the lack of widespread availability of appropriate multi-detection brain imaging devices and also to the lack of logistical support to perform emergency brain SPECT imaging for acute stroke and finally to the limitations of brain SPECT imaging compounds for detecting acute stroke in the face of confounding "luxury perfusion" masking the presence and/or extent of the area of infarction (Mountz et al. 2003).

As a result, CT and MRI have largely replaced SPECT and PET, for the detection, differential diagnosis, and prognosis assessment and follow-up of patients with acute stroke. At present, brain SPECT is still, however, used in the assessment of complex cases and also for the evaluation of cerebrovascular reserve with and without an acetazolamide challenge (Van Heertum et al. 2001). PET imaging is additionally utilized in the determination of the oxygen extraction fraction (OEF) in patients being considered for corrective carotid artery obstructive disease surgery (Grubb et al. 2003). Unfortunately, this technique is not widely employed because of the requirement for an on site cyclotron for oxygen-15 production.

3.2 SPECT and PET Brain Imaging in the Evaluation of Dementia

The role of SPECT and PET in the evaluation of neurodegenerative dementia is continuing to evolve. PET, in particular, is finding an increasing role in the early detection, differential diagnosis, prognosis and follow-up of dementia.

In the early detection of dementia, a number of investigators (Reiman et al. 2005; Ercoli et al. 2006) have reported on the value of risk stratification of PET and other biomarkers as a logical means of cost-effectively identifying those patients who are greatest risk for developing Alzheimer's disease (AD). At the present time,

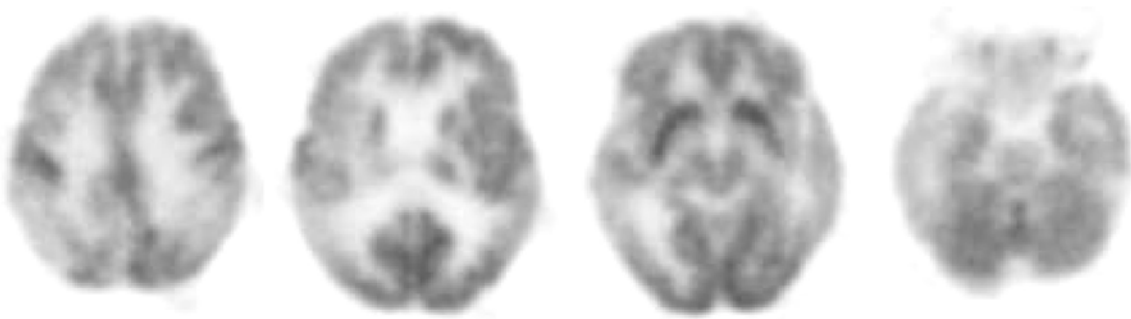

Fig. 3.1. Early dementia. Fifty-seven-year-old man who presented with "difficulty processing information" was referred for a FDG-PET scan to assess for cognitive dysfunction. Transverse plane FDG-PET images (vertex to cerebellum) reveal hypometabolism in the posterior parietal-temporal lobe (right greater than left) and the posterior cingulum. The findings when combined with the history are most compatible with early dementia of the Alzheimer type

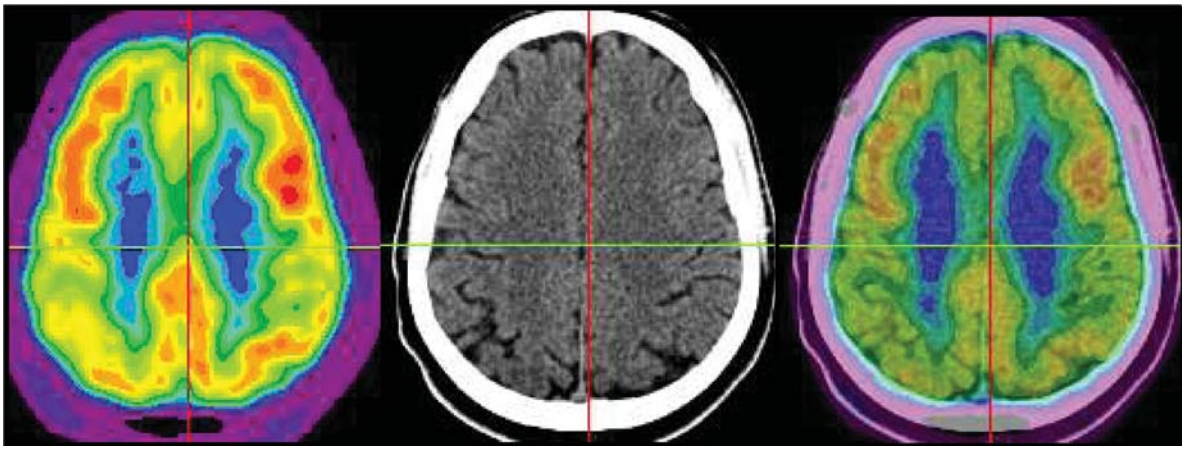

Fig. 3.2. The value of PET/CT in the evaluation of Alzheimer's disease – transverse plane FDG-PET (*left*), CT (*middle*) and fused PET/CT (*right*) images. Study reveals evidence of bilateral posterior parietal hypometabolism without evidence of significant cortical atrophy on CT

the focus of this strategy has been on identifying individuals with and without mild cognitive impairment (MCI) who are homozygous for the apolipoprotein E-ε4 (APOE-ε4) allele, a group that is considered at higher risk for developing AD (Van Heertum and Tikofsky 2003). Once identified, these patients subsequently undergo a FDG-PET scan as the next step. Patients who are likely to progress on to AD generally will demonstrate a pattern of bilateral posterior parietal lobe hypometabolism, similar to but not as profound as the degree of hypometabolism observed in AD patients at a time when the individual is still cognitively intact, as measured by neuropsychological testing (Reiman et al. 2005). As additional biomarkers are validated, it is likely that other risk stratification approaches, employing neuroimaging, will also be pursued. Other advances in the detection of dementia include the use of hybrid imaging devices such as PET/CT and in the future PET/MRI.

In addition, further advances in the development of new PET and SPECT radiopharmaceuticals are contributing to the detection of dementia. One particularly promising category of radiopharmaceuticals relates to agents that are being used to detect β-amyloid plaque deposition in-vivo. At present, two different compounds are being most widely investigated in multicenter clinical investigations. These PET compounds were developed based on the structure of two different histopathology stains, thioflavin T and Congo red, that have a high binding affinity for brain β-amyloid.

One compound commonly referred to as the "Pittsburgh compound" or [^{11}C]PIB (BTA), which results from a modification of the amyloid-binding stain thioflavin-T, appears very promising but is limited to sites with an on-site cyclotron because of the short life carbon-11 label (Mathis et al. 2002). The second compound, developed by the UCLA group, has the advantage of a fluorine-18 label ([^{18}F]FDNNP). This compound attaches to a different receptor on β-amyloid and also binds to neurofibrillary tangles (Shoghi-Jadid et al. 2002). Additional investigations will be necessary to determine the value of these compounds. Finally, more sophisticated, user-friendly, voxel-based methods of image quantification, that are tied to normative databases, are beginning to appear in the market place (Drzezga et al. 2003). This approach, similar to nuclear cardiology analysis of myocardial perfusion studies, should hopefully bring an improved level of objectivity to the visual analysis of FDG-PET studies in dementia patients.

3.3 SPECT and PET Brain Imaging in the Evaluation of Brain Tumors

There are 13,500 brain tumors newly diagnosed each year, accounting for about 2 % of all adult malignancies. Overall, gliomas make up over 90 % of all adult brain tumors with males slightly predominating (Del Sole et al. 2001). Typically, gliomas are classified using the World Health Organization (WHO) grading system, which takes into account cell type and the degree of cellular differentiation (Smirniotopoulos 1999). In children, brain tumors are typically infratentorial with medulloblastomas, arising in the posterior fossa, the most common (Farinotti et al. 1998). Supratentorial gliomas are less frequent. In addition, there are also many secondary or metastatic tumors that may involve the brain via the systemic circulation.

3.3.1 Neuroimaging

A wide variety of neuroimaging procedures are used in the evaluation of brain tumors. CT and MR are, in large

part, used as anatomic imaging techniques. Overall the accuracy of CT and MRI for detecting the presence of brain tumors is approximately 95 %; however, CT and MRI are less helpful in defining cell type and degree of malignancy (Ricci 1999). Magnetic resonance spectroscopy and nuclear medicine techniques are often useful adjunctive techniques when this type of cellular biochemical distinction becomes important to ascertain.

3.3.2 Brain SPECT Imaging

The SPECT radiopharmaceutical can be divided into a number of broad groups including: regional cerebral blood flow compounds ([^{99m}Tc]HMPAO and [^{99}Tc]ECD); cationic compounds (thallium-201, [^{99m}Tc]MIBI, [^{99m}Tc]-tetrofosmin); labeled amino acids [[^{123}I]iodo-α-methyltyrosine (IMT)]; labeled antibodies; labeled somatostatin analogs ([^{111}In]octreotide) and apoptosis compounds ([^{123}I]annexin) (Del Sole et al. 2001). Although brain SPECT is still utilized for special cases and there is an evolving role for labeled amino acid SPECT, much of SPECT imaging, for brain tumors, has been replaced by PET imaging.

3.3.3 PET Brain Imaging

PET brain imaging is most commonly performed with FDG. FDG-PET is of value for tumor detection; defining tumor extent and degree of malignancy; as well as in the assessment of tumor response, and differentiation of viable tumor versus radiation necrosis in cases where MRI cannot make the distinction or the MRI results are equivocal (Van Heertum et al. 2004). [^{11}C]methionine (MET), which is incorporated into the tumor protein synthesis pathway, is very useful for detection of brain tumors. An important characteristic of MET is that it is more accurate for detecting low-grade brain tumors than FDG (Pirotte et al. 2004). Other compounds, including [^{11}C] and [^{18}F]choline and [^{18}F]fluoro-thymidine (FLT), are currently in clinical trials to further define their clinical efficacy.

FDG-PET, after a number of decades of clinical use, has been particularly well characterized as regards clinical efficacy and known strengths and weaknesses.

3.3.4 Strengths

Since the first introduction of FDG-PET imaging, it has been recognized that the technique is very sensitive for detecting high-grade gliomas with an overall accuracy in the range of 90 – 95 %.

In addition, the degree of uptake in tumors cells has been shown to correlate directly with the degree of malignancy noted on histopathology. Some investigators (Alavi et al. 1988) have reported that the level of FDG uptake is a better measure of the malignancy potential of individual brain tumors, than actual histopathology. Specifically, patients with histological low-grade brain tumors and markedly elevated glucose metabolism have a shorter survival time than patients with low-grade tumors and lower glucose metabolism (Di Chiro 1986). The ability of FDG to assess tumor glucose metabolism is a very important aspect of brain tumor evaluation, particularly in the follow-up assessment of patients post-treatment. FDG-PET is also a very useful technique for distinguishing radiation necrosis post-treatment from viable residual or recurrent tumor in those cases where MRI is unable to make the distinction or is equivocal (Kim et al. 1992).

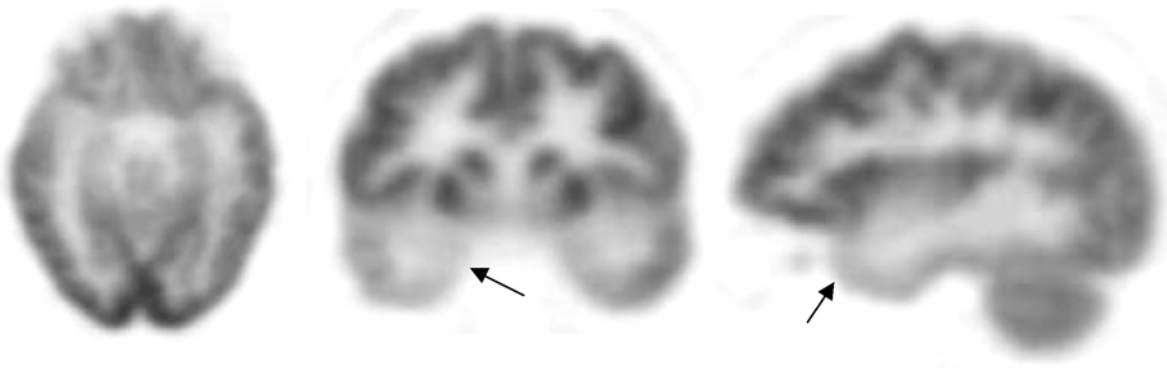

Fig. 3.3. Partial complex seizure disorder, right temporal lobe – interictal FDG-PET, in the axial, coronal and sagittal image planes, reveals localized glucose hypometabolism involving the anterior and mesial (*arrows*) right temporal lobe consistent with an interracial seizure focus

3.3.5
Weaknesses

There are also a number of clearly identified weaknesses to the use of FDG-PET in the evaluation of brain tumors.

Since the very early days of PET brain imaging, it has been recognized that the methodology is less accurate for the detection of histologic low-grade tumors (DiChiro et al. 1982). In part, this lower accuracy rate is due to the high cortical gray matter of FDG often surrounding the actual tumor. The absolute uptake of labeled glucose is also confounded by uptake in areas of inflammation and/or infection including the tumor itself during and immediately after treatment. Delaying the initial scan 6–8 weeks after completion of treatment and the performance of serial imaging at a number of time points post FDG administration are of some value for improving the accuracy of tumor detection (Spence et al. 2004).

Labeled amino acids, in particular [^{11}C]methionine (MET), can often be complementary to FDG imaging. MET has an improved accuracy rate for detecting low-grade tumors and is not hampered to the same degree as FDG by uptake in adjacent gray matter of the surrounding brain (Jacobs et al. 2005). In the future, PET brain imaging in the evaluation of brain tumors should become increasingly more sophisticated as new PET imaging compounds for the assessment of tumor proliferation, angiogenesis, receptor activity and ischemia become more readily available.

3.4
SPECT and PET Brain Imaging in the Evaluation of Seizure Disorders

3.4.1
Incidence and Prevalence – Seizure Disorders

The differences between a seizure disorder and epilepsy are defined by strict criteria. A single episodic event, which may be due to a central nervous system cause or a systemic etiology arising outside the brain, is generally defined as a seizure whereas multiple recurring seizures, from an underlying persistent cerebral dysfunction, are necessary to be defined as epilepsy (Henry and Van Heertum 2003). Each year, approximately 300,000 individuals develop first time seizures, with 120,000 of these first time seizures occurring in children under the age of 18 years. Most pediatric seizures are febrile in origin and are seen in children under the age of 5 years. Overall, approximately 5% of all individuals in the United States will have at least one seizure during their lifetime (Engel 1989).

3.4.2
Incidence and Prevalence – Epilepsy

Each year, 200,000 new cases of epilepsy are diagnosed with the greatest number of diagnosed cases occurring under the age of 2 and over the age of 65 years. The incidence of epilepsy is somewhat higher in males as compared to females and more likely to occur in socially disadvantaged populations and also in individuals with underlying risk factors such as cerebral palsy or mental retardation. There are approximately 2.7 million individuals, in the United States, who have been diagnosed as having active epilepsy. The overall prevalence of epilepsy increases with age, so that by age 20 years, 1% of the population will have developed epilepsy and by 75 years of age, the percentage of the population diagnosed as having epilepsy increases to 3% (Henry and Van Heertum 2003).

3.4.3
Clinical Diagnosis

Epilepsy is generally classified by brain location and causation/etiology. As defined in the International Classification of Epileptic Seizures, partial seizures are seizures that begin locally and subsequently may or may not remain localized. Generalized seizures, on the other hand, originate symmetrically, in multiple sites, bilaterally and are not localizable. In primary epilepsy, the seizure is the only clinical manifestation of the cerebral malfunction and there is no underlying cause for epileptic seizures apparent. Most other seizures, including most partial seizure disorders, are acquired secondary to some form of acquired cerebral injury (Tikofsky and Van Heertum 2000).

The standard epilepsy workup includes a variety of procedures and tests including video EEG monitoring, neuroimaging, preferably MRI and where necessary depth electrode measurements. While there are a significant number of patients that can be diagnosed when there is concordance of the clinical findings with video EEG and MRI results (Lee et al. 1998), there are, however, also many patients with disparate findings that require additional procedures including neuroimaging with SPECT and PET imaging and, in some instances, magnetic resonance spectroscopy or depth electrode analysis. The patients that benefit the most from surgery are individuals with medically intractable partial-onset seizures arising in the temporal lobe although on occasion extratemporal seizures are amenable to surgical treatment (Duncan 1997).

3.4.4 SPECT Brain Imaging

The optimum brain SPECT method for localizing a seizure focus is to perform ictal and interictal imaging studies, on separate days, followed by subtraction of the co-registered images. This method or some variation is reported to have an accuracy rate in the range of 89–94% (Henry and Van Heertum 2003). Unfortunately, this technique requires a level of logistical co-ordination that many institutions are unable to achieve. In particular, the patient should be observed on a continuous video EEG monitoring system in a seizure disorder unit. The intravenous injection of the SPECT radiotracer should occur in less than 2 min from the time of the seizure so as to ensure that a diagnostic SPECT study, representative of the ictal state, is obtained. The radiotracer must be readily accessible and secured on the unit in a manner that meets the requirements of local, state and federal regulatory agencies responsible for the handling of radioactive materials. In addition, the personnel responsible for injecting the radiotracer must be trained and approved to handle radioactive materials. The requirements for injection of the radiotracer for an interictal SPECT study are logistically demanding; however, it is important that the patient be documented as being seizure-free for at least 24 h prior to injection of the radiotracer. The image patterns observed with these two studies, when performed optimally, although complementary, are very different. The ictal SPECT study reveals a localized area of increased radiotracer activity at the site of the seizure activity that is reflective of the increased rCBF and metabolism present at the time of ictus. On the other hand, the pattern observed on the interictal study is one of a localized decrease in rCBF at the seizure nidus. Secondarily, one may observe additional areas of increased or decreased blood flow related to activation or inhibition of interconnected circuitry and secondary promulgation of the seizure activity (Won et al. 1999).

3.4.5 PET Brain Imaging

FDG-PET brain studies are also utilized to evaluate seizure disorder patients in the interictal state. Similar to interictal SPECT, this technique identifies the interictal seizure focus as an area of focal hypometabolism. Overall, interictal PET is more accurate than interictal SPECT with accuracy rates ranging from 65% to 79% versus 48% to 52% for SPECT (Van Heertum et al. 2004). The improved accuracy with PET, as compared to SPECT, relates, primarily, to improved spatial and contrast resolution of this technique. Interictal PET is

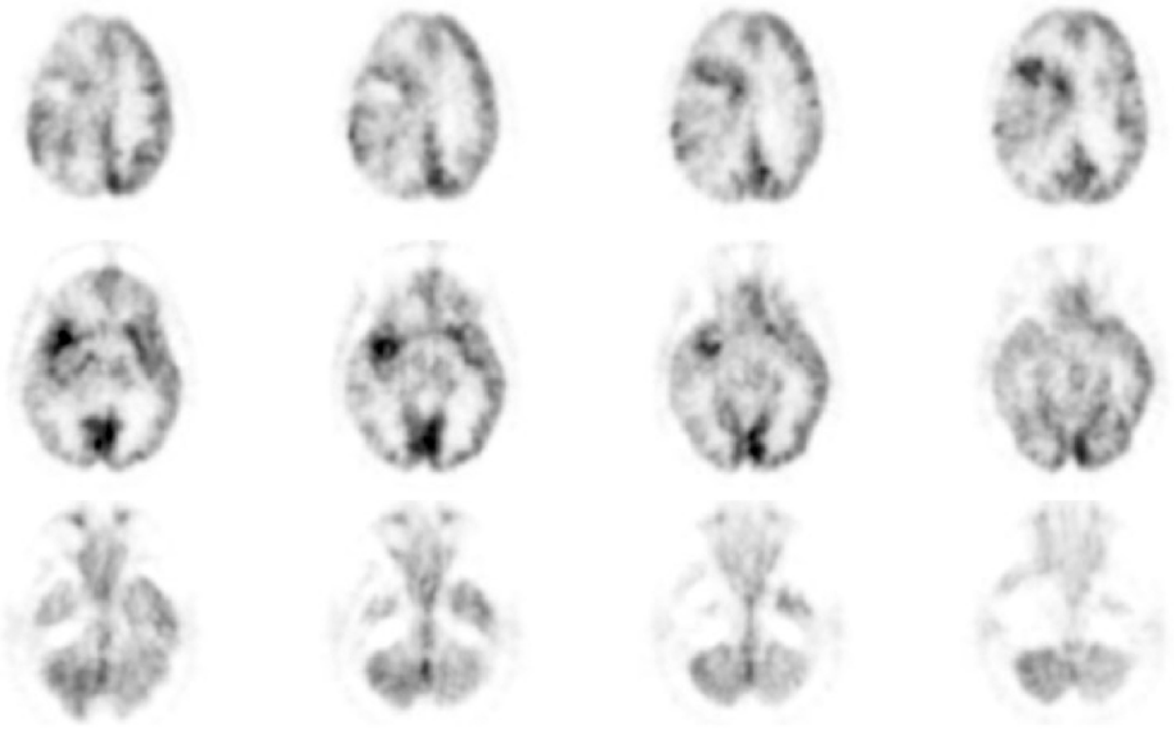

Fig. 3.4. Recurrent right fronto-temporal astrocytoma grade IV post-treatment – FDG-PET images in the transverse plane (superior to inferior) reveal evidence of a large area of mixed hypo- and hypermetabolic foci involving the right posterior frontal lobe and the right anterior to mid temporal lobe consistent with residual viable tumor post treatment

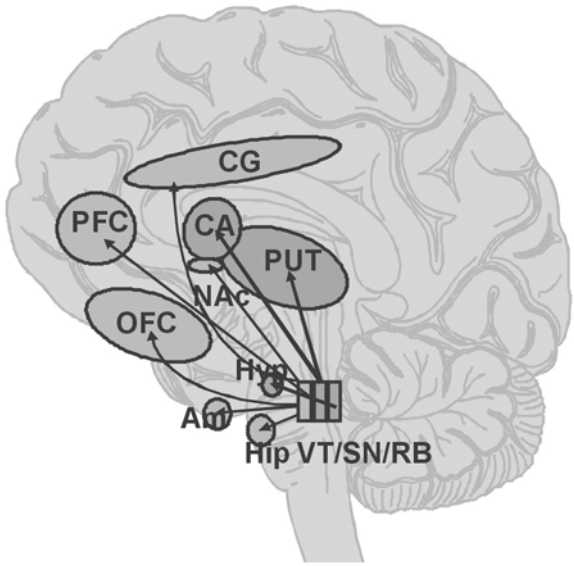

Fig. 3.5. Three major dopaminergic projections, namely, the nigrostriatal, mesolimbic and tuberoinfundibular pathways. *SN* substantia nigra, *VT* ventral tegmentum, *RB* retrobulbar area, *CA* caudate, *PUT* putamen, *NAc* nucleus accumbens, *Hip* hippocampus, *Am* amygdala, *CG* cingulate gyrus, *PFC* prefrontal cortex, *OFC* orbitofrontal cortex, *Hyp* hypothalamus

often utilized as an alternative neuroimaging procedure because it is logistically less demanding than ictal SPECT even though it is a somewhat less accurate technique (Hwanga et al. 2001). Interictal FDG-PET has also been combined with ictal SPECT imaging, with and without digital subtraction techniques, as a means of identifying seizure foci more precisely. At present, it is not clear how this method compares with the standard digital subtraction technique using ictal and interictal SPECT imaging.

In addition to FDG-PET, a number of other neuroreceptor radiotracers have been employed. The most commonly employed neuroreceptor imaging technique employed in the evaluation of epilepsy is the GABA receptor [^{11}C]flumazenil. This compound has been reported by a number of investigators to be a very reliable method for identifying seizure foci. More recently, [^{18}F]5HT$_{1A}$ (WAY) receptor imaging has also been employed for identifying reductions in serotonin receptor sited in seizure foci (Theodore 2004).

3.4.6 SPECT and PET Imaging of the Dopamine System in Movement Disorders

The dopamine system is one of the important neurotransmission systems of the central nervous system. There are three major dopaminergic projections in the brain (Fig. 3.5). The nigrostriatal pathway originates from the substantia nigra in the midbrain and projects onto the striatum that consists of the caudate and putamen; the mesolimbic pathway originates from the ventral tegmentum and projects onto the limbic system including the nucleus accumbens, hippocampus, amygdala, and the limbic cortex; and the tuberoinfundibular pathway originates from the retrobulbar midbrain to the hypothalamus and pituitary gland. These three pathways are involved in the control of movement, emotional behavior and endocrine function, respectively.

PET and SPECT allow quantitative imaging of the dopamine system. They have been used extensively in clinical research to evaluate patients with Parkinson's disease (PD) and other movement disorders such as progressive supranuclear palsy (PSP) and multiple system atrophy (MSA). These conditions are characterized pathologically by progressive degeneration of the dopamine neurons that originate in the substantia nigra and project to the striatum (Fig. 3.5). PET and SPECT imaging using radioligands, as a biomarker of the dopamine system, is a promising tool in the diagnosis and differential diagnosis of movement disorders, measuring disease progression and monitoring the efficacy of neuroprotective therapy in PD.

Currently, multi-center phase II–III clinical trials for SPECT radioligands that target the dopamine transporter (DAT) (Fig. 3.2) such as [^{123}I]altropane and [^{99m}Tc]TRODAT-1 are under way in North America to evaluate the diagnostic utility of these radioligands for

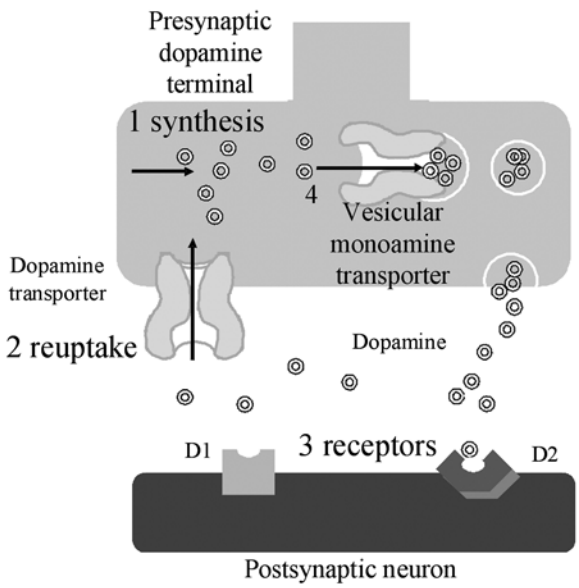

Fig. 3.6. Illustration of the dopamine synapse. There are four different kinds of PET or SPECT radioligands that reflect or bind to: *1* dopamine synthesis, *2* dopamine reuptake sites (dopamine transporter), *3* dopamine receptors and *4* monoamine reuptake or transporter sites. For specific radioligands, see Table 3.1

Table 3.1. Radioligands for PET and SPECT imaging of the dopamine system

	Target site	PET	SPECT
Presynaptic	1. Synthesis	[^{18}F]FDOPA	–
	2. Dopamine transporter	[^{11}C]cocaine, [^{11}C]methylphenidate, [^{11}C]WIN-35, 428	[^{123}I]β-CIT, [^{123}I]FP-CIT, [^{123}I]altropane,
	4. Monoamine transporter	[^{11}C]DTBZ	[^{99m}Tc]TRODAT-1
Postsynaptic	3. Receptors	–	–
	D_1	[^{11}C]SCH 23390, [^{11}C]NNC 112	–
	D_2	[^{11}C]raclopride, [^{11}C]FLB 457, [^{18}F]fallypride	[^{123}I]IBZM, [^{123}I]IBF, [^{123}I]epidepride

movement disorders. These agents therefore are expected to be in clinical use in the near future. In Europe, another SPECT DAT radioligand, [^{123}I]FP-CIT or DATSCAN, and a dopamine D_2 receptor SPECT radioligand, [^{123}I]IBZM, have been commercially available for clinical use for some time.

Many PET and SPECT radioligands have been developed for imaging of either pre- or post-synaptic components of the dopaminergic system (Fig. 3.6, Table 3.1). [^{18}F]FDOPA is a PET marker for dopamine synthesis. [^{18}F]FDOPA is converted by the aromatic amino acid decarboxylase (AADC) to [^{18}F]dopamine, which becomes trapped within the presynaptic dopamine neuron (Brooks 1998). The type 2 vesicular monoamine transporter (VMAT2) in the presynaptic dopamine and other monoaminergic neurons pumps newly synthesized or recovered monoamines into the synaptic vesicles. [^{11}C]DTBZ binds to VMAT2 on the presynaptic vesicles containing not only dopamine but also those containing serotonin and histamine (Frey et al. 1996). After release into the synapse, excess dopamine is removed from the synapse via reuptake sites (also called dopamine transporters or DAT) located on the presynaptic dopamine nerve terminals. Several cocaine-derived radioligands that bind to DAT have been developed for use with both PET and SPECT (Table 3.1). Particularly, SPECT DAT radioligands such as [^{123}I]β-CIT (Marek et al. 1996), [^{123}I]FP-CIT (Benamer et al. 2000a), [^{123}I]altropane (Fischman et al. 1998) and [^{99m}Tc]TRODAT-1 (Mozley et al. 2000) have been extensively employed in clinical research.

SPECT imaging with [^{123}I]β-CIT is usually done at 18–24 h after bolus injection of the tracer. With [^{123}I]FP-CIT, [^{123}I]altropane and [^{99m}Tc]TRODAT-1, a diagnostic scan can be performed within several hours of tracer injection, although the striatum-to-cerebellum uptake ratio is lower and time-dependent compared with [^{123}I]β-CIT. Figure 3.7 shows examples of SPECT images with different DAT radioligands in normal subjects and patients with Parkinson's disease as well as [^{18}F]FDOPA images in comparison.

For [^{18}F]FDOPA, an influx rate constant, K_i, is used as a measure of [^{18}F]FDOPA uptake. As a measure of transporter or receptor density, however, binding potential (BP) is estimated by calculating the ratio: (striatum-cerebellum)/cerebellum at equilibrium. BP is higher if the transporter (receptor) density (B_{max}) or the affinity is higher and BP is also higher if the nonspecific binding of the radioligand is lower (Ichise et al. 2001).

The three types of presynaptic radioligands, namely, [^{18}F]FDOPA (reflecting the AADC activity), [^{11}C]DTBZ (reflecting the vesicular monoamine density) and, for example, [^{99m}Tc]TRODAT-1 (reflecting DAT density) have been used as a marker for the dopamine neurons that degenerate in PD and other movement disorders such as PSP and MSA. Uptake of these radioligands generally correlates with the nigral dopamine neuron cell count (Snow et al. 1993). However, when synaptic dopamine concentrations are decreased due to loss of dopamine neurons, the AADC activity or [^{18}F]FDOPA uptake might be increased (upregulated) while DAT radioligand binding might be decreased (downregulated). On the other hand, VMAT2 is said to be free from regulations by changes in endogenous dopamine, although [^{11}C]DTBZ is not a specific marker for the dopamine neuron (Lee et al. 2000).

On the post-synaptic side, there are two classes of dopamine receptors: D_1-like receptors (D_1 and D_5) and D_2-like receptors (D_2, D_3 and D_4). The D_1-like receptors interact with G-proteins called Gs complexes resulting in the activation of adenylate cyclase, whereas D_2-like receptors interact with Gi complexes to inhibit this enzyme. Table 3.1 lists radioligands for PET imaging of D_1 and D_2 receptors and SPECT imaging of D_2 receptors.

3.4.7 Diagnostic Utility of Dopamine PET and SPECT

Patients with signs and symptoms of parkinsonism (tremor, rigidity, bradykinesia, and postural and gait disturbances) may have PD or any one of a number of other central nervous system disorders such as PSP, MSA, essential tremor, vascular parkinsonism, drug-induced parkinsonism and Alzheimer's disease. The accurate diagnosis of PD is essential for deciding on

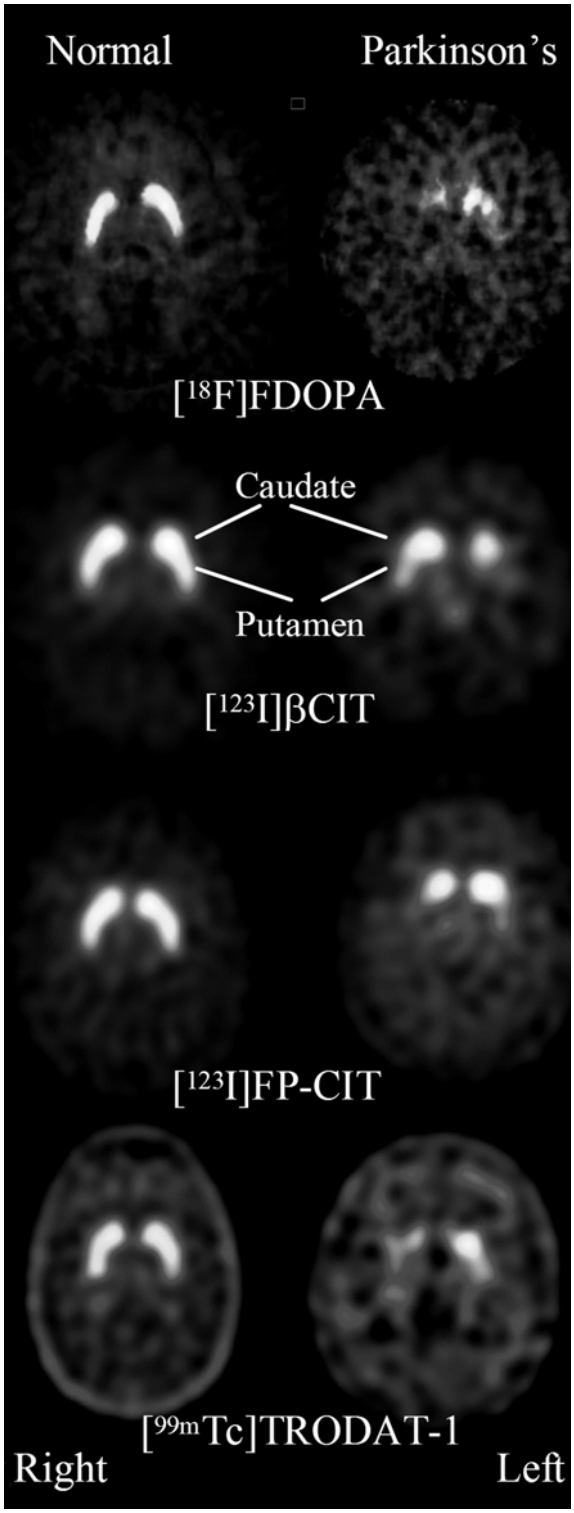

Fig. 3.7. [^{18}F]FDOPA PET images (parametric images of influx rate constant, K_i) and dopamine transporter (DAT) SPECT images using [^{123}I]β-CIT (24 h post injection), [^{123}I]FP-CIT (4 h post injection) and [^{99m}Tc]TRODAT-1 (3 h post injection) of normal controls (*left column row*) and Parkinson's disease patients (*right column*). In both columns, scans shown are from different normal individuals and Parkinson's disease patients

practical approaches to treatment as well as providing the patient and family some indication of prognosis. The most widely accepted clinical diagnosis of PD requires the presence of two of three cardinal motor signs (tremor, rigidity, and bradykinesia) and a response to L-dopa. Typically, the period of clinical observation before the rendering of a final diagnosis of PD extends over several months. However, up to 24% of cases with an ante-mortem clinical diagnosis of typical PD may have other diseases at postmortem examination (Hughes et al. 1992). Conversely, patients with atypical clinical features may turn out to have typical pathological findings of PD (Hughes et al. 1992).

Figure 3.7 (right column) shows typical reductions of striatal [^{18}F]FDOPA uptake and DAT binding with three different DAT radioligands, [^{123}I]β-CIT, [^{123}I]FP-CIT and [^{99m}Tc]TRODAT-1 in different PD patients. The reductions in striatal radioligand uptake in PD patients have shown two topographic characteristics: radioligand uptake in the striatum contralateral to the clinically more affected side is reduced more compared with the ipsilateral side and radioligand uptake is reduced more in the putamen than in the caudate (Seibyl et al. 1995; Marek et al. 1996; Ichise et al. 1999a, 1999b). These findings are consistent with those of pathological studies of PD; degeneration of nigrostriatal neurons usually progresses asymmetrically in two ways; either right or left side is more severely involved and the ventrolateral substantia nigra projecting to putamen degenerates more severely than the ventromedial substantia nigra projecting to caudate (German et al. 1989; Fearnley and Lees 1991). Reductions in putamen DAT binding show an inverse correlation with limb bradykinesia and rigidity in PD but not with rest tremor severity (Benamer et al. 2000b). In addition, dopamine transporter SPECT may be sensitive enough to detect subclinical involvement of dopamine projections in PD (Marek et al. 1996) because 40–50% losses of these projections are said to have occurred before PD patients develop parkinsonian symptoms (Fearnley and Lees 1991). In fact, hemi-PD patients, who represent the great majority of patients at initial presentation, demonstrate bilateral changes in brain imaging assessments of presynaptic dopaminergic function. Insofar as these patients go on to develop bilateral symptoms, the changes evident in brain imaging are noted prior to the manifestation of symptoms on that side of the body.

All of the presynaptic PET and SPECT radioligands discussed here differentiate clinically probable early PD from normal subjects or essential tremor patients with sensitivity over 90% and specificity of 83–100% (for recent reviews see Fischman 2005; Seibyl 2003; Marshall and Grosset 2003; Brooks 2004; Ravina et al. 2005). A positive PET or SPECT presynaptic scan thus supports a diagnosis of PD when there is diagnostic doubt clinically. For example, Jennings et al. (2004) re-

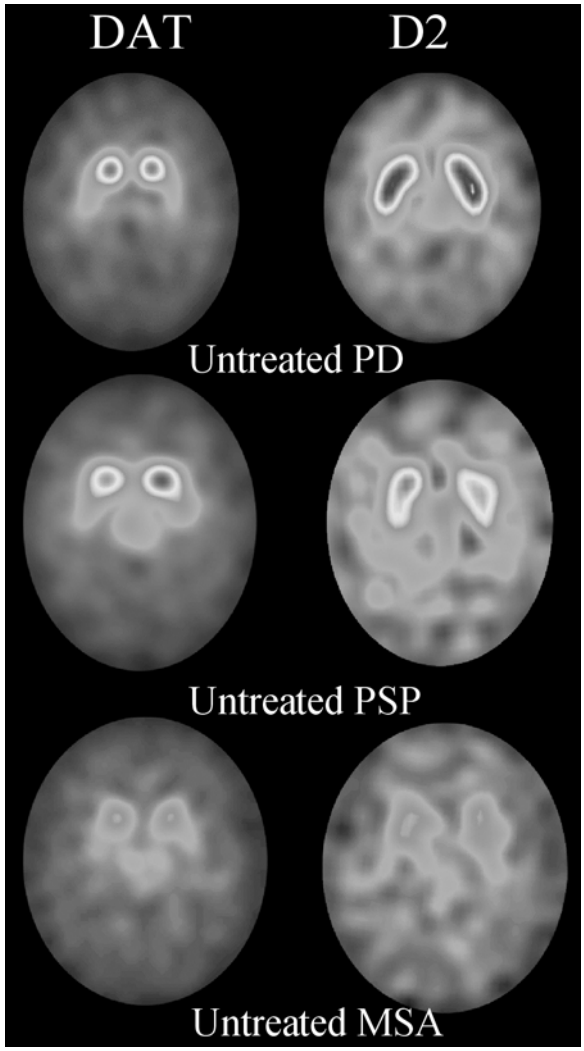

Fig. 3.8. Presynaptic dopamine transporter (DAT) images with [^{123}I]β-CIT (*left column*) and postsynaptic dopamine D_2 receptor images with [^{123}I]IBF (*right column*) in patients with untreated Parkinson's disease (PD) (*top row*), progressive supranuclear palsy (PSP) (*middle row*) and multiple system atrophy (MSA) (*bottom row*), respectively

cently evaluated the diagnostic accuracy of [^{123}I]β-CIT SPECT imaging in patients with suspected parkinsonian syndrome (PS). Diagnoses in question included essential tremor, psychogenic parkinsonism, drug-induced parkinsonism, primary dystonia, and unspecified gait disorder. When compared with the judgment of an expert movement disorders clinician 6 months after the initial visit, quantitative [^{123}I]β-CIT SPECT imaging showed 92 % sensitivity and 100 % specificity for PS in 35 subjects. Performing DAT imaging at baseline therefore appears to be a useful diagnostic tool to detect patients thought to have PS at baseline but who, after follow-up, do not have PS. Currently, several large-scale multi-center clinical trials are being carried out in North America to evaluate the diagnostic utility of DAT SPECT imaging using a similar study design to that of Jennings et al. (2004).

Dopamine neurons also degenerate in other parkinsonian syndromes such as MSA and PSP. Although the regional asymmetry or unevenness of DAT radioligand or [^{18}F]FDOPA distribution characteristically found in PD is said to be lacking in these parkinsonian syndromes (Otsuka et al. 1991), none of the presynaptic imaging techniques can reliably differentiate between these conditions. Here, PET/SPECT imaging studies designed to evaluate the postsynaptic dopamine D_2 receptor have shown that striatal dopamine D_2 receptor binding is intact in PD but it can be reduced in MSA and PSP and other movement disorders such as Huntington's disease (Ichise et al. 1993, 1999b; van Royen et al. 1993; Schwartz et al. 1992; Buck et al. 1995; Brooks et al. 1992) (Fig. 3.8). D_2 receptors may be upregulated in patients with untreated PD (Ichise et al. 1999b). On the other hand, in treated PD patients, striatal D_2 sites are either normal or reduced (Kim et al. 2002; Brooks et al. 1992), reduced levels occurring particularly in chronically treated patients who have developed a fluctuating response to therapy. Thus, the knowledge obtained from postsynaptic scans about the status of D_2 receptors in patients with parkinsonism can predict therapy response to dopamine agonists because these drugs require intact D_2 receptors to be effective (Schwarz et al. 1992). Additionally, [^{18}F]fluorodeoxyglucose ([^{18}F]FDG) PET as well as MRI can be helpful in distinguishing these conditions, the latter showing abnormal putamen and pontine signal on T2 or diffusion-weighted images (Antonini et al. 1997, 1998; Eidelberg et al. 1993; Schultz et al. 1999; Seppi et al. 2003).

3.4.8 PET and SPECT as a Biomarker of Disease Progression

PET and SPECT presynaptic radioligands described here are a biomarker of certain components of the dopamine neurotransmission. Therefore, these radioligands can potentially be used as a "state" marker, which should allow objective monitoring of disease progression in vivo in patients with PD and other parkinsonian syndromes. However, for these imaging techniques to provide valid estimates of disease progression, several factors need to be considered. First, the imaging technique must be highly reproducible; with [^{18}F]FDOPA PET and DAT SPECT, the test/retest reproducibility is excellent (test/retest variability < 10 %) (Marek et al. 1996; Brooks 2004). Second, PET and SPECT measurements should not be influenced by dopaminergic medications. In animal models, supratherapeutic doses of dopaminergic medications in time-limited studies have shown regulation of presynaptic target sites. The relevance of these studies to hu-

man imaging of these targets sites remains unclear, and controlled human imaging studies of sufficient subject number are just now being conducted. In fact, the overwhelming majority of the few small human trials which have looked at this issue have not demonstrated regulation of presynaptic target sites by dopaminergic (L-dopa or dopamine agonists) medications in PD (Innis et al. 1999; Ceravolo et al. 2002; Turjanski et al. 1999). Finally, [^{18}F]FDOPA and DAT radioligands may overestimate and underestimate, respectively, the terminal dopamine neuron density as the nigral cell loss progresses. With these caveats, [^{18}F]FDOPA PET and DAT SPECT studies have shown that the rate of decline of [^{18}F]FDOPA uptake or DAT binding in the putamen is faster at ~10% per year in PD patients on L-dopa than in healthy subjects at ~1% per year (Seibyl 2003; Brooks 2004).

PET and SPECT imaging of the presynaptic nigrostriatal dopamine system as a "state" marker of PD may have then the potential to be used in clinical trials of putative neuroprotective therapy to monitor its efficacy. For example, two clinical trials, CALM-PD CIT (Parkinson Study Group 2002) and REAL-PET (Whone et al. 2003), recently used [^{123}I]β-CIT and [^{18}F]FDOPA, respectively, to assess the disease modifying potential of the dopamine agonists, pramipexole in the former and ropinirole in the latter, as compared with L-dopa in early PD patients treated with the respective medications. In the CALM-PD CIT, after 46 months, there was a one-third reduction in the relative rates of decline of [^{123}I]β-CIT binding in the agonist (pramipexole)-treated group. Similarly, in the REAL-PET, there was also a one-third reduction in the rate of decline of [^{18}F]FDOPA uptake in the agonist (ropinirole) group over the L-dopa group at as early as 24 months, suggesting the neuroprotective potential of the agonists over L-dopa. Interestingly in both studies, however, clinical measures of PD severity, quality of life and global function were better in the L-dopa group than in the agonist groups. The discrepancy between imaging measures and clinical measures in the evaluation of disease progression may be due to the fact that many medications being evaluated as "disease-modifying" are also potent symptomatic treatments which cannot be completely washed out. Hence, for L-dopa, it has been suggested that a washout on the order of several months may be necessary to truly evaluate a PD patient's native illness. The interpretation of the REAL-PET and the CALM-PD studies is confounded by the lack of a placebo control. Therefore, it appears difficult to definitively conclude that DA agonists are protective or L-dopa toxic, some combination of these, or there is another explanation entirely. There is a distinction between imaging as surrogate marker or primary endpoint in clinical trials and biomarkers as adjunctive endpoints (Ravina et al. 2005). It is sometimes useful to stress the fact that imaging data may be best seen as complementary to the clinical data, interrogating the system at a different point than a clinical assessment and hence providing different information.

3.5 SPECT and PET Imaging of the Dopamine System in Psychiatric Disorders

Despite being of limited diagnostic utility in psychiatric disorders, PET and SPECT imaging techniques of neurotransmission systems have been shown to be a valuable research tool to further our understanding of the pathophysiological mechanisms of important psychiatric disorders such as schizophrenia, depression and substance abuse (Parsey and Mann 2003; Frankle and Laruelle 2002; Devous 2005; Volkow et al. 2003). Furthermore, these techniques can play an essential role in understanding drug action and new drug development in psychiatry (Brooks 2005; Talbot and Laruelle 2002). In addition to imaging the dopamine system, recent advances in radioligand developments have increasingly allowed imaging of other neurotransmission systems, particularly the serotonin (5-HT) system, which is thought to be implicated in the pathophysiology of several psychiatric disorders.

Radioligands designed to image the 5-HT system as in the case for the dopamine system are classified into presynaptic imaging of the serotonin transporter (SERT) and 5-HT synthesis, and post-synaptic 5-HT receptors, although 5-HT$_{1A}$ receptors are found on both the presynaptic 5-HT cell bodies autoreceptors) and post-synaptic neurons. Table 3.2 lists several radioligands developed for imaging of the 5-HT system. PET imaging with [^{11}C]DASB for example allows quantitative imaging of the detailed regional distribution of SERT in human and animal brains (Fig. 3.9). Recent advances in radioligand developments expand the feasibility of studying other neurotransmission systems relevant to psychiatric disorders, for example, substance P/NK1 receptors ([^{18}F]SPARQ), $\alpha_4\beta_2$ nicotinic receptors ([^{123}I] or [^{18}F]A-85380) and muscarinic M_2 receptors ([^{18}F]FP-TZTP).

Table 3.2. Radioligands for PET and SPECT imaging of the serotonin (5-HT) system

	Target site	PET	SPECT
Presynaptic	Synthesis	[^{11}C]methyl-tryptophan	–
	Serotonin transporter	[^{11}C]DASB, [^{11}C]McN 5652	[^{123}I]β-CIT, [^{123}I]ADAM
Postsynaptic	Receptors	–	
	5-HT$_{1A}$	[^{11}C]WAY, [^{18}F]FCWAY	–
	5-HT$_{2A}$	[^{18}F]altanserin	-

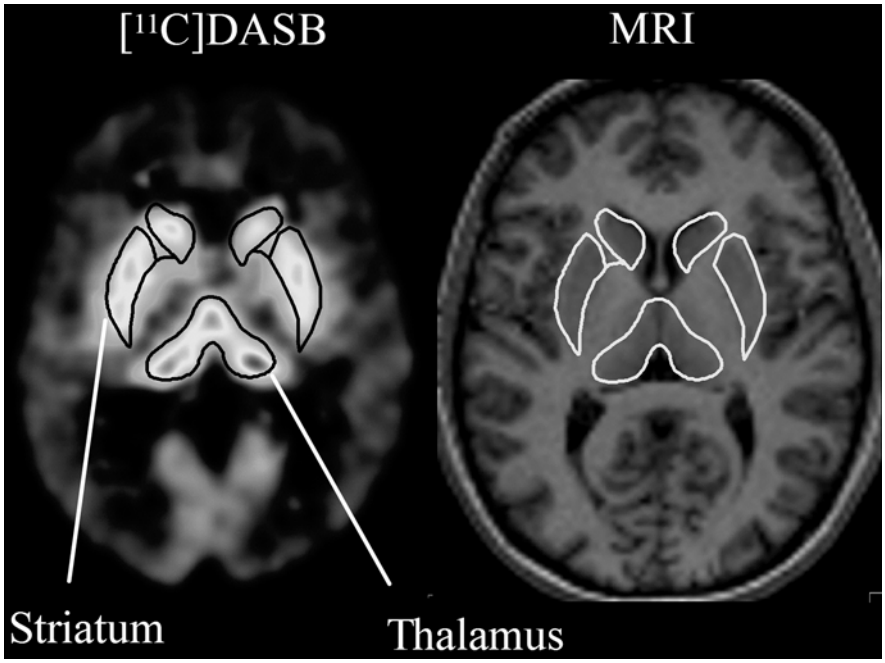

Fig. 3.9. Transaxial [^{11}C]DASB binding potential (*BP*) image (*left*) and coregistered magnetic resonance image (MRI) (*right*) with anatomically defined regions of interest templates placed over the striatum and thalamus. The serotonin transporter *BP* image was generated by voxel-wise fitting of dynamic [^{11}C]DASB PET data (Ichise et al. 2003)

3.5.1 PET and SPECT as a Tool to Understand Pathophysiology

The dopamine system has been closely linked to the pathophysiology of schizophrenia. Here, the mesolimbic dopamine pathway as opposed to the nigrostriatal pathway (Fig. 3.1) plays an important role in psychiatric disorders. Recent evidence from PET imaging studies of the dopamine system in schizophrenia suggests that dopamine D_1 receptor availability is increased in the prefrontal cortex due to a compensatory upregulation secondary to sustained deficiency of tonic release of mesocortical dopamine. This dopamine deficiency in the limbic system appears responsible for negative symptoms of schizophrenia including impairments of working memory (Abi-Dargham et al. 2002). On the other hand, dopamine D_2 PET studies to examine extrastriatal D_2 receptor sites with [^{11}C]FLB 457 have shown decreased dopamine D_2 receptor binding in the anterior cingulate cortex, where decreased D_2 binding correlated negatively with positive symptoms of schizophrenia (Suhara et al. 2002). These findings support the hypothesis that there is dysregulation of dopamine release in schizophrenia such that while tonic dopamine release is decreased, phasic release of mesocortical dopamine is increased. The latter findings are also consistent with the findings of dopamine D_2 receptor imaging studies that have shown that patients with schizophrenia show abnormally increased release of dopamine in response to amphetamine challenge (Laruelle 2005).

In major depression, abnormal 5-HT transmission has been linked to its pathophysiology. SERT is found on the 5-HT cell bodies in the raphe complex and on the 5-HT nerve endings in the striatum, thalamus, hypothalamus, amygdala and limbic cortical regions (Fig. 3.9). SERT is a critical modulator of 5-HT neurotransmission, a marker of serotonergic innervations and the site of action of commonly used antidepressant drugs, selective serotonin reuptake inhibitors (SSRIs). Therefore, in vivo imaging of the SERT has been of intense interest as a tool to study 5-HT function in psychiatric disorders. PET and SPECT imaging studies using these [^{11}C]McN5652 and [^{123}I]β-CIT have shown decreased SERT binding in the raphe, midbrain, amygdala, and ventral striatum (Parsey and Mann 2003). However, [^{123}I]β-CIT also binds to DAT, and [^{11}C]McN5652 shows regionally different degrees of nonspecific binding. Furthermore, limbic cortical SERT binding with [^{11}C]McN5652 cannot be reliably estimated due to low specific signals in the cortex. [^{11}C]DASB is a recently developed PET radioligand for SERT imaging. [^{11}C]DASB allows accurate quantitative voxel-wise parametric imaging of SERT binding (Fig. 3.5) (Ichise et al. 2003).

In addition to SERT, 5-HT receptors play a pivotal role in 5-HT neurotransmission. For example, therapeutic actions of SSRIs are related to the initial inhibition of 5-HT_{1A} receptors on the cell body of 5-HT neurons in the raphe (presynaptic autoreceptors) that subsequently leads to enhanced 5-HT transmission at the target sites (hippocampus) involving peripheral 5-HT_{1A} receptors (postsynaptic receptors). PET studies of 5-HT_{1A} receptors have found decreased 5-HT_{1A} binding in the mid brain and hippocampus in patients with

major depression (Parsey and Mann 2003). Decreased 5-HT_{1A} binding is consistent with the findings of animal models of chronic stress, where hypercortisolism as a result of prolonged stressful events is known to cause neuronal damage particularly in the hippocampus. Corticosteroids or exposure to chronic unpredictable stress in rats reduces 5-HT_{1A} mRNA, and 5-HT_{1A} receptor number, in the hippocampus.

In substance abuse research, many PET and SPECT imaging studies, particularly those conducted by Volkow and colleagues at the Brookhaven National Laboratory, have made an enormous contribution to our understanding of the pathophysiological brain mechanisms of substance abuse (Volkow et al. 2003, 2004). These investigators have focused on imaging of the dopamine system, because drugs of abuse such as cocaine, methamphetamine, nicotine and methylenedioxymethamphetamine (MDMA, ecstasy) all directly or indirectly increase brain dopamine. Dopamine is involved in the regulation and motivation of behaviors that are indispensable for survival (see the mesolimbic dopamine pathway in Fig. 3.1). However, the ability of drugs of abuse to increase dopamine by itself does not explain the process of addiction. Here, PET studies have consistently shown long lasting decreases in dopamine D_2 receptors in cocaine abusers, for example. PET studies in cocaine abusers also show significant reductions in dopamine release in response to a stimulant challenge. This led to the hypothesis that decreases in brain dopamine D_2 receptors coupled with decreases in dopamine release could result in an understimulation of reward circuits which could put subjects at greater risk for seeking drug stimulation as a means to compensate for this deficit and to temporarily activate these reward circuits. These findings reported in cocaine-addicted subjects generalize to other addictions such as alcoholics, heroine abusers and methamphetamine abusers. Currently research in substance abuse is being expanded to delineate the unique differences among the various drugs of abuse. For example, ecstasy (MDMA) not only increases brain dopamine but also serotonin (5-HT). Recent SERT PET studies suggest that ecstasy may cause acutely widespread reductions in central SERT binding sites. This acute neurotoxic effect of ecstasy, however, is reversible after withdrawal (Thomasius et al. 2003; Buchert et al. 2004).

3.5.2 PET and SPECT in Drug Action and Development of New Drugs

PET and SPECT imaging of neuroreceptors and transporters has been used to study antipsychotic or antidepressant drug action by examining the relationship between neuroreceptor or transporter occupancy of psychiatric drugs and clinical response. Although it is still not fully clear what level of receptor binding is required to achieve the minimum clinically effective therapeutic response, occupancy of over 70 % is generally recommended for D_2 antagonists. However, atypical neuroleptics, such as clozapine, are clinically effective when only occupying 50 % of D_2 receptors (Brooks 2005; Talbot and Laruelle 2002). Similarly, minimum therapeutic doses of antidepressants (SSRIs) occupy 80 % of central SERT binding sites according to a recent [^{11}C]DASB PET study (Meyer et al. 2004). Here, the drug occupancy refers to the percentage of receptor sites occupied by a drug with a particular dosing regimen.

In the development of novel drugs for psychiatric illnesses, pharmaceutical companies have been frequently employing PET and SPECT imaging techniques (Brooks 2005; Talbot and Laruelle 2002). One such way is to determine the dose-occupancy profiles of novel drugs using existing radioligands and so help guide dose selection for phase I and II trials. Another way of making use of PET imaging in drug development involves microdosing techniques where multiple candidate drugs are prepared as radioligands (by usually [^{11}C]-labeling) and tested simultaneously. Because subpharmacological doses are being administered (< 20 μg) on only one or two occasions, the toxicology requirements for administration of these novel radiotracers in man are less stringent than for pharmacological drugs. PET can then assess the plasma, regional brain, and other organ pharmacokinetics in man ahead of therapeutic trials. Thus, phase I studies in drug development allow for the assessment of the penetration of investigational agents across the BBB in humans and determination of the selectivity of binding to the appropriate target. Also, it is important to stress that screening out of candidate agents is important from a financial perspective, that is, killing a drug in phase I prior to initiation of costly phase II studies is a useful outcome of phase I microdosing studies.

3.6 Brain Death Scintigraphy

Brain death is defined as the irreversible loss of all brain and brainstem functions including the capacity to breathe, even though the heart continues to beat and spinal functions may persist. The concept that brain death is equivalent to death of the individual has been widely accepted, although discussions of brain death continue not without reference to metaphysical, cultural, religious, legal and medical implications (Engelhardt 1999). In the United States, this concept of brain death is the basis of the Uniform Determination of Death Act (1993, 1997), and every jurisdiction in the US has come to accept neurological criteria to define death (Wijdicks 2001; Morenski et al. 2003).

The diagnosis of brain death requires demonstration of the irreversible cessation of cerebral hemispheric and brain stem function. The diagnosis of brain death is primarily clinical (apnea, deep coma, loss of all brain stem reflexes). Irreversibility of this condition is confirmed by repeated examinations. The American Academy of Neurology (1995) now recommends an observation period of 6 h for uncomplicated cases in adults. The duration of observation between examinations of brain death for pediatric patients is based on age and varies accordingly (12–48 h). For further details on the clinical diagnostic criteria and neurologic examinations of brain death, the reader is referred to the excellent reviews by Wijdicks (2001) and Morenski et al. (2003).

Confirmatory tests including cerebral angiography, brain scintigraphy, electroencephalography (EEG) and transcranial Doppler can be used to confirm the irreversibility of brain death in the presence of confounding factors such as hypothermia or drug intoxication, especially when the clinical history is unknown. Of the confirmatory tests, cerebral angiography and transcranial Doppler can assess only larger intracranial vessels, the former may damage potential donor organs for transplantation, and EEG findings may be equivocal in the presence of centrally acting drugs. Brain scintigraphy on the other hand is safe, reliable, and widely available, and it is not affected by centrally acting drugs such as the barbiturates. In particular, brain scintigraphy with lipophilic tracers such as [^{99m}Tc]HMPAO (hexamethylpropylene amine oxime) and [^{99m}Tc]ECD (ethyl cysteinate dimer) that cross the intact blood brain barrier and are retained in the brain has the advantage of demonstrating absence or presence of brain parenchymal perfusion. An unequivocally positive radionuclide brain scan can shorten an observation period between examinations of brain death to as little as 2 h (Morenski et al. 2003; Newberg et al. 2002).

The procedure guideline for brain death scintigraphy published by the Society of Nuclear Medicine (Donohoe et al. 2003) states that there is no clear evidence that brain-specific tracers such as [^{99m}Tc]HMPAO and [^{99m}Tc]ECD are more accurate than traditional nonspecific agents such as [^{99m}Tc]DTPA (diethylene-triamine-penta-acetic acid). However, brain scintigraphy with brain-specific agents can be interpreted independently of the quality of the bolus injection and delayed planar or tomographic images can be interpreted in a straightforward manner without any confusing situations that can occasionally occur with images obtained with non-diffusible tracers, for example, due to jugular and sagittal sinus reflux (Lee et al. 1987).

Complete absence of brain perfusion on brain scintigraphy with [^{99m}Tc]HMPAO or [^{99m}Tc]ECD ("hollow skull sign," Abdel-Dayem et al. 1989) is diagnostic of brain death (Fig. 3.10). To date, no false positive test results have been reported (Morenski et al. 2003; Newberg et al. 2002). However, partial perfusion in the cerebrum or more commonly in the cerebellum may be found in patents with a clinical diagnosis of brain death. For example, Kurtek et al. (2000) reported [^{99m}Tc]HMPAO scan findings in 23 patients who satisfied their clinical criteria of brain death. Of these, 19 patients showed complete absence of brain perfusion while four patients showed varying degrees of perfusion in the cerebrum and cerebellum. However, repeat scans within 24 h showed complete absence of brain perfusion in these four patients. Brain scintigraphy can also be easily performed in children. However, Conrad and Sinha (2003) in their review article warn that the number of cases currently published with lipophilic tracers in the pediatric age group is relatively small and an understanding of the age related maturity pattern of brain perfusion is essential to avoid errors of interpretation.

In summary, the diagnosis of brain death is primarily clinical. Brain scintigraphy is an important confirmatory test of brain death that can be used to shorten an observation time in the presence of confounding factors especially when the clinical history is unknown. Brain scintigraphy with [^{99m}Tc]HMPAO or [^{99m}Tc]ECD appears the method of choice for scintigraphic diagnosis of brain death at many centers (Morenski et al. 2003; Newberg et al. 2002; Spieth et al. 1994, 2004; Kurtek et al. 2000). For details on the methodology of brain death scintigraphy, the reader is referred to the procedure guideline mentioned above and an excellent review article by Conrad and Sinha (2003).

3.7 Radionuclide Cerebrospinal Fluid Flow Studies

The nuclear imaging approach is an optimal method for the assessment of cerebrospinal fluid (CSF) flow dynamics. The principal technique utilized, for observing CSF flow, is radionuclide cisternography. Radionuclide cisternography is primarily used to track CSF flow from the region of the lower level lumbar spine up to the convexity of the brain where CSF is reabsorbed (Alzaracki et al. 1973). Under normal conditions, CSF is secreted by the choroid plexus located in the lateral ventricles, into the intraventricular system. The CSF then flows out of the ventricular system into the intrathecal space surrounding the brain and spinal cord. The normal pattern of CSF flow, after leaving the ventricles, is both into the spinal canal and around the brain. CSF flows retrograde from the spinal canal to the basilar cisterns, through the sylvian fissures and over the convexity of the brain where it is absorbed in the arachnoid villi located in the parasagittal regions (Schossberger and Touya 1976).

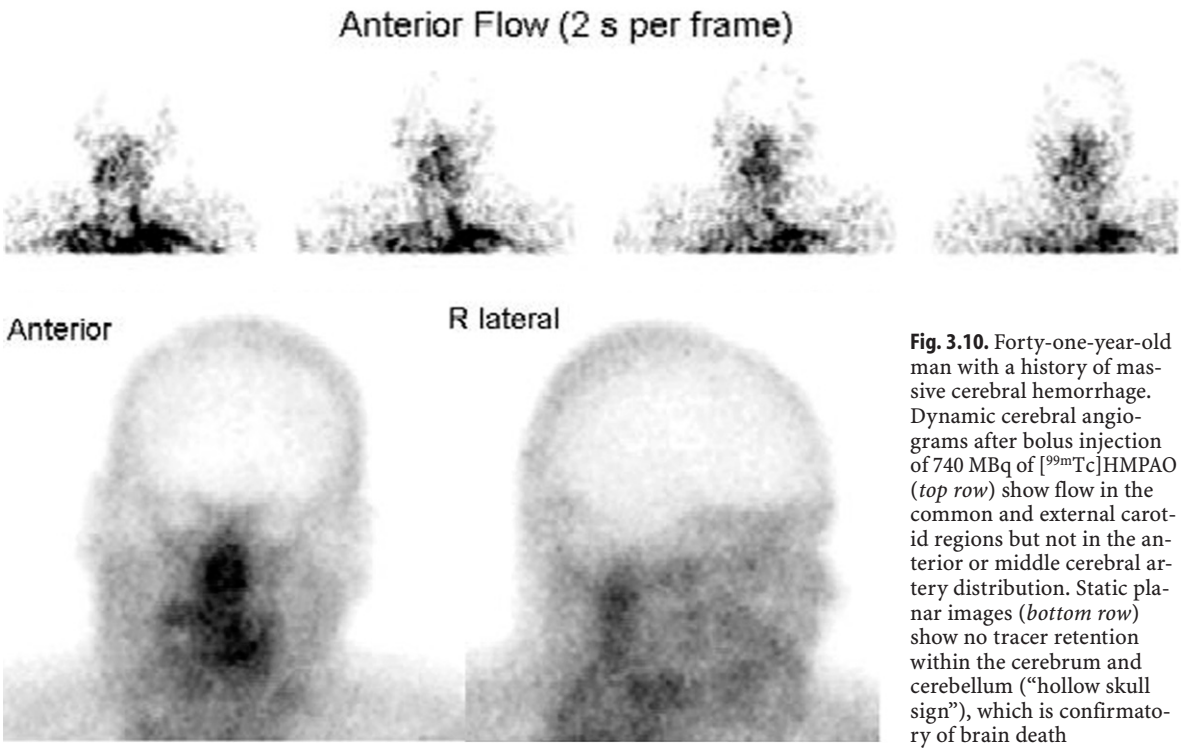

Fig. 3.10. Forty-one-year-old man with a history of massive cerebral hemorrhage. Dynamic cerebral angiograms after bolus injection of 740 MBq of [^{99m}Tc]HMPAO (*top row*) show flow in the common and external carotid regions but not in the anterior or middle cerebral artery distribution. Static planar images (*bottom row*) show no tracer retention within the cerebrum and cerebellum ("hollow skull sign"), which is confirmatory of brain death

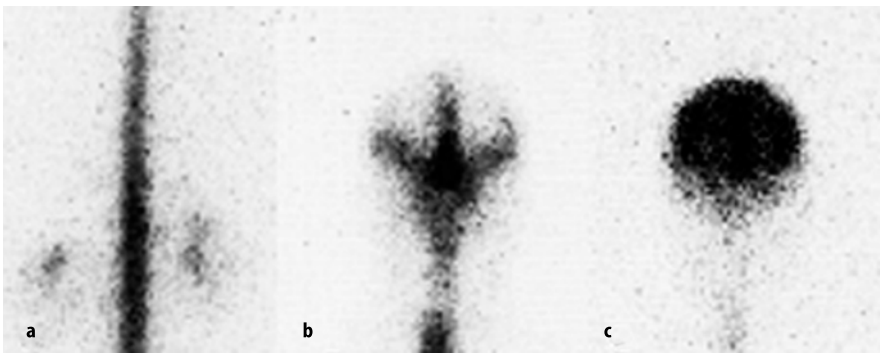

Fig. 3.11. Normal CSF flow pattern: Images at 2 h (**a**) reveal radiotracer, in CSF, ascending up the thoraco-lumbar spinal canal; at 6 h (**b**) the radiotracer is in the basilar cisterns and at 24 h (**c**) the radiotracer is being reabsorbed in the arachnoid villi at the convexity of the brain

Radionuclide cisternography involves the injection of radiotracer into the intrathecal space usually at the level of the lumbar spine. ^{111}In-DTPA is the most commonly used radiopharmaceutical. The typical dose, which is prepared in a small volume of less than 1 ml, approximates 18.5 MBq. The dose is administered using a small gauge spinal needle so as to avoid leakage back over the injection needle tract. Following administration of the radiotracer, the retrograde passage of CSF is tracked using the gamma camera. Typically, the radiotracer arrives at the level of the basilar cisterns by 4 h and then progresses around the brain by two pathways. The sylvian fissure is the major flow pathway with a proportionately lesser amount of CSF flow occurring directly anteriorly and posteriorly up to convexities where CSF re-absorption occurs by 24 h (Fig. 3.11). The usual imaging times are at 4–6, 24 and, if necessary, 48 h. Under normal circumstances, there is no evidence of retrograde CSF flow into the ventricles (Schossberger and Touya 1976).

There are, however, a number of CSF flow patterns that are viewed as borderline types of flow patterns. These pathways, through a number of compensatory mechanisms, maintain a normal CSF flow dynamic environment. The transependymal passage of CSF directly across the ventricular lining where it is reabsorbed in the brain substance is the main compensatory mechanism utilized for CSF reabsorption. In this condition, the ventricles are visualized early on at 4–6 h (ventricular penetration) but are cleared of radiolabeled CSF by 24 h (Bartfelt et al. 1975). Another pattern of altered, but compensated normal, CSF flow occurs when the predominant flow to the convexities is by a direct anterior or posterior flow route, mainly in the interhemispheric fissure, rather than via the sylvian fissures.

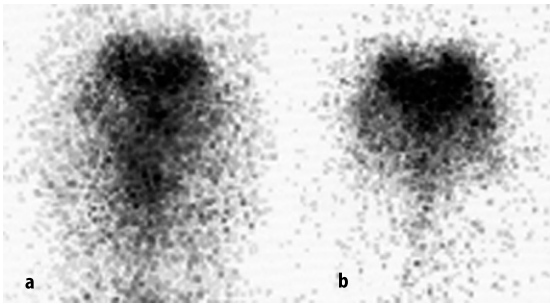

Fig. 3.12. Normal pressure hydrocephalus pattern: Images at 24 h (**a**) demonstrate radiotracer in the lateral ventricles, "ventricular penetration," and at 48 h (**b**) persistence of radiotracer in the lateral ventricles, "ventricular stasis" and no movement of the radiotracer beyond the basilar cisterns consistent with extra-ventricular obstruction to CSF flow

In communicating hydrocephalus (Fig. 3.12), the lateral ventricles are visualized early in the study "ventricular penetration" and the radiotracer remains in the ventricular system beyond 24 h, "ventricular stasis." Another aspect of the altered CSF flow pattern, observed in communicating hydrocephalus, is delayed or even complete obstruction of CSF movement, around the brain. The observed impediment to CSF flow may occur at any level all the way up to the parasagittal arachnoid villa (Bartfelt et al. 1975). Unilateral or bilateral delayed, but typically not obstructed, CSF flow, without ventricular penetration or stasis, may be seen in cortical atrophy or prior cerebral infarction without communicating hydrocephalus. The type of information that is available from radionuclide cisternography in the communicating hydrocephalic patient is useful to the neurosurgeon in helping to decide on the type of shunting procedure to be performed. In particular, radionuclide cisternography is very informative in normal pressure hydrocephalus, a form of communicating hydrocephalus, where the opening CSF spinal tap pressure level is within the normal range. Radionuclide cisternography when combined with surgical packing is also, on occasion, very helpful in identifying the presence and site of a CSF leak (Primeau et al. 1988). The imaging is especially useful when combined with SPECT imaging and measures of the amount of radioactivity present in surgical gauze pledgets (Servadei et al. 1998).

The second technique used for the assessment of CSF dynamics is radionuclide ventriculography. This procedure is used to check the patency of the afferent and efferent limbs of a ventricular shunt as well as function of the shunt pump. ^{99m}TcDTPA is the radiotracer typically used for this procedure. For assessment of the distal limb of the shunt, the radiotracer is injected directly into the shunt reservoir, using a low pressure injection technique, and follow-up drainage from the reservoir and distal limb is monitored over time. Under normal circumstances, clearance from the reservoir and distal limb is less than 10 min. The drainage from the distal ventriculo-peritoneal (V-P) limb should be unimpeded and without evidence of hold up at the distal drainage point into the peritoneum. The distal limb may be kinked, partially or even completely obstructed. These types of observed changes will, in general, require neurosurgical intervention, including possible shunt revision or shunt replacement. Radionuclide ventriculography can also be used to assess the function of the proximal limb of the shunt. This approach requires a higher-pressure injection of the radiotracer into the shunt reservoir. The higher-pressure injection should result in retrograde flow of the radiotracer out of the patent proximal shunt limb into the ventricle, which is then monitored for clearance over. Although an individual experienced with shunts should perform all types of injections into the shunt reservoir, particular care should be exercised when employing the high-pressure injection technique to achieve backflow from the shunt reservoir into the proximal limb of the shunt and the lateral ventricle.

References

Abdel-Dayem HM, Bahar RH, Sigurdsson GH, Sadek S, Olivecrona H, Ali AM (1989) The hollow skull: A sign of brain death in Tc-99m HM-PAO brain scintigraphy. Clin Nucl Med 14:912 – 916

Abi-Dargham A, Mawlawi O, Lombardo I, Gil R, Martinez D, Huang Y, Hwang DR, Keilp J, Kochan L, Van Heertum R, Gorman JM, Laruelle M (2002) Prefrontal dopamine D1 receptors and working memory in schizophrenia. J Neurosci 22:3708 – 3719

Academy of Neurology (1995) Practice parameters for determining brain death in adults (summary statement): report of the Quality Standards Subcommittee of the American Academy of Neurology. Neurology 45:1012 – 1014

Alavi JB, Alavi A, Chawluc J, Kushner M, Powe J, Kickey W, Reivich M (1988) Positron emission tomography in patients with gliomas. A predictor of prognosis. Cancer 62:1074 – 1078

Alazaki NP, Halpern SE, Ashburn WL, Coel M (1973) Hyberbaric cisternography: experience in humans. J Nucl Med 14:226 – 229

Antonini A, Leenders KL, Vontobel P, Maguire RP, Missimer J, Psylla M, Gunther I (1997) Complementary PET studies of striatal neuronal function in the differential diagnosis between multiple system atrophy and Parkinson's disease. Brain 120:2187 – 2195

Antonini A, Kazumata K, Feigin A, Mandel F, Dhawan V, Margouleff C, Eidelberg D (1998) Differential diagnosis of parkinsonism with [18F]fluorodeoxyglucose and PET. Mov Disord 13:268 – 274

Bartfelt D, Jordan CE, Strecker EP, James AE (1975) Comparison of ventricular enlargement and radiopharmaceutical retention: a cisternographic-pneumoencephalographic comparison. Radiology 116:111 – 115

Benamer HT, Patterson J, Wyper DJ, Hadley DM, Macphee GJ, Grosset DG (2000a) Correlation of Parkinson's disease severity and duration with I-123-FP-CIT SPECT striatal uptake. Mov Disord 15:692 – 698

Benamer TS, Patterson J, Grosset DG, Booij J, de Bruin K, van Royen E, Speelman JD, Horstink MH, Sips HJ, Dierckx RA, Versijpt J, Decoo D, Van Der Linden C, Hadley DM, Doder M, Lees AJ, Costa DC, Gacinovic S, Oertel WH, Pogarell O, Hoeffken H, Joseph K, Tatsch K, Schwarz J, Ries V (2000b) Accurate differentiation of parkinsonism and essential tremor using visual assessment of [^{123}I]-FP-CIT SPECT imaging: The [^{123}I]-FP-CIT study group. Mov Disord 15: 503 – 510

Brooks DJ (1998) Positron emission tomography studies in movement disorders. Neurosurg Clin N Am 9:263 – 282

Brooks DJ (2004) Neuroimaging in Parkinson's disease. Neurorx 1:243 – 254

Brooks DJ (2005) Positron emission tomography and single-photon emission computed tomography in central nervous system drug development. Neurorx 2:226 – 236

Brooks DJ, Ibanez V, Sawle GV (1992) Striatal D2 receptor status in patients with Parkinson's disease, striatonigral degeneration, and progressive supranuclear palsy, measured with 11C-raclopride and positron emission tomography. Ann Neurol 31:184 – 192

Buchert R, Thomasius R, Wilke F, Petersen K, Nebeling B, Obrocki J, Schulze O, Schmidt U, Clausen M (2004) A voxel-based PET investigation of the long-term effects of "Ecstasy" consumption on brain serotonin transporters. Am J Psychiatry 161:1181 – 1189

Buck A, Westera G, Sutter M, Albani C, Kung HF, vonSchulthess GK (1995) Iodine-123-IBF SPECT evaluation of extrapyramidal diseases. J Nucl Med 6:1196 – 1200

Ceravolo R, Piccini P, Bailey DL, Jorga KM, Bryson H, Brooks DJ (2002) ^{18}F-dopa PET evidence that tolcapone acts as a central COMT inhibitor in Parkinson's disease. Synapse 43:201 – 207

Conrad GR, Sinha P (2003) Scintigraphy as a confirmatory test of brain death. Semin Nucl Med 33:312 – 323

Di Chiro G (1986) Positron emission tomography using [18F] fluorodeoxyglucose in brain tumors: a powerful diagnostic and prognostic tool. Invest Radiol 22:360 – 371

Di Chiro G, DeLaPaz RL, Brooks RA, Sokoloff L, Kornblith PL, Smith BH, Patronas NJ, Kufta CV, Kessler RM, Johnston GS, Manning RG, Wolf AP (1982) Glucose utilization of cerebral gliomas measured by [18F]fluorodeoxyglucose and positron emission tomography. Neurology 32:1323 – 1329

Del Sole A, Falini A, Ravasi L, Ottobrini L, De Marchis D, Bombardieri E, Lucignani G (2001) Anatomical and biochemical investigation of primary brain tumours. Eur J Nucl Med 28:1851 – 1872

Devous MD (2005) Single-photon emission computed tomography in neurotherapeutics. Neurorx 2:237 – 249

Donohoe KJ, Frey KA, Gerbaudo VH, Mariani G, Nagel JS, Shulkin B (2003) Procedure guideline for brain death scintigraphy. J Nucl Med 44:846 – 851

Drzezga A, Lautenschlager N, Siebner H, Riemenschneider M, Willoch F, Minoshima S, Schwaiger M, Kurz A (2003) Cerebral metabolic changes accompanying conversion of mild cognitive impairment into Alzheimer's disease: a PET follow-up study. Eur J Nucl Med Mol Imaging 30:1104 – 1113

Duncan JS (1997) Imaging and epilepsy. Brain 120:339 – 377

Eidelberg D, Takikawa S, Moeller JR, Dhawan V, Redington K, Chaly T, Robeson W, Dahl JR, Margouleff D, Fazzini E (1993) Striatal hypometabolism distinguishes striatonigral degeneration from Parkinson's disease. Ann Neurol 33:518 – 527

Engel J, Jr (1989) Seizures and epilepsy. FA Davis Publishers, Philadelphia

Engelhardt HT Jr (1999) Redefining death: the mirage of consensus. In: Youngner SJ, Arnold RM, Shapiro R (eds) The definition of death: contemporary controversies. Johns Hopkins University Press, Baltimore, pp 319 – 331

Ercoli L, Siddarth P, Huang SC, Miller K, Bookheimer SY, Wright BC, Phelps ME, Small G (2006) Perceived loss of memory ability and cerebral metabolic decline in persons with the apolipoprotein E-IV genetic risk for Alzheimer disease. Arch Gen Psychiatry 63:442 – 448

Farinotti M, Ferrarini M, Solari A, Filippini G (1998) Incidence and survival of childhood CNS tumours in the region of Lombardy, Italy. Brain 121:1429 – 1436

Fearnley JM, Lees AJ (1991) Aging and Parkinson's disease: substantia nigra regional selectivity. Brain 114:2283 – 2301

Fischman AJ (2005) Role of [^{18}F]-dopa-PET imaging in assessing movement disorders. Radiol Clin N Am 43:93 – 106

Fischman AJ, Bonab AA, Babich JW, Palmer EP, Alpert NM, Elmaleh DR, Callahan RJ, Barrow SA, Graham W, Meltzer PC, Hanson RN, Madras BK (1998) Rapid detection of Parkinson's disease by SPECT with altropane: a selective ligand for dopamine transporters. Synapse 29:128 – 141

Frankle WG, Laruelle M (2002) Neuroreceptor imaging in psychiatric disorders. Ann Nucl Med 16:437 – 446

Frey KA, Koeppe RA, Kilbourn MR, Vander Borght TM, Albin RL, Gilman S, Kuhl DE (1996) Presynaptic monoaminergic vesicles in Parkinson's disease and normal aging. Ann Neurol 40:873 – 884

German DC, Manaye K, Smith WK, Woodward DJ, Saper CB (1989) Midbrain dopaminergic cell loss in Parkinson's disease: computer visualization. Ann Neurol 26:507 – 514

Grubb RL Jr, Powers WJ, Derdeyn CP, Adams HP Jr, Clarke WR (2003) The Carotid Occlusion Surgery Study. Neurosurg Focus 14:1 – 7

Henry TR, Van Heertum RL (2003) Positron emission tomography and single photon emission computed tomography in epilepsy. Care Semin Nucl Med 33:88 – 104

Hughes AJ, Daniel SE, Kilford L, Lees AJ (1992) Accuracy of clinical diagnosis of idiopathic Parkinson's disease: a clinico-pathological study of 100 cases. J Neurol Neurosurg Psychiatry 55:181 – 184

Hughes AJ, Daniel SE, Blankson S, Lees AJ (1993) A clinicopathologic study of 100 cases of Parkinson's disease. Arch Neurol 50:140 – 148

Hwanga S-I, Kima JH, Parka SW, Hana MH, Yua IK, Leea SH, Leea DS, Leea SK, Chunga C-K, Chang K-H (2001) A comparative analysis of MR imaging, positron emission tomography, and ictal single-photon emission CT in patients with neocortical epilepsy. AJNR 22:937 – 946

Ichise M, Toyama H, Fornazzari L, Ballinger JR, Kirsh JC (1993) Iodine-123-IBZM dopamine D2 receptor and technetium-99m-HMPAO brain perfusion SPECT in the evaluation of patients with and subjects at risk for Huntington's disease. J Nucl Med 34:1274 – 1281

Ichise M, Kim YJ, Erami SS, Ballinger JR, Vines D, Tanaka F, Lang AE (1999a) Functional morphometry of the striatum in Parkinson's disease on three-dimensional surface display of I-123-CIT SPECT data. J Nucl Med 40:530 – 538

Ichise M, Kim YJ, Ballinger JR, Vines D, Erami SS, Tanaka F, Lang AE (1999b) SPECT imaging of pre- and post-synaptic dopaminergic alterations in dopa-untreated PD. Neurology 52:1206 – 1214

Ichise M, Meyer JH, Yonekura Y (2001) An introduction to PET and SPECT neuroreceptor quantification models. J Nucl 42:755 – 763

Ichise M, Liow JS, Lu JQ, Takano A, Model K, Toyama H, Suhara T, Suzuki K, Innis RB, Carson RE (2003) Linearized reference tissue parametric imaging methods: application to [^{11}C]DASB positron emission tomography studies of the serotonin transporter in human brain. J Cereb Blood Flow Metab 23:1096 – 1112

Innis RB, Marek KL, Sheff K, Zoghbi S, Castronuovo J, Feigin A, Seibyl JP (1999) Effect of treatment with L-dopa/carbido-

pa or L-selegiline on striatal dopamine transporter SPECT imaging with [^{123}I]β-CIT. Mov Disord 14:436 – 442
Jacobs AH, Kracht LW, Gossmann A, Ruger MA, Thomas AV, Thiel A, Herholz K (2005) Imaging in neurooncology. NeuroRx 2(2):333 – 47
Jennings DL, Seibyl JP, Oakes D, Eberly S, Murphy J, Marek K (2004) [^{123}I]β-CIT and single-photon emission computed tomographic imaging vs. clinical evaluation in Parkinsonian syndrome: unmasking an early diagnosis. Arch Neurol 61:1224 – 1229
Kim EE, Chung SK, Haynie TP, et al. (1992) Differentiation of residual or recurrent tumors from post-treatment changes with F-18 FDG PET. Radiographics 12:269 – 279
Kim YJ, Ichise M, Ballinger JR, Vines D, Erami SS, Tatschida T, Lang AE (2002) Combination of dopamine transporter and D2 receptor SPECT in the diagnostic evaluation of PD, MSA, and PSP. Mov Disord 17:303 – 312
Kurtek RW, Lai KK, Tauxe WN, Eidelman BH, Fung JJ (2000) Tc-99m hexamethylpropylene amine oxime scintigraphy in the diagnosis of brain death and its implications for the harvesting of organs used for transplantation. Clin Nucl Med 25:7 – 10
Laruelle M (2005) Imaging synaptic neurotransmission with in vivo binding competition techniques: a critical review. J Cereb Blood Flow Metab 20:423 – 451
Lee VW, Hauck RM, Morrison MC, Peng TT, Fischer E, Carter A (1987) Scintigraphic evaluation of brain death: significance of sagittal sinus visualization. J Nucl Med 28:1279 – 1283
Lee DH, Gao F-Q, Rogers JM, Gulka I, Mackenzie IRA, Parrent AG, Kubu CS, Munoz DG, McLachlan RS, Warren T, Blume WT, Girvin JP (1998) MR in temporal lobe epilepsy: analysis with pathologic confirmation. AJNR 19:19 – 27
Lee CS, Samii A, Sossi V, Ruth TJ, Schulzer M, Holden JE, Wudel J, Pal PK, de la Fuente-Fernandez R, Calne DB, Stoessl AJ (2000) In vivo positron emission tomographic evidence for compensatory changes in presynaptic dopaminergic nerve terminals in Parkinson's disease. Ann Neurol 47:493 – 503
Marek K, Seibyl JP, Zoghbi SS, Zea-Ponce Y, Baldwin RM, Fussell B, Charney DS, van Dyck C, Hoffer PB, Innis RP (1996) [^{123}I]β-CIT SPECT imaging demonstrates bilateral loss of dopamine transporters in hemiparkinsons disease. Neurology 46:231 – 237
Marshall V, Grosset D (2003) Role of dopamine transporter imaging in routine clinical practice. Mov Disord 18:1415 – 1423
Mathis CA, Bacskai BJ, Kajdasz ST, McLellan ME, Frosch MP, Hyman BT, Holt DP, Wang Y, Huang GF, Debnath ML, Klunk WE (2002) A lipophilic thioflavin-T derivative for positron emission tomography (PET) imaging of amyloid in brain. Bioorg Med Chem Lett 12:295 – 298
Meyer JH, Wilson AA, Sagrati S, Hussey D, Carella A, Potter WZ, Ginovart N, Spencer EP, Cheok A, Houle S (2004) Serotonin transporter occupancy of five selective serotonin reuptake inhibitors at different doses: an [^{11}C]DASB positron emission tomography study. Am J Psychiatry 161: 826 – 835
Morenski JD, Oro JJ, Tobias JD, Singh A (2003) Determination of death by neurological criteria. J Intensive Care Med 18:211-221
Mountz JM, Liu H-G, Deutsch G (2003) Neuroimaging in cerebrovascular disorders: measurement of cerebral physiology after stroke and assessment of stroke recovery. Semin Nucl Med 33:56 – 76
Mozley PD, Schneider JS, Acton PD, Plossl K, Stern MB, Siderowf A, Leopold NA, Li PY, Alavi A, Kung HF (2000) Binding of [^{99m}Tc]TRODAT-1 to dopamine transporters in patients with Parkinson's disease and in healthy volunteers. J Nucl Med 41:584 – 589
Newberg A, Alavi A, van Rhijn S, Cotter A, Reilly P (2002) Radiologic diagnosis of brain death. JAMA 288:2121 – 2122
Otsuka M, Ichiya Y, Hosokawa S, Kuwabara Y, Tahara T, Fukumura T, Kato M, Masuda K, Goto I (1991) Striatal blood flow, glucose metabolism and ^{18}F-dopa uptake: difference in Parkinson's disease and atypical parkinsonism. J Neurol Neurosurg Psychiatry 54:898 – 904
Parkinson Study Group (2002) Dopamine transporter brain imaging to assess the effects of pramipexole vs levodopa on Parkinson disease progression. JAMA 287:1653 – 1661
Parsey RV, Mann JJ (2003) Applications of positron emission tomography in psychiatry. Semin Nucl Med 33:129 – 135
Pirotte B, Goldman S, Massager N, David P, Wikler D, Vandesteene A, Salmon I, Brotchi J, Levivier M (2004) Comparison of 18F-FDG and 11C-methionine for PET-guided stereotactic brain biopsy of gliomas. J Nucl Med 45:1293 – 1298
Primeau M, Carrier L, Miletter PC, Chartrand R, Picard D, Picard M (1988) Spinal cerebrospinal fluid leak demonstrated by radioisotopic cisternography. Clin Nucl Med 13:701 – 703
Ravina B, Eidelberg D, Ahlskog JE, Albin RL, Brooks DJ, Carbon M, Dhawan V, Feigin A, Fahn S, Guttman M, Gwinn-Hardy K, McFarland H, Innis R, Katz RG, Kieburtz K, Kish SJ, Lange N, Langston JW, Marek K, Morin L, Moy C, Murphy D, Oertel WH, Oliver G, Palesch Y, Powers W, Seibyl J, Sethi KD, Shults CW, Sheehy P, Stoessl AJ, Holloway R (2005) The role of radiotracer imaging in Parkinson disease. Neurology 64:208 – 215
Reiman EM, Chen K, Alexander GE, Caselli RJ, Bandy D, Osborne D, Saunders AM, Hardy J (2005) Correlations between apolipoprotein E epsilon4 gene dose and brain-imaging measurements of regional hypometabolism. Proc Natl Acad Sci 102(23):8299 – 302
Ricci PE (1999) Imaging of adult brain tumors. Neuroimaging Clin North Am 9:651 – 669
Schossberger PF, Touya JJ (1976) Dynamic cisternography in normal dogs and in human beings. Neurology 26:254 – 260
Schulz JB, Skalej M, Wedekind D, Luft AR, Abele M, Voigt K, Dichgans J, Klockgether T (1999) Magnetic resonance imaging-based volumetry differentiates idiopathic Parkinson's syndrome from multiple system atrophy and progressive supranuclear palsy. Ann Neurol 45:65 – 74
Schwarz J, Tatsch K, Arnold G, Gasser T, Trenkwalder C, Kirsch CM, Oertel WH (1992) ^{123}I-iodobenzamide-SPECT predicts dopaminergic responsiveness in patients with de novo parkinsonism. Neurology 42:556 – 561
Seibyl JP (2003) Imaging studies in movement disorders. Semin Nucl Med 33:105 – 113
Seibyl JP, Marek KL, Quinlan D, Sheff K, Zoghbi S, Zea-Ponce Y, Baldwin RM, Fussell B, Smith EO, Charney DS, Innis RB (1995) Decreased single-photon emission computed tomographic [^{123}I]β-CIT striatal uptake correlates with symptom severity in Parkinson's disease. Ann Neurol 38:589 – 598
Seppi K, Schocke MF, Esterhammer R, Kremser C, Brenneis C, Mueller J, Boesch S, Jaschke W, Poewe W, Wenning GK (2003) Diffusion-weighted imaging discriminates progressive supranuclear palsy from PD, but not from the parkinson variant of multiple system atrophy. Neurology 60:922 – 927
Servadei R, Moscatelli G, Giuliani G, Cremonini AM, Piazza G, Agostine M, Riva P (1998) Cisternography in combination with single photon emission tomography for the detection of the leakage site in patients with cerebrospinal fluid rhinorrhea: preliminary report. Act Neurochir (Wien) 140:1183 – 1189
Shoghi-Jadid K, Small GW, Agdeppa ED, Kepe V, Ercoli LM, Siddarth P, Read S, Satyamurthy N, Petric A, Huang SC, Barrio JR (2002) Localization of neurofibrillary tangles and beta-amyloid plaques in the brains of living patients with Alzheimer disease. Am J Geriatr Psychiatry 10(1):24 – 35
Smirniotopoulos JG (1999) The new WHO classification of brain tumors. Neuroimaging Clin North Am 9:595 – 613

Snow BJ, Tooyama I, McGeer EG Yamada T, Calne DB, Takahashi H, Kimura H (1993) Human positron emission tomographic [^{18}F]fluorodopa studies correlate with dopamine cell counts and levels. Ann Neurol 34:324 – 330

Spence AM, Muzi M, Mankoff DA, O'Sullivan SF, Link JM, Lewellen TK, Lewellen B, Minoshima S, Swanson K, Krohn KA (2004) ^{18}F-FDG PET of gliomas at delayed intervals: improved distinction between tumor and normal gray matter. J Nucl Med 45:1653 – 1659

Spieth ME, Ansari AN, Kawada TK, Kimura RL, Siegel ME (1994) Direct comparison of Tc-99m DTPA and Tc-99m HMPAO for evaluating brain death. Clin Nucl Med 19:867 – 872

Spieth ME, Devadas GC, Gauger BS (2004) Comment on: Procedure guideline for brain death scintigraphy. J Nucl Med 45:922

Suhara T, Okubo Y, Yasuno F, Sudo Y, Inoue M, Ichimiya T, Nakashima Y, Nakayama K, Tanada S, Suzuki K, Halldin C, Farde L (2002) Decreased dopamine D2 receptor binding in the anterior cingulate cortex in schizophrenia. Arch Gen Psychiatry 59:25 – 30

Talbot PS, Laruelle M (2002) The role of in vivo molecular imaging with PET and SPECT in the elucidation of psychiatric drug action and new drug development. Eur Neuropsychopharm 12:503 – 511

Theodore WH (2004) Recent advances and trends in epilepsy imaging: pathogenesis and pathophysiology. Rev Neurol Dis 1:53 – 59

Thomasius R, Petersen K, Buchert R, Andresen B, Zapletalova P, Wartberg L, Nebeling B, Schmoldt A (2003) Mood, cognition and serotonin transporter availability in current and former ecstasy (MDMA) users. Psychopharmacology 167: 85 – 96

Tikofsky RS, Van Heertum RL (2000) Seizure disorders. In: Van Heertum RL, Tikofsky RS (eds) Functional cerebral SPECT and PET imaging, 3rd edn. Lippincott Williams & Wilkins, Philadelphia, pp 189 – 228

Turjanski N, Lees AJ, Brooks DJ (1999) Striatal dopaminergic receptor dysfunction in patients with restless legs syndrome: 18F-dopa and 11C-raclopride PET studies. Neurology 52:932 – 937

Uniform Determination of Death Act, 12 Uniform Laws Annotated (ULA) 589 (West 1993 and West Supp. 1997)

Van Heertum RL, Tikofsky RS (2003) Positron emission tomography and single-photon emission computed tomography brain imaging in the evaluation of dementia. Semin Nucl Med 33:77 – 85

Van Heertum RL, Ichise M, Drocea C, Lobotes K, Fawwaz RA (2001) PET and SPECT brain imaging in the evaluation of neurologic disease. Radiol Clin N Am 39:1007 – 1033

Van Heertum RL, Greenstein EA, Tikofsky RS (2004) 2-Deoxyfluorglucose–positron emission tomography imaging of the brain: current Clinical applications with emphasis on the dementias. Semin Nucl Med 34:300 – 312

van Royen E, Verhoeff NF, Speelman JD, Wolters EC, Kuiper MA, Janssen AG (1993) Multiple system atrophy and progressive supranuclear palsy. Diminished striatal D2 dopamine receptor activity demonstrated by ^{123}I-IBZM single photon emission computed tomography. Arch Neurol 50: 513 – 516

Volkow ND, Fowler JS, Wang GJ (2003) Positron emission tomography and single-photon emission computed tomography in substance abuse research. Semin Nucl Med 33:114 – 128

Volkow ND, Fowler JS, Wang GJ (2004) The addicted human brain viewed in the light of imaging studies: brain circuits and treatment strategies. Neuropharmacology 47 Suppl 1:3 – 13

Wijdicks EF (2001) The diagnosis of brain death. N Engl J Med 344:1215 – 1221

Whone AL, Watts RL, Stoessl AJ, Davis M, Reske S, Nahmias C, Lang AE, Rascol O, Ribeiro MJ, Remy P, Poewe WH, Hauser RA, Brooks DJ; REAL-PET Study Group (2003) Slower progression of Parkinson's disease with ropinirole versus levodopa: the REAL-PET study. Ann Neurol 54:93 – 101

Won HJ, Chang K-H, Cheon J-E, Kim HD, Lee DS, Moon MH, Kim I-O, Lee SK, Chung C-K (1999) Comparison of MR imaging with PET and ictal SPECT in 118 patients with intractable epilepsy. AJNR 20:593 – 599

Heart

4

M.D. Cerqueira, M.J. Vidigal Ferreira

Radionuclide techniques are used for cardiovascular imaging to assess perfusion, function, metabolism, innervation and infarction (Klocke et al. 2003). Single photon emission computed tomographic (SPECT) techniques predominate and in comparison to alternative imaging methods such as positron emission tomography (PET), cardiac magnetic resonance imaging and cardiac computerized tomography, SPECT offers the advantages listed in Table 4.1. As practiced in the United States and Europe, myocardial perfusion imaging predominates and accounts for the majority of nuclear cardiology. This concise overview will focus predominately on assessment of myocardial perfusion and assessment of left ventricular function using either equilibrium radionuclide angiocardiography (ERNA) or first-pass radionuclide angiography (FPRNA). Imaging of myocardial innervation is developing as a new technique for risk assessment in patients with heart failure and those being considered for ventricular defibrillators. Infarct imaging is not widely performed.

Table 4.1. Advantages of SPECT over competing cardiovascular imaging modalities

1. Extensive body of literature supporting efficacy and prognostic value
2. Standardized protocols for performing studies
3. Published guidelines for utilization and appropriateness criteria
4. Widely available in hospital and outpatient setting
5. Proven cost effectiveness for diagnosis, management and risk assessment

4.1 Myocardial Perfusion Imaging

4.1.1 Historical Perspective

Myocardial perfusion imaging has evolved over 30 years to the point where it can now provide diagnostic and prognostic information in nearly all patient groups. Early studies were performed with K-43 in animal models and in man, but it was only with the availability of thallium-201 (Tl-201) in the mid 1970s that the technique using planar imaging became widely utilized for detecting the presence and extent of coronary artery disease (CAD). In the mid 1980s SPECT was introduced and became the predominant method of acquisition. All the early studies were performed using exercise stress. Since not all patients are capable of exercising, the introduction of dipyridamole, adenosine and dobutamine for pharmacologic stress in the 1980s and 1990s allowed perfusion studies to be performed in nearly all patients. Tl-201 is not the ideal perfusion tracer and in the late 1980s the technetium-99m (Tc-99m) labeled perfusion tracer, sestamibi, became available followed in the mid 1990s by Tc-99m tetrofosmin. These two tracers now account for the majority of perfusion studies. Perfusion imaging was shown to be capable of not only diagnosing the presence or absence of CAD, but of also providing accurate information on risk assessment and prognosis in patients with known or suspected CAD. In the mid 1990s ECG gating of the perfusion data methods were introduced that allowed global and regional functional information to be obtained during acquisition of the high dose Tc-99m perfusion data sets. It has subsequently been shown that these computer algorithms are accurate with Tl-201 and with the low dose portion of 1-day Tc-99m studies. Nearly all SPECT perfusion studies are now performed with ECG gated assessment function.

4.1.2 Basis of Myocardial Perfusion Imaging

Detection of CAD is based on the heterogeneity in blood flow between a normal coronary vessel and one with an anatomic stenosis or abnormal physiological function. Following exercise or pharmacologic stress, blood flow increases in normal coronary arteries. In vessels with either a critical luminal stenosis, variously defined as 50 – 80 % luminal cross sectional narrowing, or abnormal functional flow reserve, three things may occur: there is no increase in flow, the increase is less than in a normal vessel or occasionally there may even be a constrictive effect and a decrease in coronary artery blood flow. This diminished coronary flow reserve

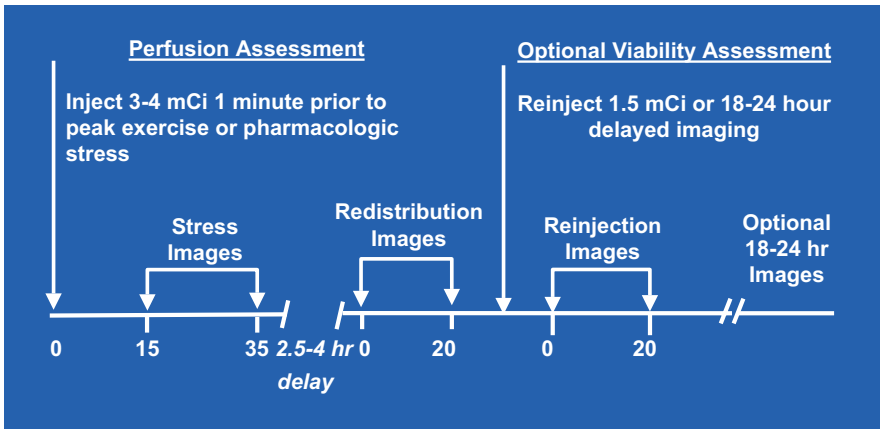

Fig. 4.1. Thallium-201 protocol with options for viability assessment

due to anatomic narrowing or physiological dysfunction is not an all-or-none phenomenon; rather, flow reserve decreases gradually as the severity of the coronary stenosis progresses. The most severe stenoses, >85%, typically have no flow reserve. Vessels with a <50% stenosis have no anatomic basic for diminished flow reserve but may have physiological abnormalities such as endothelial dysfunction, resulting in failure to produce nitrous oxide, that fail to augment or may actually decrease flow with exercise or other form of stress. Given this framework, radionuclide perfusion imaging requires a measurement of flow in the resting state and after exercise or pharmacologic stress that increases coronary blood flow and results in flow heterogeneity between normal vessels and those with anatomic narrowing or physiological impairment.

4.1.3 Radiopharmaceuticals and Imaging Protocols

The following sections will describe the characteristics of each of the radiopharmaceuticals and how they are used in the most commonly performed imaging protocols. The recommendations are based on the guidelines published by the American Society of Nuclear Cardiology (2001) and regularly updated (www.ASNC.ORG).

4.1.3.1 Thallium-201

Thallium-201 is a K^+ analog that is transported across cell membranes by the Na/K ATPase system (Taillefer 2003). Initial myocardial uptake is proportional to blood flow over a wide physiological range and is dependent on the presence of viable myocardial cells. Following the rapid high initial uptake, Tl-201 re-equilibrates with the lower concentration in the blood in a time dependent fashion. This is called washout or redistribution and like the initial uptake is directly proportional to blood flow to the area and the presence of functioning myocytes. In the typical imaging sequence using Tl-201, shown in Fig. 4.1, the patient has a stress study with dynamic exercise or pharmacologic stress with Tl-201 injected at peak stress. The patient must be imaged within 10–15 min of completion of stress to avoid early redistribution and a resulting decrease in sensitivity. This is followed 2.5–4 h later by a redistribution set of images. Areas of myocardium supplied by normal coronary arteries have a high and uniform uptake on both the stress and redistribution images. Areas of infarction have fixed defects with very low or absent uptake on both the initial stress images as there are a diminished number of myocytes to take up the Tl-201 and there is no change on the redistribution images. Following stress, areas distal to a flow limiting critical anatomic or physiologic coronary stenosis have low uptake of Tl-201 relative to the areas of myocardium with normal coronary blood supply. Areas of ischemia and infarction look identical on the post stress images. However, with ischemia the redistribution images show improvement in the ischemic areas and this allows the differentiation to be made between infarct and ischemic myocardium.

One of the major advantages of using Tl-201 is that it is also an excellent marker of myocardial viability (Udelson et al. 2004). The high and nearly linear initial myocardial uptake following stress makes Tl-201 a better marker of myocardial blood flow than the Tc-99m tracers, which have a low extraction fraction across the coronary bed and plateau at lower flow rates. Tl-201 uptake and redistribution over time is a marker of the K^+ blood pool and of viable myocardium. In areas where blood flow is severely reduced following stress, there may be very low uptake of Tl-201 initially despite the presence of living myocytes. Even the 3–4 h redistribution images may still be abnormal. However, over 18–24 h or following re-injection of an additional dose to boast blood levels, if there are viable myocytes with

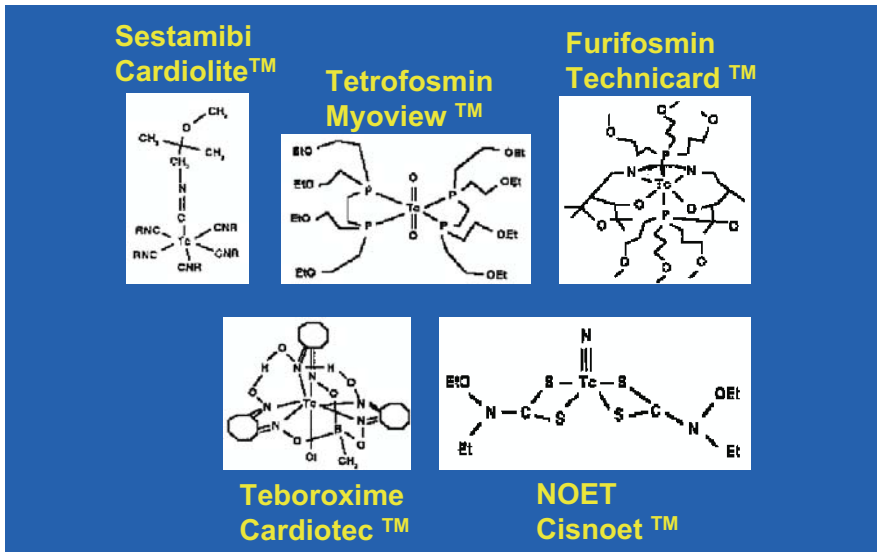

Fig. 4.2. Structures and chemical and brand names of Tc-99m labeled myocardial perfusion tracers

an intact Na/K ATPase system, Tl-201 is eventually taken up and these areas will be clearly identified as hibernating myocardium and not infarction.

Assessment of viability is especially important in patients with congestive heart failure, known cardiomyopathies or recent myocardial infarction. In patients where myocardial viability assessment is of critical clinical importance and PET is not available, several approaches using Tl-201 are shown in Fig. 4.1 that can be used to further improve on the accuracy of the regular stress/redistribution sequence. These approaches include a rest injection followed 3 – 4 h later by redistribution images; re-injection of Tl-201 before the redistribution imaging in a stress redistribution sequence; or delayed imaging at 18 – 24 h in the typical stress/redistribution sequence. A rest/3 – 4 h redistribution Tl-201 protocol can also be used for viability assessment but this does not provide information on ischemia. With the dual isotope approach to be described, both ischemia and hibernation can be identified.

4.1.3.2 Technetium-99m Radiotracers

The available Tc-99m radiopharmaceuticals used for myocardial perfusion imaging are shown in Fig. 4.2. Tc-99m tracers were developed to overcome the limitations of Tl-201. Only two Tc-99m tracers are in clinical use: Tc-99m sestamibi (Cardiolite) and Tc-99m tetrofosmin (Myoview). The advantages of Tc-99m radiotracers over Tl-201 are shown in Table 4.2. The monoenergetic 140 keV higher energy of Tc-99m versus the 69 – 83 keV range of Tl-201 results in improved resolution with less overall attenuation and scatter during imaging. Tc-99m has a half-life of 6 h in comparison to the 72 h of Tl-201. The shorter half-life allows administration of a higher Tc-99m dose resulting in high-count images. As an example, 4 mCi of Tl-201 is administered compared to 30 mCi of the Tc-99m radiotracers. The higher counts obtained with a Tc-99m radiopharmaceutical and the lack of redistribution allows ECG triggered gated acquisition, ECG gated SPECT, for assessment of function. The minimal redistribution of Tc-99m tracers following injection allows greater flexibility as to when acquisition can be performed; as soon as 10 min or as far out as 4 h following stress.

Table 4.2. Advantages of Tc-99m radiotracers over thallium-201

1. Greater availability
   a) Tc-99m kit preparation versus cyclotron production
2. Improved radiation characteristics
   a) 140 keV vs 60 – 80 keV
   b) 6 h vs 72 h half-life
3. Administer larger dose
   a) 30 mCi vs 2.5 – 4.0 mCi
   b) Higher count rates
4. Functional assessment
   a) Ability to do FPRNA
   b) ECG gated acquisition
5. Minimal redistribution
   a) Greater imaging flexibility with stress
   b) Emergency Department studies for acute chest pain

Tc-99m Sestamibi and Tetrofosmin. Both are monovalent hydrophilic cations, which makes them very lipophilic and facilitates entry into cells. Uptake is dependent on blood flow, plasma and mitochondrial derived membrane electrochemical gradients, cellular pH and intact energy pathways (Taillefer 2003). Chemical

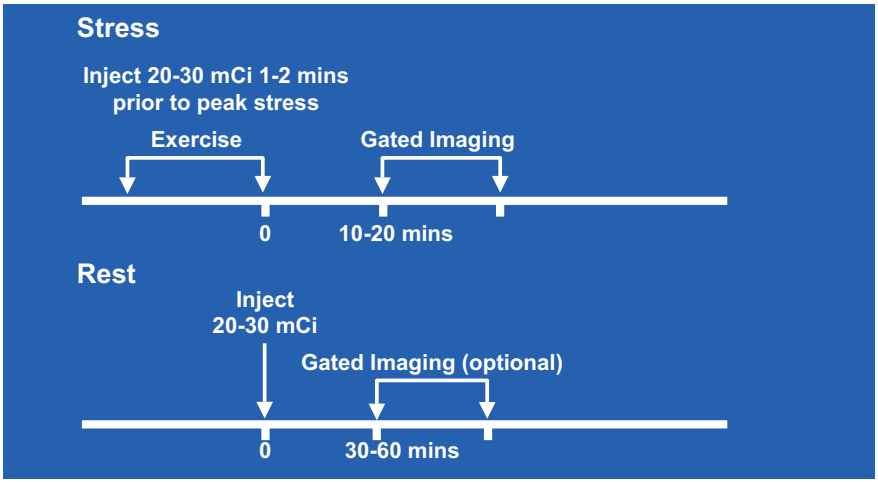

Fig. 4.3. Two-day stress/rest Tc-99m protocol

or structural conversion of the molecule is not required and inhibitors of Na^+, K^+ and Ca^{2+} transport do not prevent uptake or retention in myocytes. Once inside the myocyte they remain trapped with the greatest concentration in the mitochondria and there is minimal washout. Following intravenous injection they are cleared from blood by the liver, concentrated in the gallbladder and excreted through the common bile duct into the GI tract. The initial high liver uptake does not allow the inferior wall to be seen clearly early post injection and requires waiting 30 – 60 min following resting or pharmacologic stress injection to get adequate visualization. Clearance post exercise is rapid and image acquisition can be started as soon as 10 – 20 min following injection.

Tc-99m Radiotracer Imaging Protocol Options. The clearance characteristics of Tc-99m sestamibi and tetrofosmin are sufficiently similar that recommendations for imaging are identical with some variation between injection time and when to image due to differences in liver clearance between the two tracers (American Society of Nuclear Cardiology 2001).

Protocol options include a 2-day protocol, a 1-day split dose protocol (stress/rest or rest/stress sequence) and a dual isotope approach using Tl-201 at rest. The diagnostic accuracy results reported in the literature did not report significant differences between the various protocols or between these agents and Tl-201 (Klocke et al. 2003).

Two Day Protocol (Fig. 4.3). The maximal dose of Tc-99m, 20 – 30 mCi, is used for both images and provides high counts and better image quality. This protocol is mandatory in obese patients and allows a true rest ejection fraction (EF) to be calculated as well as a post stress measurement, which provides additional value. Due to result delay and patient inconvenience, this protocol is not used widely. The stress study should be done first and if normal the resting study is not needed. Stress first provides results sooner and has a lower radiation exposure. In obese patients with soft tissue attenuation and low counts, gating and attenuation correction improves specificity and decreases the number of patients needing to return for a rest study (Thompson et al. 2005).

One Day Studies. For logistical reasons, stress and rest studies are usually performed using a 1-day protocol as shown in Figs. 4.4 and 4.5. This requires administration of a low dose, one-third of the total dose or 8 – 12 mCi, for the first study and a larger dose, two-thirds of the total dose or 20 – 30 mCi, for the second study and waiting as long as possible between studies, usually 1.5 – 2.5 h, to allow for physical decay of Tc-99m. Using this approach, when the second set of images is acquired there is relatively little remaining activity from the first injection. The one-day rest/stress sequence, shown in Fig. 4.4, is the most frequently performed protocol in the US. The disadvantage of this sequence is that the low dose is given at rest when blood flow is lowest and there will be less myocardial uptake. The higher stress dose, administered when blood flow is maximal, will give higher counts and better quality images. The gated post stress image in patients with extensive ischemia may give a lower EF, due to residual myocardial stunning, than a true resting ejection fraction (Johnson et al. 1997). In patients with ischemia, a lower post stress EF is a better predictor of higher cardiac death and infarction rate than the size and severity of the defect alone (Sharir et al. 2001). The 1-day stress/rest protocol in Fig. 4.5 administers the lower dose when myocardial blood flow is the highest, during stress, and background activity in the subdiaphragmatic area is low due to a decrease in mesenteric blood flow associated with stress. If the stress study is normal, the rest study is not needed.

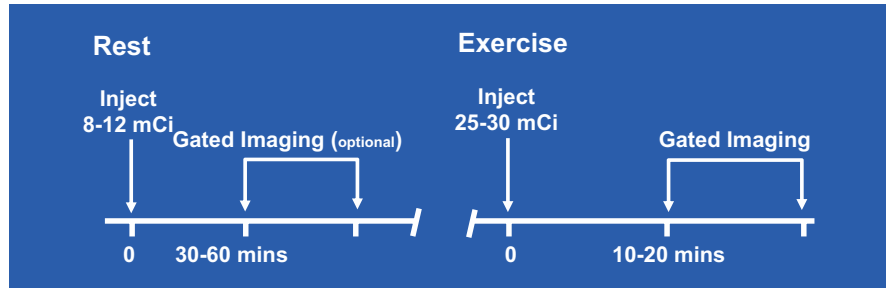

Fig. 4.4. One-day rest/stress Tc-99m protocol

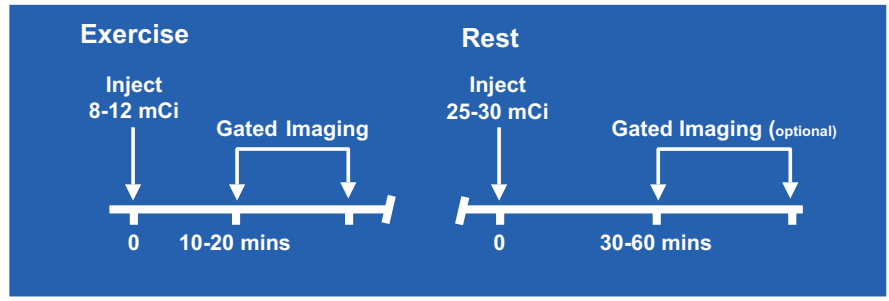

Fig. 4.5. One-day stress/rest Tc-99m protocol

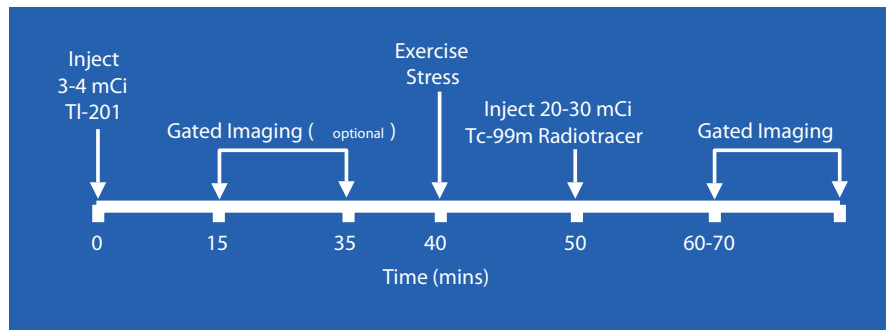

Fig. 4.6. Separate acquisition dual isotope study using Tl-201 at rest and Tc-99m for stress

Separate Acquisition Dual Isotope Tl-201/Tc-99m Radiotracer Protocol. The timing and sequence for a Tl-201/Tc-99m radiotracer dual isotope separate acquisition protocol is displayed in Fig. 4.6. For the resting Tl-201 study, the patient should be fasting and a dose of 3 – 4 mCi of Tl-201 injected. Imaging should be delayed for 10 – 15 min. For stress the patient is injected with 20 – 30 mCi of a Tc-99m tracer. The separate acquisition approach takes advantage of the two distinct and separate energy levels of Tl-201 and Tc-99m. During the second acquisition, the gamma camera selectively acquires data centering on the higher energy Tc-99m window. Although there is residual Tl-201 present from the resting study, the lower energy Tl-201 photons are excluded by the higher Tc-99m window.

When using the dual isotope approach and viability is in question, a rest-4-h redistribution Tl-201 study should be performed prior to performing the stress study (Dilsizian and Bonow 1993). Patients can also be injected with Tl-201 the evening before to give an approximate 12-h Tl-201 acquisition the following morning. This is an excellent method for the identification of myocardial viability. When the Tc-99m stress study has already been performed and questions of viability remain, delayed Tl-201 imaging cannot be performed on the same day due to the down scatter of the Tc-99m into the Tl-201 energy window. Patients can return the next day for imaging when decay of the Tc-99m has occurred and the distribution of Tl-201 can be imaged to assess viability. The low counts require additional acquisition time to get adequate quality images.

4.1.3.3 Pharmacologic Stress Agents and Protocols

All myocardial perfusion imaging studies should be done using dynamic exercise stress whenever possible to obtain exercise duration, heart rate and blood pressure response that are important for diagnosis and management but not available from pharmacologic stress (Cerqueira 1996a). Pharmacologic stress is reserved for patients who are unable to exercise or are unable to achieve at least 85 % of the maximal age-adjusted heart rate or reach an ischemic endpoint on the

Table 4.3. Properties of adenosine, dipyridamole and dobutamine

	Adenosine	Dipyridamole	Dobutamine
Half-life	< 10 s	33 – 62 min	2 min
Mean time to peak coronary flow velocity	55 s	6.5 min	≤ 10 min
Onset of action	Seconds	2 min	1 – 2 min
Mechanism of action	Direct	Indirect	Indirect
Patients with side effects requiring medical intervention	0.6 %	16 %	NA

basis of symptoms or ECG changes. Sensitivity of MPI decreases in patients who achieve < 85 % of the predicted heart rate (Iskandrian et al. 1989). If the myocardial perfusion images are normal, it cannot be certain if they are truly normal or due to an inadequate level of stress achieved during submaximal exercise. Alternatively, if there is ischemia, it is never certain if the full extent of ischemia was detected.

The three pharmacologic agents in common use are listed in Table 4.3 and include the vasodilators, adenosine and dipyridamole, and the adrenergic stimulant dobutamine. The vasodilators produce maximal coronary hyperemia, creating flow heterogeneity by causing a greater increase in blood flow in normal coronary arteries than in arteries with flow limiting stenosis. Dobutamine increases not only blood flow, but heart rate and blood pressure, and may create true ischemia.

Vasodilator Mechanism of Action. Adenosine is produced inside many cell types where it has no effect on blood flow. It is actively transported into the extracellular space where it is capable of binding and stimulating a series of adenosine (A) receptors (Cerqueira 2004). Inactivation of extracellular adenosine whether endogenously produced or exogenously administered is < 10 s due to reuptake by the same transport system and active metabolism. Dipyridamole blocks this reuptake mechanism and increases coronary blood flow by increasing extracellular concentration of endogenously produced adenosine. Adenosine nonselectively stimulates all A receptors. The A_{2a} receptors, present on vascular smooth muscle and endothelial cells, enhance arterial wall smooth muscle dilation and increase coronary blood flow. Adenosine also stimulates the A1, A2b and A3 receptors, which cause flushing, nonischemic cardiac chest pain, atrioventricular nodal block and bronchospasm, undesirable side effects in the context of perfusion imaging. Caffeine and aminophylline bind but do not stimulate the adenosine receptor and thereby block the effects of adenosine. If caffeine is present when adenosine is administered, the vasodilatory effects are blocked; flow heterogeneity is not created and in patients with CAD this may result in a false negative test. This blocking effect, however, is helpful when side effects are present and administration of aminophylline blocks the adenosine receptors and reverses the side effects.

Side Effects. Side effects have been reported to occur in 50 % of patients receiving dipyridamole with reversal required in 12 %, and in 80 % of patients receiving adenosine with < 1 % receiving aminophylline reversal (Cerqueira et al. 1994; Ranhosky and Kempthorne-Rawson 1990). Vasodilators cause a 10 mm Hg decrease in systolic and diastolic blood pressure with a compensatory 12 – 15 beat per minute increase in heart rate (Cerqueira et al. 1994). The most common cardiac side effects with dipyridamole include chest pain (20 %), ECG changes (16 %) and ST depression (7.5 %). With adenosine, the cardiac side effects include chest pain (35 %), transient A-V nodal block (7.6 %) and ST-T wave changes (5.7 %). The majority of reported chest pain is not ischemic, but due to nonselective stimulation of bradykinin pain receptors by adenosine. Patients with ECG changes consistent with ischemia are felt to have a higher dependence on collateral vessel blood flow, which may be decreased due to coronary steal associated with a marked increase in coronary flow in normal vessels during vasodilation and a resultant decrease in collateral flow. At some institutions, it is standard practice to reverse the effects of dipyridamole in all patients using aminophylline. The effective half-life of dipyridamole is 30 min, which is longer than the half-life of aminophylline, and this means additional doses may be required to prevent recurrence of side effects. Adenosine can be reversed by stopping the infusion.

Safety of Pharmacologic Stress Testing. Dipyridamole and adenosine have been used extensively and have an excellent overall safety record. Although general side effects are common, cardiac and severe adverse events are rare. When considering that patients referred for pharmacologic stress testing are generally more debilitated, overall safety is comparable to that reported for conventional dynamic exercise stress testing (Cerqueira et al. 1994). Severe adverse complications such as death and myocardial infarction in association with pharmacologic stress testing are uncommon. In a retrospective review of 73,806 patients from 59 centers in 19 countries there were 9 reported cardiac deaths and 13 nonfatal myocardial infarctions using intravenous dipyridamole (Lette et al. 1995). In a prospective registry that included 9,256 patients receiving intravenous adenosine, there were no deaths and 1 pa-

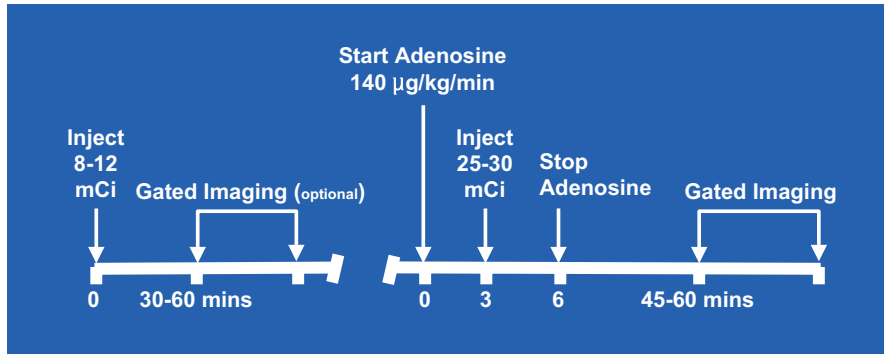

Fig. 4.7. Protocol for adenosine pharmacologic stress testing using a 1-day rest/stress Tc-99m imaging sequence

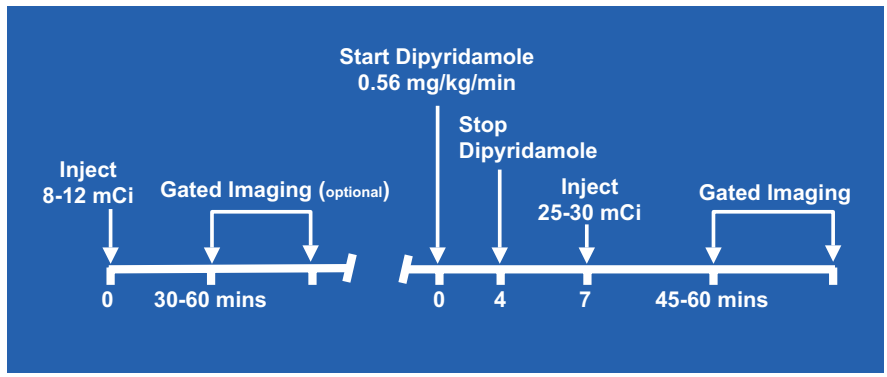

Fig. 4.8. Protocol for dipyridamole pharmacologic stress testing using a 1-day rest/stress Tc-99m imaging sequence

tient had a myocardial infarction (Cerqueira et al. 1994).

Efficacy. The reported diagnostic accuracy using adenosine or dipyridamole has been shown to be comparable to exercise. In early studies performed mostly using planar Tl-201 imaging in which each patient was studied twice with exercise and dipyridamole, sensitivity was in the 80 % range and specificity in the range of 90 %. There were no differences between the two forms of stress (Leppo 1996). The published studies looking at the accuracy of adenosine stress did not in general perform stress twice and used predominately SPECT imaging with Tl-201 or the Tc-99m tracers. The average sensitivity for pharmacologic stress with vasodilators was 87 % and the specificity was 74 % (Leppo 1996). Based on extensive publications and practical clinical experience in everyday use, the accuracy of vasodilator pharmacologic stress is accepted as being equivalent to exercise stress.

Adenosine and Dipyridamole Pharmacologic Stress Protocols. Figures 4.7 and 4.8 demonstrate imaging protocols for using adenosine and pharmacologic stress in combination with a one-day Tc-99m protocol. Patients should fast a minimum of 8 h and medications and foods containing caffeine stopped for 12 – 24 h. Methylxanthines and dipyridamole need to be stopped for 48 h prior to testing as they inhibit the vasodilatory effects of the adenosine and dipyridamole and patients taking dipyridamole can have a severe response to adenosine. Patients with 2° A-V nodal block (Mobitz Type II) or 3° A-V nodal block without a functioning pacemaker should not receive adenosine due to the potential A-V node blocking effects. Patients with a prolonged PR interval or Wenckebach block can be tested safely. The use of vasodilator stress is recommended in all patients with a left bundle branch block (LBBB) as the use of exercise leads to a higher rate of false positive studies due to septal defects (American Society of Nuclear Cardiology 2001).

Adenosine is infused at a rate of 140 µm/kg per minute for 4 or 6 min with the radiotracer injected at minutes 2 or 3 and the infusion continued a minimum of 1 min to allow maximal extraction, especially of the Tc-99m tracers, which have a lower extraction fraction than Tl-201 across the coronary bed. If the patient has evidence of ischemia by symptoms or profound ECG changes, the radiotracer can be administered earlier, but the infusion must be maintained a minimum of 1 min to allow radiotracer extraction at the high coronary blood flow rates. Performing low level exercise during adenosine infusion decreases side effects and improves image quality and is recommended in all patients capable of walking on a treadmill.

Dipyridamole is infused at a rate of 0.56 mg/kg of body weight over 4 min to a maximum total dose of 60 mg. Tl-201 or a Tc-99m radiotracer can be administered by bolus injection 3 – 4 min following completion of the infusion or earlier if the patient has evidence of

Table 4.4. Typical SPECT perfusion acquisition parameters

1. Dose (recommendations for 70-kg patient, adjust accordingly based on weight): Tc-99m 30 mCi for one day or dual isotope and 8–12 and 24–36 for one day split dose protocol; Tl-201 2–5-3.5 mCi
2. Position: supine in general, prone imaging to minimize diaphragmatic attenuation
3. Energy windows: Tc-99m 140±15% keV; Tl-201 centered on 70 keV peak and also on higher 135–167 keV
4. Collimators: Tc-99m low-energy high-resolution (LEHR); Tl-201 low energy all purpose (LEAP); dual isotope LEHR
5. Orbit: 180° from 45° RAO to 45° LPO using circular or noncircular (elliptical or body-contoured) orbits
6. Pixel size: 6.4±0.4 mm for 64×64 matrix
7. Acquisition type: step-and-shot or continuous
8. Number of projections: 64 over 180° for Tc-99m and 32 for Tl-201
9. Total time: dependent on number of detectors but should get adequate number of counts in under 20 min to avoid patient motion

ischemia by symptoms or profound ECG changes. Maximal coronary hyperemia is delayed due to the need to allow endogenous adenosine levels to increase following the inhibition of the reuptake mechanism by dipyridamole. Aminophylline administration is required more often due to the longer half-life, and side effects may recur due to the shorter half-life of aminophylline.

Catecholamines. Dobutamine is used infrequently for myocardial perfusion imaging. The protocol requires 3-min stepwise infusion stages of increasing doses of dobutamine and takes longer than vasodilator stress (Hays et al. 1993). Patients with hypertension, abdominal aortic aneurysms, poorly controlled supraventricular arrhythmias or ventricular arrhythmias should not be studied. Although some nuclear cardiology laboratories use it exclusively, at most centers it is used predominately in patients with severe and poorly controlled lung disease and in patients who have ingested caffeine on the day of testing and vasodilators cannot be used.

4.1.4 SPECT Image Acquisition

The recommendations for acquisition are summarized in Table 4.4. The parameters will vary depending on the equipment used and patient considerations such as gender and weight. Light weight, small footprint, 90° fixed field of view camera systems are ideal for nuclear cardiology procedures and have allowed placement in non-hospital settings. The limitations of such systems is that they cannot be used for general nuclear medicine procedures other than brains and large patients are a problem. The listed parameters were established to obtain the maximal counts for best image quality.

4.1.5 Processing Protocols

Once the acquisition is completed, the results need to be reviewed to determine whether the patient can leave or additional acquisition is required. SPECT processing can be performed by technologists or physicians but requires careful review by both: the technologists before the patient leaves to see if re-imaging is required and the physician at the time of interpretation in order to see if technical factors will influence the perfusion images. Communication between the two is important in order to get the best possible results. The basic steps of the process are listed in Table 4.5. Orientation and segmentation should be in accordance with published guidelines (Cerqueira et al. 2002). Technical advances in computer processing are providing more options that should result in better image quality.

Table 4.5. Typical SPECT processing protocols

1. Filtering: low pass filters such as Hanning or Butterworth with cutoff adjusted to the signal-to-noise ratio
2. Reconstruction: generally filtered back projection with a ramp filter. Faster processors make iterative techniques possible which avoid "ramp filter" artifacts caused by GI activity
3. Reorientation: oblique angle reformation relative to the long axis of the heart is recommended
4. Display for cine review of rotating projection images and interpretation should be performed on a workstation

4.1.6 Quantitative Analysis of Perfusion

Visual analysis is the recommended method of interpretation, but quantitative methods may be useful to provide over reads. The steps for performing quantitative analysis are outlined in Table 4.6. These steps are critical to get good results. Poor definition of the borders is likely to result in errors. The most difficult problem with using quantitative analysis is overcoming the fear of not calling abnormalities when they are identified as abnormal by quantitation. This fear may be related to concerns about liability or an over eager need to be sensitive and not miss any disease. In either case, it is important to reach a decision based on visual interpretation before reviewing the quantitation. Many recognize that it is more sensitive and less specific and areas identified as abnormal are given a second look just in case something was missed. Problems with scaling, boundary definitions, inappropriate alignment and

Table 4.6. Perfusion quantitation

1. Define limits: apex, basal plane and search limits for epicardial borders need to be manually defined
2. Scaling and normalization to the heart
3. Polar plot generation
4. Database comparison using gender appropriate normal files and generally using 2.5 standard deviations below the normal mean to define abnormal perfusion
5. Generating blackout, severity and reversibility maps

scatter lead to erroneous quantitative results that lead to patients being inappropriately labeled as having CAD.

4.1.7 ECG Gating

Since being introduced in the early 1990s, ECG gating is now a critical element of all SPECT studies and more than 90 % of all perfusion studies are performed with gating (Germano et al. 1995). Gating can be performed with both Tl-201 and Tc-99m agents. However, due to the higher count rates achieved with Tc-99m perfusion tracers, these are the preferred agents for ECG gated SPECT.

Gated SPECT Acquisition. Gated SPECT studies are acquired using 8 or 16 time frames in the heart cycle. It has been demonstrated that 16 frames are more accurate for ejection fraction calculation, but at the expense of poor image quality as each of the 16 frames only has one-half the counts contained in the 8-frame acquisition. Ejection fraction measured using 8 frames will give values that are approximately 3 ejection fraction units lower than when 16-frame acquisition is performed. Sixteen-frame acquisition allows analysis of filling and ejection rates that can be used for assessment of diastolic function (Akincioglu et al. 2005).

For arrhythmia rejection, it is best to avoid selection of parameters that will compromise the perfusion information or prolong the acquisition. Thus, accepting all beats will guarantee high-count perfusion images without increasing the imaging time, but this may compromise the results of the ejection fraction calculation. To guarantee optimal perfusion information, a ±50 % acceptance window around the pre-study sampled heart rate will give the most counts. Newer systems allow separate perfusion and gated windows to be acquired, in which case a tighter acceptance window can be used to get the most accurate ejection fraction without compromising the perfusion data. Patients in atrial fibrillation with a narrow RR interval have accurate EF measurements. If more than 1 out of every 6 beats is an APC or PVC, EF measurements are not reliable.

Gated SPECT Wall Motion Analysis. Areas that have normal wall motion and thickening may be associated with normal myocardium, the two-thirds of segments having ischemia on perfusion imaging, or anatomic variants such as apical thinning, or areas with breast or diaphragm attenuation. Since gated Tc-99m studies are acquired a minimum of 15 min following peak exercise stress, regional wall motion in most patients with ischemia usually returns to normal by the time of imaging. If there is profound ischemia, areas of myocardium may continue to have persistent wall motion abnormalities that are detected during gated acquisition in as many as one-third of cases (Johnson et al. 1997). One of the most important benefits of gated SPECT acquisition is helping to differentiate attenuation due to the diaphragm or breast from areas of old myocardial infarction or scar (Choi et al. 1998). Areas of scar have absent or diminished motion and thickening while areas with decreased activity due to attenuation will show normal motion and thickening. Patients with prior heart surgery will show akinesis or hypokinesis of the septum because of the surgery in the absence of ischemia or infarction.

Validation of Gated SPECT EF with Blood Pool Imaging. In addition to improving diagnostic accuracy during subjective visual image interpretation, gated Tc-99m measurements of global ejection fraction and regional wall thickening have been validated using equilibrium blood pool imaging, cardiac catheterization and cardiac MR (Everaert et al. 1996, 1998; Gunning et al. 1997; Mochizuki et al. 1997). These studies found excellent agreement across EF values ranging from 12 to 88. Small hearts gave very high EF values due to the poor spatial of the SPECT systems.

4.1.8 Acquisition Options

Attenuation correction may be performed using either a sealed source such as Gd-153 or an X-ray or CT based method for acquiring the transmission maps. The results to date on both methods have not resolved the true value of either method for improving accuracy (Masood et al. 2005). In addition to attenuation, scatter degrades image quality and needs to be corrected as well as the loss of resolution as a function of distance between the organ and the detector.

4.1.9 Image Interpretation and Reporting

As listed in Table 4.6, accurate interpretation of SPECT MPI studies involves a systematic approach that starts with technical quality control performed on the rotating projection images, rest/stress perfusion and func-

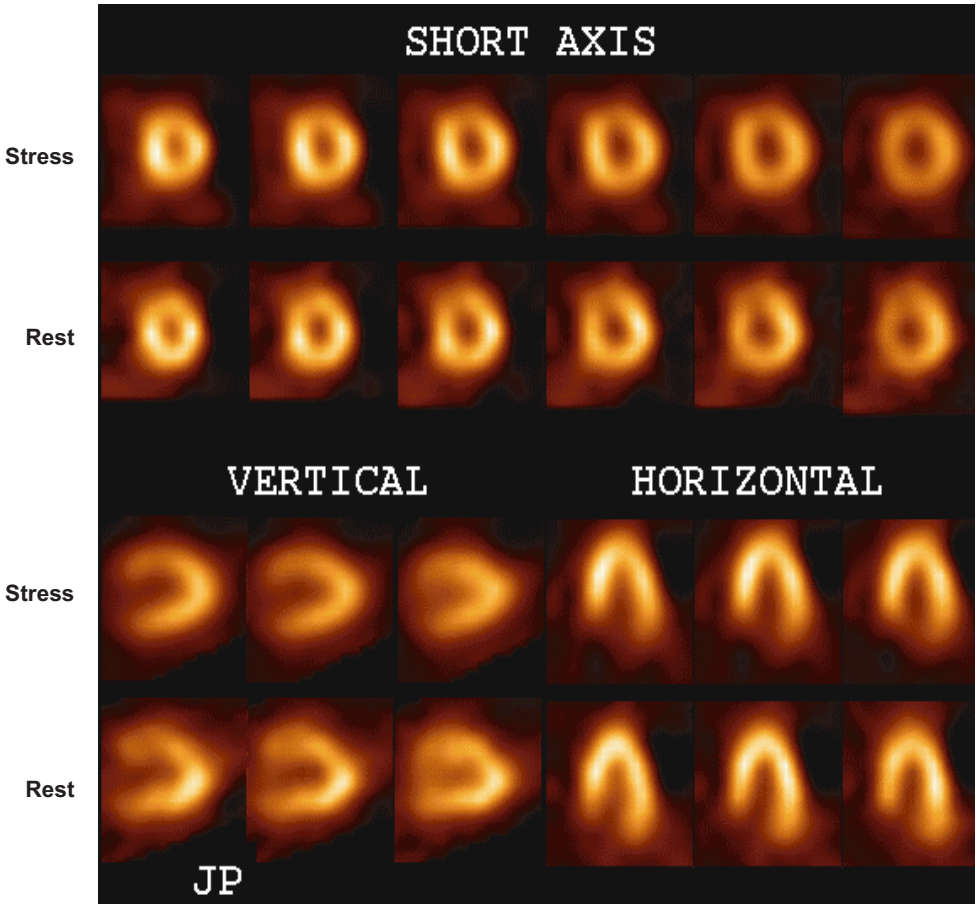

Fig. 4.9. Three view stress and rest Tc-99m/Tl-201 study that shows diminished perfusion on both

Table 4.7. Essential items to review on the rotating projection images as part of the quality control prior to interpretation of myocardial perfusion images

1. Patient motion
2. Count density
3. Sources of attenuation such as breast and diaphragm
4. Extracardiac activity: liver, gallbladder, stomach and bowel
5. Lung uptake
6. Cardiac chamber size: rest, stress and any change between them due to transient ischemic dilation
7. Pathologic soft-tissue uptake

tion comparison, reaching a conclusion based on the imaging information, reviewing the clinical indications and the stress test results and reconciling all this data to reach a final conclusion (Cerqueira 1996b; Hendel et al. 2003). An important part of this process is the initial quality control that must be done on an interactive workstation that allows image manipulation and modification. The items listed in Table 4.7 must be systematically examined on every study to identify technical factors that may influence the perfusion data seen on the aligned slices. False positive SPECT MPI studies very often are due to poor quality acquisition data that in the process of filtering, reconstruction and display, perfusion defects are created and not recognized.

Once this initial quality control has been performed, the matched stress and rest slices must be aligned and reviewed ideally using at least two color scales. The first one used should be linear, preferably gray scale, that displays the data spectrum in a continuous manner. Color scales have different characteristics that require careful correlation with coronary angiography or patient outcomes to determine the accuracy of diagnosis. An example of a SPECT perfusion study is shown in Fig. 4.9 in a female patient who was 5'5" (1.63 cm) tall and weighed 275 lbs (125 kg). Three views are shown and there is a clear anterior wall defect on the stress and rest views. Is this due to breast attenuation or an old infarction? Listing a long differential is not helpful for clinicians, but using ECG gating (Fig. 4.10) to show that the wall moves and thickens makes this most consistent with attenuation and the study can be interpreted as normal after obtaining from the clinical history and

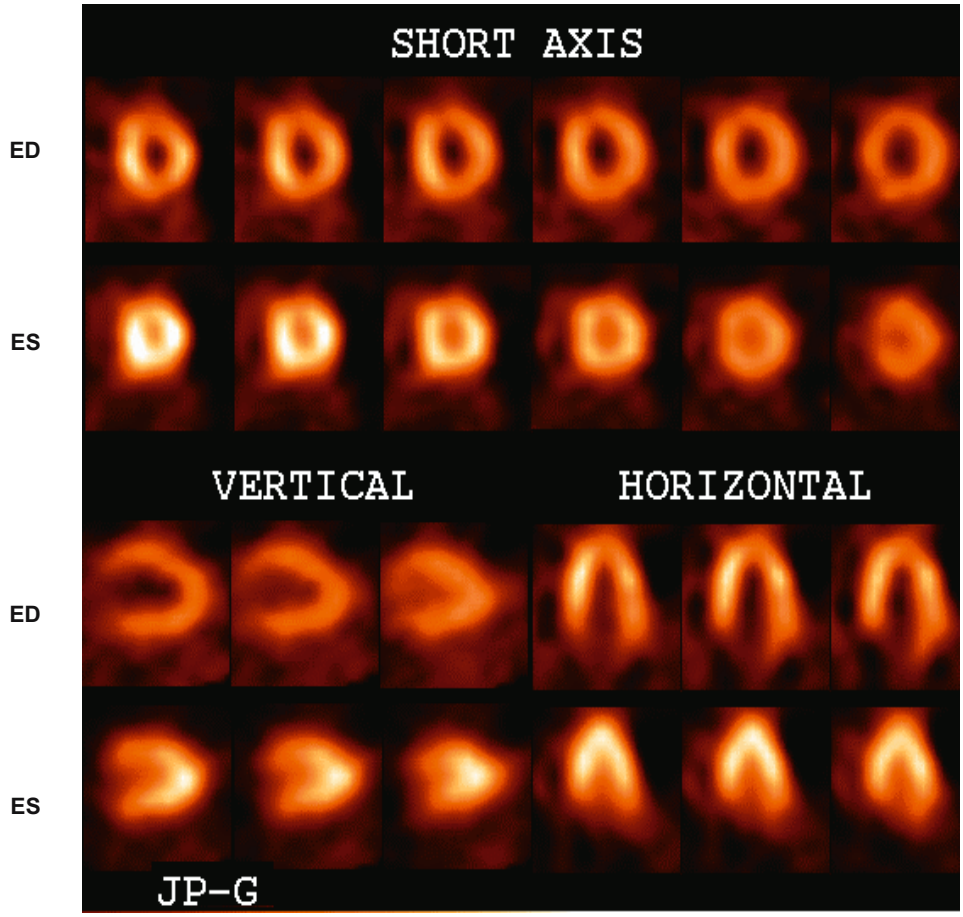

Fig. 4.10. End diastolic and systolic frames in the same patient as in Fig. 4.9 showing that there is movement and thickening or brightening in the anterior wall most consistent with breast attenuation and not infarction

ECG that the patient had no history of infarction, exercised to 91 % of the maximal age predicted heart rate and had no chest pain or ECG changes of ischemia.

Figure 4.11 shows a patient with a clear reversible anterior wall area of ischemia. Figure 4.12 shows lateral wall ischemia and Fig. 4.13 demonstrates an inferior wall infarction with surrounding ischemia.

4.1.10 Generating a Report

The final product of all the above steps is a report for the referring physician that conveys an accurate, unambiguous and clinically relevant assessment of the probability that the patient has abnormal myocardial blood flow (Cerqueira 1996b; Hendel et al. 2003). It is beyond the scope of this concise review to cover this most important detail.

4.1.11 Clinical Indications

4.1.11.1 Diagnosis of CAD

Sensitivity and specificity for MPI have been extensively reported using planar Tl-201 to more recent publications using the Tc-99m tracers with SPECT, quantitative analysis and the use of ECG gating (Iskandrian et al. 1997; Mahmarian et al. 1990). The accuracy is heavily influenced by the populations being studied and post test referral bias. In a meta-analysis using primarily planar Tl-201 studies weighted by sample size, a sensitivity of 87 % and a specificity of 64 % were reported (Fleischmann et al. 1998). In an analysis including more contemporary studies with Tc-99m SPECT and gating, the sensitivity was found to be 87 % and the specificity was 73 % (Klocke et al. 2003). Tc-99m radiotracers provide the best quality gated images, and are the most commonly used.

It is recommended that treadmill testing be used

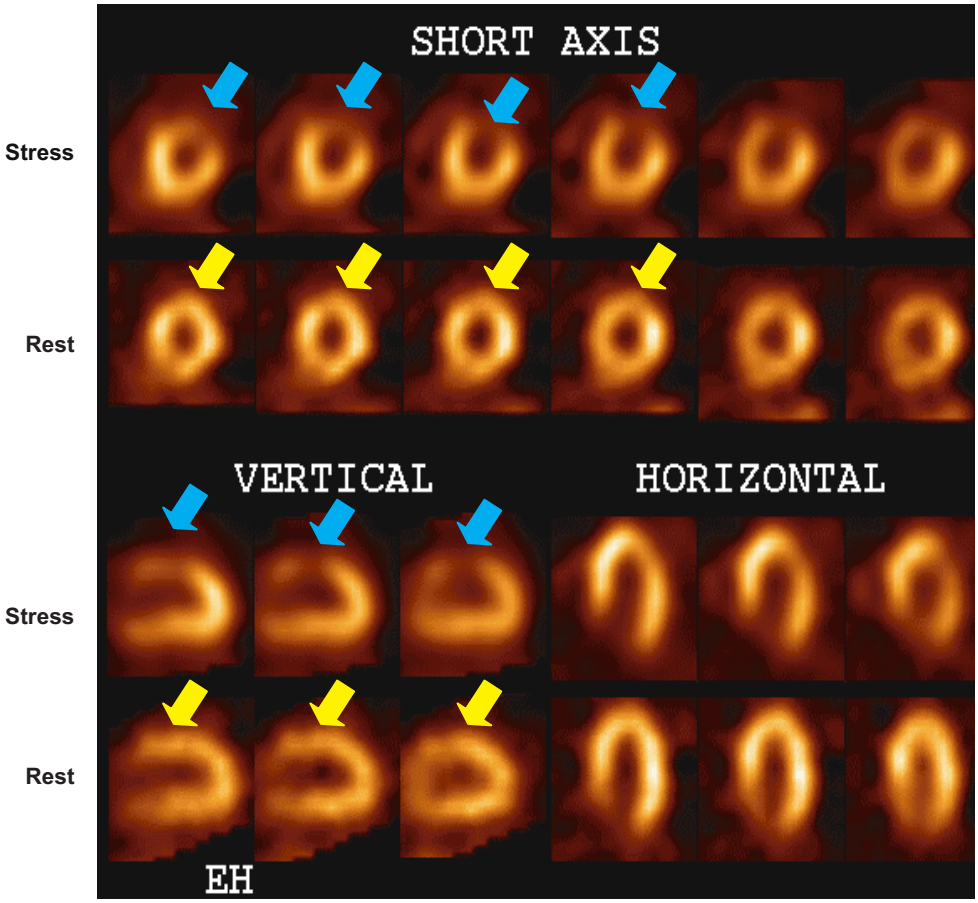

Fig. 4.11. Three view Tc-99m/Tl-201 study in a patient with a clear anterior defect on stress (*blue arrows*) and a normal resting set of images (*yellow arrows*) consistent with left anterior descending distribution ischemia

first in a stepwise approach for patients with an intermediate risk for CAD who have a normal baseline ECG and are capable of performing dynamic exercise (Gibbons et al. 2002). For patients who are unable to exercise, SPECT MPI is capable of providing diagnostic and prognostic information that cannot be gotten from treadmill testing. However, such patients have more risk factors and even if the perfusion study is normal, the occurrence of cardiac death is higher than in patients who are capable of exercising (Hachamovitch et al. 1998). In patients who have positive ECG changes of ischemia, SPECT MPI provides additional information for management, especially in the intermediate risk category (Shaw et al. 1999a). In a study with 4,649 intermediate Duke Treadmill Score patients who had normal perfusion, the 7-year cardiac mortality was very low at 1.5 % and the cumulative frequency of catheterization was 17 % (Gibbons et al. 1999).

SPECT is recommended in patients with abnormal ST segments, LBBB, ventricular paced rhythms, pre-excitation, left ventricular hypertrophy (LVH) or prior revascularization (Gibbons et al. 2002, 2003). The effects of referral bias, testing in patients with prior revascularization and the documented occurrence of abnormal perfusion in patients without obstructive CAD but functionally abnormal flow reserve, all influence the accuracy of testing when comparing it to the "gold standard," coronary angiography. For that reason, accuracy of testing for the detection of disease and assessment of prognosis will be discussed in the context of recognized specific patient populations that can influence the results of testing.

Ethnic and Racial Differences. Most of the published data on SPECT is in Caucasian males capable of performing dynamic exercise. When tests are performed in other groups, SPECT accuracy and prognosis results vary and usually lose accuracy and prognostic value (Akinboboye et al. 2001; Shaw et al. 2005). Many of these groups have a higher cardiovascular risk factor profile and other potential factors influencing test performance such as LVH and arrhythmic death. African Americans have overall lower test accuracy and worse prognosis across the range of ischemia. Whereas the

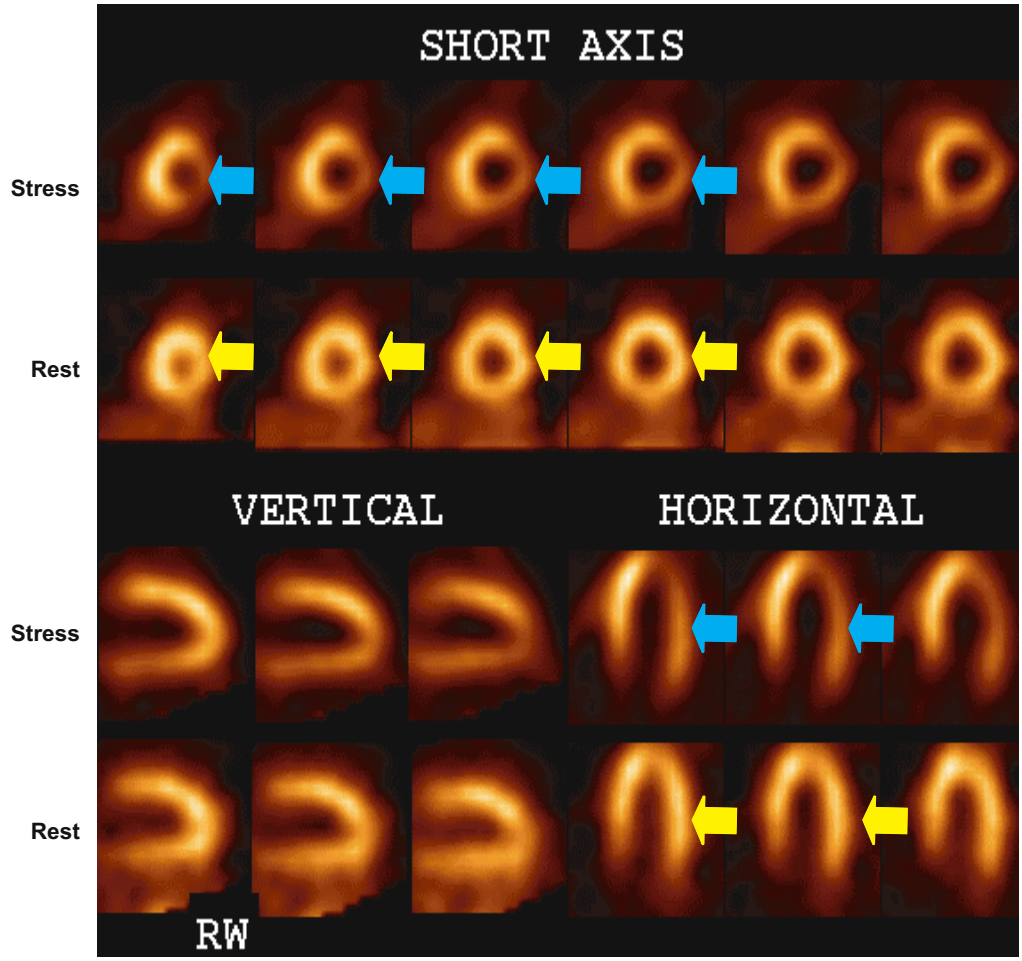

Fig. 4.12. Three view Tc-99m/Tl-201 study in a patient with a lateral wall defect on stress (*blue arrows*) and a normal resting set of images (*yellow arrows*) consistent with left anterior descending distribution lateral wall ischemia

death and MI rate in Caucasians is < 1 % with a normal SPECT MPI, two studies have shown it to be 2 %/year in African Americans.

Women. SPECT diagnostic and prognostic accuracy in women is influenced by gender differences in the prevalence of CAD and technical limitations, primarily breast attenuation, that lower study accuracy due to lower specificity (Taillefer et al. 1997). Low specificity was a major limitation in the early studies using planar Tl-201 that was overcome with the availability of SPECT, ECG gating and the use of attenuation correction. Using these advanced techniques, gender differences in the performance of testing for diagnosis have been minimized, but not totally eliminated, and the specificity is comparable to those reported for stress echocardiography (Taillefer et al. 1997). Similarly, the prognostic value of SPECT MPI has been shown to be accurate in women undergoing exercise or pharmacologic stress testing.

LBBB/Pacemakers, Left Ventricular Hypertrophy, Patients with Nonspecific ST-T Wave Changes. For patients in these categories, treadmill testing does not provide accurate diagnostic or prognostic information and SPECT MPI is indicated for evaluation. Patients with LBBB with exercise MPI have a low specificity in the LAD distribution due to a septal defect caused by diminished septal blood flow at high heart rates in the absence of obstructive CAD (Wagdy et al. 1998). If there are associated perfusion defects in the apex or anterior wall, specificity is improved but the use of vasodilator stress improves diagnostic accuracy and gives prognostic information. Overall prognosis is worse in such patients but imaging is predictive of events. In 245 patients the 3-year survival was 27 % in high risk scans and 87 % in low risk scans (Wagdy et al. 1998). Less well documented is the effect of pacemakers on SPECT accuracy and prognosis, but such patients are treated in the same way as those with LBBB and prognostic value of SPECT is retained (Giola et al. 1997). In the presence

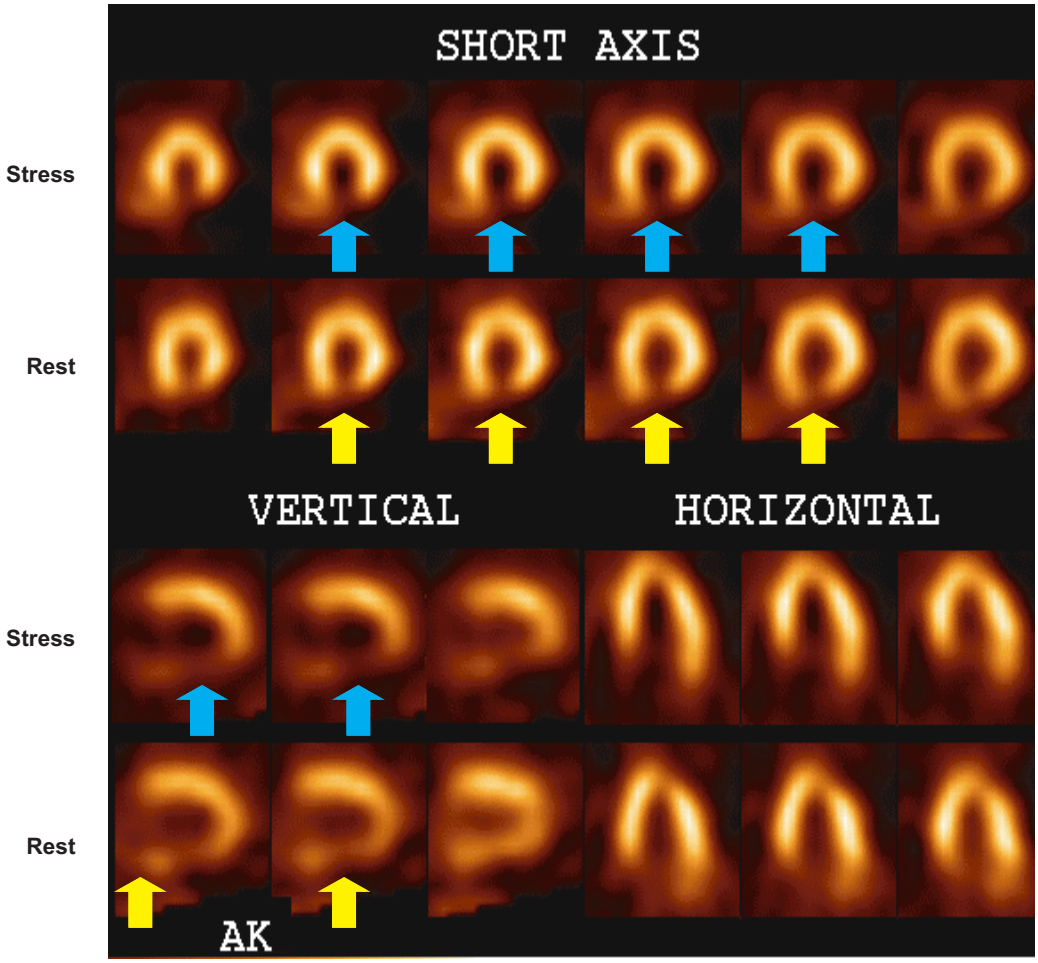

Fig. 4.13. Three view Tc-99m/Tl-201 study in a patient with a large inferior wall perfusion defect on stress (*blue arrows*) and a persistent but smaller defect on the resting set of images (*yellow arrows*) consistent with right coronary artery infarction and peri-infarct ischemia

of LVH, hypertension or nonspecific ST-T wave changes on the resting ECG, SPECT retains diagnostic and prognostic value (Amanullah et al. 2000; Elhendy et al. 2001). Well trained athletes with LVH by echocardiography have been reported to have a higher incidence of false positive studies due to "hot spot" scaling problems (Bartram et al. 1998).

Asymptomatic Patients. Although testing is not recommended in asymptomatic patients, SPECT can detect the presence of disease and give prognostic information (Blumenthal et al. 1996, 2003). Testing may be appropriate in high risk occupations such as aviators, firemen and policemen with multiple risk factors (Gibbons et al. 2002).

Diabetes. Patients with diabetes mellitus (DM) are at a very high risk for having critical coronary stenosis and cardiovascular events (Diabetes mellitus: a major risk factor for cardiovascular disease 1999). Despite the diffuse nature of vessel involvement with a higher occurrence of balanced disease, SPECT has diagnostic and prognostic value (Giri et al. 2002; Kang et al. 1999a, 1999b; Wackers et al. 2004). In a retrospective analysis, event free survival was found to be lower in diabetics across all categories of ischemia (Kang et al. 1999b). In a prospective study involving 1,123 carefully screened asymptomatic diabetics, half were randomized to SPECT imaging and 118 (22%) were found to have silent ischemia on SPECT, of which 33 (6%) had moderate or large perfusion defects. The high prevalence of silent ischemia was higher than expected. All patients in this study are being prospectively followed to determine if imaging will influence management and long term survival.

4.1.11.2 Chest Pain in the Emergency Department

Patients presenting to an emergency department (ED) within several hours of chest pain and a nondiagnostic ECG can be risk stratified based on acute injection of a Tc-99m perfusion tracer. Patients with a perfusion abnormality are at high risk for having infarction or unstable angina and deserve very aggressive medical and interventional management. Such patients will have abnormal perfusion due to occlusion or spasm of an unstable vessel and the perfusion abnormalities can be detected prior to elevation of serum enzyme markers (Tatum et al. 1997; Heller et al. 1998; Udelson et al. 2002). The closer to the time of chest pain the isotope is injected, the greater the sensitivity of the study. Injection 2 h after symptoms is less reliable. Studies have a very high negative predictive value and patients discharged have a very low likelihood of having cardiac events. If the acute study is normal, it can be used as the resting image for comparison following exercise or pharmacologic stress to exclude underlying CAD in such patients. In a prospective randomized controlled study comparing imaging to conventional ED care to such care with imaging, imaging significantly lowered hospitalization rates from 52 % to 42 % (Udelson et al. 2002).

4.1.11.3 Myocardial Perfusion Imaging Before and After Revascularization

Radionuclide Imaging Before Revascularization Interventions. SPECT is used to assess the highly variable physiological relationship between coronary lesion severity and coronary flow reserve. Even in the presence of flow limiting stenosis, if exercise or pharmacologic stress perfusion is normal, patients are at low risk for cardiac events (Brown and Rowen 1993). Using SPECT as a gatekeeper for referral to coronary angiography has been shown not only to be cost effective, but in no circumstance does it place patients at a higher risk for cardiac death or nonfatal myocardial infarction in comparison to the more expensive and invasive approach of performing angiography on all patients (Shaw et al. 1999b). It also has a role in determining the sequence and number of grafted vessels in high risk coronary artery bypass graft (CABG) patients and for identification of the culprit lesion at the time of percutaneous coronary intervention (PCI).

Radionuclide Imaging After Percutaneous Coronary Intervention. In asymptomatic patients routine SPECT is not indicated at any time in the first 2 years following a procedure (Brindis et al. 2005). In the first few months after a procedure it has been shown that < 30 % of symptomatic patients have documented stenosis (McPherson et al. 1999). In addition, peri-procedural changes in the treated area may result in perfusion defects even in the absence of restenosis, and testing in symptomatic patients the first 4 – 6 weeks following a procedure is not recommended due to the occurrence of false positives (Jain et al. 1988). If ischemia is detected beyond the immediate period of the procedure, the prognostic value of SPECT persists and the occurrence of cardiac death and MI is increased in patients with large amounts of ischemia (Ho et al. 1999). With the placement of drug eluting stents to prevent restenosis, delayed healing, prolonged inflammation and exercise induced paradoxic coronary vasoconstriction of the adjacent segment have been reported.

Radionuclide Imaging after CABG. Even with the altered anatomy following CABG, SPECT retains diagnostic and prognostic accuracy early and late for detection of stenosis in grafts as well as in the native vessel (Miller et al. 1998; Palmas et al. 1995; Zellweger et al. 2001). Routine testing in asymptomatic patients is not recommended (Brindis et al. 2005). The extent and severity of perfusion abnormalities detected by SPECT is predictive of death in both symptomatic and asymptomatic patients in the first 5 years after surgical revascularization (Zellweger et al. 2001). Beyond 5 years, it has been shown that the presence of ischemia is the strongest predictor of mortality (Palmas et al. 1995; Lauer et al. 1998; Nallamothu et al. 1997). In 9,000 asymptomatic patients, the presence of ischemia predicted a 3 % annual mortality (Lauer et al. 1998).

4.1.11.4 Radionuclide Imaging Before Noncardiac Surgery

Risk assessment prior to noncardiac surgery requires a thorough review of the clinical, demographic and surgical indications of risk rather than nonselective use of SPECT (Eagle et al. 2002). Major predictors of increased perioperative risk include recent acute MI, unstable angina pectoris, decompensated congestive heart failure, significant arrhythmias, high degree of atrioventricular block and severe valvular disease. In such patients SPECT is not indicated. Pharmacologic perfusion imaging with dipyridamole or adenosine is an effective method for risk assessment (Klocke et al. 2003; Mangano and Goldman 1995). The negative predicative value in both vascular and nonvascular surgery cases was 96 – 100 %, but the positive predictive value of any ischemia ranged from 4 % to 20 % in vascular patients. Perfusion markers of high risk include a large area of ischemia, perfusion defects in multiple vascular territories, left ventricular dilatation, or increased lung Tl-201 uptake, and such patients are candidates for angiography. The ACC/AHA guidelines recommend cor-

onary angiography should be performed in patients for whom the results of noninvasive testing indicate a high risk of cardiac events or who have angina pectoris that is unresponsive to medical therapy. In low risk patients with low risk surgery, SPECT is not indicated.

4.2 Assessment of Ventricular Function

4.2.1 Historical Perspective

Used widely in the late 1970s and 1980s for the detection of CAD in combination with bicycle exercise stress and for resting global and regional function, the use of ERNA and FPRNA declined in the 1990s. This was due to the increasing use of planar and SPECT perfusion imaging with ECG gating for CAD detection and the competition from echocardiography, which provides more clinically relevant information. These factors, in combination with the declining availability of the multicrystal and small field of view cameras that are optimal for high quality studies, have resulted in resting ERNA studies being performed almost exclusively for the monitoring of anthracycline induced cardiotoxicity. It is not likely that the use of these techniques will increase in the future. The American Society of Nuclear Cardiology has published and is revising detailed guidelines for the performance and interpretation of these methods (American Society of Nuclear Cardiology 2001).

4.2.2 Equilibrium Radionuclide Angiocardiography

The nomenclature for this technique includes MUGA (name of an early software program), equilibrium gated blood pool imaging and radionuclide ventriculography. It can be used determine global and regional right ventricular (RV) and left ventricular (LV) function at rest and following exercise or pharmacologic stress. Analysis of the time activity curve provides information on systolic and diastolic function. Both planar and tomographic methods have been used for acquisition, but planar predominates due to ease of use and extensive experience.

4.2.2.1 Technique

Radiopharmaceutical and Red Blood Cell Labeling. The basic technique uses 2–3 mg of stannous pyrophosphate to create a favorable oxidation/reduction environment inside red blood cells (RBC) so that when 20–35 mCi of Tc-99m pertechnetate is administered it binds to hemoglobin and remains attached. Labeling can be accomplished in three ways: in vivo, modified in vivo/in vitro and in vitro. There are differences in the efficiency of labeling, defined as the percentage of total radioactivity attached to RBCs, versus the time and expense required to perform the technique. Heparin and dextrose have been shown to decrease labeling efficiency. The use of Tc-99m from an old generator results in high background activity due to high amounts of Tc-99 which compete for the stannous ions and allow a higher percentage of non-RBC labeling.

In Vivo. This is the simplest, fastest and least expensive labeling method but gives the lowest labeling efficiency. The stannous pyrophosphate is given intravenously followed 15 min later by Tc-99m, which can be given as a rapid bolus for first pass radionuclide angiography (FPRA). This method achieves only 80–90% RBC labeling and the background activity is higher due to labeling of structures outside the vascular space such as the stomach and thyroid.

Modified In Vivo/In Vitro. The stannous pyrophosphate is given intravenously and 20–30 min later an aliquot of blood is withdrawn into a syringe containing the Tc-99m pertechnetate and this is gently shaken for 10 min before being injected back into the patient. The labeling efficiency approaches 95%.

In Vitro. An aliquot of blood is withdrawn, centrifuged and the RBC pellet washed, incubated first with stannous pyrophosphate followed by the Tc-99m before being re-injected into the patient. There are commercial kits available which give a labeling efficiency of >97% using this method.

Instrumentation and Procedure. Table 4.8 lists the acquisition parameters for rest and exercise studies. Rest studies allow longer acquisition times and can be performed with a high resolution collimator. A collimator with 30° angulation allows optimal separation of the left atrium from the LV in the LAO position, especially in patients with a horizontally positioned heart. Stress studies are limited to a 2-min acquisition at rest and peak stress and in such situations a low energy all-purpose collimator gives a higher count rate. Cameras should be peaked at 140±10 keV. The heart rate is sampled prior to acquisition to establish the time interval for each frame and a ±10–15% arrhythmia rejection window should be used with elimination of the early beat as well as the next beat, which has a longer filling period. List mode acquisition allows 10-ms temporal resolution and maximal flexibility in image processing, but is memory intensive and many of the current programs do not make it easy to acquire or process studies. Buffered beat techniques with forward and backward reconstruction of the time activity curve to eliminate drop-off in counts

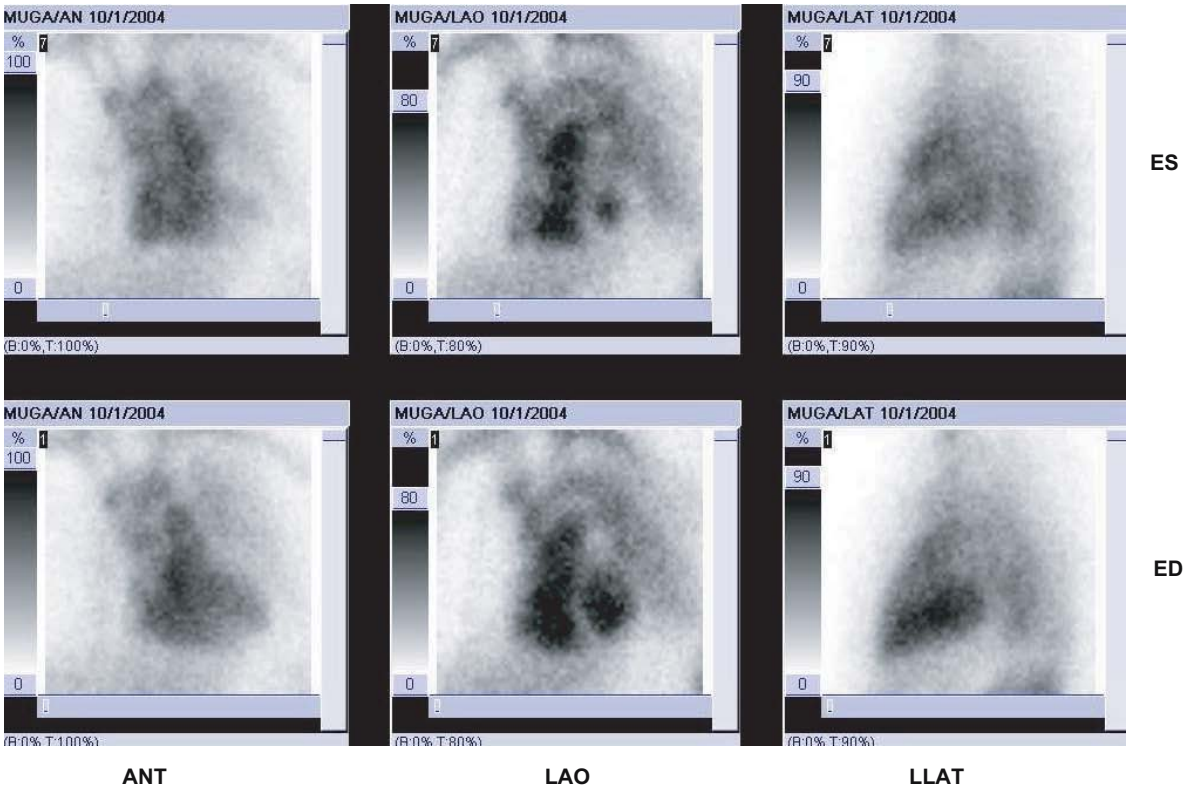

Fig. 4.14. Three planar ERNA images at ED and ES

Table 4.8. Typical equilibrium radionuclide angiocardiography acquisition parameters

1. Collimator: for resting studies a parallel hole high resolution collimator or a slant hole collimator to get better separation of left atrium from left ventricle on left anterior oblique. Rest/stress studies require low-energy all-purpose (LEAP) to get more counts
2. Energy window: 140±10 %
3. Arrhythmia rejection: ±10 – 15 % of mean R-R interval with rejection of next beat
4. Acquisition method: frame mode or buffered beat. List mode optional but cumbersome
5. Frame rate: minimum of 16 – 32 frames for rest and stress
6. Count density: 20,000 counts/cm over center of left ventricle
7. Positioning: best RV/LV separation on left anterior oblique (LAO) plus anterior and lateral usually 45° to either side of LAO. Exercise studies compares LAO views at rest and peak stress
8. Quality control: view cine-loop and R-R histogram
9. Interpretation: cine review of all three views

provide greater flexibility when diastolic function analysis is required. In order to measure the minimum volume in the time activity curve at end systole, a minimum of 16 frames is required to get an accurate EF in patients with fast heart rates at rest or during exercise stress. Rest studies with very slow heart rates require up to 32 frames to get accurate EF measurements.

Acquisition can be set up based on acquiring a fixed number of beats, time or counts. Whichever method is used, it is necessary to acquire a minimum of 20,000/cm over the center of the LV to get sufficient information density for an accurate EF calculation. The patient is positioned and three views are acquired. The most important view for calculating the EF is the left anterior oblique (LAO), which provides the best septal separation between the two ventricles, usually 45°. Once this view has been acquired, the camera head is rotated 45° anteriorly and 45° towards the left lateral to get orthogonal views.

Once the images have been acquired, the images are temporally and spatially smoothed and three views in a cine loop should be reviewed in gray scale for a visual assessment of global and regional function to correlate with the quantitative EF. These three views are shown in Fig. 4.14. The beat-length histogram should be reviewed for adequacy of ECG gating.

Calculation of an EF requires measuring counts or volume from the LAO view in the isolated LV at end diastole (ED) and end systole (ES) after correcting for the background activity. Figure 4.15 shows how the septum separates the LV from surrounding structures at ED

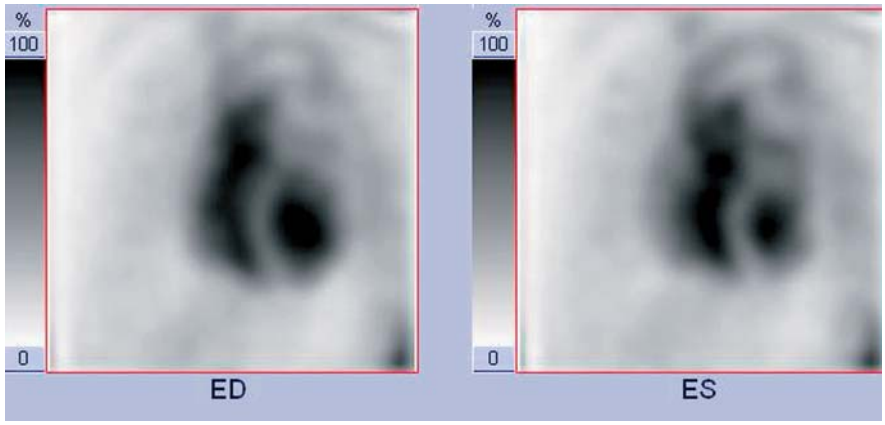

Fig. 4.15. End diastolic (ED) and end systolic (ES) frames on equilibrium radionuclide angiocardiography in the left anterior oblique position showing optimal separation of the two ventricular chambers

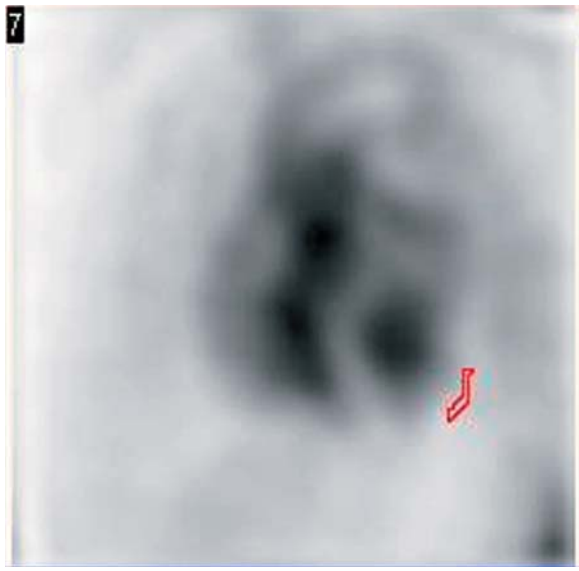

Fig. 4.16. Left anterior oblique at end systole showing where to place the background regions of interest required to get an accurate ejection fraction measurement

and ES. The left atrium can be seen popping up behind the LV on the ES frame. Background correction is necessary to eliminate the effects of blood pool activity in the structures overlaying and adjacent to the LV that do not change cyclically the way they do in the LV as a function of contraction. This background region is placed in the LAO view adjacent to the heart anywhere from 2 to 5 o'clock with care to avoid the left atrium, descending thoracic aorta, gastric free Tc-99m pertechnetate uptake or spleen and the lower counts found over a gastric bubble. This is shown in Fig. 4.16. Putting the background area in any of these regions will lead to erroneous results. The formula for calculating EF, LVEF = [(Background Corrected ED counts – Background Corrected ES counts/Background Corrected ED counts]) × 100), is used for measurements. Although methods are available for calculating absolute ventricular volumes, they are not used routinely for clinical studies.

Analysis of systolic and diastolic function using emptying and filling rates can be performed on the time activity curves as shown in Fig. 4.17.

Exercise Studies. To detect CAD, dynamic exercise can be performed using upright or supine bicycle exercise following RBC labeling. The patient is positioned on the bicycle with the camera in the LAO position and a 2-min acquisition is performed for a baseline measurement. Incremental exercise is performed in 3-min stages during which the patient exercises for 1 min

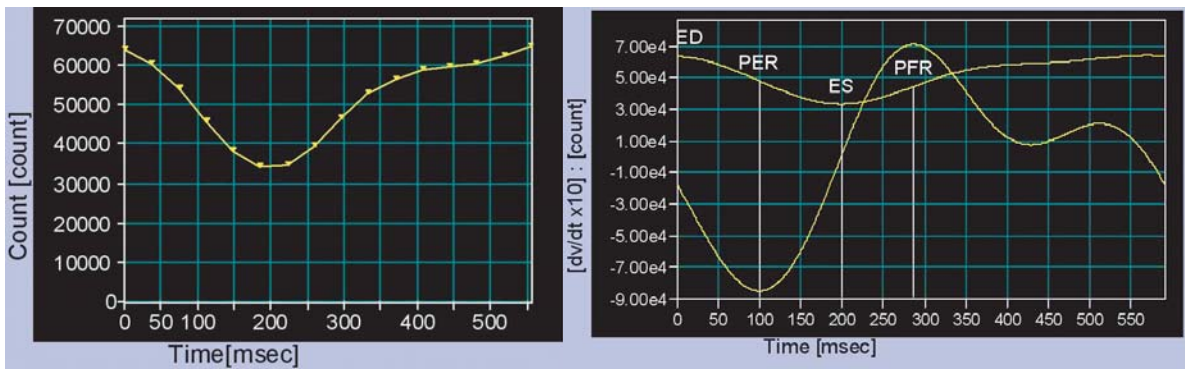

Fig. 4.17. Time activity curve and the 1st derivative curve used to derive emptying and filling for assessment of systolic and diastolic left ventricular function

before a 2-min acquisition is acquired for each stage until the patient reaches symptom limited maximal exercise. In patients without CAD or other forms of heart disease, with peak exercise there is a minimum augmentation in global EF by at least 5 EF units from the baseline measurement. In patients with critical flow limiting stenosis, EF may drop, stay the same or fail to augment by at least 5 EF units. Attempts to look at regional wall motion rather than the global EF response to improve sensitivity have not been successful due to the limited regional wall motion assessment available from the single LAO planar view.

4.2.2.2 Clinical Indications

Assessment of LV Function. ERNA is capable of providing accurate measurements of LV global and regional function. Although RV EF can be measured, overlap of the right atrium does not allow complete isolation of counts or volume in the RV and this introduces error depending on the position of the two chambers. Assessment of diastolic and systolic filling and emptying rates requires accurate time activity curves for analysis which conventional frame mode acquisition does not provide. Echocardiography using Doppler based velocity measurements can provide such information more readily.

Detection of CAD. With the availability of SPECT myocardial perfusion imaging, this technique is not used widely. Since the EF response to exercise may be abnormal in patients with nonischemic cardiomyopathies and other forms of cardiac muscle disease, specificity was low. In a composite of the published literature, a sensitivity of 86 % and a specificity of 79 % has been reported (Gibbons 1991). For patients unable to exercise, vasodilator stress does not provide sufficient accuracy in the ability to induce global or regional functional changes.

Monitoring Chemotherapeutic Cardiotoxicity. ERNA continues to have a role in the serial monitoring of adults receiving anthracyclines or trastuzumab for the treatment of cancer (Schwartz et al. 1987). This approach allows patients to receive the highest possible doses of these drugs for effective tumor treatment at the lowest possible risk of developing cardiotoxicity, which in early studies could be as deadly as the tumor being treated. A baseline EF is measured prior to treatment with anthracyclines. If the EF is less than 30 %, alternative agents should be considered. EF values of 30 – 50 % can be treated with a higher risk of toxicity but an EF measurement should be performed prior to each dose and treatment stopped if there is a decrease. For patients with EF > 50 %, a repeat measurement should be made at a total dose of 450 mg/min/m^2. If the EF remains normal treatment can be continued. If the EF drops by greater than 10 EF units but the absolute value remains above 45 %, treatment can be continued with measurements prior to each dose. If the EF drops by > 15 EF units or the absolute value falls below 45 %, this is considered moderate to severe toxicity and alternative chemotherapeutic drugs should be considered. Attempts to develop less toxic drugs or to pretreat patients with agents to lower cardiotoxicity have been unsuccessful and serial monitoring is still required. In this setting the reproducibility and quantitative nature of the technique offers advantages over echocardiography (van Royen et al. 1996).

4.2.3 First Pass Radionuclide Angiography

First pass radionuclide angiography (FPRNA) can be used to assess left and right ventricular function at rest or during stress. It provides information on wall motion, ejection fraction and assessment of systolic and systolic parameters. It is best performed with dedicated multicrystal or digital systems capable of delivering a minimum of 150,000 counts/s to provide sufficient information density. A bolus of radioactivity is injected into the venous system and multiple serial images are acquired at a 25 – 100 ms frame rate that allows the radioactivity to be tracked from when it enters the RV to when it exits from the LV. Using individual or summed time frames, measurements of global and regional RV and LV function can be performed. If there are atrial or ventricular shunts present, these may sometimes be detected and measured. Despite these unique features, the lack of adequate equipment and payer reimbursement for performing studies, it is seldom performed.

4.2.3.1 Instrumentation and Procedure

Table 4.9 lists the typical instrumentation and acquisition parameters. Studies performed independently of Tc-99m perfusion studies are best performed using Tc-99m diethylenetriaminopentoacetic acid (DTPA), which is cleared by the kidneys and is sufficiently far from the heart to not cause interference in case a second bolus injection is required. The injection site should be in a large vein to allow rapid, compact bolus administration. Patients are positioned upright or supine in the anterior or a shallow right anterior oblique (RAO) position for rest or exercise studies. For patients performing treadmill exercise stress, radioactive markers are placed on the chest and used for motion correction.

Table 4.9. Typical first-pass radionuclide angiography acquisition parameters

1. Radiopharmaceutical: 10 – 25 mCi at rest and exercise of Tc-99m diethylaminetriaminepentaacetic acid (DTPA) or Tc-99m sestamibi or tetrofosmin
2. Injection site: antecubital vein or external jugular using 14 – 18 gauge cannula
3. Injection rate: slow for assessment of RV function and rapid for assessment of function or detection of shunts
4. Position: upright or supine in anterior or 20°–30° right anterior oblique
5. ECG gating: multicrystal – no; single crystal – yes; shunt – no
6. Energy window: 120 – 160 keV
7. Window time frame: 25 – 50 ms for rest or stress RV and LV function; 50 – 100 ms for shunts
8. Single crystal collimators: high or ultra-high sensitivity for LV, LV and shunt

4.3 Heart Failure and Assessment of Viability

4.3.1 Introduction

For patients with heart failure due to ischemic or nonischemic causes, hypertrophic cardiomyopathy, hypertensive heart disease or valvular heart disease, radionuclide techniques have proven value. These techniques are useful for initial assessment of LV and RV systolic and diastolic function and for the assessment of myocardial viability and/or underlying ischemia in those patients being considered for revascularization who do not have angina (Klocke et al. 2003).

4.3.2 SPECT Methods

Regions of myocardial dysfunction may consist of scar, hibernating, stunned, ischemic, or infiltrated myocardium. As shown by histologic analysis, many times there is a continuum of all of these states, and radionuclide perfusion tracer uptake in such patients needs to have a linear relationship with the extent of viability and the probability of functional recovery after revascularization (Perrone-Filardi et al. 1995). Resting uptake of Tl-201 and the two T-99m tracers is capable of identifying areas of myocardium that will show functional recovery after revascularization, but accuracy is best when a threshold of 60 % is used for Tl-201 and 55 % for the Tc-99m tracers (Acampa et al. 2002). There were no differences between the three tracers using these thresholds.

4.3.3 PET Methods

An alternative method of viability assessment measures preserved metabolic activity at rest using F-18 FDG or C-11 labeled fatty acids (Allman et al. 2002; Di Carli et al. 1995; Tarakji et al. 2006). Such studies use a perfusion tracer, usually N-13 ammonia, O-15 water or Rb-82, and compare it to the marker of viability. Areas that have a perfusion/metabolism mismatch, severely diminished or absent perfusion but preserved or enhanced metabolic activity, have a high probability of regaining function after revascularization and improving long term survival, 88 % vs 50 % with medical treatment. Not only was survival improved, but heart failure symptoms were less after revascularization (Di Carli et al. 1994). The benefits of revascularization were shown in a larger group of patients who benefited from revascularization regardless of the amount of viability.

4.3.4 Neurocardiac Imaging

We still need new tracers and perhaps what is needed is to move forward a tracer with which we have some experience, I-123 MIBG for imaging of cardiac innervation (Arora et al. 2003). This agent could be extremely useful for the management of heart failure patients with regards to medical management as well as with the selection for expensive interventions such as implantable cardioverter-defibrillator (ICD) placement (Chambers et al. 2002). In order to make I-123 MIBG widely available, new sources of I-123 production will need to be developed and this will open up the possibility of developing new agents that are iodinated rather than Tc-99m or positron labeled. This makes the chemistry easier and could overcome many of the limitations we have faced using Tc-99m.

References

Acampa W, Cuocolo A, Petretta M, et al. (2002) Tetrofosmin imaging in the detection of myocardial viability in patients with previous myocardial infarction: comparison with sestamibi and Tl-201 scintigraphy. J Nucl Cardiol 9(1):33 – 40

Akinboboye OO, Idris O, Onwuanyi A, et al. (2001) Incidence of major cardiovascular events in black patients with normal myocardial stress perfusion study results. J Nucl Cardiol 8(5):541 – 547

Akincioglu C, Berman DS, Nishina H, et al. (2005) Assessment of diastolic function using 16-frame 99mTc-sestamibi gated myocardial perfusion SPECT: normal values. J Nucl Med 46(7):1102 – 1108

Allman KC, Shaw LJ, Hachamovitch R, et al. (2002) Myocardial viability testing and impact of revascularization on prognosis in patients with coronary artery disease and left ventricular dysfunction: a meta-analysis. J Am Coll Cardiol 39(7): 1151 – 1158

Amanullah AM, Berman DS, Kang X, et al. (2000) Enhanced prognostic stratification of patients with left ventricular hypertrophy with the use of single-photon emission computed tomography. Am Heart J 140(3):456 – 462
American Society of Nuclear Cardiology (2001) Updated imaging guidelines for nuclear cardiology procedures, part 1. J Nucl Cardiol 8(1):G5–G58
Arora R, Ferrick KJ, Nakata T, et al. (2003) I-123 MIBG imaging and heart rate variability analysis to predict the need for an implantable cardioverter defibrillator. J Nucl Cardiol 10(2):121 – 131
Bartram P, Toft J, Hanel B, et al. (1998) False-positive defects in technetium-99m sestamibi myocardial single-photon emission tomography in healthy athletes with left ventricular hypertrophy. Eur J Nucl Med 25(9):1308 – 1312
Blumenthal RS, Becker DM, Moy TF, et al. (1996) Exercise thallium tomography predicts future clinically manifest coronary heart disease in a high-risk asymptomatic population. Circulation 93(5):915 – 923
Blumenthal RS, Becker DM, Yanek LR, et al. (2003) Detecting occult coronary disease in a high-risk asymptomatic population. Circulation 107(5):702 – 707
Brindis RG, Douglas PS, Hendel RC, et al. (2005) ACCF/ASNC appropriateness criteria for single-photon emission computed tomography myocardial perfusion imaging (SPECT MPI): a report of the American College of Cardiology Foundation Quality Strategic Directions Committee Appropriateness Criteria Working Group and the American Society of Nuclear Cardiology endorsed by the American Heart Association. J Am Coll Cardiol 46(8):1587 – 1605
Brown KA, Rowen M (1993) Prognostic value of a normal exercise myocardial perfusion imaging study in patients with angiographically significant coronary artery disease. Am J Cardiol 71(10):865 – 867
Cerqueira MD (1996a) Pharmacologic stress versus maximal-exercise stress for perfusion imaging: which, when, and why? J Nucl Cardiol 3(6):S10 – 14
Cerqueira MD (1996b) The user-friendly nuclear cardiology report: what needs to be considered and what is included. J Nucl Cardiol 3(4):350 – 355
Cerqueira MD (2004) The future of pharmacologic stress: selective A2A adenosine receptor agonists. Am J Cardiol 94(2A):33D–40D; discussion 40D–42D
Cerqueira MD, Verani MS, Schwaiger M, et al. (1994) Safety profile of adenosine stress perfusion imaging: results from the Adenoscan Multicenter Trial Registry. J Am Coll Cardiol 23(2):384 – 389
Cerqueira MD, Weissman NJ, Dilsizian V, et al. (2002) Standardized myocardial segmentation and nomenclature for tomographic imaging of the heart. A statement for healthcare professionals from the Cardiac Imaging Committee of the Council on Clinical Cardiology of the American Heart Association. Int J Cardiovasc Imaging 18(1):539 – 542
Chambers MG, Narula J, Cerqueira MD (2002) The economic burden of heart failure and implantable cardioverter defibrillators: The value of noninvasive imaging of high-risk patients. J Nucl Cardiol 9(5 Suppl):71S–80S
Choi JY, Lee KH, Kim SJ, et al. (1998) Gating provides improved accuracy for differentiating artifacts from true lesions in equivocal fixed defects on technetium 99m tetrofosmin perfusion SPECT. J Nucl Cardiol 5(4):395 – 401
Di Carli MF, Davidson M, Little R, et al. (1994) Value of metabolic imaging with positron emission tomography for evaluating prognosis in patients with coronary artery disease and left ventricular dysfunction. Am J Cardiol 73(8):527 – 533
Di Carli MF, Asgarzadie F, Schelbert HR, et al. (1995) Quantitative relation between myocardial viability and improvement in heart failure symptoms after revascularization in patients with ischemic cardiomyopathy. Circulation 92(12):3436 – 3444
Diabetes mellitus: a major risk factor for cardiovascular disease. A joint editorial statement by the American Diabetes Association; The National Heart, Lung, and Blood Institute; The Juvenile Diabetes Foundation International; The National Institute of Diabetes and Digestive and Kidney Diseases; and The American Heart Association. Circulation 100(10):1132 – 1133
Dilsizian V, Bonow RO (1993) Current diagnostic techniques of assessing myocardial viability in patients with hibernating and stunned myocardium. Circulation 87(1):1 – 20
Eagle KA, Berger PB, Calkins H, et al. (2002) ACC/AHA guideline update for perioperative cardiovascular evaluation for noncardiac surgery – executive summary: a report of the American College of Cardiology/American Heart Association Task Force on Practice Guidelines (Committee to Update the 1996 Guidelines on Perioperative Cardiovascular Evaluation for Noncardiac Surgery). J Am Coll Cardiol 39(3):542 – 553
Elhendy A, van Domburg RT, Sozzi FB, et al. (2001) Impact of hypertension on the accuracy of exercise stress myocardial perfusion imaging for the diagnosis of coronary artery disease. Heart 85(6):655 – 661
Everaert H, Franken PR, Flamen P, et al. (1996) Left ventricular ejection fraction from gated SPET myocardial perfusion studies: a method based on the radial distribution of count rate density across the myocardial wall. Eur J Nucl Med 23(12):1628 – 1633
Everaert H, Vanhove C, Franken PR (1998) Gated SPET myocardial perfusion acquisition within 5 minutes using focussing collimators and a three-head gamma camera. Eur J Nucl Med 25(6):587 – 593
Fleischmann KE, Hunink MG, Kuntz KM, et al. (1998) Exercise echocardiography or exercise SPECT imaging? A meta-analysis of diagnostic test performance. JAMA 280(10):913 – 920
Germano G, Kiat H, Kavanagh PB, et al. (1995) Automatic quantification of ejection fraction from gated myocardial perfusion SPECT. J Nucl Med 36(11):2138 – 2147
Gibbons RJ (1991) Rest and exercise radionuclide angiography for diagnosis in chronic ischemic heart disease. Circulation 84(3 Suppl):I93 – 99
Gibbons RJ, Hodge DO, Berman DS, et al. (1999) Long-term outcome of patients with intermediate-risk exercise electrocardiograms who do not have myocardial perfusion defects on radionuclide imaging. Circulation 100(21):2140 – 2145
Gibbons RJ, Balady GJ, Bricker JT, et al. (2002) ACC/AHA 2002 guideline update for exercise testing: summary article. A report of the American College of Cardiology/American Heart Association Task Force on Practice Guidelines (Committee to Update the 1997 Exercise Testing Guidelines). J Am Coll Cardiol 40(8):1531 – 1540
Gibbons RJ, Abrams J, Chatterjee K, et al. (2003) ACC/AHA 2002 guideline update for the management of patients with chronic stable angina – summary article: a report of the American College of Cardiology/American Heart Association Task Force on practice guidelines (Committee on the Management of Patients with Chronic Stable Angina). J Am Coll Cardiol 41(1):159 – 168
Gioia G, Bagheri B, Gottlieb CD, et al. (1997) Prediction of outcome of patients with life-threatening ventricular arrhythmias treated with automatic implantable cardioverter-defibrillators using SPECT perfusion imaging. Circulation 95(2):390 – 394
Giri S, Shaw LJ, Murthy DR, et al. (2002) Impact of diabetes on the risk stratification using stress single-photon emission computed tomography myocardial perfusion imaging in patients with symptoms suggestive of coronary artery disease. Circulation 105(1):32 – 40

Gunning MG, Anagnostopoulos C, Davies G, et al. (1997) Gated technetium-99m-tetrofosmin SPECT and cine MRI to assess left ventricular contraction. J Nucl Med 38(3):438 – 442
Hachamovitch R, Berman DS, Shaw LJ, et al. (1998) Incremental prognostic value of myocardial perfusion single photon emission computed tomography for the prediction of cardiac death: differential stratification for risk of cardiac death and myocardial infarction. Circulation 97(6):535 – 543
Hays JT, Mahmarian JJ, Cochran AJ, et al. (1993) Dobutamine thallium-201 tomography for evaluating patients with suspected coronary artery disease unable to undergo exercise or vasodilator pharmacologic stress testing. J Am Coll Cardiol 21(7):1583 – 1590
Heller GV, Stowers SA, Hendel RC, et al. (1998) Clinical value of acute rest technetium-99m tetrofosmin tomographic myocardial perfusion imaging in patients with acute chest pain and nondiagnostic electrocardiograms. J Am Coll Cardiol 31(5):1011 – 1017
Hendel RC, Wackers FJ, Berman DS, et al. (2003) American Society of Nuclear Cardiology Consensus Statement: reporting of radionuclide myocardial perfusion imaging studies. J Nucl Cardiol 10(6):705 – 708
Ho KT, Miller TD, Holmes DR, et al. (1999) Long-term prognostic value of Duke treadmill score and exercise thallium-201 imaging performed one to three years after percutaneous transluminal coronary angioplasty. Am J Cardiol 84(11):1323 – 1327
Iskandrian AS, Heo J, Kong B, et al. (1989) Effect of exercise level on the ability of thallium-201 tomographic imaging in detecting coronary artery disease: analysis of 461 patients. J Am Coll Cardiol 14(6):1477 – 1486
Iskandrian AE, Heo J, Nallamothu N (1997) Detection of coronary artery disease in women with use of stress single-photon emission computed tomography myocardial perfusion imaging. J Nucl Cardiol 4(4):329 – 335
Jain A, Mahmarian JJ, Borges-Neto S, et al. (1988) Clinical significance of perfusion defects by thallium-201 single photon emission tomography following oral dipyridamole early after coronary angioplasty. J Am Coll Cardiol 11(5):970 – 976
Johnson LL, Verdesca SA, Aude WY, et al. (1997) Postischemic stunning can affect left ventricular ejection fraction and regional wall motion on post-stress gated sestamibi tomograms. J Am Coll Cardiol 30(7):1641 – 1648
Kang X, Berman DS, Lewin H, et al. (1999a) Comparative ability of myocardial perfusion single-photon emission computed tomography to detect coronary artery disease in patients with and without diabetes mellitus. Am Heart J 137(5):949 – 957
Kang X, Berman DS, Lewin HC, et al. (1999b) Incremental prognostic value of myocardial perfusion single photon emission computed tomography in patients with diabetes mellitus. Am Heart J 138(6):1025 – 1032
Klocke FJ, Baird MG, Lorell BH, et al. (2003) ACC/AHA/ASNC guidelines for the clinical use of cardiac radionuclide imaging – executive summary: a report of the American College of Cardiology/American Heart Association Task Force on Practice Guidelines (ACC/AHA/ASNC Committee to Revise the 1995 Guidelines for the Clinical Use of Cardiac Radionuclide Imaging). J Am Coll Cardiol 42(7):1318 – 1333
Lauer MS, Lytle B, Pashkow F, et al. (1998) Prediction of death and myocardial infarction by screening with exercise-thallium testing after coronary-artery-bypass grafting. Lancet 351(9103):615 – 622
Leppo JA (1996) Comparison of pharmacologic stress agents. J Nucl Cardiol 3(6):S22 – 26
Lette J, Tatum J, Fraser S, et al. (1995) Safety of dipyridamole testing in 73,806 patients: The Multicenter Dipyridamole Safety Study. J Nucl Cardiol 2(1):3 – 17
Mahmarian JJ, Boyce TM, Goldberg RK, et al. (1990) Quantitative exercise thallium-201 single photon emission computed tomography for the enhanced diagnosis of ischemic heart disease. J Am Coll Cardiol 15(2):318 – 329
Mangano DT, Goldman L (1995) Preoperative assessment of patients with known or suspected coronary disease. N Engl J Med 333(26):1750 – 1756
Masood Y, Liu YH, Depuey G, et al. (2005) Clinical validation of SPECT attenuation correction using x-ray computed tomography-derived attenuation maps: multicenter clinical trial with angiographic correlation. J Nucl Cardiol 12(6): 676 – 686
McPherson JA, Robinson PS, Powers ER, et al. (1999) Angiographic findings in patients undergoing catheterization for recurrent symptoms within 30 days of successful coronary intervention. Am J Cardiol 84(5):589 – 592, A588
Miller TD, Christian TF, Hodge DO, et al. (1998) Prognostic value of exercise thallium-201 imaging performed within 2 years of coronary artery bypass graft surgery. J Am Coll Cardiol 31(4):848 – 854
Mochizuki T, Murase K, Tanaka H, et al. (1997) Assessment of left ventricular volume using ECG-gated SPECT with technetium-99m-MIBI and technetium-99m-tetrofosmin. J Nucl Med 38(1):53 – 57
Nallamothu N, Johnson JH, Bagheri B, et al. (1997) Utility of stress single-photon emission computed tomography (SPECT) perfusion imaging in predicting outcome after coronary artery bypass grafting. Am J Cardiol 80(12):1517 – 1521
Palmas W, Bingham S, Diamond GA, et al. (1995) Incremental prognostic value of exercise thallium-201 myocardial single-photon emission computed tomography late after coronary artery bypass surgery. J Am Coll Cardiol 25(2):403 – 409
Perrone-Filardi P, Pace L, Prastaro M, et al. (1995) Dobutamine echocardiography predicts improvement of hypoperfused dysfunctional myocardium after revascularization in patients with coronary artery disease. Circulation 91(10): 2556 – 2565
Ranhosky A, Kempthorne-Rawson J (1990) The safety of intravenous dipyridamole thallium myocardial perfusion imaging. Intravenous Dipyridamole Thallium Imaging Study Group. Circulation 81(4):1205 – 1209
Schwartz RG, McKenzie WB, Alexander J, et al. (1987) Congestive heart failure and left ventricular dysfunction complicating doxorubicin therapy. Seven-year experience using serial radionuclide angiocardiography. Am J Med 82(6):1109 – 1118
Sharir T, Germano G, Kang X, et al. (2001) Prediction of myocardial infarction versus cardiac death by gated myocardial perfusion SPECT: risk stratification by the amount of stress-induced ischemia and the poststress ejection fraction. J Nucl Med 42(6):831 – 837
Shaw LJ, Hachamovitch R, Peterson ED, et al. (1999a) Using an outcomes-based approach to identify candidates for risk stratification after exercise treadmill testing. J Gen Intern Med 14(1):1 – 9
Shaw LJ, Hachamovitch R, Berman DS, et al. (1999b) The economic consequences of available diagnostic and prognostic strategies for the evaluation of stable angina patients: an observational assessment of the value of precatheterization ischemia. Economics of Noninvasive Diagnosis (END) Multicenter Study Group. J Am Coll Cardiol 33(3):661 – 669
Shaw LJ, Hendel RC, Cerquiera M, et al. (2005) Ethnic differences in the prognostic value of stress technetium-99m tetrofosmin gated single-photon emission computed tomography myocardial perfusion imaging. J Am Coll Cardiol 45(9):1494 – 1504

Taillefer R (2003) Kinetics of myocardial perfusion imaging radiotracers. In: Iskandarian A, Verani MS (eds) Nuclear cardiac imaging, 3rd edn. Oxford, New York, pp 51 – 73

Taillefer R, DePuey EG, Udelson JE, et al. (1997) Comparative diagnostic accuracy of Tl-201 and Tc-99m sestamibi SPECT imaging (perfusion and ECG-gated SPECT) in detecting coronary artery disease in women. J Am Coll Cardiol 29(1):69 – 77

Tarakji KG, Brunken R, McCarthy PM, et al. (2006) Myocardial viability testing and the effect of early intervention in patients with advanced left ventricular systolic dysfunction. Circulation 113(2):230 – 237

Tatum JL, Jesse RL, Kontos MC, et al. (1997) Comprehensive strategy for the evaluation and triage of the chest pain patient. Ann Emerg Med 29(1):116 – 125

Thompson RC, Heller GV, Johnson LL, et al. (2005) Value of attenuation correction on ECG-gated SPECT myocardial perfusion imaging related to body mass index. J Nucl Cardiol 12(2):195 – 202

Udelson JE, Beshansky JR, Ballin DS, et al. (2002) Myocardial perfusion imaging for evaluation and triage of patients with suspected acute cardiac ischemia: a randomized controlled trial. JAMA 288(21):2693 – 2700

Udelson JE, Bonow RO, Dilsizian V (2004) The historical and conceptual evolution of radionuclide assessment of myocardial viability. J Nucl Cardiol 11(3):318 – 334

van Royen N, Jaffe CC, Krumholz HM, et al. (1996) Comparison and reproducibility of visual echocardiographic and quantitative radionuclide left ventricular ejection fractions. Am J Cardiol 77(10):843 – 850

Wackers FJ, Young LH, Inzucchi SE, et al. (2004) Detection of silent myocardial ischemia in asymptomatic diabetic subjects: the DIAD study. Diabetes Care 27(8):1954 – 1961

Wagdy HM, Hodge D, Christian TF, et al. (1998) Prognostic value of vasodilator myocardial perfusion imaging in patients with left bundle-branch block. Circulation 97(16): 1563 – 1570

Zellweger MJ, Lewin HC, Lai S, et al. (2001) When to stress patients after coronary artery bypass surgery? Risk stratification in patients early and late post-CABG using stress myocardial perfusion SPECT: implications of appropriate clinical strategies. J Am Coll Cardiol 37(1):144 – 152

5 Lung

M. Bajc, B. Jonson, H.C. Steinert

5.1 Conventional and SPECT Lung Imaging

M. Bajc, B. Jonson

5.1.1 Introduction and Historical Perspective

Scintigraphic lung studies are designed to demonstrate patterns of ventilation and perfusion.

In the healthy individual there is a balance between regional perfusion and ventilation to achieve optimal gas exchange. When a pulmonary disease causes a deficiency in both ventilation and perfusion, they are "matched." Mismatch implies an imbalance between perfusion and ventilation. The single most important application of lung scintigraphy is the evaluation of patients with suspected pulmonary embolism (PE). The value of scintigraphy in the detection of PE was first demonstrated by Wagner in 1964, using ^{131}I-human serum albumin (HSA) for perfusion scintigraphy and a rectilinear scanner for imaging (Wagner 1976).

Studies of pulmonary ventilation and perfusion are still commonly based on planar imaging although the introduction of single photon emission tomography (SPECT) over 20 years ago was the start of a new era in nuclear medicine, making planar imaging obsolete in several fields. When the issue is identification and quantification of focal or regional aberrations of organ function, SPECT is the method of choice. Examples are brain function or myocardial perfusion. In spite of the undeniable advantage of ventilation/perfusion tomography (V/P_{SPECT}), this technique is only slowly becoming accepted in the diagnostics of PE (Corbus et al. 1997; Lemb and Pohlabeln 2001; Palmer et al. 2001; Reinartz et al. 2001, 2004; Bajc et al. 2004). Lung scintigraphy is being severely challenged by contrast enhanced tomography (CT) of the pulmonary arteries. The arguments against lung scintigraphy go back to a study named PIOPED (The PIOPED Investigators 1990; Gottschalk et al. 1993b). PIOPED was based upon planar imaging with techniques already obsolete in the 1980s when the study was performed. The technique and the interpretation criteria led to a very high rate of non-diagnostic findings. Unfortunately, studies comparing up to date CT and ventilation/perfusion scintigraphy are still often based on less than optimal scintigraphic methods.

5.1.2 Radiopharmaceuticals

5.1.2.1 Ventilation Scintigraphy

Ventilation can be performed with radioactive gases (Fazio and Jones 1975) or labeled aerosols (Taplin et al. 1974; Kohn et al. 1985). One particular aerosol is Technegas, regarded as a "pseudo-gas" because of its very small particle size, giving aerodynamic properties simulating a gas (Burch et al. 1984, 1986).

The radioactive gases include xenon and krypton (^{133}Xe, ^{127}Xe and ^{81m}Kr).

Xenon-133 is still a widely used isotope. Its half-life of 5 days makes it suitable for distribution. Ventilation in relation to regional lung volume can be studied from the time course during wash-in of ^{133}Xe while in the first phase the patient is breathing air with a constant concentration of xenon. The next phase is "steady state," in which regional activity represents gas volume.

In the third phase of pure air breathing, wash-out, delayed clearance of ^{133}Xe shows gas trapping in obstructive lung disease. Imaging is often performed in only one or two projections in order to limit radiation exposure. The low photon energy of ^{133}Xe of 81 keV makes it a less suitable tracer due to the high attenuation and inferior intrinsic resolution that degrades the images.

Krypton-81m, produced from a rubidium (^{81}Ru) generator, has the ideal energy of 190 keV and a half-life of 13 s. The short half-life implies that inhaled ^{81m}Kr disappears by decay within the alveolar space rather than by exhalation. During steady state inhalation the regional concentration of ^{81m}Kr therefore reflects regional ventilation. Multiple views are easily obtained and tomography is feasible. The ^{81}Ru parent has a half-life of 4.6 h so that a generator can be used for only one day. Limited commercial accessibility, high cost and

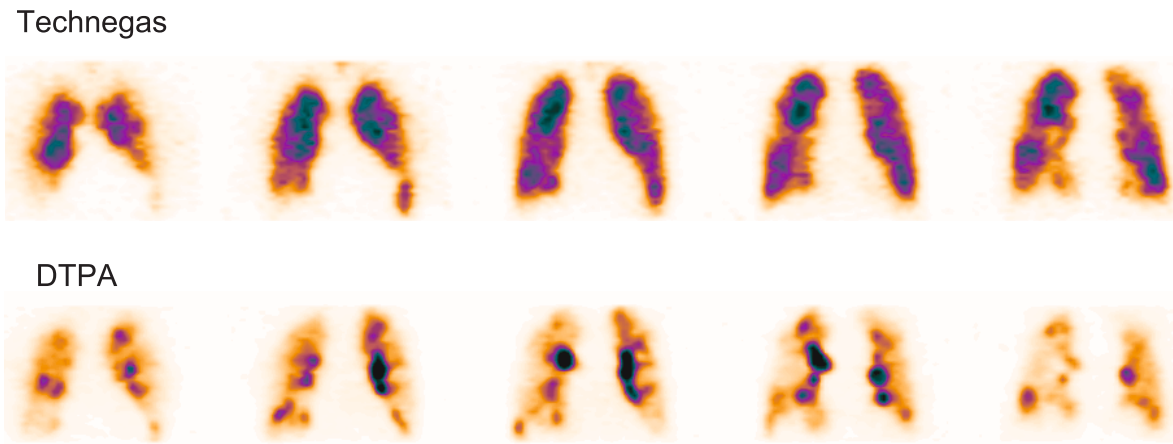

Fig. 5.1. Patient with COPD. Frontal slices: ventilation study with Technegas and DTPA

impracticality of the daily generator are some of reasons why ^{81m}Kr has gained limited clinical utility.

Radioaerosols are an alternative to radioactive gases. Diethylene triamine penta-acetate (DTPA) labeled with technetium-99m is a frequently used agent (Engeler et al. 1995; Kao et al. 1996; Kuni et al. 1993; Tagil et al. 2000). Commercial nebulizers are available that provide particles of appropriate size. The ideal ones are in the range of 0.1 – 0.5 µm. Particles larger than 2 – 3 µm tend to settle out on large airways. The aerosol deposition and distribution depend on the aerodynamic properties of the aerosol determined mostly by particle size (Agnew et al. 1982; Isawa et al. 1996; Senden et al. 1997; Strong and Agnew 1989). Regional activity therefore reflects not only ventilation. Liquid particles are hydrophilic and grow in size within the conducting airways. The frequently used aerosol of ^{99m}Tc-labeled Technegas has hydrophobic particles with a constant size of 0.005 – 0.2 µm. These penetrate to the alveolar level nearly as a gas. Technegas is advantageous, compared to other aerosols, particularly in patients with obstructive lung disease (Fig. 5.1).

5.1.2.2 Perfusion Scintigraphy

Perfusion scintigraphy is accomplished by microembolization with radio-labeled particles injected in a peripheral vein. The commercially used particles are macroaggregate of human albumin (MAA), marked with ^{99m}Tc. They are 15 – 100 µm in size and will lodge in the pulmonary capillaries and precapillary arterioles. The particle distribution accurately illustrates regional perfusion. When performing the study an important concern is the number of particles given. A minimum of 60,000 particles is required to obtain an even distribution of activity reflecting regional perfusion (Heck and Duley 1974). Normally, about 400,000 labeled particles are injected. Bearing in mind that there are over 280 billion pulmonary capillaries and 300 million precapillary arterioles, the routinely administered particles will result in obstruction of only a very small fraction of pulmonary vessels. However, a special preparation of 100,000 – 200,000 particles is usually given to patients with known pulmonary hypertension, right to left heart shunt or after a single lung transplantation.

5.1.3 V/P$_{SPECT}$ Method

5.1.3.1 Acquisition

Lung scintigraphy should always include ventilation and perfusion studies in order to increase the specificity and the pattern recognition for other lung diseases than PE. Some centers add ventilation only when perfusion scans are pathological. For several reasons we routinely study both ventilation and perfusion. One reason is that we gain time as a preliminary judgment of perfusion is needless. With an efficient technique and effective organization, the time is 1 h from referral to report with planar (Tagil et al. 2000) and tomographic techniques (Palmer et al. 2001). Other reasons are that small perfusion defects can be more safely detected and that ventilation defects commonly lead to diagnoses other than PE and may explain the patient's symptoms.

In our set-up, a large field-of-view dual-head gamma camera with low energy all-purpose collimators and a 64×64 matrix is used with 128 projections over 360°. The ventilation study routinely starts with inhalation of aerosolized Technegas, with the patient in the supine position until about 30 MBq reaches the lung (usually 2 – 3 breaths). For the same purpose inhaled aerosolized ^{99m}Tc-DTPA (TechneScan DTPA, Mallin-

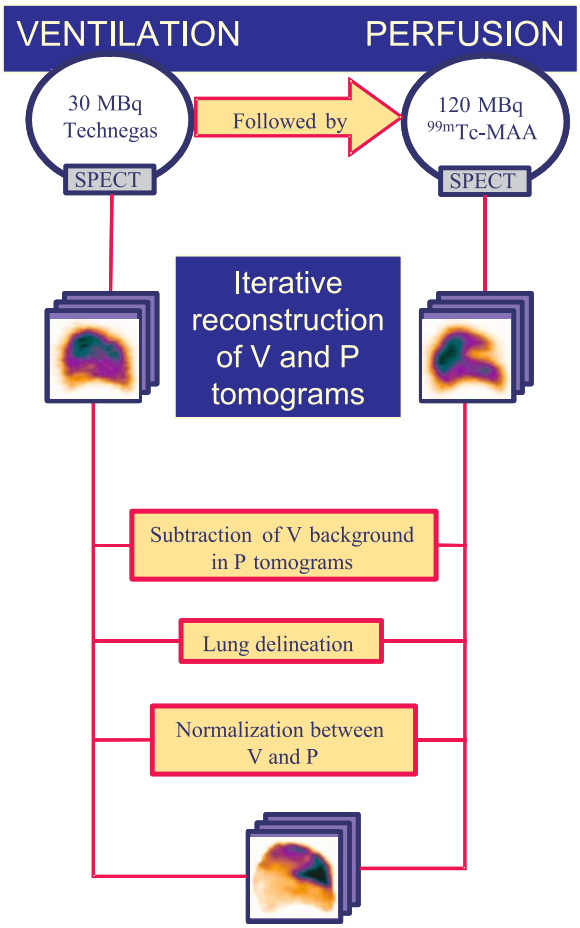

Fig. 5.2. The qV/P_{SPECT} method according to Palmer et al. (2001) and Bajc et al. (2004)

ckrodt Medical, Petten, Holland) might be used by spontaneous breathing from a pressurized air driven nebulizer. Each projection takes 10 s. Immediately thereafter and without patient movement, 100–120 MBq ^{99m}Tc-MAA (TechneScan LyoMAA, Mallinckrodt Medical) is given intravenously for the perfusion study. Perfusion tomography follows in the same way except that each projection takes 5 s. During the examination the patient is in the supine position, carefully maintained between ventilation and perfusion acquisitions. Immobilization that lasts only 20 min is well tolerated by all patients. Examination in the supine position is comfortable even for critically ill patients and convenient for the staff.

Iterative reconstruction is performed using OSEM (ordered subset expectation maximization) with eight subsets and two iterations. In processing the images the ventilation background is subtracted from the perfusion tomograms and a normalized V/P image set calculated, $V/P_{quotient}$. Computed normalized V/P images facilitate diagnosis and quantification of PE extension, giving the quantitative term V/P SPECT, qV/P_{SPECT} (Fig. 5.2). The algorithms for $V/P_{quotient}$ were developed by Palmer et al. (2001) and further amended by Bajc et al. (2004). The main consideration in the creation of $V/P_{quotient}$ images was to scale smoothened ventilation and perfusion data sets to display $V/P_{quotient}$ in a fixed linear scale allowing separation of normal regions from such with mismatch.

$V/P_{quotient}$ facilitates the recognition and quantification of PE (Figs. 5.3, 5.5a, 5.6) as well as identification of other patterns like heart failure (Fig. 5.8a). It is particularly valuable in complex cases with heterogeneous ventilation (Fig. 5.7). Quantification is becoming important for choice of therapy, i.e., thrombolysis or conventional anticoagulants, and more importantly for identifying patients suitable for outpatient treatment and follow-up of patients with PE (Olsson et al. 2006).

5.1.4 Clinical Application

In disease, scintigraphy often shows changes in ventilation or perfusion or both. Vascular occlusive disease like PE causes perfusion defects in areas with intact ventilation. If the findings of ventilation and perfusion are disconcordant, there is a so-called mismatch, which is a basis of PE diagnosis (Fig. 5.3). Ventilation studies show disturbances in other lung diseases than PE, such as pneumonia, tumors and obstructive disease. Such findings are valuable, providing additional specificity and significance to the pattern identified in perfusion studies.

5.1.4.1 Pulmonary Embolism

In PE, a perfusion defect is due to an embolus blocking blood flow, while ventilation remains normal because there is no corresponding blockage in the airway. The distinction of whether a given perfusion defect is matched or mismatched is fundamental. The next step is to characterize the perfusion defects. Perfusion defects due to blockage of a pulmonary artery should reflect the branching of pulmonary circulation and its classical segmental anatomy. A segmental defect is shaped as a wedge with its base on the pleura.

On qV/P_{SPECT} images it is rather simple to identify segmental and subsegmental patterns of perfusion defects. Figure 5.3 shows multiple perfusion defects in a 72-year-old woman with a history of frequent pneumonia, now with chest pain and breathlessness. PE extension was estimated initially to be 65 %. She was treated with low-molecular-weight heparin and warfarin. Only 4 days later perfusion was significantly improved and was normalized after 1 month.

Figure 5.4 shows frontal slices from a 40-year-old man with a swollen leg in whom ultrasound was nega-

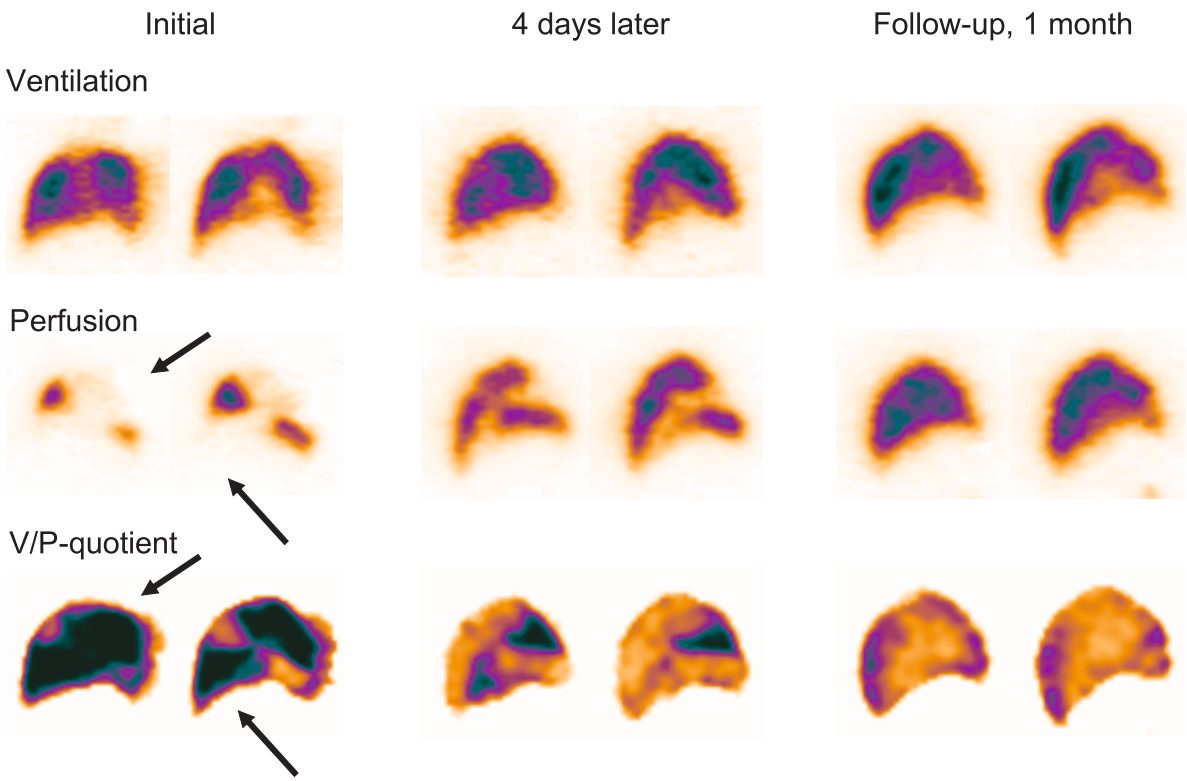

Fig. 5.3. Patient with massive PE, initially and at 4 days and 1 month follow-up. Sagittal slices: *left panel:* in acute stage, multiple areas with absent perfusion (*arrows*) and preserved ventilation well delineated in $V/P_{quotient}$ images (*arrows*). *Middle panel:* follow-up after 4 days shows major improvement in perfusion. *Right panel:* nearly normal perfusion at 1 month follow-up

tive. Suspected PE was confirmed in terms of both large and subsegmental perfusion defects. Extension was estimated to be 35 %.

In planar images, visualization of a solitary segmental perfusion defect within the middle lobe or the lingula is difficult or impossible (Morrell et al. 1993a, 1993b). Only from the combined information from ventilation and perfusion images, amplified in $V/P_{quotient}$ images, it is possible to identify these changes. A 30-year-old woman had quite non-specific symptoms. Figure 5.5a shows perfusion defects in the middle lobe and in the lingula, which were most easily delineated in $V/P_{quotient}$ images. The diagnosis was supported by near normal findings after 2 weeks of therapy (Fig. 5.5b). These changes can also be nicely observed by 3D surface rendered volume images as seen in patients with PE in the lingula (Fig. 5.6).

5.1.4.2 Interpretation: Probabilistic Versus Holistic

The PIOPED study was designed to assess the diagnostic usefulness of V/P scintigraphy for the diagnosis of acute PE (The PIOPED Investigators 1990; Gottschalk et al. 1993a). The findings were assessed as high, intermediate and low probability depending on the size of perfusion defects and findings in ventilation scans and chest X-ray. On the whole, high probability reflected perfusion defects in two segments, and low and very low probability denoted non-segmental perfusion defects or >3 small segmental perfusion defects with a normal chest X-ray. Normal probability denoted no perfusion defect. Intermediate probability did not fall into the above categories.

PIOPED criteria have caused confusion in nuclear and clinical medicine (Gray 2002). For decisions about therapy, the utility of a report in terms of "Yes" or "No" to the question "PE?" is greater than the usefulness of the probability of PE. This is particularly the case if such probability is based only upon predefined rigid criteria for PE. According to Bayes' theorem, true probability is grossly influenced by prior probability. Therefore all available information should be taken into account.

An important step in this direction was the PISA-PED study (Miniati et al. 1996). By using clinical evaluation, ECG interpretation, chest X-ray, measurement of PaO_2 and $PaCO_2$ and by recognition of perfusion patterns typical for PE, the number of non-diagnostic examinations decreased significantly even without ventilation studies. Their clinical diagnostic algorithm test included the identification of three relevant symptoms: sudden onset of dyspnea, chest pain or fainting and their association with ECG or chest X-ray. High or in-

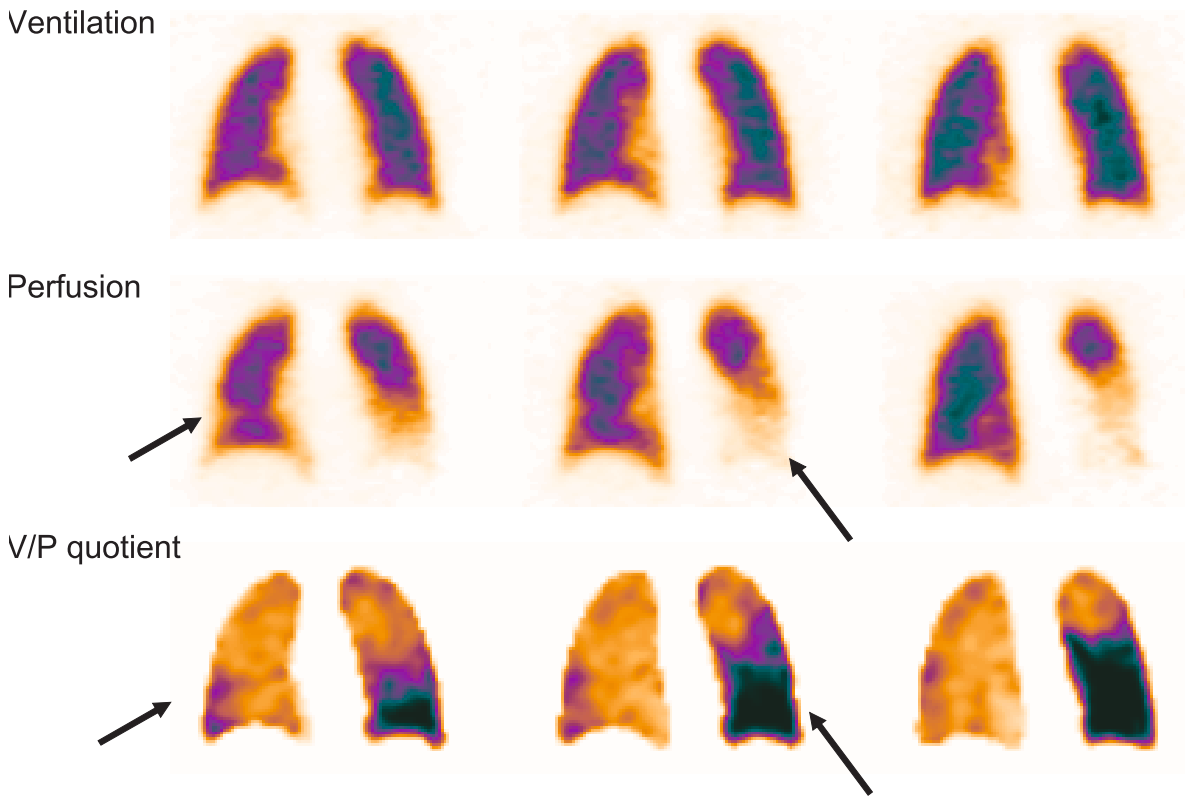

Fig. 5.4. Patient with medium sized PE. Frontal slices: the subsegmental perfusion defects in the right lung (*arrow*) nicely delineated in $V/P_{quotient}$ images (*arrow*). Lobar defect in the left lung (*arrow*)

termediate clinical probability combined with perfusion scan suggestive for PE yielded a 98% positive predictive value for PE. A low pretest probability paired with an abnormal scan not suggestive for PE had a 99% negative predictive value for PE. Nevertheless, we consider ventilation studies important because they help to explain perfusion defects not caused by PE and reflect functional changes not reflected by X-ray.

Freeman et al. argued that "the experts' successful interpretation of lung scans exceeds the best accuracy achievable by algorithms, which, by definition, are distillations of decision making into finite linear steps. The subjective interpretation of the whole is superior to any possible attempt to define its discrete parts" (Freeman et al. 2001).

A holistic interpretation of scintigraphic images in our setting includes:

1. Clinical information
2. Chest X-ray when available
3. Recognition of patterns typical for PE based upon segmental charts, and
4. Recognition of patterns of other diseases than PE (Bajc et al. 2002a, 2004; Palmer et al. 2001)

Several schemes are used to structure clinical information to estimate the pretest probability. Well's score is frequently recommended (Table 5.1) (Wells et al. 2001). The score is based upon generally available information and does not delay diagnostics. The general use of this score would facilitate comparisons between studies of diagnostic strategies.

To meet the requirements of our clinicians, the degree of PE is routinely quantified. In addition, the total

Table 5.1. Score for clinical probability of PE

Clinical feature	Score
Clinical signs and symptoms of DVT (objectively measured leg swelling and pain with palpation in the deep vein system)	3.0
Heart rate > 100 beats/min	1.5
Immobilization for ≥ 3 consecutive days (bed rest except to go to bathroom) or surgery in previous 4 weeks	1.5
Previously objectively diagnosed pulmonary embolism or DVT	1.5
Hemoptysis	1.0
Cancer (with treatment within previous 6 months or palliative treatment)	1.0
Pulmonary embolism likely or more likely than alternative diagnoses (on the basis of history, physical examination, chest radiography, ECG, and blood tests)	3.0

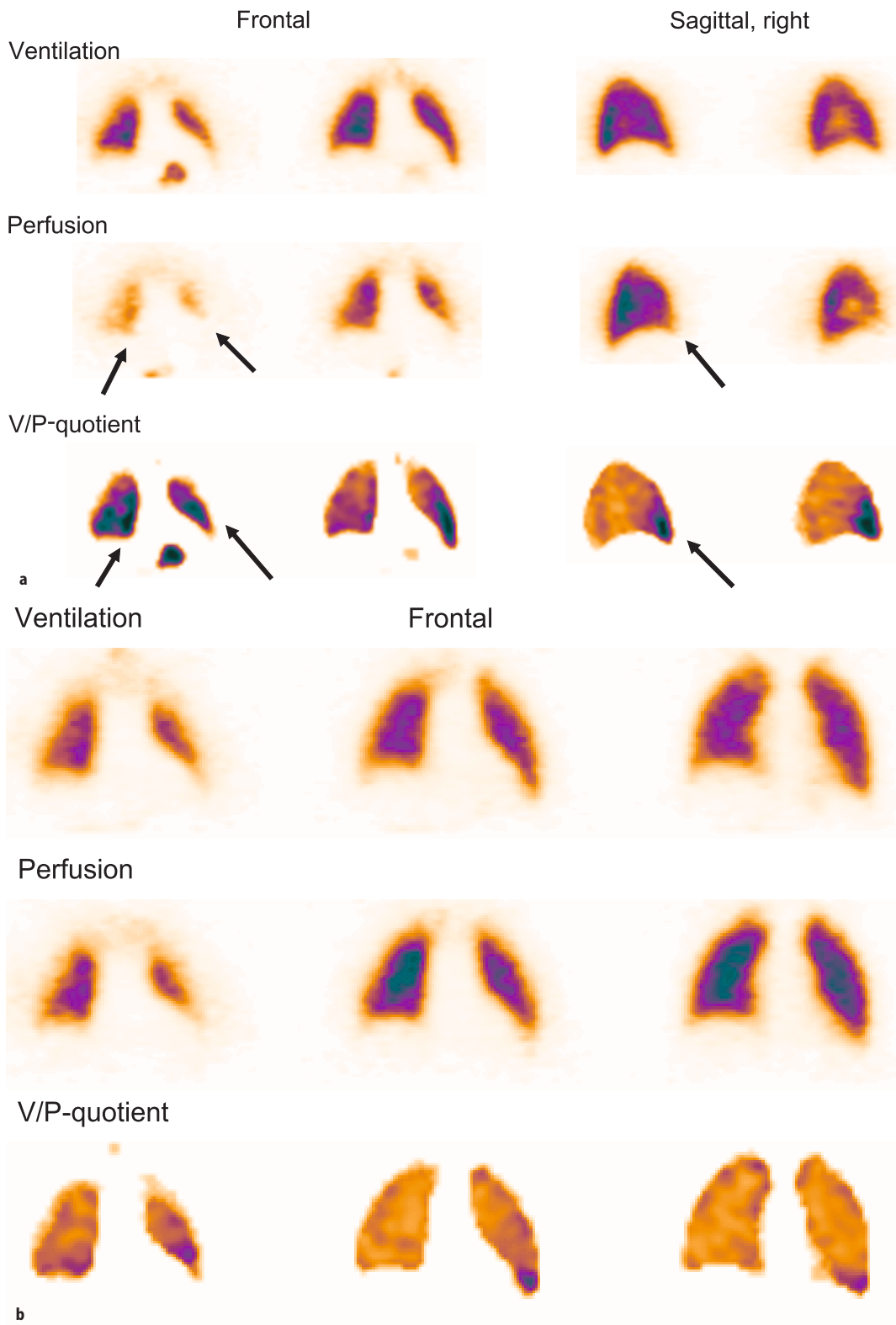

Fig. 5.5a, b. Patient with PE in middle lobe and lingula. **a** Frontal slices: *left panel:* in acute stage perfusion defects are observed in the right middle lobe and in lingula in left lung (*arrows*), most obvious in $V/P_{quotient}$ images (*arrow*). Sagittal slices: *right panel:* perfusion defects in middle lobe, mismatch easily detected in $V/P_{quotient}$ images (*arrow*). **b** Frontal slices: nearly normal perfusion 2 weeks after therapy with low molecular heparin

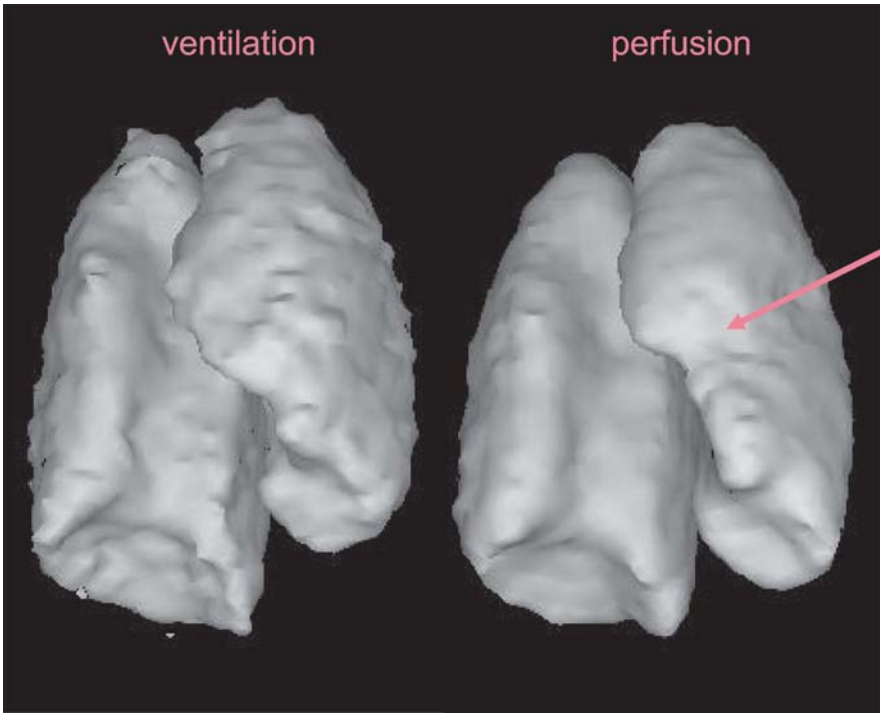

Fig. 5.6. Patient with PE in lingula: 70-year-old woman developed PE after operation. 3D surface rendered images show perfusion defect (*arrow*) in lingula

lung function reduction is validated. For these purposes ventilation and perfusion defects are quantified in terms of "RoVent" points (reduction of ventilation), "RoPer" points (reduction of perfusion) and mismatch points (Olsson et al. 2006). A segmental reduction or a subsegmental total deficiency of function is attributed 1 point, segmental total deficiency 2 points. Each lung comprises according to our charts 9 segments, representing 18 points. Mismatch defects are expressed as mismatch points, which after division by 36 give the fraction of the lung that is embolized. All areas with ventilation or perfusion defects are summed for estimation of total lung function.

Within the holistic principle of image reading we have applied the following guidelines for PE diagnosis:

1. No embolism: maximum 1 mismatch point.
2. Embolism: segmental or subsegmental defects giving at least 2 mismatch points. The reader considers the number of mismatched areas, their distinctness, peripheral or central position, as well as segmental or non-segmental orientation.
3. Other pathology than PE: perfusion and ventilation defects, matched or reversed mismatch, with patterns typical for other lung diseases.
4. Non-diagnostic for PE: complex V/P defects rendering the judgment of mismatch impossible or non-typical V/P defects.

Signs of obstructive or parenchymal lung disease and heart failure are included in the reports.

5.1.4.3 Pitfalls

Artifacts might be technical. Withdrawing blood into the syringe with ^{99m}Tc-MAA may cause aggregation of particles, creating hot spots in the images. So may failure to re-suspend ^{99m}Tc-MAA particles prior to administration. Problems with planar imaging related to superposition of lung regions with normal perfusion, which shine through hidden embolized regions, are eliminated by V/P_{SCINT}.

Technegas, as shown in Fig. 5.1, is in general preferred over liquid aerosols in patients with chronic obstructive pulmonary disease (COPD). However, in some patients with emphysema Technegas particles are trapped in bullae, causing a pattern that may be mistaken for a mismatch. The pattern can in most cases be differentiated from the segmental pattern typical for PE.

When interpreting the findings, it is important to be aware that mismatch findings not having a segmental character do not usually represent PE. Non-segmental mismatch defects imply that perfusion defects do not conform to segments and are not wedge shaped. Non-segmental patterns are observed in patients with tumor, mediastinal adenopathy, post-radiation therapy and heart failure. Tomography greatly facilitates the identification of segmental defects. This is particularly the case when using rotating volume-rendered images.

Importantly, total absence of perfusion in one lung without any other mismatch region is generally caused by pathology other than PE, such as a central tumor or abscess.

5.1.4.4 Selection of Therapeutic Strategy

Management of PE was previously confined to in-hospital therapy, using thrombolysis, heparin injections and oral anticoagulants for an extended period of time.

Twenty to 50 % of patients with deep venous thrombosis have concomitant PE, which is not usually diagnosed because symptoms of PE are lacking. Outpatient hospital therapy of patients with deep venous thrombosis, which is perceived as a safe routine, implies also that many patients with PE are treated at home. Home treatment of patients with diagnosed PE has been suggested (Beer et al. 2003; Kovacs et al. 2000). In order to select a therapeutic strategy the degree of PE obviously needs to be estimated. Very extensive PE may motivate thrombolysis, while PE with limited extension may be treated at home. Intermediate cases and patients with co-morbidity need in-hospital treatment.

Obviously, quantification requires studies of the whole lung with methods allowing recognition of large and small emboli. qV/P_{SPECT} is the ideal method for this purpose as segmental and subsegmental emboli are detected with high sensitivity (Bajc et al. 2002b, 2004) and can be quantified in terms of mismatch points. In a prospective study, Olsson et al. (2006) studied 102 outpatients with up to a moderate degree of PE (40 %). After only 5 days, embolism diminished by 44 % and there was no thromboembolic mortality in the trial. At late follow-up, PE had not recurred in patients showing resolution after 5 days. After our positive experience, outpatient treatment in our hospital is now perceived as a safe routine in patients selected on the basis of qV/P_{SPECT} and relevant clinical information. Since 2004, more than 300 patients with up to 40 % extension of PE have been treated as outpatients.

5.1.4.5 Follow-up

Follow-up is a frequently overlooked aspect of diagnostic strategies although it is essential for both clinical and scientific reasons. Follow-up is needed, in order to:

1. Assess the need for repeated thrombolytic therapy after each infusion of such drugs.
2. Assess the need for prolonged oral anticoagulation beyond 6 months, in case of extensive remnants of PE.
3. Allow differentiation between new and old PE on suspicion of recurring PE.
4. Explain physical incapacity after PE in the case of permanently deranged lung function.
5. Evaluate and compare drugs and therapeutic strategies.

For follow-up, qV/P_{SPECT} is the only suitable method for the following reasons:

- Detection of all emboli requires that the whole lung is examined with a sensitive method.
- The cumulative radiation dose is much lower than for CT, which is a central issue when the indication is relative.
- The functional impairment of lung units due to non-perfusion increases dead space and pulmonary vascular resistance. In severe cases it strains the right heart.

To study efficacy of treatment in individual patients or in scientific materials, the same method should obviously be used for diagnosis and for follow-up. This is a further strong argument in favor of qV/P_{SPECT} as the primary diagnostic method for PE.

5.1.5 Computed Tomographic Angiography in Diagnosis of Pulmonary Embolism

Computed tomography (CT) was introduced in the early 1990s as a powerful method for the "direct" visualization of emboli. For this purpose data are collected as the patient moves through the gantry, after i.v. injection of iodine contrast. The initial single detector CT produced 5-mm scans at 1 s per gantry rotation and was performed from the aortic arch to below the inferior pulmonary vessels, covering about 15 cm of the lung field. Initial results showed a sensitivity of 65 – 90 % and a specificity of about 90 % (Goodman 2001). It has been shown that thinner sections, 2 mm, provide a better demonstration of segmental and subsegmental arteries (Remy-Jardin et al. 1997). To further improve the visualization of peripheral arteries and detection of small emboli, dynamic developments in CT technology during the past few years have improved the generation of multi-detector CT from 4 to 64 slices. They allow coverage of the entire chest with submillimeter resolution and within a short single breath-hold. An overview of CT angiography for the diagnosis of PE was recently presented by Schoepf and Costello (2004).

5.1.5.1 Interpretation

The vascular signs of PE are based on the presence of partial or complete filling defects within the contrast-enhanced lumen of the pulmonary artery.

5.1.5.2 Pitfalls

According to Aviram et al. (2004), one should observe pitfalls which may occur for a variety of reasons. "These include technical problems caused by respiratory motion artifact, improper bolus timing, streak artifact, and patient body habitus. In addition, misinterpretation of normal bronchovascular anatomy may lead to an erroneous diagnosis."

5.1.5.3 Sensitivity and Specificity of V/P_{SPECT} and CT in Diagnosis of PE

Notwithstanding that the PIOPED study (The PIOPED Investigators 1990) was performed with an inferior technique and inflexible suboptimal interpretation criteria, the results are still cited as arguments against lung scintigraphy for the diagnosis of PE. In particular, PIOPED had a rate of non-diagnostic scintigraphies of 65 %. A reduction in the number of non-diagnostic reports to 10 % can be achieved even with planar lung V/P scintigraphy with adequate acquisition (Barghouth et al. 2000) and a holistic interpretation strategy (Bajc et al. 2002a). With V/P_{SPECT}, this number is further reduced to below 4 %, as found in recent studies (Corbus et al. 1997; Lemb and Pohlabeln 2001; Reinartz et al. 2001; Bajc et al. 2004; Reinartz et al. 2004).

The sensitivity of qV/P_{SPECT} was tested in a porcine model using latex emboli, labeled with ^{201}Tl to enable precise localization of the emboli, which were 2.2 – 3.7 mm in diameter and caused only subsegmental defects. For the planar technique, sensitivity and specificity were 67 % and 80 % and for SPECT 93 % and 94 %, respectively (Bajc et al. 2002b). A study by Baile (Baile et al. 2000), using a methacrylate cast of the porcine pulmonary vessels as the independent standard, showed with angiography and CT sensitivities of 87 % and 82 % for emboli sized about 4 mm. They concluded that angiography as the gold standard can be misleading. They also underlined the fact that CT was performed under apnea, which is often not possible in the clinic. Together, these animal studies indicate that qV/P_{SPECT} has a sensitivity superior to scintigraphic planar technique, angiography and CT.

In a clinical study, 53 % more mismatch points were identified with qV/P_{SPECT} compared to the planar technique (Bajc et al. 2004). Similar results have been found by others (Reinartz et al. 2004). SPECT eliminates superimposed structures, and clarifies the segmental and subsegmental nature of perfusion defects caused by PE.

Powell reported that the sensitivity and specificity of CT for central PE are about 90 % (Powell and Muller 2003). Perrier et al. (2001) found in broad-based clinical material that CT had a sensitivity of 70 % for PE and a specificity of 91 %. They concluded: "clinical CT should not be used alone for suspected PE but could replace angiography in combined strategies that include ultrasonography and lung scanning." Likewise, van Strijen et al. (2005) found in a multicenter prospective study that sensitivity of CT was 69 % while specificity was 84 % and "concluded that the overall sensitivity of spiral CT is too low to endorse its use as the sole test to exclude PE" and that "this holds true even if one limits the discussion to patients with larger PE in segmental or larger pulmonary artery branches." Our experience supports the latter idea (Bajc 2005). Also, CT as a second procedure following scintigraphy has limited value (van Strijen et al. 2003). Multislice CT seems to improve resolution, but sensitivity for small PE appears not to be improved (Remy-Jardin et al. 2002).

The recently published Prospective Investigation of Pulmonary Embolism Diagnosis II trial (PIOPED II) was a prospective multicenter investigation study to assess accuracy of multidetector CT alone, and combined with venous-phase imaging for diagnosis of PE and clinical assessment using the Wells score (Table 5.1) (Stein et al. 2006). Sensitivity of CT alone was only 83 %, a disappointment according to Perrier and Bounameaux (2006). The authors conclude: "The false negative rate of 17 percent for CTA alone indicates the need for additional information to rule out PE." Furthermore, in confirmation with previous studies, the positive predictive value for PE in a main lobar artery was 97 % but only 68 % for a segmental vessel and 25 % for a subsegmental branch. When clinical assessment was taken into account the positive predictive value of abnormal CT was 92 – 96 % in patients with intermediate or high probability but only 58 % in patients with low probability for PE. About 20 % of patients with suspected PE could not undergo CT because of renal failure or allergy to contrast agents. Six percent of CT studies were non-interpretable because of insufficient quality.

PIOPED II confirms that CT has important limitations with respect to applicability. Sensitivity and specificity are low in large groups of patients, even if pretest probability is taken into account. The absolute gain by combination with venous-phase imaging was modest. Notably, the radiation exposure was not discussed. The euphoria in the beginning of the CT era is fading under the influence of true evidence.

A problem associated with the limited sensitivity of CT and incomplete coverage of the total lung is that the degree of embolism and lung function deficiency cannot be quantified. Quantification that is important for therapy selection is not achieved.

Some researchers speculate that subsegmental emboli are of little importance for otherwise healthy people and may be left untreated. The advocates for less sensitive methods for diagnosing PE too quickly neglect the potential importance of these emboli (BTS

Guidelines 2003). Small emboli are important because they: (1) may be a first and only sign of silent deep venous thrombosis, (2) may precede larger ones, (3) if repeated, may lead to chronic pulmonary hypertension, (4) form a threat to patients with limited cardiopulmonary reserve, (5) are clinically essential for quantification and choice of therapy, and (6) are important in scientific therapy evaluation.

Thus, each embolus is relevant, irrespective of size. Before subsegmental emboli are left untreated, prospective controlled studies are required.

5.1.5.4 Alternative Diagnosis

It is argued that in the presence of negative CT for PE, CT has the advantage of providing the clinicians with an alternative diagnosis when identifying abnormalities liable to explain the patient's symptoms and that this information cannot be suggested by other imaging modalities (van Strijen et al. 2005). Alternative diagnoses include pneumonia, malignancy, pleural fluid and cardiac failure (Richman et al. 2004, van Strijen et al. 2005). Importantly, when other disease dominates the images, coexisting PE can easily be overlooked. The likelihood for PE increases in patients with several diseases as shown by Hampson (1995) and in the ICOPER study (Elliott et al. 2000).

Also V/P scintigraphy can show other diagnosis than PE (Friedman and Braunwald 1966; Garg et al. 1983; Li et al. 1994; Sostman and Gottschalk 1992). In many centers, this opportunity is not clinically exploited.

5.1.6 Ancillary Findings with V/P_{SPECT}

5.1.6.1 Reverse Mismatch Defects

Reverse mismatch is a zone where the alveoli are overperfused in relation to their ventilation (Palmaz et al. 1984; Gottschalk et al. 1993b). This phenomenon produces shunts (venous admixture) due to inequality of ventilation and perfusion. The degree of shunt can be estimated from the ensuing abnormally high pO_2 and pCO_2 differences between alveolar gas and arterial blood (West 1974). With tomographic functional imaging of $V/P_{quotient}$, it is possible to locate areas with reverse mismatch and to explain abnormalities in gas exchange non-invasively. It has been found that abnormal V/P ratios determined by SPECT correlate well with abnormalities in alveolar-arterial oxygen pressure differences (Sando et al. 1997).

5.1.6.2 Chronic Obstructive Pulmonary Disease

A dominant finding in chronic obstructive pulmonary disease (COPD) is matched areas with defects in ventilation and perfusion. Ventilation defects are commonly more prominent than those of perfusion. Perfused but non-ventilated lung, i.e., reverse mismatch, is another common finding, explained by failure of blood flow diversion from hypoxic lung segments (Chapman et al. 1983; Gottschalk et al. 1993b). Garg et al. (1983) found a significant correlation between the degree of abnormalities on aerosol ventilation imaging and pulmonary function tests. In our clinical routine, ventilation scintigraphy frequently provides the first indication of COPD. As shown in Fig. 5.1, Technegas penetrates better to the lung periphery compared to DTPA aerosols, which is particularly important in COPD.

Pulmonary embolism is quite frequent in COPD. However, in a recent study "the clinical symptoms supporting the suspicion of PE, such as hemoptysis, chest pain, and edema of the lower limbs, did not definitively indicate PE in this group" (Tillie-Leblond et al. 2006). The authors also showed a 25% prevalence of PE in patients with COPD hospitalized for severe exacerbation. Similar results were found previously (Mispelaere et al. 2002). PE accounts for approximately 10% of death in stable COPD patients (Schonhofer and Kohler 1998). With V/P_{SPECT} both diagnoses may be made simultaneously. The ruling according to PIOPED that pathology of ventilation implies that scintigraphy is non-diagnostic with respect to PE is a particularly obsolete belief (The PIOPED Investigators 1990). Figure 5.7 shows a combination of COPD and PE in an 80-year-old heavy smoker. Dyspnea led to suspicion of heart failure. qV/P_{SPECT} showed uneven ventilation typical for COPD. In addition, multiple bilateral perfusion defects were observed in ventilated regions. In $V/P_{quotient}$ images mismatch corresponding to PE of 70% of the pulmonary parenchyma was observed. Notably, reverse mismatch was also evident. This is typical in cases with COPD and extensive PE, probably reflecting that pulmonary hypertension counteracts and supersedes vasoconstriction caused by hypoxia.

5.1.6.3 Heart Failure

In patients with heart failure, redistribution of perfusion towards upper lung regions was described in 1966 by Friedman and Braunwald. Patients with pulmonary venous hypertension due to congestive heart failure, mitral valve disease, and chronic ischemic heart disease usually develop interstitial edema and perivascular fibrosis, primarily in the lung bases. Inversion of flow from the lower to the upper lung regions is ob-

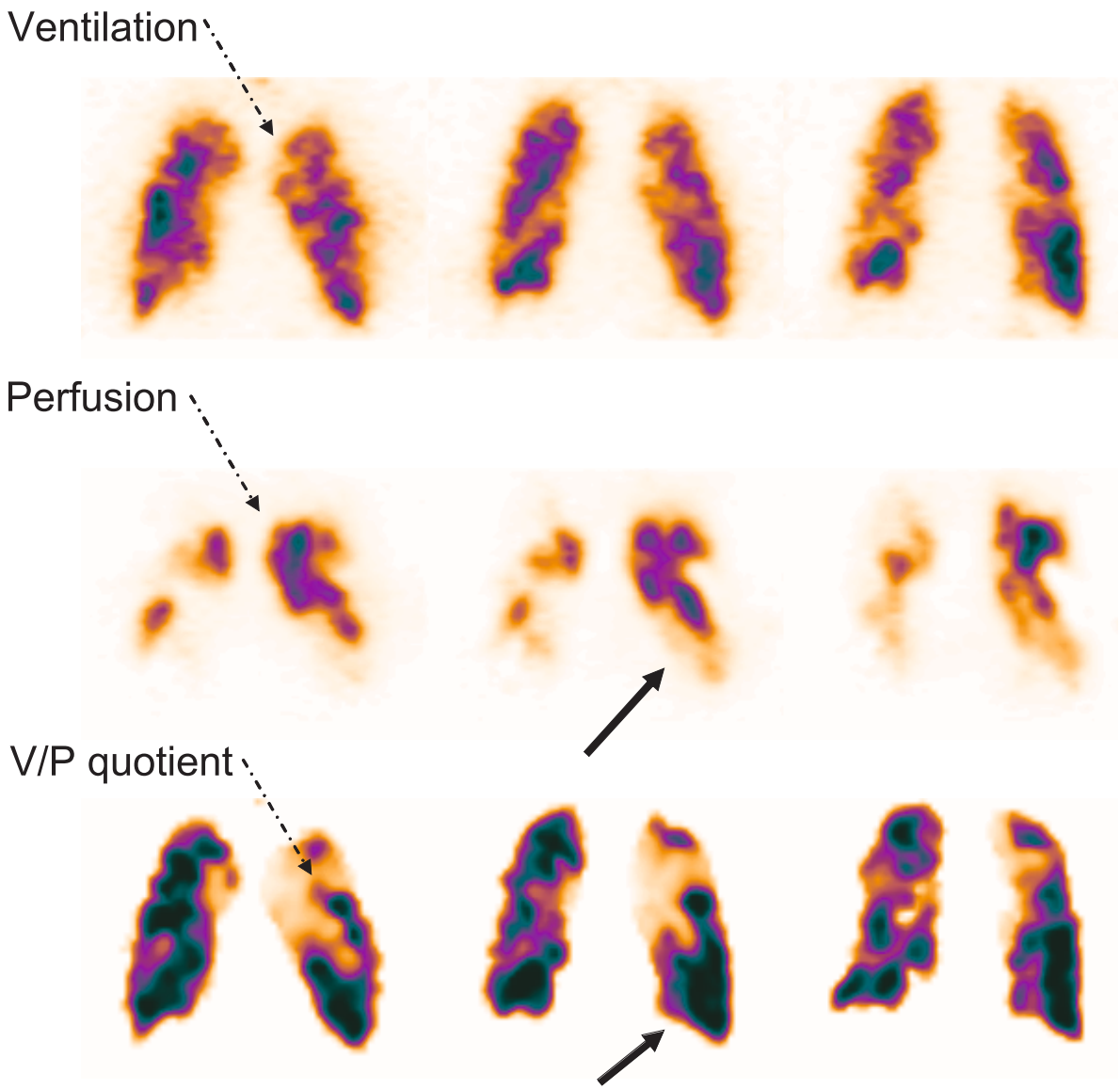

Fig. 5.7. Patient with COPD and extensive PE. Frontal slices: multiple perfusion defects with mismatch (*arrows*) but also reverse mismatch (*interrupted arrows*)

served when alveolar space is flooded by edema fluid (Mohsenifar et al. 1989; Pistolesi et al. 1988; Slama et al. 2000; Surette et al. 1975; Tsang et al. 1986). As ventilation is usually not affected to the same grade as perfusion, mismatch is common, although not of segmental character. In about 5–10% of our patients, signs of heart failure have been observed and reported.

A 50-year-old man had experienced pain in the left chest, increasing weariness and breathlessness for 2 weeks. Chest X-ray showed infiltrate in the left lung but no other pathology. Clinical and laboratory findings for infection were normal. PE was suspected. qV/P_{SPECT} identified redistribution of ventilation and perfusion towards the anterior regions (Fig. 5.8a). Ventilation was less affected, causing mismatch on VP quotient images, although not segmental. Scintigraphic diagnosis was heart failure but not PE. Two weeks after treatment for heart failure, ventilation and perfusion gradient were normalized but the patient developed pneumonia in the right lung as seen in Fig. 5.8b.

5.1.6.4 Pneumonia

Pneumonia is inflammation of the lung parenchyma associated with alveolar filling by exudates. Since a non-ventilated pneumonic region often maintains some perfusion, it causes shunting and hypoxemia. The

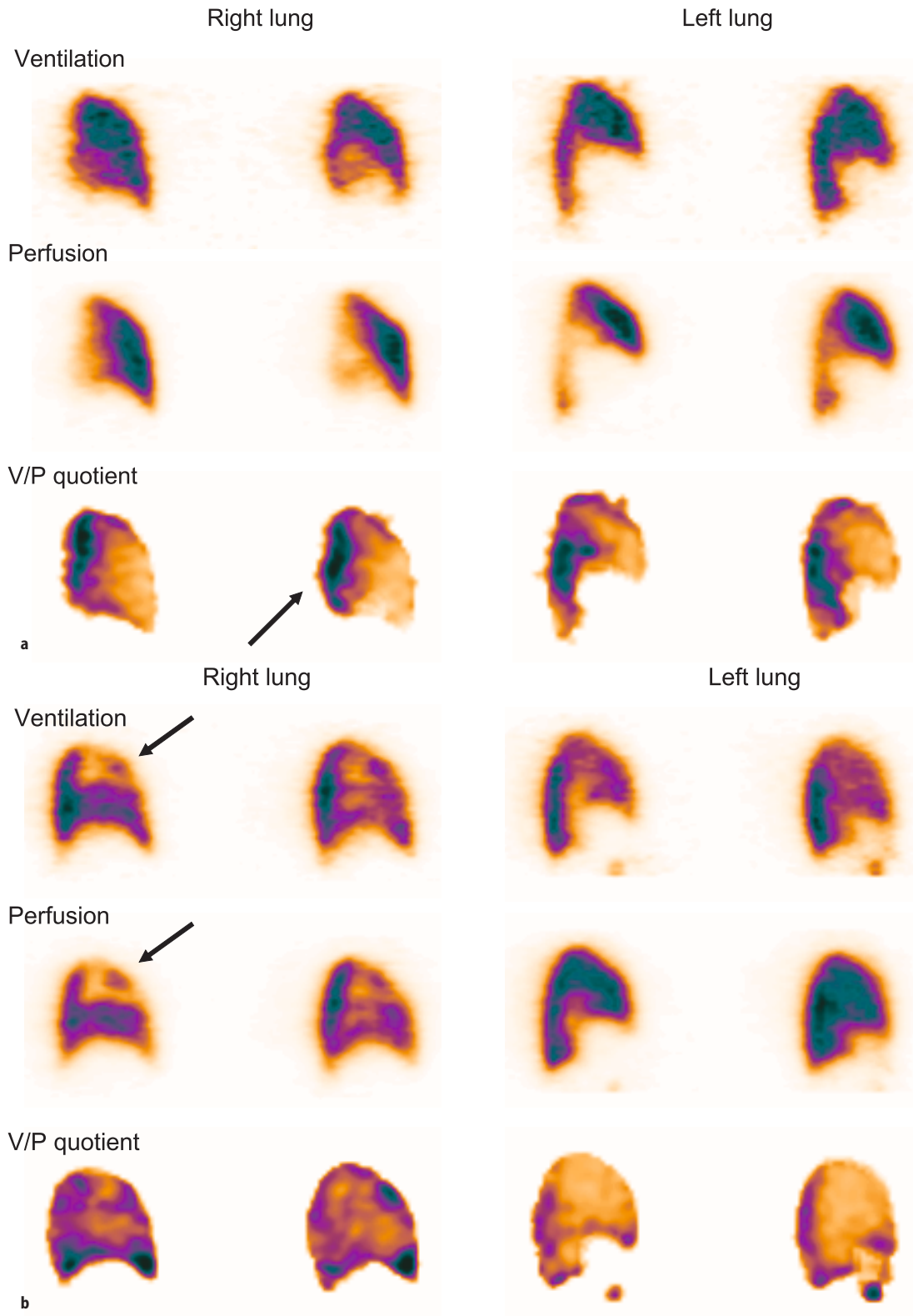

Fig. 5.8a, b. Patient with heart failure. **a** Sagittal slices of the right lung in acute stage. Non-segmental mismatch nicely visualized on $V/P_{quotient}$ images (*arrow*). **b** Sagittal slices of right (*left panel*) and left lung (*right panel*) 2 weeks after therapy. Normalization of ventilation/perfusion gradient is observed bilaterally. In the meantime, the patient developed pneumonia, which is identified as a ventilation and perfusion defect in right upper lobe (*arrows*)

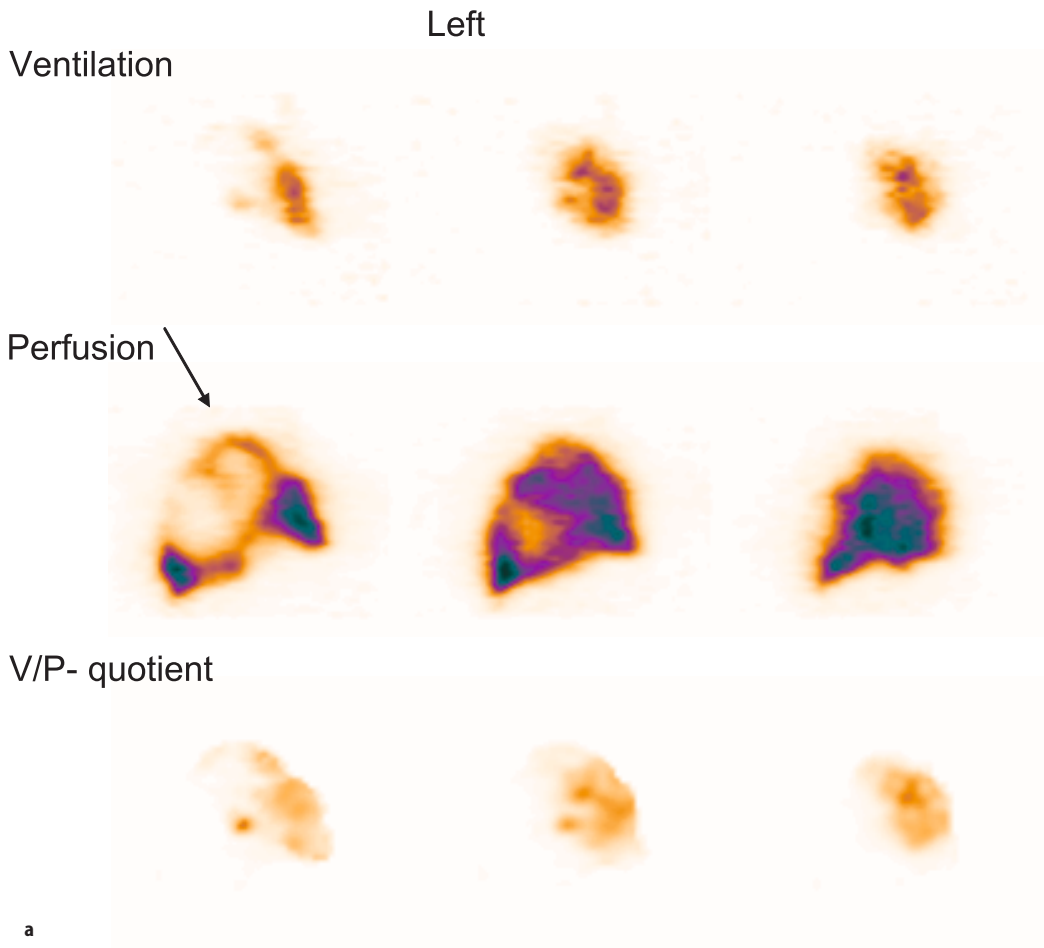

Fig. 5.9a, b. Patient with extensive bilateral pneumonia. **a** Sagittal slices of the left lung show almost absent ventilation. Perfusion is better preserved as is obvious from corresponding images. A stripe sign is typical for pneumonia (*arrow*). **b** Chest X-ray showing pleural effusion on the left side

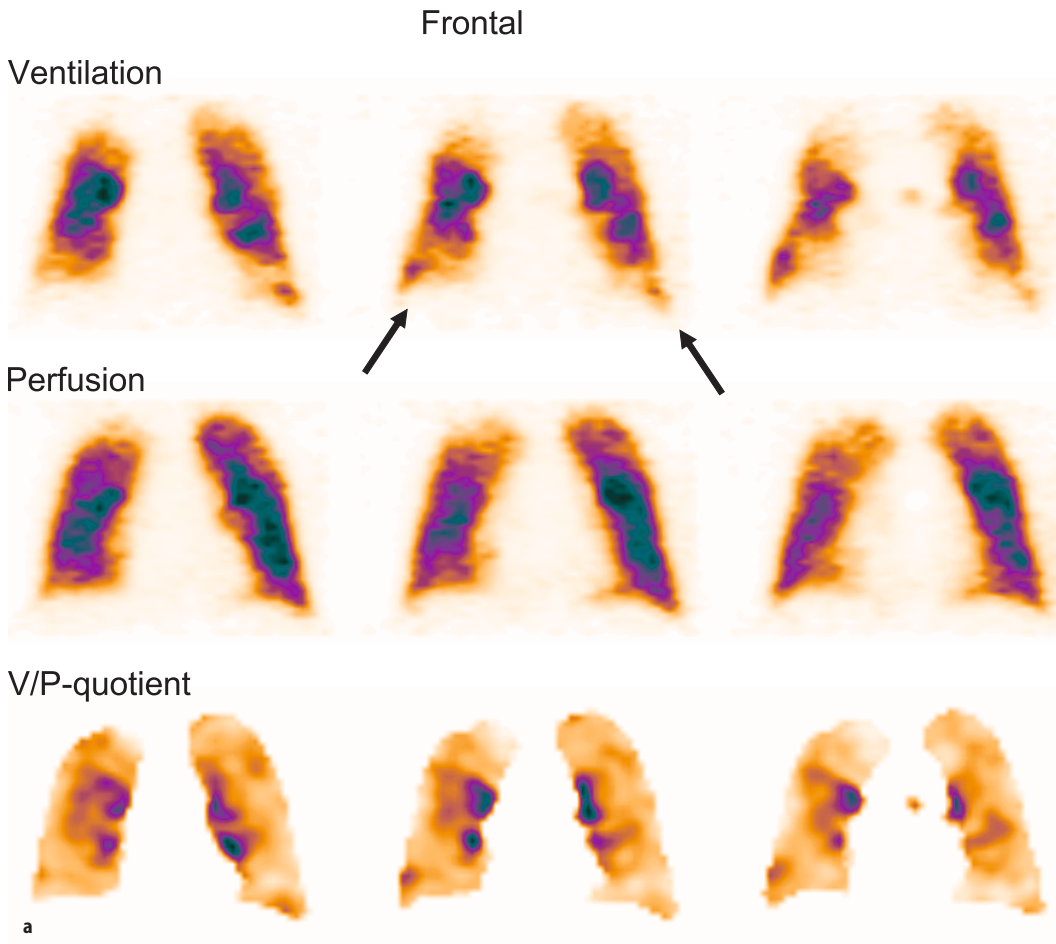

Fig. 5.10a–c. Patient with pneumonia and COPD. **a** Frontal slices from a 65-year-old man with COPD. In ventilation images is non-homogeneous distribution of Technegas with central deposition of aerosol, typical for COPD. Perfusion is less affected. **b** Sagittal slices; ventilation is decreased/absent in posterior region (*arrows*), while perfusion is less affected, reverse mismatch, typical for pneumonia. **c** Chest X-ray shows atelectasis and infiltrate in right lung

most frequent finding is a matched defect (Li et al. 1994). However, ventilation defects usually exceed perfusion defects, causing reverse mismatch (Carvalho and Lavender 1989). Li et al. (1984) suggested the presence of reverse mismatch as a sign of chest infection, finding it in 81 % of all reverse mismatches.

A 79-year-old man who felt general illness, shivering, and low blood pressure, had a chest X-ray which showed pleural effusion in the left lung with suspicion of parenchymal changes (Fig. 5.9a). D-dimer was increased. qV/P_{SPECT} showed bilateral ventilation reduction, with almost absent ventilation in the left lung (Fig. 5.9b) and much better preserved perfusion. A stripe sign was observed. Diagnosis after qV/P_{SPECT} was extended pneumonia that was confirmed at autopsy.

In pneumonia the "stripe sign" has often been described and highlighted (Sostman and Gottschalk 1982, 1992). This sign refers to a stripe adjacent to the pleural surfaces in which perfusion is relatively well maintained compared to a more pronounced central perfusion defect. Compared to planar imaging, the identification of a stripe sign is facilitated by V/P_{SPECT} as overlying structures do not mask the finding (Pace and Goris 1998).

Figure 5.10a–c shows a finding of a 65-year-old man with known COPD with sudden development of chest pain and tachycardia. Coronary angiography was normal.

Due to PE suspicion, qV/P_{SPECT} was performed. COPD was diagnosed on the basis of a typical ventilation pattern and pneumonia on the basis of absent/reduced ventilation in the posterior and basal regions with better preserved perfusion (Fig. 5.10a, b). Chest X-ray showed atelectasis in the right lung and infiltrate (Fig. 5.10c).

The likelihood for PE increases in patients with coexisting diseases as shown by Hampson (1995) and in the ICOPER study (Elliott et al. 2000). In the ICOPER

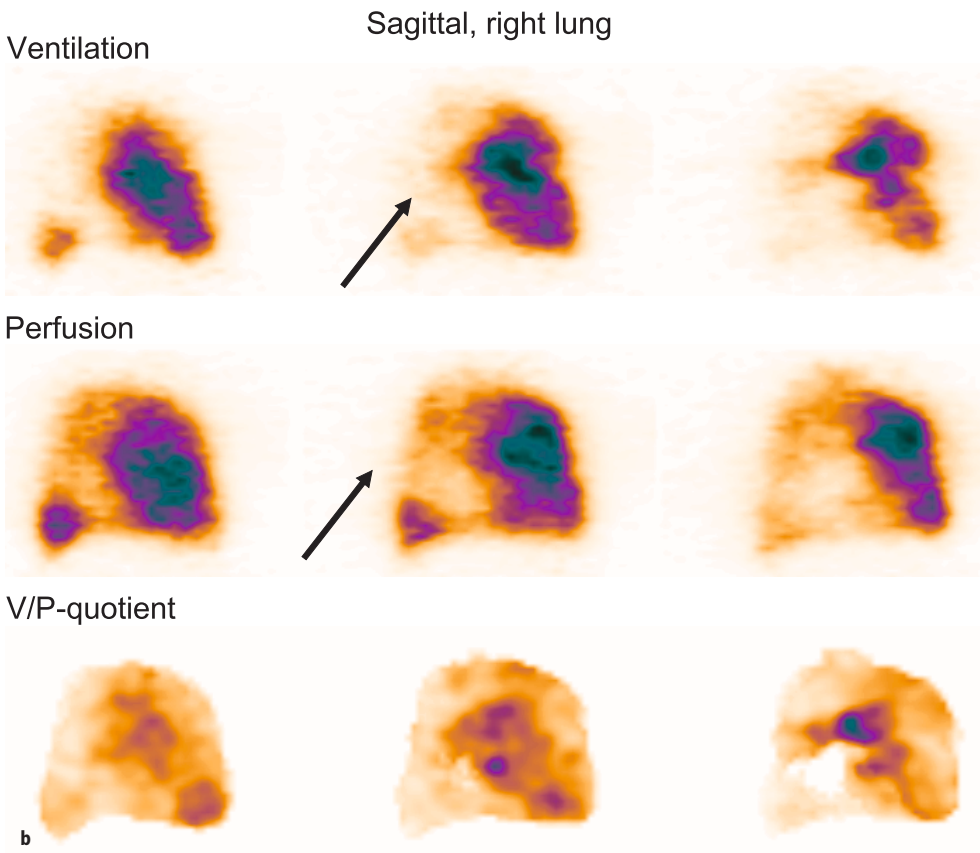
Sagittal, right lung
Ventilation
Perfusion
V/P-quotient
b

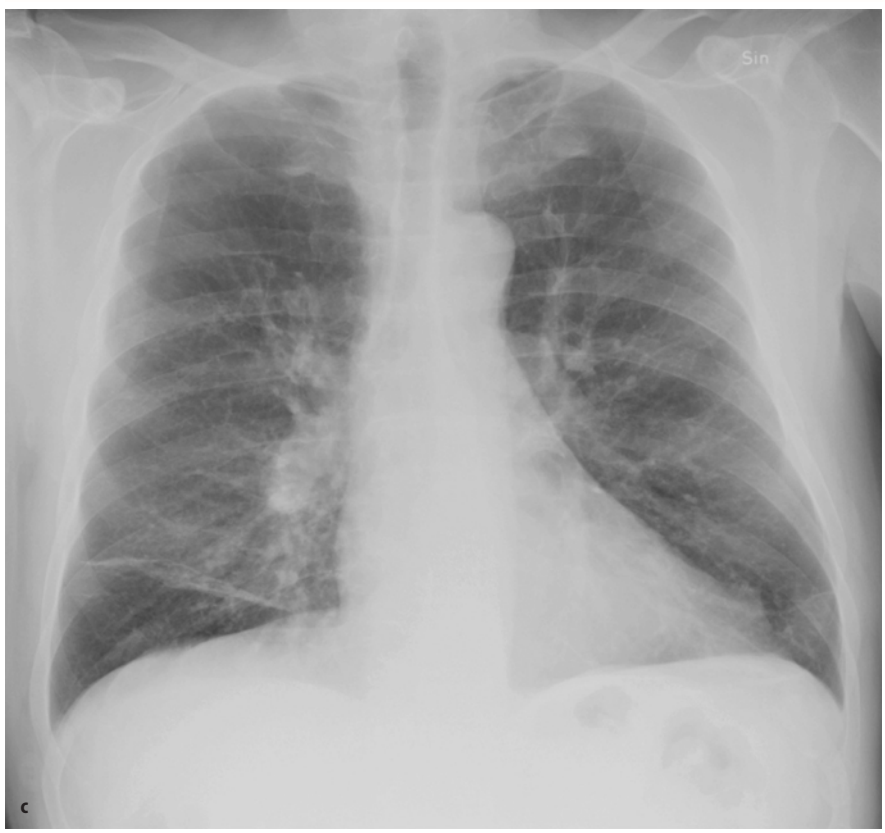
Sin
c

Fig. 5.10b, c

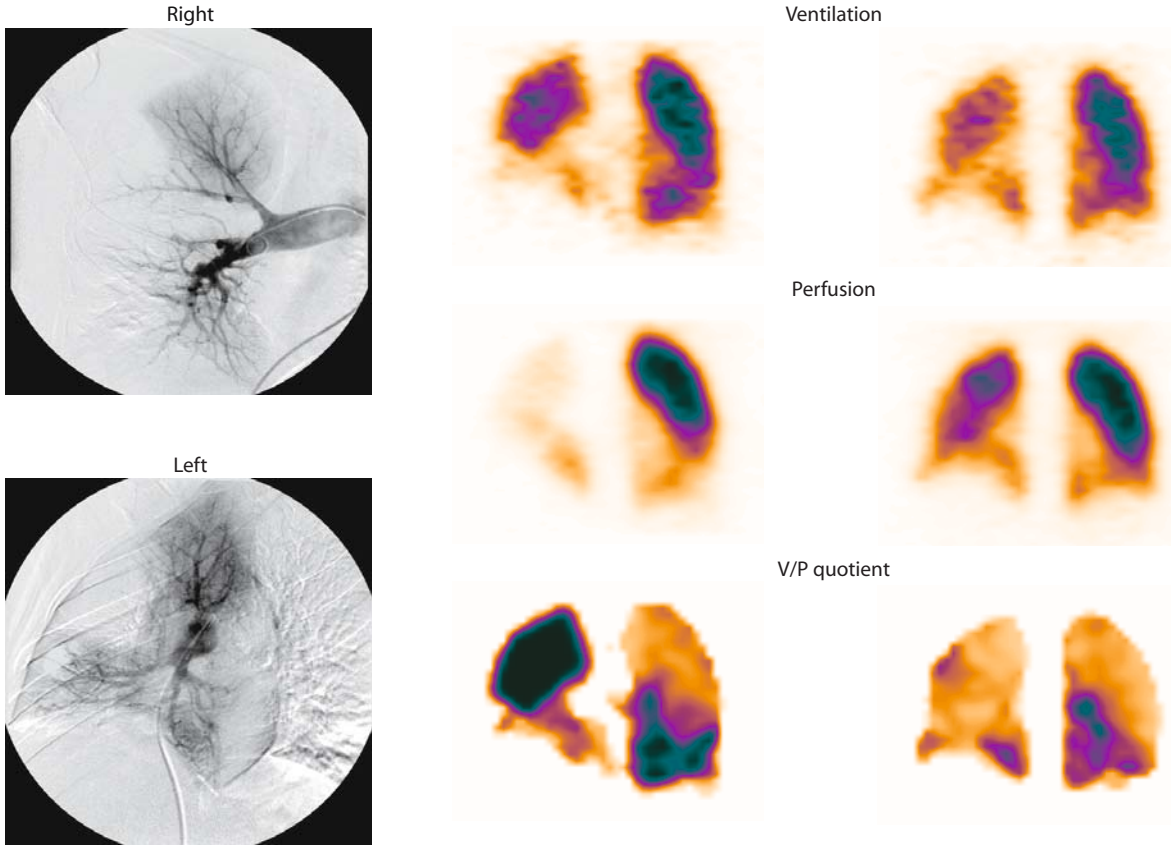

Fig. 5.11. Patient with pneumonia and extensive PE. *Left panel:* angiography; *middle panel:* initial V/P_{SPECT}; frontal slices, *right panel:* V/P_{SPECT} at 1 month follow-up. Pneumonia is indicated by absence of ventilation and perfusion (*matched changes*) in right lower lobe (*interrupted arrows*). PE was diagnosed from absent perfusion with preserved ventilation in areas well delineated on $V/P_{quotient}$ images (*drawn arrows*)

study, among 2,000 patients with confirmed PE, only 25 % had a normal chest X-ray. Infiltrates were present in 17 %. In 288 patients with autopsy proven PE, pneumonia was observed in 17 % (Mandelli et al. 1997).

A young female was diagnosed with pneumonia in three multislice CT studies in two university hospitals. When she became critically ill, qV/P_{SPECT} showed signs of pneumonia but also of PE. Extensive PE was diagnosed on the basis of widespread mismatch (Fig. 5.11) (Bajc 2005). Angiography, motivated by conflicting findings in CT and qV/P_{SPECT}, confirmed PE. After therapy, starting with repeated thrombolytic injections, she became well and follow-up scintigraphy showed nearly total recovery. An underlying disease may suggest alternative explanations for the patient's symptoms and may distract from life-threatening PE. Regarding the clinical probability and the diagnosis of acute PE, it is important to "think outside the box" (Farzaneh-Far et al. 2006).

5.1.7 Positron Emission Tomography

5.1.7.1 Ventilation and Perfusion

Positron emission tomography (PET) involves the administration of a radioisotope that decays by emitting a positron. The positron annihilates with an electron into two 511-keV antiparallel photons. By coincidence detection, annihilation photons are registered by external crystals arranged in rings around the object. Positron emitting isotopes have a half-life of a few seconds up to hours (^{19}Ne $t_{1/2}$ = 17 s, ^{15}O $t_{1/2}$ = 2 min, ^{11}C $t_{1/2}$ = 20 min, ^{13}N $t_{1/2}$ = 10 min, ^{18}F $t_{1/2}$ = 110 min). ^{19}Ne can be used in a way analogous to that of ^{81m}Kr for studies of regional ventilation (Valind et al. 1987; Brudin et al. 1994). These cyclotron produced isotopes are often incorporated into biologically relevant substances and can be used for many research purposes.

Gallium-68 produced from a generator can be incorporated into microspheres for perfusion studies. $^{13}N_2$

can be used for studies of ventilation/perfusion ratio when infused intravenously and for ventilation studies when administered by inhalation (Rhodes et al. 1989; Schuster 1998; Musch and Venegas 2005). $^{13}N_2$ was used by Vidal Melo (Vidal Melo et al. 2003) for quantitative assessment of a regional V/P relationship after PE.

5.1.7.2 Radiation Exposure

Doses of 30 MBq and 120 MBq for ventilation and perfusion SPECT, respectively, allow excellent V/P_{SPECT} quality at an effective radiation dose of 1.8 mSv (ICRP 53 1998). Estimation of exposure is relatively easy when short-lived isotopes are used in nuclear medicine. In contrast, for X-ray technologies this is much more difficult because of differences in equipment, the size of exposed fields and several other factors. Single slice CT for PE may give an effective dose of 5 – 10 mSv (ICRP 2000). To reduce the dose to such levels the examination field is limited to about 15 cm or 50 % of the total length of the lung. The female breast may receive 20 – 35 mSv, an exposure that may significantly increase the risk of breast cancer particularly in young women (Remy-Jardin et al. 1998; Nickoloff and Aldersson 2001). This problem has recently been emphasized in a study by Parker et al. (2005). These authors emphasize the public health issue related to the collective dose associated with very large numbers of CT scans and the individual dose in association with frequently performed multiple pulmonary CT angiograms in the same patient.

5.1.7.3 Algorithm for Evaluation of Patients Suspected of Having PE

Clinical diagnosis is both problematic and unreliable and in 70 % of cases there is no correct diagnosis (Tilli et al. 2006). Different diagnostic strategies for PE have been evaluated. They frequently combine clinical assessment, plasma D-dimer measurement, lower limb venous ultrasonography and helical CT (Musset et al. 2002; Perrier et al. 2004; Wells et al. 2001). Such strategies are complicated and involve multiple rounds of tests and are thus time consuming, costly and difficult to apply in clinical practice. Moreover, angiography and ventilation perfusion scintigraphy are needed to reach a definite diagnosis in some patients (Perrier et al. 2004). In the Christopher study (van Belle et al. 2006), evaluation of patients with suspected PE was based on clinical probability, D-dimer and CT. Radiation exposure was avoided in one-third of patients. Of 1,505 patients without PE in whom CT was performed or intended, 20 suffered a thromboembolic event, of whom 8 died in PE during 3 months follow-up. The strategy was considered safe. However, the significance of negative findings by multidetector CT must be confirmed, particularly as sensitivity is low. D-dimer for PE diagnosis is of low utility, particularly in the elderly and in inpatients (Sohne et al. 2005). Parker et al. (2005) showed in a large clinical study that D-dimer has a sensitivity of 52 %, a specificity of 40 % and a negative predictive value of 71 %. These authors also stressed that the high radiation exposure of CT is important in designing a diagnostic strategy.

Clinical information with a clinical pretest probability such as the Wells score (Table 5.1) combined with a holistic interpretation of high quality V/P_{SPECT} offers a simple strategy to all patients suspected of PE. This simple based algorithm reflects clinical reality based on the beneficial experience of more than 5,000 examined patients, 962 patients treated and followed up for PE since 2002. The examination is feasible for all patients. There are no contraindications and the radiation dose is low. It has a high diagnostic accuracy and there are few non-diagnostic reports. It has an impact on the selection of therapeutic strategy and is suitable for follow-up.

5.1.8 Concluding Remarks

V/P_{SPECT}, performed and interpreted according to the state of the art, has unquestionable advantages over CT. V/P_{SPECT} is the preferable method for diagnosis and the only method for routine follow-up of PE. An obvious limitation is its much lower availability than CT. Nuclear medicine has the responsibility and the challenge to provide optimal care for patients with suspected PE by making high quality V/P_{SPECT} more available.

High quality V/P_{SPECT} can be performed at low cost within 1 h. A holistic interpretation gives results superior to CT with respect to sensitivity, specificity and less than 4 % of non-diagnostic findings (Corbus et al. 1997; Lemb and Pohlabeln 2001; Reinartz et al. 2001; Bajc et al. 2004; Reinartz et al. 2004).

With an increasing number of tomographic gamma cameras, V/P_{SPECT} should be applied in each hospital by using the standard software offered together with modern systems. The calculation of $V/P_{quotient}$ according to our technique is a further step forward that merits implementation in new systems (Olsson et al. 2006).

V/P_{SPECT} and CT are both essential elements in the diagnosis of PE, the former because of its higher accuracy, lower radiation dose and feasibility in all patients, the latter because of its higher availability. Furthermore, close cooperation between clinicians, nuclear medicine and diagnostic radiology is essential to achieve the optimal diagnosis and therapy for PE.

References

Agnew JE, Francis RA, Pavia D, Clarke SW (1982) Quantitative comparison of 99Tcm-aerosol and 81Krm ventilation images. Clin Phys Physiol Meas 3:21 – 30

Aviram G, et al. (2004) Pitfalls in the diagnosis of acute pulmonary embolism on spiral computer tomography. Curr Probl Diagn Radiol 33:74 – 84

Baile EM, et al. (2000) Spiral computed tomography is comparable to angiography for the diagnosis of pulmonary embolism. Am J Respir Crit Care Med 161:1010 – 1015

Bajc M, et al. (2002a) Comparison of ventilation/perfusion scintigraphy and helical CT for diagnosis of pulmonary embolism; strategy using clinical data and ancillary findings. Clin Physiol Funct Imaging 22:392 – 397

Bajc M, et al. (2002b) Lung ventilation/perfusion SPECT in the artificially embolized pig. J Nucl Med 43:640 – 647

Bajc M (2005) Value of ventilation/perfusion SPECT detecting extensive pulmonary embolism in a patient with pneumonia. Thromb Haemost 93:993 – 994

Bajc M, Olsson C-G, Palmer J, Jonson B (2004a) Quantitative ventilation/perfusion SPECT (QV/P_{SPECT}): a primary method for diagnosis of pulmonary embolism. In: Freeman L (ed) Nuclear medicine annual. Lippincott, Williams & Wilkins, Philadelphia, pp 173 – 186

Bajc M, et al. (2004b) Diagnostic evaluation of planar and tomographic ventilation/perfusion lung images in patients with suspected pulmonary emboli. Clin Physiol Funct Imaging 24:249 – 256

Barghouth G, et al. (2000) Combination of clinical and V/Q scan assessment for the diagnosis of pulmonary embolism: a 2-year outcome prospective study. Eur J Nucl Med 27:1280 – 1285

Beer JH, et al. (2003) Outpatient treatment of pulmonary embolism is feasible and safe in a substantial proportion of patients. J Thromb Haemost 1:186 – 187

Brudin LH, et al. (1994a) Interrelationships between regional blood flow, blood volume, and ventilation in supine humans. J Appl Physiol 76:1205 – 1210

Brudin LH, et al. (1994b) Relationships between regional ventilation and vascular and extravascular volume in supine humans. J Appl Physiol 76:1195 – 1204

BTS Guidelines for the management of suspected acute pulmonary embolism (2003) Thorax 58:470 – 484

Burch WM, Tetley IJ, Gras JL (1984) Technetium-99m "pseudogas" for diagnostic studies in the lung. Clin Phys Physiol Meas 5:79 – 85

Burch WM, et al. (1986) Lung ventilation studies with technetium-99m Pseudogas. J Nucl Med 27:842 – 846

Carvalho P, Lavender JP (1989) The incidence and etiology of the ventilation/perfusion reverse mismatch defect. Clin Nucl Med 14:571 – 576

Chapman CN, Sziklas JJ, Spencer RP, Rosenberg RJ (1983) Pulmonary perfusion "without ventilation". J Nucl Med 24:1149 – 1150

Corbus HF, et al. (1997) Diagnostic usefulness of lung SPET in pulmonary thromboembolism: an outcome study. Nucl Med Commun 18:897 – 906

Elliott CG, Goldhaber SZ, Visani L, DeRosa M (2000) Chest radiographs in acute pulmonary embolism. Results from the International Cooperative Pulmonary Embolism Registry. Chest 118:33 – 38

Engeler CE, et al. (1995) Regional alterations in lung ventilation in end-stage primary pulmonary hypertension: correlation between CT and scintigraphy. AJR Am J Roentgenol 164:831 – 835

Farzaneh-Far R, Schwarzberg T, Mushlin SB (2006) Clinical problem-solving. Thinking outside the box. N Engl J Med 354:2376 – 2381

Fazio F, Jones T (1975) Assessment of regional ventilation by continuous inhalation of radioactive krypton-81m. Br Med J 3:673 – 676

Freeman LM, Krynyckyi B, Zuckier LS (2001) Enhanced lung scan diagnosis of pulmonary embolism with the use of ancillary scintigraphic findings and clinical correlation. Semin Nucl Med 31:143 – 157

Friedman WF, Braunwald E (1966) Alterations in regional pulmonary blood flow in mitral valve disease studied by radioisotope scanning. A simple nontraumatic technique for estimation of left atrial pressure. Circulation 34:363 – 376

Garg A, Gopinath PG, Pande JN, Guleria JS (1983) Role of radio-aerosol and perfusion lung imaging in early detection of chronic obstructive lung disease. Eur J Nucl Med 8:167 – 171

Goodman LR (2001) Venous thromboembolic disease: CT evaluation. Q J Nucl Med 45:302 – 310

Gottschalk A, et al. (1993a) Ventilation-perfusion scintigraphy in the PIOPED study. Part I. Data collection and tabulation. J Nucl Med 34:1109 – 1118

Gottschalk A, Sostman HD, et al. (1993b) Ventilation-perfusion scintigraphy in the PIOPED study. Part II. Evaluation of the scintigraphic criteria and interpretations. J Nucl Med 34:1119 – 1126

Gray HW (2002) The natural history of venous thromboembolism: impact on ventilation/perfusion scan reporting. Semin Nucl Med 32:159 – 172

Hampson NB (1995) Pulmonary embolism: difficulties in the clinical diagnosis. Semin Respir Infect 10:123 – 130

Heck LL, Duley JW (1974) Statistical considerations in lung imaging with 99mTc albumin particles. Radiology 113:675 – 679

ICRP 53 (1998) Radiation dose to patients from radiopharmaceuticals (addendum 2 to ICRP publication 53). Ann ICRP 28:1 – 126

ICRP (2000) Managing patient dose in computed tomography. A report of the International Commission on Radiological Protection. Ann ICRP 30:7 – 45

Isawa T, Lee BT, Hiraga K (1996) High-resolution electron microscopy of technegas and pertechnegas. Nucl Med Commun 17:147 – 152

Kao CH, et al. (1996) Evaluation of lung ventilation and alveolar permeability in cirrhosis. J Nucl Med 37:437 – 441

Kohn H, et al. (1985) Dry aerosol of monodisperse millimicrospheres for ventilation imaging: production, delivery system, and clinical results in comparison with 81m-krypton and 127-xenon. Eur J Nucl Med 10:411 – 416

Kovacs MJ, et al. (2000) Outpatient treatment of pulmonary embolism with dalteparin. Thromb Haemost 83:209 – 211

Kuni CC, Ducret RP, Nakhleh RE, Boudreau RJ (1993) Reverse mismatch between perfusion and aerosol ventilation in transplanted lungs. Clin Nucl Med 18:313 – 317

Lemb M, Pohlabeln H (2001) Pulmonary thromboembolism: a retrospective study on the examination of 991 patients by ventilation/perfusion SPECT using Technegas. Nuklearmedizin 40:179 – 186

Li DJ, Stewart I, Miles KA, Wraight EP (1994) Scintigraphic appearances in patients with pulmonary infection and lung scintigrams of intermediate or low probability for pulmonary embolism. Clin Nucl Med 19:1091 – 1093

Mandelli V, Schmid C, Zogno C, Morpurgo M (1997) "False negatives" and "false positives" in acute pulmonary embolism: a clinical-postmortem comparison. Cardiologia 42: 205 – 210

Miniati M, et al. (1996) Value of perfusion lung scan in the diagnosis of pulmonary embolism: results of the Prospective Investigative Study of Acute Pulmonary Embolism Diagnosis (PISA-PED). Am J Respir Crit Care Med 154:1387 – 1393

Mispelaere D, et al. (2002) [Pulmonary embolism and sibilant

types of chronic obstructive pulmonary disease decompensations]. Rev Mal Respir 19:415 – 423
Mohsenifar Z, Amin DK, Shah PK (1989) Regional distribution of lung perfusion and ventilation in patients with chronic congestive heart failure and its relationship to cardiopulmonary hemodynamics. Am Heart J 117:887 – 891
Morrell NW, et al. (1993a) The limitations of posterior view ventilation scanning in the diagnosis of pulmonary embolism. Nucl Med Commun 14:983 – 988
Morrell NW, et al. (1993b) The underestimation of segmental defect size in radionuclide lung scanning. J Nucl Med 34: 370 – 374
Musch G, Venegas JG (2005) Positron emission tomography imaging of regional pulmonary perfusion and ventilation. Proc Am Thorac Soc 2:508 – 529
Musset D, et al. (2002) Diagnostic strategy for patients with suspected pulmonary embolism: a prospective multicentre outcome study. Lancet 360:1914 – 1920
Nickoloff EL, Alderson PO (2001) Radiation exposures to patients from CT. AJR 177:285 – 287
Olsson CG, et al. (2006) Outpatient tinzaparin therapy in pulmonary embolism quantified with ventilation/perfusion scintigraphy. Med Sci Monit 12:PI9 – 13
Pace WM, Goris ML (1998) Pulmonary SPECT imaging and the stripe sign. J Nucl Med 39:721 – 723
Palmaz JC, et al. (1984) Reverse ventilation-perfusion mismatch. Clin Nucl Med 9:6 – 9
Palmer J, Bitzen U, Jonson B, Bajc M (2001) Comprehensive ventilation/perfusion SPECT. J Nucl Med 42:1288 – 1294
Parker MS, et al. (2005) Female breast radiation exposure during CT pulmonary angiography. AJR Am J Roentgenol 185: 1228 – 1233
Perrier A, Bounameaux H (2006) Accuracy or outcome in suspected pulmonary embolism. N Engl J Med 354:2383 – 2385
Perrier A, et al. (2001) Performance of helical computed tomography in unselected outpatients with suspected pulmonary embolism. Ann Intern Med 135:88 – 97
Perrier A, et al. (2004) Diagnosing pulmonary embolism in outpatients with clinical assessment, D-dimer measurement, venous ultrasound, and helical computed tomography: a multicenter management study. Am J Med 116:291 – 299
Pistolesi M, et al. (1988) Factors affecting regional pulmonary blood flow in chronic ischemic heart disease. J Thorac Imaging 3:65 – 72
Powell T, Muller NL (2003) Imaging of acute pulmonary thromboembolism: should spiral computed tomography replace the ventilation-perfusion scan? Clin Chest Med 24: 29 – 38
Reinartz P, et al. (2001) Optimizing ventilation-perfusion lung scintigraphy: parting with planar imaging. Nuklearmedizin 40:38 – 43
Reinartz P, et al. (2004) Tomographic imaging in the diagnosis of pulmonary embolism: a comparison between V/Q lung scintigraphy in SPECT technique and multislice spiral CT. J Nucl Med 45:1501 – 1508
Remy-Jardin M, et al. (1997) Peripheral pulmonary arteries: optimization of the spiral CT acquisition protocol. Radiology 204:157 – 163
Remy-Jardin M, et al. (1998) Spiral CT of pulmonary embolism: diagnostic approach, interpretive pitfalls and current indications. Eur Radiol 8:1376 – 1390
Remy-Jardin M, et al. (2002) CT angiography of pulmonary embolism in patients with underlying respiratory disease: impact of multislice CT on image quality and negative predictive value. Eur Radiol 12:1971 – 1978
Rhodes CG, et al. (1989) Quantification of regional V/Q ratios in humans by use of PET. I. Theory J Appl Physiol 66:1896 – 1904
Richman PB, et al. (2004) Prevalence and significance of nonthromboembolic findings on chest computed tomography angiography performed to rule out pulmonary embolism: a multicenter study of 1,025 emergency department patients. Acad Emerg Med 11:642 – 647
Sando Y, Inoue T, Nagai R, Endo K (1997) Ventilation/perfusion ratios and simultaneous dual-radionuclide single-photon emission tomography with krypton-81m and technetium-99m macroaggregated albumin. Eur J Nucl Med 24:1237 – 1244
Schoepf UJ, Costello P (2004) CT angiography for diagnosis of pulmonary embolism: state of the art. Radiology 230: 329 – 337
Schonhofer B, Kohler D (1998) Prevalence of deep-vein thrombosis of the leg in patients with acute exacerbation of chronic obstructive pulmonary disease. Respiration 65:173 – 177
Schuster DP (1998) The evaluation of lung function with PET. Semin Nucl Med 28:341 – 351
Senden TJ, et al. (1997) The physical and chemical nature of technegas. J Nucl Med 38:1327 – 1333
Slama K, et al. (2000) Unilateral lung edema: effects on pulmonary gas exchange, hemodynamics, and pulmonary perfusion distribution. J Appl Physiol 89:1513 – 1521
Sohne M, Kamphuisen PW, van Mierlo PJ, Buller HR (2005) Diagnostic strategy using a modified clinical decision rule and D-dimer test to rule out pulmonary embolism in elderly in- and outpatients. Thromb Haemost 94:206 – 210
Sostman HD, Gottschalk A (1982) The stripe sign: a new sign for diagnosis of nonembolic defects on pulmonary perfusion scintigraphy. Radiology 142:737 – 741
Sostman HD, Gottschalk A (1992) Prospective validation of the stripe sign in ventilation-perfusion scintigraphy. Radiology 184:455 – 459
Sostman HD, Neumann RD, Gottschalk A, Greenspan RH (1983) Perfusion of nonventilated lung: failure of hypoxic vasoconstriction? AJR Am J Roentgenol 141:151 – 156
Stein et al. (2006) Multidetector computed tomography for acute pulmonary embolism. N Engl J Med 354:2317 – 2327
Strong JC, Agnew JE (1989) The particle size distribution of technegas and its influence on regional lung deposition. Nucl Med Commun 10:425 – 430
Surette GD, Muir AL, Hogg JC, Fraser RG (1975) Roentgenographic study of blood flow redistribution in acute pulmonary edema in dogs. Invest Radiol 10:109 – 114
Tagil K, et al. (2000) Efficient lung scintigraphy. Clin Physiol 20:95 – 100
Taplin GV, Poe ND, Isawa T, Dore EK (1974) Radioaerosol and xenon gas inhalation and lung perfusion scintigraphy. Scand J Respir Dis Suppl 85:144 – 158
The PIOPED Investigators (1990) Value of the ventilation/perfusion scan in acute pulmonary embolism. Results of the prospective investigation of pulmonary embolism diagnosis (PIOPED). JAMA 263:2753 – 2759
Tilli P, et al. (2006) Diagnostic and therapeutic approach to acute pulmonary embolism in an emergency department. Eur Rev Med Pharmacol Sci 10:91 – 98
Tillie-Leblond I, et al. (2006) Pulmonary embolism in patients with unexplained exacerbation of chronic obstructive pulmonary disease: prevalence and risk factors. Ann Intern Med 144:390 – 396
Tsang JY, Baile EM, Hogg JC (1986) Relationship between regional pulmonary edema and blood flow. J Appl Physiol 60:449 – 457
Valind SO, Rhodes CG, Jonson B (1987) Quantification of regional ventilation in humans using a short-lived radiotracer – theoretical evaluation of the steady-state model. J Nucl Med 28:1144 – 1154
van Belle A, et al. (2006) Effectiveness of managing suspected

pulmonary embolism using an algorithm combining clinical probability, D-dimer testing, and computed tomography. JAMA 295:172 – 179
van Strijen MJ, et al. (2003) Diagnosis of pulmonary embolism with spiral CT as a second procedure following scintigraphy. Eur Radiol 13:1501 – 1507
van Strijen MJ, et al. (2005a) Helical computed tomography and alternative diagnosis in patients with excluded pulmonary embolism. J Thromb Haemost 3:2449 – 2456
van Strijen MJ, et al. (2005b) Accuracy of single-detector spiral CT in the diagnosis of pulmonary embolism: a prospective multicenter cohort study of consecutive patients with abnormal perfusion scintigraphy. J Thromb Haemost 3:17 – 25
Vidal Melo MF, et al. (2003) Quantification of regional ventilation-perfusion ratios with PET. J Nucl Med 44:1982 – 1991
Wagner HN, Jr (1976) The use of radioisotope techniques for the evaluation of patients with pulmonary disease. Am Rev Respir Dis 113:203 – 218
Wells PS, et al. (2001) Excluding pulmonary embolism at the bedside without diagnostic imaging: management of patients with suspected pulmonary embolism presenting to the emergency department by using a simple clinical model and d-dimer. Ann Intern Med 135:98 – 107
West J (1974) Respiratory physiology. Williams & Wilkins, Baltimore

5.2 PET and PET/CT in Lung Cancer

H.C. Steinert

5.2.1 Introduction

Lung cancer is the most common type of cancer and is the leading cause of cancer deaths in the United States for both women and men. The common types of lung cancer are non-small cell lung cancer (NSCLC) and small cell lung cancer (SCLC). Accurate tumor staging is essential for choosing the appropriate treatment strategy in lung cancer. In NSCLC, surgical resection offers the best chance for cure. However, curable surgical resection is only possible for early stages of NSCLC (no contralateral mediastinal lymph node metastases, no distant metastases). Patients with SCLC are treated with chemotherapy and radiation treatment. Malignant pleural mesothelioma (MPM) is the most common cancer of the pleura. MPM usually develops at least 20 – 30 years after asbestos exposure. The treatment consists of a tri-modality therapy, including chemotherapy, radical surgery, and radiation treatment. Even though the 5-year survival rate of patients with lung cancer and pleural cancer remains low, treatments are improving and newer agents appear promising. Therefore, the accurate assessment of the extent of disease is critical to determine whether the patient is treated by surgical resection, chemotherapy, radiation therapy, or a combination of these therapies. Positron emission tomography (PET) imaging and integrated PET/CT (positron emission tomography and computed tomography) imaging play an import role in the evaluation of patients with lung cancer. In this chapter, the role of PET imaging and PET/CT imaging in patients with NSCLC, SCLC, and MPM is discussed.

5.2.2 Radiopharmaceuticals

PET imaging is a molecular imaging technique that requires radiopharmaceuticals. By far the most widely used radiopharmaceutical for tumor staging with PET is ^{18}F-fluorodeoxyglucose (FDG), which is an analogue of glucose. FDG is transported across cell membranes by glucose transporter proteins and is phosphorylated by hexokinase like glucose. Once phosphorylated, FDG-6-phosphate is metabolically trapped. Thus FDG labels cellular glucose uptake and metabolism. ^{18}F for labeling FDG is produced in a cyclotron. The physical half-life of ^{18}F-labeled compounds is 110 min. Thus, central production and regional shipment of FDG is possible.

5.2.3 PET Imaging

PET imaging is based on the detection of the two annihilation photons which are produced when a positron is emitted from a radioisotope. ^{18}F is the most widely used PET radionuclide. The positrons emitted by the radioisotope are not stable in matter. Positrons are the antimatter counterparts of electrons, having the same mass and the opposite (positive) charge of the electron. Once produced, the positron leaves the nucleus and gradually loses energy in the surrounding tissue. When most of its energy is lost, the positron annihilates with a nearby electron. The annihilation reaction results in two photons with an energy of 511 keV, and they leave the annihilation site in opposite directions at an angle of almost exactly 180°. In a PET scanner, the two emitted photons are detected by a ring scintillation detector consisting of thousands of detector elements. Simultaneous detection of two 511-keV photons in any two detectors in the ring indicates that an annihilation occurred on a line connecting those detectors. Such an event represents a coincidence. Each coincidence is recorded, and the final raw data sample is based on the detector pairs. These raw data represent projections of the radiotracer in the body, and are subsequently reconstructed into cross-sectional images.

Attenuation, the loss of true events through absorption, influences the quality of PET images. In order to obtain homogeneous images, an attenuation correction of the PET data, which are called emission data,

has to be done. In conventional PET scanners, attenuation is measured by using photons from a rotation radioactive source. The photons are registered by the detectors of the PET scanner. However, the photon flux of these sources is very low and attenuation correction scans are thus lengthy procedures. In clinical routine, an emission PET scan lasts about 30 min. For an attenuation correction scan, called a transmission scan, about 15 min has to be added. The attenuation data are introduced into the image reconstruction process of the emission images and result in attenuation corrected PET images.

The efficiency of PET for detecting emitted photons is far higher than that for single photon imaging as SPECT (single photon emission computed tomography). However, the fraction of all emitted photon pairs that are detected is small (< 1 %). Even with the low detection efficiency, PET imaging is the most sensitive way to detect small concentrations of tracers in the body. The system resolution of a modern PET scanner for patient imaging is 4 – 5 mm.

5.2.4 Integrated PET/CT Imaging

Today, PET and CT are combined into a single inline imaging system, where the patient is moved from the CT to the PET gantry by table motion. The integrated PET/CT devices offer several advantages over a PET scanner alone. The attenuation correction can be performed more accurately by CT data, resulting in a better quality of PET images. Since CT imaging takes only several seconds, the total imaging time is shortened. The PET (metabolic) and CT (morphologic) information are perfectly co-registered. This is of major importance because PET scans provide little anatomic information. Several studies have demonstrated that the diagnostic accuracy of integrated PET/CT imaging is higher compared to the conventional visual correlation of PET and CT on separate units in staging lung cancer (Lardinois et al. 2003; Antoch et al. 2003; Shim et al. 2005). It is likely that the synergistic effects obtained when adding CT to PET are responsible for the almost explosive growth of PET/CT imaging worldwide.

At our institution the following PET/CT protocol is used: Patients fast for at least 4 h prior to the scanning. Oral CT contrast agent is given 15 min before the injec-

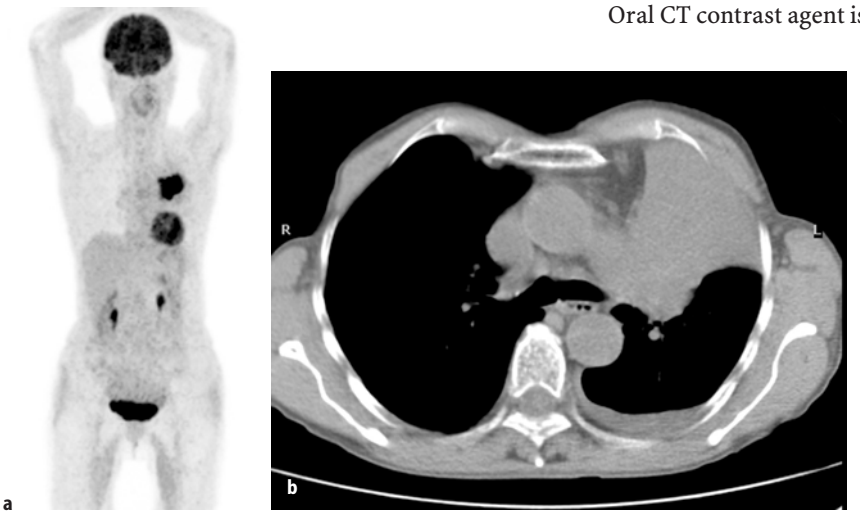

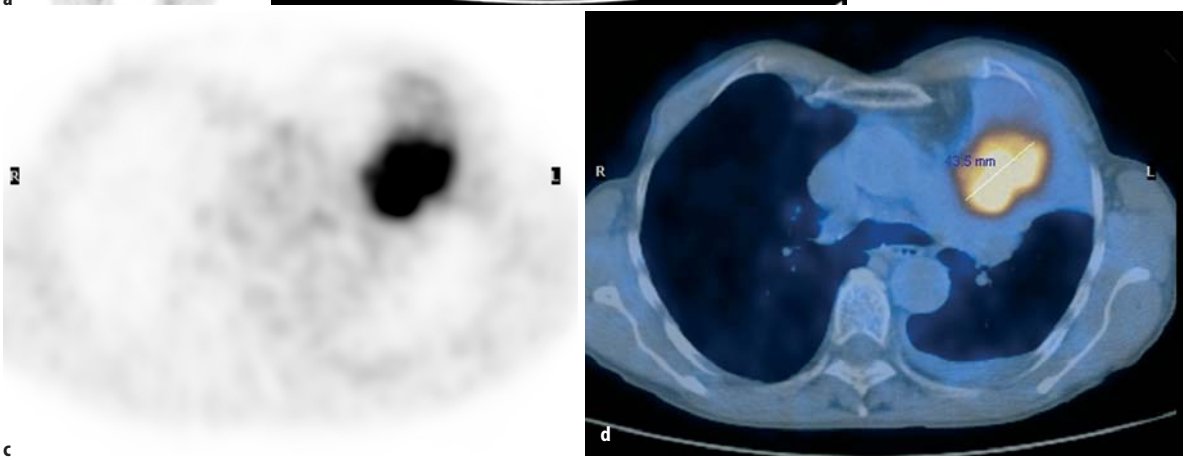

Fig. 5.12a–d. A 70-year-old woman with a lung cancer in the left upper lobe. PET/CT with FDG was performed for preoperative staging. **a** Maximum intensity projection (MIP) PET scan; **b** axial unenhanced low-dose CT scan; **c** axial CT-attenuation corrected PET scan; and **d** axial co-registered PET/CT scan. With PET/CT the primary tumor in the atelectasis could be clearly localized. No mediastinal metastases and no distant metastases were found. The patient was referred to surgery

tion of a standard dose of 350 – 400 MBq of FDG. After the FDG injection, patients rest at least 45 min. Patients are examined in the supine position. An intravenous contrast agent is not given routinely. After bladder voiding just prior to scanning, we first perform a low dose CT scan at 80 mA, 140 kV, 0.5 s/tube rotation, slice thickness 4.25 mm, scan length 867 mm, and a data-acquisition time of 22.5 s. Our CT scanner is a state of the art four-slice MDCT. Patients are instructed to expire and hold their breath when the CT scanner scans this body region. Immediately following the CT acquisition, a PET emission scan is acquired with an acquisition time of 3 min per cradle position with a one-slice overlap. The six to seven cradle positions from the upper legs to the head result in an acquisition time of approximately 24 – 27 min. Starting PET scanning in the upper legs rather than the head avoids a potential major PET/CT mismatch in the bladder region. This is due to bladder filling between CT data acquisition and the relatively lengthy PET scan, if started at the head.

After this "baseline" PET/CT data acquisition, additional standard CT protocols can be performed depending upon the clinical requirements. In patients with central lung tumors, we also perform a CT scan enhanced with an intravenous contrast agent, which can better delineate the tumor in relation to the vessels. Other groups have advocated the use of contrast enhanced CT scans from the beginning and as the only CT scan. It is our opinion that contrast enhanced CT should not be performed routinely for PET/CT imaging. In many settings, CT contrast is not needed, as FDG is mostly a much better "contrast agent" for the tumor than the contrast agents used in CT. The additional radiation burden to a patient with a low dose CT at 40 mAs is in the range of 2 – 3 mSv, and that of PET around 8 – 9 mSv. Thus, a PET/CT examination with the above protocol has a lower radiation dose compared to a standard CT.

The CT data is used for the attenuation correction and the images are reconstructed using a standard iterative algorithm (OSEM). The acquired images are viewed with software providing multiplanar reformatted images of PET alone, CT alone and fused PET/CT with linked cursors.

5.2.5 Non-Small Cell Lung Cancer

There are four main histologic types of NSCLC: adenocarcinoma, squamous cell carcinoma, large cell carcinoma, and mixed carcinoma. Adenocarcinomas typically develop in the periphery of the lung and are most common in women and in nonsmokers. Adenocarcinomas have a high incidence of early metastases and tend to grow more rapidly than squamous cell carcinomas. Bronchioalveolar cell carcinoma (BAC) is a subtype of adenocarcinoma. BACs typically grow along the alveolar spaces without invasion of the stroma. BAC can appear as a solitary pulmonary nodule, a pneumonia-like consolidation or as multiple nodules throughout the lung. Squamous cell carcinomas are strongly associated with smoking. In general, they have the best prognosis because of their slow growth rate and their low incidence of distant metastases. They tend to become large and develop a central necrosis. Metastases to regional lymph nodes are common. Squamous cell carcinoma is the most common cause of Pancoast tumors. These occur typically at the apex of the lung and are associated with Horner's syndrome and bone destruction. Large cell carcinomas are also strongly associated with smoking. They tend to grow rapidly, metastasize early and are associated with a poor prognosis. Staging of NSCLC is based on the TNM system and requires accurate characterization of the primary tumor (T stage), regional lymph nodes (N stage), and extrathoracic metastases (M stage).

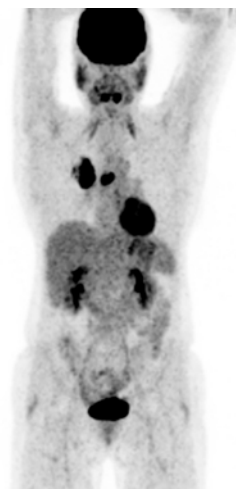

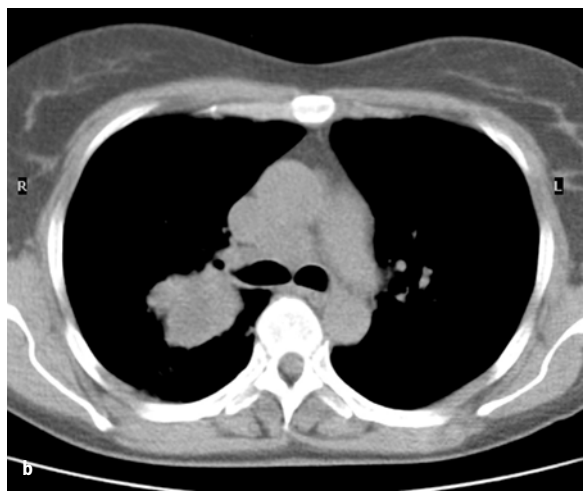

Fig. 5.13a–d. A 51-year-old woman with a lung cancer in the right upper lobe. PET/CT with FDG was performed for preoperative staging. **a** Maximum intensity projection (MIP) PET scan; **b** axial unenhanced low-dose CT scan.

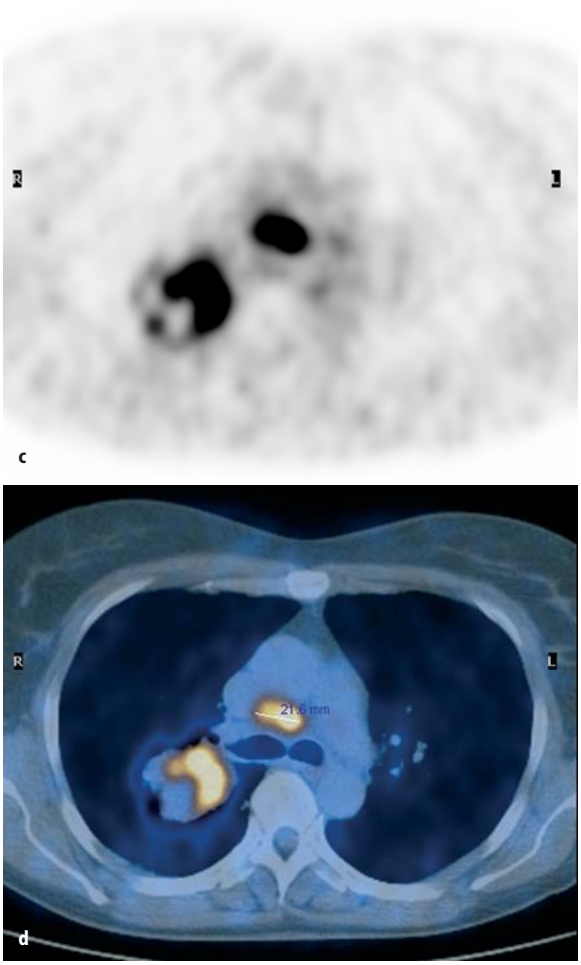

Fig. 5.13. c axial CT-attenuation corrected PET scan; and **d** axial co-registered PET/CT scan. PET/CT showed the necrotic primary tumor and precarinal lymph node metastases. No distant metastases were detected. The patient was referred to surgery

Both CT and PET using FDG play an important role in the diagnosis and staging of patients with NSCLC. CT provides excellent morphological information, but has significant limitations in differentiating between benign and malignant lesions either in an organ or in lymph nodes. It has been shown that FDG PET is highly accurate in classifying lung nodules as malignant or benign. Whole-body PET improves the rate of detection of mediastinal lymph-node metastases as well as extrathoracic metastases when compared to CT, MRI, ultrasound or bone scanning. Since modern PET scanners have a fairly high resolution (< 6 mm), even small lesions less than 1 cm can be detected. This represents a critical advantage of PET over CT and MR. It has been shown that integrated PET/CT provides more than the sum of PET and CT (Lardinois et al. 2003; Antoch et al. 2003; Shim et al. 2005). Due to precise CT correlation with the extent of FDG uptake, the location of even small lesions can be exactly defined. The information from a PET/CT scan guides the surgeon to the lesions.

5.2.5.1 Solitary Pulmonary Nodule

A solitary pulmonary nodule (SPN) is a circumscribed round or oval lesion in the lung parenchyma less than 3 cm in diameter. About 60 % of SPNs are benign and 40 % are malignant. Benign SPNs represent infectious or inflammatory nodules, adenomas, and hamartomas. In 20 – 30 % of patients, an SPN is the initial presentation of a lung cancer (Erasmus et al. 2000). Therefore, the early definitive diagnosis of an SPN is important for treatment management. Traditionally, a benign diagnosis for an SPN is made through a series of conventional radiographs or CT. If the SPN resolves or remains stable over time, it is considered to be a benign finding. The major drawback to the follow-up examinations is the time needed to establish the diagnosis. At least one follow-up study after 3 – 6 months is necessary to rule out growth of the SPN. Invasive transbronchial or transthoracic needle aspiration biopsy can be performed to clarify the diagnosis. The complications include pneumothorax and hemorrhage. Another limitation is that biopsies can miss the lesion or are non-diagnostic.

Many studies have demonstrated that FDG PET or PET/CT is a useful method to distinguish between benign and malignant SPN. PET was found to be 97 % sensitive and 78 % specific for malignancy (Gould et al. 2001; Hellwig et al. 2001). The standardized uptake value (SUV) is a semiquantitative measurement of the intensity of the FDG accumulation. An SUV cut-off of 2.5 is used for distinguishing between benign and malignant lesions. Particularly in SPN with indeterminate radiographic findings, FDG PET or PET/CT has a high clinical impact. PET or PET/CT is also useful in patients with SPN, where biopsy may be risky. If PET or PET/CT does not show an increased FDG accumulation, then the lesion is observed by CT to definitely establish a benign nature. It has to be recognized that FDG PET or PET/CT may show negative results for pulmonary carcinoid tumors, bronchiolo-alveolar lung carcinomas, and mucinous tumors (Higashi et al. 1998; Yap et al. 2002). Lesions with increased FDG accumulation should be considered malignant, although false-positive results have been reported in cases of inflammatory and infectious processes, such as histoplasmosis, aspergillosis, or active tuberculosis. However, most FDG active SPNs are malignant and should be resected.

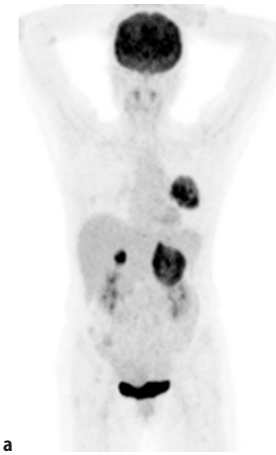

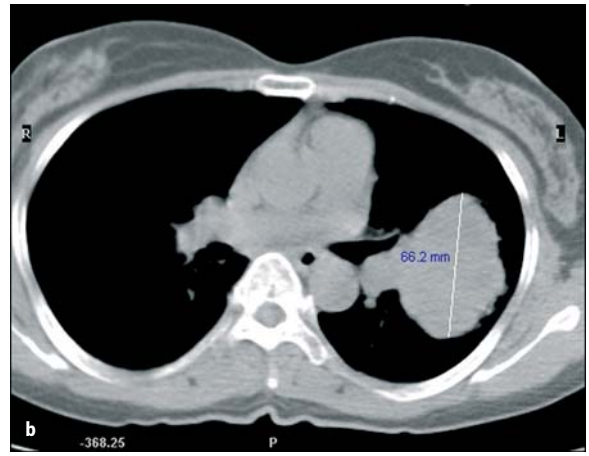

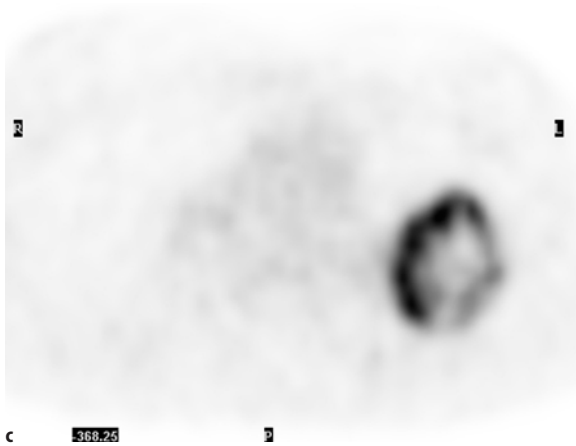

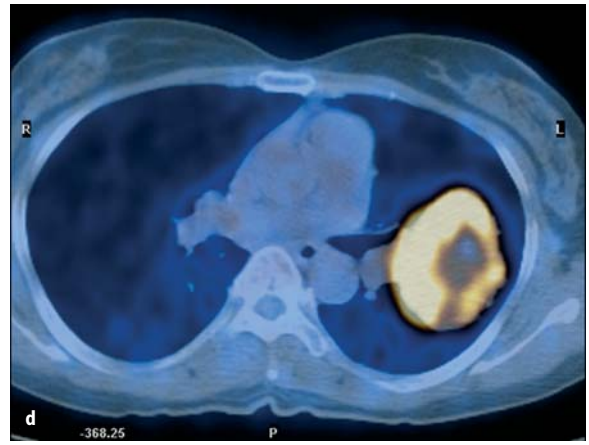

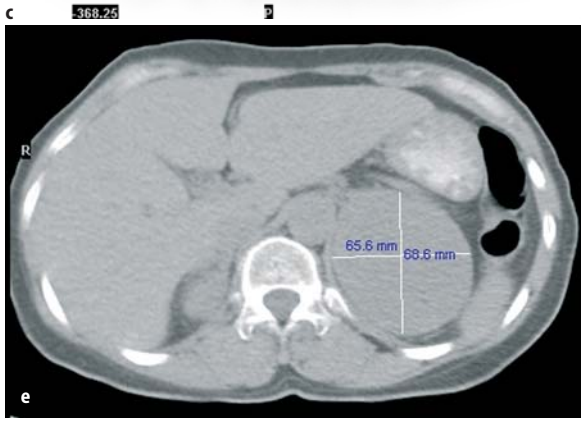

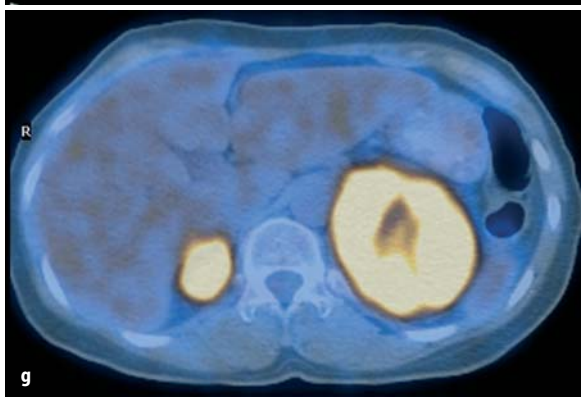

Fig. 5.14a–g. A 51-year-old woman with a lung cancer in the left upper lobe and suspicion of metastases in the adrenal glands. **a** Maximum intensity projection (MIP) PET scan; **b, e** axial unenhanced low-dose CT scans; **c, f** axial CT-attenuation corrected PET scans; and **d, g** axial co-registered PET/CT scans. PET/CT showed the primary tumor and bilateral metastases of the adrenal glands. No mediastinal lymph node metastases were found. The patient was referred to chemotherapy

5.2.5.2 Staging of the Primary Tumor

Surgical resection is the only treatment for cure in patients with NSCLC. The infiltration of the primary tumor into the chest wall, the mediastinum, or great vessels may limit the resectability. Without image fusion, the use of PET in the diagnosis of a tumor invasion in the surrounding tissue is limited. It has been shown that integrated PET/CT is superior to CT alone, PET alone, and visual correlation of PET and CT in T staging of patients with NSCLC (Lardinois et al. 2003;

Shim et al. 2005). Due to the exact anatomic correlation of the extent of FDG uptake, the delineation of the primary tumor can be defined precisely. Therefore the diagnosis of chest wall infiltration and the mediastinal invasion by the tumor is improved. Lesions with chest wall infiltration are classified as stage T3 and are potentially resectable. Surgical treatment requires en bloc resection of the primary tumor and the contiguous chest wall. Particularly in patients with poor cardiopulmonary reserve, the preoperative determination of chest wall infiltration is desirable in order to avoid extended en bloc resection. Integrated PET/CT provides important information on mediastinal infiltration as well. However, PET/CT imaging is unable to distinguish contiguity of tumor with the mediastinum from the direct invasion of the walls of mediastinal structures. It has been shown that FDG PET is a useful tool for the differentiation between tumor and peritumoral atelectasis. This is particularly important for the planning of radiotherapy in patients with lung cancer associated with an atelectasis (Fig. 5.12). The information provided by FDG PET results in a change in the radiation field in approximately 30–40% of patients (Nestle et al. 1999).

5.2.5.3 Mediastinal Lymph Node Staging

Accurate mediastinal staging is essential for the therapy management of patients with NSCLC. Patients with ipsilateral mediastinal lymph node metastases (N2 disease) are considered to have potentially resectable disease (Fig. 5.13). In the case of ipsilateral bulky mediastinal metastases or contralateral mediastinal lymph node metastases (N3 disease), surgery is generally not indicated. CT and MRI have substantial limitations in depicting mediastinal lymph node metastases. Normal sized lymph nodes may prove to have metastases upon histologic examination, and nodal enlargement can be due to reactive hyperplasia or other nonmalignant conditions. The sensitivity and specificity of determining lymph node metastases for non-small cell lung cancer by CT is 60–70% (Webb et al. 1991; McLoud et al. 1992). Thus, in 30–40% of cases, CT scanning will erroneously suggest the presence of mediastinal lymph node metastases and will miss lymph node metastases in 30–40% of cases.

Multiple studies have demonstrated that FDG PET is significantly more accurate than CT in the determination of nodal status (Steinert et al. 1997; Vansteenkiste et al. 1998; Pieterman et al. 2000). With modern PET even small lesions (<1 cm) with an increased FDG accumulation can be detected. This represents a critical advantage of PET over CT and MRI. Several meta-analyses comparing PET and CT in the mediastinal staging of NSCLC have been performed. Dwamena et al. (1999) calculated a mean sensitivity and specificity of 0.79 and 0.91, respectively, for PET, and 0.60 and 0.77, respectively, for CT. These results were confirmed in another meta-analysis including more than 1,000 patients (Hellwig et al. 2001).

However, inflammatory mediastinal lymph nodes which accumulate FDG may occur and lead to false positive results. Thus, histopathological correlation of FDG accumulating mediastinal lymph nodes is recommended. With the information of PET and PET/CT, the surgeon is guided to the suspicious lymph node. The site of lymph node metastases should be recorded according to the lymph node station-mapping system of the American Thoracic Society (Mountain and Dresler 1997).

In our experience, integrated PET/CT imaging will become the new standard of mediastinal staging. Still, microscopic foci of metastases within normal sized lymph nodes cannot be detected with any imaging modality. It has to be recognized that FDG PET or PET/CT up to 4 weeks after induction therapy is less accurate in mediastinal staging than in staging of untreated NSCLC due to inflammatory lymph nodes or microscopic nodal tumor involvement (Akhurst et al. 2002). For restaging after chemotherapy, PET or PRT/CT imaging should be performed after an interval of 4–8 weeks.

5.2.5.4 Staging of Distant Metastases

Whole-body PET or PET/CT is an excellent method to screen for extrathoracic metastases (Fig. 5.14). Our group has shown that in 15% of patients with NSCLC whole-body PET or PET/CT detects previously unknown and unsuspected extrathoracic metastases (Weder et al. 1998). In a meta-analysis of 581 patients, sensitivity, specificity, and accuracy of FDG PET were 94%, 97% and 96%, respectively (Hellwig et al. 2001). Due to the detection of unknown metastases, PET and PET/CT changes therapeutic management in about 20% of patients. The most common sites of distant metastases are the liver, adrenal glands, bone, and the brain. With the exception of the brain, PET or PET/CT is more accurate than current imaging modalities for accurate M staging of patients (Erasmus et al. 1997; Marom et al. 1999).

However, FDG is not tumor specific but is also taken up in lymphoid tissue or inflammatory cells (Fig. 5.15). Recently, our group analyzed 350 PET/CT examinations in patients with NSCLC for single extrapulmonary lesions (Lardinois et al. 2005). In 72 patients (21%), a solitary extrapulmonary lesion with an increased FDG accumulation was found. Histopathological confirmation was performed in 69 of these patients; 50% of the lesions represented metastases of NSCLC,

25% of lesions were unknown secondary cancer, and 25% of lesions were benign as acute fracture, colon adenoma or Warthin's tumor.

It is well known that active muscles accumulate FDG. In some patients with lung cancer an intense focal FDG accumulation is seen in the lower anterior neck just lateral to the midline. Co-registered PET/CT images revealed that this focal FDG uptake is frequently localized in the internal laryngeal muscles (Kamel et al. 2002). This finding is a result of compensatory laryngeal muscle activation caused by contralateral recurrent laryngeal nerve palsy due to direct nerve invasion by lung cancer of the left mediastinum or lung apices. The knowledge of this finding is important to avoid false positive PET results.

5.2.5.5 Recurrent Lung Cancer

Despite radical therapy, the overall 5-year survival rate for patients with NSCLC remains low. Progression of disease may occur as intrathoracic recurrence or metastases. The differentiation of recurrent lung cancer and post-therapeutic changes remains a problem for radiological imaging. Thus, some patients may undergo a biopsy to determine tumor viability, although invasive procedures including transthoracic needle biopsy and open lung biopsy carry associated risks. Furthermore, due to sampling errors, these procedures do not always provide a definitive answer. A high accuracy of FDG PET or PET/CT in distinguishing recurrent disease from benign treatment effects has been reported (Patz et al. 1994; Inoue et al. 1995; Hicks et al. 2001; Keidar et al. 2004). PET/CT is helpful in selecting biopsy sites to confirm recurrent disease. Patients should be evaluated a minimum of 2 months after completion of therapy. Otherwise post-therapeutic healing processes or radiation pneumonitis may result in false positive FDG findings. These abnormal findings return to normal at variable times without further intervention.

5.2.5.6 Therapy Monitoring

The early prediction of tumor response is of much interest in patients with advanced NSCLC. Tumor progression during first-line chemotherapy occurs in approximately one-third of the patients. Thus a significant percentage of patients undergo several weeks of toxic and costly therapy without benefit. It has been shown that effective chemotherapy causes a rapid reduction of the SUV in the primary tumor during the course of therapy (Weber et al. 2003). In patients without metabolic response, the drug regimen may be changed to second-line therapy, thereby reducing the morbidity and costs from ineffective therapy. PET has also been evaluated to assess the response after radiation treatment in patients with NSCLC (MacManus et al. 2003). In this study, PET scans were performed at a median of 70 days after completion of radiation treatment. PET imaging allowed differentiation of viable tumor or fibrotic tissue. PET response was significantly associated with survival duration. PET and PET/CT may have a wide application in measuring treatment response in patients with NSCLC. Because prognostic information can be obtained at an early time point, therapies could be modified depending on the PET response.

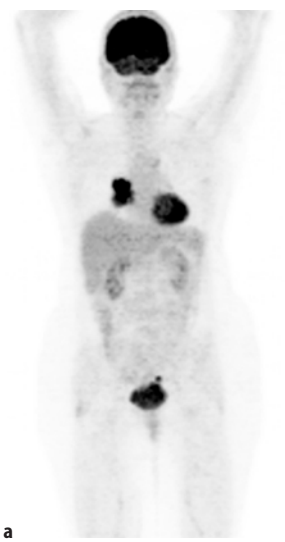

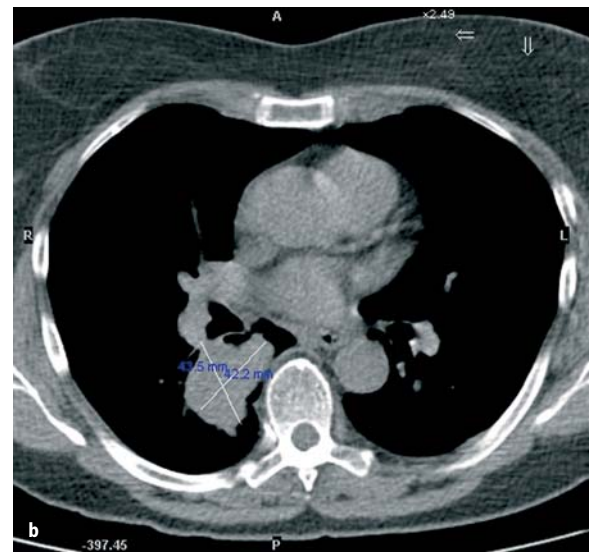

Fig. 5.15a–g. A 57-year-old woman with a lung cancer in the right lower lobe. **a** Maximum intensity projection (MIP) PET scan; **b, e** axial unenhanced low-dose CT scans; **c, f** axial CT-attenuation corrected PET scans; and **d, g** axial co-registered PET/CT scans. PET/CT demonstrated the lung cancer in the apical right lower lobe. No mediastinal metastases were found. In the sigmoid, cranial to the bladder, a lesion with an increased FDG accumulation was found. A colonoscopy and histologic correlation of the lesion was performed. The finding represented a benign colon adenoma. The patient was referred to surgery of the lung cancer

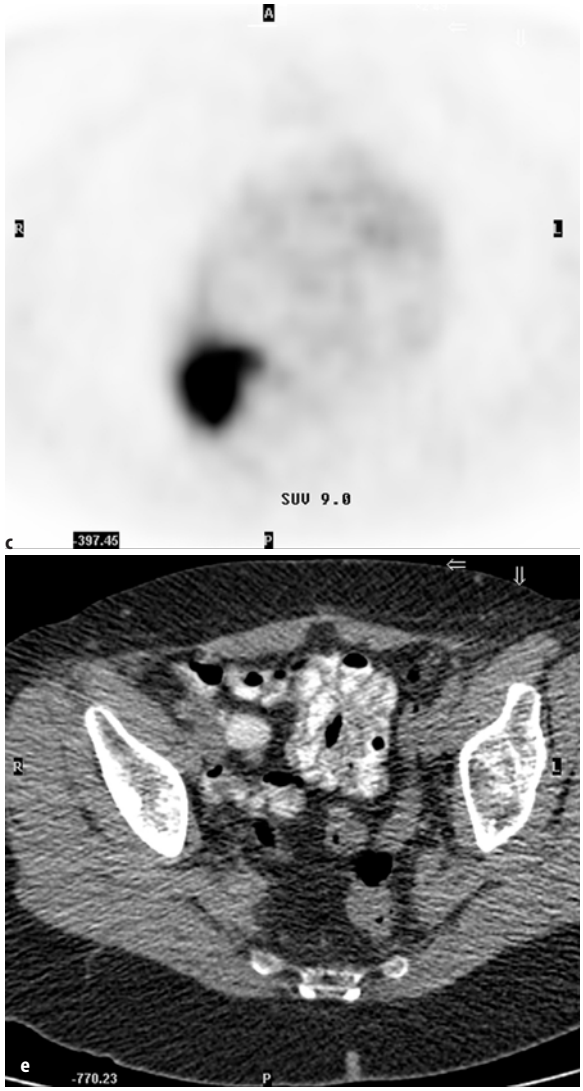

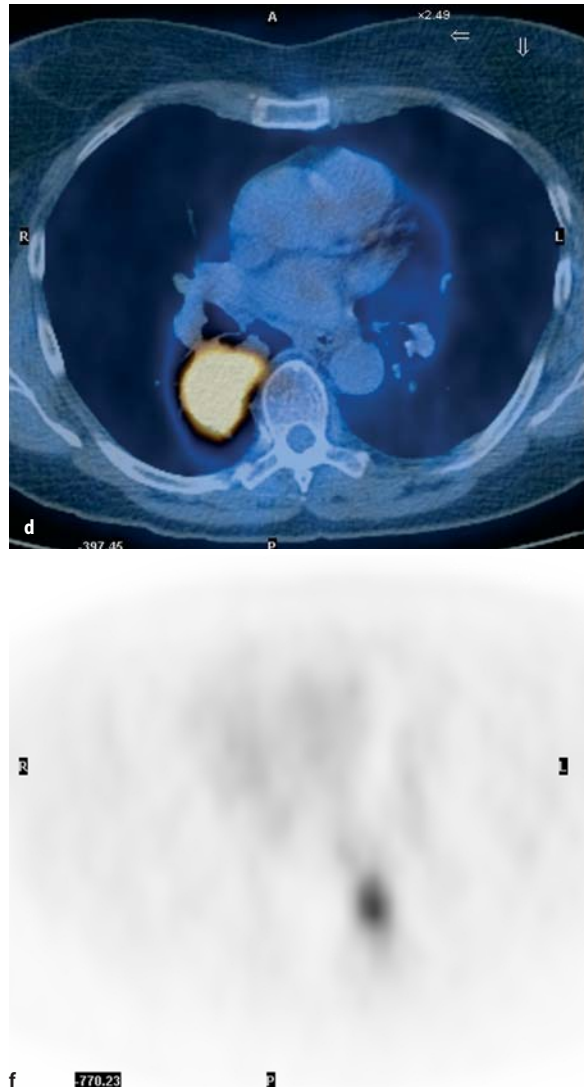

Fig. 5.15c–g

5.2.6 Small Cell Lung Cancer

Small cell lung cancer (SCLC) is the most aggressive lung cancer. SCLC is characterized by rapid growth and early metastases, which are present in 60 – 80 % of cases at the time of diagnosis. The staging procedures for SCLC do not differ from those for NSCLC. The primary role for imaging is to separate accurately limited disease (LD) from extended disease (ED). In patients with disease confined to the thorax, radiation treatment will be performed. Patients with extended disease are managed with chemotherapy. Integrated PET/CT imaging is an accurate method for the assessment of the total tumor extent and plays an important role in the planning of radiation treatment (Kamel et al. 2003). It is useful for accurate target definition by reducing the probability of overlooking involved areas. FDG PET is superior to conventional staging in the detection of all involved

sites, and particularly in the assessment of mediastinal lymph node metastases.

5.2.7 Malignant Pleural Mesothelioma

Malignant pleural mesothelioma (MPM) is the most common neoplasm of the pleura and directly linked to asbestos exposure. MPM usually develops at least 20 – 30 years after asbestos exposure. Imaging is particularly helpful in preoperative staging of MPM. Similarly to lung cancer, excellent FDG uptake in malignant pleural mesothelioma (MPM) has been previously described (Schneider et al. 2000). Our first experience suggests that PET/CT imaging is a promising method for MPM, as the extent of the tumor can be precisely defined. Integrated PET/CT imaging is helpful in identifying the optimal biopsy site, thereby increasing the diagnostic accuracy of the histological examination.

References

Akhurst T, Downey RJ, Ginsberg MS, et al. (2002) An initial experience with FDG-PET in the imaging of residual disease after induction therapy for lung cancer. Ann Thorac Surg 73:259 – 266

Antoch G, Stattaus J, Nemat AT, et al. (2003) Non-small cell lung cancer: dual modality PET/CT in preoperative staging. Radiology 229:526 – 533

Dwamena BA, Sonnad SS, Angobaldo JO, Wahl RL (1999) Metastases from non-small cell lung cancer: mediastinal staging in the 1990s – meta-analytic comparison of PET and CT. Radiology 213:530 – 536

Erasmus JJ, Patz EF, McAdams HP, et al. (1997) Evaluation of adrenal masses in patients with bronchogenic carcinoma using 18F-fluorodeoxyglucose positron emission tomography. AJR 168:1357 – 1362

Erasmus JF, Connolly JE, McAdams HP (2000) Solitary pulmonary nodules: Part 1. Morphologic evaluation for differentiation of benign and malignant lesions. Radiographics 20: 43 – 58

Gould MK, Maclean, CC, Kuschner WG, et al. (2001) Accuracy of positron emission tomography for diagnosis of pulmonary nodules and mass lesions: a meta-analysis. JAMA 285: 914 – 924

Hellwig D, Ukena D, Paulsen F, et al. (2001) Meta-analysis of the efficacy of positron emission tomography with F-18-fluorodeoxyglucose in lung tumors. Pneumologie 55: 367 – 377

Hicks RJ, Kalff V, MacManus MP, et al. (2001) The utility of 18F-FDG PET for suspected recurrent non-small cell lung cancer after potentially curative therapy: impact on management and prognostic stratification. J Nucl Med 42:1605 – 1613

Higashi K, Ueda Y, Seki H, et al. (1998) Fluorine-18-FDG PET imaging is negative in bronchoalveolar lung carcinoma. J Nucl Med 39:1016 – 1020

Inoue T, Kim E, Komaki R, et al. (1995) Detecting recurrent or residual lung cancer with FDG-PET. J Nucl Med 36: 788 – 793

Kamel E, Goerres GW, Burger C, von Schulthess GK, Steinert HC (2002) Detection of recurrent laryngeal nerve palsy in patients with lung cancer using PET-CT image fusion. Radiology 224:153 – 156

Kamel EM, Zwahlen D, Wyss MT, et al. (2003) Whole-body (18)F-FDG PET improves the management of patients with small cell lung cancer. J Nucl Med 44:1911 – 1917

Keidar Z, Haim N, Guralnik L, et al. (2004) PET/CT using 18F-FDG in suspected lung cancer recurrence: diagnostic value and impact on patient management. J Nucl Med 45:1640 – 1646

Lardinois D, Weder W, Hany TF, et al. (2003) Staging of non-small-cell lung cancer with integrated positron-emission tomography and computed tomography. N Engl J Med 348: 2500 – 2507

Lardinois D, Weder W, Roudas M, et al. (2005) Etiology of solitary extrapulmonary positron emission tomography and computed tomography findings in patients with lung cancer. J Clin Oncol 23:6846 – 6853

MacManus MP, Hicks RJ, Matthews JP, et al. (2003) Positron emission tomography is superior to computed tomography for response-assessment after radical radiotherapy or chemoradiotherapy in patients with non-small cell lung cancer. J Clin Oncol 21:1285 – 1292

Marom EM, McAdams HP, Erasmus JJ (1999) Staging non-small cell lung cancer with whole-body PET. Radiology 212:803 – 809

McLoud TC, Bourgouin PM, Greenberg RW, et al. (1992) Bronchogenic carcinoma: Analysis of staging in the mediastinum with CT by correlative lymph node mapping and sampling. Radiology 182:319 – 32

Mountain CF, Dresler CM (1997) Regional lymph node classification for lung cancer staging. Chest 11:1718 – 1723

Nestle U, Walter K, Schmidt S, Licht N, et al. (1999) 18F-deoxyglucose positron emission tomography (FDG-PET) for the planning of radiotherapy in lung cancer: high impact in patients with atelectasis. Int J Radiat Oncol Biol Phys 44: 593 – 597

Patz EF, Lowe VJ, Hoffman JM, et al. (1994) Persistent or recurrent bronchogenic carcinoma: detection with PET and 2-[F-18]-2-deoxy-D-glucose. Radiology 191:379 – 382

Pieterman RM, van Putten JWG, Meuzelaar JJ, et al. (2000) Preoperative staging of non-small-cell lung cancer with positron-emission tomography. N Engl J Med 343:254 – 261

Schneider DB, Clary-Macy C, Challa S, et al. (2000) Positron emission tomography with F18-fluorodeoxyglucose in the staging and preoperative evaluation of malignant pleural MPM. J Thorac Cardiovasc Surg 120:128 – 133

Shim SS, Lee KS, Kim BT, et al. (2005) Non-small cell lung cancer: prospective comparison of integrated FDG PET/CT and CT alone for preoperative staging. Radiology 236:1001 – 1019

Steinert HC, Hauser M, Allemann F, et al. (1997) Non-small cell lung cancer: nodal staging with FDG PET versus CT with correlative lymph node mapping and sampling. Radiology 202:441 – 446

Vansteenkiste JF, Stroobants SG, De Leyn PR, et al. (1998) Lymph node staging in non-small cell lung cancer with FDG PET scan: a prospective study on 690 lymph node stations from 68 patients. J Clin Oncol 16:2142 – 2149

Webb WR, Gatsonis C, Zerhouni E, et al. (1991) CT and MR imaging in staging non-small cell bronchogenic carcinoma: Report of the Radiology Diagnostic Oncology Group. Radiology 178:705 – 713

Weber WA, Peterson V, Schmidt B, et al. (2003) Positron emission tomography in non-small cell lung cancer: prediction

of response to chemotherapy by quantitative assessment to glucose use. J Clin Oncol 21:2651 – 2657
Weder W, Schmid R, Bruchhaus H, Hillinger S, von Schulthess GK, Steinert HC (1998) Detection of extrathoracic metastases by positron emission tomography in lung cancer. Ann Thorac Surg 66:886 – 893
Yap CS, Schiepers C, Fishbein MC, et al. (2002) FDG-PET imaging in lung cancer: how sensitive is it for bronchioloalveolar carcinoma? Eur J Nucl Med Mol Imaging 29:1166 – 1173

Liver, Spleen and Biliary Tree

6

L.S. Zuckier, L.M. Freeman

6.1 Brief Introduction and Historical Perspective

Nuclear medicine occupies a unique niche amongst various imaging modalities by virtue of its ability to evaluate functional and physiologic parameters in a non-invasive and quantitative manner. Although at one time scintigraphic studies were used as primary modalities to address anatomic questions, these tasks are currently performed by the higher-resolution modalities ultrasound (US), computed tomography (CT), and magnetic resonance (MR) imaging. In current practice, nuclear medicine retains a more limited though unique role in the functional and physiologic characterization of tissue (Zuckier and Freeman 2003).

Within the solid gastrointestinal (GI) tract, colloid imaging of the liver visualizes the distribution of reticuloendothelial (RE) system cells which phagocytize intravascular particulate material from the blood while hepatobiliary scintigraphy evaluates the uptake and excretion of bile by hepatocytes. Specific radiopharmaceuticals such as ^{18}F-FDG, ^{123}I- or ^{131}I-MIBG, ^{67}Ga-gallium citrate and ^{111}In-Octreotide are used to evaluate metabolic and receptor characteristics of tissues relevant to various pathological processes that affect the liver and spleen. Radiolabeled red blood cells (RBCs) are used to quantitate the blood flow and intravascular blood pool within the liver, thereby confirming the diagnosis of intrahepatic hemangioma. These applications summarized in Table 6.1 will be featured in the chapter below.

6.2 Biliary Excretion

The initial indication for biliary scintigraphy, to evaluate the etiology of acute right upper quadrant pain, remains current today. A second and expanding indication for this technique is the non-invasive evaluation of bile flow to assess extravasation or obstruction in the post-surgical and post-traumatic patient.

Table 6.1. Physiological correlates of radiopharmaceutical behavior in the liver

Radiopharmaceutical	Parameter	Physiologic correlate
^{99m}Tc-SC	Uptake	Kupffer cell function
^{99m}Tc-HIDA	Uptake	Hepatocyte function
^{99m}Tc-HIDA	Liver washout	Presence of biliary radicals
^{99m}Tc-RBC	Visualization on flow images	Hepatic artery supply
^{99m}Tc-RBC	Visualization on delayed images	Intravascular volume
^{133}Xe gas	Uptake	Lipid solubility
^{67}Ga citrate	Uptake	Transferrin binding
^{111}In-Octreoscan	Uptake	Somatostatin (sstr2) receptor
^{18}F-FDG	Uptake	Glucose (Glut) transporter
^{123}I- or ^{131}I-MIBG	Uptake	Catecholamine-producing cells

6.2.1 Radiopharmaceuticals

Attributes of an ideal radiopharmaceutical for evaluation of bile flow include labeling with a radionuclide of favorable imaging and dosimetry characteristics, rapid liver extraction and transit into the biliary system, little or no absorption from the intestine, and minimal renal excretion (Wistow et al. 1977). ^{99m}Tc-labeled iminodiacetic acid (IDA) derivatives approach these ideal criteria. Typically 185 MBq (5 mCi) of the DISIDA (2, 6-diisopropylacetanilido-iminodiacetic acid) or BRIDA (bromo-2, 4, 6-trimethylacetanilido-iminodiacetic acid) analogues are used for biliary scintigraphy; the latter has an advantage of superior liver extraction and is therefore favored in patients with more severe hepatic dysfunction. While the IDA analogues generally resemble bilirubin in their uptake and excretion, they are not conjugated as is bilirubin.

6.2.2 Methodology (Balon et al. 2001)

Clinical information of relevance prior to a hepatobiliary study includes history of previous surgeries, recent bilirubin and liver enzyme levels, and current medications, with special attention to opioids which increase the sphincter of Oddi tone and thereby alter biliary kinetics. Time of most recent food ingestion is also important as eating profoundly alters the pattern of gallbladder (GB) filling.

For evaluation of right-upper quadrant pain, patients are generally imaged after a 2- or preferably 4-h period of fasting, designed to avoid post-prandial contraction of the GB. Patients who are on total parenteral nutrition or have not eaten for over 24 h may have tumefactive bile ("sludge") in the GB which also impedes GB filling. In this situation, a 3–5 min IV injection of 10–20 ng/kg of sincalide (CCK-8, the terminal octapeptide of cholecystokinin) may be administered approximately 1/2–1 h prior to radiopharmaceutical (Table 6.2). This serves to contract and empty the GB, allowing for subsequent filling with IDA.

Radiopharmaceutical is injected intravenously, and anterior images over the liver and upper abdomen are obtained at intervals of 5 min or less using a large-field-of-view gamma-camera. Wherever possible, continuous computer acquisition, at approximately 1 frame per minute, is obtained for subsequent presentation of the data in cine mode. In traditional protocols, imaging is continued for up to 4 h post-injection, until the bowel and GB are visualized or no significant activity remains within the liver (Fig. 6.1). On rare occasions, such as when hepatic uptake is impaired, delayed imaging, up to 24 h, may be helpful.

Rather than continuing the study through 4 h, an alternate accelerated method of biliary scintigraphy can

Drug	Dose, route	Mechanism	Use
Cholecystokinin-8	10–20 ng/kg/3 min, IV	Stimulates contraction of the GB and relaxes sphincter of Oddi	1. Evacuation of sludge from GB prior to study 2. Evaluation of percent GB emptying post-stimulus (ejection fraction)
Morphine sulfate	40–100 µg/kg slowly over 2–3 min, IV	Constricts sphincter of Oddi	Divert IDA from CBD into GB, thereby reducing period of biliary scintigraphy
Phenobarbital	5 mg/kg daily in two divided doses × 5 days, PO	Induces hepatic enzymes	Used to promote liver excretion of IDA in differentiation of neonatal hepatitis from biliary atresia

Table 6.2. Pharmacologic interventions in biliary scintigraphy (after Saremi et al. 2002)

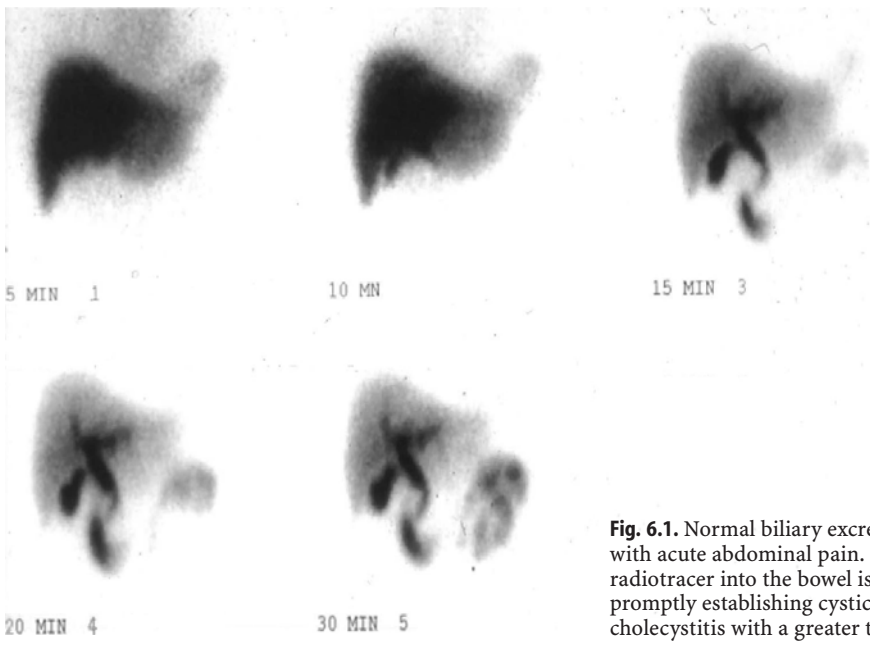

Fig. 6.1. Normal biliary excretion study in a 43 year old man with acute abdominal pain. Prompt uptake and excretion of radiotracer into the bowel is noted. The gall bladder also fills promptly establishing cystic duct patency ruling out acute cholecystitis with a greater than 90% accuracy

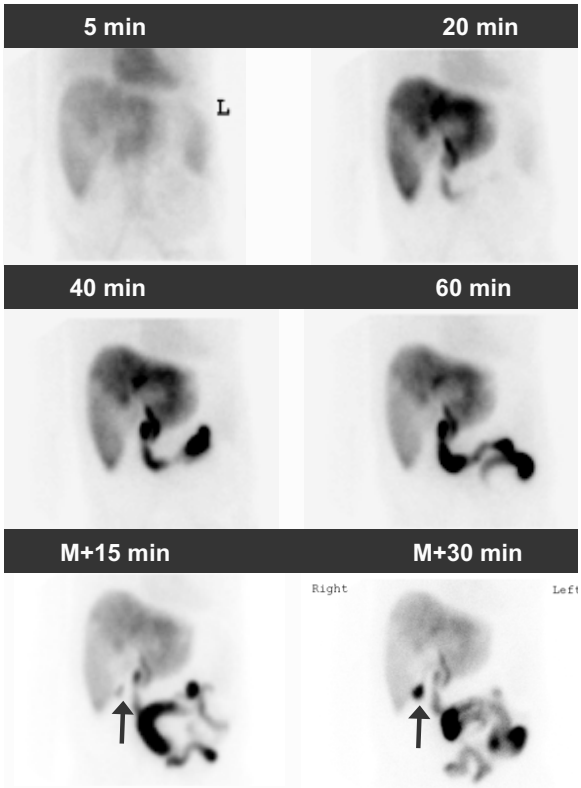

Fig. 6.2. Morphine augmented cholescintigraphy in a 53-year-old male with history of gallstones and right upper quadrant pain. Imaging through 1 h demonstrated prolonged cardiac blood pool activity and slightly inhomogeneous uptake within the liver, consistent with a known history of liver dysfunction. Increasing activity is noted in the bowel between 20 min and 1 h. At this juncture, 2 mg of morphine sulfate was administered intravenously and additional images were obtained, demonstrating filling of the GB (*arrows*). These findings indicate chronic cholecystitis

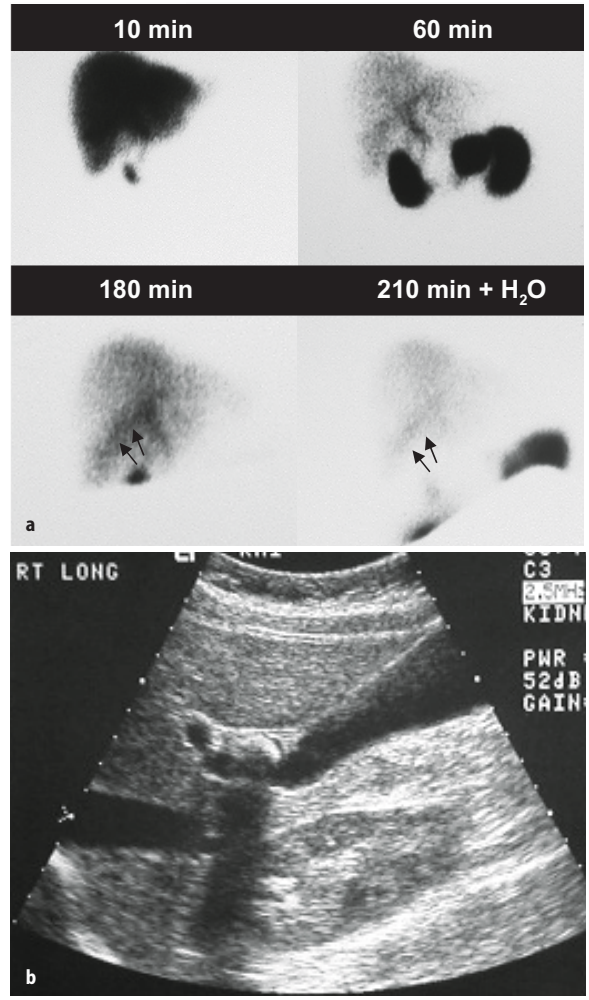

Fig. 6.3. Acute cholecystitis in a 27-year-old woman who presented with right upper quadrant pain. Biliary excretion study (**a**) reveals prompt uptake by the liver and rapid excretion into the small bowel with no visualization of the GB through 3½ h. Of note, there is a suggestion of a faint "stripe" of activity in the region of the GB fossa (*arrows*), suggesting acute gangrenous cholecystitis. To eliminate the confounding possibility of duodenal activity adjacent to the GB fossa, water was given to the patient following the 3-h view. Additionally, the bowel is shielded by a lead cape on the 3½-h view. Ultrasound study (**b**) demonstrates stones in the region of the neck of the GB. (Reprinted from Zuckier and Freeman 2003 with permission)

be performed if by 1 h activity is noted within the duodenum but no GB is evident. A quantity of 0.04 – 0.1 mg/kg of morphine sulfate (Table 6.2) is administered intravenously over 2 – 3 min. This serves to constrict the sphincter of Oddi, thereby shunting bile into the GB (Fig. 6.2). Imaging is terminated 30 min following morphine administration, which is functionally equivalent to continuing through the standard 4-h period.

At times it may be difficult to ascertain if a collection of activity medially placed in the right upper quadrant is related to bowel or in fact is contained within the GB. In addition to obtaining oblique views which may be helpful, patients can be imaged following ingestion of a small amount of water. This serves to wash out the activity within the duodenum but would not affect activity in the GB (Fig. 6.3).

6.2.3 Clinical Indications and Interpretation

In the normal patient, hepatic uptake of a ^{99m}Tc-labeled iminodiacetic acid derivative is prompt, with observable blood-pool activity in the heart clearing by 5 min post-injection. There is likewise rapid excretion of radiopharmaceutical by the liver, through the biliary tree, and into the duodenum and GB, both of which visualize within the first hour (Fig. 6.1). Transient reflux of activity into the stomach may be seen and a small amount of

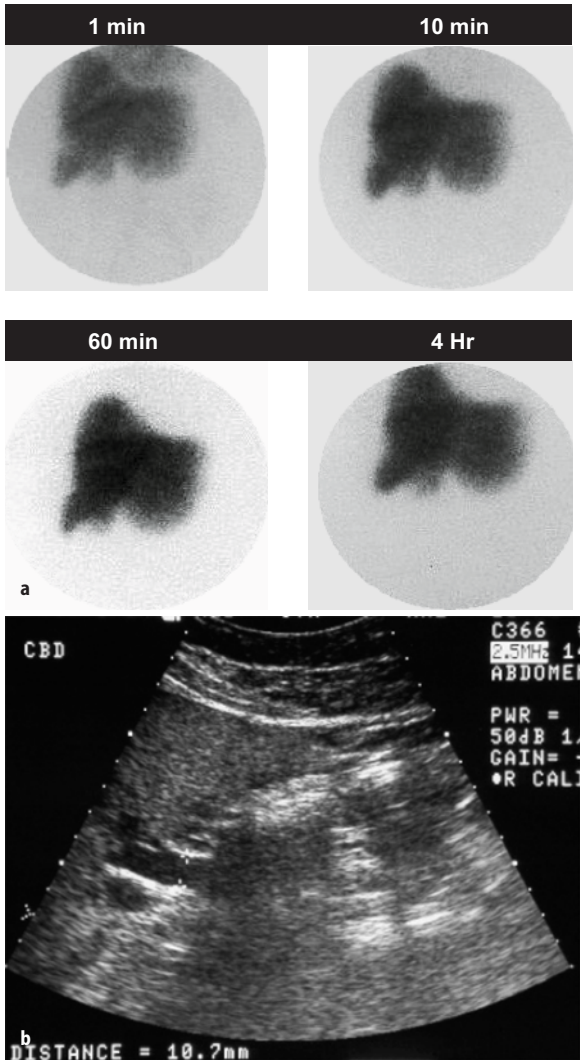

Fig. 6.4. Common bile duct obstruction in a woman who presented with right upper quadrant pain and with suspicion of acute cholecystitis. A fixed "hepatogram" pattern is present through 4 h (**a**), consistent with the diagnosis of CBD obstruction. Correlative ultrasound performed the following day (**b**) demonstrates mild dilation of the CBD to a diameter of 10.7 mm. (Reprinted from Zuckier and Freeman 2003 with permission)

activity is frequently noted in the urinary tract. Over time, activity proceeds distally into the small and large bowel while the liver activity diminishes to background levels. Criteria of evaluation include the rate of uptake and excretion of the radiotracer by the liver, the timing of visualization of the bowel and GB, and the appearance of abnormal collections of activity within the abdomen. Deviations from the norm are associated with various disease states, as described below.

6.2.3.1 Disorders of Hepatic Uptake and Excretion into Bowel

Uptake by the liver may be impaired, evidenced by slow clearance of the blood pool, and increased vicarious excretion of radiotracer by the kidneys. This abnormality may be primary, due to parenchymal disease such as hepatitis, or secondary, due to obstruction at the level of the common hepatic or common bile duct (CBD). At times it may be difficult to distinguish between intrinsic hepatic disease and obstruction as in both cases activity is retained in the liver and does not proceed distally into the bowel (Fig. 6.4).

In hepatitis, impairment of hepatic uptake and excretion is variable. In mild dysfunction, decreased liver extraction may be evidenced by prolongation of blood pool activity (typically beyond 5 min) and an increase in vicarious excretion by the kidneys. In patients with severe dysfunction, liver uptake may be diminished to the point where the liver is poorly defined, and no biliary excretion is noted. Generally, performance of hepatobiliary studies in patients with total bilirubin above 15 to 20 mg/dl is of little value in that insufficient activity will be excreted into the biliary tree to yield information regarding its patency. Instances where uptake of radiopharmaceutical by the liver is relatively preserved in contrast to severely decreased hepatic excretion may be rarely seen as an idiosyncratic reaction to medications such as isoniazid and halothane. This unusual combination is termed "intrahepatic cholestasis" and can be confusing in that it simulates relatively acute high-grade obstruction of the biliary tree.

In very early mechanical obstruction of the biliary tree, liver uptake and excretion remain intact, and excreted activity within the dilated biliary tree may be observed to the level of obstruction. As high-grade obstruction of the biliary tree progresses over hours to days from acute to subacute and chronic, liver uptake and excretion of radiopharmaceutical become increasingly impaired to the point where no activity is observed in the bile ducts, which can even appear as linear photon deficiencies. With prolonged obstruction, the degree of hepatic dysfunction becomes profound, no activity is excreted into the ducts, and it is impossible to differentiate mechanical obstruction from hepatitis.

When partial CBD obstruction is present, ductal prominence and stasis as well as delayed biliary to bile transit may occur, with appearance of the bowel delayed beyond 60 min. This latter finding is non-specific and can be seen with a variety of intra-abdominal pathologies as well as following opioid administration or in patients administered CCK-8 prior to scintigraphy (Kim et al. 1990). Chronic cholecystitis may also be associated with this finding in some cases.

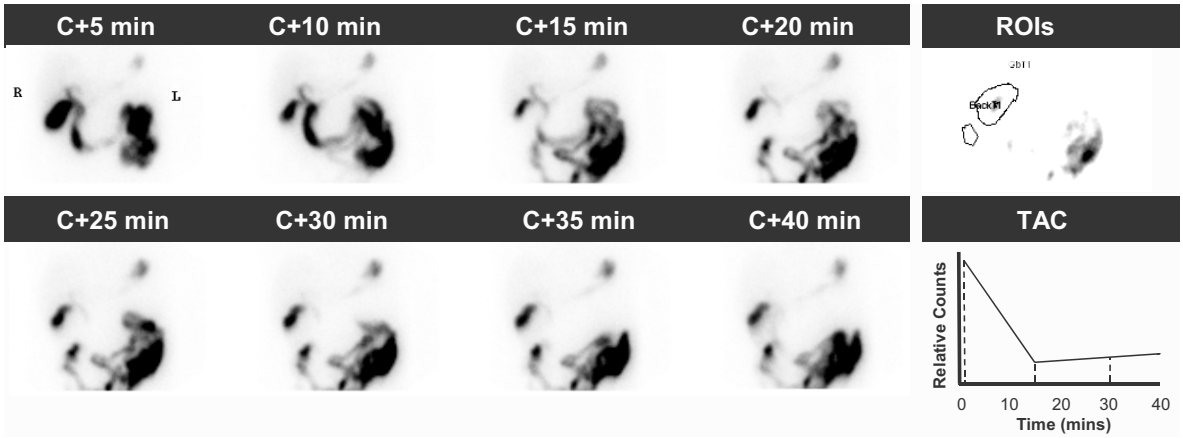

Fig. 6.5. Normal GB ejection fraction. Two micrograms of CCK-8 was administered at 1 h by slow infusion and images were obtained over 40 min. There is prompt and excellent emptying of the GB. Time-activity curve (*TAC*) demonstrates an ejection fraction of 85 %, which peaks at 12 min post-infusion

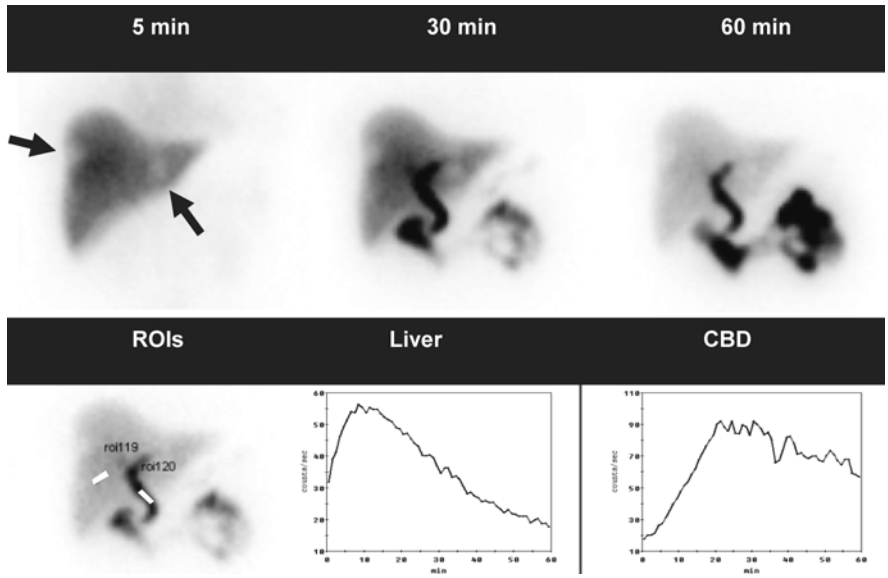

Fig. 6.6. Twenty-eight-year-old female with recurrent right-sided abdominal pain following cholecystectomy. Representative images at 5, 30 and 60 min are displayed (*top row*). Regions of interest (ROIs) were applied as per the method of Sostre (Sostre et al. 1992) in order to generate a quantitative score. TACs of indicated regions over the liver and common bile duct are displayed. For this patient, analysis does not support the diagnosis of sphincter of Oddi dysfunction. Incidentally noted are focal defects within the liver parenchyma due to two known hemangiomas (*arrows*)

6.2.3.2 Disorders of Gallbladder Visualization

The primary parameter evaluated on IDA scanning in patients with right upper quadrant pain and suspected cholecystitis is filling of the GB. Assuming sufficient radiotracer reaches the bowel, the GB normally fills between 10 min and 1 h post-injection of radiopharmaceutical. Delayed visualization, between 1 and 4 h, is most commonly ascribed to chronic cholecystitis. Complete non-visualization through 4 h in an acutely ill patient is both highly sensitive and specific for acute cholecystitis, reflecting cystic duct obstruction (Weissmann et al. 1979). This is usually caused by impaction of a stone in the cystic duct; however, acute acalculous cholecystitis will also cause non-visualization of the GB (Weissmann et al. 1983a). It should be cautioned that in the presence of CBD obstruction or severe hepatic dysfunction non-visualization of the GB is not diagnostic as there is insufficient flow of activity into the bowel to make any determination of cystic duct patency.

The morphine-enhanced IDA study, as discussed above, shortens the total examination time to 1.5 h instead of the 4 h needed to reliably differentiate acute from chronic cholecystitis. Filling of the GB within 30 min following morphine is analogous to delayed visualization on a 4-h study and suggests chronic cholecystitis (Fig. 6.2). If no filling of the GB occurs by 30 min post-administration, the cystic duct is demonstrated to be obstructed, consistent with the diagnosis of acute cholecystitis (Fink-Bennett et al. 1991; Kim et al. 1993).

An important finding, suggestive of complicated acute cholecystitis, is the "rim" or "stripe" sign which consists of a band of increased activity at the lower margin of the liver in the region of the GB fossa (Fig. 6.3). This finding is postulated as being due to adjacent cholestasis in inflamed regional hepatocytes, or to actual leakage from a GB perforation. When present, the rim sign has high specificity for complicated acute cholecystitis and is predictive of increased morbidity (Smith et al. 1985; Meekin et al. 1987).

6.2.3.3 Functional Disorders of the Gallbladder

In patients with biliary colic and biliary dyskinesia, routine standard biliary scintigraphy may be normal. In these cases, an additional provocative test may be necessary to confirm suspected pathology. In one such technique, radiopharmaceutical is administered and the GB is allowed to fill for 60 min. At this point, 10–20 ng/kg of CCK-8 is administered intravenously over a minimum of 3 min (Table 6.2) and GB emptying is monitored for 30 min using regions of interest and time-activity curves (Fig. 6.5). In normal patients, a decrease of activity within the GB of greater than 35–40% is observed, while in patients with biliary dyskinesia, the GB ejection fraction (EF) remains lower. In another variation of this technique, CCK-8 is infused over a more prolonged period of 30 min, designed to reduce nausea associated with more-rapid CCK-8 administration and to diminish false-positive results (Krishnamurthy and Krishnamurthy 1996). With slower CCK-8 infusion, GB EF normally exceeds 40%. In instances where CCK-8 has not been available, standardized fatty meals have been used to stimulate GB contraction (Krishnamurthy and Brown 2002; Ziessman et al. 2003). It must be remembered that physiologic quantitative studies are complicated, and must be interpreted within the entire clinical context including pharmacologic effects of other medications (Ziessman 1999).

Occasionally, right upper quadrant pain persists following cholecystectomy. In these circumstances, quantitative scintigraphy may be used to assess the physiologic transit of radiotracer from the liver to the bowel, thereby evaluating function of the sphincter of Oddi. Scoring systems have been proposed as a means of objectively and non-invasively predicting which patients would benefit from sphincterotomy (Fig. 6.6) (Sostre et al. 1992).

6.2.3.4 Post-operative and Post-traumatic Patients

Because of the ability to track bile flow, biliary scintigraphy is effective in monitoring extravasation of bile following surgery (Trerotola et al. 1992) or trauma (Zeman et al. 2006). Biliary scintigraphy is therefore used in symptomatic post-laparoscopic cholecystectomy patients, where reduced surgical exposure may lead to complications such as retained stones, transection, or ligation of the CBD (Estrada et al. 1991) (Fig. 6.7). Scintigraphy is useful in visualizing the expected flow of radiotracer from the liver into the bowel. Delayed images are helpful in facilitating visualization of extravasated activity and can portray loculated collections and free intraperitoneal leaks (Fig. 6.7), while decubitus views are used to demonstrate free flow of intraperitoneal activity.

Following trauma, collections may be observed on CT or US; however, their etiology may be unclear. Cholescintigraphy is a simple tool which helps define a collection in relationship to biliary excretion (Fig. 6.8). Flow of activity into a biloma is typically slow and visu-

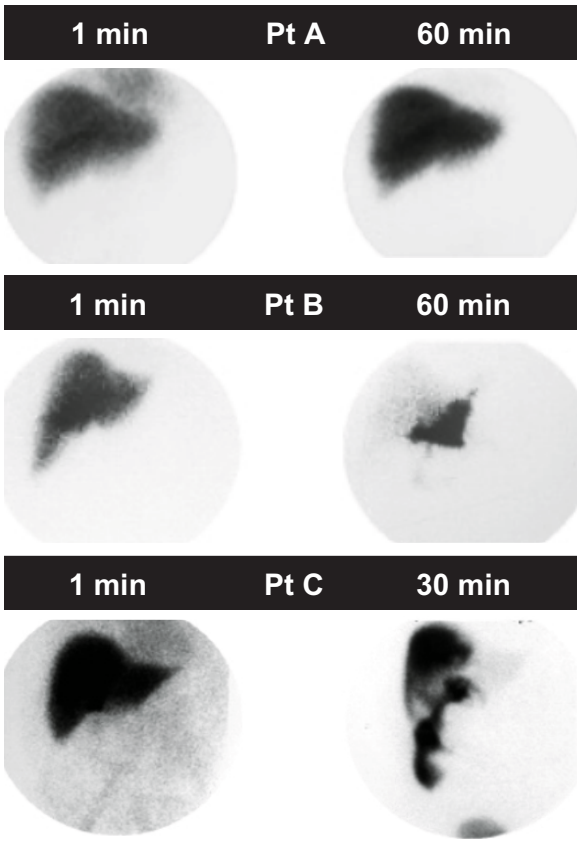

Fig. 6.7. Representative biliary scintigraphic images in three symptomatic post-laparoscopic cholecystectomy patients. Patient A is a 23-year-old female, 6 days post-procedure, who has increasing nausea, vomiting, and pain. A CBD obstructive pattern is noted. Patient B is a young female studied 10 days post-procedure. A relatively confined leak into the lesser sac is noted with negligible activity proceeding into the small bowel. Patient C also evidences a leak, which appears freely flowing down the right paracolic gutter. (Reprinted from Zuckier and Freeman 2003 with permission)

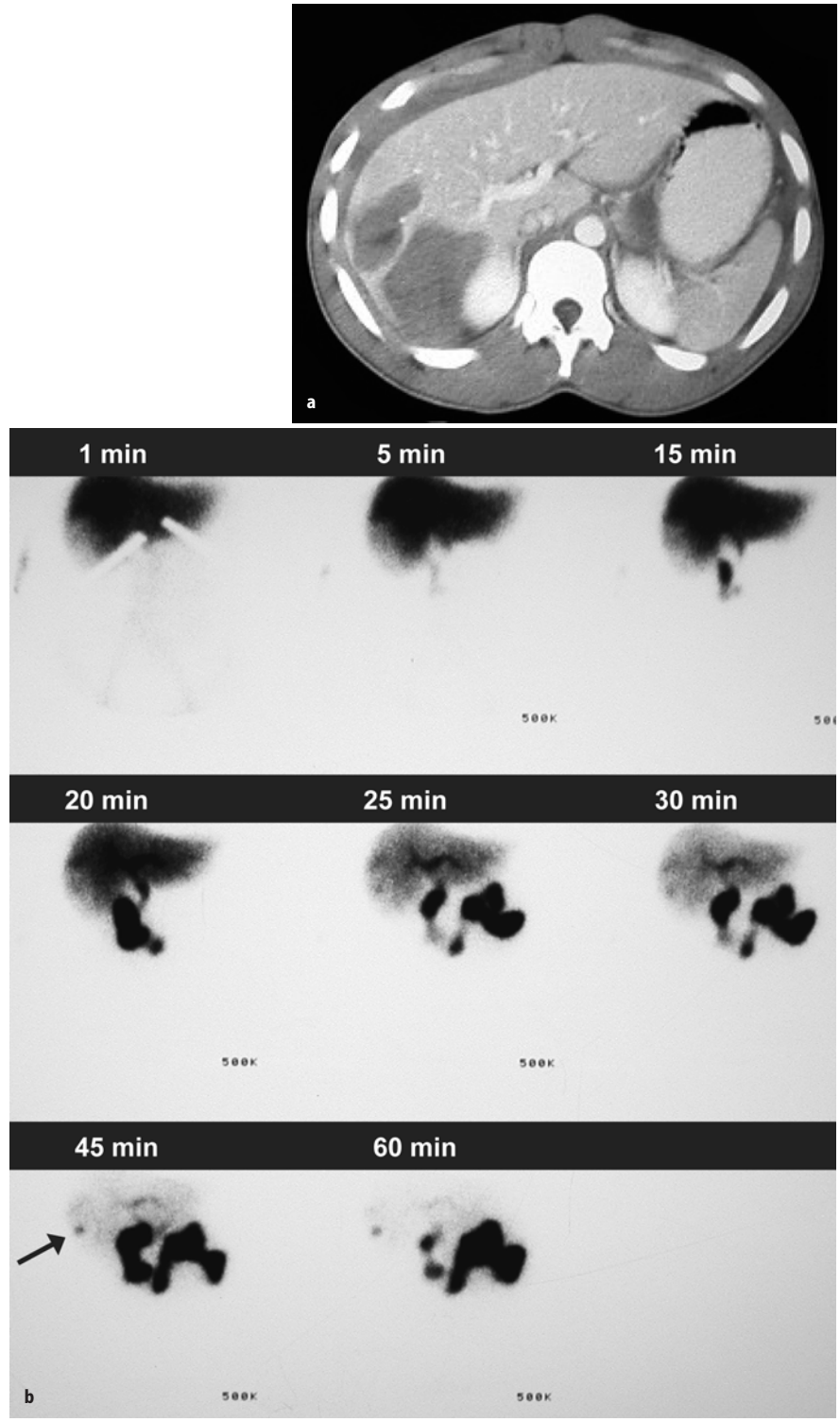

Fig. 6.8. Biloma following penetrating injury to the abdomen in an 18-year-old male who sustained a stab wound to his right flank. CT (**a**) demonstrates a large hemoperitoneum, laceration of the anterior and posterior segments of the right lobe of the liver, and a hematoma in Morrison's pouch. Biliary scintigraphy performed the following day (**b**) initially demonstrates presence of a photon-poor collection in the lateral aspect of the right lobe; however, over the hour course of imaging a small focus of bile extravasation within the region of the collection is noted (*arrow*). The majority of the bile is excreted into the small bowel. (Reprinted from Zuckier and Freeman 2003 with permission)

alization may only appear on delayed images following gradual accumulation of radiopharmaceutical within the collection and maximal wash-out of activity from the normal liver (Zuckier and Freeman 2003). Scintigraphy can be used to quantitate the degree of bile leak and thereby assess significance of injury (Weissmann et al. 1983b) (Fig. 6.9). If the majority of bile flow progresses through the biliary tree into the duodenum,

conservative management, rather than surgical repair, is usually attempted.

6.2.3.5 Biliary Atresia

A specialized use of biliary scintigraphy is in the differentiation of biliary atresia from neonatal hepatitis. Infants are typically prepared by pretreatment with 5 mg/kg/day of phenobarbital, given orally in two divided doses, over a minimum of 3 – 5 days, designed to induce hepatic enzymes and maximize excretion of radiopharmaceutical (Majd et al. 1981; Fink-Bennett 1991)

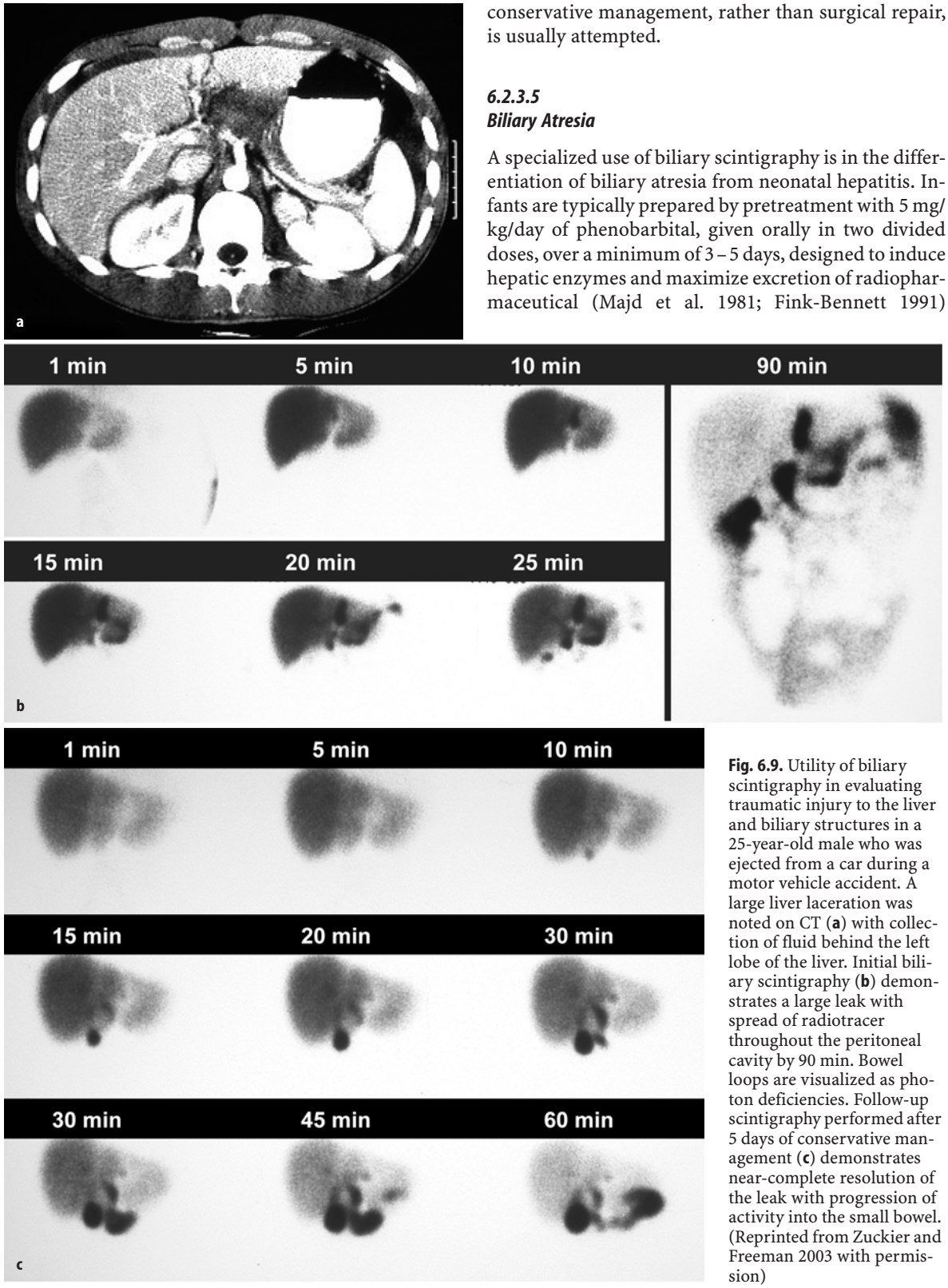

Fig. 6.9. Utility of biliary scintigraphy in evaluating traumatic injury to the liver and biliary structures in a 25-year-old male who was ejected from a car during a motor vehicle accident. A large liver laceration was noted on CT (**a**) with collection of fluid behind the left lobe of the liver. Initial biliary scintigraphy (**b**) demonstrates a large leak with spread of radiotracer throughout the peritoneal cavity by 90 min. Bowel loops are visualized as photon deficiencies. Follow-up scintigraphy performed after 5 days of conservative management (**c**) demonstrates near-complete resolution of the leak with progression of activity into the small bowel. (Reprinted from Zuckier and Freeman 2003 with permission)

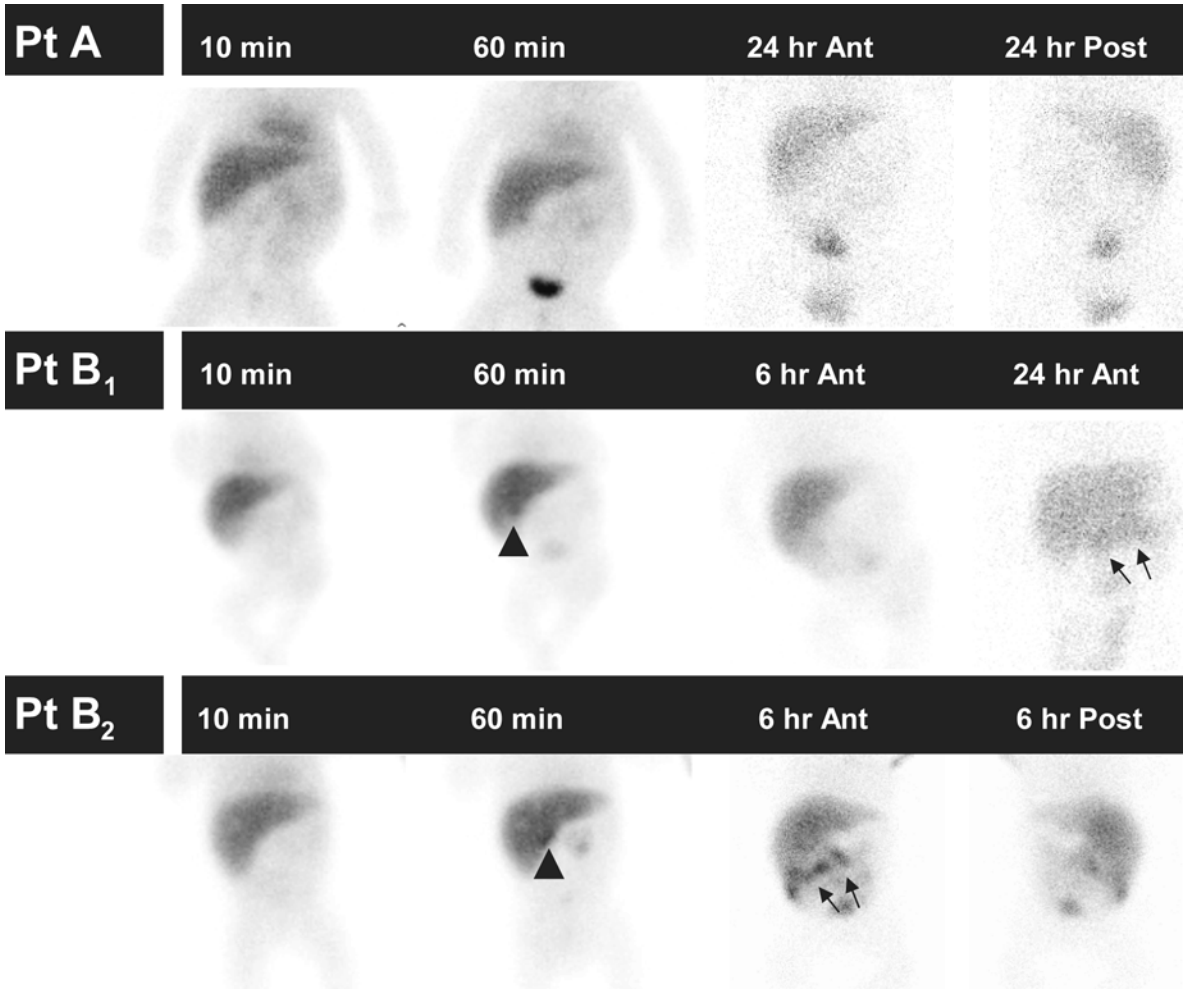

Fig. 6.10. Three separate studies performed on two infants to exclude biliary atresia. Patients were all administered phenobarbital prior to imaging in order to enhance excretion (see text and Table 6.2). Patient A: 4-month-old baby boy, delivered at a gestational age of 26 weeks, who presented with cholestatic jaundice. Persistent cardiac blood pool activity is noted up to 60 min of imaging, suggestive of hepatocellular dysfunction. Absence of gastrointestinal excretion of radiotracer in both early as well as 24-h delayed images is consistent with either biliary atresia or severe hepatocellular dysfunction. Activity within the kidneys, urinary system and diaper should not be confused with bowel excretion. Patient B is a 41-day-old baby girl who presented with increased bilirubin. Initial study (B_1) demonstrates relatively prompt uptake of radiotracer by the liver. The cardiac blood pool activity has cleared by 5 min. There is no evidence of radiotracer excretion into the GI system at the end of 1 h although the GB is faintly observed (*arrowhead*). Delayed images obtained at 6 h demonstrate vague activity into the intestine while further delayed images obtained at 24 h confirm gastrointestinal excretion (*arrows*). Biliary atresia can therefore be excluded. Study was repeated 6 weeks thereafter (B_2). At this juncture, the GB is better visualized on the 60-min image (*arrowhead*) and bowel excretion is clearly noted on 6-h delayed images (*arrows*). These findings exclude biliary atresia

(Table 6.2). For infants and children, 2–7 MBq/kg (0.05–0.2 mCi/kg) of radiopharmaceutical is typically administered with a minimum of 15–20 MBq (0.4–0.5 mCi) (Balon et al. 2001). BRIDA is preferred to DISIDA due to its higher liver extraction. Imaging begins immediately post-injection and extends intermittently through several hours. If no bowel activity is observed, patients return for delayed imaging through 24 h. Any activity noted within the bowel or GB indicates patency of the CBD and excludes the diagnosis of biliary atresia (Lee et al. 2000) (Fig. 6.10). When no bowel excretion is visualized, findings are ambiguous, as lack of excretion may be due to either severe neonatal hepatitis or biliary atresia. In this instance, liver biopsy will be necessary to establish the diagnosis.

6.2.3.6 Characterization of Liver Masses

Biliary scintigraphy can contribute to the characterization of liver lesions (Table 6.1). Uptake of hepatobiliary radiopharmaceutical indicates presence of functioning

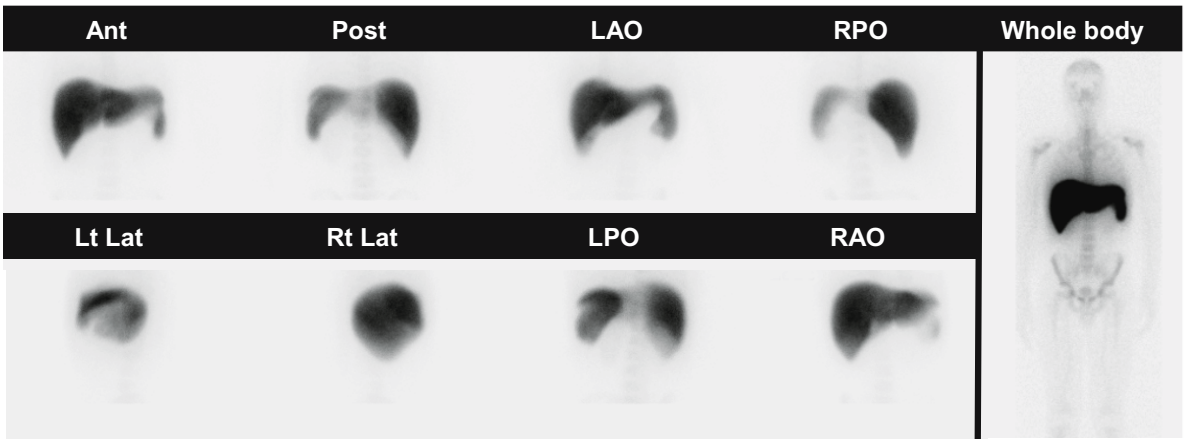

Fig. 6.11. Normal appearance of liver-spleen sulfur colloid scan in a 15-year-old boy. Standard planar views are shown in the *left panel*. Anterior whole-body view at increased intensity (*right panel*) illustrates the relative distribution of activity

hepatocytes and thereby excludes masses of non-hepatic origin. If within a mass of hepatic origin the biliary radicals are not well developed, excretion of activity will be impaired, evidenced by slow washout and persistent activity on delayed imaging. For this reason, hepatocellular carcinoma (HCC) typically is best seen on delayed imaging several hours post-injection due to the combination of relatively reduced initial uptake by the tumor but slow washout and retention (Lee et al. 1984; Hasegawa et al. 1986). In general, uptake within HCC correlates strongly with degree of tumor differentiation (Calvet et al. 1988). Slow washout of biliary radiopharmaceutical has also been noted in hepatic adenoma and FNH (Drane et al. 1987). In cases where aspiration biopsy is inconclusive in differentiating well-differentiated HCCs from cirrhotic reactive changes, some have suggested utility in using delayed IDA imaging to differentiate well-differentiated HCCs, which may retain radiopharmaceutical, from cirrhotic reactive changes, which should not (Lee et al. 1985; Hasegawa et al. 1986; Middleton 1996). Unfortunately, no such distinction can be made scintigraphically between hepatic adenomas and HCCs, both of which may retain radiopharmaceutical.

6.3 Reticuloendothelial System Imaging of the Liver and Spleen

6.3.1 Radiopharmaceuticals

The distribution of the RE system is visualized following intravenous administration of radiolabeled colloids. Particles of SC range in size from 100 nm to approximately 1 μm. In the average patient, 80–90% of injected SC is phagocytized by the RE cells of the liver (Kupffer cells), 5–10% by the spleen, and the remainder by the bone marrow (Chilton and Brown 1990) (Fig. 6.11). A quantity of 110–185 MBq (3–5 mCi) of ^{99m}Tc-sulfur colloid (SC) is injected intravenously for imaging of the liver; when imaging of the marrow is intended, the amount used is typically raised to 370 MBq (10 mCi) to compensate for its low marrow uptake. As a rule, smaller particles are preferentially taken up by marrow while larger particles are phagocytized by the spleen. When more-targeted imaging of the spleen is necessary (see Sect. 6.3.3.3), imaging can therefore be performed after injection of relatively large ^{99m}Tc-labeled heat-damaged RBCs, prepared by incubation of the labeled cells for 20 min in a waterbath at 49–50 °C (Royal et al. 2003).

6.3.2 Methodology (Royal et al. 2003)

Imaging of the liver and spleen commences approximately 10–15 min following SC injection. Planar views of the liver and spleen are taken in multiple obliquities (anterior, posterior, right lateral, right anterior oblique, right posterior oblique). An image which includes a lead marker of standardized size placed on the costal margin is usually obtained. The left anterior oblique view, helpful in separating the left lobe of the liver from the spleen, left posterior oblique and left lateral views are often added for imaging of the spleen. If ectopic splenic tissue is being evaluated, more extensive views of the entire abdomen, and possibly of the thorax as well (Yammine et al. 2003), should be obtained (Fig. 6.12). On a large field of view camera, the anterior image is usually acquired for approximately 500,000 to 1 million counts; other views are acquired for the same amount of time to facilitate comparison. SPECT imaging is especially helpful in resolving three-dimensional distributions of activity and in enabling comparison with findings on anatomic modalities, such as CT, US and MRI.

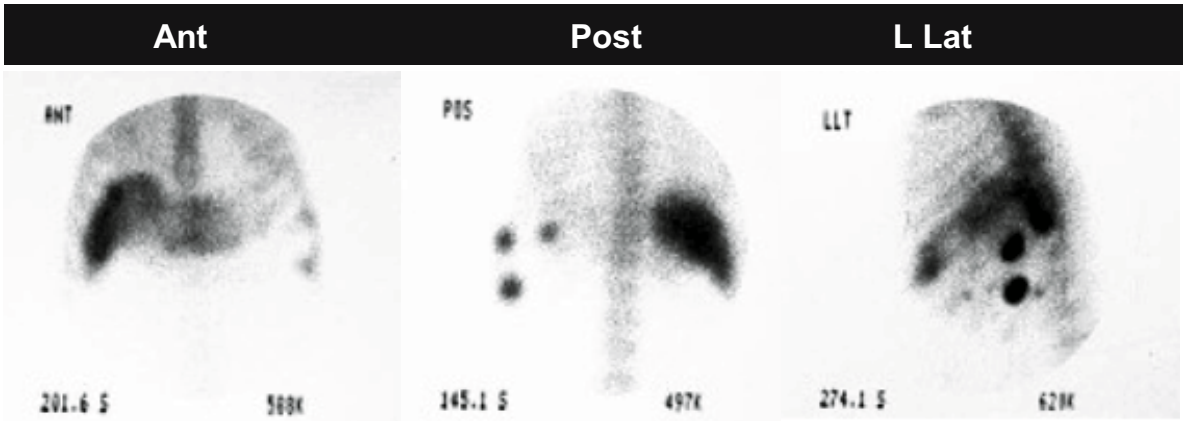

Fig. 6.12. Splenosis noted on a ^{99m}Tc-sulfur colloid study in a patient with cirrhosis and a remote history of abdominal trauma and splenectomy. In place of the spleen, three intense foci of activity are noted in the left upper quadrant of the abdomen, representing areas of functioning splenic tissue. Size and function of the spleen cannot be used to assess diffuse hepatic disease in the patient with splenectomy however other signs may be observed. Uptake of colloid within the marrow is markedly increased and tertiary uptake in the lung is also noted. The liver appears small and there is separation of the lateral aspect of the liver from the rib margin (Helman's sign), suggesting ascites. (Reprinted from Zuckier and Freeman 2003 with permission)

6.3.3 Clinical Indications and Interpretation

Colloid studies of the liver are currently performed to assess diffuse hepatic disease and less frequency to evaluate focal processes within the liver. Colloid splenic imaging is primarily performed to identify functional splenic tissue. These applications are discussed below.

6.3.3.1 Diffuse Parenchymal Disease of the Liver

Phagocytosis of particulate matter in the blood is an intrinsic function of the Kupffer cells of the liver (Waxman 1982). The distribution of RE activity normally appears more intense in the liver than in the spleen, and marrow activity is generally only faintly appreciated. Variations in distribution of SC can therefore be used as a measure of hepatic activity. In this sense, colloid scintigraphy yields information regarding physiologic function in addition to anatomy (McClees and Gedgaudas-McClees 1984). For evaluation of diffuse parenchymal liver disease, criteria of interpretation include hepatic size, splenic size, and the relative distribution of colloid between various sites within the RES. Standardized technique is important as size of the colloid particles, and the prandial state of the patient, affect quantitative parameters including the ratio of counts in the liver and spleen (Hoefs et al. 2005).

Features of the liver spleen scan that correlate best with diffuse hepatocellular disease include moderate to severe inhomogeneous liver uptake, increased bone marrow uptake, and reversal of the normal liver-to-spleen uptake ratios (Geslien et al. 1976) (Fig. 6.12). Colloid "shift" is not specific for hepatic dysfunction; factors including portal hypertension, hypersplenism, marrow-active anemia as a response to chemotherapy, and malignant melanoma may also result in this finding (Royal et al. 2003). Splenomegaly is not a specific finding in hepatic disease, because other pathology, such as lymphoma, can alter splenic size (Geslien et al. 1976; Kim 1979).

6.3.3.2 Focal Processes Within the Liver

At one time, colloid scintigraphy had a role in identifying space-occupying lesions of the liver; today its use in identifying and characterizing focal processes within the liver is uncommon. Most true space-occupying processes within the liver, such as metastases and abscesses, are devoid of Kupffer cells, with resultant defects noted on SC imaging (Fig. 6.13). In contrast, processes that simulate space-occupying lesions on radiographic studies, but do not disturb Kupffer cell function, such as regenerating nodules or fatty change within the liver, retain SC uptake (Lisbona et al. 1986; Baker et al. 1986). Many investigators report sensitivity on the order of 80–85% for detecting liver metastases (Alderson et al. 1983); surface lesions less than 2 cm, and deep lesions less than 3–4 cm in diameter, may not be well visualized on planar scintigraphy due to spatial limitations of the gamma camera (Davis and McCarroll 1994). At low disease prevalence, SPECT has been shown to offer only a marginal benefit over planar scintigraphy (Fawcett and Sayle 1989). SPECT slightly improves the detection of small lesions, but may cause a concomitant decrease in specificity, as small normal structures, such as vessels or ducts, may become visible and resemble lesions (Davis and McCarroll 1994). Advent of SPECT-CT systems may obviate this confusion

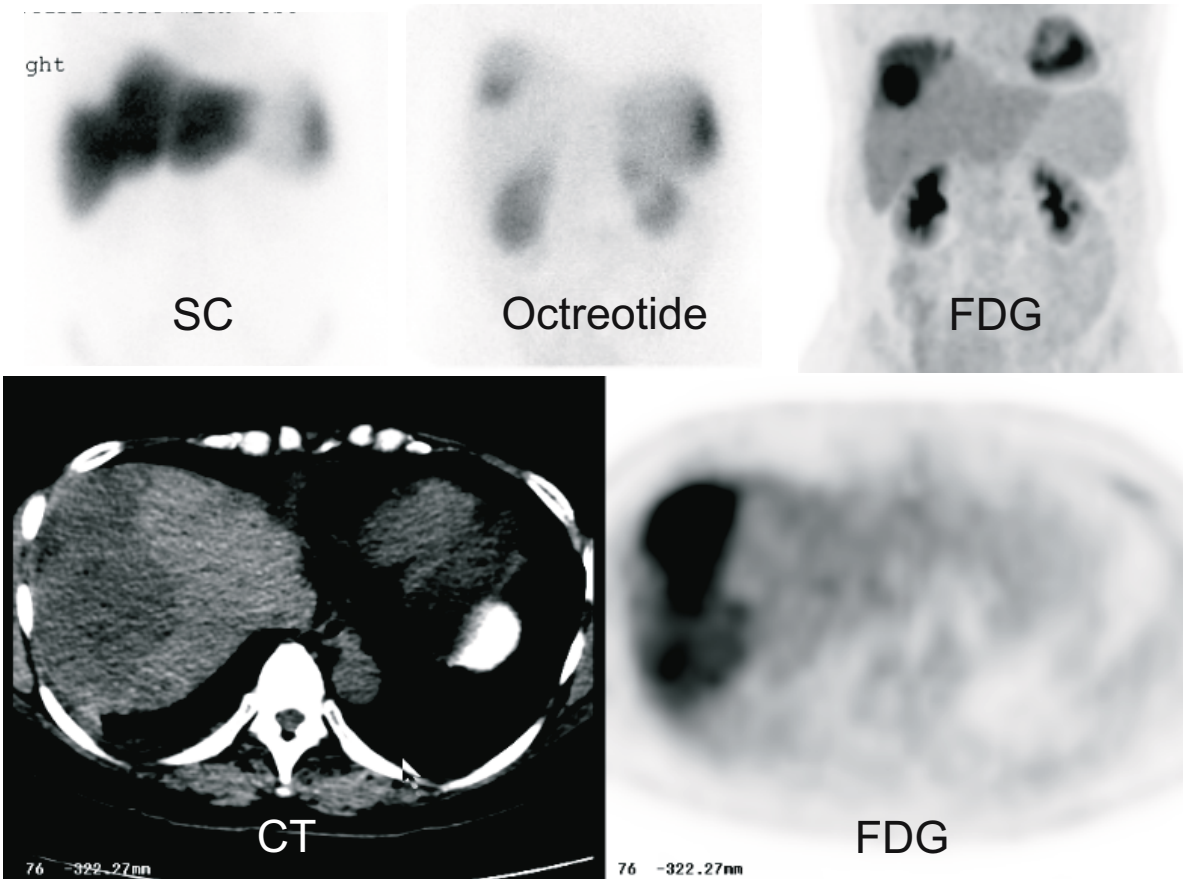

Fig. 6.13. Forty-eight-year-old female with history of pancreatic carcinoid tumor metastatic to liver. Anterior ^{99m}Tc-sulfur colloid image demonstrates a defect in the superior aspect of the liver. Focal uptake is noted on ^{111}In-octreotide anterior planar image and ^{18}F-FDG anterior MIP image, consistent with metastatic carcinoid tumor. On the *lower panels*, transaxial PET-CT images illustrate FDG uptake corresponding to a low-density liver metastasis

and optimize tomographic colloid studies by combining physiology and anatomic detail.

Primary masses originating within the liver include HCC, focal nodular hyperplasia (FNH) and hepatic adenoma. HCC is devoid of uptake on SC studies. In FNH, lesions have variable degrees of Kupffer cell function, and consequently variable colloid uptake has been described in these lesions ranging from decreased (in 30% of lesions), to normal (30%), to supra-normal (30%) and even intense (10%) (Welch et al. 1985). Recent scintigraphic and pathologic literature has also documented possible presence of Kupffer cells in hepatic adenomas (Lubbers et al. 1987; Rubin and Lichtenstein 1993), with moderate uptake in up to one-quarter of the patients studied. Masses with uptake above normal are believed to be relatively pathognomonic for FNH (Fig. 6.14).

In addition to FNH, several vascular derangements may lead to focal regions of increased SC uptake within the liver (Table 6.3). In superior vena cava (SVC) obstruction, a venous injection of SC into the upper extremities must bypass the occluded SVC and reach the heart via porto-systemic collaterals, typically through the internal mammary vein that connects to the paraumbilical and left portal vein (Tetalman et al. 1978; Dickson 2005). Adjacent regions of the liver, specifically the medial segment of the left lobe, receive relatively enriched amounts of colloid and consequently appear intense on subsequent imaging (Fig. 6.15). In obstruction of the inferior vena cava (IVC), a similar finding has been noted following injection of radiotracer via the lower extremities though injection via the upper

Table 6.3. Focal "hot spots" in the liver

Disorder	Region	Mechanism
Budd-Chiari syndrome	Caudate lobe	Direct drainage by accessory vein
SVC or IVC obstruction	Quadrate lobe	Collateral pathway to left portal vein
Focal nodular hyperplasia	Variable	Presence of excessive Kupffer cells
Ethanol abuse	Left lobe	"Streamlining" of toxins to right lobe

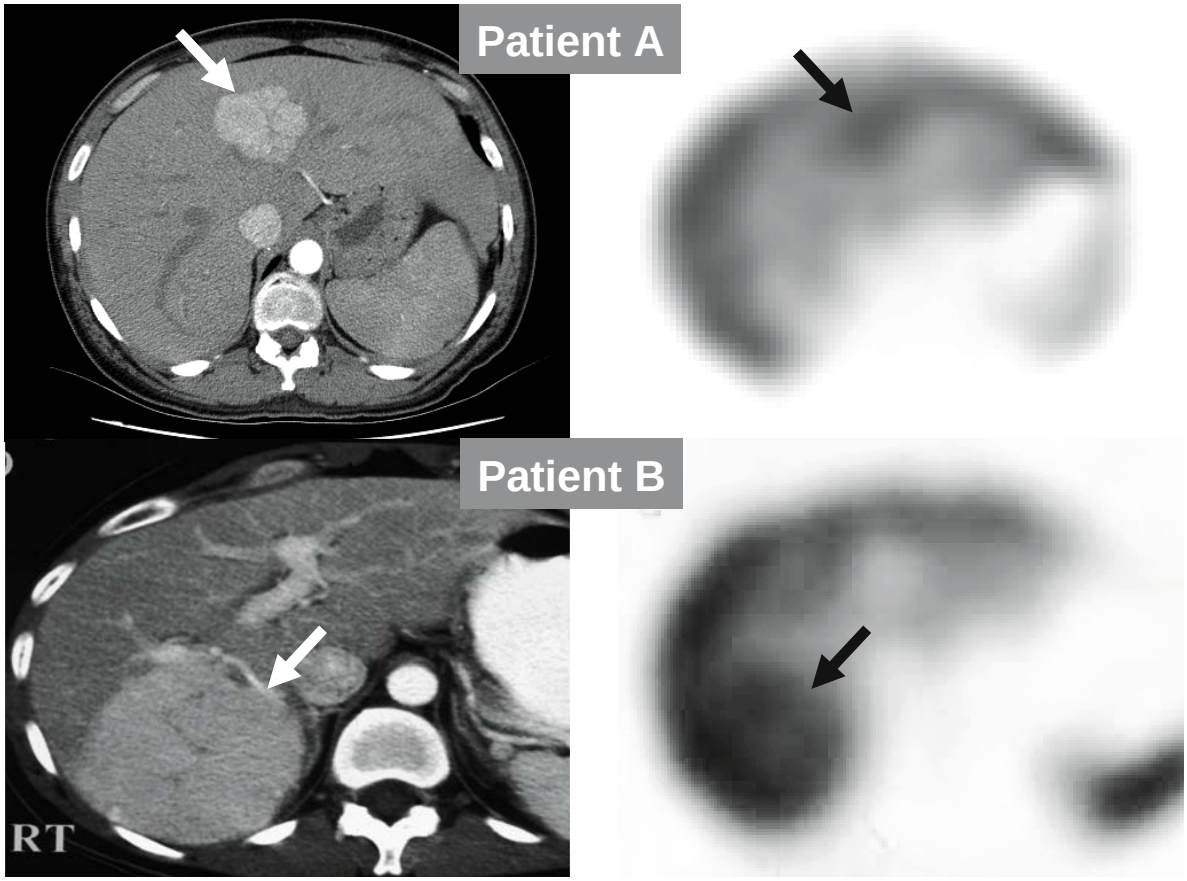

Fig. 6.14. Two examples of relatively intense uptake of SC in FNH. On SPECT imaging, the center of the liver normally appears less intense than the periphery due to the effect of photon attenuation. Patient A is a 38-year-old woman with abdominal discomfort noted to have an enhancing lesion within the right lobe of the liver (*arrow*) on CT scan. Tomographic image from a liver spleen colloid scan shows an area of increased colloid uptake relative to the surrounding liver, pathognomonic of FNH. Patient B is a 42-year-old woman with a liver mass incidentally detected on sonography. An area of relatively intense SC uptake is seen corresponding to the enhancing mass seen on arterial phase CT

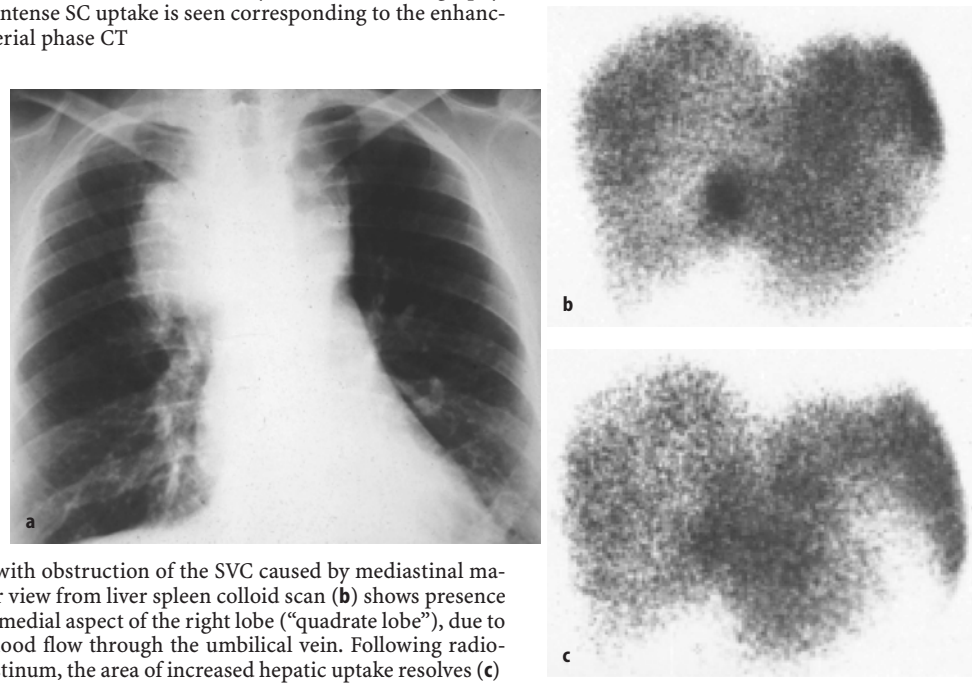

Fig. 6.15. Adult male with obstruction of the SVC caused by mediastinal malignancy (**a**). Anterior view from liver spleen colloid scan (**b**) shows presence of a hot region in the medial aspect of the right lobe ("quadrate lobe"), due to collateralization of blood flow through the umbilical vein. Following radiotherapy to the mediastinum, the area of increased hepatic uptake resolves (**c**)

extremities will result in a normal distribution of activity (Muramatsu et al. 1994).

In Budd-Chiari syndrome, hepatic venous drainage into the SVC is obstructed thereby impairing overall liver function. In contrast, liver parenchyma in the region of the caudate lobe often drains directly into the adjacent SVC via accessory veins. This segment thereby exhibits relatively intact uptake of colloid in comparison to the remainder of the affected liver, a finding coined the "bullseye" sign (Meindok and Langer 1976).

An additional cause of relatively increased uptake within the liver may be seen in alcoholic liver disease, which preferentially affects the right lobe of the liver resulting in an "intrahepatic colloid shift" from the severely affected right lobe to the relatively preserved left lobe. This phenomenon is believed to be due to asymmetric "streamlining" of toxic portal venous blood within the lobes of the liver (Shreiner and Barlai-Kovach 1981).

6.3.3.3 Splenic Imaging

Utility of colloid imaging of the spleen derives from a relatively high degree of tissue specificity based on the-functional nature of the examination. Because larger particles preferentially localize in the spleen, denatured RBCs appear to be superior to SC for splenic imaging (Armas 1985; Massey and Stevens 1991), although this more-complicated procedure is not routinely employed.

Splenic imaging may be performed in children to rule out congenital asplenia or polysplenia. SPECT imaging is especially valuable for this purpose because of the ability to resolve splenic uptake adjacent to the liver as distinct from the liver itself (Oates et al. 1995). Other indications for splenic imaging include confirming presence of functional splenic tissue in cases of splenic autotransplantation following splenic trauma (Fig. 6.12) or absence of such tissue in patients who have been treated previously with splenectomy for conditions such as idiopathic thrombocytopenic purpura (ITP) (Massey and Stevens 1991). Splenic imaging can also be performed in order to characterize incidentally noted abdominal masses, which are thought to represent accessory spleens or splenic tissue (Fig. 6.16).

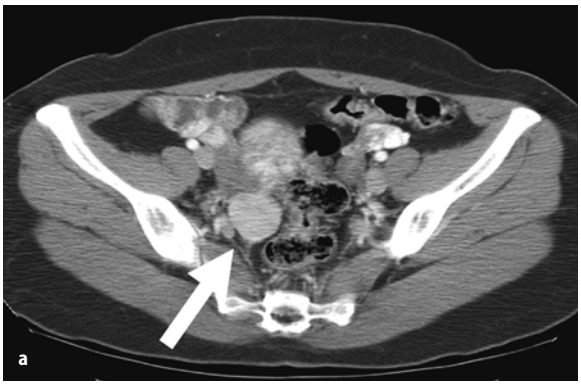

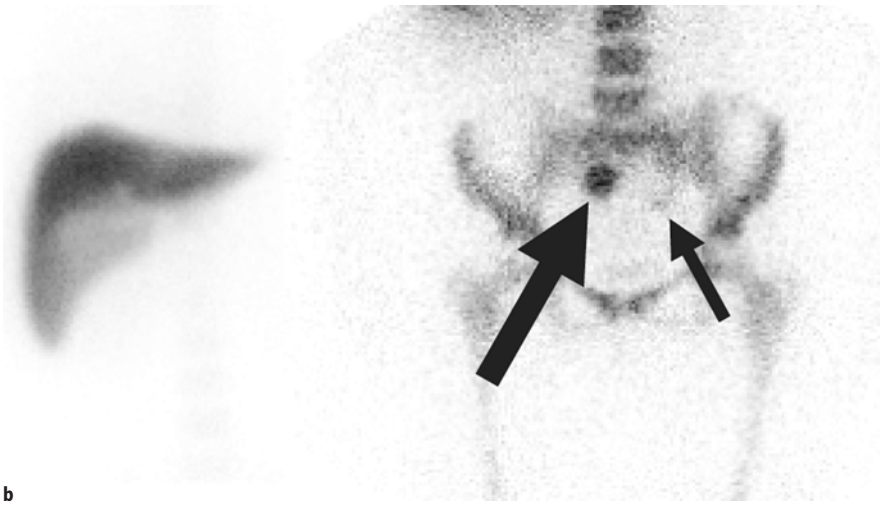

Fig. 6.16. Contrast enhanced CT scan (**a**) in this 36-year-old Hispanic female demonstrates several enhancing masses within the abdomen and pelvis (one such pelvic mass is illustrated by *arrow*). History was significant for a motor vehicle accident several years earlier with probable splenectomy. Colloid study demonstrates absence of orthotopic spleen (**b**). When viewed at increased intensity, a prominent focus of colloid accumulation is noted anterior to the right SI joint corresponding to the region of the enhancing mass (*large arrow*) with a smaller focus noted inferior to the left SI joint (*small arrow*), both of which are caused by splenosis

6.4 Hemangioma Imaging

The most common benign lesion of the liver is hemangioma, occurring in up to 7 % of the population and representing a frequent incidental finding in the course of imaging of the abdomen (Ishak and Rabin 1975). Hemangiomas are typically less than 3 cm in diameter; when larger than 4 cm, they bear the designation "giant" (Nelson and Chezmar 1990). As a rule, hemangiomas do not require any medical intervention or treatment, and a non-invasive and specific means of characterizing these lesions would serve to obviate further concern. Imaging of the liver with ^{99m}Tc-labeled RBCs fulfills this role.

6.4.1 Radiopharmaceuticals

For identification of hemangioma, 750 MBq (20 mCi) of ^{99m}Tc-RBCs is used, optimally labeled by the in-vitro method. Methods of RBC labeling are common to other scintigraphic applications, such as GI bleeding studies, and are discussed elsewhere in this book.

6.4.2 Methodology (Royal et al. 2003)

Prior to hemangioma imaging it is important to identify location of the suspect lesion, most commonly by reference to the previously obtained CT, US or MRI study. Where no prior images are available for consultation, a low-dose SC study can be performed immediately preceding RBC imaging to define the defect; however, this procedure is usually of little value where other cross-sectional images are available for consultation. Generally, imaging consists of three phases: arterial perfusion (flow), immediate blood pool, and delayed blood pool (Middleton et al. 1994). Arterial perfusion imaging, typically obtained at 1 frame per second during injection of the labeled RBCs, reveals useful information about regional distribution of hepatic arterial blood flow and should be performed in the view potentially suited to portray the lesion while avoiding overlap with normal vascular structures. Immediate blood pool images are then acquired for 1 to 2 million counts each, in this optimal projection as well as in standard anterior, posterior and right lateral views. Delayed blood pool images, designed to portray the maximal wash-in of RBCs into the hemangioma, are acquired approximately 2 – 3 h following injection in similar projections to the immediate blood pool images. SPECT will often be necessary to visualize small lesions, especially when deep within the liver parenchyma or not detected on planar views (Kudo et al. 1989), and is useful for comparison to other cross-sectional imaging modalities.

6.4.3 Clinical Indications and Interpretation

Classic findings in hemangioma are absent visualization during arterial perfusion imaging, while on blood pool imaging the lesion becomes more intense than surrounding normal liver, a phenomenon termed the "perfusion-blood pool mismatch" (Rubin and Lichtenstein 1993) (Fig. 6.17). Activity greater than adja-

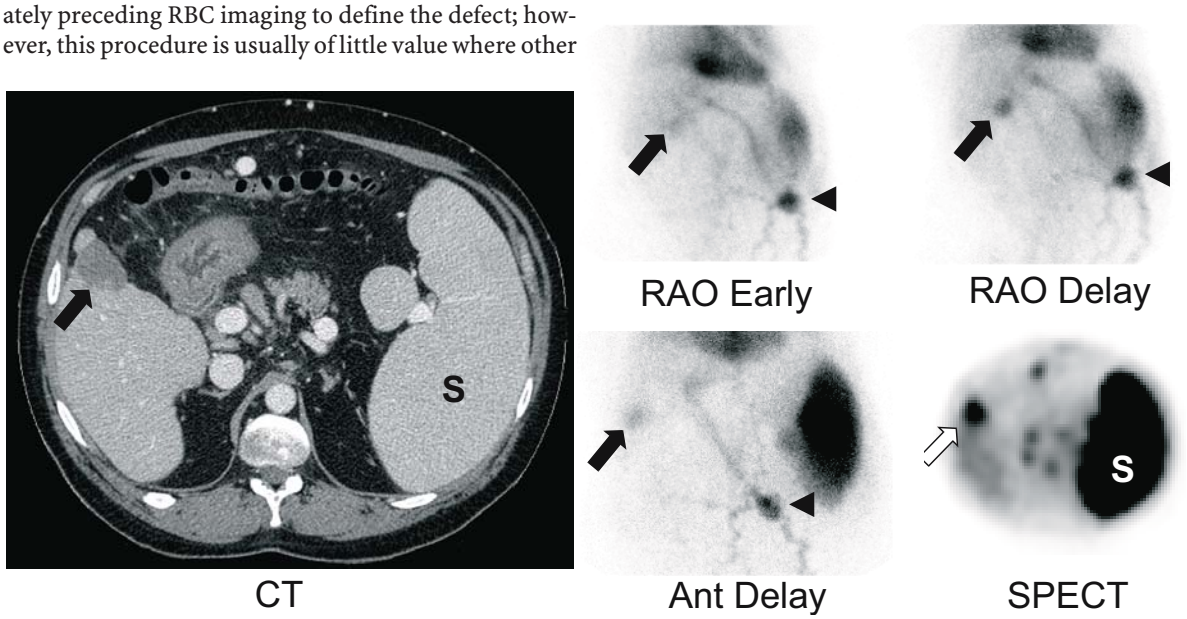

Fig. 6.17. Fifty-year-old male with hepatitis C and alcoholic cirrhosis. CT scan of the abdomen (*left panel*) suggests hemangioma of the liver (*arrow*). Multiple venous collaterals are noted throughout the abdomen. Images from RBC hemangioma study (*right panels*) demonstrate presence of intense blood pool in the region of the lesion, increasing between the early and delayed images. The spleen (*S*) is enlarged and multiple venous anastomoses over the abdomen are noted (*arrowhead*, caput medusae)

cent liver is observed on the 2–3 h delayed image but may even be noted on the immediate blood pool images.

Overall imaging accuracy for detecting hemangiomas is reported to be 90%, especially if SPECT is used for smaller lesions. Sensitivity for characterizing hemangiomas greater than 2–3 cm in diameter is high; smaller lesions can be best detected when peripheral and SPECT is performed (Kudo et al. 1989; Ziessman et al. 1991; Royal et al. 2003). In giant cavernous hemangiomas, RBC SPECT has been shown to be useful in differentiation from other large liver masses and is superior to US (Tsai et al. 2002). False negative results have been rarely seen in hemangiomas with extensive fibrosis and thrombosis (Rabinowitz et al. 1984) or when attempting to visualize lesions below the effective resolution. False positive studies demonstrating increased blood pool have been rarely described in patients with hemangiosarcoma (Ginsberg et al. 1986), and very rarely in HCC. In a meta-analysis of 365 patients with 254 hemangiomas (Middleton et al. 1994), the unusual combination of early flow and delayed intense filling was present in 16 lesions (4.4%). Twelve of these cases were determined to be hemangioma, while 4 were diagnosed as HCC. In an effort to increase specificity, the authors recommended restricting the diagnosis of hemangioma to lesions that do not evidence increased arterial perfusion, even though sensitivity will be slightly reduced. When increased arterial flow is present, as in the 4.4% of examinations in their meta-analysis, additional diagnostic studies and biopsy are then needed to make a definitive diagnosis.

6.5 ^{18}F-Fluorodeoxyglucose PET

6.5.1 Introduction

^{18}F-Fluorodeoxyglucose (FDG) PET has become a mainstay of oncologic imaging (Khandani and Wahl 2005). It is therefore not surprising that this modality has been successfully used in evaluating tumors of the liver and GI tract (Fig. 6.13). Normal liver tissue normally exhibits moderate FDG uptake with Standardized Uptake Values (SUVs) typically on the order of 2.0. Increased FDG uptake in tumor cells has been shown to be due to increased expression of glucose transporter (GLUT) molecules on the cell surface, increased activity of hexokinase, and reduced levels of glucose-6-phosphatase (Bombardieri et al. 2001).

In a prospective blinded study published in 1998, FDG PET was reported as detecting all liver metastases from adenocarcinoma and sarcoma greater than 1 cm in diameter (Delbeke et al. 1998). In this pioneering study, 8 of 8 cholangiocarcinomas were likewise successfully characterized as malignant; however, HCC had elevated FDG uptake in only 16 of 23 patients. The following discussion will expand upon these observations.

6.5.2 Liver Metastases

Indeed, FDG PET has proved exceptionally useful in the evaluation of liver metastases from a variety of primary malignancies. A meta-analysis which reviewed 111 published data sets compared non-invasive imaging methods in the detection of hepatic metastases from colorectal, gastric and esophageal cancers (Kinkel et al. 2002). At equivalent specificity, FDG PET was the most sensitive non-invasive imaging modality for the diagnosis of hepatic metastases.

In patients with colorectal carcinoma, FDG scanning has been shown to be superior to CT in detecting hepatic and extrahepatic metastases and has utility both in patients considered for resection of solitary hepatic metastases and in restaging of patients with colorectal carcinoma (Wiering et al. 2005). Five year survival following resection of hepatic metastases from colorectal cancer in patients screened and selected by FDG PET was superior to historical controls without PET imaging (Fernandez et al. 2004). Following radiofrequency ablation of liver metastases FDG PET appears superior to contrast CT scanning in early recognition of incomplete tumor destruction (Donckier et al. 2003; Barker et al. 2005) or of recurrence (Anderson et al. 2003).

6.5.3 Benign Hepatic Lesions and HCC

Most benign hepatic lesions, with the notable exception of abscesses, have low FDG uptake. In a series of 8 patients with proven FNH, FDG uptake was universally decreased or normal (Kurtaran et al. 2000). A lesion to background ratio of 2.0 and SUV cut-off of 3.5 has been shown to be useful in discriminating malignant from benign lesions (Delbeke et al. 1998). In spite of these generalities, hepatic adenomas (Patel et al. 1997), regenerating nodules (Bohm et al. 2004) and FNH (Aznar et al. 2005) may occasionally have elevated FDG uptake with reported SUVs as high as 4.2–4.5, potentially leading to false positive interpretation for malignancy.

The relatively low sensitivity of FDG PET in detecting primary HCC has been postulated as due to relatively increased activity of glucose-6-phosphatase within the malignant cells, thereby leading to washout of FDG and decreased tumor to background ratios (Fig. 6.18). Sensitivity of FDG PET appears relatively

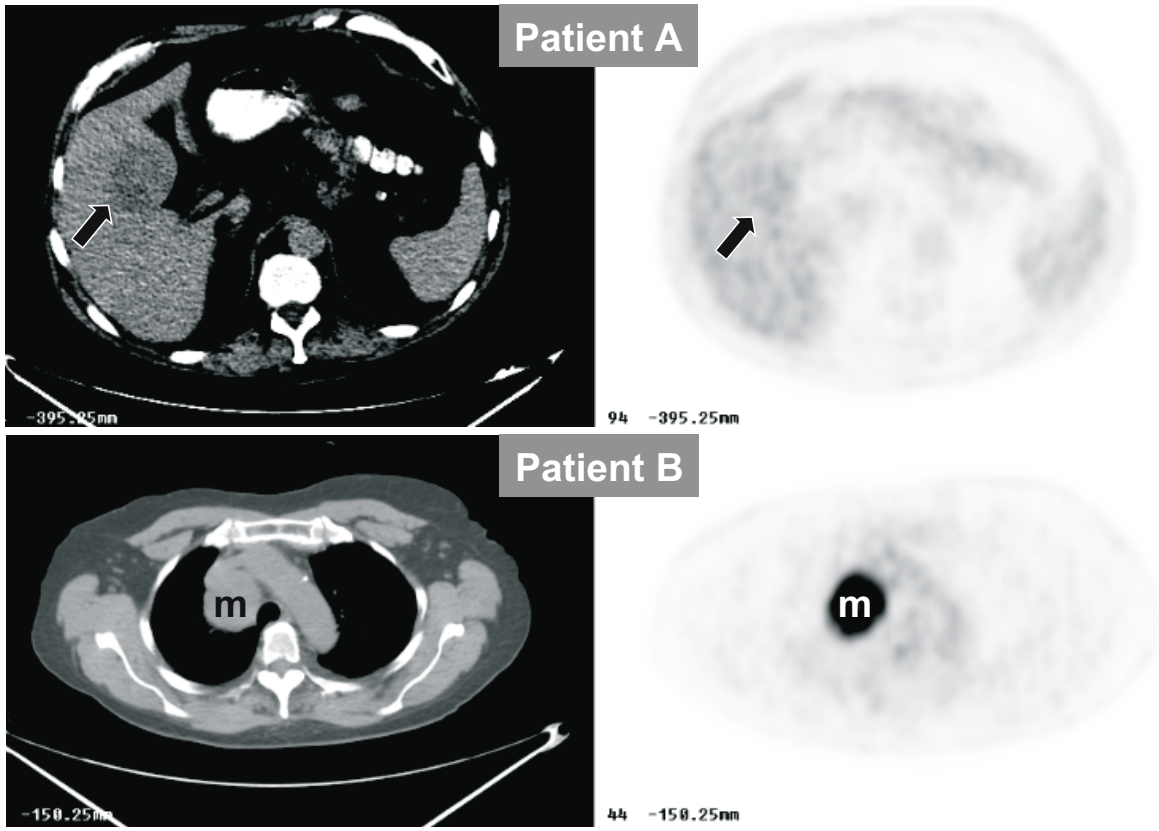

Fig. 6.18. Variable appearance of HCC on FDG PET scans. PET-CT images in upper panels are from a 58-year-old male (patient A) with newly diagnosed HCC. CT demonstrates presence of a low attenuation lesion in the liver (*arrow*); however, this area is isointense to liver on PET. On *lower panels*, thoracic PET-CT images are displayed of a 66-year-old female (patient B) with history of HCC, status post-resection. There is a large right paratracheal mass (*m*) with intense FDG radiotracer uptake, consistent with metastatic HCC

higher in patients with moderately or poorly differentiated HCC, in large tumors, or those with markedly elevated AFP levels (Trojan et al. 1999). In the case of poorly differentiated HCC, metastases may be more FDG-avid than the primary tumor (Fig. 6.18) (Khandani and Wahl 2005). It appears that delayed imaging at 2 h has higher diagnostic sensitivity than conventional imaging at 1 h (Lin et al. 2005). In spite of the stated limitations, FDG PET imaging is reported as contributing clinically to a large fraction of the patients studied (Wudel, Jr. et al. 2003).

6.5.4 Cholangiocarcinoma

It has been suggested that hilar and extrahepatic cholangiocarcinomas are less FDG-avid than the peripheral intrahepatic variety of this tumor (Kim et al. 2003; Khandani and Wahl 2005). Sensitivity for detecting mucinous tumors is reduced as compared to tubular variety of adenocarcinoma (Fritscher-Ravens et al. 2001). Nodular tumors are also considerably more detectable than the infiltrating type (Kato et al. 2002; Anderson et al. 2004). Chronic inflammation has been associated with false positive studies (Fritscher-Ravens et al. 2001) and, similarly, FDG uptake was associated with biliary stents in 7 of 12 patients (Anderson et al. 2004). Nonetheless, FDG PET was shown to be able to correctly discriminate between primary sclerosing cholangitis with and without cholangiocarcinoma (Anderson et al. 2004; Rosenbaum et al. 2006). Sensitivity for detecting regional or hepatoduodenal lymph node metastases has varied (Kluge et al. 2001; Kim et al. 2003), possibly related to technical factors and experience of the readers (Fig. 6.19). Sensitivity for distant metastases appears to be in the 65–70% range, with some variation in sensitivity for detecting carcinomatosis (Kluge et al. 2001; Anderson et al. 2004). The ability of FDG PET to detect distant metastases has had an impact on patient management in 20–30% of patients (Fritscher-Ravens et al. 2001; Anderson et al. 2004).

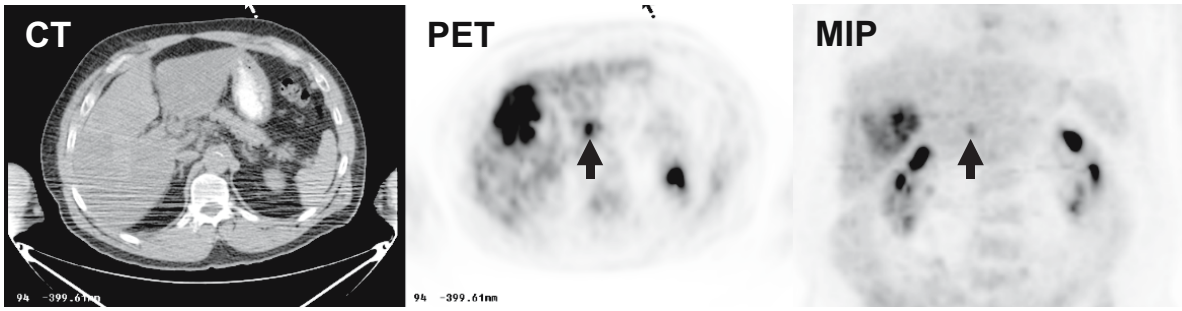

Fig. 6.19. PET-CT images from a 63-year-old male with peripheral cholangiocarcinoma. Intense uptake of FDG is noted in the primary intrahepatic lesion and a portal lymph node metastasis is clearly visible (*arrow*)

6.5.5 Gallbladder Carcinoma

FDG PET appears to have a role in the initial evaluation of GB masses. In several studies, sensitivity for detecting carcinoma was 75–80% while specificity was approximately 85% (Koh et al. 2003; Rodriguez-Fernandez et al. 2004). Lesions were considered positive when intensity exceeded that of liver (Koh et al. 2003) or SUV was greater than 2.5 (Rodriguez-Fernandez et al. 2004). False negative cases included relatively small lesions, a mucinous adenocarcinoma, and a patient with diabetes mellitus, which is postulated to reduce sensitivity. False positive cases included xanthogranulomatous cholecystitis, a tuberculoid granulomatous reaction, and a polypoid lesion with adenomyomatosis. Because acute inflammation can lead to FDG uptake, it is suggested that FDG PET should only be used to diagnose carcinoma when acute inflammation is not present (Koh et al. 2003). In fact, specificity of FDG PET in detecting GB carcinoma is poor when C-reactive protein is elevated and improves significantly when these patients are excluded from analysis (Nishiyama et al. 2006). Imaging at 2.5 h post FDG administration may be superior to standard imaging at 1 h due to increased lesion uptake and contrast (Nishiyama et al. 2006).

FDG PET has also proved helpful for detecting residual GB carcinoma following cholecystectomy, with sensitivity for detecting residual disease of 78% and specificity of 80% (Anderson et al. 2004). Sensitivity for detecting extrahepatic metastases was only 50%, and FDG PET performed especially poorly in patients with carcinomatosis.

6.5.6 Pancreatic Malignancy

FDG PET has been shown to be accurate in differentiating malignant from benign pancreatic cysts, with similar sensitivity to CT and superior specificity (Sperti et al. 2005). An appropriate SUV cutoff level of 2.0 appears optimal to differentiate benign from malignant pancreatic lesions (Delbeke et al. 1999). A more challenging application of FDG-PET is in discriminating between pancreatic malignancy and mass-forming pancreatitis (Fig. 6.20). The latter can result in focal FDG uptake with intensity indistinguishable from malignancy (Shreve 1998). Other groups have shown adequate sensitivity and specificity for diagnosing pancreatic primary malignancies when patients with elevated serum amylase levels (Papos et al. 2002) or elevated C-reactive protein and plasma glucose levels (Diederichs et al. 2000) were excluded. Accuracy in detecting loco-regional lymph node involvement has been limited in published studies (Hustinx 2004; Rosenbaum et al. 2006) and detection of peritoneal metastasis is limited (Diederichs et al. 2000). FDG-PET has been shown to be accurate in detecting distal metastases including liver metastases greater than 1 cm in diameter (Frohlich et al. 1999; Nakamoto et al. 1999), in post-surgical surveillance (Jadvar and Fischman 2001) and has also been successfully applied for prognostic purposes (Sperti et al. 2003). In clinical series, management has been altered in a large fraction of patients studied (Delbeke et al. 1999). Reduction in tumor uptake of FDG at 1 month following chemotherapy has been shown to correlate with improved overall survival (Maisey et al. 2000).

An interesting feature of pancreatic diseases is the not uncommon association with insulin deficiency. As performance of FDG-PET scanning is adversely affected by elevated glucose levels, some care must be exercised in eliminating patients with grossly elevated titers (Bombardieri et al. 2001). False negative findings are reported with tumors smaller than 1 cm in diameter (Diederichs et al. 2000), and in highly differentiated GI tumors (Bombardieri et al. 2001). False positive uptake in the liver has been noted in the presence of marked intrahepatic cholestasis (Frohlich et al. 1999), in addition to patients with inflammation and pancreatitis as discussed above. Dual-phase scanning has been proposed by several authors to improve diagnostic accuracy of FDG PET (Hustinx 2004). Using this technique, inflammatory lesions generally decrease with time while neoplasms increase or remain stable.

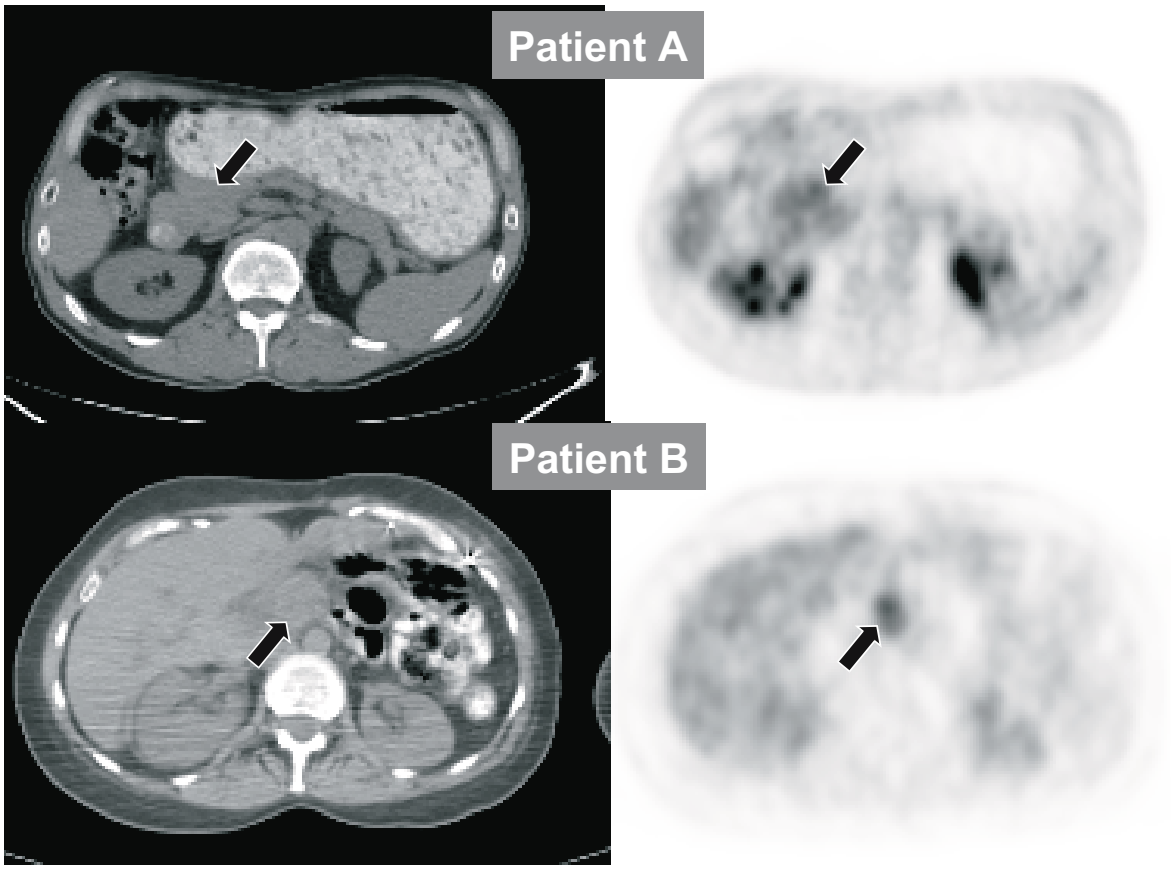

Fig. 6.20. Benign and malignant pancreatic masses may be difficult to differentiate on FDG PET-CT. Patient A is a 61-year-old male with newly diagnosed pancreatic mass (*arrow*), ultimately shown to be due to focal pancreatitis. There is gastric outlet obstruction secondary to mass effect. Irregular, focal FDG uptake is noted, which is difficult to differentiate from malignancy. Patient B is a 50-year-old female recently found to have obstructive jaundice and a mass in the head of the pancreas. The patient is status post-splenectomy for unrelated reasons. Focal FDG uptake is seen corresponding to this region suggestive of a metabolic neoplastic process (*arrow*).

6.5.7 Artifacts

A consideration in FDG PET imaging is the potential "stunning" of uptake which can occur following chemotherapy. The duration of this phenomenon is not well known, but may extend as long as 4–6 weeks and mandates deferring imaging to as late as feasible in the cycle of clinical management (Khandani and Wahl 2005). An important technical pitfall in PET-CT imaging of the liver is mis-registration of the FDG uptake between PET and the anatomic CT image, produced at least in part by differences in breath holding between the two modalities (Osman et al. 2003; Nakamoto et al. 2003; Sarikaya et al. 2003). This is especially prevalent at the dome of the liver, where an intrahepatic lesion may appear to be situated in the lung base, or, conversely, a lung lesion may appear to be intrahepatic. Careful inspection of CT images is therefore mandated when analyzing FDG-avid lesions in this region. Frequency and degree of artifact may be reduced by application of special breath-hold techniques (Beyer et al. 2003).

It should be remembered that FDG PET is a relatively new technology and is still evolving. For example, the impact of image fusion is not fully reflected in the quoted medical literature. Limitations in detection of subtle metastases in some of the previously published studies may become less relevant with proliferation of high resolution systems and PET-CT fusion (Rosenbaum et al. 2006). Furthermore, as a diagnostic discipline, PET-CT reading still resides on the "learning curve." For this reason, published sensitivities and specificities should be viewed as lower limits of current performance.

6.6 Other Ancillary Techniques

6.6.1 Hepatic Arterial Perfusion Scintigraphy

Hepatic arterial perfusion scintigraphy (HAPS) was initially developed and is still used as a means of confirming proper placement of hepatic artery chemother-

apy infusion catheters prior to delivery of arterial chemotherapy to intrahepatic tumors (Thrall 1984; Civelek et al. 1993). A quantity of 40–100 MBq (1–3 mCi) of ^{99m}Tc-macroaggregated albumin (MAA) is injected through an infusion catheter placed in the hepatic artery, resulting in trapping of radiopharmaceutical within the downstream perfused capillary bed. The rate of injection should be less than 1 ml/min to avoid creating artifactual perfusion patterns. The distribution of activity is subsequently imaged using planar or SPECT scintigraphy, including views of the lungs to identify intrahepatic arteriovenous fistulas. This technique has been adopted as a sensitive means of detecting intrahepatic metastases based on the differences in perfusion of normal liver parenchyma, largely via the portal vein, versus intrahepatic metastases, via the hepatic artery. Metastatic lesions as small as 0.5–1.0 cm in size may be detected as "hot spots" (Drane 1991). Small lesions have been identified that were not seen by CT or CT arterial portography and which could only be confirmed at blind resection or biopsy (Vogel et al. 1994). While effective, HAPS is not commonly performed for detection of intrahepatic malignancy due to the invasiveness of placing an injection catheter into the hepatic artery.

Based on similar physiologic principles, treatment with ^{90}Y-containing glass microspheres (TheraSphere) has been introduced as a means of delivering localized radiation to sites of hepatocellular carcinoma (Salem et al. 2005).

6.6.2 ^{133}Xenon Gas

Though not commonly performed today, radioactive xenon has historically been used to identify focal fatty changes in the liver, based on retention of the radioactive gas within the liver on delayed washout studies (Ahmad et al. 1977; Lisbona et al. 1988). When the liver exhibits only a moderate degree of hepatic steatosis, a normal SC examination appears to be a more reliable (Baker et al. 1986) and available means of excluding pathology.

6.6.3 ^{123}I- and ^{131}I-Metaiodobenzylguanadine

^{123}I- and ^{131}I-metaiodobenzylguanadine (MIBG) is used in the imaging of pheochromocytomas, paragangliomas, neuroblastoma, carcinoid and medullary thyroid tumors and can be helpful in evaluating lesions metastatic to the liver (Kaltsas et al. 2004; Pashankar et al. 2005). MIBG is a guanidine derivative, structurally similar to norepinephrine, that concentrates within secretory granules of catecholamine-producing cells. Correlation with anatomic imaging is important in achieving accuracy (Pfannenberg et al. 2003).

The ^{123}I-labeled analog has superior imaging and dosimetry characteristics, and is preferred if available. Some authors have reported relatively higher concentration of MIBG in normal parenchyma of the left lobe of the liver as compared to the right, possibly due to a greater presence of catecholamines and a higher sympathetic nerve density (Jacobsson et al. 2005). MIBG imaging may be useful in selecting patients slated for therapy with therapeutic amounts of ^{131}I-MIBG (Ezuddin and Fragkaki 2005).

6.6.4 ^{111}In-Octreotide (Octreoscan)

^{111}In-octreotide represents a receptor binding radiopharmaceutical that is used in the staging of various endocrinologic tumors and can detect presence of liver metastases (Figs. 6.13, 6.21). This ^{111}In-labeled somatostatin analog binds to the sstr2 receptor that is present on the extracellular membrane of numerous neuroendocrine tumor types (Bombardieri et al. 2001). Overall, reported sensitivity of ^{111}In-octreotide is 80–90% for gastrinomas, 70% for carcinoids, 40% for insulinomas and 30% for glucagonomas (Drane 1998). Somatostatin receptor scintigraphy has been shown to be superior to FDG PET for diagnosing and staging carcinoid tumors; the latter should be reserved for patients with negative results on octreotide scintigraphy (Belhocine et al. 2002).

6.6.5 ^{67}Ga-Citrate

Since the 1970s, ^{67}Ga-citrate has been known to accumulate in both malignant and infectious processes that affect the liver (Lomas et al. 1972). More recently, the mechanism of localization of ^{67}Ga-citrate in tumors has been understood to be receptor based, reflecting increased presence of transferrin receptors to which circulating ^{67}Ga-transferrin complexes bind (Larson et al. 1980). Comparison to SC imaging is recommended (Davis and McCarroll 1994), as a gallium-avid tumor may appear isointense to normal liver and would therefore be difficult to diagnose on gallium scan alone though it would be readily identifiable when compared to the defect on a SC study.

Approximately 90–95% of HCCs are reported to have ^{67}Ga-citrate uptake and this radiopharmaceutical can serve an important ancillary role in making this diagnosis (Lomas et al. 1972; Suzuki et al. 1974; Hauser and Alderson 1978) (Fig. 6.22). In addition to HCC, other tumor types that are frequently ^{67}Ga-citrate avid include lymphoma, and metastases from lung carcinoma, melanoma, colorectal carcinoma, sarcoma and testicular neoplasms. A variety of abscesses concentrate gallium citrate and this application is discussed elsewhere in this book under the topic of infection imaging.

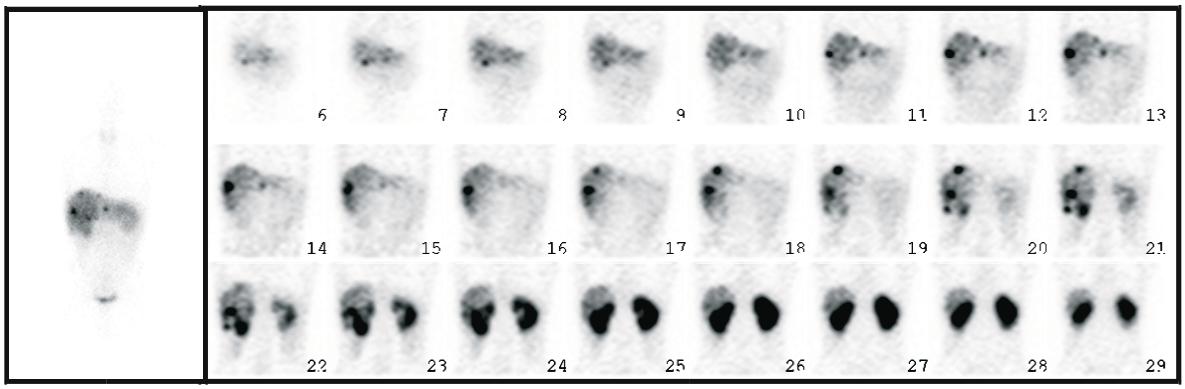

Fig. 6.21. Forty-two-year-old male with history of carcinoid tumor. Whole body image (*left panel*) and sequential coronal SPECT images (*right panel*) were obtained 24 h following injection of ^{111}In-octreotide. Numerous foci of radiopharmaceutical uptake are noted which stud the liver. Physiologic excretion of octreotide is noted on posterior tomographic images through the kidneys (*frames 22–29*)

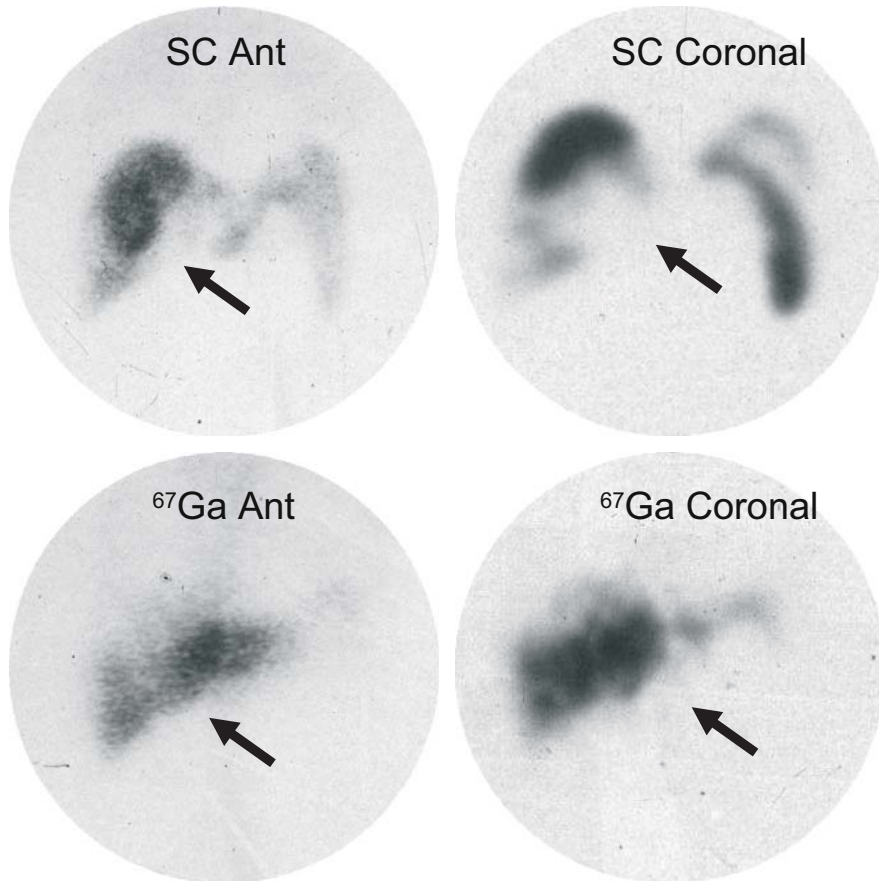

Fig. 6.22. Sixty-three-year-old alcoholic with markedly elevated alpha-fetal protein. Sulfur colloid images (*upper panels*) demonstrate heterogeneous defects within the liver, especially inferiorly (*arrows*). The spleen appears enlarged on the coronal SPECT image (*right upper panel*). Gallium-67 citrate images (*lower panels*) demonstrate gallium-avid HCC replacing hepatic tissue in region of defects noted on the colloid study. (Reprinted from Middleton et al. 1994, with permission)

6.6.6 Immunologic Imaging Agents

Antibody imaging agents were once touted as promising agents for imaging tumors, and since 1992 several FDA-approved agents have been introduced and marketed for colon, lung, prostate and ovarian carcinoma (Zuckier and DeNardo 1997). At present, only the prostate specific membrane antigen (PSMA) directed antibody ^{111}In-capromab pendetide (Prostascint) remains commercially available as an imaging agent, and this radiopharmaceutical is of relatively little utility in evaluation of liver masses which infrequently derive from this malignancy. To a large degree, the success of PET imaging in staging colorectal, ovarian and lung carcinoma has supplanted the use of radiolabeled antibodies in these indications.

6.7 Summary and Future Developments

Scintigraphic imaging retains a role in the functional and non-invasive evaluation of the solid GI tract. In the near future, the area of greatest growth which will likely impact on this modality is the continued development of novel PET radiopharmaceuticals that target those tumors presently not well localized by the currently available radiopharmaceutical ^{18}F-FDG (Rosenbaum et al. 2006). Increasing experience and knowledge will also lead to increased integration of radionuclide studies into diagnostic and treatment algorithms, especially in the realm of oncology. Through fusion of scintigraphic images with CT, hybrid imaging seeks to combine the advantages of both anatomic and functional imaging. Penetration of image fusion into single-photon scintigraphy will also serve to combine the functional strength of scintigraphic imaging with the superior resolution of anatomic radiologic modalities.

References

Ahmad M, Witztum KF, Fletcher JW, Hendershott LR, Klos D, George EA, Donati RM (1977) Xenon-133 accumulation in hepatic steatosis. J Nucl Med 18:881 – 5

Alderson PO, Adams DF, McNeil BJ, Sanders R, Siegelman SS, Finberg HJ, Hessel SJ, Abrams HL (1983) Computed tomography, ultrasound, and scintigraphy of the liver in patients with colon or breast carcinoma: a prospective comparison. Radiology 149:225 – 30

Anderson GS, Brinkmann F, Soulen MC, Alavi A, Zhuang H (2003) FDG positron emission tomography in the surveillance of hepatic tumors treated with radiofrequency ablation. Clin Nucl Med 28:192 – 7

Anderson CD, Rice MH, Pinson CW, Chapman WC, Chari RS, Delbeke D (2004) Fluorodeoxyglucose PET imaging in the evaluation of gallbladder carcinoma and cholangiocarcinoma. J Gastrointest Surg 8:90 – 7

Armas RR (1985) Clinical studies with spleen-specific radiolabeled agents. Semin Nucl Med 15:260 – 75

Aznar DL, Ojeda R, Garcia EU, Aparici F, Sanchez PA, Flores D, Martinez C, Sopena R (2005) Focal nodular hyperplasia (FNH): a potential cause of false-positive positron emission tomography. Clin Nucl Med 30:636 – 7

Baker MK, Schauwecker DS, Wenker JC, Kopecky KK (1986) Nuclear medicine evaluation of focal fatty infiltration of the liver. Clin Nucl Med 11:503 – 6

Balon HR, Brill DR, Fink-Bennett DM, Freitas JE, Krishnamurthy GT, Ziessman HA, Lang O, Robinson PJ (2001) Society of Nuclear Medicine procedure guideline for hepatobiliary scintigraphy 3.0. Society of Nuclear Medicine Procedure Guidelines. Society of Nuclear Medicine

Barker DW, Zagoria RJ, Morton KA, Kavanagh PV, Shen P (2005) Evaluation of liver metastases after radiofrequency ablation: utility of 18F-FDG PET and PET/CT. AJR Am J Roentgenol 184:1096 – 102

Belhocine T, Foidart J, Rigo P, Najjar F, Thiry A, Quatresooz P, Hustinx R (2002) Fluorodeoxyglucose positron emission tomography and somatostatin receptor scintigraphy for diagnosing and staging carcinoid tumours: correlations with the pathological indexes p53 and Ki-67. Nucl Med Commun 23:727 – 34

Beyer T, Antoch G, Blodgett T, Freudenberg LF, Akhurst T, Mueller S (2003) Dual-modality PET/CT imaging: the effect of respiratory motion on combined image quality in clinical oncology. Eur J Nucl Med Mol Imaging 30:588 – 96

Bohm B, Voth M, Geoghegan J, Hellfritzsch H, Petrovich A, Scheele J, Gottschild D (2004) Impact of positron emission tomography on strategy in liver resection for primary and secondary liver tumors. J Cancer Res Clin Oncol 130:266 – 72

Bombardieri E, Aliberti G, de Graaf C, Pauwels E, Crippa F (2001) Positron emission tomography (PET) and other nuclear medicine modalities in staging gastrointestinal cancer. Semin Surg Oncol 20:134 – 46

Calvet X, Pons F, Bruix J, Bru C, Lomena F, Herranz R, Brugera M, Faus R, Rodes J (1988) Technetium-99m DISIDA hepatobiliary agent in diagnosis of hepatocellular carcinoma: relationship between detectability and tumor differentiation. J Nucl Med 29:1916 – 20

Chilton HM, Brown ML (1990) Radiopharmaceuticals for abdominal and gastrointestinal imaging: reticuloendothelial, hepatobiliary, and intestinal. In: Swanson DP, Chilton HM, Thrall JH (eds) Pharmaceuticals in medical imaging. Macmillan Publishing Co., New York, pp 462 – 500

Civelek AC, Sitzmann JV, Chin BB, Venbrux A, Wagner HN, Jr., Grochow LB (1993) Misperfusion of the liver during hepatic artery infusion chemotherapy: value of preoperative angiography and postoperative pump scintigraphy. AJR Am J Roentgenol 160:865 – 70

Davis LP, McCarroll K (1994) Correlative imaging of the liver and hepatobiliary system. Semin Nucl Med 24:208 – 18

Delbeke D, Martin WH, Sandler MP, Chapman WC, Wright JK, Jr., Pinson CW (1998) Evaluation of benign vs malignant hepatic lesions with positron emission tomography. Arch Surg 133:510 – 5

Delbeke D, Rose DM, Chapman WC, Pinson CW, Wright JK, Beauchamp RD, Shyr Y, Leach SD (1999) Optimal interpretation of FDG PET in the diagnosis, staging and management of pancreatic carcinoma. J Nucl Med 40:1784 – 91

Dickson AM (2005) The focal hepatic hot spot sign. Radiology 237:647 – 8

Diederichs CG, Staib L, Vogel J, Glasbrenner B, Glatting G, Brambs HJ, Beger HG, Reske SN (2000) Values and limitations of 18F-fluorodeoxyglucose-positron-emission tomography with preoperative evaluation of patients with pancreatic masses. Pancreas 20:109 – 16

Donckier V, Van Laethem JL, Goldman S, Van Gansbeke D, Feron P, Ickx B, Wikler D, Gelin M (2003) [F-18] fluorodeoxyglucose positron emission tomography as a tool for early recognition of incomplete tumor destruction after radiofrequency ablation for liver metastases. J Surg Oncol 84:215 – 23

Drane WE (1991) Nuclear medicine techniques for the liver and biliary system. Update for the 1990s. Radiol Clin North Am 29:1129 – 50

Drane WE (1998) Scintigraphic techniques for hepatic imaging. Update for 2000. Radiol Clin North Am 36:309 – 18

Drane WE, Krasicky GA, Johnson DA (1987) Radionuclide imaging of primary tumors and tumor-like conditions of the liver. Clin Nucl Med 12:569

Estrada WN, Zanzi I, Ward R, Negrin JA, Margouleff D (1991) Scintigraphic evaluation of postoperative complications of laparoscopic cholecystectomy. J Nucl Med 32:1910 – 1

Ezuddin S, Fragkaki C (2005) MIBG and FDG PET findings in a patient with malignant pheochromocytoma: a significant discrepancy. Clin Nucl Med 30:579 – 81

Fawcett HD, Sayle BA (1989) SPECT versus planar liver scintigraphy: is SPECT worth it? J Nucl Med 30:57 – 9

Fernandez FG, Drebin JA, Linehan DC, Dehdashti F, Siegel BA, Strasberg SM (2004) Five-year survival after resection of hepatic metastases from colorectal cancer in patients screened

by positron emission tomography with F-18 fluorodeoxyglucose (FDG-PET). Ann Surg 240:438 – 47
Fink-Bennett D (1991) Augmented cholescintigraphy: its role in detecting acute and chronic disorders of the hepatobiliary tree. Semin Nucl Med 21:128 – 39
Fink-Bennett D, Balon H, Robbins T, Tsai D (1991) Morphine-augmented cholescintigraphy: its efficacy in detecting acute cholecystitis. J Nucl Med 32:1231 – 3
Fritscher-Ravens A, Bohuslavizki KH, Broering DC, Jenicke L, Schafer H, Buchert R, Rogiers X, Clausen M (2001) FDG PET in the diagnosis of hilar cholangiocarcinoma. Nucl Med Commun 22:1277 – 85
Frohlich A, Diederichs CG, Staib L, Vogel J, Beger HG, Reske SN (1999) Detection of liver metastases from pancreatic cancer using FDG PET. J Nucl Med 40:250 – 5
Geslien GE, Pinsky SM, Poth RK, Johnson MC (1976) The sensitivity and specificity of 99mTc-sulfur colloid liver imaging in diffuse hepatocellular disease. Radiology 118:115 – 9
Ginsberg F, Slavin JD, Jr, Spencer RP (1986) Hepatic angiosarcoma: mimicking of angioma on three-phase technetium-99m red blood cell scintigraphy. J Nucl Med 27:1861 – 3
Hasegawa Y, Nakano S, Ibuka K, Hashizume T, Noguchi A, Sasaki Y, Imaoka S, Fujita M, Kawamoto S, Kasugai H (1986) Specific diagnosis of hepatocellular carcinoma by delayed hepatobiliary imaging. Cancer 57:230 – 6
Hauser MF, Alderson PO (1978) Gallium-67 imaging in abdominal disease. Semin Nucl Med 8:251 – 70
Hoefs JC, Sheikh MY, Guerrero H, Milne N (2005) Factors affecting the quantitative liver-spleen scan in normal individuals. Dig Dis Sci 50:283 – 9
Hustinx R (2004) PET imaging in assessing gastrointestinal tumors. Radiol Clin North Am 42:1123 – 39, ix
Ishak KG, Rabin L (1975) Benign tumors of the liver. Med Clin North Am 59:995 – 1013
Jacobsson H, Jonas E, Hellstrom PM, Larsson SA (2005) Different concentrations of various radiopharmaceuticals in the two main liver lobes: a preliminary study in clinical patients. J Gastroenterol 40:733 – 8
Jadvar H, Fischman AJ (2001) Evaluation of pancreatic carcinoma with FDG PET. Abdom Imaging 26:254 – 9
Kaltsas G, Rockall A, Papadogias D, Reznek R, Grossman AB (2004) Recent advances in radiological and radionuclide imaging and therapy of neuroendocrine tumours. Eur J Endocrinol 151:15 – 27
Kato T, Tsukamoto E, Kuge Y, Katoh C, Nambu T, Nobuta A, Kondo S, Asaka M, Tamaki N (2002) Clinical role of (18)F-FDG PET for initial staging of patients with extrahepatic bile duct cancer. Eur J Nucl Med Mol Imaging 29:1047 – 54
Khandani AH, Wahl RL (2005) Applications of PET in liver imaging. Radiol Clin North Am 43:849 – 60
Kim CK, Palestro CJ, Solomon RW, Molinari DS, Lee SO, Goldsmith SJ (1990) Delayed biliary-to-bowel transit in cholescintigraphy after cholecystokinin treatment. Radiology 176:553 – 6
Kim CK, Juweid M, Woda A, Rothstein RD, Alavi A (1993) Hepatobiliary scintigraphy: morphine-augmented versus delayed imaging in patients with suspected acute cholecystitis. J Nucl Med 34:506 – 9
Kim EE (1979) Focal splenic defect. Semin Nucl Med 9:320 – 1
Kim Y-J, Yun M, Woo JL, Kim KS, Lee JD (2003) Usefulness of 18F-FDG PET in intrahepatic cholangiocarcinoma. Eur J Nucl Med Mol Imaging 30:1467 – 72
Kinkel K, Lu Y, Both M, Warren RS, Thoeni RF (2002) Detection of hepatic metastases from cancers of the gastrointestinal tract by using noninvasive imaging methods (US, CT, MR imaging, PET): a meta-analysis. Radiology 224:748 – 56
Kluge R, Schmidt F, Caca K, Barthel H, Hesse S, Georgi P, Seese A, Huster D, Berr F (2001) Positron emission tomography with [(18)F]fluoro-2-deoxy-D-glucose for diagnosis and staging of bile duct cancer. Hepatology 33:1029 – 35
Koh T, Taniguchi H, Yamaguchi A, Kunishima S, Yamagishi H (2003) Differential diagnosis of gallbladder cancer using positron emission tomography with fluorine-18-labeled fluoro-deoxyglucose (FDG-PET). J Surg Oncol 84:74 – 81
Krishnamurthy S, Krishnamurthy GT (1996) Cholecystokinin and morphine pharmacologic intervention during Tc-99m HIDA cholescintigraphy: a rational approach. Semin Nucl Med 26:16 – 24
Krishnamurthy GT, Brown PH (2002) Comparison of fatty meal and intravenous cholecystokinin infusion for gallbladder ejection fraction. J Nucl Med 43:1603 – 10
Kudo M, Ikekubo K, Yamamoto K, et al. (1989) Distinction between hemangioma of the liver and hepatocellular carcinoma: value of labeled RBC-SPECT scanning. AJR Am J Roentgenol 152:977 – 83
Kurtaran A, Becherer A, Pfeffel F, Muller C, Traub T, Schmaljohann J, Kaserer K, Raderer M, Schima W, Dudczak R, Kletter K, Virgolini I (2000) 18F-fluorodeoxyglucose (FDG)-PET features of focal nodular hyperplasia (FNH) of the liver. Liver 20:487 – 90
Larson SM, Rasey JS, Allen DR, Nelson NJ, Grunbaum Z, Harp GD, Williams DL (1980) Common pathway for tumor cell uptake of gallium-67 and iron-59 via a transferrin receptor. J Natl Cancer Inst 64:41 – 53
Lee VW, O'Brien MJ, Devereux DF, Morris PM, Shapiro JH (1984) Hepatocellular carcinoma: uptake of 99mTc-IDA in primary tumor and metastasis. AJR Am J Roentgenol 143:57 – 61
Lee VW, O'Brien MJ, Morris PM, Devereux DF, Shapiro JH (1985) The specific diagnosis of hepatocellular carcinoma by scintigraphy. Multiple radiotracer approach. Cancer 56: 25 – 36
Lee C-H, Wang P-W, Lee T-T, Tiao M-M, Huang F-C, Chuang J-H (2000) The significance of functioning gallbladder visualization on hepatobiliary scintigraphy in infants with persistent jaundice. J Nucl Med 41:1209 – 13
Lin WY, Tsai SC, Hung GU (2005) Value of delayed 18F-FDG-PET imaging in the detection of hepatocellular carcinoma. Nucl Med Commun 26:315 – 21
Lisbona R, Rush CL, Derbekyan V, Novales-Diaz JA (1986) Radiocolloid liver imaging in hepatic steatosis. Clin Nucl Med 11:183 – 7
Lisbona R, Mishkin S, Derbekyan V, Novales-Diaz JA, Roy A, Sanders L (1988) Role of scintigraphy in focally abnormal sonograms of fatty livers. J Nucl Med 29:1050 – 6
Lomas F, Dibos PE, Wagner HN, Jr (1972) Increased specificity of liver scanning with the use of 67 gallium citrate. N Engl J Med 286:1323 – 9
Lubbers PR, Ros PR, Goodman ZD, Ishak KG (1987) Accumulation of technetium-99m sulfur colloid by hepatocellular adenoma: scintigraphic-pathologic correlation. AJR Am J Roentgenol 148:1105 – 8
Maisey NR, Webb A, Flux GD, Padhani A, Cunningham DC, Ott RJ, Norman A (2000) FDG-PET in the prediction of survival of patients with cancer of the pancreas: a pilot study. Br J Cancer 83:287 – 93
Majd M, Reba RC, Altman RP (1981) Effect of phenobarbital on 99mTc-IDA scintigraphy in the evaluation of neonatal jaundice. Semin Nucl Med 11:194 – 204
Massey MD, Stevens JS (1991) Residual spleen found on denatured red blood cell scan following negative colloid scans. J Nucl Med 32:2286 – 7
McClees EC, Gedgaudas-McClees RK (1984) Screening for diffuse and focal liver disease: the case for hepatic scintigraphy. J Clin Ultrasound 12:75 – 81
Meekin GK, Ziessman HA, Klappenbach RS (1987) Prognostic

value and pathophysiologic significance of the rim sign in cholescintigraphy. J Nucl Med 28:1679 – 82
Meindok H, Langer B (1976) Liver scan in Budd-Chiari syndrome. J Nucl Med 17:365 – 8
Middleton ML (1996) Scintigraphic evaluation of hepatic mass lesions: emphasis on hemangioma detection. Semin Nucl Med 26:4 – 15
Middleton ML, Milstein DM, Freeman LM (1994) Hepatic mass lesions: Scintigraphic update with emphasis on hemangioma detection. In: Freeman LM (ed) Nuclear medicine annual 1994. Raven Press, New York, pp 55 – 90
Muramatsu T, Miyamae T, Mashimo M, Suzuki K, Kinoshita S, Dohi Y (1994) Hot spots on liver scans associated with superior or inferior vena caval obstruction. Clin Nucl Med 19:622 – 9
Nakamoto Y, Higashi T, Sakahara H, Tamaki N, Kogire M, Imamura M, Konishi J (1999) Contribution of PET in the detection of liver metastases from pancreatic tumours. Clin Radiol 54:248 – 52
Nakamoto Y, Tatsumi M, Cohade C, Osman M, Marshall LT, Wahl RL (2003) Accuracy of image fusion of normal upper abdominal organs visualized with PET/CT. Eur J Nucl Med Mol Imaging 30:597 – 602
Nelson RC, Chezmar JL (1990) Diagnostic approach to hepatic hemangiomas. Radiology 176:11 – 3
Nishiyama Y, Yamamoto Y, Fukunaga K, Kimura N, Miki A, Sasakawa Y, Wakabayashi H, Satoh K, Ohkawa M (2006) Dual-time-point 18F-FDG PET for the evaluation of gallbladder carcinoma. J Nucl Med 47:633 – 8
Oates E, Austin JM, Becker JL (1995) Technetium-99m-sulfur colloid SPECT imaging in infants with suspected heterotaxy syndrome. J Nucl Med 36:1368 – 71
Osman MM, Cohade C, Nakamoto Y, Marshall LT, Leal JP, Wahl RL (2003) Clinically significant inaccurate localization of lesions with PET/CT: frequency in 300 patients. J Nucl Med 44:240 – 3
Papos M, Takacs T, Tron L, Farkas G, Ambrus E, Szakall S, Jr, Lonovics J, Csernay L, Pavics L (2002) The possible role of F-18 FDG positron emission tomography in the differential diagnosis of focal pancreatic lesions. Clin Nucl Med 27:197 – 201
Pashankar FD, O'Dorisio MS, Menda Y (2005) MIBG and somatostatin receptor analogs in children: current concepts on diagnostic and therapeutic use. J Nucl Med 46 Suppl 1:55S–61S
Patel PM, Alibazoglu H, Ali A, Fordham E, LaMonica G (1997) 'False-positive' uptake of FDG in a hepatic adenoma. Clin Nucl Med 22:490 – 1
Pfannenberg AC, Eschmann SM, Horger M, Lamberts R, Vonthein R, Claussen CD, Bares R (2003) Benefit of anatomical-functional image fusion in the diagnostic work-up of neuroendocrine neoplasms. Eur J Nucl Med Mol Imaging 30:835 – 43
Rabinowitz SA, McKusick KA, Strauss HW (1984) 99mTc red blood cell scintigraphy in evaluating focal liver lesions. AJR Am J Roentgenol 143:63 – 8
Rodriguez-Fernandez A, Gomez-Rio M, Llamas-Elvira JM, Ortega-Lozano S, Ferron-Orihuela JA, Ramia-Angel JM, Mansilla-Rosello A, Martinez-del-Valle MD, Ramos-Font C (2004) Positron-emission tomography with fluorine-18-fluoro-2-deoxy-D-glucose for gallbladder cancer diagnosis. Am J Surg 188:171 – 5
Rosenbaum SJ, Stergar H, Antoch G, Veit P, Bockisch A, Kuhl H (2006) Staging and follow-up of gastrointestinal tumors with PET/CT. Abdom Imaging 31:25 – 35
Royal HD, Brown ML, Drum DE, Nagle CE, Sylvester JM, Ziessman HA (2003) Society of Nuclear Medicine procedure guideline for hepatic and splenic imaging 3.0. Society of Nuclear Medicine Procedure Guidelines. Society of Nuclear Medicine
Rubin RA, Lichtenstein GR (1993) Hepatic scintigraphy in the evaluation of solitary solid liver masses. J Nucl Med 34: 697 – 705
Salem R, Lewandowski RJ, Atassi B, Gordon SC, Gates VL, Barakat O, Sergie Z, Wong C-YO, Thurston KG (2005) Treatment of unresectable hepatocellular carcinoma with use of ^{90}Y microspheres (TheraSphere): safety, tumor response, and survival. J Vasc Interv Radiol 16:1627 – 39
Saremi F, Jadvar H, Siegel ME (2002) Pharmacologic interventions in nuclear radiology: indications, imaging protocols, and clinical results. Radiographics 22:477 – 90
Sarikaya I, Yeung HW, Erdi Y, Larson SM (2003) Respiratory artefact causing malpositioning of liver dome lesion in right lower lung. Clin Nucl Med 28:943 – 4
Shreiner DP, Barlai-Kovach M (1981) Diagnosis of alcoholic cirrhosis with the right-to-left hepatic lobe ratio: concise communication. J Nucl Med 22:116 – 21
Shreve PD (1998) Focal fluorine-18 fluorodeoxyglucose accumulation in inflammatory pancreatic disease. Eur J Nucl Med 25:259 – 64
Smith R, Rosen JM, Gallo LN, Alderson PO (1985) Pericholecystic hepatic activity in cholescintigraphy. Radiology 156: 797 – 800
Sostre S, Kalloo AN, Spiegler EJ, Camargo EE, Wagner HN, Jr (1992) A noninvasive test of sphincter of Oddi dysfunction in postcholecystectomy patients: the scintigraphic score. J Nucl Med 33:1216 – 22
Sperti C, Pasquali C, Chierichetti F, Ferronato A, Decet G, Pedrazzoli S (2003) 18-Fluorodeoxyglucose positron emission tomography in predicting survival of patients with pancreatic carcinoma. J Gastrointest Surg 7:953 – 9
Sperti C, Pasquali C, Decet G, Chierichetti F, Liessi G, Pedrazzoli S (2005) F-18-fluorodeoxyglucose positron emission tomography in differentiating malignant from benign pancreatic cysts: a prospective study. J Gastrointest Surg 9:22 – 8
Suzuki T, Matsumoto Y, Manabe T, Honjo I, Hamamoto K (1974) Proceedings: Serum alpha-fetoprotein and Ga67 citrate uptake in hepatoma. AJR Am J Roentgenol 120:627 – 33
Tetalman MR, Kusumi R, Gaughran G, Baba N (1978) Radionuclide liver spots: indicator of liver disease or a blood flow phenomenon. AJR Am J Roentgenol 130:291 – 6
Thrall JH (1984) Hepatic arterial chemotherapy: pharmacokinetic rationale and radionuclide perfusion imaging. Nuclear Medicine Annual:211 – 26
Trerotola SO, Savader SJ, Lund GB, Venbrux AC, Sostre S, Lillemoe KD, Cameron JL, Osterman FA, Jr (1992) Biliary tract complications following laparoscopic cholecystectomy: imaging and intervention. Radiology 184:195 – 200
Trojan J, Schroeder O, Raedle J, Baum RP, Herrmann G, Jacobi V, Zeuzem S (1999) Fluorine-18 FDG positron emission tomography for imaging of hepatocellular carcinoma. Am J Gastroenterol 94:3314 – 9
Tsai CC, Yen TC, Tzen KY (2002) The value of Tc-99m red blood cell SPECT in differentiating giant cavernous hemangioma of the liver from other liver solid masses. Clin Nucl Med 27:578 – 81
Vogel SB, Drane WE, Ros PR, Kerns SR, Bland KI (1994) Prediction of surgical resectability in patients with hepatic colorectal metastases. Ann Surg 219:508 – 14
Waxman AD (1982) Scintigraphic evaluation of diffuse hepatic disease. Semin Nucl Med 12:75 – 88
Weissmann HS, Frank MS, Bernstein LH, Freeman LM (1979) Rapid and accurate diagnosis of acute cholecystitis with 99mTc-HIDA cholescintigraphy. AJR Am J Roentgenol 132: 523 – 8
Weissmann HS, Berkowitz D, Fox MS, Gliedman ML, Rosenblatt R, Sugarman LA, Freeman LM (1983a) The role of tech-

netium-99m iminodiacetic acid (IDA) cholescintigraphy in acute acalculous cholecystitis. Radiology 146:177 – 80
Weissmann HS, Byun KJ, Freeman LM (1983b) Role of Tc-99m IDA scintigraphy in the evaluation of hepatobiliary trauma. Semin Nucl Med 13:199 – 222
Welch TJ, Sheedy PF, Johnson CM, Stephens DH, Charboneau JW, Brown ML, May GR, Adson MA, McGill DB (1985) Focal nodular hyperplasia and hepatic adenoma: comparison of angiography, CT, US, and scintigraphy. Radiology 156: 593 – 5
Wiering B, Krabbe PFM, Jager GJ, Oyen WJG, Ruers TJM (2005) The impact of fluor-18-deoxyglucose-positron emission tomography in the management of colorectal liver metastases. Cancer:2658 – 70
Wistow BW, Subramanian G, Heertum RL, Henderson RW, Gagne GM, Hall RC, McAfee JG (1977) An evaluation of 99mTc-labeled hepatobiliary agents. J Nucl Med 18:455 – 61
Wudel LJ, Jr, Delbeke D, Morris D, Rice M, Washington MK, Shyr Y, Pinson CW, Chapman WC (2003) The role of [18F]fluorodeoxyglucose positron emission tomography imaging in the evaluation of hepatocellular carcinoma. Am Surg 69:117 – 24
Yammine JN, Yatim A, Barbari A (2003) Radionuclide imaging in thoracic splenosis and a review of the literature. Clin Nucl Med 28:121 – 3
Zeman RK, Lee CH, Stahl R, Viscomi GN, Baker C, Cahow CE, Dobbins J, Neumann R, Burrell MI (2006) Strategy for the use of biliary scintigraphy in non-iatrogenic biliary trauma. Radiology 151:771 – 7
Ziessman HA (1999) Cholecystokinin cholescintigraphy: victim of its own success? J Nucl Med 40:2038 – 42
Ziessman HA, Silverman PM, Patterson J, Harkness B, Fahey FH, Zeman RK, Keyes JW, Jr (1991) Improved detection of small cavernous hemangiomas of the liver with high-resolution three-headed SPECT. J Nucl Med 32:2086 – 91
Ziessman HA, Jones DA, Muenz LR, Agarval AK (2003) Cholecystokinin cholescintigraphy: methodology and normal values using a lactose-free fatty-meal food supplement. J Nucl Med 44:1263 – 6
Zuckier LS, DeNardo GL (1997) Trials and tribulations: oncological antibody imaging comes to the fore. Semin Nucl Med 27:10 – 29
Zuckier LS, Freeman LM (2003) Selective role of nuclear medicine in evaluating the acute abdomen. Radiol Clin North Am 41:1275 – 88

7 Kidney

A.T. Taylor

Radionuclide renal scintigraphy provides important functional data to assist in the diagnosis and management of patients with a variety of known or suspected diseases involving the kidney, ureters and bladder. Several different radiopharmaceuticals are available for radionuclide renography, multiple quantitative indexes can be generated, and protocols often vary depending on institutional preference and the clinical presentation. The nuclear medicine physician needs to obtain a clear understanding of the clinical question so that the renal study can be optimized to answer the clinician's question as clearly as possible.

7.1 Radiopharmaceuticals

The radiopharmaceuticals available for assessment of renal function and anatomy can be grouped into three broad categories: those excreted by glomerular filtration, those primarily excreted by tubular secretion, and those retained in the renal tubules for long periods of time.

7.1.1 Tc-99m DTPA (Glomerular Filtration)

Glomerular filtration is an important measure of renal function; each day the glomeruli filter about 160 liters of water and a kilogram of salt. Technetium-99m diethylene triamine pentaacetic acid (DTPA) is the only renal radiopharmaceutical available for routine imaging that is purely filtered by the glomerulus and can be used to measure glomerular filtration rate (GFR). In normal subjects, the extraction fraction of DTPA (the percentage of the tracer extracted with each pass through the kidney) is approximately 20 %; this extraction fraction is relatively low compared to the extraction fraction of tubular tracers (40 – 80 %) and this difference has important clinical implications particularly in selecting a radiopharmaceutical for patients with azotemia or suspected obstruction.

7.1.2 Cr-51 EDTA (Glomerular Filtration)

Cr-51 EDTA (ethylene diamine tetraacetic acid) is cleared by glomerular filtration and is used to measure GFR using plasma sample techniques (see "Clearances" below).

7.1.3 I-123 and I-131 OIH (Tubular Secretion)

I-123 and I-131 orthoiodohippurate (OIH) are cleared primarily by the proximal tubules although a small component is filtered by the glomeruli. The clearance of OIH is approximately 500 – 600 ml/min in subjects with normal kidneys; this clearance is often described as the effective renal plasma flow (ERPF) (Eshima and Taylor 1992). There is a common misconception that the ERPF (OIH clearance) is equivalent to renal plasma flow or, at least, proportional to renal plasma flow. The clearance of OIH is often proportional to renal plasma flow but OIH clearance (and the clearance of other Tc-99m tubular tracers) has two components: (1) the tracer must be delivered to the kidney (renal plasma flow) and (2) the tracer must be extracted from the plasma by the proximal tubules. These two components do not always change in a parallel fashion. The main disadvantages of I-131 OIH are the suboptimal imaging characteristics of many cameras for the high-energy 364-keV photon of I-131 and the I-131 beta emission which can result in radiation doses as high as 1 Sv (100 rem) to the kidneys of patients with impaired renal function (Marcus and Kuperus 1985; Stabin et al. 1992). For these reasons, I-131 OIH is not recommended for routine use. I-123 OIH is an excellent renal radiopharmaceutical, but it is limited by the logistics associated with the 13-h half-life of I-123 and lack of availability in many countries.

7.1.4 Tc-99m MAG3 (Tubular Secretion)

The clearance of Tc-99m mercaptoacetyltriglycine (MAG3) is highly correlated with the clearance of OIH

and the MAG3 clearance can be used as an independent measure of renal function. MAG3 is highly protein bound and is cleared almost exclusively by the proximal renal tubules (Bubeck et al. 1990; Eshima and Taylor 1992). The extraction fraction is 40 – 50 % (Schaap et al. 1988; Bubeck et al. 1990), more than twice that of DTPA. Because of its more efficient extraction, MAG3 is preferred over DTPA in patients with suspected obstruction and impaired renal function (Taylor et al. 1990; Al-Nahhas et al. 1988; Taylor et al. 1994; Taylor et al. 1987; O'Reilly et al. 1996; Gordon et al. 2000, 2001).

The MAG3 clearance averages about 300 ml/min/1.73 m^2 in adults under age 40 and tends to decrease at a rate of about 3 – 4 ml/year after age 40 (Russell et al. 1996). The clearance of MAG3 is only 50 – 60 % that of OIH but MAG3 is more highly protein bound than OIH and tends to remain in the intravascular compartment; for this reason, blood pool activity in the heart, spleen and liver are often prominent on the early images, especially in patients with impaired function. Moreover, in contrast to OIH, MAG3 does not enter the red cells to any significant degree (Eshima and Taylor 1992; Bubeck et al. 1990; Russell et al. 1988). For these two reasons, a greater proportion of MAG3 remains in the plasma, and the increased plasma concentration compensates for the lower extraction fraction so that MAG3 is excreted from the body at essentially the same rate as OIH. Because of the similar rates of excretion, the renogram curves of MAG3 and OIH are almost identical.

The reproducibility of the MAG3 clearance has been a focus of debate. MAG3 clearance measurements based on blood samples have shown mixed results (Piepsz et al. 1988; Kotzerke et al. 1997; Kanazawa et al. 1998); however, in one study of a large series of patients, the coefficient of variation was only 8.5 %, which is certainly adequate for most clinical uses (Russell and Dubovsky 1999). Although plasma sample techniques are considered to have greater accuracy than camera based clearance measurements (Blaufox et al. 1996), clearances that rely on blood samples have sources of error (timing of plasma samples, correction for radioactive decay, dilution of standards, pipetting errors) that are largely avoided by camera based techniques (see below for a discussion of clearances). Camera-based clearances appear to be reproducible and superior to the creatinine clearance for monitoring changes in renal function (Klingensmith et al. 1994; Russell and Dubovsky 1999; Taylor et al. 1999; Halkar et al. 2007).

In normal subjects, approximately 0.5 % of the injected dose of MAG3 accumulates in the gallbladder by 30 – 60 min post-injection and 1 % of the dose is present in the GI tract by 3 h (Taylor et al. 1988). Elimination of MAG3 via the gallbladder can increase when patients have impaired renal function and it can be accentuated by kit impurities (Taylor et al. 1988; Shattuck et al. 1994). The gallbladder is not a problem on early images but on very rare occasions can simulate pelvic or calyceal activity on delayed images; if this question arises, it can be resolved by a lateral image. Bowel activity can also be observed and can present a problem in interpretation if delayed images are obtained to search for a urine leak (Taylor et al. 1999).

7.1.5 Tc-99m L,L and D,D-EC (Tubular Secretion)

Tc-99m L,L- and D,D-ethylenedicysteine (EC) are both excellent renal radiopharmaceuticals with clearances slightly higher than MAG3 (Van Nerom et al. 1993; Kabasakal et al. 1995; Taylor et al. 1997a). LL-EC is available in several countries as a kit formulation and is clinically comparable to MAG3.

7.1.6 Tc-99m DMSA (Cortical Retention)

Tc-99m DMSA (dimercaptosuccinic acid) is an excellent cortical imaging agent. Approximately 40 % of the injected dose binds to the renal tubules within 1 h after injection; the remainder is slowly excreted in the urine over the subsequent 24 h. DMSA is used when high resolution anatomic images are required, such as the detection of pyelonephritis. Cortical scans can also confirm a suspected column of Bertin, measure relative function and identify functioning renal tissue in patients with congenital abnormalities.

7.1.7 Tc-99m GH (Cortical Retention and GFR)

Tc-99m GH (glucoheptonate) is cleared both by GFR and the renal tubules. In patients with normal renal function, most of the dose is rapidly excreted; however, 10 – 15 % of the injected dose remains bound to the renal tubules and high resolution delayed static images can be obtained. GH tends to be used when DMSA is unavailable. It should not be used to evaluate suspected renal obstruction.

7.1.8 Tc-99m MDP (GFR)

Tc-99m MDP (methylenediphosphonate) is not usually considered a renal imaging agent; however, it is cleared by GFR and measurements of relative renal uptake (relative GFR) can be obtained at the time of a bone scan injection using standard renal software.

7.2 Technical Issues and Quality Control

7.2.1 Patient Information

Adequate patient information is not always provided. A simple and focused questionnaire given to the patient on arrival in the department can generate useful information to help the nuclear medicine physician place the scan results in an appropriate clinical context. A simple targeted questionnaire could ask for current medications, a description of any kidney abnormality, renal function if known, and any history of heart disease, diabetes, atherosclerosis, hypertension, kidney infection, renal trauma, renal surgery or prior radiation therapy to the area of the kidney.

7.2.2 Hydration

For routine renography, patients should be well hydrated. Dehydration can lead to calyceal or pelvic retention and prolong the excretory phase of the renogram curve. Outpatients should be instructed to drink plenty of fluids prior to coming for the test and the nursing staff should be requested to hydrate inpatients. To facilitate hydration, patients can also be given 5–10 ml of water/kg immediately on arrival in the nuclear medicine department, preferably 30–60 min before the exam. If a two stage ACEI examination is scheduled, it is important to continue hydration between the studies. Despite these efforts, hydration may still be suboptimal (Lindh et al. 1998). The state of hydration can be evaluated when the patient arrives by collecting a urine sample and measuring the specific gravity. A specific gravity greater than 1.015 suggests dehydration.

7.2.3 Image Over the Injection Site

If part of the dose is infiltrated, the effect is variable depending on the rapidity of reabsorption of the infiltrated dose; however, single sample clearances are apt to be incorrect and the excretory phase of the renogram

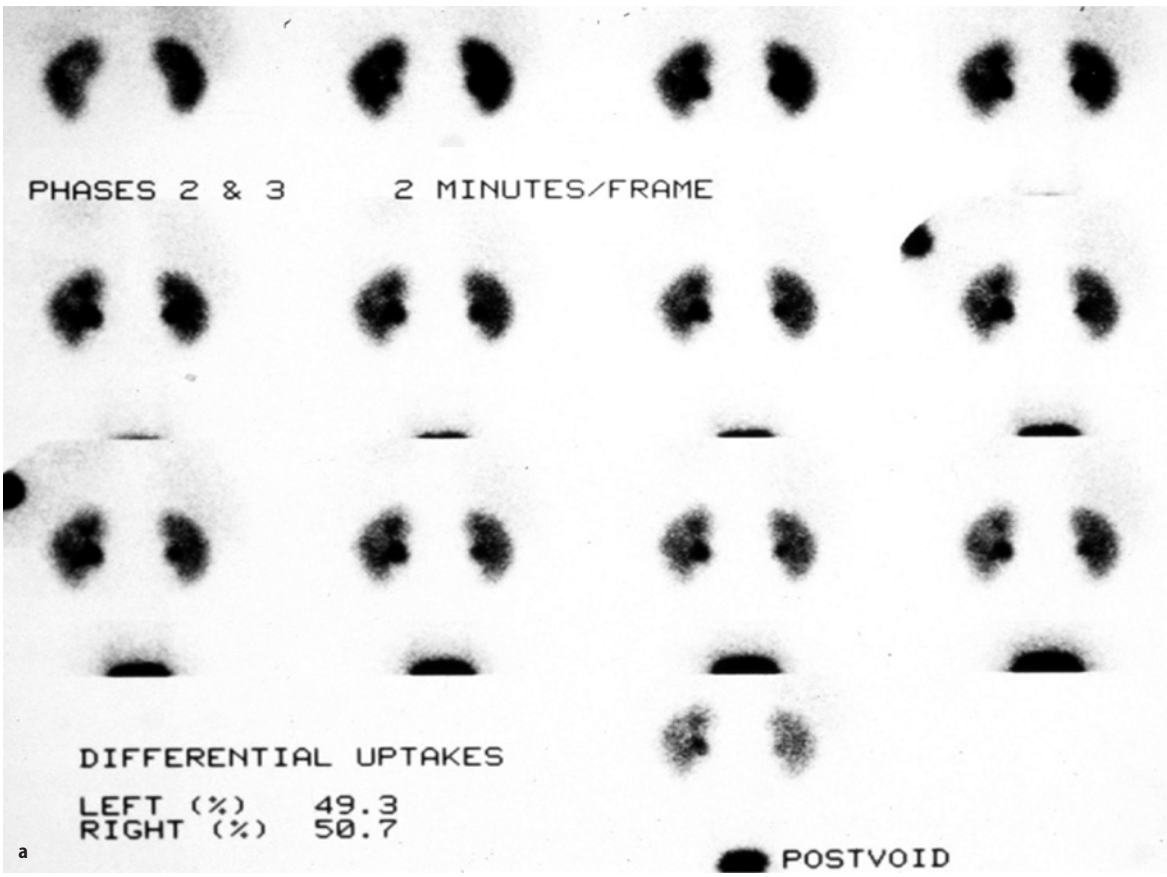

Fig. 7.1. a Two-minute sequential renal images and a post-void image were obtained following the intravenous injection of approximately 370 MBq of MAG3. There is marked infiltration of the dose noted in the left arm at 16–18 and 18–20 min post-injection. The software estimated that 18% of the dose was infiltrated based on dividing the counts in the site of infiltration at the completion of the study by the counts injected.

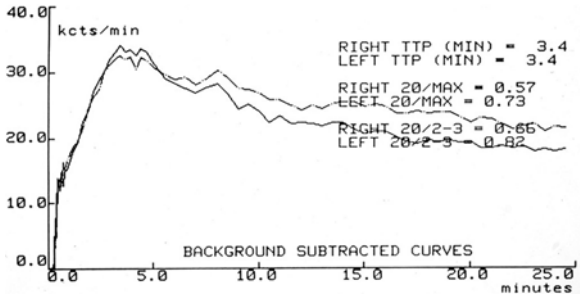

Fig. 7.1. b The renogram curves appear to show slow washout of the tracer with cortical 20 min/maximum count ratios of 0.57 and 0.73 (normal is less than 0.35). The apparent slow washout was due to the gradual absorption of infiltrated MAG3. A repeat study was normal

curve may be prolonged (Slavin et al. 1996) (Fig. 7.1). A spurious increase in the grade of the renogram curve from 0–2 or 1–2 grades (Fig. 7.2) due to infiltration could result in an erroneous interpretation of an ACEI renogram (see below). A quantitative estimate of infiltration can be obtained if the decay corrected counts in the injection site are divided by the injected counts. If the infiltration exceeds 0.5%, plasma sample clearances may be erroneous and caution should be exercised before reporting the value. Infiltration can also be evaluated qualitatively by imaging the injection site. Finally, the likelihood of infiltration appears to be reduced if the radiopharmaceutical is injected through a small indwelling catheter versus direct venipuncture.

7.2.4 Minimizing the Radiation Dose to the Patient

The patient should always be instructed to void at the conclusion of the study. In normal well-hydrated subjects, approximately 70% of the injected dose of OIH and MAG3 reaches the bladder by 30 min post-injection (Taylor et al. 1988). Although the radiation dose from MAG3 and DTPA is low (Table 7.1), emptying the bladder at the conclusion of a MAG3 study can reduce the radiation dose to the whole body, bladder and ovaries by more than 50% compared to voiding 4 h after tracer injection (Stabin et al. 1992).

Table 7.1. Radiation dose estimates for Tc-99m DTPA and MAG3[a]. Bladder voided at 30 min, then at 4 h, then every 4 h thereafter

Organ	DTPA mSv	(rem)	MAG3 mSv	(rem)
Kidneys	0.14	(0.014)	0.14	(0.014)
Ovaries	0.13	(0.013)	0.086	(0.009)
Red marrow	0.045	(0.005)	0.018	(0.002)
Bone surfaces	0.068	(0.007)	0.025	(0.003)
Testes	0.088	(0.009)	0.050	(0.006)
Urinary bladder wall	1.9	(0.19)	1.7	(0.17)
Uterus	0.24	(0.024)	0.109	(0.011)
Total body	0.049	(0.005)	0.024	(0.002)
Effective dose equivalent	0.20	(0.020)	0.15	(0.015)

[a] 37 MBq (1 mCi) of Tc-99m DTPA or MAG3

7.2.5 Postvoid Images of the Kidneys

A postvoid image of the kidneys can be a useful adjunct to the standard renogram and can be particularly useful in evaluating the adult and pediatric patient with suspected obstruction. This image should be obtained after the adult patient has assumed an upright position to void or after an infant has been held in an upright position for about 5 min so that gravity can assist drainage of any residual stasis related to the patient's supine position (Donoso et al. 2003; Wong et al. 2000; Piepsz et al. 2002; Gordon et al. 2001; Anderson et al. 1997; Frokier et al. 2006).

7.3 Quantitative Measurements

7.3.1 Relative Uptake

The relative renal uptake of each radiopharmaceutical provides a measure of relative function and is an important parameter in the interpretation of most studies. The measurement is usually made in the 1–2, 1–2.5 or 2–3 min period post-injection for DTPA, MAG3, and OIH and needs to be completed prior to any drainage from the renal pelvis. Background subtraction using a C-shaped, elliptical or perirenal region of interest appears to be superior to no background or inferior background regions of interest (Taylor et al. 1994a; Prigent et al. 1999; Peters et al. 1988) and an automated background subtraction probably improves reproducibility (Halkar et al. 1996). Differences in the renal depth of the two kidneys can affect the relative uptake due to differences in attenuation but this is rarely a clinically important problem. In a recent study where renal depth was determined by CT in 201 patients without abdominal pathology, the average difference in renal depth between the two kidneys was 0.61 cm. If the two kidneys have equal function, lie at a depth of 7 cm and the effective attenuation coefficient is 0.12, a 0.6 cm difference in renal depth would change the relative uptake from 50/50 to 52/48. The difference in renal depth was less than 2.0 cm in 99% of the patients and a difference in 2.0 cm would change the relative uptake from 50/50 to 56/44. A recent study using MAG3 with automated C-shaped perirenal background regions of interest to measure relative function in 106 potential renal donors showed that all values were $\geq 40\%$ and $\leq 60\%$ (Esteves et al. 2006).

7.3.2
Whole Kidney Versus Cortical Regions of Interest

The whole kidney region of interest (ROI) consists of an ROI placed around the whole kidney including the renal pelvis. Quantitative values generated using this ROI will be affected by retention of tracer in the kidney and collecting system; retention may be due to pathological states such as diabetic nephropathy or obstruction or may occur in non-pathological states such as a non-obstructed dilated collecting system or mild dehydration. To obtain a better assessment of parenchymal function, cortical or parenchymal regions of interest may be assigned over the renal cortex (parenchyma) that exclude any activity retained in the pelvis or calyces. Cortical regions of interest often provide a better assessment of renal function but have reduced counts compared to whole kidney ROIs and are more susceptible to artifact due to motion or reduced counts in a poorly functioning kidney.

7.3.3
Time to Peak Height

The time to the peak height (T_{max}) of the renogram curve is a useful measurement, particularly in the evaluation of patients with suspected renovascular hypertension (see below). In general, the peak should occur by 5 min after injection, but retention of the radiopharmaceutical in the renal calyces or pelvis can alter the shape of the renogram and affect the T_{max} measurement.

7.3.4
20 Min/Max Count Ratios

As renal function deteriorates, there is often a flattening of the renogram curve with a prolonged time to peak and delayed washout (Fig. 7.2). The degree of abnormality can be quantitated by a measurement of residual cortical activity using the ratio of the counts at 20 or 30 min to the maximum (peak) counts. These or similar ratios may also prove to be useful in monitoring patients with suspected urinary tract obstruction or renovascular hypertension (Piepsz et al. 2000; Anderson et al. 1997; Taylor et al. 1996; Blaufox et al. 1998). Using background subtracted parenchymal regions of interest (activity within the collecting system excluded from the ROI), the 20 min/max count ratio in a series of potential renal donors studied with MAG3 was 0.19 ± 0.07 for the right kidney and 0.19 ± 0.04 for the left kidney (Esteves et al. 2006). If the patient is not dehydrated and the 20 min/max count ratio for the cortical ROI exceeds 0.35 (greater than 2 standard deviations above the mean), the kidney is likely to be abnormal.

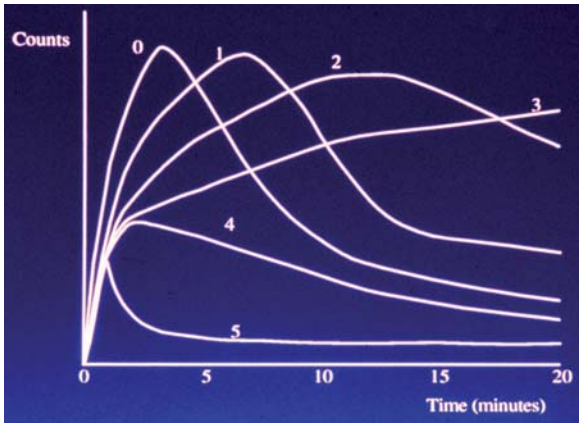

Fig. 7.2. Common renogram patterns used for the visual interpretation of ACEI renography. *Type 0:* normal. *Type 1:* time to peak (T_{max}) is >5 min and 20 min/max count ratio is >0.3 for background subtracted OIH and MAG_3 curves. *Type 2:* There are more exaggerated delays in time to peak and in parenchymal washout. *Type 3:* Progressive parenchymal accumulation (no washout detected). *Type 4:* Renal failure pattern, but with measurable renal uptake. *Type 5:* Renal failure pattern, representing blood background activity only

7.3.5
Prevoid/Maximum, Postvoid/Maximum, Prevoid/1 – 2 Min and Postvoid/1 – 2 Min Count Ratios

These simple indices correlate with the more computational intensive measurement of output efficiency to evaluate obstruction and can provide a useful adjunct to the interpretation of diuresis renography (Chaiwatanarat et al. 1993; Piepsz et al. 2002; Donoso et al. 2003). They can be easily derived from the renogram curve and/or a post-void image of the kidneys; the post-void image should be obtained after the patient assumes an upright posture so that gravity can assist drainage from the collecting system. Infants should be held in an erect position for 5 min before the post-void image is obtained.

7.3.6
Residual Urine Volume

The patient population referred for renography often includes older males and patients with diabetes. Patients with prostatic hypertrophy may have substantial post-void residuals and patients with diabetes may present with a diabetic cystopathy, bladder distention and an increased risk of reflux and pyelonephritis. Residual urine volume can be measured based on the counts in pre- and post-void ROIs over the bladder and a measurement of the voided volume (Strauss and Blaufox 1970). Calculation of residual urine volume is a routine measurement at some institutions and can provide additional information for the referring clinician.

7.4 Renal Function

An assessment of renal function is often a critical element in the management of patients with renal disease. The most common measure of renal function in clinical practice is the serum creatinine and it can be used to estimate the GFR; however, a number of factors (muscle mass, diet, age, certain drugs, illness, tubular secretion) can affect the serum creatinine and the serum creatinine is not a sensitive measurement for detecting early renal disease (Levey et al. 1991; Manjunath et al. 2001). In fact, there is a wide range of values for serum creatinine for all levels of GFR and the serum creatinine can remain within the normal range despite a GFR 60 – 80 % below normal (Levey et al. 1991). The creatinine clearance provides a more sensitive method for monitoring renal function but formal measurement of creatinine clearance with blood and 24-h urine samples is cumbersome, inconvenient for patients and often unreliable (Rosenbaum 1970; Brown and O'Reilly 1995). Moreover, repeated measurements of creatinine clearance in stable patients have been shown to have a disappointingly high 25 % coefficient of variation (standard deviation/mean) (Brochner-Mortensen and Rodbro 1974).

Measurement of renal function at the time of the scan can aid in the interpretation of a radionuclide study and provide a baseline for monitoring changes. From a clinical point of view, it is often more important to know if the renal function is stable, improving or deteriorating than to know a precise clearance measurement; depending on the clinical question, reproducibility may be much more important than accuracy. A DTPA scan can be combined with a measurement of GFR, an OIH scan can be combined with a measurement of ERPF and a MAG3 scan can be combined with a measurement of the MAG3 clearance. Since the MAG3 and OIH clearances are highly correlated over a wide range of renal function, some institutions use a conversion factor to convert the MAG3 clearance into an OIH equivalent. The two most widely used techniques to measure clearances are plasma sample and camera based techniques.

7.4.1 Plasma Sample Clearances

The clearances of OIH and MAG3 can be estimated from the dose injected and the amount of radioactivity in a single blood sample obtained approximately 45 min after injection (Russell et al. 1996; Bubeck 1993; Blaufox et al. 1996). Since DTPA is cleared more slowly than OIH or MAG3, its clearance (GFR) must be estimated from the dose injected and the activity in one or more plasma samples obtained 1 – 4 h after injection (Blaufox et al. 1996; Russell 1993). If carefully performed, clearance measurements based on plasma samples are more accurate than camera-based clearances, but plasma sample clearances require meticulous technique and attention to detail. Standards must be accurately prepared, dilutions carefully made, and the Tc-99m samples corrected for decay. In addition, the time of injection and the time of drawing the blood must be accurately recorded, and plasma samples must be carefully obtained without contamination by saline, heparin, or plasma from an earlier time. If the measurement is performed by a poorly trained or inexperienced individual, technical errors are often made and the results are spurious. The Radionuclides in Nephrourology Consensus Report provides specific details regarding the recommended methodology for plasma sample clearances (Blaufox et al. 1996).

7.4.2 Camera Based Clearances

With nuclear medicine evolving toward increasing camera and computer sophistication and with pressures to increase the procedure volume, many technologists and physicians no longer have adequate training and/or time to obtain reliable plasma sample clearances. To address this need, camera clearance methods that do not require blood samples have been developed for DTPA, OIH and MAG3 (Schlegel and Hamway 1976; Gates 1982; Taylor et al. 1997b; Inoue et al. 1999). Camera based approaches to measure the renal uptake of DTPA, OIH and MAG3 have been reviewed in a recent consensus report (Prigent et al. 1999). The integral method has an accuracy comparable to the other camera based methods, is simpler to perform (Prigent et al. 1999; Bocher 2001) and requires a measurement of the injected counts and counts in the kidney in an interval from 1 – 2, 1 – 2.5 or 2 – 3 min post-injection.

The methodology is illustrated by a current camera-based approach to calculate the MAG3 clearance; briefly, processing software determines the percent injected dose in each kidney from 1 – 2.5 min post-injection and uses an algorithm derived from a multi-center trial to convert the sum of the percent injected dose in the left and right kidneys to a global MAG3 clearance (ml/min/1.73 m^2) (Taylor et al. 1995; Taylor et al. 1997b). The pre-injection and post-injection syringes containing the 37 – 74 MBq (1 – 2 mCi) dose are counted on the camera; counts in the post-injection syringe are corrected for decay and subtracted from the counts in the pre-injection syringe to determine counts injected. To obtain percent injected dose in each kidney, kidney counts from 1 – 2.5 min post-injection are corrected for background, infiltration, attenuation and renal depth and divided by the counts injected. If a larger dose such as 370 MBq (10 mCi) is to be given, there is a risk of

dead time losses if the syringe containing 370 MBq is counted on the camera. The injected counts can be determined without dead time losses by use of an attenuator (Bocher et al. 2001) or by counting a small dose (37 MBq) on the camera and multiplying the counts in the small dose by the ratio of the injected dose to the small dose, both measured in a dose calibrator.

Not surprisingly, camera clearance methods have problems of their own. Two common sources of error are the estimation of renal depth for attenuation correction and background subtraction. In regard to background subtraction errors, OIH and MAG3 have an inherent advantage over DTPA because they are extracted more than twice as efficiently as DTPA. Because of the more efficient extraction, the kidney to background ratio is much higher for OIH and MAG3 than DTPA and any potential error introduced by over- or under-subtraction of background is substantially reduced. Renal depth is usually estimated from a nomogram based on height and weight (Tonnesen et al. 1974; Taylor et al. 1993). To the degree that a population derived nomogram fails to fit a particular individual, the clearance measurement will vary from the true clearance. An alternative approach is to measure the renal depth based on a lateral image but this requires extra steps, and defining an accurate renal outline on a lateral view 30 min following the injection of OIH or MAG3 can be problematic, particularly in patients with good renal function. The sources of error due to background, self attenuation and renal depth tend to be reflected in a wider confidence interval associated with the accuracy of camera-based clearance compared to plasma sample clearances.

Commercial camera-based techniques are currently available for measuring GFR (DTPA), effective renal plasma flow (OIH) and the MAG3 clearance. In evaluating commercial software, it is important to confirm that the vendor has (1) incorporated the appropriate quality control features (a check for dose infiltration, avoidance of dead time loses, preferably automated and reproducible peri-renal background regions of interest, and a standardized time zero that is constant between studies) and (2) provided citable validation studies to confirm that there have been no coding errors and that the software is performing as claimed.

7.5 Renal Transplantation

Renal transplantation is the preferred treatment for end-stage renal disease but the use of renal scintigraphy to evaluate the potential donor and the transplant recipient varies from center to center. Some centers use a renal scan to screen potential donors to ensure that both kidneys are functioning normally; other centers rely primarily on other imaging procedures. A normal renal scan in the immediate post-transplant period reliably excludes clinically important complications such as vascular occlusion, urine leak and obstruction (Dubovsky et al. 1999). In cadaveric transplants, a scan in the immediate postoperative period can assess the presence of acute transplant nephropathy (ATN, acute tubular necrosis), which is related to ischemic damage that occurs before the donor's death and/or during the preservation period prior to transplantation. The kidney with ATN typically shows relatively preserved perfusion with reduced function but perfusion can be also decreased in severe cases; the functional impairment usually resolves without therapy (Dubovsky et al. 1999).

Scan interpretation requires knowledge of the clinical course and a review of prior scans, if available. Sequential scans with monitoring of renal function can identify early graft failure and ACEI renography can detect renovascular hypertension as a late cause of deteriorating renal function; however, an isolated scan demonstrating prolonged transit and reduced function cannot reliably distinguish between rejection, ATN or calcineurin-inhibitor (cyclosporine and tacrolimus) toxicity (Dubovsky and Russell 1991; Dubovsky et al. 1999). Chronic transplant nephropathy represents cumulative and incremental damage to nephrons from both immunologic and non-immunologic causes; calcineurin-inhibitor nephrotoxicity appears to be the chief cause of late histologic injury associated with a continuing decline in renal function (Nankivell et al. 2003). When transplant patients present with a decline in renal function, imaging studies are obtained if the clinician suspects complications relating to renal blood flow, urine leak, urinoma, obstruction, abscess, hematoma or lymphoma whereas renal biopsy is usually obtained to distinguish between rejection and calcineurin-inhibitor nephrotoxicity.

7.6 Diuresis Renography

Obstruction to urinary outflow may lead to obstructive uropathy (dilatation of the calices, pelvis or ureters) and obstructive nephropathy (damage to the kidney itself). Urine outflow obstruction may be suspected based on clinical findings, the incidental detection of a dilated renal collecting system, or diagnosis of previous obstruction in a patient referred for follow-up. Diuresis renography is the only widely available study that can evaluate renal function and urodynamics in a single test. This noninvasive test is based on a high endogenous rate of urine flow stimulated by the administration of furosemide. Interpretation of the test is based on the rate of washout of the radiopharmaceutical from the collecting system in the upper urinary tract.

7.6.1 Technical Issues Relating to Diuresis Renography

7.6.1.1 Pre-test Voiding

The patient should void immediately prior to the examination. A full bladder may affect upper tract emptying and give false positive results (O'Reilly et al. 1996; Hvistendahl et al. 1998).

7.6.1.2 Choice of Radiopharmaceutical

A recent International Consensus Committee on Diuresis Renography concluded that MAG3 is "the current agent of choice" and that DTPA "is not recommended for diuresis renography" (O'Reilly et al. 1996). The Pediatric Committee of the EANM also recommended tubular agents over DTPA (Gordon et al. 2000, 2001) because of the fact that MAG3, EC and OIH are much more efficiently extracted by the kidney than DTPA. Tubular agents such as MAG3 are particularly useful in infants and patients with impaired renal function (Fig. 7.3) (Taylor et al. 1994b).

7.6.1.3 Hydration

Intravenous hydration should be considered if the recommendations for oral hydration under "Technical Issues and Quality Control" have been followed and the urine specific gravity remains high (>0.015). An infusion of 0.9% sodium chloride administered at a rate of 360 ml/m^2 over 30 min before the scintigraphic study may reduce the number of false positive or indeterminate studies (Howman-Giles et al. 1987). Infants should be given water or formula ad libitum beginning 2 h before the study (Members of Fetal Urology 1992). Some experts also recommend that infants receive an IV infusion of diluted normal saline (D5, 0.3 or 0.25% saline) given at a rate of 15 ml/min over 30 min, beginning 15 min before the injection of furosemide although the necessity of this approach in all cases has been questioned and aggressive oral hydration is probably sufficient in the majority of patients (O'Reilly et al. 1996; Members et al. 1992; Gordon et al. 2001).

7.6.1.4 Timing of Furosemide Administration

Multiple protocols have been used for diuretic renography; they differ in the timing of furosemide and in the use of one or two acquisitions. The 1996 Santa Fe Consensus Report recommended that the time of furosemide be specified; typical times for furosemide administration are the F–15, F=0 and F+20 protocols where the furosemide is administered 15 min before, simultaneously with or 20 min after the tracer administration. The Consensus Report recommended a 35-min acquisition with furosemide administered 20 min into the

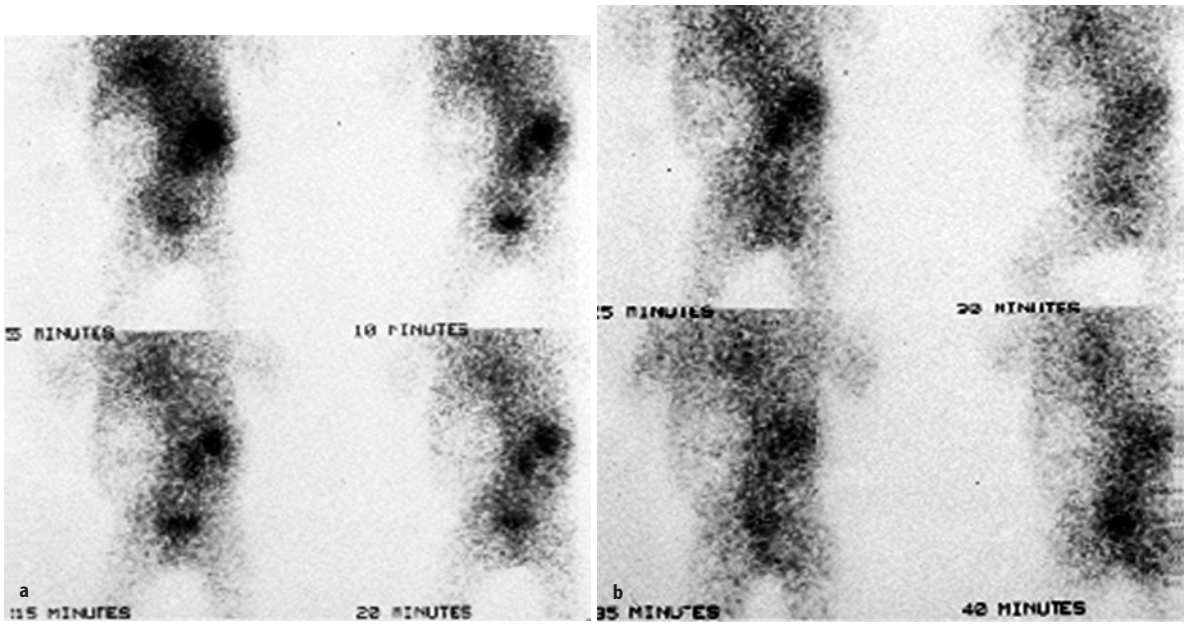

Fig. 7.3. A 3-day-old female infant underwent ultrasonography at age 3 days because of a rising creatinine. Renal ultrasonography showed a large, multicystic, dysplastic left kidney and marked dysplastic changes, peripheral cysts and mild hydronephrosis of the right kidney with a dilated right ureter. Voiding cystoureterography showed no evidence of reflux. A Tc-99m DTPA scan (74 MBq) was obtained 4 days after birth. Sequential 5-min images for 20 min are displayed in **a**. The patient received 1 mg of furosemide and sequential 5-min images from 25–40 min are shown in **b**.

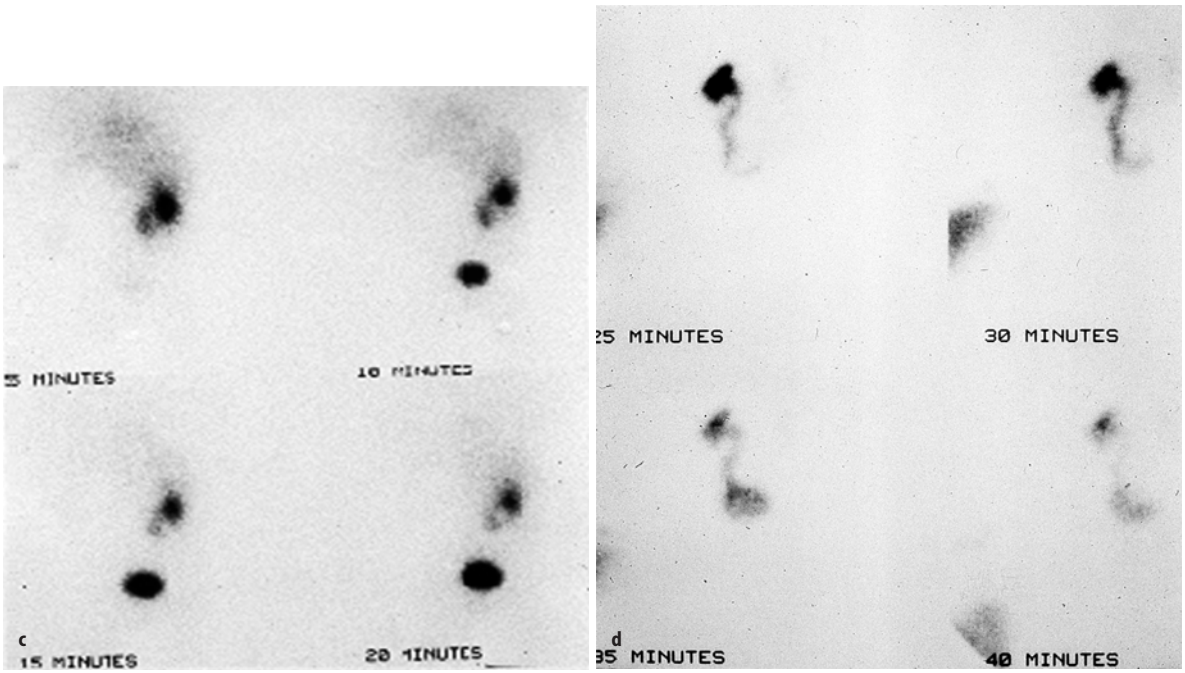

Fig. 7.3 (*Cont.*) There is poor kidney definition and the study was repeated with 74 MBq of Tc-99m MAG3 3 days later. Sequential 5-min images for 20 min are displayed in **c.** Furosemide was administered and sequential 5-min images from 25 – 40 min are shown in **d.** The MAG3 is already in the renal pelvis and upper ureter by 5 min; there is an excellent kidney to background ratio and the tracer washes out rapidly following furosemide thus excluding obstruction. The higher extraction fraction of MAG3 contributed to the superior image quality and led to greater diagnostic certainty. (Reproduced with permission, Taylor et al. 1994b)

study (O'Reilly 1996). A disadvantage of this protocol is that a percentage of patients (30 % in one series) will not complete the acquisition because of a need to void (Liu et al. 2005). The study can be divided into two separate acquisitions, a 20 – 25 min baseline acquisition followed by patient voiding and then a second 15 – 20 min acquisition concurrently with furosemide administration. If the baseline study is normal, obstruction can be excluded and the furosemide acquisition can be omitted (Kuyvenhoven et al. 2003). Since the test is based on the washout of the tracer from the collecting system, some physicians want to see retention of the radiopharmaceutical clearly visible in the collecting system (calyces, pelvis or ureters) at the time of furosemide administration. If there is no radiopharmaceutical retention in the collecting system, the activity entering the kidney from the blood may largely replace the activity leaving the kidney, resulting in a prolonged $T_{½}$ even if the kidney is completely normal. All three protocols are acceptable and appear to give comparable results in the majority of patients (Adeyoju et al. 2001; Wong et al. 1999).

7.6.1.5 Patient Position

Imaging is usually performed with the patient supine. The supine position allows a more accurate estimate of relative renal function since the kidneys are more likely to lie at the same depth. If the patient is initially imaged in a sitting or reclining position, one of the kidneys may change position leading to a difference in relative uptake which is due to differences in attenuation rather than differences in relative function. Gravity assisted drainage is important for the interpretation of selected studies, and routine acquisition of post-void images (see below) is a recommended component of the acquisition protocol (Gordon et al. 2000, 2001; Frokier et al. 2006).

7.6.1.6 Postvoid Images

If a large proportion of the radiopharmaceutical remains in the collecting system at the end of the study, the patient should be asked to get off the table, stand up, go to the toilet and void. After the patient voids, an additional image of the kidney is obtained after the patient returns to the supine position to maintain a consistent geometry; measurements to quantitate postvoid emptying or gravity assisted drainage may facili-

tate interpretation of the study (Wong et al. 2000; Piepsz et al. 2002; Adeyoju et al. 2001). Infants should be held in an upright position for about 5 min to allow gravity to assist drainage and then another image of the kidney should be obtained (Wong et al. 2000; Gordon 2001). If the post-void image is obtained with the patient upright, a ptotic kidney may give a false impression of adequate emptying. Prompt drainage of radiopharmaceutical from the collecting system excludes obstruction and obviates administration of furosemide in a dual acquisition protocol (Fig. 7.4). A second advantage of having the patient void prior to administering furosemide is simply to empty the bladder; a full bladder can slow drainage from the upper urinary tract. In adults or infants who cannot empty their bladders, use of a catheter will minimize false-positive or indeterminate findings.

7.6.1.7 Dose of Furosemide

The recommended dose of furosemide is 0.5 mg/kg or 40 mg in an adult and 1.0 mg/kg in a child with a maximum dose of 20 mg (Members et al. 1992; O'Reilly et al. 1996; Gordon et al. 2001). Furosemide is secreted by the proximal tubule and reaches its site of action in the tubular lumen of the thick ascending loop of Henle via the tubular fluid. In patients with impaired renal function, secretion of furosemide is proportionally reduced because of the underlying kidney disease; in addition, endogenous organic acids accumulate in chronic renal insufficiency and competitively inhibit the organic transport system of the proximal tubule further reducing the secretion of furosemide. To counteract these effects, a larger dose of furosemide must often be given to

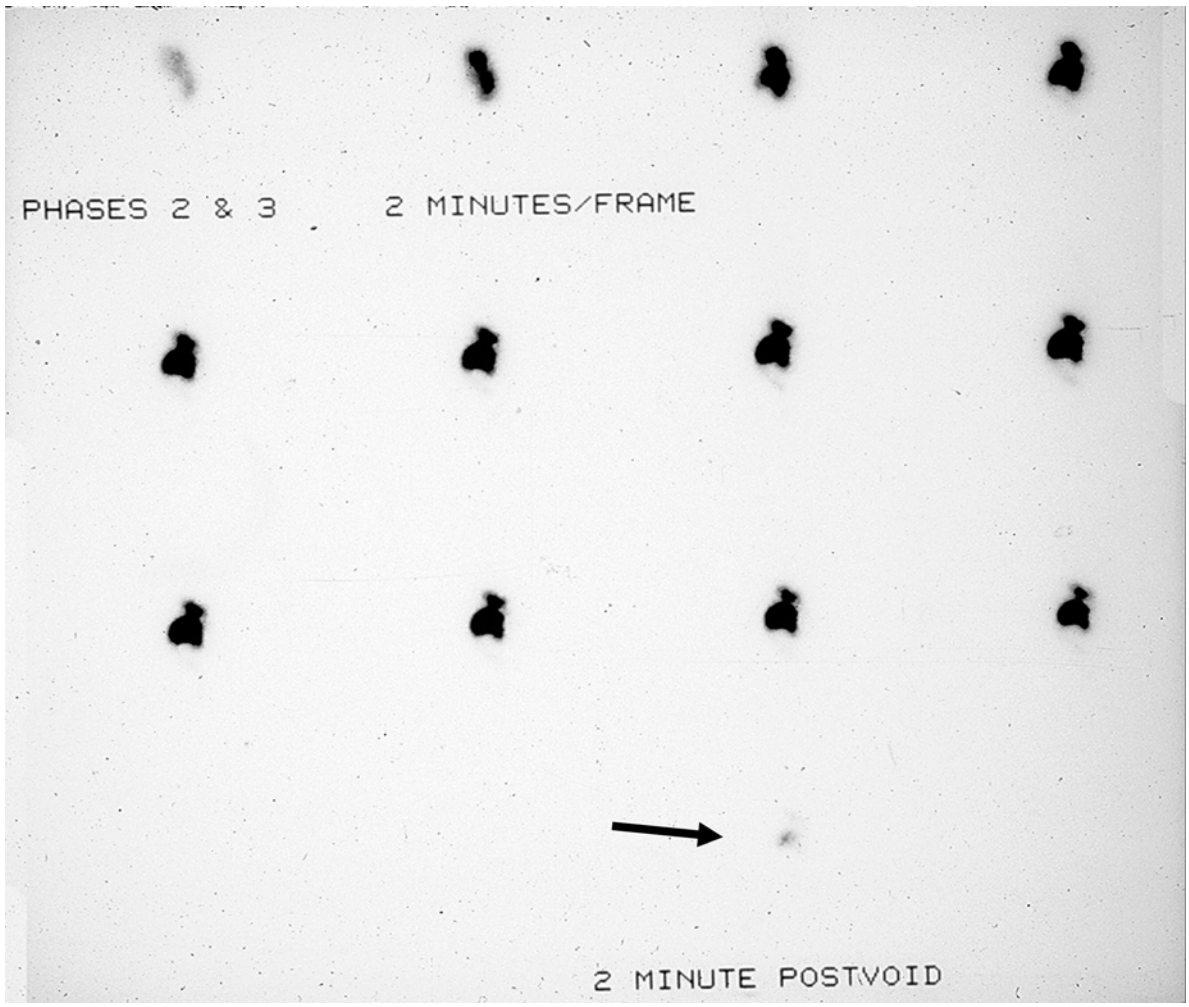

Fig. 7.4. A CT scan obtained in a middle aged male with abdominal pain showed congenital absence of the right kidney and a dilated left renal pelvis. A MAG3 renal scan was performed with approximately 185 MBq of Tc-99m MAG3 and 2-min images were obtained by a post-void image (*arrow*). Following assumption of an upright posture and voiding, urine rapidly drained from the kidney excluding obstruction, obviating the need for furosemide and illustrating the value of the post-micturition image

attain an effective level of diuretic in the tubular fluid (Fig. 7.5) (Brater 1998; Hunsche et al. 2004). Thrall and Ziessman (1995) recommend 60 mg of furosemide for a creatinine of 2.0 mg/dl and 80 mg for a creatinine of 3.0 mg/dl, but these recommendations are probably conservative.

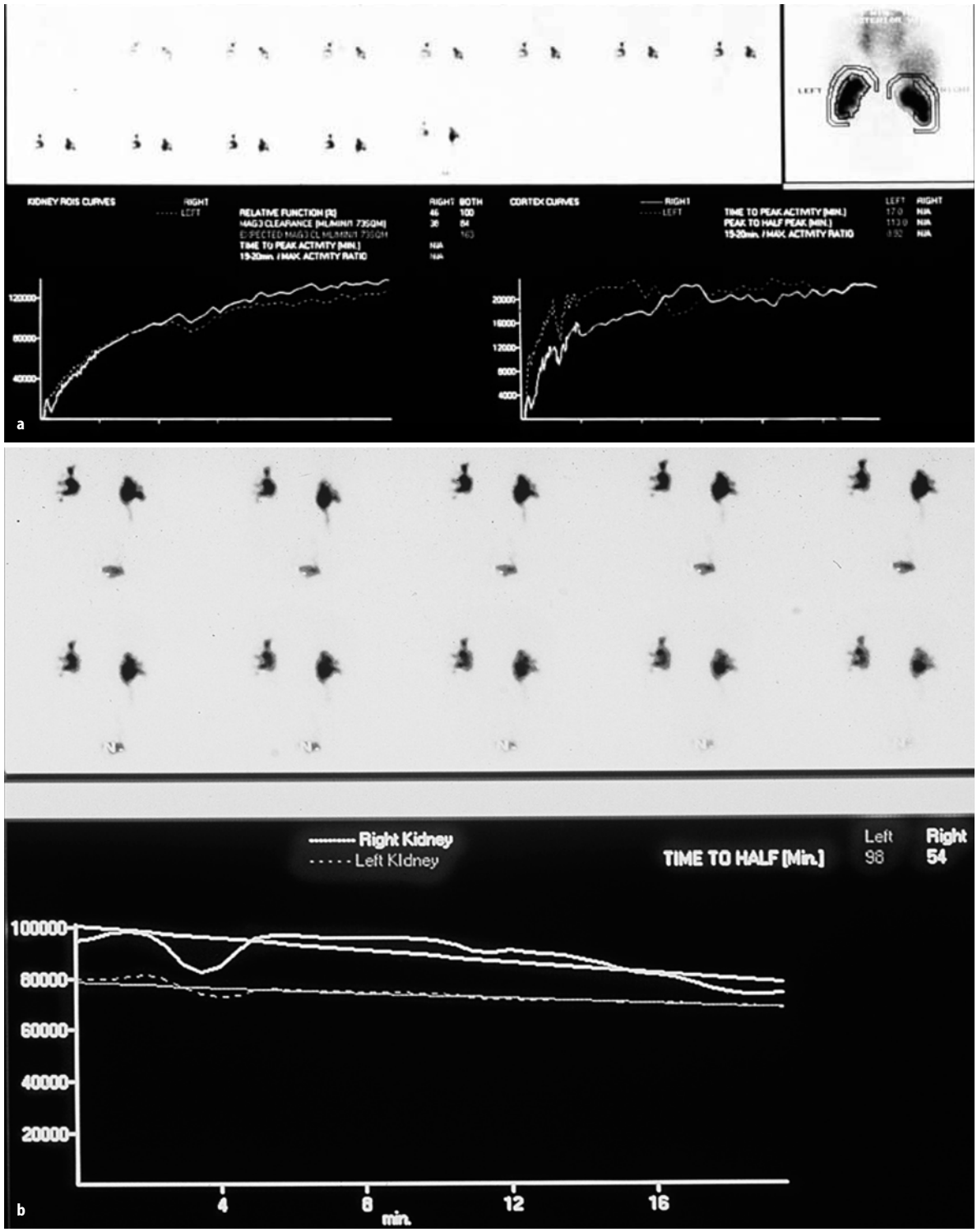

Fig. 7.5a–b

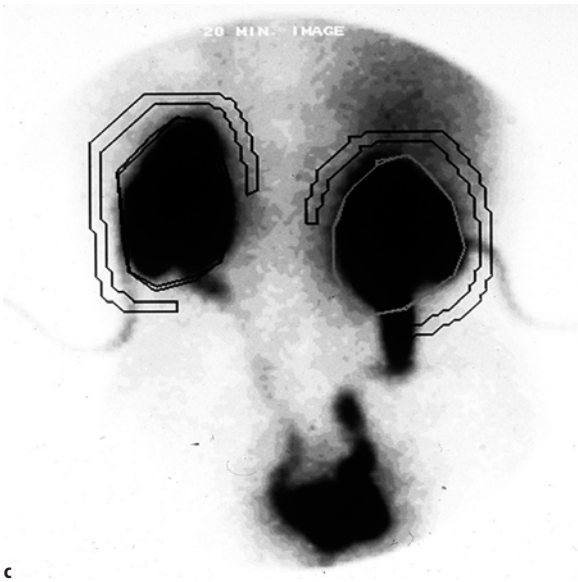

c

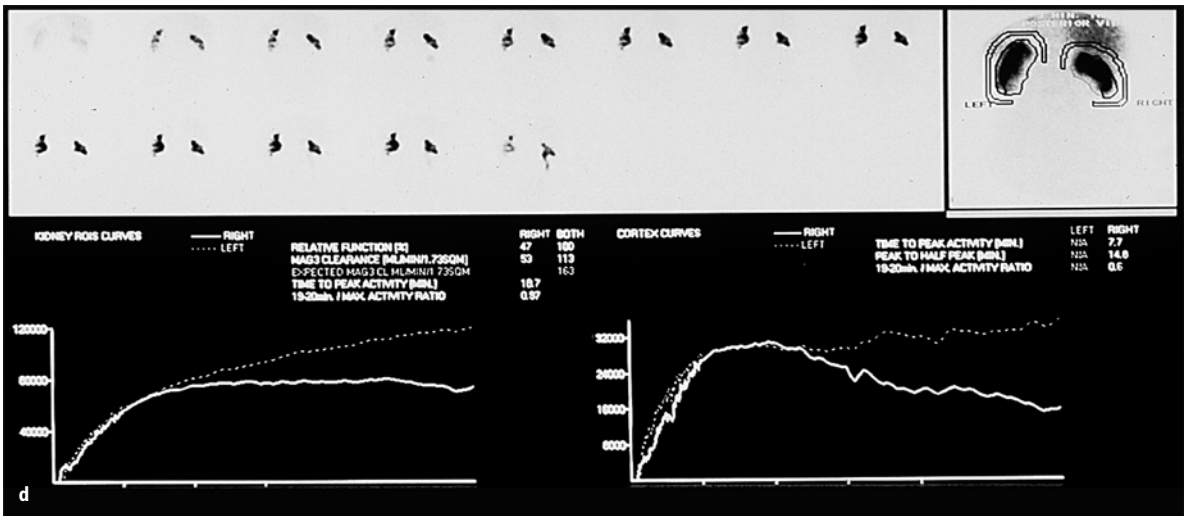

d

Fig. 7.5. a A 77-year-old man with a complicated medical history had bilateral obstruction and bilateral nephrostomies placed in 1995. Four years later, he was observed to be voiding normally as well as draining from his nephrostomy tubes and he was referred for diuresis MAG3 renography to determine if obstruction was still present or if the nephrostomy tubes could be removed. His creatinine had been stable at 2.0 mg/dl. Following the injection of 280 MBq of Tc-99m MAG3, sequential 2-min images were obtained for 24 min (*upper left panel*); the last image in the sequence is a postvoid image. The *upper right panel* shows a 1–2.5-min image with whole kidney, cortical, and background regions of interest. Whole kidney renogram (*lower left panel*) shows a prolonged time to peak activity bilaterally (*N/A* indicates that the time to peak and the 19/20 to max ratio were not reached during the period of the examination on the left). On the right, the time to peak and the 19/20 to max ratio were 18.7 and 0.97 min, respectively. The relative function was 53 % on the left and 47 % on the right. The camera-based MAG3 clearance was 113 ml/min/1.73 m^2, compared with an expected MAG3 clearance value of 163 ml/min/1.73 m^2. The renogram obtained with a cortical region of interest (*lower right*) shows a prolonged time to peak activity bilaterally (*N/A* indicates that the time to peak, the peak to half peak, and the 19/20 to max ratio were 7.7, 14.8 and 0.6 min, respectively. **b** Forty milligrams of furosemide was administered and sequential 2-min images were obtained for 20 min after furosemide administration (*upper left panel*). The kidneys shows prominent pelvic retention. The time activity curve (*lower panel*) shows minimal excretion with prolonged half-times of 98 min on the left and 54 min on the right, consistent with obstruction. **c** By increasing the intensity, the percutaneous nephrostomy tubes (*arrows*) and the ureters could be visualized, although they were not apparent on the standard image display. The nephrostomy tubes had not been clamped; consequently, the patient was still in his baseline state and could not have been obstructed even though the scan appearance was that of obstruction. **d** The study was repeated with 366 MBq of MAG3 and the nephrostomy tubes were clamped. Sequential 2-min Tc-99m MAG3 images were obtained for 24 min (*upper left panel*); the last image in the sequence is a postvoid image. The *upper right panel* shows a 1–2.5-min image with whole kidney, cortical, and background regions of interest. Whole kidney renogram (*lower left panel*) shows a prolonged time to peak activity bilaterally (*N/A* indicates that the time to peak and the 19/20 to max ratio were not reached during the period of the examination on both sides). The relative function was 54 % on the left and 46 % on the right. The camera-based MAG3 clearance was 84 ml/min/1.73 m^2, compared with an expected MAG3 clearance value of 163 ml/min/1.73 m^2. The renogram obtained with a cortical region of interest (*lower right*) shows a prolonged time to peak activity bilaterally (*N/A* indicates that the time to peak, the peak to half peak, and the 19/20 to max ratio were 17, 113, and 0.92 min, respectively

7.6.1.8 Region of Interest Selection for the Diuretic Portion of the Study

For the diuretic portion of the study, some experts assign an ROI over the whole kidney; others recommend placing ROIs around the dilated collecting system (O'Reilly et al. 1996; Members et al. 1992; Thrall et al. 1981; Kass and Majd 1985). Placement of the ROI around the dilated pelvis and collecting system rather than the whole kidney provides a better assessment of the response to furosemide (Connolly et al. 2000), but $T_{½}$ measurements still vary depending on the method of calculation (see below).

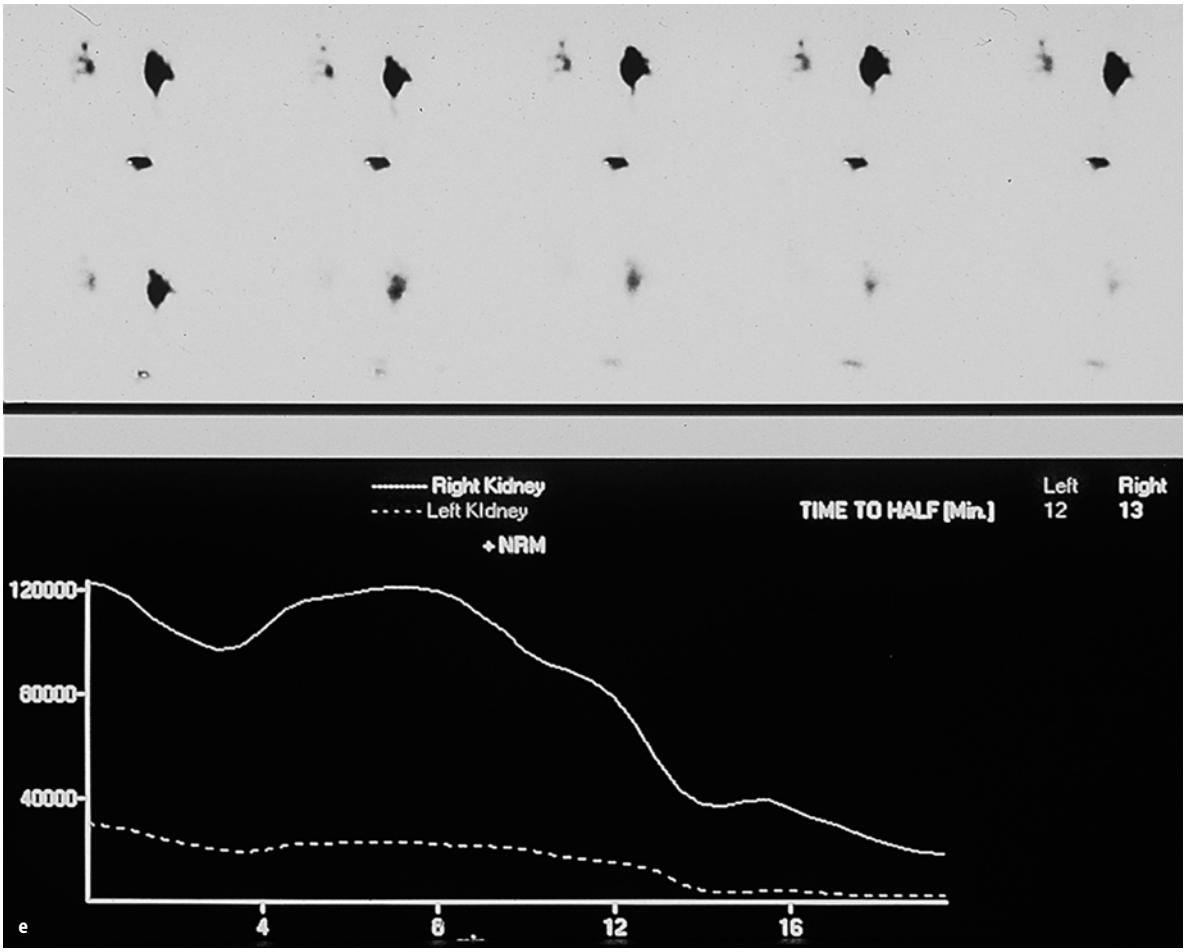

Fig. 7.5 (*Cont.*) **e** Forty milligrams of furosemide was not sufficient to cause an adequate diuresis to exclude obstruction in the initial study and because the patient had an elevated creatinine of 2.0 mg/dl, 80 mg of furosemide was administered. The *upper panel* (sequential 2-min images obtained for 20 min after furosemide administration) and the time activity curves (*lower panel*) show no signs of obstruction with prompt washout of the tracer from the right kidney; the left kidney had largely emptied before furosemide administration. The $T_{½}$ was 12 min for the left kidney and 13 min for the right kidney. The nephrostomies were removed and the patient's renal function has remained stable for 3 years. (Reproduced with permission, Hunsche et al. 2004)

7.6.1.9 Calculating the $T_{½}$

Measurement of the $T_{½}$ has not been standardized and the $T_{½}$ will vary depending on the placement of the ROI (whole kidney or dilated collecting system) and it will also vary depending on whether the measurement begins at the start of the data acquisition, the time the diuretic is injected or at the beginning of the diuretic response. The $T_{½}$ will also be affected by the algorithm (linear or exponential) used to fit the washout curve (Members et al. 1992).

7.6.1.10 Adequacy of Diuresis

The patient should void at the beginning and end of the diuretic acquisition. Dividing the volume of urine voided at the conclusion of the diuretic acquisition by the time in minutes between the two voiding periods gives an estimate of the urine flow rate. If the patient has normal renal function and 40 mg of furosemide is administered at the time of radiopharmaceutical injection, the patient should produce 200 – 300 ml of urine by the end of the 20 – 30 min (Brown et al. 1992). A poor diuretic response may indicate dehydration or impaired renal function and result in false-positive or indeterminate findings. Measuring the voided volume alerts the nuclear medicine physician to an inadequate diuresis.

The rate of urine flow will decrease as renal function decreases, but urine flow rates as high as 4 ml/min have been reported for kidneys with creatinine clearances reduced to 20% of normal (Kletter and Nurnberger 1989; Upsdell et al. 1988). This flow rate often makes it possible to exclude obstruction even in kidneys with

poor renal function, particularly if the renal pelvis is not excessively dilated. As renal function further deteriorates, an abnormal response cannot be used to distinguish obstruction from a poorly functioning kidney that failed to respond to furosemide. Conversely, if the kidney has a near normal clearance, it should have a good diuretic response and collecting system retention following furosemide is much more suspicious for obstruction.

7.6.2 Interpretation

7.6.2.1 Interpreting the $T_{½}$

Some experts interpret the study by visually analyzing the washout curve while others prefer to evaluate the rate of washout by measuring the $T_{½}$ (O'Reilly et al. 1996). It is important to emphasize that normal values for $T_{½}$ depend on the radiopharmaceutical, the delay between administering the radiopharmaceutical and administering furosemide, the method of hydration, the presence or absence of a bladder catheter, the dose of furosemide, region of interest selection, the interval used to make the measurement and the method of calculating the $T_{½}$. For these reasons, normal values for the $T_{½}$ tend to be institution specific; nevertheless, there is general agreement that prompt clearance of the radiopharmaceutical from the renal collecting system with a $T_{½}$ under 10 min is a normal response. Depending on the technique, a $T_{½}$ between 10 and 20 min is often considered indeterminate, and a $T_{½}$ greater than 20 min is suspicious for obstruction. However, the $T_{½}$ value alone should never be the sole criterion for determining the presence or absence of obstruction; the $T_{½}$ must always be interpreted in the context of the whole set of images, curves, and quantitative indices including total function, relative function and the voided volume as well as any clinical information or diagnostic studies that may be available.

7.6.2.2 Alternatives to the $T_{½}$

Some experts recommend that the $T_{½}$ not even be used to assess drainage in asymptomatic children with unilateral utereropelvic junction dilation (Frokier et al. 2006). Instead, techniques which consider renal function, gravity and an empty bladder are recommended. These include more complex measurements such as output efficiency and simpler measurements such as normalized residual activity (NORA, prevoid/maximum, postvoid/maximum, prevoid/1 – 2 min and postvoid/1 – 2 min count ratios) and the pelvic excretion efficiency (PEE) (Chaiwatanarat et al. 1993; Anderson et al. 1997; Piepsz et al. 2000).

7.6.2.3 Non-diagnostic Studies

Despite optimal technique, a certain number of studies (approximately 10 – 15 %) will be difficult to interpret because of an intermediate diuretic response. From a clinical point of view, it is important to decrease the number of tests that are non-diagnostic and to recognize the conditions other than obstruction that may lead to an abnormal diuretic response. Equivocal or false-positive results can occur due to a distended bladder (Hvistendahl et al. 1998), the failure of a poorly functioning kidney to respond to furosemide, or slow washout of the radiopharmaceutical due to the reservoir effect of a grossly dilated collecting system (Kletter and Nurnberger 1989; Brown et al. 1992).

The response to furosemide usually begins 2 – 4 min after injection, but the maximum diuresis is usually not reached until 15 – 18 min after injection. In equivocal cases, some investigators recommend repeating the study with the F–15 renogram so that the patient will be in a state of maximum diuresis at the time the radiopharmaceutical is administered (Upsdell et al. 1992). In selected cases, an equivocal F+20 study will become normal or obstructed following an F–15 renogram (Upsdell et al. 1992).

7.6.2.4 Relative Function

The purpose of intervention is to preserve renal function. Unless it is acute, obstruction usually causes a loss of function in the affected kidney. If the relative renal function is 50/50 in a patient with suspected unilateral obstruction, it may be appropriate to observe the patient and repeat the study even if the quantitative data such as the $T_{½}$ are abnormal or equivocal.

7.6.3 Diuresis Renography in Acute Renal Colic

Unenhanced (non-contrast) helical CT is a valuable test in the management of the patient presenting with acute renal colic; the test can detect a ureteral stone with a high degree of accuracy but unenhanced helical CT cannot predict the presence or absence of obstruction. The addition of a diuretic renal scan can determine the presence or absence of obstruction and direct patient management (Sfakianakis et al. 2000; Loberboym et al. 2000; Bird et al. 2002). If additional data show that a renal scan leads to better patient outcomes and/or reduces medical costs, then diuresis renography may develop an increasingly important role in the management of patients presenting with an acute renal colic.

7.7 Renovascular Hypertension and ACE Inhibition Renography

Renovascular hypertension (RVH) is estimated to affect <0.5–3% of the unselected hypertension population and up to 15–30% of patients referred to a subspecialty center because of refractory hypertension (Prigent 1993). Renovascular hypertension is part of the spectrum of renovascular disease which also includes renal artery stenosis and azotemic renal vascular disease (ARVD). Renovascular hypertension is defined as a functionally significant renal artery stenosis that leads to an elevated blood pressure due to a reduction of perfusion pressure distal to the stenosis and activation of the renin-angiotensin system. ARVD refers to the gradual loss of kidney function associated with severe occlusive disease of the renal artery. Pathological findings associated with ARVD include intrarenal vascular lesions, glomerulosclerosis and atrophy while clinical findings may include hypertension and azotemia. Patients with ARVD may or may not have co-existing renovascular hypertension; however, revascularization is sometimes undertaken in these patients in an attempt to improve or stabilize renal function although the long term utility of this approach versus current medical therapy is still debated.

Renal artery stenosis (RAS) is common in the aging population; as many as 30–50% of normotensive patients with advancing age may have moderate or even severe RAS (Eyler et al. 1962; Holley et al. 1964; Dustan et al. 1964); similarly, RAS may be an associated but non-etiologic finding in patients with essential hypertension. Consequently, it comes as no surprise that revascularization of a stenotic artery in a hypertensive patient does not always result in amelioration of the hypertension. In fact, three randomized studies comparing revascularization with medical therapy suggest that angioplasty appears to have little advantage over antihypertensive drug therapy (Plouin et al. 1998; Webster et al. 1998; Van Jaarsvelt et al. 2000). Alternatively, however, the data in these three studies can also be interpreted as demonstrating the need to determine the hemodynamic significance of a renal artery stenosis prior to revascularization (Taylor 2006). The goals of angiotensin converting enzyme inhibition (ACEI) renography are twofold: (1) to detect those patients with hypertension who have a functionally significant renal artery stenosis as the cause of their hypertension and who would benefit from revascularization, and (2) to determine which hypertensive patients do not have RVH and obviate the expense and risk of a revascularization procedure.

ACE inhibition renography has been shown to be cost effective in a carefully selected population with a prevalence of RVH of 11.6% but it is probably most cost effective in patients with a moderate to high risk of renovascular hypertension (Blaufox et al. 1996; Helin et al. 1998). Clinical features which indicate patients with a moderate or high risk of renovascular hypertension include abrupt onset of hypertension in patients under age 30 or over age 55, severe hypertension resistant to medical therapy in a compliant patient, bruits in the abdomen or flank, occlusive disease in other vascular beds, unexplained azotemia or worsening renal function during therapy with ACE inhibitors. To best utilize the test and maximize the congruence between the performance of the test and the expectations of the referring physicians, it is important to distinguish between renal artery stenosis, renovascular hypertension and ARVD.

The protocols and the criteria for findings indicative of renovascular hypertension have tended to vary from center to center. The lack of standardization coupled with the fact that many reported studies use stenosis of the renal artery, not blood pressure response to revascularization (i.e., true renovascular hypertension), as the end point, make it more difficult to draw definitive conclusions. In an attempt to address these issues, an international consensus committee on ACE inhibitor renography was established by the Ninth International Symposium of Radionuclides in Nephrourology. The 1996 guidelines published by the consensus committee and updated in 2003 form the basis for the following recommendations (Taylor 1996, 2003).

7.7.1 Pathophysiology of Renovascular Hypertension and ACE Inhibition

A functionally significant renal artery stenosis causes a decrease in the perfusion pressure to the afferent arterioles of the glomeruli resulting in a decrease in the transglomerular pressure gradient; the fall in the transglomerular pressure gradient leads to a decrease in glomerular filtration and a decrease in sodium delivery to the distal tubule. The decrease in perfusion pressure and the resulting reduction in distal tubule sodium delivery stimulate the juxtaglomerular apparatus to release renin which cleaves angiotensin I from angiotensinogen; angiotensin I is then converted to angiotensin II by angiotensin converting enzyme. Angiotensin II is a potent vasoconstrictor and acts preferentially on the efferent glomerular arteriole. Constriction of the efferent arteriole raises the transglomerular pressure gradient and can maintain GFR even in the face of a moderate reduction in perfusion pressure resulting from a functionally significant renal artery stenosis.

In patients with renovascular hypertension, ACE inhibitors have two important mechanisms of action: (1)

ACE inhibitors block the conversion of angiotensin I to angiotensin II and thereby interfere with the angiotensin II mediated constriction of the efferent arteriole. (2) ACE inhibitors inhibit kininase II, a dipeptidylcarboxypeptidase that inactivates bradykinin; consequently, bradykinin accumulates following ACE inhibition. Bradykinin is a potent vasodilator and causes selective efferent arteriolar dilation (Gainer et al. 1998; Karanakis et al. 2002; Kon et al. 1993). This second mechanism is probably quite important since only 60 % of angiotensin II is synthesized by ACE dependent pathways in the human renal cortex and neither acute nor chronic ACE inhibition completely eliminates angiotensin II from the plasma (Nussberger et al. 1985; Sandberg and Hong 2000).

The reduction in GFR induced by ACE inhibition can be detected by renography. For DTPA, the primary effect is a reduction in renal uptake of DTPA by the affected kidney. For tubular tracers such as MAG3 or OIH, renovascular hypertension is best detected by cortical retention following ACE inhibition (Fig. 7.6) although a change in relative uptake or a decrease in absolute uptake of the OIH or MAG3 by the affected kidney is an important finding when it occurs (Taylor and Eshima 1994; Taylor et al. 1996; Blaufox et al. 1998; Müller-Suur et al. 1998). The cortical retention of MAG3 and OIH is secondary to the decrease in glomerular filtration induced by ACE inhibition; with the decrease in GFR, there is decreased flow in the renal tubules and delayed washout of the radionuclide from the tubules and tubular lumen (Visscher et al. 1996). Cortical retention can be quantitated by measuring the T_{max} and the 20 or 30 min/maximum ratio (Taylor et al. 1996; Blaufox et al. 1998).

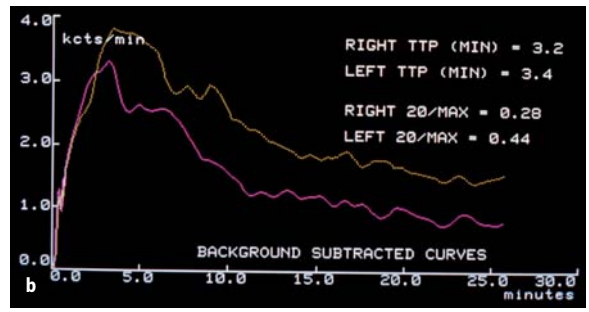

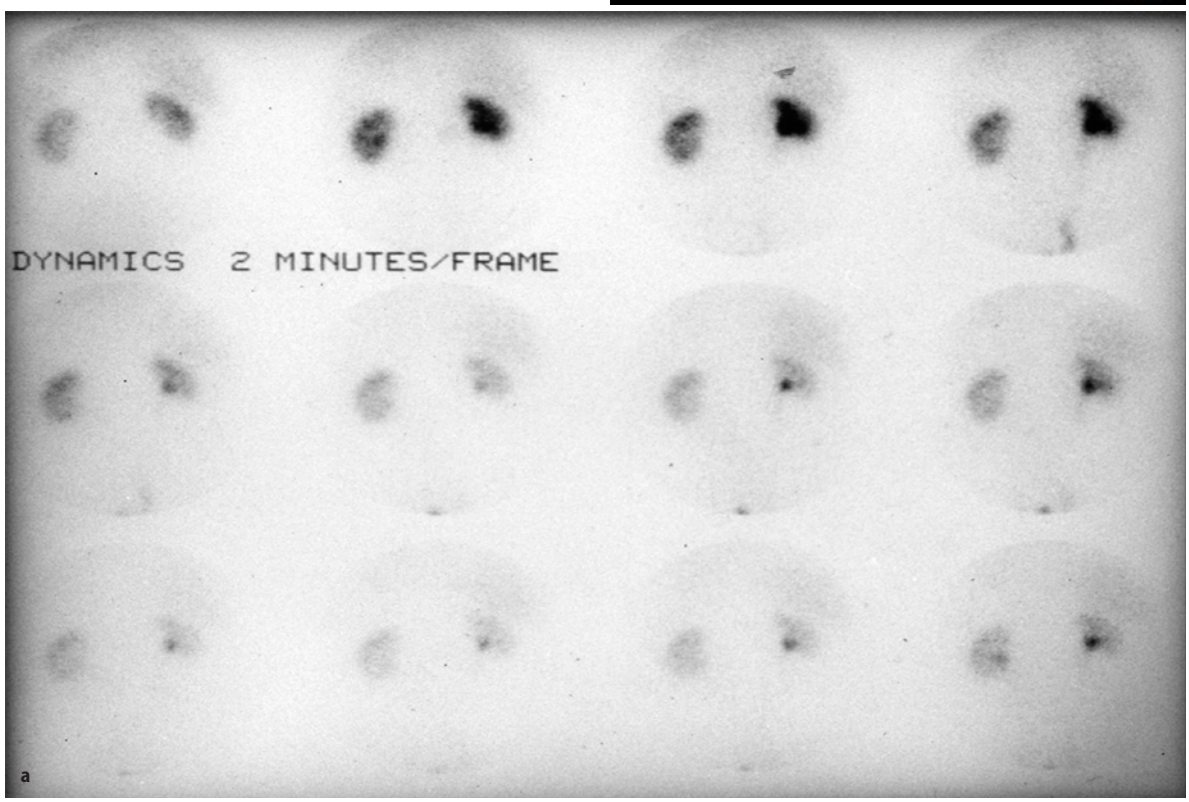

Fig. 7.6. A 78-year-old man who presented with dizziness, a creatinine of 1.7 mg/dl and blood pressure of 230/120 was referred for ACEI renography. **a** A baseline scintigram was obtained with 1.2 mCi of MAG3. Images obtained at 2-min intervals for 24 min show prompt uptake and washout of the tracer. **b** The relative uptake was 52 % in the right kidney and 48 % in the left kidney. The background subtracted cortical renogram curves show a normal T_{max} for both kidneys; however, there is an abnormal 20 min/max ratio of 0.44 for the left kidney (normal < 0.35)

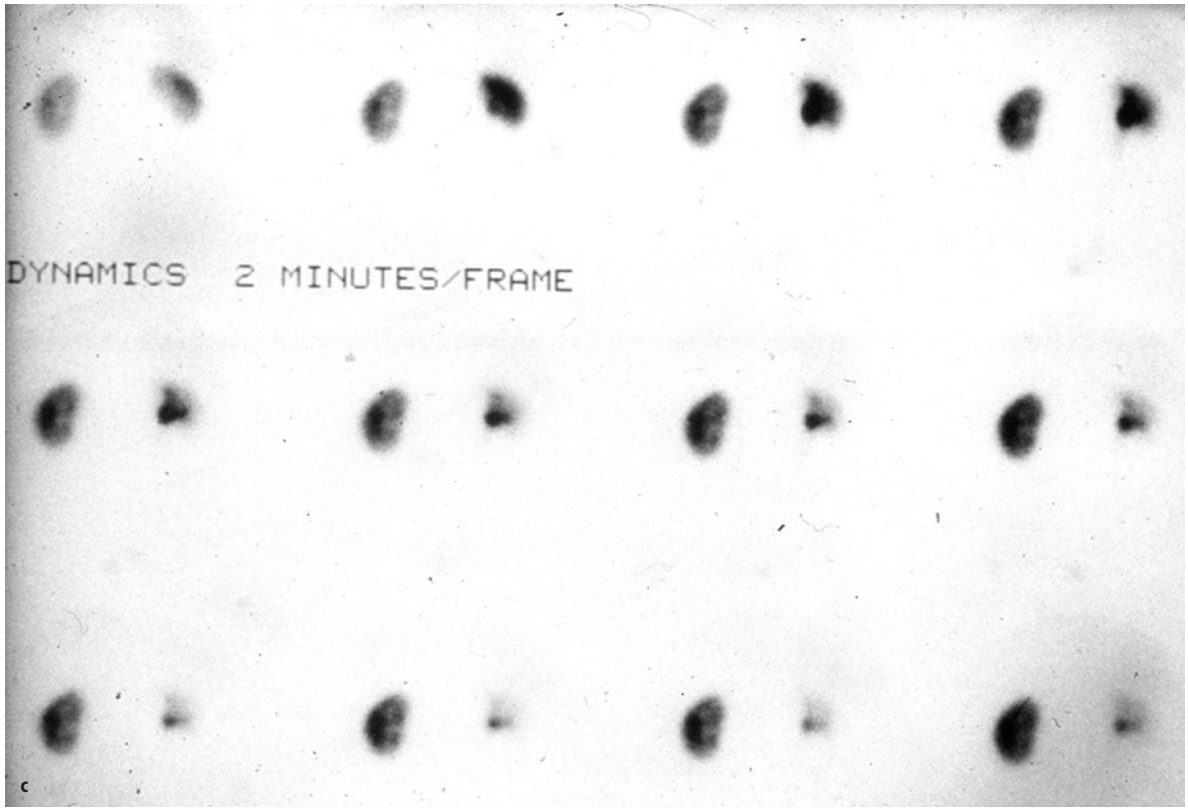

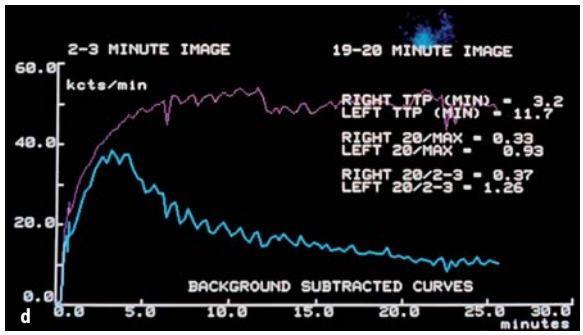

Fig. 7.6 (*Cont.*) **c** Following completion of the baseline study, the patient was given 50 mg of captopril and a second MAG3 scintigram was obtained with 9.3 mCi, approximately 1.5 h later. The sequential 2-min images show cortical retention in the left kidney; however, the right kidney appears normal. **d** Following captopril, the left cortical renogram curve has become markedly abnormal; the time to peak has increased to 11.7 min and the 20 min/max ratio has increased from 0.44 to 0.93. Although the cortical renogram curves are noisier than whole kidney renogram curves, the 20 min/max ratio for the right cortical ROI has increased from a baseline high normal value of 0.28 to an elevated value of 0.37 although this is not considered to be a significant change. Angiography demonstrated bilateral renal artery stenosis. A revascularization procedure was not performed

7.7.2 Technical Issues Relating to ACE Inhibition Renography

7.7.2.1 Diet and Hydration

Ideally, patients should be instructed to arrive well hydrated and receive 5 – 10 ml/kg of water on arrival in the department, preferably 30 – 60 min before the study. If baseline and ACEI studies are to be performed on the same day, hydration should be continued between studies.

Food may delay gastric emptying and interfere with the absorption of captopril. If captopril is to be given as the ACE inhibitor, the patient should be instructed not to eat any solids after midnight before the exam; however, instructions should clearly distinguish between avoiding solid food and the importance of hydration. Low-sodium diets need to be avoided for several days prior to the test to avoid extracellular volume depletion which might accentuate a hypotensive response following ACE inhibitor administration.

7.7.2.2 Medications

ACE Inhibitors and Angiotensin II Receptor Blockers (ARBs). The majority of ACE inhibition studies have been performed with captopril but enalaprilat is an ac-

ceptable alternative (Taylor et al. 1996, 2003; Erbslöh-Möller et al. 1991). Limited data suggest that chronic ACE inhibition may reduce the sensitivity of the test (Setaro et al. 1991; Visscher et al. 1995) and the consensus recommendation is to discontinue captopril for 4 days prior to the study and discontinue the longer half-life ACE inhibitors for 7 days (Taylor et al. 1996, 2003). Since ACE inhibitors and ARBs both block the vasoconstrictive effect of angiotensin II on the efferent vessels in patients with RVH, it was thought that chronic ARB administration might also reduce the sensitivity of the ACE inhibition renography. Recent data, however, indicate that it is probably not necessary to discontinue the ARB class of drugs (Karankias et al. 2002). Captopril renograms were obtained in 26 hypertensive patients with normal or near normal renal function who were receiving angiotensin II receptor blockers; in this patient population, the sensitivity of ACE inhibition renography for renovascular hypertension was 92% and specificity was 100%, values comparable to those obtained in patients not taking ARBs (Taylor 2000; Karankias et al. 2002). Finally, a recent study showed that ARB renography is considerably less sensitive than captopril renography for detecting RAS in hypertensive patients or for detecting RVH (Picciotto et al. 2003). The superiority of ACE inhibitors over the ARBs in detecting renovascular hypertension probably derives from the action of ACE inhibitors on kininase II (see above).

Diuretics. Chronic diuretic administration increases the likelihood of volume depletion which may reduce the specificity of the test and increase the risk of a hypotensive response. These concerns can be minimized if diuretics are discontinued for 2–3 days prior to the study.

Calcium Channel Blockers. Calcium channel blockers have been associated with bilaterally symmetrical abnormal renogram curves in the absence of renal artery stenosis (Claveau-Tremblay 1998; Ludwig et al. 2003). As an alternative to discontinuing another drug, a reasonable option is to ensure adequate hydration and to note the use of a calcium channel blocker. In the rare setting where bilateral symmetrical abnormalities occur in the absence of dehydration, hypotension or infiltration, the ACEI component of the test could be repeated after discontinuation of calcium channel blockers.

7.7.2.3 Choice of Radionuclide

In patients with azotemia, tubular agents such as MAG3 or I-123 OIH are the agents of choice (Taylor et al. 1996; Blaufox et al. 1998; Sfakianakis et al. 1993). In patients with normal renal function, MAG3 and DTPA appear to give comparable results.

7.7.2.4 Choice of ACE Inhibitor

Captopril (25–50 mg crushed and administered orally with 250 ml of water) has been used in most published studies. A 25-mg tablet is sufficient unless the patient has delayed gastric emptying or poor absorption from the gastrointestinal tract. Food can interfere with the absorption of captopril, and patients should not eat before captopril scintigraphy. The peak activity of captopril does not occur until approximately 60 min after ingestion; for this reason, the radiopharmaceutical should be given 1 h after captopril. A second approach is to inject enalaprilat (Vasotec, 40 μg/kg IV over 3–5 min, maximum dose of 2.5 mg), wait a minimum of 15 min, and then inject the radiopharmaceutical (Erbslöh-Möller et al. 1991; Kopecky et al. 1990; Black et al. 1991). Intravenous injection of enalaprilat avoids the possibility of a false negative test due to delayed gastric emptying in a diabetic patient or poor absorption and the patient is usually under continuous observation after enalaprilat injection as the technologist prepares for the study. A potential disadvantage is possibly a greater risk of a hypotensive response and the need for venous access. Both ACE inhibitors are acceptable (Taylor 1996, 2003).

7.7.2.5 Blood Pressure

Blood pressure must be monitored. Asymptomatic hypotension secondary to ACE inhibition can result in bilateral symmetrical abnormalities in the renogram curves (Fig. 7.7). This phenomenon is uncommon and may occur in approximately 1–3% of patients referred for ACEI renography; it appears to be most likely to occur in patients who are volume or salt depleted (Fanti et al. 1998; Stavropoulos et al. 1999). ACE inhibitors can also cause a major hypotensive episode, although the prevalence appears to be quite low in well-hydrated patients. The hypotension can usually be reversed by placing the patient supine, raising the patient's legs, and infusing normal saline. Some centers establish an IV line before scintigraphy; this precaution is important for high risk patients such as those with angina, recent myocardial infarction, a history of transient ischemic attacks, recent stroke and patients receiving enalaprilat or furosemide. Before the patient leaves the department, it is probably wise to document that the standing blood pressure is greater than 70% of the baseline blood pressure and that the patient is asymptomatic. A statement to this effect can be included in the report.

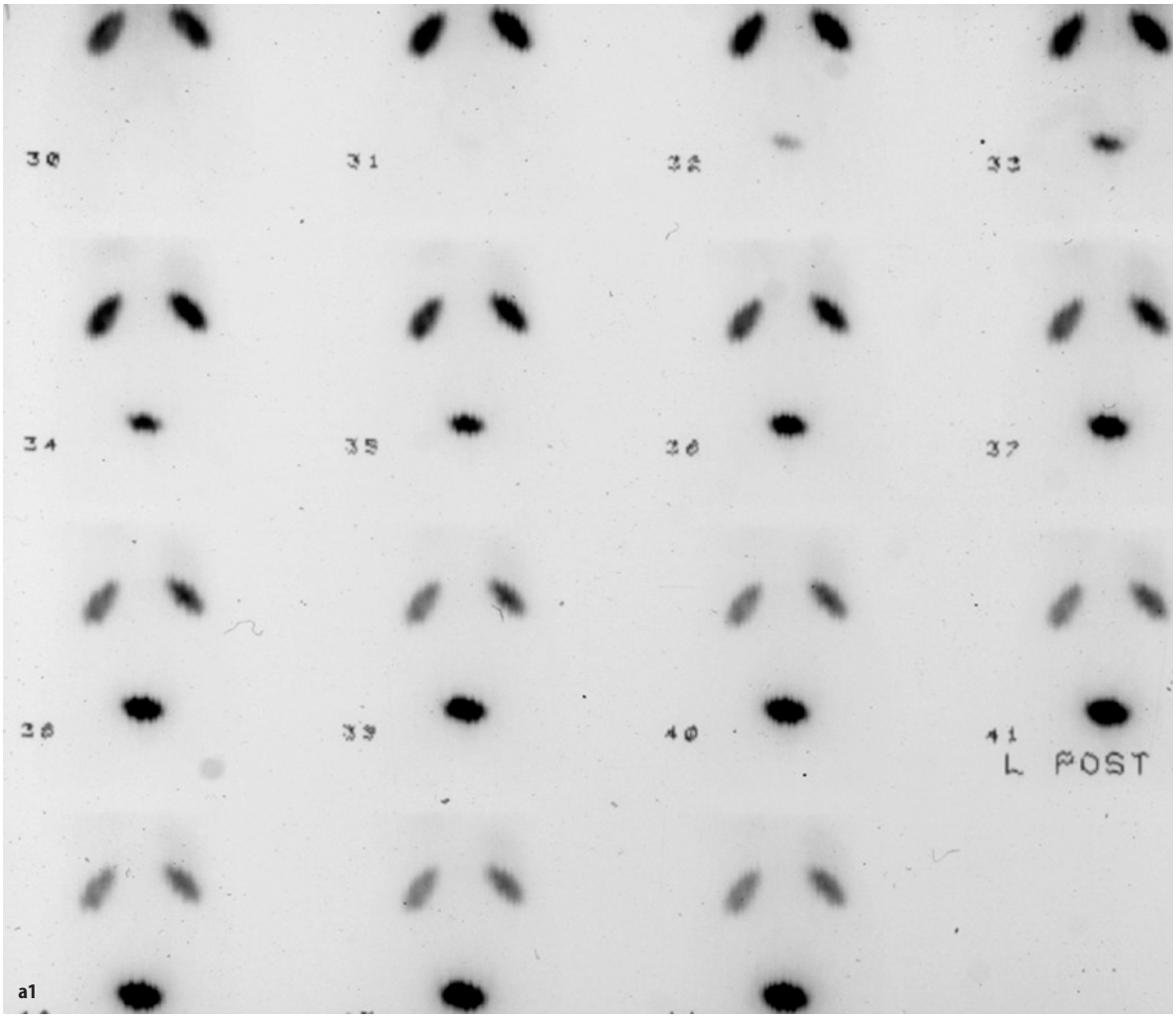

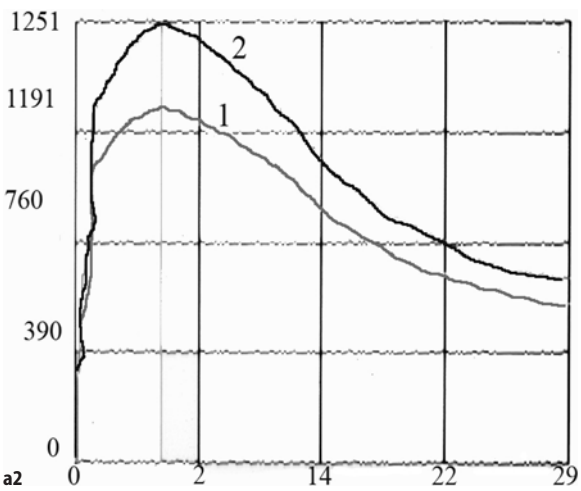

Fig. 7.7. A middle age male with refractory hypertension was referred for ACE inhibition renography. **a** Sequential 2-min images and whole kidney renogram curves were obtained following a baseline injection of approximately 1.0 (37 MBq) of MAG3.

7.7.2.6 One Versus a Two Day Protocol

Some centers begin with captopril or enalaprilat renography because a normal study following ACE inhibition renography obviates the need for a baseline study. If the ACE inhibition study is abnormal, the specificity can be improved by obtaining a baseline renogram; however, because of the administration of the ACE inhibitor, the patient will have to return for the baseline study on another day. In some centers an abnormal ACEI study coupled with a high clinical probability for renovascular hypertension is justification for angiography.

A second approach is to use a low dose (37 MBq or 1 mCi) of MAG3 or DTPA for the baseline study, administer the ACE inhibitor and then obtain a second study with a significantly higher dose (approximately 370 MBq or 10 mCi). This protocol requires two studies on the same day and requires the patient to spend a longer time in the department, but the complete study is finished in a single day. The first approach is less costly

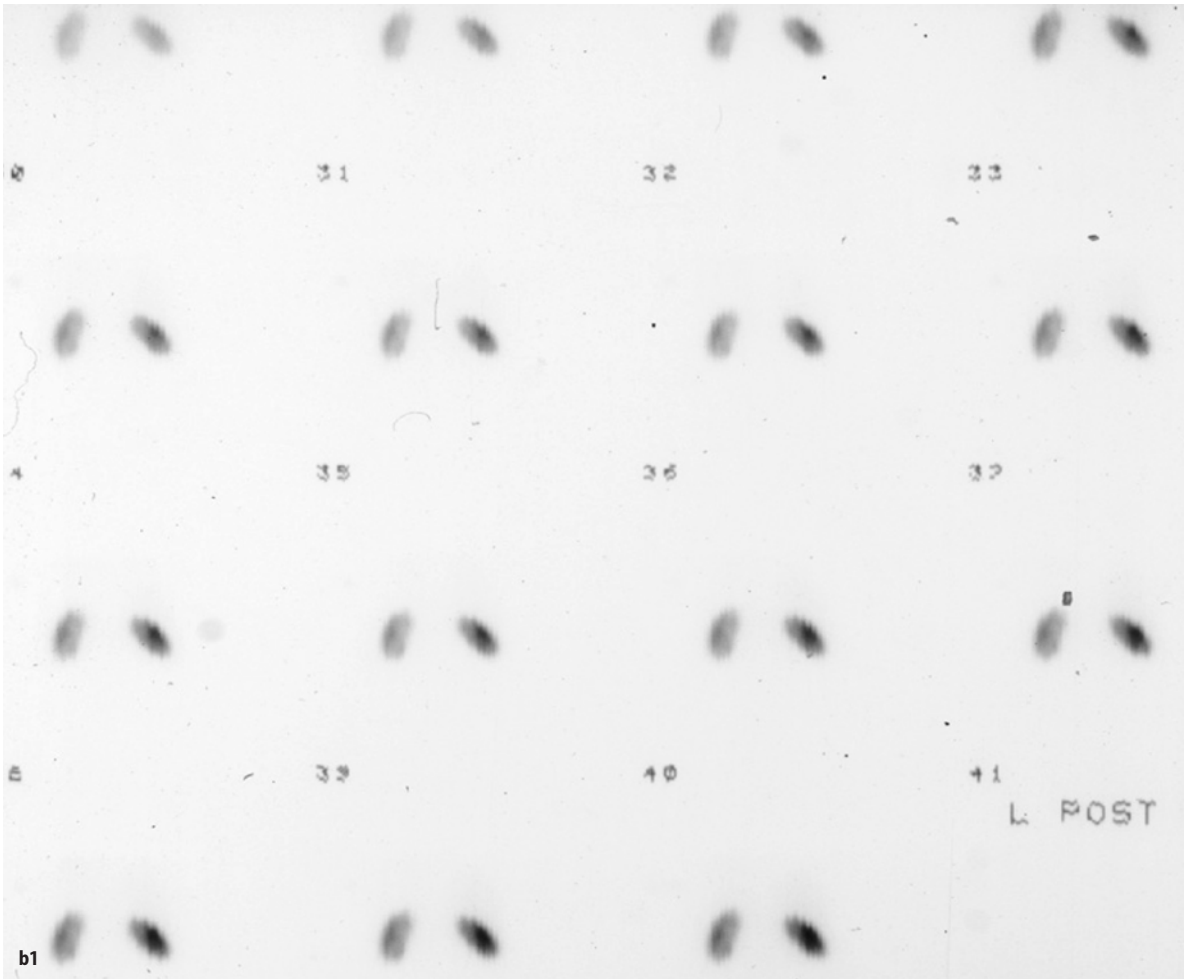

b1

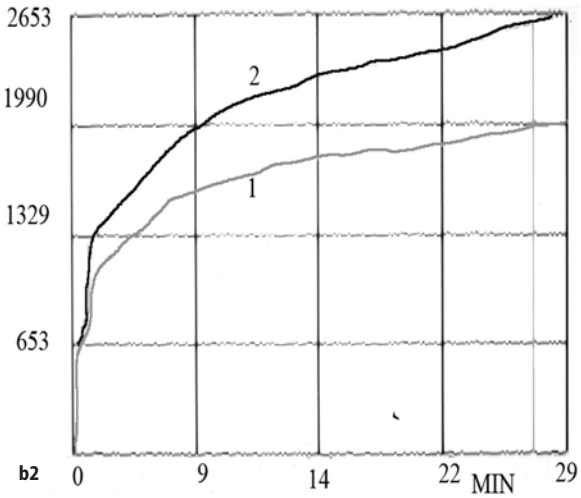

b2

Fig. 7.7 (*Cont.*) **b** The patient received 50 mg of captopril and 10 mCi (370 MBq) was injected 1 h later. The 2-min images demonstrate parenchymal retention with bilateral rising whole kidney renogram curves. Usually, renovascular hypertension produces asymmetrical abnormalities. On further review, the patient's pre-captopril blood pressure was 165/71 but it fell to 102/41 during the study even though the patient remained asymptomatic.

if the time required for the patient to return on a second day for a baseline test is not factored into the calculation.

7.7.2.7 Furosemide-Augmented ACEI Renography

With MAG3 or OIH, the diagnosis of renovascular hypertension is primarily based on cortical retention of the radiopharmaceutical; physiologic retention of these radioactive agents in the calices can distort both the visual and quantitative analysis (T_{max} and the 20 – 30 min/maximum ratio). To minimize retention of tracer in the collecting system, some centers advocate furosemide-augmented captopril or enalaprilat renography for the detection of renovascular hypertension (Sfakianakis et al. 1993; Erbslöh-Möller et al. 1991; Caglar et al. 1998). Furosemide is a loop diuretic and acts distal to the proximal tubules, where MAG3 and OIH are secreted. Consequently, furosemide can wash the radiopharmaceutical out of the calices and pelvis, but it does not affect cortical retention (Sfakianakis et al. 1993). A disad-

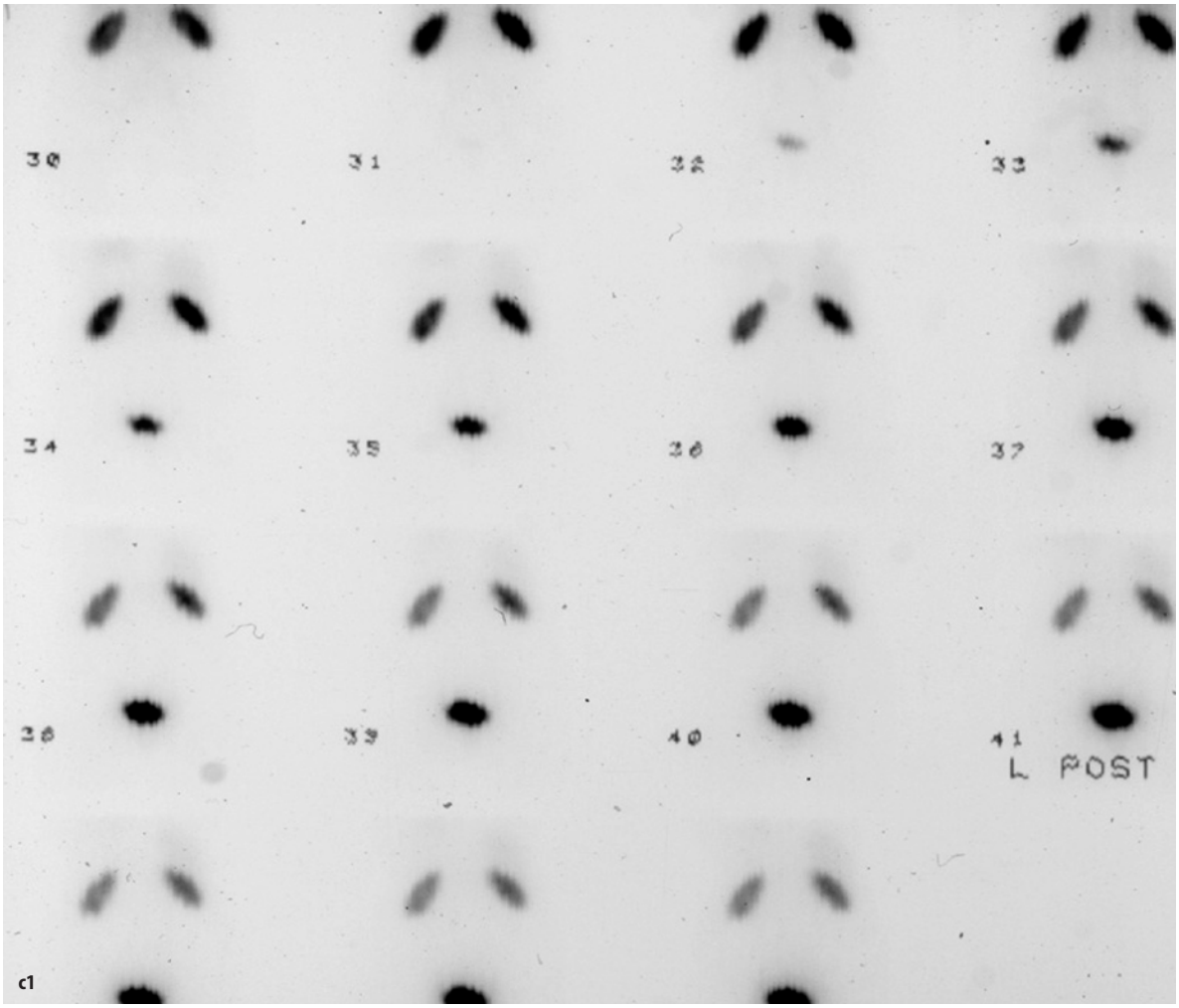

c1

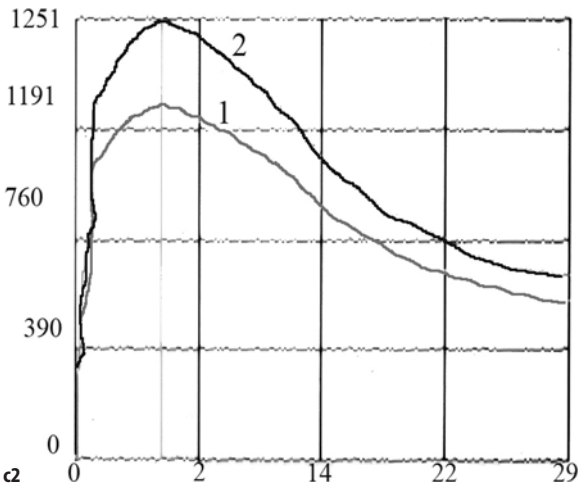

c2

Fig. 7.7 (*Cont.*) **c** Several days later the study was repeated with 50 mg of captopril and intravenous hydration to maintain blood pressure. The 2-min sequential images and renogram curves are normal. Bilateral symmetrical abnormalities following ACE inhibition are a non-specific finding and are often due to volume depletion and hypotension

vantage of furosemide is volume depletion and a greater risk of significant hypotension. The Consensus Committee considered the use of furosemide to be a local option but not a necessary component of ACEI renography; if furosemide is administered, an IV line should be placed in case supplemental hydration is necessary (Taylor et al. 1996, 2003).

7.7.3 Diagnostic Criteria

Two recent consensus panels have recommended that the test be interpreted as high, low or intermediate probability for renovascular hypertension (Nalley et al. 1991; Taylor et al. 1996).

High Probability. Unilateral deterioration of the renogram curve and/or change in relative function following ACE inhibition compared to the baseline study.

Intermediate (Indeterminate) Probability. Small poorly functioning kidney or kidneys with abnormal baseline renograms (Grade III–V) which are unchanged following ACE inhibition.

Low Probability. A normal ACE inhibition renogram or Grade II renogram which is unchanged or improves following ACE inhibition.

A change in the shape of the renogram curve may be evaluated quantitatively by a prolongation of the 20 or 30 min/max ratio and/or a prolongation of the time to peak. For tubular tracers, a unilateral increase in the 20 min/max ratio of 0.15 (0.30 – 0.45) or greater for parenchymal (cortical) ROIs represents the 90% confidence limit for a significant change (Taylor et al. 1996; Blaufox et al. 1998). The confidence limit is slightly lower for 30 min/max ratios and higher for whole kidney ROIs. A prolongation of the time to peak of 120 s for a cortical ROI is significant at the 90 – 95% confidence limit. It is important to note, however, that a change from 5 to 7 min is much more significant than a change from 15 to 17 min. Renograms derived from the cortical ROIs minimize the error or diagnostic difficulty that can be introduced by retention of the tracer in the collecting system. A change in the relative uptake of MAG3 or OIH by 10 percentage points (50/50 to 40/60) is uncommon even in a patient with RVH but it is highly significant when it occurs.

The principal diagnostic criterion for DTPA is a change in the relative uptake. A reduction in the relative uptake greater than 10 percentage points (50/50 to 60/40) is a highly significant change and 5 – 9 percentage points is considered to be an intermediate response (Taylor et al. 1996; Fommei et al. 1993; Dey et al. 1993), although a recent study performed under carefully controlled conditions suggests that smaller changes in relative uptake may be significant (Blaufox et al. 1998). Parenchymal retention of DTPA following ACE inhibition can also be an important diagnostic finding and can be quantitated by a delay in the time to peak or an increase in the 20 – 30 min/max ratios although, in general, changes have to be much more pronounced than with MAG3 and OIH to be significant (Taylor et al. 1996; Sfakianakis et al. 1993, 1997).

7.7.4 Sensitivity and Specificity

The sensitivity and specificity depend on the patient selection (see below), the analysis of the patient with an indeterminate scan and the difficulty in determining the response to revascularization; the response to revascularization may be affected by restenosis, a change in medications, and the lack of a systematic approach to determining the blood pressure response. Most studies report sensitivities and specificities in the range of 80 – 90% although many studies use an inappropriate gold standard and compare the results of ACE inhibition renography to the presence or absence of renal artery stenosis rather than the blood pressure response to revascularization. Different diagnostic criteria as well as different populations of patients probably explain some of the variation in results. Better results are often obtained when the end point is normalization or reduction in blood pressure following revascularization rather than the presence or absence of renal artery stenosis (Taylor et al. 1996; Fommei et al. 2003; Mittal et al. 1996; Kahn et al. 1994; Fommei et al. 1994; Geyskes et al. 1991; Dondi et al. 1992; Taylor 2000).

Intermediate probability results present a problem for analysis; they can be included with the positive studies, in which case sensitivity is increased at the expense of specificity; they can be included with the low probability studies, increasing specificity at the expense of sensitivity, or they can all be counted as incorrect, or they can even be omitted from the data analysis. The sensitivities and specificities will vary depending on the frequency of intermediate probability studies in the study population and how these results are handled in the data analysis.

Results are improved by appropriate patient selection. In selecting patients for ACE inhibition renography and in communicating with the referring physician, *it is essential to distinguish between the hypertensive patient with azotemic renovascular disease (ARVD) and the hypertensive patient without ARVD because results differ in these two patient populations.*

7.7.4.1 Hypertensive Patients with Azotemic Renovascular Disease

Current data indicate that the test is not as accurate in patients with azotemic renovascular disease (ARVD). Fortunately, these patients are not difficult to identify. The likelihood that a patient has severe atherosclerotic vascular disease involving one or both kidneys is substantially increased if the patient is azotemic or if the patient is already known to have a small kidney. These patients will have a high percentage of intermediate probability test results. This is not necessarily a problem if the referring physician understands the likelihood of an intermediate result when such a patient is referred for ACEI renography. An intermediate test result in the appropriate clinical setting may be sufficient to refer a patient for angiography. False negative results are uncommon but when they occur, they appear to be more likely in azotemic patients with bilateral disease, probably due to suppression of the renin angiotensin system.

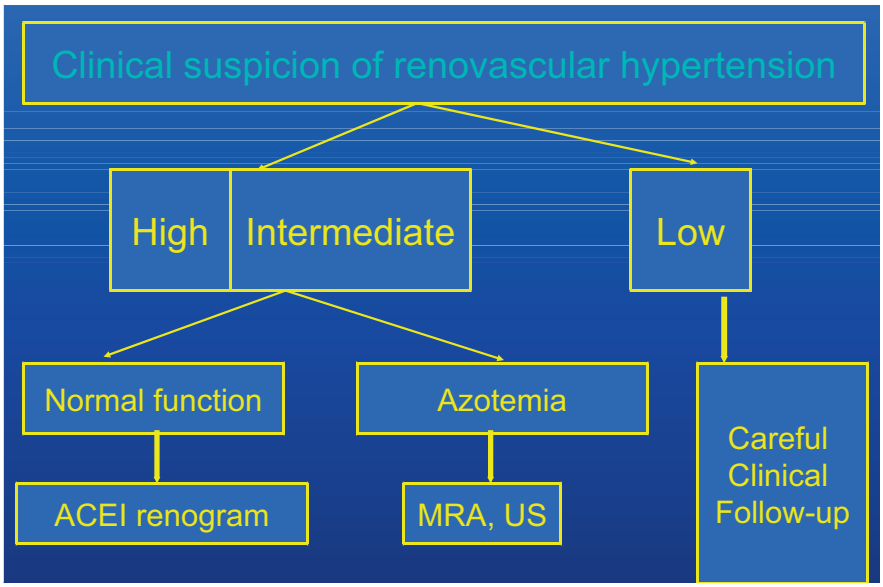

Fig. 7.8. Algorithm for the diagnosis of renovascular hypertension

7.7.4.2 Hypertensive Patients Without Azotemic Renovascular Disease

The probability is considered high (greater than 90 %) when marked deterioration of the renogram curve occurs after ACE inhibition, compared to baseline findings (Taylor et al. 1996; Blaufox et al. 1998; Taylor 2000). Normal findings on ACE inhibition renography indicate a low probability (less than 10 %) for renovascular hypertension. Abnormal baseline findings that improve after ACE inhibition also indicate low probability for renovascular hypertension. In the patient population that does not have a small poorly functioning kidney and that has normal or near normal renal function, the sensitivity, specificity, and positive and negative predictive value of ACE inhibition renography probably exceed 90 %. A proposed algorithm for investigating suspected RVH is shown in Fig. 7.8 (Taylor 2006).

7.8 The Role of Positron Emission Tomography in Renal Imaging

Renal blood flow can be determined with O-15 water ($H_2{}^{15}O$), N-13 ammonia, rubidium-82 and copper-64 or copper-62 pyruvaldehyde bis (N4-methyl)thiosemicarbazone (PTSM). The use of PET tracers to monitor renal blood flow has the potential to serve as a useful measurement in the study of renal physiology and pharmacology. Carbon-11 acetate is a marker of oxidative metabolism and it is efficiently extracted by the kidney. Carbon-11 acetate is converted to carbon-11 acetyl-CoA and enters the Krebs cycle where it is metabolized, releasing the carbon-11 as carbon-11 CO_2. Although carbon-11 acetate is not excreted into the urine, its role in imaging renal metabolism or renal pathology has so far been limited. Fluorine-18 fluorodeoxyglucose (FDG) is an increasingly important PET imaging agent in oncology but it is not optimal for imaging renal pathology because it is filtered by the glomerulus and, unlike glucose, it is not reabsorbed from the tubular lumen; consequently, fluorine-18 FDG accumulates in the renal pelvis and bladder potentially obscuring ^{18}F-FDG avid pathology in the kidney or region of the bladder.

A promising application of PET in the kidneys is the study of the angiotensin receptor subtype, AT1R. AT1R mediates most of the physiological effects of angiotensin II including renal blood flow, glomerular filtration, sodium and water reabsorption, myocardial contractility and aldosterone secretion and studies are currently being conducted to monitor AT1R expression using positron labeled drugs with a high selectivity and affinity for the receptor (Szabo and Matthews 2006). The use of PET to monitor AT1R expression in humans potentially provides an important in vivo window for investigating the mechanisms of human hypertension and other AT1R modulated diseases.

7.8.1 Fluorine-18 FDG Imaging in Renal Carcinoma

The assessment of a renal mass is best performed with sonography, CT or MRI. Purely cystic lesions are benign; more complex cystic renal masses require observation or removal depending on the characteristics of the cystic mass. The primary staging of masses suspicious for renal cell carcinoma is performed primarily with CT. F-18 FDG PET is not commonly used to assess

a renal mass because the normal F-18 FDG in the kidney may mask uptake by a renal cell carcinoma; in addition, most renal cell carcinomas are slow growing and tend to be less FDG avid. PET may be helpful in the evaluation of equivocal findings on conventional imaging (Schöder and Larson 2004). FDG PET may play a greater role in restaging to detect recurrent or metastatic disease. Recent studies suggest that FDG PET has a sensitivity in the range of 60–70 %; consequently, a negative study cannot not exclude disease (Majhail et al. 2003; Jadvar et al. 2004).

References

Adeyoju AA, Burke D, Atkinson C, et al. (2001) The choice of timing for diuresis renography for the assessment of equivocal pelviureteric obstruction. Br J Urol Int 88:1–5

Al-Nahhas AA, Jafri RA, Britton KE, et al. (1988) Clinical experience with 99m Tc-MAG3, mercaptoacetyltriglycine, and a comparison with 99mTc-DTPA. Eur J Nucl Med 14:453–462

Anderson PJ, Rangarajan V, Gordon I (1997) Assessment of drainage in PUJ obstruction: pelvic excretion efficiency as an index of renal function. Nucl Med Commun 18:823–826

Bird VG, Gomez-Martin O, Leveillee RJ, Sfakianakis GN, Rivas LA, Amendola MA (2000) A comparison of unenhanced helical computerized tomography findings and renal obstruction determined by furosemide ^{99m}technetium mercaptoacetyltriglycine diuretic scintirenography for patients with acute renal colic. J Urol 167:1597–1603

Black HR, Bourgoignie JJ, Pickering T, Svetkey L, Saddler MC, et al. (1991) Report of the working party group for patient selection and preparation. Am J Hypertens 4:745S–456S

Blaufox MD, Middleton ML, Bongiovanni J, Davis BR (1996a) Cost efficacy of the diagnosis and therapy of renovascular hypertension. J Nucl Med 37:171–177

Blaufox MD, Aurell M, Bubeck B, et al. (1996b) Report of the radionuclides in nephrourology committee on renal clearance. J Nucl Med 37:1883–1890

Blaufox MD, Fine EJ, Heller S, et al. (1998) Prospective study of simultaneous orthoiodohippurate and diethylenetriaminepentaacetic acid captopril renography. J Nucl Med 39: 522–528

Bocher M, Shrem Y, Tappiser A, Klein M, Schecter D, Taylor A, Jr, Chisin R (2001) Technetium-99m-MAG3 clearance: comparison of camera based methods. Clin Nucl Med 26: 745–750

Brater CD (1998) Diuretic therapy. N Engl J Med 339:387–395

Brochner-Mortensen J, Rodbro P (1976) Selection of routine method for determination of glomerular filtration rate in adult patients. Scand J Clin Lab Invest 36:35–43

Brown SCW, O'Reilly PH (1995) Glomerular filtration rate measurement: a neglected test in urological practice. Br J Urol 75:296–300

Brown SCW, Upsdell SM, O'Reilly PH (1992) The importance of renal function for the interpretation of diuresis renography. Br J Urol 69:121–125

Bubeck B (1993) Renal clearance determination with one blood sample: improved accuracy and universal applicability by a new calculation principle. Semin Nucl Med 23:73–86

Bubeck B, Brandau W, Weber E, et al. (1990) Pharmacokinetics of technetium-99m-MAG3 in humans. J Nucl Med 31: 1285–1293

Caglar M, Moretti JL, Buchet P, et al. (1998) Enalapril plus frusemide MAG3 scintigraphy in hypertensive patients with atherosclerosis and moderate renal insufficiency. Nucl Med Commun 19:1135–1140

Chachati A, Meyers A, Godon JP, Rigo P (1987) Rapid method for the measurement of differential renal function: validation. J Nucl Med 28:829–836

Chaiwatanarat T, Padhy AK, Bomanji JB (1993) Validation of renal output efficiency as an objective parameter in the evaluation of upper urinary tract obstruction. J Nucl Med 34:845–848

Claveau-Tremblay R, Turpin S, Debraekeleer M, et al. (1998) False-positive captopril renography in patients taking calcium antagonists. J Nucl Med 39:1621–1626

Connolly LP, Zurakowski D, Peters CA, et al. (2000) Variability of diuresis renography interpretation due to method of post-diuretic renal pelvic clearance half-time determination. J Urol 164:467–471

Dey HM, Hoffer PB, Lerner E, et al. (1993) Quantitative analysis of the technetium-99m-DTPA captopril renogram: contribution of washout parameters to the diagnosis of renal artery stenosis. J Nucl Med 34:1416–1419

Dondi M, Fanti S, De Fabritiis A, et al. (1992) Prognostic value of captopril renal scintigraphy in renovascular hypertension. J Nucl Med 33:2040–2044

Donoso G, Kuyvenhoven JD, Ham H, Piepsz A (2003) 99mTc-MAG3 diuretic renography in children: a comparison between F0 and F+20. Nucl Med Commun 24:1189–1193

Dubovsky EV, Russell CD (1991) Diagnosis of renovascular hypertension after renal transplantation (Suppl). Am J Hypertension 4:724–730

Dubovsky EV, Russell CD, Bischof-Deloye A, et al. (1999) Report of the radionuclides in nephrourology committee for evaluation of transplanted kidney (review of techniques). Semin Nucl Med 29:175–188

Dustan HP, Mumphries AW, Dewolfe VG, Page IH (1964) Normal arterial pressure in patients with renal arterial stenosis. JAMA187:1028–1029

Erbslöh-Möller B, Dumas A, Roth D, Sfakianakis G, Bourgoignie JJ (1991) Furosemide I-131 hippuran renography after angiotensin-converting enzyme inhibition for the diagnosis of renovascular hypertension. Am J Med 90:23–29

Eshima D, Taylor A, Jr (1992) Technetium-99m (99mTc) mercaptoacetyltriglycine: Update on the new 99m Tc renal tubular function agent. Semin Nucl Med 22:61–73

Esteves FP, Taylor A, Manatunga A, et al. (2006) Tc-99m-MAG3 renography: Normal values for MAG3 clearance and curve parameters, excretory parameters and residual urine volume. AJR 187:W610–W617

Eyler WR, Clark MD, Garman JE, Rian RL, Meininger DE (1962) Angiography of the renal areas including a comparative study of renal arterial stenosis in patients with and without hypertension. Radiology 78:879–892

Fanti S, Dondi M, Guidalotti PL, et al. (1998) Bilateral symmetrical induced changes in captopril scintigraphy. J Nucl Med 39:86P

Fommei E, Ghione S, Hilson AJW, et al. (1993) Captopril radionuclide test in renovascular hypertension: A European multicentre study. Eur J Nucl Med 20:625–644

Fommei E, Ghione S, Hilson AJW, et al. (1994) Captopril radionuclide test in renovascular hypertension: European multicenter study. In: O'Reilly PH, Taylor A, Nally JV (eds) Radionuclides in nephrourology, vol 1. Field and Wood, Blue Bell, PA

Frokier J, Eskild-Jensen A, Dissing T (2006) Antenatally detected hydronephrosis: the nuclear medicine techniques. In: Prigent A, Piepsz A (eds) Functional imaging in nephrourology. Taylor and Francis, London, pp 103–115

Gainer JV, Morrow JD, Loveland A, King DJ, Brown NJ (1998) Effect of bradykinin-receptor blockade on the response to

angiotensin-converting-enzyme inhibitor in normotensive and hypertensive subjects. N Engl J Med 339:1285 – 1292
Garcia EV, Taylor A, Halkar RK, et al. (2006) RENEX: An expert system for the interpretation of 99mTc-MAG3 scans to detect renal obstruction. J Nucl Med 47:320 – 329
Gates GF (1982) Glomerular filtration rate: estimation from fractional renal accumulation of Tc-99m DTPA (stannous). AJR 138:565 – 570
Gates GF (1983) Split renal function testing using Tc-99m DTPA: rapid technique for determining differential filtration. Clin Nucl Med 8:400 – 407
Geyskes GG, deBruyn AJG (1991) Captopril renography and the effect of percutaneous transluminal angioplasty on blood pressure in 94 patients with renal artery stenosis. Am J Hypertens 4:685S–689S
Gordon I, Colarinha P, Fettich J, Fischer S, Frøkiær J, Hahn K, Kabasakal L, Mitjavila M, Olivier P, Piepsz A, Porn U, Sixt R, van Velzen J (2000) Guidelines for Standard and Diuretic Renogram in Children. In: EANM Web Journal. http://www.eanm.org/. Auspices of the Paediatric Committee of the European Association of Nuclear Medicine
Gordon I, Colarinha P, Fettich J, Fischer S, Frøkiær J, Hahn K, Kabasakal L, Mitjavila M, Olivier P, Piepsz A, Porn U, Sixt R, van Velzen J (2001) Guidelines for Standard and Diuretic Renogram in Children. Eur J Nucl Med 28:BP31 – 36
Halkar RK, Chrem Y, Galt, Jr, et al. (1996) Interoperator variability in quantitating the MAG3 renal uptake based on semiautomated and manual regions of interest. J Nucl Med 37:293P
Halkar R, Taylor A, Manatunga A, et al. (2007) Monitoring renal function: a prospective study comparing camera-based clearance and creatinine clearance. Urology 69:426 – 430
Helin KH, Tikkanen I, von Knorring JE, et al. (1998) Screening for renovascular hypertension in a population with relatively low prevalence. J Hypertension 16:1523 – 1529
Holley KE, Hunt JC, Brown AL, Jr, et al. (1964) Renal artery stenosis: a clinical-pathologic study in normotensive and hypertensive patients. Am J Med 37:14 – 22
Howman-Giles R, Uren R, Roy LP, et al. (1987) Volume expansion diuretic renal scan in urinary tract obstruction. J Nucl Med 28:824 – 828
Hunsche A, Press H, Taylor A (2004) Increasing the dose of furosemide in patients with azotemia and suspected obstruction. Clin Nucl Med 26:149 – 153
Hvistendahl JJ, Pedersen TS, Schmidt F, et al. (1998) Renal function is modulated by a vesico-renal reflex mechanism during elevated bladder pressure in the pig. Nucl Med Commun 19:502
Inoue Y, Ohtake T, Yokoyama I, Yoshikawa K, Asai S, Ohtomo K (1999) Evaluation of renal function from 99mTc-MAG3 renography without blood sampling. J Nucl Med 40:793 – 798
Jadvar H, Kherbache HM, Pinski JK, Conti PS (2004) Diagnostic role of [F-18]-FDG positron emission tomography in restaging renal cell carcinoma. Clin Nucl Med 29:811 – 812
Kabasakal L, Atay S, Vural AV, et al. (1995) Evaluation of Tc-99m-L,L-ethylenedicysteine in renal disorders and determination of extraction ratio. J Nucl Med 36:1398 – 1403
Kahn D, Ben-Haim S, Bushnell DL, et al. (1994) Captopril-enhanced Tc-99m MAG3 renal scintigraphy in subjects with suspected renovascular hypertension. Nucl Med Commun 15:515 – 528
Kanazawa T, Shimizu M, Seto H, et al. (1998) Reproducibility of ^{99}Tcm-MAG3 clearance in normal volunteers with the two-sample method: comparison with OIH. Nucl Med Commun 19:899 – 903
Karanikas G, Becherer A, Wiesner K, Dudczak R, Kletter K (2002) ACE inhibition is superior to angiotensin receptor blockade for renography in renal artery stenosis. Eur J Nucl Med 29:312 – 318
Kass EJ, Majd M (1985) Evaluation and management of upper urinary tract obstruction in infancy and childhood. Urol Clin North Am 12(1):133 – 141
Kletter K, Nurnberger N (1989) Diagnostic potential of diuresis renography: Limitation by the severity of hydronephrosis and by impairment of renal function. Nucl Med Comm 10:51 – 61
Klingensmith WC, Briggs DE, Smith WI (1994) Technetium-99m-MAG3 renal studies: normal range and reproducibility of physiologic parameters as a function of age and sex. J Nucl Med 35:1612 – 1617
Kon V, Fogo A, Ichikawa I, et al. (1993) Bradykinin causes selective efferent arteriolar dilation during angiotensin I converting enzyme inhibition. Kidney Int 44:545 – 550
Kopecky RT, McAfee JG, Thomas FD, et al. (1990) Enalaprilat-enhanced renography in a rat model of renovascular hypertension. J Nucl Med 31:501 – 507
Kotzerke J, Glatz S, Grillenberger K, et al. (1997) Reproducibility of a single-sample method for ^{99}Tcm-MAG3 clearance under clinical conditions. Nucl Med Commun 18:352 – 357
Kuyvenhoven J, Piepsz M, Ham H (2003) When could the administration of furosemide be avoided? Clin Nucl Med 28:732 – 737
Levey AS, Madaio MP, Perrone RD (1991) The kidney. In: Brenner BM, Rector FC (eds) Laboratory assessment of renal disease: clearance, urinalysis and renal biopsy. WB Saunders, Harcourt Brace, Jovanovich, Philadelphia, PA, pp 919 – 968
Lindh A, Malmgren M, Ekberg S, Stenstrom M, Granerus G (1998) Analysis of the diuretic response to 7 ml/kg hydration prior to captopril renography. Eur J Nucl Med 25:1190
Liu Y, Ghesani NV, Skurnick JH, Zukier LS (2005) The F+0 protocol for diuretic renography results in fewer interrupted studies due to voiding than the F–15 protocol. J Nucl Med 46:317 – 320
Lorberboym M, et al. (2000) The role of renal scintigraphy and unenhanced helical computerized tomography in patients with ureterolithiasis. Eur J Nucl Med 27:441 – 446
Ludwig V, Martin WH, Delbeke D (2003) Calcium channel blockers: a potential cause of false-positive captopril renography. Clin Nucl Med 28:108 – 112
Majhail NS, Urbain JL, Albani JM, et al. (2003) F-18 fluorodeoxyglucose positron emission tomography in the evaluation of distant metastases from renal cell carcinoma. J Clin Oncol 21:3995 – 4000
Manjunath G, Sarnak MJ, Levery AS (2001) Estimating the glomerular filtration rate; dos and don'ts for assessing kidney function. Postgrad Med 110(6):55 – 62
Marcus CS, Kuperus JH (1985) Pediatric renal I-123 orthoiodohippurate dosimetry. J Nucl Med 26:1211 – 1214
Members of the Society for Fetal Urology and Pediatric Nuclear Medicine Council Members, Society of Nuclear Medicine (1992) The "well tempered" diuretic renogram: a standard method to examine the asymptomatic neonate with hydronephrosis or hydroureteronephrosis. J Nucl Med 33:2047 – 2051
Mittal BR, Kumar P, Arora P, et al. (1996) Role of captopril renography in the diagnosis of renovascular hypertension. Am J Kidney Dis 28:209 – 213
Müller-Suur R, Tidgren B, Lundberg HJ (1998) Effect of captopril on MAG3 clearance in patients with and without renal artery stenosis and after PTRA. Eur J Nucl Med 25:845
Nally JW, Jr, Chen C, Fine E, et al. (1991) Diagnostic criteria of renovascular hypertension with captopril renography. Am J Hypertens 4:749S–752S
Nankivell BJ, Borrows RJ, Fung CL, O'Connell PJ, Allen RDM, Chapman JR (2003) The natural history of chronic allograft nephropathy. N Engl J Med 349:2326 – 2333

Nussberger J, Brunner DB, Waeber B, Brunner HR (1985) Plasma angiotensin under sustained converting enzyme inhibition with enalapril in normal humans. J Hypertens 3:S269–S270
O'Reilly P, Aurell M, Britton K, et al. (1996) Consensus on diuresis renography for investigating the dilated upper urinary tract. J Nucl Med 37:1872 – 1876
Peters AM, George P, Ballardie F, et al. (1988) Appropriate selection of background for 99mTc-DTPA. Nucl Med Commun 9:973 – 985
Picciotto G, Sargiotto A, Petrarulo M, Rabbia C, De Filippi PG, Roccatello D (2003) Reliability of captopril renography in patients under chronic therapy with angiotensin II (AT1) receptor antagonists. J Nucl Med 44:1574 – 1581
Piepsz A, Tondeur M, Kinthaert J, et al. (1988) Reproducibility of technetium-99m-mercaptoacetylglycine clearance . Eur J Nucl Med 23:195 – 198
Piepsz A, Tondeur M, Ham HR (2000) NORA: A simple and reliable parameter for estimating renal output with or without frusemide challenge. Nucl Med Commun 21:317 – 323
Piepsz A, Kuyvenhoven JD, Tondeur M, Ham H (2002) Normalized residual activity: usual values and robustness of the method. J Nucl Med 43:33 – 38
Plouin PF, Chatellier G, Darne B, Raynaud A (1998) Blood pressure outcome of angioplasty in atherosclerotic renal artery stenosis: a randomized trial. Essai Multicentrique Medicaments vs Angioplastie (EMMA) Study Group. Hypertension 31(3):823 – 829
Prigent A (1993) The diagnosis of renovascular hypertension: the role of captopril renal scintigraphy and related issues. Eur J Nucl Med 20:625 – 644
Prigent A, Piepsz A, Müller-Suur R (1998) The true clinical significance of renography in nephro-urology. Eur J Nucl Med 25:307 – 312
Prigent A, Cosgriff P, Gates GF, et al. (1999) Consensus report on quality control of quantitative measurements of renal function obtained from renogram. Semin Nucl Med 29: 146 – 159
Rosenbaum JL (1970) Evaluation of clearance studies in chronic kidney disease. J Chron Dis 22:507 – 514
Russell CD (1993) Optimum sample times for single-injection, multi-sample renal clearance methods. J Nucl Med 10: 1761 – 1765
Russell CD, Dubovsky EV (1999) Reproducibility of single-sample clearance of 99mTc-mercaptoacetyltriglycine and 131I-orthohippurate. J Nucl Med 40:1122 – 1124
Russell CD, Thorstad B, Yester MV, et al. (1988) Comparison of technetium-99m MAG3 with iodine-131 hippuran by a simultaneous dual channel technique. J Nucl Med 29:1189 – 1193
Russell CD, Taylor AT, Dubovsky EV (1996) Measurement of renal function with technetium-99m-MAG3 in children and adults. J Nucl Med 37:588 – 593
Sandberg K, Hong J (2000) Kidney angiotensin receptors and their role in renal pathophysiology. Semin Nephrol 20:402 – 416
Schaap GH, Alferink THR, deJong RBJ, et al. (1988) Tc-99m MAG3: dynamic studies in patients with renal diseases. Eur J Nucl Med 14:28 – 31
Schlegel JU, Hamway SA (1976) Individual renal plasma flow determination in 2 minutes. J Urol 116:282 – 285
Schöder H, Larson SM (2004) Positron emission tomography for prostate, bladder and renal cancer. Semin Nucl Med 34:274 – 292
Setaro JF, Saddler MC, Chen CC, et al. (1991) Simplified captopril renography in diagnosis and treatment of renal artery stenosis. Hypertension 18:289 – 298
Sfakianakis GM, Bourgoignie JJ, Georgiou M, et al. (1993) Diagnosis of renovascular hypertension with ACE inhibition scintigraphy. Radiol Clin North Am 31:831 – 848
Sfakianakis GN, Cohen DJ, Braunstein RH, et al. (2000) MAG3-F0 scintigraphy in decision making for emergency intervention in renal colic after helical CT positive for a urolith. J Nucl Med 41:1813 – 1822
Shattuck LA, Eshima D, Taylor AT, Anderson T, Graham DL, Latino FA, Payne SE (1994) Evaluation of the hepatobiliary excretion of Tc-99m MAG3 and reconstitution factors affecting the radiochemical purity. J Nucl Med 35:349 – 355
Slavin JD, Jung WK, Spencer RP (1996) False-positive study with Tc-99m DTPA caused by infiltration of dose. Clin Nucl Med 21:978 – 980
Stabin M, Taylor A, Eshima D, Wooten W (1992) Radiation dosimetry for technetium-99m-MAG3, technetium-99m-DTPA, and iodine-131-OIH based on human biodistribution studies. J Nucl Med 33:33 – 40
Stavropoulos SW, Sevigny SA, Ende JF, Drane WE (1999) Hypotensive response to captopril: a potential pitfall of scintigraphic assessment for renal artery stenosis. J Nucl Med 40:406 – 411
Strauss BS, Blaufox MD (1970) Estimation of residual urine and urine flow rates without ureteral catheterization. J Nucl Med 11:81 – 84
Szabo Z, Matthews WB (2006) Positron emission tomography imaging of the kidneys. In: Prigent A, Piepsz A (eds) Functional imaging in nephrourology. Taylor and Francis, London, pp 197 – 210
Taylor A (2000) Functional testing: ACEI renography. Semin Nephrol 20:437 – 444
Taylor A (2006) ACE inhibition renography in the evaluation of suspected renovascular hypertension. In: Prigent A, Piepsz A (eds) Functional imaging in nephrourology. Taylor and Francis, London, pp 149 – 164
Taylor A, Eshima D (1994) Renal artery stenosis and ischemia: effect on renal blood flow and extraction fraction. Hypertension 23:96 – 103
Taylor A, Eshima D, Christian P, Milton W (1987) Evaluation of Tc-99m mercaptoacetyltriglycine in patients with impaired renal function. Radiology 162:365 – 370
Taylor A, Eshima D, Christian PE, et al. (1988) A technetium-99m MAG3 kit formulation: preliminary results in normal volunteers and patients with renal failure. J Nucl Med 29:616 – 622
Taylor A, Jr, Ziffer JA, Eshima D (1990) Comparison of Tc-99m MAG3 and Tc-99m DTPA in renal transplant patients with impaired renal function. Clin Nucl Med 15:371 – 378
Taylor A, Lewis C, Giacometti A, et al. (1993) Improved formulas for the estimation of renal depth in adults. J Nucl Med 34:1766 – 1769
Taylor A, Thakore K, Folks R, Halkar R, Manatunga A (1994a) Background subtraction in Tc-99m-MAG3 renography. J Nucl Med 35:2054 – 2055
Taylor A, Clark S, Ball T (1994b) Comparison of Tc-99m MAG3 and Tc-99m DTPA scintigraphy in neonates. Clin Nucl Med 19:575 – 580
Taylor A, Corrigan PL, Galt J, et al. (1995) Measuring technetium-99m-MAG3 clearance with an improved camera-based method. J Nucl Med 36:1689 – 1695
Taylor, Nally J, Aurell M, et al. (1996) Consensus report on ACE inhibitor renography for detecting renovascular hypertension. J Nucl Med 37:176 – 1882
Taylor A, Hansen L, Eshima D, et al. (1997a) Comparison of technetium-99m-L,L-EC isomers in rats and humans. J Nucl Med 38:821 – 826
Taylor A, Manatunga A, Morton K, et al. (1997b) Multicenter trial validation of a camera based method to measure Tc-99m mercaptoacetyltriglycine or Tc-99m MAG3 clearance. Radiology 204:47 – 54
Taylor A, Myrick S, Grant S, Issa M, Halkar R, Alazraki NP

(1999) A prospective study to compare the reproducibility of camera based MAG3 and creatinine clearance measurements. J Nucl Med 40:52P
Taylor, Blaufox MD, Dubovsky EV, et al. (2003) Society of Nuclear Medicine procedure guideline for diagnosis of renovascular hypertension. www.snm.org
Thrall JH, Koff SA, Keyes JW, Jr. (1981) Diuretic radionuclide renography and scintigraphy in the differential diagnosis of hydroureteronephrosis. Semin Nucl Med 11:89 – 104
Thrall JH, Ziessman HA (1995) Nuclear medicine: The requisites. Mosby-Year Book, St. Louis, MO, p 300
Tonnesen KH, Munck O, Hald T, et al. (1974) Influence on the radiorenogram of variation in skin to kidney distance and the clinical importance hereof. In: Zum Winkel K, Mlaufox MD, Funck-Bretano JL (eds) Proceedings of the International Symposium on Radionuclides in Nephrourology. Thieme, Stuttgart, pp 79 – 86
Upsdell SM, Leeson SM, Brooman PJC, et al. (1988) Diuretic-induced urinary flow rates at varying clearances and their relevance to the performance and interpretation of diuresis renography. Br J Urol 61:14 – 18
Upsdell SM, Testa HJ, Lawson RS (1992) The F-15 diuresis renogram in suspected obstruction of the upper urinary tract. Br J Urol 69:126 – 131
van Jaarsveld BC, Krijnen P, Pieterman H, Derkx FH, Deinum J, Postma CT, Dees A, Woittiez AJ, Bartelink AK, Man in 't Veld AJ, Schalekamp MA (2000) The effect of balloon angioplasty on hypertension in atherosclerotic renal-artery stenosis. Dutch Renal Artery Stenosis Intervention Cooperative Study Group. N Engl J Med 342(14):1007 – 1014
Van Nerom CG, Bormans GM, De Roo MF, Verbruggen AM (1993) First experience in healthy volunteers with Tc-99m-L,L-ethylenedicysteine: a new renal imaging agent. Eur J Nucl Med 20:738 – 746
Visscher CA, de Zeeuw D, Huisman RM (1995) Effect of chronic ACE inhibition on the diagnostic value of renography for renovascular hypertension: a preliminary report. Nephrol Dial Transplant 10:263 – 265
Visscher CA, de Zeeuw D, de Jong PE, et al. (1996) Angiotensin-converting enzyme inhibition-induced changes in hippurate renography and renal function in renovascular hypertension. J Nucl Med 37:482 – 488
Webster J, Marshall F, Abdalla M, Dominiczak A, Edwards R, Isles CG, Loose H, Main J, Padfield P, Russell IT, Walker B, Watson M, Wilkinson R (1998) Randomised comparison of percutaneous angioplasty vs continued medical therapy for hypertensive patients with atheromatous renal artery stenosis. Scottish and Newcastle Renal Artery Stenosis Collaborative Group. J Hum Hypertens 12(5):329 – 335
Wilcox CS (1996) Ischemic nephropathy: noninvasive testing. Semin Nephrol 16:43 – 52
Wong DC, Rossleigh MA, Farnsworth RH (1999) F+0 diuresis renography in infants and children. J Nucl Med 40:1805 – 1811
Wong DC, Rossleigh MA, Farnsworth RH (2000) Diuretic renography with the addition of quantitative gravity-assisted drainage in infants and children. J Nucl Med 41:1030 – 1036

Lower Genitourinary Tract

8

Tzu-Chen Yen, Cheng-Keng Chuang, Chyong-Huey Lai

Conventional radionuclide techniques have, for many years, played a role in evaluating vesico-ureteral reflux and suspected testicular torsion. More recently, the advent of prostate immunoscintigraphy, positron emission tomography (PET) and PET/computed tomography (CT) has broadened nuclear medicine's role to the area of oncologic diagnosis, as well. This chapter will first discuss the older standard techniques and follow with the oncologic applications in both the male and female genitourinary tract.

8.1 Radionuclide Cystography

Urinary tract infection (UTI) is a common problem in childhood and may lead to unwanted sequelae such as renal scarring, hypertension, and renal failure. Vesicoureteral reflux (VUR) is the most common urologic anomaly in children, occurring in about 1% of newborns. In children with UTI, the incidence of VUR ranges between 30% and 45%. VUR predisposes children to acute pyelonephritis by transporting bacteria from the bladder to the kidney. If the child has repeated infections, a strong family history of VUR or persistent hydronephrosis or ureteral dilatation on postnatal ultrasonography, cystography is recommended for the detection of VUR. The radiographic voiding cystourethogram (VCUG) is the generally accepted referencing method. Radionuclide cystography has a lower gonadal radiation dose and is as sensitive as VCUG. However, it cannot provide the same anatomical detail as VCUG. Abnormalities such as ectopic ureterocele and duplicated collecting systems will be detected more readily with the radiographic study. In the follow-up studies where the anatomical detail is not required and the presence or absence of reflux is the primary consideration, radionuclide cystography becomes the method of choice.

There are two kinds of radionuclide cystography in clinical practice: direct radionuclide cystography (DRC) and indirect radionuclide cystography (IRC). DRC utilizes catheterization and instillation of radionuclide-containing fluid to distend the urinary bladder. Images are to be taken throughout bladder filling, voiding, and after voiding for detecting VUR. IRC does not require bladder catheterization, but only cooperative toilet-trained children can undergo this procedure. For DRC, the patient is catheterized and a slow fluid instillation is required to avoid premature micturition. The end of fluid instillation into the bladder is achieved when the patient develops discomfort, spontaneously voids, or when the fluid instillation is stopped by the elevated pressure in the bladder. Detectable reflux is classified into three grades: grade 1, with activity limited to the ureter; grade 2, with activity reaching the collecting system with little activity in the ureter; grade 3, with activity in the dilated collecting system and in the dilated tortuous ureter (Fig. 8.1). Postvoid residual volume in the bladder can also be quantified as will be described in the following section. One of the major reasons that DRC is preferable to IRC is that 21% of reflux occurs only during the filling phase and not during voiding (Conway et al. 1972).

Indirect cystography (IRC) is performed at the completion of a conventional upper urinary tract evaluation with Tc-99m DTPA or MAG-3. Care must be taken to assure that the kidneys have emptied prior to commencing the voiding portion of the examination. The child must be older in order to cooperate. He or she is positioned on a portable potty with the camera detector head against their back. Images are obtained continuously while the child is voiding. The advantages of this method over DRC are the avoidance of catheterization and the ability to evaluate the upper urinary tract. However, the disadvantages are the need for an older cooperative child, a potentially longer wait to empty the upper tract (particularly if renal disease is present) and, most importantly, as mentioned above, the fact that up to 21% of cases of reflux occurring only during bladder filling may be missed if only the voiding phase is studied.

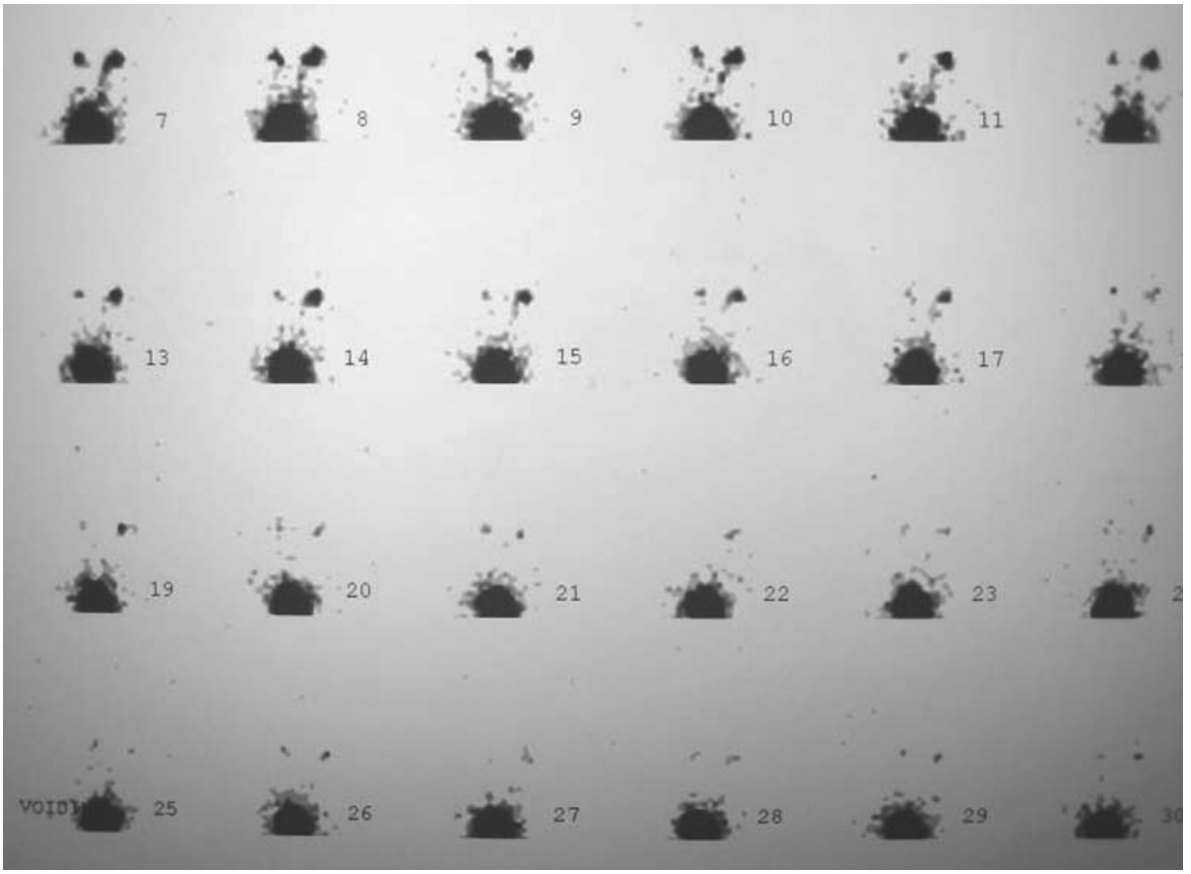

Fig. 8.1. Direct radionuclide cystography of a 6-year-old boy revealed the presence of bilateral vesicoureteral reflux at voiding

8.1.1 Determination of Residual Urine

As part of the reflux study or, alternatively, evaluating patients with prostatic enlargement, one can easily determine post-voiding residual bladder volume. The procedure starts with performing a conventional renal scan. At the completion of the study, the kidneys should be relatively empty and the bladder full. Counts are obtained over the bladder. The patient then voids into a container and the volume of voided urine is determined. Post-void counts are then obtained over the bladder. Using these values, residual urine is then calculated using the following formula:

$$\frac{\text{Voided Volume} \times \text{Final Count}}{\text{Initial Count} - \text{Final Count}} \qquad (8.1)$$

8.1.2 Testicular Scintigraphy

About 80% of patients with acute scrotal pain have non-surgical conditions such as epididymitis or torsion of the appendix testis, while testicular torsion may account for the remainder. Testicular torsion is a surgical emergency since successful detorsion within 6 h results in nearly 100% testicular viability. Detorsion at 12 h results in only 20% viability. The diagnosis of testicular torsion can be suspected clinically based upon the history and physical examination. If the etiology of an acute scrotal pain remains equivocal, color Doppler ultrasonography or testicular scintigraphy can be undertaken. Decreased testicular perfusion usually indicates testicular torsion, while epididymitis shows increased blood flow to the affected side (Fig. 8.2). However, decreased perfusion can also be seen in patients with hydrocele, abscess, hematoma, or scrotal hernia. It is also important to keep in mind that false-negative sonographic or nuclear scan results may occur with spontaneous detorsion and partial or intermittent torsion. Another pattern that may be seen is a photon deficient scrotum with a surrounding rim of increased activity (Fig. 8.3). This pattern has been referred to as a delayed or late torsion. It results from increased flow from the internal pudendal vessels to the dartos surrounding the testicle. The internal pudendal artery does not travel through the spermatic cord and is, therefore, not involved in the torsion. This creates a "bull's-eye" appearance in this late torsion image.

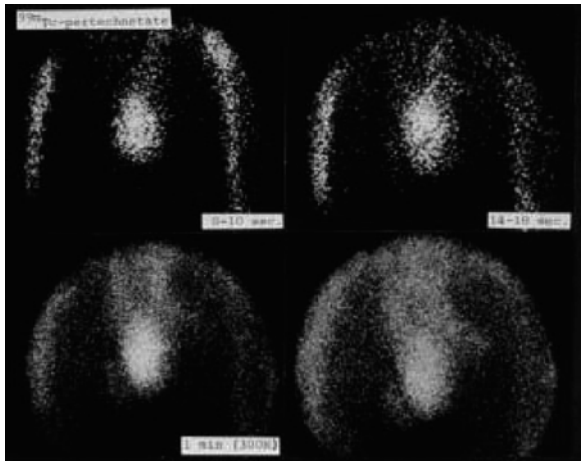

Fig. 8.2. A 9-year-old boy had severe left scrotal pain. Testicular scintigraphy revealed markedly increased activity over the entire left scrotal contents consistent with acute epididymitis

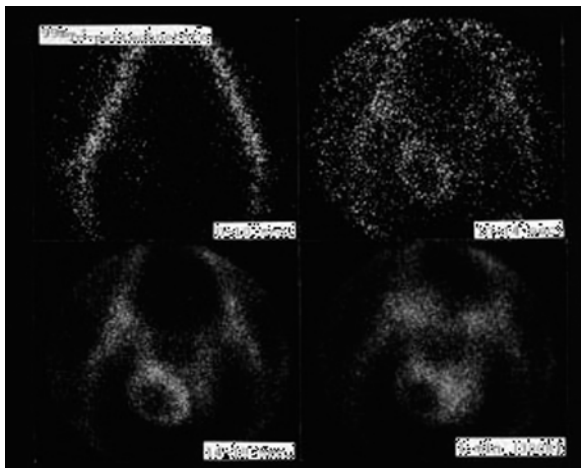

Fig. 8.3. An 8-year-old boy had right scrotal pain and swelling for 2 days. Testicular scintigraphy revealed decreased blood pool activity over the right testicle with increased radiotracer activity surrounding it, indicating delayed torsion

The non-specificity of a "cold" area is illustrated in Fig. 8.4. It is essential that the scintigraphic findings are correlated with history and physical findings in order to arrive at the correct diagnosis.

For testicular scintigraphy, Tc-99m pertechnetate is administered intravenously as a rapid bolus. Radionuclide angiography can be acquired with 3–4 s frames. Static blood-pool imaging of the scrotum is then obtained. The penis is usually taped to the skin over the pubis, and a lead shield can be placed underneath the scrotum to reduce background interference from the thighs and bladder. It is advisable to obtain an additional pin-hole image to achieve higher resolution. A line source can be used to mark the median scrotal raphe for better image interpretation.

8.2 Malignancies of the Male Genital System

8.2.1 Prostate Cancer

Prostate cancer is the most common cancer in men. In the United States, more than 230,000 new patients of prostate cancer were diagnosed in 2005 and about 30,000 men will die from this disease in the same period. A 50-year-old man has a 42% chance of developing prostate cancer during his lifetime and a 3% risk of death due to it. Widespread screening with prostate specific antigen (PSA) has led to earlier detection of this cancer, rendering more patients detected at a curable stage. Accurate staging at initial detection is essential for the selection of appropriate treatment. Localized prostate cancer can be treated with radical prostatectomy or radiation therapy, while non-contiguous metastatic disease is typically treated with hormonal therapy. Digital rectal examination, transrectal ultrasound, and MRI are used for assessment of local tumor.

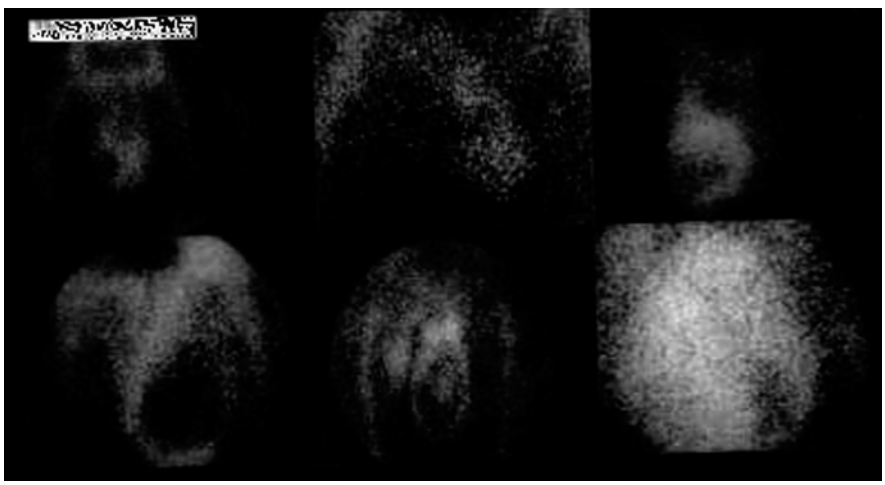

Fig. 8.4. The non-specificity of photon deficient lesions is evident in these six different patients: testicular torsion (*upper left*), appendix testis torsion (*upper middle*), hematoma (*upper right*), inguinal hernia (*lower left*), hydrocele (*lower middle*), prosthetic testicle (*lower right*). Careful attention to the history and physical findings is essential to clarify the etiology of the cold area in each patient

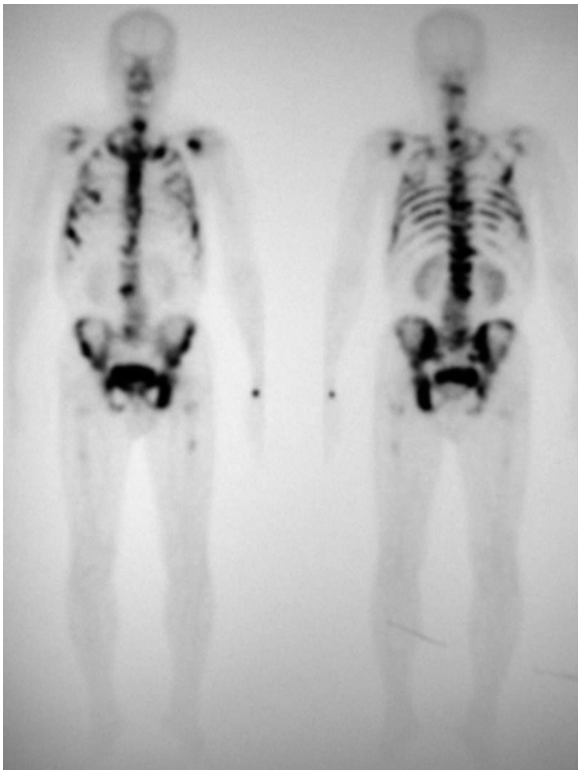

Fig. 8.5. Skeletal scintigraphy in an 80-year-old man with clinical stage T3 prostate cancer and PSA level of 26.2 ng/ml shows the presence of multiple bone metastases

The detection of bone metastasis, which is the most frequent distant metastasis and is predominantly osteoblastic, can be performed using skeletal scintigraphy. Figure 8.5 shows a skeletal scintigraph in a patient with prostate cancer who has multiple bone metastases. Generally, a bone scan is only recommended if the PSA level exceeds 10 ng/mg. Conventional imaging modalities, including CT, MRI and sonography, have limitations in the detection of small metastatic lymph nodes, in the differentiation of benign and malignant lesions, and in the uncovering of recurrent or metastatic foci at PSA relapse. In addition, there is a wide variation of tumor biology in prostate cancer, ranging from low-grade, indolent tumors to very aggressive, rapidly lethal carcinomas. Gleason scoring is a histologic grading of tumor differentiation, with the higher scores (>7) signifying the more aggressive, de-differentiated lesions with a poorer prognosis.

Increased popularity of PET and PET/CT as well as clinical and basic studies utilizing new tracers will definitely expand its clinical utility in the future. In general, fluorodeoxyglucose (FDG) has not performed as well in prostatic cancer as it has in many other areas of oncologic diagnosis, such as the gynecologic malignancies discussed later in this chapter. Acetate, choline, and methionine labeled with positron-emitting isotopes have also been shown to be promising in many circumstances. In addition to staging, recurrence detection and restaging, PET or PET/CT with these newer agents has the potential to be of assistance in prognosis, risk stratification for optimal treatment selection, and monitoring or assessment of therapeutic response.

Immunoscintigraphy with capromab pendetide (Prostascint) has provided an additional means of detecting lymph node metastases. Although it has been used in high risk patients at initial presentation, its main application has been in post-prostatectomy patients with recurrent PSA elevations. This will be discussed in the section on recurrent disease.

8.2.1.1 Initial Staging

Since prostate cancers are often slow-growing and have lower rates of glycolysis, these cancers usually have lower FDG uptake. Additionally, it is important to keep in mind that benign prostatic hyperplasia (BPH) and prostatitis may also be associated with elevated FDG uptake. It is thus problematic to differentiate between benign and malignant prostatic processes. The strong FDG activity in the urine also makes the distinction between the prostate and the bladder difficult. So FDG-PET probably has no role in the detection or exclusion of primary prostate cancer. However, the study by Oyama et al. suggested a correlation between higher FDG accumulation and higher Gleason grades of prostate cancer (Oyama et al. 2001). FDG-PET might detect some unsuspected foci of metastasis at initial staging. More aggressive tumor cells with enhanced glycolysis will be more easily detected by FDG-PET. In addition, FDG-PET may have implications in assessing the aggressiveness of local or metastatic tumor cells, and thus may have implications in the selection of optimal treatment.

Carbon-11 choline was first used by Hara et al. (1998) to image prostate cancer patients. Its mechanism of uptake is related to the synthesis of phosphatidylcholine and other phospholipids as essential components of the cell membrane. The standardized uptake value (SUV) of tracer uptake in tumor is high while its accumulation in the bladder and rectal wall is low. Farsad et al. (2005) performed a sextant-based analysis in 36 patients with prostate cancer. The sensitivity, specificity, and accuracy of C-11 choline PET/CT were 66%, 81%, and 71%, respectively. Prostate disorders other than cancer may also accumulate C-11 choline. Thus, this tracer is not suited for detecting or excluding primary prostate cancer. Sutinen et al. (2004) found no correlation between the tumor uptake of C-11 choline and the histological grade, Gleason score, or PSA. However, it may have some utility in the detection of lymph node or distant metastasis. In a prospective study of 67

prostate cancer patients by de Jong et al. (2003), the sensitivity, specificity, and accuracy of C-11 choline PET for detecting metastatic pelvic lymph nodes were 80 %, 96 %, and 93 % respectively. F-18 fluorocholine with its longer half-life for imaging also has been developed. A preliminary study showed its potential to be the same as C-11 choline in the detection of lymph node metastases and recurrent disease (Schmid et al. 2005).

Carbon-11 acetate was studied as a tracer for renal imaging by Shreve et al. (1995). They found the clearance rate of C-11 acetate in renal cell carcinoma is substantially reduced. Oyama et al. (2002) studied 22 patients at initial staging and found that C-11 acetate is more sensitive than FDG for detecting prostate cancer. However, the study of Kato et al. (2002) revealed that, like C-11 choline, it is difficult to discriminate prostate cancer from BPH or normal prostate tissue by using this tracer. Increased acetate accumulation is probably related to enhanced lipid synthesis and is not specific for cancers. However, its higher sensitivity may have some value in the detection of metastatic or recurrent disease. Preliminary application of F-18 fluoroacetate was also reported with the advantage of acquiring delayed imaging (Matthies et al. 2004).

Carbon-11 methionine has also been studied in prostate cancer. Its accumulation in tumor cells is related to increased amino acid metabolism. Further studies of comparison and complementary utility of the above-mentioned tracers are needed. At present, it is clear that the utility of PET in the initial staging of prostate cancer is limited to those patients with more advanced disease.

In addition to distant metastasis, the presence or absence of lymph node metastasis is also important for treatment selection and prognosis prediction of prostate cancer. Local lymph node spread in the pelvis without distant metastasis may potentially be curable if early treatment is instituted. Extensive pelvic lymphadenectomy, in addition to radical prostatectomy, has been proposed as the treatment of choice in this situation. However, this may result in complications such as lymphocele, lymphedema, deep vein thrombosis and pulmonary embolism. As a result, a reliable method to detect lymph node metastasis is important. Zuckier et al. (1990) introduced a method for prostatic sentinel lymph node (SLN) localization. Wawroschek et al. (2003) performed studies of SLN in 350 patients with clinically organ-confined prostate cancer; lymph node metastasis was present in 25 % of patients and the SLN technique with subsequent biopsy had a sensitivity of 97 %. Figure 8.6 shows a sentinel node study after injection of a colloid tracer directly into the prostate bed. However, this technique is highly demanding and may need a substantial learning curve. Harisinghani et al. (2003) studied 80 patients with clinical stage T1-T3 prostate cancer using MRI with lymphotropic superparamagnetic nanoparticles. All 33 patients with lymph node metastasis were detected. In the node-by-node analysis, this new method had a sensitivity of 90.5 % while the conventional MRI had a sensitivity of 35.4 %. This newly developed MRI method seems quite promising.

As mentioned above, Prostascint studies have also been used to detect lymph node metastases in newly presenting, high risk patients. In a commercially sponsored study in 224 pre-operative patients, positive results were found in 85 %. In 40 %, lesions were confined to the prostate or peri-prostatic area while 44 % had extra-prostatic, intra-pelvic lesions and 16 % had extra-pelvic lesions clearly out of the surgical field.

8.2.1.2 Recurrent Disease

In prostate cancer, most recurrent disease presents as biochemical failure, that is, an increase in the serum PSA values. Transrectal ultrasound and MRI can be used to detect local recurrence with limited success. The sensitivity of conventional MRI for detecting lymph node metastasis is also low. Skeletal scintigraphy can be used to detect bone metastasis but the presence of bone metastases seems to be rare in the initial

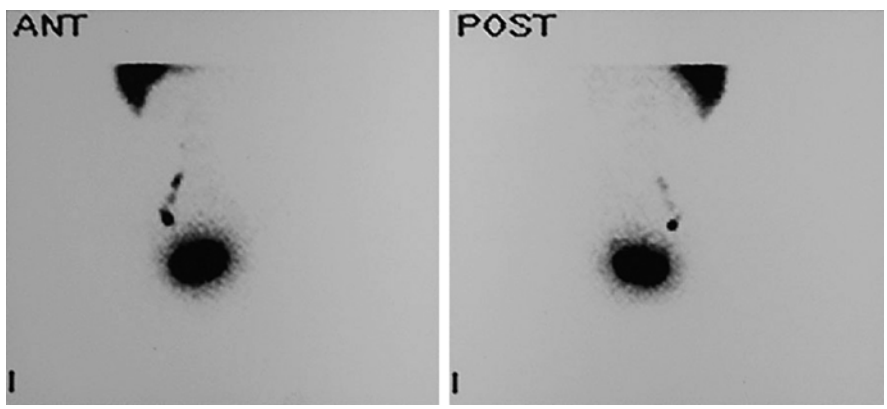

Fig. 8.6. Visualization of right iliac nodes after injecting Tc-99m labeled sulfur colloid particles into the prostate showed sentinel lymph nodes in the right iliac region

situation of PSA relapse after successful primary treatment.

Immunoscintigraphy

Immunoscintigraphy with radiolabeled antibody to prostate-specific membrane antigen (PSMA), using In-111 capromab pendetide (Prostascint: Cytogen Co., Princeton, NJ), has been utilized. Its sensitivity for local recurrence in the prostatic bed is 49–77% and its specificity is 35–71% (Lamb and Faulds 1998). Although this is not highly sensitive, it is still considerably better than the 15% sensitivity obtained with CT. It must be kept in mind that blind biopsy of the prostate fossa is also not very sensitive, with only 50% of positive cases being detected on initial sampling. Thus, Prostascint and biopsy performed together yield much better results.

The overall sensitivity of the study as shown in a large, commercially sponsored study was 72% (187 of 259 patients). Of the positive studies, 31% had disease confined to the prostate fossa and contiguous area (Fig. 8.7), 29% had disease outside the fossa, but within the pelvis, and 40% had extrapelvic disease. Interestingly, in this latter group, 16% had both pelvic and extrapelvic involvement whereas a striking 24% had disease only in the abdomen or above (Fig. 8.8). These latter cases represent "skip" metastases. Saitoh et al. postulated that these "skip" metastases may be due to any of three possible mechanisms. These are:

1. Streamlining via lymphatics bypassing pelvic nodes
2. Hematogenous rather than lymphatic spread through the para-vertebral venous plexus of Batson, directly seeding extrapelvic nodes
3. Direct extension from vertebral bony metastases

The demonstration of extra-pelvic metastases has a very significant impact on management decisions, since the disease has progressed to a point where it is outside both the surgical and usual radiotherapy treatment field. Kahn et al. (1998) have reported on the results of salvage radiotherapy to the prostate fossa following recurrent PSA elevations. Durable complete responses were much more frequent (70% of patients) when the study was normal or disease was confined to the fossa. Only 22% of patients showed a positive response to radiation when extra-pelvic disease was present on the study.

Prostascint studies are performed after a slow intravenous infusion of 5 mCi of indium-111 labeled antibody over a 3–5 min period. The patient returns at 72–96 h. Blood is drawn and the red cells are labeled with 20 mCi of ^{99m}Tc using either in vitro or in vivo methodology. Dual acquisition whole body as well as SPECT pelvic and abdominal images are obtained simultaneously using the ^{111}In and ^{99m}Tc photopeaks. The images may be co-registered if the appropriate software is available. The blood pool images are necessary to help distinguish blood vessels from adjacent lymph nodes, particularly in the pelvis.

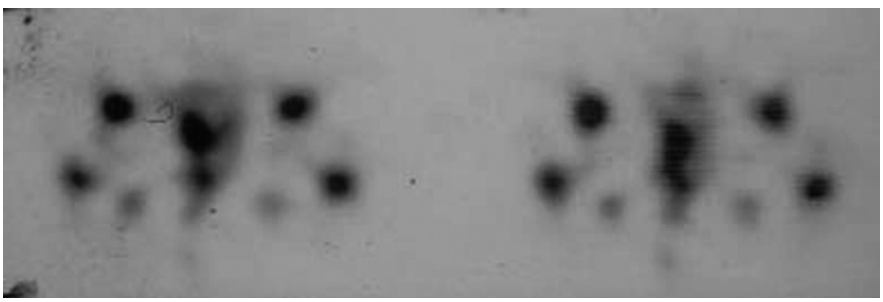

Fig. 8.7. Indium-111 capromab pendetide imaging revealed radiotracer uptake in the prostatic bed, suggesting local recurrence in a patient with PSA relapse

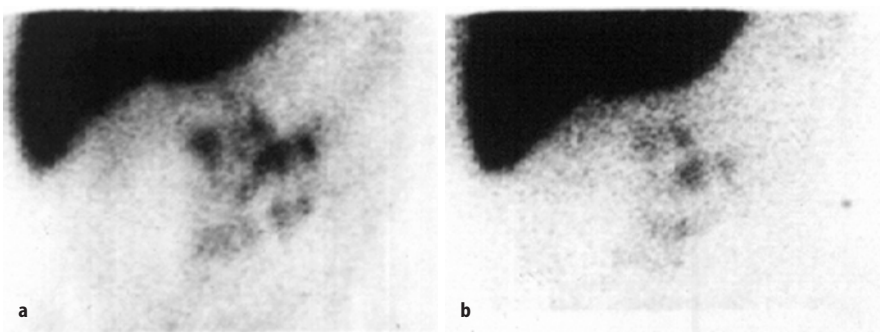

Fig. 8.8. a Prostascint study showing "skip" metastases to abdominal node (**b**). Four-month follow-up with patient on anti-androgen therapy

PET Studies

Salminen et al. (2002) studied 15 prostate cancer patients with suspicious recurrence using FDG-PET. In 13 patients with recurrence, FDG-PET was true positive in 10 patients. FDG-PET tends to detect true-positive lesions if the PSA level is high. Nunez et al. (2002) studied 12 patients with newly noticed disease progression. The lesion-based sensitivities of FDG-PET and C-11 methionine PET for bone metastases were 6c% and 70%, respectively, while the sensitivities for abdominal and pelvic soft tissue lesions were 30% and 70%, respectively.

In a study of 100 patients with PSA relapse by Picchio et al. (2003), C-11 choline PET was superior to FDG-PET and complementary to conventional imaging. In the study by de Jong et al. (2003), C-11 choline PET detected recurrent sites in 78% of the patients with PSA relapse after radiotherapy and in 38% of the patients with PSA relapse after radical prostatectomy. Schmid et al. (2005) studied nine patients with biochemical failure using F-18 fluorocholine and found evidence of recurrence or metastasis in all nine patients.

Kotzerke et al. (2002) studied patients with suspected relapse after prostatectomy. C-11 acetate PET detected 13 abnormal sites in 16 patients with local recurrence proven by biopsy. Fricke et al. (2003) studied C-11 acetate PET in 24 patients with suspected relapse or metastasis and lesions were detected in 20 patients. They found that C-11 acetate seems to be more useful than FDG in the detection of local recurrence and regional lymph node metastasis, whereas FDG appears to be more accurate in visualizing distant metastasis. Oyama et al. (2003) suggested that C-11 acetate PET is of little use if the PSA level is lower than 3 ng/ml.

8.2.1.3 Monitoring of Treatment Response

PSA has been a reference tumor marker for the monitoring of disease progression and treatment response in prostate cancer. However, imaging studies can yield additional information for the localization and response of individual lesions. FDG-PET has been studied in many cancers for the monitoring of treatment response with promising results. For bone metastasis, skeletal scintigraphy has been considered unreliable in the assessment of treatment response since many responding lesions remain persistently active on follow-up studies because of a "flare" phenomenon. It is very difficult to distinguish osteoblastic response to tumor from response to healing. Morris et al. (2002) studied 17 patients with progressive metastatic prostate cancer. They concluded that FDG-PET can discriminate active osseous disease from scintigraphically quiescent lesions and post-treatment changes in the SUV tend to correlate with changes in PSA. Oyama et al. (1999) studied FDG-PET in ten patients before and 1–5 months after the initiation of hormone therapy. They found the glucose utilization by tumors was suppressed by androgen ablation in both primary and metastatic lesions. Kurdziel et al. (2003) also observed a reduction of SUV in FDG-PET during anti-angiogenic therapy.

Oyama et al. (2004) also studied an androgen-dependent prostate tumor model in mice with microPET imaging using F-18 fluorothymidine and found this can be used for monitoring the therapeutic effect of androgen ablation. In a preliminary study by DeGrado et al. (2000), the uptake of F-18 fluorocholine by tumors was markedly reduced during androgen ablation. It seems that both FDG and other tracers may have potential utility in the assessment of treatment effect, and thus may help in the therapeutic selection or modification. As mentioned previously, prostate cancer has a wide variation of tumor biology and aggressiveness. Individualized therapy will be a future direction and studies in the nuclear medicine will certainly play a significant role.

8.2.2 Testicular Cancer

Testicular cancer is more frequent in young men and is highly curable in its early stage. Accurate staging is important for management selection. CT is the most commonly used imaging modality for primary staging. However, it has significant false-negative and false-positive rates. Studies have shown the superiority of FDG-PET over CT. Albers et al. (1999) studied 37 patients with clinical stage I and II testicular germ cell tumors. They found FDG-PET to have higher sensitivity and specificity than CT and to be useful in the assessment of patients with clinical stage II disease. However, FDG-PET can be false-negative in small metastatic lymph nodes and mature teratoma. Cremerius et al. (1999) studied 50 patients with germ cell tumors with similar conclusions.

Although cisplatin-based combination chemotherapy can achieve long-term survival in about 80% of patients, some patients have residual masses after chemotherapy. For these residual masses, surgical results showed viable tumors in 10–20% of cases, mature teratoma in 30–40%, and fibrosis or necrosis in 40–50%. FDG-PET can differentiate residual mass in germ cell tumor after chemotherapy. Hain et al. (2000) studied 55 patients with germ cell tumors with residual masses or unexplained elevation of tumor markers. For residual masses FDG-PET had a positive predictive value of 96% and a negative predictive value of 90%. For unexplained tumor marker elevation, the positive predictive value was 92% but the negative predictive value was

50 %. FDG-PET has limitation in the detection of small viable or micrometastatic tumors. However, FDG-PET is usually still the first imaging modality for early detection of recurrent foci in the follow-up of these patients. Sugawara et al. (1999) studied 21 patients and correctly differentiated viable tumors from mature teratoma and necrosis or scar. In addition, they suggested that mature teratoma can be further differentiated using kinetic rate constants.

Bokemeyer et al. (2002) studied 23 patients with relapsed germ cell tumors. FDG-PET acquired after 2 – 3 cycles of induction chemotherapy but before the start of high-dose chemotherapy was used for early prediction of treatment response. FDG-PET predicted the outcome in 91 % of patients, as compared to 59 % for CT and 48 % for tumor marker. The utility of FDG-PET in testicular cancer seems promising and further prospective studies with a larger number of patients are warranted.

8.2.3 Penile Cancer

Squamous cell carcinomas constitute the majority of penile cancer. FDG-PET is usually sensitive for detecting squamous cell carcinomas, such as head and neck cancers. Scher et al. (2005) studied 13 patients with suspected penile cancer or recurrence with FDG-PET/CT. The sensitivity and specificity for primary lesion detection were both 75 %. Two small primary lesions were missed due to small size, although they can be delineated in retrospective review. FDG-PET detected four out of five patients with lymph node metastasis and missed one patient with a micrometastatic lymph node. The main utility of FDG-PET in penile cancer is in the detection of regional or distant metastases.

The earliest study of sentinel lymph node (SLN) started with penile cancer. Kroon et al. (2005) reported their experience in 10 years with 140 clinically node-negative patients. Sentinel node metastasis was found in 31 patients, while another 6 patients had developed regional tumor recurrence, resulting in a false-negative rate of 16 %. However, they think the false-negative rate could be lowered with more experienced technique and more extended pathological sectioning and staining. By combining FDG-PET and SLN techniques, patients with penile cancer may have more precise staging before surgery.

8.3 Urological Malignancies

8.3.1 Renal Cell Carcinoma

Unlike glucose, FDG is excreted through the kidney into the urine without reabsorption. This makes its application in the urologic malignancies such as renal cell carcinoma (RCC) and bladder cancer more prone to inaccuracy. Ramdave et al. (2001) studied FDG-PET in 17 patients with known or suspected RCC. FDG-PET was true positive in 15, true negative in 1, and false negative in 1. FDG-PET detected unsuspected metastasis in two patients. In eight patients with suspected recurrence or metastasis, FDG-PET upstaged three patients and excluded recurrence in one patient. FDG-PET was more accurate than CT in detection of local recurrence or metastasis. Kang et al. (2004) studied 66 patients and found a lower sensitivity of 60 % for detecting primary RCC. Some renal cell carcinomas seem to have lower FDG uptake. Further prospective studies and kinetic analyses are required.

Safaei et al. (2002) studied the utility of FDG-PET for restaging in 36 patients with advanced renal cell cancer. FDG-PET correctly classified the clinical stage in 32 patients (89 %). Majhail et al. (2003) studied 24 patients with suspected RCC metastases. A total of 33 distant metastatic sites were identified and the lesion-based sensitivity of FDG-PET was 64 %. FDG-PET is not sensitive enough and may not detect small lesions. However, the specificity of FDG-PET seemed high and the need for a biopsy may be alleviated in selected situations. Whether other radiotracers will have better or complementary utility remains to be investigated.

8.3.2 Bladder Cancer

As with prostate cancer and renal cancer, the utility of FDG-PET in bladder cancer is significantly limited by the urinary excretion of FDG. Kosuda et al. (1997) performed a preliminary assessment of 12 patients with suspected residual or recurrent bladder cancer. FDG-PET was true-positive in eight patients and false-negative in four patients. In a recent study of patients with invasive transitional cell carcinoma of bladder by Drieskens et al. (2005), the sensitivity, specificity, and accuracy of FDG-PET for detecting regional and distant metastatic disease were 53 %, 72 %, and 65 %, respectively. By adding the information of CT, the sensitivity, specificity, and accuracy increased to 60 %, 88 %, and 78 %. Staging was improved in 15 % of patients as compared with CT staging. In addition, the sensitivity of FDG-PET for lymph node metastasis was 50 %, as compared with 42 % for CT. More accurate lymph node staging is needed. However, SLN technique is difficult to perform in bladder cancer. Whether MRI with lymphotropic superparamagnetic nanoparticles can have promising results in this field can be answered in the near future.

Evaluating PET by clinical benefit is specific to the individual tumor and an attractive new end point. We advocate that whether PET scan improves outcome for

a specific cancer can only be proven by means of well-designed prospective studies, best including randomized controlled trials. More independent prospective studies are necessary to evaluate the role of PET in lower genitourinary tract cancer patients.

8.4 Gynecologic Cancer

8.4.1 Cervical Cancer

Cervical cancer is one of the most common female malignancies and also a leading cause of cancer-related death among women in developing countries. Early-stage (International Federation of Gynecology and Obstetrics [FIGO] IB and IIA) cervical cancer can be cured on an average rate of 80%. Approximately 30–50% of patients with stage IIB to IV will ultimately fail after definitive treatment. Primary treatment, relapse pattern, and characteristics at presentation are determinants for prognosis after recurrence. Regardless of the mode of primary treatment, the 5-year survival rates of patients with persistent/recurrent cervical cancer are between 3.2% and 15% (Hong et al. 2004; Lai 2004; Waggoner 2003).

8.4.1.1 Primary Staging

Optimal primary treatment based on an adequate assessment of disease extent is more rewarding than a deliberate post-treatment surveillance and aggressive salvage therapy (Lai 2004). The clinical value of 18-fluorodeoxyglucose positron emission tomography (FDG-PET) for primary staging seems promising in locally advanced untreated cervical cancer (Grigsby et al. 2001, 2005; Rose et al. 1999; Tsai et al. 2004; Yen et al. 2003, 2004). Rose et al. (1999) reported a prospective study of locally advanced cervical cancer ($n=32$) assessed by surgical staging before definitive radiation, in which FDG-PET scanning had a sensitivity (SN) of 75%, specificity (SP) of 92%, positive predictive value (PPV) of 75%, and a negative predictive value (NPV) of 92% for para-aortic lymph node (LN) metastasis. Grigsby et al. (2001) retrospectively investigated 101 cervical cancer patients before primary chemoradiation. CT demonstrated abnormally pelvic LNs in 20% and para-aortic LNs in 7%, while PET detected abnormal FDG uptake at pelvic LNs in 67% and para-aortic LNs in 21% and supraclavicular LNs in 8%. The 2-year progression free rates were 64% for CT (–), PET (–); 18% for CT (–), PET (+); and 14% for CT (+), PET (+) ($P<0.0001$). In another study, Grigsby et al. (2005) found no significant difference in the 5-year cause-specific survival (78% vs. 74%, $P=0.99$) and overall survival (85% vs 81%, $P=0.91$) between RT alone ($n=15$) and CCRT ($n=50$) groups for those without extracervical spread. Using dual-phase PET technique (adding 3-h delayed images to the 40-min scans) and area under the curve (AUC) of the receiver-operating characteristic curve (ROC) to evaluate the diagnostic efficacy, we found that dual-phase scans are superior to 40-min scans or CT-MRI in detecting metastasis in untreated advanced primary as well as recurrent cervical cancer patients (Yen et al. 2004).

In contrast, the value of FDG-PET in early-stage resectable cervical cancer is controversial. Reinhart et al. (2001) reported a prospective study of 35 FIGO stage IB-II cervical cancer patients who underwent RH-PLND. On a patient basis, LN staging resulted in a sensitivity of 91% with PET and 73% with MRI ($P>0.05$). On an LN-site basis, PET achieved a positive-predictive value of 90% and an MRI of 64% ($P<0.05$). In Reinhart's series, of these 11 pelvic LN metastases, PET detected 10 and MRI detected 8. As a matter of fact, of the MRI-negative patients ($n=27$), only three had histologically proven pelvic LN metastasis and PET detected two of them. In our recent study (Chou et al. 2006), 60 patients with untreated cervical cancer stage IA2–IIA, cervical carcinoma, MRI-defined negative for LN metastasis, were enrolled. The gold standard of LN metastasis was histological. There were 16.7% (10/60) pelvic LN metastases and 1.7% (1/60) para-aortic (PA) LN metastases histologically. FDG-PET demonstrated the single PALN metastasis (1/1) but detected only one of the 10 (10%) pelvic LN metastases. The PET false-negative pelvic LN micrometastases measured 4.0×3.0 mm (range, 0.5×0.5 to 7×6 mm).

8.4.1.2 Post-therapy Surveillance or Re-staging of Tumor Recurrence

Its contribution to post-treatment surveillance has been varied according to the selecting criteria, among which those with unexplained tumor marker (such as squamous cell carcinoma antigen [SCC-Ag]) elevation seem to be valuable (Chang et al. 2004), whereas routine post-therapy surveillance in asymptomatic patients is associated with low cost-effectiveness (Ryu et al. 2003). For re-staging potentially curable recurrent cervical cancer, additional PET is potentially beneficial. In our previous study (Lai et al. 2004), a total of 22 (55%) patients had treatment modified due to PET findings. PET (SN 92%) was significantly superior to CT/MRI (SN 60%) (AUC: 0.962 vs 0.771, $P<0.0001$) in identifying metastatic lesions. For those receiving primary surgery, a significantly better 2-year overall survival rate was noted for study patients when compared with those restaged without PET (HR=0.21; 95% CI 0.05–0.83, $P=0.020$).

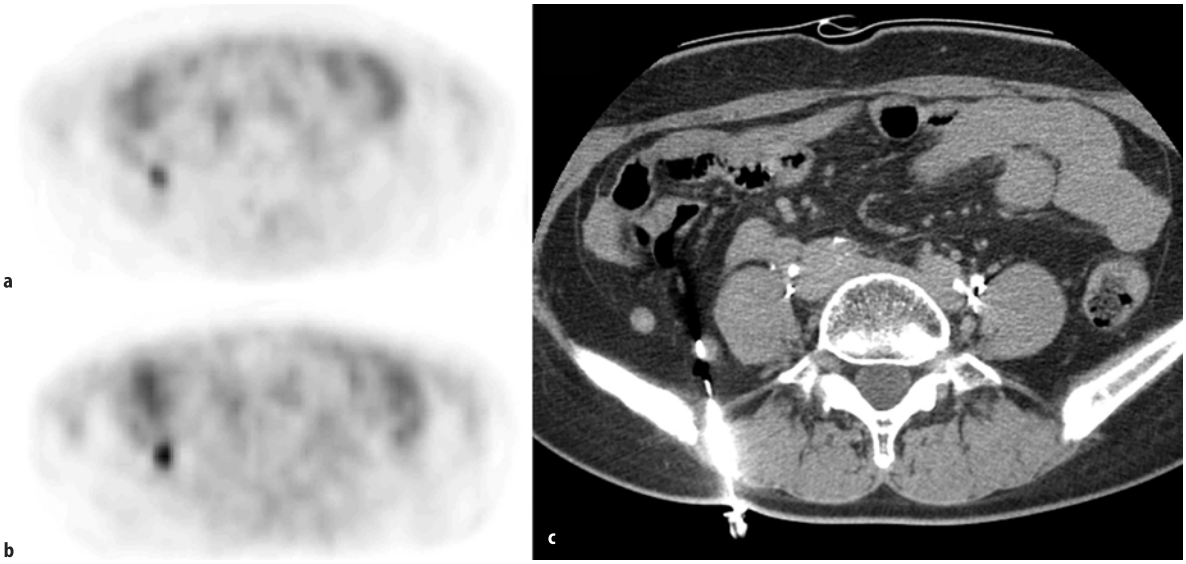

Fig. 8.9. This 48-year-old female patient had cervical cancer of FIGO stage IIb. One year after primary therapy with radical surgery and concurrent chemoradiation, recurrent lymph nodes were found at the left neck, and radical neck dissection with adjuvant radiotherapy was performed. Follow-up CT scan half a year later revealed no evidence of tumor recurrence at the neck region; however, PET scan at 40 min (**a** with lesion SUV = 3.01) and 3 h (**b** with lesion SUV = 4.05) disclosed an FDG-avid lesion in the right lower abdomen. CT-guided core needle biopsy confirmed it to be a metastatic carcinoma (**c**). She then received curative surgery for this sole-site secondary recurrence

8.4.2 Vaginal Cancer

Vaginal cancer is a rare gynecologic cancer, with an etiology and mode of spread similar to cervical cancer. In a prospective study, FDG-PET and CT were used for primary staging in 21 untreated and two vaginal tumors resected. Of the 21 cases with intact primary vaginal tumor, CT visualized the primary tumor in 9 (43%), 3 with positive groin LN, and 1 with positive pelvic LN. PET identified all 21 (100%) intact primary vaginal cancers, 4 with positive groin LN, and 2 with positive pelvic LN (Lamoreaux et al. 2005).

8.4.3 Ovarian Cancer

Ovarian cancer accounts overall for half of all deaths related to female genital cancer (Boyle et al. 2003). Prognosis of ovarian cancer is closely related to the initial stage when diagnosed. Morphologic imaging modalities may play a role in delineating disease extent before surgical exploration. CT and MRI are considered to be useful for retroperitoneal lymph nodes and predicting probability of optimal cytoreduction in those apparently advanced ovarian cancer patients (Qayyum et al. 2005). Although some investigators consider FDG-PET useful in differential diagnosis of malignancy, most studies have proved it to be of little value for this purpose. Moreover, a physiologically increased uptake of FDG in normal ovary is not infrequently seen (Fenchel et al. 2002; Grab et al. 2000; Hubner et al. 1993; Lerman et al. 2004; Rieber et al. 2001; Yoshida et al. 2004).

CA125 is an important tumor marker for epithelial ovarian cancer. Generally, FDG-PET may provide benefits for those with plateaued or increasing abnormal serum CA 125 (>35 U/ml), CT-MRI defined localized recurrence feasible for local destructive procedures (such as surgery, radiotherapy, or radiofrequency ablation), and clinically suspected recurrent or persistent cancer for which CT-guided biopsy cannot be performed (Kurokawa et al. 2002; Sironi et al. 2004). Overall, the SN of PET for recurrent disease is quite high when CA-125 is elevated, or there is an abnormal examination or abnormal conventional imaging, so that PET is confirmatory of patient status. However, there is no evidence that an early institution of salvage therapy improves overall survival.

8.4.4 Endometrial Cancer

Endometrial cancer is one of the most common gynecologic cancers. The FIGO staging requires a surgical staging. The overall survival rate of patients with endometrial cancer is high because most patients had early-stage disease at the time of diagnosis (Boyle et al. 2003). Nevertheless, the prognosis is poor in advanced or recurrent endometrial carcinoma, especially when extrapelvic sites are involved, or there is previously irradiated site failure or multifocal metastases (Kao 2004).

MRI-CT can be used to evaluate cancer extension and provide important information for treatment planning (Manfredi et al. 2004). Preoperative serum CA-125 may play a role in predicting extrauterine spread of clinically localized endometrial cancer (Dotters 2000; Duk et al. 1986). The role of FDG-PET in endometrial cancer is relatively less defined because of the lack of data in the literature (Belhocine et al. 2002; Chao et al. 2006; Horowitz et al. 2004; Nakahara et al. 2001; Saga et al. 2003; Torizuka et al. 2003). For the assessment of FDG avidity of endometrial cancer, there were only two reports providing the data of SUV: one report of five patients with a mean SUV of 18.8 ± 9 (Lerman et al. 2004) and the other of nine patients with a range of 3.8 – 16.8 (Torizuka et al. 2003). Lerman et al. (2004) found that the benign endometrial pathology (SUV mean 4.5 ± 2.1) and postmenopausal (SUV mean 1.7 ± 0.5) endometrial uptake varied substantially. Most PET imaging studies in gynecologic cancer are performed using FDG (Hubner et al. 1993).

In a retrospective case series ($n = 34$), Belhocine et al. noted that FDG-PET had an SN of 96 % and an SP of 78 % for post-therapy surveillance with 35 % altered treatment (Belhocine et al. 2002). Saga et al. evaluated 30 scans in the post-operative patients revealing an SN of 100 % with 33.3 % treatment plan modified (Saga et al. 2003). Horowitz et al. (2004) have recently reported a prospective study for the role of FDG-PET in primary staging. A total of 11 % (2 of 18) patients had pathological nodal metastasis. PET predicted that three patients had positive nodes, which turned out two true-positives and one false-positive.

In our prospective study (Chao et al. 2006), patients with histologically confirmed primary advanced (FIGO stage III/IV) or suspicious/documented recurrent endometrial cancer, with poor prognostic features (serum CA 125 > 35 U/ml or unfavorable cell types), or surveillance after salvage therapy were enrolled. A minimum SUV of true-positive central pelvic lesions was 5.7 (mean 13.2 ± 7.1), whereas it could be as low as 1.5 (mean 11.1 ± 6.4) for metastatic lesions, indicating a great variation in the uptake of endometrial cancer. The clinical impact of FDG-PET scanning was classified as (1) negative: if PET led to unnecessary, additional invasive procedures; (2) no change: same findings as MRI-CT, the false-positive and false-negative FDG-PET findings did not affect surgical staging or treatment, or detecting an incurable relapse; or (3) positive: (a) treatment modified owing to correct staging with upstaged or down-staged against MRI-CT, (b) confirmation of sole site involvement for distant recurrences (stick to curative treatment), (c) early detection of curable recurrence or re-recurrence, (d) deferring exploration for the false-positives of MRI-CT, or (e) change to palliation avoiding a futile salvage attempt. The clinical impact was positive in 29 (6c.3 %) of the 60 scans, 22.2 % for primary staging, 73.1 % for post-therapy surveillance, and 57.1 % after salvage therapy, respectively. FDG-PET plus MRI-CT was significantly superior to MRI-CT alone in overall lesion detection (AUC: 0.949 vs 0.872; $P = 0.004$), pelvic nodal/soft tissue ($P = 0.06$c) or extrapelvic metastasis ($P = 0.010$), while FDG-PET alone was only marginally superior by AUC ($P = 0.063$). Our results showed that FDG-PET coupled with MRI-CT may facilitate optimal management of endometrial cancer in well-selected cases.

8.4.5 Vulvar Cancer

The status of inguinal LN plays an important role in stage, treatment, and prognosis of patients with vulvar cancer. The groin LN metastasis is common even with superficial depth invasion. Local recurrences at the vulva are most likely and usually amenable to salvage surgery, but regional and distant recurrences are difficult to detect, appropriate management difficult to apply and have poor prognosis (Heaps et al. 1990; Sedlis et al. 1987).

Scanty studies have been reported in the management of vulvar cancer using FDG-PET. More data is needed. In a prospective series of 15 patients with primary vulvar squamous carcinoma, FDG-PET was performed prior to groin dissection. Six patients had posi-

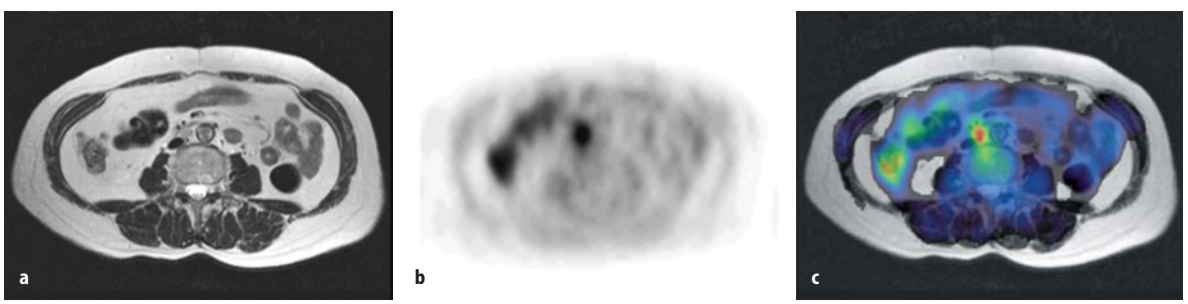

Fig. 8.10. The MRI study of this 70-year-old woman with endometrial adenocarcinoma disclosed only primary tumor. FDG-PET revealed an additional lesion of right para-aortic lymph node (PALN) (**a** MRI imaging; **b** PET imaging; **c** MRI-PET fusion imaging). The histopathology proved PALN metastasis. PET led to up-staging

tive scans, suggesting eight groins containing metastatic cancer. On a groin basis, they were SN of 67 %, SP of 95 %, PPV of 86 %, and NPV of 86 % (Cohn et al. 2002).

8.4.6 Gestational Trophoblastic Neoplasias

Gestational trophoblastic neoplasia (GTN) is quite unique in biological behavior and clinical management. GTN includes hydatidiform mole, invasive mole, choriocarcinoma, and placental site trophoblastic tumor (PSTT). Human chorionic gonadotropin (hCG) is an excellent tumor marker for GTN. GTNs should be treated according to the prognostic grouping. Chemotherapy is unnecessary if the serum hCG values regressed well after molar evacuation. Almost 100 % low-risk and non-metastatic GTNs could be cured with standard management. The prognosis is good even for metastatic GTN. However, some of the high-risk and persistent/recurrent GTNs harboring chemotherapy-resistant tumor cells remain a problem, and PSTT represents a relatively chemoresistant form of GTNs (Bower et al. 1997; Feltmate et al. 2001; Newlands et al. 1998). Several case reports have investigated the role of PET in GTN (Dose et al. 2000; Hebart et al. 1996; Sironi et al. 2003; Truenbach et al. 1997; Zhuang et al. 2001), and the findings and treatment outcome were encouraging; however, these reports were limited to confirmation of malignant lung lesions, ruling out false-positive persistent mass by CT (resection was perormed despite no FDG uptake and normal serum β-hCG, and the final pathology showed non-viable cells), and to assess response to chemotherapy for high-risk GTN.

Our preliminary results (Chang et al. 2006) suggest that FDG-PET is potentially useful in selected GTN by providing a precise metastatic mapping of tumor extent before chemotherapy, monitoring response, and localizing viable tumors after chemotherapy. The diagnosis of GTT could be based on clinical imaging and elevated serum hCG without histological proof. Tissue proof of metastases is regarded unnecessary for its exquisite chemosensitivity and high vascularity. The evaluation of a diagnostic tool, such as PET, is usually via comparison of the diagnostic efficacy (SN, SP, etc.), or the ROC method, and is not as applicable for GTN. Therefore the clinical impact of additional PET was defined as positive if there was: (1) modified management after the PET study due to the disclosure of chemoresistant lesions; (2) ruling out of false-positive CT lesions and avoidance of unnecessary surgery/radiotherapy or chemotherapy; (3) detection of additional lesion(s) not found by conventional imaging in high-risk GTN or PSTT at the start of primary chemotherapy; (4) confirmation of a complete treatment response for PSTT or after salvage therapy for recurrent/resistant GTN; or (5) localization of tumor for post-molar unexplained abnormal β-hCG regression. The impact of the PET results was considered negative when it showed false-negative or false-positive results, with or without the consequence of unnecessary treatment or treatment delay. When PET failed to localize the tumor for recurrent/resistant GTN whose CT was also negative, or post-molar unexplained abnormal β-hCG, it was determined to have no clinical impact. In our pilot study, a total of 14 patients were recruited, and 16 PET scans were performed with one patient having 3 serial studies. The benefits of additional PET were seen in 7 out of the 16 (43.8 %).

References

Albers P, Bender H, Yilmaz H, et al. (1999) Positron emission tomography in the clinical staging of patients with Stage I and II testicular germ cell tumors. Urology 53:808 – 811

Belhocine T, de Barsy C, Hustinx R, et al. (2002) Usefulness of (18)F-FDG PET in the post-therapy surveillance of endometrial carcinoma. Eur J Nucl Med Mol Imaging 29:1132 – 1139

Bokemeyer C, Kollmannsberger C, Oechsle K, et al. (2002) Early prediction of treatment response to high-dose salvage chemotherapy in patients with relapsed germ cell cancer using [(18)F]FDG PET. Br J Cancer 86:506 – 511

Bower M, Newlands ES, Holden L, et al. (1997) EMA/CO for high-risk gestational trophoblastic tumours: results from a cohort of 272 patients. J Clin Oncol 15:2636 – 2643

Boyle P, Leon ME, Maisonneuve P, Autier P (2003) Cancer control in women. Update 2003. Int J Gynecol Obstet 83 Suppl 1:179 – 202

Chang TC, Law KS, Hong JH, et al. (2004) Positron emission tomography for unexplained serum SCC-Ag elevation in cervical cancer patients – a phase II study. Cancer 101:164 – 171

Chang TC, Yen TC, Ma SY, et al. (2006) 18F-fluoro-D-deoxyglucose positron emission tomography of trophoblastic tumor: a pilot study. Eur J Nucl Med Mol Imaging. doi: 10.1007/s00259-005-1873-1

Chao A, Chang YC, Hsueh S, et al. (2006) F-18 fluorodeoxyglucose positron emission tomography in the management of endometrial cancer. Eur J Nucl Med Mol Imaging 33:36 – 44

Chou HH, Chang TC, Yen TC, et al. (2006) Low value of 2-fluoro-2-deoxy-d-glucose positron emission tomography in primary staging of early-stage cervical cancer prior to radical hysterectomy. J Clin Oncol 24:123 – 128

Cohn DE, Dehdashti F, Gibb RK, et al. (2002) Prospective evaluation of positron emission tomography for the detection of groin node metastases from vulvar cancer. Gynecol Oncol 85:179 – 184

Conway JJ, King LR, Belman AB, et al. (1972) Detection of vesicoureteral reflux with radionuclide cystography. Am J Roentgenol 115:720

Cremerius U, Wildberger JE, Borchers H, et al. (1999) Does positron emission tomography using 18-fluoro-2-deoxyglucose improve clinical staging of testicular cancer? – Results of a study in 50 patients. Urology 54:900 – 904

de Jong IJ, Pruim J, Elsinga PH, et al. (2003a) 11C-choline positron emission tomography for the evaluation after treatment of localized prostate cancer. Eur Urol 44:32 – 38

de Jong IJ, Pruim J, Elsinga PH, et al. (2003b) Preoperative staging of pelvic lymph nodes in prostate cancer by 11C-choline PET. J Nucl Med 44:331 – 335

DeGrado TR, Wang S, Holden JE, et al. (2000) Synthesis and preliminary evaluation of (18)F-labeled 4-thia palmitate as a

PET tracer of myocardial fatty acid oxidation. Nucl Med Biol 27:221 – 231
Dose J, Bohuslavizki K, Huneke B, et al. (2000) Detection of intramural choriocarcinoma of the uterus with 18F-FDG-PET. A case report. Clin Positron Imaging 3:37 – 40
Dotters DJ (2000) Preoperative CA 125 in endometrial cancer: is it useful? Am J Obstet Gynecol 182:1328 – 1334
Drieskens O, Oyen R, Van Poppel H, et al. (2005) FDG-PET for preoperative staging of bladder cancer. Eur J Nucl Med Mol Imaging 32:1412 – 1417
Duk JM, Aalders JG, Fleuren GJ, de Bruijn HW (1986) CA 125: a useful marker in endometrial carcinoma. Am J Obstet Gynecol 155:1097 – 1102
Farsad M, Schiavina R, Castellucci P, et al. (2005) Detection and localization of prostate cancer: correlation of 11C-choline PET/CT with histopathologic step-section analysis. J Nucl Med 46:1642 – 1649
Feltmate CM, Genest DR, Wise L, et al. (2001) Placental site trophoblastic tumour: a 17-year experience at the New England Trophoblastic Disease Center. Gynecol Oncol 82: 415 – 419
Fenchel S, Grab D, Nuessle K, et al. (2002) Asymptomatic adnexal masses: correlation of FDG PET and histopathologic findings. Radiology 223:780 – 788
Freeman LM, Krynyckyi BR, Li Y, et al. (2002) The role of ^{111}In Capromab Pendetide (Prostascint^{R}) immunoscintigraphy in the management of prostate cancer. Q J Nucl Med 46: 131 – 137
Fricke E, Machtens S, Hofmann M, et al. (2003) Positron emission tomography with 11C-acetate and 18F-FDG in prostate cancer patients. Eur J Nucl Med Mol Imaging 30:607 – 611
Grab D, Flock F, Stohr I, et al. (2000) Classification of asymptomatic adnexal masses by ultrasound, magnetic resonance imaging, and positive emission tomography. Gynecol Oncol 77:454 – 459
Grigsby PW, Siegel BA, Dehdashti F (2001) Lymph node staging by positron emission tomography in patients with carcinoma of the cervix. J Clin Oncol 19:3745 – 3749
Grigsby PW, Mutch DG, Rader J, et al. (2005) Lack of benefit of concurrent chemotherapy in patients with cervical cancer and negative lymph nodes by FDG-PET. Int J Radiat Oncol Biol Phys 61:3441 – 3449
Hain SF, O'Doherty MJ, Timothy AR, et al. (2000) Fluorodeoxyglucose positron emission tomography in the evaluation of germ cell tumours at relapse. Br J Cancer 83:863 – 869
Hara T, Kosaka N, Kishi H (1998) PET imaging of prostate cancer using carbon-11-choline. J Nucl Med 39:990 – 995
Harisinghani MG, Barentsz J, Hahn PF, et al. (2003) Noninvasive detection of clinically occult lymph-node metastases in prostate cancer. N Engl J Med 348:2491 – 2499
Heaps JM, Fu YS, Montz FJ, et al. (1990) Surgical-pathologic variables predictive of local recurrence in squamous cell carcinoma of the vulva. Gynecol Oncol 38:309 – 314
Hebart H, Erley C, Kaskas B, et al. (1996) Positron emission tomography helps to diagnose tumour emboli and residual disease in choriocarcinoma. Ann Oncol 7:416 – 418
Hong JH, Tsai CS, Lai CH, et al. (2004) Recurrent squamous cell carcinoma of cervix following definitive radiotherapy. Int J Radiat Oncol Biol Phys 60:249 – 257
Horowitz NS, Dehdashti F, Herzog TJ, et al. (2004) Prospective evaluation of FDG-PET for detecting pelvic and para-aortic lymph node metastasis in uterine corpus cancer. Gynecol Oncol 101:164 – 171
Hubner KF, McDonald TW, Niethammer JG, et al. (1993) Assessment of primary and metastatic ovarian cancer by positron emission tomography (PET) using 2-[18F]deoxyglucose (2-[18F]FDG). Gynecol Oncol 51:197 – 204
Kahn D, Williams RD, Manyak MJ, et al. (1998) ^{111}In Capromab Pendetide in the evaluation of patients with residual or recurrent prostate cancer after radical prostatectomy. J Urol 159:2041 – 2047
Kang DE, White RL, Jr, Zuger JH, et al. (2004) Clinical use of fluorodeoxyglucose F 18 positron emission tomography for detection of renal cell carcinoma. J Urol 171:1806 – 1809
Kao MS (2004) Management of recurrent endometrial cancer. Chang Gung Med J 27:639 – 645
Kato T, Tsukamoto E, Kuge Y, et al. (2002) Accumulation of [11C]acetate in normal prostate and benign prostatic hyperplasia: comparison with prostate cancer. Eur J Nucl Med Mol Imaging 29:1492 – 1495
Kosuda S, Kison PV, Greenough R, et al. (1997) Preliminary assessment of fluorine-18 fluorodeoxyglucose positron emission tomography in patients with bladder cancer. Eur J Nucl Med Mol Imaging 24:615 – 620
Kotzerke J, Volkmer BG, Neumaier B, et al. (2002) Carbon-11 acetate positron emission tomography can detect local recurrence of prostate cancer. Eur J Nucl Med Mol Imaging 29:1380 – 1384
Kroon BK, Horenblas S, Meinhardt W, et al. (2005) Dynamic sentinel node biopsy in penile carcinoma: evaluation of 10 years experience. Eur Urol 47:601 – 606
Kurdziel KA, Figg WD, Carrasquillo JA, et al. (2003) Using positron emission tomography 2-deoxy-2-[18F]fluoro-D-glucose, 11CO, and 15O-water for monitoring androgen independent prostate cancer. Mol Imaging Biol 5:86 – 93
Kurokawa T, Yoshida Y, Kawahara K, et al. (2002) Whole-body PET with FDG is useful for following up an ovarian cancer patient with only rising CA-125 levels within the normal range. Ann Nucl Med 6:491 – 493
Lai CH (2004) Management of recurrent cervical cancer. Chang Gung Med J 72:711 – 719
Lai CH, Huang KG, See LC, et al. (2004) Restaging of recurrent cervical cancer with dual-phase positron emission tomography. Cancer 100:544 – 552
Lamb HM, Faulds D (1998) Capromab pendetide. A review of its use as an imaging agent in prostate cancer. Drugs Aging 12:293 – 304
Lamoreaux WT, Grigsby PW, Dehdashti F, et al. (2005) FDG-PET evaluation of vaginal cancer. Int J Radiat Oncol Biol Phys 62:733 – 737
Lerman H, Metser U, Grisaru D, et al. (2004) Normal and abnormal 18F-FDG endometrial and ovarian uptake pre- and postmenopausal patients: assessment by PET/CT. J Nucl Med 45:266 – 271
Majhail NS, Urbain J-L, Albani JM, et al. (2003) F-18 fluorodeoxyglucose positron emission tomography in the evaluation of distant metastases from renal cell carcinoma. J Clin Oncol 21:3995 – 4000
Manfredi R, Mirk P, Maresca G, et al. (2004) Local-regional staging of endometrial carcinoma: role of MR imaging in surgical planning. Radiology 231:372 – 378
Matthies A, Ezziddin S, Ulrich E-M, et al. (2004) Imaging of prostate cancer metastases with 18F-fluoroacetate using PET/CT. Eur J Nucl Med Mol Imaging 31:797
Morris MJ, Akhurst T, Osman I, et al. (2002) Fluorinated deoxyglucose positron emission tomography imaging in progressive metastatic prostate cancer. Urology 59:913 – 918
Nakahara T, Fujii H, Ide M, et al. (2001) F-18 FDG uptake in endometrial cancer. Clin Nucl Med 26:82 – 83
Newlands ES, Bower M, Holden L, et al. (1998) Management of resistant gestational trophoblastic tumours. J Reprod Med 43:111 – 118
Nunez R, Macapinlac HA, Yeung HWD, et al. (2002) Combined 18F-FDG and 11C-methionine PET scans in patients with newly progressive metastatic prostate cancer. J Nucl Med 43:46 – 55

Oyama N, Akino H, Suzuki Y, et al. (1999) The increased accumulation of [18F]fluorodeoxyglucose in untreated prostate cancer. Jpn J Clin Oncol 29:623 – 629
Oyama N, Akino H, Suzuki Y, et al. (2001) FDG PET for evaluating the change of glucose metabolism in prostate cancer after androgen ablation. Nucl Med Commun 22:963 – 969
Oyama N, Akino H, Kanamaru H, et al. (2002) 11C-acetate PET imaging of prostate cancer. J Nucl Med 43:181 – 186
Oyama N, Miller TR, Dehdashti F, et al. (2003) 11C-acetate PET imaging of prostate cancer: detection of recurrent disease at PSA relapse. J Nucl Med 44:549 – 555
Oyama N, Ponde DE, Dence C, et al. (2004) Monitoring of therapy in androgen-dependent prostate tumor model by measuring tumor proliferation. J Nucl Med 45:519 – 525
Picchio M, Messa C, Landoni C, et al. (2003) Value of [11C]choline-positron emission tomography for re-staging prostate cancer: a comparison with [18F]fluorodeoxyglucose-positron emission tomography. J Urol 169:1337 – 1340
Qayyum A, Coakley FV, Westphalen AC, Hricak H, Okuno WT, Powell B (2005) Role of CT and MR imaging in predicting optimal cytoreduction of newly diagnosed primary epithelial ovarian cancer. Gynecol Oncol 96:301 – 306
Ramdave S, Thomas GW, Berlangieri SU, et al. (2001) Clinical role of F-18 fluorodeoxyglucose positron emission tomography for detection and management of renal cell carcinoma. J Urol 166:825 – 830
Reinhardt MJ, Ehitt-Braun C, Vogelgesang D, et al. (2001) Metastatic lymph nodes in patients with cervical cancer: detection with MR imaging and FDG-PET. Radiology 218:776 – 782
Rieber A, Nussle K, Stohr I, et al. (2001) Preoperative diagnosis of ovarian tumors with magnetic resonance imaging: Comparison with transvaginal sonography, positive emission tomography and histologic findings. Am J Roentgenol 177:123 – 129
Rose PG, Adler LP, Rodriguez M, Faulhaber PF, Abdul-Karim FW, Miraldi F (1999) Positron emission tomography for evaluating para-aortic nodal metastasis in locally advanced cervical cancer before surgical staging: a surgicopathologic study. J Clin Oncol 17:41 – 45
Ryu SY, Kim MH, Choi SC, Choi CW, Lee KH (2003) Detection of early recurrence with 18F-FDG PET in patients with cervical cancer. J Nucl Med 44: 347 – 352
Safaei A, Figlin R, Hoh CK, et al. (2002) The usefulness of F-18 deoxyglucose whole-body positron emission tomography (PET) for re-staging of renal cell cancer. Clin Nephrol 57:56 – 62
Saga T, Higashi T, Ishimori T, et al. (2003) Clinical value of FDG-PET in the follow up of post-operative patients with endometrial cancer. Ann Nucl Med 17:197 – 203
Saitoh H, Yoshida KL, Uchijima Y, et al. (1990) Two different lymph node metastatic patterns of a prostate cancer. Cancer 65:1843 – 1845
Salminen E, Hogg A, Binns D, et al. (2002) Investigations with FDG-PET scanning in prostate cancer show limited value for clinical practice. Acta Oncol 41:425 – 429
Scher B, Seitz M, Reiser M, et al. (2005) 18F-FDG PET/CT for staging of penile cancer. J Nucl Med 46:1460 – 1465
Schmid DT, John H, Zweifel R, et al. (2005) Fluorocholine PET/CT in patients with prostate cancer: initial experience. Radiology 235:623 – 628
Sedlis A, Homesley H, Bundy BN, et al. (1987) Positive groin lymph nodes in superficial squamous cell vulvar cancer. Am J Obstet Gynecol 156:1159 – 1164
Shreve P, Chiao PC, Humes HD, et al. (1995) Carbon-11-acetate PET imaging in renal disease. J Nucl Med 36:1595 – 1601
Sironi S, Picchio M, Mangili G, et al. (2003) [^{18}F]fluorodeoxyglucose positron emission tomography as a useful indicator of metastatic gestational trophoblastic tumour: preliminary results in three patients. Gynecol Oncol 91:226 – 230
Sironi S, Messa C, Mangili G, et al. (2004) Integrated FDG PET/CT in patients with persistent ovarian cancer: correlation with histologic findings. Radiology 233:433 – 440
Sugawara Y, Zasadny KR, Grossman HB, et al. (1999) Germ cell tumor: differentiation of viable tumor, mature teratoma, and necrotic tissue with FDG PET and kinetic modeling. Radiology 211:249 – 256
Sutinen E, Nurmi M, Roivainen A, et al. (2004) Kinetics of [(11)C]choline uptake in prostate cancer: a PET study. Eur J Nucl Med Mol Imaging 31:317 – 324
Torizuka T, Kanno T, Futatsubashi M, et al. (2003) Imaging of gynecologic tumors: comparison of (11)C-choline PET with (18)F-FDG PET. J Nucl Med 44:1051 – 1056
Truenbach J, Pereira PL, Huppert PE, et al. (1997) Primary choriocarcinoma of the pulmonary artery mimicking pulmonary embolism. Br J Radiol 70:843 – 845
Tsai CS, Chang TC, Lai CH, et al. (2004) Preliminary report of using FDG-PET to detect extrapelvic lesions in cervical cancer patients with enlarged pelvic lymph nodes on MRI/CT. Int J Radiat Oncol Biol Phys 58:1506 – 1512
Waggoner SE (2003) Cervical cancer. Lancet 361:2217 – 2225
Wawroschek F, Vogt H, Wengenmair H, et al. (2003) Prostate lymphoscintigraphy and radio-guided surgery for sentinel lymph node identification in prostate cancer. Technique and results of the first 350 cases. Urol Int 70:303 – 310
Yen TC, Ng KK, Ma SY, et al. (2003) Value of dual-phase 2-fluoro-2-deoxy-d-glucose positron emission tomography in cervical cancer. J Clin Oncol 21:3651 – 2658
Yen TC, See LC, Ma SY, et al. (2004) Defining priority of utilizing 18F-fluoro-D-deoxyglucose positron emission tomography for recurrent cervical cancer. J Nucl Med 45:1632 – 1639
Yoshida Y, Kurokawa T, Kawahara K, et al. (2004) Incremental benefits of FDG positron emission tomography over CT alone for the preoperative staging of ovarian cancer. Am J Roentgenol 182:227 – 233
Zhuang H, Yamamoto AJ, Ghesani N, et al. (2001) Detection of choriocarcinoma in the lung by FDG positron emission tomography. Clin Nucl Med 26:723
Zuckier LS, Finklestein M, Kreutzer ER, et al. (1990) Technetium-99m antimony sulphide colloid lymphoscintigraphy of the prostate by direct transrectal injection. Nucl Med Commun 11:589 – 596

Gastrointestinal System

9

H.A. Ziessman

9.1 Introduction

Radionuclide methods are ideally suited for evaluation of gastrointestinal disease because of the functional nature of the methodology. Many gastrointestinal radionuclide tests have stood the test of time. For decades, the gastric emptying study has been the gold standard for quantification of gastric motility. Motility studies of the esophagus and intestinal tract, although less commonly requested, provide valuable diagnostic and therapeutic information at many centers. The gastrointestinal bleeding study can noninvasively localize a site of active hemorrhage and guides specific intervention and therapy. Meckel's scan can detect ectopic gastric mucosa as a cause of rectal bleeding in children, and radionuclide methods confirm gastroesophageal reflux with high sensitivity, particularly in neonates and young children.

Newer radionuclide studies are an important growing aspect of nuclear medicine gastrointestinal imaging. For example, somatostatin receptor imaging, In-111 pentetreotide, is now routinely used to localize gastroenteropancreatic tumors and carcinoid tumors. F-18 fluorodeoxyglucose (FDG) positron emission tomography (PET) is the area of most rapid growth in nuclear medicine and has become routine for the staging and restaging of various gastrointestinal tumors, as well as evaluating the response to therapy.

This chapter will review the gamut of modern day gastrointestinal nuclear medicine procedures, including those mentioned above and other numerous but less commonly used radionuclide studies. Emphasis will be on clinical indications, radiopharmaceutical mechanisms of uptake and distribution, proper methodology, and diagnostic criteria.

9.2 Gastrointestinal Motility

Radionuclide methodology is ideally suited to study esophageal, gastric, and intestinal motility. For decades the radionuclide gastric emptying study has been regarded as the standard, in spite of many older and newer competitive methodologies. The esophageal swallow study has demonstrated value, but is most commonly used to evaluate the effectiveness of therapy, e.g., in patients with achalasia. The gastroesophageal reflux study is a highly sensitive and simple methodology used by pediatricians to confirm the clinically suspected diagnosis. Intestinal motility studies have been slow to gain a clinical foothold but are increasingly being requested by referring clinicians.

9.2.1 Esophageal Motility

The esophagus is essentially a muscular tube with sphincters at its proximal and distal ends. It transports ingested food from the mouth to the stomach, clears regurgitated substances, and prevents acid reflux and tracheobronchial aspiration. Dysphagia and dyspepsia are the most common clinical symptoms of esophageal motor dysfunction.

The diagnosis of esophageal motility disorders is most commonly made with contrast radiography and esophageal manometry. Barium-swallow studies demonstrate anatomical lesions and mucosa changes, but provide only a qualitative assessment of motility. Esophageal manometry is the generally accepted diagnostic standard because it provides quantification of peristaltic contraction, sphincter pressure, and upper and lower sphincter relaxation. Advantages of the radionuclide esophageal motility study are that it is noninvasive, physiologic, and easy to perform (Mariani et al. 2004). Lack of specificity is its disadvantage.

Achalasia is a rather common cause of esophageal dysmotility and in most nuclear medicine practices the most common referral diagnosis. The primary abnormality is the inability of the lower esophageal sphincter to relax and the loss of esophageal body peristalsis due to degeneration of neurons in the esophageal wall. Food is retained in the esophagus, resulting in dilatation and symptoms of weight loss, nocturnal regurgitation, cough and aspiration. Radiographic studies show retention of contrast in the distended esophagus, a narrowed sphincter, and very delayed clearance. Manome-

try is usually diagnostic, demonstrating an absence of peristalsis in the distal two-thirds of the esophagus, elevated lower esophageal sphincter pressure, and poor sphincter relaxation with swallowing.

Scleroderma is a smooth muscle connective tissue disorder producing fibrosis and vascular obliteration of esophageal muscle and its innervation. Contrast barium studies show a dilated aperistaltic esophagus. Manometry can confirm decreased or absent lower esophageal sphincter pressure and contraction amplitude. *Diffuse esophageal spasm* presents as intermittent chest pain and dysphagia. Manometry shows normal peristalsis interspersed with frequent high-pressure nonpropagated waves. The *nutcracker esophagus* is a common cause of angina-like pain. This is a manometric diagnosis that has normally propagated but high-amplitude peristaltic waves in the distal esophagus.

Although radionuclide transit studies can show characteristic findings in some of these diseases, the scintigraphic pattern of delayed esophageal transit is often nonspecific as to etiology. Since the gastroenterologists diagnose these diseases with manometric measurements, the role of scintigraphy is usually to evaluate the effectiveness of therapy.

Radiopharmaceuticals. Tc-99m sulfur colloid (Tc-99m SC), Tc-99m nanocolloid and Tc-99m diethylenetriaminepentaacetic acid (Tc-99m DTPA) are used for esophageal motility scintigraphy. Seven to 11 MBq (200 – 300 μCi) is mixed in 10 ml of liquid, often water. Some data suggests that semi-solid boluses have increased sensitivity for detecting abnormal transit.

Methodology. Esophageal transit methodologies vary between institutions. Acquisition can be either anterior or posterior. The posterior view allows for easier administration of the bolus and closer observation of the patient. Imaging can be performed with the patient sitting upright; however, the supine position eliminates the effect of gravity. Gravity is the primary mechanism of emptying in achalasia. Dynamic images should be acquired with a rapid framing rate, e.g., 1 – 3 s per frame, in 64 × 64 byte mode. Multiple swallows are recommended to ensure representative data.

Image Analysis and Quantification. Qualitative image analysis with cinematic display is often sufficient to diagnose abnormal esophageal transit (Fig. 9.1a). However, a strength of the radionuclide method is quantification. This is particularly valuable for evaluating the effectiveness of therapy and comparing serial studies. Time-activity curves can be generated by drawing esophageal regions of interest (ROIs) that include the entire esophagus or proximal, middle and distal thirds. Different quantitative methodologies have been described (Tatsch et al. 1996). One method determines *residual activity* in the esophagus at the end of the study (Fig. 9.1b). Alternatively, a *transit time*, e.g., the time from entry of the bolus into the esophagus until all but 10 % of activity clears, has been used. An abnormal liquid transit time is typically > 15 s and abnormal semisolid swallow is > 5 % residual at 20 min (Fig. 9.1). The data can be assimilated into a single image for easy viewing, called a *condensed dynamic image,* with one spatial (vertical) and one temporal dimension.

Clinical Indications and Accuracy. The sensitivity of radionuclide transit studies for detecting abnormal motility is generally not felt to be acceptable for excluding most esophageal motility disorders (33 – 75 %), perhaps with the exception of achalasia (90 %). The latter also has a high positive predictive value, but it is less for other diseases (50 – 75 %). Thus, transit studies are usually used to judge therapeutic response.

9.2.2 Gastric Motility

Radionuclide gastric emptying studies have long been the standard method for measuring gastric motility. Scintigraphic analysis of gastric motility is noninvasive, reproducible, simple to perform, accurate and quantitative. The physiology of gastric emptying can be accurately characterized and quantified. From a functional standpoint, the stomach has two distinct regions. The proximal stomach (fundus) is responsible for liquid emptying, while the distal stomach (antrum) controls solid emptying. Thus, liquids and solids empty differently.

The fundus acts as a reservoir and accepts large volumes of food with only minimal increase in pressure (receptive relaxation). Its muscular contractions are tonic in character, causing liquids to empty in an exponential manner, i.e., the larger the volume, the more rapid the emptying. There is no delay before emptying begins. Nutrients slow the rate of liquid emptying.

Rhythmic muscular contractions sweep down the antrum in a ring-like manner, pushing solid food particles towards the pylorus. Those particles less than 1 – 2 mm in size pass through, but larger particles are retropelled back towards the fundus and repeatedly ground up, until small enough to pass through the pylorus. Thus, there is a delay before emptying begins, which is called the *lag phase*. Solid emptying is slower than liquid emptying, partially but not exclusively due to the lag phase. As might be expected, the lag phase is lost after surgical antrectomy. Once solid emptying begins, the pattern of emptying is continuous and linear (%/min) in character. The rate of emptying depends on the size and contents of the meal. Increasing the amounts of nutrients slows emptying, the degree depending on the type and amount.

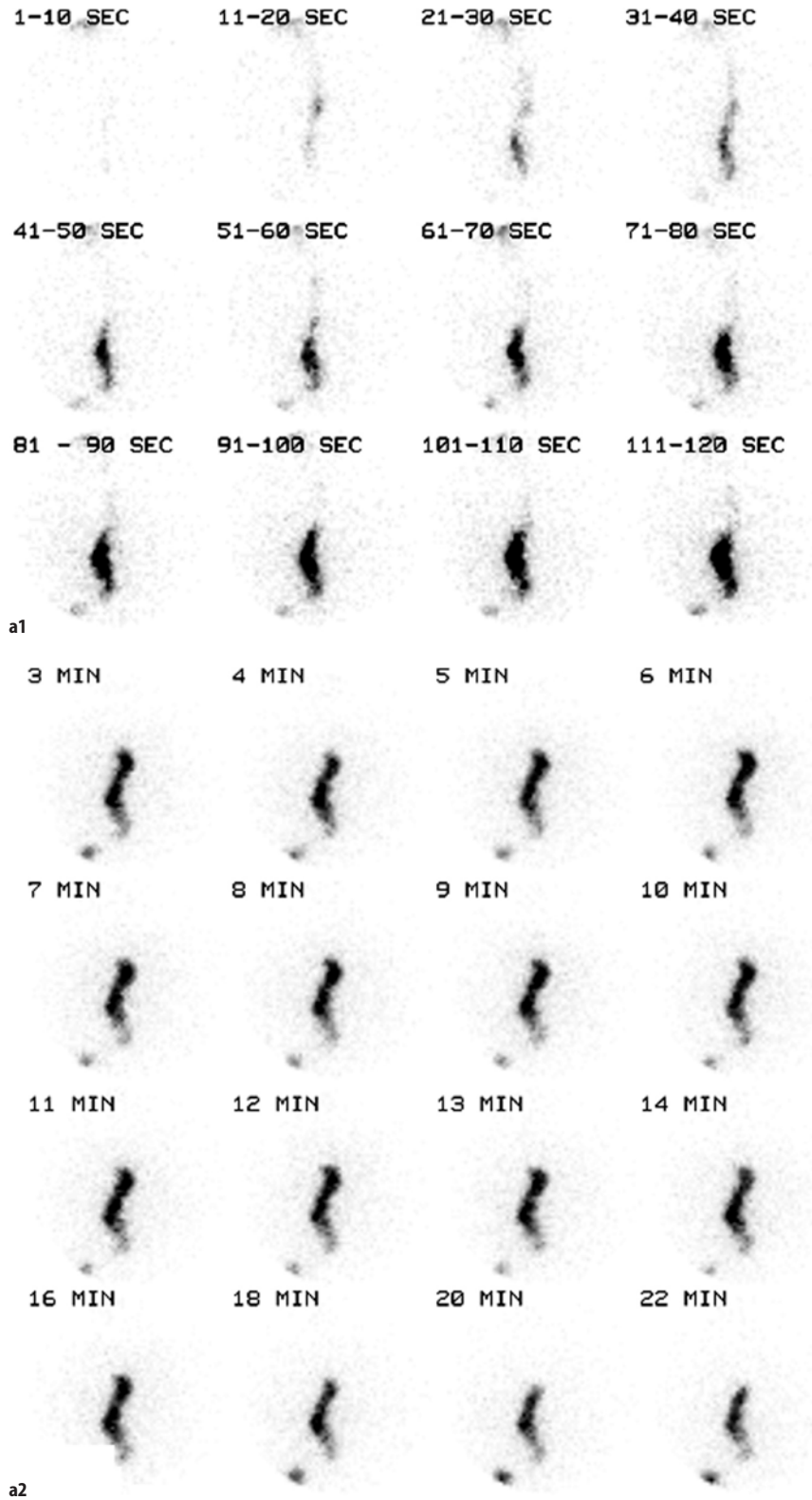

Fig. 9.1. Achalasia. **a** Semi-solid esophageal swallow study. Sequential 10-s images for 2 min followed 1-min images for 22 min. There is very poor emptying from the esophagus

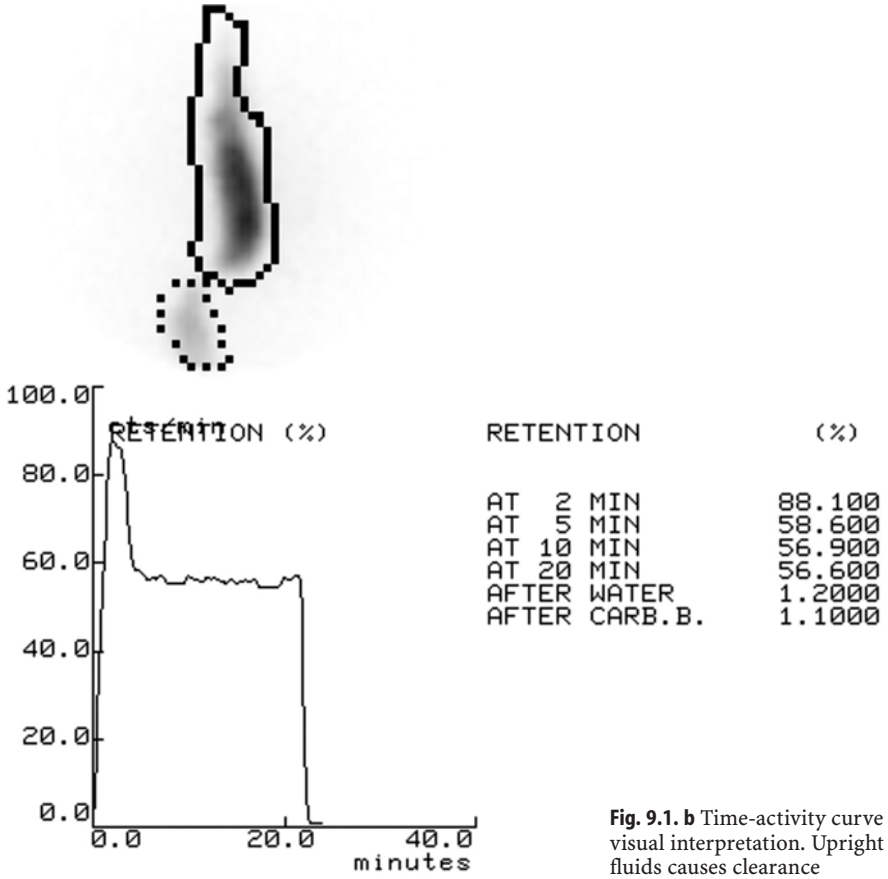

Fig. 9.1. b Time-activity curve and quantification confirms visual interpretation. Upright positioning and ingestion of fluids causes clearance

Clinical Indications. Symptoms of delayed gastric emptying include post-prandial nausea, vomiting, bloating, and abdominal discomfort. Poor emptying may be caused by an anatomical obstruction or a functional *gastroparesis* (Table 9.1). A contrast upper gastrointestinal series or endoscopy is needed to exclude obstruction. Emptying may be delayed during an acute illness, e.g., viral gastroenteritis, trauma, or metabolic derangements such as hyperglycemia. However, patients are usually referred with chronic symptomatology. The list of causes of gastroparesis is long and can be categorized as either metabolic, neurologic, muscular, or systemic disease causes. The most frequent etiologies are diabetic gastroenteropathy and non-ulcer dyspepsia. Many commonly used therapeutic drugs, e.g., nicotine, opiates, and alcohol, inhibit emptying (Table 9.2). Delayed emptying can exacerbate the symptoms of gastroesophageal reflux and counteract effective therapy.

Table 9.1. Causes of abnormal gastric emptying

Delayed	Rapid
Diabetic gastroenteropathy	Diabetic gastroenteropathy
Non-ulcer dyspepsia	Pyloroplasty, hemigastrectomy
Hypothyroidism	Hyperthyroidism
Gastric ulcer	Zollinger-Ellison syndrome (gastrinoma)
Pernicious anemia	
Amyloidosis	
Connective tissue disorders (e.g., SLE)	
Post-vagotomy	
Tumor-associated gastroparesis	
Myotonic dystrophy	
Familial dysautonomia	
Hyperglycemia	
Uremia	
Hypercalcemia	
Gastroenteritis	

Table 9.2. Drugs that delay gastric emptying

Nifedipine
Beta adrenergic agonists
Isoproterenol
Theophylline
Sulcralfate
Anticholinergics
Diazepam
Tricyclic antidepressants
Phenothiazine
Levodopa
Progesterone
Alcohol
Nicotine

Diabetic gastroenteropathy occurs in patients with long-standing insulin-dependent diabetes. The pathophysiology is vagal nerve damage as part of a generalized autonomic neuropathy. Delayed emptying can exacerbate the problem of diabetic glucose control. Although most patients with diabetic gastroenteropathy have delayed emptying, a minority have rapid emptying. *Non-ulcer dyspepsia* is an increasingly common clinical diagnosis. It is considered a functional disease without known cause. Many have *H. pylorii* infection and approximately 40 % of patients with non-ulcer dyspepsia have delayed gastric emptying. A variety of chronic systemic diseases are associated with delayed gastric emptying, including Parkinson's disease, amyloidosis, myotonic dystrophy, and HIV infection (Table 9.1).

Radiopharmaceuticals and Meals. To accurately quantify solid emptying, the radiotracer must be tightly bound to the solid meal. Early investigators used an excellent method of labeling. Tc-99m sulfur colloid was injected into the vein of a live chicken, which was taken up by Kupffer cells. The chicken was sacrificed and the liver cooked and mixed with stew for volume and palatability. Labeling efficiency and stability were both quite high, approximately 98 %. Being impractical for most clinics, ex-vivo methods of labeling chicken liver were subsequently described and successfully used. However, today most clinics radiolabel egg albumen with Tc-99m SC, by frying or scrambling the eggs or egg substitute with the radiopharmaceutical. It is often served as an egg sandwich. Labeling efficiency is approximately 85 %.

Measuring simultaneous solid and liquid emptying is feasible using a dual isotope study, e.g., by radiolabeling a liquid phase with In-111 DTPA. The natural history of abnormal gastric emptying is that the solid phase becomes abnormal before the liquid phase. In severe disease, both are delayed. Thus on a clinical basis, only solid emptying is required. Dual isotope studies are usually reserved for research purposes. A clear liquid study may be useful in a patient intolerant of solids but able to retain liquids (Fig. 9.2).

Methodology. Various methodologies have been used. Meal composition, patient positioning, instrumentation, frequency of data acquisition, study length, and quantitative methods all vary between institutions. In general, the patient is asked to fast overnight or for at least 4 h prior to the study. The meal should be ingested within 5 – 10 min, after which imaging commences. The study can be acquired standing, sitting, and supine. For accurate quantification, it is not important which method is used, except that the methodology should always be the same and normal values derived and validated for that methodology.

From a physiological standpoint, the most accurate method of quantification would be to calculate a lag phase and the rate of emptying (Ziessman et al. 2001). Thus many protocols acquire 1-min frames for 60 – 120 min or longer. However, the clinical value of the lag phase is controversial and unproven. Other protocols call for less frequent image acquisition, e.g., every 20 – 30 min for 2 – 3 h. Many protocols have established normal values based on a half-time of emptying or the percent emptying from time zero to the end of the study. To some extent this takes into consideration both phases of emptying (Ziessman et al. 1996). What is most important is that the method used should be standardized, in regard to the meal, patient position, frequency of acquisition, the attenuation correction method, and that normal values be used that have been established for that method.

Increasingly, gastroenterologists argue that the physiologic information obtained from frequent image acquisition is not generally necessary. Rather what is needed is a simple screening test that is standardized across different institutions. With this in mind, a protocol has been published that calls for imaging, at time 0, 1 h, 2 h, and 4 h (Tougas et al. 2000). Using this acquisition protocol and an egg-substitute meal, normal values have been established for 123 normal subjects from multiple institutions in several countries. The normal values are 10 %, 65 %, and 90 % at 1, 2, and 4 h, respectively (Fig. 9.3). Some data suggests that the longer imaging period of 4 h provides a higher sensitivity for detection of abnormal emptying compared to 2 h (Ziessman et al. 2007; Camerilli et al. 1998; Parkman et al. 1996).

Decay correction is mandatory for accurate quantification of gastric emptying because of the short half-life of Tc-99m and the relatively long study time. *Attenuation correction* should also routinely be performed because of the variable soft tissue attenuation as the meal moves from the relatively posterior (fundus) to the more anterior (antrum). The lack of attenuation correction results in an underestimation of gastric emptying of 10 – 50 %. This is a serious and frequent problem in obese patients. The need for attenuation correction is less in thin patients, but significant errors occur which are not predictable prior to the study. Thus attenuation correction should be routine for all solid gastric emptying studies. However, it is not necessary for liquid emptying.

The standard method for attenuation correction is the *geometric mean method* (square root of the product of the anterior and posterior views). If only a single-headed camera is available, the opposing images must be acquired sequentially. An alternative method has been described and successfully used where images are obtained in the left anterior oblique (LAO) view (*LAO method*). In that projection, the stomach contents move roughly parallel to the head of the gamma camera, thus

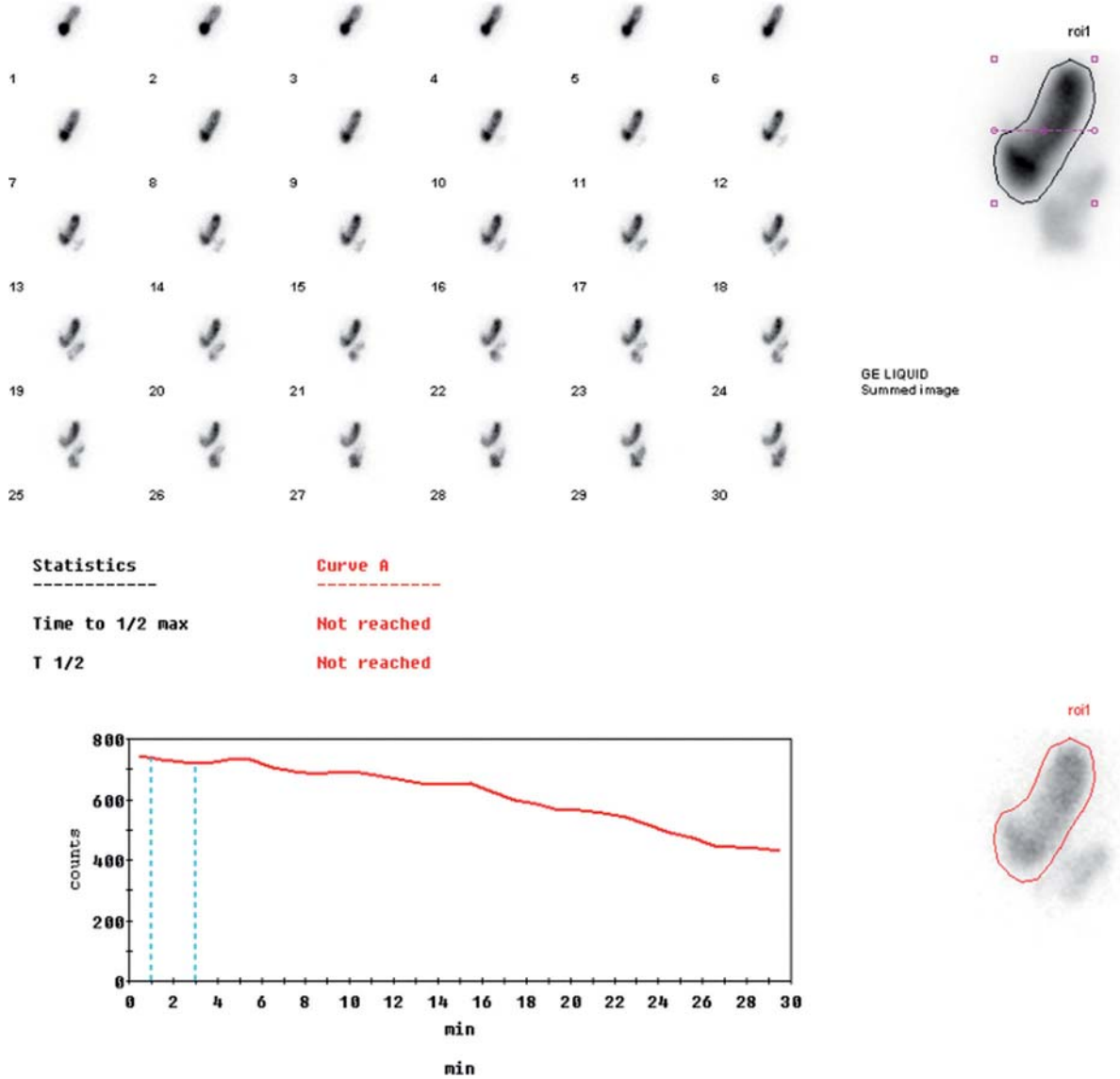

Fig. 9.2. Delayed liquid gastric emptying. One-minute frames for 30 min after ingestion of 500 cc of water. Emptying is very delayed, never reaching a half-time of emptying. Normal half-time of emptying is 10 – 20 min

minimizing the effect of attenuation. The LAO method requires no mathematical correction for attenuation (Fahey et al. 1989).

9.2.3 Intestinal Motility

The clinical indications and value of intestinal motility studies are evolving. *Small intestinal transit* dysmotility often produces symptoms similar to gastric dysmotility, e.g., bloating, early satiety, dyspepsia, and nausea. Associated diarrhea soon after eating may suggest a small bowel motility disorder. Delayed small bowel transit is seen in patients with chronic intestinal pseudoobstruction, i.e., obstruction without mechanical cause due to poor muscular contractility. Constipation is the most common indication for a *large intestinal transit* study. Some patients have diffuse colonic dysmotility, while others have delayed transit limited to the rectosigmoid region, and others with similar symptoms have normal transit. Treatment differs and thus the potential for this study.

Various radiologic methods and non-imaging breath tests have been used over the years. Most have serious limitations. The radionuclide method offers the distinct advantages of physiologic imaging. One methodologic problem is that, unlike gastric emptying, small or large bowel input is not instantaneous, but

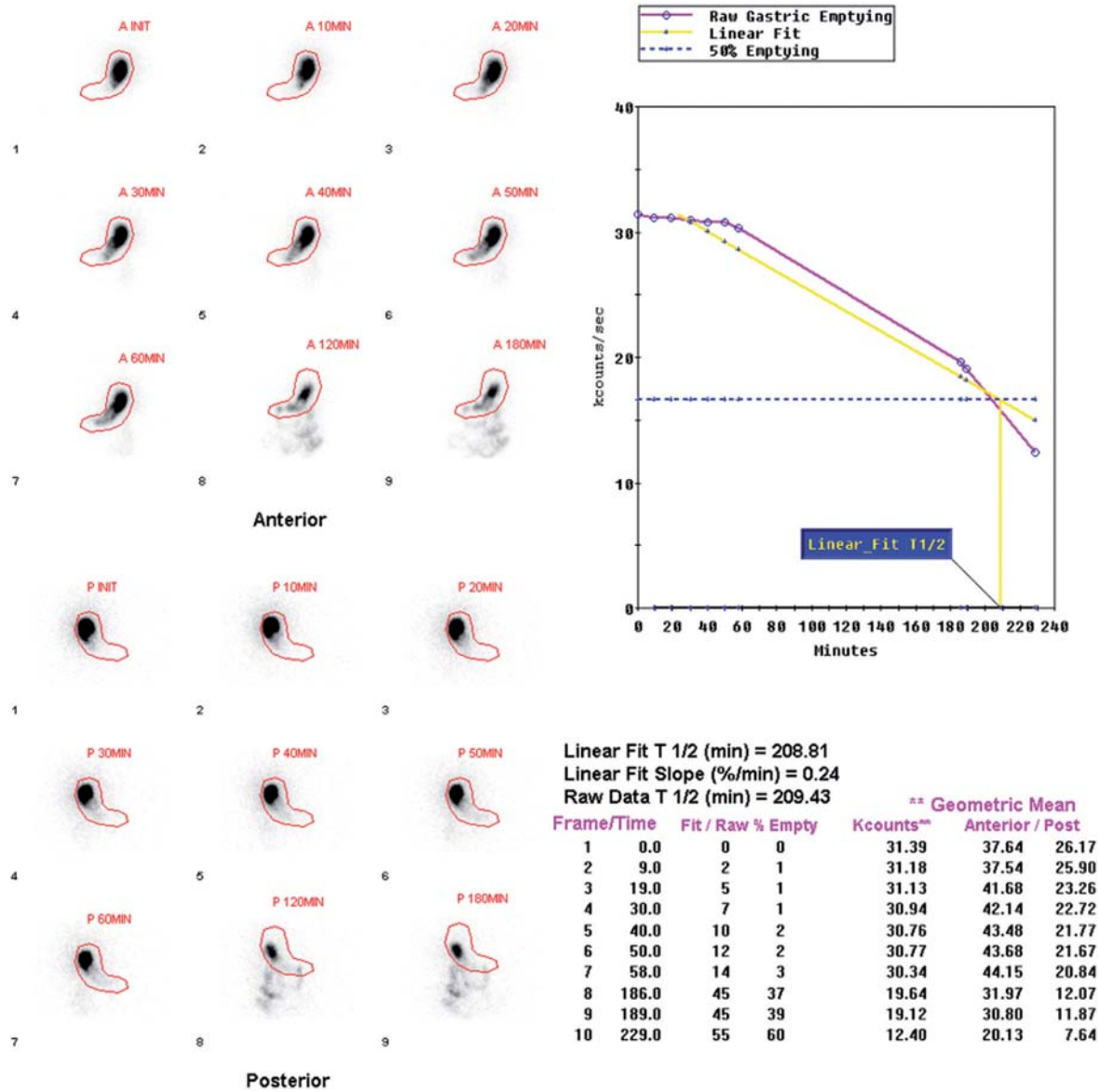

Frame/Time		Fit / Raw % Empty		Kcounts**	Anterior / Post	
1	0.0	0	0	31.39	37.64	26.17
2	9.0	2	1	31.18	37.54	25.90
3	19.0	5	1	31.13	41.68	23.26
4	30.0	7	1	30.94	42.14	22.72
5	40.0	10	2	30.76	43.48	21.77
6	50.0	12	2	30.77	43.68	21.67
7	58.0	14	3	30.34	44.15	20.84
8	186.0	45	37	19.64	31.97	12.07
9	189.0	45	39	19.12	30.80	11.87
10	229.0	55	60	12.40	20.13	7.64

Fig. 9.3. Delayed solid gastric emptying. After ingestion of an egg sandwich, images were obtained for every 10 min × 10, then every hour × 3 for a total of 4 h. Emptying is very delayed with only 60 % emptying at 4 h (normal > 90 %)

rather occurs over time. Placing the radiotracer directly in the small or large bowel obviates this problem, but is invasive and not generally acceptable. Another problem is that study length is long, which is a logistical problem for many clinics.

Simplified studies have been proposed that can be used to evaluate whole gut transit, including the stomach, small bowel, and large bowel. One approach is that of the Temple University group (Maurer et al. 1995), who have developed a 4 day test (but few imaging times), utilizing a dual isotope test meal, a 500 μCi Tc-99m SC egg sandwich and 300 ml of water mixed with 4.5 MBq (125 μCi) of In-111 DTPA. Anterior and posterior imaging is performed with Tc-99m at 0, 1, 2, and 4 h to measure solid and liquid gastric emptying, and a 6 h image for small bowel transit determination. Small bowel transit is defined as the percent arrival of total activity at the terminal ileum-cecum at 6 h. Colonic transit is measured at 24, 48 and 72 h and a geometric centroid of activity calculated. Details and normal values should be referenced (Bonapace et al. 2000).

Another approach is that of the Mayo Clinic group (Camilleri et al. 1998). A major difference with their methodology is the use of In-111 radiolabeled resin pellets (Amberlite IR 120), a radiopharmaceutical that does not disintegrate until it reaches the terminal ileum or proximal colon. Colonic transit is measured as the geometric center of activity. After the pellets have emp-

tied from the stomach, Tc-99m labeled resin pellets (Amberlite IR-410) mixed with eggs are administered and used to measure the percent gastric retention at 2 and 4 h and small bowel transit at 6 h (Camilleri et al. 1998).

9.3 Gastroesophageal Reflux

In adults gastroesophageal reflux causes symptoms of heartburn and chronic reflux that can result in esophagitis, bleeding, perforation, Barrett's esophagus, and cancer. In infants and young children, the symptoms are different, i.e., respiratory, iron deficiency anemia, and failure to thrive. Although reflux occurs in normal infants, it usually resolves by 7–8 months. Even when persistent, most children have a benign course. However, some children have serious sequelae, with strictures, recurrent pneumonia and inanition.

Barium esophagography can detect mucosal damage, stricture, and tumor, but has poor sensitivity for detection of reflux. Endoscopy allows for direct visualization of the esophageal mucosa and biopsy of suspicious areas; however, histopathologic evidence of eso-

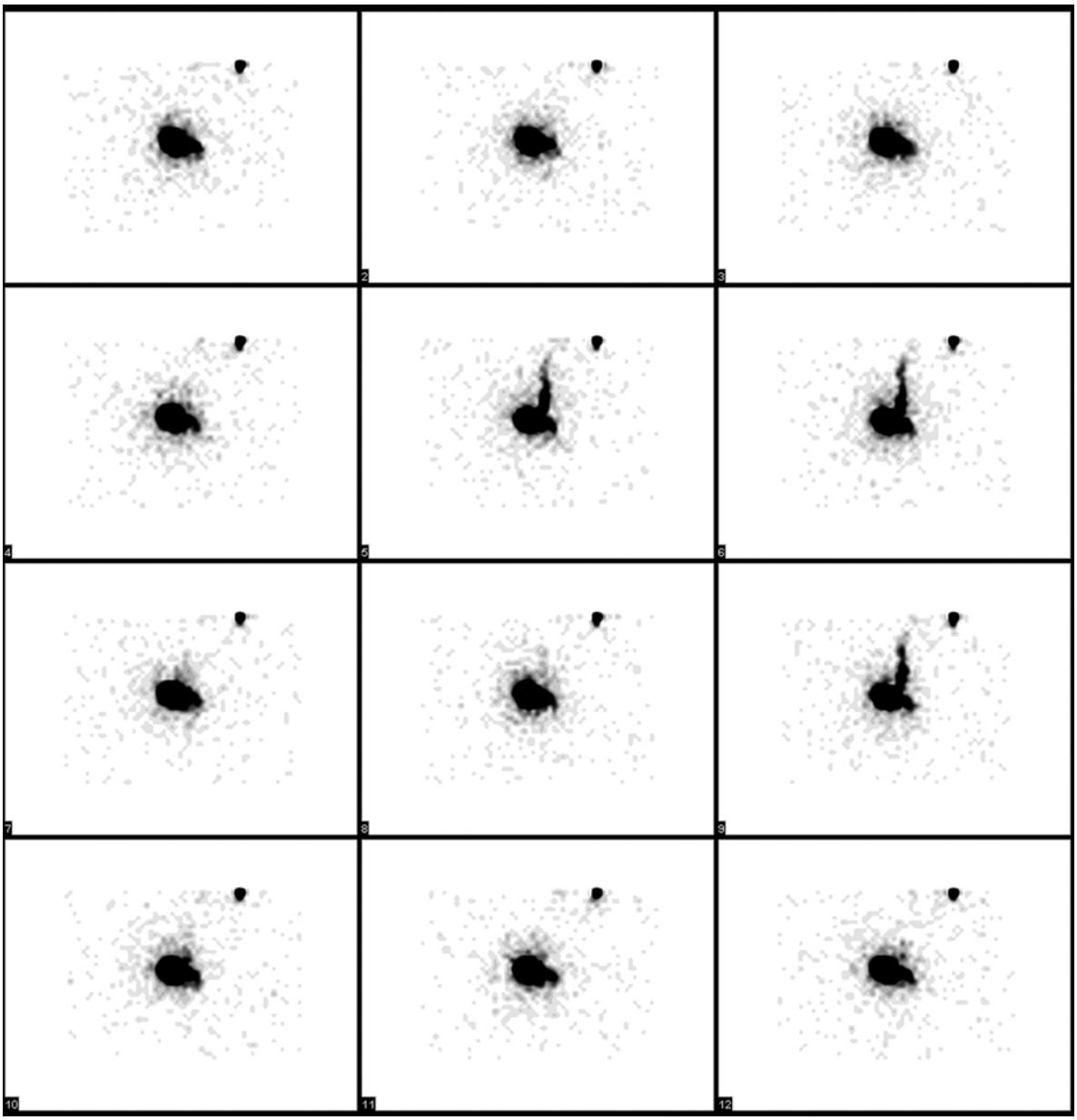

Fig. 9.4. Gastroesophageal reflux. After ingestion of milk, 5-s frame sequential images are acquired. High-level reflux events are seen, both a long one (15 s) and a short one (5 s). The study was acquired for 60 min in total. A hot marker is placed at the level of the mouth

phagitis is not sensitive for the diagnosis of reflux. The Bernstein acid infusion test (hydrochloric acid 0.1 N) can reproduce reflux symptoms and confirm their esophageal origin. The Tuttle acid reflux test is considered by some to be the gold standard for confirming gastroesophageal reflux. A pH electrode is positioned in the distal esophagus and the patient monitored for 24 h. An abrupt fall in pH is diagnostic of a reflux event. However, placement of the probe is technically demanding and requires inpatient observation.

Radionuclide scintigraphy is a sensitive noninvasive method for detecting gastroesophageal reflux and increasingly requested by pediatricians to confirm their clinical suspicion. The test is noninvasive, simple to perform, quantitative, and results in a relatively low radiation absorbed dose. Maximum sensitivity is achieved by using a frequent framing rate, usually 5 – 10 s in length for 60 min. Furthermore, detection of reflux events is greatest when the stomach is full and decreases as it empties (Shay et al. 1991). Although performed most commonly in neonates and young children, the protocol works well for older children and even adults. Tc-99m sulfur colloid, 0.3 – 0.5 μCi, is mixed with the normal infant meal volume, formula or milk. In adults, milk or orange juice is used.

Interpretation of the study requires review of all images. Reflux events are easily identified with scintigraphy (Fig. 9.4). Many quantitative methods have been described, some of them rather complex. A simple method is to define events as low or high and short or long. High events are defined as activity refluxing greater than 50 % of the length of the esophagus. Long events are defined as those greater than 10 s in length. Normal values are not established, but the higher and longer reflux events are the most clinically significant ones. Low events and short events are not infrequent in normal neonates.

Quantification of gastric emptying can be performed during the reflux study. Although normal values have never been established for neonates or young children, normal is generally considered to be approximately 50 % at 1 h and 75 % at 2 h. Images are often obtained at 2 h to detect evidence of pulmonary aspiration. Sensitivity for detection is not high, but when seen is significant. When aspiration is suspected, a *salivagram* may detect it sometimes even when the reflux study is negative for aspiration (Heyman et al. 1989). A small volume of tracer is placed in the infant's posterior pharynx and the study acquired at a fast framing rate, followed by static imaging.

9.4 *Helicobacter pylori* Infection and the C-14 Urea Breath Test

The Nobel prize in medicine in 2005 was awarded to two Australians for the discovery that infection with *Helicobacter pylori*, a gram negative bacterium, is the cause of gastric and duodenal ulcer disease. Treatment with antibiotics reverses the abnormal histologic changes and results in ulcer healing. This was a major advance because priorly, gastrectomy for ulcer disease was a common surgical procedure for patients unresponsive to anti-acid medication.

The C-14 urea breath test is used to detect the presence of *H. pylori* infection. The initial diagnosis is usually made by gastric biopsy. Serological markers fall too slowly to be diagnostically helpful to determine the effectiveness of therapy. The C-14 urea breath test can determine if the infection has been eradicated by antibiotic therapy. This test is widely available, simple to perform, noninvasive, and inexpensive.

In the presence of the bacterial enzyme urease, orally administered urea is hydrolyzed to carbon dioxide and ammonia. The C-14 radioactive beta emitter is detected in the breath as labeled CO_2. The test has high accuracy. False negative results may occur because of recent use of antibiotics or bismuth containing medications. False positive results occur in patients with achlorhydria, contamination with oral urease-containing bacteria, and colonization with another *Helicobacter*, e.g., *H. felis*.

9.5 Gastrointestinal Bleeding

Bleeding from the gastrointestinal tract can be life-threatening and prompt localization of the bleeding site allows for appropriate and effective therapy. *Upper gastrointestinal bleeding* can be suspected by the history and clinical examination, e.g., melena, and confirmed with gastric intubation and localized at endoscopy. However, localization of the site of *lower gastrointestinal bleeding* is more difficult. Barium radiography and colonoscopy are not possible during active bleeding.

Contrast angiography is the gold standard for gastrointestinal bleeding localization. However, it is invasive and there must be active hemorrhage at the time of contrast injection to localize a bleeding site. Gastrointestinal bleeding is typically intermittent and the clinical determination of whether a patient is actively bleeding is unreliable because symptoms and clinical findings often are noted after the bleeding has stopped. False negative angiography may result. The *radionuclide gastrointestinal bleeding study* is more sensitive

than contrast angiography by a factor of 10. Scintigraphy can detect bleeding rates of approximately 0.1 ml/min, compared to 1 cc/min with contrast angiography. Only 2 – 3 ml of blood is required for detection (Thorne et al. 1987). The radionuclide test has two purposes. First, it gives assurance that the patient is indeed actively bleeding. Second, it can localize the approximate site of hemorrhage, giving the angiographer information on the likely vascular origin of the bleed, e.g., celiac, superior or inferior mesenteric artery. This saves time and contrast media during angiography and increases the likelihood of a diagnostic study.

9.5.1 Radiopharmaceuticals

Tc-99m sulfur colloid (Tc-99m SC) was the first radiopharmaceutical used for gastrointestinal bleeding studies. After intravenous injection, Tc-99m SC extravasates into the bowel lumen at the site of active hemorrhage. Because intraluminal activity increases with each recirculation (serum half-life of 3 min) and the radiotracer is rapidly extracted by reticuloendothelial cells of the liver, spleen, and bone marrow, background is rapidly reduced and a high target to background ratio results. Diagnosis can often be made during the 30-min study. The disadvantage of this method is that, similar to angiography, the patient must be actively bleeding at the time of injection.

Tc-99m labeled red blood cells (Tc-99m RBCs) have become the standard radiopharmaceutical used for gastrointestinal bleeding studies because the problem of intermittent bleeding is addressed. Although the target-to-background is less than with Tc-99m SC, the use of Tc-99m RBCs allows for a considerably longer imaging time, potentially up to 24 h.

Methodology. Tc-99m must be tightly labeled to the red blood cell. Any free Tc-99m pertechnetate will be taken up and excreted by saliva and gastric mucosa and will transit the gastrointestinal tract, potentially simulating bleeding. Tc-99m pertechnetate normally freely diffuses in and out of the red blood cell. Stannous ion (tin), in the form of *stannous pyrophosphate or stannous chloride,* reduces Tc-99m pertechnetate intracellularly so that it can bind to the beta chain of hemoglobin.

Different methods of labeling red blood cell have been used over the years. In vivo labeling was the first method used. It was attractive in that it only requires an intravenous injection of stannous ion followed 20 – 30 min later by Tc-99m pertechnetate. The binding occurs in vivo. Although this method is simple to perform, labeling efficiency is only about 75 %, and considerable free pertechnetate inevitably results. Thus, a *modified in vivo (in-vitro)* method was developed. The stannous ion is initially injected intravenously. After 20 – 30 min, 3 – 5 ml of blood is withdrawn through an intravenous line into a syringe containing Tc-99m pertechnetate and anticoagulant, either heparin or acid-citrate-dextrose (ACD) solution. Without disconnecting the syringe and using gentle agitation for 10 min, radiolabeling occurs. The contents of the syringe are then reinjected. Labeling efficiency is approximately 85 %.

Table 9.3. Labeling efficiency of various methods of red blood cell labeling

Method	Labeling efficiency
In vivo	75 – 80 %
In vivtro (modified in vivo)	85 – 90 %
In vitro	98 %

However, the method with the highest labeling efficiency is the in-vitro technique of radiolabeling red blood cells (Table 9.3). Labeling efficiency is greater than 97 %. Although this can be done in a laboratory setting, a simple commercial kit method is available. Blood is drawn and added to a reaction vial containing stannous chloride. Sodium hypochlorite is added to oxidize excess extracellular stannous ion and then removed with a sequestering agent. Tc-99m pertechnetate is added and reduced by the stannous ion within the cell. After 20 min of room temperature incubation, the Tc-99m labeled red blood cells are injected.

Investigations comparing the Tc-99m SC and Tc-99m red blood cell imaging methods have all shown the superiority of the RBC method. In a large multi-center comparison study of 100 patients, the site of bleeding was diagnosed with Tc-99m SC in 5 patients compared to 38 patients using the labeled RBC study (Bunker et al. 1984). Other studies have shown similar results.

Methodology. After in vitro radiolabeling of red blood cells, the radiopharmaceutical is injected intravenously. A flow study, 1 – 3 s/frame × 1 min, is acquired, followed by dynamic imaging, 1 frame/min × 90. Static images of the neck and left lateral pelvis are then obtained. A frequent framing rate is essential for localizing a site of bleeding. Delayed imaging can be as needed, but should always be acquired dynamically.

Interpretation. Specific criteria are mandatory for accurate diagnosis of the bleeding site. These include: (1) activity is seen where none was initially; (2) the activity increases over time; and (3) the activity moves in a pattern that conforms anatomically to small or large intestines.

The flow phase can help define vascular structures (aneurysm, kidney, uterus) that might be confused with a bleeding site, occasionally detect a site of hemorrhage not well seen on delayed images (e.g., in the re-

Table 9.4. Criteria for localization of site of gastrointestinal bleeding

1. Focal activity appears out of nowhere
2. Activity increases with time
3. Transit of activity conforms to intestinal pattern

gion of the bladder), or show a vascular blush in an area not actively bleeding caused by angiodysplasia or malignancy.

Continuous dynamic imaging increases the likelihood of localizing a site of bleeding. Blood can move rapidly antegrade and/or retrograde. Greater than 75 % of bleeding sites are localized in the first 60 – 90 min of the study. It is wise to delay interpretation and continue imaging until certain about the site of origin. Delayed imaging can be beneficial if it is acquired in a similar dynamic manner and the same strict diagnostic criteria are used for interpretation (Table 9.4).

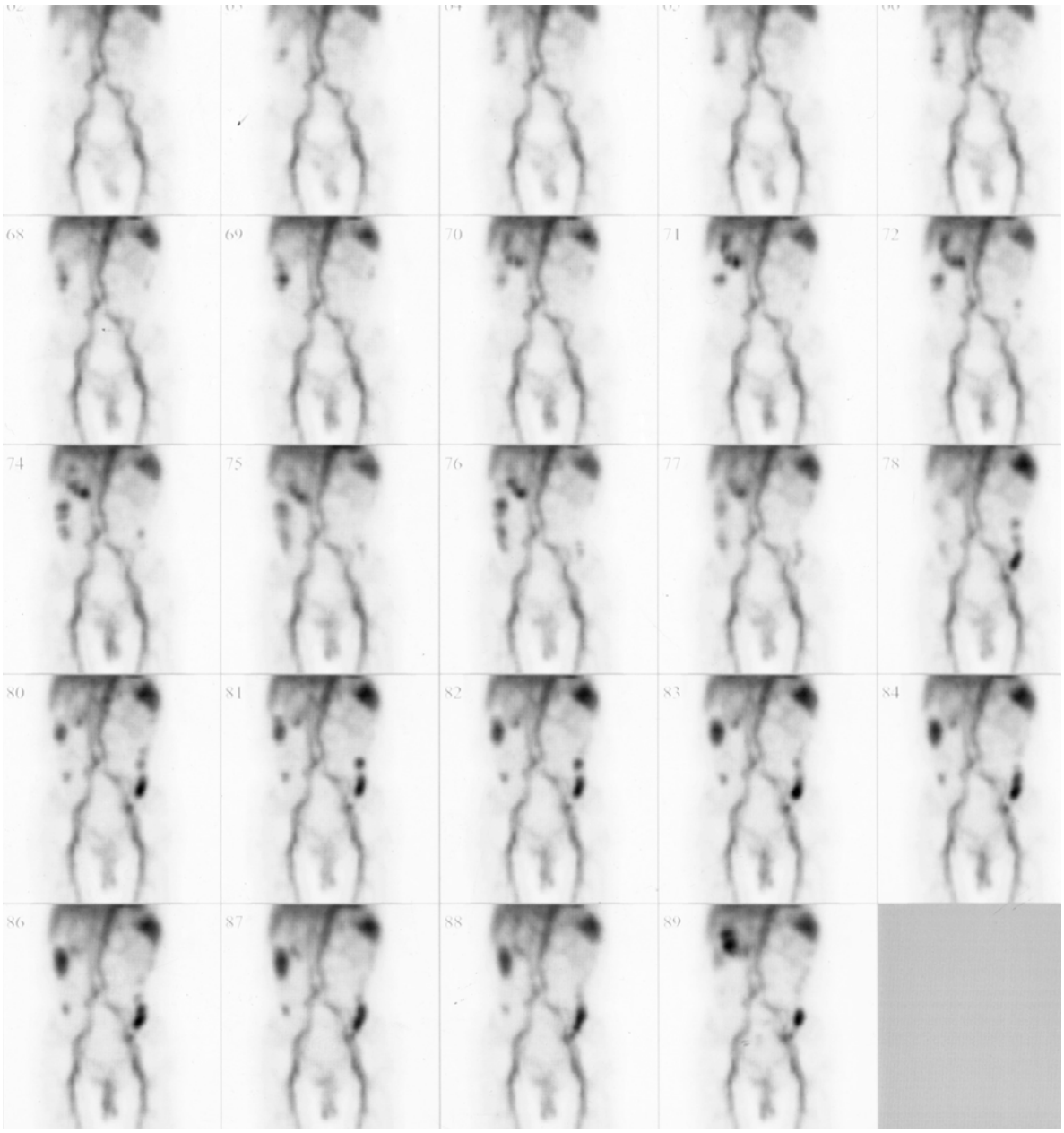

Fig. 9.5. Hepatic flexure colonic bleed. Early images show faint activity in the right upper quadrant. Over 30 min, the activity moves across the upper abdomen and down to the left lower quadrant in a pattern consistent with right colonic bleeding. Some retrograde movement is noted

Sometimes when searching for a lower intestinal site of gastrointestinal bleeding, an upper gastrointestinal bleeding site will inadvertently be detected. However, this must be carefully differentiated from free Tc-99m pertechnetate secretion and transit. Images of the salivary glands and thyroid glands can be helpful to confirm or exclude free Tc-99m. A recent intravenous contrast study may cause lack of thyroid uptake, but salivary gland uptake will be seen with free Tc-99m pertechnetate.

Cinematic display of the 90 min dynamic study should be routine because it improves diagnostic bleeding site localization (Maurer et al. 1992). The pattern of intestinal transit of activity enables differentiation of small bowel from large bowel. Large intestinal bleeding moves along the periphery of the abdomen in elongated bowel loops (Fig. 9.5). Small bowel is more central and activity progresses rapidly in a curvilinear serpent-like pattern (Fig. 9.6). The left lateral pelvic view can aid differentiating activity in the rectum from that in the bladder or penis.

Common interpretative pitfalls (Table 9.5) include the presence of free pertechnetate or genitourinary activity, misinterpreting rectal bleeding as bladder or penile activity as bleeding, and not using the same methodology and diagnostic criteria for delayed image interpretation. The presence of activity on delayed images is diagnostic of prior bleeding, but gives no information on the site of hemorrhage. Bleeding during menses should be considered in a female of reproduc-

Table 9.5. Common pitfalls for interpretation of RBC gastrointestinal bleeding

Free Tc-99m pertechnetate
Genitourinary activity (normal kidneys with urinary transit)
Genitourinary activity (ectopic, pelvic kidney)
Uterine bleeding
Penile blood pool activity
Gallbladder (hemoglobin metabolic products with uremia)
Fixed activity (hemangioma, aneurysm, varices, accessory spleen)

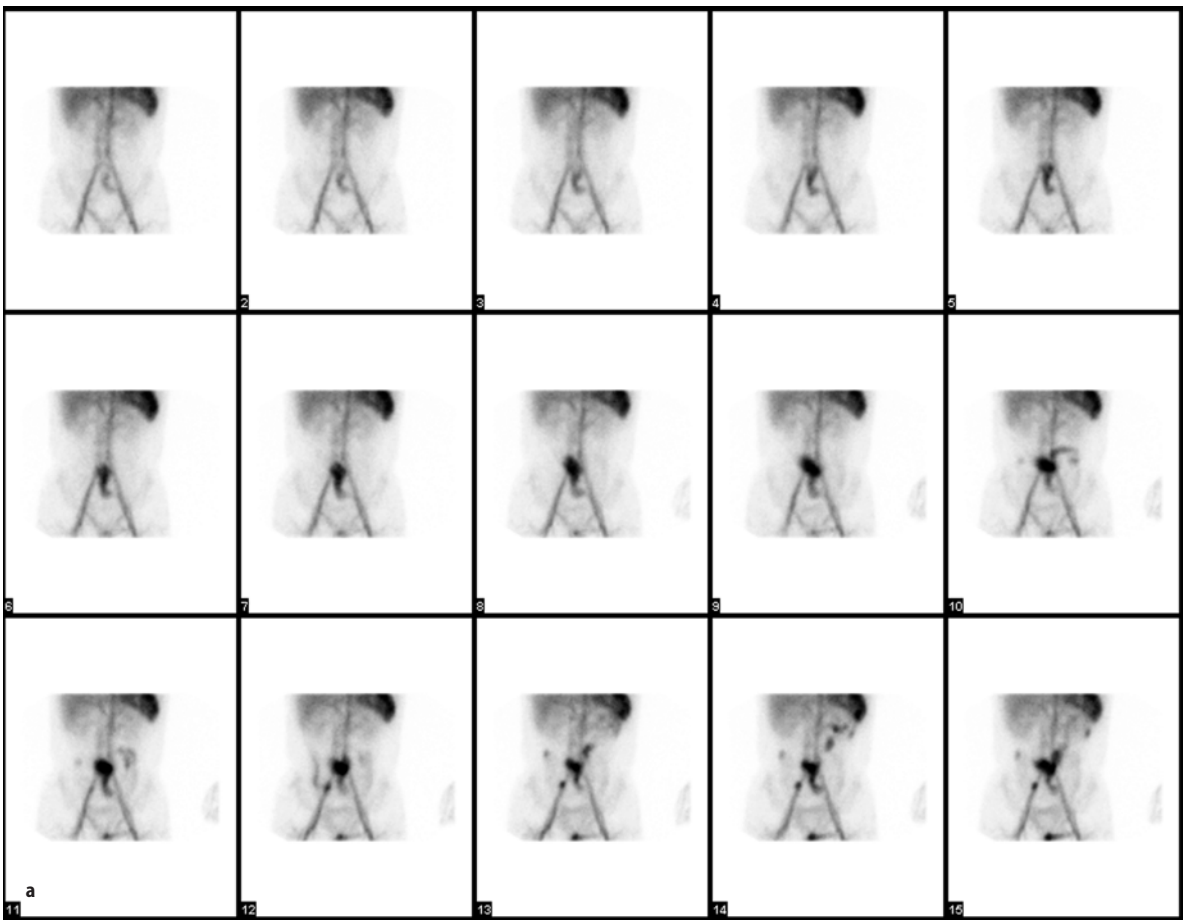

Fig. 9.6. Small intestinal bleed. **a** After in-vitro red blood cell labeling and infusion of the radiopharmaceutical, 1 min per frame images were obtained. Initially low level activity is seen in the midline abdomen just below the aortic bifurcation. This activity slowly increases in intensity and begins to move in a circuitous pattern during the initial 30-min acquisition

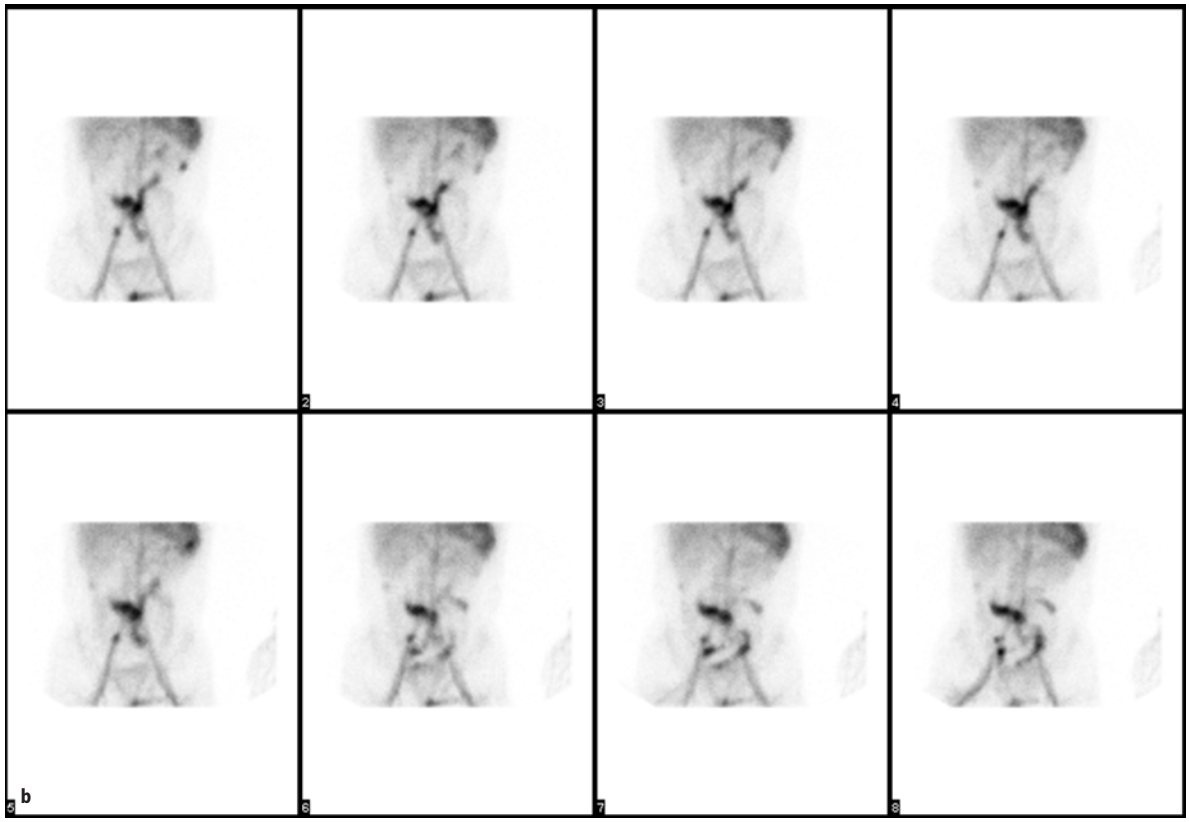

Fig.9.6. b During the second 30-min sequence of selected sequential images the small bowel pattern becomes increasingly obvious. The study was discontinued at 60 min

tive age with the presence of pelvic activity. Other potential pitfalls include hemangiomas, accessory spleens, and aneurysms. The latter are fixed abnormalities and do not truly meet diagnostic criteria for active bleeding.

The overall accuracy of the Tc-99m RBC gastrointestinal cell bleeding study is controversial, because published results have varied widely, from very accurate to very inaccurate. Detecting the site of hemorrhage is dependent on using proper methodology and using proper interpretive criteria as described (McKusick et al. 1981). Some published series have not done this. Furthermore, opportunity to detect an active site of bleeding is highest in patients imaged early in the course of bleeding, e.g., when they present to the emergency room. When the study is performed later in the hospital course after other patient workup, diagnostic yield is reduced. Thus imaging should be performed as early in the hospital course as possible. Finally, the criteria used as confirmation of the site of bleeding are of varied quality. Angiographic demonstration is best. However, a minority of patients in published studies have angiographic correlation. Delayed diagnosis by other methods of polyps, diverticuli, etc., on contrast studies may or may not be related to the etiology.

9.6 Heterotopic Gastric Mucosa

Although the term *ectopic* gastric mucosa is commonly used, this refers to an organ that has migrated, e.g., ectopic kidney, while *heterotopic* refers to a tissue at its site of origin, e.g., gastrointestinal duplications, Barrett's esophagus, post-operative retained gastric antrum, and Meckel's diverticulum. *Meckel's diverticulum* is the most common clinical presentation of heterotopic (ectopic) gastric mucosa.

Radiopharmaceutical. Tc-99m pertechnetate is taken up by the mucosa of the gastric fundus, although gastric parietal cells were initially suspected to be responsible for uptake. However, Tc-99m uptake occurs in gastric tissue with no parietal cells, and autoradiographic studies have localized the Tc-99m uptake to the mucin rather than the parietal cell.

Meckel's Diverticulum. This congenital anomaly is found on the antimesenteric side of the small intestine, usually 80 – 90 cm from the ileocecal valve. The diverticulum is caused by failed closure of the embryonic omphalomesenteric duct, which connects the yolk

sac to the primitive foregut through the umbilical cord. Heterotopic gastric mucosa is present in 10–30% of patients with Meckel's divertici, in 60% of symptomatic patients, and in 98% of those with gastrointestinal bleeding. Most symptomatic patients are children, often under 2 years of age. However, it can present in older children and adults. The gastric mucosal secretions cause peptic ulceration of the diverticulum or adjacent ileum, with resulting pain, bleeding, and/or perforation.

The diagnosis is often missed on small bowel radiography because of a narrow ostium that fills poorly and empties rapidly. Surgery is definitive and resection therapeutic. The Tc-99m pertechnetate scan (Meckel's scan) is the most reliable preoperative diagnostic method.

Methodology. Barium contrast studies should not be performed for several days prior to the study. Patients are advised to have nothing by mouth for 4–6 h prior to the study to minimize stomach size. Potassium perchlorate should not be administered to block the thyroid because it will also prevent gastric uptake. Premedication with cimetidine, 20 mg/kg orally for 2 days prior to the study, is routine in many clinics. The H_2-receptor antagonist cimetidine inhibits release of Tc-99m pertechnetate from the gastric mucosa. The drug is safe and generally recommended, although, in fact, little data substantiates its benefit (Diamond et al. 1991). Pentagastrin has been used in the past to stimulate gastric secretion, but has side effects and is no longer commercially available. Glucagon can be used to paralyze the bowel. Voiding prior to, during and at end of study is suggested since the bladder (cold or hot) may obscure diverticular mucosal uptake.

The imaging field of view should be from the xiphoid to symphysis pubis. Tc-99m pertechnetate, 30–100 μCi/kg, is injected intravenously. Flow images, 1–3 s/frame, are acquired for 1 min, followed by 1-min frames for 60 min. Post-void images and left and right anterior oblique and posterior view images are suggested.

Interpretation. Meckel's diverticuli appear as focal areas of uptake, usually in the right lower quadrant (Fig. 9.7). Diverticular uptake usually occurs simultaneously with gastric uptake. Upright or oblique images can be helpful in differentiating a Meckel's diverticu-

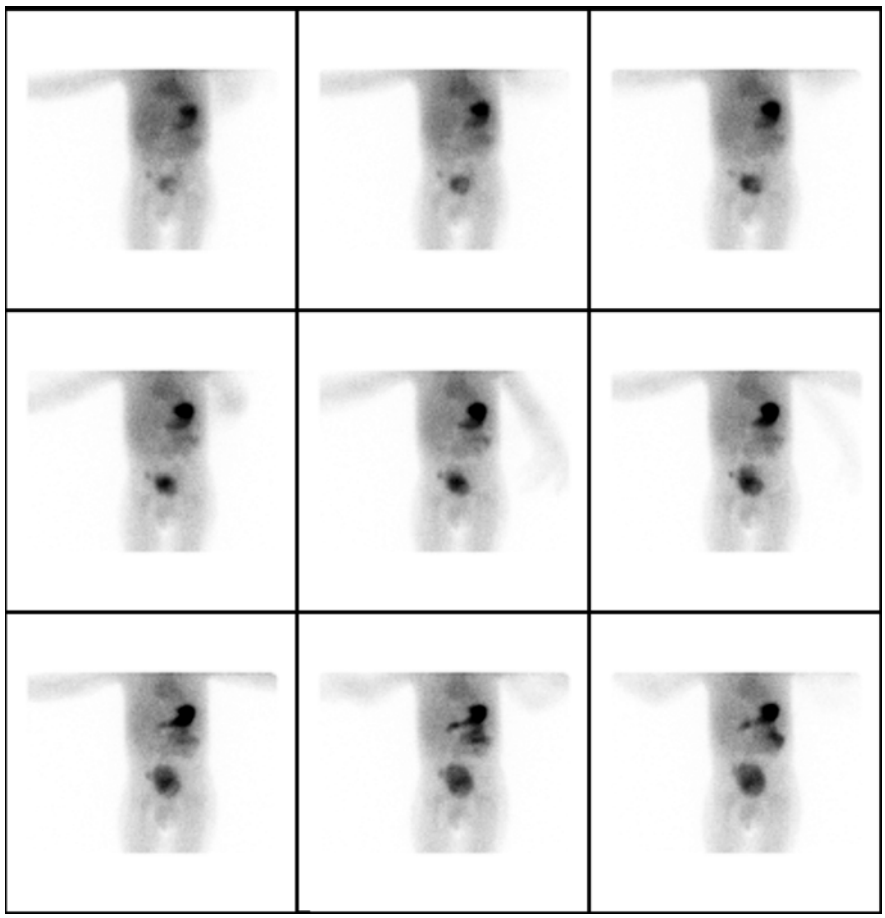

Fig. 9.7. Meckel's diverticulum. Two-year-old child with rectal bleeding. After intravenous injection of Tc-99m pertechnetate, sequential images were obtained. Focal activity can be seen adjacent to the bladder in the right lower quadrant, initially increasing in activity with time, becoming closer to the bladder as it fills. Meckel's diverticulum was confirmed at surgery

Table 9.6. Causes for false positive Meckel's diverticulum

Urinary tract activity (extrarenal pelvis, hydronephrosis, vesicoureteral reflux, horseshoe kidney)
Vascular (aneurysm of intraabdominal vessel, hemangioma, arteriovenous malformation)
Gastroenteric duplication cysts
Inflammation (Crohn's disease, ulcerative colitis, appendicitis)
Small bowel obstruction (intussusception, volvulus)

lum from urinary activity, the most common cause for a false positive study.

False negative studies may occur because of small size (<2 cm^2), rapid mucosal washout, or impaired blood supply, e.g., intussusception or volvulus. Overall accuracy of the Meckel's scan is reported to be high (Sfankianakis and Haas 1982); however, a large number of causes for false positive studies are reported (Emanian et al. 2001). These generally fall into one of several categories, e.g., urinary tract activity, vascular (hemangiomas, A-V malformation), hyperemia and inflammatory (inflammatory bowel disease, appendicitis), neoplasm (carcinoid, lymphoma), obstruction, and other causes for ectopic gastric mucosa, e.g., gastrointestinal duplications (Table 9.6).

Thirty to 50 % of gastrointestinal duplications contain gastric mucosa. The duplications are cystic or tubular congenital abnormalities with mucosa, smooth muscle, and alimentary epithelium attached to any part of the gastrointestinal trace, often in the ileum. Twenty percent occur in the mediastinum. Tc-99m pertechnetate scans have been used to diagnose a retained gastric antrum after Billroth II gastrojejunostomy or a Barrett's esophagus. This purpose is rarely requested in current practice.

9.7 Shilling Test

The Shilling test is a time-tested standard non-imaging radionuclide technique used to diagnose intestinal B_{12} malabsorption. It is most commonly ordered for patients suspected of having pernicious anemia. Vitamin B_{12} is absorbed from the terminal ileum only if it is complexed with intrinsic factor, produced by gastric parietal cells in the stomach. For the non-imaging study, B_{12} is labeled with cobalt-57 (Co-57). An intramuscular dose of unlabeled (cold) B_{12} is administered first in order to saturate tissue and plasma binding sites, ensuring renal excretion of all absorbed Co-57 B_{12}. The urine is collected at 24 and 48 h. The utility of the 48 h sample is limited to patients with renal insufficiency to insure time full excretion. The fraction of the administered dose that is excreted in the urine is reported to be normally greater than 8 – 9 %. This is Stage I of the test.

An abnormally low result is diagnostic of B_{12} malabsorption, but is not specific as to etiology, e.g., the lack of intrinsic factor (pernicious anemia), or primary intestinal malabsorption (e.g., sprue, bacterial overgrowth), or pancreatic insufficiency. A Stage II study is needed for this differential diagnosis. If pernicious anemia is suspected, the test is then performed with ingestion of radiolabeled B_{12} with intrinsic factor. If the history suggests bacterial overgrowth, a course of antibiotics can be given prior to the second study. If pancreatic insufficiency is suspected as the cause, pancreatic enzymes can be administered. A commercial dual isotope study has been used with suspected pernicious anemia, utilizing Co-58 labeled B_{12} and Co-57 labeled B_{12} bound to intrinsic factor.

9.8 Somatostatin Receptor Imaging

The hormone somatostatin is a 14-amino-acid polypeptide found in the brain, where it acts as a neurotransmitter, and in the gastrointestinal tract and pancreas, where it inhibits release of growth hormone, insulin, glucagon, gastrin, serotonin, and calcitonin. It has an antiproliferative effect on tumors, inhibiting angiogenesis and various growth factors.

Somatostatin receptors are integral membrane glycoproteins located on many normal cells of neuroendo-

Table 9.7. Somatostatin receptor distribution in normal tissues and associated tumors

Normal tissue cells	Tumor
Anterior pituitary	Adenomas (GH, TSH)
Pancreatic islet cells	Islet cell tumors
Gastrointestinal endocrine cells	Carcinoid tumors
Undifferentiated neuroendocrine carcinomas	
Endocrine cells in miscellaneous sites	Neuroendocrine tumors of ovary, cervix, endometrium, breast, kidney, larynx, paranasal sinuses, salivary glands
Adrenal medulla	Pheochromocytoma Neuroblastoma Paraganglionoma
Thyroid cells	Medullary carcinomas
Skin	Merkel cell carcinomas Melanomas
Bronchopulmonary endocrine cells	Small cell lung cancer
Leptomeninges	Meningiomas
Glial cells	Well-differentiated glial-derived tumors
Activated leukocytes	Lymphomas, granulomas, autoimmune diseases

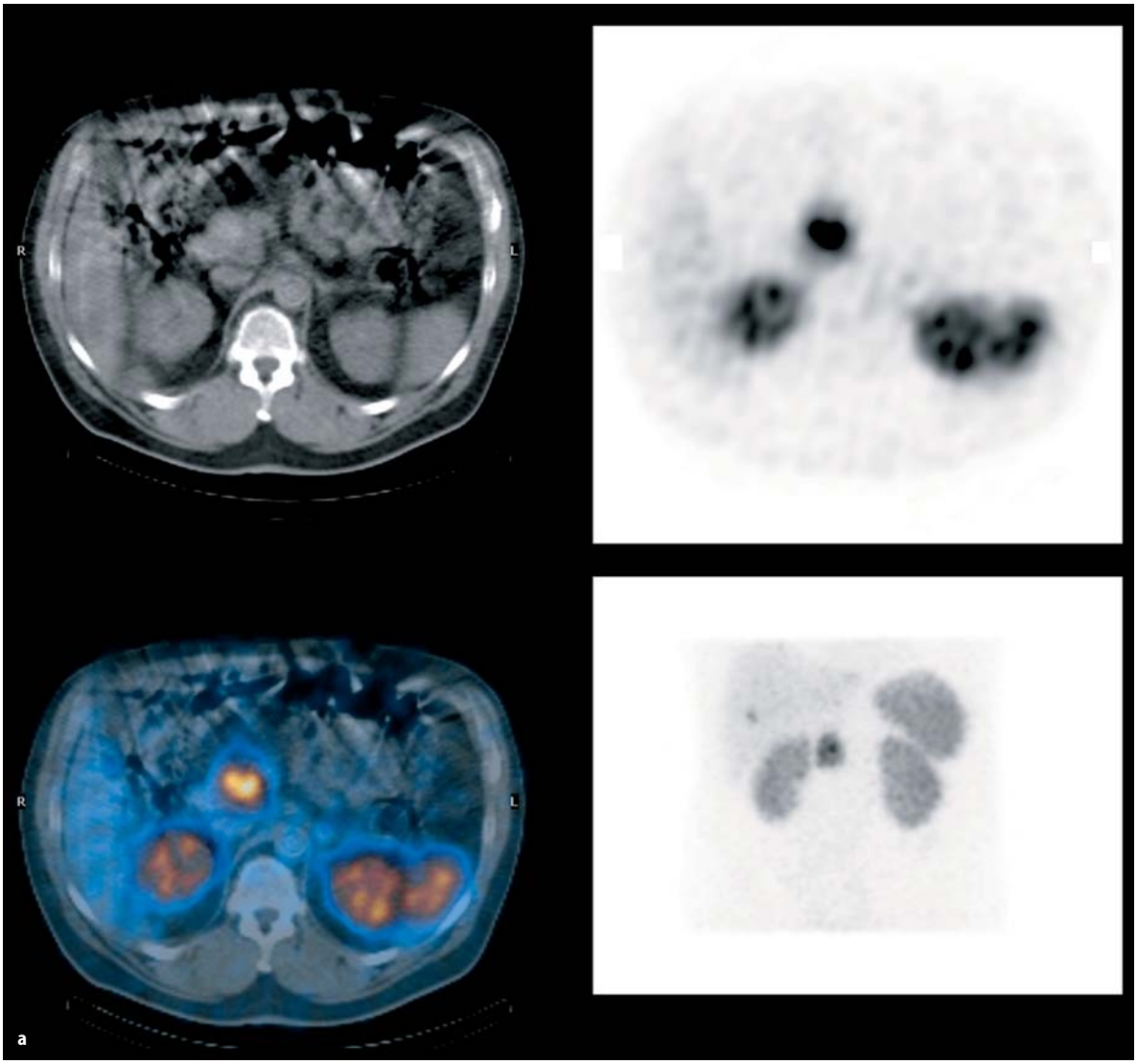

Fig. 9.8. Indium-111 pentreotide imaging of neuroendocrine tumor. Fifty-one-year-old female with a surgically confirmed neuroendocrine tumor in the head of the pancreas. **a** PET CT demonstrates that the primary tumor has somatostatin receptors. The MIP view shows the primary tumor and probable second tumor in the liver. PET CT localizes the In-111 pentreotide uptake to the head of the pancreas

crine origin, e.g., pancreatic islet cells, thyroid C-cells and anterior pituitary somatograph cells. They are also located on non-neuroendocrine cells, e.g., activated lymphocytes. Five somatostatin receptor types (SSTR 1 – 5) have been described.

In addition to normal tissue distribution, these receptors are found in neuroendocrine tumors derived from neural crest cells belonging to the amine precursor uptake and decarboxylation (APUD) system that produce bioactive proteins, e.g., catecholamines and serotonin. SSTR2 is expressed in neuroendocrine tumors and is the receptor that In-111 pentetreotide binds to with high affinity. Somatostatin receptors are also found on other types of tumors, e.g., tumors of the central nervous system, breast, lung, and lymphoma.

Although there are many tumors of many organ systems with somatostatin receptors (Table 9.7), only the *gastroenteropancreatic and carcinoid* tumors will be discussed in this chapter on gastrointestinal nuclear medicine. The tumors include *pancreatic islet cell tumors* named after the hormone they secrete, e.g., gastrinomas, insulinomas, glucagonomas, stomatostinomas, and VIPomas and *carcinoid tumors* that can be found in the stomach, duodenum, jejunum, appendix, cecum, colon, and rectum.

Gastroenteropancreatic tumors are relatively rare, 1 to 8 per 1,000 population. They are usually highly differentiated, slow growing, and can be quite small. Most

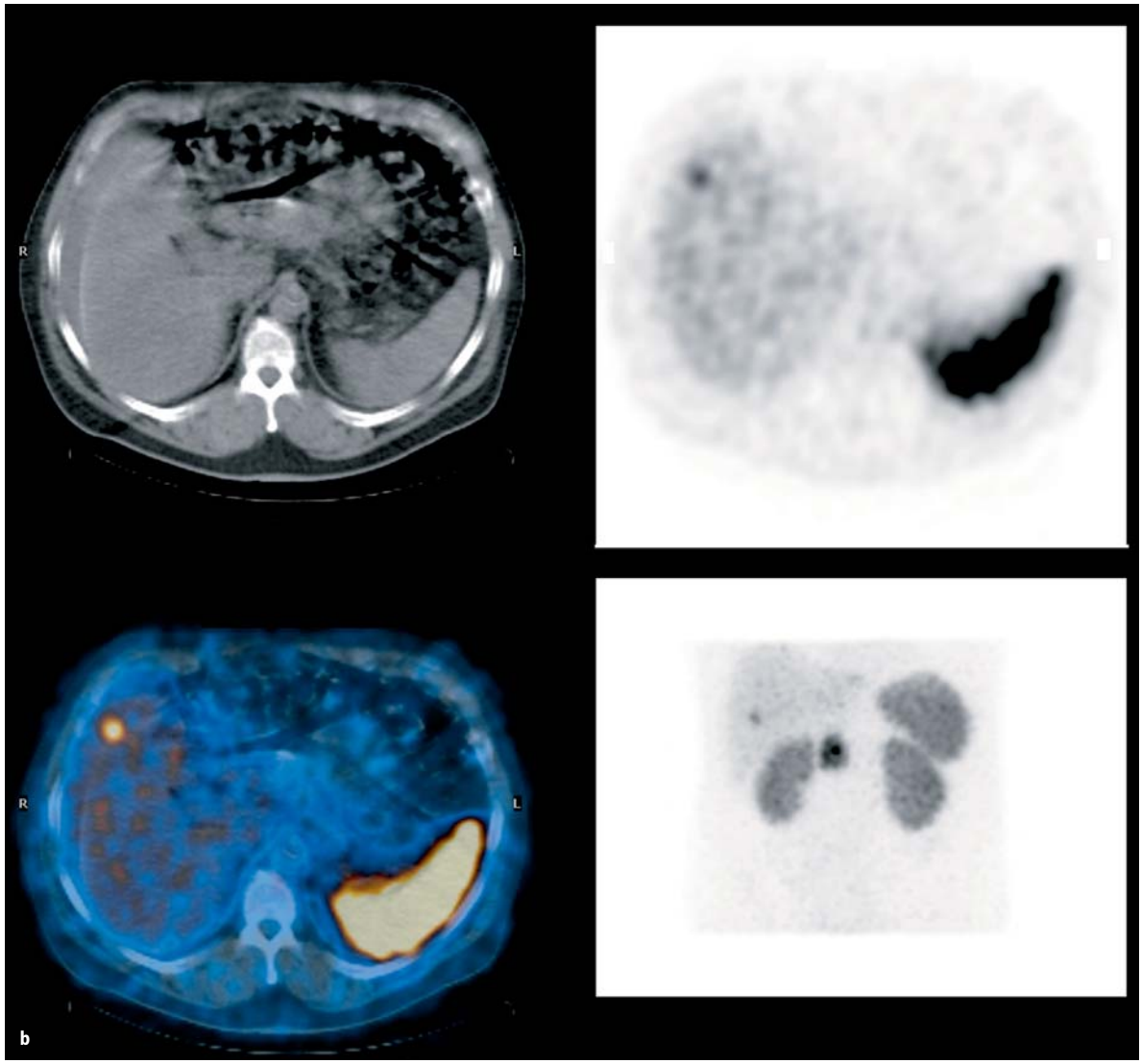

Fig. 9.8. b PET CT localizes a small focus of uptake to the right lobe of the liver, confirmed to be metastatic tumor

have high concentrations of somatostatin receptors. Symptoms are oftentimes prominent, secondary to the hormonal activity expressed, e.g., hypoglycemia (insulinoma), gastric ulcers (gastrinoma), severe diarrhea, and flushing [5-hydroxyindoleacetic acid (5-HIAA) of carcinoid tumors]. Often they have metastasized by the time of diagnosis, most commonly to the liver, lymph nodes, bone, lungs, and skin.

Gastrointestinal carcinoid tumors derive either from the foregut (stomach, duodenum), midgut (distal ileum, proximal colon), or hindgut (distal colon, rectum). The midgut carcinoids with liver metastases are the ones that cause the *carcinoid syndrome*, with symptoms of flushing, diarrhea, wheezing, and valvular right heart disease.

The pharmacologic drug, octreotide, is commonly used therapeutically to control symptoms in patients with the carcinoid syndrome. The first somatostatin receptor radionuclide imaging agent, I-123 tyr^3 octreotide, was introduced in 1987. However, it was a suboptimal imaging agent with considerable gastrointestinal clearance. In-111 labeled pentetreotide, an octreotide analogue, subsequently became available and is now routinely used for imaging of somatostatin receptor positive tumors (Krenning et al. 1993). DTPA serves as the chelator binding In-111 to pentreotide. The radionuclide In-111 has two photopeaks (172 and 247 keV), both with high abundance (89% and 94%). It also emits Auger electrons, which gives the radiopharmaceutical therapeutic potential as well. A Tc-99m labeled compound has been developed (Tc-99m depreotide); however, In-111 pentetreotide is more sensitive for gastroenteropancreatic tumor detection because of its longer physical half-life (2.8 days), which permits de-

layed imaging, thus more time for background clearance, and an improved target-to background ratio.

Highest uptake of In-111 pentetreotide occurs in the kidneys and spleen. It is cleared mostly by the genitourinary system. The liver has less uptake and variable hepatobiliary clearance. The gallbladder can sometimes be seen. Thyroid uptake is not uncommonly seen. Whether this is normal variation or secondary to chronic thyroiditis is uncertain.

The usual administered dose of In-111 pentetreotide is 200 MBq (5 mCi). The spleen receives the highest radiation dose, approximately 15 cGy/200 MBq (15 rads/5 mCi), followed by the kidneys (10.8 cGy). Whole body imaging at 24 h and SPECT of the abdomen is standard. SPECT increases tumor detectability compared to planar imaging. Delayed imaging at 48 h is only occasionally helpful in confirming or excluding tumor by allowing time for bowel clearance. SPECT CT is increasingly being used to enhance diagnostic certainty of localization (Figs. 9.8, 9.9).

For carcinoid and gastrinoma tumors, tumor detection sensitivity is high (80–90%), somewhat lower for VIPomas and glucagonomas (75%), but even lower for insulinomas (50%). Other imaging modalities, e.g., ultrasonography, MRI, and CT, all have a considerably lower tumor detection rate than In-111 pentreotide scintigraphy (Bombardieri et al. 2004). Generally gastroenteropancreatic tumors are quite small and difficult to detect by standard methods.

Somatostatin receptor imaging is used to select patients who will be likely to respond favorably to octreotide therapy. In some cases, scintigraphy preempts sur-

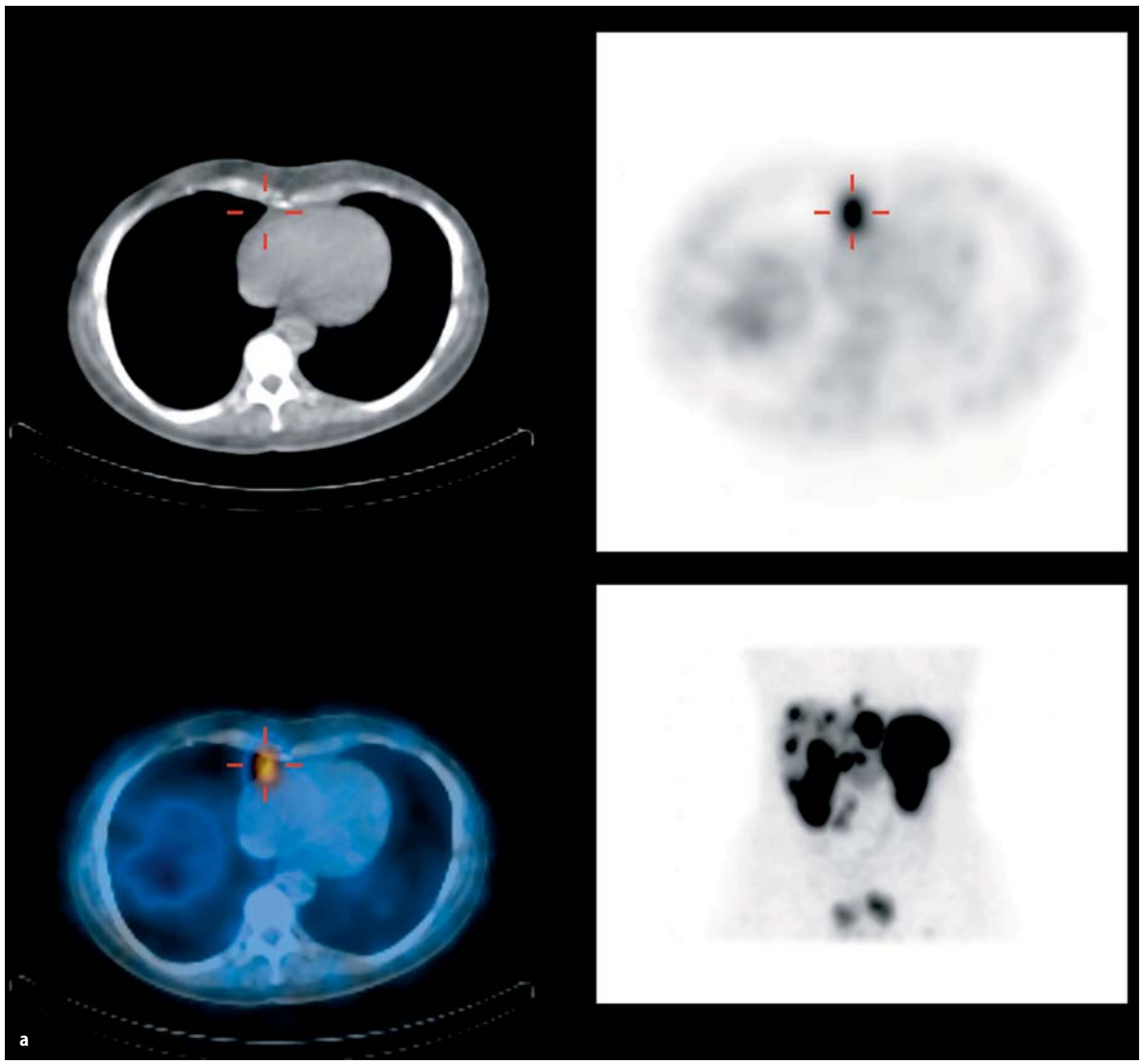

Fig. 9.9. Metastatic carcinoid tumor. **a** MIP image shows multiple metastases to the liver, abdomen, and pelvis. One focus of uptake above the diaphragm is clarified by the SPECT CT scan, consistent with a metastatic pericardial lymph node

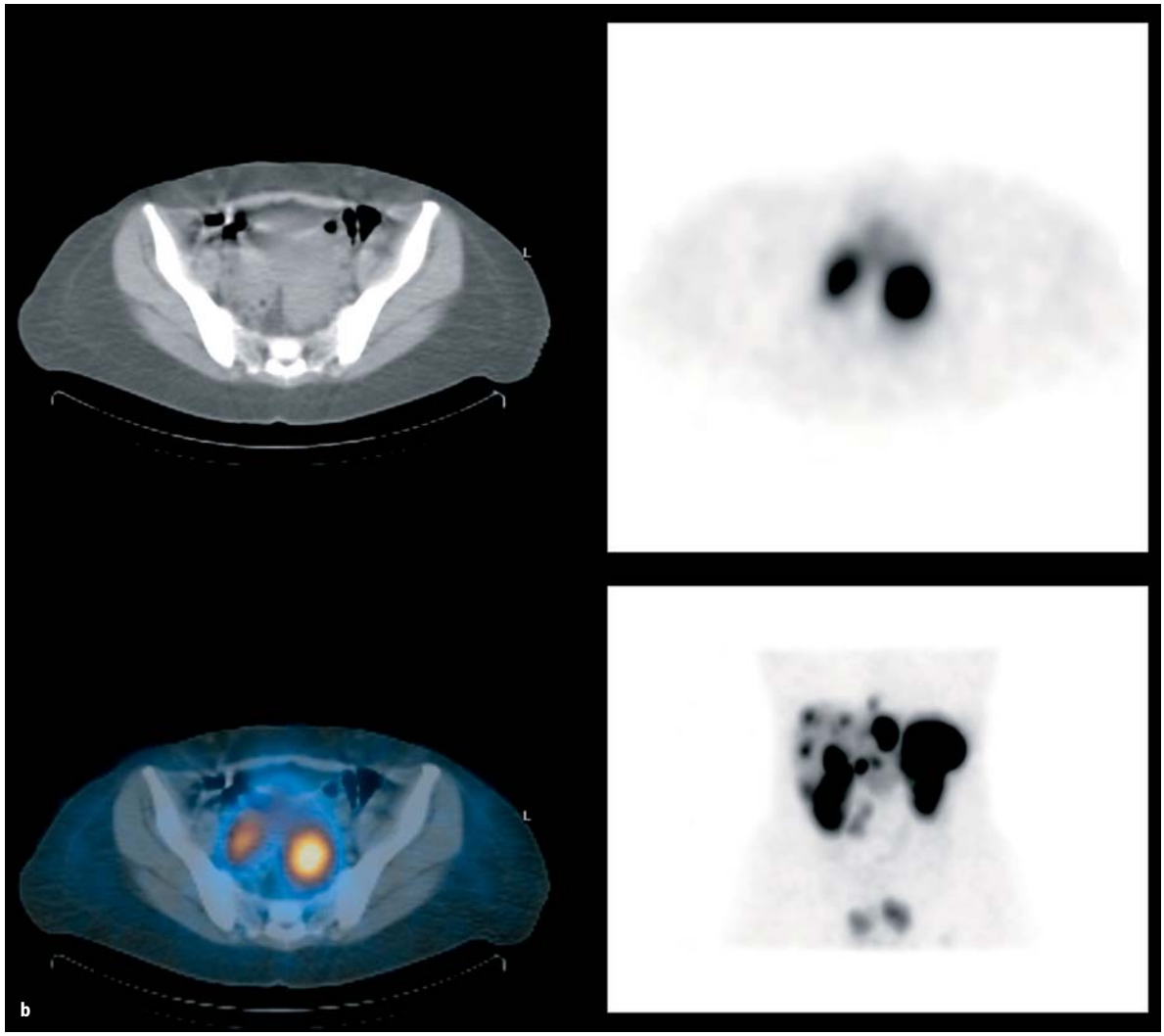

Fig. 9.9. b SPECT CT shows that the two foci of uptake in the pelvis fuse with adnexal regions. Bilateral ovarian metastases were subsequently confirmed

gery in patients whose tumors have metastasized and can direct the choice of therapy in patients with inoperable tumors. In-111 pentetreotide imaging positively impacts patient management in 25–45% of patients (Lebtahi et al. 1997). False positive studies may occur in patients due to an accessory spleen, recent cerebrovascular accident, surgical incisions, or inflammatory lesions.

F-18 FDG PET is usually negative in well-differentiated tumors. However, poorly differentiated tumors may be FDG PET positive. These latter patients typically have negative In-111 pentreotide studies. The single-photon agent I-123 MIBG is taken up in some tumors, but is inferior to In-111 pentetreotide.

Single and dual photon (PET) radiopharmaceuticals are under investigation. Single-photon somatostatin-analogue peptides being investigated include In-111 DOTA lanreotide (MAURITIUS) and Tc-99m vapreotide. PET tracers under investigation include C-11 5-HTP and F-18 DOPA, I-124 MIBG and Cu-64 TETA-octreotide.

9.9 Positron Emission Tomography of Gastrointestinal Disease

F-18 FDG PET and FDG PET-CT tumor imaging is enjoying rapid growth and playing an important role in the staging, restaging, and response to therapy of various gastrointestinal malignancies, including tumors of the esophagus, colorectal cancer, pancreatic carcinoma, cholangocarcinoma, and gastrointestinal stromal tumors.

9.9.1 Colorectal Cancer

Cancers of the colon and rectum are the third leading cause of death, after lung and breast and prostate cancers. Although FDG PET imaging presently has little role in initial tumor staging, it is increasingly being used for restaging, preoperative evaluation prior to hepatic tumor resection, and for evaluating response to therapy (Delbeke and Martin 2004).

FDG uptake in primary colorectal cancer is generally high (Fig. 9.10), with the exception of mucinous adenocarcinoma, where sensitivity is the range of 60%. The sensitivity of FDG PET as a screening tool for colorectal cancer is poor compared to colonoscopy, because of the generally small size of the polyps. In newly diagnosed primary colorectal cancer, FDG PET detection sensitivity for local lymph node involvement is less than 30%, similar to CT (Abdel-Nabi et al. 1998). Most patients with newly diagnosed colorectal cancer require surgery to prevent obstruction and the incidence of clinically unsuspected distant metastases is not high. Thus, there is not commonly a need for preoperative FDG PET. Occasionally, an incidental primary colorectal cancer can be suspected when evaluating a patient for a known malignancy (Fig. 9.11).

Over seventy percent of primary colorectal cancers are thought to be resectable with curative intent at the time of surgery. However, a third of these patients have disease recurrence within 2 years. Serial serum carcinoembryonic antigen (CEA) is used clinically to monitor patients for recurrence; however, its sensitivity is only 59% and it provides no localizing information. It is not uncommon for patients to present with a rising CEA, but have normal conventional imaging, including CT. FDG PET can detect the recurrent tumor in over two-thirds of these patients (Flanagan et al. 1998).

The sensitivity of CT for detecting metastatic recurrences is approximately 70%, compared to FDG PET, which has repeatedly been shown to be greater than 95% (Huebner et al. 2000). Twenty percent of colorectal recurrences are in the liver. Although CT portography has a higher accuracy than CT for detecting metastases to the liver, FDG PET has superior accuracy, 92% for FDG PET, 80% for CT portography, and 78% for CT (Table 9.8) (Delbeke et al. 1997).

Patients with a single liver metastasis are potentially curable by surgical resection; however, only 25% are in fact cured. Extrahepatic metastases are generally a contraindication to surgical resection; however, preopera-

Table 9.8. Comparative accuracy of FDG PET and CT in recurrent colorectal cancer

Author	Date	Patients	Sensitivity		Specificity	
			PET	CT	PET	CT
Delbeke	1997	61	93	79	86	58
Valk	1999	115	93	69	98	96
Whiteford	2000	105	87	68	66	59
Gambhir[a]	2001	1387	93	71	96	89

[a] Literature summary review

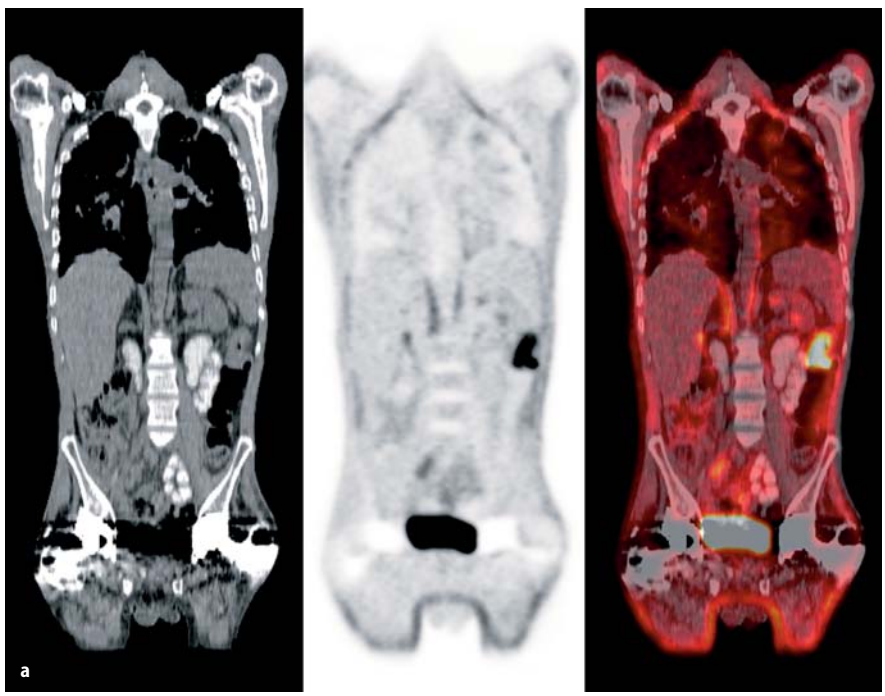

Fig. 9.10. Primary colorectal cancer on FDG PET. Newly diagnosed splenic flexure cancer. PET-CT shows high uptake in a primary cancer in coronal (**a**) and transverse (**b**) slices. No local or distant metastases were seen

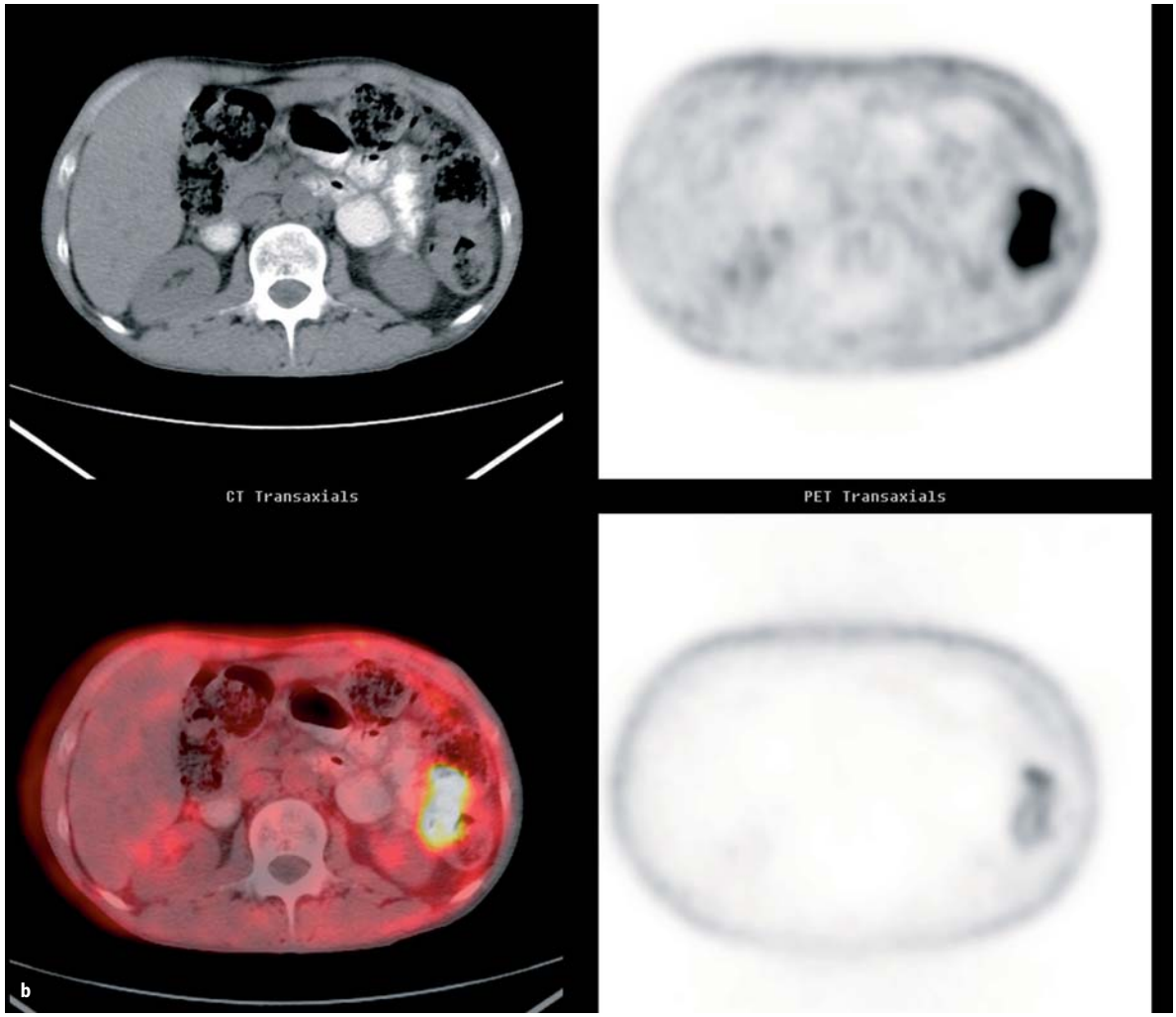

Fig. 9.10. (*Cont.*)

tive detection is poor by conventional methods. CT underestimates the number of lobes involved by one-third, commonly misses peritoneal and mesenteric metastases, and has great difficulty in differentiating post-surgical changes from local recurrence. FDG PET can also differentiate post-operative fibrosis from recurrent tumor with high accuracy (Ito et al. 1992). An improved method is desirable for selection of patients who might benefit from hepatic resection.

Hybrid PET-CT is rapidly becoming the standard method of PET imaging. In addition to decreasing the time required for acquisition of transmission images used for attenuation correction, PET-CT improves the certainty of tumor detection and location. One published investigation has shown that FDG PET-CT reduced equivocal and probable interpretations by 50 %, increased definite interpretations by 25 % and improved staging from 78 % to 89 % (Cohade et al. 2003).

Beyond high sensitivity and specificity, PET CT changes patient management. Multiple investigations have shown that FDG PET has a clinical impact in 30 – 40 % of patients, making it possible to avoid unnecessary surgery and allowing earlier evaluation for treatment by detecting recurrences before detected by CT (Wiering et al. 2005).

Increasing data suggests that response to chemotherapy can be predicted with FDG PET, usually within 3 weeks after chemotherapy, and perhaps earlier, and 6 months after radiation therapy. FDG uptake significantly decreases after effective therapy (Fig. 9.12). FDG PET is used to monitor the effectiveness of radiation therapy, chemotherapy, and regional liver therapy, e.g., chemoembolization, radiofrequency ablation, and radioactive microspheres.

PET FDG is now an accepted method of evaluating patients with suspected or known colorectal cancer. It does not replace other imaging modalities, including

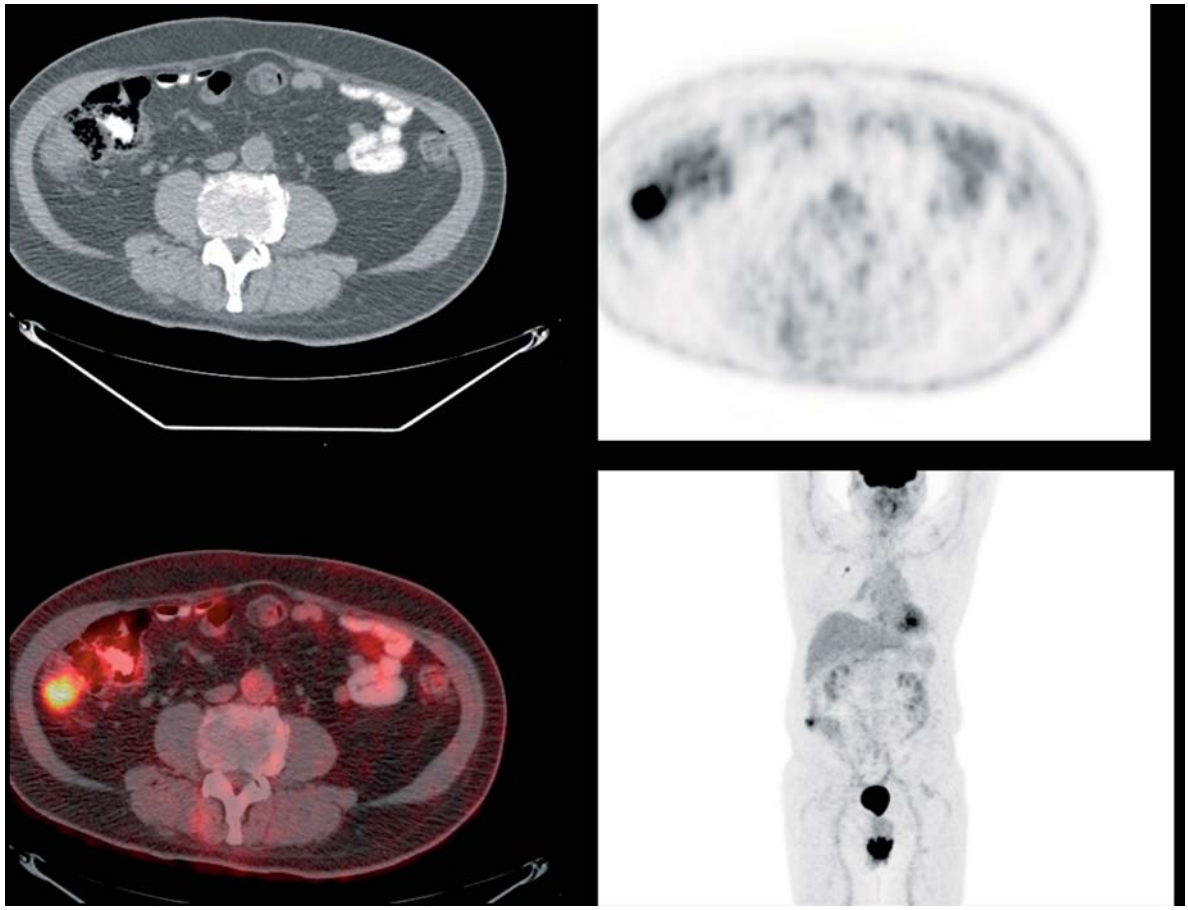

Fig. 9.11. Incidental colorectal cancer on FDG PET. Follow-up exam post-chemotherapy in a patient with small cell lung cancer. Focal uptake is seen in the right lower quadrant on the MIP view. In the transverse view, the FDG uptake fuses with a soft tissue mass in the cecum

CT, but is indicated for staging of recurrent disease, particularly when the patient is being considered for resection, differentiation of post-treatment changes from recurrent tumor, evaluating equivocal changes on other imaging modalities, and for monitoring therapy.

9.9.2 Cancer of the Esophagus

Esophageal cancer is often clinically silent until an advanced stage. Early stage disease is surgically curable; however, up to 80 % of patients have local metastases and 50 % have distant metastases at initial diagnosis. The overall 5-year survival rate is 10 %. Worldwide, squamous cell carcinoma is the most common histopathology, although its incidence is decreasing, probably because of population dietary changes. On the other hand, adenocarcinoma of the esophagus is increasing in the Western world. It is associated with gastroesophageal reflux, esophageal metaplasia, and Barrett's esophagus.

Prognosis depends on the magnitude of disease at initial diagnosis. Prognostic indicators include the extent of the primary tumor (T staging), regional node metastases (N) and distant metastases (M). Surgical resection can be curative in early disease; however, nonsurgical therapy in metastatic disease is rarely curative. Regional metastases occur anywhere from the cervical chain, down to mediastinal, gastrohepatic, and celiac nodes. Neoadjuvant chemotherapy (before surgery) is increasingly being used in patients thought to have resectable disease because it improves local tumor control, prevents distant disease, and decreases tumor burden, allowing for complete resection.

FDG uptake is usually quite high in primary esophageal cancer. Sensitivity for detection is greater than 95 %. However, FDG PET cannot provide important staging information on the depth of invasion and periesophageal tissue invasion (T staging), and has relatively poor sensitivity (50 – 75 %) for determining nodal involvement. Five-year survival in patients without nodal involvement approaches 75 %, but in those with nodal disease, survival is approximately 10 %.

An important role for FDG PET in primary staging is in the detection of distant metastases, commonly lo-

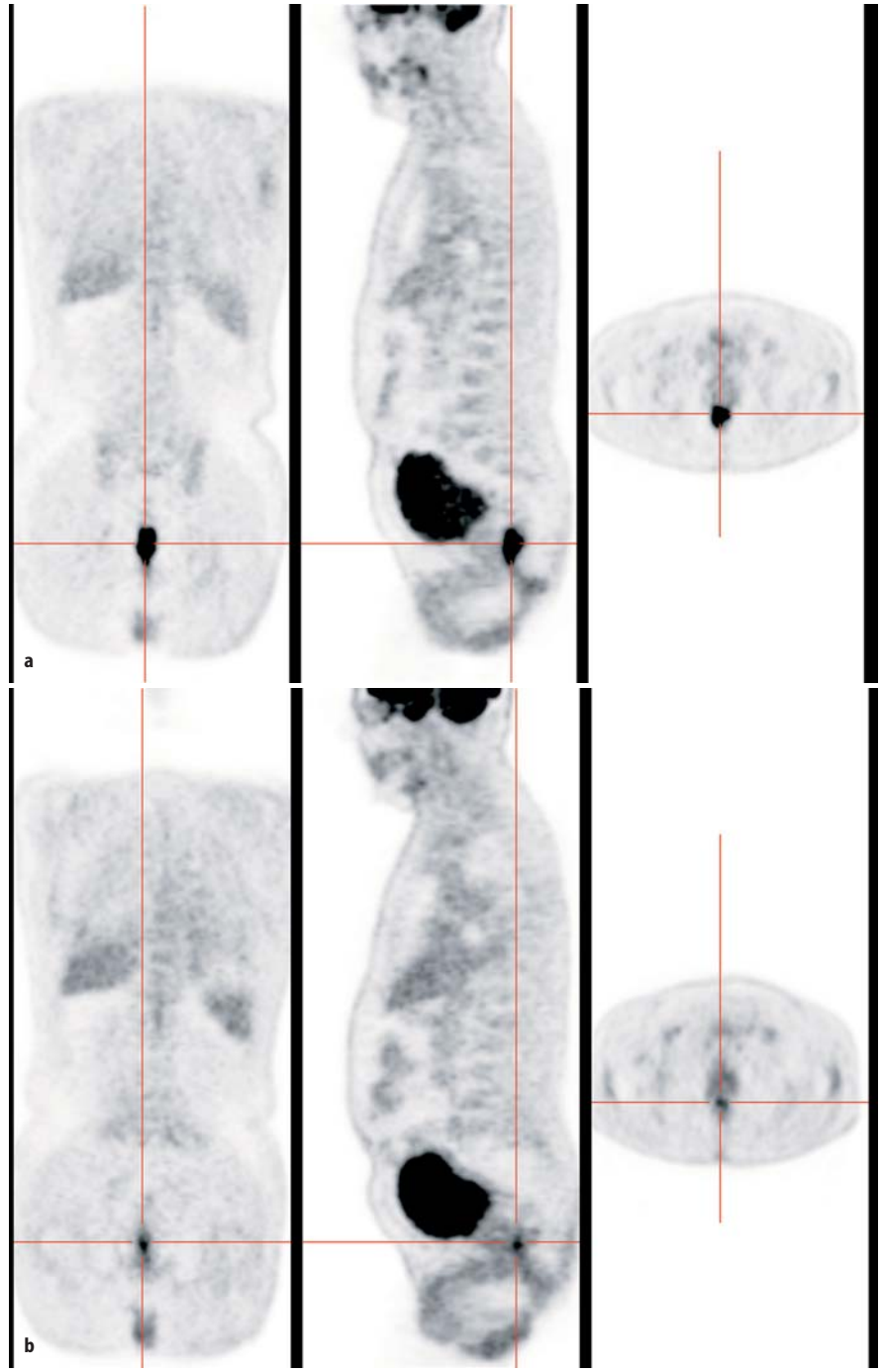

Fig. 9.12. Rectal cancer pre (**a**) and post (**b**) neoadjuvant chemotherapy. The tumor has shown an incomplete but definite response to therapy

cated in the liver and lung (Fig. 9.13). Probably the main impact of FDG PET is improved detection of occult stage IV disease. One exception may be in the brain, where MRI is superior. Small lung metastases may be better detected by CT. Sensitivity and specificity of FDG PET for distant esophageal metastases is generally high, 80–90%, respectively, compared to CT, with a sensitivity and specificity of 50–75%, respectively (Dehdashti and Siegel 2004). FDG PET imaging upstages as many as 15% of patients.

For detection of recurrences of esophageal cancer, FDG PET has a high accuracy, although it has a poor specificity for anastomotic recurrences (Table 9.9) (Flamen et al. 2000). For the detection of systemic metastases, the sensitivity is in the range of 94% compared to 81% for conventional imaging, with similar specificity

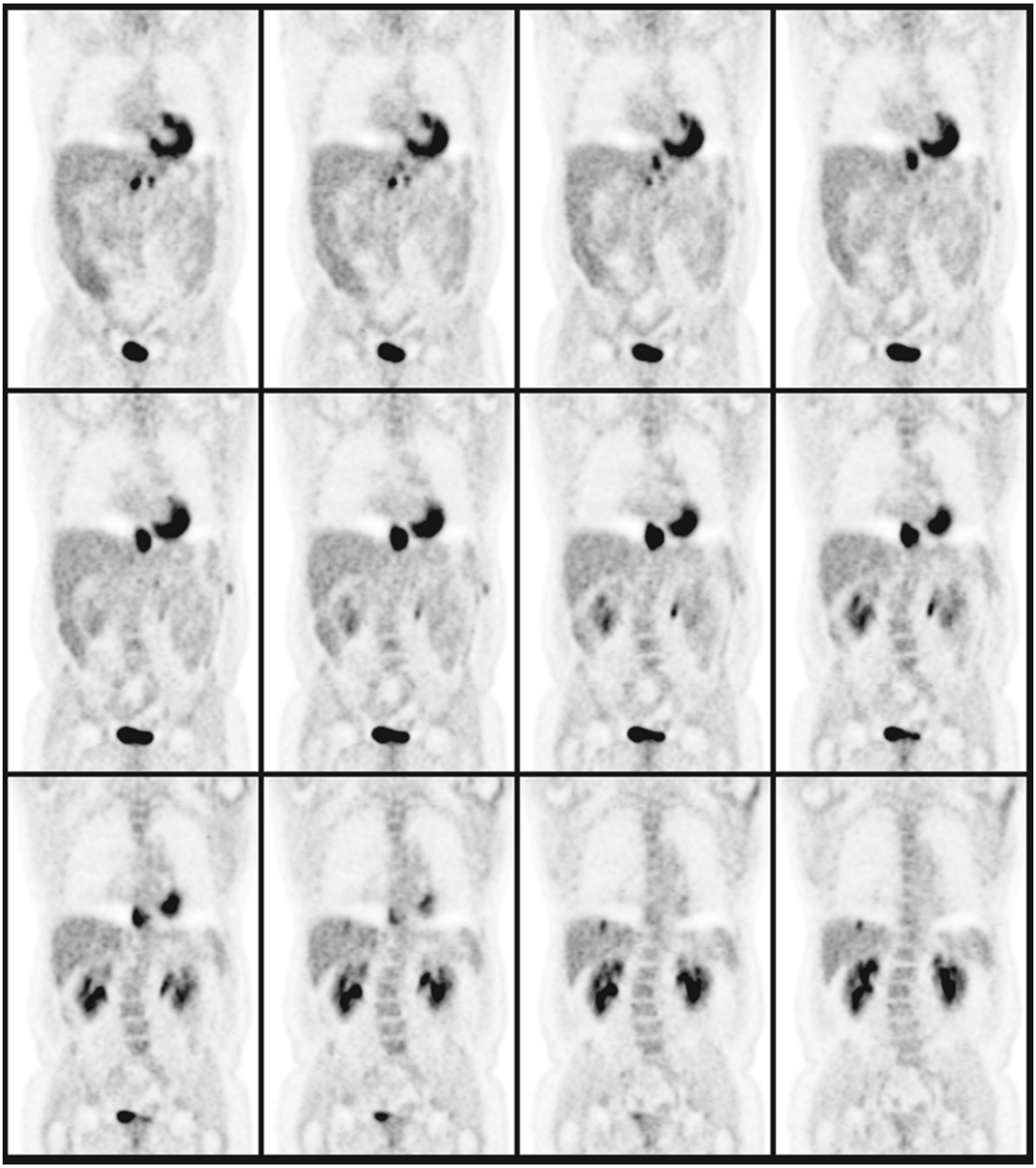

Fig. 9.13. Staging esophageal cancer with FDG PET. Newly diagnosed 62-year-old patient referred for FDG PET for staging. In addition to uptake in the primary tumor in the distal esophagus adjacent to the heart, metastases are detected in gastrohepatic and celiac nodes just below the diaphragm. A small metastasis is also seen in the right lobe of the liver

Table 9.9. Comparative accuracy of FDG PET and CT in metastatic esophageal cancer

Author	Patients	Sensitivity		Specificity		Accuracy	
		PET	CT	PET	CT	PET	CT
Luketich	100	69	46	93	94	84	63
Yueng	22	80	68	95	81	86	73

(Gambhir et al. 2001). As in all areas of PET imaging, PET CT improves the overall accuracy, for differentiating benign from malignant disease and for precise localization (Bar-Shalom et al. 2005)

FDG PET is a good indicator of prognosis and has a promising role in monitoring the effectiveness of therapy. In one study, a 35% decrease in SUV distin-

guished responders from non-responders with a sensitivity of 93 % and specificity of 95 % (Weber et al. 2001). FDG PET has been used to assess response to neoadjuvant therapy (Kato et al. 2002). Despite aggressive therapy for metastases, poor survival and common recurrence, the disease free survival time can be prolonged.

9.9.3 Pancreatic Cancer

Carcinoma of the pancreas is the third most common gastrointestinal malignancy and fourth most common of cancer related deaths in the United States. Early diagnosis and resection is curative; however, the tumor is unresectable in most patients at the time of diagnosis. Sensitivity for detection with PET is high, greater than 90 % (Delbeke et al. 2004). FDG PET has good accuracy for differentiating benign from malignant disease. However, pancreatitis can produce false positive studies and hyperglycemia, false negatives (Diederich et al. 1998).

Only anatomic imaging can demonstrate the relationships between tumor, adjacent organs, and vascular structures (T stage). Neither can FDG PET reliably detect regional metastases (N) with high sensitivity. The main role of PET in diagnosis is in the detection of liver and distant metastases (M). Overall accuracy is approximately 83 % for PET and 63 % for CT (Gambhir et al. 2001). FDG PET can alter management in almost 45 % of patients (Delbeke et al. 1999). FDG PET has been successfully used to evaluate the response to neoadjuvant therapy with initially unresectable disease.

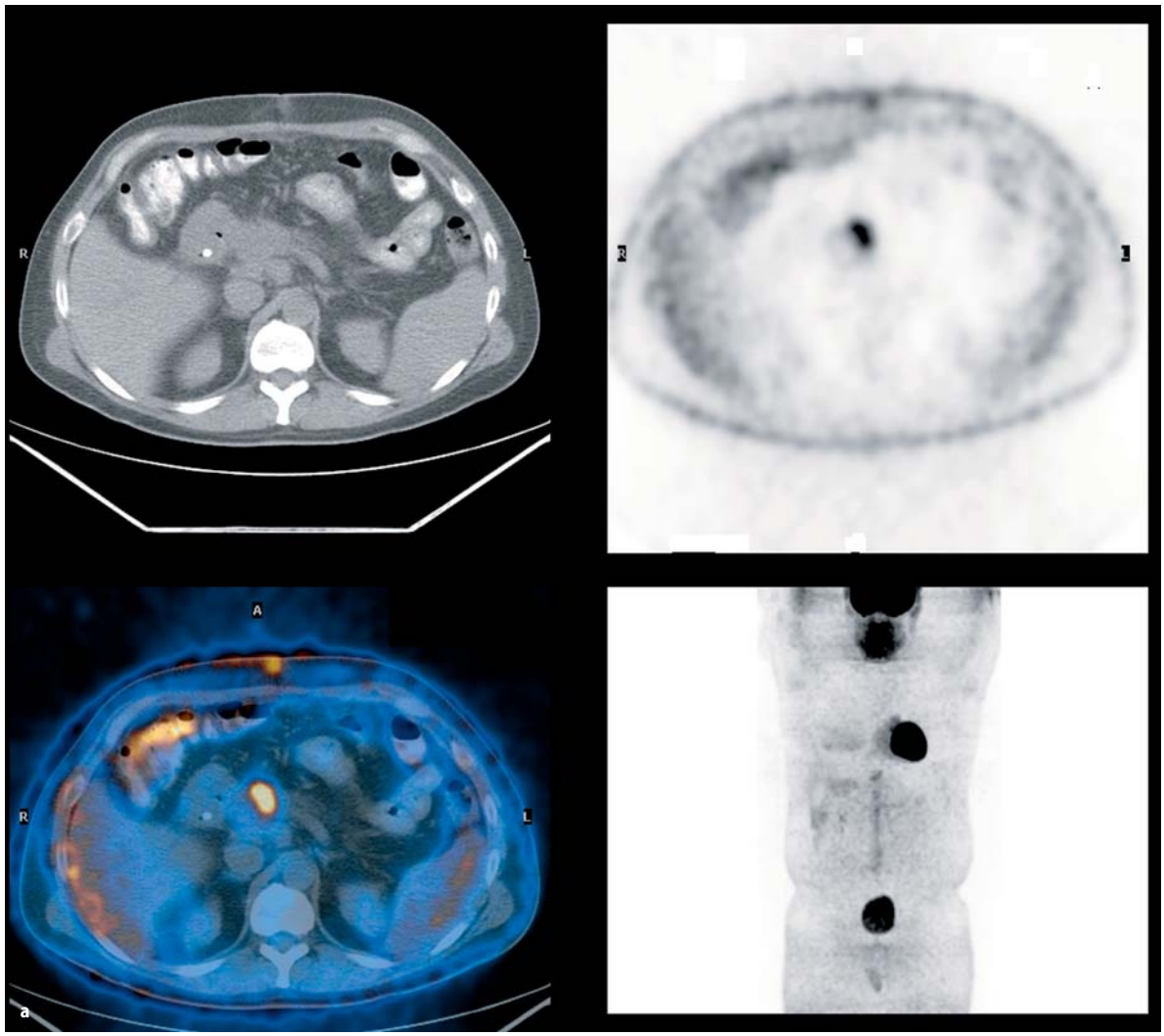

Fig. 9.14. Pancreatic cancer pre- and post-chemotherapy. Stage III unresectable adenocarcinoma of the pancreatic head and neck. **a** Pre-chemotherapy

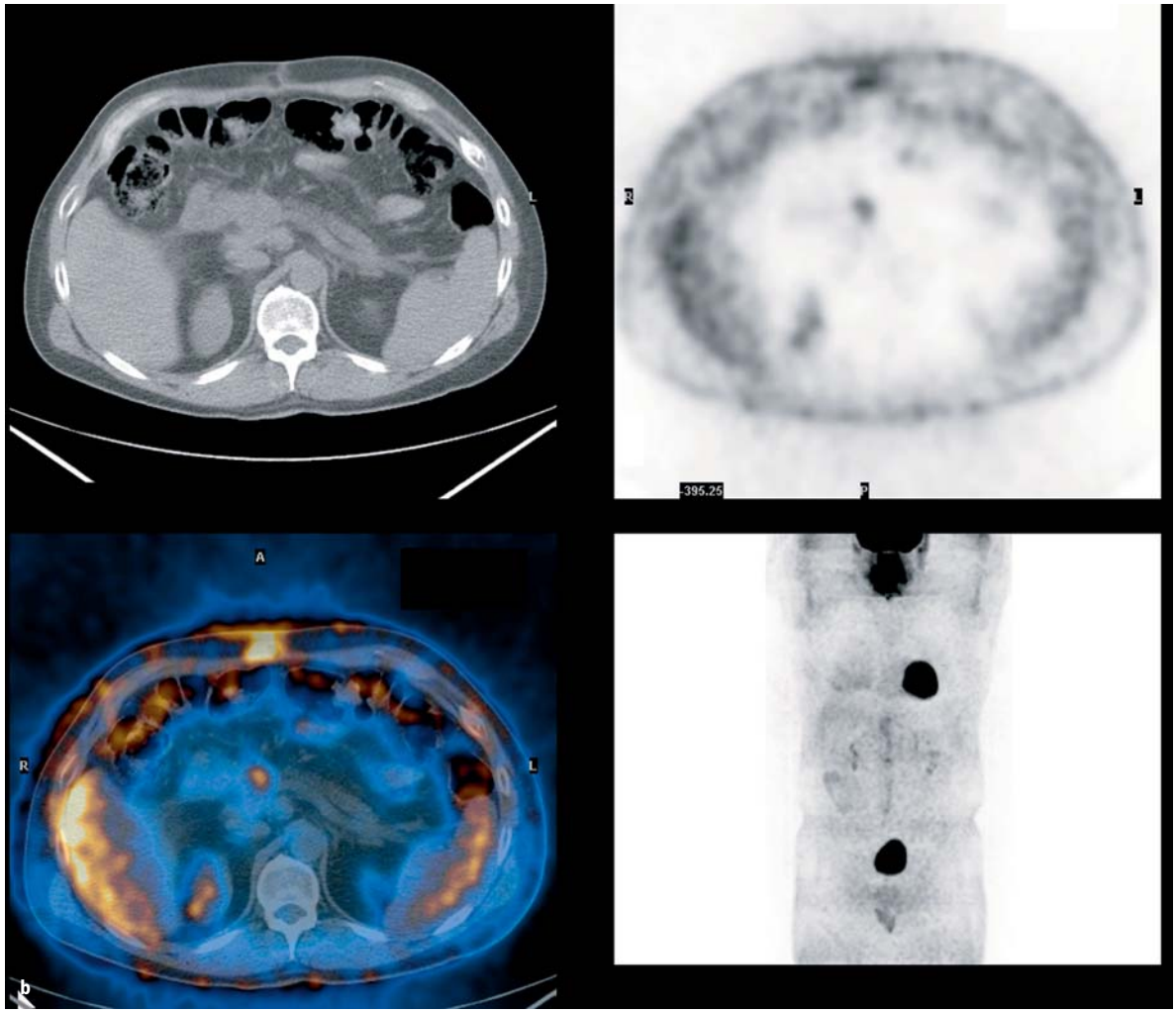

Fig. 9.14. b post-chemotherapy, 4 months later. There has been a significant decrease in CT size and amount of FDG uptake in the tumor

FDG PET detects recurrent disease better than other imaging modalities. It is useful in differentiating post-operative changes from recurrence. Its major impact is in identification of recurrent nodal or distant metastatic disease. The absence of FDG uptake 1 month following chemotherapy is an indicator of improved survival (Maisey et al. 2000). FDG PET is useful when CT identifies an uncertain region in the resected pancreatic bed difficult to differentiate from post-operative fibrosis, evaluation of new hepatic lesions, or the patient with rising serum tumor markers. Preliminary studies show that FDG PET is predictive of response to therapy and survival (Fig. 9.14).

9.9.4 Gastrointestinal Stromal Tumors

These rare mesenchymal tumors of the gastrointestinal tract represent only 0.1 – 0.3 % of all gastrointestinal tumors, 1 – 3 % of gastric neoplasms, and 20 % of small intestinal neoplasms. Seventy percent are benign and 30 % malignant. Malignant tumors tend to recur and metastasize to the liver and peritoneum, less commonly to the lungs, pleura, retroperitoneum, bone, and subcutaneous tissue. Median survival is 12 – 19 months.

Gastrointestinal stromal malignant tumors are generally resistant to chemotherapy and radiation therapy. However, most patients have a dramatic response to the tyrosine kinase inhibitor, imatinib mesylate (Gleevac, Novartis Pharmaceuticals Corp., Basel, Switzerland), with long lasting disease stability.

Both CT and FDG PET have high sensitivity and specificity for primary tumor detection, greater than 90 %. In approximately 25 % of patients, FDG PET can detect a good response to therapy earlier than CT (Antoch et al. 2004). In 5 % CT detects the response first. FDG PET correctly characterizes response to therapy at 1 month in 95 % of patients, and 100 % at 3 and 6 months.

References

Abdel-Nabi H, Doerr RJ, Lamonica DM, et al. (1998) Staging of primary colorectal carcinomas with fluorine-18 fluorodeoxyglucose whole body PET: correlation with histopathologic and CT findings. Radiology 206:775 – 760

Antoch G, Kanja J, Bauer S, et al. (2004) Comparison of PET, CT, and dual-modality PET/CT imaging for monitoring of Imatinib (STI571) therapy in patients with gastrointestinal stromal tumors. J Nucl Med 45:357 – 365

Bar-Shalom R, Guralnik L, Tsalic M, et al. (2005) The additional value of PET/CT over PET in FDG imaging of esophageal cancer. Eur J Nucl Med Mol Imag 32:918 – 924

Bombardieri E, Seregni E, Villano C, et al. (2004) Position of nuclear medicine techniques in the diagnostic workup of neuroendocrine tumors. Q J Nucl Med Mol Imaging 48: 150 – 163

Bonapace ES, Maurer AH, Davidoff S, et al. (2000) Whole gut transit scintigraphy in the clinical evaluation of patients with upper and lower gastrointestinal symptoms. Am J Gastroenterol 95:2838 – 2847

Bunker SR, Lull RJ, Tanasescu DE, et al. (1984) Scintigraphy of gastrointestinal hemorrhage: superiority of 99mTc red blood cells over 99mTc sulfur colloid. AJR 143:543 – 548

Camilleri M, Hasler W, Parkman HP, et al. (1998) Measurement of gastrointestinal motility in the GI laboratory. Gastroenterology 115:747 – 762

Cohade C, Osman M, Leal J, et al. (2003) Direct comparison of 18F-FDG PET and PET/CT in patients with colorectal carcinoma. J Nucl Med 44:1797 – 1803

Dehdashti F, Siegel BA (2004) Neoplasms of the esophagus and stomach. Semin Nucl Med 34:198 – 208

Delbeke D, Martin WH (2004) PET and PET-CT for evaluation of colorectal carcinoma. Semin Nucl Med 34:209 – 223

Delbeke D, Pinson CW (2004) Pancreatic tumors: role of imaging in the diagnosis, staging, and treatment. J Hepatobil Pancreat Surg 11:4 – 10

Delbeke D, Vitola J, Sandler MP, et al. (1997) Staging recurrent metastatic colorectal carcinoma with PET. J Nucl Med 38:1196 – 1201

Delbeke D, Chapman WC, Pinson CW, et al. (1999) F-18 fluorodeoxyglucose imaging with positron emission tomography has a significant impact on diagnosis and management of pancreatic ductal adenocarcinoma. J Nucl Med 40:1784 – 1792

Diederich CG, Staib L, Glatting G, et al. (1998) FDG PET: Elevated plasma glucose reduces both uptake and detection rate of pancreatic malignancies. J Nucl Med 39:1030 – 1033

Diamond RH, Rothstein RD, Alavi A (1991) The role of cimetidine enhanced Tc-99m pertechnetate imaging for visualizing Meckel's diverticulum. J Nucl Med 32:1422 – 1424

Emanian SA, Shalaby-Rana E, Majd M (2001) The spectrum of heterotopic gastric mucosa in children detected by Tc-99m pertechnetate scintigraphy. Clin Nucl Med 26:529 – 535

Fahey FH, Ziessman HA, Collin MJ, et al. (1989) Left anterior oblique projection and peak-to-scatter ratio for attenuation compensation of gastric emptying studies. J Nucl Med 30: 233 – 239

Flamen P, Lerut A, Van Cutsem E, et al. (2000) The utility of positron emission tomography for the diagnosis and staging of recurrent esophageal cancer. J Thorac Cardiovasc Surg 120:1085 – 1092

Flanagan FL, Dehdashti F, Ogunbiyi OA, et al. (1998) Utility of FDG-PET for investigating unexplained plasma CEA elevation in patients with colorectal cancer. Ann Surg 227:319 – 323

Gambhir S, Czernin J, Schwimmer J, et al. (2001) A tabulated summary of the FDG PET literature. J Nucl Med 42:S1 – 39

Heyman S, Respondek M (1989) Detection of pulmonary aspiration in children by radionuclide "salivagram". J Nucl Med 30:697 – 699

Huebner RH, Park KC, Shepherd JE, et al. (2000) A meta-analysis of the literature for whole body FDG PET detection of colorectal cancer. J Nucl Med 41:1177 – 1189

Ito K, Kato T, Tadakoro M, et al. (1992) Recurrent rectal cancer and scar: differentiation with PET and MR imaging. Radiology 182:549 – 452

Kato H, Kuwano H, Nakajima M, et al. (2002) Usefulness of positron emission tomography for assessing the response of neoadjuvant chemoradiotherapy in patients with esophageal cancer. Am J Surg 184:279 – 283

Kim J-H, Czernin J, Allen-Auerbach MS, et al. (2005) Comparison between 18F-FDG PET, in-line PET/CT, and software fusion for restaging of recurrent colorectal cancer. J Nucl Med 46:587 – 595

Krausz Y, Keidar Z, Kogan I, et al. (2003) SPECT/CT hybrid imaging with 111In-pentetreotide in assessment of neuroendocrine tumors. Clin Endocrinol 59:565 – 573

Krenning EP, Kwekkeboom DJ, Bakker WH, et al. (1993) Somatostatin receptor scintigraphy with [111In-DTPA-d-Phe] and [123I-Tyr3]-octreotide: the Rotterdam experience with more than 1000 patients. Eur J Nucl Med 20:716 – 731

Lebtahi R, Cadiot G, Sarda L, et al. (1997) Clinical impact of somatostatin receptor scintigraphy in the management of patients with neuroendocrine gastroenteropancreatic tumors. J Nucl Med 38:853 – 858

Maisey NR, Webb A, Flux GD, et al. (2000) FDG-PET in the prediction of survival of patients with cancer of the pancreas: a pilot study. Br J Cancer 83:287 – 293

Mariani G, Boni G, Barreca M, et al. (2004) Radionuclide gastroesophageal motor studies. J Nucl Med 45:1004 – 1028

Maurer AH, Kevsky B (1995) Whole gut transit scintigraphy in the evaluation of small bowel and colon transit disorders. Semin Nucl Med 25:326 – 338

Maurer AH, Rodman MS, Vitti RA, et. al. (1992) Gastrointestinal bleeding: improved localization with cine scintigraphy. Radiology 185:187 – 192

McKusick KA, Froelich J, Callahan RJ, et al. (1981) 99mTc red blood cells for detection of gastrointestinal bleeding: experience with 80 patients. AJR Am J Roentgenol 137:1113 – 1118

Orenstein SR, Klein HA, Rosenthal MS (1993) Scintigraphy versus pH probe for quantification of pediatric gastroesophageal reflux: A study using concurrent multiplexed data and acid feedings. J Nucl Med 34:1228 – 1234

Parkman HP, Maurer AH, Caroline DF, et al. (1996) Optimal evaluation of patients with nonobstructive esophageal dysphagia manometry, scintigraphy, or videoesophagography. Dig Dis Sci 41:1355 – 1368

Sfankianakis GN, Haas GM (1982) Abdominal scintigraphy for ectopic gastric mucosa: a retrospective analysis of 143 studies. AJR Am J Roentgenol 138:7 – 12

Shay SS, Eggli D, Johnson L, et al. (1991) Simultaneous esophageal pH monitoring and scintigraphy during the postprandial period in patients with severe reflux esophagitis. Dig Dis Sci 36:558 – 564

Tatsch K, Voderholzer W, Weiss MJ, et al. (1996) Reappraisal of quantitative esophageal scintigraphy by optimizing results with ROC analyses. J Nucl Med 1799 – 1905

Thorne DA, Datz FL, Remley K, Christian PE (1987) Bleeding rates necessary for detecting acute gastrointestinal bleeding with technetium-99m labeled red blood cells in an experimental model. J Nucl Med 28:514 – 520

Tougas G, Eaker EY, Abell TL, et al. (2000) Assessment of gastric emptying using a low fat meal: establishment of international control values. Am J Gastroenterol 95:1456 – 1462

Valk PE, Abella-Columna E, Haseman MK, et al. (1999) Whole-

body PET imaging with 18F fluorodeoxyglucose in management of recurrent colorectal cancer. Arch Surg 134:503 – 511
Weber WA, Ott K, Becker K, et al. (2001) Prediction of response to preoperative chemotherapy in adenocarcinomas of esophagogastric junction by metabolic imaging. J Clin Onc 19:3058 – 3065
Whiteford MH, Whiteford HM, Yee LF, et al. (2000) Usefulness of FDG-PET scan in the assessment of suspected metastatic or recurrent adenocarcinoma of the colon and rectum. Dis Colon Rectum 43:759 – 767
Wiering B, Krabbe PFM, Jager GJ, et al. (2005) The impact of fluor-18-deoxyglucose-positron emission tomography in the management of colorectal liver metastases. A systematic review and metaanalysis. Cancer 104:2658 – 70
Ziessman HA, Atkins FB, Vermulakonda US, et al. (1996) Lag phase quantification for solid gastric emptying studies. J Nucl Med 37:1639 – 1643
Ziessman HA, Atkins FB, Vemalakonda US, et al. (1996) Lag phase quantification for solid gastric emptying studies. J Nucl Med 37:1639 – 1643
Ziessman HA, Fahey FH, Atkins FB, Tall J (2004) Standardization and quantification of radionuclide solid gastric emptying studies. J Nucl Med 45:760 – 764
Ziessman Ha, Goetze S, Bonta D, Ravich W (2007) Experience with a new standardized 4-hr gastric emptying protocol. J Nucl Med 48:568 – 572

Musculoskeletal System

10

G. Gnanasegaran, G. Cook, I. Fogelman

10.1 Introduction

Bone scintigraphy is used as a common screening test for suspected bone metastases because of its high sensitivity, availability, low cost, and ability to scan the entire skeleton. Historical data and clinical experience has established bone scintigraphy as the reference standard in the search for skeletal metastatic disease and many indications have become established for benign skeletal disorders (Table 10.1). Chiewitz and Hevesy first described the use of radionuclides to study the skeleton in 1935 where phosphorus-32 (^{32}P) activity was measured in rat organs with a Geiger-Müller counter and where uptake of ^{32}P from blood to bone was noted, suggesting that skeletal metabolism is a dynamic process. Fleming and colleagues produced the first radionuclide skeletal images in 1961 using ^{85}Sr (Fleming et al. 1961) and this radioisotope was commonly used for bone scanning and the study of skeletal kinetics. Although ^{87m}Sr was introduced as an alternative bone scanning agent with a more suitable gamma ray for imaging of 388 keV and half-life of 2.8 h, the introduction of ^{18}F-fluoride and then ^{99m}Tc labelled compounds superseded this. In 1971, Subramanian and McAfee successfully prepared technetium-99m-polyphosphates. However, it was later found that the bone localising properties were due to pyrophosphate (Subramanian and McAfee 1971; Davis and Jones 1976). Since then there have been many developments in both radiopharmaceuticals and scanning techniques to aid evaluation of metastatic bone disease. In recent years technetium-99m (^{99m}Tc) labelled diphosphonates have become the most widely used radiopharmaceuticals, particularly ^{99m}Tc-methylene diphosphonate (MDP). Improvements in gamma camera design, including the increased availability of tomographic scintigraphy [single photon emission computed tomography (SPECT)], have also helped nuclear medicine techniques which provide functional information and maintain their clinical utility in spite of the major advances in cross-sectional anatomical imaging techniques such as computed tomography (CT) and magnetic resonance imaging (MRI). In recent years there has been increasing interest in the use of positron emission tomography (PET) tracers in the investigation of various aspects of skeletal disease but especially in the diagnosis of bone metastases.

The positron emitting ion, ^{18}F-fluoride, was first described as a scanning agent in 1962 by Blau. Its rapid blood clearance, high skeletal uptake and convenient half-life (~110 min) showed advantages over previous scanning agents. The 511 keV annihilation photons are not ideal for conventional gamma cameras, which are optimised for ^{99m}Tc (140 keV), and although the use of ^{99m}Tc bone seeking agents has taken over in the last two decades, ^{18}F-fluoride was an important bone-scanning agent in the early days of clinical nuclear medicine. Recently both ^{18}F-fluorodeoxyglucose (^{18}FDG), as a tumour specific tracer, and ^{18}F-fluoride ion, as a non-specific bone tracer, have been assessed and early results

Table 10.1. General clinical application of bone scintigraphy

Investigation of bone pain
Metastatic tumour
Benign bone tumour
Trauma
Avascular necrosis
Infection
Osteomalacia
Paget's disease
Investigation of malignancy
Initial staging
Discordant scan/X-ray findings
Assessment of extent of disease
Monitoring progress of disease
Assessment of response to therapy
Hypertrophic pulmonary osteoarthropathy
Primary bone tumours
Investigation of benign bone disease
Orthopedic disorders
Sports/exercise related injuries
Metabolic bone disease – Paget's disease, hyperparathyroidism
Infection
Benign bone tumours
Degenerative disease
Miscellaneous
Vascular abnormalities
Abnormalities of the renal and urinary tract
Soft tissue accumulation of diphosphonate

suggest that both agents may have a role to play in the clinical management of patients.

10.2 Radiopharmaceuticals and Mechanisms of Uptake

Initially ^{99m}Tc-polyphosphates and -pyrophosphates were employed but subsequently diphosphonates such as hydroxyethylidene diphosphonate (HEDP) and methylene diphosphonate (MDP) were introduced (Subramanian and McAfee 1971; Subramanian et al. 1972). Uptake of diphosphonates depends on local blood flow, osteoblastic activity and extraction efficiency. The actual mechanism of uptake is still not fully understood but diphosphonates are probably incorporated into the hydroxyapatite crystal on the bone surface. ^{99m}Tc-MDP is the most widely used bone agent, giving optimal contrast between normal and diseased bone but similar, alternative ^{99m}Tc-diphosphonate tracers exist (Fogelman 1982). Excretion of ^{99m}Tc-MDP is primarily renal and 70 % of the administered dose is eliminated by 6 h.

Other single photon radiopharmaceuticals have been used in the assessment of both primary and metastatic bone tumours and are most commonly non-specific tumour agents rather than acting as bone tracers (Elgazzar et al. 1989; Caner et al. 1992). Thallium-201 (^{201}Tl), an analogue of potassium, enters tumour cells via the Na^+/K^+ ATPase pump, but as well as reflecting the metabolic status of the cell, uptake also depends on blood flow. ^{99m}Tc labelled sestamibi (^{99m}Tc-MIBI) shows a similar distribution to ^{201}Tl but has a different mechanism of accumulation and is thought to reflect cell viability being mainly associated with mitochondria intracellularly. ^{99m}Tc-pentavalent dimercaptosuccinic acid [^{99m}Tc(V) DMSA] uptake has also been described in bone metastases, the exact mechanism of uptake being uncertain (Lam et al. 1997). However, compared to the diphosphonates and tumour-specific tracers, these are rarely used in clinical practice to specifically evaluate the skeleton.

Positron emission tomography tracers that are currently available and have potential roles for assessing skeletal metastases include ^{18}F-fluoride ion and fluorine-18 labelled deoxyglucose (^{18}FDG). The mechanism of uptake of ^{18}F-fluoride is similar to other bone tracers used in nuclear medicine and depends on both regional blood flow and osteoblastic activity. It is preferentially deposited at sites of high bone turnover and remodelling by chemisorption onto bone surfaces, exchanging with hydroxyl groups in hydroxyapatite crystal of bone to form fluoroapatite (Blau et al. 1972).

As tumour uptake of ^{18}FDG depends on glycolysis and membrane glucose transporters, both of which are known to be increased in malignant tissue (Warburg 1954; Yamamoto et al. 1990), the mechanism of uptake and hence the information available from this tracer in the skeleton are significantly different to ^{18}F-fluoride. The uptake of ^{18}FDG is relatively tumour specific but obviously not restricted to tumour involving the skeleton and has the advantage of demonstrating all metastatic sites in a cancer patient, whether they are in soft tissue or bone.

In addition to non-specific skeletal tracers there are a number of radiopharmaceuticals, which exist for specific types, or groups, of tumours and which in addition to evaluating soft tissue metastases can be helpful in assessing the skeleton. Examples include iodine-131 (^{131}I) for differentiated thyroid cancer metastases, ^{123}I- or ^{131}I-metaiodobenzylguanidine (mIBG) and ^{111}In-pentetreotide for neuroendocrine tumours.

10.3 Scintigraphy Techniques

In practice bone scans with diphosphonates are obtained between 2 and 4 h after injection (and with ^{18}F-fluoride at 1 – 2 h), but if renal function is significantly impaired (without concomitant renal osteodystrophy and associated skeletal remodelling) then scans may be performed at a later time to allow further clearance of ECF and vascular activity.

Although in the past, many ^{99m}Tc-MDP bone scans have been acquired as multiple overlapping spot views of the skeleton, modern dual-headed gamma cameras allow high resolution, whole-body images of the entire skeleton in a short acquisition time, including both anterior and posterior images. Most modern gamma camera systems also have the ability to acquire additional SPECT images, allowing an increased sensitivity for lesion detection because of the resultant improvement in contrast compared to planar imaging and a better three-dimensional localisation of abnormalities, which aids specificity. It has been suggested that SPECT imaging not only increases sensitivity in the detection of vertebral metastases in cancer patients but by being able to examine the pattern and position of lesions tomographically that it may be possible to improve differentiation between metastases and coincidental benign lesion (Bushnell et al. 1995; Han et al. 1998). A 3-phase bone scan is primarily used to evaluate patients with suspected bone infections. Phase 1 involves intravenous (IV) injection of a radiolabelled tracer and short sequential imaging of the blood flow at the region of concern or interest. In the second phase (2 – 5 min post-injection), an image of the blood pool is obtained followed by the third phase, which includes delayed skeletal images 3 or 4 h later of the specific area.

PET imaging depends on the detection of two coincident 511 keV gamma rays, which are emitted at 180° from one another following the annihilation of a positron (a positively charged, anti-matter equivalent of an electron from an unstable nucleus). The synchronous detection of the two photons allows accurate placement of the point of emission and with standard image reconstruction algorithms, tomographic images can be acquired and displayed. There are a number of advantages over conventional nuclear medicine techniques. PET shows higher spatial resolution and accurate, absolute quantitation, the latter because of the ability to accurately correct for the effects of attenuation of photons within the body. The dual-imaging modality PET/CT is a relatively new investigation method that has not been extensively studied in the context of the skeleton.

10.4 Scintigraphic Patterns, Variants and Artifacts

A normal bone scan will show higher activity concentration in the parts of the skeleton predominated by trabecular bone, e.g. spine, compared to the shafts of long bones that are predominantly cortical bone. Urinary bladder activity, renal activity, and minimal soft-tissue activity are also normally present (Fig. 10.1). To obtain optimum contrast in all areas of the skeleton, this variation in activity may necessitate viewing images at different intensity settings to optimise contrast at different skeletal sites. Although uptake of labelled diphosphonate on a bone scan is not specific for metastases, by studying the pattern and distribution of lesions it is often possible to infer the aetiology of abnormalities without requiring further correlative imaging, although a number of cases will remain problematic.

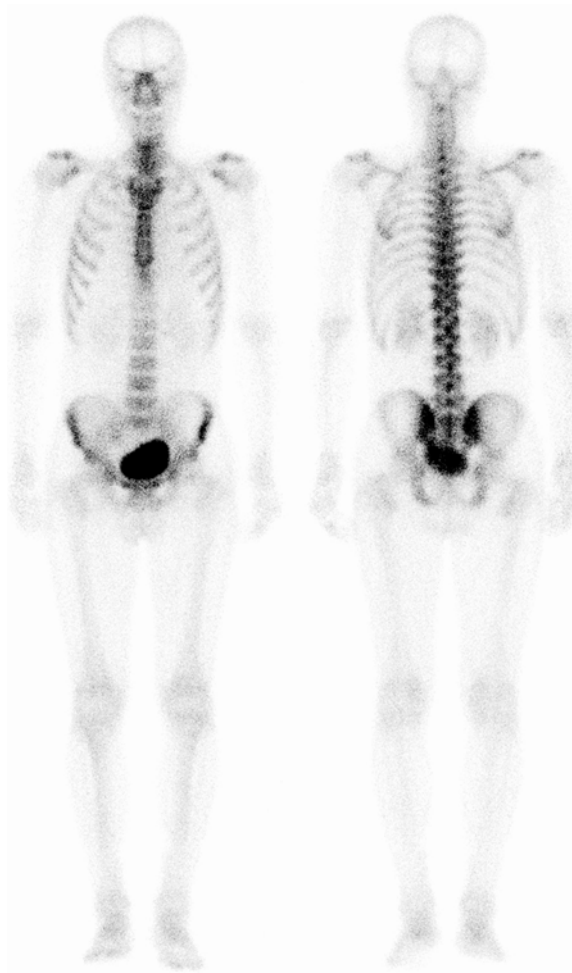

Fig. 10.1. Normal scan: whole body bone scan showing symmetrical distribution of tracer throughout the skeleton. Urinary bladder activity and renal activity is also normally observed

The majority of bone metastases are distributed irregularly in the axial skeleton and ribs and there is seldom any confusion in this situation. A small proportion (< 10 %) affect the appendicular skeleton and this is most commonly seen in clinical practice in carcinoma of the lung, prostate and breast (Tofe et al. 1975). An unexpected finding from scanning the peripheries, particularly in patients with bronchogenic carcinoma, may be the observation of hypertrophic pulmonary osteoarthropathy (HPOA) (Fig. 10.2). This typically appears as symmetrical increased uptake of tracer in the cortices ("tram lines"), generally seen in the femora and tibiae.

Rarely, when bone metastases are very extensive, a bone scan on first inspection may appear normal due to the confluent nature of the lesions. However, the "superscan", so called because of the apparent good quality of the scan due to diffusely increased skeletal uptake, has a number of distinguishing features (Fig. 10.3). In addition to the apparent high quality of the scan, the soft tissues, particularly the kidneys, may be inconspicuous or invisible due to the increased ratio between skeletal and soft tissue accumulation. Metabolic bone diseases may also cause a superscan but that caused by malignancy may be differentiated on close inspection where some irregularity of uptake and indeed more focal abnormality is usually visible. This is more apparent in the ribs or the ends of the long bones.

To increase the specificity of bone scan interpretation it is necessary to have a knowledge of normal variants which may mimic metastases and of other skeletal disorders which may cause confusion. One example is of increased tracer accumulation at the manubriosternal junction. This is a relatively common normal variant but may cause difficulty in patients with carcinoma of the breast, as the sternum is a common site for early metastatic disease. Clues that a lesion at this site is not

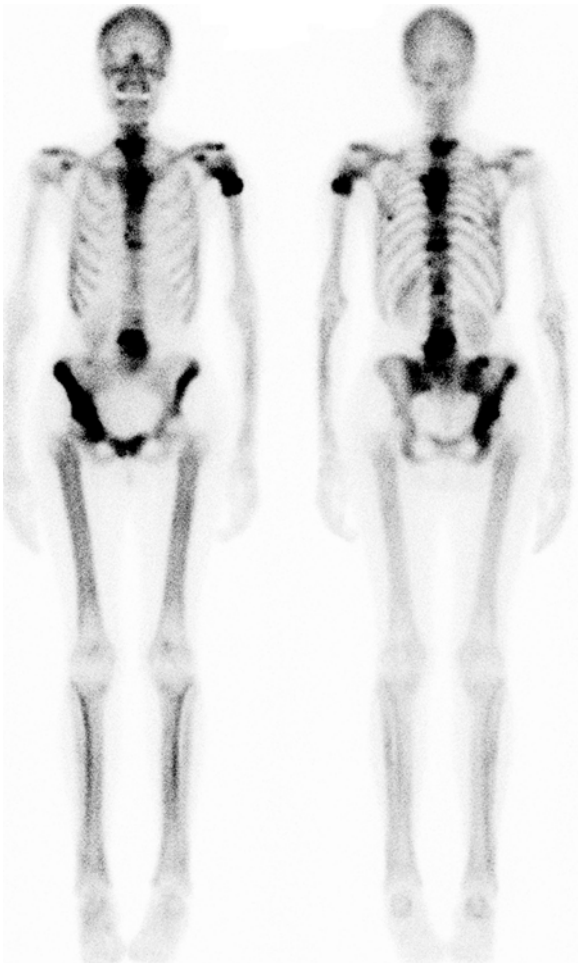

Fig. 10.2. Hypertrophic pulmonary osteoarthropathy (HPOA): characteristic pericortical uptake involving the long bones of the lower limbs. Multiple foci of abnormal accumulation are demonstrated in the proximal left humerus, multiple vertebrae, ribs and right hemi-pelvis, characteristic of multiple metastases from underlying lung cancer

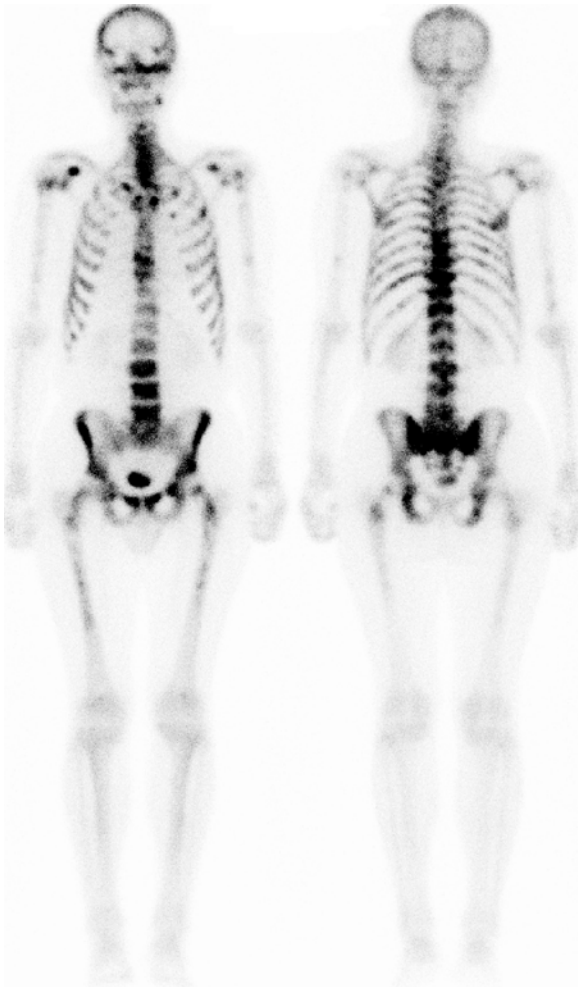

Fig. 10.3. Superscan of malignancy: disseminated metastatic involvement from underlying breast cancer, showing diffuse involvement of multiple ribs and spine, with some patchy uptake in the femora. The kidneys are not visualised. The scan pattern is consistent with 'superscan' of malignancy

benign are asymmetry and/or lack of linearity. When doubtful or if there are local symptoms or signs then further imaging may be required. The sternum is often difficult to adequately visualise with radiography and localised CT or MRI are often more helpful in this circumstance.

Other variants, which should be recognised, include activity at the confluence of sutures at the pterion in the skull, the deltoid muscle insertion on the humerus and symmetrical muscle insertion in the posterior ribs of paraspinal muscles causing a stippled appearance. On occasion the tip of the scapula overlying a rib may mimic a focal abnormality. It is useful to take an extra view with the arms raised, thereby moving the tip of the scapula outside the line of the ribs. Bladder and renal collecting system activity is usually appreciated even if patients void prior to scanning.

The appearance of a lesion may aid interpretation. A single focal rib lesion is often the result of trauma, which may not even be recalled by the patient, but a lesion extending along the length of a rib is usually malignant in nature. However, Baxter et al. (1995) have suggested that a single rib hot spot in a patient with a known malignancy may turn out to have a malignant aetiology in a surprisingly large number of patients (41 %). Even focal abnormalities at the anterior ends of ribs, a position where abnormalities are often considered to be benign in the majority of cases, showed a large number of confirmed metastases (36 %). However, these findings differ from those previously reported by Tumeh et al. in a similar retrospective study, where only 10 % of solitary rib lesions proved to be malignant (Tumeh et al. 1985) and indeed seems a gross overesti-

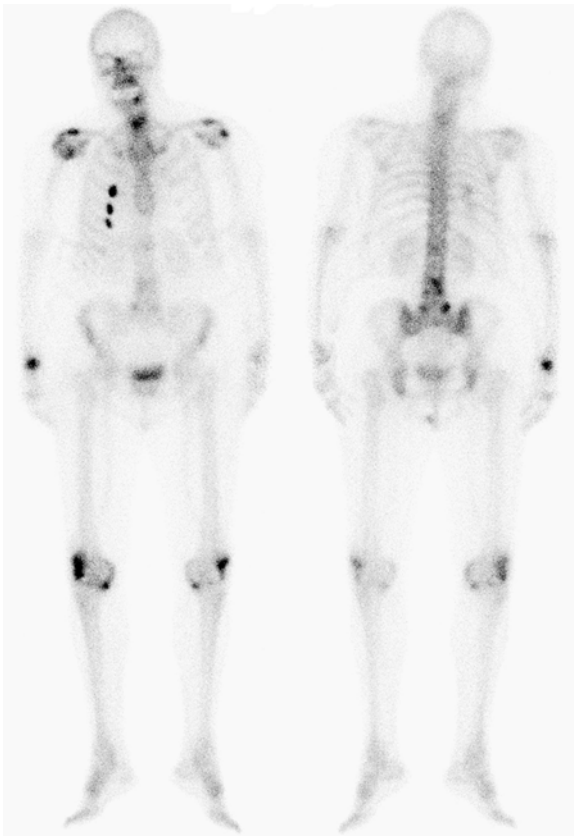

Fig. 10.4. Rib fractures: the whole body bone scan shows intense uptake in the right three to five ribs anteriorly typical for rib fractures. Elsewhere there are degenerative changes

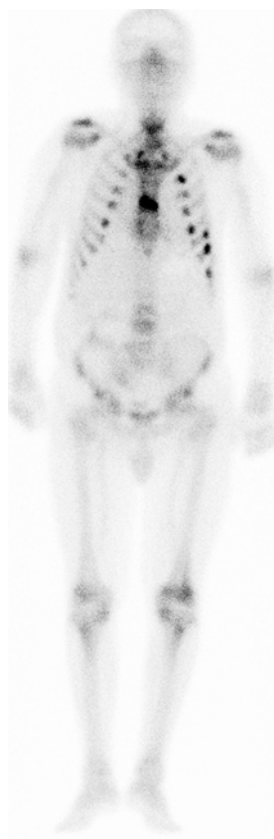

Fig. 10.5. Traumatic fracture: whole body bone scan shows increased uptake involving multiple ribs bilaterally and linear intense uptake in the body of the sternum in a patient who received CPR following a cardiac arrest

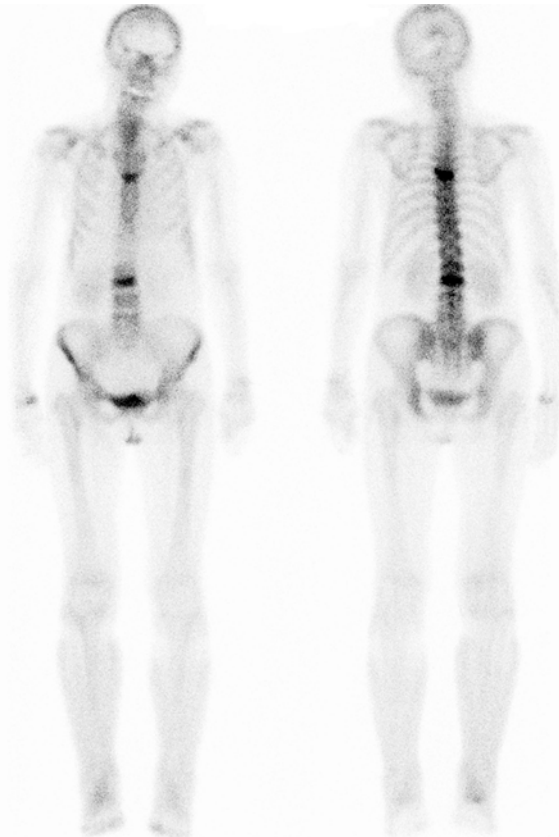

Fig. 10.6. Compression fractures/collapse: whole body bone scan of an elderly male showing linear intense uptake in the T7 thoracic and L3 vertebrae with loss of vertebral contour. The scan appearances are compatible with vertebral fracture/collapse, which is likely to be benign. However, in patients with known malignancy pathological fracture cannot absolutely be excluded

mate based on our personal experience. A linear array of rib lesions in adjacent ribs remains a situation where one may be confident of a traumatic aetiology (Figs. 10.4, 10.5).

The interpretation of hot spots, whether solitary or multiple, may be especially problematic in the spine as there is a high prevalence of benign abnormalities such as degenerative disease, which may be indistinguishable without further investigation. In the scenario of a single spinal hot spot in patients with a known primary tumour, Coakley et al. (1995) found that just over one-half (57 %) turned out to be benign on subsequent clinical and imaging follow-up.

Vertebral body fractures have a characteristic appearance on bone scintigraphy showing a linear pattern of increased tracer accumulation. However, it is not possible to differentiate fractures due to benign diseases such as osteoporosis from malignant collapse (Fig. 10.6). MRI is probably the best current method for differentiating benign from malignant causes. A follow-up bone scan after a few months that shows reducing activity at a vertebral fracture site suggests a benign cause.

10.5 Clinical Application of Bone Scans in Specific Cancers

10.5.1 Breast Cancer

The skeleton is the most common distant site to which breast cancer spreads, 8% of patients being affected, rising to between 50% and 85% in those with advanced disease (Coleman and Rubens 1987; Galasko 1986). The majority of bone metastases from breast cancer are either lytic or of a mixed pattern with a smaller proportion being purely sclerotic (Fig. 10.7). Bone scintigraphy is very sensitive with a false negative rate of 2% (Coleman et al. 1988a). However, some controversy has existed as to the precise role of bone scanning in patients at different stages of disease and the use of bone scintigraphy still varies between institutions. The positive bone scan is a poor prognostic factor (McKillop et al. 1978). The median survival of patients with bone metastases is only 24 months (Coleman et al. 1987). In breast cancer, the role of bone scintigraphy has been evaluated in the initial staging, routine/symptomatic follow-up and evaluation of effectiveness of treatment (Bitran et al. 1980; Coleman et al. 1988b) (Fig. 10.8).

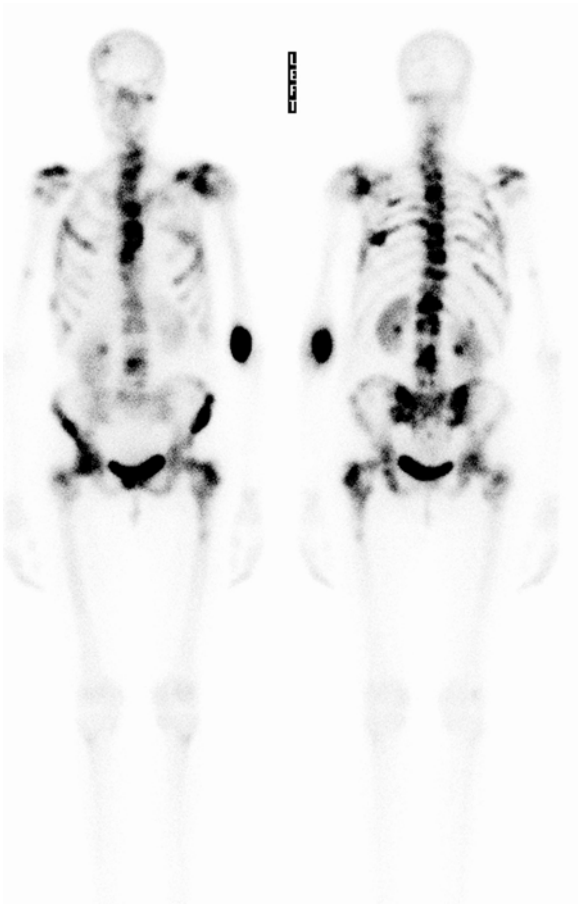

Fig. 10.7. Breast cancer metastases: whole body bone scan showing disseminated metastatic involvement of skeleton involving skull, multiple ribs bilaterally, multiple vertebrae, pelvis and long bones

10.5.2 Prostate Cancer

Prostate cancer is one of the commonest cancers in men and 85% of patients dying from this cancer have bone metastases (Narayan 1995). Knowledge of the presence of bone metastases has a huge impact on the treatment of prostate cancer. The majority of bone metastases are osteoblastic and appear sclerotic on X-ray. Because of the osteoblastic nature of the majority of prostate metastases, the bone scan is exquisitely sensitive. Prostate cancer most commonly involves well vascularised areas of the skeleton such as the vertebral col-

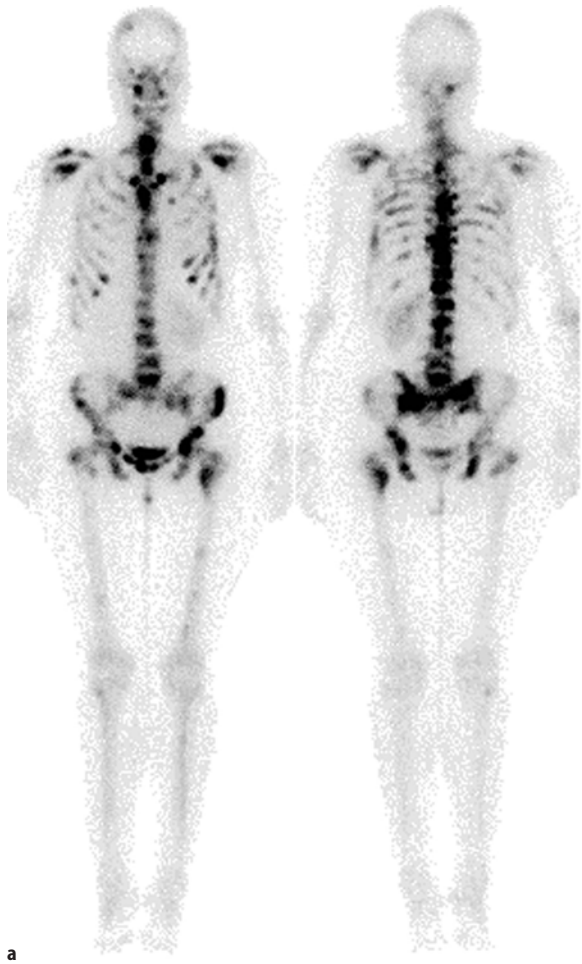

a

Fig. 10.8. Disease regression: **a** disseminated metastatic disease from cancer involving multiple ribs, spine, sacroiliac joints, femora and **b** 18 months later shows significant improvement with resolution of lesions in the spine, pelvis and ribs following treatment

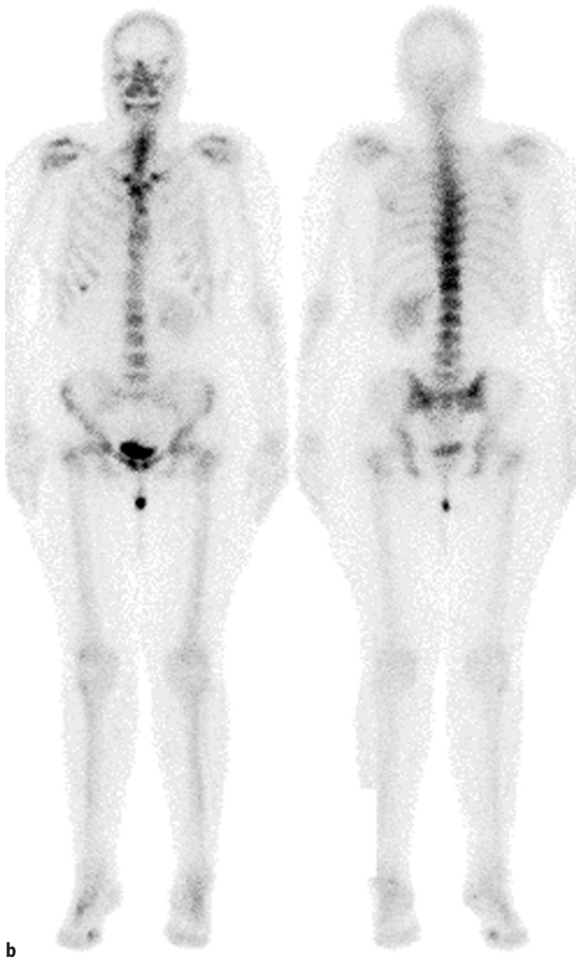

b

Fig. 10.8. (*Cont.*)

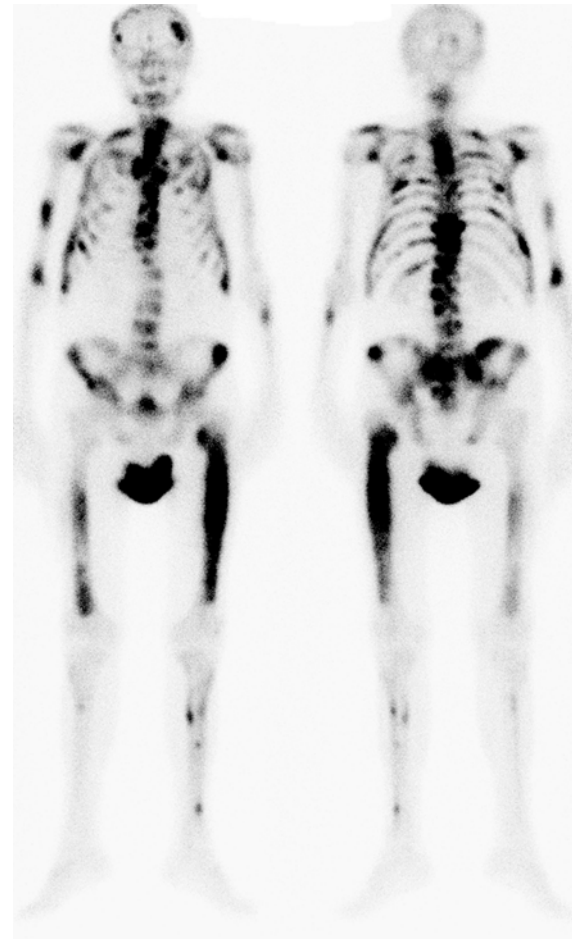

Fig. 10.9. Prostate cancer: disseminated metastatic involvement of the skull, multiple ribs, vertebrae, humeri, femora, left tibia, sacroiliac joints and pelvis

umn, pelvis, skull, and long bones (Fig. 10.9). Debate exists with regard to the mechanism of spread. Some authors suggest that the low-pressure Batson's venous plexus is involved while others dispute this (Dearnaley 1994; Batson 1942). Metastatic carcinoma of the prostate is one of the commonest causes of a malignant superscan seen in bone scintigraphy. As with breast cancer, the areas where bone scintigraphy has been evaluated include initial staging, both routine and symptomatic follow-up and the evaluation of the effectiveness of treatment (Fig. 10.10). There has been ongoing debate and investigation into the need for staging bone scans in prosate cancer (O'Sullivan and Cook 2002). Using PSA (prostate specific antigen), Gleason score and clinical stage, it is possible to place patients into three risk categories such as low, medium and high. This information can help decide which patients require a bone scan for staging and also in the interpretation of equivocal lesions (Zelefsky et al. 1995; O'Sullivan and Cook 2002). As an independent factor, PSA also provides a readily available tool for risk assessment in these patients. Although there is some uncertainty whether a level of PSA of 10 or 20 ng/ml should be used as an upper threshold for performing scintigraphy, a level of less than 10 ng/ml is very rarely associated with bone metastases at presentation (Lee 2000).

10.5.3 Other Genitourinary Tumours

Renal cell carcinoma metastasises to bone relatively frequently. At presentation the incidence of bone metastases varies in reported series from 7.5% to 32% (Fogelman and McKillop 1991) but the majority of patients have either clinical or biochemical evidence of metastases. There would not therefore seem to be a need for routine scintigraphy of asymptomatic patients at presentation. If patients are symptomatic and have bone disease, the bone scan may not alter surgical management of the primary tumour but may be valuable in

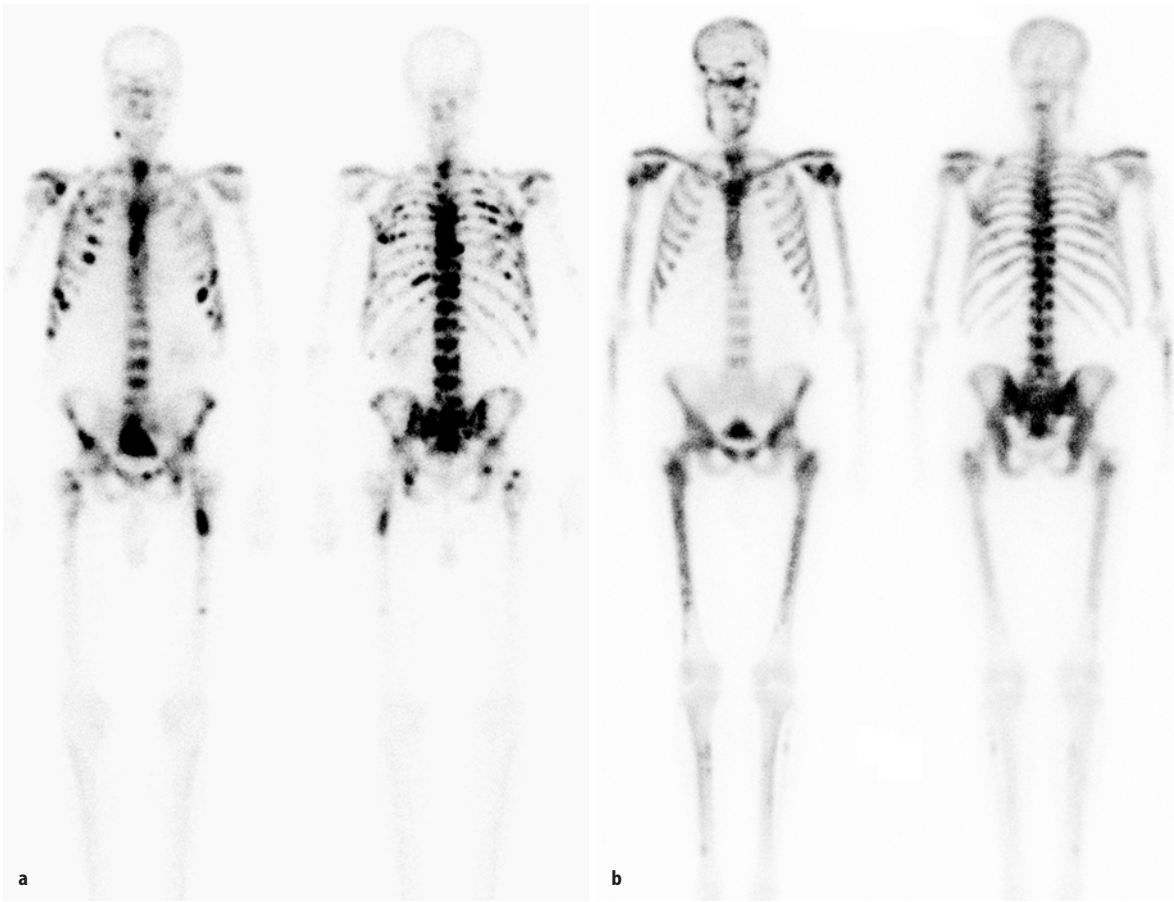

Fig. 10.10. Disease progression: **a** disseminated metastatic disease from prostate cancer involving multiple ribs, spine, sacroiliac joints, humeri, and femora which has progressed into a superscan of malignancy in 15 months (**b**) with diffuse involvement of the skeleton

confirming and localising lesions and assessing the extent prior to local or systemic palliative therapy. Metastases from renal carcinoma are mostly lytic and frequently do not excite much in the way of an osteoblastic response. Lesions may therefore be inconspicuous on bone scan and a careful review for cold lesions should be made (Kim et al. 1983). Tumours such as bladder, cervical, ovarian and uterine carcinomas have a low incidence of bone metastases at presentation and therefore the routine scanning of asymptomatic patients is not justified. The role of bone scintigraphy in these tumours would seem to be in the assessment and treatment follow-up of patients with clinical suspicion of bone involvement.

10.5.4 Lung Cancer

The reported rates of positive bone scans in patients presenting with lung cancer vary widely (2–19%) (Fogelman and McKillop 1991), and this may reflect differences in the proportion of tumour types in the populations studied. Certainly, small cell carcinoma, which is seldom treated surgically, appears to have a higher incidence of bone involvement at presentation, approaching 50% (Bitran et al. 1981; Levenson et al. 1981) (Fig. 10.11). The prognosis of those with a positive bone scan at presentation is extremely poor, where nearly all patients are dead by 12 months (Gravenstein et al. 1979). Practice may change as clinical PET scanning becomes more widely available as whole body imaging with ^{18}FDG can assess local and distant metastatic spread to soft tissues and bone. This technique is also more sensitive than current staging techniques with CT alone, demonstrated in a series of 35 non-small cell lung cancers which were otherwise operable, where 18% had management changed to a non-surgical regime because of the detection of previously unsuspected metastases (Lewis et al. 1994).

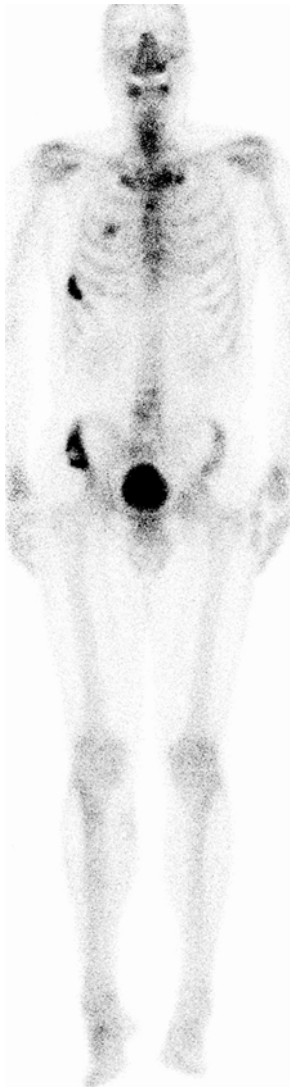

Fig. 10.11. Lung cancer. Whole-body scan shows abnormal uptake in the ribs and right iliac crest (note the photopenic area in the centre due to an osteolytic lesion) suggestive of multiple metastases. Some patchy uptake is also present in the left strenoclavicular joint due to degenerative disease at that site

10.5.5 Neuroblastoma

This solid, childhood tumour frequently metastasises to the skeleton, and bone scintigraphy has been demonstrated as a sensitive method for assessment of the skeletal involvement. Obtaining very good quality studies is important in this disease if false negative interpretations are to be avoided. Photopenic lesions may occur, which can be difficult to resolve in the smaller paediatric skeleton (Fawcett and McDougall 1980), and symmetrical, diffuse uptake of tracer next to the joints, seen as blurring of the borders of epiphyseal activity, requires high-resolution images for detection. Uptake of ^{99m}Tc-MDP is often noted in the primary tumour and soft tissue metastases (Howman-Giles et al. 1979; Podrasky et al. 1983). Although ^{123}I-mIBG is a specific tracer for staging and follow-up of neuroblastoma, false negatives have been noted in relation to the skeleton, and full assessment with both ^{99m}Tc-MDP and ^{123}I-mIBG is recommended (Gordon et al. 1990).

10.5.6 Miscellaneous Tumours

Due to the low incidence of bone involvement at presentation in many of the commoner cancers such as bowel, thyroid, melanoma, head and neck tumours, bone scintigraphy is usually only performed in those with suspicion of bone involvement and in the treatment assessment of those with proven bone metastases.

10.6 Clinical Applications of Bone Scan in Metabolic Bone Disease

10.6.1 Osteoporosis

In clinical management of the metabolic bone diseases, the isotope bone scan is most useful in osteoporotic patients, in whom it has a valuable role in evaluation and management (Cook et al. 2002). The bone scan has no role in the diagnosis of osteoporosis per se, but may be used in established osteoporosis to confirm or exclude recent vertebral fracture. The characteristic appearance of this type of fracture is of intense, linearly increased tracer uptake at the affected level (Fig. 10.12). It should be noted that although the bone scan may become positive immediately after a fracture, it could take up to 2 weeks for the scan to become abnormal, especially in the elderly. Subsequently there is a gradual reduction in tracer uptake, with the scan normalising between 3 and 18 months after the incident, the average being between 9 and 12 months (Fogelman and Carr 1980a). Because of this, the bone scan also is extremely useful in assessing the age of fractures. If a patient complains of back pain with multiple vertebral fractures on radiographs, and the bone scan is normal, then this essentially excludes recent fracture as a cause of symptoms. An isotope bone scan also may be valuable in patients in whom back pain persists for longer than one would expect after vertebral fracture. It is common to find that there has been an additional unsuspected vertebral or sacral fracture or a rib fracture in close proximity to spine. In addition, we are increasingly becoming aware that osteoporotic patients with chronic back pain may have unsuspected abnormalities affecting the facet joints (Cook et al. 2002; Ryan et al. 1992a). To identify abnormalities in the facet joints, SPECT imaging is essential. On planar imaging alone, it is not usually possible to separate activity in the facet joints from associated activity in the vertebral body caused by fracture.

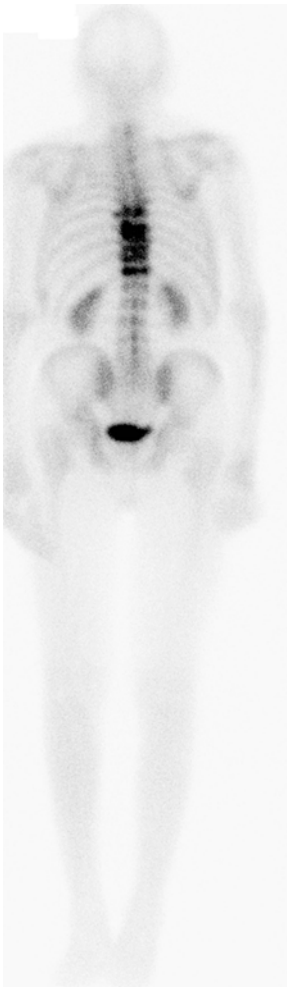

◁ **Fig. 10.12.** Multiple osteoporotic fractures: whole body bone scan of an elderly male with osteoporosis showing multiple foci of linear, intense uptake in the thoracic vertebrae with loss of vertebral contour

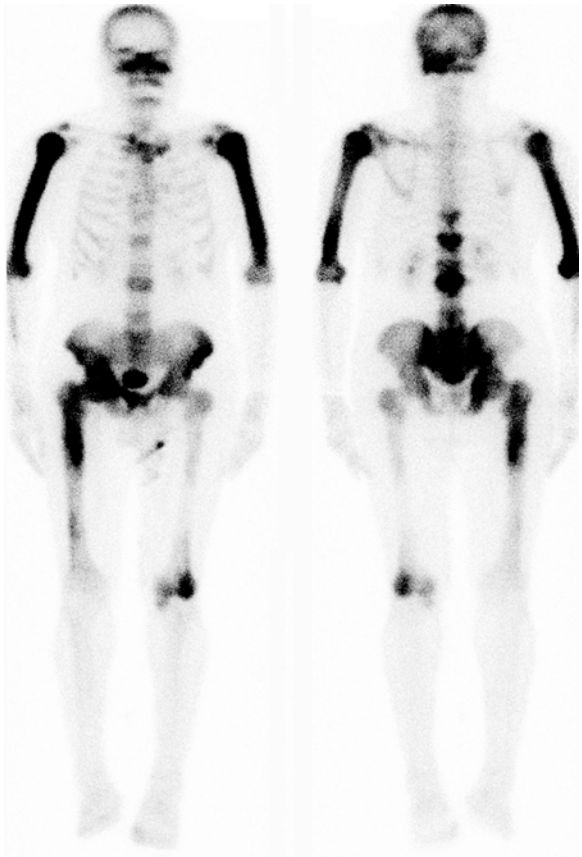

▷ **Fig. 10.13.** Polyostotic Paget's disease: whole body bone scan showing multiple areas of intense increased uptake in the skull, humeri, right femur, lumbar spine and pelvis

10.6.2 Paget's Disease

The isotope bone scan is invaluable in the assessment of patients with suspected Paget's disease, both for diagnosis and to define the extent of skeletal involvement. The majority of patients with Paget's disease have polyostotic disease (80–90%) (Fig. 10.13). The bone scan is a convenient way to evaluate the whole skeleton and has shown a greater sensitivity for detecting affected sites than having radiographic skeletal surveys (Fogelman and Carr 1980b). Characteristically, affected bones show intensely increased activity, which starts at the end of a bone and spreads either proximally or distally, often showing a "V" or "flame-shaped" leading edge. Another clue that a scintigraphic abnormality is due to Paget's disease rather than other focal skeletal pathology is that the whole bone is often involved, which is most often seen in the pelvis, scapula, and vertebrae (Figs. 10.14–

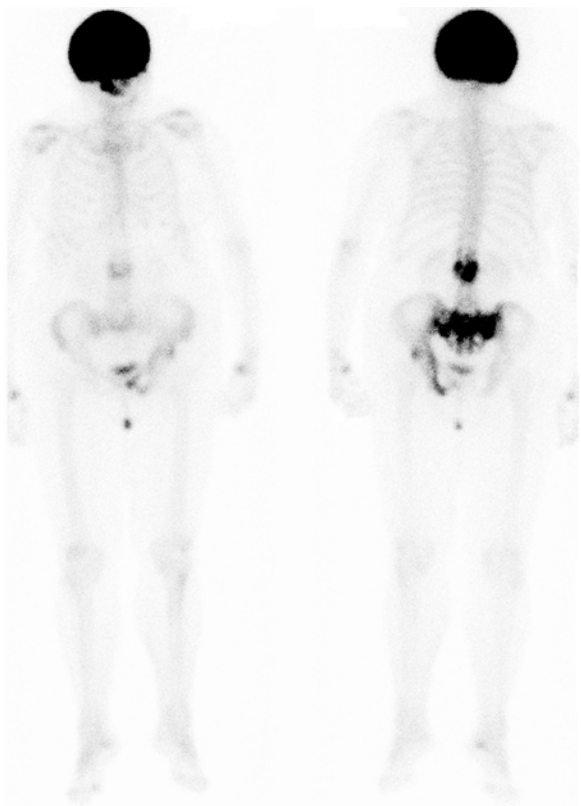

▷ **Fig. 10.14.** Polyostotic Paget's disease: whole body bone scan showing intense accumulation in the skull, L3 lumbar vertebra, sacrum and less prominently in the left hemi-pelvis

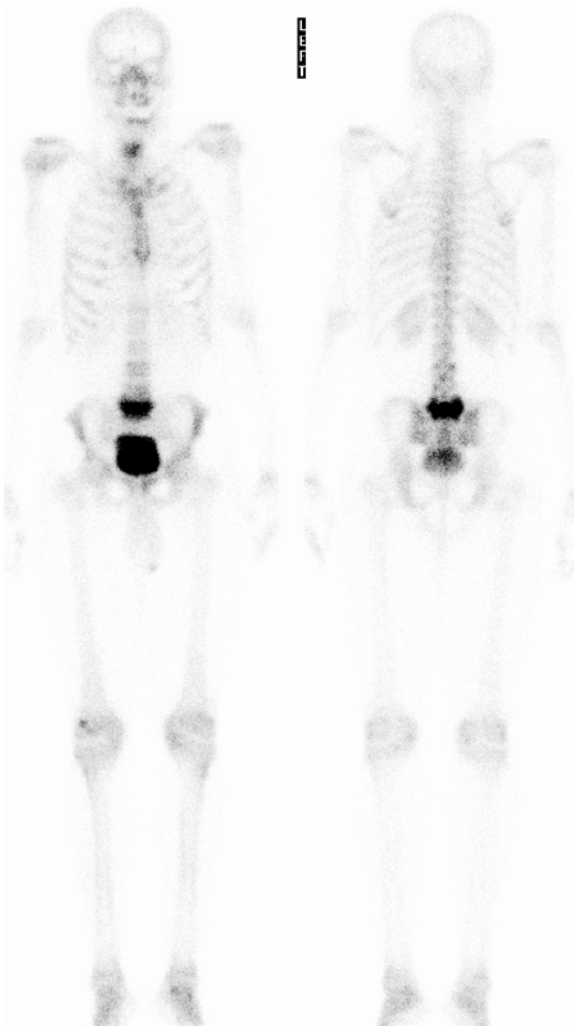

Fig. 10.15. Monostotic Paget's disease: whole body bone scan showing intense accumulation in L5 vertebra, typical for Paget's disease

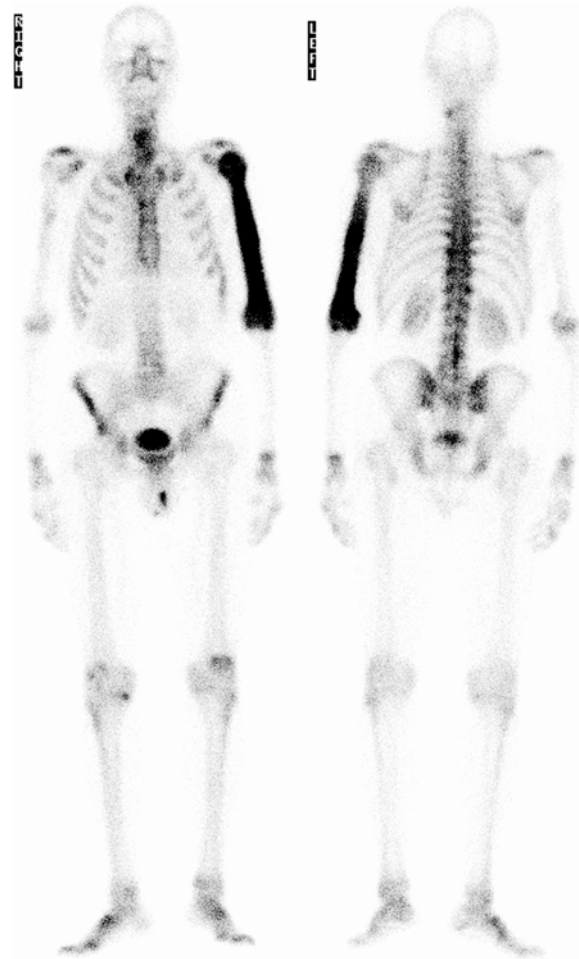

Fig. 10.16. Monostotic Paget's disease: whole body bone scan showing intense accumulation in the left humerus due to Paget's disease

10.16). In the vertebrae, the characteristic finding is of abnormal tracer accumulation throughout the vertebra, affecting the body and posterior elements, including the spinous and transverse processes. The radionuclide bone scan is useful for the evaluation of the extent of the disease and response to the treatment. The radionuclide bone scan may occasionally identify complications of Paget's disease.

10.6.3 Hyperparathyroidism

Most cases of primary hyperparathyroidism are asymptomatic and are unlikely to be associated with changes on bone scintigraphy. The diagnosis is a biochemical one, and the bone scan therefore has no routine role in diagnosis. Bone scans are often used to help differentiate the causes of hypercalcaemia; in particular, hyperparathyroidism versus malignancy (although hypercalcaemia in the latter may also be due to humoral factors related to PTH, etc.) and so typical features of metabolic bone disorders should be recognised. In hyperparathyroidism there is increased skeletal turnover, and in the more severe cases, commonly seen as part of renal osteodystrophy, this will be evident scintigraphically. A bone scan may show a number of features in hyperparathyroidism, but the most important is the generalised increased uptake throughout the skeleton, that may be identified because of increased contrast between bone and soft tissues. Other typical metabolic features that have been described in bone scans in metabolic bone diseases include a prominent calvarium and mandible, beading of the costochondral junctions, and a "tie" sternum.

10.6.4 Renal Osteodystrophy

Renal osteodystrophy is due to a combination of bone disorders as a consequence of chronic renal dysfunction and often demonstrates the most severe cases of metabolic bone disease. It may comprise osteoporosis, osteomalacia, adynamic bone and secondary hyperparathyroidism in varying degrees. The bone scan appearance generally reflects the degree of hyperparathyroidism and in severe cases leads to a 'metabolic' super scan, and uptake of diphosphonate in areas of ectopic calcification also may be seen although it is now relatively uncommon. A clue in differentiating this type of scintigraphic pattern from others is that there may be a lack of bladder activity in view of renal failure.

10.6.5 Osteomalacia

Patients with osteomalacia usually demonstrate similar features on a bone scan as described in hyperparathyroidism, although in the early stages of the disease, it may appear normal (Fogelman et al. 1978). ^{99m}Tc-MDP can detect Looser's zones or pseudofractures with high sensitivity, especially in ribs where X-ray may not be helpful (Ryan and Fogelman 1997; Mari et al. 1999). The pseudofractures are often noted in the ribs, which is the most common site seen on the bone scan. The distribution is usually symmetrical and perpendicular to the bone surface (Mari et al. 1999).

10.7 Clinical Application of Bone Scan in Sports/Exercise Related Injuries

Sports-induced injuries include a host of musculotendinous abnormalities, such as stress fractures, shin splints, arthritis, muscle injuries, etc. (Table 10.2). Approximately 50 % of all sports injuries are secondary to overuse and result from repetitive microtrauma that causes local tissue damage (Wilder and Sethi 2004; Murray 1998a). Sports-induced injuries are generally due to biomechanical abnormalities (malalignments, muscle imbalance/weakness, inflexibility/instability), poor technique, improper equipment, and changes in duration or frequency of activity (Wilder and Sethi 2004). The pathogenesis of stress fracture is multifactorial and usually involves repetitive submaximal stress (Boden and Osbahr 2000).

Bone scintigraphy with ^{99m}Tc-MDP has been used with increasing frequency in detecting sports-induced injuries especially stress fractures, because of its high sensitivity and its ability to show abnormalities in bone metabolism well before they are manifested radiographically (Drubach et al. 2001) (Fig. 10.17). Its sensi-

Table 10.2. Common clinical applications of bone scan in sports medicine

Soft tissue injury	Tendons (Achilles tendon), plantar fasciitis, impingement syndromes, shin splints, compartment syndromes, De Quervain's tenosynovitis
Bone injuries	Stress fractures involving tibia, fibula, hip/pelvis Stress fractures of small bones in the feet, scaphoid fractures, etc.
Injuries to the vertebral column	
Meniscal injuries	
Ligament injuries	

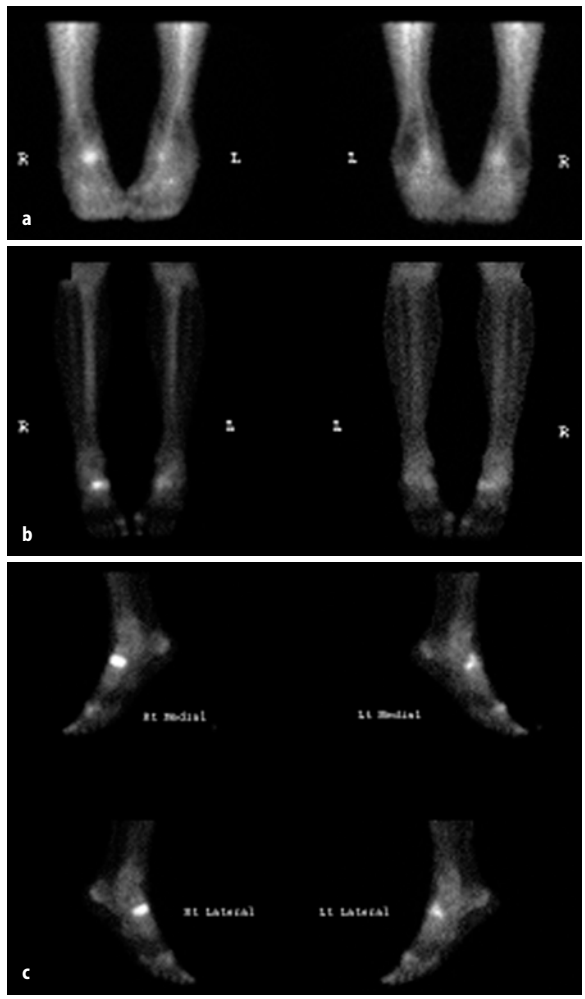

Fig. 10.17. Stress fractures: 28-year-old male footballer with increasing pain in the right foot. No previous injury or problems with lower limbs. **a** Blood pool images show increased vascularity over the medial aspect of the right foot and the delayed images (**b, c**) show intense uptake at this site due to a navicular fracture

tivity for this diagnosis approaches 100 % (Drubach et al. 2001).

Bone scintigraphy is also used to differentiate stress fractures from shin splints in the tibia. Tibial stress fracture accounts for half of all reported stress fractures (McBryde 1985). Increased perfusion and blood flow are typically present in acute stress fracture. The delayed images often reveal focal fusiform uptake in the lesion, which is usually seen medially at the junction of the middle and distal thirds of the tibia (Rupani et al. 1985; Love et al. 2003) (Fig. 10.18).

Shin splints are due to excessive exertion of the tibialis and soleus muscles of the legs, which gives rise to periostitis at the tibial insertions of these muscles (Love et al. 2003). In shin splints, blood flow and blood pool images are usually normal. However, delayed images reveal longitudinally oriented linear areas of increased uptake of varying intensity that involve one-third or more of the posterior tibial cortex (Love et al. 2003; Holder and Michael 1984) (Fig. 10.19). The differentiation of stress fracture from shin splints is important because their treatments are different (Love et al. 2003).

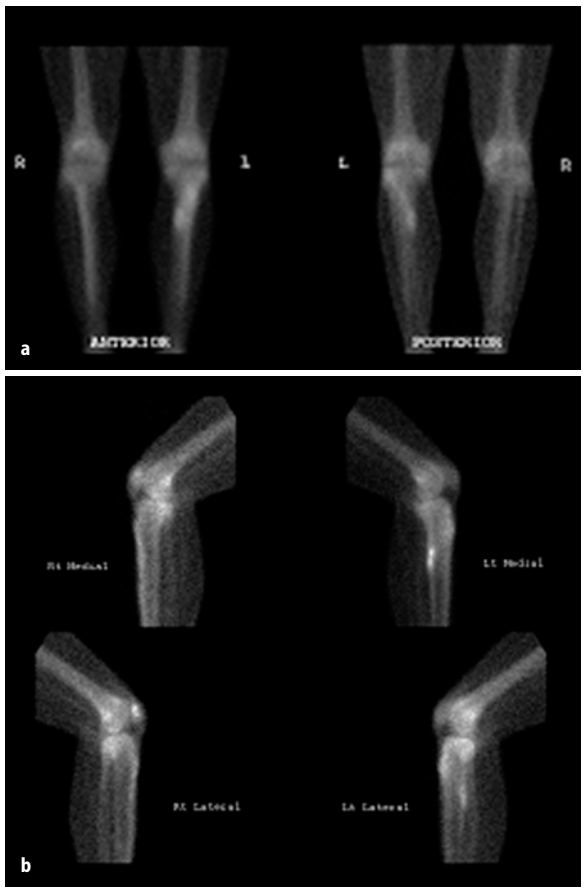

Fig. 10.18. Stress fracture: 32 year old (triathlete), complaining of pain in the left tibia over the previous 2 months. The delayed images (**a, b**) show focal intense uptake at the medial aspect of the upper left tibia

Plantar fasciitis, a form of localised reactive periostitis, develops during events such as running and aerobics that involve extensive foot dorsiflexion. Pain and tenderness are concentrated at the site of the insertion of the long plantar tendon into the inferior aspect of the calcaneus. The typical radionuclide bone scan appearance of this entity is that of focally increased (intense) activity, at the site of the tendon insertion (Murray 1998; Love et al. 2003; Aburano et al. 1990; Intenzo et al. 1991). With bone scintigraphy, reflex sympathetic dystrophy usually manifests as diffuse, uniformly increased uptake throughout the affected region. In childhood cases and occasionally in adults the uptake can be reduced (Goldsmith et al. 1989; Turpin et al. 1996).

Fig. 10.19. Shin splints: 29-year-old female marathon runner complaining of increasing pain in both tibiae over the previous 3 months. There is increased tracer uptake seen extending along the posterior aspect of both tibiae (**b, c**). The appearances are those of a periosteal reaction due to 'shin splints'

10.8 Clinical Applications of Bone Scan in Infection and Evaluation of Joint Prostheses

^{99m}Tc-MDP bone scintigraphy is used as a complementary imaging procedure in evaluation of infection. It is routinely used in the evaluation for osteomyelitis in a diabetic patient. Early diagnosis and treatment of the condition can reduce the likelihood of complications. Three-phase bone scan is reported to have an accuracy of over 90 % (Palestro and Torres 1997). The classic appearance of osteomyelitis on three-phase bone scans consists of focal hyperperfusion, focal hyperemia, and focally increased bone uptake (Love et al. 2003; Palestro and Torres 1997). However, fractures, tumours, and joint neuropathy may also mimic osteomyelitis on a three-phase bone scan, thus reducing the specificity of the technique (Love et al. 2003; Palestro and Torres 1997). Labelled white blood cell (WBC) imaging is reported to be more sensitive and specific in diagnosing pedal osteomyelitis than bone scintigraphy alone (Palestro 1994). ^{99m}Tc-HMPAO labelled white cells are generally more sensitive for the detection of acute osteomyelitis than of chronic osteomyelitis. It is also useful in paediatric groups, where ^{99m}Tc-MDP has low specificity (Peters 1994). However, ^{111}In-labelled WBC is preferred for imaging chronic osteomyelitis as 24-h imaging is feasible (Palestro and Torres 1997; Seabold and Nepola 1999), which is important in the presence of low-grade infection. But false-positive WBC scans have occurred in Charcot's (neuropathic) joints, probably attributable to inflammation and haematopoietically active bone marrow (Palestro and Torres 1997).

^{99m}Tc-MDP-bone scintigraphy is used to evaluate patients with painful joint replacement/prosthesis (Fig. 10.20). The commonest indication is to differentiate loosening from infection. Differentiating the aseptically loosened from the infected joint prosthesis is not always easy. Levitsky et al. reported a sensitivity of 33 %, a specificity of 86 %, a positive predictive value of 30 %, and a negative predictive value of 88 % in 72 total

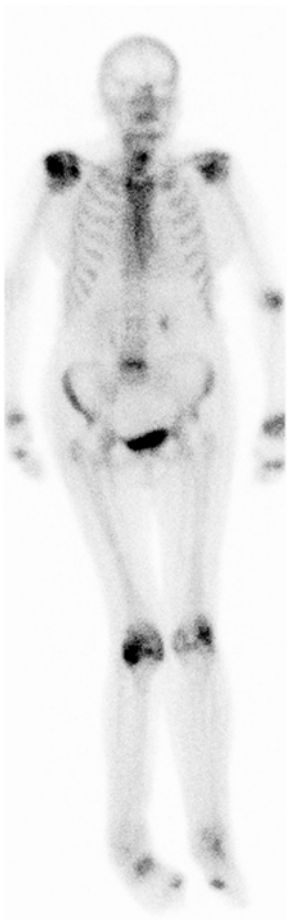

Fig. 10.20. Severe osteoarthritis with bilateral total hip replacement (THR): whole body bone scan shows abnormal uptake involving multiple joints, shoulders, knees and L5 vertebra. Bilateral hip replacements are also noted, which show normal tracer distribution on blood pool (not shown) and delayed images

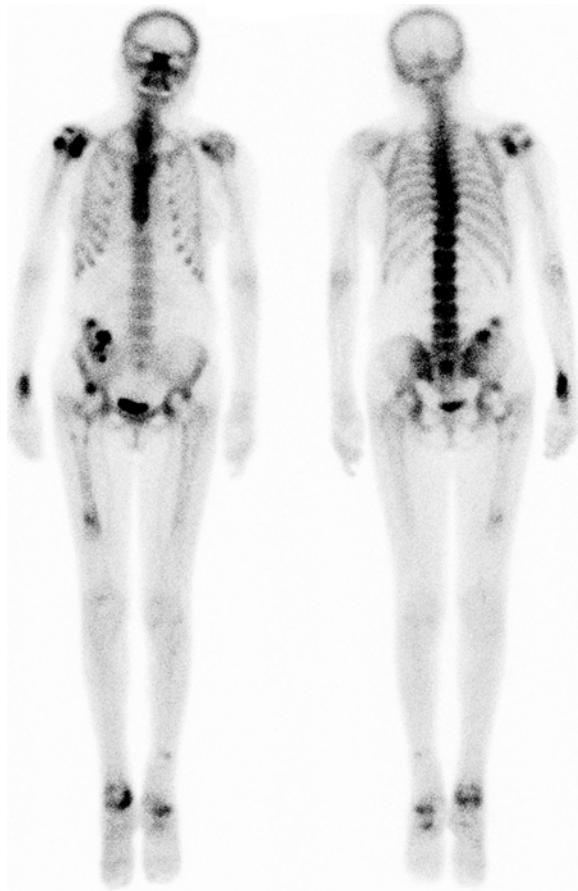

Fig. 10.21. Loosening of hip prostheses: patient presented with right-sided hip pain 2 years after total hip replacement (THR). The delayed whole body images show bilateral THRs, right shoulder replacement, and a right ankle prosthesis. Increased metabolic activity with normal blood pool (not shown) in the acetabular components bilaterally and at the tip of right femoral component is consistent with loosening. The uptake noted in the right shoulder and ankle is consistent with degenerative changes. A right transplant kidney is also noted and the patient has been treated for avascular necrosis

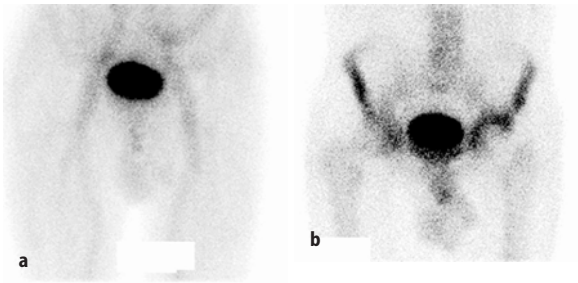

Fig. 10.22. Loosening of left THR: patient with left THR (performed 4 years previously) with pain in the left hip. The delayed images (**b**) *on the left* show increased accumulation in the acetabular component of the prosthesis with normal blood pool (**a**), which is compatible with loosening of the acetabular component

joint replacements examined with bone scintigraphy (Levitsky et al. 1991). In bone scintigraphy, focally increased radionuclide uptake around the prosthesis is commonly considered to represent loosening (Figs. 10.21, 10.22), while diffusely increased uptake in blood pool and delayed phase is commonly considered to represent infection (Palestro and Torres 1997; Williamson et al. 1979; Stumpe et al. 2004). However, infection may also be present in prostheses with focal uptake patterns (Mountford and Coakley 1989; Aliabadi et al. 1989). Bone scintigraphy within 12 months of an arthroplasty procedure may be of limited value in ruling out loosening and infection due to existent inflammatory changes following surgery (Stumpe et al. 2004). Type, location of the prosthesis and the amount of time elapsed between implantation and imaging must be taken into account during interpretation (Love et al. 2001). Hip and knee replacements can be cemented or cementless. In patients with a cemented hip prosthesis the majority of the asymptomatic patients will have a normal bone scan beyond 1 year and about 10% will have persistent increased uptake beyond this period (Utz et al. 1986). In patients with a cementless hip prosthesis, the persistent uptake is more prevalent beyond 1-year post-replacement (Oswald et al. 1989, 1990). In patients with knee replacements, persistent peri prosthetic uptake beyond 1-year post-implantation is also noted (89% of tibial components and 63% of femoral components) (Rosenthal et al. 1987; Hofmann et al. 1990). Hofmann et al. found that a single post-operative bone scan could not differentiate loosening from early bone remodelling (Hofmann et al. 1990).

^{111}In-Labelled WBC scintigraphy in general is a good agent for diagnosing infection in prosthesis. However, diagnostic accuracy of labelled white cell imaging can be limited as it accumulates in normal reticuloendothelial bone marrow (Peters 1994; Palestro and Torres 1997). Implantation of prosthesis may alter the bone marrow distribution at the site of intervention. However, inability to distinguish labelled leukocyte uptake in infection from uptake in bone marrow is a problem. This issue can be overcome by performing additional bone marrow imaging with ^{99m}Tc-sulphur colloid. Both labelled leukocytes and sulphur colloid accumulate in the bone marrow whereas there is mismatch in infection when leukocytes accumulate but sulphur colloid does not (Palestro et al. 1990, 1991). The reported sensitivity, specificity, and accuracy of labelled leukocytes plus sulphur colloid bone marrow imaging is 96%, 97%, and 97%, respectively (Palestro et al. 1990).

10.9 Clinical Application of Bone SPECT

In patients with chronic low back pain the addition of SPECT to bone scintigraphy is a useful adjunct that some departments perform routinely. SPECT has been shown to be more sensitive than plain film radiology, with most SPECT lesions corresponding to identifiable disease on computed tomography (CT) (Ryan et al. 1992b) (Table 10.3). One-third of lesions may not be visible on planar scintigraphy (Ryan et al. 1992b) (Fig. 10.23). Lesions can be accurately located to the vertebral bodies or posterior vertebral elements (Ryan et al. 1992c). It was noted that the main benefit occurred in lesions localised to the posterior aspect of the vertebra where radiographs failed to detect abnormalities in the majority of cases, even when additional oblique views were available.

SPECT has been found to be particularly valuable in the investigation of facet syndrome as a cause of low back pain (Holder et al. 1995; Dolan et al. 1996) (Fig. 10.24). Not only is it a sensitive method for detecting facet joint related pain compared to planar imaging but also it can predict those patients who are more likely to benefit from local facet joint injections or denervation (Dolan et al. 1996). As clinical features are often non-specific in facet joint related pain, bone SPECT is also helpful in identifying the cause of pain in those without a facetal aetiology (Holder et al. 1995). Pars interarticularis defects, thought to be due to a repeated stress phenomenon causing spondylolysis, are a signif-

Table 10.3. Clinical applications of bone SPECT

Patients with chronic low back pain
Facet syndrome (as a cause of low back pain)
Pars interarticularis
Evaluation of symptomatic patients following spinal surgery
Osteoporosis and chronic back pain
Investigation of metastatic disease in the spine
Avascular necrosis (AVN)
Diagnosis of meniscal tears
Temporomandibular joint (TMJ) dysfunction
Skull SPECT in malignant otitis externa in diabetic patients
Calculation of tracer uptake per volume of bone

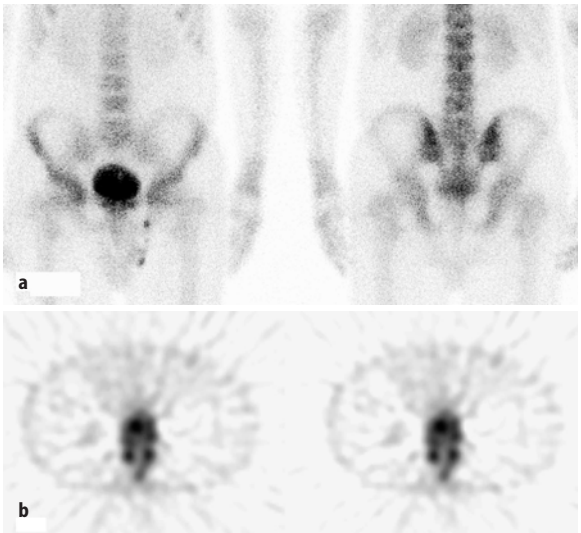

Fig. 10.23. Normal planar and positive SPECT: facet joint disease in a patient with low-back pain. The local views of spine show no abnormality (**a**). However, SPECT (**b**) of lumbosacral spine shows increased tracer uptake in the facet joints at the level of L5 vertebra, suggesting active inflammatory disease at this site. Note also some increased uptake in the vertebral body due to degenerative disease

icant cause of back pain, particularly in young people actively participating in sport. Bone SPECT is able to identify more lesions than radiographs (Bellah et al. 1991; Read 1994; Bodner et al. 1988; Collier et al. 1985; Dutton et al. 2000) and a normal SPECT scan makes spondylolysis an unlikely cause of back pain. SPECT scans may be helpful in guiding management, by correlating the presence or absence of abnormal metabolic activity with pars defects identified on CT.

Bone SPECT of the lumbar spine may contribute to the evaluation of symptomatic patients following spinal surgery. SPECT is more sensitive than planar imaging alone (Slizofski et al. 1987) and is valuable in precisely locating the level of maximum instability or cause of symptoms distal from the operative site (Lusins et al. 1989; Gates et al. 1999). Bone scintigraphy with SPECT is not hampered by artefacts caused by surgical metal-work as are CT and MRI. It is able to identify pseudoarthroses by the persistence of focal activity more than a year after surgery.

SPECT may also be helpful in the early diagnosis of sacroiliitis, where in conjunction with MRI, objective and complementary evidence for inflammatory activity may be gained before radiographic changes (Hanly et al. 1994). It is likely that the addition of a SPECT acquisition may be helpful in the investigation of metastatic disease in the spine. Not only is it possible to detect more lesions with SPECT but by being able to accurately locate the position and observe the pattern of a lesion it may be possible to differentiate benign from malignant lesions in the spine.

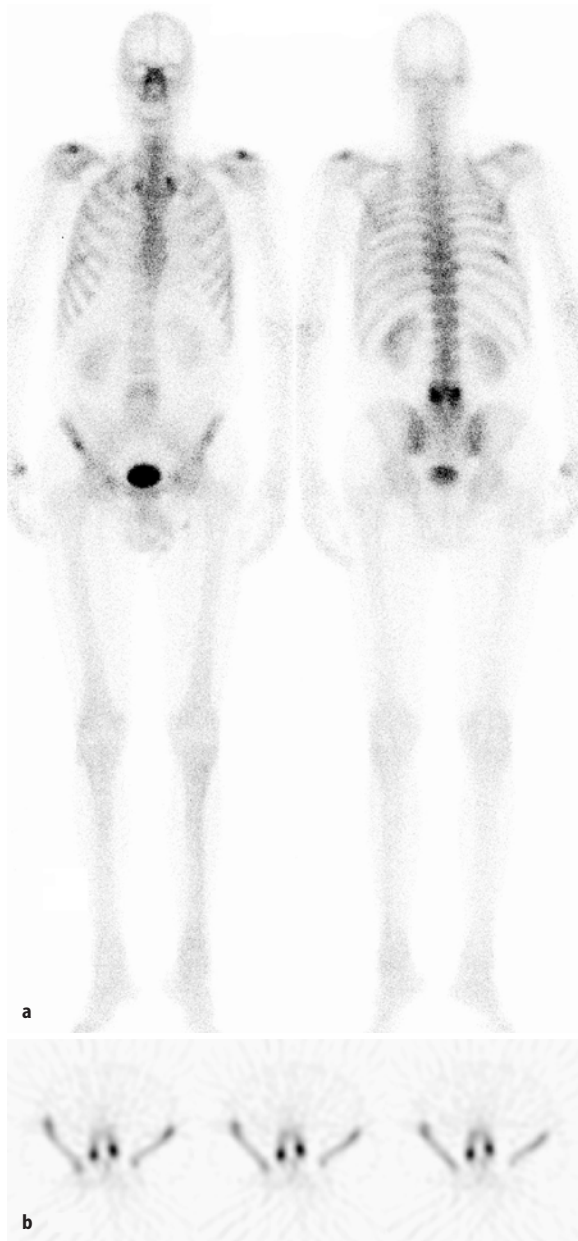

Fig. 10.24. Facet joint disease in a patient with low back pain: **a** Whole body bone scan and SPECT (**b**) of lumbosacral spine show intense uptake in the facet joints of L5. Increased uptake of tracer is also seen in the right ninth ribs posteriorly, which was traumatic in nature

Studies of the hips with SPECT have been related to the investigation of avascular necrosis (AVN). Both idiopathic AVN in children (Legg-Calve-Perthes disease) and secondary AVN may be identified by SPECT bone scanning, with sensitivities approaching 90 % being reported (Siddiqui et al. 1993; Stulberg et al. 1989; Collier et al. 1985; Kim et al. 1993).

In the knees the major interest in the use of SPECT is in the diagnosis of meniscal tears. Despite being pri-

marily a soft tissue injury, increased bone uptake is seen probably as a result of altered joint mechanics due to the deficient meniscus with increased activity at the sites of increased stress. In the appropriate clinical setting, high sensitivities of approximately 90 % have been reported with consistently better results than planar imaging alone (Murray et al.1990; Collier et al. 1985). The most specific pattern for a meniscal tear is an increase in vascularity on equilibrium images, abutting femoral and tibial condyle activity on delayed tomographic slices and a crescentic region of uptake on transaxial tibial slices corresponding to the injured meniscus (Ryan et al. 1993). Specific patterns have also been described in other ligamentous knee injuries including anterior cruciate ligament tears (Murray et al. 1990; Cook et al. 1996) and lateral collateral ligament injury (Cook and Fogelman 1996).

Temporomandibular joint (TMJ) dysfunction has a high prevalence and bone SPECT has been proposed as a method to evaluate patients with this disorder. SPECT has been reported as being more sensitive than planar scintigraphy (Kraznow et al. 1987) as well as X-ray tomography (Toni et al. 1992).

Skull SPECT is helpful in malignant otitis externa in diabetic patients. Not only does SPECT appear to be more sensitive than CT (Strashun et al. 1984) but also it may be possible to differentiate those with bone involvement from the less serious type where only soft tissues are affected (Hardoff et al. 1994).

The addition of tomography to bone scintigraphy allows accurate calculation of tracer uptake per volume of bone. By expressing regional activity in units of MBq/ml, it is possible to quantify bone turnover in different skeletal regions conceptually. This is still primarily a research application rarely carried out in clinical practice.

There is now clear evidence that SPECT adds to the diagnostic utility of bone scans, especially in the lumbar spine. Now that most departments with modern gamma cameras are able to make SPECT acquisitions, it should be possible to make use of the extra information available to improve accuracy in interpretation.

10.10 Positron Emission Tomography in Skeletal Disease

^{18}FDG is the most widely used oncological PET tracer but to date there has been little work on the use of PET specifically in bone. ^{18}FDG-PET has the advantage of better spatial resolution than conventional bone scans, and even if one is primarily interested in bone it does provide additional information regarding soft tissue disease (Fig. 10.25).

In breast carcinoma, the literature is far from clear as to whether ^{18}FDG-PET is more sensitive than the conventional bone scan in identification of bone me-

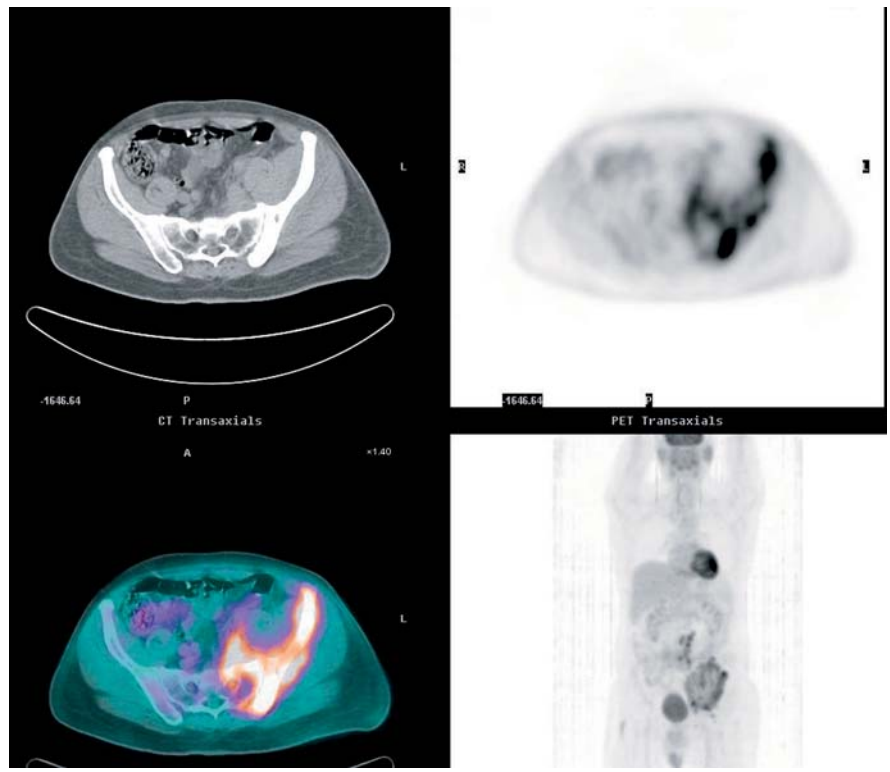

Fig. 10.25. Bone lymphoma: ^{18}F-FDG PET/CT scan in a patient with lymphoma involving the left hemi-pelvis and adjacent soft tissue

tastases. However, early observations in the use of this technique in women with metastatic breast cancer showed that significantly more bone metastases are detected compared to ^{99m}Tc-MDP scintigraphy. This may be due to a combination of the physical advantages of PET and because ^{18}FDG localises in tumour rather than bone and so may detect metastases before they are large enough to cause a bone reaction.

Lonneux et al. studied women with breast cancer who were treated with surgery, both with and without chemotherapy and radiotherapy. They concluded ^{18}FDG-PET was more sensitive than the bone scan in detecting skeletal metastases (Lonneux et al. 2000). A study from Ohta in patients with breast cancer found that both ^{18}FDG-PET and the bone scan had identical sensitivity (77.7%) but that ^{18}FDG-PET was more specific (97.6% vs 80.9%) (Ohta et al. 2001). Cook et al. found that patients who had either lytic or a mixed pattern of disease had a higher number of lesions identified on ^{18}FDG-PET than on the isotope bone scan but for the sub-group with sclerotic lesions a lower number was seen (Cook et al. 1998). It has been suggested that while there may be differences in the glycolytic rate between these types of metastases, sclerotic lesions have much smaller tumour volume relative to the size of the whole skeletal lesion and may therefore simply be less likely to be identified.

Prostate cancer is now established as the "classic" cancer with false negative results on ^{18}FDG-PET. These observations concur with those of Shreve et al., who noted only 65% sensitivity for the detection of skeletal metastases from prostate cancer, which is predominantly osteoblastic, when using ^{18}FDG compared to ^{99m}Tc-MDP (Shreve et al. 1996). However, Morris et al. in their study in patients with progressive metastatic prostate cancer concluded that ^{18}FDG-PET could discriminate active osseous disease from scintigraphically quiescent lesions (Morris et al. 2002). In patients with lung cancer, both the Bury and Gayed studies reached essentially identical conclusions, i.e. that both techniques had similar sensitivity for the detection of bone metastases but that ^{18}FDG-PET was more specific (Bury et al. 1998; Gayed et al. 2003).

There is relatively little in the literature relating to lymphoma and the skeleton, but ^{18}FDG-PET seems to perform better than the bone scan (Moog et al. 1999) and there is an increasing body of evidence relating to the valuable role of ^{18}FDG-PET in myeloma (Schirrmeister et al. 2002; Fogelman et al. 2005; Bredella et al. 2005), where it is clearly better than the bone scan (although this is hardly an area where the bone scan shines) and this is presumably because ^{18}FDG is identifying marrow-based disease at an early stage. There is very little data in the literature regarding the use of ^{18}FDG-PET in monitoring the response of bone metastases to therapy and it is probable that future studies will confirm its role (Figs. 10.26, 10.27).

Recent reports on use of ^{18}F-labelled NaF (^{18}F-PET) in detection of bone metastases are encouraging and it

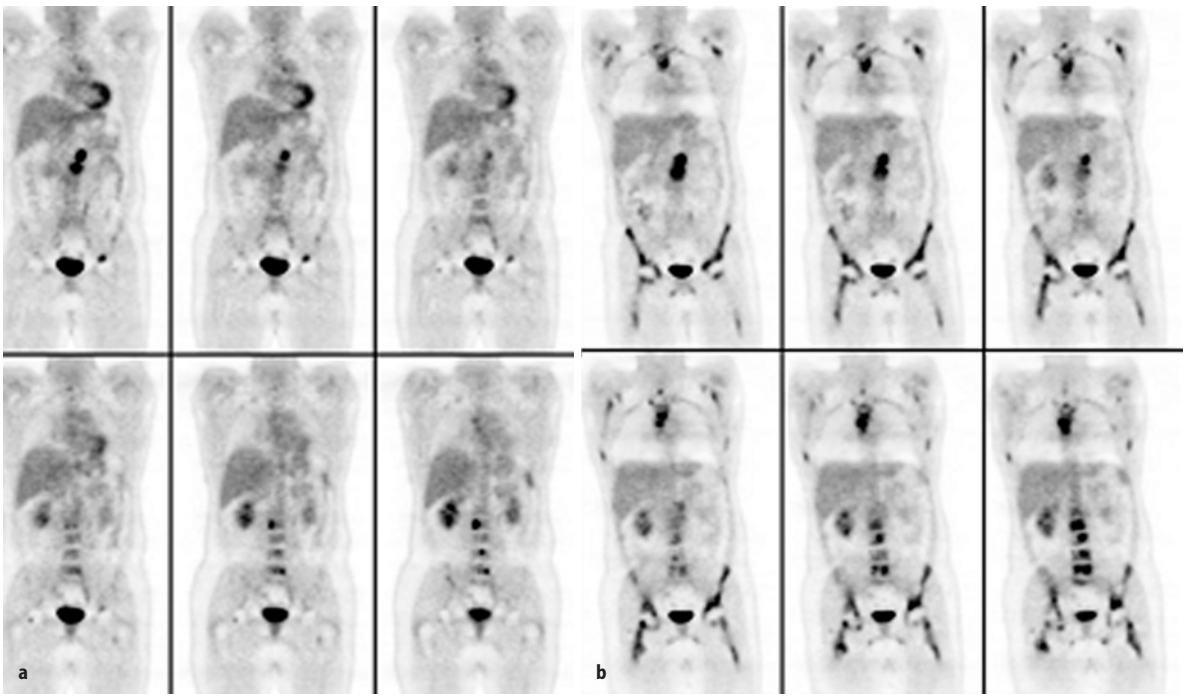

Fig. 10.26. Non-Hodgkin's lymphoma (NHL): **a** ^{18}F-FDG PET scan in NHL with bone marrow and nodal involvement; **b** progression with widespread intense focal FDG uptake in bone marrow and nodes after transformation into a high-grade lymphoma

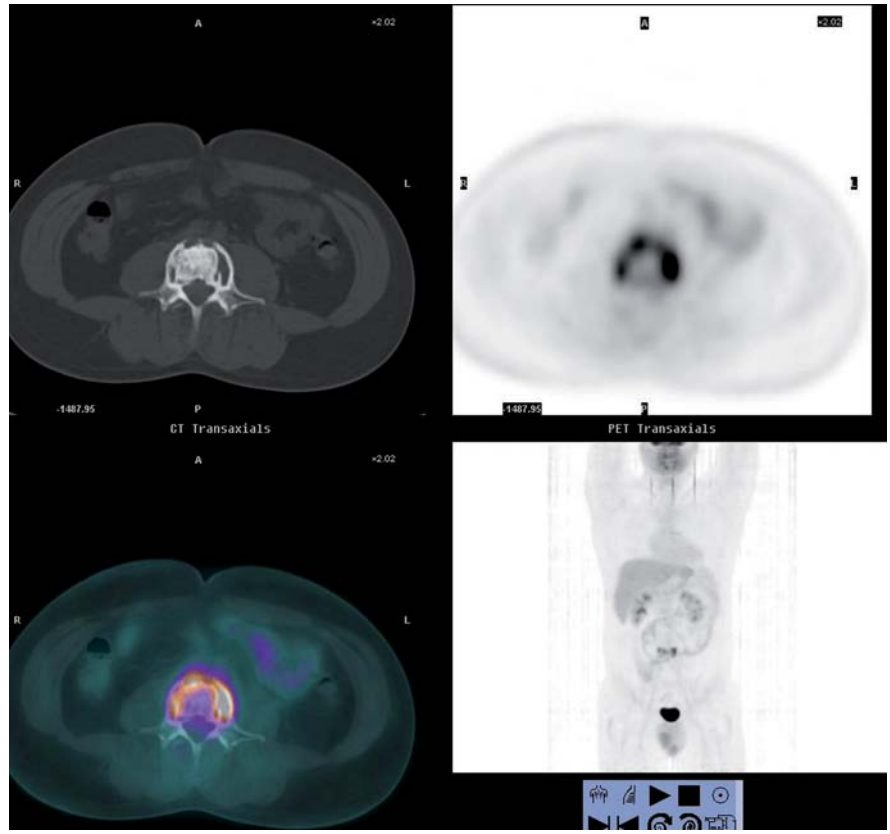

Fig. 10.27. Plasmacytoma: ^{18}F-FDG PET/CT scan in a patient with a treated plasmacytoma (with radiotherapy) in the lumbar spine with rising tumour markers. CT shows sclerotic changes due to previous treatment and PET reveals new disease in the surrounding marrow

has been shown to be significantly more accurate in detecting bone metastases than ^{99m}Tc-MDP scans (Schirrmeister et al. 1999a). Uptake of the fluoride ion (^{18}F) is twofold higher than that of ^{99m}Tc-polyphosphonates (Even-Sapir et al. 2004). However, it is difficult to differentiate benign from malignant ^{18}F-fluoride uptake (Cook and Fogelman 2000). The high sensitivity of ^{18}F-fluoride for both benign and malignant lesions may pose a diagnostic dilemma (Even-Sapir et al. 2004).

^{18}F-Fluoride is reported to be more sensitive than ^{99m}Tc-MDP bone scan, mainly for the detection of lytic lesions, which may not be always identified on a bone scan (Schirrmeister 1999b, 2002). However, as yet it has not been shown to be cost effective and not readily available for routine use.

A lesion-based comparison by Schirrmeister et al. with ^{18}F-PET indicated that the sensitivity of planar bone scan in detecting vertebral bone metastases was as low as 40 %. However, the sensitivity ranged from 80 % to 90 % in the skull, thorax, and extremities (Schirrmeister et al. 1999a), though recent studies have suggested that the sensitivity of ^{99m}Tc-MDP might be improved by additional SPECT imaging and it is reported to be less expensive (Schirrmeister et al. 2001). In the assessment of entire vertebral column two SPECT acquisitions will be necessary and this increases the acquisition time and also the risk of movement during acquisition. These factors can reduce spatial localisation with SPECT when compared with ^{18}F-PET (Schirrmeister et al. 2001). Overall the problem seems to be more technical than biological; hence, ^{18}F-PET will become more attractive in the future, though the reported accuracies of ^{18}F-PET and of SPECT were not statistically significant (Schirrmeister et al. 2001). But this was a small study and it is probable that future studies will confirm the advantages of ^{18}F-PET.

References

Aburano T, Yokoyama K, Taki J, Nakajima K, Tonami N, Hisada K (1990) Tc-99m MDP bone imaging in inflammatory enthesopathy. Clin Nucl Med 15:105 – 106

Aliabadi P, Tumeh SS, Weissman BN, McNeil BJ (1989) Cemented total hip prosthesis: radiographic and scintigraphic evaluation. Radiology 173:203 – 206

Batson O (1942) The role of the vertebral veins in metastastic processes. Ann Intern Med 16:38 – 45

Baxter AD, Coakley FV, Finlay DB, West C (1995) The aetiology of solitary hot spots in the ribs on planar bone scans. Nucl Med Commun 16:834 – 837

Bellah RD, Summerville DA, Treves ST, et al. (1991) Low back pain in adolescent athletes: detection of stress injury to the pars interarticularis with SPECT. Radiology 180:509 – 512

Bitran JD, Bekerman C, Desser RK (1980) The predictive value of serial bone scans in assessing response to chemotherapy in advanced breast cancer. Cancer 45:1562 – 1568

Bitran JD, Beckerman C, Pinsky S (1981) Sequential scintigraphic staging of small cell carcinoma. Cancer 47:1971 – 1975
Blau M, Nagler W, Bender MA (1962) Fluorine-18: a new isotope for bone scanning. J Nucl Med 3:332 – 4
Blau M, Ganatra R, Bender MA (1972) 18F-fluoride for bone imaging. Semin Nucl Med 2:31 – 7
Boden BP, Osbahr DC (2000) High-risk stress fractures: evaluation and treatment. J Am Acad Orthop Surg 8:344 – 353
Bodner RJ, Heyman S, Drummond DS, Gregg JR (1988) The use of SPECT in the diagnosis of low back pain in young patients. Spine 13:1155 – 1160
Bredella MA, Steinbach L, Caputo G, Segall G, Hawkins R (2005) Value of FDG PET in the assessment of patients with multiple myeloma. AJR Am J Roentgenol 184:1199 – 204
Bury T, Barreto A, Daenen F, Barthelemy N, Ghaye B, Rigo P (1998) Fluorine-18 deoxyglucose positron emission tomography for the detection of bone metastases in patients with non-small cell lung cancer. Eur J Nucl Med 25:1244 – 1247
Bushnell DL, Kahn D, Huston B, Bevering CG (1995) Utility of SPECT imaging for determination of vertebral metastases in patients with known primary tumors. Skeletal Radiol 24: 13 – 16
Caner B, Kitapcl M, Unlu M, Erbengi G, Calikoglu T, Gogus T, Bekdik C (1992) Technetium-99m-MIBI uptake in benign and malignant bone lesions: a comparative study with technetium-99m-MDP. J Nucl Med 33:319 – 324
Chiewitz P, Hevesy G (1935) Radioactive indicators in the study of phosphorus metabolism in rats. Nature 136:754 – 5
Coakley FV, Jones AR, Finlay DB, Belton IP (1995) The aetiology and distinguishing features of solitary spinal hot spots on planar bone scans. Clin Radiol 50:327 – 330
Coleman RE, Rubens RD (1987) The clinical course of bone metastases from breast cancer. Br J Cancer 55:61 – 66
Coleman RE, Rubens RD, Fogelman I (1988a) A reappraisal of the baseline bone scan in breast cancer. J Nucl Med 29: 1045 – 1049
Coleman RE, Mashiter G, Whitaker KB, Moss DW, Rubens RD, Fogelman I (1988b). Bone scan flare predicts successful systemic therapy for bone metastases. J Nucl Med 29:1354 – 1359
Collier BD, Carerra GF, Johnson RP, Isitman AT, Hellman RS, Knobel J, Finger WA, Gonyo JE, Malloy PJ (1985a) Detection of femoral head avascular necrosis in adults by SPECT. J Nucl Med 26:979 – 987
Collier BD, Johnson RP, Carrera GF, Isitman AT, Veluvolu P, Knobel J, Hellman RS, Barthelemy CR (1985b) Chronic knee pain assessed by SPECT: comparison with other modalities. Radiology 157:795 – 802
Collier BD, Johnson RP, Carrera GF, Meyer GA, Schwab JP, Flatley TJ, Isitman AT, Hellman RS, Zielonka JS, Knobel J (1985) Painful spondylolysis or spondylolisthesis studies by radiography and SPECT. Radiology 154:207 – 211
Cook GJR, Fogelman I (1996) Lateral collateral ligament tear of the knee: appearances on bone scintigraphy with SPECT. Eur J Nucl Med 23:720 – 722
Cook GJR, Fogelman I (2000) The role of positron emission tomography in the management of bone metastases. Cancer 88:2927 – 2933
Cook GJR, Fogelman I (2001) The role of positron emission tomography in skeletal disease. Semin Nucl Med 31:50 – 61
Cook GJR, Ryan PJ, Clarke SEM, Fogelman I (1996) Anterior cruciate ligament tear: findings on SPECT bone scintigraphy of the knee. J Nucl Med 37:1353 – 1356
Cook GJ, Houston S, Rubens R, Maisey MN, Fogelman I (1998) Detection of bone metastases in breast cancer by 18FDG PET: differing metabolic activity in osteoblastic and osteolytic lesions. J Clin Oncol 16:3375 – 3379
Cook GJR, Hannaford E, Lee M, Clarke SEM, Fogelman I (2002) The value of bone scintigraphy in the evaluation of osteoporotic patients with back pain. Scand J Rheumatol 31:245 – 248
Davis MA, Jones AL (1976) Comparison of 99mTc-labeled phosphate and phosphonate agents for skeletal imaging. Semin Nucl Med 6:19 – 31
Dearnaley DP (1994) Cancer of the prostate. Br Med J 308: 780 – 4
Desmet AA, Dalinka MK, Alazraki N, Berquist TH, Daffner RH, el-Khoury GY, Goergen TG, Keats TE, Manaster BJ, Newberg A, Pavlov H, Haralson RH 3rd, McCabe JB, Sartoris D (2000) Diagnostic imaging of avascular necrosis of the hip. American College of Radiology. ACR Appropriateness Criteria Radiology 215:247 – 254
Dolan AL, Ryan PJ, Arden NK, Stratton R, Wedley JR, Hamann W, Fogelman I, Gibson T (1996) The value of SPECT scans in identifying back pain likely to benefit from facet joint injection. Br J Rheumatol 35:1269 – 1273
Drubach LA, Connolly LP, D'Hemecourt PA, Treves ST (2001) Assessment of the clinical significance of asymptomatic lower extremity uptake abnormality in young athletes. J Nucl Med 42:209 – 12
Durie BG, Waxman AD, D'Agnolo A, Williams CM (2002) Whole-body (18)F-FDG PET identifies high-risk myeloma. J Nucl Med 43:1457 – 1463
Dutton JA, Hughes SP, Peters AM (2000) SPECT in the management of patients with back pain and spondylolysis. Clin Nucl Med 25:93 – 96
Elgazzar AH, Malki AA, Abdel-Dayem HM, Sahweil A, Razzak S, Jahan S, El-Sayed M, Omar YT (1989) Role of thallium-201 in the diagnosis of solitary bone lesions. Nucl Med Commun 10:477 – 485
Even-Sapir E, Metser U, Flusser G (2004) Assessment of malignant skeletal disease: initial experience with 18F-fluoride PET/CT and comparison between 18F-fluoride PET and 18F-fluoride PET/CT. J Nucl Med 45:272 – 8
Fawcett HD, McDougall IR (1980) Bone scan in extraskeletal neuroblastoma with hot primary and cold skeletal metastases. Clin Nucl Med 5:49 – 50
Fleming WH, McIraith JD, King ER (1961) Photoscanning of bone lesions utilising strontium-85. Radiology 77:635 – 636
Fogelman I (1982) Diphosphonate bone scanning agents – current concepts. Eur J Nucl Med 7:506 – 509
Fogelman I, Carr D (1980a) A comparison of bone scanning and radiology in the evaluation of patients with metabolic bone disease. Clin Radiol 31:321 – 326
Fogelman I, Carr D (1980b) A comparison of bone scanning and radiology in the assessment of patients with symptomatic Paget's disease. Eur J Nucl Med 5:417 – 421
Fogelman I, McKillop JH (1991) The bone scan in metastatic disease. In: Rubens RD, Fogelman I (eds) Bone metastases: diagnosis and treatment. Springer-Verlag, London, pp 31 – 35
Fogelman I, McKillop JH, Bessent RG, Boyle IT, Turner JG, Greig WR (1978) The role of bone scanning in osteomalacia. J Nucl Med 19:245 – 248
Fogelman I, Cook G, Israel O, Van der Wall H (2005) Positron emission tomography and bone metastases. Semin Nucl Med 35:135 – 42
Galasko CSB (1986) Incidence and distribution of skeletal metastases. In: Galasko CSB (ed) Skeletal metastases. Butterworth, London, pp 14 – 21
Galasko CSB, Weber DA (1984) Avascular necrosis. In: Galasko CSB, Weber DA (eds) Radionuclide scintigraphy in orthopaedics. Churchill Livingstone, Edinburgh, pp 200 – 209
Gates GF, McDonald RJ (1999) Bone SPECT of the back after lumbar surgery. Clin Nucl Med 24:395 – 403

Gayed I, Vu T, Johnson M, Macapinlac H, Podoloff D (2003) Comparison of bone and 2-deoxy-2-[18F]fluoro-D-glucose positron emission tomography in the evaluation of bony metastases in lung cancer. Mol Imaging Biol 5:26 – 31

Goldsmith DP, Vivino FB, Eichenfield AH, Athreya BH, Heyman S (1989) Nuclear imaging and clinical features of childhood reflex neurovascular dystrophy: comparison with adults. Arthritis Rheum 32(4):480 – 5

Gordon I, Peters AM, Gutman A, Morony S, Dicks-Mireaux C, Pritchard J (1990) Skeletal assessment in neuroblastoma – the pitfalls of iodine-123-MIBG scans. J Nucl Med 31:129 – 134

Gravenstein S, Peltz MA, Poreis W (1979) How ominous is an abnormal scan in bronchogenic carcinoma. JAMA 241: 2523 – 2524

Han LJ, Au-Yong TK, Tong WC, Chu KS, Szeto LT, Wong CP (1998) Comparison of bone SPECT and planar imaging in the detection of vertebral metastases in patients with back pain. Eur J Nucl Med 25:635 – 638

Hanly JG, Mitchell MJ, Barnes DC, MacMillan L (1994) Early recognition of sacroiliitis by MRI and SPECT. J Rheumatol 21:2088 – 2095

Hardoff R, Gips S, Uri N, Front A, Tamir A (1994) Semiquantitative skull planar and SPECT bone scintigraphy in diabetic patients: differentiation of necrotizing (malignant) external otitis from severe external otitis. J Nucl Med 35:411 – 415

Hofmann AA, Wyatt RWB, Daniels AU, Armstrong L, Alazraki N, Taylor A Jr (1990) Bone scan after total knee arthroplasty in asymptomatic patients. Clin Orthop 251:183 – 188

Holder LE, Michael RH (1984) The specific scintigraphic pattern of "shin splints in the lower leg": concise communication. J Nucl Med 25:865 – 869

Holder LE, Machin JL, Asdourian PL, et al. (1995) Planar and high resolution SPECT bone imaging in the diagnosis of facet syndrome. J Nucl Med 36:37 – 44

Howman-Giles R, Gilday DL, Ash JM (1979) Radionuclide skeletal survey in neuroblastoma. Radiology 131:497 – 502

Intenzo CM, Wapner KL, Park CH, Kim SM (1991) Evaluation of plantar fasciitis by three-phase bone scintigraphy. Clin Nucl Med 16:325 – 328

Kim EE, Bledin AG, Gutierrez C, Haynie TP (1983) Comparison of radionuclide images and radiographs for skeletal metastases from renal cell carcinoma. Oncology 40:284 – 286

Kim KY, Lee SH, Moon DH, Nah HY (1993) The diagnostic value of triple head SPECT in avascular necrosis of the femoral head. Int Orthop 17:132 – 138

Kosuda S, Kaji T, Yokoyama H, Yokokawa T, Katayama M, Iriye T, Uematsu M, Kusano S (1996) Does bone SPECT actually have lower sensitivity for detecting vertebral metastases than MRI? J Nucl Med 37:975 – 978

Kraznow AZ, Collier BD, Kneeland JB, Carrera GF, Ryan DE, Gingrass D, Sewall S, Hellman RS, Isitman AT, Froncisz W, et al. (1987) Comparison of high resolution MRI and SPECT bone scintigraphy for non-invasive imaging of the temporomandibular joint. J Nucl Med 28:1268 – 1274

Lam AS, Kettle AG, O'Doherty MJ, Coakley AJ, Barrington SF, Blower PJ (1997) Pentavalent 99Tcm-DMSA imaging in patients with bone metastases. Nucl Med Commun 18:907 – 914

Lee N, Fawaaz R, Olsson CA, Benson MC, Benson MC, Petrylak DP, Schiff PB, Bagiella E, Singh A, Ennis RD (2000) Which patients with newly diagnosed prostate cancer need a radionuclide bone scan? An analysis based on 631 patients. Int J Radiat Oncol Biol Phys 48:1443 – 6

Levenson RM, Sauerbrunn FJL, Ihde DC, Bunn PA, Cohen MH, Minna JD (1981) Small cell lung cancer: radionuclide bone scans for assessment of tumour extent and response. AJR 137:31 – 35

Levitsky KA, Hozack WJ, Balderston RA, Rothman RH, Gluckman SJ, Maslack MM, Booth RE, Jr (1991) Evaluation of the painful prosthetic joint: relative value of bone scan, sedimentation rate, and joint aspiration. J Arthroplasty 6:237 – 244

Lewis P, Griffin S, Marsden P, Gee T, Nunan T, Malsey M, Dusek J (1994) Whole body ^{18}F-fluorodeoxyglucose positron emission tomography in preoperative evaluation of lung cancer. Lancet I:1265 – 1266

Lonneux M, Borbath II, Berliere M, Kirkove C, Pauwels S (2000) The place of whole-body PET FDG for the diagnosis of distant recurrence of breast cancer. Clin Positron Imaging 3:45 – 49

Love C, Tomas MB, Marwin SE, Pugliese PV, Palestro CJ (2001) Role of nuclear medicine in diagnosis of the infected joint replacement. Radiographics 21:1229 – 1238

Love C, Din AS, Tomas MB, Kalapparambath TP, Palestro CJ (2003) Radionuclide bone imaging: an illustrative review. Radiographics 23:341 – 358

Lusins JO, Danielski EF, Goldsmith SJ (1989) Bone SPECT in patients with persistent back pain after lumbar spine surgery. J Nucl Med 30:490 – 496

Mari C, Catafau A, Carrio I (1999) Bone scintigraphy and metabolic bone disease. Semin Nucl Med 27:291 – 305

McBryde AM, Jr (1985) Stress fractures in athletes. Clin Sports Med 4:737 – 752

McKillop JH (1987) Bone scanning in metastatic disease. In: Fogelman I (ed) Bone scanning in clinical practice. Springer-Verlag, Berlin, pp 41 – 60

McKillop JH, Blumgart LH, Wood CB, Fogelman I, Furnival CM, Greig WR, Citrin DL (1978) The prognostic and therapeutic implications of the positive radionuclide bone scan in clinically early breast cancer. Br J Surg 65:649 – 652

Moog F, Kotzerke J, Reske SN (1999) FDG PET can replace bone scintigraphy in primary staging of malignant lymphoma. J Nucl Med 40:1407 – 1413

Morris MJ, Akhurst T, Osman I, Nunez R, Macapinlac H, Siedlecki K, Verbel D, Schwartz L, Larson SM, Scher HI (2002) Fluorinated deoxyglucose positron emission tomography imaging in progressive metastatic prostate cancer. Urology 59:913 – 918

Mountford PJ, Coakley AJ (1989) Role of technetium-99m phosphonate bone and indium-111 leukocyte scanning for detecting the infected hip prosthesis. J Nucl Med 30:562 – 563

Murray IPC (1998a) Bone scintigraphy in trauma. In: Murray IPC, Ell PJ (eds) Nuclear medicine in clinical diagnosis and treatment, 2nd edn. Churchill Livingstone, Edinburgh, pp 1241 – 1267

Murray IPC (1998b) Vascular manifestations. In: Murray IPC, Ell PJ (eds) Nuclear medicine in clinical diagnosis and treatment, 2nd edn. Churchill Livingstone, Edinburgh, pp 1223 – 1240

Murray IPC, Dixon J, Kohan L (1990) SPECT for acute knee pain. Clin Nucl Med 15:828 – 840

Narayan P (1995) Neoplasms of the prostate gland. In: Tanagho EA, McAninch JW (eds) Smith's general urology, 14 edn. Appleton and Lange, Norwalk, p 392

Ohta M, Tokuda Y, Suzuki Y, Kubota M, Makuuchi H, Tajima T, Nasu S, Suzuki Y, Yasuda S, Shohtsu A (2001) Whole body PET for the evaluation of bony metastases in patients with breast cancer: comparison with 99Tcm-MDP bone scintigraphy. Nucl Med Commun 22:875 – 879

O'Sullivan JM, Cook GJ (2002) A review of the efficacy of bone scanning in prostate and breast cancer. Q J Nucl Med 46:152 – 9

Oswald SG, Van Nostrand D, Savory CG, Anderson JH, Callaghan JJ (1989) Three-phase bone scan and indium white cell scintigraphy following porous coated hip arthroplasty: A prospective study of the prosthetic tip. J Nucl Med 30: 1321 – 1331

Oswald SG, Van Nostrand D, Savory CG, Anderson JH, Callaghan JJ (1990) The acetabulum: a prospective study of three-phase bone and indium white blood cell scintigraphy following porous-coated hip arthroplasty. J Nucl Med 31: 274 – 280

Palestro CJ (1994) Musculoskeletal infection. In: Freeman LM (ed) Nuclear medicine annual. Raven Press, New York, pp 91 – 119

Palestro CJ, Torres MA (1997) Radionuclide imaging in orthopedic infections. Semin Nucl Med 27:334 – 345

Palestro CJ, Kim CK, Swyer AJ, Capozzi JD, Solomon RW, Goldsmith SJ (1990) Total-hip arthroplasty: periprosthetic indium-111-labelled leukocyte activity and complementary technetium-99-m sulfur colloid imaging in suspected infection. J Nucl Med 31:1950 – 1955

Palestro CJ, Swyer AJ, Kim CK, Goldsmith SJ (1991) Infected knee prostheses: diagnosis with In-111 leukocyte, Tc-99m sulfur colloid, and Tc-99m MDP imaging. Radiology 179:645 – 648

Peters AM (1994) The utility of 99mTc-HMPAO-leukocytes for imaging infection. Semin Nucl Med 2:110 – 127

Podrasky AER, Stark DD, Hattner RS, Gooding GA, Moss AA (1983) Radionuclide bone scanning in neuroblastoma: skeletal metastases and primary tumour localisation of 99m-Tc MDP. AJR 141:469 – 472

Read MT (1994) SPECT scanning for adolescent back pain. A sine qua non? Br J Sports Med 28:56 – 57

Roland J, van den Weygaert D, Krug B, Brans B, Scalliet P, Vandevivere J (1995) Metastases seen on SPECT imaging despite a normal planar bone scan. Clin Nucl Med 20:1052 – 1054

Rosenthal L, Lepanto L, Raymond F (1987) Radiophosphate uptake in asymptomatic knee arthroplasty. J Nucl Med 28: 1546 – 1549

Rupani HD, Holder LE, Espinola DA, Engin SI (1985) Three-phase radionuclide bone imaging in sports medicine. Radiology 156:187 – 196

Ryan PJ, Fogelman I (1997) Bone scintigraphy in metabolic bone disease. Semin Nucl Med 27:291 – 305

Ryan PJ, Evans P, Gibson T, Fogelman I (1992a) Osteoporosis and chronic back pain: a study with SPECT bone scintigraphy. J Bone Miner Res 7:1455 – 1460

Ryan PJ, Evans PA, Gibson T, Fogelman I (1992b) Chronic low back pain: comparison of bone SPECT with radiography and CT. Radiology 182:849 – 854

Ryan PJ, Gibson T, Fogelman I (1992c) The identification of spinal pathology in chronic low back pain using SPECT. Nucl Med Commun 13:497 – 502

Ryan PJ, Taylor M, Grevitt M, et al. (1993) Bone single-photon emission tomography in recent meniscal tears: an assessment of diagnostic criteria. Eur J Nucl Med 20:703 – 707

Schirrmeister H, Guhlmann A, Elsner K, Kotzerke J, Glatting G, Rentschler M, Neumaier B, Trager H, Nussle K, Reske SN (1999a) Sensitivity in detecting osseous lesions depends on anatomic localization: planar bone scintigraphy versus 18F PET. J Nucl Med 40:1623 – 1629

Schirrmeister H, Guhlnamm A, Kotzerke J, Santjohanser C, Kuhn T, Kreienberg R, Messer P, Nussle K, Elsner K, Glatting G, Trager H, Neumaier B, Diederichs C, Reske SN (1999b) Early detection and accurate description of extent of metastatic bone disease in breast cancer with fluoride ion and positron emission tomography. J Clin Oncol 17:2381 – 2389

Schirrmeister H, Glatting G, Hetzel J, Nussle K, Arslandemir C, Buck AK, Dziuk K, Gabelmann A, Reske SN, Hetzel M (2001) Prospective evaluation of clinical value of planar bone scan, SPECT and ^{18}F-labeled NaF PET in newly diagnosed lung cancer. J Nucl Med 42:1800 – 1804

Schirrmeister H, Bommer M, Buck AK, Muller S, Messer P, Bunjes D, Dohner H, Bergmann L, Reske SN (2002) Initial results in the assessment of multiple myeloma using 18F-FDG PET. Eur J Nucl Med Mol Imaging 29:361 – 366

Seabold JE, Nepola JV (1999) Imaging techniques for evaluation of postoperative orthopedic infections. Q J Nucl Med 43(1):21 – 8

Sedonja I, Budihna NV (1999) The benefit of SPECT when added to planar scintigraphy in patients with bone metastases in the spine. Clin Nucl Med 24:407 – 413

Shreve PD, Grossman HB, Gross MD, Wahl RL (1996) Metastatic prostate cancer: initial findings of PET with 2-deoxy-2-[F-18]fluoro-D-glucose. Radiology 199:751 – 756

Siddiqui AR, Kopecky KK, Wellman HN, Park HM, Braunstein EM, Brandt KD, Klatte EC, Capello WN, Leapman SB, Filo RS (1993) Prospective study of MRI and SPECT bone scans in renal allograft recipients: evidence for self-limited subclinical abnormality of the hips. J Nucl Med 34:381 – 386

Slizofski WJ, Collier BD, Flately TJ, Carrera GF, Hellman RS, Isitman AT (1987) Painful pseudoarthrosis following lumbar spine fusion: detection by combined SPECT and planar bone scintigraphy. Skel Radiol 16:136 – 141

Strashun AM, Nejatheim M, Goldsmith SJ (1984) Malignant otitis externa; early scintigraphic detection. Radiology 150: 541 – 545

Stulberg BN, Levine M, Bauer TW, et al. (1989) Multimodality approach to osteonecrosis of the femoral head. Clin Orthop Rel Res 240:181 – 193

Stumpe KDM, Nötzli HP, Zanetti M, Kamel EM, Hany TF, Gorres GW, von Schulthess GK, Hodler J (2004) FDG PET for differentiation of infection and aseptic loosening in total hip replacements: comparison with conventional radiography and three-phase bone scintigraphy. Radiology 231:333 – 341

Subramanian G, McAfee JG (1971) A new complex of Tc-99m for skeletal imaging. Radiology 99:192 – 196

Subramanian G, McAfee JG, Bell EG, Belhobek GH, Pflanze W, Feiglin DH, Roth AI (1972) 99m Tc-labeled polyphosphate as a skeletal imaging agent. Radiology 102:701 – 4

Tofe AJ, Francis MD, Harvey WJ (1975) Correlation of neoplasms with incidence and localisation of skeletal metastases. An analysis of 1355 diphosphonate bone scans. J Nucl Med 16:986 – 989

Toni MG, Calderazzi A, Battolia L, De Gaudio C, Mita A (1992) SPECT in the study of pathology of the temporomandibular joint. The authors personal experience. Radiol Med 84:549 – 552

Tumeh SS, Beadle G, Kaplan WD (1985) Clinical significance of solitary rib lesions in patients with extraskeletal malignancy. J Nucl Med 26:1140 – 1143

Turpin S, Taillefer R, Lambert R, Leveille J (1996) Cold" reflex sympathetic dystrophy in an adult. Clin Nucl Med 21:94 – 7

Utz JA, Lull RJ, Galvin EG (1986) Asymptomatic total hip prosthesis: natural history determined using Tc-MDP bone scans. Radiology 161:509 – 512

Warburg O (1954) On the origin of cancer cells. Science 123: 306 – 314

Wilder RP, Sethi S (2004) Overuse injuries: tendinopathies, stress fractures, compartment syndrome, and shin splints. Clin Sports Med 23:55 – 81

Williamson BR, McLaughlin RE, Wang GW, Miller CW, Teates CD, Bray ST (1979) Radionuclide bone imaging as a means of differentiating loosening and infection in patients with a painful total hip prosthesis. Radiology 133:723 – 725

Yamamoto T, Seino Y, Fukumoto H, Koh G, Yano H, Inagaki N, Yamada Y, Inoue K, Manabe T, Imura H (1990) Over-expression of facilitative glucose transporter genes in human cancer. Biochem Biophys Res Commun 170:223 – 230

Zelefsky MJ, Leibel SA, Kutcher GJ, Kelson S, Ling CC, Fuks Z (1995) The feasibility of dose escalation with three-dimensional conformal radiotherapy in patients with prostatic carcinoma. Cancer J Sci Am 1:142

Malignant Melanoma and Soft Tissue Sarcomas 11

C. Menzel, H. Palmedo, F. Grünwald, H.-J. Biersack

11.1 Malignant Melanoma

Malignant melanoma (MM) of the skin has increased dramatically throughout the world during recent years. The overall increase in incidence has been dominated by new cases in the developed countries, with most patients being diagnosed in North America and Western Europe and, relative to population size, a large number of cases in Australia and New Zealand. While it is obvious that a combination of light-colored populations and increasing exposure to ultraviolet radiation has led to an increased risk of the development of malignant melanomas, it remains largely unknown in detail which factors are responsible for the transformation of a rarely proliferating melanocyte into a highly aggressive, often fatal tumor. Recently it has been shown that surface anomalies on the melanoma cells are responsible for a loosely bound architecture of tumor clones, leading to the easy development of metastatic disease. For these reasons there is an increasing need for advanced diagnostic strategies and new therapy modalities.

11.1.1 Introduction

The clinical spectrum of malignant melanoma includes any combination of a variety of features including variations of color, irregular surface, irregular perimeter, bleeding and ulceration. These lesions may sometimes be difficult to diagnose due to their, e.g., small size and difficult localization. A good way to further classify these tumors is to follow their growth patterns.

11.1.1.1 Superficial Malignant Melanoma

Superficial malignant melanoma (SMM) represents by far the majority of cases (>70%). In general, there is normally a history of a preexisting nevus at the locus of the primary MM. This nevus – the so-called precursor lesion – often shows a longer history (years) of slow changes in color, color pattern or size – with a more aggressive change in the time immediately (weeks) prior to the final diagnosis. During the early phase of SMM these lesions may show patches of amelanotic regression. Showing irregular margins, the lesion generally remains flat. With time vertical growth may dominate and also lead to an irregular surface.

11.1.1.2 Nodular Malignant Melanoma

Nodular malignant melanoma (NMM) represents about one-third of all MMs. They commonly evolve from previously unaffected skin, rather than developing out of a preexisting nevus. Their growth rate and further course is more aggressive than SMM. Clinically they present with a mostly darker color, more homogeneously distributed and with a nodular, elevated shape.

11.1.1.3 Lentigo Maligna Melanomas

Due to their different growth patterns, lentigo maligna melanomas (LMMs) appear to represent a third entity of MM. They are mostly tumors of elderly patients who show up with a history of very long preexistence (up to 10–15 years) of a lesion, often located facially. Lesions are typically tan with different shades of brown and black.

Screening for melanomas seems to be of benefit, if the relatively long phase of slow, mostly radial growth of MM is taken into account. This phase is thought to last at least months or years in a considerable number of patients, making yearly screening an option. Screening also offers the option of resection of precursor lesions, so called dysplastic nevi, for which there is a particular suspicion of them developing into full MM in patients with a history of previous MM located elsewhere. Tumor thickness is the factor limiting the patient's prognosis. Table 11.1 gives an overview of the AJCC staging system for MM.

Table 11.1. AJCC staging system for malignant melanoma

Stage	Characterization
IA	Localized melanoma 0.75 mm or level II (T1N0M0)
IB	Localized melanoma 0.76 – 1.5 mm or level III (T2N0M0)
IIA	Localized melanoma 1.5 – 4.0 mm or level IV (T3N0M0)
IIB	Localized melanoma > 4.0 mm or level IV (T4N0M0)
III	Limited nodal metastases involving only 1 lymph node region or less than 5 in-transit metastases without lymph node metastases
IV	Advanced regional metastases (any T, N2M0) or distant metastases (any T, any N, M1 or M2)

11.1.2 Radiopharmaceuticals

Conventional nuclear medicine imaging does not really offer competitive strategies for the staging and therapy control of advanced MM. This does not hold true of course for the superior characterization of a sentinel lymph node done with radioisotopes. In the late 1980s and early 1990s there were some approaches with technetium-99m-labeled antibodies directed against melanoma surface antigens. These, however, were not really a success. Other imaging modalities include scintigraphy with ^{99m}Te-labeled biphosphonates for detection of bone metastases, the use of tumor-seeking tracers such as thallium-201 and the receptor-ligand ^{123}I-iodobenzamide. The latter has not increased diagnostic accuracy compared to conventional nuclear medicine techniques while the tumor-seeking conventional tracers were found to be clearly inferior to FDG-PET.

Several radiopharmaceuticals suitable for PET imaging have been investigated for MM. FDG is by far the best evaluated tracer in this indication. Its unique abilities in taking advantage of the tumor metabolism itself have already been described elsewhere in this book; however, it is noteworthy that MM in particular are aggressive tumors with one of the highest glucose metabolisms. This allows FDG-PET to image metastatic disease at very small morphological sizes. The cellular uptake in MM cells has recently been studied in detail by Yamada and coworkers. They found FDG not only to be related to multi-drug resistance gene expression in MM but further to be immediately influenced by the hexokinase activity in the cells. In contrast, no correlation between FDG uptake and the expression of the glucose transporter GLUT 1 was found.

11.1.3 Methodology

Malignant melanoma is one of the tumors with the most unpredictable distribution throughout the body. Virtually any combination of metastatic disease can be found, ranging from a single metastasis in a locoregional lymph node, to dozens of metastases within one parenchymal organ (e.g., liver) without any evidence of other tumor sites, to hundreds of metastases distributed throughout the whole body. Thus, in MM it is particularly important to conduct whole body imaging and not trunk imaging only, which is the widely accepted compromise for most other tumors being imaged by PET.

While stand alone PET with FDG is definitely unsuitable to rule out brain metastases, the high uptake of MM still makes it a useful approach to at least include the brain in a scan sequence. This is also important to include viscerocranial structures in the scan. To rule out small metastases within the brain, MR imaging remains the standard. For PET-CT it still remains to be shown that the combined information is equally valuable to brain MRI in this indication. Given these thoughts, it is obvious to further include the complete lower extremities in the scan. Using conventional PET it is justified to do emission scans of the lower extremities only in order to keep the total scan time within tolerable limits for the patient. It is generally accepted to start the PET scan about 45 – 60 min after i.v. injection of a body weight adjusted amount of FDG. Normally the scan should start at the pelvis or upper thigh to avoid too much activity within the bladder during the scan itself. This scan should be done up to the vertex. Transmission (T) and emission (E) scans are done for, e.g., 8 min (T) and 5 min (E) per bed position, e.g., using a TEETTEET sequence.

If PET-CT is available, the scan protocol is modified. Normally the scan would be initiated with an investigation of the trunk starting with the pelvis or upper thigh and moving upwards to the throat with the arms raised. Emission scans of, e.g., 3 – 5 min per bed position, would be preceded by CT scans after oral and intravenous contrast enhancement. Care should be taken here to use contrast media of medium density only to avoid unnecessary artifact in the emission scan due to attenuation caused by the contrast media itself. This scan is then followed by a second investigation of the head and neck region (with arms next to the body) and, if necessary, followed by a scan of the legs. The CT scans are acquired during breath hold within the normal expiration position to allow exact fusion of CT and PET images. Table 11.2 gives an overview of the scan protocols of PET and PET-CT.

11.1.4 Clinical Indications (Including Pitfalls and Variations)

FDG-PET is unsuitable for the early detection of malignant melanoma primaries in the skin. This method will miss most primary tumors due to their limited size,

Table 11.2. Examples of scanning protocols for PET and PET-CT

	PET Brain	PET-CT Trunk	Legs	Brain	Trunk	Legs
Activity (MBq)	4.0 MBq/kg (370 MBq max.)	4.0 MBq/kg (370 MBq max.)				
Latency[a]	45 – 60 min	45 – 60 min				
Scan sequence	1st		2nd	2nd	1st	3rd
Start	1st pelvis upwards to vertex (T+E) 2nd legs downwards (E only)	1st: pelvis upwards to throat[b] incl. CE 2nd: head and throat[c] 3rd: legs downwards				
Scan duration	60 – 80 min		20 min	10	30	20 min
Total scan time	80 – 100 min	60 min				

[a] Between injection and scan start, [b] Arms raised, CE: i.v. and oral contrast enhancement, [c] Arms down

and occult lymph node metastases are often missed too. Therefore FDG-PET cannot be substituted for isotope guided sentinel lymph node biopsy. Therefore, FDG-PET is not recommended in clinical stages I and II of melanoma. Wagner et al. and Belhocine et al. both demonstrated that subclinical micrometastatic disease was only detected in about 15 % of cases. Comparisons of these findings are always limited by the different nature of the methods that are evaluated. PET and SLN biopsy have a completely different approach towards the pathology. While PET directly targets tumor metabolism, SLN biopsy focuses on a certain structure which may or may not be affected by metastatic disease. Both have their advantages and limitations. For example, in the case of severe metastatic involvement of the SLN, lymphatic drainage could be misdirected to a histopathologically still normal non-SLN. PET would not have misinterpreted this case. In contrast, PET is certainly not able to detect microscopic metastases. Although PET thus should not employed as a routine investigation here, it may well reveal relevant information in selected cases in early stage MM too.

Normally, however, stage I or II melanoma is not considered a routine application for PET using FDG. Small primary tumors as well as micrometastatic involvement of the sentinel lymph node are likely not detected due to its small volume (Wagner et al. 2001). Whilst the specificity of PET is generally good, tumor volumes below 80 cm^3 are detected with rapidly decreasing sensitivity.

In stage III melanomas, PET gains an increasingly greater clinical importance with the advance of the tumor burden within the patient. Crippa et al. studied PET results with a focus on lymph node metastases. The overall efficacy of FDG-PET in the diagnosis of involved lymph nodes was also good. Sensitivity was 95 %, specificity 84 %, accuracy 91 %, positive predictive value 92 %, and negative predictive value 89 % (16/18). Metastases were shown histologically in 114 of 647 surgically removed lymph nodes. FDG-PET detected 100 % of metastases of 10 mm or more in diameter, 83 % of metastases between 6 and 10 mm, but only 23 % of metastases of 5 mm or less in diameter. On a lesion-by-lesion analysis, Harris et al. (2005) found FDG-PET had a sensitivity of 92 %, a specificity of 88 %, and an accuracy of 91 %. PET in particular correctly influenced the clinical decision-making process in 40 of 126 patient studies (32 %), particularly assisting in the selection of patients for surgery.

The overall prognosis of advanced stage or recurrent melanoma is poor. The median survival of metastatic melanoma is about 6 – 9 months. However, gaining local control by tumor surgery is highly recommended in non-cerebral, well accessible metastases and the combination of surgery and interleucin-2-based immunotherapy may even achieve durable complete remissions in a number of patients. Thus an exact staging algorithm is essential for these patients and FDG-PET is known to improve the quality of this staging. For example, compared to a full battery of conventional structural imaging (CT/MRI), PET still seems to be of higher sensitivity and specificity for the detection of advanced stage or recurrent malignant melanoma. In a recent study by Finkelstein et al., a single FDG-PET scan was found to be slightly more precise than the different scans applied by conventional imaging modalities. Furthermore, the combined use of structural and functional imaging allowed an even better detection of metastatic sites (sensitivity 88 %, specificity 91 %, positive predictive value 91 %, negative predictive value 88 %).

The pitfalls of PET have recently been described in detail by Abouzied and coworkers. They showed a number of situations in which a physiological or a pathological, yet not malignancy related, hot-spot may confuse or compromise a proper evaluation of a PET scan done for MM staging. Missing an otherwise positive metastatic lesion often occurs if these lesions are small in size and within the vicinity of structures that typically take up high amounts of FDG such as the brain and at times the myocardium. Especially with regard to a potentially cerebral metastasis, it has to be remembered that PET with FDG is unsuitable for ruling

out cerebral metastatic disease. However, the brain should routinely remain a part of the evaluation of patients suffering from melanoma since larger metastases are often detected as well and viscerocranial disease is better detected by PET.

11.1.5 FDG-PET Versus Conventional Radiological Imaging

It is well known for a number of tumors that PET imaging with FDG is clearly superior to the complete test battery of conventional radiological imaging. The performance radiology relies on two dominant parameters; these are the size of a lesion and its contrast (enhancement) compared to surrounding structures. FDG-PET relies on contrast due to glucose-transporter mediated uptake, and FDG in particular leads to a high tumor uptake in relation to a low uptake of surrounding tissue. PET is less influenced by size, namely small subcentimeter lesions can easily be detected and – at times – large tumors with slow proliferation rate may be missed. For these reasons, FDG-PET is superior to conventional imaging in all regions of the body except for the detection of tiny lung metastases (here CT takes full advantage of its superior resolution while it is not negatively influenced by dense tissue) and except for the detection of small brain metastases (here MRI shows its superior ability in characterizing proton-density differences while PET is negatively influenced by the high physiological FDG uptake of the brain).

In all other regions of the body, especially the viscerocranium, the neck and mediastinum, the axillae and extremities, the abdomen and pelvis and the bone marrow, FDG-PET has proven to be superior to conventional imaging as long as the indication targets a tumor with a significant density of glucose transporter proteins and thus a high metabolic rate. This holds true for a large number of malignancies described elsewhere in this book, especially including the melanomas.

11.1.6 Future Developments

Future developments in staging and restaging of melanomas are focusing on increasing the diagnostic accuracy of non-invasive imaging. In terms of PET this is leading to the development of more specific radiopharmaceuticals, and attention has been drawn to the application of metabolites of melanin synthesis. Melanin is the polymerized form of indole-5,6-chinone, which itself is a molecule formed from DOPA and the amino acids tyrosine/phenylalanine, respectively. These compounds, being attached to positron emitters, are becoming increasingly available. Initial investigations using iodine-123 α-methyltyrosine (123IMT) have shown specific uptake in melanocytes. 123IMT has shown low sensitivity in initial patient studies. Thus its clinical use has never been recommended (Boni et al. 1997). In contrast, first results using ^{18}F-DOPA and DOPA-related compounds may show better results in the future (Mishima et al. 1997).

Recently, McQuade et al. published results of PET imaging with ^{64}Cu- and ^{86}Y-DOTA-ReCCMSH(Arg11) for an early detection of melanoma. They used a cyclized peptide analogue of α-MSH (melanocyte stimulation hormone) and concluded from animal experiments that this approach could have the potential to become a tracer also for the early stages of MM.

11.2 Soft Tissue Tumors

Soft tissue tumors comprise a variety of benign and malignant lesions which are – for a number of reasons – difficult to measure regarding their incidence. This is due to the fact that most "soft" tumors of the skin remain either in loco or undergo unbiopsied resection. The overwhelming number of lesions (>99%) are of benign histological differentiation. These lesions often arise after a trauma or injury. Focusing on malignant lesions, there may be a history of exposure to carcinogens or radiation of the affected area. It should be kept in mind – however – that the patient's history, as well as the growth rate of the lesion, is generally nonspecific regarding the lesion's aggressiveness.

Neoplasms of mesenchymal tissues represent not only a proliferation of fibroblasts and the formation of collagen, they also often show cells with features typical for histiocytes. Neoplasms of fibrous tissue are mostly solitary tumors with collagen excess. The nodular fasciitis is included in this subgroup of benign tumors with collagen excess and patchy perivascular infiltrations. The term fibromatosis describes roughly the same histological pattern but indicates the often multifocal aspect of this disease. These nodules are difficult to distinguish from surrounding tissue and often show a benign local tumor growth. However, a locally aggressive, destructive growth may evolve. Fibrosarcomas, in contrast, show high cellularity and fewer fibers.

Benign lipomas, by far the most frequent tumor of mesenchymal tissue, consist entirely of mature fat cells. Liposarcomas vary from this pattern to an extent that reflects their differentiation. While highly differentiated liposarcomas are almost of identical structure to lipomas and are of good prognosis, dedifferentiated liposarcomas at times may show only few fat cells associated with an aggressive biological behavior, locally destructive growth and rapid evolvement of metastases. Tumors of other soft tissues have a similar systematology. Benign leiomyomas and – in the case of connective tissue involvement – leiomyofibromas show a fully ma-

ture cellular pattern with or without central necrosis or calcifications. The malignant variants of the leiomyosarcomas may show any degree of dedifferentiation, a consequent increase in cellularity and mitotic activity and a consequently aggressive biology. Rhabdomyomas/rhabdomyosarcomas and tumors of the vascular tissue (angiomas/angiosarcomas) have a similar systematology.

11.2.1 Introduction

Soft tissue tumors can be benign, malignant or intermediate, and it is important to consider age, sex and location of the lesion found as well as the patient's history so as to apply the appropriate imaging strategy. An overview of the most frequent types of lesions is given in Tables 11.3 and 11.4.

While ultrasound is generally involved in the majority of superficial lesions, any detailed investigation of – especially deeply located – lesions is the domain of MRI. With MRI a morphological characterization of the lesion and its relations to surrounding tissues can be done with superior quality. It must, however, be kept in mind that signal characteristics differ largely and in general there is no differentiation of benign and malignant lesions possible with MRI.

Conventional nuclear medicine has been applied with soft tissue tumors for decades now and has an established role especially in those tumors arising from the bone tissue. Using three phase bone scans, the tumor perfusion, vascularity and calcification can be investigated as well as the reaction of the surrounding bone. At times, even parenchymal metastases from these tumors may be detected using bone scintigraphy, e.g., lung metastases of osteosarcoma. Although a number of such uptake phenomena have been described over the years, this finding remains rare and limited to those tumors which may show signs of calcification.

A different approach is that of so called tumor scintigraphy employing tracers that detect tumors due to their metabolic activity. Gallium-67 citrate and thallium-201 chloride have been used for decades now. In recent years these tracers have been substituted by substances of the technetium-99m sestamibi "family," which apply high photon flux, necessary for good imaging quality and a lower radiation burden in addition to favorable pharmaceutical characteristics. These substances have shown to be of benefit in soft tissue tumors, especially in situations in which there is a PET scan unavailable.

11.2.2 Radiopharmaceuticals and Indications

11.2.2.1 PET Studies

Due to the large number of different lesions and gradings, there remains a considerable lack of large, well designed trials to define the relative additional contributions of PET to the primary diagnosis, the therapy control and the follow-up of these tumors. However, the current literature has shown that PET with FDG is useful for various indications.

Taking the various limitations of conventional structural imaging into account, PET is very useful in the differentiation of malignant from benign tissue. This is especially so in the situation of tumor recurrence after multimodal therapy. In a large study by Schulte et al., more than 100 soft tissue lesions were evaluated. After biopsy, these lesions could be classified into malignant (e.g., 39 high-grade sarcomas) and benign (e.g., 36 benign or tumorlike lesions). Interestingly, most lesions showed at least some FDG uptake. Schulte used a tumor-to-background-ratio (TBR) of 3 or more to define malignancy. Those TBRs below 1.5 were considered benign. The sensitivity of FDG-PET was 97 % and the specificity was 65.7 %. Most high-TBR lesions were found to be sarcomas. Only aggressive benign tumors had a similarly high FDG uptake. It seems that only lipomas show no considerable uptake, while a moderate FDG uptake may either be due to a benign lesion or represent low-grade sarcomas. In general, however, FDG uptake will correlate to the grade of malignancy as has been confirmed in a number of mainly smaller studies. This is important as it leads to the consequence that PET should guide the biopsy to the tumor area of probably highest malignancy. In addition, it was shown that FDG uptake reflects the grade of malignancy regardless of the cellular origin of the soft tissue tumor. Nieweg et al., for example, found no differences in tumor uptake in various types of soft tissue sarcoma.

Schwarzbach et al. recently confirmed these findings, now using the more accepted standard uptake value (SUV) for relative grading of different soft tissue sarcomas. PET proved a prognostic parameter after surgical resection of the sarcomas. According to the increase in SUV, PET could predict overall survival, recurrence-free survival, and local tumor control.

Another application of FDG-PET in soft tissue tumors is for the follow-up of patients during a therapy regimen in order to differentiate responders from non-responders at an early stage. Several studies have been conducted in this regard. Jones et al. (1996) studied different neoadjuvant therapy concepts with PET and correlated findings to histopathological results. In neoadjuvant therapies consisting of radiotherapy and hyper-

Table 11.3. Frequent benign soft tissue tumors by anatomic location and age (from Kransdorf 1995a, b)

Age (years)	Hand/wrist		Arms		Axilla/shoulder		Foot/ankle		Legs		Hip, groin, buttocks		Head and neck		Trunk		Retroperitoneum	
0–5	Hemangioma	15%	Fibrous hamartoma of infancy	16%	Fibrous hamartoma of infancy	29%	Granuloma annulare	30%	Granuloma annulare	23%	Fibrous hamartoma of infancy	20%	Nodular fasciitis	20%	Hemangioma	18%	Lipoblastoma	37%
6–15	Fibrous histiocytoma	14%	Fibrous histiocytoma	23%	Fibrous histiocytoma	34%	Fibromatosis	23%	Hemangioma	22%	Nodular fasciitis	27%	Nodular fasciitis	33%	Nodular fasciitis	28%	Lymphangioma	37%
16–25	GCTTS	20%	Nodular fasciitis	35%	Fibrous histiocytoma	36%	Fibromatosis	22%	Fibrous histiocytoma	24%	Neurofibroma	16%	Nodular fasciitis	21%	Nodular fasciitis	24%	Fibromatosis	20%
26–45	Fibrous histiocytoma	18%	Nodular fasciitis	38%	Lipoma	28%	Fibromatosis	21%	Fibrous histiocytoma	25%	Lipoma	17%	Lipoma	29%	Lipoma	19%	Schwannoma	23%
46–65	GCTTS	23%	Nodular fasciitis	20%	Lipoma	58%	Fibromatosis	25%	Lipoma	23%	Lipoma	35%	Lipoma	46%	Lipoma	44%	Schwannoma	19%
>66	GCTTS	21%	Lipoma	22%	Lipoma	58%	Fibromatosis	14%	Lipoma	26%	Lipoma	21%	Lipoma	50%	Lipoma	42%	Schwannoma	26%

GCTTS giant cell tumor of tendon sheath

Table 11.4. Frequent malignant soft tissue tumors by anatomic location and age (from Kransdorf 1995a, b)

Age (years)	Hand/wrist		Arms		Axilla/shoulder		Foot/ankle		Legs		Hip, groin, buttocks		Head and neck		Trunk		Retroperitoneum	
0–5	Fibrosarcoma	45%	Fibrosarcoma	29%	Fibrosarcoma	56%	Fibrosarcoma	45%	Fibrosarcoma	45%	Fibrosarcoma	32%	Fibrosarcoma	37%	Fibrosarcoma	26%	Fibrosarcoma	20%
6–15	Epithelioid sarcoma	21%	Angiomatoid MFH	33%	Angiomatoid MFH	21%	Synovial sarcoma	21%	Synovial sarcoma	22%	Angiomatoid MFH	21%	Rhabdomyosarcoma	26%	Angiomatoid MFH	15%	Rhabdomyosarcoma	31%
16–25	Epithelioid sarcoma	29%	Synovial sarcoma	23%	Synovial sarcoma	18%	Synovial sarcoma	30%	Synovial sarcoma	22%	Synovial sarcoma	18%	MFH	19%	DFSP	23%	Fibromatosis	20%
26–45	MFH	18%	MFH	28%	DFSP	33%	Synovial sarcoma	26%	Liposarcoma	28%	Liposarcoma	18%	MFH	30%	DFSP	30%	Leiomyosarcoma	32%
46–65	MFH	19%	MFH	46%	MFH	35%	MFH	25%	MFH	43%	Liposarcoma	24%	DFSP	28%	MFH	31%	Liposarcoma	33%
>66	MFH	35%	MFH	60%	MFH	50%	Karposi's sarcoma	37%	MFH	55%	MFH	46%	MFH	34%	MFH	44%	Liposarcoma	39%

MFH malignant fibrous histiocytoma, *DFSP* dermatofibrosarcoma protuberans

thermia, they found circumscript regions of reduced uptake within the FDG.

Schütze et al. also evaluated response to neoadjuvant therapy. Patients with a baseline tumor $SUV_{max} \geq 6$ and < 40 % decrease in FDG uptake were at high risk of systemic disease recurrence estimated to be 90 % at 4 years from the time of initial diagnosis. Patients whose tumors had a ≥ 40 % decline in the SUV_{max} in response to chemotherapy were at a significantly lower risk of recurrent disease and death after complete resection and adjuvant radiotherapy.

Non-FDG based PET studies in sarcomas are rare. Some studies with ^{11}C-methionine have been conducted which demonstrated no additional value over FDG. Korkmaz et al. reported a sensitivity/specificity of 77 %/87 % for ^{11}C-methionine compared to 93 %/97 % for FDG.

11.2.2.2 Conventional Nuclear Medicine

Prior to the availability of PET, a number of radiopharmaceuticals for scintigraphy and SPECT have been evaluated. The most widely used substances are phosphate compounds to detect or rule out bone involvement. It was suggested that their uptake also correlates with tumor perfusion and microscopic calcifications. These findings have not played a relevant role in the diagnostic work-up of soft tissue sarcomas. However, it should be kept in mind that a variety of benign and malignant tumors of the soft tissues may eventually show some uptake in bone scans. Metastatic disease to the bones is rare. Chew et al. found only five patients with bone metastases in a cohort of 80 soft tissue sarcoma patients. While routine screening for bone metastases is thus avoidable, the role of phosphate compounds remains to demonstrate the relationship of the soft tissue tumor mass and the bone structures in the immediate vicinity of the primary lesion. If the tumor affects the bone normally, an increased uptake can be expected. Sometimes, however, aggressive tumors may also penetrate and destroy the bone without the induction of an increased uptake.

Other authors investigated tumor seeking compounds, mainly Tc-99m-sestamibi and thallium-201. Both radiopharmaceuticals mainly reflect tumor activity: thallium-201 by its similarity to potassium, Tc-99m sestamibi by its affinity to mitochondrial membranes. The latter has been evaluated in more detail due to its superior imaging characteristics and its lower radiation exposure. Tc-99m sestamibi vascular influx may be measured and used to study tumor vascularity; its uptake reflects tumor activity/viability and – most interestingly today – it was shown that this substance is a good indicator of multi-drug resistance (MDR). Both in vitro and in vivo studies have shown that Tc-99m sestamibi is washed out of tumor cells in close relation to the expression of the MDR1 gene. Thus decreased uptake due to increased, active efflux of Tc-99m sestamibi allows the imaging of a process that affects the washout of cytostatic drugs. In this light, Tc-99m setamibi must be inferior with regard to tumor detection when compared with FDG-PET. In a study of 48 patients, Garcia et al. found the sensitivities and specificities to be 82 %/80 % for sestamibi and 98 %/90 % for FDG-PET. Sestamibi failed to localize nine tumors which were FDG positive; four of them showed multi-drug resistance.

11.2.3 Methodology

Imaging soft tissue sarcomas with FDG-PET does not differ from its application in other malignancies.

11.2.4 Pitfalls and Variations

A general problem with the soft tissue tumor is its overall great heterogeneity compared to other tumor entities. For this reason, the results published for FDG-PET vary in relation to the cohort investigated. Low grade soft tissue tumors may be missed by PET and this must be kept in mind. Other aspects which influence the results and capabilities of PET using FDG remain the same as have been described in other chapters of this book, namely uptake due to benign functional activations or inflammation. If PET is used to monitor therapy, this may also be a problem since it has been shown that there may remain some tumor uptake even in the situation of full tumor response to therapy. In these patients a – generally faint – uptake may remain within the vicinity of the tumor. Biopsies have shown that this phenomenon is related to the formation of benign fibrous tissue (Jones et al. 1996).

11.2.5 FDG-PET Versus Conventional Radiological Imaging

PET with FDG is equally sensitive in the detection of local recurrences compared to MRI, but provides a much better specificity. Especially in soft tissues, MRI has a great impact in the clear documentation of normal and abnormal morphology. However, local surgery, radiation therapy or chemotherapy often alter morphology significantly. This leads to a clearly reduced specificity for MRI which is confused by regenerative processes unrelated to a tumor recurrence. In a larger series, Korkmatz et al. (1993) demonstrated that PET and MRI/CT had a similar sensitivity (93 % each) for the detection of a tumor recurrence while PET showed a significantly better specificity (97 % PET vs. 70 % MRI/CT). Interestingly, in the same cohort the additional use of ^{11}C-methionine added no further information.

References

Abouzied MM, Crawford ES, Nabi HA (2005) 18F-FDG imaging: pitfalls and artifacts. J Nucl Med Technol 33(3):145 – 55

Bastiaannet E, Oyen WJ, Meijer S, Hoekstra OS, Wobbes T, Jager PL, Hoekstra HJ (2006) Impact of [18F]fluorodeoxyglucose positron emission tomography on surgical management of melanoma patients. Br J Surg 93(2):243 – 9

Belhocine T, Pierard G, Brassinne de la M, Lehaye T, Rigo P (2002) Staging of regional node in AJCC stage I and II melanoma. 18FDG imaging versus sentinel node detection. Oncologist 7(4):271 – 8

Boni R, Steinert H, Huch Boni R, Von Schulthess GK, Meyer J, Dummer R, Burg G, Westera G (1997) Radioiodine-labelled alpha-methyl-tyrosine in malignant melanoma: cell culture studies and results in patients. Br J Dermatol 137(1):96 – 100

Brenner W, Klomp HJ, Bohuslavizki KH, Szonn B, Kampen WU, Henze E (1999) Limited sensitivity of iodine-123 – 2-hydroxy-3-iodo-6-methoxy-N-[(1-ethyl-2-pyrrolidinyl)methyl] benzamide whole-body scintigraphy in patients with malignant melanoma: a comparison with thallium-201 imaging. Eur J Nucl Med 26(12):1567 – 71

Chew FS, Hudson TM, Enneking WF (1981) Imaging of soft tissue neoplasms. Semin Nucl Med 11(4):266 – 76

Crippa F, Leutner M, Belli F, Gallino F, Greco M, Pilotti S, Cascinelli N, Bombardieri E (2000) Which kinds of lymph node metastases can FDG PET detect? A clinical study in melanoma. J Nucl Med 41(9):1491 – 4

Finkelstein SE, Carrasquillo JA, Hoffman JM, Galen B, Choyke P, White DE, Rosenberg SA, Sherry RM (2004) A prospective analysis of positron emission tomography and conventional imaging for detection of stage IV metastatic melanoma in patients undergoing metastasectomy. Ann Surg Oncol 11(8): 731 – 8

Garcia R, Kim EE, Wong FC, Korkmaz M, Wong WH, Yang D, Podoloff DA (1996) Comparison of fluorine-18-FDG PET and technetium-99m-MIBI SPECT in evaluation of musculoskeletal sarcomas. J Nucl Med 37(9):1476 – 9

Ghanem N, Altehoefer C, Hogerle S, Nitzsche E, Lohrmann C, Schafer O, Kotter E, Langer M (2005) Detectability of liver metastases in malignant melanoma: prospective comparison of magnetic resonance imaging and positron emission tomography. Eur J Radiol 54(2):264 – 70

Harris MT, Berlangieri SU, Cebon JS, Davis ID, Scott AM (2005) Impact of 2-deoxy-2[F-18]fluoro-D-glucose positron emission tomography on the management of patients with advanced melanoma. Mol Imaging Biol 23:1 – 5

Jones DN, McCowage GB, Sostman HD, Bizel DM, Layfield L, Charles HC, Dewhirst M, Prescott DM, Friedman HS, Harrelson JM, Scully SP, Coleman RE (1996) Monitoring of neoadjuvant chemotherapy response of soft-tissue sarcoma using fluorine-18-FDG PET. J Nucl Med 37:1438 – 1444

Korkmaz M, Kim EE, Wong F, Haynie T, Wong WH, Tilbury R, Benjamin R (1993) FDG and methionine PET in differentiation of recurrent or residual musculoskeletal sarcomas from posttherapy changes. J Nucl Med 34:33P

Kransdorf MJ (1995a) Benign soft-tissue tumors in a large referral population: distribution of specific diagnoses by age, sex, and location. AJR Am J Roentgenol 164(2):395 – 402

Kransdorf MJ (1995b) Malignant soft-tissue tumors in a large referral population: distribution of diagnoses by age, sex, and location. AJR Am J Roentgenol 164(1):129 – 34

Larisch R, Schulte KW, Vosberg H, Ruzicka T, Muller-Gartner HW (1998) Accumulation of iodine-123-iodobenzamide in melanotic and amelanotic melanoma metastases in vivo. J Nucl Med 39(6):996 – 1001

McQuade P, Miao Y, Yoo J, Quinn TP, Welch MJ, Lewis JS (2005) Links imaging of melanoma using 64Cu- and 86Y-DOTA-ReCCMSH(Arg11), a cyclized peptide analogue of alpha-MSH. J Med Chem 48(8):2985 – 92

Mishima Y, Imahori Y, Honda C, Hiratsuka J, Ueda S, Ido T (1997) In vivo diagnosis of human malignant melanoma with positron emission tomography using specific melanoma-seeking 18F-DOPA analogue. J Neurooncol 33(1 – 2): 163 – 9

Nieweg O, Pruim J, Willemsen ATM, Hoekstra AJ, Paans AMJ, Vaalburg W, Molenaar WM, Odloff J, Schaffordt Koops H (1996) Fluorine-18-fluorodeoxyglucose PET imaging of soft tissue sarcoma. J Nucl Med 37:257 – 261

Schulte M, Brecht-Krauss D, Heymer B, Guhlmann A, Hartwig E, Sarkar MR, Diederichs CG, Von Baer A, Kotzerke J, Reske SN (2000) Grading of tumors and tumorlike lesions of bone: evaluation by FDG PET. J Nucl Med 41(10):1695 – 701

Schütze SM, Rubin BP, Vernon C, Hawkins DS, Bruckner JD, Conrad EU 3rd, Eary JF (2005) Use of positron emission tomography in localized extremity soft tissue sarcoma treated with neoadjuvant chemotherapy. Cancer 103(2):339 – 48

Schwarzbach MH, Hinz U, Dimitrakopoulou-Strauss A, Willeke F, Cardona S, Mechtersheimer G, Lehnert T, Strauss LG, Herfarth C, Buchler MW (2005) Prognostic significance of preoperative [18-F] fluorodeoxyglucose (FDG) positron emission tomography (PET) imaging in patients with resectable soft tissue sarcomas. Ann Surg 241(2):286 – 94

Wagner JD, Schauwecker DS, Davidson D, Wenck S, Jung SH, Hutchins G (2001) FDG-PET sensitivity for melanoma lymph node metastases is dependent on tumor volume. J Surg Oncol 77(4):237 – 42

Wagner JD, Schauwecker D, Davidson D, Logan T, Coleman JJ 3rd, Hutchins G, Love C, Wenck S, Daggy J (2005) Inefficacy of F-18 fluorodeoxy-D-glucose-positron emission tomography scans for initial evaluation in early-stage cutaneous melanoma. Cancer 104(3):570 – 9

Yamada K, Brink I, Bisse E, Epting T, Engelhardt R (2005a) Factors influencing [F-18] 2-fluoro-2-deoxy-D-glucose (F-18 FDG) uptake in melanoma cells: the role of proliferation rate, viability, glucose transporter expression and hexokinase activity. J Dermatol 32(5):316 – 34

Yamada K, Brink I, Engelhardt R (2005b) Factors influencing [F-18] 2-fluoro-2-deoxy-D-glucose (F-18 FDG) accumulation in melanoma cells: is FDG a substrate of multidrug resistance (MDR)? J Dermatol 32(5):335 – 45

Sentinel Node Biopsy and Occult Lesion Localization in Early Breast Cancer

12

G. Paganelli, G. Trifirò, L. Ravasi, C. de Cicco

12.1 Sentinel Node Biopsy in Early Breast Cancer

12.1.1 Introduction

Sentinel lymph node (SLN) localization and biopsy represent one of the most important recent developments in surgery, which has been reflected in important changes in the management of patients affected by early infiltrating breast carcinoma. Sentinel lymph node biopsy (SLNB) was first applied in melanoma patients by Morton and colleagues (Morton et al. 1992). Subsequently, the technique was proposed as a method of disease staging in breast cancer patients (Giuliano et al. 1997), so that less aggressive surgical treatment would less compromise the patient's quality of life. In fact, removal of axillary nodes in the presence of breast cancer is performed for staging and not with curative intent (Fisher et al. 2002), and axillary dissection (AD) is burdened by a significant rate of immediate and delayed possible complications such as lymphedema, paresthesia, pain and restriction of arm motion (Shaw and Rumball 1990; Kissin et al. 1986). In this context, SLNB has been proposed as an alternative to routine axillary clearance for nodal status determination.

The idea of the "sentinel lymph node" implies that lymphatic metastasis is not a random event. It is rather based on an orderly and predictable pattern of lymph flow draining from the primary site to the regional lymph node basin. Sequential progression of tumor cells is assumed to occur, with the first SLN filtering the afferent lymph and thereby entrapping the tumor cells. Experimental evidence and clinical data support the hypothesis that there is an orderly and predictable pattern of lymphatic drainage from the breast to the regional lymph nodes and progressive involvement of the axillary lymph nodes.

Based on the significant morbidity that AD may lead to and the evidence of the 60% of patients found to be free from metastatic disease after surgery, SNB has now been accepted as a standard procedure for patients bearing a clinically staged T1N0 or T2N0 breast cancer.

SLNB allows a complete histopathological examination of the SLN, and it can be performed with the patient under local anesthesia with no significant side effects.

Several studies have shown that lymphoscintigraphy (LS) combined with gamma probe-guided surgery is a more sensitive procedure than blue dye mapping for identifying and removing the SLN in breast cancer patients (Veronesi et al. 1997).

12.1.2 Radiopharmaceuticals Employed

Three types of radiocolloid preparations are commonly employed for lymphoscintigraphy combined with intraoperative gamma-probe sentinel node identification. ^{99m}Tc-sulfur colloid is the most commonly employed agent in the United States, either unfiltered (with particles ranging in size from about 15 to 5,000 nm) or filtered. Different pore sizes (100 nm or 220 nm) have been proposed for such microfiltration, aiming at using particles ranging from about 50 to 100 nm or from 50 to 200 nm. Although some authors still claim the superiority of the unfiltered over the filtered preparation (Hill et al. 1999; Cody and Borgen 1999), the prevailing trend now favors the routine use of filtered ^{99m}Tc-sulfur colloid for sentinel lymph node studies.

Most European investigators use ^{99m}Tc-nanocolloid human albumin (HSA) (95% of the particles < 80 nm). At present, this radiopharmaceutical offers the best range of particle size and the additional benefits of instant labeling at room temperature and stability. It is also the only generally available colloid, but not throughout Europe, as each country has different rules on the usage of human or animal derived protein.

^{99m}Tc-antimony trisulfide (3–30 nm) is commercially available in Australia and Canada, where it is widely employed for sentinel lymph node procedures. Even though antimony sulfide is commercially available in Europe, it is not widely used due to the greater availability (and better results in SLN visualization) of ^{99m}Tc-nanocolloid HSA. Radiocolloids with most particles between 200 and 1000 nm represent the best com-

promise between fast and efficient lymphatic drainage and satisfactory retention in the SLN; unfortunately, compounds with such characteristics are not commercially available for clinical routine examinations.

12.1.3 Methodology

To optimize the administration of the radiopharmaceutical for lymphatic mapping and sentinel lymph node biopsy in breast cancer surgery, the following parameters need to be taken into account: (a) injection site, (b) injected volume, and (c) injected activity.

Common corollaries of the intratumoral route are a large volume of the injectate (> 4 ml) and a rather high dose of injected activity of radiocolloid (37 – 370 MBq). The purpose of injecting a large volume is to increase intratumoral pressure, to force lymph flow from the tumor, thereby enhancing the likelihood of visualizing the lymphatic pathways and draining lymph node(s). The virtual absence of a lymphatic system within the tumor requires the administration of a rather large amount of radioactivity because the percentage of intratumorally injected radiocolloid leaving the tumor is minimal. However, administration of rather large volumes may lead to distortion of tissues and lymphatics, and may unpredictably affect the radiocolloid clearance. Therefore, large volume intratumoral injections are not recommended.

Most investigators presently favor interstitial administration of radiocolloids for sentinel lymph node biopsy through the extratumoral route, which includes the peritumoral and the subdermal injection technique.

The rationale of peritumoral and subdermal administration is to inject the radiotracer in a site immediately adjacent to the tumor, i.e., in the space where an assumed healthy lymphatic system is the only possible drainage pathway for fluids, particles and cells leaving the tumor via the extravascular route. In this approach, the radiocolloid is given in deposits around the tumor circumference in aliquots of about 0.2 ml, containing 7 – 12 MBq of ^{99m}Tc-labeled colloid. Similarly to the intratumoral and subdermal approaches, 25-gauge or even 27-gauge needles are commonly used for injection, the only difference being the length of the needle bore according to depth of the injection.

Massaging the injection site for a few minutes after injection may improve radiocolloid migration to the sentinel node.

Imaging is a crucial component of any procedure of SLNB in breast cancer, as it provides important unique information such as possible lymphatic drainage towards the internal mammary chain, a pattern that would be undetected with intraoperative gamma-probe counting (Pijpers et al. 1997). The SLN technique is particularly helpful for distinguishing true additional sentinel nodes on different lymphatic pathways if more than a single sentinel lymph node in the axilla is visible.

Generally, the lymphoscintigraphy is performed during the afternoon prior to the surgery day, about 15 – 18 h before surgery. This timing is convenient for the routine in the Nuclear Medicine Department and consistent with the lymphatic drainage for radiocolloids from the physiopathological point of view.

With the ^{99m}Tc-labeled colloids, the energy setting of the gamma camera should be centered on the 140-keV emission peak of ^{99m}Tc, with a 20 % window. The use of a high-resolution collimator and of an acquisition matrix of 128 × 128 pixels is highly recommended.

The patient should be positioned supine, the arm completely abducted to allow for the head of the gamma camera to be placed as close as possible to the axilla. In patients with large breasts, moving the breast away from the axillary and parasternal regions reduces the attenuation effect of soft breast tissue and enhances the radioactive focus, i.e., the sentinel node, which takes up less than 1 % of the injected activity.

An anterior scintigraphic view and the oblique anterior view are acquired to investigate the internal mammary chain and to better distinguish between the injection site and focal spots, corresponding to the draining axillary lymph nodes, respectively.

Finally, the last step of the examination consists of marking the skin-projected-sentinel node position with an indelible marker. Such a position is found with the aid of a radioactive point source and/or preferably by using the gamma probe for counting the spot(s) visualized by lymphoscintigraphy.

12.1.4 Clinical Indications

Although the variables involved in any possible combination in the procedure of radioguided SLNB are many, the results reported in the literature with respect to the success rate of the technique are amazingly consistent. The success rate is commonly defined as the positive radioguided identification of the sentinel node based on the combined lymphoscintigraphic and gamma-probe counting approach. In a literature search from 1997 to 2000, the success rate of radioguided procedures in localizing the sentinel node during breast cancer surgery ranged from 94 % to 97 % in studies with $n > 100$. In some studies, the success rate in sentinel node localization reached 99 % when radioguidance was combined with the vital blue dye technique.

However, our opinion is that combining blue dye and lymphoscintigraphy is not necessary for SN identification and SNB, since more than 99 % of SN visualiza-

tion, using lymphoscintigraphy only, is achievable according to the published standard method (De Cicco et al. 1998; Veronesi et al. 1997; Trifirò et al. 2004).

Another parameter of uppermost importance in sentinel lymph node biopsy is classification of tumor status of the node by intraoperative frozen section histopathology. Clearly, the most dreadful occurrence to be avoided is misclassification of the patient due to defining a sentinel lymph node as tumor-free, yet finding metastatic disease in lymph nodes of the subsequent echelons. The occurrence of such false-negative sentinel lymph nodes has been documented in the majority of the studies that also involved complete axillary node dissection and extensive histopathologic evaluation of the axilla. The incidence of this finding, which is reported to range between 4% and 8% of all patients undergoing sentinel lymph node biopsy, can be affected both by technical factors in the identification step and by the accuracy of intraoperative histopathology.

It is worth noting that the lowest incidence of false-negative sentinel lymph nodes is reported when the technique outlined above is employed for extensive histopathology of the node. Furthermore, in our own experience a false-negative sentinel lymph node has never been observed in patients with breast cancer in the early stage of growth (Veronesi et al. 1999; Mariani et al. 2000).

The crucial parameter concerning the accuracy of SLNB in breast cancer surgery is its impact on the long-term clinical outcome of patients. This issue is, at present, unsolved and will hopefully be clarified by ongoing long-term investigations involving the two-arm protocol to which eligible patients were randomly assigned. Briefly, in one arm axillary node dissection was routinely performed irrespective of the tumor status of the SLN, while in the other arm it was performed only if the sentinel node turned out to be metastatic at intraoperative frozen section histopathology. Among the 167 patients of the study, who did not undergo axillary dissection, there were no cases of axillary metastases during follow-up (Veronesi et al. 2003). On the basis of these results we decided to extend the indication of SNB to the majority of breast cancer patients, even in particular conditions which were previously considered contraindications.

12.1.5 Contraindications to Sentinel Node Identification and Biopsy

In the proceedings of the Consensus Conference (Philadelphia, 2001) on the role of SLNB in carcinoma of the breast, the panel considered SLNB to be a suitable replacement for AD in carcinomas with a diameter below 3 cm and no clinically suspicious palpable axillary nodes (Schwartz et al. 2002).

The rapid spread of SLNB has led to its use in clinical settings previously considered contraindications to SLNB. It has to be clearly stated, however, that controversial indications for SLNB should be limited to centers with extensive experience in this procedure, and should only be used after careful discussion of the available data with the patient.

Lymphoscintigraphic sentinel lymph node identification is contraindicated in patients with the following findings:

1. Palpable axillary lymph nodes or other evidence of axillary node metastatic disease
2. Breast cancer above stage T2 (>4 cm in diameter)
3. Inflammatory breast disease (mastitis)

Other conditions previously considered contraindications to LS and SNB are now, after the experience of several groups, under re-evaluation. With respect to primary chemotherapy (PC), some authors reported that the false negative rate of SLNB was greater in patients who had received PC than in those who were PC-free (Bedrosian et al. 2000; Cohen et al. 2000; Nason et al. 2000; Brady 2002). However, more recent and larger studies have shown that the identification of SLN and false-negative rates of SLNB are similar to those reported in the absence of PC (Breslin et al. 2000; Stearns et al. 2002; Mamounas 2003; Schwartz and Meltzer 2003) when the expertise is relevant. Therefore, in women with a clinically negative axilla before the start of PC, SLNB might be considered after the completion of medical treatment if no progression has occurred. In patients with suspicious axillary nodes at presentation which have been "downstaged" to N0 by medical treatment, SLNB might also be considered an option in the hands of surgeons with extensive experience in this procedure. SLNB is obviously not recommended for patients whose axillary nodes remain clinically suspicious after PC. Multifocal disease seems to be associated with a higher rate of nodal involvement than unifocal lesions of similar size (Andea et al. 2002). Multiple foci of carcinoma, particularly when located in different quadrants of the breast, have been considered a relative contraindication to SLNB because these tumors may involve more than one dominant lymphatic trunk draining to axillary nodes. This may lead to an increased false-negative rate (Anderson 2003; Reintgen et al. 2002). In our initial experience with 163 women, two out of the four patients with false-negative SLNB had multifocal disease (Pijpers et al. 1997). Ozmen et al. (2002), in a study conducted on 111 patients, 21 of whom had multifocal tumors, reported an accuracy of 93.7% with a false negative rate of 11.3% in the whole cohort of patients. Multifocality and tumor size (>2 cm) were significantly associated with decreased accuracy and increased false negative rates. Klimberg et al., however, reported that the rate of identification of

the SLN was equal following either subareolar or peritumoral injection (Klimberg et al. 1999), and therefore multicentric cancers might drain first to the subareolar area and then to the SLN in the axilla, through a network of lymphatic vessels connecting different quadrants with the subareolar area (Grant et al. 1959). Schrenk and Wayand (2001) performed SLNB with either blue dye alone or blue dye plus radiolabeled colloid injected in the subareolar area in 21 women with multicentric breast carcinoma who were prospectively evaluated and candidates for standard AD. The authors found a 100 % identification rate of SLNs and no false negative SLNBs.

Two papers from the Memorial Sloan-Kettering Cancer Center have addressed the issue of SLNB in multicentric breast cancer. In the first (Kim et al. 2002), five patients with two tumors in distinct quadrants were injected at one site with technetium-labeled sulfur colloid and at the second site with isosulfan blue dye. Having identified at least one node that was both hot and blue within the axilla in all cases, the authors suggested that the lymphatic drainage of the entire breast coincides with the drainage of the tumor bed, regardless of its location. In the second paper, Tousimis et al. (2003) studied 70 patients with multicentric/multifocal breast carcinoma who underwent mastectomy and SLNB with planned AD. The accuracy of SLNB was 96 %, the sensitivity 92 % (false negative rate 8 %); these results are comparable to those of published studies carried out in women presenting with unifocal disease. All three patients with inaccurate SLNB had dominant invasive tumor larger than 5 cm, and in one case axillary disease was palpable at surgery.

In the study by Kumar et al. (2003) on 48 patients with multicentric/multifocal breast carcinoma, success rate, sensitivity, negative predictive value and accuracy were 93 %, 100 %, 100 % and 100 % using the radiocolloid probe, 87 %, 100 %, 100 % and 100 % using blue dye, and 93.5 %, 100 %, 100 % and 100 % using combined methods. The authors concluded that SLN localization maintained a high negative predictive value in multicentric/multifocal breast cancer, as opposed to the common belief that a higher rate of false negative results occurs in this subset of patients, and they proposed its routine use instead of AD in these patients too.

Some authors have suggested that altered lymphatic drainage decreases the likelihood of successful lymphatic mapping and, indeed, that SLNB for breast cancer may be less accurate after excisional biopsy of the primary tumor (Borgstein et al. 1998; McMaster et al. 1998; Ollila and Giuliano 1998). Other authors (Wong et al. 2002; Miner et al. 1999) claim that neither biopsy type nor type of definitive surgical procedure significantly affects the accuracy of SLN biopsy for breast cancer, and that SLNB can be performed accurately after excisional biopsy and is equally effective in patients undergoing partial mastectomy or total mastectomy (Intra et al. 2005; Luini et al. 2005).

In a recent review on breast cancer during pregnancy, it has been stated that AD is preferred because nodal metastases are commonly found, nodal status affects the choice of adjuvant chemotherapy and SLNB poses an unknown risk to the fetus from the radioisotope (Woo et al. 2003). Patients with breast cancer during pregnancy are excluded from randomized studies on SLNB currently ongoing in the United States, and in the Consensus Conference on the role of SLNB in breast carcinoma the panel advised against SLNB in pregnant women until more data are available (Hurkmans et al. 2003).

Nicklas and Baker (2000) suggested that lymphoscintigraphy can be safely performed in pregnancy, with negligible risks for the fetus. In fact, the radioisotope remains trapped at the injection site or within the lymphatics, and the exposure to the fetus is essentially zero. Similarly, Morita et al. (2000) report pregnancy as not being a contraindication when performing lymphoscintigraphy in female patients.

In our opinion some practical recommendations might be followed to further minimize the exposure of the fetus, such as avoiding contact with other patients who are potential sources of radioactivity (e.g., by scheduling a pregnant patient as the first procedure of the day, and keeping the patient in a single-bed room) and decreasing the time interval between lymphoscintigraphy and surgery to reduce the administered activity. Thus in pregnant patients SLNB could be performed within 2 – 3 h post-injection of 3 – 5 MBq of ^{99m}Tc radiocolloids; with this activity the risk is reliably low (Gentilini et al. 2004).

It is worth noting that patients previously treated with breast radiotherapy after primary surgery should anyway undergo a lymphoscintigraphy. Even though chances to visualize the SLN may be lower and location may be unusual such as controlateral.

Finally, it should be underlined that introduction of the SLNB procedure in any given institution requires a combined effort which involves at least three different specialties: (1) nuclear medicine, (2) surgical oncology and (3) pathology, with the addition of health physicists.

Thus, the learning curve should be related to the team rather than to the individual specialists, who will have to gain confidence in each procedure step and rely on each other's contribution for the successful outcome of the technique.

12.2 Occult Lesion Localization in Early Breast Cancer

12.2.1 Introduction

The widespread use of mammography in screening campaigns has resulted in a greater detection of non-invasive breast neoplasms (carcinoma in situ). Some authors (Schwartz et al. 1988; Franceschi et al. 1990; Goedde et al. 1992) report intraductal carcinomas as 15 – 25 % of all breast tumors. Most intraductal carcinomas are non-palpable lesions and their number is expected to increase. Other authors (Symmonds and Roberts 1987; Tubiana et al. 1994; Schwartz et al. 1994; Brenner 2000; Liberman et al. 2001) report that 50 % of breast cancer patients under disease evaluation are likely to have a clinically occult lesion.

Surgical excision of a suspect occult lesion is suggested and highly recommended if a cluster of microcalcification is present. Here, preoperative localization is crucial since accurate location determination predicts proper radical tumor removal and prevents unnecessary exeresis of healthy tissue. Ideally, the lesion is located in the middle of the removed tissue with at least 1 cm from the lesion to the excision edges.

In 1996 here at the European Institute of Oncology, we developed a radiotracer method to enable localization of non-palpable breast lesions. The so-called "radioguided occult lesion localization" (ROLL) was thought of as a consequence of our studies on sentinel node biopsy for breast carcinoma.

Soon after its validation, ROLL became the preferred approach to preoperative localization of non-palpable breast lesions in our institute. From the very first studies (Paganelli et al. 1997; Luini et al. 1998; Luini et al. 1999; Gennari et al. 2000; De Cicco et al. 2002), several authors have reported ROLL superiority over wire localization as it provides more accurate centring of the lesion sparing healthy tissue exeresis.

12.2.2 Methodology

12.2.2.1 Injection Technique

The injection is given approximately 14 – 18 h before surgery, under US or mammographic guidance to accurately point to the center of the lesion. The patient is administered with 0.5 μg of macroaggregates of human serum albumin, particle size 10 – 150 μm (Macrotec, Amersham-Nycomed-Sorin, Italy) labeled with 7 – 10 MBq of ^{99m}Tc, diluted in 0.2 ml of saline. For microcalcifications, opacities or other anomalies revealed by mammography and not by ultrasound, mammographic equipment with a computerized stereotactic system is used to guide the injection. Mammograms are acquired with the X-ray tube oriented at +15° then at –15° to reference and reconstruct the images; a computerized system calculates the 3D co-ordinates of the lesion. Craniocaudal projections are acquired when lesions are located in the breast upper quadrants; external or internal lateral projections are acquired for lesions located in the outer or inner lower quadrants respectively. A 22G spinal needle, mounted in the stereotactic frame, is introduced into the lesion so that the position of the needle tip corresponds to the calculated co-ordinates. The correct tip location (i.e., at the center of the lesion) is checked by a new mammogram. The mandrel is then removed and the radiotracer injected, immediately followed by 0.2 ml of radiopaque contrast medium (Iomeron 300, Bracco SpA, Milan, Italy). The needle is then removed and a standard orthogonal mammogram is taken to verify the correct localization of contrast medium within the lesion. Women with diffuse microcalcifications and multifocal or multicentric lesions are excluded from the procedure.

When the occult lesion is detected ultrasonically, the radiotracer is injected under ultrasound (US) guidance. The US examination is performed with a linear probe with 7.5 – 13 MHz according to breast size. Then another probe (7.5 – 10 MHz) fitted in a needle biopsy device is employed. The needle is positioned in the device and inserted into the breast manually; the needle tip is positioned at the center of the lesion as shown by a change in echogenicity at the lesion site. Radiotracer is injected in 0.2 ml of saline. When lesions are visible by both US and mammography, the radiotracer is preferentially injected under US guidance due to greater accuracy for centering the lesion. An ink mark is written on the skin over the lesion to serve as an initial guide during scintigraphy and surgery.

12.2.2.2 Scintigraphy

Lateral and anterior scintigraphic images are usually acquired about 10 min after radiotracer injection, although this timing depends upon the requirements of the department. The lateral view is acquired when the patient is lying prone using a homemade polystyrene block to hold the breast in position. A flexible wire ^{57}Co source outlines the breast contour during acquisition.

The anterior image is obtained when the patient is standing with abducted arms, after placing a ^{57}Co point source on the nipple as a landmark. Images are acquired over about 5 min with no less than 70 kcounts in a 256 × 256-pixel matrix, zoom 1.33 (Fig. 12.1).

The scan enables the assessment of contamination. When the hot-spot appears as a small well delimited area, the patient can be referred for biopsy whereas if the radioactive uptake is spread over a large area of breast parenchyma, the localization is considered unsuccess-

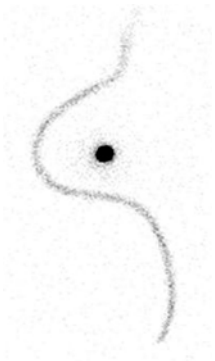

Fig. 12.1. Static scintigraphy acquired in lateral view after ^{99m}Tc-MAA injection into the lesion

ful and repeated using a different technique. If skin contamination occurs, the skin is accurately cleaned and the scan repeated.

12.2.2.3 Surgery

Patients undergo surgical excision of the lesion while under general anesthesia. The incision is guided by the skin mark, the radioactivity detected by a hand-held detecting probe (GDP), and cosmetic criteria. The GDP is also used to check the position of the hot-spot whenever required during the excision, and to establish the margins of the resection as the locus of points around the hot-spot where the count rate falls off sharply to background (1 – 1.5 cps). After lesion removal the resection cavity is checked for residual activity greater than background; if any activity is present the resection is enlarged. In case of microcalcifications, the specimen is tagged with clips on one or more margins and X-rayed to verify complete lesion removal and the concentricity of the lesions. If microcalcifications are too close to the edges and/or not correctly centered by the surgeon, radicalization of the resection line is performed. From a legal point of view, it is suggested to perform a specimen analysis to prove the lesion's existence.

12.2.3 Clinical Applications

From 2001 to 2004 we carried out 1,778 consecutive ROLL procedures. Of these 1,778 patients, 56% had clusters of microcalcifications found on mammography, and radiotracer injection was performed under X-ray stereotactic control. In the other 44% of cases, the lesions were detected by US, and the radiotracer was injected under US guidance. The procedure was generally well tolerated although needle insertion may have produced some discomfort. No allergic reactions occurred after radiopharmaceutical administration; one patient had a cutaneous erythema after contrast medium injection. In our daily practice we omit contrast medium administration in the case of patients with a history of intolerance or allergic reactions to it.

The procedure was rated successful in 1,692/1,778 (95%) of cases. The failures were caused by an absence of overlay between tracer and lesion site (61 cases) or by spread of macroaggregated albumin (MAA) over a large area of the breast parenchyma (25 cases). All the procedures performed under US guidance (783) correctly identified the lesion. The presence of radioactivity along the needle track (211 cases) did not interfere with a correct surgical excision.

In 1,680/1,692 (99%) cases, the lesion was included in the excised tissue as confirmed by the histological analyses. Out of the 898 (53%) cases of invasive breast cancer, the resection edges were disease free in 887 cases (98.8%); in 11 cases (1.2%) a radicalization of one or more margins was required.

In our experience ROLL represents a good approach to solving the problem of non-palpable tumor localization. It provides the surgeon with a quick and simple means of localizing and removing the lesion in the operating room. The surgeon is able to choose the site of surgical incision to give the best cosmetic result, the lesion is easier to identify at operation and the confidence that the abnormality has been excised is improved. The absence of side effects of this method has contributed to its success in our institute and in many other institutions (Feggi et al. 2001; Patel et al. 2004; Rampaul et al. 2004; Ronka et al. 2004; Zgajnar et al. 2004; Audisio et al. 2005). However, the procedure is not applicable in women with diffuse microcalcifications and multifocal or multicentric lesions. To provide the best results, this method requires a very strict collaboration between radiologist, nuclear medicine, surgeon and pathologist. Training the operators (30 procedures may be sufficient to reach a good level of expertise) to improve their personnel skills assures the correct performance of each step of the procedure. The best results are obtained when lesion localization is carried out under US guidance: the procedure is simple, rapid (5 – 10 min maximum) and with excellent correlation between radioactivity spot and lesion location. The echogenicity changes reflecting the presence of both the needle and tracer are a self-check to proper insertion of the needle tip in the lesion and proper tracer injection. A less friendly approach is by using X-ray stereotaxis; the injection needle may not always be inserted at the correct depth. The distance between the injected radiopaque spot and the lesion must always be checked on the standard mammogram taken after injection. It is worth underlining that very superficial lesions are difficult to center and that lesions in the central quadrant of the breast are worrisome because of a rather high risk of injecting the tracer into a galactophore duct.

Macroaggregates of albumin do not diffuse away from the injection site provided that the radiotracer has not been introduced into the lymphatic vessels or galactophorous ducts. This gives a large interval of time in which to arrange surgery, consistent with the physical decay of technetium-99m.

With respect to radioprotection, ROLL is a safe examination as it involves negligible risk for patients and hospital staff and does not require special radioprotection measures (Cremonesi et al. 1999; Rampaul et al. 2003). In brief, the mean absorbed dose to the patients' abdomen is 0.45 mGy. After 100 operations, the mean absorbed dose to the surgeons' hands is 0.45 mGy and the mean effective dose 0.09 mSv. Absorbed doses to all hospital personnel involved in the procedures are very low compared to recommended annual limits stipulated by the International Commission on Radiological Protection (IRCP).

References

Andea AA, et al. (2002) Pathologic analysis of tumor size and lymph node status in multifocal/multicentric breast carcinoma. Cancer 94:1383 – 1390

Anderson BO (2003) Sentinel lymphadenectomy in breast cancer: an update on the NCCN Clinical Practice Guidelines. J Natl Compr Cancer Network 1:S64–S70

Audisio RA, et al. (2005) Radioguided occult lesion localisation (ROLL) is available in the UK for impalpable breast lesions. Ann R Coll Surg Engl 87(2):92 – 95

Bedrosian I, et al. (2000) Accuracy of sentinel lymph node biopsy in patients with large primary breast tumors. Cancer 88:2540 – 2545

Borgstein PJ, et al. (1998) Sentinel lymph node biopsy in breast cancer: guidelines and pitfalls of lymphoscintigraphy and gamma probe detection. J Am Coll Surg 186:275 – 283

Brady EW (2002) Sentinel lymph node mapping following neoadjuvant chemotherapy for breast cancer. Breast J 8:97 – 100

Brenner RJ (2000) Lesions entirely removed during stereotactic biopsy: preoperative localization on the basis of mammographic landmarks and feasibility of freehand technique – initial experience. Radiology 214(2):585 – 590

Breslin TM, et al. (2000) Sentinel lymph node biopsy is accurate after neoadjuvant chemotherapy for breast cancer. Clin Oncol 18:3480 – 3486

Cody HS 3rd, Borgen PI (1999) State-of-the-art approaches to sentinel node biopsy for breast cancer: study design, patient selection, technique, and quality control at Memorial Sloan-Kettering Cancer Center. Surg Oncol 8:85 – 91

Cohen LF, et al. (2000) Identification and evaluation of axillary sentinel lymph nodes in patients with breast carcinoma treated with neoadjuvant chemotherapy. Am J Surg Pathol 24:1266 – 1272

Cremonesi M, et al. (1999) Radiation protection in radioguided surgery of breast cancer. Nucl Med Commun 20(10): 919 – 924

De Cicco C, et al. (1998) Lymphoscintigraphy and radioguided biopsy of the sentinel axillary node in breast cancer. J Nucl Med 39(12):2080 – 2084

De Cicco C, et al. (2002) Radioguided occult lesion localisation (ROLL) and surgical biopsy in breast cancer. Technical aspects. Q J Nucl Med 46(2):145 – 151

Feggi L, et al. (2001) An original approach in the diagnosis of early breast cancer: use of the same radiopharmaceutical for both non-palpable lesions and sentinel node localisation. Eur J Nucl Med 28(11):1589 – 1596

Fisher B, et al. (2002) Twenty-five-year follow up of a randomized trial comparing radical mastectomy, total mastectomy, and total mastectomy followed by irradiation. N Engl J Med 22:567 – 575

Franceschi D, et al. (1990) Breast biopsy for calcifications in nonpalpable breast lesions. Arch Surg 125:170 – 173

Gennari R, et al. (2000) Use of technetium-99m-labeled colloid albumin for preoperative and intraoperative localization of nonpalpable breast lesion. J Am Coll Surg 190:692 – 699

Gentilini O, et al. (2004) Safety of sentinel node biopsy in pregnant patients with breast cancer. Ann Oncol 15(9):1348 – 1351

Giuliano AE, et al. (1997) Sentinel lymphadenectomy and breast cancer. J Clin Oncol 15:2345 – 2350

Giuliano AE, et al. (2000) Prospective observational study of sentinel lymphadenectomy without further axillary dissection in patients with sentinel node-negative breast cancer. J Clin Oncol 18:2553 – 2559

Goedde TA, et al. (1992) The impact of mammography on breast biopsy. Am Surg 58:661 – 666

Grant RN, et al. (1959) The surgical significance of the subareolar plexus in cancer of the breast. Surgery 33:71 – 78

Hill AD, et al. (1999) Sentinel lymph node biopsy in breast cancer: unfiltered radioisotope is superior to filtered. J Am Coll Surg 188:377 – 381

Hurkmans CW, et al. (2003) Quality assurance of axillary radiotherapy in the EORTC AMAROS trial 10981/22023. Radiother Oncol 68:233 – 240

Intra M, et al. (2005) Second biopsy of axillary sentinel lymph node for reappearing breast cancer after previous sentinel lymph node biopsy. Ann Surg Oncol 12(11):895 – 899

Kim HJ, et al. (2002) Sentinel node drainage in multicentric breast cancers. Breast J 8:356 – 361

Kissin MW, et al. (1986) Risk of lymphedema following the treatment of breast cancer. Br J Surg 73:580 – 584

Klimberg VS, et al. (1999) Subareolar versus peritumoural injection for location of the sentinel lymph node. Ann Surg 229:860 – 864

Kumar R, et al. (2003) Retrospective analysis of sentinel node localization in multifocal, multicentric, palpable, or nonpalpable breast cancer. J Nucl Med 44:7 – 10

Liberman L, et al. (2001) Bracketing wires for preoperative breast needle localization. AJR Am J Roentgenol 177(3): 565 – 572

Luini A, et al. (1998) Radioguided surgery of occult breast lesions. Eur J Cancer 34:204 – 205

Luini A, et al. (1999) Comparison of radioguided excision with wire localisation of occult breast lesions. Br J Surg 86: 522 – 525

Luini A, et al. (2005) The sentinel node biopsy after previous breast surgery: preliminary results on 543 patients treated at the European Institute of Oncology. Breast Cancer Res Treat 89(2):159 – 163

Mamounas EP (2003) Sentinel lymph node biopsy after neoadjuvant systemic therapy [review]. Surg Clin North Am 83:931 – 942

Mariani G, et al. (2000) Mapping sentinel lymph node in breast cancer by combined lymphoscintigraphy, blue-dye and intraoperative gamma-probe. Cancer Biother Radiopharm 15:245 – 252

Mariani G, et al. (2001) Radioguided sentinel lymph node biopsy in breast cancer surgery. J Nucl Med 42:1198 – 1215

McMaster KM, et al. (1998) Sentinel-lymph-node biopsy for breast cancer – not yet the standard of care. N Engl J Med 339:990 – 995

Miner TJ, et al. (1999) Sentinel lymph node biopsy for breast cancer: the role of previous biopsy on patient eligibility. Am Surg 65:493 – 499
Morita ET, et al. (2000) Principles and controversies in lymphoscintigraphy with emphasis on breast cancer. Surg Clin North Am 80:1721 – 1739
Morton DL, et al. (1992) Technical details of intraoperative lymphatic mapping for early stage melanoma. Arch Surg 127:392 – 399
Nason KS, et al. (2000) Increased false negative sentinel node biopsy rates after preoperative chemotherapy for invasive breast carcinoma. Cancer 89:2187 – 2194
Nicklas A, Baker M (2000) Imaging strategies in pregnant cancer patients. Semin Oncol 27:623 – 632
Ollila DW, Giuliano AE (1998) Intraoperative lymphatic mapping and sentinel lymphadenectomy using isosulfan blue dye. Breast Dis 8:297 – 300
Ozmen V, et al. (2002) Increased false negative rates in sentinel lymph node biopsies in patients with multifocal breast cancer. Breast Cancer Res Treat 76:237 – 244
Paganelli G, et al. (1997) Radioguided surgery in non-palpable breast lesions [abstract]. Eur J Nucl Med 24(Suppl):893P
Patel A, et al. (2004) Radioguided occult lesion localisation (ROLL) and sentinel node biopsy for impalpable invasive breast cancer. Eur J Surg Oncol 30(9):918 – 923
Pijpers R, et al. (1997) Impact of lymphoscintigraphy on sentinel node identification with technetium-99m-colloidal albumin in breast cancer. J Nucl Med 38:366 – 368
Rampaul RS, et al. (2003) Radioisotope for occult lesion localisation (ROLL) of the breast does not require extra radiation protection procedures. Breast 12(2):150 – 152
Rampaul RS, et al. (2004) Randomized clinical trial comparing radioisotope occult lesion localization and wire-guided excision for biopsy of occult breast lesions. Br J Surg 91(12): 1575 – 1577
Reintgen D, et al. (2002) Lymphatic mapping and sentinel lymph node biopsy for breast cancer. Cancer J 8:S15–S21
Ronka R, et al. (2004) Radio-guided occult lesion localization in patients undergoing breast-conserving surgery and sentinel node biopsy. Am J Surg 187(4):491 – 496
Schrenk P, Wayand W (2001) Sentinel-node biopsy in axillary lymph-node staging for patients with multicentric breast cancer. Lancet 357:122
Shaw JH, Rumball EM (1990) Complications and local recurrence following lymphadenectomy. Br J Surg 77:760 – 764
Schwartz GF, Meltzer AJ (2003) Accuracy of axillary sentinel lymph node biopsy following neoadjuvant (induction) chemotherapy for carcinoma of the breast. Breast J 9:374 – 379
Schwartz GF, et al. (1988) Significance and staging of nonpalpable carcinomas of the breast. Surg Gynecol Obstet 166:6 – 10
Schwartz GF, et al. (1994) Mammographically detected breast cancer. Nonpalpable is not a synonym for inconsequential. Cancer 73(6):1660 – 1665
Schwartz GF, et al. (2002) Consensus Conference Committee. Proceedings of the consensus conference on the role of sentinel lymph node biopsy in carcinoma of the breast, April 19 – 22, 2001, Philadelphia, Pennsylvania. Cancer 94:2542 – 2551
Stearns V, et al. (2002) Sentinel lymphadenectomy after neoadjuvant chemotherapy for breast cancer may reliably represent the axilla except for inflammatory breast cancer. Ann Surg Oncol 9:235 – 242
Symmonds RE, Roberts JW (1987) Management of nonpalpable breast abnormalities. Ann Surg 205:520 – 528
Tousimis E, et al. (2003) The accuracy of sentinel lymph node biopsy in multicentric and multifocal invasive breast cancers. J Am Coll Surg 197:529 – 535
Trifirò G, et al. (2004) Sentinel node detection in pre-operative axillary staging. Eur J Nucl Med Mol Imaging 31 Suppl 1:S46 – 55
Tubiana M, et al. (1994) Commission of the European Communities "Europe Against Cancer" Programme. European School of Oncology Advisory Report. Management of nonpalpable and small lesions found in mass breast screening. Eur J Cancer 30:538 – 547
Veronesi U, et al. (1997) Sentinel-node biopsy to avoid AD in breast cancer with clinically negative lymph-nodes. Lancet 349:1864 – 1867
Veronesi U, et al. (1999) Sentinel lymph node biopsy and axillary dissection in breast cancer: results in a large series. J Natl Cancer Inst 91:368 – 373
Veronesi U, et al. (2003) A randomized comparison of sentinel-node biopsy with routine axillary dissection in breast cancer. N Engl J Med 349:546 – 553
Wong SL, et al. (2002) The effect of prior breast biopsy method and concurrent definitive breast procedure on success and accuracy of sentinel lymph node biopsy. Ann Surg Oncol 9:272 – 277
Woo JC, et al. (2003) Breast cancer in pregnancy: a literature review. Arch Surg 138:91 – 99
Zgajnar J, et al. (2004) Radioguided occult lesion localization (ROLL) of the nonpalpable breast lesions. Neoplasma 51(5): 385 – 389

FDG-PET and PET-CT Imaging of Head and Neck Cancers

13

Y. Menda, M.M. Graham

Head and neck cancers are generally defined as cancers involving all regions of the head and neck, except for the thyroid and central nervous system. Most of these cancers are squamous cell carcinomas. The most common sites are larynx, tongue, floor of the mouth, lip, tonsils, and salivary glands, although these carcinomas can arise at almost any location in the nasopharynx, oropharynx, or hypopharynx. Thyroid cancers and tumors of the central nervous system are usually not included in head and neck cancer classification. The estimated number of new cases in the United States for 2005 is 39,000, with approximately 11,000 deaths (American Cancer Society 2005). The male:female ratio is about 2:1. Primary risk factors for virtually all head and neck cancers are alcohol and tobacco use. Early stage head and neck tumors are treated with either surgery or radiotherapy with excellent prognosis. Locally advanced tumors without distant metastasis are typically treated with surgery and postoperative radiation and chemotherapy or with definitive combination chemoradiation therapy. If chemoradiation is used as the initial treatment, salvage surgery is performed if there is evidence of residual disease. Patients with distant metastatic disease have very poor prognosis and are usually referred for palliative chemotherapy or radiation.

13.1 Diagnosis and Conventional Imaging

A working diagnosis of malignant tumor is usually obtained after history and careful clinical exam. Histologic characterization may be determined with fine needle aspiration, which requires image guidance (CT, MRI or US) for deep-seated tumors. Flexible endoscopy with multiple biopsies is performed for tumors of the upper aerodigestive tract. Panendoscopy under general anesthesia, which includes laryngoscopy, esophagoscopy and bronchoscopy, is performed in most patients to biopsy the primary tumor and to rule out synchronous tumors. CT of the neck with intravenous contrast is often the first-line imaging study to evaluate the extent of primary tumor and for cervical nodal metastasis. MRI may be complementary to CT in staging of primary tumors and is particularly helpful to evaluate for dural involvement of nasopharyngeal and sinonasal tumors. Evaluation for distant disease with chest CT is advised with locally advanced tumors with cervical nodal metastases.

13.2 FDG-PET Imaging Technique of Head and Neck Cancer

As for other oncologic PET studies, FDG-PET scans should not be performed if serum glucose level exceeds 200 mg/dl, as high glucose levels compete with FDG resulting in lower tumor uptake of FDG (Lindholm et al. 1993). Sedation with diazepam or alprazolam during uptake phase may be very helpful to reduce normal muscle uptake in the neck. This is particularly important if the scan is not done on a hybrid PET/CT camera, because uptake in normal muscle and adipose tissue may be difficult to distinguish from pathologic uptake in cervical lymph nodes. It is also useful to discuss this problem with the patient so that they try to lie quietly in a relaxed state during the uptake period. Providing a quiet area with music and minimizing potentially interesting activity near the patient can facilitate this. Another important measure during the uptake phase is to prohibit speech, which results in increased uptake in laryngeal muscles. The uptake period should be at least 60 min and it may be advantageous to delay even longer to 90 or 120 min, since tumor to background ratio steadily increases with time (Brink et al. 2002). The resolution of the PET images can be improved by using a smaller pixel size than is routinely used for body imaging. This is particularly helpful if images are not acquired on a hybrid PET-CT scanner and electronic coregistration of PET images with CT or MRI is planned. With a 2 – 2.5 mm pixel-size, a resolution of 5 – 6 mm can be obtained, compared to 8 – 10 mm resolution routinely obtained on whole-body images. Interpretation of the PET images of head and neck is complex because many normal anatomic structures in the neck show elevated uptake of FDG compared to nearby soft tissue.

These tissues include the salivary glands, lingual, palatine, and pharyngeal tonsils, base of the tongue, floor of the mouth and the laryngeal, pterygoid and strap muscles of the neck. These are demonstrated in a recent atlas of head and neck PET imaging published in the *Seminars of Nuclear Medicine* (Graham and Menda 2005).

13.3 Staging of Head and Neck Cancers

Head and neck cancers are staged according to TNM classification (AJCC 2002). Although the description of T-stage varies with the site of the primary tumor, generally tumors less than 2 cm are staged as T1, 2 – 4 cm as T2, >4 cm as T3, and tumors involving adjacent neck structures are staged as T4. For cervical nodes, N1 denotes a single ipsilateral node less than 3 cm, N2 indicates single or multiple nodes between 3 – 6 cm, and N3 refers to node(s) greater than 6 cm in greatest dimension. Presence of metastases, which are most commonly seen in the lungs, bone and liver, is designated as M1.

Involvement of neck nodes is an important prognostic and therapeutic factor for all head and neck cancers regardless of the primary site. Therefore knowledge of nodal anatomy and the standard system for describing the location of nodes is critical for proper communication with referring surgeons (Robbins et al. 2002) (Fig. 13.1). Level I nodes are the submental (Level IA) and submandibular (Level IB) nodes and usually drain tumors of the anterior oral cavity. The jugular nodes are posterior to the sternohyoid muscle and anterior to the sternocleidomastoid muscle and include Level II, III and IV nodes. Level II nodes are between the level of the skull base and inferior hyoid bone and are further classified into IIA and IIB nodes (Fig. 13.2). Level IIA nodes are anterior, medial and lateral to the internal jugular vein and IIB nodes are posterior to the vein. Level III nodes are between the inferior border of the hyoid and inferior border of the cricoid cartilage. Level II and Level III nodal metastases can be seen with tumors of the oral cavity, the entire pharyngeal region, and larynx. Level IV nodes are inferior to the cricoid and extend to the level of the clavicle and are usually involved with tumors of the hypopharynx, larynx, cervical esophagus, or thyroid. Level V nodes are the posterior triangle nodes and are between the posterior border of the sternocleidomastoid muscle and the trapezius muscle. Level V nodes are at highest risk for metastases from nasopharynx, oropharynx and posterior scalp. Level VI nodes are the anterior compartment nodes, medial to the common carotid artery and extend from the hyoid to the manubrium and most commonly harbor metastases from thyroid cancer, larynx, hypopharynx, and cervical esophagus.

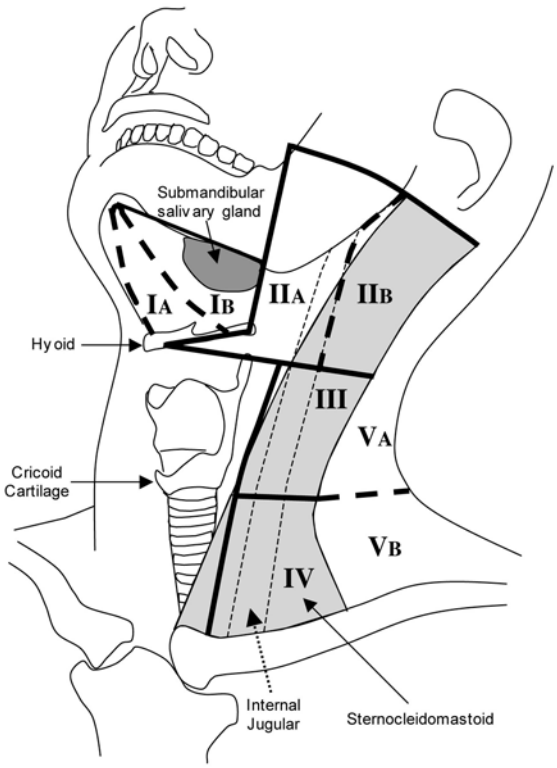

Fig. 13.1. Nodal levels of the neck according to the American Head and Neck Society and the American Academy of Otolaryngology-Head and Neck Surgery classification. (With permission from Graham M, Menda Y: Positron emission tomography/computed tomography imaging of head and neck tumors: an atlas. Semin Nucl Med 2005; 35:220 – 52)

Diagnostic criteria for cervical nodal metastases with CT or MRI are: nodal size greater than 15 mm for jugulodigastric nodes and greater than 10 mm for other neck nodes; round shape with central necrosis; presence of more than three nodes or presence of extracapsular invasion. However, more than 40 % of metastatic nodes are less than 10 mm is size (Brink et al. 2002) and many larger nodes simply represent reactive inflammatory lymph nodes. FDG uptake in a lymph node is significantly more predictive of nodal disease. In comparative studies, sensitivity and specificity of PET in detection of nodal metastases was found between 70 – 100 % and 82 – 94 % respectively, compared to 58 – 85 % and 58 – 96 % for CT/MRI (Hannah et al. 2002; Stuckensen et al. 2000; Stoeckli et al. 2002; Kresnik et al. 2001; Di Martino et al. 2000). FDG-PET may be falsely negative in small nodes less than 1 cm in diameter or in nodes completely replaced by necrosis. Small hypermetabolic nodes adjacent to muscles with FDG uptake may also not be detectable; however, these are generally resolved on integrated PET-CT scanners. False positive FDG uptake in cervical nodes may be due to inflammation. Because of significant overlap between inflammatory and

metastatic nodes, quantitation of uptake with SUV does not improve the interpretation accuracy of FDG-PET in cervical lymph nodes.

FDG-PET has also been studied in patients with a *clinically negative neck (No neck).* Only 25 – 30 % of patients with N0 neck are found to have metastatic neck nodes at surgery. This means that the majority of patients with N0 neck undergoing a potentially morbid neck dissection surgery are unlikely to have a therapeutic effect from this procedure. In three studies totaling 48 patients, where a sentinel node biopsy with immunohistochemistry was used as the gold standard, the detection rate of PET for nodal involvement in clinically N0 patients was only 0 – 30 % (Hyde et al. 2003; Stoeckli et al. 2002; Civantos et al. 2003). This may be explained by the fact that 40 % of cervical nodal metastases are less than 1 cm in size and PET detection rate for nodes less than 1 cm is only 71 % (Brink et al. 2002). Sentinel node biopsy with immunohistochemistry appears significantly more accurate in this clinical setting.

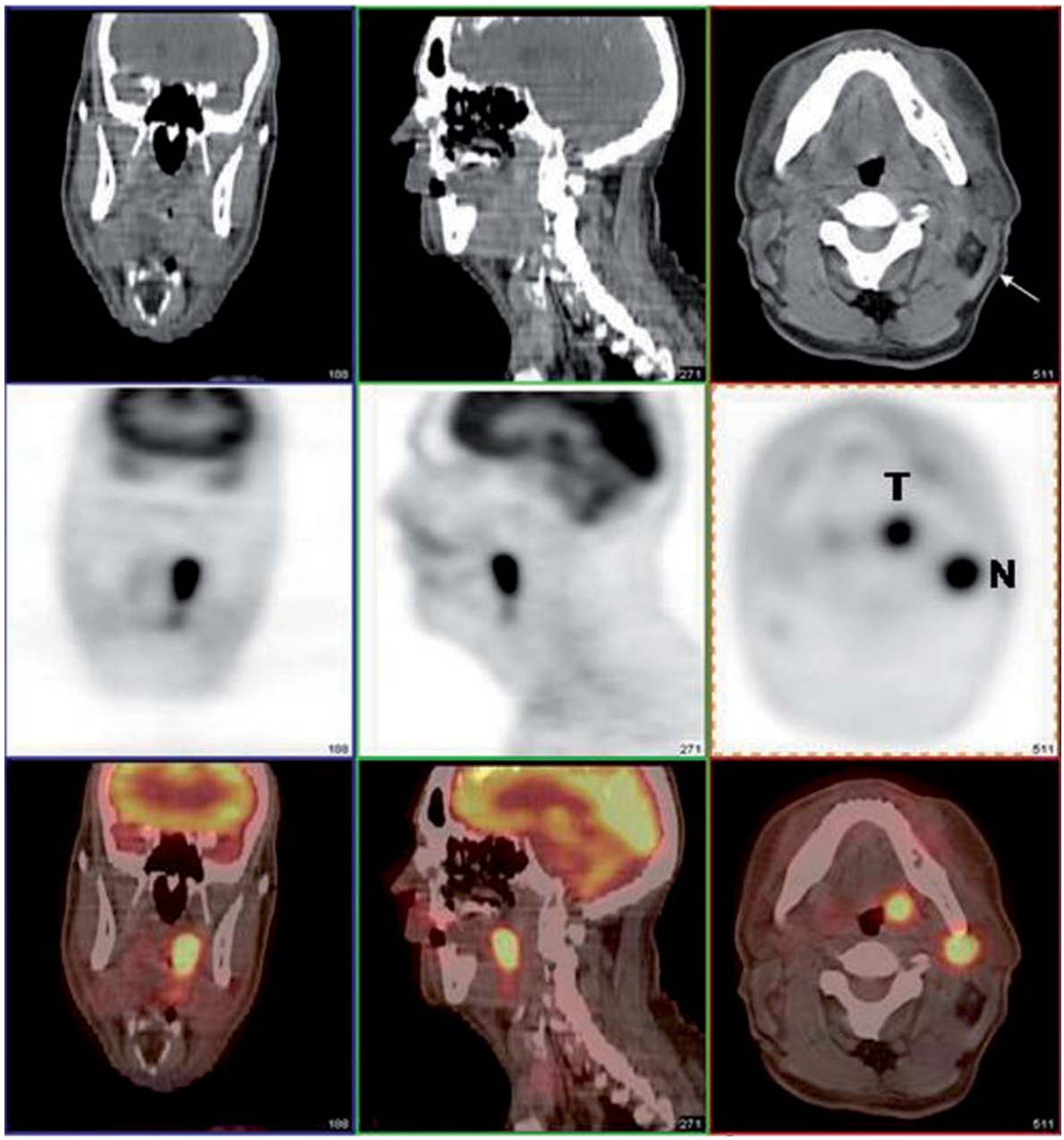

Fig. 13.2. Left tonsillar hypermetabolic tumor (*T*) with left Level IIA cervical nodal metastasis (*N*) just anterior to sternocleidomastoid muscle (*arrow*)

The main advantage of FDG PET over conventional imaging in pretherapy staging of head and neck cancer is its ability to detect synchronous tumors and metastatic disease in the chest and abdomen. A PET scan in the initial staging is most helpful in patients with advanced local disease (Stage III or IV). Several studies suggest that PET finds unexpected distant metastasis in approximately 10% of patients with locally advanced head and neck cancer (Teknos et al. 2001; Schwartz et al. 2003; Goerres et al. 2003; Sigg et al. 2003).

13.4 Carcinoma of Unknown Primary

Squamous cervical nodal metastases from an unknown primary tumor constitute 2% of newly diagnosed head and neck cancers. These patients are routinely treated with wide-field irradiation to include the entire pharyngeal axis and larynx and bilateral neck. The wide-field irradiation reduces the risk of tumor recurrence; however, it causes significant morbidity particularly in terms of xerostomia (Mendenhall et al. 2001). Correct localization of the primary tumor substantially reduces the complication risk of radiotherapy by decreasing the size of the radiation portal and may also improve survival (Mendenhall et al. 1998). Initial radiological work-up of patients with a squamous cell nodal metastasis with unknown primary includes CT and/or MRI of the neck followed by endoscopy and directed biopsies. Even after such an extensive workup the detection rate of the primary tumor is less than 50%. The most common sites of the primary tumor are tonsil and base of tongue (Mendenhall et al. 1998).

The current FDG-PET literature on carcinoma of unknown primary includes a number of small single-center studies with variable diagnostic work-up before the PET scan. These were recently reviewed by Rusthoven et al., which included 302 patients in 16 studies (Rusthoven et al. 2004). The average detection rate of the primary tumor with FDG-PET was 24.5%. Additional regional metastases were found in 15.9% and distant metastases in 11.2% of patients (Rusthoven et al. 2004). The detection rate of the primary tumor with PET is not different in studies where FDG-PET is only performed after a negative endoscopy and conventional imaging (Wong and Saunders 2003; Fogarty et al. 2003; Johansen et al. 2002; Kresnik et al. 2001; Jungehulsing et al. 2000; Greven et al. 1999; Kole et al. 1998). It seems therefore reasonable to obtain an FDG-PET as the initial imaging study in patients with carcinoma of unknown primary. If the FDG-PET scan is negative, a primary tumor is found subsequently only in 12% of patients (Rusthoven et al. 2004).

13.5 Detection of Residual and Recurrent Disease after Treatment

Early detection of recurrence of head and neck cancers is critical because the disease-free survival after salvage surgery is highly dependent on the stage of the recurrent tumor (Goodwin 2000). The 2-year disease-free survival is 67–73% for stage I or II recurrent tumor compared to 22–33% for stage III and IV disease. Diagnosis of recurrence is difficult with conventional imaging with CT or MRI because of the loss of symmetry and inflammation associated with healing. Routine biopsy of treated areas is also not recommended because of increased risk of bleeding and infection in irradiated tissue and potential false-negative biopsies due to sampling errors. Metabolic imaging with FDG-PET is more sensitive and specific than CT or MRI in detection of residual or recurrent disease, with a reported weighted average sensitivity and specificity of 86% and 73% for FDG-PET compared to 56% and 59% respectively for CT and/or MRI (Klabbers et al. 2003). A true positive FDG PET-CT for local recurrence is demonstrated in Fig. 13.3. The largest study regarding PET for local recurrence included 143 patients, who were imaged for suspected recurrence after an average of 6.9 months following completion of definitive treatment with surgery and/or radiation and chemotherapy (Wong et al. 2002). Using visual analysis (positive if uptake above background level is present outside normal structures), the sensitivity and specificity of FDG-PET in this study was 96% and 72%. False-positive FDG uptake in the post-therapy setting is seen secondary to reactive inflammatory changes from treatment, infection or osteoradionecrosis (Fig. 13.4). There is a significant overlap in SUV between recurrent tumors and post-therapy changes and no SUV cut-off has been found to outperform visual analysis by an experienced reader (Wong et al. 2002; Lapela et al. 2000). If the initial biopsy after a positive PET scan fails to demonstrate tumor, a follow-up PET scan is suggested in 2–3 months (Terhaard et al. 2001; Schoder and Yeung 2004). Tumor is very unlikely if the uptake on the follow-up PET scan is decreased (consistent with healing), whereas repeat biopsy is usually necessary if the SUV is unchanged or has increased in the interval (Schoder and Yeung 2004).

Many patients with locally advanced head and neck cancer, particularly originating from larynx and hypopharynx, are treated with initial radiation and chemotherapy for better functional preservation. These patients may subsequently undergo salvage surgery if residual disease is present. Several studies have demonstrated the value of FDG-PET in evaluating response to treatment in head and neck cancer. Greven et al. have reported a sensitivity and specificity of 100% and 90% in 28 patients with head and neck cancer who were im-

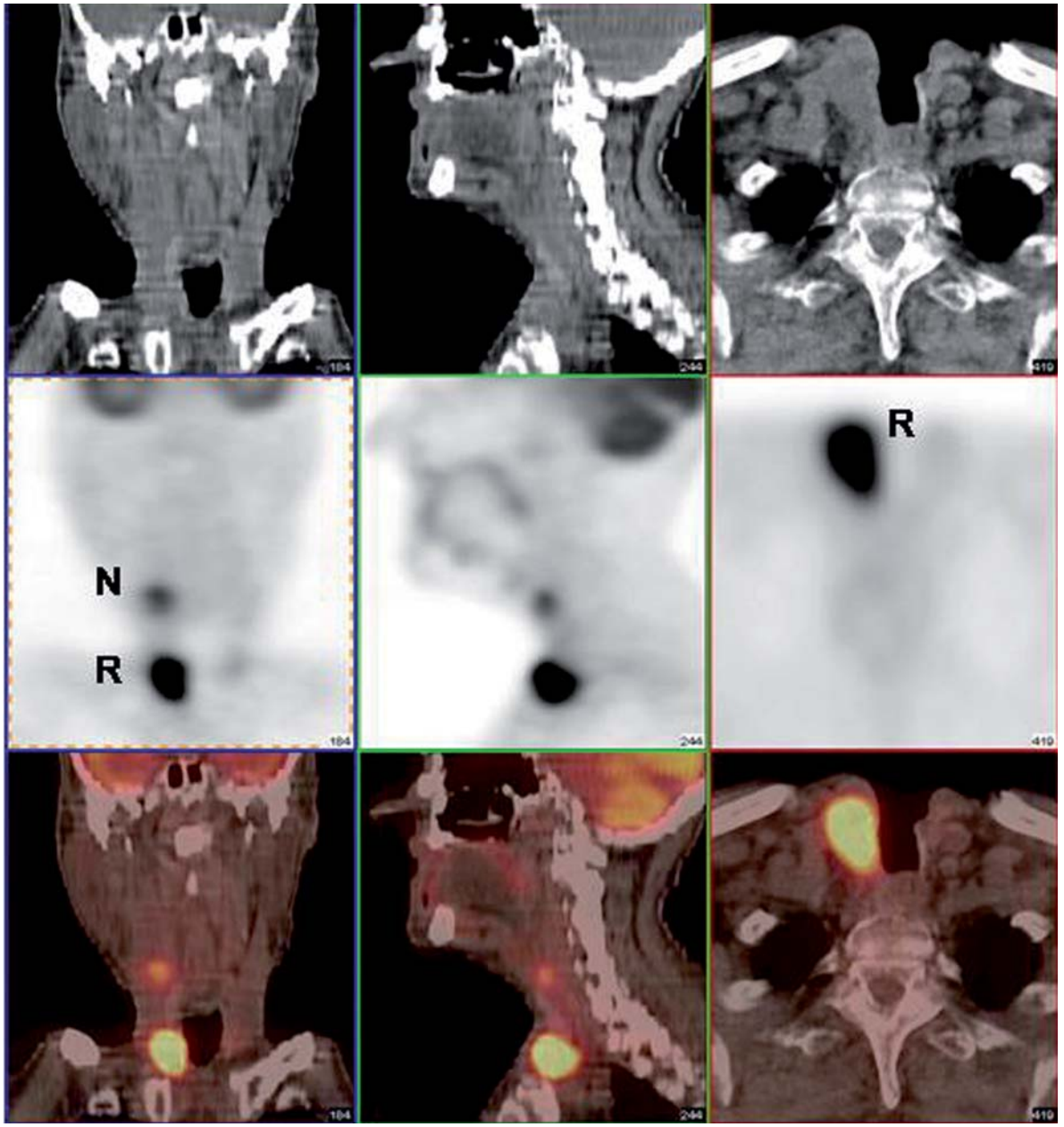

Fig. 13.3. Patient with history of laryngeal cancer, now with tracheostomy, peristomal recurrence (*R*) and right Level III nodal metastasis (*N*)

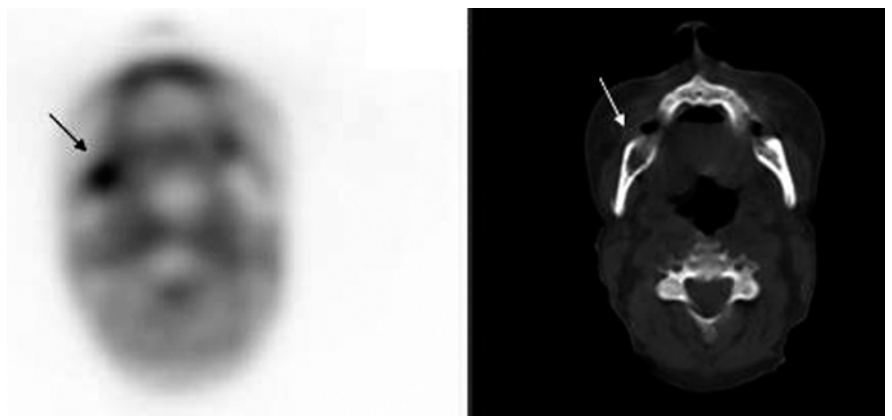

Fig. 13.4. False positive FDG uptake in osteoradionecrosis of the right mandible

aged 4 months after completion of radiotherapy (Greven et al. 2001). Our experience with 53 patients who were imaged with FDG-PET at 3 months post-treatment is in concordance with the earlier study by Greven in terms of the negative predictive value of PET (100%); however, the specificity of PET in our group was significantly lower at 43% (Yao et al. 2005). A negative FDG-PET study after chemoradiation has a very high negative predictive value even when there is residual nodal enlargement on follow-up CT. Comparing the PET scans obtained at a median of 3 months after treatment with histology from salvage surgery in 39 patients with residual nodal enlargement after chemoradiation, Porceddu et al. have reported a negative predictive value of 97% for PET and a positive predictive value of 71% (Porceddu et al. 2005). Although there is general agreement that a 3-month postradiation PET scan has an acceptable accuracy, earlier PET imaging may be desirable, as many surgeons prefer to perform the salvage surgery within 6–8 weeks after radiation, before postradiation fibrotic changes develop in the neck (Kutler et al. 2004). At least two studies have shown that 1-month post-therapy PET has an unacceptably low sensitivity. Greven et al. have reported that the sensitivity of 1-month PET for detection of residual disease was only 59% compared to 100% for 4-month posttherapy PET (Greven et al. 2001). In another study, Rogers et al. have reported a sensitivity of 45% for a 1-month post-therapy FDG-PET in comparison to the 6–8 week post-treatment surgical histopathology (Rogers et al. 2004). Data for accuracy of FDG-PET scans obtained between 1 and 3 months after therapy is limited. In a single study including 26 patients, sensitivity and specificity for FDG-PET 6–8 weeks after completion of chemoradiation was greater than 90% (Goerres et al. 2004). In summary, a PET scan performed 3–4 months after radiation or chemoradiation therapy has a high negative predictive value so that patients with negative studies can be safely followed up without intervention. A positive PET finding needs to be confirmed before management decisions are made as postradiation changes significantly lower the specificity of FDG-PET.

13.6 PET Versus PET-CT for Head and Neck Cancers

Co-registration of PET with CT allows precise anatomic definition of PET abnormalities and also improves the accuracy of PET data. This is because physiologic uptake of FDG in many normal neck structures can be easily identified through co-registration, reducing false-positive interpretations, particularly in asymmetric necks in the post-therapy setting. On the other hand, subtle areas of abnormal FDG uptake in small necrotic cervical nodes are potentially better detected after co-registration of PET images with CT. If independently acquired PET and CT data is to be co-registered using fusion software, an exact match of patient positioning for PET and CT acquisition is needed. This may be quite challenging because even slight differences in the positioning or rotation of the neck may cause significant misalignment. On an integrated PET-CT scanner, misalignment from repositioning is minimized because there is no physical motion between two studies. Another advantage of an integrated PET-CT scanner is the use of CT data for attenuation correction, which significantly reduces the acquisition time, to 25–30 min compared to 50–60 min for a whole body scan on a dedicated PET scanner. Improved performance of integrated PET-CT over dedicated PET has been shown by several groups. Schoder et al. in 68 patients with 157 lesions found an improved accuracy of PET-CT, 96% compared to 90% for PET alone, with 53% reduction in equivocal lesions and 18% change in management through PET-CT findings (Schoder et al. 2004). In another study, Syed et al. reported that PET/CT downstaged the disease and changed management in 17% of patients compared to PET alone, by correctly assigning areas of increased uptake to fat or muscle tissue (Syed et al. 2005). If the CT scan of PET-CT is to be used for diagnostic purposes, administration of intravenous contrast is necessary. Fortunately attenuation artifacts from intravenous contrast are rare and there is only modest effect of intravenous contrast on quantitation of FDG uptake in tumors (Nakamoto et al. 2003).

13.7 Radiotherapy Planning with PET-CT

Inclusion of FDG avid tumor in the radiation field will likely improve outcome of radiotherapy as tumors with high FDG uptake have a high recurrence rate and poor prognosis (Allal et al. 2004). To utilize the FDG-PET data in radiation treatment planning the study needs to be imported into the treatment planning computer and co-registered with the treatment planning CT scan. For precise co-registration, the same immobilization head mask should be used for the planning CT and the PET or PET/CT scan. In a pilot study by Ciernik et al. the co-registration of PET/CT with the planning CT images was highly successful with average deviations of 1.2 ± 0.8 mm in the x-axis, 1.5 ± 1.2 mm in the y-axis and 2.1 ± 1.1 mm in the z-axis (Ciernik et al. 2003). The radiation target volumes may be significantly modified when FDG-PET data is incorporated into radiation treatment planning (Paulino et al. 2005; Nishioka et al. 2002; Heron et al. 2004). The target volume may be increased because metabolically active tumor can be detected in normal sized nodes. On the other hand, the PET-based target volume is smaller than CT-based tar-

get volume in some patients, because the tumor may not be metabolically active in its entirety. The radiation dose and volume may be modified dramatically, from curative intent to palliation, if distant metastases are detected on the PET scan. Although the use of PET is gaining more acceptance in the radiation oncology community, questions remain that need to be addressed before PET/CT is used as a routine tool for radiotherapy planning in head and neck cancer (Paulino and Johnstone 2004). Contouring the tumor volume with PET is not standardized; the target volume on PET will be significantly overestimated with an increased window level and can be underestimated by lowering the PET window. Fifty percent of the tumor/image maximum intensity has been used for contouring by several groups (Paulino and Johnstone 2004; Scarfone et al. 2004); however, this has not been validated in large patient populations. Larger studies are also needed to demonstrate the impact of FDG-PET on the outcome of radiotherapy.

References

AJCC (American Joint Committee on Cancer) (2002) Cancer Staging Manual, 6th edn. Greene FL, Page DL, Fleming ID, et al. (eds) Springer-Verlag, New York

Allal AS, Slosman DO, Kebdani T, et al. (2004) Prediction of outcome in head-and-neck cancer patients using the standardized uptake value of 2-[18F]fluoro-2-deoxy-D-glucose. Int J Radiat Oncol Biol Phys 59:1295

American Cancer Society, Cancer Facts and Figures 2005, Retrieved from www.cancer.org, accessed on August 18, 2005

Brink I, Klenzner T, Krause T, Mix M, Ross UH, Moser E, Nitzsche EU (2002) Lymph node staging in extracranial head and neck cancer with FDG PET – appropriate uptake period and size-dependence of the results. Nuklearmedizin 41:108 – 13

Ciernik IF, Dizendorf E, Baumert BG, et al. (2003) Radiation treatment planning with an integrated positron emission and computer tomography (PET/CT): a feasibility study. Int J Radiat Oncol Biol Phys 57:853 – 63

Civantos FJ, Gomez C, Duque C, et al. (2003) Sentinel node biopsy in oral cavity cancer: correlation with PET scan and immunohistochemistry. Head Neck 25:1 – 9

Di Martino E, Nowak B, Krombach GA, et al. (2000) Results of pre-therapeutic lymph node diagnosis in head and neck tumors. Clinical value of 18-FDG positron emission tomography. Laryngorhinootologie 79:201 – 6

Fogarty GB, Peters LJ, Stewart J, et al. (2003) The usefulness of fluorine 18-labelled deoxyglucose positron emission tomography in the investigation of patients with cervical lymphadenopathy from an unknown primary tumor. Head Neck 25:138 – 45

Goerres GW, Schmid DT, Gratz KW, et al. (2003) Impact of whole body positron emission tomography on initial staging and therapy in patients with squamous cell carcinoma of the oral cavity. Oral Oncol 39:547 – 51

Goerres GW, Schmid DT, Bandhauer F, et al. (2004) Positron emission tomography in the early follow-up of advanced head and neck cancer. Arch Otolaryngol Head Neck Surg 130:105 – 9; discussion 120 – 1

Goodwin WJ, Jr (2000) Salvage surgery for patients with recurrent squamous cell carcinoma of the upper aerodigestive tract: when do the ends justify the means? Laryngoscope 110: Suppl 93:1 – 18

Graham MM, Menda Y (2005) Positron emission tomography/computed tomography imaging of head and neck tumors: an atlas. Semin Nucl Med 35:220 – 52

Greven KM, Keyes JW, Jr, Williams DW, 3rd, et al. (1999) Occult primary tumors of the head and neck: lack of benefit from positron emission tomography imaging with 2-[F-18] fluoro-2-deoxy-D-glucose. Cancer 86:114 – 8

Greven KM, Williams DW, 3rd, McGuirt WF, Sr, et al. (2001) Serial positron emission tomography scans following radiation therapy of patients with head and neck cancer. Head Neck 23:942 – 6

Hannah A, et al. (2002) Evaluation of 18 F-fluorodeoxyglucose positron emission tomography and computed tomography with histopathologic correlation in the initial staging of head and neck cancer. Ann Surg 236:208 – 17

Heron DE, Andrade RS, Flickinger J, et al. (2004) Hybrid PET-CT simulation for radiation treatment planning in head-and-neck cancers: a brief technical report. Int J Radiat Oncol Biol Phys 60:1419 – 24

Hyde NC, Prvulovich E, Newman L, et al. (2003) A new approach to pre-treatment assessment of the N0 neck in oral squamous cell carcinoma: the role of sentinel node biopsy and positron emission tomography. Oral Oncol 39:350 – 60

Johansen J, Eigtved A, Buchwald C, et al. (2002) Implication of 18F-fluoro-2-deoxy-D-glucose positron emission tomography on management of carcinoma of unknown primary in the head and neck: a Danish cohort study. Laryngoscope 112:2009 – 14

Jungehulsing M, Scheidhauer K, Damm M, et al. (2000) 2[F]-fluoro-2-deoxy-D-glucose positron emission tomography is a sensitive tool for the detection of occult primary cancer (carcinoma of unknown primary syndrome) with head and neck lymph node manifestation. Otolaryngol Head Neck Surg 123:294 – 301

Klabbers BM, Lammertsma AA, Slotman BJ (2003) The value of positron emission tomography for monitoring response to radiotherapy in head and neck cancer. Mol Imaging Biol 5:257 – 70

Kole AC, Nieweg OE, Pruim J, et al. (1998) Detection of unknown occult primary tumors using positron emission tomography. Cancer 82:1160 – 6

Kresnik E, Mikosch P, Gallowitsch HJ, et al. (2001) Evaluation of head and neck cancer with 18F-FDG PET: a comparison with conventional methods. Eur J Nucl Med 28:816 – 822

Kutler DI, Patel SG, Shah JP (2004) The role of neck dissection following definitive chemoradiation. Oncology (Huntingt) 18:993 – 8; discussion 999, 1003 – 4, 1007

Lapela M, Eigtved A, Jyrkkiö S, et al. (2000) Experience in qualitative and quantitative FDG PET in follow-up of patients with suspected recurrence from head and neck cancer. Eur J Cancer 36:858 – 67

Lindholm P, Minn H, Leskinen-Kallio S, et al. (1993) Influence of the blood glucose concentration on FDG uptake in cancer – a PET study. J Nucl Med 34:1 – 6

Mendenhall WM, Mancuso AA, Parsons JT, Stringer SP, Cassisi NJ (1998) Diagnostic evaluation of squamous cell carcinoma metastatic to cervical lymph nodes from an unknown head and neck primary site. Head Neck 20:739 – 44

Mendenhall WM, Mancuso AA, Amdur RJ, et al. (2001) Squamous cell carcinoma metastatic to the neck from an unknown head and neck primary site. Am J Otolaryngol 22:261 – 7

Nakamoto Y, Chin BB, Kraitchman DL, Lawler LP, Marshall LT, Wahl RL (2003) Effects of nonionic intravenous contrast agents at PET/CT imaging: phantom and canine studies. Radiology 227:817 – 24

Nishioka T, Shiga T, Shirato H, et al. (2002) Image fusion between 18FDG-PET and MRI/CT for radiotherapy planning of oropharyngeal and nasopharyngeal carcinomas. Int J Radiat Oncol Biol Phys 53:1051 – 7

Paulino AC, Johnstone PA (2004) FDG-PET in radiotherapy treatment planning: Pandora's box? Int J Radiat Oncol Biol Phys 59:4 – 5

Paulino AC, Koshy M, Howell R, et al. (2005) Comparison of CT- and FDG-PET-defined gross tumor volume in intensity-modulated radiotherapy for head-and-neck cancer. Int J Radiat Oncol Biol Phys 61:1385 – 92

Porceddu SV, Jarmolowski E, Hicks RJ, et al. (2005) Utility of positron emission tomography for the detection of disease in residual neck nodes after (chemo) radiotherapy in head and neck cancer. Head Neck 27:175 – 81

Robbins KT, Clayman G, Levine PA, et al. (2002) Neck dissection classification update: revisions proposed by the American Head and Neck Society and the American Academy of Otolaryngology-Head and Neck Surgery. Arch Otolaryngol Head Neck Surg 128:751 – 8

Rogers JW, Greven KM, McGuirt WF, et al. (2004) Can post-RT neck dissection be omitted for patients with head-and-neck cancer who have a negative PET scan after definitive radiation therapy? Int J Radiat Oncol Biol Phys 58:694 – 7

Rusthoven KE, Koshy M, Paulino AC (2004) The role of fluorodeoxyglucose positron emission tomography in cervical lymph node metastases from an unknown primary tumor. Cancer 101:2641 – 9

Scarfone C, Lavely WC, Cmelak AJ, et al. (2004) Prospective feasibility trial of radiotherapy target definition for head and neck cancer using 3-dimensional PET and CT imaging. J Nucl Med 45:543 – 52

Schoder H, Yeung HW (2004) Positron emission imaging of head and neck cancer, including thyroid carcinoma. Semin Nucl Med 34:180 – 97

Schoder H, Yeung HW, Gonen M, Kraus D, Larson SM (2004) Head and neck cancer: clinical usefulness and accuracy of PET/CT image fusion. Radiology 231:65 – 72

Schwartz DL, Rajendran J, Yueh B, et al. (2003) Staging of head and neck squamous cell cancer with extended-field FDG-PET. Arch Otolaryngol Head Neck Surg 129:1173 – 8

Sigg MB, Steinert H, Gratz K, et al. (2003) Staging of head and neck tumors: [18F] fluorodeoxyglucose positron emission tomography compared with physical examination and conventional imaging modalities. J Oral Maxillofac Surg 61: 1022 – 9

Stoeckli SJ, Steinert H, Pfaltz M, Schmid S (2002) Is there a role for positron emission tomography with 18F-fluorodeoxyglucose in the initial staging of nodal negative oral and oropharyngeal squamous cell carcinoma. Head Neck 24:345 – 9

Stuckensen T, Kovacs AF, Adams S, Baum RP (2000) Staging of the neck in patients with oral cavity squamous cell carcinomas: a prospective comparison of PET, ultrasound, CT and MRI. J Craniomaxillofac Surg 28:319 – 24

Syed R, Bomanji JB, Nagabhushan N, et al. (2005) Impact of combined (18)F-FDG PET/CT in head and neck tumours. Br J Cancer 92:1046 – 50

Teknos TN, Rosenthal EL, Lee D, et al. (2001) Positron emission tomography in the evaluation of stage III and IV head and neck cancer. Head Neck 23:1056 – 60

Terhaard CH, Bongers V, van Rijk PP, Hordijk GJ (2001) F-18-fluoro-deoxy-glucose positron-emission tomography scanning in detection of local recurrence after radiotherapy for laryngeal/ pharyngeal cancer. Head Neck 23:933 – 41

Wong RJ, Lin DT, Schoder H, et al. (2002) Diagnostic and prognostic value of [(18)F]fluorodeoxyglucose positron emission tomography for recurrent head and neck squamous cell carcinoma. J Clin Oncol 20:4199 – 208

Wong WL, Saunders M (2003) The impact of FDG PET on the management of occult primary head and neck tumours. Clin Oncol (R Coll Radiol) 15:461 – 6

Yao M, Smith RB, Graham MM (2005) The role of FDG PET in management of neck metastasis from head-and-neck cancer after definitive radiation treatment. Int J Radiat Oncol Biol Phys 63:991 – 9

The Endocrine System

14

E. Hindle, M. Calzada-Naucaudie, I. Keller, S. Askienazy

14.1 Thyroid Scintigraphy

Although sonography (US) and cytology (fine-needle aspiration, FNA) play the principal role in the diagnosis of thyroid nodules, thyroid scintigraphy remains an important tool for guiding clinical decisions in thyroid diseases. Thyroid scintigraphy is so used in the diagnosis of the cause of a patient's hyperthyroidism (Graves' disease, thyroid autonomy, subacute, silent and postpartum thyroiditis, etc.), in the evaluation of selected patients with thyroid nodules and in the identification of normal and ectopic thyroid tissue (neonatal hypothyroidism).

Pregnancy and breast-feeding are contraindications to thyroid scintigraphy.

14.1.1 Embryology, Anatomy and Physiology

The thyroid gland develops from the ventral wall of the pharynx and grows caudally from the base of the tongue to the level of the cricoid cartilage at the base of the neck during the first semester of gestation. A narrow isthmus unites the two lobes and sometimes a pyramidal lobe, representing the end of the thyroglossal duct, is present in the midline.

The protein by which the thyroid concentrates iodide is the sodium/iodine symporter (NIS), located on the basolateral membrane of the thyroid follicular cells. The expression of NIS, in physiological conditions, is mainly dependent on TSH and modulated by cytokines. Iodide is then translocated across the apical membrane into the colloid. The oxidation of iodide into iodine and organification of iodine in tyrosyl residues of the thyroglobulin molecule take place at the luminal surface of the apical membrane.

14.1.2 Radionuclides for Thyroid Imaging and Measurements

In view of the main role that iodine plays in the physiology and physiopathology of the thyroid gland, iodine radioisotopes are the most suited for thyroid scintiscanning. However, iodine "analogues" can be used instead of radioiodines for a majority of common indications.

The first radiopharmaceutical that was used for thyroid scanning was iodine-131 [physical half-life of 8.1 days, a relatively high-energy gamma ray (364 keV) and beta emissions]. The requirement of high energy collimators results in a poor spatial resolution. Combined with the fact that the radiation dose delivered is high, this explains why ^{131}I is unfavorable for thyroid imaging. The indication for ^{131}I scintigraphy is now mainly restricted to patients with differentiated thyroid cancer (see chapter on thyroid cancer). Some authors still use ^{131}I to obtain a full thyroid uptake curve over several days for planning ^{131}I therapy of hyperthyroidism. However, when measurement points are restricted to the initial 24 h, ^{123}I is appropriate.

The two commonly used radiopharmaceuticals for imaging are iodine-123 and technetium-99m pertechnetate as TcO_4^-.

Iodine-123 is a pure gamma emitter (gamma energy: 159 keV, absence of ÿ-emission) with a short half-life (13 h). ^{123}I is trapped by functioning thyroid, organified and retained, thus allowing for a proper determination of the iodine uptake in the gland. The activity commonly administered for imaging in adults is about 5 – 15 MBq either intravenously or orally (in this case fasting for 6 h before administration is recommended).

Compared with ^{123}I, TcO_4^- (half-life = 6 h, gamma energy: 140 keV) is not organified in the thyroid gland. Although TcO_4^- does not perfectly reflect the physiology of iodine, it has some practical advantages, namely lower cost and on-site daily availability in nuclear medicine departments. For thyroid scanning, an activity of about 37 – 74 MBq is intravenously injected. Due to the absence of organification, the thyroid radiation dose per unit activity is lower than with ^{123}I.

Although ^{123}I is the optimal radionuclide for thyroid scanning, this cyclotron product has a higher cost than TcO_4^-.

14.1.3 Thyroid Uptake of Radioiodine

Measurements of radioiodine uptake help in selecting the appropriate ^{131}I activity to be used for the treatment of hyperthyroidism.

Thyroid uptake (RAIU) with ^{123}I is performed using either scintillation counting equipment or with the region of interest technique on a gamma camera. Correction for neck "background" (radioactivity in the neck outside the thyroid) must be performed.

1. With a scintillation counting probe:

$$\text{Thyroid uptake (\%)} = \frac{(\text{Net CPM over Neck} - \text{Net CPM over thigh})}{\text{Net CPM over Dose STD} \times R \times F} \times 100 \quad (14.1)$$

Net CPM are counts/min minus room background

R is the ratio of dose administered to the dose in the standard

F is the factor that corrects for physical decay of the isotope between the time of counting the dose standard and the patient.

Various methods have been developed for correcting uptake measurements for variations in tissue attenuation in patients with large goiters or thick necks.

2. With a gamma camera, and a parallel hole collimator, using the region of interest technique:

$$\text{Thyroid uptake (\%)} = \frac{(\text{counts over thyroid} - \text{background counts})}{\text{Counts of injected activity}} \times 100 \quad (14.2)$$

In a normal subject, thyroid uptake increases progressively and reaches a plateau at 24 h. Several factors may influence the normal radioiodine uptake, the most important being the daily iodine intake. Therefore, thyroid uptake values vary largely from one country to another and for one region to another. Usual values are: 5 – 15 % at 2 h, 10 – 20 % at 6 h and 15 – 35 % at 24 h.

Among the factors that reduce uptake are the use of iodine-containing medications (amiodarone, Lugol's solution, antitussive syrups, surface disinfectants such as povidone-iodine, etc.), antithyroid drugs (propylthiouracil, carbimazole, methimazole), other medications (sulfonamides, p-aminosalicylic acid, glucocorticoids, etc.), and administration of iodinated contrast agents.

Thyroid hormones suppress TSH and therefore expression of NIS by the thyrocytes, reducing thyroid uptake. Intake of LT4 should be withheld for about 3 weeks before scintigraphy.

14.1.4 Thyroid Scintigraphy

Standard scintigraphy requires a gamma camera with pinhole and parallel collimators. Pinhole imaging demonstrates the highest spatial resolution but results in spatial distortion, which can interfere with correct correlation of a palpable nodule. On the other hand, parallel collimators, unless specially designed, cannot be put close to the thyroid gland, and therefore there is a loss of resolution, but no spatial distortion.

Imaging with TcO_4^- should be done 20 min after intravenous injection (before leakage out of the thyroid). With ^{123}I, images are usually acquired 2 – 4 h after injection).

A minimum of 100,000 – 150,000 counts should be obtained for scintigraphy of TcO_4^- and 50,000 – 100,000 counts for ^{123}I scans. An anterior image is standard and oblique images can be obtained. A clinician should examine the patient at the time of scintigraphy. The use of an external radioactive marker to delineate the nodule(s) allows the correlation between the nodule(s) and the abnormalities on the image to be firmly established.

14.1.4.1 Normal Thyroid Scintigraphy

The thyroid lobes appear as two elliptical columns slightly angled towards each other inferiorly. A slight degree of asymmetry is common and the right lobe is more often larger. Lateral margins are usually straight or convex and tracer localization should be homogeneous. Relatively less activity is present at the peripheries of the lobes where the gland is thinner. The isthmus may or may not be visualized and the pyramidal lobe appears in 10 % of patients.

14.1.4.2 Hyperthyroidism

Thyroid scanning can be very useful in differentiating the various causes of thyrotoxicosis.

Graves' Disease. Graves' disease is the most frequent cause of hyperthyroidism. It is characterized by the occurrence of TSH receptor antibodies (TRAb), which can be detected in about 80 % of cases by conventional radioreceptor antibody assays. Second generation assays have improved the sensitivity of auto-antibody testing. These antibodies stimulate the follicular cell TSH receptor, resulting in autonomous function and thyrotoxicosis.

When the clinical diagnosis is certain (in the presence of typical ocular signs and/or positivity of TRAb) and the thyroid is not nodular at palpation and US, scintigraphy is not necessary. When clinical diagnosis is uncertain, scanning is useful.

The typical scintigraphy pattern in a patient with a first episode of Graves' disease is an increased uptake with homogeneous distribution of the tracer (Fig.

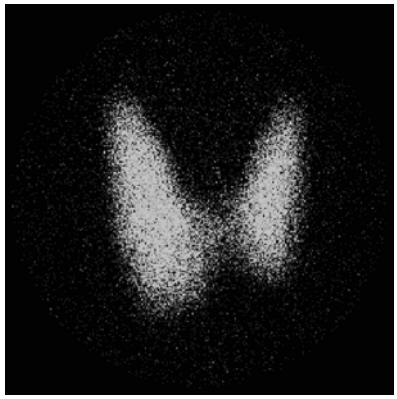

Fig. 14.1. Grave's disease – diffuse uptake on an ^{123}I study

14.1). The isthmus and the pyramidal lobe, located in the midline, are often visible. Radioiodine uptake is higher than normal. Moreover, the peak of uptake is reached earlier than in normal subjects, so that the uptake at early time points can be higher than at 24 h, translating increased turnover with a short residence time of radioiodine in the thyroid gland.

The distribution of the tracer can be heterogeneous in the case of old-standing or recurrent diagnosed Graves' disease.

In a patient with suspicion of Graves' disease, but who has coexisting thyroid nodule(s), scintigraphy is advocated. In the presence of a cold nodule, FNA is used. Some studies suggest that the risk of malignancy is higher in cold nodules of patients with Graves' disease. In rare cases, Graves' disease can coexist with a hyperfunctioning nodule (Marine-Lenhart syndrome).

Thyroid Autonomy. Thyroid autonomy is the second most frequent cause of hyperthyroidism. The probability of autonomy as the cause of hyperthyroidism increases with age, goiter volume and goiter nodularity, and is more frequent in iodine deficiency areas.

Scintigraphy can show a "hot" nodule with suppression of the remainder of the gland, together with suppressed TSH ("toxic adenoma"). This is illustrated in Fig. 14.2.

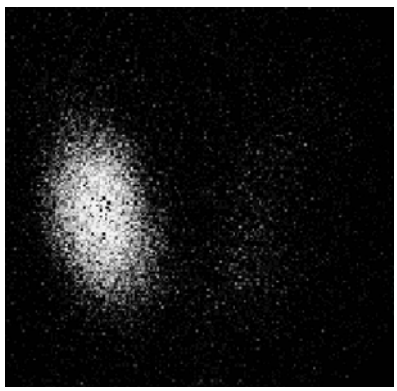

Fig. 14.2. ^{123}I study shows a toxic nodule (right lobe) with suppression of uptake in left lobe

When the nodule is hyperfunctioning, but the remaining thyroid parenchyma is not totally suppressed, TSH levels can be suppressed, decreased, or normal, and one may speak about "autonomous nodule."

Toxic multinodular goiter is scintigraphically characterized by multiple hot nodules with suppression of the surrounding stroma and suppressed TSH.

In multifocal autonomy the surrounding stroma is not totally suppressed, and TSH levels may vary from suppressed to normal. Radioiodine uptake is normal or moderately increased.

Subacute Thyroiditis. Subacute thyroiditis is an inflammatory disease of the thyroid of presumed viral origin. The inflammatory process causes the release of much of the stored thyroid hormones, which results in mild and transient thyrotoxicosis. Clinical symptoms are a painful gland "sore throat" sometimes accompanied by fever. Pain can irradiate to the ear and jaw. TSH levels are suppressed at the initial phase with hyperthyroidism and increase in erythrocyte sedimentation rate and C-reactive protein. After a thyrotoxic phase, there often follows a hypothyroid phase before the patient returns to euthyroidism.

In the initial phase, scanning shows absent or markedly decreased uptake. If scanning has been delayed, the pattern is more that of heterogeneous uptake.

Similar scan findings are seen in "silent thyroiditis" and "postpartum thyroiditis."

When thyroid scanning in a patient with hyperthyroidism shows absence of uptake one should eliminate other causes such as iodine overload (iodinated contrast media, iodine-containing drugs such as amiodarone, etc.) and thyrotoxicosis factitia due to intake of thyroid hormones. Measurement of urinary iodine and Tg (very low in the case of thyrotoxicosis factitia) are helpful.

Hyperthyroidism and Amiodarone. Amiodarone is a highly effective anti-arrhythmic drug, which contains 75 mg iodine per 200-mg tablet. Amiodarone can cause two types of hyperthyroidism.

Type 1 thyrotoxicosis is caused by excess thyroid hormone synthesis from the high iodine levels in a preexisting thyroid disease. Scintigraphy shows a persistent, although low, uptake which can be diffuse or localized.

Type 2 thyrotoxicosis is similar to the destructive release of hormone in subacute thyroiditis; scintigraphy shows absent or very low uptake.

14.1.5 Nodules

Thyroid nodules are a common clinical problem. The prevalence of palpable thyroid nodules in adults is as

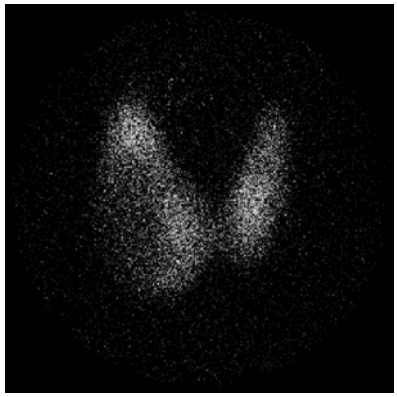

Fig. 14.3. ^{123}I study shows a "cold nodule" in right lobe

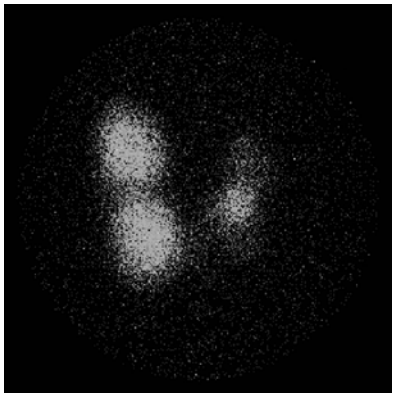

Fig. 14.4. ^{123}I study shows a multinodular goiter with interspersed functioning and hypofunctioning areas

high as 5 % in women and 1 % in men living in iodine-sufficient parts of the world.

Solitary Thyroid Nodule. The risk of thyroid cancer is about 10 % for a palpable thyroid nodule. It increases in the case of a previous history of radiation exposure, among other factors.

In the evaluation of patients with a palpable thyroid nodule (or with a non-palpable nodule larger than 1 cm), thyroid sonography and measurement of serum thyrotropin (TSH) are the initial steps.

If serum TSH is subnormal, scintigraphy should be obtained to document whether the nodule is hot, isofunctioning, or non-functioning. Because "hot" nodules rarely harbor malignancy, no additional cytologic evaluation is necessary. When the nodule is isofunctioning "warm" or non-functioning "cold" as in Fig. 14.3, fine needle aspiration (FNA) should be performed.

When TSH is normal or elevated one may go directly to FNA. However, if the cytology reading is "indeterminate," a thyroid scan should be performed because a significant number of indeterminate readings are due to "follicular" benign lesions that appear as a functioning nodule. If a concordant autonomously functioning nodule is not seen, lobectomy or total thyroidectomy should be considered.

Some authors recommend FDG-PET in cases of non-diagnostic cytology or a cytological diagnosis of "follicular proliferation." In fact FDG-PET is not able to differentiate benign from malignant thyroid nodules in all cases, but can be helpful in surgical decisions.

Multinodular Goiter. Patients with multiple thyroid nodules have the same overall risk of malignancy as those with a solitary nodule. Scintigraphy is useful, especially if TSH is low or low-normal (Fig. 14.4). Scintigraphy can determine the functionality of each nodule larger than 1 – 1.5 cm and a comparison is made with sonography data. This allows selection of the most suspicious nodules for FNA.

Autoimmune Thyroiditis. Autoimmune thyroiditis (AIT or Hashimoto's disease) is characterized by a destructive lymphocytic infiltration of the thyroid gland with or without goiter. In most patients, antibodies against thyroid peroxidase (anti-TPO) can be observed. Subclinical or manifest hypothyroidism is present in 30 – 40 % of patients. Initial transient hyperthyroidism (hashitoxicosis) can occur in 5 – 10 % due to thyroid hormone release secondary to inflammation. The differential diagnosis between Graves' disease and hyperthyroid AIT can be difficult. Scintigraphy in AIT usually shows heterogeneous uptake, but is not very specific.

14.1.6 Hypothyroidism

In an adult with clinical and biochemical evidence of primary hypothyroidism, there is seldom a reason to obtain scintigraphy.

Hypothyroidism of the newborn is often due to dysgenesis of the thyroid gland (thyroid ectopia or thyroid agenesis). Other causes are inherited disorders of the thyroid metabolism, such as iodine organification defect (peroxidase defect) and specific mutations of the genes coding for the NIS, thyroid peroxidase, thyroglobulin and pendrin. Some of these cases may appear later during childhood.

Thyroid scintigraphy is helpful for differential diagnosis. Scintigraphy can show ectopic tissue at the base of the tongue with no normal tissue in the neck (lingual thyroid), neither uptake in the neck nor ectopic tissue (agenesis of thyroid). Complete iodine transport defect (mutations in both NIS alleles) can be identified by the absence of radioiodine uptake in the thyroid and in extrathyroidal tissues that are known to express NIS (stomach, salivary glands).

14.1.6.1 The Potassium Perchlorate Discharge Test

In spite of the identification of specific mutations of the genes coding for thyroid peroxidase and pendrin, the discharge test has kept a role in establishing the diagnosis of neonatal hypothyroidism.

Potassium perchlorate prevents iodide from entering the thyroidal space by impairment of the NIS function. In a normal thyroid, the uptake of iodine will remain constant after perchlorate because organified and therefore non-dischargeable iodine cannot leave the follicular lumen. An organification defect is present if a reduction in the thyroidal uptake is noted after administration of potassium perchlorate. This test is helpful for the differential diagnosis of newborns with a suspicion of Pendred's syndrome (congenital deafness, hypothyroidism by thyroidal organification defect and goiter).

14.2 Parathyroid Imaging

Through their secretion of parathyroid hormone (PTH), the two pairs of parathyroid glands, located in the neck posterior to the thyroid gland, regulate serum calcium concentration and bone metabolism. PTH promotes the release of calcium from bone, increases absorption of calcium from the intestine and increases reabsorption of calcium in the renal tubules. In turn, the level of serum calcium concentration regulates PTH secretion, a mechanism mediated via a calcium sensing receptor on the surface of the parathyroid cells.

14.2.1 Parathyroid Scanning with ^{99m}Tc-Sestamibi (Several Imaging Protocols)

^{99m}Tc-sestamibi (methoxyisobutylisonitrile, MIBI) is a cationic lipophilic complex. Its uptake by parathyroid tumors was first reported in 1989 by Coakley et al. ^{99m}Tc-sestamibi has replaced thallium-201 for parathyroid imaging.

The major obstacle to visualization of the parathyroid tumors is that the thyroid gland is also avid for ^{99m}Tc-sestamibi. Several methods for distinguishing thyroid uptake from parathyroid uptake have been suggested, but basically there are two kinds of approach. The first approach takes advantage of differences in ^{99m}Tc-sestamibi uptake kinetics between the thyroid and parathyroid tissue "double-phase method." In the second approach, "subtraction scanning," ^{99m}Tc-sestamibi is used in combination with a second tracer taken up by the thyroid gland but not by the parathyroid glands, either iodine-123 (Weber et al. 1993; Kettle and O'Doherty 2006) or ^{99m}Tc-pertechnetate (Rubello et al. 2003).

A. The "Double-Phase Method". It has been shown that ^{99m}Tc-sestamibi is washed out from the thyroid tissue faster than from the parathyroid tissue (Fig. 14.5).

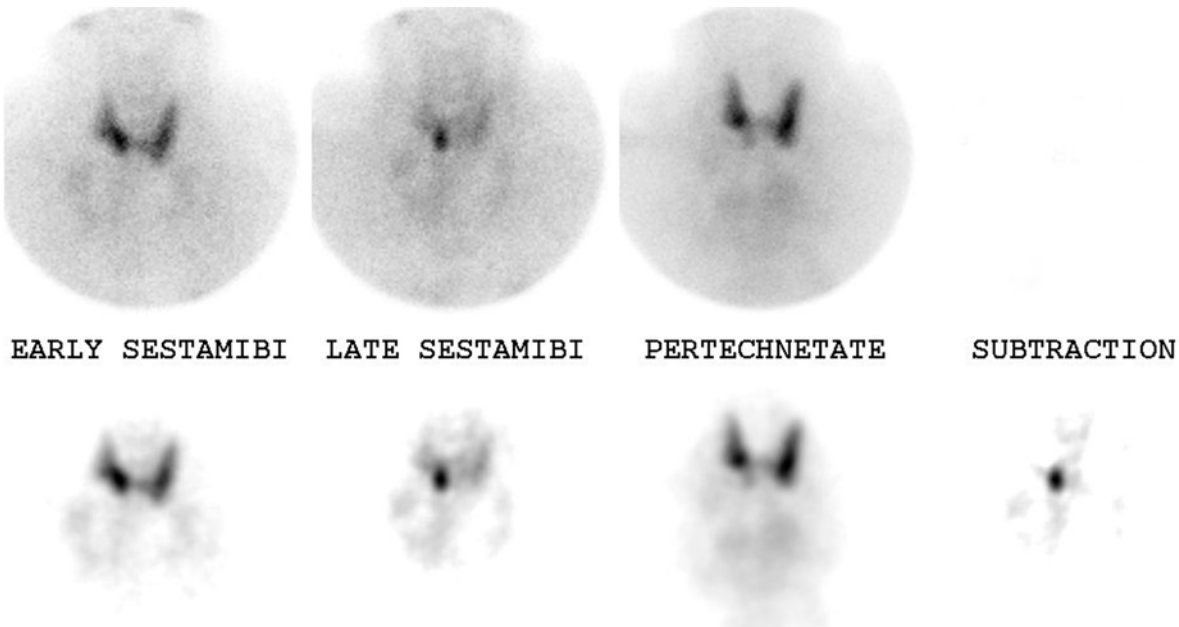

Fig. 14.5. Early (15 min) and late (2 h) sestamibi images show initial hyperconcentration and subsequent delayed washout at the low medial portion of the right lobe. Thyroid specific pertechnetate scan shows absent activity in the same location. Subtraction image confirms the abnormal focus of activity. This was a parathyroid adenoma at surgery. (Courtesy of Dr. Christopher Palestro)

It follows that foci of ^{99m}Tc-sestamibi uptake that enhance or are still visible on an image recorded 2 – 3 h after the radionuclide injection theoretically correspond to parathyroid tissue (Taillefer et al. 1992). The need for a single radionuclide and the simplicity of comparing two images recorded about 15 and 150 min after the injection have made this technique extremely popular. However, during evaluation of this technique, evidence rapidly accumulated that longer retention is not a constant feature (Giordano et al. 2001; Kettle and O'Doherty 2006; Palestro et al. 2005). Sensitivity is poor in the case of multiple parathyroid gland disease (Martin et al. 1996). Moreover, retention of ^{99m}Tc-sestamibi in some thyroid nodules may mimic parathyroid tumors (Palestro et al. 2005).

B. Subtraction Techniques. Two images of the cervical area are recorded, one showing uptake of ^{99m}Tc-sestamibi by the thyroid and parathyroid glands and the other showing uptake of the second radionuclide by the thyroid gland only. This may be ^{123}I or ^{99m}Tc-pertechnetate. A computer program is used to subtract the second image from the first, thus generating an image that reflects uptake by the parathyroid glands only (Fig. 14.6). One difficulty with subtraction imaging is maintaining the patient still during the time necessary to scan the thyroid, to inject ^{99m}Tc-sestamibi, and to record images of this second tracer. Simultaneous recording of ^{123}I and ^{99m}Tc-sestamibi can be a simple answer to these difficulties. It prevents artifacts on subtraction images due to patient motion, and shortens the imaging time (Hindié et al. 1998; Mullan 2004).

14.2.1.1 Practical Considerations for Dual-Tracer ^{99m}Tc-Sestamibi and Iodine-123 Subtraction Scintigraphy with Simultaneous Acquisition

The investigation should be done in the absence of iodine saturation. Patients on thyroid hormone replacement should withhold this treatment 2 – 3 weeks before the investigation. An injection (or an oral dose) of iodine-123 (12 MBq) is given. Two hours later, the patient is placed under a gamma camera and given an injection of ^{99m}Tc-sestamibi (600 MBq). Images are acquired simultaneously using appropriate energy windows without overlap (Hindié et al. 1998). Imaging starts with a planar image of the anterior aspect of the neck and mediastinum (300 s) using a broad field of view extending from the submandibular salivary glands to the heart to ensure detection of ectopic glands (Akerström et al. 1984). Then an enlarged image of the anterior neck (600 s) is obtained using a pinhole collimator. An image analysis computer program subtracts an increasing percentage of the iodine-123 image from the ^{99m}Tc-sestamibi image. Subtraction is considered optimal when ^{99m}Tc-sestamibi activity is identical in the thyroid gland in the neighboring tissues (Figs. 14.5, 14.6). At this time, any focus or foci of increased ^{99m}Tc-sestamibi uptake is suspicious for abnormal parathyroid glands (Figs. 14.5, 14.6). When the anterior image shows a single focus suggesting a solitary parathyroid adenoma (Fig. 6a), a lateral view is recorded to determine whether the adenoma is close to the thyroid gland body or is lateroesophageal (Fig. 14.6b). If the mediastinal view

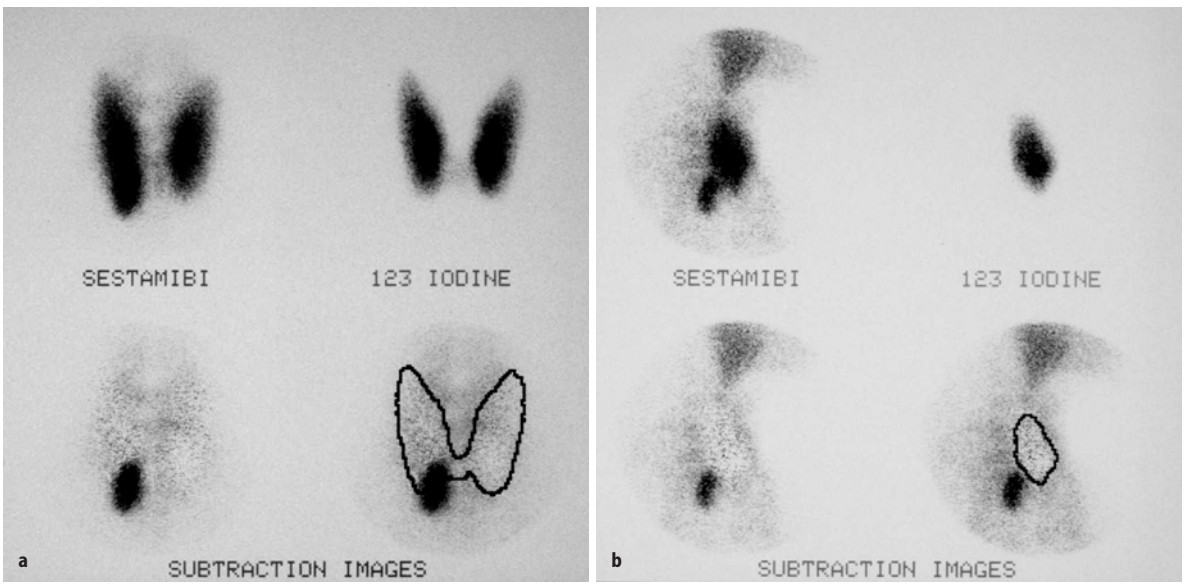

Fig. 14.6. a Subtraction scanning with simultaneous acquisition of ^{99m}Tc-sestamibi and iodine-123 in a patient with primary hyperparathyroidism. The subtraction shows a focus of selective ^{99m}Tc-sestamibi uptake at the level of the lower pole of the right lobe of the thyroid. **b** Lateral view (same patient as in **a**) shows that the lesion is slightly posterior to the thyroid gland. A parathyroid adenoma of 1,870 mg was found at surgery

shows ectopic uptake, then SPECT acquisition is necessary.

An alternative approach to using ^{123}I is to use ^{99m}Tc-pertechnetate. Direct side by side comparison or actual computer subtraction of the sestamibi-iodine or sestamibi-pertechnetate images may be performed (see below).

We will now focus on the role of parathyroid scintigraphy in patients with primary hyperparathyroidism, as well as in renal failure patients with secondary hyperparathyroidism.

14.2.2 Primary Hyperparathyroidism

Primary hyperparathyroidism (pHPT) is a surgically correctable disease with the third highest incidence of all endocrine disorders after diabetes mellitus and hyperthyroidism (Al Zahrani and Levine 1997). Primary hyperparathyroidism is caused by excessive amounts of parathyroid hormone secreted by one or more enlarged diseased parathyroid gland. Patients with pHPT may suffer from renal stones, osteoporosis, gastrointestinal symptoms, cardiovascular disease, muscle weakness and fatigue, and neuropsychological disorders. The highest occurrence of the disease is in post-menopausal women, in whom the prevalence may attain 2% (Lundgren et al. 1997).

In the past, primary hyperparathyroidism was characterized by severe skeletal and renal complications and apparent mortality. This may still be the case in some developing countries. The introduction of calcium autoanalyzers in the early 1970s led to changes in the incidence of pHPT and deeply modified the clinical spectrum of the disease at diagnosis (Heath et al. 1980). Most new cases are now biologically mild without overt symptoms (Al Zahrani and Levine 1997). Parathyroidectomy is the only curative treatment of pHPT. In the recent guidelines of the US National Institute of Health (NIH), surgery is recommended for all young individuals, and for all patients with overt symptoms (Bilezikian et al. 2002). For patients who are asymptomatic and are 50 years old or older, surgery is recommended if any of the following signs is present (serum calcium greater than 10 mg/l above the upper limits of normal; 24-h total urine calcium excretion of more than 400 mg; creatinine clearance reduced by more than 30% compared with age-matched persons; bone density that is more than 2.5 SDs below peak bone mass; T score $\leq$2.5; and patients for whom medical surveillance is either not desirable or not possible). After complete baseline evaluation, patients who are not operated on need to be monitored twice yearly for serum calcium concentration, yearly for creatinine concentration, and it is also recommended to obtain bone mass measurements on a yearly basis (Bilezikian et al. 2002). Some authors recommend parathyroidectomy for all patients with a secure diagnosis of pHPT (Utiger 1999).

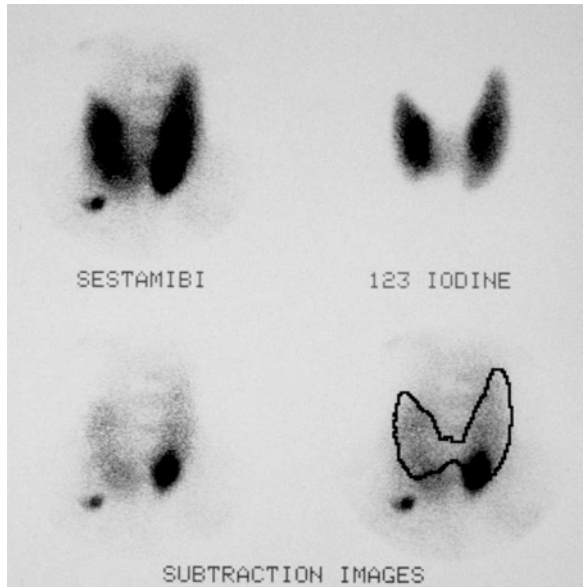

Fig. 14.7. Subtraction scanning with simultaneous acquisition of ^{99m}Tc-sestamibi and iodine-123 in a patient with primary hyperparathyroidism. The subtraction shows two foci that were confirmed at surgery: a lower right parathyroid adenoma (70 mg) and a lower left second parathyroid adenoma (2,300 mg)

Successful parathyroidectomy depends on recognition and excision of all hyperfunctioning parathyroid glands. Primary hyperparathyroidism is typically caused by a solitary parathyroid adenoma, less frequently (in about 15%) by multiple parathyroid gland disease (MGD) (Fig. 14.7) and rarely (in about 1%) by parathyroid carcinoma. Patients with MGD have either double adenomas or hyperplasia of three or all (four) parathyroid glands. Most cases of MGD are sporadic, while a small number are associated with hereditary disorders such as multiple endocrine neoplasia type 1 or type 2a, or familial hyperparathyroidism (Marx et al. 2002). Conventional surgery consists of routine bilateral exploration with identification of all four parathyroid glands. For several decades, preoperative imaging was not used before first-time surgery. Unguided bilateral exploration dissecting all potential sites in the neck achieved cure in 90–95% of patients (Russell and Edis 1982). The two main reasons for failed surgery are ectopic glands and undetected MGD (Levin and Clark 1989). In the past several years, minimally invasive surgery has become increasingly popular (see below).

The Choice of a Parathyroid Imaging Technique. The most common preoperative localization methods are radionuclide scintigraphy and ultrasound. Because high resolution ultrasound would, even in skilled hands, fail to detect the majority of ectopic glands and

the majority of MGD cases, it is not optimal for preoperative imaging as a single technique. In the study by Haber, ultrasound missed six of eight ectopic glands and five of six cases of MGD (Haber et al. 2002). Ultrasound may, however, be useful in combination with sestamibi imaging (Rubello et al. 2003).

^{99m}Tc-sestamibi scanning is now considered the most sensitive imaging technique in patients with primary hyperparathyroidism (Giordano et al. 2001; Mullan 2004; Haber et al. 2002; Kettle and O'Doherty 2006). Whatever the protocol used, sestamibi scanning would usually meet the requirement of detecting ectopic glands (eight out of eight in the study by Haber et al. 2002). However, when dealing with the ability to recognize MGD, the protocol in use will lower sensitivity. When ^{99m}Tc-sestamibi is used as a single tracer with planar imaging at two time points – "the double-phase method" – sensitivity for primary hyperplasia is very low (Taillefer et al. 1992; Martin et al. 1996), although better results can be obtained by adding SPECT. Subtraction scanning, using either ^{123}I (Borley et al. 1996; Hindié et al. 2000; Mullan 2004; Kettle and O'Doherty 2006) or ^{99m}Tc-pertechnetate (Rubello et al. 2003), in addition to ^{99m}Tc-sestamibi, greatly improves sensitivity for hyperplastic glands.

Some Points are Important to Know when Proceeding with Parathyroid Scanning.

- Imaging is not for diagnosis. The increase in calcium and PTH plasma levels establish the diagnosis.
- Imaging does not identify normal parathyroids, which are too small (20 – 50 mg) to be seen.
- Imaging should detect abnormal parathyroid(s) and indicate the approximate size and the precise relationship to the thyroid (at what level of the thyroid the parathyroid lesion is seen on anterior view; and whether it is proximal to the thyroid or deeper in the neck on the lateral or oblique view or on SPECT).
- Imaging should identify ectopic glands (add SPECT in cases of mediastinal focus, and ask for additional CT or MRI for confirmation and anatomical landmarks). A mediastinal adenoma is illustrated in Fig. 14.8.
- Optimal imaging should be able to differentiate patients with single adenoma from those with MGD.
- Imaging should identify thyroid nodules that may require concurrent surgical resection.

Imaging is Mandatory in Case of Reoperation. The two main reasons for failed surgery are ectopic glands (retro-esophageal, mediastinal, intrathyroid, in the sheath of the carotid artery, or undescended) and undetected MGD (Levin and Clark 1989). Repeat surgery is associated with a dramatic reduction in the success rate and an increase in surgical complications. Imaging is therefore mandatory before reoperation (Sosa et al. 1998). Sestamibi scanning (Coakley) has established itself as the imaging method of choice in reoperation of persistent or recurrent hyperparathyroidism (Weber et al. 1993). In these patients it is necessary to have all the information concerning the first intervention, including the number and location of parathyroids that have been seen by the surgeon and the size and histology of resected glands. Whatever the sestamibi scanning protocol used, it is necessary to provide the surgeon with the best anatomical information using both anterior and lateral (or oblique) views of the neck, and SPECT whenever useful, especially so for a mediastinal focus.

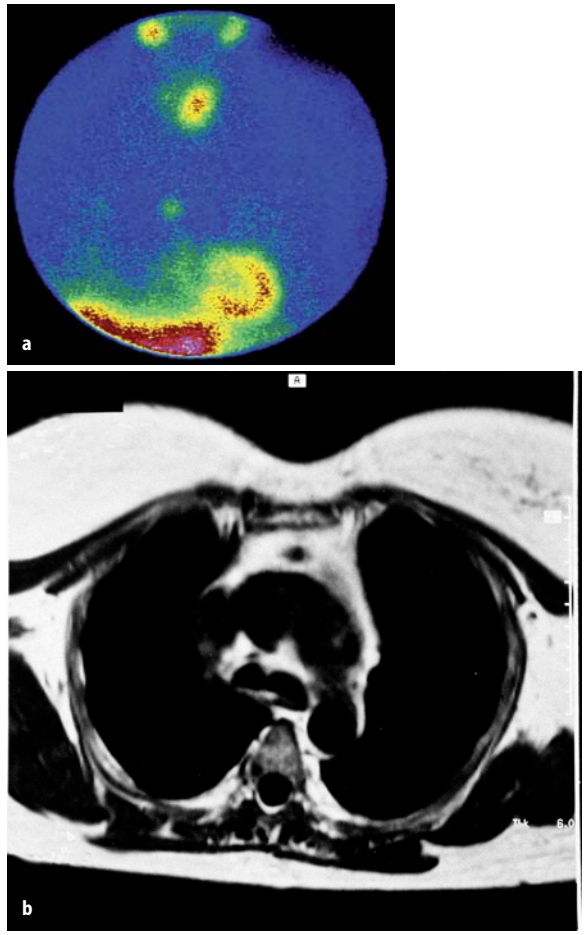

Fig. 14.8. This 61-year-old woman with primary hyperparathyroidism has a past history of right thyroid surgery for a thyroid nodule. Ultrasound examination suggested a parathyroid lesion in the region of the right thyroid bed. The ^{99m}Tc-sestamibi image (**a**) shows slight uptake in the right thyroid bed. However, there was similar uptake on the iodine-123 image (not presented), suggesting remnant thyroid tissue. The ^{99m}Tc-sestamibi sestamibi image clearly shows a small focus in the mediastinum (**a**). MRI confirmed the presence of a 15 × 8 mm nodule anterior to the ascending aorta (**b**). This lesion has hyposignal on T_1 compared to surrounding thymic fat. A 585 mg parathyroid adenoma was resected

Sestamibi results should be confirmed with a second imaging technique (usually US for a neck focus, CT or MRI for a mediastinal image) before proceeding to reoperation. The availability of hybrid instruments, that allow both SPECT and CT to be performed on the same machine with excellent image fusion, should be an ideal answer to these requirements (Krausz et al. 2006). ^{11}C-methionine, a PET tracer, may have a role before reoperation in the case of negative sestamibi scanning (Cook et al. 1998).

Scanning with Sestamibi is Increasingly Ordered on a Routine Basis for First-Time Parathyroidectomy. The first exploration is the best time to cure hyperparathyroidism. Most surgeons would then appreciate having information concerning the site of the neck on which to start dissection and concerning the possibility of ectopic parathyroid glands (Sosa et al. 1998; Liu et al. 2005). By preoperatively recognizing the rare cases (2–5%) of ectopic parathyroid tumors, the success of bilateral surgery can now be very close to 100% (Hindié et al. 1997). In the case of a mediastinal gland, the surgeon can proceed directly with first-intention thoracoscopy, avoiding unnecessary initial extensive neck surgery in searching for the elusive gland (Liu et al. 2005). Preoperative imaging would also shorten the duration of bilateral surgery (Hindié et al. 1997). By allowing the surgeon to find the offending gland earlier in the operation, the time necessary for frozen section examination can be used by the surgeon for inspection of the other parathyroids, also reducing surgeon anxiety.

Preoperative Imaging has Opened up a New Era of Minimally Invasive Parathyroid Surgery. Conventional bilateral exploration is still considered the gold standard in parathyroid surgery. However, the introduction of sestamibi scanning, the availability of intraoperative adjuncts such as the gamma probe and intraoperative monitoring of PTH, to help detect MGD, has challenged the dogma of routine bilateral exploration. When preoperative imaging points to a single well-defined focus, unequivocally suggesting a "solitary adenoma," the surgeon may now choose focused surgery instead of bilateral exploration. Focused excision can be made by open surgery through a mini-incision, and possibly under local anesthesia, or by video-assisted endoscopic surgery under general anesthesia (Lee and Inabnet 2005). Patients in whom focussed parathyroid surgery is successfully completed enjoy, as compared to bilateral surgery, a shorter operation time (often as an outpatient), the possibility of using local anesthesia, a better cosmetic scar, a less painful postoperative course, a less profound postoperative "transient" hypocalcemia, and an earlier return to normal activities. The fact that many clinicians now use a lower threshold for surgery is partly due to the perception that parathyroid surgery is easier than in the past (Utiger 1999).

Patients at specific risk of failure of minimal surgery are those with unrecognized MGD. Therefore, when choosing minimal surgery, the surgeon is committed to depicting cases of MGD either preoperatively, through an appropriate imaging protocol, or with intraoperative monitoring of PTH plasma levels, or, frequently, by combination of both. The true sensitivity of intraoperative PTH for MGD is still debated. What raises concern is that studies relying solely on intraoperative measurements report a low percentage of MGD of only 3% (Irvin), which is three to four times lower than generally observed during routine bilateral surgery. Whether this will lead to higher rates of late recurrences is not known. It would thus be important that imaging methods used to select patients for focused surgery have a high sensitivity for detecting MGD.

In this new era of focused, minimally invasive operations, the success of parathyroid surgery not only depends on an experienced surgeon but on an excellent interpretation of images. A localization study with high accuracy is mandatory to avoid converting the surgery to a bilateral exploration under general anesthesia after minimal surgery has been started. It is thus important to avoid confusion with a thyroid nodule. Precise anatomic description is also important. With enlargement and increased density, superior parathyroid adenomas can become pendulous and descend posteriorly. A lateral view (or oblique view, or SPECT) should indicate whether the adenoma is close to the thyroid or deeper in the neck (tracheo-esophageal groove, or retroesophageal). This information is useful, because visualization through the small incision is restricted. Moreover, the surgeon may choose a lateral approach to excise this gland instead of an anterior approach. To reach a high sensitivity in detecting MGD with subtraction techniques, the degree of subtraction should be monitored carefully. Progressive incremental subtraction with real-time display is a good way to choose the optimal level of subtraction (following subtraction, residual activity in the thyroid area should not be lower than in surrounding neck tissues). Oversubtraction would easily delete additional foci of activity and provide in some patients a wrong image suggestive of a single adenoma.

14.2.3 Secondary Hyperparathyroidism

Secondary hyperparathyroidism is a common complication in patients with chronic renal failure. Hypocalcemia, accumulation of phosphate, and a decrease in the active form of vitamin D lead to increased secretion of parathyroid hormone. With chronic stimulation, hyperplasia of parathyroid glands accelerates and may

develop into autonomous adenomas. The extent of parathyroid growth then becomes a major determinant of parathyroid hormone hypersecretion. Secondary hyperpathyroidism leads to renal bone disease, the development of soft tissue calcifications, vascular calcifications and increased cardiovascular risk, among other complications. When medical therapy fails, surgery becomes necessary. Surgery can be either subtotal parathyroidectomy, with resection of three glands and partial resection of the fourth gland, or total resection with grafting of some parathyroid tissue in soft tissues of the forearm in order to avoid permanent hypoparathyroidism.

Preoperative Imaging. Surgery of secondary hyperparathyroidism requires routine bilateral identification of all parathyroid tissue. Moreover, early studies based on single-tracer sestamibi scanning have reported low sensitivity of about 40 – 50 % in detecting hyperplastic glands. Inefficiency of single-tracer techniques both in secondary hyperparathyroidism and in primary hyperplasia is possibly due to more rapid wash-out of tracer from hyperplastic glands than from parathyroid adenomas. For those reasons, preoperative imaging has not yet gained universal acceptance among surgeons.

Dual-tracer subtraction imaging, planar or SPECT, provides substantial improvement in the detection rate of hyperplastic glands in renal failure patients (Hindié et al. 1999; Perié et al. 2005).

The following information can be obtained:

- The preoperative map may facilitate recognition of the position of aberrant parathyroids, also reducing the extent of dissection (Hindié et al. 1999; Fuster et al. 2006).
- Parathyroid glands with major ectopia would be missed without preoperative imaging.
- Although the usual number of parathyroid glands is four, some individuals (about 10 %) may have a supernumerary fifth gland (Akerström et al. 1984). When this information is provided by preoperative imaging it may avoid surgical failure or late recurrence (Hindié et al. 1999).
- Finally, the use of the parathyroid gland that has the lowest sestamibi uptake intensity as remnant tissue may reduce the risk of recurrent disease (Hindié et al. 1999; Fuster et al. 2006).

Image Findings in Patients with Persistent or Recurrent Secondary Hyperparathyroidism After Initial Surgery. Immediate failure and delayed recurrence are not unusual, occurring in 10 – 30 % of patients. Imaging is mandatory before reoperation. Knowledge of all the details concerning the initial intervention is necessary for interpretation. As with primary hyperparathyroidism, we recommend that lesions seen on the sestamibi scan be matched with a second radiological technique (US, or MRI) for confirmation and anatomical landmarks before reoperation.

Some aspects specific to patients reoperated on for secondary hyperparathyroidism need to be emphasized:

- Specific views of the forearm should be obtained in patients who had a parathyroid graft.
- It is not unusual that imaging in these patients shows more than one focus of activity with one corresponding to recurrent disease on the subtotally resected gland (or on grafted tissue) and the other corresponding to an ectopic or fifth parathyroid, missed at initial intervention (unpublished data).

14.3 Adrenal and Neuroendocrine Imaging

14.3.1 Adrenal Cortical Imaging

The adrenal glands secrete steroid hormones (mineralocorticoids, sex steroids and glucocorticoids) originating from cholesterol. Like any endocrine tissue, they can become overactive and/or undergo tumor transformation. Hyperplasia can be diffuse as in enzymatic or focal as in adenomas and hyperaldosteronism. Adenomas can involve each of the three layers of the gland and secrete the corresponding hormones. Non-functional nodules are observed mainly in hypertensive patients. The corticosurrenalomas are carcinomas of suprarenal origin which often result in a multi-secreting syndrome with both metastatic and locoregional extensions (vascular and ganglionary). The prognosis is determined by histopathology using the score of Weiss and is worsened by locoregional recurrence and metastases. Surgery is the treatment of choice. The adrenals are also the location of various tumors or pseudotumors, and metastases. On occasion, incidental abnormalities can be discovered in the course of performing imaging examiations, e.g., PET or CT, for other reasons. These fortuitous findings have been called “incidentalomas.”

^{131}I-6β-19-Nor-Cholesterol. This is an analogue of cholesterol transported by LDL and captured by their receptors in the three layers of the adrenal cortex. Its elimination is intestinal with an enterohepatic cycle. Its deiodination releases iodine-131. A very slow intravenous administration from 20 to 40 MBq for an adult is given at least 2 – 4 days before the acquisition of the images (may be up to 10 days). An additional localization of the kidneys by Tc-DTPA is sometimes useful. Dosimetry is unfavorable as the total body dose is approximately 2.4 mS/MBq, the target organs being the thyroid, adrenal, liver, uterus, ovaries and testes. The adverse effects are notable: anaphylactic reactions, faint-

ness and hypertension. These are accentuated in the event of a rapid intravenous injection, particularly in children less than 3 years old. Contraindications, in addition to pregnancy or nursing, relate to premature and newborns. Preparing the patient is of primary importance: thyroid saturation (a few hours before the injection and for the following 7 days) by stable iodine (100 mg of stable iodide per day in any form, e.g., Lugol's solution). One may also attempt to stimulate intestinal elimination by administering hyperosmotic laxatives and even blocking of the enterohepatic cycle (at least 48 h after the injection) by biliary salt chelators such as cholestyramine. Certain medications can increase the uptake (hypocholesterolemic agents), lower it (inhibitors of steroid synthesis, indomethacin, oral contraceptive, hypercholesterolemia) or interfere with the renin-angiotensin system. The latter group of medications includes spironolactone (to be stopped after 6 weeks), diuretics (1 week), inhibitors of the conversion enzyme and calcium inhibitors (24 h), and alpha-blockers (24 h).

If the aim of the study is to visualize an autonomous hyperfunctioning adrenal cortical lesion (such as primary hyperaldosteronism, or hyperandrogenism), corticotropic restraining (dexamethasone 4 mg/4 times per day including one dose before sleeping, to be started 7 days before the injection until the last acquisition) is indicated to inhibit normal uptake.

The indications for scintigraphy without corticotropic restraining are localization of an extra-adrenal lesion (hyperandrogenism), Cushing adenoma, or determination of whether a lesion detected on CT or MRI is malignant. The interpretation of the images has to take into account physiological uptakes (hepatic, testicular, biliary and intestinal elimination) as well as the effectiveness of the patient preparation administered prior to imaging.

The expected results vary according to indication.

Primary Hyperaldosteronism. The primitive hypersecretion of aldosterone (Fallo et al. 2006) is associated with a low rate of renin secretion and often hypokalemia. This accounts for 2% of the causes of arterial hypertension. Other positive findings include Conn's adenoma (60% of the cases), diffuse hyperplasia (25%) or macronodular hyperplasia (5%), and, rarely, a corticosuprarenaloma (<1%). CT cannot by itself make the distinction between these entities. Scintigraphy preceded by appropriate patient preparation can distinguish whether a lesion is uni- or bilateral (Fig. 14.9). In making this distinction, scintigraphy is 78–94% successful versus 67–75% for CT (Nocaudie-Calzada et al. 1999). The reference standard is adrenal venous catheterization, which is invasive and fails to make the distinction between unilateral or bilateral involvement in 10% of cases (Carr et al. 2004).

Fig. 14.9. Primary aldosteronism. Dexamethasone suppression with ^{131}I-noriodocholesterol scintigraphy performed with 37 MBq. The study was performed 7 days post-injection. Posterior abdominal view shows bilateral adrenal hyperplasia

Hypercorticism. Additional ectopic adrenals stimulated by hypercorticotropism can explain a persistent hypercorticism after bilateral adrenalectomy for Cushing disease. Cushing adenomas are adrenocortical secreting glucocorticoids, which behave autonomously independently of the contralateral adrenal gland without restraining corticotropins (Rossi et al. 2000). For *hyperandrogenism* the sensitivity of scintigraphy is 85–90% (85% for CT, 74% for MRI). Other areas that have been looked at include ovarian polycystic tumors, Stein-Leventhal syndrome and testicular tumors with Leydig cells (Mountz et al. 1988). Figures 14.9 and 14.10 show examples of primary aldosteronism and adrenal carcinoma, respectively.

14.3.1.1 Other Radiopharmaceuticals

The ability to specifically demonstrate functioning adrenocortical activity is very useful in guiding therapeutic choices. However, ^{131}I-noriodocholesterol is the one examination in nuclear medicine that is associated with adverse effects and a significant radiation burden for the patient. For these reasons, it has never received FDA approval for routine use in the United States. It also requires preparation of the patient which, in the case of hyperaldosteronism, involves hypertensive risks. Therefore, other gamma emitting radiopharmaceuticals have been considered using cholesterol LDL or metapyrone transporters. Currently ^{11}C-metomidate is under investigation. In addition, ^{18}F-FDG appears to show promise in possibly distinguishing benign from malignant lesions of the adrenal (Minn et al. 2004). Figure 14.10d and e show an FDG study in an adrenal carcinoma.

14.3.2 Adrenal Medulla: Pheochromocytomas and Paragangliomas

Pheochromocytoma is rare (1/100,000 in the general population, 1/1,000 among hypertensive patients and 4% in the event of adrenal incidentaloma). The pheo-

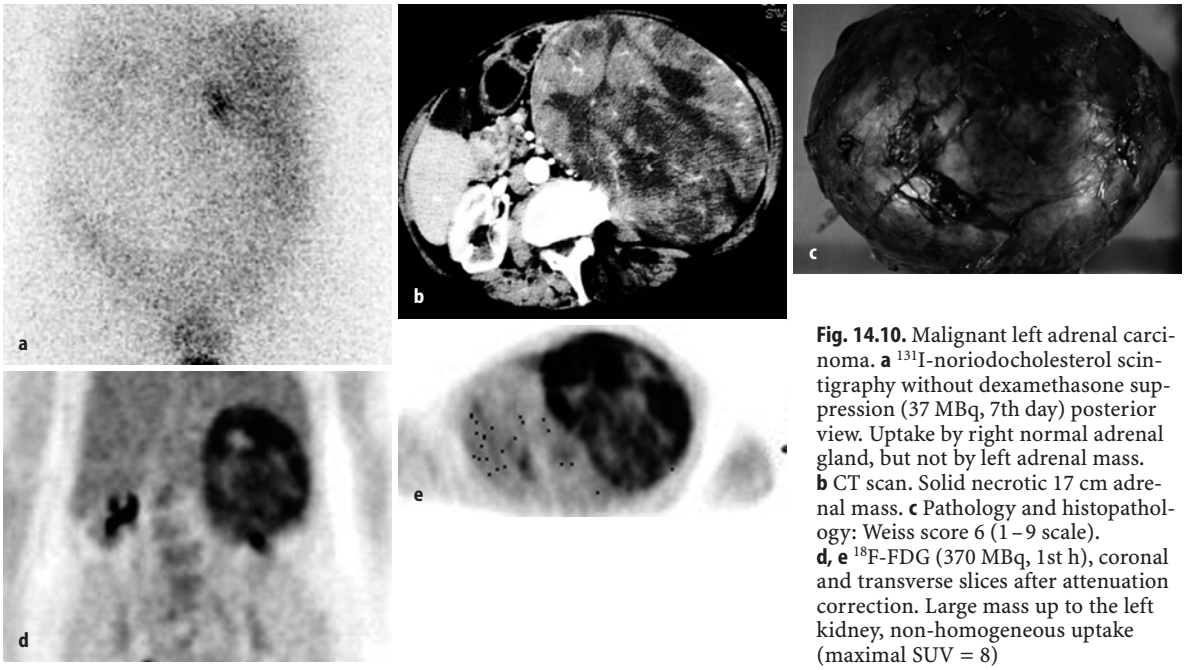

Fig. 14.10. Malignant left adrenal carcinoma. **a** ^{131}I-noriodocholesterol scintigraphy without dexamethasone suppression (37 MBq, 7th day) posterior view. Uptake by right normal adrenal gland, but not by left adrenal mass. **b** CT scan. Solid necrotic 17 cm adrenal mass. **c** Pathology and histopathology: Weiss score 6 (1–9 scale). **d, e** ^{18}F-FDG (370 MBq, 1st h), coronal and transverse slices after attenuation correction. Large mass up to the left kidney, non-homogeneous uptake (maximal SUV = 8)

chromocytoma may exist in the adrenal medulla as well as the paraganglioma. Developed from sympathetic tissue, it is considered functional if it secretes catecholamine or non-functional if it is not secreting (generally located on the head and the neck). A genetic predisposition is found in 25% of pheochromocytomas. Malignancy (10%) is more frequent in the event of SDH-B mutations (Gimenez-Roqueplo et al. 2003). Catecholamine hypersecretion is symptomatic in 50–60% of cases (sweating, palpitations, hypertension). The risks are related to the cardiovascular complications, to their extension to regional nervous and vascular networks and to their ability to recur and metastasize. Surgery is the prescribed treatment after preparation by alpha- or beta-blockers. Anesthetic precautions should also be considered. The treatment of symptomatic metastases is generally done with radiotherapy and, especially, treatment by ^{131}I-MIBG.

Meta-iodobenzylguanidine. Found in the adrenal medulla, myocardium and salivary glands, meta-iodobenzylguanidine (MIBG) labeled with iodine-131 or -123 is an analogue of adrenalin which is secreted by APUD cells (amine precursor uptake and decarboxylation). Abnormal localization occurs in pheochromocytomas, paragangliomas and neuroblastomas. Hepatic metabolism is poor with most elimination being through urinary, intestinal and pulmonary routes. After deiodation (<5%), released iodine follows its usual pathway with primary uptake by the thyroid gland. Dosimetry depends on the isotope used, with the target organs being the liver, bladder, spleen, salivary glands and adrenals: the effective total body dose is 0.2 mSv/MBq with ^{131}I and 0.015 mSv/MBq with ^{123}I. The drugs which may interfere with MIBG uptake include antidepressants, cocaine, reserpine, sympathicomimetics, alpha and beta blockers and calcium channel inhibitors. Metastatic lesions may actually be suppressed while a patient is on therapy (Fig. 14.11).

Patient preparation consists of thyroid saturation by stable iodine, oral hydration and acceleration of the intestinal transit time. Contraindications are pregnancy and breast feeding. Anaphylactic reactions are very rare. In the case of too rapid administration, especially with therapeutic doses, hypertension, abnormalities of cardiac rhythm and conduction are the risks which are related to the adrenergic effects of the MIBG. Scintigraphic acquisitions should be performed from the head to the pelvis. SPECT, with or without CT, can be done, as well. Anatomic landmarks with low activities of a Tc-labeled agent can be used, if desired. Pheochromocytomas (Fig. 14.12) and paragangliomas (Fig. 14.13) are diagnosed by MIBG with a specificity of 90–97% and a sensitivity of 80–90% if they are sporadic. The sensitivity is less (60–70%) if they are multiple (NEM2) (De Graaf et al. 2000), malignant or not secreting (head and neck) (Van der Horst-Schrivers et al. 2006). Levels of plasma metanephrines are sensitive and preferred for the diagnosis in the high-risk populations of pheochromocytoma. Levels of total urinary metanephrines are specific and recommended for screening in cases of low risk (Unger et al. 2006). MIBG scintigraphy should be added in the case of a moderate risk (Sawka et al. 2004). An increase in the plasma level

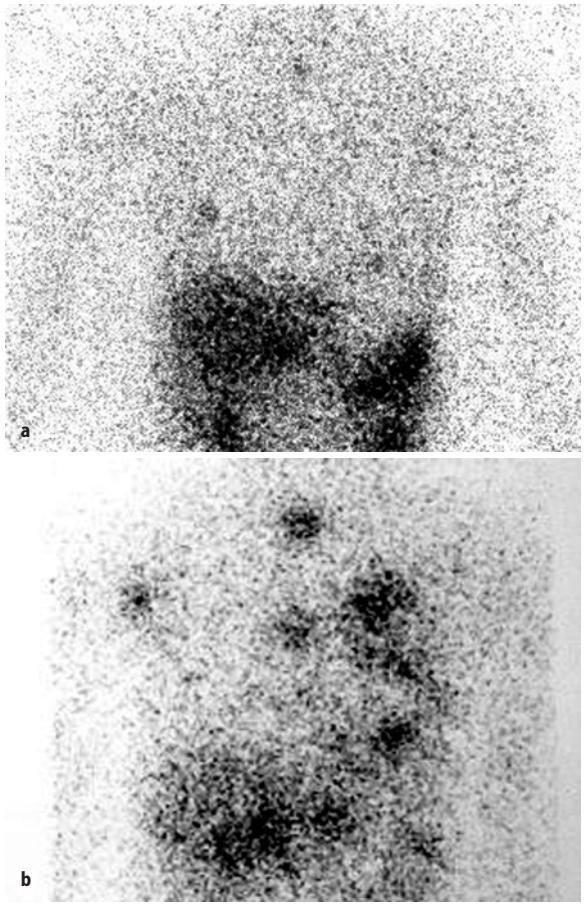

Fig. 14.11. Malignant pheochromocytoma with diffuse metastases. ^{131}I-MIBG post-therapeutic scintigraphy performed with 5 GBq, 5 days post-injection with patient on imipramine therapy (**a**) and following withdrawal of therapy (**b**). The post-withdrawal image shows diffuse metastases

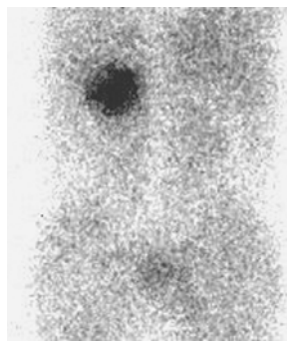

Fig. 14.12. Left adrenal (benign) pheochromocytoma (7 cm) is clearly seen on a posterior 48 h study following the administration of 37 MBq of ^{131}I-MIBG

of chromogranin-A reflects the mass of the pheochromocytoma and has a good negative predictive value (90 %) as does MIBG scintigraphy in the case of an adrenal nodule in hypertensive patients (Giovanella 2005).

Radiometabolic Treatment with ^{131}I-MIBG. This is possible using the beta emission of iodine-131. Administration from 3.7 to 7.4 GBq of ^{131}I-MIBG is carried out

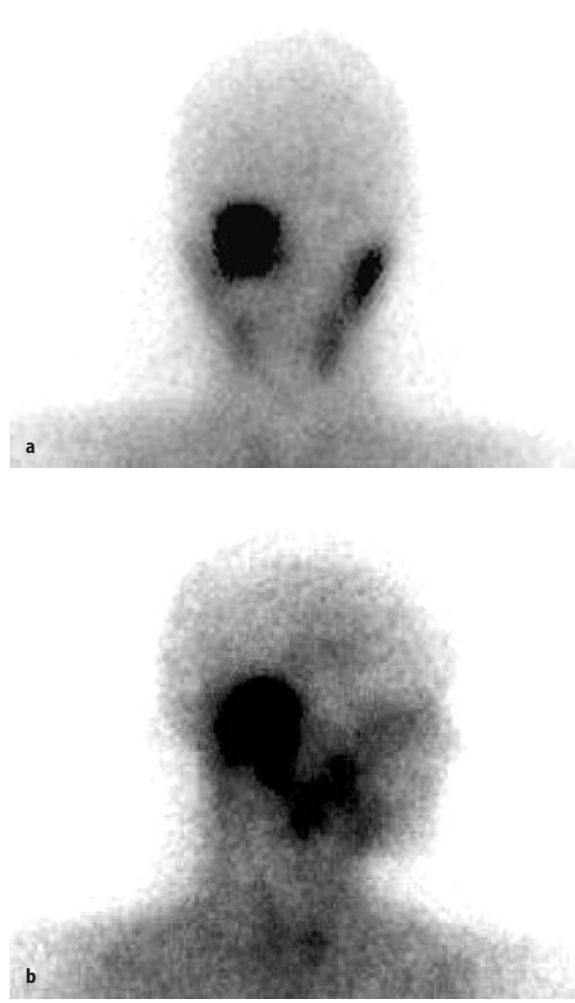

Fig. 14.13. Right tympanic paraganglioma. The study was performed on the 5th day following a therapeutic dose of 5 GBq of ^{131}I-MIBG. Anterior (**a**) and right lateral (**b**) views are shown

using a very slow intravenous infusion (60 – 90 min), under medical supervision. The patient has to be hospitalized in an isolated room for several days. The immediate cardiovascular risks can be seen in the case of too rapid an infusion because of mobilization of the secreting mass or tumoral lysis. Nauseas and vomiting may be handled with antidopaminergic treatment. Hematologic toxicity (thrombopenia and neutropenia) justifies blood count monitoring, and is related to the cumulative activity (> 30 GBq). This is especially true if there is associated chemotherapy. Renal toxicity also is increased by chemotherapy. Post-therapeutic whole body scintigraphy allows an assessment of extension (Fig. 14.14). The treatment may be repeated after 6 – 8 months depending on the hematologic state.

Therapeutic indications relate to all tumors having a sufficient MIBG uptake, with a valuable biological half-time. Therapeutic effectiveness in patients with inoperable and disseminated metastatic pheochromocytoma

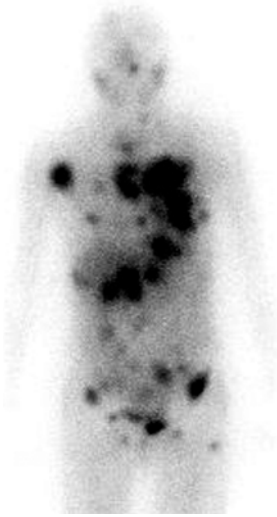

Fig. 14.14. Diffuse metastases shown on ^{131}I-MIBG whole body post-therapeutic scintigraphy (5 GBq, 5th day)

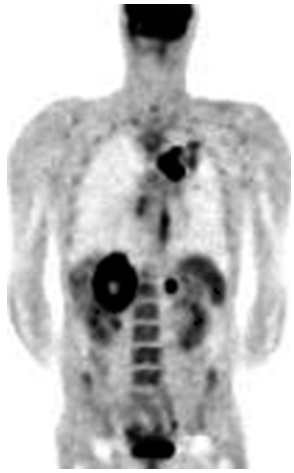

Fig. 14.15. Non-small cell lung carcinoma with several lung tumors, mediastinal lymph nodes and large necrotic right and small left adrenal metastases. The study was performed with 370 MBq of ^{18}F-FDG. A coronal slice is shown

is useful as it can significantly improve quality of life. The effect on the tumoral volume is not negligible (complete response 6%, partial 18%, stability 44%, growth 21%) and complete responses have been described with high dose regimens (Pink 2003). The reader is also referred to Chapter 25 for additional information on MIBG therapy.

14.3.2.1 Somatostatin Analogues

Pheochromocytomas and paragangliomas are rich in somatostatin receptors and thus concentrate octreotide derivatives such as ^{111}In-pentetreotide. The sensitivity for pheochromocytomas is inferior to that of MIBG imaging (25%) (Van der Harts et al. 2001), but better for paragangliomas (80%) particularly those not located in the head and neck (Muros et al. 1998). This also allows the detection of paragangliomas in the genetically predisposed patients (Duet et al. 2003). Mismatches between MIBG and Octreoscan scintigraphy may be observed, such as a positive somatostatin study in pheochromocytoma metastases associated with a negative MIBG examination (Tenenbaum et al. 1995).

Other Radiopharmaceuticals. Other radiopharmaceuticals such as positron emitters are being studied: These include ^{11}C-hydroxyepinephrine (Mann et al. 2006), ^{18}F-fluorodopamine (Mamede et al. 2006) and ^{18}F-DOPA (Hoegerle et al. 2002). The results have been variable.

14.3.3 Adrenal Incidentaloma

The term "incidentaloma" indicates an adrenal mass fortuitously discovered by abdominal imaging. The frequency of these discoveries (9% on CT) increases with age and existence of arterial hypertension or diabetes mellitus. The discovery of an adrenal incidentaloma (bilateral in 80% of cases) mandates a need to assess with additional imaging for malignancy as well as blood tests to decide between a surgical excision (which should not be delayed in case of a secreting medullary or cortical lesion), and a more conservative treatment and monitoring method (Mansmann et al. 2004). Etiologies for incidentalomas include: non-secreting adenomas (40%), corticosuprarenaloma (5%), pheochromocytoma (4%), other tumors and extra-adrenal masses, and metastases (20% in the absence of antecedent neoplasic history, 30–70% in the case of a breast, lung, or renal neoplasm, melanoma or lymphoma). Conventional imaging must be technically specific for the adrenal glands including CT with and without contrast media (wash-out study) and MRI (weighted T2 chemical-shift study) (Al-Hawary et al. 2005). MIBG confirms the diagnosis of pheochromocytoma and allows the detection of multiple or metastatic localizations (Maurea et al. 2002) (Figs. 14.14, 14.15). Noriodocholesterol may visualize functional corticosuprarenal tumors and contralateral suppression in cases of cortisolic infraclinical adenoma (Bardet et al. 1996). ^{18}FDG can show the malignancy of a corticosuprarenaloma and its extension (Leboulleux et al. 2006) or the primitive lesion in the event of metastasis (Fig. 14.15). Another interesting PET approach utilizes ^{11}C-metomidate to visualize adrenocortical tumors. If a mass is discovered and treated, monitoring is recommended at 6 months and 1 year. It can then be spaced out during the next several years (Bernini et al. 2005). The diagnostic strategy is multidisciplinary (Grumbach et al. 2003).

14.3.4 Neuroendocrine Tumors

Neuroendocrine tumors are ubiquitous and characterized by a phenotype of endocrine cells and neurons de-

pending upon their embryologic origin. Endocrine tumors with a neuronal phenotype (neuroblastoma, pheochromocytoma, paraganglioma) are distinguished from more frequent endocrine tumors with an epithelial phenotype. This latter group occurs in various localizations (appendix, colon, rectum, stomach, bronchi, intestine, pancreas, cutaneous tumor of Merckel). The term "neuroendocrine tumor" refers to tumors developed from diffuse endocrinal tissue, except for tumors having a specific denomination (medullary cancer of thyroid, etc.). The term "carcinoid" is kept for tumors likely to cause a carcinoid syndrome (serotonin). Gastro-entero-pancreatic endocrine tumors (75% of endocrine tumors) are usually low grade and slow growing and their incidence is underestimated. Pulmonary endocrine tumors are classified as typical or atypical carcinoid, low differentiated small or large cells. Endocrine tumors can also be located in other organs (thymus, breast, prostate). There are associated endocrine tumors in the event of multiple endocrine neoplasia (MEN): Variations include MEN type 1 (parathyroid, duodeno-pancreas, pituitary gland), MEN type 2 (medullary thyroid cancer), MEN 2A (pheochromocytoma(s) and parathyroidal hyperplasia) or MEN 2B (mucous neuromas, ganglioneuromas, ocular abnormalities and marfanoid morphotype). Histopathologic confirmation of the endocrine characteristics is performed by silver impregnation and immunohistochemistry. Clinically, a secondary syndrome may or may not be seen (carcinoid, Zollinger-Ellisson, hyperinsulinism, etc.). The tumoral syndrome depends on the site, growth and tumoral extension. Malignancy can only be assessed by the degree of local, locoregional or remote, ganglionic, hepatic and osseous invasion. Prognosis depends on the stage and differentiation. Stability can exist for years (even if malignant) and is best evaluated with serial studies. Treatment is surgical excision. Non-operable and progressive metastatic tumors require systemic, anti-secreting and anti-tumoral treatment, such as somatostatin analogues (even interferon or chemotherapy). The anti-secreting effect of somatostatin analogues is proven and is covered in Chapter 25.

14.3.4.1 Scintigraphy with Meta-Iodobenzylguanidine

Scintigraphy with ^{123}I or ^{131}I labeled meta-iodobenzylguanidine (MIBG) permits visualization of carcinoid tumors with a resolution of 1.0 – 1.5 cm and an overall sensitivity of 70%. By regions, the sensitivity is: 86% for abdominal extra-hepatic, 37 – 80% for intrahepatic, and 15 – 30% for intrathoracic. By tumor origin, the sensitivity is 50% for intestinal carcinoids, 9% for pancreatic or gastric lesions and even less for thymic or bronchial tumors (Kwekkeboom et al. 1993; Nocaudie-Calzada et al. 1996).

Radiometabolic Treatment with ^{131}I-MIBG. This is administered by a very slow intravenous infusion (60 – 90 min) of 3.7 – 12 GBq, repeated, if needed, every 6 months up to a cumulative activity of 20 GBq. Published results have shown for carcinoid tumors a symptomatic (49%), humoral (37%) and even tumoral (17%) response. In a recent series of 72 patients with metastatic endocrine carcinomas, there was a notable increase (38 months) in the median survival time (Safford et al. 2004). More detail on MIBG therapy may be found in Chapter 25.

14.3.4.2 Analogues of Somatostatin

Somatostatin receptors have a ubiquitous distribution in the body. Five subtypes of receptors (sst1 to sst5) have been identified, the density of which varies according to normal or pathological tissues (Reubi et al. 2001). They are transmembrane receptors, and the complex ligand-receptor is internalized (Cescato et al. 2006). The many analogues of somatostatin available or being studied vary by their affinity for the subtypes of sst. Their labeling by various radioisotopes via various chelators leads to different radiopharmaceuticals, with different pharmacokinetic and radioactive properties (Kwekkeboom et al. 1999). The scintigraphic visualization of neuroendocrine tumors depends on the tumoral density of sst having a strong affinity for the analogue, size, vascularization and homogeneity of the tumors, and the background noise function of the biodistribution of the radioanalogue.

14.3.4.3 Scintigraphy with Somatostatin Analogues

Scintigraphy with somatostatin analogues is generally performed with ^{111}In-pentetreotide (Octreoscan), which has been commercially available for more than 10 years. This study has been a major contribution to the study of neuroendocrine tumors. This ligand has a strong affinity for subtype 2 (and 3 and 5 to a lesser degree) and is captured by the endocrine tumors as well as by activated lymphocytes, renal cortex, spleen, liver, thymus, thyroid, pituitary gland and breast tissue). It is eliminated by the urinary, biliary and intestinal tracts (Fig. 14.16). In the absence of pregnancy and/or breast feeding, patients have to be hydrated orally and prepared by a laxative after the intravenous injection of approximately 185 MBq of the radiopharmaceutical. Pre-treatment by cold analogues is not a contraindication. Early and late images (from 4 to 8 h p.i.) should be acquired especially in the abdomen in order to distinguish tumoral uptake from intestinal elimination. SPECT images are also essential, particularly to explore the pancreatic area. A ^{99m}Tc liver/spleen scan can help

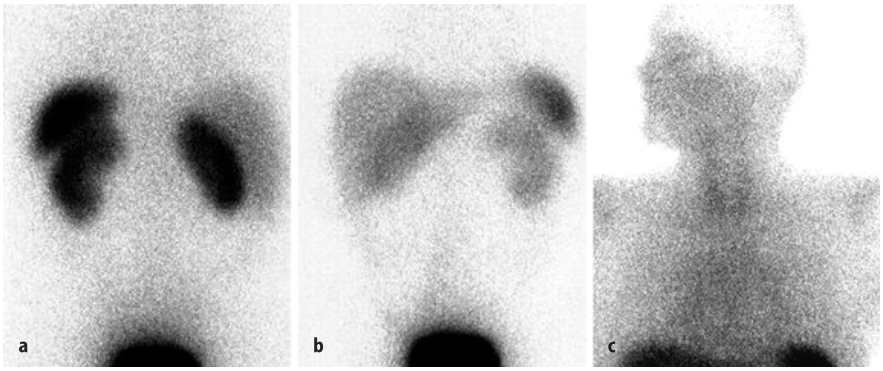

Fig. 14.16a–c. Normal ^{111}In-pentetreotide (Octreoscan) study performed 4 h after the administration of 185 MBq. Normal organs visualized include kidney, spleen, liver, thyroid as well as urinary and intestinal activity

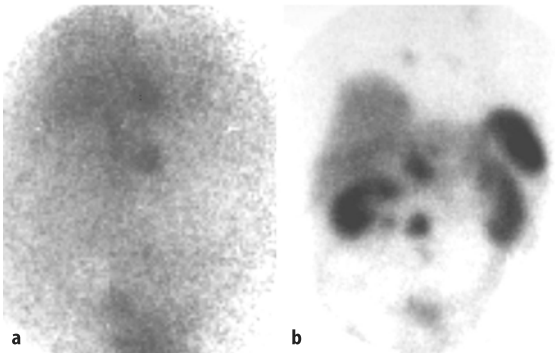

Fig. 14.17. Metastatic carcinoid tumor with abdominal lymph nodes and lung metastases. **a** ^{131}I-MIBG (37 MBq, 72th h) abdominal anterior view. **b** ^{111}In-pentetreotide (185 MBq, 24th h) abdominal anterior view

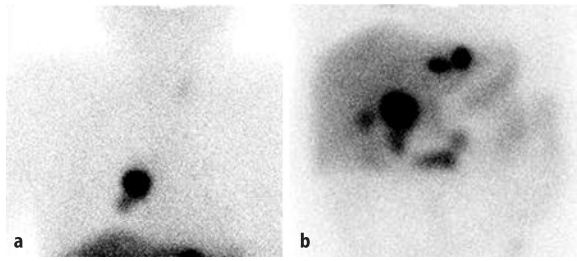

Fig. 14.18. Malignant gastrinoma with lung, liver and abdominal lymph node metastasis. The study was performed at 24 h with 185 MBq of ^{111}In-pentetreotide. Anterior images of the chest (**a**) and abdomen (**b**) are shown

contribute to the diagnosis of hepatic metastases or accessory spleen. Other neoplastic and non-neoplastic tissues are rich in somatostatin receptors: These include inflammatory foci (including post-surgery or -radiotherapy), infections and granulomatosis abnormalities (tuberculosis, sarcoidosis), foci of autoimmunity (basedowian ophthalmopathy, pituitary tumors (somatotropic), paragangliomas, pheochromocytomas, neuroblastomas and small cell pulmonary cancer) (Krenning et al. 1993). In carcinoid tumors, ^{111}In-penteotride scintigraphy shows better resolution (0.5–1.0 cm) and sensitivity (84–96%) than MIBG. This varies according to the tumor site (75% for gastric carcinoid, 33% for bronchial lesions). Discordant uptake between the two tracers in different metastases in the same patient has been shown (^{111}In-penteotride – 67–86%; and MIBG – 50–64%) (Fig. 14.17) (Nocaudie-Calzada et al. 1996; Kaltsas et al. 2001). Other comparisons between these two agents (Le Rest et al. 2001) or with F-DOPA (Becherer et al. 2004) have also been performed. These scintigraphic discordances are indicative of the functional heterogeneity that exists with these neuroendocrine tumors.

Cushing syndrome may present as an ectopic secretion of ACTH, generally by a bronchial carcinoid tumor or thymic secretion. In this scenario, the scintigraphic sensitivity with somatostatin analogues is only 30%, versus 50% for CT or MRI. The combination of the anatomic and functional imaging examinations increases the sensitivity to 70% (Pacak et al. 2004). For duodenopancreatic endocrine tumors, the sensitivity is high (50–60%) and increases to 90% when coupled with echoendoscopy. Gastrinomas and their possible metastases have an intense uptake (Fig. 14.18) even if they are occult and discovered in the framework of the MEN1 (Nikou et al. 2005). The uptake of insulinomas (sensitivity 50%) is less (Schillaci et al. 2000). Somatostatin scintigraphy is sensitive (80%) for the detection of hepatic metastases and is helped if performed in conjunction with the newer generation of CT or MRI (Dromain et al. 2005). As with other lesions, SPECT increases the number of visualized sites (Schillaci et al. 2003). For osseous metastases, it is as sensitive as ^{99m}Tc-phosphate bone scintigraphy (Lebtahi et al. 1999). It is certainly clear that scintigraphy with somatostatin analogues has enhanced diagnosis in 10–25% of the cases (Gotthardt et al. 2003).

14.3.4.4 Other Analogues

Various somatostatin radio-analogues are presently being studied (Reubi 2000): Tyr-3-octreotide (TOC) was first labeled with iodine-125 for autoradiography and, subsequently, with iodine-123 for scintigraphy. ^{99m}Tc-

depreotide has been marketed for the differentiation of benign from malignant solitary pulmonary nodules, and ^{111}In-DOTA-lanreotide has been studied in neuroendocrine tumors, but also in digestive adenocarcinomas, lymphomas, melanomas and head and neck cancers. Finally, there is ^{177}Lu-DOTA whose gamma emission allows scintigraphic visualization of foci irradiated by the beta emitting ^{64}Cu-TETA-octreotide. Another positron emitting agent, ^{86}Y-DOTA-TOC, has allowed diagnostic monitoring of the response to tumors irradiated by its analogue beta emitter ^{90}Y-DOTA-TOC.

Treatment by Somatostatin Radioanalogues. This is being studied with various analogues: the octreotide (affinity for sst2, but also 3 and 5), lanreotide or vapreotide (affinity for all except sst1, but lower uptake than the octreotide), and more recently the octreotate, remarkable for its great affinity for sst2). These therapeutic approaches are discussed in detail by Teunissen and his associates in Chapter 24.

14.3.4.5 Other Radiopharmaceuticals

Peptides or neurotransmitters such as VIP (vasointestinal peptide) (labeled with ^{123}I, ^{99m}Tc or ^{111}In) have been studied in various adenocarcinomas and insulinomas (Raderer et al. 2000). ^{18}F-DOPA is a dopamine analogue actively captured by endocrine tumors, myocardium, liver and kidneys and has a biliary and urinary elimination. The images are acquired 20 – 90 min after an intravenous injection of 300 MBq on a hydrated fasting patient. Alcohol, coffee and tobacco should be avoided prior to the study. Early studies are encouraging, showing an overall good sensitivity (65 – 85 %) in endocrine tumors as compared to the somatostatin analogues (58 – 70 %) and ^{18}F-FDG (29 %). Sensitivity was high for osseous lesions (100 %), intestinal and mesenteric lymph nodes (92 %) and hepatic metastases (80 %), but poor for pulmonary lesions (20 %) (Becherer et al. 2004). Promising results have been reported in children's insulinomas (Ribeiro et al. 2005). ^{11}C-dihydroxytryptophan is being studied for carcinoid tumors (Orlefors et al. 2005).

References

Akerström G, Malmaeus J, Bergström R (1984) Surgical anatomy of human parathyroid glands. Surgery 95:14 – 21

Al Zahrani AA, Levine MA (1997) Primary hyperparathyroidism. Lancet 349:1233 – 1238

Al-Hawary MM, Francis IR, Korobkin M (2005) Non-invasive evaluation of the incidentally detected indeterminate adrenal mass. Best Pract Res Clin Endocrinol Metab 19:277 – 292

Bardet S, et al. (1996) 131I-6 beta-iodomethylnorcholesterol scintigraphy: an assessment of its role in the investigation of adrenocortical incidentalomas. Clin Endocrinol (Oxf) 44:587 – 596

Becherer A, et al. (2004) Imaging of advanced neuroendocrine tumors with 18F-FDOPA PET. J Nucl Med 45:1161 – 1167

Becker D, Charles ND, Dworkin H, Hurley J, McDougall IR, Price D, Royal H, Sarkar S (1996) Procedure guideline for thyroid scintigraphy. J Nucl Med 37(7):1264 – 6

Belhocine T, et al. (2002) Fluorodeoxyglucose positron emission tomography and somatostatin receptor scintigraphy for diagnosing and staging carcinoid tumours: correlations with the pathological indexes p53 and Ki-67. Nucl Med Commun 23:727 – 734

Bernini GP, Moretti A, Oriandini C, Bardini M, Taurino C, Salvetti A (2005) Long-term morphological and hormonal follow-up in a single unit on 115 patients with adrenal incidentalomas. Br J Cancer 92:1104 – 1109

Bilezikian JP, Potts JT, Jr, Fuleihan Gel-H, Kleerekoper M, Neer R, Peacock M, Rastad J, Silverberg SJ, Udelsman R, Wells SA (2002) Summary statement from a workshop on asymptomatic primary hyperparathyroidism: a perspective for the 21st century. J Clin Endocrinol Metab 87:5353 – 61 [review]

Blake MA, et al. (2006) Adrenal lesions: characterization with fused PET/CT image in patients with proved or suspected malignancy – initial experience. Radiology 238:970 – 977

Borley NR, Collins REC, O'Doherty M, Coakley A (1996) Technetium 99m-sestamibi parathyroid localization is accurate enough for scan-directed unilateral neck exploration. Br J Surg 83:989 – 991

Bourguet P, et al. (2005) Understanding positron emission tomography (PET) with [18F]-FDG in clinical oncology. Information dedicated to patients and relatives. Bull Cancer 92:723 – 732

Carr CE, Cope C, Cohen DL, Fraker DL, Trerotola SO (2004) Comparison of sequential versus simultaneous methods of adrenal venous sampling. J Vasc Interv Radiol 15:1245 – 1250

Cavalieri RR, McDougall IR (1996) In vivo isotopic tests and imaging. In: Braverman LE, Utiger RD (eds) Werner and Ingbar's The Thyroid – A fundamental and clinical text, 7th edn. JB Lippincott-Raven, Philadelphia, pp 352 – 376

Cescato R, et al. (2006) Internalization of sst2, sst3, and sst5 receptors: effects of somatostatin agonists and antagonists. J Nucl Med 47:502 – 511

Coakley AJ, Kettle AG, Wells CP, O'Doherty MJ, Collins REC (1989) 99mTc sestamibi – a new agent for parathyroid imaging. Nucl Med Commun 10:791 – 794

Cook GJ, Wong JC, Smellie WJ, Young AE, Maisey MN, Fogelman I (1998) [11C]Methionine positron emission tomography for patients with persistent or recurrent hyperparathyroidism after surgery. Eur J Endocrinol 139:195 – 7

Cooper DS, Doherty GM, Haugen BR, Kloos RT, Lee SL, Mandel SJ, Mazzaferri EL, McIver B, Sherman SI, Tuttle RM (2006) The American Thyroid Association Guidelines Taskforce. Management guidelines for patients with thyroid nodules and differentiated thyroid cancer. Thyroid 16:1 – 33

De Graaf JS, Dullaart RP, Kok T, Piers DA, Zwierstra RP (2000) Limited role of meta-iodobenzylguanidine scintigraphy in imaging phaeochromocytoma in patients with multiple endocrine neoplasia type II. Eur J Surg 166:289 – 292

Dromain C, et al. (2005) Detection of liver metastases from endocrine tumors: a prospective comparison of somatostatin receptor scintigraphy, computed tomography, and magnetic resonance imaging. J Clin Oncol 23:70 – 78

Duet M, et al. (2003) Clinical impact of somatostatin receptor scintigraphy in the management of paragangliomas of the head and neck. J Nucl Med 44:1767 – 1774

Fallo F, et al. (2006) Prevalence and characteristics of the metabolic syndrome in primary aldosteronism. J Clin Endocrinol Metab 91:454 – 459

Fuster D, Ybarra J, Ortin J, Torregrosa JV, Gilabert R, Setoain X, Paredes P, Duch J, Pons F (2006) Role of pre-operative imaging using (99m)Tc-MIBI and neck ultrasound in patients with secondary hyperparathyroidism who are candidates for subtotal parathyroidectomy. Eur J Nucl Med Mol Imaging 33:467 – 73

Gimenez-Roqueplo A, et al. (2003) Mutations in the SDHB gene are associated with extra-adrenal and/or malignant phaeochromocytomas. Cancer Res 63:5615 – 5621

Giordano A, Rubello D, Casara D (2001) New trends in parathyroid scintigraphy. Eur J Nucl Med 28:1409 – 20 [review]

Giovanella L (2005) Serum chromogranin – an assay in differential diagnosis of incidentally discovered adrenal masses. Anticancer Res 25(3A):1547 – 50

Gotthardt M, et al. (2003) Influence of somatostatin receptor scintigraphy and CT-MRI on the clinical management of patients with gastrointestinal neuroendocrine tumors: an analysis in 188 patients. Digestion 68:80 – 85

Grumbach MM, et al. (2003) Management of the clinically inapparent adrenal mass ("incidentaloma"). Ann Intern Med 138:424 – 429

Haber RS, Kim CK, Inabnet WB (2002) Ultrasonography for preoperative localization of enlarged parathyroid glands in primary hyperparathyroidism: comparison with (99m)technetium sestamibi scintigraphy. Clin Endocrinol (Oxf) 57:241 – 9

Heath H, Hodgson SF, Kennedy MA (1980) Primary hyperparathyroidism. Incidence, morbidity, and potential economic impact in a community. N Engl J Med 302:189 – 193

Hegedus L (2004) Clinical practice. The thyroid nodule. N Engl J Med 351:1764 – 1771

Hindié E, Melliere D, Perlemuter L, Jeanguillaume C, Galle P (1997) Primary hyperparathyroidism: Higher success rate of first surgery after preoperative Tc-99m-sestamibi/I-123 subtraction scanning. Radiology 204:221 – 228

Hindié E, Mellière D, Jeanguillaume C, Perlemuter L, Galle P (1998) Parathyroid imaging using simultaneous double-window recording of Tc-99m-sestamibi and 123I. J Nucl Med 39:1100 – 1105

Hindié E, Ureña P, Jeanguillaume C, et al. (1999) Preoperative imaging of parathyroid glands with technetium-99m-labelled sestamibi and iodine-123 subtraction scanning in secondary hyperparathyroidism. Lancet 353:2200 – 2204

Hindie E, Melliere D, Jeanguillaume C, Urena P, deLabriolle-Vaylet C, Perlemuter L (2000) Unilateral surgery for primary hyperparathyroidism on the basis of technetium Tc 99m sestamibi and iodine 123 subtraction scanning. Arch Surg 135:1461 – 8

Hoegerle S, et al. (2002) Pheochromocytomas: detection with 18F DOPA whole body PET – initial results. Radiology 222:507 – 512

Intenzo CM, Capuzzi DM, Jabbour S, et al. (2001) Scintigraphic features of autoimmune thyroiditis. Radiographics 21:957 – 964

Kaltsas, et al. (2001) Comparison of somatostatin analog and metaiodobenzylguanidine radionuclides in the diagnosis and localization of advanced neuroendocrine tumors. J Clin Endocrinol Metab 86:895 – 902

Kettle AG, O'Doherty MJ (2006) Parathyroid imaging: how good is it and how should it be done? Semin Nucl Med 36:206 – 11

Kraimps JL, Bouin-Pineau MH, Mathonnet M, De Calan L, Ronceray J, Visset J, Marechaud R, Barbier J (2000) Multicentre study of thyroid nodules in patients with Graves' disease. Br J Surg 87:1111 – 1113

Krausz Y, Bettman L, Guralnik L, Yosilevsky G, Keidar Z, Bar-Shalom R, Even-Sapir E, Chisin R, Israel O (2006) Technetium-99m-MIBI SPECT/CT in primary hyperparathyroidism. World J Surg 30:76 – 83

Krenning EP, et al. (1993) Somatostatin receptor scintigraphy with [111In-DTPA-D-Phe1]- and [123I-Tyr3]-octreotide: the Rotterdam experience with more than 1000 patients. Eur J Nucl Med 20:716 – 731

Kwekkeboom DJ, Krenning EP, Bakker WH, Oei HY, Kooij PP, Lamberts SW (1993) Somatostatin analogue scintigraphy in carcinoid tumours. Eur J Nucl Med 20:283 – 292

Kwekkeboom DJ, Kooij PP, Bakker WH, Macke HR, Krenning EP (1999) Comparison of 111In-DOTA-Tyr3-octreotide and 111In-DTPA-octreotide in the same patient: biodistribution, kinetics, organ and tumor uptake. J Nucl Med 40: 762 – 767

Kwekkeboom DJ, et al. (2005) Radiolabeled somatostatin analog [177Lu-DOTA0,Tyr3]octreotate in patients with endocrine gastroenteropancreatic tumors. J Clin Oncol 23: 2754 – 2762

Le Rest C, Bomanji JB, Costa DC, Townsend CE, Visvikis D, Ell PJ (2001) Functional imaging of malignant paragangliomas and carcinoid tumours. Eur J Nucl Med 28:478 – 482

Leboulleux S, et al. (2006) Diagnostic and prognostic value of 18-fluorodeoxyglucose positron emission tomography in adrenocortical carcinoma: a prospective comparison with computed tomography. J Clin Endocrinol Metab 91:920 – 925

Lebtahi R, et al. (1999) Detection of bone metastases in patients with endocrine gastroenteropancreatic tumors: bone scintigraphy compared with somatostatin receptor scintigraphy. J Nucl Med 40:1602 – 1608

Lee JA, Inabnet WB 3rd (2005) The surgeon's armamentarium to the surgical treatment of primary hyperparathyroidism. J Surg Oncol 89:130 – 5 [review]

Levin KE, Clark OH (1989) The reasons for failure in parathyroid operations. Arch Surg 124:911 – 5

Lind P, Kohlfürst S (2006) Respective roles of thyroglobulin, radioiodine imaging, and positron emission tomography in the assessment of thyroid cancer. Semin Nucl Med 36: 194 – 205

Liu RC, Hill ME, Ryan JA, Jr (2005) One-gland exploration for mediastinal parathyroid adenomas: cervical and thoracoscopic approaches. Am J Surg 189:601 – 5

Lumachi F, et al. (2005) Role and cost-effectiveness of adrenal imaging and image-guided FNA cytology in the management of incidentally discovered adrenal tumours. Anticancer Res 25:4559 – 4562

Lundgren E, Rastad J, Thurfjell E, Akerström G, Ljunghall S (1997) Population-based screening for primary hyperparathyroidism with serum calcium and parathyroid hormone values in menopausal women. Surgery 121:287 – 94

Mamede M, et al. (2006) Discordant localization of 2-[18F]-fluoro-2-deoxy-D-glucose in 6-[18F]-fluorodopamine- and [(123)I]-metaiodobenzylguanidine-negative metastatic pheochromocytoma sites. Nucl Med Commun 27:31 – 36

Mann GN, et al. (2006) [11C]metahydroxyephedrine and [18F]fluorodeoxyglucose positron emission tomography improve clinical decision making in suspected pheochromocytoma. Ann Surg Oncol 13:187 – 197

Mansmann G, Lau J, Balk E, Rothberg M, Miyachi Y, Bornstein SR (2004) The clinically inapparent adrenal mass: update in diagnosis and management. Endocr Rev 25:309 – 340

Martin D, Rosen IB, Ichise M (1996) Evaluation of single isotope technetium-99m-sestamibi in localization efficiency for hyperparathyroidism. Am J Surg 172:633 – 636

Marx SJ, Simonds WF, Agarwal SK, Burns AL, Weinstein LS, Cochran C, Skarulis MC, Spiegel AM, Libutti SK, Alexander HR, Jr, Chen CC, Chang R, Chandrasekharappa SC, Collins FS (2002) Hyperparathyroidism in hereditary syndromes: special expressions and special managements. J Bone Miner Res 17 Suppl 2:N37 – 43 [review]

Maurea S, Klain M, Caraco C, Ziviello M, Salvatore M (2002) Diagnostic accuracy of radionuclide imaging using 131I nor-cholesterol or meta-iodobenzylguanidine in patients with hypersecreting or non-hypersecreting adrenal tumours. Nucl Med Commun 23:951 – 960

Meier DA, Kaplan MM (2001) Radioiodine uptake and thyroid scanning. Endocrinol Metab Clin North Am 30(2):291 – 313

Meller J, Becker W (2002) The continuing importance of thyroid scintigraphy in the era of high resolution ultra sound. Eur J Nucl Med Mol Imaging 29 (Suppl 2):S425–S438

Minn H, et al. (2004) Imaging of adrenal incidentalomas with PET using (11)C-metomidate and (18)F-FDG. J Nucl Med 45:972 – 979

Molinari AS, Irvin GL, 3rd, Deriso GT, Bott L (1996) Incidence of multiglandular disease in primary hyperparathyroidism determined by parathyroid hormone secretion. Surgery 120:934 – 7

Mountz JM, et al. (1988) Scintigraphic localization of ovarian dysfunction. J Nucl Med 29:1644 – 50

Mullan BP (2004) Nuclear medicine imaging of the parathyroid. Otolaryngol Clin North Am 37:909 – 39, xi-xii [review]

Muros MA, et al. (1998) 111In-pentetreotide scintigraphy is superior to 123I-MIBG scintigraphy in the diagnosis and location of chemodectoma. Nucl Med Commun 19:735 – 742

Nguyen C, et al. (2004) Long-term efficacy of radionuclide therapy in patients with disseminated neuroendocrine tumors uncontrolled by conventional therapy. J Nucl Med 45:1660 – 1668

Nikou GC, et al. (2005) Gastrinomas associated with NEM-1 syndrome: new insights for the diagnosis and management in a series of 11 patients. Hepatogastroenterology 52:1668 – 1676

Nocaudie-Calzada M, Huglo D, Deveaux M, Carnaille B, Proye C, Marchandise X (1996) Comparison of somatostatin analogue and metaiodobenzylguanidine scintigraphy for the detection of carcinoid tumours. Eur J Nucl Med 23:1448 – 1454

Nocaudie-Calzada M, et al. (1999) Efficacy of iodine-131 6-methyl-iodo-19-norcholesterol scintigraphy and computed tomography in patients with primary aldosteronism. Eur J Nucl Med 26:1326 – 1332

Orlefors H, et al. (2005) Whole-body (11)C-5-hydroxytryptophan positron emission tomography as a universal imaging technique for neuroendocrine tumors: comparison with somatostatin receptor scintigraphy and computed tomography. J Clin Endocrinol Metab 90:3392 – 3400

Pacak K, Ilias I, Chen CC, Carrasquillo JA, Whatley M, Nieman LK (2004) The role of [(18)F]fluorodeoxyglucose positron emission tomography and [(111)In]-diethylenetriaminepentaacetate-D-Phe-pentetreotide scintigraphy in the localization of ectopic adrenocorticotropin-secreting tumors causing Cushing's syndrome. J Clin Endocrinol Metab 89:2214 – 2221

Paganelli G, et al. (2001) Receptor-mediated radiotherapy with 90Y-DOTA-D-Phe1-Tyr3-octreotide. Eur J Nucl Med 28: 426 – 434

Palestro CJ, Tomas MB, Tronco GG (2005) Radionuclide imaging of the parathyroid glands. Semin Nucl Med 35:266 – 276 [review]

Perie S, Fessi H, Tassart M, Younsi N, Poli I, St Guily JL, Talbot JN (2005) Usefulness of combination of high-resolution ultrasonography and dual-phase dual-isotope iodine 123/technetium Tc 99m sestamibi scintigraphy for the preoperative localization of hyperplastic parathyroid glands in renal hyperparathyroidism. Am J Kidney Dis 45:344 – 52

Raderer M, et al. (2000) Value of peptide receptor scintigraphy using (123)I-vasoactive intestinal peptide and (111)In-DTPA-D-Phe1-octreotide in 194 carcinoid patients: Vienna University Experience, 1993 to 1998. J Clin Oncol 18:1331 – 1336

Reubi JC, et al. (2000) Affinity profiles for human somatostatin receptor subtypes SST1-SST5 of somatostatin radiotracers selected for scintigraphic and radiotherapeutic use. Eur J Nucl Med 27:273 – 282

Reubi JC, Waser B, Schaer JC, Laissue JA (2001) Somatostatin reception sst1-sst5 expression in normal and neoplastic human tissues using receptor autoradiography with subtype-selective ligands. Eur J Nucl Med 28(7):836 – 46. Erratum in: Eur J Nucl Med 2001;28:1433

Ribeiro MJ, et al. (2005) Characterization of hyperinsulinism in infancy assessed with PET and 18F-fluoro-L-DOPA. J Nucl Med 46:560 – 566

Rose B, et al. (2003) High-dose 131I-metaiodobenzylguanidine therapy for 12 patients with malignant pheochromocytoma. Cancer 98:239 – 248

Rossi R, et al. (2000) Subclinical Cushing's syndrome in patients with adrenal incidentaloma: clinical and biochemical features. J Clin Endocrinol Metab 85:1440 – 1448

Rubello D, Pelizzo MR, Casara D (2003) Nuclear medicine and minimally invasive surgery of parathyroid adenomas: a fair marriage. Eur J Nucl Med Mol Imaging 30:189 – 2

Russell CF, Edis AJ (1982) Surgery for hyperparathyroidism: experience with 500 consecutive cases and evaluation of the role of surgery in the asymptomatic patient. Br J Surg 69:244 – 247

Safford SD, et al. (2004) Iodine-131 metaiodobenzylguanidine treatment for metastatic carcinoid. Results in 98 patients. Cancer 101:1987 – 93

Sarkar SD (2006) Benign thyroid disease: What is the role of nuclear medicine? Semin Nucl Med 36:185 – 193

Sawka AM, Gafni A, Thabane L, Young WF, Jr (2004) The economic implications of three biochemical screening algorithms for pheochromocytoma. J Clin Endocrinol Metab 89:2859 – 66

Schillaci O, Massa R, Scopinaro F (2000) 111In-pentetreotide scintigraphy in the detection of insulinomas: importance of SPECT imaging. J Nucl Med 41:459 – 462

Schillaci O, et al. (2003) Somatostatin receptor scintigraphy in liver metastasis detection from gastroenteropancreatic neuroendocrine tumors. J Nucl Med 44:359 – 368

Schoen EJ, Clapp W, To TT, Fireman BH (2004) The key role of newborn thyroid scintigraphy with isotopic iodide (123I) in defining and managing congenital hypothyroidism. Pediatrics 114(6):e683 – 8

Seminara MD, Daniels GH (1998) Amiodarone and thyroid. Endocr Pract 4:48 – 54

Smith JR, Oates E (2004) Radionuclide imaging of the thyroid gland: patterns, pearls and pitfalls. Clin Nucl Med 29:181 – 193

Sosa JA, Powe NR, Levine MA, Udelsman R, Zeiger MA (1998) Profile of a clinical practice. Thresholds for surgery and surgical outcomes for patients with primary hyperparathyroidism: A national survey of endocrine surgeons. J Clin Endocrinol Metab 83:2658 – 2665

Sturgeon C, Shen WT, Clark OH, Duh QY, Kebebew E (2006) Risk assessment in 457 adrenal cortical carcinomas: how much does tumor size predict the likelihood of malignancy? J Am Coll Surg 202:423 – 30

Taillefer R, Boucher Y, Potvin C, Lambert R (1992) Detection and localization of parathyroid adenomas in patients with hyperparathyroidism using a single radionuclide imaging procedure with Technetium-99m-Sestamibi (double-phase study). J Nucl Med 33:1801 – 1807

Tenenbaum F, Lumbroso J, Schlumberger M, Mure A, Plouin PF, Caillou B, Parmentier C (1995) Comparison of radiolabeled octreotide and meta-iodobenzylguanidine (MIBG)

scintigraphy in malignant pheochromocytoma. J Nucl Med 36:1 – 6
Thorin-Savoure A, et al. (2005) Collision/composite tumors of the adrenal gland: pitfall of scintigraphy imaging and hormone assays in the detection of adrenal metastasis. J Clin Endocrinol Metab 90:4924 – 4929
Unger N, et al. (2006) Diagnostic value of various biochemical parameters for the diagnosis of pheochromocytoma in patients with adrenal mass. Eur J Endocrinol 154:409 – 417
Utiger RD (1999) Treatment of primary hyperparathyroidism (editorial). N Engl J Med 341:13101 – 02
Valkema R, et al. (2005) Long-term follow-up of renal function after peptide receptor radiation therapy with (90)Y-DOTA(0),Tyr(3)-octreotide and (177)Lu-DOTA(0), Tyr(3)-octreotate. J Nucl Med 46:83S–91S
Van der Harst E, et al. (2001) [(123)I]metaiodobenzylguanidine and [(111)In]octreotide uptake in benign and malignant pheochromocytomas. J Clin Endocrinol Metab 86:685 – 693
Van Der Horst-Schrivers AN, Jager PL, Boezen HM, Schouten JP, Kema IP, Links TP (2006) Iodine-123 metaiodobenzylguanidine scintigraphy in localising phaeochromocytomas – experience and meta-analysis. Anticancer Res 26:1599 – 1604
Waldherr C, et al. (2002) Tumor response and clinical benefit in neuroendocrine tumors after 7.4 GBq (90)Y-DOTATOC. J Nucl Med 43:610 – 616
Weber CJ, Vansant J, Alazraki N (1993) Value of technetium 99m sestamibi iodine 123 imaging in reoperative parathyroid surgery. Surgery 114:1011 – 1018

Nuclear Hematology

15

E.B. Silberstein

15.1 Introduction

One of the first areas of patient care to which the specialty of nuclear medicine contributed was hematology, when phosphorus-32 was employed by John Lawrence, MD at the Donner Laboratory, University of California at Berkeley, to treat leukemia and polycythemia vera. Hematologic techniques developed over a half-century ago can quantitate the survival and localize the site of destruction of erythrocytes and platelets with remarkable sensitivity. Measurement of the erythrocyte volume (EV) and plasma volume (PV) remains the cornerstone of any diagnostic algorithm for determining the cause of an elevated hematocrit/hemoglobin. And yet utilization of these techniques is diminishing.

An important reason for this, at least in the United States, is the separation between nuclear imaging studies, now dominated by radiologists, and laboratory studies, performed almost entirely by clinical pathologists. As radioassay gave way to immunological techniques and the enzyme-linked immunosorbent assay (ELISA), nuclear medicine laboratories witnessed a marked decline in their laboratory testing component. This trend often led to the abandonment of other nuclear medicine techniques requiring in vitro counting of biological samples and subsequently to a failure to train technologists in this area as the volume of such tests decreased. Clinical pathologists also tend to prefer techniques which do not carry the risk of radiation contamination and avoid the burdensome regulations imposed by the United States Nuclear Regulatory Commission. So there are too few technologists in the United States who can, for example, perform a blood volume study, which requires 5–6 h to complete. It is incumbent on the reader, therefore, not only to understand the studies to be described but to make them more widely available.

In any multi-authored text there is the opportunity for many overlapping sections, which we have tried to avoid here. Therefore this review will not deal with labeled leukocyte studies for the detection of inflammation/infection, which will be found in Dr. Corsten's chapter (Chapter 17). Spleen imaging is dealt with in Chapter 6 by Drs. Freeman and Zuckier, where a mention of marrow imaging can also be found. Lymphoma radioimmunotherapy discovered by Dr. Baum, ^{18}F-fluorodeoxyglucose PET imaging by Dr. Bombardieri, and thromboembolic disorders are discussed in Chapter 5 by Dr. Steinert et al.

15.2 Radiolabeling of Circulating Blood Cells

The ideal radioisotope for radiolabeling of any cell should have no effect on cellular anatomy or physiology. It should remain attached to the cell throughout its life, and then not be reutilized, since the latter characteristic would make cell life span artifactually prolonged. The photopeak of the radionuclide should ideally be between 100 and 250 keV to maximize efficiency of interaction with a gamma camera or gamma well counter when imaging or external counting would be helpful. Finally the physical half-life of the radionuclide employed should be appropriate for the study under consideration (McIntyre 1977).

Cells may either be labeled as a cohort (pulse labeling) or randomly. A cohort of cells which are approximately the same age are found in the marrow and, when pulse labeled, they will then mature and circulate in the blood pool together. Iron is the most common radiolabel for this purpose, but ^{75}Se-selenomethionine, ^{32}P-orthophosphate, ^{32}P- and ^{14}C-diisopropylfluorophosphate, and ^{3}H-thymidine have been employed for this purpose; none of these are now clinically useful. Random labels are easier to use, and in clinical nuclear medicine chromium-51 (as sodium chromate) (ICSH 1980a; Gray and Sterling 1950), technetium-99m (as sodium pertechnetate) (ICSH 1980a; Rehani and Sharma 1980; Smith and Richards 1976; Pavel et al. 1977), and indium-111 (as indium-oxine complex) (Rao and Dewanjee 1982) have been employed as in vitro cell tags, followed by injection of the radiolabeled cells. Of these, ^{51}Cr has by far the slowest elution rate, measured at 0.5–1.3%/day in normals (Cline and Berlin 1963), making it the radionuclide of choice. As hexavalent anionic chromate, this ion passes through the erythrocyte mem-

Table 15.1. Adult dosimetry for radiopharmaceuticals employed to measure the blood volume in mGy/MBq (CDE dosimetry)

Radionuclide	Spleen	Marrow	Blood	Liver	Testis	Ovary	EDE
^{51}Cr-RBC	1.6	0.12	–	0.24	0.06	0.09	0.26
^{125}I-HSA	0.8	0.46	5.14	–	0.54	0.54	0.16

RBC red blood cells or erythrocytes

brane and is largely bound by the beta chain of hemoglobin where it is reduced to the trivalent state. Only 5 % is membrane bound (Gray and Sterling 1950; Rehani and Sharma 1980). To avoid cellular damage by chromium, the material must be of high specific activity, in excess of 740 MBq (20 mCi) per milligram at the time of use (Cline and Berlin 1963). Human adult dosimetry for ^{51}Cr-erythrocytes and iodine-125 labeled human serum albumin (^{125}I-HSA) appears in Table 15.1. Chromium-51, with a 27.8-day half-life, decays by electron capture, emitting a beta particle with mean energy of 315 keV in 91 % of decays, with 9 % of decays as 322 keV gamma rays. Iodine-125, with an even longer physical half-life, 60 days, emits short-range Auger electrons. Hence the administered activity of both radiopharmaceuticals should be as low as possible. We administer about 5 μCi of ^{125}I-HSA and 10 – 15 μCi of ^{51}Cr-labeled erythrocytes.

A potentially problematic in vivo drug interaction is with stannous pyrophosphate, which is given intravenously to label erythrocytes with $^{99m}TcO_4$ for the radionuclide ventriculogram and which will inhibit ^{51}Cr binding to erythrocytes, unless these cells are first washed (Holt et al. 1982).We do not recommend the use of technetium-99m in ^{99m}Tc-pertechnetate as an erythrocyte label, since this radiopharmaceutical, reduced by stannous ion to the trivalent form as it labels erythrocytes, elutes at a rate of up to 10 % in 30 – 60 min, and would therefore cause falsely elevated EV; eluted pertechnetate is very rapidly cleared from the plasma (Smith and Richards 1976).

15.3 The Blood Volume

Any compartment, such as the EV or PV, may be calculated by the dilution principle, used for well over a century (Porter et al. 1983), wherein the volume to be determined is inversely proportional to the concentration of the label in the blood sample drawn after complete mixing. The underlying assumptions which must be fulfilled for these measurements to be valid are the stability of the compartment size being assessed during the measurement (i.e., a closed system), and a rate of mixing of the tracer within the compartment which is greatly in excess of the rate at which the tracer leaves the compartment, if that occurs at all. Hence the presence of bleeding or transudate into a "third space," e.g., pleural effusion, will invalidate the study, although there are techniques available to correct the latter issue of extravascular transit of the plasma tracer. Furthermore the tracer to be used must be stable, nonantigenic, sterile, nonpyrogenic, of high specific activity, and quite small in volume, with a very low amount of unbound radionuclide.

The blood volume, consisting of separate measurements of the erythrocyte and plasma volumes, is a crucial study when the hematologist must determine whether an elevated hematocrit or hemoglobin is due to contraction of the PV or expansion of the EV. This volume measurement has been referred to, erroneously, as the red cell "mass" because of potential confusion with the erythrocyte mean corpuscular volume (MCV), which is the volume of a red cell in picoliters. The correct term refers to a true volume, however, and EV will be retained in this review. In some hematologic diseases, especially in polycythemia vera, both the EV and PV are expanded, so that erythrocytosis can coexist with a normal hematocrit. Yet in a recent poll of the members of the American Society of Hematology, 22 % admitted to diagnosing polycythemia vera without benefit of the red cell and plasma volume measurements. It is clear that these tests are essential in separating a suspected case of polycythemia vera from other causes of an elevated hematocrit (Table 15.2) (Spivak 2003), despite the objections of a single author who claims that the EV measurement is rarely needed and can be replaced by an accurate interpretation of the hematocrit within the context of clinical presentation and certain laboratory tests (Tefferi 2003). In discussing the EV measurement it will be important for the reader to discern the erroneous assumptions in this latter belief.

The problems of diagnosing polycythemia vera cannot be overemphasized. While the elevated hematocrit or hemoglobin value is usually the first sign that marrow physiology may be abnormal, what else can one rely on to determine the polycythemia vera, or another cause of the elevated hematocrit, is present (Table 15.2), given the wide range of hematocrit values in normals? In fact the hematocrit only predicts an elevated red cell mass when it exceeds 60 %, and the correlation coefficient between the hematocrit and the EV is only 0.76.

In fact, polycythemia vera presents with trilineage hyperplasia only 40 % of the time, i.e., with simultaneous elevation of erythrocyte, leukocyte, and platelet counts. Approximately 20 % of the time the only clinical abnormality is erythrocytosis alone (Spivak 2003). While cellular markers of polycythemia vera do exist, such as PRV-1, impaired expression of the thrombopoietin-receptor, c-Mpl, or the newly described JKA2 kinase gene, these are not unique and have been detected

Table 15.2. Causes of erythrocytosis

Relative erythrocytosis
Hemoconcentration
Dehydration/plasma volume contraction
Androgens
Tobacco or ethanol abuse
Hypertension
Absolute erythrocytosis
Hypoxia
Carbon monoxide intoxication
Hemoglobinopathies with high oxygen affinity
High altitude
Pulmonary disease
Right-to-left shunts
Sleep apnea syndrome
Neurologic disease
Renal disease
Renal artery stenosis
Focal sclerosing or membranous glomerulonephritis
Renal transplantation
Hydronephrosis
Tumors
Hypernephroma
Hepatoma
Cerebellar hemangioblastoma
Uterine fibromyoma
Adrenal tumors, usually with Cushing's syndrome
Meningioma
Pheochromocytoma
Drugs
Androgens
Recombinant erythropoietin
Familial (with normal hemoglobin function)
Polycythemia vera

Table 15.3. Causes of altered *f* or F_{cells}*

Low *f*
Apprehension
Vasopressors
Hypertension
Hypovolemia
Dehydration
Hypothermia
Pheochromocytoma
High *f*
Splenomegaly
Anesthesia
Sedation
Sympatholytic drugs
Hypervolemia
Congestive heart failure
Late pregnancy
Elevated serum immunoglobulin

f ratio of whole body to venous hematocrit

in other myeloproliferative diseases (Tefferi and Spivak 2005). Therefore simple blood tests or clonal markers which allow the distinctive diagnosis of individual myeloproliferative disorders continue to elude us. The serum erythropoietin level will not be elevated in polycythemia vera, but it may be well within the normal range. Furthermore the measurement of EV should be considered in the presence of the following findings that do not have an obvious explanation: splenomegaly, elevated leukocyte and/or platelet counts, and portal vein thrombosis. This follows from the fact that since both the EV and the PV may be increased in polycythemia vera, a normal hematocrit value does not exclude that disorder as a cause for these laboratory and/or clinical findings. All these facts cast serious doubt on the validity of the dissenting opinion referred to above concerning the need for measurement of the red cell volume.

The whole body hematocrit may be defined by the fraction:

$$\frac{EV}{EV + PV} \qquad (15.1)$$

But there is no reason to suppose, a priori, that this ratio, reflecting distribution of these two volumes, would be identically reflected in a sample of capillary or antecubital venous blood draining skin, muscle, and bone, taken from an upper extremity. In fact we know that the hematocrit varies in different organs, with the intrasplenic hematocrit significantly higher than the venous hematocrit, while this measurement is lower than the venous value in the lungs and kidneys (Klopper et al. 1979). The ratio of the whole body to the venous hematocrit is called the Fcells or *f* ratio, and is found to be consistently 0.89 – 0.91 in normals (ICSH 1980a; Gregersen and Rawsen 1959), so that the whole body hematocrit is normally less than the venous hematocrit. This would seem to simplify the issue of blood compartment measurement, since one could potentially use only one tracer to measure a single compartment, the blood volume, using the dilution principle (to be detailed below), and then multiply this number by the hematocrit, corrected by *f*, to yield the red cell volume. However, this train of thought assumes that *f* is a constant in all disease processes, and it clearly is not, ranging from about 0.7 to 1.2 depending on the clinical circumstances (Table 15.3) (Balga et al. 2000). For example, the splenic hematocrit is always higher than the venous hematocrit, so it would be logical, and correct, to assume that diseases with splenomegaly, such as polycythemia vera (in a majority of cases), have a higher than normal *f*. There is a nonlinear relationship between the red cell volume and hematocrit when the latter exceeds 50 % (Fairbanks 2000).

For this study use of the dilution principle may be conceptualized by recognizing that with a careful injection of the contents of radiolabeled blood into a patient, allowing up to 40 – 60 min for mixing, especially in the presence of splenomegaly (Mollison 1979), and careful withdrawal of a sample of blood, the activity (*A*) in the

injecting syringe (s) must equal the activity in the patient (pt):

$$A_{sy} = A_{pt} \tag{15.2}$$

Compartmental activity = (concentration in μCi/mL) (volume in mL), so it follows that:

$$(uCi/mL)_{sy}\,(mL)_{sy} = (uCi/mL))_{pt} \times (mL)_{pt} \tag{15.3}$$

Since the first three terms of this equation are measurable, the diluted blood concentration of a given tracer after careful phlebotomy, the fourth, i.e., $(mL)_{pt}$, the patient compartment volume of interest (here EV or PV), may be calculated easily, as:

$$(mL)_{pt} = \frac{(uCi/mL)_{sy}\,(mL)_{sy}}{(uCi/mL)_{pt}} \tag{15.4}$$

Chromium-51, as sodium chromate, was found to label erythrocytes at the beta chain, with only a 1% elution rate per day for hemoglobin A (Sterling and Gray 1950). We always check the stool for blood before initiating the test, to confirm the mandatory steady state. The plasma volume is optimally measured with a human protein, and iodinated (iodine-125) human serum albumin (HSA) is commercially available for this purpose. This radiopharmaceutical should optimally have less than 2% free iodide and a protein concentration of about 2 g/dL. Albumin normally leaves and reenters the intravascular compartment fairly rapidly. The ICSH therefore recommends sampling the plasma at 10, 20, and 30 min, but we have found it necessary to obtain more samples out to 60–75 min, especially in the presence of splenomegaly. Thus one must obtain multiple blood specimens, plot the values for these times, and extrapolate to obtain the counts/mL back to the time of injection, i.e., time zero (El-Hemaidi et al. 1997).

To meet the requirement for a steady state in a reasonable fashion we require the patient to fast for 4 h. The patient should be at rest in a recumbent position for at least 15 min before initiation of the study and remain in this position until completion of all phlebotomies, as the hematocrit in supine patients is about 0.02 lower than in the sitting position (El-Hemaidi et al. 1997). The International Committee for Standardization in Hematology has detailed the methods for performing the red cell and plasma volume assays (ICSH 1980a), as well as the interpretation of the values obtained (Pearson et al. 1995). Normal values for the EV and PV have a wide range. Values presented as mL/kg body weight are suspect because in obese patients the excess fat is relatively hypovascular (Lorberboym et al. 2005), and the red cell mass needs to be related to lean body mass and/or surface area as well as weight.

In a direct comparison of the measurement of EV by the ICSH methodology versus calculating the EV from the venous hematocrit, plasma volume, and mean value of *f*, i.e.

$$EV = PV \times \frac{(\text{venous hct}) \times f}{1 - (\text{venous hct})} \tag{15.5}$$

seventeen of 146 patients (12%) with an elevated measured EV would have been lost from the polycythemia group and 29 of 118 patients (25%) with normal EV values would incorrectly meet the criteria for true erythrocytosis. Thus 46 of 264 patients, or 17%, an unacceptable error rate, would have been misclassified (Balga et al. 2000).

What normal values should one use? The Polycythemia Vera Study Group suggested that the upper limit of red cell volume for men be >36 ml/kg, and for women >32 ml/kg. These criteria have largely been abandoned because of the false negative results that obesity may cause, as noted above. The ICSH suggests that for men:

mean normal EV = (1486 × *S*) – 825
mean normal PV = 1578 × *S*,
and for women:
mean normal EV = (822 × *S*) + (1.06 × age)
mean normal PV = 1395 × *S*
where *S* = surface area in $m^2 = W^{0.425} \times h^{0.725} \times 0.007184$ (age in years, height in centimeters and weight in kilograms).

Then the suggested normal ranges lie within ±25% of the calculated mean values, yielding 99% confidence limits (Pearson et al. 1995).

An examination of several techniques for measuring EV concluded that the ^{51}Cr procedure was the best approach, with a mean coefficient of variation of 2.8%, 90% confidence limits 2.4–3.2%; a carbon monoxide inhalation method had a slightly lower mean coefficient of variation, 2.2%, but the technique is obviously more invasive (Gore et al. 2005). These are reasonable criteria, but there are several reasons why the separation of normals from patients with true erythrocytosis can never be perfect. Of greatest importance is the fact that the distribution of values for the EV in normal subjects and in patients with polycythemia vera both seem to fall in a normal, overlapping distribution, so that the upper "normal" range of EV in normals will always overlap with the lower limit of EV measurements in polycythemic patients. If one expands the normal values upward one will reduce the number of false positive tests, thus increasing specificity, where:

$$\text{specificity} = \frac{(\text{true negatives})}{\text{true negatives} + (\text{false positives})} \tag{15.6}$$

while increasing the number of misclassified patients with true erythrocytosis who have been falsely considered not to have this abnormal physiology, thus reducing sensitivity, where:

$$\text{sensitivity} = \frac{(\text{true negatives})}{\text{true negatives} + (\text{false positives})} \tag{15.7}$$

Hence this test, like virtually all others in medicine, will never have 100% sensitivity and specificity, regardless of the criteria employed.

15.4 Red Cell and Platelet Survival Studies

The long physical half-life, very slow rate of elution and lack of reutilization make ^{51}Cr-chromate the only radiopharmaceutical appropriate for measuring red cell or platelet survival (Ebaugh et al. 1953). The ICSH has recommended the ACD (acid-citrate-dextrose) technique wherein blood is mixed with ACD and centrifuged to concentrate the erythrocytes. After the supernatant plasma has been removed, ^{51}Cr is added and incubated for 15 min at 37 °C, washed in saline, then injected (ICSH 1980b). Blood is sampled from the non-injected arm over at least 5 days after injection to produce a reliable time-activity curve. We do not perform phlebotomy for 24 h after injection of the radiolabeled erythrocytes because there is usually an early loss of ^{51}Cr from cells, ranging from 6% to 9% (Ebaugh et al. 1953; Kasfiki et al. 1982), probably from cells damaged by handling and labeling. One must apply the daily correction for ^{51}Cr elution provided by the ICSH (1980b) or one will obtain a ^{51}Cr-erythrocyte survival time in normals of about 24 – 25 days, rather than the true normal mean survival of 45 – 60 days. This latter value represents the results of the random labeling of cells which have a normal survival time of 90 – 120 days. Since one does not know in a given patient whether the disappearance curve of the labeled red cell (or platelet) will be linear, exponential, or in some other form, the time activity curve is best analyzed by a weighted mean least-squares program (Kasfiki et al. 1982).

In such analyses, as with the EV and PV measurements, the system must be in a steady state, with as many cells entering the intravascular compartment per day as leave it. Although a mathematical approach to the use of the survival curve to estimate production of cells in the non-steady state has been described, there is little evidence of its clinical validity (Sanchez-Medal and Loria 1972). Thus the reticulocyte count, hemoglobin level and hematocrit should ideally have been at the same level for 4 months, the life span of the oldest erythrocyte. If there has been a diminution or cessation of production of cells for a week or more prior to initiation of the study, then only older cells will be labeled, yielding an artifactually shortened half-life. Similarly, if a hemolytic crisis is treated and hemolysis diminishes but compensatory erythropoiesis is still increasing, then labeled cells are more rapidly diluted by new, unlabeled cells, the decline in activity per milliliter of cells is artifactually rapid, and the measured survival will again be shorter than the true value. Transfusions and blood loss will also invalidate the study. During the red cell survival study we also perform a 4-day analysis of fecal blood loss (Ebaugh et al. 1958) to detect that cause of an apparent shortened red cell survival. Blood samples for this purpose are collected 60 min after injection and again 4 days later, at the completion of the fecal collection. Fecal blood loss equals the total counts per minute in the 4-day sample divided by the average counts/mL of the circulating blood from the first and last collection days. The normal average daily blood loss ranges from 0.3 to 2.8 mL, mean 1.2 ± 0.5 mL (Blahd 1971).

This study is uncommonly performed at this time, because it is not necessary to place a precise number of days on the red cell survival if brisk hemolysis is occurring, as the hematologist will observe anemia, an elevated corrected reticulocyte count and erythroid marrow hyperplasia as sufficient evidence, once gastrointestinal bleeding is simply excluded. The pathophysiologic process causing the hemolysis must be treated, regardless of the number. If there is no cause for marrow suppression the bone marrow can increase erythrocyte production 6 – 8 times over the normal rate. If erythrocyte survival is less than about one-eighth of normal therefore, less than about 11 – 13 days, anemia will result, since:

$$\text{EV} = (\text{mL of erythrocytes produced/day}) \times (\text{erythrocyte survival in days}) \quad (15.8)$$

In the study of platelet survival ^{111}In-oxine labeling has been shown to yield results essentially equivalent to those of ^{51}Cr, and, again, a weighted mean least-squares program is recommended to analyze the time-activity curve generated by the study. The considerations noted above for the clinical application of survival techniques apply to the analysis of thrombocytopenia as well, where the clinician can usually distinguish a reduction in platelet production from increased platelet destruction by evaluation of bone marrow morphology. However, the ^{111}In-oxine platelet labeling technique permits imaging of thrombi with reasonable sensitivity (Goodwin et al. 1978). The causes of shortened erythrocyte and platelet survival in the nuclear medicine literature have been summarized elsewhere (Silberstein and Singh 1984).

15.5 Surface Counting to Assess Splenic Erythrocyte Destruction

A related issue to that of red cell or platelet survival is the role of the spleen in removing abnormal cells from the circulation. Confirmation that the spleen was playing a large role in erythrocyte or platelet destruction could provide information justifying splenectomy.

Such data first appeared in a report of two patients in whom external counting showed a significant accumulation of erythrocytes and subsequent splenectomy improved the condition of each patient (Korst et al. 1955). With more experience a variety of indices of splenic sequestration have been suggested which would predict a successful response to splenectomy for hemolytic anemias. One index of sequestration was defined as the difference between the relative radioactivity (expressed as a percentage of that over the precordium) for liver or spleen at the time of the red cell survival half-life and this value at time zero, with values of 30 – 60 % suggested as normal, 60 – 100 % as indicating mild to moderate organ "sequestration" of the labeled cells, and a number over 100 % indicating a moderate to severe process (Jandl et al. 1956). The word "sequestration" as applied to this process is incorrect, since we are looking for evidence of cell destruction, not merely sequestration. A rising spleen-to-liver ratio is another predictive marker of successful splenectomy, with a positive predictive value of 81 % in 31 cases (Korst et al. 1955; Schloesser et al. 1957; Goldberg et al. 1966). A related approach has been to calculate the excess counts over spleen and liver related to the heart after precordial counts are normalized to 1000 (Hughes-Jones and Szur 1957), while another group developed a splenic localization index:

$$\frac{(\text{delta } S/P_{max} \times 10)}{S/P_0 \times d_{max}} \qquad (15.9)$$

where delta S/P_{max} is the maximum change in the spleen-to-precordium count ratio, S/P_0 is the initial ratio (counted after a 30 – 60 min equilibrium period), and d_{max} is the day on which the maximum ratio occurs (McCurdy and Rath 1958). This index, if in excess of 1.0, had a positive predictive value of 91 % in 11 cases. However, a good correlation was found in another series between splenic accumulation of ^{51}Cr-erythrocytes and a good clinical response to splenectomy in only 44 % of nine splenectomized patients and 40 % of five patients receiving splenic irradiation (Ben-Basset et al. 1967). In another small series three of five patients with autoimmune hemolytic anemia and both a normal splenic sequestration index and a spleen-to-liver ratio under 2.5 still had reduced hemolysis by splenectomy, whereas one of three patients with both indices abnormal did not. If one (but not both) index was abnormal, three of four were not helped (Parker et al. 1977).

There are several reasons for the variability of this test. One must count precisely over the liver and spleen when performing the study, so a low dosage of ^{99m}Tc-sulfur colloid should be used to localize the extent of these organs, especially when their location is not obvious on physical examination, so that the sites requiring counting can be marked on the body surface before the labeled erythrocytes are injected. The ^{99m}Tc photopeak at 140 keV should be easily separable from that of ^{51}Cr, 322 keV. Collimation must be carefully performed to avoid cross talk between liver, spleen, and precordium, especially in children. Splenomegaly without hemolysis will also cause high spleen-to-precordium counts, but with sequestration and no cell destruction the ratio will remain stable as the cells arriving and leaving this organ are essentially at equilibrium, excluding those senescent cells the spleen culls from the blood daily. Another problem in predicting the response to splenectomy has been the response of the liver to this operation, as the phagocytic hepatic Kupffer cells may take over the sequestration function that the spleen had performed, sometimes without providing evidence of this sequestration capability on the labeled erythrocyte study. The results of splenic sequestration studies in a variety of anemias have been reported elsewhere (Silberstein and Singh 1984).

A review of the various indices of splenic erythrocyte destruction suggests that the index of sequestration (Jandl et al. 1956) and a progressively rising spleen-to-liver ratio provide the most reliable information, with approximately an 85 % positive predictive value in suggesting a response to splenectomy.

15.6 In Vivo Testing for Transfusion Compatibility

Alloantibodies active between 30 and 37 °C may cause apparent incompatibility between a prospective recipient and all donors on the in vitro cross match. There are also unexplained hemolytic transfusion reactions not predicted by the in vitro cross match. In these two clinical circumstances a small infusion of radiolabeled erythrocytes proposed for transfusion may be very useful to safely determine compatibility. Earlier techniques, involving the transfusion of up to 50 mL of donor blood, were both insensitive and potentially dangerous, as the end point was the detection of hyperbilirubinemia or an elevated plasma hemoglobin (Weiner et al. 1942). Radiolabeled cells were first employed for this purpose in 1955. The ICSH recommends an injection of 0.5 ml of donor cells labeled with 5 – 20 μCi of ^{51}Cr after washing and diluting the cells to a final volume of 10 mL. Blood samples are obtained at 3, 10, and 60 min from a vein other than that used for injection (ICSH 1980b).

Compatible labeled erythrocytes should yield a counting rate in the 60 min sample which is in the range of 99.5 ± 2.5 % of injected blood, so with normal survival the lowest value likely to be seen at 60 min is about 94.5 %. The ICSH suggests a range of 94 – 104 % at 60 min, owing to elution and errors in measurement. The requirement for sampling over 60 min implies a rapid rate of destruction, i.e., greater than 5 %/h, but

longer sampling times will detect lower rates of erythrocyte destruction, even up to 24 h.

In emergent situations patients have been successfully transfused when the erythrocyte survival at 60 min is no less than 70 % and the amount of radioactivity in the plasma at 10 and 60 min does not exceed 3 % of the radioactivity injected. If the survival is in excess of 70 %, the concentration of offending antibody is usually quite low, so the destruction of a large number of incompatible cells will occur quite slowly. A delayed hemolytic transfusion reaction is, however, not fully excluded even when the 24-h survival of whole units of blood appears to be satisfactory (ICSH 1980b).

15.7 Ferrokinetics

Iron-59 was first employed to study the intricacies of iron metabolism in the 4th decade of the twentieth century (Hahn and Whipple 1936). Many thousands of studies of iron metabolism have been published since that time, usually employing the tracer iron-59. The results of these studies reveal a system of remarkable complexity, and ferrokinetic studies have proved to be challenging, exacting, time consuming, and costly. These studies should only be used clinically when the desired information cannot be obtained by other means. Considerable information can be obtained from a clinical ferrokinetic study, including plasma iron clearance and turnover, red cell iron incorporation and turnover, and even sites of extramedullary hematopoiesis. Answers also may be provided to concerns about ineffective erythropoiesis with this quantitative data.

Before injection radiolabeled iron must first be bound to transferrin, its carrier protein. A PV measurement is also required. There are other complexities to these calculations. For example, the serum iron level varies diurnally, so morning and evening blood specimens are required. If there is in vitro or in vivo hemolysis, the plasma iron time-activity curves may be contaminated with ^{59}Fe-hemoglobin in the later stages of the study. The ^{59}Fe disappearance curve is triexponential, involving iron taken up by erythrocyte precursors, iron refluxing to the plasma from extravascular sites into which transferrin has equilibrated, and also from ineffective erythropoiesis in the marrow. A fractional iron clearance rate which sums these can be estimated (Ricketts and Cavill 1975), although there is no satisfactory clinical technique for analyzing red cell ^{59}Fe curves to determine the time erythroblasts spend in the marrow, or the exact stage of development at which they may be destroyed in the marrow, the result of ineffective erythropoiesis. However, one can measure the proportion of plasma iron turnover involved in the effective production of mature, viable erythrocytes. The amount of iron involved in the effective production of mature erythrocytes can then be calculated from the plasma iron turnover, the fraction of the ^{59}Fe in erythrocytes at the end of the study, and the integral of the plasma ^{59}Fe clearance curve. The mean erythrocyte life span is the quotient of total circulating erythrocyte iron and the rate of erythrocyte iron turnover. The rate of erythrocyte production may be derived from the daily erythrocyte iron turnover and the mean cellular iron content (Cavill et al. 1977), but these calculations may "exceed the resolving power of the data obtained" (Finch and Hueber 1982).

Normally about 70 – 80 % of injected ^{59}Fe-transferrin will appear within circulating erythrocytes within 10 – 14 days. Plotting the time-activity curves from counting circulating red cells which have incorporated iron yields diagnostic information (Fig. 15.1). With iron deficiency ^{59}Fe-erythrocyte incorporation will rise more rapidly than normal and approach 90 – 100 %. Hemolytic anemias show a similar more rapid incorporation of iron into the erythrocyte than normal but the curve of labeled erythrocyte activity falls prematurely as circulating cells are destroyed. Ineffective erythropoiesis is characterized by a ^{59}Fe-erythrocyte curve which never achieves a normal incorporation level, as the cells and their precursors are prematurely destroyed in the marrow. In this condition the cells that circulate in the blood rarely have a normal life span, and even the subnormal level of iron incorporation they achieve will diminish prematurely. By external counting over the liver, spleen, and precordium (Fig. 15.2), one may obtain an indication of extramedullary hematopoiesis if the spleen/precordium or liver/precordium ratios rise within a day to ≥ 1.75 and then decrease over the next 1 – 5 days as red cells are released into the circulation. Hemolytic anemias will demonstrate liver and spleen uptake only after the precordial counts have risen first from labeled cells released into the circulating blood pool, with subsequent

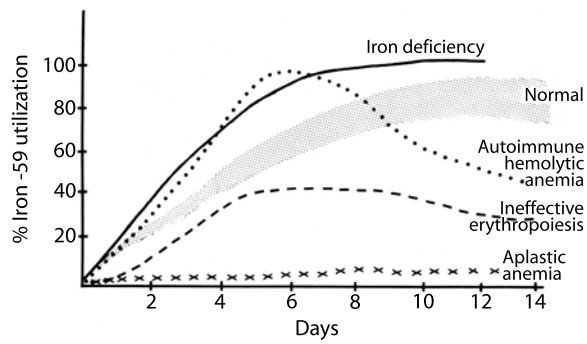

Fig. 15.1. Iron utilization time-activity curves typical of several hematological disorders. (Reproduced from *Nuclear Medicine Annual 1984* by permission of Wolters Kluwer nv)

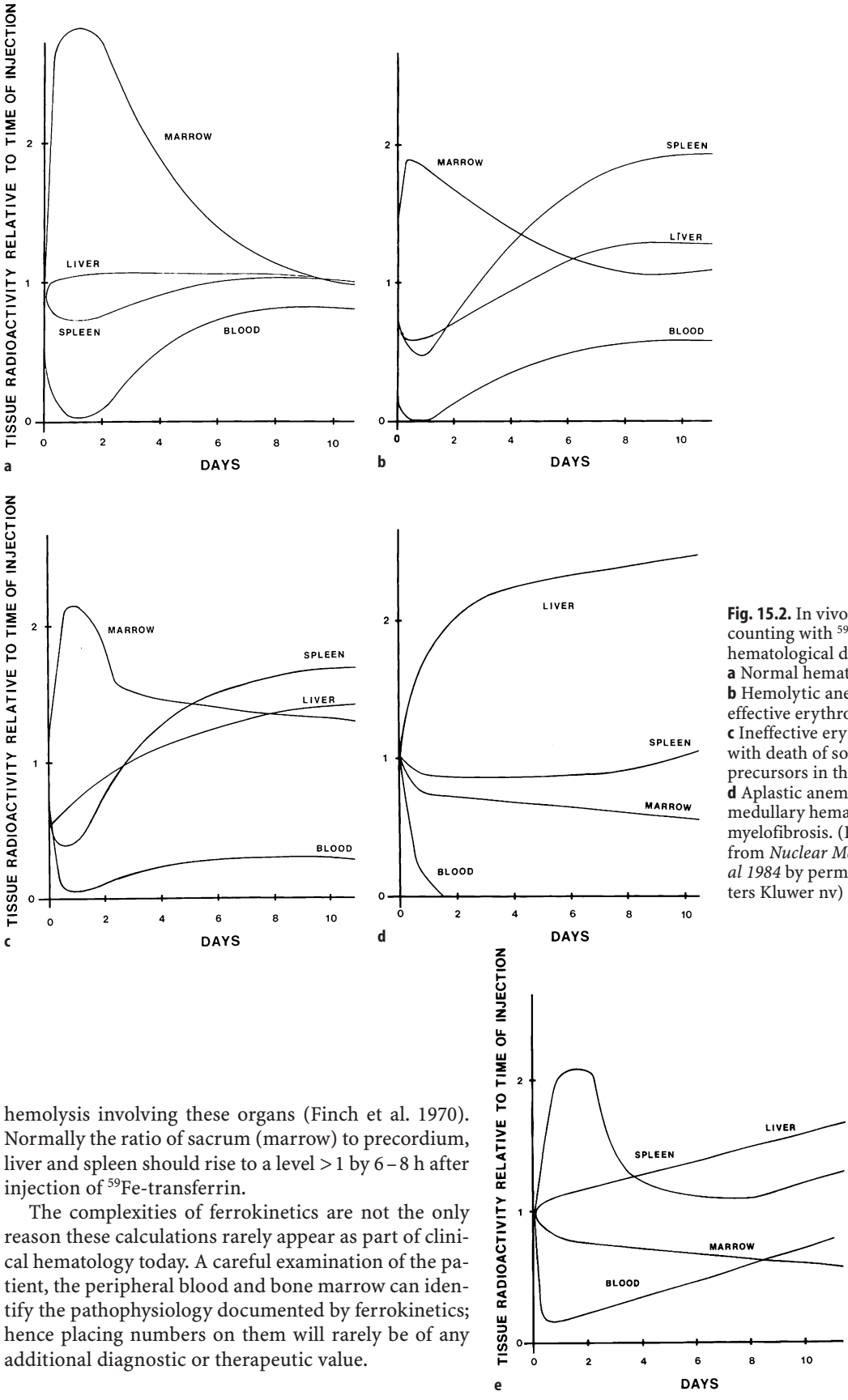

Fig. 15.2. In vivo surface counting with ^{59}Fe in several hematological disorders. **a** Normal hematopoiesis. **b** Hemolytic anemia with effective erythropoiesis. **c** Ineffective erythropoiesis with death of some red cell precursors in the marrow. **d** Aplastic anemia. **e** Extramedullary hematopoiesis with myelofibrosis. (Reproduced from *Nuclear Medicine Annual 1984* by permission of Wolters Kluwer nv)

hemolysis involving these organs (Finch et al. 1970). Normally the ratio of sacrum (marrow) to precordium, liver and spleen should rise to a level > 1 by 6 – 8 h after injection of ^{59}Fe-transferrin.

The complexities of ferrokinetics are not the only reason these calculations rarely appear as part of clinical hematology today. A careful examination of the patient, the peripheral blood and bone marrow can identify the pathophysiology documented by ferrokinetics; hence placing numbers on them will rarely be of any additional diagnostic or therapeutic value.

15.8 Marrow Scintigraphy

The bone marrow contains both mesenchymal cells, which differentiate into the stromal, reticuloendothelial system (RES), and hematopoietic stem cells and their progeny which differentiate, by stages, into mature erythrocytes, leukocytes, platelets, monocytes and macrophages. These stem cells require a special microenvironment for cell division and differentiation to occur (Kemp et al. 2005). Normal human hematopoiesis takes place after birth solely in the extravascular spaces between a highly branching network of medullary sinuses which carries blood from the osseous cortex into a large central sinus from which emissary veins return it to the systemic circulation. Developing blood cells must traverse the sinus wall to enter the circulation. This wall consists of a complete inner (luminal) layer of endothelial cells and an abluminal wall of adventitial reticular cells in an incomplete outer coat.

The marrow endothelial cells are also capable of removing particular matter from the circulation; this process is called endocytosis. The reticular cells (of the RES) have extensive, proximally branching, cytoplasmic processes that are contiguous with the sinus wall, but they are not highly phagocytic (Tamako 1969). However, the third type of phagocytic cell found in the marrow, the monocyte-derived macrophages, is quite active in this function.

Tracers designed for marrow imaging may therefore be specific for one of the types of hematopoietic cells differentiating there, or one may design a radiopharmaceutical which can be phagocytosed by one or more of the three marrow systems which remove particles from the circulation.

^{111}In-labeled leukocytes and platelets will both image hematopoietic marrow, since these cells will circulate through active marrow, but these labeled cell types are not employed to study leukocyte kinetics in depth. Since ^{111}In-leukocytes will visualize normal marrow activity, however, labeled leukocytes may localize in unexpected sites around total hip and knee prostheses, or in the feet in the presence of trauma from Charcot neuropathy, when ^{111}In-leukocyte scintigraphy is employed to search for infection, often after a bone scan is found to be abnormal at these sites. If this occurs, then a separate marrow scan must be performed to distinguish between ^{111}In-leukocyte detection of osteomyelitis and heterotopic, functioning, non-infected marrow (Palestro et al. 2004). Anti-granulocyte antibodies are no longer commercially available in the United States and will not be considered here, although these can delineate hematopoietic marrow. Positron-emitting ^{18}F-fluorodeoxyglucose (FDG) is also capable of producing impressive images of functioning marrow, even showing the presence of marrow hyperplasia in the presence of colony stimulating factors (Gundlapalli et al. 2002), and the ability of ^{18}F-FDG PET to detect bone metastases not seen on ^{99m}Tc-bisphosphonate scintigraphy is due to the imaging of hypermetabolic tumor in marrow that has not yet invaded the osseous cortex (Aydin et al. 2005). The use of positron emission tomography, and especially of ^{18}F-FDG in nuclear oncology, is the subject of a separate chapter by Dr. Bombardieri (Chapter 18) and will not be considered further under the topic of marrow imaging.

An obvious marker for hematopoietic marrow is a radioisotope of iron. However, there are no radioisotopes of iron with optimal imaging properties. Iron-52, most often employed for this purpose, has only an 8 h half-life and is a positron-emitter. It is cyclotron-produced and currently commercially unavailable in the United States. Iron-59 has also been employed, but its physical characteristics allow administration of only a small dosage (Table 15.4), so that the resultant image quality is poor. Iron clearance from the blood has a normal biologic half-time of 60 – 140 min, after which iron will be predominantly in the marrow for the next 3 – 4 days, unless there is extramedullary hematopoiesis, usually in the spleen and liver, so that scanning with radiolabeled iron may begin 8 – 12 h following the injection of transferrin-bound iron.

Radiocolloids have been employed to visualize phagocytic marrow since 1958 when gold-198 was first used for this purpose. Several colloids have been employed, but currently ^{99m}Tc-sulfur colloid and ^{99m}Tc-nanocolloid (a microaggregated human serum albumin) are the radiopharmaceuticals most in use. The

Table 15.4. Radiopharmaceuticals for bone marrow imaging

Radiopharmaceutical	Activity administered	Physical $t_{1/2}$	Photopeak (MeV)	Dosimetry (mGy/MBq) Liver	Spleen	Marrow	Gonads
^{52}Fe	3.7 MBq	8.2 h	0.165 0.511	0.8 – 5.8	0.9	11.1 – 13.0	0.3 – 1.2
^{59}Fe	1.85 MBq	45 days	1.1 1.3	22	85	12	3.5 – 7.3
^{99m}Tc-sulfur colloid	370 MBq	6 h	0.14	0.09	0.05	0.005	< 0.01

Table 15.5. Changes in pediatric marrow distribution with age

Area imaged	Marrow activity (years) 0–2	2–5	5–10	10–15
Femur	Entire	Entire	Most	Proximal
Knee	Present	Present	Present	Variable
Tibia	Entire	Proximal	None	None

former is a larger particle, with a diameter of about 100–500 nm, while the albumin colloid is smaller, with a diameter < 80 nm, although this range in size does not appear to alter colloid biodistribution in liver (85%), spleen (10–12%), and marrow (3–5%) markedly. Other than the function of these organs, other colloid variables, biophysical and chemical in nature, including colloid charge, size, number of particles, the presence of stabilizers, surface-active agents, the chemical nature of the particle surface, etc., do not have clinically significant effects on colloid distribution. The dosimetry of the radiopharmaceuticals we have discussed for marrow imaging appears in Table 15.5.

How much of a compromise does one make in employing a ^{99m}Tc-radiocolloid to image hematopoietic marrow when radioisotopes of iron more directly indicate this process? Usually the reticuloendothelial and hematopoietic marrow distribution is identical, for the stem cells need this special microenvironment to produce their progeny (Kemp et al. 2005). Exceptions to this congruence of marrow images have been noted in certain disease processes, especially after treatment, probably because stem cells have been killed or the microenvironment so altered by therapy that they cannot survive. These include a variety of congenital and acquired aplastic anemias, Hodgkin's disease or polycythemia vera after radiation or chemotherapy, and various forms of myelofibrosis (Van Dyke et al. 1967).

The normal distribution of bone marrow varies with age, involving virtually all the bones at birth, then receding with time. The pattern of pediatric marrow recession is summarized in Table 15.5. By late adolescence and adulthood hematopoiesis occur only in the central or axial skeleton and skull plus about the proximal one-third of the femur, with relatively poor uptake in the femoral head and greater trochanter) and humerus (Fig. 15.3). The mass of active ("red") marrow in an adult is about 1.5 kg for a 70 kg human at age 35–40 (Ellis 1961).

The most common pattern of altered marrow is expansion down the humerus and femur, indicating reactive erythropoiesis in the presence of chronic anemia. Photopenic areas within the skeleton will be seen in any of the myeloproliferative disorders in which secondary myelofibrosis becomes a complicating factor, especially polycythemia vera and myeloid metaplasia. Radiation causes clearly demarcated absence of marrow activity within the radiation port. After 35–45 Gy the radiocolloid marrow scan will show absent activity within the port for 6–12 months, with regeneration over the next 2 years in the majority of exposed areas (Rubin et al. 1973). Stromal regeneration always precedes stem cell recovery (Werts et al. 1980), but improvement of radiocolloid distribution does not guarantee that hematopoiesis is occurring in that site (DeGowin et al. 1974). In chronic myelogenous leukemia the marrow is markedly expanded but will show areas of irregular diminution as blast crisis intervenes. The marrow will be expanded in true, but not in spurious, erythrocytosis (caused by plasma volume contraction), but the EV, not a marrow scan, is the appropriate diagnostic test here.

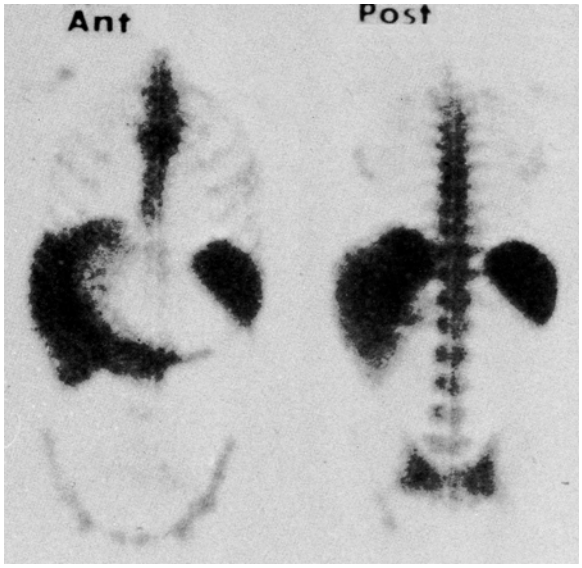

Fig. 15.3. Normal marrow scan with ^{99m}Tc-sulfur colloid in the presence of a large hepatic mass. Because of the decreased hepatic tissue in the midline, lower thoracic and upper lumbar marrow is much more easily seen than in the usual case. The intensity of liver and spleen activity, which contain 95% or more of the injected radioactivity, makes the small amount of appendicular marrow in the proximal femur and humerus very difficult to visualize here. (Reproduced from *Nuclear Medicine Annual 1984* by permission of Wolters Kluwer nv)

Metastatic disease may be detected as photopenic sites within the areas where marrow should normally occur, and the marrow scan is often, but not always, as sensitive as the bone scan for detecting skeletal metastases (Fig. 15.4) (Huggett et al. 1991), since blood-born metastatic disease usually begins in the marrow, spreading only later to the cortex. Absence of marrow activity in cancer patients can also be caused, of course, by infarction, fibrosis, focal lymphoid or fatty infiltration, hemangioma or other benign tumor, Paget's disease, etc. However, the bone scan carries several advantages over the marrow scan. The absence of marrow activity in the adult distal to the proximal humerus and femur, the difficulty seeing lower thoracic and upper lumbar vertebrae because of crosstalk from the adja-

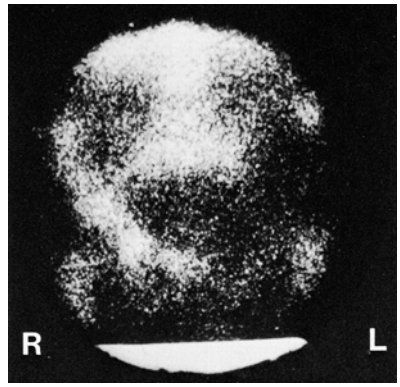

Fig. 15.4. Metastatic disease in the left ilium with a normal bone scan (not shown). (Reproduced from *Nuclear Medicine Annual 1984* by permission of Wolters Kluwer nv)

cent liver and spleen, and the lack of specificity of the findings make marrow scintigraphy a less useful technique, especially with the availability of modern MRI (Haubold-Reuter et al. 1993; Gosfield et al. 1993).

The radiocolloid marrow scan has been described as helpful in defining sites of infiltration in multiple myeloma (Shreiner and Hsu 1981), but ^{99m}Tc-sestamibi has been described as having higher sensitivity in staging this disease and following the response of myeloma to therapy (Vivva 2005). This use is likely to be replaced by the ubiquitous ^{18}F-FDG if the procedure can be reimbursed.

There remain only a few areas wherein the marrow scan can play a useful role in modern nuclear medicine. The distinction between an infected site and displacement of marrow seen with ^{111}In has been alluded to above, and the use of a ^{99m}Tc-radiocolloid is essential to solve this diagnostic dilemma. Chronic versus acute anemia can be distinguished, since the marrow scan will be normal if the onset of the anemia occurred in a week or less (Nelp and Larson 1972). In patients with myelofibrosis the marrow scan can detect sites still available for biopsy.

Myeloid metaplasia with progressive myelofibrosis is a very difficult disease to treat, with pancytopenia caused both by fibrosis of the marrow and by splenomegaly. If splenectomy is to be considered as a therapeutic option, a marrow scan will indicate if there is, in fact, any intra-osseous hematopoietic marrow remaining. If none is visualized, a reasonable assumption is that the enlarged spleen is the site of blood cell production and therefore cannot be safely removed. Marrow imaging may also indicate extramedullary masses that are sites of hematopoiesis rather than malignancy (Brown et al. 1980). At this time marrow scintigraphy with radiocolloid for the detection of skeletal metastases or infarction cannot be recommended, since better techniques, viz. bone scintigraphy and MRI, are available (Haubold-Reuter et al. 1993).

15.9 Vitamin B_{12} Absorption

In the presence of macrocytosis (mean corpuscular volume or MCV in excess of 100 fL), megaloblastic anemia, peripheral neuropathy, and even dementia, vitamin B_{12} deficiency should be entered into the differential diagnosis (Silberstein 1984a) once reticulocytosis is eliminated by quantitation and/or examination of the peripheral blood. The malabsorption of vitamin B_{12} is the most common cause of deficiency of this vitamin. Dietary deficiency is rare since B_{12} is present in not only meat but also in eggs and dairy products. Vitamin B_{12} deficiency usually follows malabsorption of the vitamin by 3–7 years because of the large hepatic store of B_{12}. The absorption of vitamin B_{12} may be studied with nuclear medicine techniques because the cobalt atom which is incorporated into the porphyrin-like corrin major ring structure may be radiolabeled, currently with ^{57}Co, although ^{58}Co and ^{60}Co have been used in the past (Table 15.6). The commercially available form of B_{12} is actually cyanocobalamin, but we shall use the abbreviation B_{12} to stand for both this and the activated adenosylcobalamin form of the vitamin.

In the presence of microgram amounts of B_{12}, absorption depends largely on the presence of a transport glycoprotein produced by gastric parietal cells called intrinsic factor. Given in milligram amounts, B_{12} can be absorbed through the intestinal wall by mass action. After oral ingestion of the radiolabeled B_{12} several methods are available to measure its absorption, including measurement of fecal excretion, external monitoring over the liver, whole body counter measurements, sequential serum B_{12} levels measured after ingestion, and a collection of urine following the ingestion of radiolabeled B_{12} and injection of a dose of nonradiolabeled B_{12}, also known as the Schilling test (Schil-

Table 15.6. Dosimetry of vitamin B_{12} labeled with cobalt radioisotopes (CDE dosimetry)

Radioisotope	Physical $t_{1/2}$	Radiation emitted	Gamma energy (MeV)	Liver dose (after flushing dose of B_{12}) (mGy/MBq)	EDE
^{57}Co	272 days	Gamma	0.12	23 – 30	0.5 – 3.0
^{58}Co	71 days	Positron	0.51	35 – 47	1.3 – 5.7
		Gamma	0.81		
^{60}Co	5.24 years	Electron	1.33	71 – 550	12 – 87
		Gamma	1.17		

ling 1953). The injected unlabeled B_{12} blocks hepatic, and, to some extent, blood receptors (the serum protein transcobalamin II) of the orally administered ^{57}Co, so that, rather than being stored, the ^{57}Co-B_{12} is excreted by the kidney at the rate of glomerular filtration. Although the whole body counter, or a shadow shield technique using a gamma camera, can quantitate the radioactivity in the body, that radioactivity will be emanating from three compartments, the gastrointestinal tract, the genitourinary tract, and the remaining tissues of the body containing vitamin which has been absorbed but not yet excreted. Since we have found that up to 16 days may be required to clear the intestine of ^{57}Co in elderly, constipated patients, repeated, time-consuming measurements may be needed, requiring equipment which is not readily available. A corollary of this delay in excretion before whole body techniques give reliable data is that fecal collections may be required for well over 2 weeks if one chooses that approach. Whole body counting is the direct method of choice (ICSH 1981) and the preferred technique in patients with urinary and/or fecal incontinence.

The Schilling test became the method of choice for measuring B_{12} absorption because of the small amount of radiation involved, apparent good separation of normals and abnormals (at least at the time of its description), and a delay of only 2 or 3 days before results become available. However, to obtain a normal result from the Schilling test, not only must the stomach secrete intrinsic factor, but the pancreas must be functioning, ileal receptors of the intrinsic factor-B_{12} complex must be intact, and the genitourinary system must be normal. An important further source of error is an inadequate urinary collection. At least a 48-h collection is required to avoid false positive results in about 20% of patients (Silberstein 1973). Since up to 6% of the ^{57}Co activity may adhere to the capsule of the vitamin being given orally, it should be dissolved before administration (Williams et al. 1980) and given with 100–200 mL of water as solvent (ICSH 1981). Just before the test the urine must be checked for radioactivity from any previous nuclear medicine test. A low 48–72 h urine excretion of B_{12} should be followed by a second stage of the Schilling test wherein intrinsic factor is mixed with the B_{12} before administration and not given as a separate capsule (McDonald et al. 1975). Correction of a first stage Schilling test showing low urinary excretion of the radiolabeled vitamin by readministration of ^{57}Co-B_{12} with added intrinsic factor confirms the diagnosis of intrinsic factor deficiency, most often due to the autoimmune disease pernicious anemia. Failure to achieve full correction of B_{12} absorption with intrinsic factor may indicate a problem of pancreatic, ileal, or genitourinary function if a failure to collect all urine specimens can be excluded. A full listing of the causes of an abnormal Schilling test appears elsewhere (Silberstein 1984a). To add to the complexities of interpretation, a deficiency of vitamin B_{12}, or of folic acid, which is also a cause of megaloblastic anemia, is actually a systemic disorder involving the intestine, so that ileal malabsorption of either vitamin may result. This phenomenon can cause a falsely abnormal second stage Schilling test which one would have expected to normalize with intrinsic factor in the presence of pernicious anemia. Therefore retesting may be required after weeks or months of treatment with the deficient vitamin (Carmel and Herbert 1967).

To avoid repeated testing of the patient with sequential first and second stage Schilling tests, the simultaneous administration of intrinsic factor bound and unbound B_{12}, labeled with different radioisotopes, has been employed. While this dual isotope procedure can more rapidly make the diagnosis of pernicious anemia, it also gives a significant number of normal patients more radiation (albeit a small amount) than they would have received with the conventional sequence of the Schilling test. Another problem with this approach is that a number of investigators have noted an exchange of the unbound ^{58}Co with the bound ^{57}Co (Briedis et al. 1971; Fairbanks et al. 1983), an occurrence which has led to incorrect or indeterminate diagnoses in as many as 20–30% of patients so tested (Pathy et al. 1979; Atrah et al. 1999).

The diagnostic accuracy of the Schilling test for B_{12} malabsorption has been challenged by the demonstration of the malabsorption of food-bound B_{12} in the presence of normal absorption of crystalline vitamin B_{12}. Studies employing B_{12} bound to chicken serum, eggs, and various meats clearly demonstrate that this phenomenon can be a cause of B_{12} deficiency (Zittoun and Zittoun 1999). A major problem in evaluating tests of B_{12} malabsorption is deciding what the gold standard for the diagnosis of B_{12} deficiency should be. The prevalence of B_{12} deficiency is higher when certain metabolites requiring B_{12} for chemical transformation are assayed along with the vitamin level itself. Serum B_{12} levels may be low normal to normal in elderly patients who have elevated serum methylmalonic acid (MMA) levels and/or serum total homocysteine levels. These metabolites are often found to be elevated because of a deficiency of activated B_{12}, adenosylcobalamin, which is involved in moving methyl groups in the two compounds. In many of these patients the usual etiologic investigations prove to be negative, but the MMA levels normalize with B_{12} therapy (Zittoun and Zittoun 1999). One-third of a group of patients with elevated serum MMA levels and biopsy-proven atrophy of the gastric body had normal absorption of crystalline and food-bound B_{12}. The food-bound B_{12} study is more sensitive than the test of crystalline B_{12} absorption, but even the adequacy of the sensitivity of the former has been called into question (Lindgren et al. 1997). Low but un-

explained B_{12} levels have also been described in lymphoproliferative diseases, especially multiple myeloma. Normalization of elevated MMA and homocysteine levels with B_{12} therapy may be a reasonable diagnostic standard for B_{12} deficiency, but these metabolites cannot themselves be used as screening tests for the condition because both are elevated even in mild renal insufficiency (Rasmussen et al. 1990). If the second stage Schilling test, involving intrinsic factor, does not correct B_{12} malabsorption, then one must add the inability to cleave food-bound B_{12} from an ingested protein as yet another cause of this abnormal test, along with B_{12} deficiency-induced B_{12} malabsorption, and the better known causes, disorders of the stomach, pancreas, ileum, and kidneys.

15.10 Radiophosphorus Therapy for Hematologic Disease

Radiophosphorus, as P-30, was the first artificial radioactive element produced by Frederick and Irene Joliot-Curie, December 31, 1933, using alpha particle bombardment (Joliot and Curie 1934). In 1934, Hevesy, employing radon as a neutron source, made the pure beta-emitter ^{32}P (maximum energy 1.71 MeV, half-life 14.3 days) in nanocurie amounts. By 1936 Ernest Lawrence could produce millicurie amounts of ^{32}P-orthophosphate with his Berkeley cyclotron. The metabolism of ^{32}P-orthophosphate has been summarized elsewhere (Silberstein 1992). ^{32}P-orthophosphate was administered intravenously to patients with chronic lymphatic and myelogenous leukemias, multiple myeloma, solid tumors and polycythemia vera beginning in 1936 with mixed results, although the hematologic neoplasms, especially polycythemia vera, often showed clear responses (Reinhard et al. 1946; Roberts and Smith 1997).

In myeloproliferative disorders, primarily polycythemia vera and essential thrombocythemia, a small role for ^{32}P-orthophosphate remains, in the treatment of patients who cannot tolerate hydroxyurea or interferon-alpha, and in the elderly patient who cannot be relied upon to take a daily chemotherapeutic agent on a regular basis (Parmentier 2003). In a study of the therapy of myeloproliferative diseases with ^{32}P-orthophosphate the median number of injections required was two, but ranged widely, from one to thirteen (Balan and Critchley 1997). Life is clearly prolonged in myeloproliferative disorders treated with ^{32}P-orthophosphate even though the radiopharmaceutical is leukemogenic (Roberts and Smith 1997; Parmentier 2003). The uses of ^{32}P-orthophosphate are explored further in Chapter 23 by Dr. Palmedo.

References

Atrah HI, Davidson RJ (1999) A survey and critical evaluation of a dual isotope (Dicopac) vitamin B12 absorption test. Eur J Nucl Med 15:57 – 60

Aydin A, Yu JQ, Zhuang H, et al. (2005) Detection of bone marrow metastases by FDG-PET and missed by bone scintigraphy in widespread melanoma. Clin Nucl Med 30:606 – 607

Balan KK, Critchley M (1997) Outcome of 259 patients with primary proliferative polycythemia (PPP) and idiopathic thrombocythaemia (IT) treated in a regional nuclear medicine department with phosphorus-32 – a 15 year review. Br J Radiol 70:1169 – 1173

Balga I, Solenthaler M, Furlan M (2000) Should the whole-body red cell mass be measured or calculated? Blood Cells Mol Dis 26:25 – 31

Ben-Bassat I, Seligsohn U, Leiba H, et al. (1967) Sequestration studies with chromium-51 labeled red cells as criteria for splenectomy. Israel J Med Sci 3:832 – 837

Blahd WH (1971) Gastrointestinal tract function. In: Blahd WH (ed) Nuclear medicine, 2nd edn. McGraw-Hill, New York, pp 350 – 381

Briedis D, McIntyre PA, Judisch J, et al. (1973) An evaluation of a dual-isotope method for the measurement of vitamin B_{12} absorption. J Nucl Med 14:135 – 141

Brown LJ, Paquelet JKR, Tetalman MR (1980) Intrathoracic extramedullary hematopoiesis: appearance on ^{99m}Tc-sulfur colloid marrow scan. Am J Roentgenol 134:1254 – 1255

Carmel R, Herbert V (1967) Correctable intestinal deficiency of vitamin B12 absorption in pernicious anemia. Ann Int Med 67(6):1201 – 7

Cavill I, Ricketts C, Napier JAF (1977) Ferrokinetics and erythropoiesis in man: an evaluation of ferrokinetic measurements. Br J Haematol 35:35 – 47

CDE Dosimetry Services, Inc. (2001) available from http://www.internaldosimetry.com/linkedpages/doseestimates.html

Cline MI, Berlin NJ (1963) The red cell chromium elution rate in patients with some hematologic diseases. Blood 21:63 – 69

DeGowin RL, Chaudhuri TK, Christie JH, et al. (1974) Marrow scanning in evaluation of hemopoiesis after radiotherapy. Arch Int Med 134:297 – 303

Ebaugh FG, Emerson CP, Ross JF, et al. (1953) The use of chromium-51 as an erythrocyte tagging agent for the determination of red cell survival in vivo. J Clin Invest 32:1260 – 1261

Ebaugh FG, Clemens T, Jr, Rodman G, et al. (1958) Quantitative measurement of gastrointestinal blood loss. I. The use of radioactive ^{51}Cr in patients with gastrointestinal hemorrhage. Am J Med 25:169 – 181

El-Hemaidi I, Nunan TO, Pearson TC (1997) Red cell mass and plasma volume measurement. Nucl Med Commun 18:189 – 190

Ellis R (1961) The distribution of active bone marrow in the adult. Phys Med Biol 5:255 – 258

Fairbanks VF (2000) Myeloproliferative disease: Polycythemia vera: The packed cell volume and the curious logic of the red cell mass. Hematology 4:381 – 395

Fairbanks VF, Wahner HW, Valley TB, et al. (1983) Spurious results from dual-isotope (Dicopac) vitamin B_{12} absorption test. Nucl Med Commun 4:17 – 23

Finch CA, Hueber H (1962) Perspectives in iron metabolism. N Engl J Med 360:1250 – 1258

Finch CA, Beubelbeiss K, Cook JD, et al. (1970) Ferrokinetics in man. Medicine 49:17 – 53

Goldberg A, Hutchinson HE, MacDonald E (1966) Radiochromium in the selection of patients with hemolytic anemia for splenectomy. Lancet 1:109 – 114

Goodwin DA, Bushberg JT, Doherty PW, et al. (1978) Indium-111-labeled autologous platelets for location of vascular thrombi in humans. J Nucl Med 19:626 – 634

Gore CJ, Hopkins WG, Burge CM (2005) Errors of measurement for blood volume parameters: a meta-analysis. J Appl Physiol 99:1745 – 1758
Gosfield E, Alavi A, Kneeland B (1993) Comparison of radionuclide bone scan and magnetic resonance imaging in detecting spinal metastases. J Nucl Med 34:2191 – 2198
Gray SJ, Sterling K (1959) The tagging of red cells and plasma proteins with radioactive chromium. J Clin Invest 29:1604 – 1612
Gregersen MI, Rawson RA (1959) Blood volume. Physiol Rev 309:377 – 344
Gundlapalli S, Ohja B, Mountz JM (2002) Granulocyte colony-stimulating factor. Clin Nucl Med 27:140 – 141
Hahn PF, Whipple GH (1936) Iron metabolism. Am J Med Sci 191:24 – 43
Haubold-Reuter BG, Duewell S, Schilcher BR, et al. (1993) The value of bone scintigraphy, bone marrow scintigraphy and fast spin-echo magnetic resonance imaging in staging of patients with malignant solid tumors: a prospective study. Eur J Nucl Med 20:1063 – 1069
Holt JT, Spitalnik SL, Wilson G (1982) Inhibition of chromium-51 RBC labeling by stannous pyrophosphate. J Nucl Med 23:934 – 935
Huggett SM, Nimalaraj T, Costa DC, et al. (1991) Nanocolloid imaging in early bone or marrow metastatic spread. J Nucl Med Tech 19:33 – 35
Hughes-Jones NC, Szur L (1957) Determination of the sites of red cell destruction using ^{51}Cr-labelled red cells. Br J Haematol 3:320 – 331
International Committee for Standardization in Hematology (1980a) Recommended methods for measurement of red cell and plasma volume. J Nucl Med 21:793 – 800
International Committee for Standardization in Hematology (1980b) Recommended method for radioisotope red cell survival studies. Br J Haematol 45:659 – 666
International Committee for Standardization in Hematology (1981) Recommended methods for the measurement of vitamin B_{12} absorption. J Nucl Med 22:1091 – 1093
Jandl JH, Greenberg MS, Yonemoto RH, et al. (1956) Clinical determination of the sites of red cell sequestration in hemolytic anemia. J Clin Invest 35:842 – 867
Joliot F, Curie I (1934) Artificial production of a new kind of radioelement. Nature 133:201 – 202
Kasfiki AG, Antipas SE, Dimitriou PA (1982) Mathematical analysis of ^{51}Cr-labeled red cell survival curves in congenital hemolytic anemias. Eur J Nucl Med 7:181 – 183
Kemp KC, Hows J, Donaldson C (2005) Bone marrow-derived mesenchymal cells. Leuk Lymphoma 46:1531 – 1544
Klopper JF, Spencer RP, Srivastava SC, et al. (1979) Studies on determination of the regional hematocrit in dogs. Int J Nucl Med Biol 6:68 – 72
Korst DR, Clatanioff DV, Schilling RF (1955) External scintillation counting over the liver and spleen after transfusion of radioactive erythrocytes. Clin Res Proc 3:195 – 196
Lindgren A, Bagge E, Cederblad A, et al. (1997) Schilling and protein-bound cobalamin absorption tests are poor instruments for diagnosing cobalamin malabsorption. J Intern Med 241:477 – 484
Lorberboym M, Rahimi-Levine N, Lipszyc H, et al. (2005) Analysis of red cell mass and plasma volume in patients with polycythemia. Arch Pathol Lab Med 129:89 – 91
McCurdy PR, Rath CE (1958) Splenectomy in hemolytic anemia: results predicted by body scanning after injection of ^{51}Cr-tagged red cells. N Engl J Med 259:459 – 493
McDonald JWD, Barr RM, Barton WB (1975) Spurious Schilling test results obtained with intrinsic factor enclosed capsules. Ann Intern Med 83:827 – 829
McIntyre PA (1977) Newer developments in nuclear medicine applicable to hematology. In: Brown EB (ed) Progress in hematology, vol 10. Grune and Stratton, New York, pp 381 – 409
Mollison PL (1979) Blood volume. In: Mollison PL (ed) Blood transfusion in clinical medicine, 6th edn. Blackwell Scientific, Oxford, pp 88 – 92
Nelp W, Larson SM (1972) Patterns in clinical bone marrow imaging. J Nucl Med 13:456 – 457
Palestro C, El Espera I, Blondet C, Moullart V, et al. (2004) The usefulness of ^{99m}Tc sulfur colloid bone marrow scintigraphy combined with ^{111}In leukocyte scintigraphy in prosthetic joint infection. Nucl Med Commun 25:171 – 175
Parker AC, Macpherson AIS, Richmond J (1977) Value of radiochromium investigation in autoimmune hemolytic anemia. Br Med J 1:208 – 209
Parmentier C (2003) Uses and risks of phosphorus-32 in the treatment of polycythaemia vera. Eur J Nucl Med Mol Imaging 30:1413 – 1417
Pathy MS, Kirkman S, Molloy MJ (1979) An evaluation of simultaneously administered free and intrinsic factor bound radioactive cyanocobalamin in the diagnosis of pernicious anemia in the elderly. J Clin Pathol 32:244 – 250
Pavel DG, Zimmer AM, Patterson VN (1977) In vivo labeling of red blood cells with ^{99m}Tc: a new approach to blood cell visualization. J Nucl Med 18:305 – 308
Pearson TC, Guthrie DL, et al. (1995) Interpretation of measured red cell mass and plasma volume in adults: Expert panel on radionuclides of the International Committee for Standardization in Hematology. Br J Haematol 89:748 – 756
Porter WC, Dees SM, Freitas JE, et al. (1963) Acid-citrate-dextrose compared with heparin in the preparation of in vivo/in vitro technetium-99m red blood cells. J Nucl Med 23: 383 – 387
Rao SA, Dewanjee MR (1982) Comparative evaluation of red cell labeling parameters of three lipid soluble-111In chelates: effect of lipid solubility on membrane incorporation and stability constant on transchelation. Eur J Nucl Med 7:282 – 285
Rasmussen K, Vyberg B, Pedersen KO, et al. (1990) Methylmalonic acid in renal insufficiency. Evidence of accumulation and implications for diagnosis of cobalamin deficiency. Clin Chem 36:1523 – 1524
Rehani MM, Sharma SK (1980) Site of Tc-99m binding to the red cell. J Nucl Med 21:676 – 678
Reinhard EH, Moore CV, Bierbaum OS, et al. (1946) Radioactive phosphorus as a therapeutic agent. A review of the literature and analysis of the results of treatment of 155 patients with various blood diseases, lymphomas and other malignant neoplastic diseases. J Lab Clin Med 31:107 – 195
Ricketts C, Cavill I (1975) Ferrokinetics: methods and interpretation. Clin Nucl Med 3:159 – 164
Roberts BE, Smith AH (1997) Use of radioactive phosphorus in hematology. Blood Rev 11:146 – 153
Rubin P, Landman S, Meyer E, et al. (1973) Bone marrow regeneration and extension after extended field irradiation in Hodgkin's disease. Cancer 32:699 – 711
Sanchez-Medal L, Loria A (1972) Erythrocytic production in the anemias. I. The use of the survival curve for predicting production in the nonsteady state. J Nucl Med 13:111 – 114
Schilling RF (1953) Intrinsic factor studies. II. The effect of gastric juice on the urinary excretion of radioactivity after oral administration of radioactive vitamin B_{12}. J Lab Clin Med 42:860 – 866
Schloesser LL, Korst DR, Clatanoff DV, Schilling R (1957) Radioactivity over the spleen and liver following infusion of chromium-51-labelled erythrocytes in hemolytic anemia. J Clin Invest 36:1470 – 1485
Shreiner DP, Hsu Y (1981) Comparison of reticuloendothelial scans with bone scans in malignant disease. Clin Nucl Med 6:101 – 104

Silberstein (1973) Value of 48- or 72-hour urine collection in performing the Schilling test. J Nucl Med 14:692 – 694
Silberstein EB (1984a) Nuclear hematology: the erythron. In: Freeman L (ed) Nuclear medicine annual 1984. Raven Press, New York, p 196
Silberstein EB (1984b) Nuclear hematology: the erythron. In: Freeman L (ed) Nuclear medicine annual 1984. Raven Press, New York, p 200
Silberstein EB (1991) Phosphorus-32 radiopharmaceuticals for the treatment of painful osseous metastases. Semin Nucl Med 22:17 – 27
Silberstein EB, Singh A (1984) Quantitative nuclear hematology. In: Silberstein EB, McAfee JG (eds) Differential diagnosis in nuclear medicine. McGraw-Hill, New York, pp 224 – 225
Smith TD, Richards P (1976) A simple kit for the preparation of ^{99m}Tc-labeled red blood cells. J Nucl Med 17:126 – 132
Spivak JL (2003) Diagnosis of the myeloproliferative disorders: Resolving phenotypic mimicry. Semin Hematol 40 (Suppl I):1 – 5
Sterling K, Gray SJ (1950) Determination of the circulating red cell volume in man by radioactive chromium. J Clin Invest 32:1614 – 1619
Tamako Y (1969) An electron microscopic study of non-phagocytic reticulum cells in human bone marrow. I. Cells with intracytoplasmic fibrils. Acta Haematol Japan 32:275 – 286
Tefferi A (2003) Polycythemia vera: A comprehensive review and clinical recommendations. Mayo Clin Proc 78:174 – 194
Tefferi A, Spivak JL (2005) Polycythemia vera: scientific advances and current practice. Semin Hematol 42: 206 – 220
Van Dyke D, Shkurkin C, Price D, et al. (1967) Differences in distribution of erythropoietic and reticuloendothelial marrow in hematologic disease. Blood 30:364 – 374
Vivva G, Balleari E, Carletto M, et al. (2005) Staging and therapy monitoring of multiple myeloma by ^{99m}Tc-sestamibi scintigraphy: a five year single center experience. J Exp Clin Cancer Res 24:355 – 361
Weiner AS, Silverman IJ, Aronson W (1942) Hemolytic transfusion reactions. II. Prevention, with special reference to a new biological test. Am J Clin Pathol 12:241 – 248
Werts ED, Gibson DP, Knapp SA, et al. (1980) Stromal cell migration precedes hemopoietic repopulation of the bone marrow after irradiation. Radiat Res 81:20 – 30
Williams PJ, Silberstein EB, Hughes JA, et al. (1980) Modification of the Schilling test for pediatric studies. J Nucl Med Tech 8:165 – 167
Zittoun J, Zittoun R (1999) Modern clinical testing strategies in cobalamin and folate deficiency. Semin Hematol 36:35 – 46

16 Hodgkin's Disease and Lymphomas

L. Kostakoglu, M. Coleman, S.J. Goldsmith

16.1 Introduction

Lymphomas represent a diverse range of diseases with evolving pathologic classification and therapy strategies. Essentially, the lymphomas are classified into two main groups, Hodgkin's disease (HD) and non-Hodgkin's lymphoma (NHL). For both disease entities accurate determination of extent of disease at initial staging and restaging is key for optimal management. More than 75% of all newly diagnosed patients with adult HD can be cured with combination chemotherapy and/or radiation therapy. As for NHL, effective drug combinations can produce prolonged disease-free survival in the majority of patients. A functional or metabolic diagnostic imaging modality can contribute to the assessment of a patient in various ways. Functional imaging can complement anatomic imaging modalities, mainly CT, and thereby enhances the accuracy of defining the extent of disease prior to therapy. In the post-therapy setting, the ability to differentiate residual viable disease from benign post-therapy changes could impact patient management and outcome, particularly if it helps to select patients who would require additional therapy or a change in treatment regimen. The limitations associated with anatomic imaging modalities, mainly with computed tomography (CT), to identify disease in the lymph nodes as well as in the extra-nodal sites have long been recognized. Functional imaging techniques such as Ga-67 single photon emission tomography (SPECT) have complemented CT, particularly in the post-therapy setting, although the sensitivity of this imaging technique is suboptimal in infra-diaphragmatic disease and low grade lymphomas. Thallium-201 and Tc-99m-sestamibi SPECT have been proposed as alternative imaging studies in the assessment of low-grade lymphomas. Nonetheless, similar restrictions apply to both of these radiotracers when imaging intra-abdominal lymphomas. Since the advent of ^{18}F-fluorodeoxyglucose positron emission tomography (FDG-PET), sufficient evidence has accumulated to demonstrate that FDG-PET is a more accurate imaging modality compared to conventional imaging studies in the staging and restaging as well as in the evaluation of treatment response in lymphomas. Recently, the accuracy of FDG-PET imaging has significantly improved with the introduction of combined modality PET-CT fusion technology. The main advantage of PET-CT fusion imaging is the ability to correlate two contemporaneous imaging modalities for a comprehensive examination that combines anatomic data with metabolic information in the same imaging session.

This chapter summarizes the data on the usefulness of various functional imaging techniques with a special emphasis on FDG-PET imaging at staging, restaging, and monitoring response to therapy.

16.2 Classification and Staging

The proper staging and management of lymphomas depend on an accurate pathological diagnosis, classification and determination of extent of disease. Most malignancies arise as localized disease within the tissue of origin; in contrast, lymphoma is regarded as a systemic disease due to the widespread distribution of the lymphoid tissues and tendency of lymphoid cells to migrate. Thus, the TNM staging system, which requires the knowledge of the exact origin of the malignancy, cannot be used in lymphomas. The established classification system, the Revised European-American Classification of Lymphoid Neoplasms (REAL) (National Cancer Institute 1982), and the subsequently adopted and updated World Health Organization (WHO) (Jaffe et al. 1999) classification integrate the cytogenetic, molecular, and immunologic information. This integrated system – WHO/REAL classification – is currently in routine clinical use for both HD and NHL (Table 16.1) (Harris et al. 2000).

The Ann Arbor staging system originally developed for HD disease was adapted also for staging of NHLs (Lister et al. 1989; Rosenberg 1977). This staging system focuses on the number of involved sites, disease location, and the presence or absence of systemic symptoms. There are basically four stages of lymphomas as demonstrated in Table 16.1.

Table 16.1. REAL/WHO classification system

Hodgkin's lymphoma	Non-Hodgkin's lymphoma
Classic	**Indolent**
Nodular sclerosis (NS)	B-cell CLL/small lymphocytic lymphoma
Mixed cellularity (MC)	Marginal zone lymphoma
Lymphocyte-rich (LR)	MALT
Lymphocyte-depleted (LD)	Splenic marginal zone lymphoma
	Nodal marginal zone lymphoma
Nodular lymphocyte-predominant (NLP)	Lymphoplasmacytoid lymphoma/immunocytoma
	Follicle center lymphoma, follicular type
	Aggressive
	Diffuse, large cell lymphoma
	Mediastinal large cell lymphoma
	Primary effusion lymphoma
	Mantle cell lymphoma[b]
	Burkitt's lymphoma/high-grade Burkitt's-like
	Precursor B-cell leukemia/lymphoma

CLL chronic lymphocytic leukemia, *MALT* mucosa-associated lymphoid tissue, *hpf* high-powered field

[a] Among all B-cell NHL in adult Americans

[b] Subtype may exhibit either indolent or aggressive clinical behavior

International Prognostic Index (IPI) and Score (IPS). The Ann Arbor staging system is not highly accurate in identifying prognostic subgroups which usually determines the therapy strategy (The Non-Hodgkin's Lymphoma Classification Project 1997). Consequently, a pretreatment predictive model, International Prognostic Index (IPI) was developed for patients with aggressive NHL (The International Non-Hodgkin's Lymphoma Prognostic Factors Project 1993) to provide useful information for determination of proper therapy for subgroups based on risk profile. Using the IPI, there are five adverse risk factors: age > 60 years, tumor stage III or IV, the number of extranodal sites > 1, performance status 2, and serum lactate dehydrogenase level > 1 × normal. Subsequently, for advanced HD, the International Prognostic Score (IPS) was described based on the number of adverse prognostic factors present at diagnosis (Hasenclever and Diehl 1998). In the IPS, seven factors are considered for adverse prognostic effects: a serum albumin level < 4 g/dl, a hemoglobin level < 10.5 g/dl, male sex, age ≥ 45 years, stage IV disease by Ann Arbor classification, leukocytosis (a white-cell count ≥ 15,000/mm^3), and lymphocytopenia (a lymphocyte count < 600/mm^3, a count < 8% of the white-cell count, or both).

16.3 Clinically Relevant Issues About Lymphomas

The lymphomas are traditionally divided into two broad categories, HD and NHLs, based on the therapeutic and management implications. NHL accounts for more than 85% of the lymphomas. NHL is a heterogenous group of lymphoproliferative malignancies with varying patterns of behavior from indolent to rapidly fatal (Armitage 1993). In clinical practice, the NHLs are classified into low-grade (indolent) and aggressive subtypes. Aggressive lymphomas constitute approximately 60% of NHL series (http://www.cancer.gov/cancertopics/types/non-hodgkins-lymphoma) while indolent lymphomas account for approximately 40% of new diagnoses. HD accounts for 10–15% of lymphomas and is composed of two different entities, classical HD representing 95% of cases and nodular lymphocyte-predominant HD making up 5% of cases. Classical HD is further subdivided into nodular sclerosis (most common), mixed cellularity, lymphocyte rich and lymphocyte depletion types. Patients with nodular lymphocyte-predominant HD usually present with isolated peripheral lymph node involvement. These patients have a clinical course resembling NHL with an indolent growth pattern, which thus is considered to have a different biology than classical HD.

Unlike HD, NHL is much less predictable and has a far greater predilection to have a disseminated pattern. Only 10% of patients with low grade follicular NHL have localized disease at diagnosis (Anderson et al. 1982) and the majority of patients with aggressive lymphomas have advanced-stage disease.

In both HD and NHL, prognosis and treatment depend on histological type and grade as well as disease stage. For patients with non-bulky early-stage classical HD (favorable prognosis), radiation therapy alone has been the primary treatment. However, the late effects of radiation therapy consisting of occurrence of solid tumors and cardiovascular disease render this therapy modality a less attractive option for patients with favorable prognosis. The use of combination therapy with non-alkylating agents and involved field radiotherapy (IF RT) has proven more effective to reduce the relapse rate compared to the use of radiotherapy alone (Tubiana et al. 1989). For patients with bulky stage I–II disease, treatment usually consists of a full course of chemotherapy followed by IF RT. Patients with advanced stage disease are treated with full-course chemotherapy, with the consideration of delivering IF RT to bulky disease sites.

Accurate staging is particularly important in initial staging to determine extent of disease to modify therapy protocols. With polychemotherapy the cure rate for HD is greater than 80 % of patients with first line therapy. The detection of additional disease sites would have a significant impact on management of both aggressive NHL and classical HD patients in whom a stage migration occurs from apparently early stage to advanced stage. In these patients, number of chemotherapy cycles can be modified and/or combined modality therapy can be initiated in addition to or in lieu of radiotherapy alone. Furthermore, detection of unknown disease sites and better definition of metabolically active tumor volume could alter radiotherapy fields and gross tumor volume alike. Nonetheless, this is an evolving area and FDG-PET based changes in therapy planning require further evaluation. The lymphocyte-predominant HD has a relatively indolent course and radiation therapy alone can be an option for these patients (Diehl et al. 1999); thus, imaging findings are less conducive to a dramatic change in management in this subtype of HD. It is generally accepted that there is little therapeutic benefit in distinguishing between stage III and stage IV disease, since the treatment options are nearly identical.

Evaluation of therapy response is equally important in both HD and NHL to determine whether fewer cycles of chemotherapy can be administered in rapidly responding patients to avoid unnecessary therapy and morbidity. Moreover, imaging can determine whether or not radiation therapy is indicated for an individual lymphoma patient. This is essential as unnecessary use of radiation may lead to development of untoward effects such as cardiac disease, pulmonary fibrosis and secondary malignancies while appropriate use could potentially decrease the risk of recurrence and allow for administration of fewer chemotherapy cycles (Ng et al. 2002) than the conventional 6 cycles.

16.4 Imaging in Lymphomas

The traditional imaging modality of choice for the diagnosis and staging of lymphoma is CT, which may be accompanied by sonography or endoscopy in some selected cases. MRI is a competitive technique which can provide images of the abdomen of somewhat comparable diagnostic quality using faster acquisition sequences. Additionally, MRI offers advantages including better tissue discrimination, lack of ionizing radiation and use of contrast agents with less risk of systemic effects (Hoane et al. 1994; Jung et al. 2000; Ferrucci 1998). Nevertheless, the diagnostic accuracy of both CT and MRI depends on lymph node enlargement and multiplicity; thus, false negative results are obtained in normal size lymph nodes that harbor lymphoma. Alternatively, in lymph nodes that are enlarged due to reactive changes they can give rise to false positive findings.

16.4.1 Differences Between HD and NHL on Imaging

An important feature of HD is its tendency to spread in an orderly fashion to contiguous areas of lymph nodes. The disease involves the chest in more than 70 % of patients. Superior mediastinal lymph nodes are involved in more than 90 % of patients. Extranodal disease is rare. Isolated lung involvement does not usually occur in the absence of mediastinal disease. Pulmonary and chest wall involvement is often the result of direct extension of disease from neighboring lymph nodes. Bulky disease is usually accompanied by pleural effusion. In the abdomen, HD is mostly confined to the upper abdomen and retroperitoneal lymph nodes. When the spleen is enlarged in HD, the risk of liver involvement may be as high as 30 %.

NHL shows a non-contiguous and widespread pattern at initial staging. Extranodal involvement of the liver, bone marrow and gastrointestinal tract is common. In the abdomen, disease can be at any lymph node station including mesenteric LNs. In infradiaphragmatic disease, the lymph nodes are almost always enlarged unlike HD, which can present with sub-centimeter lymph nodes harboring active disease. Lymphoma of the retropharyngeal lymphoid tissue and tonsils (i.e., Waldeyer's ring) is usually accompanied by cervical lymph node involvement. The salivary gland involvement is the result of systemic disease. In indolent NHL, hilar and mediastinal lymph nodes are often involved but large mediastinal masses are rare. Hepatomegaly in NHL tends to suggest lymphomatous involvement more than in HD.

16.5 Gallium-67 Scintigraphy

Gallium-67 is a ferric ion (Fe^{3+}) analogue with a 78-h half-life, and photopeaks of 93 (37 %), 185 (20 %), 300 (17 %), and 394 (5 %) keV. For tumor imaging, a dose of 10 mCi of Ga-67 citrate is recommended. Once injected, it binds to iron-binding plasma proteins, including transferrin and lactoferrin. The Ga-67 accumulation in tumors is mediated by various factors associated with tumor composition and physiology. Tumor-associated transferrin receptors (CD-71), anaerobic tumor metabolism leading to the dissociation of Ga-transferrin complex in low-pH conditions, increased tumor perfusion and vascular permeability (Larson et al. 1980; Vallabhajosula et al. 1983; Nejmeddine et al. 1998). A positive correlation between the density of transferrin re-

Table 16.2. Ann Arbor staging system of lymphomas

Stage I Involvement of a single lymph node region **or** involvement of a single extralymphatic organ
Stage II Involvement of two or more lymph node regions on the same side of the diaphragm **or** localized involvement of an extralymphatic organ or site plus an involved lymph node region on the same side of the diaphragm
Stage III Involvement of lymph nodes involved on **both sides of the diaphragm** can be accompanied by extralymphatic organ involvement including the spleen
Stage IV Diffuse or disseminated involvement of one or more extralymphatic organs with or without associated lymph node involvement

The presence or absence of the following symptoms should be noted with each stage designation: A = asymptomatic; B = fever, sweats, or weight loss greater than 10% of body weight; bulky disease (X) (tumor larger than 10 cm) portends worse prognosis for each stage of HD; "E" denotes extranodal disease contiguous or proximal to the known nodal site

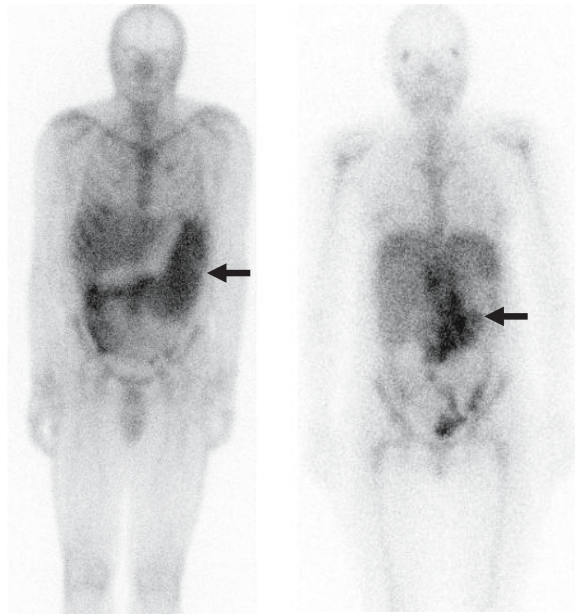

Fig. 16.1. Sixty-year-old male recently diagnosed with follicular low grade non-Hodgkin's lymphoma underwent a pre-therapy Ga-67 imaging study. Anterior planar image (*left panel*) reveals diffusely increased Ga-67 uptake in an enlarged spleen, which may represent splenic involvement by lymphoma. Otherwise, there is no evidence of nodal lymphoma elsewhere in the body although the patient had involvement of supra- and infradiaphragmatic lymph nodes on both CT and FDG-PET studies (not shown). Twenty-two-year-old female with abdominal Hodgkin's disease: The anterior Ga-7 planar image (*right panel*) demonstrates increased radiotracer uptake in the paraaortic and iliac lymph nodes, consistent with active lymphoma. Note the physiologic bowel uptake in both patients

ceptors and the Ga-67 uptake as well as a negative correlation between Ga-67 uptake by the anti-transferrin receptor antibodies has been considered accountable for Ga-67 accumulation for all lymphoid cell lines, indicating that the mechanism of Ga-67 uptake is highly dependent on transferrin receptors (Nejmeddine et al. 1998).

SPECT is an integral part of Ga-67 scintigraphy providing higher sensitivity by diminishing false negative results (Kostakoglu et al. 1992; Front et al. 1990) (Table 16.2). The recently introduced dual-modality imaging systems that combine SPECT and CT into one session have a potential to increase accuracy, particularly by decreasing false positive findings and thus improving specificity.

16.5.1 Clinical Applications

Gallium-67 imaging has long been an established diagnostic means in the evaluation of response to therapy in aggressive NHL and HD. Its use at initial diagnosis is not necessary for evaluation of extent of disease; however, a baseline study is required to subsequently assess response to therapy.

The sensitivity of Ga-67 scintigraphy exceeds 85% in aggressive NHL both in intermediate and high grade lymphomas (~95%), as well as in HD (~95%) (Front et al. 1990; Mansberg et al. 1999; Johnston et al. 1974). Among aggressive lymphomas, Ga-67 has been reported to be more sensitive in histiocytic NHL (~70%) than in lymphocytic NHL (~50%) (Johnston et al. 1974). In low grade lymphoma, however, Ga-67 is not always a reliable imaging modality, particularly in the small lymphocytic subtype and mucosa-associated lymphoid tissue lymphoma (MALT) (Cabanillas et al. 1977; Setoin et al. 1997) (Fig. 16.1). Using more recent large field dual head cameras, the sensitivity of Ga-67 scintigraphy was found to be higher in low-grade lymphomas, particularly in follicular subtype, predominantly follicular, small cleaved cell, and follicular, mixed small cleaved and large cell (84% and 91%, respectively). Nonetheless, the site sensitivity was still below 70% (Ben-Haim et al. 1996). One issue that warrants emphasis is that Ga-67 avid lesions in a patient with known indolent lymphoma may indicate transformation to high-grade lymphoma. Tl-201, Tc-99m sestamibi and In-111 octreotite have been used to detect low-grade NHL with a higher sensitivity. The role of these radiotracers will be discussed in the relevant sections.

16.5.2 Initial Staging

The overall sensitivity for Ga-67 imaging is between 75% and 90% in NHL and higher in HD at 85–95% (Mclaughlin and Southee 1994; Bar-Shalom et al. 2001). Considering its limitations in the abdomen, Ga-67 imaging is more sensitive in the neck and mediastinum than in the abdomen and retroperitoneal regions. Conceivably, due to physiologic bowel excretion of Ga-67, the sensitivity in the infradiaphragmatic disease can be as low as 60% (Devizzi et al. 1997; Turner et al. 1978; Bartold et al. 1997). In a comparative study, the accuracy for ultrasonography and Ga-67 scintigraphy in the identification of intra-abdominal lymphoma was 87.5% and 82%, respectively (Brascho et al. 1980). Although Ga-67 with SPECT has proven to have a high sensitivity in the mediastinum, in a comparative study, Ga-67 scintigraphy was found to be less sensitive than CT and MRI (90% vs. >95%, respectively) (Devizzi et al. 1997). In the neck, Ga-67 scintigraphy has an intermediate sensitivity at approximately 80% (32). Although the neck is one of the superficial compartments of the body, characteristic to lymphoma, the involved lymph nodes tend to be smaller in size, often below the resolution of gamma camera (<1.0–1.5 cm).

16.5.3 Extranodal Lymphoma

For the detection of extranodal lymphoma, MR imaging is the imaging modality of choice to assess involvement in the brain, spinal cord and bone marrow; while CT allows excellent evaluation of lung disease. Common major problems still remain with residual tumor masses after therapy.

The overall Ga-67 scan sensitivity in extranodal lymphoma is 70–83%. However, the sensitivity for lymphoma of the skin, intestine and testis is reportedly low (0–25%) (Hsu et al. 2002). In a study of 92 patients with extranodal lymphoma, the Ga-67 imaging results changed staging or treatment in 8% of patients. Similar to nodal lymphoma, the sensitivity is lower in low-grade than in aggressive NHL and in lesions measuring less than 2 cm (Nishiyama et al. 2003).

MALT is by far the most common extranodal primary NHL. Low-grade gastric MALT lymphoma can be cured by eradication of *Helicobacter pylori;* but radiotherapy and/or chemotherapy and/or surgery are the effective methods of treatment for high-grade gastric MALT lymphoma. The Ga-67 citrate scan was found to be valuable for the differentiation of the two subgroups of gastric MALT. In the low-grade group, 75% of patients had negative results while in the high grade group, all patients had positive results (Hsu et al. 2002; Hussain et al. 1998).

Ga-67 findings in patients with hepatic or splenic lymphoma vary between focally increased uptake and grossly non-uniform hepatic uptake (Ben-Haim et al. 1996) (Fig. 16.2). Hepatomegaly or splenomegaly alone is nonspecific as only 15% of patients with hepatomegaly are reported to have hepatic involvement (Zornoza and Ginaldi 1981). The sensitivity and specificity of Ga-67 scintigraphy in bone lymphoma are reportedly high at 93% and 91%, respectively (Israel et al. 2002b).

With the advent of the SPECT and CT fusion technology, precise anatomic localization of lesions and differentiation of physiologic from abnormal uptake, particularly in the subdiaphragmatic area, has become less challenging (Fig. 16.3). In one series, SPECT/CT provided additional anatomical information over SPECT alone by better characterizing lesions in 54% of patients, thus leading to reconsideration of the therapeutic approach in 33% of subjects (Palumbo et al. 2005).

Briefly, at initial staging of lymphoma, as a single imaging technique, Ga-67 scintigraphy cannot substitute for CT or MR due to its limited spatial resolution. Furthermore with the establishment of FDG-PET imaging in the staging of lymphoma, its role has been significantly diminished in the realm of lymphoma imaging.

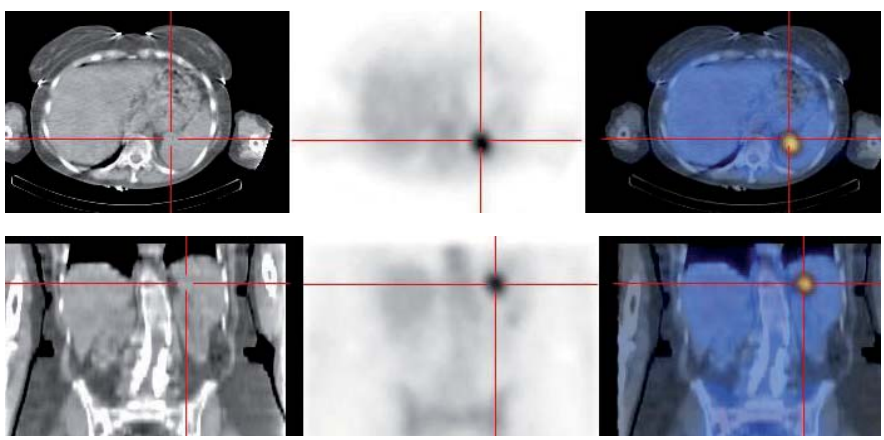

Fig. 16.2. Patient with a diagnosis of diffuse large cell lymphoma underwent pretherapy Ga-67 SPECT/CT imaging, to evaluate for the extent of disease. Axial (*top panel*) and coronal (*lower panel*) images of low dose CT (*left*), Ga-67 (*middle*) and SPECT-CT fusion (*right*) images demonstrate a discrete area of intensely increased Ga-67 uptake in a mass corresponding to the spleen, consistent with active lymphoma

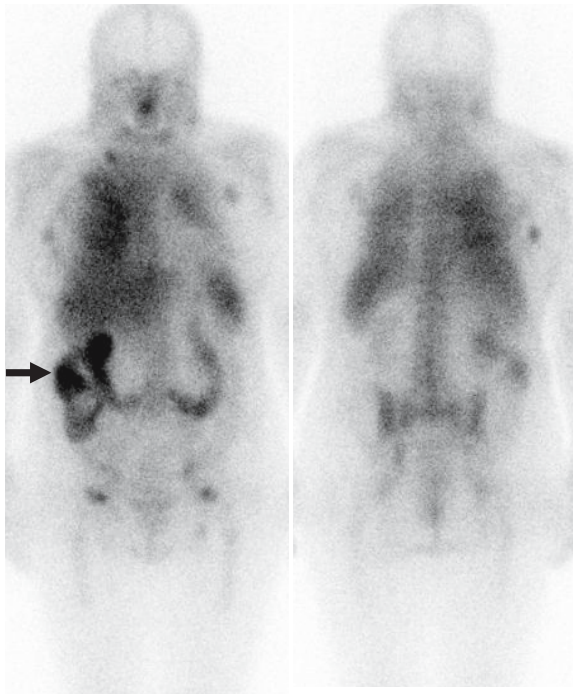

Fig. 16.3. Sixty-five-year-old patient with a history of thoracic and abdominal non-Hodgkin's lymphoma, stage III, underwent Ga-67 scintigraphy, following four cycles of therapy referred for restaging. Anterior and posterior whole body Ga-67 images demonstrate asymmetrical and heterogeneously increased pulmonary uptake, consistent with *Pneumocystis carinii* infection. This finding has resolved over time on antiobiotic therapy (not shown). Additionally, there is intense radiotracer uptake in the hepatic flexure (*arrow*). On delay images at 72 h the uptake in this location was persistent, although it has decreased in intensity (not shown). This finding was consistent with physiologic bowel uptake rather than a malignant process based on patient's clinical presentation. The foci of uptake in the right supraclavicular, bilateral axillary and inguinal regions are consistent with residual lymphoma

16.5.4 Post-Therapy Evaluation

As a consequence of its ability to differentiate between residual viable tumor and therapy induced fibrotic changes, Ga-67 has been widely accepted as an effective imaging modality in the identification of residual disease and investigation of response to therapy.

Ga-67 uptake is a sign of residual tumor activity after therapy. Ga-67 scintigraphy has shown high predictive value in differentiating between patients with a favorable and those with an unfavorable prognosis, the outcome being more favorable in patients with a negative scan and varying according to the number of chemotherapy cycles required before a negative scan is obtained.

Ga-67 scintigraphy operates at a reasonably high sensitivity and a specificity (both at 75–95%) in the differentiation of residual viable disease from post-therapy sterile masses (Fig. 16.4). Both the sensitivity and specificity of Ga-67 imaging to identify recurrent lymphoma during follow-up is approximately 90% although some series reported sensitivities as high as 95% (Bar-Shalom et al. 2001; Front et al. 1997; Rehm 2001). In a large series, the pretreatment agreement between CT and Ga-67 SPECT ranged from 75% to 100%. A greater variation in agreement was observed once chemotherapy was started, the sites with the least agreement being in the mediastinum. When the CT scan showed persistent abnormality even after Ga-67 SPECT turned negative after chemotherapy, the chances of mediastinal recurrence or progression occurred only in 15% of patients (Ha et al. 2000). Due to spatial resolution limits of gamma cameras, minimal detectable lesion is at best 1.0–1.5 cm depending on the Ga-67 avidity of the lesion. Thus, some patients with negative Ga-67 imaging during follow-up or after therapy can still have disease recurrence despite a negative post-therapy Ga-67 scan.

In a retrospective study, at restaging, Ga-67 SPECT and CT correctly identified active disease sites in 96% and 68%, respectively, in patients with biopsy proven recurrent HD. When CT was equivocal, Ga-67 SPECT identified recurrent disease in 87.5% of patients (Kostakoglu et al. 1992). Similarly, Ga-67-SPECT proved superior to spiral CT for identifying residual nodal disease with a sensitivity of 94% vs. 83% and a specificity of 100% vs. 92.5% in HD and aggressive NHL (Stroszczynski et al. 1997).

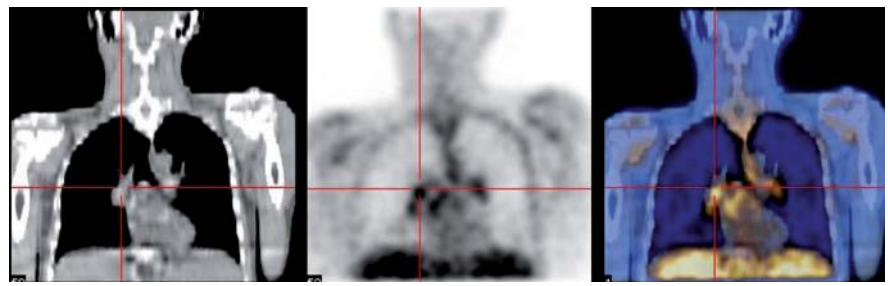

Fig. 16.4. Patient with a history of stage II mediastinal non-Hodgkin's lymphoma underwent Ga-67 scintigraphy after completion of first line therapy. The coronal chest images, CT (*left*), Ga-67 (*middle*), and fusion (*right*), demonstrate that there is intense accumulation of the radiotracer in the bilateral hilar and subcarinal regions, consistent with residual viable lymphoma. The patient subsequently progressed and required second line therapy

The non-specific hilar Ga-67 uptake following therapy is a well-recognized phenomenon which can be seen in many as 80 % of patients (Front et al. 1992). When the hila demonstrate symmetric and low grade Ga-67 uptake, this finding is deemed to be of benign etiology with a negative predictive value of ≥ 95 %. By the same token, asymmetrically increased Ga-67 uptake is a hallmark of recurrent disease with a positive predictive value of ≥ 85 % (Nikpoor et al. 2000; Gunay et al. 2004).

16.5.5 Evaluation of Response to Therapy

Sequential Ga-67 scanning can be performed before, during, or after therapy to determine whether or not a response-based management change is warranted. Following induction therapy, persistent Ga-67 uptake is a poor prognostic factor in HD and NHL, and it is an accurate predictor of both response to therapy and the overall outcome (Table 16.3) (Fig. 16.5). Several investigators reported that early restaging Ga-67 scans are more predictive of failure-free survival than final restaging Ga-67 scans. The patients who need more cycles of therapy to become Ga-67 negative are found to be more prone to develop recurrent disease (Janicek et al. 1997). A positive Ga-67 scintigraphy during chemotherapy course as an indicator of treatment failure and poor outcome suggests consideration of different therapy options. A positive Ga-67 study after completion of therapy should raise concern, even in the absence of other supporting clinical evidence. In both aggressive NHL and HD, Ga-67 imaging is a good predictor of outcome after one cycle of chemotherapy (Front et al. 1999; Front et al. 2000). In HD, failure-free survival differed significantly between patients with positive and patients with negative Ga-67 imaging after one cycle of chemotherapy but not at midtreatment. In marked contrast, failure-free survival was not significantly different between patients with positive and patients with negative CT scans at midtreatment. In patients with negative Ga-67 imaging, 92 % after one cycle and 82 % at midtreatment remained in complete remission. Among patients with positive Ga-67 studies after one cycle, 57 % relapsed (Front et al. 1999). In aggressive NHL, Ga-67 findings after one cycle of chemotherapy and at midtreatment were predictive of outcome in patients with aggressive NHL. There was no significant difference in failure-free survival between patients with positive and negative CT findings during treatment (Front et al. 2000). Thus, early Ga-67 imaging during the course of chemotherapy identifies patients who may benefit from more aggressive treatment.

In a more recent study, in aggressive NHL patients, 5-year failure free survival (FFS) was predicted by Ga-67 SPECT after one cycle of chemotherapy and at midtreatment. Positive Ga-67 scintigraphy after the first cycle and at mid-treatment predicted a therapy failure in 64 % and 77 % of patients, respectively. Furthermore, Ga-67 scintigraphy was a better predictor than the conventionally established prognostic score, IPI, for both overall response and failure-free survival (Israel et al. 2002a). Similarly, in a study of HD patients, at midtreatment, freedom-from-progression rate was 86 % and 19 % for patients with negative and positive Ga-67

Table 16.3. Gallium-67 scintigraphy in the evaluation of therapy response and residual disease

Authors	Patient no.	Entity	Chemo cycles	PPV (%)	NPV (%)
Front	31	HD	1 cycle	57	92
Front	51	NHL	1 cycle	71	81
			3 cycles	74	63
Israel	139	NHL	1 cycle	64	83
			3 cycles	77	66
Janicek	30	NHL	2 cycles	82	94
Ionescu	53	HD	3 – 4 cycles	81	86
Salloum	101	HD	Completion	[b]	83.5
Front	43	HD	Completion	80	84
	56	aNHL	Completion	73	84
Bogart	60	HD	Completion	[c]	78
Vose	66	aNHL	Completion[a]	75	47
	77	LGL	Completion[a]	76	45

PPV positive predictive value, *NPV* negative predictive value, *NHL* non-Hodgkin's lymphoma including low-grade lymphoma, *HD* Hodgkin's disease, *LGL* low-grade lymphoma, *aNHL* aggressive NHL

[a] Patients were evaluated after high-dose chemotherapy and bone marrow transplant

[b] Inadequate number of patients to determine PPV

[c] PPV not given but there was no difference in overall survivals between Ga positive or negative patients

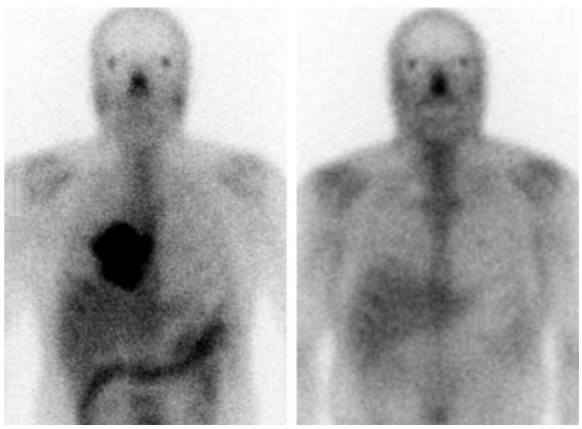

Fig. 16.5. Patient with a history of thoracic non-Hodgkin's lymphoma underwent Ga-67 scintigraphy prior to and after completion of induction therapy. The pre-therapy anterior Ga-67 image (*left*) reveals that there is intensely increased Ga-67 uptake in the anterior mediastinum consistent with active lymphoma. The post-therapy anterior Ga-67 image (*right*) demonstrates that there is complete resolution of disease in the mediastinum. The patient has been progression free for more than 48 months

scans, respectively. The 5-year overall survival rate differed significantly between Ga-67 negative (91 %) and positive (25 %) groups (Ionescu et al. 2000). Hence, positive Ga-67 early during treatment may be used as an independent test in selecting chemosensitive patients from those with chemoresistance for early therapeutic modifications. This is particularly important in high risk patients with HD, for whom the management plan includes combination chemotherapy with radiotherapy. In these patients, the role of imaging is crucial to optimize the subsequent radiotherapy planning.

The negative predictive value of Ga-67 imaging may vary greatly among patients with different pretreatment risk categories. Approximately 15 % of patients with mediastinal HD relapse at the original disease site despite a negative post-therapy Ga-67 study (54). Based on the pretreatment risk categories, negative predictive value of a post-therapy Ga-67 scintigraphy equals 95 % in early stage lymphoma while the corresponding value can be lower than 70 % for advanced stage disease (Gasparini et al. 1993; Bogart et al. 1998; Salloum et al. 1997).

Ga-67 SPECT imaging obtained after high-dose chemotherapy and autologous stem-cell transplantation may be useful for the evaluation of disease activity and to predict the eventual outcome. In one study, the 1-year failure free survival for patients with a positive post-therapy Ga-67 scintigraphy was 15 % compared with a 3-year failure free survival of 47 % for those with a negative scan. The corresponding values for CT scan were not significantly different (36 % vs. 39 %) (Vose et al. 1996).

In summary, a positive gallium scan is highly predictive of failure and poor outcome, and treatment should thus be modified; however, relapse may occur in patients with a negative gallium scan.

16.5.6 Conclusions

Gallium-67 scintigraphy remains a useful modality in the absence of FDG/PET imaging. Nevertheless, Ga-67 imaging lacks sensitivity in small size disease, abdominal lymphoma and in low-grade lymphoma. Ga-67 scintigraphy has important post-therapy implications. A positive post-therapy Ga-67 scintigraphy is consistently associated with poor prognosis while a negative result suggests a favorable prognosis. False negative results, however, may arise due to resolution limits.

16.6 Thallium-201 and Tc-99m Sestamibi Imaging in Lymphoma

Thallium-201 is mainly a myocardial perfusion agent; however, its oncologic applications have been well recognized in the assessment of tumor detection and viability (Waxman 1991; Iskandrian et al. 1987; Abdel-Dayem 1997). The Tl-201 uptake in tumor cells is regulated through blood flow, the sodium-potassium adenosinetriphosphatase system (Na-K-ATPase), co-transport system, calcium ion channel mechanisms, and increased cell membrane permeability. Because of the similarities between Tl-201 and potassium, tumor cells with high Na-K-ATPase activity can accumulate Tl-201 and potassium ions into high concentration. Cytotoxic therapy affects the activity of Na-K-ATPase on tumor cells, thus decreasing the uptake of Tl-201 (Waxman et al. 1996; Lin et al. 1995; Elgazzar et al. 1993; Dadparvar et al. 2002).

Tc-99m sestamibi (MIBI) is a lipophilic cationic metallopharmaceutical that accumulates within the mitochondria through electrical potentials of the membrane bilayers. MIBI accumulates preferentially in malignant cells due to a higher transmembrane electric potential owing to a higher metabolic rate in malignant cells. The ability of cancer cells to become simultaneously resistant to different drugs, a phenomenon known as multidrug resistance (MDR), remains a significant impediment to successful chemotherapy. The retention of MIBI within the cell is also related to transmembrane transporter proteins including the P-glycoprotein pump system (Pgp) and the multidrug resistance protein (MRP) (Piwnica-Worms et al. 1995; DelVecchio et al. 1997; Kostakoglu et al. 1997). Consequently, the wash-out of MIBI from cells has been utilized to evaluate multi-drug resistance MDR phenotype of malignant tumors and to predict response to chemotherapy (Kao et al. 2001; Fonti et al. 2004).

The optimal post-injection time interval for both Tl-201 and MIBI for tumor imaging is 20 – 60 min. Delayed images at 3 – 4 h are recommended to obtain images with high tumor-to-background ratios. A SPECT study should be acquired to better define anatomic site/s in relation to disease involvement. The specificity of SPECT studies has been improved greatly using integrated SPECT-CT systems for more accurate anatomic definition and potentially for better patient management.

16.6.1 Clinical Applications

Imaging with Tl-201 chloride and MIBI has shown promise in imaging low grade lymphomas demonstrating significantly greater tumor avidity compared to Ga-

67 imaging. In patients with low grade lymphoma, the patient and site sensitivity for Ga-67 imaging are only 56 % and 32 %, respectively (Waxman et al. 1996). Conversely, the sensitivity of Tl-201 was 100 %, for both patients and sites in the same patient population. Interestingly, within lymphoma subgroups, Tl-201 was found to be more avid for low-grade NHL than for aggressive NHL or HD. There are also reported results supporting the combined use of Tl-201 and Ga-67 scintigraphy to increase overall patient sensitivity (Mansberg et al. 1999; Waxman et al. 1996; Roach et al. 1998). In one study, the use of both agents increased the overall patient sensitivity from 67 % (for Ga-67 only) to 82 % and improved the overall site detection by approximately 40 %. Notably, Tl-201 scintigraphy is not dependable in the evaluation of abdominal disease due to the gastrointestinal excretion of the radiotracer.

Tl-201 SPECT has also been used in the differentiation of CNS lymphoma from infectious processes. Unlike Ga-67, Tl-201 rarely accumulates in inflammatory or infectious sites (Skiest et al. 2000) (Fig. 16.6). In 56 HIV-infected patients with focal CNS lesion/s on anatomic imaging, patients with CNS lymphoma had significantly higher lesion/contralateral scalp ratios compared to patients without lymphoma (1.03 vs. 0.67) (Skiest et al. 2000; Iranzo et al. 1999). Based on ROC analysis a cut-off of 0.90 for the lesion/scalp uptake ratios yielded a sensitivity and specificity of 86 % and 83 %, respectively, for the diagnosis of CNS lymphoma (71). By combining Tl-201 SPECT with serum toxoplasma IgG, diagnostic accuracy can be improved.

Several studies report the usefulness of MIBI scintigraphy in the prediction of chemotherapy response in untreated adult lymphomas exploiting the characteristics of MIBI as a transport substrate for the Pgp and MRP related drug resistance mechanisms (Kao et al. 2001; Liang et al. 2002; Ohta et al. 2001; Lazarowski et al. 2006; Song et al. 2003). The patients with faster MIBI efflux (wash-out) and those with negative or decreased MIBI activity tend to have unfavorable response to chemotherapy compared to those with sufficient MIBI accumulation irrespective of the lymphoma type. These findings are consistent with the proven inverse relationship between the Pgp levels and the magnitude of MIBI uptake and the rate of washout from the tumor cells. The results of one lymphoma series showed a stronger relationship between MIBI uptake and chemosensitivity in low grade NHL than high grade NHL and HD (Lazarowski et al. 2006). Additionally, the percent retention of MIBI showed a significant negative correlation with the IPI score in patients with NHL (Song et al. 2003). Based on these results one can conclude that the slow tumor clearance of MIBI can differentiate responding and nonresponding tumors. Nonetheless, there are considerable discrepancies among various data which could be attributed to the presence of subsets of cells with varying degrees of Pgp expression and co-existence of multiple drug resistance mechanisms or poor penetration of MIBI due to reduced blood flow in necrotic tumors.

16.6.2 Conclusions

Currently the strength of Tl-201 imaging lies in its ability to differentiate CNS lymphoma from toxoplasmosis in immunocompromised patients. Although superior to Ga-67 scintigraphy, Tl-201 still lacks high sensitivity in low-grade lymphomas. Because of its close association with multidrug resistance, MIBI scintigraphy can provide information in the prediction of chemotherapy response and could guide the design of the therapy protocols. Nevertheless, evaluation of multidrug resistance poses a challenge because of the multifaceted problems that stem from non-specificity of MIBI imaging, tumor heterogeneity, co-existence of various resistance mechanisms, and in clinical practice lack of effective reversal agents.

16.7 In-111 Octreotide Imaging in Lymphoma

Indium-111 pentetreotide (In-111 DTPA-D-Phe) scintigraphy is useful in diagnosing and following tumors with increased expression of somatostatin receptors (predominantly somatostatin receptor subtypes 2 and 5) (Weiner and Thakur 2005). Somatostatin receptor imaging (SRI) with this octapeptide can be performed in both neuroendocrine and some non-neuroendrocrine tumors. The presence of cellular somatostatin receptors, particularly of subtype 2, has been reported in lymphomas (Ferone et al. 2005; Leners et al. 1996; Van Hagen et al. 1993).

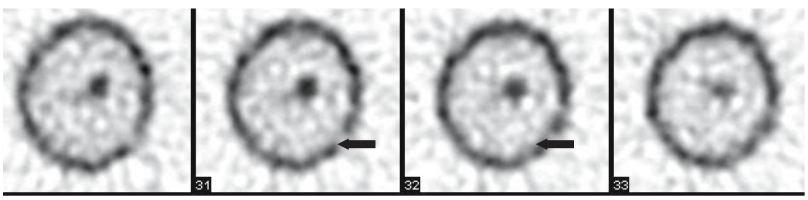

Fig. 16.6. Patient with HIV positive serology diagnosed with a brain lesion on a CT scan, referred for Tl-201 imaging to differentiate between toxoplasmosis and CNS lymphoma. The Tl-201 SPECT axial images reveal a focus of increased uptake in the left parietal cortex (*arrow*) corresponding to the lesion seen on the CT scan, consistent with CNS lymphoma. The patient was subsequently treated with chemotherapy for lymphoma and responded favorably

16.7.1 Clinical Applications

The sensitivity of somatostatin receptor scintigraphy in the diagnosis of somatostatin neuroendocrine tumors can exceed 90%, but due to the variable expression of specific receptor subtypes in lymphomas the sensitivity of this imaging method is hampered. The sensitivity of In-111-octreotide for detecting HD is 70–95% and varies between 98% for supradiaphragmatic lesions and 67% for infradiaphragmatic lesions (Lipp et al. 1995; Lugtenburg et al. 2001). The sensitivity for NHL, however, is determined to be significantly lower at 35–80% (Ferone et al. 2005; Leners et al. 1996; Van Hagen et al. 1993). This is mainly ascribed to the low receptor density present on B lymphocytes compared to neuroendocrine cells; ligand-induced internalization and differential receptor regulation may also participate in this phenomenon. Notably, the sensitivity of SRI scintigraphy in low grade NHL is relatively high and can vary from 62% for supradiaphragmatic lesions to 44% for infradiaphragmatic lesions (Leners et al. 1996).

With the currently available somatostatin analogs, SRI does not offer a sufficiently sensitive means to impact patient management. SRI may be necessary, however, in those patients who would undergo radionuclide-labeled SS analog-based therapy, although these therapy modalities are of research curiosity rather than in routine use. In a recent study, a selective expression of sst_2 and sst_3 receptors was demonstrated in lymphomas; however, the magnitude of expression was relatively low. Although these findings do not appear to be promising, further investigation may demonstrate that even with a low receptor density high response rates can be obtained in these highly radiosensitive tumors (Dalm et al. 2004; Reubi et al. 2005). SRI can also be used to select the proper patient subgroup in those patients with paraneoplastic syndromes, who could subsequently be treated with somatostatin analogs.

16.7.2 Conclusions

SRI is not used as a routine test as part of the initial staging of lymphoma, while it is better suited to characterize somatostatin receptor expressing lymphomas than to identify the extent of disease. Thus, it may be useful to determine the proper patient subpopulation that would benefit from therapy with radiolabeled somatostatin receptor analogues. Currently several new ligands and neuropeptide receptors are under investigation to overcome the limitations associated with current SRI applications and multireceptor targeting of tumors.

16.8 FDG-PET in Imaging Lymphoma

16.8.1 Indolent Vs. Aggressive Lymphomas

FDG-PET imaging has an established role in the evaluation of aggressive NHL and HD with extensive supporting evidence. Increased use of glucose through glycolysis is characteristic for lymphomas although glucose utilization may vary among various subtypes (Table 16.4). In HD, FDG uptake is usually lower in nodular lymphocyte predominance subtype compared to nodular sclerosis and mixed cellularity subtypes (mean SUVmax: 8 vs. 11 and 15, respectively) (Hutchings et al. 2006b). The intensity of tumor FDG uptake may also help in differentiating between indolent and aggressive entities (Figs. 16.7, 16.8). FDG uptake is lower in indolent compared to aggressive lymphomas both at initial staging and at relapse (mean SUV, 6.3 ± 2.7 vs. 18.1 ± 10.9 and 7.0 ± 3.1 vs. 19.6 ± 9.3, respectively) (Schoder et al. 2005). A receiver operating characteristic (ROC) analysis demonstrated that an SUV of >10 excluded indolent lymphoma with a specificity of 81%. Segregating SUVs into two distinct categories for the differentiation of aggressive and indolent lymphomas may be accurate for the majority of cases but there is always an overlap between subtypes due to the outliers for both groups. Also one of the inherent problems is the underestimation of SUV measurements in small size tumors (~1.0 cm). In cases with a transformation

Table 16.4. FDG-PET imaging in subtypes (REAL/WHO classification) of lymphomas

Subtype	FDG uptake characteristics
HD	
Classical HD (most common)	High ≥95% positive
Lymphocyte-predominance HD	FDG uptake may be < classical HD
NHL	
DLCL (most common)	High ≥95% positive
Follicular (second most common)	Moderate ≤90% positive
Transformed follicular	High ≥95% positive
Small lymphocytic lymphoma/chronic	Low to undetectable 50–70% positive
Lymphocytic leukemia (CLL/SLL)	
Extranodal marginal zone/MALT	Low-to-undetectable to high ≤70% positive
Nodal marginal zone	High FDG uptake ≥95%
Burkitt's	High FDG uptake ≥95% positive
T/natural killer cell	High FDG uptake[a]
Peripheral T-cell	Low-to-undetectable FDG uptake[a]
Mantle cell	High-to-moderate FDG uptake[a]

[a] Not well studied

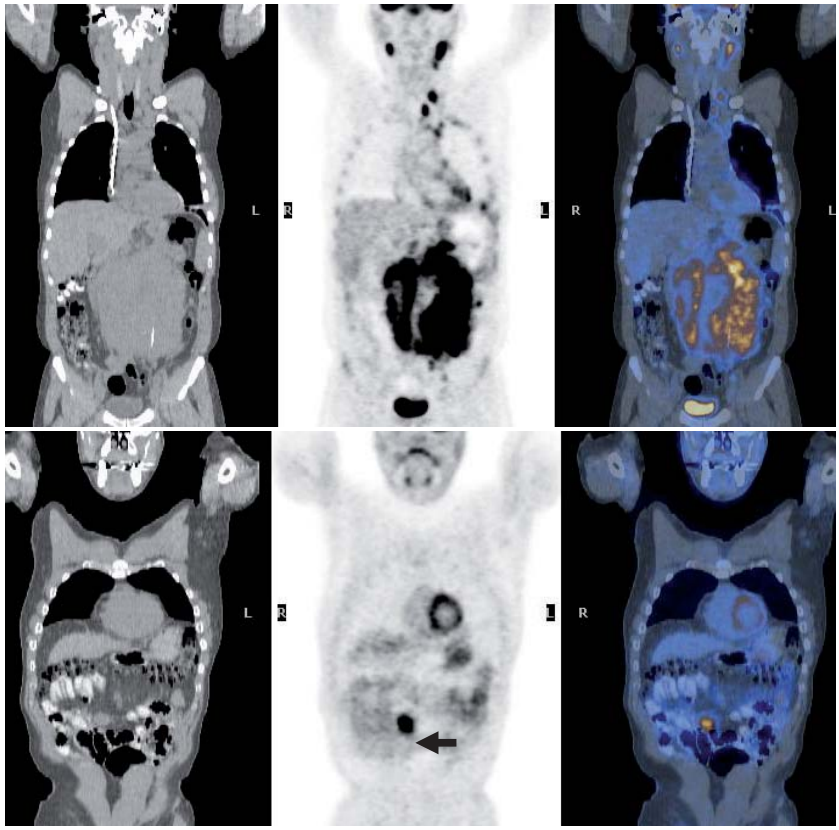

Fig. 16.7. Patient diagnosed with aggressive non-Hodgkin's disease (*upper panel*) underwent a pre-therapy FDG-PET imaging study simultaneously acquired with a CT scan, to evaluate for the extent of disease. Coronal FDG-PET/CT images demonstrate multiple small foci of abnormal FDG uptake in the cervical, left paratracheal, supradiaphragmatic, retroperitoneal, common iliac and mesenteric lymph node stations, all consistent with stage III high-grade lymphoma (SUVmax: 26). Patient diagnosed with mantle cell lymphoma (*lower panel*) underwent a pre-therapy FDG-PET imaging study simultaneously acquired with a CT scan to determine extent of disease. Coronal FDG-PET/CT images demonstrate a large focus of abnormal FDG uptake in a mesenteric lymph node right of the midline (*arrow*), consistent with active lymphoma (SUVmax 7.8). The difference in FDG avidity is obvious as reflected by the SUVmax of lesions

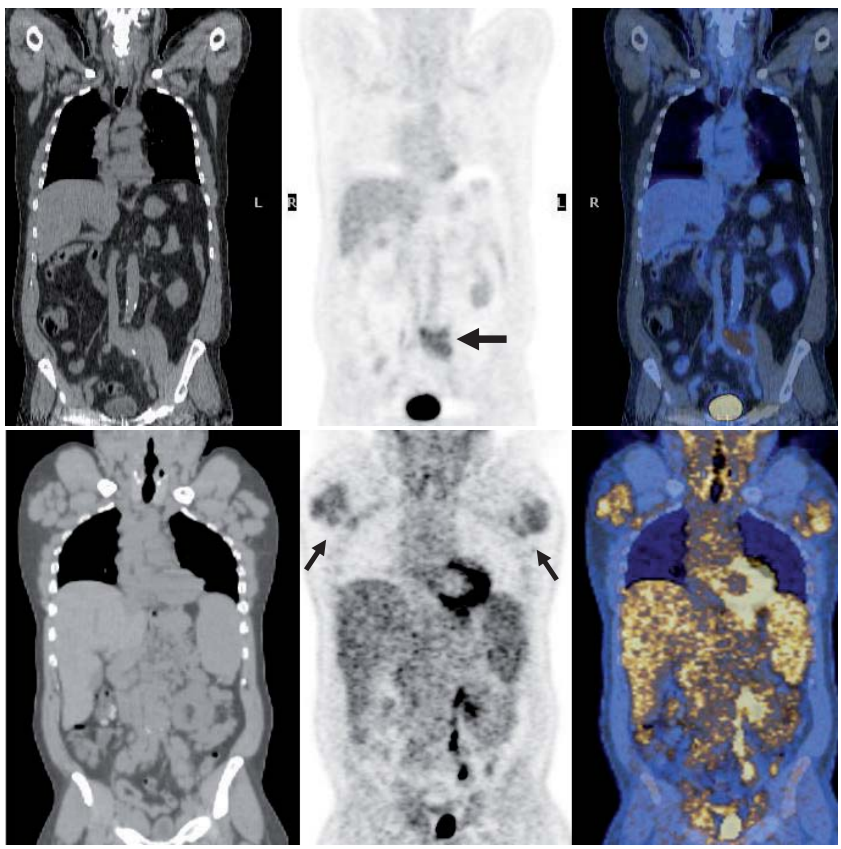

Fig. 16.8. Patient diagnosed with follicular non-Hodgkin's lymphoma (indolent) underwent a pre-therapy FDG-PET imaging study simultaneously acquired with a CT scan, to evaluate for the extent of disease. Coronal FDG-PET/CT images demonstrate a focus of abnormal FDG uptake in a conglomerate mass in the left lower quadrant (*arrow*), consistent with follicular lymphoma (SUVmax: 4.8). The patient is diagnosed with chronic lymphocytic leukemia/small lymphocytic lymphoma (CLL/SLL) (indolent lymphoma) (*lower panel*) and underwent a pre-therapy FDG-PET imaging study simultaneously acquired with a CT scan, to evaluate for the extent of disease. Coronal FDG-PET/CT images demonstrate multiple foci of abnormal FDG uptake in the bilateral axillary regions, consistent with low grade lymphoma (*arrows*) (SUVmax: 3.5). Note the difference in metabolic activity between these two cases and those in Fig. 16.7

to a more aggressive subtype FDG uptake characteristics may help identify an area of high grade transformation admixed within indolent disease and thereby may impact management. While the capability of FDG-PET has not been prospectively assessed for this purpose, simultaneously obtained multiple biopsies from sites with higher SUVs relative to other sites may lead to definition of FDG characteristics that reflect high-grade transformation.

Due to the variability in therapy schemes in indolent subtypes many clinicians do not believe that management would be significantly influenced by the determination of extent of disease; thus, in this patient population, the role of PET has not been well defined. In staging of indolent lymphoma, the usefulness of FDG-PET may, indeed, depend on the histologic subtype (Jerusalem et al. 2001; Karam et al. 2006). In a recent study, the sensitivity of FDG-PET in follicular, marginal zone and small lymphocytic (CLL/SLL) lymphoma were 94%, 71%, and 53%, respectively (Karam et al. 2006) (Fig. 16.8). However, FDG-PET outperformed CT alone in the depiction of extranodal sites in marginal zone lymphoma (85% vs. 57% sensitivity). FDG-PET appears to be less reliable in the detection of extranodal marginal zone lymphoma (MALT) with a sensitivity of 60–70% (Hoffmann et al. 2003; Nathwani et al. 1999). A recent study reported that FDG-PET visualized nodal marginal zone lymphoma in a high proportion of patients whereas FDG uptake was undetectable in extranodal marginal zone lymphoma (Hoffmann et al. 2003). These results do not simply reflect the different growth characteristics but probably reflect the disparate metabolic features. In fact, the proliferation indices of the two groups did not differ significantly (Nathwani et al. 1999).

Mantle cell lymphoma is a rare type of lymphoma demonstrating clinical features of aggressive and molecular features of low-grade lymphomas (Table 16.4) (Fig. 16.7). The diagnostic sensitivity of FDG-PET for mantle cell lymphoma is ≥90% (Hoffmann et al. 2003; Shrikanthan et al. 2004). In this subtype, FDG uptake characteristics are more or less similar to that seen in follicular low-grade lymphoma. Also in this patient population, one should be mindful of extranodal involvement observed in approximately 90% of patients and which may involve unusual areas such as skin, GIT, breast and lung.

16.8.2 Initial Staging

FDG-PET is more sensitive than Ga-67 scintigraphy (Kostakoglu et al. 2002a; Bar-Shalom et al. 2003; Wirth et al. 2002) and is usually in agreement with CT or MRI in the majority of cases with a reported sensitivity of 79–100% (Table 16.5) (Fig. 16.9). FDG-PET can manifest additional disease sites in up to 30% of patients with aggressive NHL or HD (Jerusalem et al. 1999a, 1999b; Hoh et al. 1997; Thill et al. 1997; Mainolfi et al. 1998; Cremerius et al. 1998; Stumpe et al. 1998; Moog et al. 1997, 1998; Bangerter et al. 1998, 1999; Buchmann et al. 2001; Menzel et al. 2002; Weihrauch et al. 2002; Naumann et al. 2004). One should keep in mind that, in the absence of exhaustive biopsy confirmation, the true

Table 16.5. FDG-PET pretherapy evaluation compared to conventional imaging modalities

Authors	Study	Patient no.	Patient group	Modality	Sensitivity (%)	Specificity (%)
Hoh	Retrospective	18	NHL/HD	FDG-PET	94	NA
				CM	83	NA
Thill	Retrospective	27	NHL/HD	FDG-PET	100	NA
				CT	77	NA
Mainolfi	Prospective	98	NHL/HD	FDG-PET	[a]	NA
				CM		
Bangerter	Retrospective	89	NHL/HD	FDG-PET	98	90
				CT	[b]	[b]
Wiedmann	Prospective	20	HD	FDG-PET	[a]	NA
				CM		
Moog	Retrospective	60	NHL/HD	FDG-PET	90	86
				CT		
Buchmann	Prospective	52	NHL/HD	FDG-PET	99	100
				CT	83	100
Weihrauch	Prospective	22	HD	FDG-PET	88	100
				CT	74	100
Bangerter	Prospective	44	HD	FDG-PET	86	NA
				CT	[a]	NA
Wirth	Retrospective	50	NHL/HD	FDG	95	NA
				Ga-67	88	NA
				CM	90	NA
Partridge	Retrospective	44	HD	FDG-PET	100[a]	NA
				CT	53	

HD Hodgkin's disease, *NHL* non-Hodgkin's, *CM* conventional modalities, *CT* ultrasound, *MRI* endoscopy or laparoscopy

[a] FDG-PET sensitivity not given but at worst FDG-PET findings were in agreement with CT and at best detected more sites than did CT

[b] FDG-PET findings were compared to the findings on CT imaging (CT as the reference); most sites were not biopsy confirmed

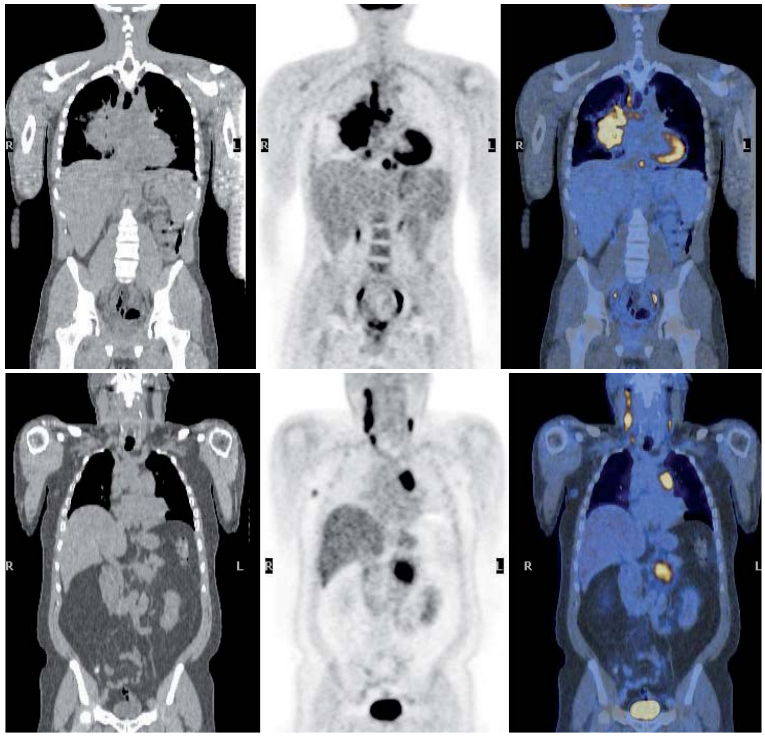

Fig. 16.9. Patient with a diagnosis of mediastinal Hodgkin's lymphoma underwent a pre-therapy FDG-PET imaging study simultaneously acquired with a CT scan, for staging. Coronal images of CT (*left*), PET (*middle*) and PET-CT fusion (*right*) demonstrate increased FDG uptake in the right anterior mediastinum and hilum as well as in the supradiaphragmatic lymph nodes, consistent with stage II lymphoma. Note the physiologic uptake in the ureters in the upper abdomen. Otherwise there is no abnormal uptake in the infradiaphragmatic nodal and extranodal regions. The patient with a recent diagnosis of aggressive non-Hodgkin's lymphoma underwent a pre-therapy FDG-PET imaging study simultaneously acquired with a CT scan, for staging. Coronal images of CT (*left*), PET (*middle*) and PET-CT fusion (*right*) demonstrate increased FDG uptake in the bilateral cervical regions, left precarinal and hilar region, right axilla, left para-aortic, and right iliac lymph node stations, consistent with stage III lymphoma

positive rate for FDG-PET will not be definitively unraveled. Nonetheless, long-term follow-up has been universally accepted as a validation means; consequently most results published in the literature have been verified by long-term follow-up data. Overall, compared to conventional staging the accuracy of FDG-PET is 10–15% higher at initial staging (Buchmann et al. 2001; Menzel et al. 2002; Weihrauch et al. 2002; Naumann et al. 2004).

FDG-PET changes staging in 15–25% of patients (Buchmann et al. 2001; Menzel et al. 2002; Weihrauch et al. 2002; Naumann et al. 2004). Upstaging occurs more often than downstaging by virtue of revealing more extensive disease. However, upstaging from early stage to advanced stage or vice versa is not frequently experienced in daily practice.

The integrated PET-CT systems allow for more accurate lesion localization. However, currently, many centers do not use intravenous contrast due to the concerns related to attenuation artifacts. Thus, one may think that there is a potential risk of missing an enlarged lymph node in PET negative cases on a non-contrast PET-CT study. A retrospective study addressing this issue reported that PET-CT performed with nonenhanced CT is more sensitive and specific than is contrast-enhanced CT for evaluation of lymph node and organ involvement in lymphoma especially regarding exclusion of disease (Schaefer et al. 2004). Provided that most disease sites were in the mediastinum, these results are not surprising as mediastinal lymph nodes can be detected without the aid of intravenous contrast. In this regard, contrast enhancement is more crucial in the abdomen, to separate lymph nodes from vessels and bowel loops.

16.8.3 FDG-PET in Extranodal Lymphoma

The results obtained, thus far, in extranodal lymphoma are similar to those with nodal lymphoma. A multitude of studies have reported that FDG-PET may provide more information about the extent of disease in cases with extranodal lymphoma compared to CT (Thill et al. 1997; Moog et al. 1998; Wiedmann et al. 1999; Rodriguez et al. 1997).

FDG-PET can differentiate primary lymphomas of the CNS from infectious processes with a reported accuracy of 89% (Hoffman et al. 1993; Heald et al. 1996; Erez et al. 2006) (Fig. 16.10). Distinguishing infectious etiology such as toxoplasmosis can be a challenge for morphological imaging studies including CT and MRI. Due to the low sensitivity and specificity of polymerase chain reaction test for toxoplasmosis and Epstein-Barr virus titers for lymphoma, patients with AIDS and CNS lesions are empirically treated with pyrimethamine and sulfadiazine for 2–4 weeks. On FDG-PET imaging,

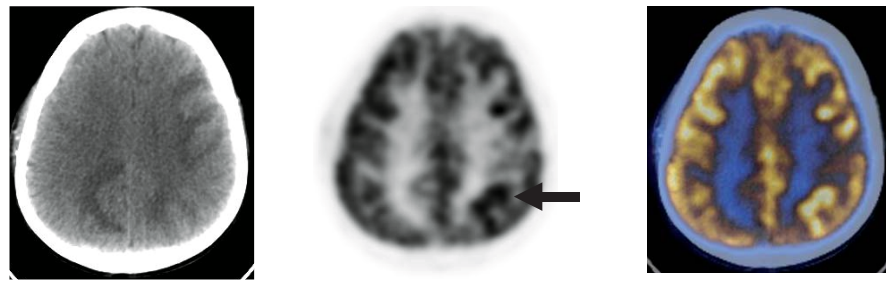

Fig. 16.10. Patient with a history of HIV positive serology, recently found to have a cerebral lesion in the left parieto-occipital lobe, referred for FDG-PET imaging to differentiate between toxoplasmosis and CNS lymphoma. There is FDG uptake in a lesion corresponding to the left posterior parieto-occipital cortex demonstrating a rim uptake, relatively higher than that in the adjacent gray matter, consistent with CNS lymphoma (*arrow*). The patient was subsequently discontinued on empirical therapy with antibiotics and started on chemotherapy

a lesion with an FDG uptake higher than the adjacent gray matter is highly suggestive of a malignant process. Thus, these lesions should be biopsied for confirmation rather than empirically treated as infectious. As alluded to in the previous section, Tl-201 is also known as a valuable imaging tool in the differentiation of CNS lymphoma from infectious causes (Skiest et al. 2000). In a recent study FDG-PET proved superior to Tl-201 SPECT in the differentiation of CNS lymphomas from toxoplasmosis with an accuracy of 100 % vs. 44 % (Erez et al. 2006). With the increasing availability of FDG-PET, this test should supplant Tl-201 SPECT as imaging study of choice following conventional imaging (MRI or CT) of CNS lesions in AIDS patients. Difficulty arises, however, when CNS lymphoma undergoes necrosis or is below the resolution limits of PET systems.

The detection of bone marrow (BM) involvement identifies a group of high-risk patients and changes disease management. Hence, this is particularly important in early stage patients given the trend towards less intensive treatment in this group of patients. The incidence of BM involvement at diagnosis varies according to the subtype of lymphoma. In general, the incidence is rather low in patients with HD (1 – 2 %) while it is common in low-grade lymphoma (mainly follicular cell subtype, 60 – 70 %), chronic lymphocytic leukemia and mantle cell lymphoma (90 – 100 %) (DeVita and Canellos 1999). In aggressive NHL (mainly diffuse large cell lymphoma), BM infiltration is observed in 25 – 40 % of patients (Shipp et al. 1997). BM biopsy is the mainstay of BM evaluation despite its association with a high rate of false-negative findings due to sampling errors. MRI is especially useful in detecting BM involvement; however, benign entities such as hemangiomas, inflammatory processes, and post-therapy changes diminish its specificity by mimicking lymphoma features. BM is a metabolically active organ, and depending on the marrow turnover, the degree of FDG uptake varies between faintly noticeable to prominent. Overall, focal FDG uptake suggests pathological BM activity, a pattern more commonly seen in HD patients (Fig. 16.11). In aggressive NHL, the degree of BM involvement may range from a few cells to complete marrow replacement. In cases with the latter condition, FDG uptake is usually diffuse and somewhat heterogeneous but never specific. Diffusely increased FDG uptake is also seen in patients with BM hyperplasia, particularly following administration of colony stimulating factors (e.g., G-CSF) (Abdel-Dayem et al. 1999; Gundlapalli et al. 2002) (Fig. 16.11). Consequently, FDG-PET is an effective means for the detection of extranodal lymphoma, but the sensitivity in detecting BM infiltration is usually suboptimal regardless of the subtype of lymphoma (Hoffmann et al. 2003; Elstrom et al. 2003; Carr et al. 1998). A sensitivity of 81 % and a specificity of 100 % have been reported for FDG-PET in the detection of BM involvement with BM biopsy confirmation (Moog et al. 1998). In patients with negative BM biopsy, FDG-PET may reveal focal BM infiltration distal to the biopsy site owing to the virtue of evaluating the entire body at one acquisition (Moog et al. 1998; Carr et al. 1998). Overall, the negative predictive value for FDG-PET in the detection of BM involvement is higher than the positive predictive value. Nevertheless, a minimal degree of BM involvement can result in false negative findings due to the inherent resolution limits of FDG-PET imaging.

Primary bone lymphoma is a separate entity that accounts for less than 5 % of all primary bone tumors. Although there is no series of cases performed using FDG-PET, our experience is that FDG avidly accumulates in all primary bone lesions or osseous extension of lymphoma (Park et al. 2005).

In cases of splenic involvement, the diagnostic efficiency of FDG-PET is superior to that of CT (Fig. 16.12). FDG-PET localizes approximately 25 % more lesions than does CT in the liver and spleen (98, 102). Furthermore, FDG-PET was found to be significantly more sensitive and accurate than Ga-67 imaging in the identification of splenic involvement in HD patients (97 % vs. 78 %) (Rini et al. 2002).

With the advent of PET-CT imaging, the accuracy of lesion detection has significantly improved. The addition of CT to PET improves mainly specificity but also sensitivity, and the addition of PET to CT increases sensitivity and specificity in tumor imaging. In a recent

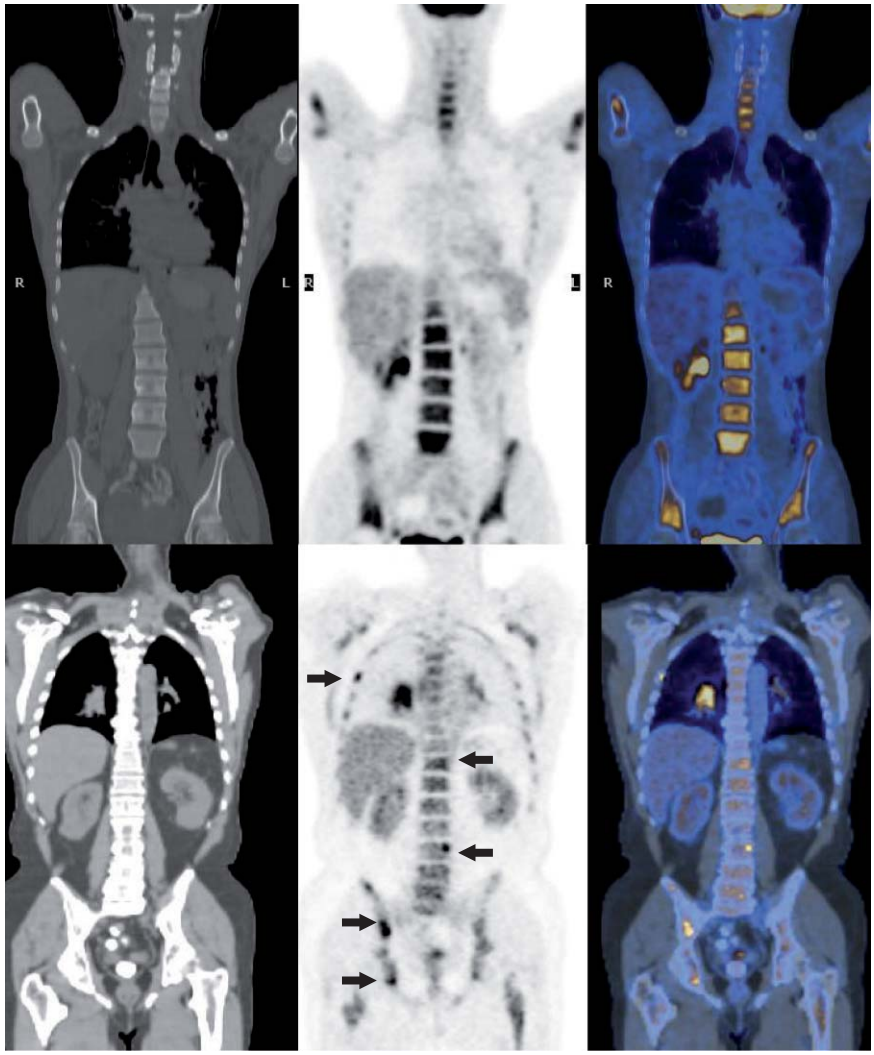

Fig. 16.11. Patient with a recent diagnosis of Hodgkin's lymphoma referred for evaluation of therapy response after four cycles of therapy (*upper panel*). The patient was administered granulocyte colony stimulating factor (GCSF) a week prior to the PET study. Coronal PET/CT images demonstrate intensely increased FDG uptake in the axial and visualized appendicular skeleton, corresponding to the bone marrow space, consistent with reactive bone marrow changes related to the recent administration of GCSF. Possible underlying bone marrow involvement cannot be evaluated with certainty due to the reactive changes in the bone marrow. Note the relatively increased FDG uptake in the spleen which may be due to extramedullary hematopoiesis induced by GCSF. Patient with a diagnosis of stage IV Hodgkin's lymphoma referred for evaluation of therapy response after three cycles of therapy (*lower panel*). The patient was administered granulocyte colony stimulating factor (GCSF) 5 days prior to the PET study. Coronal PET/CT images demonstrate intensely increased FDG uptake in the axial and visualized appendicular skeleton as well as discrete foci of increased FDG uptake in several ribs, multiple vertebral bodies and pelvic bones (*arrows*), consistent with bone/bone marrow involvement as well as reactive bone marrow changes due to GCSF. Note the residual lymphoma in the bilateral hilar regions, more prominent on the right side, innumerable foci of increased FDG uptake in the axial and visualized appendicular skeleton, consistent with bone/bone marrow involvement by lymphoma. Note the heterogeneously increased uptake in the medial aspect of the spleen, consistent with splenic involvement

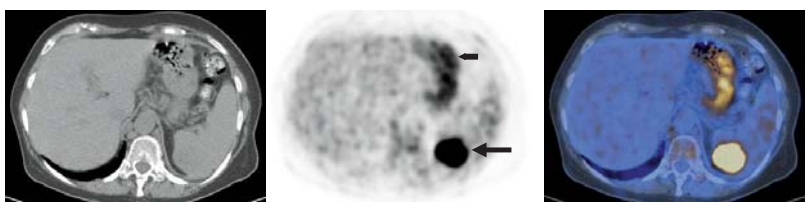

Fig. 16.12. Patient diagnosed with aggressive non-Hodgkin's lymphoma, referred for a FDG-PET study to determine the extent of disease. Axial images of CT (*left*), PET (*middle*), and PET-CT fusion (*right*) demonstrate intensely increased FDG uptake in a focus corresponding to the medial aspect of the spleen (*large arrow*), consistent with splenic involvement by lymphoma. Note the physiologic uptake in the stomach (*small arrow*)

study, PET-CT acquired with no contrast enhancement, detected extranodal disease in the bone and spleen while contrast enhanced CT was false negative at these sites (Schaefer et al. 2004). In the same study, in 79 % of patients who had no extranodal involvement there was complete agreement between PET-CT and contrast enhanced CT. Since PET-CT studies have evolved to include intravenous contrast administration, potential false negative CT findings with noncontributory PET findings should now be of a lesser concern.

16.8.4 FDG-PET Influence on Patient Management at Initial Staging

The accuracy of staging impacts management in aggressive NHL and HD than in indolent and mantle cell lymphomas as the latter entities usually present with advanced stage disease. Additionally, the additional information provided by FDG-PET is felt to be more useful in patients presenting with early stage disease than in advanced stage disease as treatment strategy may be altered by detection of unexpected disease sites in the former patient population but not in the latter (Diehl et al. 2003).

The superior sensitivity of FDG-PET results in a change of initial stage in 10–40% of patients with NHL and HD by virtue of revealing more extensive disease (Jerusalem et al. 1999a, 1999b; Hoh et al. 1997; Thill et al. 1997; Mainolfi et al. 1998; Cremerius et al. 1998; Stumpe et al. 1998; Moog et al. 1997, 1998; Bangerter et al. 1998, 1999; Buchmann et al. 2001; Menzel et al. 2002; Weihrauch et al. 2002; Naumann et al. 2004; Partridge et al. 2000; Schoder et al. 2001).

Based on the significance of change in stage for therapeutic strategy, FDG-PET findings may result in treatment modifications in up to 25% of aggressive NHL or HD patients. In one study PET helped in the decision algorithm in 62% of the patients included in the study. In a recent study, the projected analysis that focused on the suggested change in treatment strategy revealed that management would have been changed in approximately 20% of patients (Naumann et al. 2004). Among patients with early stage disease, in 20% treatment would have been intensified.

The study design often dictates the significance of findings. The limitations of the previous studies are that they were often retrospective and included a mixture of NHL and HD patients without in depth analysis for these histologic subtypes. More importantly, a clear definition of positive and negative findings were not available in most studies. The results from the first generation PET scanners were not separated from those obtained later on from more advanced scanners.

16.8.5 Restaging

Residual masses in patients with lymphoma after chemotherapy remain a problem. As many as 80% of patients with HD and 30% of those with NHL have residual masses after treatment. However, relapses occur in only a small percentage of these patients (~15–20%). A multitude of studies have demonstrated that FDG-PET is an effective imaging modality, proving more accurate than CT in the differentiation of post-therapy inert masses from active residual disease (Table 16.6). FDG-PET based identification of patients who would require salvage chemotherapy precedes clinically overt relapse. The specificity of FDG-PET is approximately 90% while the respective value for CT is in the range of 17–39% in the differentiation of residual viable disease from post-therapy benign changes (Hueltenschmidt et al. 2001; Cremerius et al. 1999; Weihrauch et al. 2001; Naumann et al. 2001; Mikhaeel et al. 2000; de Wit et al. 2001; Zinzani et al. 1999; Jerusalem et al. 2003; Cremerius et al. 1998; Dittmann et al. 2001). In a comparative study of PET-CT and contrast enhanced CT, the sensitivity and specificity were 85% vs. 69% and 100% vs. 86% (Schaefer et al. 2004). This study is, however, limited due to the preponderance of thoracic lesions and the small number of patients.

Table 16.6. FDG-PET studies in the detection of residual or recurrent lymphoma

Authors	Study	Patient no.	Patient group	PPV (%)	NPV (%)
Stumpe	Retrospective	43	HD	94	88
Jerusalem	Prospective	54	NHL/HD	100	86
Huelten-schmidt	Prospective	63	NHL/HD	83	96
Cremerius	Retrospective	41	NHL/HD	84	86
Weihrauch	Prospective	28	HD	60	95
Naumann	Prospective	58	NHL/HD	62.5	96
Mikhaeel	Retrospective	45	NHL	100	83
De Wit	Prospective	37	HD	46	96
Dittman	Retrospective	44	HD	87.5	94
Mikhaeel	Prospective	32	HD	100	93
Cremerius	Prospective	22	NHL	72	72
Becherer	Prospective	16	NHL/HD	87	87

PPV positive predictive value, *NPV* negative predictive value, *NHL* non-Hodgkin's lymphoma, *HD* Hodgkin's disease
† Either PPV or NPV or both not given
‡ All patients had intra-abdominal lymphoma

Despite reported high negative predictive values obtained FDG-PET by various investigators, false negative findings are inevitable in cases with residual microscopic disease. One major question is whether negative post-therapy FDG-PET can avoid RT after first-line therapy. This conundrum can only be solved by multicenter prospective randomized trials comparing the progression-free survival (PFS) in post-therapy PET negative patients who receive no RT with those who receive RT. Nevertheless, positive predictive value of FDG-PET is more vital in the context of identifying patients who would need immediate therapy changes or additional treatment after first-line therapy.

False positive findings can occasionally be obtained in infectious or inflammatory processes; however, the pattern of FDG uptake in these situations is recognizable in most cases unless granulomatous disease coexists with lymphoma. Post-therapy FDG accumulation in the region of original disease should be recognized as compelling evidence for further therapy due to the

superior positive predictive value of FDG-PET (>90%) compared to CT in the post-therapy setting.

16.8.6 Prediction of Therapy Outcome After Completion of Therapy

In early stage HD or aggressive NHL, up to 90% of patients respond to therapy; however, advanced stage lymphoma confers unfavorable prognosis with a cure rate of less than 50% in newly diagnosed patients (Brandt et al. 2001; Coiffier et al. 1991; Canellos 2004). Assessment of therapy response is, therefore, more imperative in patients with advanced stage disease than those with early stage in terms of considering alternative therapy options. In early stage patients, however, imaging-based response evaluation may shorten number of therapy cycles, and, thus, may decrease treatment related untowards long-term complications.

FDG-PET has an emerging role in assessing response, both at completion of and during treatment (Jerusalem et al. 1999a; Weihrauch et al. 2001; Naumann et al. 2001; Mikhaeel et al. 2000; de Wit et al. 2001; Zinzani et al. 1999; Spaepen et al. 2001; Kostakoglu et al. 2002b). According to the results of published studies, the majority of patients with positive post-therapy FDG-PET findings succumb to progressing disease. On the contrary, residual post-therapy CT masses are associated with a relapse rate of less than 50% (Jerusalem et al. 1999a; Mikhaeel et al. 2000; Spaepen et al. 2001). In this respect, false positive results continue to be of primary concern; thus, biopsy confirmation of all post-therapy positive findings is warranted before initiation of second-line therapy. Jerusalem et al calculated from data of 17 studies in end-of-treatment evaluation, a sensitivity of 76%, a specificity of 94%, a PPV of 82%, an NPV 92%, and an accuracy of 89% (Jerusalem et al. 2005) (Figs. 16.13, 16.14). Segregating data into two disease entities, another systematic review revealed that the pooled sensitivity and specificity for detection of residual disease in HD and NHL were 84% and 90%, vs. 72% and 100%, respectively, after first-line chemotherapy. These data suggested that in the case of a 50% probability of persistent tumor after first-line therapy for aggressive NHL, the probability of having persistent viable tumor after a positive PET scan was 97%, vs.

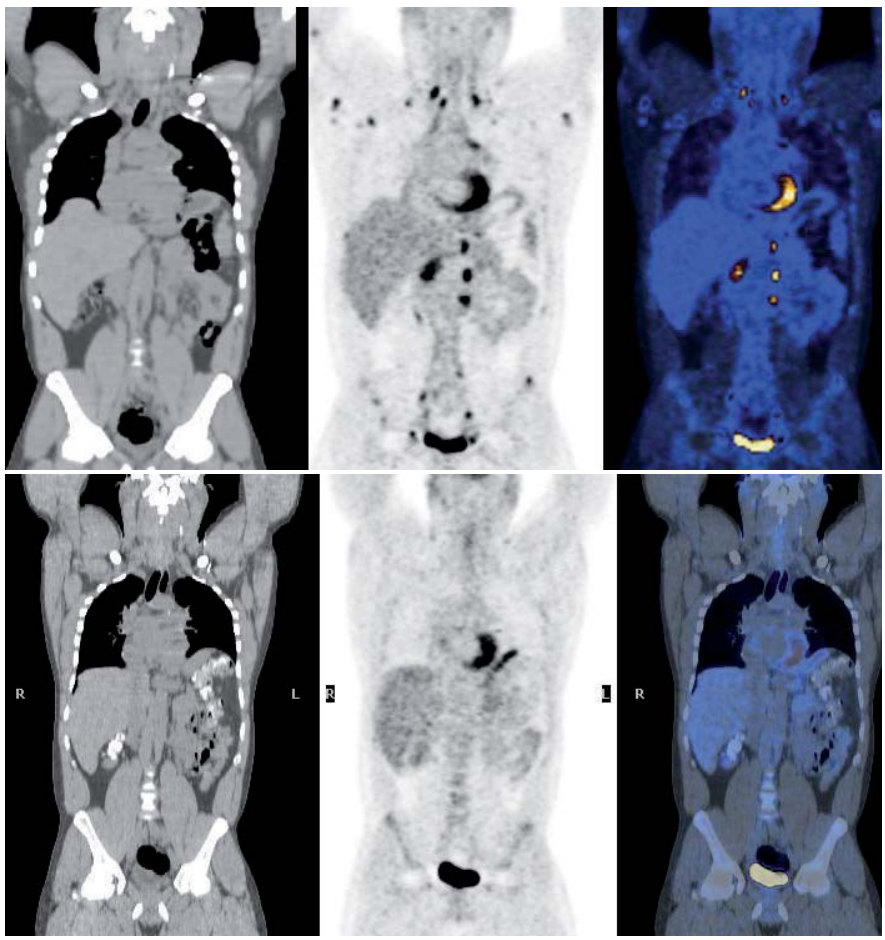

Fig. 16.13. Patient with non-Hodgkin's lymphoma underwent a PET-CT study prior to and immediately following completion of therapy to evaluate response to therapy. Pre-therapy coronal images (*upper panel*) of CT (*left*) and PET (*right*) demonstrate increased FDG uptake in multiple lymph nodes in the supraclavicular, axillary, paratracheal, left precarinal, retroperitoneal, iliac and inguinal lymph nodes consistent with active lymphoma (stage III). Post-therapy coronal images (*lower panel*) of CT (*left*) and PET (*right*) demonstrate complete resolution of disease in the cervical, chest and abdominal/pelvic regions with no evidence of residual uptake. These findings are consistent with a favorable response to therapy. The PFS has not been reached for this patient after a follow-up of 36 months

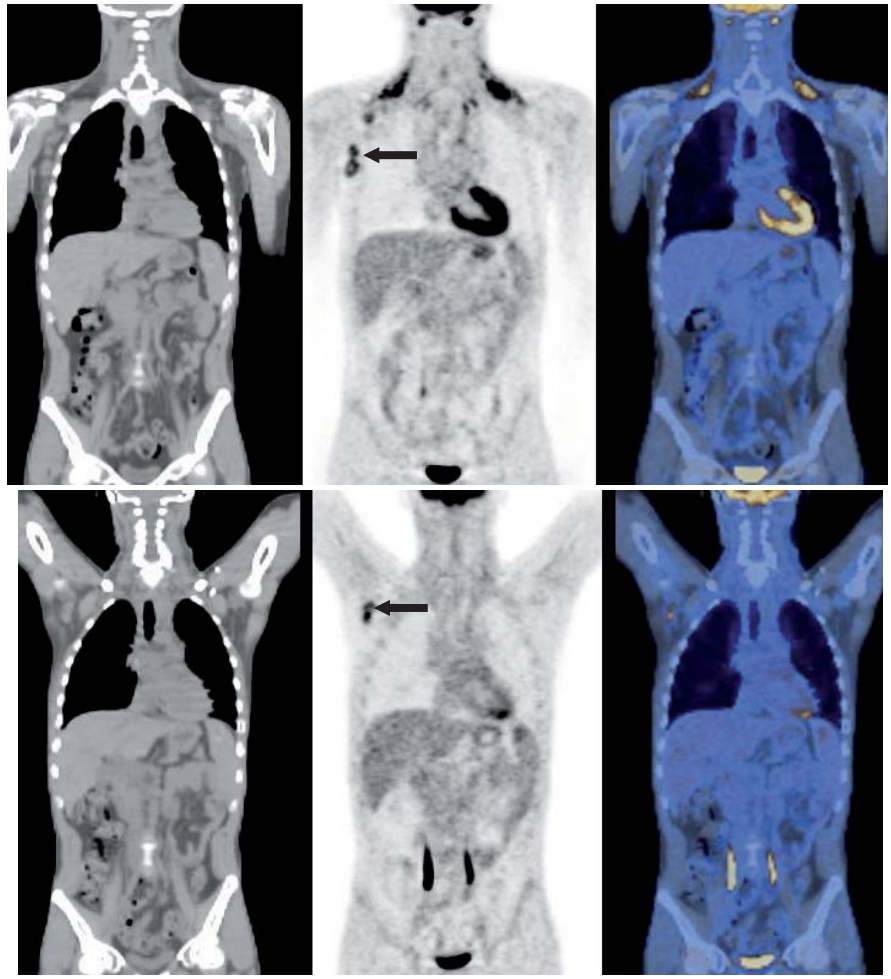

Fig. 16.14. Patient with non-Hodgkin's lymphoma underwent a PET-CT study prior to and immediately following completion of therapy to evaluate response to therapy. Pre-therapy axial images (*upper panel*) of CT (*left*) and PET (*right*) demonstrate multiple foci of increased FDG uptake in the right axilla, consistent with lymphoma (*arrow*). Post-therapy axial images (*lower panel*) of CT (*left*) and PET (*right*) demonstrate persistent FDG uptake in the right axilla, in the region of original disease (*arrow*). These findings are consistent with unfavorable response to therapy. The patient was subsequently placed on an alternative therapy. Note the physiologic uptake in the bilateral ureters in the post-therapy image

22% in the case of a negative PET result. Applying a 15% pre-test probability of relapse in HD, the corresponding numbers were 60% vs. 3% (Zijlstra et al. 2006).

16.8.7 Early Prediction of Response During Therapy

Rapidity of response to therapy as a means to measure chemosensitivity has been suggested as a predictor of response (Armitage et al. 1986; Haw et al. 1994; Verdonck et al. 1995). As a consequence of being a metabolic imaging modality well-suited for early assessment of therapy, interim FDG-PET after a few cycles or at midtreatment was reported to predict PFS in patients with aggressive NHL and HD (Mikhaeel et al. 2002; Spaepen et al. 2002; Haioun et al. 2005; Hutchings et al. 2006a) (Table 16.7). Persistent FDG uptake during chemotherapy is associated with relapse rates ranging from 70% to 100% while the relapse rate in patients with complete resolution of FDG uptake during therapy is below 10%. In early evaluation of chemosensitivity during the course of therapy, data analyzed from seven studies, Jerusalem et al. calculated for PET an overall sensitivity of 79%, a specificity of 92%, a PPV of 90%, an NPV of 81%, and an accuracy of 85% (Jerusalem et al. 2005). Furthermore, multivariate analysis revealed that FDG-PET at two cycles and mid-treatment was a stronger prognostic factor for PFS compared with conventional risk factors before treatment in HD and NHL (Hutchings et al. 2006a).

Table 16.7. FDG-PET in the early evaluation of response to therapy

Authors	Chemo cycles	Median follow-up (months)	PPV	NPV
Mikhaeel et al.	2–4	30	87%	100%
Jerusalem et al.	2–5	17	100%	67%
Kostakoglu et al.	1	19	87%	87%
Spaepen et al.	3–4	36	100%	84%
Hutchings et al.	2	23	69%	95%
Haioun et al.	2	24	44%	87%
Kostakoglu et al.	1	21	87.5%	100%

Kostakoglu et al. reported that 2-year progression-free survival for PET-negative patients after one cycle of therapy was 100 %, compared with only 12.5 % in those with a positive result (Kostakoglu et al. 2006). These investigators also reported that PET findings obtained after the first cycle correlated better with PFS than ^{18}F-FDG PET findings obtained after completion of chemotherapy (Kostakoglu et al. 2002b, 2006). The false negative results that are obtained more often after completion of therapy may be due to slowly responding but eventually relapsing disease. Most recently, a prospective study of HD reported that for prediction of PFS, interim FDG-PET was as accurate after two cycles as later during treatment and superior to CT at all times. In regression analyses, early interim FDG-PET was stronger than established prognostic factors. Other significant prognostic factors were stage and extranodal disease. A positive early interim FDG-PET is highly predictive of progression in patients with advanced-stage or extranodal disease (Hutchings et al. 2006a). Similarly, in a prospective recent study of NHL patients, outcome differed significantly between PET-negative and PET-positive groups after two cycles; the 2-year estimates of event-free survival reached 82 % and 43 %, respectively (Haioun et al. 2005). Predictive value of "early PET" was observed in both the lower-risk and higher-risk groups, indicating prognostic independence from the established risk factors (i.e., IPI). After one cycle of chemotherapy, similar results were obtained.

The results of most studies were analyzed dichotomously in two categories as responders (no FDG uptake) vs. nonresponders (residual FDG uptake). Semiquantitative studies using standardized uptake values (SUV) may be more appropriate but standardization of methodology is necessary between the two imaging periods. Furthermore, one should bear in mind that SUV cut-off values may be different depending on the patient population and therapy modality.

16.8.8 Bone Marrow Transplantation

For patients with relapsed lymphoma, high-dose chemotherapy (HDT) with autologous stem cell transplantation (SCT) is the treatment of choice (Philip et al. 1995). The outcomes after HDT/SCT, however, can be significantly different between chemosensitive and chemoresistant patients. Hence differentiation of these two patient populations is important for the identification of the optimal group that would benefit from HDT/SCT (Cremerius et al. 2002; Becherer et al. 2002; Schot et al. 2006). An analysis of published data revealed for PET a sensitivity, specificity, PPV and NPV of 84 %, 83 %, 84 %, and 83 %, respectively (Jerusalem et al. 2005). Superior PPVs are obtained if PET is performed just prior to transplantation (> 87 %) compared with those performed early during the administration of salvage therapy (PPV = 65 %) (Schot et al. 2006). This is not surprising since resistant clones can only become apparent when the sensitive ones are killed. One should keep in mind that co-existing inflammatory disease is more frequently seen in this population and can cause false-positive PET results. Further studies are necessary to define the optimal timing of PET and response criteria before this technique can be used as a standard practice to determine patient eligibility for HDT/SCT.

These results provide grounds for future trials to evaluate the prognosis in patients who are administered abbreviated courses of chemotherapy with or without combined RT given at lower radiation doses in cases with negative FDG-PET results.

Recently introduced PET-CT systems provide important information particularly in the post-therapy setting; metabolic findings that are overlooked due to the subtlety of metabolic changes on FDG-PET may result in the detection of residual disease after correlation with the simultaneously acquired CT data. Furthermore, equivocal CT findings which are suggestive of either recurrent tumor or post-therapy changes can now be distinguished with the guidance of the additional information obtained from FDG-PET data.

PET-CT imaging may also play an important role in radiation therapy planning. The metabolic activity obtained from PET superimposed on anatomic images from CT can delineate the key regions to be irradiated and exclude the vital organs such as great vessels and the heart from the field of radiation. For deeply seated disease sites which are not amenable to clinical examination, PET-CT may play a unique role defining the exact location of disease. In particular, for midline masses associated with pneumonia when CT findings may be misleading, the metabolic information contributed by PET may be crucial. Although in pneumonia there will be a certain degree of FDG uptake, the pattern of uptake may exclude the sites of disease involvement and demonstrate the margins of lymphoma mass.

It is crucial, however, to consider the limitations of FDG PET imaging to avoid false positive or negative findings. Provided that current FDG PET systems have a spatial resolution of 5 – 8 mm, FDG uptake can be underestimated in structures less than 1.0 – 1.6 cm (twice the spatial resolution). Hence, it is important to understand that FDG-PET cannot exclude minimal residual disease. In some cases positive findings do not necessarily represent residual disease. Physiological uptake can be misinterpreted, particularly by an inexperienced observer. Additionally, activated macrophages, leukocytes or granulation tissue demonstrate FDG avidity. Spaepen et al. have shown in a tumor mouse model that a transient increase in inflammatory cells may result in overestimation of the fraction of viable

cancer cells (Spaepen et al. 2003). Thus, interim FDG-PET should be performed as close as possible to the subsequent cycle (0–4 days prior) to avoid false positive findings due to therapy related inflammatory changes. After completion of therapy, optimal timing is suggested at 4–6 weeks after the last cycle of chemotherapy therapy. When radiotherapy is involved, a post-therapy period of 3–4 months should elapse for assessment of therapy effects. It is not possible to decide to stop a treatment based only on a negative ^{18}F-FDG PET. It may be indicated to repeat ^{18}F-FDG PET during routine follow-up to avoid uncertainties regarding the presence of residual disease at completion of treatment.

16.9 Pitfalls in Lymphoma Imaging

16.9.1 Sarcoid-Like Granulomas

Sarcoid-like reactions in enlarged hilar and mediastinal lymph nodes as well as in lung nodules can be identified in lymphoma patients after therapy, particularly in the HD population (de Hemricourt et al. 2003). In the case of HD, these noncaseating epithelioid-cell granulomata may occur synchronous to the disease or many years later. This inflammatory manifestation may arise directly in direct relation with the tumor or distant to the lesion. It is deemed that the granulomatous formations represent a secondary reaction to the chronic stimulation of tumoral antigens disseminated through the body or as a particular side effect of certain drugs including bleomycin and more rarely vinblastine and doxorubicin (Brincker 1986; Talcott et al. 1987).

16.9.2 Benign Lymphoproliferative Disorders

The benign lymphoproliferative disorders (LPD) most frequently manifest in the thorax either in the lymph nodes or in the bronchus associated lymphoid tissue of the lung (Koss 1995). Entities such as plasma cell granuloma, post-transplant lymphoproliferative disorders, lymphoid interstitial pneumonia and lymphomatoid granulomatosis involve the pulmonary parenchyma, while Castleman's disease, infectious mononucleosis and angioimmunoblastic lymphadenopathy involve intrathoracic lymph nodes. It is important to differentiate the "'benign" forms of LPD from the aggressive lymphomas. There is a considerable overlap between benign LPD and NHL, especially in the immunocompromised patients. One might assume that the FDG uptake would be lower in this benign form of LPD than that seen in aggressive NHL and HD (Reddy and Graham 2003; Murphy et al. 1997). It is expected that in the indolent forms of NHL, the differentiation between benign LPD and lymphoma may not be possible.

16.9.3 Thymic Uptake

Thymic hyperplasia is a common phenomenon after treatment, especially in children with an incidence of approximately 20% (Weinblatt et al. 1997; Ferdinand et al. 2004; Kawano et al. 2004). This phenomenon is characterized by lymph follicles demonstrating large nuclear centers and infiltration of plasma cells following thymic aplasia secondary to inhibition of lymphocyte proliferation. In one study, Brink et al. found increased FDG uptake in 73% of the children with malignancy prior to chemotherapy and in 75% of the children with malignancy following chemotherapy. However, they also found increased uptake in 5% of the adults with lymphoma following chemotherapy. These findings support the idea that, although thymic uptake may be a normal finding in children, it may also be expected in young adults after therapy (Ferdinand et al. 2004).

In a study of pediatric patients, thymic FDG uptake after chemotherapy was significantly higher than during chemotherapy (Kawano et al. 2004). A significant relationship between thymic FDG uptake and interval after completion of chemotherapy was observed. Post-therapy thymic uptake may persist for 6–18 months.

16.9.4 BM Uptake After Administration of Colony Stimulators

Following administration of granulocyte colony-stimulating factor or granulocyte-macrophage colony-stimulating factor, the BM demonstrates diffuse, increased FDG accumulation (Abdel-Dayem et al. 1999; Gundlapalli et al. 2002). However, diffuse bone marrow FDG uptake can also be caused by bone marrow involvement by lymphoma, which may be indistinguishable from hematopoietic cytokine-mediated FDG bone marrow uptake. Of note, colony stimulating factors can also cause increased splenic uptake, which should not be misinterpreted as splenic involvement by lymphoma.

16.9.5 Post-Transplantation Period

Following bone marrow transplantation (BMT), patients can develop cellular immunodeficiency until the full engraftment of transplanted marrow. These patients are susceptible to infections including idiopathic interstitial pneumonitis, *Pneumocystis carinii*, cytomegalovirus, and aspergillus (Armitage 1994). Additionally, acute graft vs. host disease (GVHD) often occurs during the first 3 months following an allogeneic

BMT (Ichiki et al. 2006). To minimize the risk of graft rejection and GVHD, allogeneic BMT patients are given immunosuppressants to prevent GVHD before and after transplant. Use of these drugs, however, increases the risk of infection. Therefore, caution should be exercised when interpreting FDG-PET images in immunocompromised patients.

16.9.6 AIDS Related Lymphoma

AIDS related lymphomas are characterized by the presence of B-symptoms (weight loss, night sweats, and fevers) in approximately 90 % of patients, advanced clinical stage in greater than 60 %, and clinical aggressiveness with poor therapeutic outcomes. Extranodal involvement is a particularly distinctive feature, with the gastrointestinal tract being the most common location. Other sites of involvement include the central nervous system, the bone marrow, the oral cavity, the lungs, and the skin. Recently, a primary effusion lymphoma has been described in association with HIV (Weinblatt et al. 1997). FDG-PET imaging findings reveal aggressive features, mainly demonstrating significantly high SUV values in the involved sites.

16.9.7 Conclusions

FDG-PET is at least as sensitive as CT and more specific for the detection of active lymphoma; thus, FDG-PET has become a standard procedure in routine clinical practice as an adjunct to CT. In centers with integrated PET-CT instruments, staging of lymphoma can be performed at one session using this modality only. In the post-therapy setting, FDG-PET plays a crucial role in the accurate assessment of post-therapy residual masses. Persistent FDG uptake seen in initially involved sites should be a basis for consideration of providing alternative therapy after biopsy confirmation. In advanced stage disease, negative PET results do not exclude minimal residual disease and/or the risk of late relapse. These patients might benefit from repeated follow-up scans. Patients with early-stage lymphoma and a negative FDG-PET scan after therapy are considered in CR and follow-up imaging is indicated only if recurrent disease is suspected. Prospective, randomized studies with large numbers of patients are needed to determine the role of early interim post-therapy FDG-PET in changing the therapeutic management.

References

Abdel-Dayem HM (1997) The role of nuclear medicine in primary bone and soft tissue tumors. Semin Nucl Med 27:355 – 363

Abdel-Dayem HM, Rosen G, El-Zeftawy H, Naddaf S, Kumar M, Atay S, Cacavio A (1999) Fluorine-18 fluorodeoxyglucose splenic uptake from extramedullary hematopoiesis after granulocyte colony-stimulating factor stimulation. Clin Nucl Med 24:319 – 322

Anderson T, Chabner B, Young R, et al. (1982) Malignant lymphomas: the histology and staging of 473 patients at the National Cancer Institute. Cancer 50:2699 – 2707

Armitage JO (1993) Treatment of non-Hodgkin's lymphoma. N Engl J Med 328:1023 – 1030

Armitage JO (1994) Bone marrow transplantation. N Engl J Med 330:827 – 838

Armitage JO, Weisenburger DD, Hutchins M, et al. (1986) Chemotherapy for diffuse large-cell lymphoma – rapidly responding patients have more durable remissions. J Clin Oncol 4:160 – 164

Bangerter M, Moog F, Buchmann I, et al. (1998) Whole-body 2-[18F]-fluoro-2-deoxy-D-glucose positron emission tomography (FDG-PET) for accurate staging of Hodgkin's disease. Ann Oncol 9:1117 – 1122

Bangerter M, Kotzerke J, Griesshammer M, Elsner K, Reske SN, Bergmann L (1999) Positron emission tomography with 18-fluorodeoxyglucose in the staging and follow-up of lymphoma in the chest. Acta Oncol 38:799 – 804

Bar-Shalom R, Mor M, Yefremov N, Goldsmith SJ (2001) The value of Ga-67 scintigraphy and F-18 fluorodeoxyglucose positron emission tomography in staging and monitoring the response of lymphoma to treatment. Semin Nucl Med 31:177 – 190

Bar-Shalom R, Yefremov N, Haim N, et al. (2003) Camera-based FDG PET and ^{67}Ga SPECT in evaluation of lymphoma: comparative study. Radiology 227:353 – 360

Bartold SP, Donohue KJ, Fletcher JW, et al. (1997) Procedure guideline for gallium scintigraphy in the evaluation of malignant disease. Bartold SP J Nucl Med 38:990 – 994

Bastion Y, Berger F, Bryon PA, Felman P, Ffrench M, Coiffier B (1991) Follicular lymphomas: assessment of prognostic factors in 127 patients followed for 10 years. Ann Oncol 2 Suppl 2:123 – 129

Becherer A, Mitterbauer M, Jaeger U, et al. (2002) Positron emission tomography with [18F]2-fluoro-D-2-deoxyglucose (FDG-PET) predicts relapse of malignant lymphoma after high-dose therapy with stem cell transplantation. Leukemia 16:260 – 267

Ben-Haim S, Bar-Shalom R, Israel O, et al. (1996) Utility of gallium-67 scintigraphy in low-grade non-Hodgkin's lymphoma. J Clin Oncol 14:1936 – 1942

Bogart JA, Chung CT, Mariados NF, Vermont AI, Lemke SM, Grethlein S, Graziano SL (1998) The value of gallium imaging after therapy for Hodgkin's disease. Cancer 82:754 – 759

Brandt L, Kimby E, Nygren P, Glimelius B (2001) A systematic overview of chemotherapy effects in Hodgkin's disease. Acta Oncol 40:185 – 197

Brascho DJ (1980) Hodgkin's disease and non-Hodgkin's lymphoma. In: Brasco DJ, Strawber TH (eds) Abdominal ultrasound in the cancer patient. Wiley, New York

Brincker H (1986) Sarcoid reactions in malignant tumors. Cancer Treat Rev 13:147 – 156

Buchmann I, Reinhardt M, Elsner K, et al. (2001) 2-(fluorine-18)fluoro-2-deoxy-D-glucose positron emission tomography in the detection and staging of malignant lymphoma. A bicenter trial. Cancer 91:889 – 999

Cabanillas F, Zornoza J, Haynie TP, et al. (1977) Comparison of

lymphangiograms and gallium scans in the non-Hodgkin's lymphomas. Cancer 39:85 – 88
Canellos GP (2004) Lymphoma: present and future challenges. Semin Hematol 41(4 Suppl 7):26 – 31
Carr R, Barrington SF, Madan B, O'Doherty MJ, Saunders CA, van der Walt J, Timothy AR (1998) Detection of lymphoma in bone marrow by whole-body positron emission tomography. Blood 91:3340 – 3346
Coiffier B, Gisselbrecht C, Vose JM, et al. (1991) Prognostic factors in aggressive malignant lymphomas. Description and validation of prognostic index that could identify patients requiring a more intensive therapy. J Clin Oncol 9:211 – 219
Cremerius U, Fabry U, Neuerburg J, Zimny M, Osieka R, Büll U (1998) Positron emission tomography with 18F-FDG to detect residual disease after therapy for malignant lymphoma. Nucl Med Commun 19:1055 – 1063
Cremerius U, Fabry U, Kroll U, Zimny M, Neuerburg J, Osieka R, Büll U (1999) Clinical value of FDG PET for therapy monitoring of malignant lymphoma – results of a retrospective study in 72 patients. Nuklearmedizin 38:24 – 30
Cremerius U, Fabry U, Wildberger JE, et al. (2002) Pre-transplant positron emission tomography using fluorine-18-fluoro-deoxyglucose predicts outcome in patients treated with high-dose chemotherapy and autologous stem cell transplantation for non-Hodgkin's lymphoma. Bone Marrow Transplant 30:103 – 111
Dadparvar S, Hussain R, Esteves F, et al. (2002) Thallium-201 imaging in evaluation of Hodgkin's disease. Cancer J 8: 469 – 475
Dalm VA, Hofland LJ, Mooy CM, et al. (2004) Somatostatin receptors in malignant lymphomas: targets for radiotherapy? J Nucl Med 45:8 – 16
de Hemricourt E, De Boeck K, Hilte F, et al. (2003) Sarcoidosis and sarcoid-like reaction following Hodgkin's disease. Report of two cases. Mol Imaging Biol 5:15 – 19
de Wit M, Bohuslavizki KH, Buchert, Bumann D, Clausen M, Hossfeld DK (2001) ^{18}FDG-PET following treatment as valid predictor for disease-free survival in Hodgkin's lymphoma. Ann Oncol 12:29 – 37
Del-Vecchio S, Ciarmiello A, Pace L, et al. (1997) Fractional retention of Tc-99m-Sestamibi as an index of P-glycoprotein expression in untreated breast cancer patients. J Nucl Med 38:1348 – 1351
DeVita VT, Jr, Canellos GP (1999) The lymphomas. Semin Hematol 36 (4 Suppl 7):84 – 94
Devizzi L, Maffioli L, Bonfante V, et al. (1997) Comparison of gallium scan, computed tomography, and magnetic resonance in patients with mediastinal Hodgkin's disease. Ann Oncol 8 Suppl 1:53 – 56
Diehl V, Sextro M, Franklin J, et al. (1999) Clinical presentation, course, and prognostic factors in lymphocyte-predominant Hodgkin's disease and lymphocyte-rich classical Hodgkin's disease: Report from the European Task Force on Lymphoma Project on Lymphocyte-Predominant Hodgkin's Disease. J Clin Oncol 17:776 – 783
Diehl V, Stein H, Hummel M, Zollinger R, Connors JM (2003) Hodgkin's lymphoma: biology and treatment strategies for primary, refractory, and relapsed disease. Hematology 225 – 247
Dittmann H, Sokler M, Kollmannsberger C, et al. (2001) Comparison of 18FDG-PET with CT scans in the evaluation of patients with residual and recurrent Hodgkin's lymphoma. Oncol Rep 8:1393 – 1399
Elgazzar AH, Fernandes-Ulloa M, Silberstein EB (1993) Tl-201 as a tumour-localizing agent: current status and future considerations. Nucl Med Commun 14:96 – 103
Elstrom R, Guan L, Baker G, et al. (2003) Utility of FDG-PET scanning in lymphoma by WHO classification. Blood 101: 3875 – 3876
Erez V, Kostakoglu L, Goldsmith SJ (2006) Superiority of F-18 FDG over Tl-201 SPECT in the evaluation of AIDS-associated brain lesions. J Nucl Med 47:238P
Ferdinand B, Gupta P, Kramer EL (2004) Spectrum of thymic uptake at 18F-FDG PET. Radiographics 24:1611 – 1616
Ferone D, Semino C, Boschetti M, Cascini GL, Minuto F, Lastoria S (2005) Initial staging of lymphoma with octreotide and other receptor imaging agents. Semin Nucl Med 35:176 – 85
Ferrucci JT (1998) Advances in abdominal MR imaging. Radiographics 18:1569 – 1586
Fonti R, Del Vecchio S, Zannetti A, et al. (2004) Functional imaging of multidrug resistant phenotype by 99mTc-MIBI scan in patients with multiple myeloma. Cancer Biother Radiopharm 19:165 – 170
Front D, Israel O, Epelbaum R, et al. (1990) Ga-67 SPECT before and after treatment of lymphoma. Radiology 175: 515 – 519
Front D, Ben-Haim S, Israel O, Epelbaum R, Haim N, Even-Sapir E, Kolodny GM, Robinson E (1992) Lymphoma. predictive value of Ga-67 scintigraphy after treatment. Radiology 182:359 – 363
Front D, Bar-Shalom R, Israel O (1997) The continuing clinical role of gallium 67 scintigraphy in the age of receptor imaging. Semin Nucl Med 27:68 – 74
Front D, Bar-Shalom R, Mor M, et al. (1999) Hodgkin's disease: prediction of outcome with ^{67}Ga scintigraphy after one cycle of chemotherapy. Radiology 210:487 – 491
Front D, Bar-Shalom R, Mor M, et al. (2000) Aggressive non-Hodgkin lymphoma: early prediction of outcome with ^{67}Ga scintigraphy. Radiology 214:253 – 257
Gasparini MD, Balzarini L, Castellani MR, et al. (1993) Current role of gallium scan and magnetic resonance imaging in the management of mediastinal Hodgkin lymphoma. Cancer 72:577 – 582
Gunay EC, Salanci BV, Barista I, Caner B (2004) Lung hilar Ga-67 uptake in patients with lymphoma following chemotherapy. Ann Nucl Med 18:391 – 397
Gundlapalli S, Ojha B, Mountz JM (2002) Granulocyte colony-stimulating factor: confounding F-18 FDG uptake in outpatient positron emission tomographic facilities for patients receiving ongoing treatment of lymphoma. Clin Nucl Med 27:140 – 141
Ha CS, Choe JG, Kong JS, Allen PK, Oh YK, Cox JD, Edmund E (2000) Agreement rates among single photon emission computed tomography using gallium-67, computed axial tomography and lymphangiography for Hodgkin's disease and correlation of image findings with clinical outcome. Cancer 89:1371 – 1379
Haioun C, Itti E, Rahmouni A, et al. (2005) [18F]fluoro-2-deoxy-D-glucose positron emission tomography (FDG-PET) in aggressive lymphoma: an early prognostic tool for predicting patient outcome. Blood 106:1376 – 1381
Harris N, Jaffe E, Diebold J, et al. (2000) The World Health Organization Classification of Hematological Malignancies Report of the Clinical Advisory Committee Meeting. Mod Pathol 13:193 – 207
Hasenclever D, Diehl V (1998) A prognostic score for advanced Hodgkin's disease. International Prognostic Factors Project on Advanced Hodgkin's Disease. N Engl J Med 339: 1506 – 1514
Haw R, Sawka CA, Franssen E, Berinstein HL (1994) Significance of a partial or slow response to front-line chemotherapy in the management of intermediate-grade or high-grade non-Hodgkin's lymphoma: a literature review. J Clin Oncol 12:1074 – 1084
Heald AE, Hoffman JM, Bartlett JA, Waskin HA (1996) Differentiation of central nervous system lesions in AIDS patients using positron emission tomography (PET). Int J STD AIDS 7:337 – 346

Hoane BR, Shields AF, Porter BA, et al. (1994) Comparison of initial lymphoma staging using computed tomography (CT) and magnetic resonance (MR) imaging. Am J Hematol 47:100 – 105

Hoffman JM, Waskin HA, Schifter T, et al. (1993) FDG-PET in differentiating lymphoma from non-malignant central nervous system lesions in patients with AIDS. J Nucl Med 34:567 – 575

Hoffmann M, Kletter K, Becherer A, et al. (2003) 18F-fluorodeoxyglucose positron emission tomography (18F-FDG-PET) for staging and follow-up of marginal zone B-cell lymphoma. Oncology 64:336 – 340

Hoh CK, Glaspy J, Rosen P, et al. (1997) Whole-body FDG-PET imaging for staging of Hodgkin's disease and lymphoma. J Nucl Med 38:343 – 348

Hsu CH, Sun SS, Kao CH, Lin CC, Lee CC (2002) Differentiation of low-grade gastric MALT lymphoma and high-grade gastric MALT lymphoma: the clinical value of Ga-67 citrate scintigraphy – a pilot study. Cancer Invest 20:939 – 943

Hueltenschmidt B, Sautter-Bihl ML, Lang O, et al. (2001) Whole body positron emission tomography in the treatment of Hodgkin disease. Cancer 91:302 – 10

Hussain R, Christie DR, Gebski V, Barton MB, Gruenewald SM (1998) The role of the gallium scan in primary extranodal lymphoma. J Nucl Med 39:95 – 98

Hutchings M, Loft A, Hansen M, et al. (2006a) FDG-PET after two cycles of chemotherapy predicts treatment failure and progression-free survival in Hodgkin lymphoma. Blood 107:52 – 59

Hutchings M, Loft A, Hansen M, Ralfkiaer E, Specht L (2006b) Different histopathological subtypes of Hodgkin lymphoma show significantly different levels of FDG uptake. Hematol Oncol [Epub ahead of print]

Ichiki Y, Bowlus CL, Shimoda S, Ishibashi H, Vierling JM, Gershwin ME (2006) T cell immunity and graft-versus-host disease (GVHD). Autoimmun Rev 5:1 – 9

Ionescu I, Brice P, Simon D, et al. (2000) Restaging with gallium scan identifies chemosensitive patients and predicts survival of poor-prognosis mediastinal Hodgkin's disease patients. Med Oncol 17:127 – 134. http://www.cancer.gov/cancertopics/types/non-hodgkins-lymphoma

Iranzo A, Marti-Fabregas J, Domingo P, et al. (1999) Absence of thallium-201 brain uptake in progressive multifocal leukoencephalopathy in AIDS patients. Acta Neurol Scand 100:102 – 105

Iskandrian AS, Heo J, Askenase A, Segal BL, Helfant RH (1987) Thallium imaging with single photon emission computed tomography. Am Heart J 114:852 – 865

Israel O, Mekel M, Bar-Shalom R, Epelbaum R, et al. (2002b) Bone lymphoma: ^{67}Ga scintigraphy and CT for prediction of outcome after treatment. J Nucl Med 43:1295 – 303

Israel O, Mor M, Epelbaum R, et al. (2002a) Clinical pretreatment risk factors and Ga-67 scintigraphy early during treatment for prediction of outcome of patients with aggressive non-Hodgkin lymphoma. Cancer 94:873 – 878

Jaffe E, Harris N, Diebold J, Muller-Hermelink H-K (1999) World Health Organization classification of neoplastic diseases of the hematopoietic and lymphoid tissues. A progress report. Am J Clin Pathol 111(Suppl 1):S8–S12

Janicek M, Kaplan W, Neuberg D, et al. (1997) Early restaging gallium scans predict outcome in poor-prognosis patients with aggressive non-Hodgkin's lymphoma treated with high-dose CHOP chemotherapy. J Clin Oncol 15:1631 – 1637

Jerusalem G, Beguin Y, Fassotte MF, Najjar F, Paulus P, Rigo P, Fillet G (1999a) Whole-body positron emission tomography using 18F-fluorodeoxyglucose for post-treatment evaluation in Hodgkin's disease and non-Hodgkin's lymphoma has higher diagnostic and prognostic value than classical computed tomography scan imaging. Blood 94:429 – 433

Jerusalem G, Warland V, Najjar F, Paulus P, Fassotte MF, Fillet G, Rigo P (1999b) Whole-body 18F-FDG PET for the evaluation of patients with Hodgkin's disease and non-Hodgkin's lymphoma. Nucl Med Commun 20:13 – 20

Jerusalem G, Beguin Y, Najjar F, Hustinx R, Fassotte MF, Rigo P, Fillet G (2001) Positron emission tomography (PET) with 18F-fluorodeoxyglucose (18F-FDG) for the staging of low-grade non-Hodgkin's lymphoma (NHL). Ann Oncol 12:825 – 830

Jerusalem G, Beguin Y, Fassotte MF, et al. (2003) Early detection of relapse by whole-body positron emission tomography in the follow-up of patients with Hodgkin's disease. Ann Oncol 14:123 – 130

Jerusalem G, Hustinx R, Beguin Y, Fillet G (2005) Evaluation of therapy for lymphoma. Semin Nucl Med 35:186 – 196

Johnston G, Benua RS, Teates CD, Edwards CL, Kniseley RM (1974) ^{67}Ga-citrate imaging in untreated Hodgkin's disease: preliminary report of Cooperative Group. J Nucl Med 15:399 – 403

Jung G, Heindel W, von Bergwelt-Baildon M, et al. (2000) Abdominal lymphoma staging: is MR imaging with T2-weighted turbo-spin-echo sequence a diagnostic alternative to contrast-enhanced spiral CT? J Comput Assist Tomogr 24:783 – 787

Kao CH, Tsai SC, Wang JJ, Ho YJ, Ho ST, Changlai SP (2001) Technetium-99m-sestamethoxyisobutylisonitrile scan as a predictor of chemotherapy response in malignant lymphomas compared with P-glycoprotein expression, multidrug resistance-related protein expression and other prognosis factors. Br J Haematol 113:369 – 374

Karam M, Novak L, Cyriac J, Ali A, Nazeer T, Nugent F (2006) Role of fluorine-18 fluoro-deoxyglucose positron emission tomography scan in the evaluation and follow-up of patients with low-grade lymphomas. Cancer 107:175 – 183

Kawano T, Suzuki A, Ishida A, et al. (2004) The clinical relevance of thymic fluorodeoxyglucose uptake in pediatric patients after chemotherapy. Eur J Nucl Med Mol Imaging 31:31 – 36

Koss MN (1995) Pulmonary lymphoid disorders. Semin Diagn Pathol 12:158 – 171

Kostakoglu L, Yeh SD, Portlock C, et al. (1992) Validation of gallium-67-citrate single-photon emission computed tomography in biopsy-confirmed residual Hodgkin's disease in the mediastinum. J Nucl Med 33:345 – 350

Kostakoglu L, Elahi N, Kiratli P, et al. (1997) Clinical validation of the influence of P-glycoprotein on Tc-99m-sestamibi uptake in malignant tumors. J Nucl Med 38:1003 – 1008

Kostakoglu L, Leonard JP, Kuji I, et al. (2002a) Comparison of fluorine-18 fluorodeoxyglucose positron emission tomography and Ga-67 scintigraphy in evaluation of lymphoma. Cancer 94:879 – 888

Kostakoglu L, Coleman M, Leonard JP, et al. (2002b) PET predicts prognosis after one cycle of chemotherapy in aggressive lymphoma and Hodgkin's disease. J Nucl Med 43:1018 – 1027

Kostakoglu L, Goldsmith SJ, Leonard JP, et al. (2006) FDG-PET after one cycle of chemotherapy accurately predicts response to therapy in large cell non-Hodgkin's lymphoma and Hodgkin's disease. Cancer (in press)

Larson SM, Rasey JS, Allen DR, Nelson NJ, Grunbaum Z, Harp GD, Williams DL (1980) Common pathway for tumor cell uptake of gallium-67 and iron-59 via a transferrin receptor. J Natl Cancer Inst 64:41 – 53

Lazarowski A, Dupont J, Fernandez J, et al. (2006) 99mTechnetium-sestamibi uptake in malignant lymphomas. Correlation with chemotherapy response. Lymphat Res Biol 4:23 – 28

Leners N, Jamar F, Fiasse R, Ferrant A, Pauwels S (1996) Indium-111-pentetreotide uptake in endocrine tumors and lymphoma. J Nucl Med 37:916 – 922

Liang JA, Shiau YC, Yang SN, Lin FJ, Kao A, Lee CC (2002) Prediction of chemotherapy response in untreated malignant lymphomas using technetium-99m methoxyisobutylisonitrile scan: comparison with P-glycoprotein expression and other prognostic factors. A preliminary report. Jpn J Clin Oncol 32(4):140 – 5

Lin J, Leung WT, Ho SKW, et al. (1995) Quantitative evaluation of thallium-201 uptake in predicting chemotherapeutic response of osteosarcoma. Eur J Nucl Med 22:553 – 555

Lipp RW, Silly H, Ranner G, et al. (1995) Radiolabeled octreotide for the demonstration of somatostatin receptors in malignant lymphoma and lymphadenopathy. J Nucl Med 36: 13 – 18

Lister TA, Crowther D, Sutcliffe SB, et al. (1989) Report of a committee convened to discuss the evaluation and staging of patients with Hodgkin's disease: Cotswolds meeting. J Clin Oncol 7:1630 – 1636

Lugtenburg PJ, Krenning EP, Valkema R, Oei HY, Lamberts SW, Eijkemans MJ, van Putten WL, Lowenberg B (2001) Somatostatin receptor scintigraphy useful in stage I–II Hodgkin's disease: more extended disease identified. Br J Haematol 112:936 – 944

Mainolfi C, Maurea S, Varrella P, Alaia C, Imparato C, Alfano B, Aate G, Bazzicalupo L (1998) Positron emission tomography with fluorine-18-deoxyglucose in the staging and control of patients with lymphoma. Comparison with clinico-radiologic assessment. Radiol Med 95:98 – 104

Mansberg R, Wadhwa SS, Mansberg V, et al. (1999) Tl-201 and Ga-67 scintigraphy in non-Hodgkin's lymphoma. Clin Nucl Med 24:239 – 242

Mclaughlin AF, Southee AE (1994) Gallium scintigraphy in tumor diagnosis and management. In: Murray IPC, Ell PJ (eds) Nuclear medicine in clinical diagnosis and treatment, vol 1. Churchill Livingstone, New York, pp 711 – 727

Menzel C, Dobert N, Mitrou P, Mose S, Diehl M, Berner U (2002) Positron emission tomography for the staging of Hodgkin's lymphoma. Acta Oncol 41:430 – 436

Mikhaeel NG, Timothy AR, O'Doherty MJ, Hain S, Maisey MN (2000) 18-FDG-PET as a prognostic indicator in the treatment of aggressive non-Hodgkin's lymphoma – comparison with CT. Leuk Lymphoma 39:543 – 553

Mikhaeel NG, Mainwaring P, Nunan T, Timothy AR (2002) Prognostic value of interim and post treatment FDG-PET scanning in Hodgkin lymphoma [abstract]. Ann Oncol 13 (Suppl 2):21

Moog F, Bangerter M, Diederichs CG, Guhlmann A, Kotzerke J, Merkle E (1997) Lymphoma: role of FDG-PET in nodal staging. Radiology 203:795 – 800

Moog F, Bangerter M, Diederichs CG, Guhlmann A, Merkle E, Frickhofen N, Reske SN (1998) Extranodal malignant lymphoma: detection with FDG PET versus CT. Radiology 206:475 – 481

Murphy SP, Nathan MA, Karwal MW (1997) FDG-PET appearance of pelvic Castleman's disease. J Nucl Med 38:1211 – 1212

Nathwani B, Anderson JR, Armitage JO, et al. (1999) Marginal zone B-cell lymphoma: A clinical comparison of nodal and mucosa-associated lymphoid tissue types. J Clin Oncol 17: 2486 – 2492

National Cancer Institute (1982) National Cancer Institute sponsored study of classifications of non-Hodgkin's lymphomas: summary and description of a working formulation for clinical usage. The Non-Hodgkin's Lymphoma Pathologic Classification Project. Cancer 49:2112 – 2135

Naumann R, Vaic A, Beuthien-Baumann B, et al. (2001) Prognostic value of positron emission tomography in the evaluation of post-treatment residual mass in patients with Hodgkin's disease and non-Hodgkin's lymphoma. Br J Haematol 115:793 – 800

Naumann R, Beuthien-Baumann B, Reiss A, Schulze J, Hanel A, Bredow J (2004) Substantial impact of FDG-PET imaging on the therapy decision in patients with early-stage Hodgkin's lymphoma. Br J Cancer 90:620 – 625

Nejmeddine F, Caillat-Vigneron N, Escaig F, Moretti JL, Raphael M, Galle P (1998) Mechanism involved in gallium-67 (Ga-67) uptake by human lymphoid cell lines. Cell Mol Biol 44:1215 – 1220

Ng AK, Bernardo MV, Weller E, et al. (2002) Second malignancy after Hodgkin disease treated with radiation therapy with or without chemotherapy: long-term risks and risk factors. Blood 100:1989 – 1996

Nikpoor N, Aliabadi P, Diaz L, Mannting F (2000) Long-term follow-up of residual mediastinal-hilar Ga-67 uptake after treatment for Hodgkin's and non-Hodgkin's lymphomas: what degree of Ga-67 uptake is significant? Clin Nucl Med 25:959 – 962

Nishiyama Y, Yamamoto Y, Toyama Y, Satoh K, Nagai M, Ohkawa M (2003) Usefulness of ^{67}Ga scintigraphy in extranodal malignant lymphoma patients. Ann Nucl Med 17:657 – 662

Ohta M, Isobe K, Kuyama J, et al. (2001) Clinical role of Tc-99m-MIBI scintigraphy in non-Hodgkin's lymphoma. Oncol Rep 8:841 – 845

Palumbo B, Sivolella S, Palumbo I, Liberati AM, Palumbo R (2005) ^{67}Ga-SPECT/CT with a hybrid system in the clinical management of lymphoma. Eur J Nucl Med Mol Imaging 32:1011 – 1017

Park YH, Choi SJ, Ryoo BY, Kim HT (2005) PET imaging with F-18 fluorodeoxyglucose for primary lymphoma of bone. Clin Nucl Med 30:131 – 134

Partridge S, Timothy A, O'Doherty MJ, et al. (2000) 2-Fluorine-18-fluoro-2-deoxy-D glucose positron emission tomography in the pretreatment staging of Hodgkin's disease: Influence on patient management in a single institution. Ann Oncol 11:1273 – 1279

Philip T, Guglielmi C, Hagenbeek A, et al. (1995) Autologous bone marrow transplantation as compared with salvage chemotherapy in relapses of chemotherapy-sensitive non-Hodgkin's lymphoma. N Engl J Med 333:1540 – 1545

Piwnica-Worms D, Rao VV, Kronauge JF, Croop JM (1995) Characterization of multidrug resistance P-glycoprotein transport function with an organotechnetium cation. Biochemistry 34:12210 – 20

Reddy MP, Graham MM (2003) FDG positron emission tomographic imaging of thoracic Castleman's disease. Clin Nucl Med 28:325 – 326

Rehm PK (2001) Radionuclide evaluation of patients with lymphoma. Radiol Clin North Am 39:957 – 978

Reubi JC, Macke HR, Krenning EP (2005) Candidates for peptide receptor radiotherapy today and in the future. J Nucl Med 46 Suppl 1:67S–75S

Rini JN, Manalili EY, Hoffman MA, Karayalcin G, Mehrotra B, Tomas MB, Palestro CJ (2002) F-18 FDG versus Ga-67 for detecting splenic involvement in Hodgkin's disease. Clin Nucl Med 27:572 – 577

Roach PJ, Cooper RA, Arthur CK, Ravich RB (1998) Comparison of thallium-201 and gallium-67 scintigraphy in the evaluation of non-Hodgkin's lymphoma. Aust N Z J Med 28:33 – 38

Rodriguez M, Ahlstrom H, Sundin A, Rehn S, Sundstrom C, Hagberg H, Glimelius B (1997) 18F FDG PET in gastric non-Hodgkin's lymphoma. Acta Oncol 36:577 – 584

Rosenberg S (1977) Validity of the Ann Arbor staging system classification for the non-Hodgkin's lymphomas. Cancer Treat Rep 61:1023 – 1027

Salloum E, Brandt DS, Caride VJ, et al. (1997) Gallium scans in the management of patients with Hodgkin's disease: a study of 101 patients. J Clin Oncol 15:518 – 527

Schaefer NG, Hany TF, Taverna C, Seifert B, Stumpe KD, von Schulthess GK, Goerres GW (2004) Non-Hodgkin lymphoma and Hodgkin disease: coregistered FDG PET and CT at staging and restaging – do we need contrast-enhanced CT? Radiology 232:823 – 829

Schoder H, Meta J, Yap C, et al. (2001) Effect of whole-body (18)F-FDG PET imaging on clinical staging and management of patients with malignant lymphoma. J Nucl Med 42:1139 – 1143

Schoder H, Noy A, Gonen M, Weng L, Green D, Erdi YE, Larson SM, Yeung HW (2005) Intensity of 18fluorodeoxyglucose uptake in positron emission tomography distinguishes between indolent and aggressive non-Hodgkin's lymphoma. J Clin Oncol 23:4643 – 4651

Schot BW, Pruim J, van Imhoff GW, Sluiter WJ, Vaalburg W, Vellenga E (2006) The role of serial pre-transplantation positron emission tomography in predicting progressive disease in relapsed lymphoma. Haematologica 91:490 – 495

Setoin FJ, Pons F, Herranz R, et al. (1997) Ga-67 scintigraphy for the evaluation of recurrences and residual masses in patients with lymphoma. Nucl Med Commun 18:405 – 411

Shipp M, Mauch PM, Harris NL (1997) Non-Hodgkin's lymphomas. In: Devita VT, Hellman S, Rosenberg SA (eds) Cancer principles and practice of oncology. Lippincott, Philadelphia, PA, pp 2165 – 2220

Shrikanthan S, Zhuang HM, Schuster S, Alavi A (2004) FDG-PET imaging in diagnosis of mantle cell lymphoma. J Nucl Med 45:93P

Skiest DJ, Erdman W, Chang WE, Oz OK, Ware A, Fleckenstein J (2000) SPECT thallium-201 combined with *Toxoplasma* serology for the presumptive diagnosis of focal central nervous system mass lesions in patients with AIDS. J Infect 40:274 – 281

Song HC, Lee JJ, Bom HS, Chung IJ, Kim HJ, Park YK, Kim EE (2003) Double-phase Tc-99m MIBI scintigraphy as a therapeutic predictor in patients with non-Hodgkin's lymphoma. Clin Nucl Med 28:457 – 462

Spaepen K, Stroobants S, Dupont P, et al. (2001) Prognostic value of positron emission tomography (PET) with fluorine-18 fluorodeoxyglucose ([^{18}F]FDG after first line chemotherapy in non-Hodgkins lymphoma: Is ([^{18}F]FDG PET a valid alternative to conventional diagnostic methods? J Clin Oncol 19:414 – 419

Spaepen K, Stroobants S, Dupont P, et al. (2002) Early restaging positron emission tomography with 18F-fluorodeoxyglucose predicts outcome in patients with aggressive non-Hodgkin's lymphoma. Ann Oncol 13:1356 – 1363

Spaepen K, Stroobants S, Dupont P, et al. (2003) [(18)F]FDG PET monitoring of tumour response to chemotherapy: does [(18)F]FDG uptake correlate with the viable tumour cell fraction? Eur J Nucl Med Mol Imaging 30:682 – 688

Stroszczynski C, Amthauer H, Hosten N, et al. (1997) Use of Ga-67 SPECT in patients with malignant lymphoma after primary chemotherapy for further treatment planning: comparison with spiral CT. Rofo Fortschr Geb Rontgenstr Neuen Bildgeb Verfahr 167:458 – 466

Stumpe KD, Urbinelli M, Steinert HC, Glanzmann C, Buck A, von Schulthess GK (1998) Whole-body positron emission tomography using fluorodeoxyglucose for staging of lymphoma: effectiveness and comparison with computed tomography. Eur J Nucl Med 25:721 – 728

Talcott JA, Garnick MB, Stomper PC, et al. (1987) Cavitary lung nodules associated with combination chemotherapy containing bleomycin. J Urol 138: 619 – 620

The International Non-Hodgkin's Lymphoma Prognostic Factors Project (1993) A predictive model for aggressive non-Hodgkin's lymphoma. N Engl J Med 329:987 – 994

The Non-Hodgkin's Lymphoma Classification Project (1997) A clinical evaluation of the International Lymphoma Study Group Classification of Non-Hodgkin's Lymphoma. Blood 89:3909 – 3918

Thill R, Neuerburg J, Fabry U, et al. (1997) Comparison of findings with 18-FDG PET and CT in pretherapeutic staging of malignant lymphoma. Nuklearmedizin 36:234 – 239

Tubiana M, Henry-Amar M, Carde P, et al. (1989) Toward comprehensive management tailored to prognostic factors of patients with clinical stage I and II in Hodgkin's disease. The EORTC lymphoma group controlled trials. Blood 73:47 – 56

Turner DA, Fordham EW, Ali A, et al. (1978) Gallium-67 imaging in the management of Hodgkin's disease and other malignant lymphomas. Semin Nucl Med 8:205 – 218

Vallabhajosula S, Goldsmith SJ, Lipszyc H, Chahinian AP, Ohnuma T (1983) ^{67}Ga-transferrin and ^{67}Ga-lactoferrin binding to tumor cells: specific versus nonspecific glycoprotein-cell interaction. Eur J Nucl Med 8:354 – 357

Van Hagen PM, Krenning EP, Reubi JC, et al. (1993) Somatostatin analogue scintigraphy of malignant lymphomas. Br J Haematol 83:75 – 79

Verdonck LF, van Putten WL, Hagenbeek A, Schouten HC, et al. (1995) Comparison of CHOP chemotherapy with autologous bone marrow transplantation for slowly responding patients with aggressive non-Hodgkin's lymphoma. N Engl J Med 332:1045 – 1051

Vose JM, Bierman PJ, Anderson JR, et al. (1996) Single-photon emission computed tomography gallium imaging versus computed tomography: predictive value in patients undergoing high-dose chemotherapy and autologous stem-cell transplantation for non-Hodgkin's lymphoma. J Clin Oncol 14:2473 – 2479

Waxman AD (1991) Thallium 201 in nuclear oncology. In: Freeman LM (ed) Nuclear medicine annual. Raven, New York, p 193

Waxman AD, Eller D, Ashook G, et al. (1996) Comparison of gallium-67-citrate and thallium-201 scintigraphy in peripheral and intrathoracic lymphoma. J Nucl Med 37:46 – 50

Weihrauch MR, Re D, Scheidhauer K, et al. (2001) Thoracic positron emission tomography using 18F-fluorodeoxyglucose for the evaluation of residual mediastinal Hodgkin's disease. Blood 98:2930 – 2934

Weihrauch MR, Re D, Bischoff S, Dietlein M, Scheidhauer K, Krug B (2002) Whole-body positron emission tomography using 18F-fluorodeoxyglucose for initial staging of patients with Hodgkin's disease. Ann Hematol 81:20 – 25

Weinblatt ME, Zanzi I, Belakhlef A, Babchyck B, Kochen J (1997) False-positive FDG-PET imaging of the thymus of a child with Hodgkin's disease. J Nucl Med 38:888 – 890

Weiner RE, Thakur ML (2005) Radiolabeled peptides in oncology: role in diagnosis and treatment. Biodrugs 19:145 – 163

Wiedmann E, Baican B, Hertel A, et al. (1999) Positron emission tomography (PET) for staging and evaluation of response to treatment in patients with Hodgkin's disease. Leuk Lymphoma 34:545 – 551

Wirth A, Seymour JF, Hicks RJ, et al. (2002) Fluorine-18 fluorodeoxyglucose positron emission tomography, gallium-67 scintigraphy, and conventional staging for Hodgkin's disease and non-Hodgkin's lymphoma. Am J Med 112:262 – 268

Zijlstra JM, Lindauer-van der Werf G, Hoekstra OS, Hooft L, Riphagen II, Huijgens PC (2006) 18F-fluoro-deoxyglucose positron emission tomography for post-treatment evaluation of malignant lymphoma: a systematic review. Haematologica 9:522 – 529

Zinzani PL, Magagnoli M, Chierichetti F, et al. (1999) The role of positron emission tomography (PET) in the management of lymphoma patients. Ann Oncol 10:1181 – 1184

Zornoza J, Ginaldi S (1981) Computed tomography in hepatic lymphoma. Radiology 138:405 – 410

Scintigraphic Detection of Infection and Inflammation

17

C.P. Bleeker-Rovers, F.J. Vos, F.H.M. Corstens

17.1 Brief Introduction and Historical Perspective

Nuclear medicine techniques have a lot to offer in visualization of infectious and inflammatory foci. Quite often these techniques do not lead immediately to a definitive diagnosis, i.e., a histological or a microbiological diagnosis. However, they point to parts in the body where a particular metabolic process is ongoing, leading to elevated uptake of a radiopharmaceutical. With the help of other techniques, such as puncture, biopsy and culture, a definitive diagnosis can be obtained. In other words, scintigraphic imaging helps to elucidate the cause of the disease, and facilitates prompt installation of a tailored therapeutic regimen. Furthermore, with these techniques it is possible to monitor the effect of therapy.

There are several reasons why imaging of infection and inflammation will become increasingly important in the next decade. The population is ageing, and the application of implants and transplants is increasing. The number of immune compromised patients is growing, mainly because of frequent use of chemotherapeutic agents leading to neutropenia. Furthermore, the increased use of antibiotics is leading to insensitivity for some of these pharmaceuticals.

At present inflammation is defined as the reaction of tissue to any injury, aiming at bringing serum molecules and cells of the immune system to the area where the injury takes place. Infection is defined as any injury caused by microorganisms. The injury leading to inflammation can vary from trauma, to ischemia, to neoplasm, and can be caused by infectious agents such as bacteria, viruses, fungi and parasites, but also by foreign particles, such as in asbestosis.

Injury induces the production of inflammatory mediators, being either vasoactive or chemotactic. Vasoactive mediators lead to increased vascular permeability, with edema and efflux of components from the intravascular to the extravascular space. Chemotactic mediators induce recruitment and stimulation of inflammatory cells, being mainly granulocytes in acute inflammation, while microphages and lymphocytes are predominant in chronic types of inflammation. For the

Table 17.1. Overview of characteristics of radiopharmaceuticals used for imaging inflammatory processes

Physiological characteristics	Targeting mechanism	Tracer class	Radiolabeled compound
Enhanced vascular permeability	Non-specific uptake		^{67}Ga-citrate Non-specific immunoglobulins
Endothelial activation	Antigen binding	Antibodies	F(ab')$_2$-anti-E-selectin
Enhanced influx of granulocytes	Granulocyte influx		Radiolabeled granulocytes
	Antigen binding	Antibodies	Anti-NCA-95 IgG: BW 250/183 Anti-SSEA-1 IgM: LeuTech Anti-NCA-90 Fab': sulesomab, LeukoScan
	Receptor binding	Cytokines	IL-8
Enhanced influx of mononuclear cells	Receptor binding	Cytokines	IL-2
Presence of microorganisms	Affinity for microorganisms	Antimicrobial agents	Ciprofloxacin: Infecton
Increased metabolic requirements	Enhanced glucose uptake		FDG

purpose of scintigraphic imaging of inflammation and infection, various pathways can be used (Table 17.1). Non-specific radiolabeled compounds show increased extravasation at the site of inflammation by utilizing the locally enhanced vascular permeability. Examples are ^{67}Ga-citrate and radiolabeled non-specific immunoglobulins. The second approach to imaging inflammation is to utilize the influx of leukocytes, either by radiolabeling the patient's leukocytes ex vivo or by directly targeting leukocyte antigens or receptors in vivo via administration of radiolabeled antigranulocyte monoclonal antibodies or receptor-binding ligands (chemotactic peptides, cytokines and complement factors). Most of these radiolabeled compounds preferentially bind to granulocytes and are thus most suitable in conditions with a large influx of granulocytes such as in acute inflammatory and infectious processes. Radiolabeled interleukin-2 (IL-2) is suitable for imaging chronic inflammatory processes, because the IL-2 receptor is preferentially expressed on T-lymphocytes. Alternatively, imaging of activated endothelium is possible and this involves targeting activated endothelial adhesion molecules, for example anti-E-selectin. The mechanism of ^{18}F-fluorodeoxyglucose (FDG) uptake in inflammatory cells is related to leukocytes using glucose as an energy source only after activation during the metabolic burst. The accumulation of FDG in cells with increased glucose metabolism is specific. Increased glucose metabolism, however, is also present in malignant cells, so FDG uptake is not specific for inflammatory processes as such. A new class of radiolabeled compounds consists of radiolabeled antibiotics and microbial peptides, which directly bind to microorganisms. The specific nature of uptake of these radiolabeled compounds in inflammatory processes is still a matter of debate, however.

In the context of the design of ideal radiopharmaceuticals for the imaging of infection and inflammation, it is desirable to formulate a wishlist of desiderata. The radiopharmaceutical should be taken up rapidly and well retained at the site of inflammation/infection, together with a quick wash-out from the background, in order to achieve a good target to background ratio (contrast). Uptake in normal organs such as liver, spleen, bone, bone marrow, gastrointestinal tract and kidneys should be low. The preparation of the radiopharmaceutical should be quick and easy, preferably with technetium-99m as the radionuclide. For a diagnostic agent it is obvious that there should be no toxicity and also no immune response after administration of the radiopharmaceutical. It would be most helpful to have a radiopharmaceutical that allows discrimination between infection and sterile inflammation. Unfortunately we have to face the fact that none of the currently used agents for the scintigraphic detection and localization of infection/inflammation meets all of the desiderata as listed above. So, there is the need to develop new and better agents. In order to be able to differentiate between normal and abnormal appearances on scintigraphic images it is important to understand the mechanisms of uptake of individual radiopharmaceuticals in normal and in diseased tissues and organs. Such understanding makes it possible to select the most appropriate radiopharmaceutical in a particular disease entity.

This chapter focuses in Sect. 17.2 on well-established and widely available radiopharmaceuticals as well as on "new" radiolabeled compounds in which human data are available. Section 17.3 is dedicated to the value of FDG PET in the diagnosis of infectious and inflammatory processes.

17.2 Single Photon Radiopharmaceuticals for Imaging Infectious and Inflammatory Processes

17.2.1 Non-specific Radiolabeled Compounds

17.2.1.1 ^{67}Ga-citrate

After injection, ^{67}Ga-citrate accumulates as an iron analogue through binding to circulating transferrin. This complex extravasates at the site of inflammation due to locally enhanced vascular permeability. In the inflamed tissue, ^{67}Ga is transferred to lactoferrin that is locally excreted by leukocytes or to siderophores produced by microorganisms. Physiologically 10 – 25 % of the radionuclide is excreted via the kidneys during the first 24 h. After 24 h the principal route of excretion is hepatobiliary. After 48 h about 75 % of the injected dose remains in the body and is equally distributed among the liver, bone, bone marrow and soft tissues. ^{67}Ga-citrate has been used extensively in clinical practice in several pathological conditions demonstrating high sensitivity for both acute and chronic infection and non-infectious inflammation. There are several shortcomings that limit its clinical application, however. Specificity is poor due to the physiological bowel excretion and accumulation in malignant tissues and in areas of bone modeling. In addition, the radiopharmaceutical has unfavorable imaging characteristics such as a long physical half-life (78 h) and multiple high-energy gamma radiation (93 – 889 keV), causing high radiation absorbed doses. Moreover, optimal imaging often requires delayed imaging up to 72 h after injection. These unfavorable characteristics and the development of newer radiopharmaceuticals have resulted in replacement of ^{67}Ga-citrate scintigraphy in the majority of inflammatory conditions by scintigraphy with labeled leukocytes. Leukocyte scanning, however, is of

limited value in patients with suspected vertebral osteomyelitis. Sequential gallium imaging appears to be a better way to diagnose this condition. Also, in immunocompromised patients, ^{67}Ga-citrate imaging is the procedure of choice for detecting opportunistic respiratory tract infections. Finally, ^{67}Ga-citrate scintigraphy is still the gold standard for radionuclide imaging in patients with fever of unknown origin (FUO), where it is able to detect both acute and chronic inflammatory conditions and neoplasms (Palestro 1994). However, its limited specificity and the generally unfavorable characteristics when compared to FDG PET will in patients with FUO most probably result in the near future in replacement of this technique by FDG PET.

17.2.1.2 Non-specific Immunoglobulins

Initially it was thought that human polyclonal immunoglobulin (HIG) was retained in inflammatory processes by interaction with Fc-γ receptors expressed on infiltrating leukocytes. Later it was shown, however, that radiolabeled HIG accumulates primarily in inflammatory foci by non-specific extravasation due to locally enhanced vascular permeability. HIG has been labeled with ^{111}In and ^{99m}Tc for clinical use. Disadvantages of the use of ^{111}In are a relatively high radiation burden, suboptimal gamma radiation for in vivo imaging, often limited availability and high costs. ^{99m}Tc is a more attractive alternative in most cases because of its short half-life (6 h), availability and lower costs. Both agents have slow blood clearance and physiological uptake in the liver and spleen. A general limitation is the long time span of 24 h between injection and diagnosis. In a comparative study, it was shown that ^{99m}Tc-HIG labeled using hydrazinonicotinamide (HYNIC) as the chelator, has in vivo characteristics highly similar to those of ^{111}In-HIG. In most cases it appeared to be suited to replace the ^{111}In-labeled compound. ^{99m}Tc-HIG imaging, however, has more limited sensitivity than ^{111}In-HIG scintigraphy in chest disease and in chronic inflammatory processes. Direct comparison of ^{111}In-HIG and ^{111}In-leukocytes patients with various subacute infections showed a slightly, but significantly better, overall accuracy of ^{111}In-HIG scintigraphy (Oyen et al. 1991). The major indication for imaging with raiolabeled HIG seems to be localization of acute infection or inflammation of the musculoskeletal system (Nijhof et al. 1997). Furthermore ^{99m}Tc-HIG scintigraphy appears to be an effective method for monitoring of disease activity in patients with rheumatoid arthritis (Liberatore et al. 1992). In addition, ^{111}In-HIG scintigraphy is clinically useful in pulmonary infection, particularly in immunocompromised patients (Oyen et al. 1992). In conclusion, ^{111}In- or ^{99m}Tc-HIG scintigraphy can be successfully used in various infectious and inflammatory diseases with a diagnostic accuracy comparable to that of radiolabeled leukocytes. When facilities for labeling leukocytes are not available or in severely granulocytic patients, HIG scintigraphy can be a good alternative for radiolabeled leukocytes. However, commercial kits are not available, impeding its general use in most clinics.

17.2.1.3 Limitations of Non-specific Radiolabeled Compounds in Infection/Inflammation Imaging

Although infectious and inflammatory processes can be visualized with radiolabeled compounds without a specific interaction between the agent and a tissue component in the inflammatory focus, this method has several limitations. Extravasation of molecules via diffusion is a slow process requiring prolonged high blood levels to allow for sufficient accumulation in the target tissue. High blood levels, however, entail relatively high background levels, especially in well-perfused tissues. Furthermore, in chronic inflammatory processes the vascular permeability tends to normalize. Finally, because non-specific radiolabeled compounds accumulate as a result of a common feature of infection and inflammation, these agents cannot distinguish between infection and inflammation. It must be emphasized, however, that all radiolabeled compounds accumulate to some extent in this non-specific way in inflammatory foci. This mechanism is of particular importance in evaluating new radiolabeled compounds, because non-specific accumulation can be erroneously interpreted as being specific.

17.2.2 More Specific Radiolabeled Compounds

17.2.2.1 Imaging of Endothelial Cell Activation

Anti-E-selectin Antibodies and Antibody Fragments

E-selectin is an endothelial adhesion molecule exclusively expressed on the luminal surface of activated endothelial cells and capable of binding to different populations of leukocytes. The endothelial expression of E-selectin is stimulated by interleukin-1 (IL-1), tumor necrosis factor α, and bacterial lipopolysaccharide. A $F(ab')_2$ antibody fragment, derived from an anti-E-selectin monoclonal antibody (Mab), has been synthesized and labeled with ^{111}In. Uptake of ^{111}In-$F(ab')_2$-anti-E-selectin was demonstrated in the inflamed joints of patients with rheumatoid arthritis. Compared with ^{111}In-HIG, ^{111}In-$F(ab')_2$-anti-E-selectin provided superior images in these patients (Chapman et al. 1996). Imaging with ^{111}In-$F(ab)_2$-anti-E-selectin also identified areas of inflammation in Crohn's disease and ulcerative colitis, concordant with the results of ^{99m}Tc-leukocyte

scanning (Bhatti et al. 1998). More recently, diagnostic accuracy of ^{99m}Tc-F(ab')$_2$-anti-E-selectin proved to be comparable to ^{111}In-F(ab')$_2$-anti-E-selectin and higher than diagnostic accuracy of conventional bone scanning in patients with rheumatoid arthritis (Jamar et al. 2002). Another study from the same group showed that imaging with ^{111}In-anti-E-selectin-Mab is also a sensitive method for assessment of disease activity in patients with rheumatoid arthritis and that targeting is more intense and specific than using ^{99m}Tc-HIG.

17.2.2.2 Imaging of Infiltrating Granulocytes

Radiolabeled Leukocytes

Imaging using ex vivo labeled autologous leukocytes was developed in the 1970s by McAfee and Thakur. A blood sample of approximately 50 ml is collected and leukocytes are separated in vitro from red blood cells. These leukocytes are then labeled with radioactive isotopes (^{111}In or ^{99m}Tc) and reinjected. Using standard labeling procedures, only a few granulocytes are damaged by labeling, whereas most lymphocytes are mutilated. The damaged cells are rapidly cleared from the circulation after reinjection. After intravenous administration, the radiolabeled leukocytes initially sequestrate in the lungs with subsequent rapid clearance from the (normal) lungs. The radiolabel rapidly clears from the blood and in most cases uptake in granulocytic infiltrates is high while a substantial portion of the leukocytes accumulate in the spleen and the liver. Autologous leukocytes can be labeled with ^{111}In using oxine. The use of HMPAO, a lipophilic chelator, allows for efficient labeling of white blood cells with ^{99m}Tc. In contrast to ^{111}In-oxine, some of the ^{99m}Tc-HMPAO is released from the leukocytes after injection and subsequently excreted via the kidneys (within minutes) and the hepatobiliary system (after several hours). ^{99m}Tc-labeled leukocytes have replaced ^{111}In-labeled leukocytes for most indications, because of the more optimal radiation characteristics. As a result of the biodistribution of ^{99m}Tc-HMPAO-labeled leukocytes, the use of ^{111}In-labeled leukocytes is preferred for evaluation of the kidneys, bladder and gallbladder. ^{111}In-labeled leukocytes are also preferred if late images are needed as in chronic infection. Radiolabeled leukocytes do provide a good diagnostic accuracy. The preparation of this radiopharmaceutical, however, is laborious: isolating and labeling a patient's white blood cells takes a well-trained technician 2 – 3 h. In addition, the need to handle potentially contaminated blood can result in transmission of blood-borne pathogens, such as hepatitis virus and human immunodeficiency virus, to technicians or patients. The principal clinical indications for radiolabeled leukocytes include inflammatory bowel disease, osteomyelitis, follow-up of patients with infections of vascular or orthopedic prostheses and soft tissue infections (Peters 1994). There has always been concern that chronic infections could be missed using radiolabeled leukocytes, because these infections generate a smaller granulocyte response compared to acute infections. However, a study in 155 patients demonstrated that sensitivity of labeled leukocytes for detection of acute infections (90 %) was not significantly different from sensitivity for detection of chronic infections (86 %) (Datz and Thorne 1986).

Anti-granulocyte Antibodies and Antibody Fragments

Ever since it became clear that infectious and inflammatory foci could be visualized by radiolabeled autologous leukocytes, investigators have tried to develop a method aiming to label white blood cells in vivo. The use of radiolabeled monoclonal antibodies against surface antigens as present on granulocytes has the advantage that labeling procedures are easier and do not require handling of potentially contaminated blood. Disadvantages of the use of Mab, however, are the high molecular weight, resulting in slow diffusion into sites of inflammation, a long plasma half-life and uptake in the liver due to clearance by the reticuloendothelial system. A long interval is often required between administration of radiolabeled antibodies and acquisition of images in order to improve target-to-background ratios. Use of Mab of murine origin sometimes induces production of human antimouse antibodies (HAMA), which can lead to allergic reactions and altered pharmacokinetics when repeated injections are given. This is, of course, a major limitation for follow-up studies. The use of antibody fragments (Fab' or F(ab')$_2$) or humanization of the antibodies could overcome most of these limitations. Theoretically, immunogenicity will be lower, blood clearance will be faster and accumulation in inflammatory foci will be higher. Moreover, since Fab' antibody fragments have an intrinsic lower affinity for the epitope, bone marrow uptake is lower, which is an advantage for imaging of infections of the central skeleton. Although radiolabeled anti-granulocyte antibodies and antibody fragments are generally looked at as radiolabeled compounds for specific targeting of infiltrating granulocytes, recent studies have demonstrated that they localize in infectious processes to a large extent by non-specific extravasation due to locally enhanced vascular permeability. Binding of the antibodies to infiltrating leukocytes may contribute to the retention of the radiolabel in the inflammatory focus.

Anti-Non-specific-Cross-reacting Antigen-95. One of the most widely used anti-granulocyte antibodies is the commercially available murine anti-NCA-95 IgG

(BW 250/183), labeled with ^{99m}Tc. This antibody recognizes the non-specific cross-reacting antigen 95 (NCA-95) expressed on human granulocytes and (pro)myelocytes. It has been used successfully for imaging of various infectious and inflammatory processes including subacute infectious endocarditis (Morguet et al. 1994), lung abscesses (Peltier et al. 1993), septic loosening of hip and knee prostheses (Boubaker et al. 1995; Klett et al. 2003) and diabetic foot infections (Dominguez-Gadea et al. 1993). Peripheral bone infections were also adequately visualized (Peltier et al. 1993), but sensitivity decreased in cases where the focus was located closer to the spine because of physiological bone marrow uptake, so imaging with ^{99m}Tc-anti-NCA-95 is less suitable for diagnosing vertebral osteomyelitis. Pulmonary infections other than abscesses were not visualized (Peltier et al. 1993). ^{99m}Tc-anti-NCA-95 scanning appeared to be a safe and reliable method for detecting infectious foci in neonates and infants with fever of unknown origin (Gratz et al. 1998). The preparation was also used in the evaluation of patients with inflammatory bowel disease, but it appeared to be less accurate than radiolabeled leukocytes partly due to non-specific bowel uptake (Gyorke et al. 2000; Papos et al. 1996). Due to the relatively slow blood clearance, imaging 24 h after injection is generally necessary for correct localization of the inflammatory process. The major drawback of radiolabeled anti-NCA-95, however, is the production of HAMA after the first injection.

Anti-Stage Specific Embryonic Antigen-1. Another Mab, anti-stage specific embryonic antigen-1 (anti-SSEA-1) IgM (LeuTech), recognizes CD15 antigens on granulocytes with high affinity ($K_d = 10^{-11}$ mol/l). The in vivo binding exceeds 50 %, suggesting involvement of more specific accumulation in inflammatory sites, such as in vivo migration of leukocytes from the circulation to the focus. ^{99m}Tc-anti-SSEA-1 IgM was successfully used in patients with various inflammatory and infectious diseases, such as osteomyelitis, diabetic foot ulcers and post-surgical infection (Thakur et al. 2001) with similar diagnostic accuracy when compared to radiolabeled leukocytes. Imaging with ^{99m}Tc-anti-SSEA-1 IgM also proved to be a highly sensitive test for detection of appendicitis in equivocal cases (Kipper et al. 2000). ^{99m}Tc-anti-SSEA-1 IgM is a convenient radiolabeled compound (imaging after 1 h, easy preparation) and no HAMA production has been found. Disadvantages are high liver uptake and transient mild neutropenia that has been observed after ^{99m}Tc-anti-SSEA-1 injection in several patients. This adverse effect can also be caused by other Mabs as well as some cytokines. In most cases, however, this does not represent a clinical problem and does not impair image quality.

Anti-Non-specific-Cross-reacting Antigen-90 Fab'. ^{99m}Tc-labeled anti-NCA-90 Fab' (sulesomab, LeukoScan), which binds to NCA-90 surface antigen on granulocytes, is a commercially available infection imaging agent. Promising results have been obtained in the scintigraphic detection of endocarditis (Gratz et al. 2000) and nonclassic appendicitis (Barron et al. 1999; Passalaqua et al. 2004). ^{99m}Tc-anti-NCA-90 Fab' proved to be no alternative for radiolabeled leukocytes in patients with inflammatory bowel disease due to limited sensitivity (Kerry et al. 2005). Non-specific bowel activity is often present, especially in the delayed images. At first, scintigraphy using ^{99m}Tc-anti-NCA-90 Fab' appeared to provide rapid localization of bone and soft tissue infections with a negligible HAMA response rate and accuracy comparable to that of leukocyte scanning. In other studies, however, ^{99m}Tc-anti-NCA-90 Fab' scintigraphy was found to be less specific for the diagnosis of musculoskeletal infections than leukocyte scanning. In addition, false-negative results were found in several patients with chronic infections (Gratz et al. 2003). In diabetic foot infections, sensitivity (67 %) and specificity (85 %) of ^{99m}Tc-anti-NCA-90 Fab' scintigraphy were higher than sensitivity and specificity of ^{67}Ga scintigraphy, although sensitivity was not optimal (Delcourt et al. 2005). These studies suggest that ^{99m}Tc-anti-NCA-90 Fab' scintigraphy could be used for imaging of acute orthopedic infections, with its greatest strength being a high negative predictive value. Positive studies may require further correlative imaging.

Cytokines

Cytokines are (glyco)proteins acting via interaction with specific cell surface receptors expressed mainly on leukocytes, but also on other cell types. Cytokine receptors are usually expressed at low levels on resting cells, but their expression is upregulated during activation. Cytokines potentially can be used to specifically target leukocytes in vivo, because they bind to specific receptors with high affinity in the nanomolar range, they have low molecular weights (< 25 kDa) and plasma clearance is rapid. Finally, many cytokines are of human origin and are therefore readily available and supposedly non-immunogenic.

Interleukin-8. Interleukin-8 (IL-8) is a small protein (8.5 kDa) belonging to the CXC subfamily of chemokines or chemotactic cytokines, in which the first two cysteines are separated by one amino acid. IL-8 binds with high affinity ($0.3 - 4 \times 10^{-9}$ mol/l) to two different receptors (CXCR1 and CXCR2) expressed on granulocytes and promotes chemotaxis of these cells. In a pilot study in eight patients, it was shown that ^{123}I-IL-8 could visualize osteomyelitis and cellulitis correctly (Gross et al. 2001). Recently, a ^{99m}Tc-labeled IL-8 preparation

was developed using HYNIC as a chelator resulting in a significantly higher specific activity. Protein doses to be administered were lowered substantially due to much higher specific activity of this new ^{99m}Tc-IL-8 preparation, ameliorating concerns about the influence on leukocyte counts in patients. Studies in neutropenic and normal rabbits with turpentine-induced abscesses have shown that accumulation of ^{99m}Tc-IL-8 in the abscess is a highly specific, neutrophil-driven process and that the total fraction of ^{99m}Tc-IL-8 that accumulates in the inflamed tissue is extremely high (up to >15% of injected dose) (Rennen et al. 2003). Recently, the first clinical study using ^{99m}Tc-IL-8 scintigraphy in 20 patients suspected of different infectious diseases was completed (Bleeker-Rovers et al. 2007). In our institution, injection of ^{99m}Tc-IL-8 was well tolerated. ^{99m}Tc-IL-8 rapidly cleared from the blood and most other organs. In 10 of 12 patients with an infection, ^{99m}Tc-IL-8 localized the infection 4 h p.i. In the patients with non-infectious disorders, no focal accumulation of ^{99m}Tc-IL-8 was found. ^{99m}Tc-IL-8 scintigraphy could thus be a promising new tool for detection of infections in patients.

17.2.2.3 Imaging of Infiltrating Mononuclear Cells

Interleukin-2

Interleukin-2 is a glycoprotein with a molecular weight of 15.5 kDa, which is synthesized and secreted by T-lymphocytes after specific antigen stimulation. During inflammation, activated lymphocytes express high-affinity IL-2 receptors and become a target for radiolabeled IL-2. IL-2 has been labeled with ^{123}I and ^{99m}Tc to enable imaging of chronic infection or inflammation. In several rat models of autoimmune diabetes and in rats with renal allografts, ^{123}I-IL-2 adequately detected areas of lymphocytic infiltration. Specific accumulation of ^{123}I-IL-2 has been confirmed by ex vivo autoradiography (Signore et al. 1987). ^{123}I-IL-2 has also been used successfully in patients with type 1 diabetes. ^{99m}Tc-IL-2 was able to identify a subgroup of patients with type 1 diabetes with persistent inflammation at the time of diagnosis that might benefit from the use of immunomodulating drugs to preserve β-cell function (Signore et al. 1999). In patients with active Crohn's disease, ^{123}I-IL-2 allowed imaging of activated T-lymphocytes infiltrating the gut wall. The uptake of ^{123}I-IL-2 decreased after corticosteroid therapy, so this technique could be valuable in monitoring the effect of therapy (Signore et al. 2000a). Scintigraphic results using ^{123}I-IL-2 in patients with celiac disease were consistent with the histologically determined number of infiltrating IL-2 receptor-positive cells in the jejunal mucosa (Signore et al. 2000b). ^{99m}Tc-IL-2 also strongly accumulates in the thyroid glands of patients with Hashimoto's thyroiditis and Graves' disease (Procaccini et al. 1999). No side effects were observed. These results suggest that radiolabeled IL-2 could be a suitable radiopharmaceutical for in vivo targeting of mononuclear cell infiltration as present in several autoimmune diseases.

17.2.2.4 Imaging of Microorganisms

Ciprofloxacin

Ciprofloxacin is a fluoroquinolone that binds to bacterial DNA gyrase, which is present in all dividing bacteria. Since it binds only to living bacteria, even to most bacteria that are resistant to this antibiotic, the use of ^{99m}Tc-labeled ciprofloxacin (Infecton) theoretically allows distinction between sterile inflammation and infection. ^{99m}Tc-ciprofloxacin is mainly excreted via the kidneys, it has low liver metabolism and bowel uptake is usually very low. The lack of bone marrow uptake is particularly useful for the detection of bone infections. In patients with known or suspected sites of various bacterial infections, sensitivity of scintigraphy with ^{99m}Tc-ciprofloxacin varied from 70% to 85% and specificity was approximately 80–95% (Britton et al. 2002). Comparison between ^{99m}Tc-ciprofloxacin and leukocyte imaging gave comparable sensitivities and specificity was 96% and 77%, respectively (Vinjamuri et al. 1996). ^{99m}Tc-ciprofloxacin was shown to be a very sensitive and quite specific marker of bone and joint infections (Sonmezoglu et al. 2001; Yapar et al. 2001): sensitivity of ^{99m}Tc-ciprofloxacin imaging was higher when compared to scintigraphy with ^{99m}Tc-HMPAO leukocytes (Sonmezoglu et al. 2001) and three-phase bone scanning in combination with ^{67}Ga-citrate scintigraphy (Yapar et al. 2001). In patients suspected of postoperative spine infections, ^{99m}Tc-ciprofloxacin SPET showed a sensitivity of 100% and a specificity of 74%. An interval of at least 6 months after surgery decreased the likelihood of false positives (De et al. 2004). ^{99m}Tc-ciprofloxacin has also been used successfully in patients with suspected infections of hip or knee prostheses (Larikka et al. 2002). Lately, the specificity of ^{99m}Tc-ciprofloxacin has been discussed extensively. In patients with suspected osteoarticular infections and patients with osteoarticular diseases without signs of infection, ^{99m}Tc-ciprofloxacin scintigraphy did not discriminate between infected and aseptic osteoarticular diseases and articular uptake was seen in many control patients (Sarda et al. 2003).

17.3 Positron Emission Tomography for Imaging of Infectious and Inflammatory Processes: Imaging of Enhanced Glucose Uptake Using FDG

FDG accumulates in tissues with a high rate of glycolysis, which not exclusively occurs in neoplastic cells. FDG uptake is present in all activated leukocytes (granulocytes, monocytes as well as lymphocytes), enabling imaging of acute and chronic inflammatory processes. The mechanism of FDG uptake in activated leukocytes is related to the fact that these cells use glucose as an energy source only after activation during the metabolic burst. FDG, like glucose, passes the cell membrane. Phosphorylated FDG is not further metabolized and remains trapped inside the cell in contrast to phosphorylated glucose that enters the glycolytic pathway. ^{18}F is a positron-emitting radionuclide with a physical half-life of 110 min. After annihilation of a positron with an electron, two 180°-opposed gamma rays are emitted simultaneously, which can subsequently be detected by a positron emission tomography (PET) camera. Increased uptake and retention of FDG have been shown in lesions with a high concentration of inflammatory cells, such as granulocytes and activated macrophages. In an experimental rat model of turpentine-induced inflammation, FDG uptake was elevated even more in chronic inflammation than in an acute inflammatory process (Yamada et al. 1995). In another rat model of *Escherichia coli* infection, FDG uptake in the infectious process was higher than uptake of ^{67}Ga-citrate, radiolabeled thymidine, methionine and human serum albumin (Sugawara et al. 1999).

17.3.1 Fever of Unknown Origin

The value of FDG PET has been studied in several studies in 292 patients with FUO (Bleeker-Rovers et al. 2004; Blockmans et al. 2001; Buysschaert et al. 2004; Kjaer et al. 2004; Lorenzen et al. 2001; Meller et al. 2000) (Table 17.2), showing an overall helpfulness of FDG PET corrected for a study population of 36%, which is very high compared to radiological techniques and ^{67}Ga-citrate scintigraphy. Although comparing these studies is difficult, because FDG PET was performed at different stages of the diagnostic process, no structured diagnostic protocol was used and the patient characteristics differed, FDG PET appears to be a valuable new imaging technique in these patients. The impossibility of differentiating between malignancy and infection or inflammation appears to be an advantage rather than a drawback in the investigation of patients with FUO. Another major advantage of FDG PET in the work-up of patients with FUO is the vascular FDG uptake in patients with vasculitis. From two prospective studies comparing FDG PET with ^{67}Ga-citrate scintigraphy in a total of 58 patients with FUO, it was concluded that FDG PET was superior to ^{67}Ga-citrate scintigraphy because the diagnostic yield is at least comparable to that of ^{67}Ga-citrate scintigraphy and the results are available within hours instead of days (Blockmans et al. 2001; Meller et al. 2000). Based on the results of these studies and resulting from the favorable characteristics of FDG PET, conventional scintigraphic techniques may be replaced by FDG PET in the investigation of patients with FUO in institutions where this technique is available.

Table 17.2. Review of the literature on the utility of FDG PET in patients with FUO

First author (year)	Study design	FDG PET technique	Conclusions
Meller (2000)	Prospective ($n=20$): comparison FDG PET and ^{67}Ga-citrate ($n=18$)	Dual-headed coincidence camera	FDG PET helpful in 55%, PPV 92%, NPV 75%, FDG PET superior to ^{67}Ga-citrate
Blockmans (2001)	Prospective (n=58): comparison to ^{67}Ga-citrate ($n=40$)	Full ring PET scanner	FDG PET helpful in 41%, FDG PET superior to ^{67}Ga-citrate
Lorenzen (2001)	Retrospective ($n=16$)	Full ring PET scanner	FDG PET helpful in 69%, PPV 92%, NPV 100%
Bleeker-Rovers (2004)	Retrospective ($n=35$)	Full ring PET scanner	FDG PET helpful in 37%, PPV 87%, NPV 95%
Kjaer (2004)	Prospective ($n=19$): comparison to ^{111}In-granulocyte	Full ring PET scanner	FDG PET helpful in 16%, PPV 30%, NPV 67%, ^{111}In-granulocyte scintigraphy helpful in 26%
Buysschaert (2004)	Prospective ($n=74$)	Full ring PET scanner	FDG PET helpful in 26%
Bleeker-Rovers (2007)	Prospective, multicenter ($n=70$)	Full ring PET scanner	FDG PET helpful in 33%, PPV 70%, NPV 95%

PPV positive predictive value, *NPV* negative predictive value, *ESR* erythrocyte sedimentation rate, *CRP* C-reactive protein

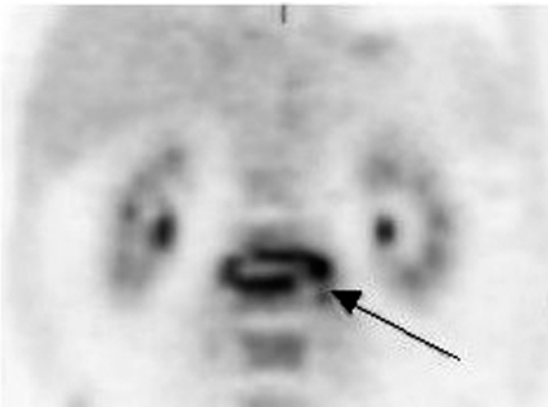

Fig. 17.1. This 64-year-old man presented with lower back pain and fever. Blood cultures grew group G streptococci. MRI was normal, but PET showed increased FDG uptake in L1 and L2. One week later spondylodiscitis was confirmed by a second MRI

17.3.2 Osteomyelitis and Spondylodiscitis

FDG PET has been used successfully in diagnosing acute osteomyelitis (Kalicke et al. 2000), but it has no added value to physical examination, laboratory results, three-phase bone scanning and MRI in the absence of complicating factors. The diagnosis of chronic osteomyelitis is more complex. In patients with chronic osteomyelitis, excellent accuracy and interobserver agreement was found for FDG PET comparable to scintigraphy with antigranulocyte antibodies and ^{111}In-labeled leukocytes (Meller et al. 2002a). In the central skeleton, accuracy of FDG PET was even higher than for antigranulocyte antibody scintigraphy. The usefulness of antigranulocyte antibody or radiolabeled leukocyte scintigraphy is low in the central skeleton due to physiological uptake in normal bone marrow. In several studies, FDG PET enabled correct visualization of spondylodiscitis. FDG PET proved to be superior to MRI, ^{67}Ga-citrate scintigraphy and three phase bone scan in these patients (Gratz et al. 2002; Stumpe et al. 2002). FDG PET was also able to differentiate between mild infection and degenerative changes (Stumpe et al. 2002). PET images are not disturbed by the presence of metallic implants, which is a major advantage when compared to CT and MRI. In addition, FDG PET is a very sensitive tool even for chronic and low-grade infections. In conclusion, FDG PET is very useful in cases of suspected osteomyelitis of the central skeleton, spondylodiscitis or chronic low-grade infections of the peripheral skeleton.

17.3.3 Prosthetic Joint Infection

Diagnosing prosthetic joint infection is very difficult, because radiographic methods and three-phase bone scanning cannot differentiate adequately between septic and aseptic loosening. FDG PET is very sensitive in detecting infected joint prostheses, but specificity varies from approximately 50% to 95% (Kisielinski et al. 2003; Schiesser et al. 2003). In a prospective study comparing FDG PET to ^{99m}Tc-labeled leukocytes in combination with bone scintigraphy in patients with a hip prosthesis suspected of infection and in controls with asymptomatic hip prostheses, the combined analysis of bone scintigraphy and leukocyte scintigraphy resulted in a comparable sensitivity, but a lower specificity for FDG PET (Vanquickenborne et al. 2003). It is concluded that FDG PET has a high sensitivity in diagnosing infected joint prostheses. Specificity, however, is lower than specificity of combined leukocyte scintigraphy and bone scanning. This limited specificity probably results from persisting FDG uptake around the prosthesis for many years after arthroplasty, even in uncomplicated cases (Kisielinski et al. 2003). Location of FDG uptake is probably important since FDG uptake along the interface between bone and prosthesis appears to be more specific for infection (Chacko et al. 2002).

17.3.4 Vascular Infections

In detecting blood vessel graft infection, FDG PET seemed to have higher sensitivity than conventional imaging techniques in a small number of patients. In a recent study systematically comparing CT and focal FDG uptake on PET in patients suspected of vascular graft infection, FDG PET showed better sensitivity and specificity (Fukuchi et al. 2005). Other endovascular foci, such as septic thrombophlebitis or septic arteritis, can also be successfully diagnosed by FDG PET. In a retrospective study, acute thrombosis did not lead to increased FDG uptake in 27 patients with proven acute or chronic thrombosis (Miceli et al. 2004).

17.3.5 Metastatic Infectious Foci

Secondary metastatic infection is a well-known complication of blood stream infections. Timely identification of metastatic complications, although critical, is often difficult. In a retrospective study in 40 patients with a high suspicion of metastatic complications after blood stream infection, FDG PET diagnosed a clinically relevant new focus in 45% of cases while on average four conventional diagnostic tests had been performed before FDG PET (Bleeker-Rovers et al. 2005). FDG PET appears to have a promising role in detecting metastatic infectious foci in patients with a high level of clinical suspicion.

17.3.6 Postoperative Infections

FDG uptake in physiological wound healing is expected to diminish over time. In one study exploring the value of FDG PET in 18 patients suspected of postoperative infections, sensitivity and specificity of infection imaging in areas outside the region of surgical trauma were 86% and 100%. Sensitivity of infection imaging in the area the surgical wound was 100%, while specificity was only 56% (Meller et al. 2002b). The interval between surgery and FDG PET was significantly shorter in patients with false positive results. Further studies on the degree, pattern and duration of physiological FDG uptake after surgery are warranted.

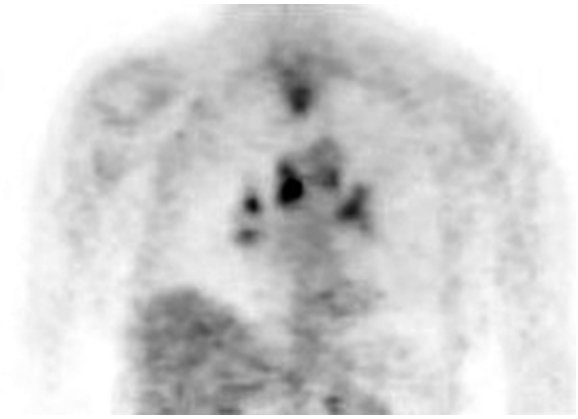

Fig. 17.2. This 71-year-old woman presented with fever of unknown origin. Chest CT was normal, but PET showed increased FDG uptake in mediastinal and hilar lymph nodes. Lymph node biopsy confirmed the diagnosis of sarcoidosis

17.3.7 Miscellaneous Infectious Diseases

In children with chronic granulomatous disease, a primary immunodeficiency leading to granuloma formation and numerous infections, FDG PET was able to differentiate active infected lesions from chronic granuloma (Gungor et al. 2001). In patients with echinococcosis, a serious parasitic infection, FDG PET correctly identified the active lesions and appeared to be helpful in assessing response to treatment (Reuter et al. 1999). Successful use of FDG PET in detection of infected liver and renal cysts in patients with autosomal dominant polycystic kidney disease has also been reported (Bleeker-Rovers et al. 2003b).

17.3.8 The Immunocompromised Host

Mahfouz et al. retrospectively studied 248 PET scans ordered in patients with multiple myeloma either for staging disease progression or infection work-up (Mahfouz et al. 2005). FDG PET identified 165 infectious foci even in patients with severe neutropenia. In 46 patients, infection was not identified by a regular diagnostic work-up. In this study, FDG PET contributed to patient care in 46% of all patients. FDG PET also appears to be a promising imaging technique in the early detection of complications and for the differential diagnosis of central nervous system lesions in patients with HIV or AIDS (Santiago et al. 1999). A possible pitfall of FDG PET in these patients, however, is the difficulty in differentiating between persisting generalized lymphadenopathy and lymphoma.

17.3.9 Vasculitis

Increased FDG uptake has been found in patients with giant cell arteritis, Takayasu arteritis, periaortitis due to Wegener's granulomatosis, polyarteritis nodosa and unspecified large vessel vasculitis (Belhocine et al. 2003; Bleeker-Rovers et al. 2003a; Meller et al. 2003a, 2003b; Salvarani et al. 2005; Scheel et al. 2004). In a prospective study, vascular FDG uptake was seen in 76% of 25 patients with biopsy-proven temporal arteritis or polymyalgia rheumatica (Blockmans et al. 2000). In several studies including patients with aortitis due to giant cell aortitis or Takayasu arteritis, FDG PET identified more vascular regions involved in the inflammatory process when compared to MRI (Meller et al. 2003a; Scheel et al. 2004; Walter et al. 2005). During follow-up, FDG uptake decreased in correlation with clinical response and inflammatory markers (Bleeker-Rovers et al. 2003a; Scheel et al. 2004). It was shown that sensitivity of FDG PET increased with higher CRP levels (Walter et al. 2005). Sensitivity of FDG PET could also be increased by coregistration with enhanced CT (Kobayashi et al. 2005). When compared to matched control groups, specificity of FDG PET was high (Kobayashi et al. 2005; Walter et al. 2005). In conclusion, FDG PET appears to be useful for diagnosing and determining the extent of various types of vasculitis. Furthermore, FDG PET could become a useful tool for evaluating the effect of treatment.

17.3.10 Inflammatory Bowel Disease

High FDG uptake has been reported in areas with inflammation in patients with inflammatory bowel disease (Bicik et al. 1997; Neurath et al. 2002). Specificity of FDG PET was comparable to MRI and antigranulocyte antibody scintigraphy in 59 patients with Crohn's disease, but sensitivity of FDG PET was significantly higher (Neurath et al. 2002). FDG PET also correctly detected histologically confirmed eosinophilic colitis, collagenous colitis and bacterial colitis in a small num-

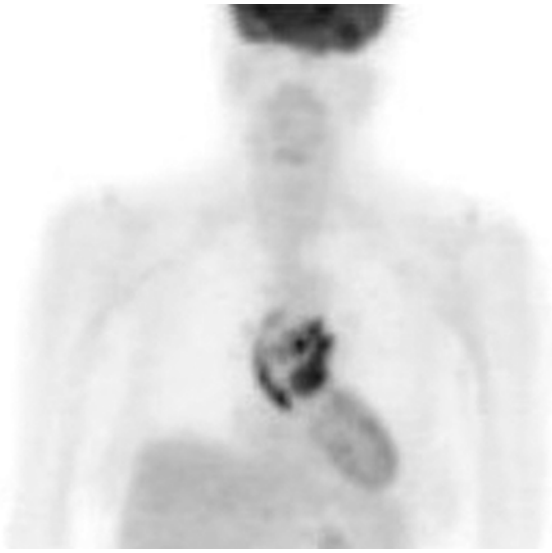

Fig. 17.3. A patient with giant cell arteritis of the ascending thoracic aorta

ber of patients (Kresnik et al. 2002). FDG PET could become a useful tool to detect disease activity in the terminal ileum and colon in patients with inflammatory bowel disease, but physiological, non-specific bowel uptake could be an important problem in clinical practice. More data are needed to justify routine application of PET in the management of inflammatory bowel disease.

17.3.11 Sarcoidosis and Rheumatoid Arthritis

In several patients with sarcoidosis, FDG uptake in hilar and mediastinal lymph nodes and erythema nodosum has been described (Brudin et al. 1994; Lewis and Salama et al. 1994). FDG uptake levels appeared to reflect disease activity (Brudin et al. 1994). FDG PET does not have a major role in the initial diagnosis of sarcoidosis, because conventional diagnostic techniques are very well able to establish this diagnosis in most cases. FDG PET may prove to be useful in evaluating response to treatment, but larger prospective studies are needed to define the role of FDG PET in these patients. In patients with rheumatoid arthritis, FDG PET allowed quantification of metabolic changes in joint inflammation comparable to volumetric changes visualized with MRI, but FDG uptake was not associated with treatment outcome (Palmer et al. 1995).

17.4 Conclusions and Future Developments

Scintigraphy using autologous leukocytes, labeled with ^{111}In or ^{99m}Tc, is still considered the "gold standard" nuclear medicine technique for the imaging of infection and inflammation, but the range of radiolabeled compounds available for this indication is expanding rapidly. A gradual shift from basic, non-specific, cumbersome and even hazardous techniques to more intelligent approaches, based on small agents binding to their targets with high affinity, is ongoing. In general, the lower molecular weight should also lead to enhanced blood clearance reducing blood pool activity. New agents should also obviate the need to handle blood as this presents potential hazards of transmission of hepatitis virus or human immunodeficiency virus to both patients and medical personnel. Radiolabeled compounds are being designed, enabling specific distinction between infection and non-infectious inflammatory disease and between acute and chronic processes. The ideal agent will thus be determined by the clinical situation. The advantages of ^{99m}Tc as a radionuclide will be fully explored. Labeling with high specific activity will reduce the doses used, resulting in less undesirable agonistic activities. Undesirable agonistic activities will also be alleviated by chemical modification of the agonist. Furthermore, FDG PET may prove to be as useful in the rapid detection and management of infectious and inflammatory diseases as it is in the management of malignant diseases.

References

Barron B, Hanna C, Passalaqua AM, Lamki L, Wegener WA, Goldenberg DM (1999) Rapid diagnostic imaging of acute, nonclassic appendicitis by leukoscintigraphy with sulesomab, a technetium 99m-labeled antigranulocyte antibody Fab' fragment. LeukoScan Appendicitis Clinical Trial Group. Surgery 125(3):288 – 96

Belhocine T, Blockmans D, Hustinx R, Vandevivere J, Mortelmans L (2003) Imaging of large vessel vasculitis with (18)FDG PET: illusion or reality? A critical review of the literature data. Eur J Nucl Med Mol Imaging 30(9):1305 – 13

Bhatti M, Chapman P, Peters M, Haskard D, Hodgson HJ (1998) Visualising E-selectin in the detection and evaluation of inflammatory bowel disease. Gut 43(1):40 – 7

Bicik I, Bauerfeind P, Breitbach T, von Schulthess GK, Fried M (1997) Inflammatory bowel disease activity measured by positron-emission tomography. Lancet 350(9073):262

Bleeker-Rovers CP, Bredie SJ, van der Meer JW, Corstens FH, Oyen WJ (2003a) F-18-fluorodeoxyglucose positron emission tomography in diagnosis and follow-up of patients with different types of vasculitis. Neth J Med 61(10):323 – 9

Bleeker-Rovers CP, Sevaux RG, Van Hamersvelt HW, Corstens FH, Oyen WJ (2003b) Diagnosis of renal and hepatic cyst infections by 18-F-fluorodeoxyglucose positron emission tomography in autosomal dominant polycystic kidney disease. Am J Kidney Dis 41(6):E18–E21

Bleeker-Rovers CP, de Kleijn EM, Corstens FH, van der Meer JW, Oyen WJ (2004) Clinical value of FDG PET in patients with fever of unknown origin and patients suspected of focal infection or inflammation. Eur J Nucl Med Mol Imaging 31(1):29 – 37

Bleeker-Rovers CP, Vos FJ, Mudde AH, Dofferhoff ASM, de Geus-Oei L-F, Rijnders AJ, Krabbe PFM, Corstens FHM, van der Meer JWM, Oyen WJG (2007) A prospective multi-center study of the value of FDG-PET as part of a structured diagnostic protocol in patients with fever of unknown origin. Eur J Nucl Med Mol Imaging 34(5):694 – 703

Bleeker-Rovers CP, Rennen HJJM, Boerman OC, Wymenga AB, Visser EP, Bakker JH, van der Meer JWM, Corstens FHM, Oyen WJG (2007) ^{99m}Tc-labeled interleukin-8 for the scintigraphic detection of infection and inflammation: first clinical evaluation. The Journal of Nuclear Medicine 48(3):337 – 343

Blockmans D, Stroobants S, Maes A, Mortelmans L (2000) Positron emission tomography in giant cell arteritis and polymyalgia rheumatica: evidence for inflammation of the aortic arch. Am J Med 108(3):246 – 9

Blockmans D, Knockaert D, Maes A, De Caestecker J, Stroobants S, Bobbaers H, Mortelmans L (2001) Clinical value of [(18)F]fluoro-deoxyglucose positron emission tomography for patients with fever of unknown origin. Clin Infect Dis 32(2):191 – 6

Boubaker A, Delaloye AB, Blanc CH, Dutoit M, Leyvraz PF, Delaloye B (1995) Immunoscintigraphy with antigranulocyte monoclonal antibodies for the diagnosis of septic loosening of hip prostheses. Eur J Nucl Med 22(2):139 – 47

Britton KE, Wareham DW, Das SS, Solanki KK, Amaral H, Bhatnagar A, Katamihardja AH, Malamitsi J, Moustafa HM, Soroa VE, Sundram FX, Padhy AK (2002) Imaging bacterial infection with (99m)Tc-ciprofloxacin (Infecton). J Clin Pathol 55(11):817 – 23

Brudin LH, Valind SO, Rhodes CG, Pantin CF, Sweatman M, Jones T, Hughes JM (1994) Fluorine-18 deoxyglucose uptake in sarcoidosis measured with positron emission tomography. Eur J Nucl Med 21(4):297 – 305

Buysschaert I, Vanderschueren S, Blockmans D, Mortelmans L, Knockaert D (2004) Contribution of (18)fluoro-deoxyglucose positron emission tomography to the work-up of patients with fever of unknown origin. Eur J Intern Med 15(3):151 – 6

Chacko TK, Zhuang H, Stevenson K, Moussavian B, Alavi A (2002) The importance of the location of fluorodeoxyglucose uptake in periprosthetic infection in painful hip prostheses. Nucl Med Commun 23(9):851 – 5

Chapman PT, Jamar F, Keelan ET, Peters AM, Haskard DO (1996) Use of a radiolabeled monoclonal antibody against E-selectin for imaging of endothelial activation in rheumatoid arthritis. Arthritis Rheum 39(8):1371 – 5

Datz FL, Thorne DA (1986) Effect of chronicity of infection on the sensitivity of the In-111-labeled leukocyte scan. AJR Am J Roentgenol 147(4):809 – 12

De WF, Gemmel F, Van LK, De WO, Poffijn B, Dierckx RA, van de WC (2004) 99mTc-ciprofloxacin planar and tomographic imaging for the diagnosis of infection in the postoperative spine: experience in 48 patients. Eur J Nucl Med Mol Imaging 31(2):233 – 9

Delcourt A, Huglo D, Prangere T, Benticha H, Devemy F, Tsirtsikoulou D, Lepeut M, Fontaine P, Steinling M (2005) Comparison between Leukoscan (Sulesomab) and Gallium-67 for the diagnosis of osteomyelitis in the diabetic foot. Diabetes Metab 31(2):125 – 33

Dominguez-Gadea L, Martin-Curto LM, de la CH, Crespo A (1993) Diabetic foot infections: scintigraphic evaluation with 99Tcm-labelled anti-granulocyte antibodies. Nucl Med Commun 14(3):212 – 8

Fukuchi K, Ishida Y, Higashi M, Tsunekawa T, Ogino H, Minatoya K, Kiso K, Naito H (2005) Detection of aortic graft infection by fluorodeoxyglucose positron emission tomography: comparison with computed tomographic findings. J Vasc Surg 42(5):919 – 25

Gratz S, Behr TM, Herrmann A, Meller J, Conrad M, Zappel H, Becker W (1998) Immunoscintigraphy (BW 250/183) in neonates and infants with fever of unknown origin. Nucl Med Commun 19(11):1037 – 45

Gratz S, Raddatz D, Hagenah G, Behr T, Behe M, Becker W (2000) 99mTC-labelled antigranulocyte monoclonal antibody FAB' fragments versus echocardiography in the diagnosis of subacute infective endocarditis. Int J Cardiol 75(1): 75 – 84

Gratz S, Dorner J, Fischer U, Behr TM, Behe M, Altenvoerde G, Meller J, Grabbe E, Becker W (2002) 18F-FDG hybrid PET in patients with suspected spondylitis. Eur J Nucl Med Mol Imaging 29(4):516 – 24

Gratz S, Schipper ML, Dorner J, Hoffken H, Becker W, Kaiser JW, Behe M, Behr TM (2003) LeukoScan for imaging infection in different clinical settings: a retrospective evaluation and extended review of the literature. Clin Nucl Med 28(4): 267 – 76

Gross MD, Shapiro B, Fig LM, Steventon R, Skinner RW, Hay RV (2001) Imaging of human infection with (131)I-labeled recombinant human interleukin-8. J Nucl Med 42(11): 1656 – 9

Gungor T, Engel-Bicik I, Eich G, Willi UV, Nadal D, Hossle JP, Seger RA, Steinert HC (2001) Diagnostic and therapeutic impact of whole body positron emission tomography using fluorine-18-fluoro-2-deoxy-D-glucose in children with chronic granulomatous disease. Arch Dis Child 85(4):341 – 5

Gyorke T, Duffek L, Bartfai K, Mako E, Karlinger K, Mester A, Tarjan Z (2000) The role of nuclear medicine in inflammatory bowel disease. A review with experiences of aspecific bowel activity using immunoscintigraphy with 99mTc antigranulocyte antibodies. Eur J Radiol 35(3):183 – 92

Jamar F, Houssiau FA, Devogelaer JP, Chapman PT, Haskard DO, Beaujean V, Beckers C, Manicourt DH, Peters AM (2002) Scintigraphy using a technetium 99m-labelled anti-E-selectin Fab fragment in rheumatoid arthritis. Rheumatology (Oxford) 41(1):53 – 61

Kalicke T, Schmitz A, Risse JH, Arens S, Keller E, Hansis M, Schmitt O, Biersack HJ, Grunwald F (2000) Fluorine-18 fluorodeoxyglucose PET in infectious bone diseases: results of histologically confirmed cases. Eur J Nucl Med 27(5):524 – 8

Kerry JE, Marshall C, Griffiths PA, James MW, Scott BB (2005) Comparison between Tc-HMPAO labelled white cells and Tc LeukoScan in the investigation of inflammatory bowel disease. Nucl Med Commun 26(3):245 – 51

Kipper SL, Rypins EB, Evans DG, Thakur ML, Smith TD, Rhodes B (2000) Neutrophil-specific 99mTc-labeled anti-CD15 monoclonal antibody imaging for diagnosis of equivocal appendicitis. J Nucl Med 41(3):449 – 55

Kisielinski K, Cremerius U, Reinartz P, Niethard FU (2003) Fluorodeoxyglucose positron emission tomography detection of inflammatory reactions due to polyethylene wear in total hip arthroplasty. J Arthroplasty 18(4):528 – 32

Kjaer A, Lebech AM, Eigtved A, Hojgaard L (2004) Fever of unknown origin: prospective comparison of diagnostic value of 18F-FDG PET and 111In-granulocyte scintigraphy. Eur J Nucl Med Mol Imaging 31(5):622 – 6

Klett R, Kordelle J, Stahl U, Khalisi A, Puille M, Steiner D, Bauer R (2003) Immunoscintigraphy of septic loosening of knee endoprosthesis: a retrospective evaluation of the antigranulocyte antibody BW 250/183. Eur J Nucl Med Mol Imaging 30:1463 – 6

Kobayashi Y, Ishii K, Oda K, Nariai T, Tanaka Y, Ishiwata K, Nu-

mano F (2005) Aortic wall inflammation due to Takayasu arteritis imaged with 18F-FDG PET coregistered with enhanced CT. J Nucl Med 46(6):917 – 22
Kresnik E, Gallowitsch HJ, Mikosch P, Wurtz F, Alberer D, Hebenstreit A, Kogler D, Gasser J, Igerc I, Kumnig G, Gomez I, Lind P (2002) (18)F-FDG positron emission tomography in the early diagnosis of enterocolitis: preliminary results. Eur J Nucl Med Mol Imaging 29(10):1389 – 92
Larikka MJ, Ahonen AK, Niemela O, Junila JA, Hamalainen MM, Britton K, Syrjala HP (2002) Comparison of 99mTc ciprofloxacin, 99mTc white blood cell and three-phase bone imaging in the diagnosis of hip prosthesis infections: improved diagnostic accuracy with extended imaging time. Nucl Med Commun 23(7):655 – 61
Lewis PJ, Salama A (1994) Uptake of fluorine-18-fluorodeoxyglucose in sarcoidosis. J Nucl Med 35(10):1647 – 9
Liberatore M, Clemente M, Iurilli AP, Zorzin L, Marini M, Di Rocco E, Colella AC (1992) Scintigraphic evaluation of disease activity in rheumatoid arthritis: a comparison of technetium-99m human non-specific immunoglobulins, leucocytes and albumin nanocolloids. Eur J Nucl Med 19(10): 853 – 7
Lorenzen J, Buchert R, Bohuslavizki KH (2001) Value of FDG PET in patients with fever of unknown origin. Nucl Med Commun 22(7):779 – 83
Mahfouz T, Miceli MH, Saghafifar F, Stroud S, Jones-Jackson L, Walker R, Grazziutti ML, Purnell G, Fassas A, Tricot G, Barlogie B, Anaissie E (2005) 18F-fluorodeoxyglucose positron emission tomography contributes to the diagnosis and management of infections in patients with multiple myeloma: a study of 165 infectious episodes. J Clin Oncol 23(31): 7857 – 63
Meller J, Altenvoerde G, Munzel U, Jauho A, Behe M, Gratz S, Luig H, Becker W (2000) Fever of unknown origin: prospective comparison of [18F]FDG imaging with a double-head coincidence camera and gallium-67 citrate SPET. Eur J Nucl Med 27(11):1617 – 25
Meller J, Koster G, Liersch T, Siefker U, Lehmann K, Meyer I, Schreiber K, Altenvoerde G, Becker W (2002a) Chronic bacterial osteomyelitis: prospective comparison of (18)F-FDG imaging with a dual-head coincidence camera and (111)In-labelled autologous leucocyte scintigraphy. Eur J Nucl Med Mol Imaging 29(1):53 – 60
Meller J, Sahlmann CO, Lehmann K, Siefker U, Meyer I, Schreiber K, Altenvoerde G, Becker W (2002b) [F-18-FDG hybrid camera PET in patients with postoperative fever]. Nuklearmedizin 41(1):22 – 9
Meller J, Grabbe E, Becker W, Vosshenrich R (2003a) Value of F-18 FDG hybrid camera PET and MRI in early Takayasu aortitis. Eur Radiol 13(2):400 – 5
Meller J, Strutz F, Siefker U, Scheel A, Sahlmann CO, Lehmann K, Conrad M, Vosshenrich R (2003b) Early diagnosis and follow-up of aortitis with [(18)F]FDG PET and MRI. Eur J Nucl Med Mol Imaging 5(30):730 – 6
Miceli M, Atoui R, Walker R, Mahfouz T, Mirza N, Diaz J, Tricot G, Barlogie B, Anaissie E (2004) Diagnosis of deep septic thrombophlebitis in cancer patients by fluorine-18 fluorodeoxyglucose positron emission tomography scanning: a preliminary report. J Clin Oncol 22(10):1949 – 56
Morguet AJ, Munz DL, Ivancevic V, Werner GS, Sandrock D, Bokemeier M, Kreuzer H (1994) Immunoscintigraphy using technetium-99m-labeled anti-NCA-95 antigranulocyte antibodies as an adjunct to echocardiography in subacute infective endocarditis. J Am Coll Cardiol 23(5):1171 – 8
Neurath MF, Vehling D, Schunk K, Holtmann M, Brockmann H, Helisch A, Orth T, Schreckenberger M, Galle PR, Bartenstein P (2002) Noninvasive assessment of Crohn's disease activity: a comparison of 18F-fluorodeoxyglucose positron emission tomography, hydromagnetic resonance imaging, and granulocyte scintigraphy with labeled antibodies. Am J Gastroenterol 97(8):1978 – 85
Nijhof MW, Oyen WJ, van Kampen A, Claessens RA, van der Meer JW, Corstens FH (1997) Evaluation of infections of the locomotor system with indium-111-labeled human IgG scintigraphy. J Nucl Med 38(8):1300 – 5
Oyen WJ, Claessens RA, van der Meer JW, Corstens FH (1991) Detection of subacute infectious foci with indium-111-labeled autologous leukocytes and indium-111-labeled human nonspecific immunoglobulin G: a prospective comparative study. J Nucl Med 32(10):1854 – 60
Oyen WJ, Claessens RA, Raemaekers JM, de Pauw BE, van der Meer JW, Corstens FH (1992) Diagnosing infection in febrile granulocytopenic patients with indium-111-labeled human immunoglobulin G. J Clin Oncol 10(1):61 – 8
Palestro CJ (1994) The current role of gallium imaging in infection. Semin Nucl Med 24(2):128 – 41
Palmer WE, Rosenthal DI, Schoenberg OI, Fischman AJ, Simon LS, Rubin RH, Polisson RP (1995) Quantification of inflammation in the wrist with gadolinium-enhanced MR imaging and PET with 2-[F-18]-fluoro-2-deoxy-D-glucose. Radiology 196(3):647 – 55
Papos M, Nagy F, Narai G, Rajtar M, Szantai G, Lang J, Csernay L (1996) Anti-granulocyte immunoscintigraphy and [99mTc]-hexamethylpropyleneamine-oxime-labeled leukocyte scintigraphy in inflammatory bowel disease. Dig Dis Sci 41(2):412 – 20
Passalaqua AM, Klein RL, Wegener WA, Crawford JA, Crow JP, Andrews DA, Goldenberg DM (2004) Diagnosing suspected acute nonclassic appendicitis with sulesomab, a radiolabeled antigranulocyte antibody imaging agent. J Pediatr Surg 39(9):1338 – 44
Peltier P, Potel G, Lovat E, Baron D, Chatal JF (1993) Detection of lung and bone infection with anti-granulocyte monoclonal antibody BW 250/183 radiolabelled with 99Tcm. Nucl Med Commun 14(9):766 – 74
Peters AM (1994) The utility of [99mTc]HMPAO-leukocytes for imaging infection. Semin Nucl Med 24(2):110 – 27
Procaccini E, Chianelli M, Pantano P, Signore A (1999) Imaging of autoimmune diseases. Q J Nucl Med 43(1):100 – 12
Rennen HJ, Boerman OC, Oyen WJ, Corstens FH (2003) Kinetics of (99m)tc-labeled interleukin-8 in experimental inflammation and infection. J Nucl Med 44(9):1502 – 9
Reuter S, Schirrmeister H, Kratzer W, Dreweck C, Reske SN, Kern P (1999) Pericystic metabolic activity in alveolar echinococcosis: assessment and follow-up by positron emission tomography. Clin Infect Dis 29(5):1157 – 63
Salvarani C, Pipitone N, Versari A, Vaglio A, Serafini D, Bajocchi G, Salvo D, Buzio C, Greco P, Boiardi L (2005) Positron emission tomography (PET): evaluation of chronic periaortitis. Arthritis Rheum 53(2):298 – 303
Santiago JF, Jana S, Gilbert HM, Salem S, Bellman PC, Hsu RKS, Naddaf S, Abdel-Hayem HM (1999) Role of fluorine-18-fluorodeoxyglucose in the work-up of febrile AIDS patients: experience with dual head coincidence imaging. Clin Positron Imaging 2(6):301 – 9
Sarda L, Cremieux AC, Lebellec Y, Meulemans A, Lebtahi R, Hayem G, Genin R, Delahaye N, Huten D, Le Guludec D (2003) Inability of 99mTc-ciprofloxacin scintigraphy to discriminate between septic and sterile osteoarticular diseases. J Nucl Med 44(6):920 – 6
Scheel AK, Meller J, Vosshenrich R, Kohlhoff E, Siefker U, Muller GA, Strutz F (2004) Diagnosis and follow up of aortitis in the elderly. Ann Rheum Dis 63(11):1507 – 10
Schiesser M, Stumpe KD, Trentz O, Kossmann T, von Schulthess GK (2003) Detection of metallic implant-associated infections with FDG PET in patients with trauma: correlation with microbiologic results. Radiology 226(2):391 – 8
Signore A, Parman A, Pozzilli P, Andreani D, Beverley PC

(1987) Detection of activated lymphocytes in endocrine pancreas of BB/W rats by injection of 123I-interleukin-2: an early sign of type 1 diabetes. Lancet 2(8558):537 – 40

Signore A, Chianelli M, Parisella MG, Capriotti G, Giacalone P, Di Leve G, Barone R (1999) In vivo imaging of insulitis in autoimmune diabetes. J Endocrinol Invest 22(2):151 – 8

Signore A, Chianelli M, Annovazzi A, Bonanno E, Spagnoli LG, Pozzilli P, Pallone F, Biancone L (2000a) 123I-interleukin-2 scintigraphy for in vivo assessment of intestinal mononuclear cell infiltration in Crohn's disease. J Nucl Med 41(2): 242 – 9

Signore A, Chianelli M, Annovazzi A, Rossi M, Maiuri L, Greco M, Ronga G, Britton KE, Picarelli A (2000b) Imaging active lymphocytic infiltration in coeliac disease with iodine-123-interleukin-2 and the response to diet. Eur J Nucl Med 27(1):18 – 24

Sonmezoglu K, Sonmezoglu M, Halac M, Akgun I, Turkmen C, Onsel C, Kanmaz B, Solanki K, Britton KE, Uslu I (2001) Usefulness of 99mTc-ciprofloxacin (Infecton) scan in diagnosis of chronic orthopedic infections: comparative study with 99mTc-HMPAO leukocyte scintigraphy. J Nucl Med 42(4):567 – 74

Stumpe KD, Zanetti M, Weishaupt D, Hodler J, Boos N, von Schulthess GK (2002) FDG positron emission tomography for differentiation of degenerative and infectious endplate abnormalities in the lumbar spine detected on MR imaging. AJR Am J Roentgenol 179(5):1151 – 7

Sugawara Y, Gutowski TD, Fisher SJ, Brown RS, Wahl RL (1999) Uptake of positron emission tomography tracers in experimental bacterial infections: a comparative biodistribution study of radiolabeled FDG, thymidine, L-methionine, 67Ga-citrate, and 125I-HSA. Eur J Nucl Med 26(4):333 – 41

Thakur ML, Marcus CS, Kipper SL, Ahdoot R, Diggles L, Pham HL, Minami C, Rhodes, Patel MC, Smith T (2001) Imaging infection with LeuTech. Nucl Med Commun 22(5):513 – 9

Vanquickenborne B, Maes A, Nuyts J, Van Acker F, Stuyck J, Mulier M, Verbruggen A, Mortelmans L (2003) The value of (18)FDG PET for the detection of infected hip prosthesis. Eur J Nucl Med Mol Imaging 30(5):705 – 15

Vinjamuri S, Hall AV, Solanki KK, Bomanji J, Siraj Q, O'Shaughnessy E, Das SS, Britton KE (1996) Comparison of 99mTc infecton imaging with radiolabelled white-cell imaging in the evaluation of bacterial infection. Lancet 347(8996): 233 – 5

Walter MA, Melzer RA, Schindler C, Muller-Brand J, Tyndall A, Nitzsche EU (2005) The value of [18F]FDG PET in the diagnosis of large-vessel vasculitis and the assessment of activity and extent of disease. Eur J Nucl Med Mol Imaging 32(6): 674 – 81

Yamada S, Kubota K, Kubota R, Ido T, Tamahashi N (1995) High accumulation of fluorine-18-fluorodeoxyglucose in turpentine-induced inflammatory tissue. J Nucl Med 36(7): 1301 – 6

Yapar Z, Kibar M, Yapar AF, Togrul E, Kayaselcuk U, Sarpel Y (2001) The efficacy of technetium-99m ciprofloxacin (Infecton) imaging in suspected orthopaedic infection: a comparison with sequential bone/gallium imaging. Eur J Nucl Med 28(7):822 – 30

18 The Relevance of PET in Diagnostic Oncology

E. Bombardieri, A. Alessi, C. Villano, A. Gerali, F. Crippa

18.1 Introduction

The characteristic feature of nuclear medicine is that it provides functional images of organs, tissues and both normal and pathological processes, revealing the uptake and the biodistribution of several radiopharmaceuticals according to their pathway of flux, concentration and metabolism. There is a strong relationship between nuclear medicine and oncology since in general nuclear medicine images are able to give both morphological information and data on molecular and cellular activity. The major advantages of this *functional imaging* are that this biological characterization is carried out by the direct observation in vivo of the patient (Bombardieri et al. 1999).

The most important requirements of modern oncology for diagnosis are:

1. The necessity of defining the presence of a malignant tumor by the earliest and most effective method, since the possibility of curing cancer is related to an early diagnosis and to the tumor extension
2. The necessity of characterizing the neoplasm in terms of biology, proliferation, aggressiveness, differentiation, and receptor status, since more or less aggressive treatments should be modulated within the same group of cancers even at the same stage according to prognostic parameters that can identify the susceptibility to a specific treatment (Chu and Devita 2001).

Besides these two primary issues, there are also other needs in oncology, which are no less essential, such as: evaluation of the size of tumor mass and involvement of other structures, the study of treatment response (during the course and at the end of the treatment), and the discovery of relapses. There is no doubt that the conventional radiologic modalities (X-rays, US, CT, MRI) today play a primary role in oncology. Some of them show a very high resolution down to 1 – 2 mm and are able to accurately describe the morphology of the lesions, their topographic relationships with the surrounding anatomical structures, and to provide information about the benign and malignant nature of the disease. However, conventional radiology sometimes fails to differentiate benign from malignant alterations, vital neoplasms from the scar or inflammatory tissue, and is not able to interpret the distortion due to the previous treatment, and to give functional information about the tumor biology. The added value of nuclear medicine consists in giving answers to many issues that are critical in the diagnostic work-up of patients and which are essential for the management.

The characteristic of nuclear medicine is that by using various metabolic radiopharmaceuticals it gives functional images of cancer which can be successfully integrated with the anatomical ones.

18.2 PET is an Example of a Necessary Examination in Oncology

In recent years there has been a very impressive increase in the number of clinical applications for PET. Initially PET studies were mainly focused on basic research, investigating brain and heart metabolism and function. The technological improvements and the advent of whole body PET instruments encouraged the greatest development of clinical PET that has been observed in oncology (Hoch et al. 1997). At present almost 90 % of the clinical activity in standard PET centers all over the world consists of oncologic PET studies. Also the number of neurologic, neuropsychiatric and cardiac applications has progressively increased, albeit to a lesser extent. The most important reason why PET is successful in oncology is that it provides much diagnostic information very useful for the clinical management of patients. The whole body examination permits a rapid image to be taken of the entire body and represents an ideal tool for staging cancer (Fig. 18.1). Several studies on the diagnostic value of FDG-PET across different oncological types (lung cancer, colorectal cancer, melanoma, lymphoma, head and neck cancer, breast tumors, brain tumors, ovarian, cervical and uterine cancer, bladder cancer, gastro-esophageal cancer, hepatocellular cancer, muscle and connective tissue tumors, pancreatic cancer, prostate can-

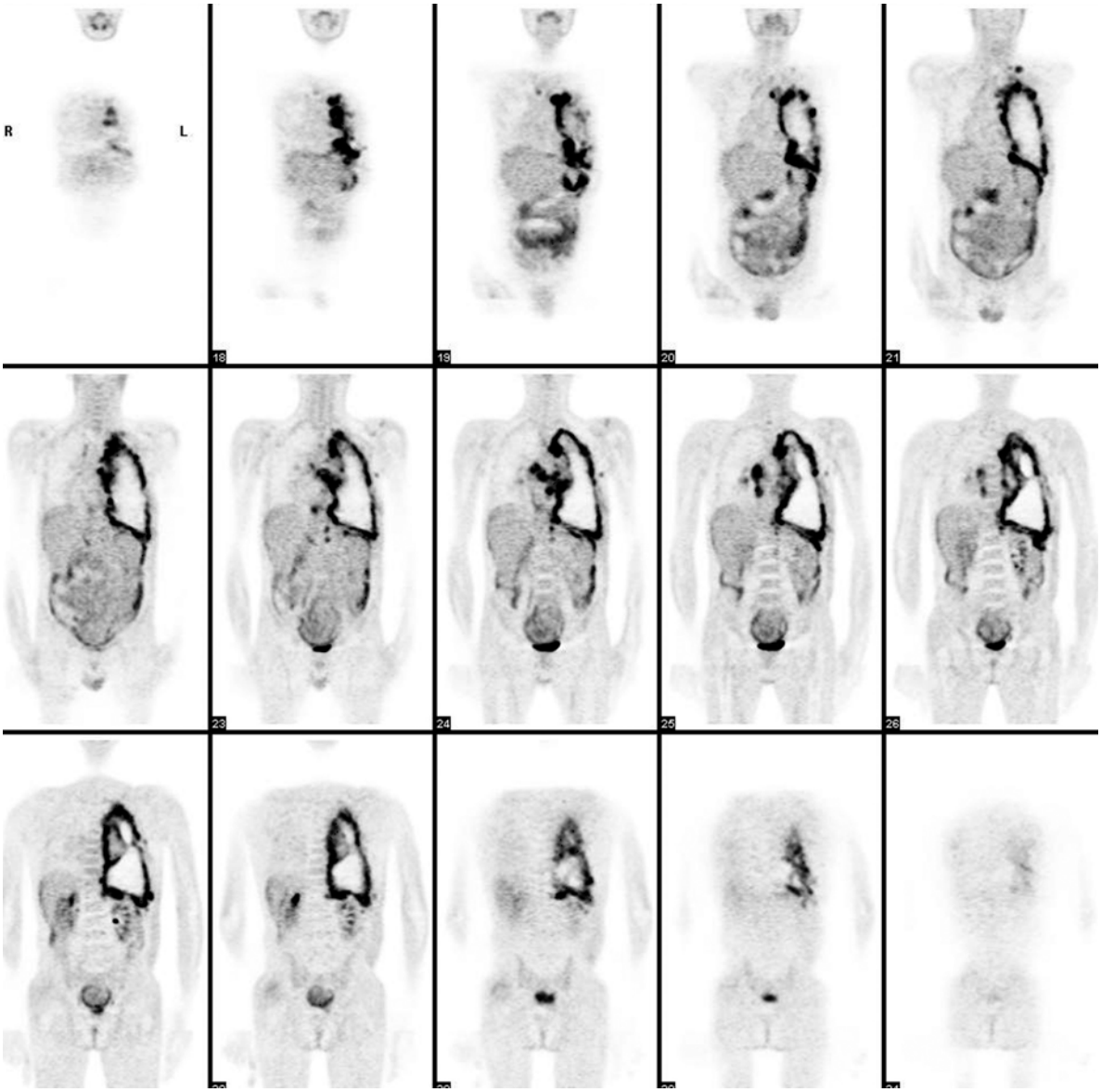

Fig. 18.1. A 54-year-old man with mesothelioma. FDG-PET was performed for pre-therapy staging, showing abnormal foci of FDG uptake in the left pleural structures, left diaphragm, mediastinum and bilateral hilar lymph-nodes. PET also detected several abdominal foci of abnormal FDG uptake, very consistent with peritoneal seedlings of the disease

cer, renal cell cancer, testicular cancer, and thyroid cancer) have estimated a very good sensitivity and accuracy (higher than 90 %) (Gambhir et al. 2001). The diagnostic validity of PET in comparison with the conventional radiologic tools (such as US, CT and MRI) is often superior. Another reason why PET has found such wide application in oncology is the intrinsic requirements of oncology itself, which needs both an improved detectability of lesions with respect to the morphologic limits of conventional radiology and new parameters to describe the behavior of cancer tissue in terms of metabolism, differentiation, proliferation, and grade of malignancy.

Neoplastic cells have metabolic characteristics that coincide with the availability of ^{18}F-fluorodeoxyglucose (FDG), which is the most suitable radiopharmaceutical for PET. FDG is used worldwide for the vast majority of clinical PET studies, particularly in oncology (Delbeke 1999; Wahl et al. 1991). Of course, FDG is not the only possible radiopharmaceutical for oncology. It is known that the avidity of tumors for FDG is not always optimal in all cancer types. Some tumors such as neuroendocrine tumors and other well-differentiated tumor types show a limited uptake of FDG. Furthermore, FDG shows a high degree of unspecific uptake in any cell type with a high glycolytic activity. FDG accumulates in

infectious and inflammatory processes (e.g., abscesses, TB, sarcoidosis, active granulomatosis, etc.) and this sometimes prevents the discrimination between tumor tissue and certain benign or inflammatory alterations (Stumpe et al. 2000). FDG also shows physiologic uptake in some normal tissues (brain, myocardium and other muscles, kidney and urinary system, gastrointestinal tract as well as thymus tissue); for instance, the high uptake of FDG by normal cortex makes FDG-PET relatively insensitive for the detection of small brain metastases (Engel et al. 1996).

18.3 Other Radiopharmaceuticals than FDG

For all the aforementioned reasons, other radiopharmaceuticals than FDG may in some cases be more appropriate for imaging certain cell pathways or specific structures. Several radiopharmaceuticals are available which explore various metabolic pathways such as amino acid uptake, ^{11}C-methyl-l-methionine (^{11}C-MET), ^{18}F-fluoroethyl-l-tyrosine (^{18}F-FET), ^{18}F-α-methyltyrosine (18F-FMT), nucleic acid synthesis, ^{18}F-fluorothymidine (^{18}F-FLT), dopamine synthesis, ^{18}F-fluoro-dihydroxy-phenylalanine (^{18}F-FDOPA), cancer cell hypoxia, ^{18}F-fluoromisonidazole (^{18}F-FMISO), hormone receptor expression ^{18}F-fluoroethinyl estradiol (^{18}F-FES), membrane metabolism, ^{11}C or ^{18}F-choline (^{11}C, ^{18}F-CHOL), etc. (Krohn 2001; Lewis and Welth 2001; Varandolo et al. 2000; Townsend and Beyer 2003; Mason and Mathis 2003; McQuade et al. 2003).

These PET tracers have been successfully evaluated by different authors in oncology; however, their use has not yet entered current clinical practice, except in a limited number of PET centers equipped with cyclotron and radiochemistry facilities.

Where PET is available, its main applications in oncology cover a number of indications involving different clinical steps in the diagnostic work-up of cancer patients. At present the most frequent clinical indications are:

1. To measure the extent of the primary tumor and eventually depict distant metastases
2. To evaluate the response after cancer treatment (early and delayed)
3. To detect suspected recurrences and re-stage relapsed patients
4. To differentiate malignant cancer cells from other non-malignant processes (Gambhir et al. 1998; Messa et al. 2004)

Other applications are not as common in the clinical routine as those already mentioned but they have been investigated and are adopted when required in different cancer types to:

1. To establish the grade of malignancy or to characterize the cancer cell
2. To predict tumor response
3. To identify the primary site in the presence of a tumor of unknown origin
4. To localize biopsy sites
5. To plan radiotherapeutic treatment by defining the biological target volume (Bombardieri et al. 2003)

PET shows certain limitations in diagnostic sensitivity and is not able to identify microscopic disease. This is due to the resolution of PET scanners, which is not less than 4 – 5 mm. Of course this problem in the future can be partially overcome as the technology of PET will continue to improve both from a instrumentation and a radiopharmaceutical standpoint. In spite of this limit the lesion detectability of PET is good, often higher than that of CT and MRI. This makes PET cost-effective even considering the relatively high cost of a PET facility. Different economic analyses (cost-analysis, cost-effectiveness analysis, cost-utility analysis) have been published and they demonstrate the advantages of the clinical use of PET (Bombardieri et al. 1997b; Scott et al. 1998; Gambhir et al. 1998). An impressive body of information shows that PET is able to provide unique information in patients with cancer that cannot be obtained with other current techniques. The practical advantages of PET compared to conventional morphologic modalities allow clinicians to change the management of patients on the basis of the FDG-PET results. The average management changes across all oncologic indications have been estimated to be around 30 %. This is particularly true in cancer with a high relapse rate after so-called radical surgery, for instance in patients with small metastatic localizations not identified by conventional modalities. Some groups of patients should not undergo an attempt at curative surgery without a previous PET scan, as the preoperative demonstration of non-resectable tumor may avoid unnecessary surgery. Beside this, PET also has the potential to evaluate the response of cancer to therapy, even at an early stage, e.g., after one or two cycles of chemotherapy. This permits a change to more effective treatment in patients who are not responding, avoiding morbidity from inappropriately prolonged treatment.

18.4 The Development of the Integration of PET-CT Imaging

PET is usually performed in association with computed tomography (CT), which is the standard imaging technique for the majority of cancer patients. The combined evaluation of PET and CT improves the diagnosis of the staging cancer in a more accurate way. In clinical

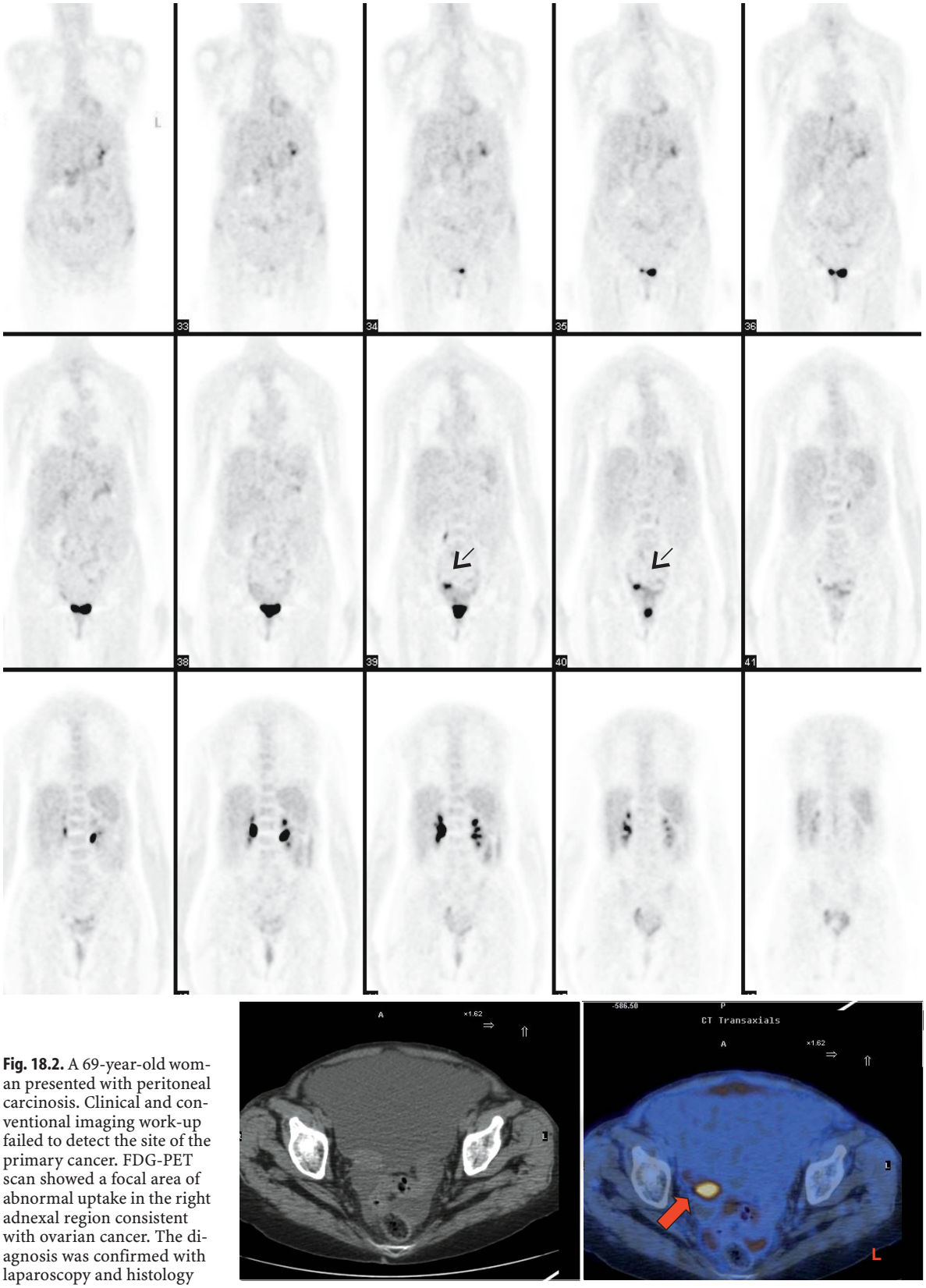

Fig. 18.2. A 69-year-old woman presented with peritoneal carcinosis. Clinical and conventional imaging work-up failed to detect the site of the primary cancer. FDG-PET scan showed a focal area of abnormal uptake in the right adnexal region consistent with ovarian cancer. The diagnosis was confirmed with laparoscopy and histology

practice the current indication of PET is when patients have already been assessed with CT, MRI or US and there is the need to clarify the nature of a suspected lesion or to look for lesions not detected by the conventional modalities even if clinically suspected. Several methods of integrating functional PET and images with morphological information provided by CT or MRI have been proposed. This combination is sometimes referred to as "anatomo-metabolic imaging" (Wechalekar et al. 2005).

Over the past decade a number of software-based algorithms have been proposed that allow the registration and combined display of PET and CT images. These solutions are good for the brain but generate many positioning errors in the whole body studies. An alternative approach is the fusion of the hardware components to allow the acquisition of anatomical and functional information in a single scan session without repositioning patients. Recently the industry has developed integrated PET-CT scanners that provide, in a single patient sitting, both the data from a CT scanner and information recorded by a PET scanner. The image fusion is performed, CT data being merged with PET data. The information coming from CT is also used for the attenuation correction. In this way a whole-body PET-CT study can be obtained in about 25 min. This approach has improved patient acceptance and throughput (Fig. 18.2).

Multimodality imaging today seems a very appealing approach and probably in the forseeable future it will become routine. In fact PET-CT offers several advantages over PET, and this can have a great impact on clinical practice. Briefly PET-CT reduces the acquisition time, improves the anatomical localization of tumor spread and gives the possibility to stage cancer patients in one single step. Over 500 combined PET-CT tomographs are operational worldwide today. An increasing number of publications are demonstrating the benefits of PET-CT imaging and substantiating the hypothesis of its improved diagnostic accuracy and clinical value. For these reasons PET-CT scanners are rapidly replacing conventional dedicated PET tomographs and the clinical success of the first PET-CT hybrid instruments has given a tremendous impulse to the technological research. The next generation of PET-CT technology is looking at the use of new acquisition and data-processing software, innovative detector designs, and adoption of gating mechanisms. The final goal is to cover large volumes and reduce the time for a whole body-PET examination to 10 – 15 min and, at the same time, to introduce into the routine respiratory/cardiac gating to better localize and define the margins of the lesions. Also the project to develop the PET-MRI system is ongoing and under evaluation, and the first satisfactory progress has been achieved in this area with small animal scanners. Of course these advances should also be flanked by the development of new radiopharmaceuticals.

The daily application of whole body PET-CT in oncology is generally the same as in the dedicated PET instruments, thus including tumor diagnosis, staging and restaging, follow-up, treatment monitoring and radiotherapy planning. In particular an application of great interest is image guided radiotherapy. Being able to gate the PET and the CT acquisition in a combined PET-CT design allows the target volumes to be defined more precisely. Several items of clinical evidence show that PET-CT is generally superior to PET, and this can have a great impact on clinical practice (Ell 2006; Taki et al. 1999).

18.5 Brain Tumors

Brain tumors (meningiomas, glioblastomas and astrocytomas) and metastatic brain tumors are one of the first oncological indications of PET. Nuclear medicine modalities with gamma emitting radiopharmaceuticals have shown to be able to image tumor lesions on the basis of alterations of the blood-brain barrier, tumor perfusion, tumor proliferation and metabolism (^{67}Ga-EDTA, ^{99m}Tc-DTPA, ^{201}Th chloride, ^{99m}Tc-HMPAO, ^{99m}Tc-sestamibi, ^{99m}Tc-tetrofosmin, ^{123}I-α-methyltyrosine) (Taki et al. 1999; Maffioli et al. 1996; Arbab et al. 1996). The assessment of the biodistribution of these radioactive tracers can be currently performed with single photon emission computed tomography (SPECT). Of the positron emitting radiopharmaceuticals for brain tumors, the most frequently used is ^{18}F-FDG followed by some amino acid tracers such as ^{11}C-MET and ^{18}F-FET (Laverman et al. 2002).

PET has a role in tumor imaging for several clinical tasks: (a) detection of viable tumor tissue; (b) tumor delineation; (c) selecting the best biopsy site; (d) noninvasive tumor grading; (e) evaluation of tumor response; and (f) therapy planning. The diagnosis of brain tumor is currently performed by means of anatomic imaging modalities, X-ray CT and/or MRI scan, with and without the administration of contrast agents and with different acquisition sequences (MRI). In particular conditions the anatomic imaging techniques are not able to give all the necessary information relating to the presence, growth, characteristics and biologic activity of a tumor. Several studies with FDG showed an elevated uptake of the tracer in tumors, but it appeared that the uptake of FDG was related to the grade of malignancy. Thus low-grade gliomas were not easily identified by ^{18}F-FDG while ^{11}C-MET and ^{18}F-FET are able to detect brain tumor boundaries with a high accuracy, both of primary lesions and recurrences, regardless of

their pathologic grading (Derlon et al. 1997; Kaschten et al. 1998; Mineura et al. 1997).

Radiolabeled amino acid seems to be superior to TC and MRI for staging all types of gliomas. As an alternative to FDG-PET, PET with radiolabeled amino acids is able to visualize amino acid transport, which is faster in tumors. These tracers might be more tumor specific than FDG since the amino acid uptake in macrophages and other inflammatory cells is low. The use of ^{11}C-MET may prevent a number of problems related to the tumor/non-tumor uptake ratio encountered with FDG, including the difficult differential diagnosis with other cerebral disorders such as infections, radiation necrosis or edema that may cause abnormal FDG uptake. ^{11}C-MET uptake is correlated to cell proliferative activity and to microvessel density, and the intensity of MET uptake can represent a prognostic parameter. Another promising radiopharmaceutical is ^{11}C-choline (CHOL), a tracer that has a higher uptake in glioblastoma cells than in normal brain tissue (Shinoura et al. 1997; Coleman et al. 2000).

Hemodynamic parameters can be measured by PET with oxygen-15. By means of mathematical modeling approaches with sequential studies using $^{15}O_2$, $C^{15}O_2$ and $C^{15}O$, functional images of cerebral blood flow (CBF), oxygen extraction (OER), oxygen metabolic rate ($rCMRO_2$) and regional blood volume (CBV) can be derived. These studies have shown that in brain tumors the blood flow is variable, while the oxygen metabolism was found to be depressed in patients with gliomas (Lammertsma et al. 1985; Tyler et al. 1987). In the presurgical assessment, nuclear medicine usually lacks the anatomic information required to define treatment margins with the accuracy needed for surgery and radiotherapy planning. Nevertheless, functional brain mapping with $H_2{}^{15}O$-PET associated with MET or FDG has been proposed as a way to define the higher cortical functions near a brain tumor, with the aim of achieving radical resections with a reduced risk of neurologic impairment (Gupta et al. 1999).

As has been mentioned above, the relationships between the grade of malignancy and the uptake of positron emitting tracers have been extensively investigated. Some reports have related the grade of malignancy of gliomas to the rate of FDG uptake and have shown that, while low-grade astrocytomas have a low FDG uptake, anaplastic astrocytomas and glioblastomas exhibit a very elevated uptake of this radiopharmaceutical (Derlon et al. 2000). So FDG-PET has been proposed as a useful tool to assess tumor grade also in oligodendrogliomas and gangliogliomas. With regards to the radiolabeled amino acid, a highly significant difference in the uptake has been demonstrated between low-grade and high-grade oligodendrogliomas, and in some recent studies it was found that MET was even better than FDG in grading this type of tumor.

CT and MRI imaging of brain tumors give single or multiple lesions heterogeneous in cellular composition where there is a mixture of active disease, non-specific inflammation, necrosis or edema. In these areas it is hard to identify the cancer components by radiological methods. In such cases FDG-PET has been proposed as a "metabolic biopsy" guide to depict the highly active area, since the anaplasia and/or proliferating cells determine an elevated uptake of glucose (Hanson et al. 1991). More recently MET-PET has also been applied to guide a stereotactic biopsy in a brain tumor. In comparison to FDG, this tracer seems to have the advantage of a better detection of non-anaplastic tumor sites and brain regions with infiltrating neoplastic cells (Pirotte et al. 2004).

In spite of the large number of potential applications, the most common use of FGD-PET in the clinical routine consists of the evaluation of patients post-treatment. Clinical evidence demonstrates that FDG-PET imaging succeeds in differentiating the residual tumor from the effects of surgery. A decrease in FDG uptake in a tumor a few weeks or months after surgery suggests a good response to treatment, indicating a reduced number of viable cells or a reduced metabolism of damaged cells (Kim et al. 1992). In the same way after intensive irradiation or chemotherapy, MRI and CT cannot distinguish tumor progression from radiation injury or necrosis. On the contrary FDG uptake indicates the presence of viable tumors (at least in those tumors where a high uptake of FDG was observed before therapy), and absent FDG uptake suggests that necrosis is present (Ishikawa et al. 1993). Recent observations demonstrated in low-grade gliomas a relationship between glucose metabolism (as assessed by FDG-PET) and risk of malignant evolution. It was concluded that the presence of areas of increased FDG uptake in histologically proven low-grade gliomas is predictive of a deleterious evolution in most cases (De Witte et al. 1996). In this field the experience with alternative tracers is still limited; however, a quantitative evaluation of MET uptake in patients with low-grade gliomas showed that a low tumor uptake in the baseline study had a significantly better prognosis than those with a high uptake (Nuutinen et al. 2000).

18.6 Head and Neck Cancer

Staging head and neck cancer is important for treatment planning and prognosis. CT and MRI are currently the first choice among the diagnostic tools, but their accuracy is not sufficient to solve the clinical problems. These methods in 5–15% of cases do not identify the primary tumor in patients with evidence of disease. FDG-PET can be successful in the detec-

tion of primary unknown tumors. However, PET represents an additional diagnostic benefit in patients with a negative diagnostic work-up, since the identification of an unknown primary lesion by FDG-PET can prevent extensive morbidity from the incorrect treatment (Jungehulsing et al. 2000). Moreover, FDG-PET can detect additional local and/or distant metastases, thus improving the accuracy of staging in these patients.

When FDG-PET is used in the initial evaluation of a known neoplastic lesion, it shows a diagnostic accuracy comparable to that of CT or MRI for the detection of primary tumor. FDG-PET images do not provide clear information on anatomic details that may be useful for treatment planning (i.e., local and perineural spread, deep infiltration, bone destruction). The use of CT or MRI-PET coregistration techniques, when it is possible, could improve the diagnostic accuracy, even if these procedures are difficult to manage in a routine work-up. FDG-PET at cancer presentation appears to play a complementary role to CT and MRI for the first diagnosis; even PET can occasionally clarify equivocal results obtained with other imaging techniques. On the contrary in detecting local nodal diseases, the accuracy of PET so far is better than that of CT, MRI and US (Adams et al. 1998b; Kau et al. 1999). False negative FDG-PET results can be expected only in the case of microscopic lymph node involvement. It is well known that the presence or absence of regional lymph node involvement is one of the most important prognostic parameters for head and neck cancer. The hybrid PET-CT system has shown to be useful in upstaging patients with negative cervical lymph nodes at CT or MRI examinations; in the same way also patients with advanced disease are usually upstaged with PET-CT (Myers et al. 1998; Hughes et al. 2004).

Another very useful application of FDG-PET is the evaluation of patients after treatment. Head and neck tumors bring several diagnostic problems as post-surgery or post-radiotherapy anatomic changes, edema and fibrosis may reduce the diagnostic reliability of CT or MRI. PET may help to establish the radicality of surgical node dissection and is very useful in studying both lymph nodes and soft tissues and bones. Moreover it should be considered that post-radiotherapy necrosis can make it difficult to perform reliable biopsies of lesions suspected of being persistent or recurrent tumor. FDG-PET has proved to be a valid non-invasive modality for studying patients after radiotherapy and distinguishing residual or recurrent tumor from post-irradiation effects on soft-tissue uptake. In this setting FDG-PET is more accurate than CT or MRI (Lonneux et al. 2000; Lapela et al. 2000).

The hybrid PET-CT system has been studied in monitoring the responses to therapy (surgery, chemotherapy, radiotherapy) since this examination is able to differentiate between the post-therapeutic abnormalities and tumor tissue. A 4 months post-radiotherapy scan is a better predictor of the presence of cancer (Greven et al. 2001). The use of FDG-PET-CT has a significant impact on tumor staging and determination of radiotherapy treatment volume and dose (Koshy et al. 2005; Schwartz et al. 2005).

FDG-PET has showed to be a reliable method for early prediction of therapy outcome in preliminary studies of patients with advanced head and neck cancer. The FDG uptake in cancer tissues before and during treatment can predict the response to chemotherapy. Early evaluation can be carried out after 1 week of radiotherapy or during the course of chemotherapy (Hicks et al. 2005b). Some interesting experience has been gained using PET with other radiopharmaceuticals, such as ^{18}F-MISO, used as markers of tumor hypoxia, but until now they have not found a large current application.

18.7 Lung Cancer

Lung cancer imaging is obtained currently with radiological techniques, especially high resolution CT (spiral, multi-slice CT), which provides excellent morphologic information about the pulmonary and thoracic structures. The conventional radiological methods show limitations in determining the nature of suspicious focal opacities, in the evaluation of mediastinal involvement, in the assessment of viability of previously treated lesions and in the diagnosis of tumor relapse. The nuclear medicine examinations with gamma emitting tracers have been established over the years for the preoperative functional evaluation (scintigraphic perfusion and ventilation), staging and detection of recurrences or differentiation of proliferating tumor (^{99m}Tc-sestamibi-SPECT, ^{201}Tl-SPECT, ^{67}Ga-SPECT, etc.) (Chiti et al. 1999). PET has had a great impact on the diagnosis and staging of lung cancer, and the areas in which PET has shown to be useful include: diagnosis of lung, nodules, thoracic and extrathoracic staging, evaluation of recurrences, and monitoring of response to therapy.

Evaluation of solitary pulmonary nodules is usually performed by chest X-rays followed by CT. At present CT is of help in characterizing the suspected lesions evident in standard X-rays. When a nodule is not benign according to the CT image results, further evaluation is required (Hartman 2005). Several studies have shown the great effectiveness of FDG-PET in classifying solitary pulmonary nodules (Paulus et al. 1995; Lowe et al. 1997). This has been confirmed by multi-institutional studies which have included a large number of patients with solitary lung masses and indefinite diagnosis after

CT examination. PET showed a sensitivity ranging from 95% to 99% for tumor detection. Semiquantitative evaluation of FDG uptake can be used to distinguish malignancy; usually a standardized uptake value (SUV) value of 2.5 or higher is considered indicative of malignancy. The general opinion is that this approach does not give different results from those obtained with a simple visual analysis. False positive findings occur in the presence of infectious and inflammatory processes (granulomatosis, tuberculosis, fungal diseases), but most acute infectious diseases do not accumulate FDG. False negative results occur in tumors with a low level of metabolic activity (bronchioalveolar cell carcinoma) or in small nodules (the detection limit is around 5–6 mm with dedicated PET scanners). FDG-PET in many cases allows the differential diagnosis of solitary pulmonary nodules, thus avoiding tissue sampling in patients with non-metabolically active lesions while prompting a biopsy in the case of nodules that take up FDG. The use of PET prevents unnecessary thoracotomies, resulting also in cost savings. An open question is: should PET be applied to all patients with solitary pulmonary nodules or only to a selected group of patients? Particular characteristics of pulmonary nodules can predict malignancy and constitute an absolute indication for surgical resection.

Preoperative study of mediastinal lymph nodes with PET has an impact both on the surgical and/or medical strategies and has a great prognostic value. Since size is not correlated with tumor involvement, morphologic imaging does not show sufficient sensitivity for depicting node metastases. Several prospective studies demonstrate that the diagnosis of lymph node involvement by FDG-PET is more accurate than by CT. It should be stressed that in a study with histological control the use of PET resulted in a 96% accuracy versus a rate of only 79% for CT (Steinert et al. 1997). These data have been confirmed by other similar studies (Magnani et al. 1999; Baum et al. 1999). A large number of investigators conclude that in the staging and management of NSCLC the combination of FDG-PET with CT is more economic and it results also in a marginal increase in life expectancy as compared to conventional staging with CT alone.

Imaging fusion with PET-CT has been shown to prevent unnecessary surgery in 20% of patients evaluated as being operable with other criteria (Lardinois et al. 2003; Verboom et al. 2003). This means that PET-CT results in changing the management of 30% of patients (Keidar et al. 2005).

Another important characteristic of PET is that it is a whole-body scanning modality able to find extrathoracic metastases in addition to primary tumors and lymph node metastases. The metastases of lung cancer are imaged with good contrast and this results in a very high diagnostic accuracy of PET. For example, PET seems to be more specific than bone scan in identifying the site of skeletal metastases. Also adrenal metastases are visualized with high accuracy, and so are liver, abdominal, and parenchymal lung metastases. The detection of previously unknown distant metastases leads to a change in therapeutic management in about 20% of patients (Marom et al. 1999).

Several experiences report that FDG-PET may also play a role in the assessment of therapy results, as changes in metabolism always precede changes in morphology (Fig. 18.3). The determination of tumor changes has a much greater accuracy with PET than with CT (Herbert et al. 1996). Post-irradiation changes have to subside for PET to provide an accurate semiquantitative assessment of tumor viability with a lesser chance of false positive results. Inflammatory changes in the first few weeks after radiation therapy can cause a problem. Therefore PET should not be performed until 3 months after radiation therapy. In the same way, PET can be used also to assess the efficacy of chemotherapy (MacManus et al. 2005).

There is a clinical role for integrated PET-CT in the definition of treatment volume in radiation treatment planning. In fact PET-CT based radiation treatment planning is a useful tool resulting in the modification of gross tumor volume in about 50% of patients (Ashamalla et al. 2005). Several authors confirmed that the co-registration of PET and CT images leads to a change in the definition of the clinical target volume in the majority of patients; this may significantly modify the management and the radiation treatment modality in patients (Messa et al. 2005). The outcome after radiotherapy can be predicted on the basis of the kinetics and uptake of ^{18}F-MISO in tumor tissue. High SUV and an accumulation type curve are highly suggestive of an incomplete response (Eschmann et al. 2005).

FDG uptake in cancer can be assumed to be a prognostic indicator. The FDG SUV correlates with prognostic parameters, such as tumor stage and grade. However, SUV alone cannot be considered as an independent predictor of survival (Kieninger et al. 2006).

As an alternative radiopharmaceutical to FDG other PET radiopharmaceuticals are ^{11}C-MET and ^{18}F-FLT; however, the limited experience in this field did not demonstrate a real superiority of these examinations in visualizing tumors. FLT showed an interesting correlation between tumor uptake and cell proliferation, so it can be proposed as a parameter for chemotherapy monitoring (Ishimori et al. 2004; Yap et al. 2006).

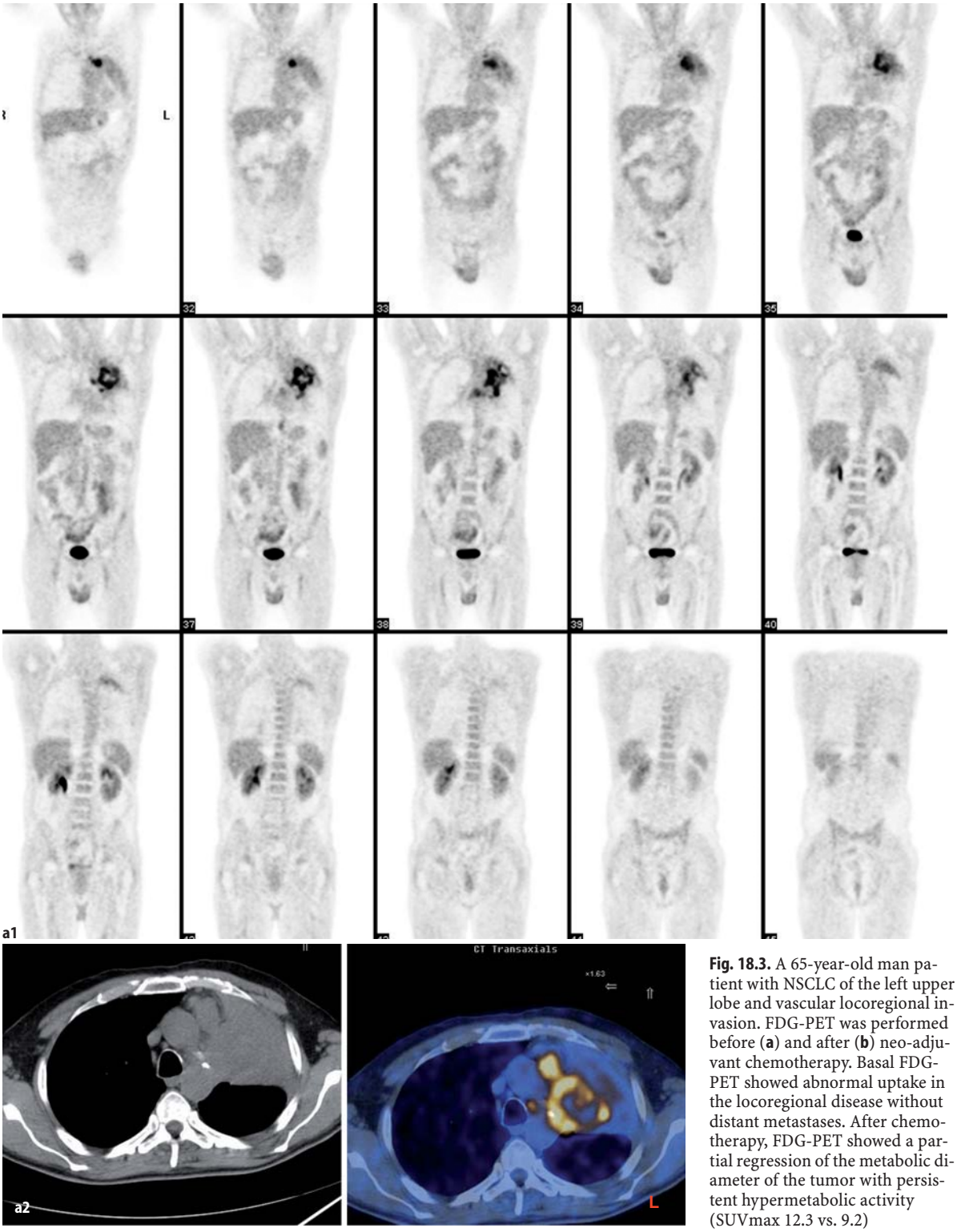

Fig. 18.3. A 65-year-old man patient with NSCLC of the left upper lobe and vascular locoregional invasion. FDG-PET was performed before (**a**) and after (**b**) neo-adjuvant chemotherapy. Basal FDG-PET showed abnormal uptake in the locoregional disease without distant metastases. After chemotherapy, FDG-PET showed a partial regression of the metabolic diameter of the tumor with persistent hypermetabolic activity (SUVmax 12.3 vs. 9.2)

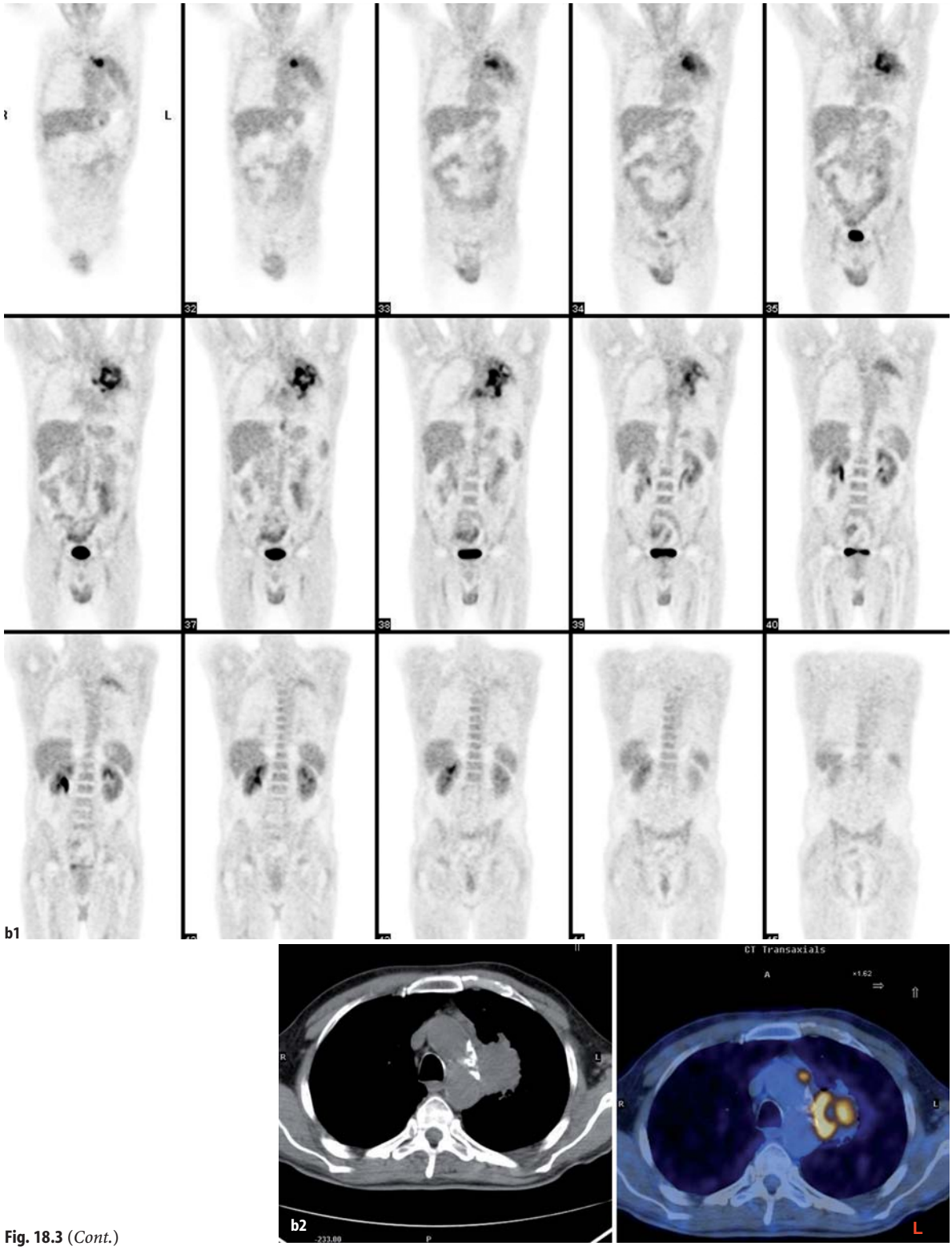

Fig. 18.3 (*Cont.*)

18.8 Gastrointestinal Cancer

The most frequent gastrointestinal (GI) cancers are colon-rectum, stomach, pancreas, liver, bile duct, and esophagus. The most common tumor type is adenocarcinoma. Among the GI epithelial cancers one can identify a particular type of tumor called neuroendocrine tumor. Neuroendocrine tumors of the GI tract are now referred to as neuroendocrine gastroenteropancreatic (GEP) tumors and they often express somatostatin (SST) receptors. PET imaging of most epithelial GI tumors is based on FDG because epithelial GI tumors – like nearly all malignant tumors – are characterized by an accelerated rate of glycolysis. Other PET tracers of interest but without current usefulness in GI cancer include ^{11}C-MET, labeled chemotherapeutic agents such as^{18}F-FET, ^{18}F-FU, ^{11}C-thymdine and radiolabeled DNA precursors, as well as other agents that trace tumor blood flow and tumor hypoxia (Vansteenkiste et al. 1997; Bombardieri et al. 2001; Tewson and Krohon 1998; Wester et al. 1999; Hayashi et al. 1998).

FDG has not proven to be an ideal radiopharmaceutical for neuroendocrine tumors (Eriksson et al. 1999; Adams et al. 1998a). In fact, in a number of tumors FDG-PET has revealed an increased glucose metabolism only in poorly differentiated GEP tumors. These less differentiated neuroendocrine cancers usually do not express SST receptors. This means that FDG can be considered a suitable tracer for tumors that are SST receptor negative and its uptake may have prognostic value since it provides information about tumor aggressiveness. New radiopharmaceuticals based on precursors different from glucose analogs have been developed, namely 5-hydroxytryptophan (5HTP) and L-dihydroxyphenylalanine (DOPA) labeled with ^{11}C (Adams et al. 1998a; Sundin et al. 2000). ^{18}F-DOPA seems more suitable than the precursors labeled with ^{11}C and FDG in imaging GEP tumors (Hoegerle et al. 1999, 2001). Other tracers for the detection of neuroendocrine neoplasms expressing somatostatin receptors are under development; one of these is ^{64}Cu-TETA-octreotide and the other one, which is very promising, is ^{68}Ga-DOTATOC (Anderson et al. 2001; Koukouraki et al. 2006; Bombardieri et al. 2004).

18.8.1 Colorectal Cancer

The tools available today to stage and assess colon cancer relapses lack accuracy and sometimes result in diagnostic and therapeutic delay. Circulating tumor markers are useful even though they show 65 % sensitivity for recurrences. Conventional X-ray can detect local recurrence but has insufficient sensitivity (less than 50 %) for overall recurrence detection. Similar results have been reported for colonoscopy (Delbeke et al. 1997). CT is the best conventional modality routinely used to localize recurrences but often fails in depicting metastases to the peritoneum, lymph nodes and mesentery. Moreover, radiology is not always successful in differentiating postoperative changes from tumor recurrences.

Much evidence indicates an important role for PET in colorectal cancer. FDG-PET is suitable for detecting recurrences, metastases and also primary tumors (Dobos and Rubesin 2002; Kanyari et al. 2005). At present the most common clinical use of PET is focused on patients with known or suspected recurrent colorectal carcinoma. In fact FDG-PET is used mainly in restaging patients with colorectal cancer, especially those with rising CEA levels or with equivocal lesions on conventional imaging (Erturk et al. 2006; Lamy et al. 2005). The clinical and economic impact of PET appears most clearly in the evaluation of postoperative recurrence (Ruhlmann and Oehr 1999; Delbeke and Valk 2001). FDG-PET shows a higher accuracy in comparison with CT and CT portography in detecting and localizing liver metastases. In addition, as whole-body FDG-PET imaging allows the evaluation of the entire body it can identify disease in the chest, abdomen, and pelvis. Outside the liver, FDG-PET is especially helpful in detecting distant nodal and peritoneal involvement.

The diagnosis of recurrences and the evaluation of tumor resectability was shown to be cost-effective when the conventional strategy (CT and CEA test) was compared to FDG-PET (Valk et al. 1999). For this reason all patients facing the problem of resection of recurrent or metastatic colorectal carcinoma should undergo FDG-PET preoperatively.

FDG-PET is used successfully in monitoring the response to therapy since it can distinguish local recurrences from scars after radiotherapy, discriminating between responders and non-responders to chemotherapy, and monitoring the effectiveness of liver chemoembolization (Yoshika et al. 1999; Vitola et al. 1996; Wiering et al. 2005). The indication for chemotherapy after surgery depends on the presence of viable residual tumor tissue. The response to chemotherapy in patients with hepatic metastases can be predicted by PET. Responders may be distinguished from non-responders after some cycles of chemotherapy by measuring FDG uptake. Also regional therapy to liver by chemoembolization can be monitored with FDG-PET imaging.

We use FDG-PET to evaluate both the viability of residual tumor and the results of previous therapeutic interventions. On this basis PET may have an impact on further treatment strategies. Of course one should take into account that FDG-PET also has limitations in the imaging of colorectal cancers. False negative results depend on the small volume of the tumor mass, which

leads to underestimation of the FDG concentration in lesions smaller than 1 cm in diameter. False positive results may be due to the presence of granulomatous or inflammatory lesions related to recent surgery or placement of catheters or drains. An interesting finding is that an elevated glucose metabolism can be observed in colon adenomas, and the detectability increases with the increase in adenoma size. This should not be seen only as false positive information but could be of interest as it is known that adenomas are premalignant lesions.

Integrated PET-CT images compared to PET alone, or PET correlated with CT at a different time, have shown improvement of lesion detection, improvement of localization of foci of FDG uptake, and precise localization of the malignant foci (soft tissue versus skeleton, liver versus bowel or lymph nodes, etc.). In particular PET-CT imaging in restaging colorectal cancer patients leads to a greater sensitivity in the interpretation of anatomic localization of metastases (Strunk et al. 2005). PET-CT fusion images influence clinical management, orienting further procedures and excluding the need for other decisions. PET-CT has the potential to give information to guide the biopsy. The imaging with an integrated system may be important for the interpretation of lesions in the abdomen and pelvis because of the absence of anatomical landmarks. In many situations it is possible to reduce the frequency of equivocal lesion findings and the number of definite locations increase. This approach is able to change patient management in approximately 35 % of patients. In spite of similar evidence about the incremental value of integrated PET-CT images, there are still discussions about the proposal to use PET-CT as the imaging of first choice in colon cancer staging (Strunk et al. 2005; Arulampalam et al. 2001, 2004; Huebner et al. 2000; Dietlein et al. 2003; Lonneux 2005).

18.8.2 Pancreatic Cancer

Pancreatic carcinoma has a very poor prognosis since its diagnosis is often based on non-specific symptoms and by indirect signs on morphologic imaging (US or CT). Its diagnosis can be obtained by endoscopic cholangiopancreatography, endoscopic US, laparoscopy and percutaneous biopsy. Surgical cure is possible only with an early diagnosis since the candidates for surgery are patients with cancer limited within the pancreatic capsule (Freeny 2001).

FDG imaging of pancreatic cancer has been successful because glucose transporters and glycolytic enzymes are often overexpressed in malignant compared to benign tumors or chronic pancreatitis. A number of studies have shown a significantly increased FDG uptake in pancreatic malignancies (Zimny et al. 1997; Froehlich et al. 1999; Ksperk et al. 2001). Many reports have demonstrated the diagnostic superiority of FDG-PET over CT and US. However, FDG-PET in the differential diagnosis of a pancreatic mass has limited value, as the presence of FDG uptake corresponding to a pancreatic mass cannot be considered fully diagnostic (Jadvar and Fischman 2001; Sendler et al. 2000; Diederichs et al. 2000). It is very difficult to make the discrimination between pancreatic tumors and mass-forming pancreatitis. False negative findings have been reported in patients with small lesions (less than 1 cm in size) and a highly differentiated histotype. The diagnostic accuracy of a PET examination is highly dependent on glucose levels. In subjects with diabetes mellitus and blood glucose levels > 130 mg/dl, the sensitivity of FDG-PET falls below 50 % (Diederichs et al. 1998). Some authors use the semiquantitative evaluation of FDG uptake to improve the accuracy, but this parameter seems to be of limited value (Imdahl et al. 1999).

The major advantages of PET consist of detecting the locoregional involved lymph nodes and of visualizing distant metastases in liver, lung, peritoneum and bone. Therefore FDG-PET has an important role in staging pancreatic cancer, in particular for detection of liver metastasis as this is decisive for the surgical curability of such patients. Pancreatic cancer metastases to the liver > 1 cm in diameter can be detected with a sensitivity of 97 % and a specificity of 95 %. Visualization of lesions < 1 cm using PET is possible only in 43 % of cases, with a remarkable specificity of 95 % (Froehlich et al. 1999; Nishiyama et al. 2005). The image fusion achieved with PET-CT represents an important staging procedure prior to pancreatic resection for cancer, since it significantly improves patient selection and is cost-effective (Heinrich et al. 2005).

An interesting potential application of FDG-PET is the quantitation of tumor uptake as a prognostic parameter. In this way SUV can be considered a metabolic staging, since a high glycolytic activity has been proved to be associated with cell proliferation and biological aggressiveness of the tumor (Hoh 1999). In a Japanese study a multivariate analysis of survival indicated that SUV was an independent prognostic factor for patients with unresectable pancreatic cancer (Nakata et al. 2001). FDG-PET can be used also as an early test to predict the response to chemotherapy. In fact, the absence of FDG uptake at 1 month following chemotherapy means a clear improvement of the overall survival (Maisey et al. 2000). Several studies have been performed to evaluate the advantages of FDG by using alternative radiopharmaceuticals such as ^{11}C-acetate or ^{18}F-FET, in order to allow to a better discrimination between tumors and inflammatory tissues (Rasmussen et al. 2004; Pauleit et al. 2005). These tracers seem to be more promising for tumor characterization than for imaging; however, they need further evaluation in large series of patients.

18.8.3 Esophageal Cancer

Patients with esophageal cancer are usually diagnosed at an advanced stage, as the tumor may grow without any signs or symptoms. Chest X-ray, barium swallow, CT and MRI are the methods currently used for the initial diagnosis. All these modalities have a low negative predictive value, and they usually fail to detect abdominal lymph node metastases and liver metastases.

Although the ability of FDG-PET to visualize primary tumors has been well demonstrated, its main clinical value is to assess the extent of disease, and to depict the progression to contiguous structures, the nodal involvement and the presence of liver metastases. PET is more specific than CT and endoscopic US for locoregional lymph nodal metastases, and its use can influence the management of the patients. Therefore FDG-PET is a powerful instrument for preoperative staging since it has been demonstrated that PET examination can prevent unnecessary surgical exploration (Pramesh and Mistry 2005; van Westreenen et al. 2005a). In addition PET imaging has great value in the diagnosis of distant metastatic sites, features that may substantially affect patient management (Liberale et al. 2004; Blackstock et al. 2006). The accuracy of PET in evaluating tumor resectability is superior to that of CT, and the combined modalities achieve an accuracy close to 90 – 95 %.

Very interesting results have been obtained with the measurement of FDG uptake as a prognostic parameter. The SUV assumes a prognostic value, but is not an independent factor that can be used to assess survival. FDG-PET can also predict the response to chemotherapy early in the course of the treatment. FDG-PET is more accurate than conventional imaging with CT and US in evaluating response to chemotherapy and radiation therapy. Measuring the decrease of the FDG uptake during chemotherapy, it is possible to classify patients with responding and non-responding tumors (Rizk et al. 2006; Wieder et al. 2005; van Westreenen et al. 2005b).

PET-CT fusion imaging can avoid the potential pitfalls in the interpretation of ^{18}F-FDG accumulation in the distal esophagus (Rampin et al. 2005). The additional value of PET-CT consists of improving the accuracy of small tumor detection, since fusion is of special value for the correct interpretation of cervical and abdominopelvic sites, for the assessment of disease in locoregional lymph nodes before surgery and in regions with post-surgical anatomical distortion (Goh et al. 2005). FDG-PET can have a role in guiding biopsy for the diagnosis of esophageal cancer recurrence (von Rahden et al. 2006).

PET-CT image fusion has been demonstrated to have an impact on image treatment planning and management of esophageal carcinoma for conformational radiotherapy (Moureau-Zabotto et al. 2005; Vrieze et al. 2004).

The visualization of tumor and the detection of small value metastatic disease with PET can be obtained by the use of ^{11}C-choline. This radiopharmaceutical seems to be superior to FDG in discovering metastases located in the mediastinum. ^{18}F-FLT is another radiopharmaceutical that has been studied in esophageal cancer patients in order to improve the diagnostic performances of PET (Kobori et al. 1999).

18.8.4 Neuroendocrine GEP Tumors

GEP tumors are neoplasms that originate from neuroendocrine cells distributed in the GI tract epithelium (carcinoids, islet cell carcinomas, insulinomas, glucagonomas and VIPomas). Nuclear medicine modalities have been currently adopted in staging, restaging and treatment monitoring for the management of this group of diseases. The nuclear imaging of choice for these patients is ^{111}In-pentetreotide scintigraphy, based on the affinity of somatostatin analogues for somatostatin receptors expressed by cancer cells. However, not all GEP tumors present somatostatin receptors on their membranes, and the ones that do not cannot be imaged with somatostatin receptor scintigraphy but can be studied by other nuclear medicine modalities. Unfortunately FDG is not fully suitable as a tracer for neuroendocrine tumors due to their low metabolism. Only the clinically most aggressive neuroendocrine tumors show an intense FDG uptake (Adams et al. 1998a; Pasquali et al. 1998). In these cases, when the FDG uptake is evident, FDG-PET has a prognostic value, and a PET scan is able to detect some metastatic lesions that are not revealed by conventional imaging modalities. Alternative radiopharmaceuticals have been developed to image GEP tumors, e.g., ^{11}C-hydroxytryptophan (5HTP), ^{11}C-DOPA, and ^{18}F-DOPA. Other radiopharmaceuticals for neuroendocrine neoplasms expressing somatostatin receptors are under study such as ^{64}Cu-TETA-octreotide and ^{68}Ga-DOTATOC (Vansteenkiste et al. 1997; Anderson et al. 2001; Koukouraki et al. 2006; Bombardieri et al. 2004; Ahlstrom et al. 1995).

For example, ^{18}F-DOPA has been shown to detect 65 % of carcinoids, FDG-PET only 29 %, and somatostatin-receptor scintigraphy 57 %. Although the morphologic procedures were most sensitive for organ metastases, ^{18}F-DOPA-PET was superior in the localization of primary tumors and lymph node staging. These results stress the value of PET radiochemistry in providing specific tracers for specific metabolism; however, at present similar approaches are being carried out as clinical research and are possible only in those PET centers with cyclotron facilities and highly specialized

teams of skilled radiochemists. ^{68}Ga-DOTATOC in limited series of patients has been compared to ^{111}In-pentetreotide, and it seems to be superior especially in detecting small tumors and cancer bearing only a low density of somatostatin receptors. In particular it offers excellent imaging properties and very high tumor to background ratios.

18.9 Lymphomas

Lymphomas can be distinguished in Hodgkin's disease (HD) and non-Hodgkin's lymphomas (NHL). The extent of disease is commonly evaluated with the following tools: clinical examination, laboratory tests, US, CT and/or MRI, and bone marrow biopsy. The prognosis of HD and NHL in recent years has substantially improved. All imaging techniques have greatly contributed to this achievement since the choice of the type and intensity of treatment depends on accurate staging and risk assessment at diagnosis.

At present the two most commonly used nuclear medicine procedures in the management of lymphoma patients are ^{67}Ga-SPECT and FDG-PET (Reske and Buchmann 2001; Draisma et al. 1998). FDG-PET is clearly superior to ^{67}Ga-SPECT: the spatial resolution of PET is higher, ^{67}Ga-SPECT has a lower sensitivity for intra-abdominal tumors and low-grade NHL, the scintigraphy protocols of gallium scanning take more time, and patient compliance is generally worse (Cheson et al. 1999).

In the initial staging of HD and NHL, conventional imaging techniques such as CT, US and MRI provide detailed morphologic information to define the clinical stage and a satisfactory basis for subsequent follow-up evaluation. The CT scan gives adequate information about possible organ involvement in addition to the extent of nodal disease, while MRI is the imaging modality of choice to assess central nervous system (CNS) involvement. A large number of publications have demonstrated over the past years that ^{67}Ga-SPECT is an accurate tool to image and stage initial supradiaphragmatic lymphomas (Zinzani et al. 1999; Bartold et al. 1997). However, an increasing body of evidence confirms that FDG-PET is able to demonstrate additional nodal and extranodal lesions not detected by conventional morphologic imaging, resulting in upstaging of 13 % of cases. In comparison to the ^{67}Ga scan, FDG-PET has shown superior sensitivity also in the assessment of abdominal lesions, in detecting bone marrow infiltration, and in visualizing involved lymph nodes, soft tissues and parenchymal organs (Kostakoglu et al. 2004).

The accuracy of PET is high in all types of lymphomas except for some types such as marginal zone lymphoma and small lymphocyte lymphoma which appear to have less reliable PET positive findings. PET imaging is highly sensitive in patients with more aggressive lymphoma, and the FDG uptake may have implications for grade of disease, transformation and degree of response. A lot of clinical evidence has demonstrated that FDG-PET is useful both in staging HD and NHL at presentation of disease, in evaluating tumor response after the first treatment, in detecting relapses and also as a prognostic evaluation (Meignan et al. 2006; Hicks et al. 2005a).

Multiple studies have supported the use of PET for accurate staging and restaging of HD and NHL.

FDG-PET has good but not conclusive concordance with the results of bone marrow biopsy for the detection of bone marrow infiltration, since few data are not concordant with pathology. So PET may only complement the results of bone marrow biopsy (Pakos et al. 2005).

Residual mediastinal mass may occur with various types of lymphoma. The diagnostic and prognostic value of ^{67}Ga-SPECT in the evaluation of residual lymphoma masses has been established by many trials (Delcambre et al. 2000; Gasparini et al. 1998). A positive FDG scan in patients with mediastinal masses in both HD and NHL indicates a significantly higher risk of relapses. In this application FDG-PET revealed a higher positive predictive value and negative predictive value than the CT scan. FDG-PET has a very great value in assessing response to therapy and predicting survival in lymphoma patients (Fig. 18.4). In fact in recent years several studies have reported the excellent accuracy and predictive value of FDG-PET when performed either during treatment ("early assessment") or after treatment, which proved to be far better than that of CT

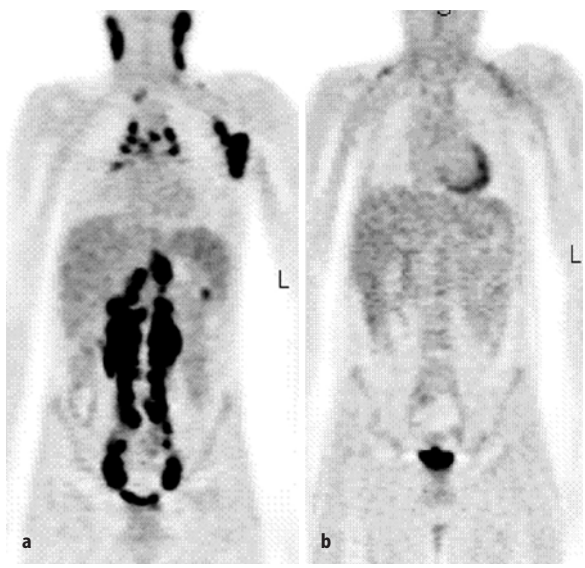

Fig. 18.4. A 27-year-old man with NH lymphoma with FDG-PET before (**a**) and after (**b**) chemotherapy, showing complete remission of multiple foci of abnormal FDG uptake

and ^{67}Ga-SPECT. Early assessment with FDG-PET (after one or two courses of chemotherapy) has been shown to be successful by measuring the changes in the FDG uptake prior to and during chemotherapy (Römer et al. 1998). This evaluation is extremely important in lymphoma both to confirm the efficacy of the therapy and to select non-responder patients for more aggressive therapeutic regimens. FDG-PET is currently used in treatment monitoring since a persistent abnormal FDG uptake after any treatment is highly predictive of residual or recurrent disease (Jerusalem et al. 1999; Hutchings et al. 2006).

FDG-PET findings after therapy are predictors of prognosis, since the clinical results show a high rate of disease free survival in PET negative patients and low rates of free disease survival in PET positive patients. Kaplan-Maier analysis in patients with high grade NHL after two or three cycles of chemotherapy indicated that progression free survival and overall survival were related to the presence or absence of FDG minimal residual uptake (Mikhaeel et al. 2005).

Some studies have also described an interesting role of FDG-PET in the pre-transplant evaluation of aggressive lymphoma. The data show a clear correlation between a pre-transplant negative scan and overall survival and progression-free survival. This means that PET imaging results may be predictive of outcome in patients undergoing high-dose therapy and transplant.

In addition, ^{18}F-FDG PET is a valuable diagnostic tool for therapy planning in radio-oncology with a high impact on therapeutic decision-making in initial staging as well in restaging. Especially in a curative setting it should be used for definition of target volumes (Dietl and Marienhagen 2005).

The high accuracy of FDG-PET might also result in cost savings because of better planning of further diagnostic procedures and treatment (Heald et al. 1996; Klose et al. 2000; Rigacci et al. 2005). Data indicate that FDG-PET has a relevant impact on the management of patients, contributing to changes in clinical staging in about 40 % of patients and changes in treatment in more than 50 % of cases.

PET today has achieved a strategic importance in the diagnostic work-up of lymphoma patients. There is a general consensus about the high-risk patients who may have at least three systematic FDG-PET examinations: one for staging, one for early assessment to confirm the efficacy of chemotherapy, and one at approximately 6 weeks following completion of therapy to detect residual disease (Talbot et al. 2001). With regard to the low-risk patients it has been discussed whether or not at disease presentation FDG-PET should be considered a staging procedure. In the case of diagnostic doubts PET of course will complement radiological imaging.

The combined PET-CT imaging is better than CT in the diagnosis of both nodal and extranodal disease, and can detect disease in normal-sized lymph nodes that are overlooked by CT. As a consequence PET-CT upstages approximately 40 % of all cases of lymphoma. PET-CT is also better than CT alone for the purpose of post-therapy evaluation owing to its greater predictive value. Much evidence demonstrates that a positive post-treatment study is associated with poorer prognosis, while a scan performed after the first cycle of treatment is often predictive of response, especially in cases of aggressive HD and NHL (Burton et al. 2004; Hillner et al. 2004; Hart et al. 2005).

18.10 Breast Cancer

The importance of PET in the management of breast cancer patients has been demonstrated by several papers. FDG-PET has shown great diagnostic efficacy mainly in determining tumor extent (staging and restaging). Other indications can be assessing the benign or malignant nature of a breast mass, evaluating the response of the tumor to treatment and characterizing the tumor biology (Adler and Bakale 2001; Wahl 1998; Landheer et al. 2005).

FDG-PET in tumor staging appears to be superior to the other conventional imaging modalities in localizing tumor lesions, as significantly more lesions can be detected at different sites, allowing the diagnosis of a significant number of metastases which would have been missed or not correctly diagnosed by CT, US, MRI and bone scintigraphy. Soft tissue lesions of the liver, lung, and lymph nodes and lytic or mixed-lytic and sclerotic bone metastases accumulate FDG (Wahl 1998; Weir et al. 2005; Isasi et al. 2005). FDG-PET is considered the most sensitive imaging modality in detecting lymph node metastases and it might be useful also for the visualization of parasternal and mediastinal lymph nodes when the primary tumor is located in the internal quadrant of the breast (Fig. 18.5) (Bellon et al. 2000).

The diagnostic accuracy of whole-body FDG-PET during the follow-up can limit the number of tests for the patients at high risk of metastases. Whole-body PET is fundamental when the recurrence of the disease is suspected because of the presence of clinical symptoms or a progressive increase in tumor marker levels (Crippa et al. 1992; Lamy et al. 2005). A condition after treatment is the brachial plexopathy that occurs in a small proportion of cases and may be due either to fibrosis secondary to therapy or to new malignant growth. This condition is difficult to study with morphological imaging since these patients sometimes show normal CT and MRI findings. FDG-PET is able to differentiate plexopathy induced by treatment from plexopathy caused by a malignant growth (Hathaway et al. 1999; Ahmad et al. 1999).

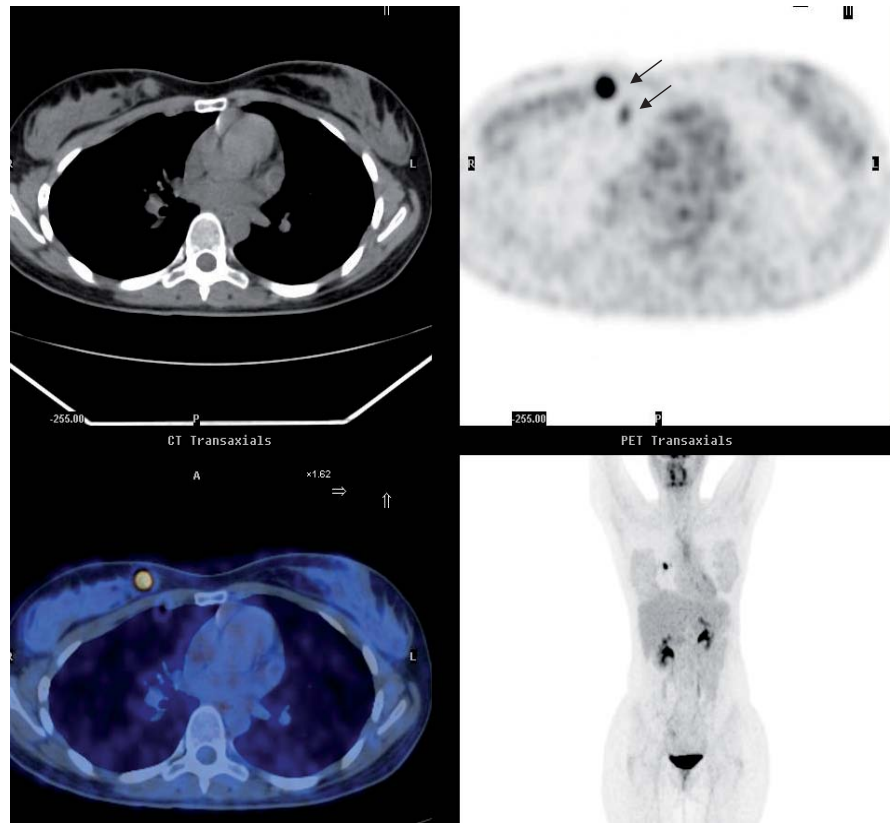

Fig. 18.5. A 26-year-old woman with breast cancer in staging. FDG PET-CT showed focal areas of abnormal uptake in the primary tumor and internal mammary lymph node

The detection of axillary lymph node involvement is an area in which nuclear medicine methods have become of much value because of the limits of the non-nuclear medicine techniques (Bombardieri et al. 1998). Clinical examination is an unreliable diagnostic tool, and conventional radiographic modalities lack accuracy. Many studies evaluated FDG-PET in axillary lymph node staging among a total of more than 300 patients, with a variable sensitivity and specificity (Bender et al. 1997; Gimenez et al. 1999; Adler et al. 1997). However, the most relevant studies with PET including those with the largest numbers of patients showed an overall sensitivity and specificity of around 80 – 90 %. The largest study on axillary staging has been performed by our group at our institute including a series of 167 consecutive patients with breast tumors, who underwent axillary dissection and pathological diagnosis. The overall sensitivity, specificity, and accuracy of lymph node staging with FDG-PET was 94.4 %, 86.3 % and 89.8 %, respectively (Greco et al. 2001). The negative predictive value ranged from 93.5 % to 97.3 % and the positive predictive value from 54.5 % to 94.1 %. What is very important in our series was the very high predictive value of negative FDG-PET (over 95 %), especially in the light of the current discussion about the need for surgical procedures for axillary staging. It may be hypothesized that in women at low risk of axillary metastasis (for example, those bearing tumors ≤ 10 mm) axillary node dissection could be omitted on the basis of a negative FDG-PET result. FDG-PET positive nodes are highly predictive of metastasis in breast cancer (Kumar et al. 2006). It should be mentioned that in staging axillary involvement other valid nuclear medicine techniques are currently used, namely lymphoscintigraphy and the intraoperative detection of the sentinel lymph node with a gamma probe. This technique is considered very reliable and highly sensitive and has found a place in current clinical management since it is also able to detect metastases very small in size (a few millimeters in diameter or micrometastases). It is clear that these two modalities are completely different: PET is a non-invasive imaging technique, the other one a technique with a surgical component; PET also provides functional and biologic information regarding the tumor and the whole body, while assessment of the sentinel lymph node is only aimed at the diagnosis of axillary node involvement.

This potential use of FDG-PET in preoperative staging prompts consideration about the cost/benefit issue. Similar findings were described in the US by the Institute for Clinical PET (ICP), which confirmed the savings that could be attained by the use of FDG-PET to guide the surgical strategy in patients with stage I and II breast cancer (Institute for Clinical PET 1994). The use of a PET management strategy for the staging of

breast cancer is expected to be a cost-effective approach (Sloka et al. 2005).

FDG-PET at the presentation of breast masses shows a diagnostic sensitivity ranging from 67 % to 100 % and a specificity ranging from 75 % to 100 % (Bombardieri et al. 1997a; Yutani et al. 1999). It must be stressed that the highest sensitivity and specificity have been observed in tumors 10 mm in size, clinically palpable and with a high probability of malignancy. For non-palpable tumors or small breast masses the sensitivity and specificity are lower (70 – 95 % and 70 – 90 %, respectively). Fibrocystic changes and inflammatory processes often do not show any significant FDG uptake, even if false positive imaging has been observed in patients with fibroadenoma, severe fibrocystic mastopathy, ductal ectasia, tubular angiomyoepithelioma or cystosarcoma phyllodes. In spite of these very interesting results it must be said that the differential diagnosis of any breast alteration should be routinely performed by means of mammography and/or ultrasonography, while MRI is still under evaluation. There is general consensus that FDG-PET must not be considered the first-choice modality in the diagnosis of primary breast masses in view of the high diagnostic efficacy of mammography together with its low cost. However, nuclear medicine modalities may be useful only in those particular conditions where mammography and other conventional morphologic techniques are unable to solve diagnostic ambiguities, for example in breasts with implants that are difficult to explore radiologically, dense breasts, or breasts with morphologic distortions due to previous treatment (surgery, chemotherapy or radiotherapy) (Bombardieri et al. 1997a; Bender et al. 1998).

FDG-PET can monitor metabolic changes in tissues. A decrease in tissue of FDG uptake after therapy occurs from 8 to 60 days from the beginning of chemotherapy or radiotherapy, while a significant reduction in tumor size requires much more time (Weber et al. 2000). The metabolic response of the tumor precedes the volumetric response because the anticancer treatment primarily influences the tumor metabolism, and only at a later stage is it followed by a decrease in tumor mass. Experimental data have shown that the reduction of SUV precedes the morphologic decrease in tumor diameter. Unchanged or enhanced FDG uptake indicates tumor progression while a decline in FDG uptake is a biochemical signal in patients who are responsive to treatment (Schelling et al. 2000). This finding should be used both to assess the efficacy of treatment following its completion and to measure the subclinical response of the tumor in order to predict the degree of clinical response (Nair et al. 2000).

The hybrid PET-CT system is useful in re-staging, in the detection of nodal disease and in the visualization of distant metastases in non-suspected sites. It also appears better than PET or CT alone in the evaluation of response to the treatment, and the absence of metabolic response on PET-CT means a worse prognosis (Tatsumi et al. 2005; Fueger et al. 2005).

As an alternative to FDG, ^{11}C-labeled tyrosine (TYR) was successful in visualizing breast cancer and was shown to correlate with the protein synthesis rate (Kole et al. 1997). MET-PET had some use in evaluating tumor response after chemotherapy. Comparative imaging pre- and post-therapy showed a decreasing uptake in stable or regressing tumors, whereas enhanced uptake was associated with cancer progression and non-response (Houvinen et al. 1993).

PET allows the biological characterization in vivo of breast cancer and this can be of great interest for oncologists, given the influence that some prognostic parameters may have on the decision regarding future therapies. A positive correlation was found between FDG uptake and tumor histology, microscopic tumor growth patterns, and tumor cell proliferation. No relationship was found between FDG uptake and tumor size, axillary node status, fibrotic and cystic compounds, presence of inflammatory cells, steroid receptor status, and expression of GLUT-1 (Avril et al. 2001). A study has been carried out in our institute on the correlations between SUV and tumor histology, receptor status, labeling index (LI) and tissue expression of cytosolic p53 (Crippa et al. 1998). SUV was significantly higher in infiltrating ductal carcinomas than in lobular carcinomas, and higher in grade 3 than in grade 1 – 2 carcinomas. No significant association between SUV, receptor status, and labeling index was observed. With regard to the correlation between SUV and p53, patients with p53 levels >0.5 ng/mg of protein had a significantly higher median SUV than patients with a p53<0.5 ng/mg. This kind of study clearly shows that FGD-PET may provide important information in vivo in a non-invasive way that could have potential prognostic interest.

18.11 Melanoma

Melanoma is a potentially curable tumor if detected early and resected. The most important prognostic factor is the stage of the disease at presentation. About 20 % of patients with nodal metastases but without distant metastases can be cured by surgery resection. In addition, the resection of isolated metastasis (in brain, lung and liver) in selected groups of patients improves survival. Diagnostic tests for staging and monitoring melanoma include X-rays, US of lymph node basins and abdomen, CT and MRI (for brain metastases). Lymphoscintigraphy with sentinel node biopsy is becoming an increasingly common procedure for staging since melanoma usually metastasizes to regional lymph nodes before distant spreading.

FDG-PET is a very sensitive technique for melanoma detection as melanoma cells actively accumulate glucose. Moreover, PET is a whole body scan technique, and this is very useful since melanoma usually widely metastasizes the body. Our experience and data from the literature show that FDG-PET reveals a good diagnostic sensitivity (79–92%) in detecting lymph node metastases (Wagner et al. 1997; Strauss 2000; Klein et al. 2000). The value of FDG-PET in the baseline lymph node staging remains limited since lymphatic mapping with sentinel node biopsy is a safe and accurate method to assess for regional node metastases, where there is no palpable regional lymphoadenopathy and no suspicion of distant metastases. Sentinel node biopsy is much more sensitive than PET in detecting microscopic lymph node metastases (Kumar et al. 2005).

However, PET imaging has a very important role in the evaluation of patients with aggressive primary melanoma with suspected distant metastases, in follow-up of patients with previously excised melanoma, and in restaging of patients with known distant metastases to evaluate for treatment response. PET in association with CT can detect occult disease (Fig. 18.6) (Brady et al. 2006; Hafner et al. 2004). Several reports have shown that FDG-PET is more sensitive than CT in detecting nodal involvement, because metastatic lymph nodes are very small and sometimes under the limits of detectability of radiological imaging. The accuracy of FDG-PET for the diagnosis of distant metastases in patients with recurrent disease is even superior to that for lymph nodes. The sensitivity of PET for liver metastases, soft tissues, abdominal metastases, skeletal metastases and cutaneous metastases is better than that of CT (Swetter et al. 2000; Mijnhout et al. 2001). CT does not routinely evaluate the lesions in supraclavicular area, neck, or upper and lower extremities, sites that are easily imaged by PET, including peritoneal diffusion. It must be said that PET has no great efficacy, only in detecting small pulmonary nodules and in visualizing small cerebral metastases in the cortex (Friedman and Wahl 2004). Lung and brain metastases continue to be better evaluated with CT than PET. The advantage of PET-CT imaging in these patients is the evaluation of small lung nodules not detected by PET.

The detection limits of FDG-PET consist of the micrometastatic involvement. In this regard in our institute we evaluated before surgery 56 lymph node basins in 38 patients with a clinical or instrumental diagnosis of lymph node metastases from melanoma (Crippa et al. 2000). All lymph node basins underwent node dissection from melanoma. The FDG-PET results were compared with the postoperative histopathological results. The efficacy of FDG-PET with a dedicated PET scanner in the diagnosis of involved lymph nodes was good, as the sensitivity was 95%, specificity 84% and overall accuracy 91%. Metastases were shown histologically in 114 of 647 surgically removed lymph nodes. FDG-PET detected 100% of metastases greater than 10 mm in diameter but only 23% of metastases smaller than 5 mm. Moreover, FDG-PET showed high sensitivity only for metastases with more than 50% neoplastic involvement or with capsular infiltration. Even if FDG-PET demonstrated a good diagnostic specificity, some false positive results occurred. Another study investigated the detectability of lesions by PET in relation with lymph-node volume from direct measurements of metastatic nodules in formalin fixed specimens. FDG-PET was reliable in detecting lymph node tumor deposits greater than approximately 80 mm^3 volume, but its sensitivity fell rapidly below this mass (Wagner et al. 2001).

This amount of tumor volume is mostly likely to occur in patients with stage III or IV disease. On the basis of these findings, FDG-PET cannot be recommended as a replacement for sentinel node biopsy at stage I and II of malignant melanoma. FDG-PET can be used routinely to stage disease at the time of initial presentation in patients with primary lesions at high risk of incidence of regional node and distant metastatic disease. The demonstration of metastatic disease by FDG-PET may suggest the need for a direct biopsy rather than sentinel node biopsy. Sentinel node biopsy can be performed if the findings on FDG-PET are negative.

FDG-PET is indicated in the follow-up of high-risk patients after surgery and at high risk of relapse, or in those patients with recurrent disease since the metastases can be multiple and sometimes are not diagnosed on the conventional radiological examinations. FDG-PET can also be used to evaluate the nature of lesions observed with CT that are difficult to evaluate bioptically or when the biopsy has given a non-diagnostic result. FDG-PET can be considered a very reliable technique for the study of the response of multiple widespread lesions to chemotherapy or immunotherapy. PET is used to check the entire body and the changes in FDG uptake reflect the biologic activity of the metastatic tumor (Segall and Johnson 2001).

Integrated PET/CT in melanoma patients, even if superior to CT alone, is not useful for initial staging or in early disease, but it is of value for re-staging of more advanced disease or detecting melanoma relapses (Ishimori et al. 2005; Reinhardt et al. 2006; Schoder et al. 2004). Alternative radiopharmaceuticals to FDG have been developed in order to visualize melanoma lesions with negative FDG findings. One of these tracers is ^{18}F-DOPA, which seems to provide different information from FDG and can help to identify viable melanoma metastases and select patients who would benefit from further treatments (Dimitrakopoulou-Strauss et al. 2001).

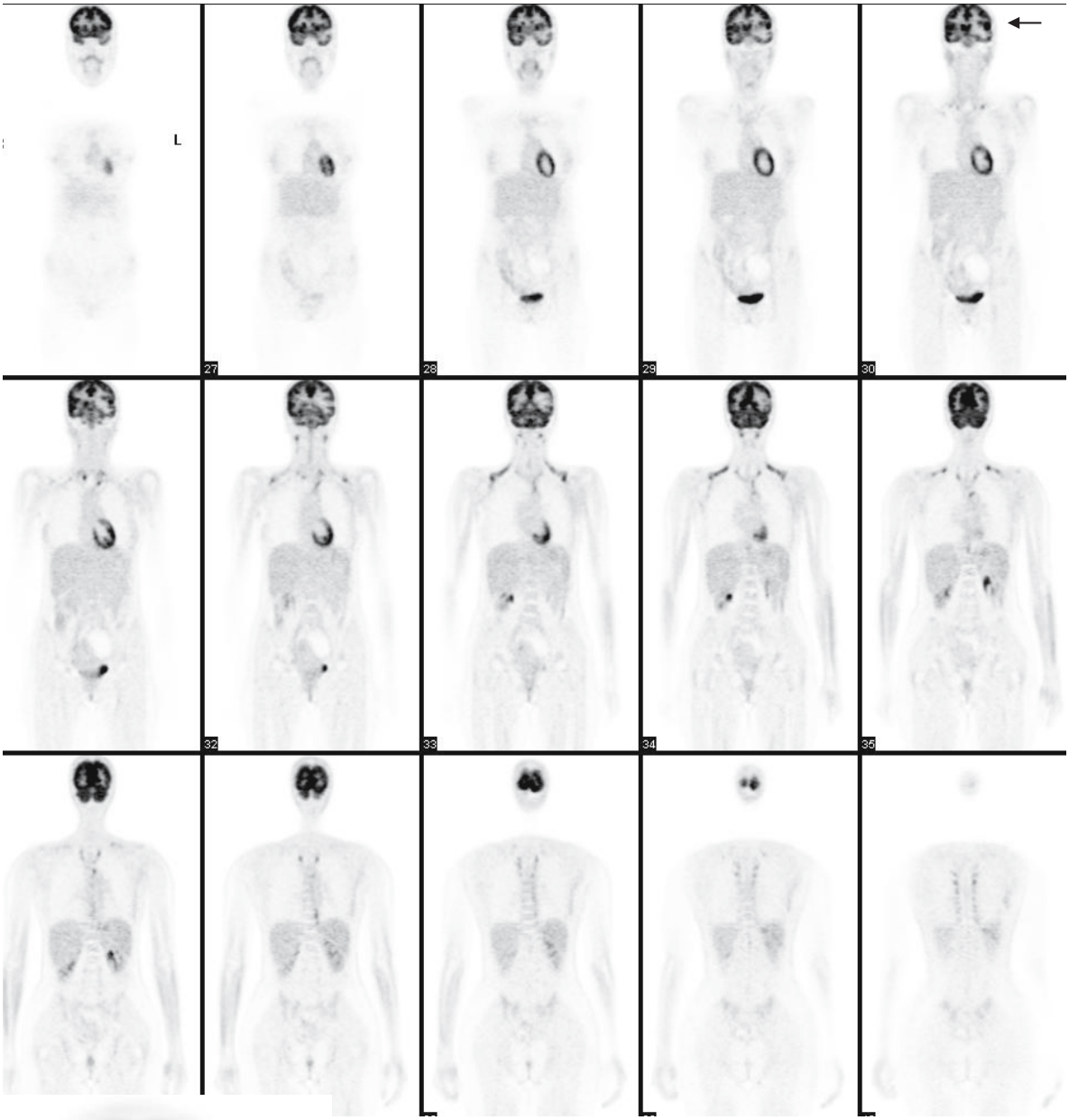

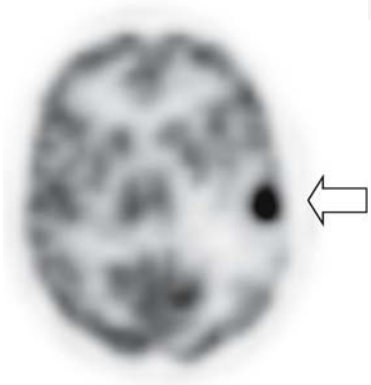

Fig. 18.6. A 48-year-old patient with cutaneous melanoma of the back with lymph node metastases in the right axilla. FDG-PET was performed after surgery as a follow-up procedure and it showed a focal area of abnormal uptake in the brain (left parietal region) very consistent with metastasis. The PET finding was confirmed by MR. FDG-PET was negative in the other body regions

18.12 Other Cancers

A large number of cancer patients may benefit from PET, including a wide variety of different cancer types such as muscle and connective tissue tumors, renal cell cancer, bladder cancer and testicular cancer. In all these cancer types PET is useful mainly in staging tumors in order to determine the extent of disease before planning a resection and in assessing the effectiveness of the different treatment (Ak et al. 2000). The relapses from testicular germ cell tumors often produce AFP and HCG; thus PET should be guided by a progressive rise of these tumor markers, even without any evident clinical or instrumental signs of disease. In these conditions PET is successful in detecting and localizing the sites of cancer relapse. At our institute we have gained wide experience with the use of PET guided by tumor marker elevations, mainly in breast cancer (PET guided by CA 15.3), gastrointestinal tract cancer (CEA and CA 19.9), testicular tumors (AFP and HCG), and also ovarian (CA 125), prostate (PSA) and thyroid cancer (TG) (Seregni and Bombardieri 1999).

18.12.1 Ovarian Cancer

Early diagnosis of ovarian cancer at stage I or II is relatively infrequent. Most tumors are not detected until the disease is at an advanced stage (stage III–IV). For this reason ovarian cancer has the highest mortality rate among gynecologic cancers and the even apparently early-stage tumors present with local recurrence and/or distant metastases after primary treatment. The current diagnostic approaches are physical examination, US and CT. US is the most widely used imaging technique for the diagnosis of carcinoma and may allow the detection of a mass not apparent on clinical examination. CT scan with injection of contrast agents allows exploration of the entire abdominal and pelvic cavities, particularly the visceral component. The tumor marker CA 125 has an important role in ovarian cancer management (Soper 2001). There is general consensus that one of the most useful applications of the CA 125 test consists of its serial measurements during the follow-up in order to detect the preclinical recurrence of the disease. This results in an earlier diagnosis than with radiologic procedures; the latter should be used in the case of a progressive rise of CA 125 to confirm and locate the site of the lesion(s). The most available nuclear medicine diagnostic imaging procedure is PET. Much research has been done on antibody imaging in ovarian cancer and only one product has been licensed in the US (^{111}In-satumomab pendetide) but is not available in Europe (Pinkas et al. 1999; Bohdiewicz 1998). The general results from clinical trials with immunoscintigraphy show a sensitivity ranging from 80 % for masses larger than 2 cm to approximately 50 % for smaller masses. Immunoscintigraphy is not reliable in the detection of small lesions. At present FDG-PET is the best nuclear medicine modality for imaging recurrent ovarian cancer and several clinical trials have demonstrated that the diagnostic value of FDG-PET in ovarian cancer management is very high, with an overall accuracy of about 90 %. All clinical studies on FDG-PET have reported a high and comparable sensitivity (range 80 – 93 %) in the detection of primary and recurrent ovarian cancer (Pandit-Taskar 2005). It should be noted that the data from the literature are sometimes discordant with regard to the specificity (54 – 82 %), probably due to a variable proportion of inflammatory processes in the patient populations. False negative results for very small lesions have been reported in some studies, which may be explained by the spatial resolution of current PET scanners (about 4 – 5 mm for the best instruments), the presence of hypometabolic tumors (e.g., mucinous carcinoma) and technical problems, e.g., respiratory or peristaltic movements during acquisition and physiologic FDG uptake and clearance in the alimentary and urinary tracts (Trampal et al. 2000; Nakamoto et al. 2001; Rose et al. 2001). FDG-PET has shown to be a very important tool in detecting the recurrences in epithelial ovarian cancer (Fig. 18.7). The sensitivity of the combination PET and CA 125 is very high, 97.5 % with very few false negative results (Murakami et al. 2006). For these reasons the use of PET has to be recommended in patients with a clinical suspicion of recurrence and/or elevated CA 125 and negative results at conventional diagnostic work-up (Takekuma et al. 2005).

Sequential FDG-PET examinations predicted patient outcome as early as after the first cycle of neoadjuvant chemotherapy and were more accurate than clinical or pathological response criteria including changes in tumor marker CA 125. For this reason FDG-PET ap-

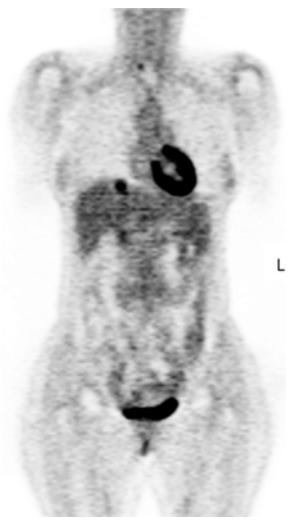

Fig. 18.7. A 69-year-old woman with ovarian cancer was treated with surgery and chemotherapy. In the follow-up a blood test indicated rising CA 125 levels. A FDG-PET study showed a focal area of abnormal uptake in the liver (IV–VIII segment) very consistent with metastasis

pears a very promising tool for early prediction of response to chemotherapy (Avril et al. 2005).

Combined PET-CT demonstrates a very high positive predictive value in identifying recurrent ovarian cancer in retroperitoneal lymph nodes, when conventional CT findings are negative or equivocal. In patients with recurrent ovarian cancer, PET-CT permits the exact anatomical localization of pathological tracer uptake and can thus direct further treatments to the precise site of tumor recurrence. Hence PET-CT should be considered for follow-up of patients with ovarian cancer (Bristow et al. 2005; Hauth et al. 2005).

18.12.2 Testicular Cancer

Testicular cancer is classified into seminoma and non-seminomatous cell tumors. The diagnosis of primary tumor is often done by clinical examination, US and the tumor marker test. However, the staging is very important because a comprehensive evaluation is necessary to define the extent of disease in order to determine the appropriate treatment. The currently used tumor imaging for staging is CT and MRI. In recent years PET has been demonstrated to be reliable for in vivo detection of cancer of the reproductive tract (Reinhardt et al. 2002). PET has shown to be useful both for the initial diagnosis of cancer and in defining the presence or absence of disease in patients with residual masses (Kumar et al. 2004). The association of FDG-PET and tumor marker determination can be useful, after surgery, in discovering the presence of a tumor relapse non-detected by other conventional radiological modalities. Clinical evidence demonstrated that FDG-PET is successful both in non-seminomatous germ cell and in seminoma tumors (Lassen et al. 2003; Lenzo et al. 2004). FDG-PET also shows ability for the early prediction of response in patients with relapsed metastatic germ cell tumors and undergoing salvage high-dose chemotherapy. The outcome of high-dose treatment is correctly predicted by PET-CT and PET is superior to CT alone and tumor markers (Bokemeyer et al. 2002).

18.12.3 Prostate Cancer

Nuclear medicine has an important role in staging and restaging prostate carcinoma. For many years ^{99m}Tc-MDP bone scanning has been a valid tool for the study of bone metastases, in association with serum measurement of PSA. Bone scan is still the procedure of choice in patients at risk and those with elevated levels of PSA (Corstens 2001). Labeled monoclonal antibodies have been found to have some utility. Capromab pentetide showed poor sensitivity for small volume disease, so it may not eliminate the need for staging a lymph node dissection to evaluate disease spread (Valliappan et al. 1999; Haseman et al. 2000). Immunoscintigraphy has not been demonstrated to be reliable in determining the local extent of the primary tumor and in detecting locoregional tumor relapses. The most important value in immunoscintigraphy is to identify lymph node metastases in high-risk patients with a negative bone scan.

FDG-PET is a useful diagnostic modality. However, several papers have demonstrated that FDG-PET is not a useful test in the evaluation of clinically organ-confined prostate cancer. Several authors used FDG-PET for staging pelvic lymph nodes and detecting distant metastases (Liu et al. 2001; Heicappell et al. 1999). With respect to bone scan, whole-body PET not only detects skeletal lesions but also lesions in soft tissues and parenchymal organs. Moreover, attention should be paid to the fact that the FDG clearance follows the urinary tract, and this affects the visualization of the lesions in the abdominal and pelvic area that can be masked by the physiological concentrations of FDG. In addition, the glucose uptake may be affected by androgen ablation, and this is a critical issue in patients undergoing hormone therapy (Oyama et al. 2001). Patients who could benefit from FDG-PET imaging are patients who are untreated, who have had an incomplete response to therapy, or who have increasing PSA levels (Sung et al. 2003). An alternative tracer to FDG for prostate cancer is ^{11}C-CHOL. Choline is not eliminated through the kidney and the urinary tract, so this radiopharmaceutical has better characteristics for visualizing prostatic cancer. However, at tumor presentation PET may not be of use, since there is not a reliable differential ^{11}C-CHOL uptake in BPH and prostate cancer. ^{11}C-CHOL may be of value in staging, in detecting pelvic recurrences and in monitoring prostate cancer. In particular it seems useful for re-staging prostatectomy cases with increasing serum PSA levels. This radiopharmaceutical seems to be superior to ^{18}F-FDG PET and complementary to conventional imaging (Yoshida et al. 2005; Picchio et al. 2003). The fluorinated choline analog, ^{18}F-CHOL, can be a more suitable radiopharmaceutical for clinical use, due to the longer half-life of ^{18}F. A comparison has been made in a series of prostate cancer patients between FDG-PET and ^{8}F-CHOL-PET. In patients with advanced disease more lesions were seen in the ^{18}F-CHOL scans, and the SUVs were higher than in the FDG scans. ^{18}F-CHOL has demonstrated to be an interesting imaging modality for detecting local recurrences and lymph node metastases (Schmid et al. 2005; Kwee et al. 2005). ^{11}C-MET or ^{11}C-acetate has been evaluated in the diagnosis of intraprostatic nodules with short dynamic scanning and multicore biopsy. They show a high detection rate in patients with increased PSA and repeated negative biopsies. ^{11}C-acetate gives a rate of cancer identification superior to that of FDG-

PET and seems to be a very effective radiopharmaceutical for detection of recurrent prostate carcinoma (Toth et al. 2005; Oyama et al. 2003; Dimitrakopoulou-Strauss and Strauss 2003; Kotzerke et al. 2002).

PET and PET-CT have been used in monitoring the effectiveness of cancer therapy (Morris et al. 2005). CT information obtained from the PET-CT instrument can also be used for the purpose of volume planning for radiotherapy, and the available PET information can be used in the same way to better delineate tumor margins or to distinguish viable from non-viable tumor.

18.12.4 Thyroid Cancer

The iodine-131 whole-body scan is at present the most frequently used test for monitoring patients without palpable disease or elevated serum thyroglobulin under L-T4 therapy. The radioiodine scan has the main advantage of finding disease that may be amenable to ^{131}I therapy. However, patients who have elevated thyroglobulin levels while on L-T4 therapy or after TSH stimulation but a negative ^{131}I whole-body scan require other imaging procedures such as ^{99m}Tc-sestamibi, ^{201}Tl-, or ^{99m}Tc-tetrofosmin. A lot of clinical evidence has shown that FDG-PET can be of great value in the postoperative follow-up of differentiated thyroid cancer. In cases of elevated serum thyroglobulin levels but negative whole-body scan, FDG-PET has become the method of choice to detect ^{131}I-negative recurrences and metastases (Haugen and Lin 2001; Shiga et al. 2001; Khan et al. 2003) (Fig. 18.8). Comparison of the results with FDG-PET, ^{131}I whole-body scintigraphy and other diagnostic tools gave a sensitivity for FDG-PET of 75 % in the whole patient group (222 patients) and 85 % in the group of patients with negative radioiodine scans (166 patients). On the contrary the sensitivity and specificity of ^{131}I whole-body scan were 53 % and 92 %, respectively (Grunwald et al. 1999). We may conclude that FDG-PET should be proposed as a first-line evaluation in patients with persistent disease but negative findings on whole-body scan after treatment (Helal et al. 2001; Hooft et al. 2001; Schluter et al. 2001).

A second important clinical application of FDG-PET is the detection of recurrent cervical lymph nodes of differentiated thyroid carcinoma, since PET has proved to be very reliable in discovering locoregional lymph node metastases (Lind et al. 2000). A recent report

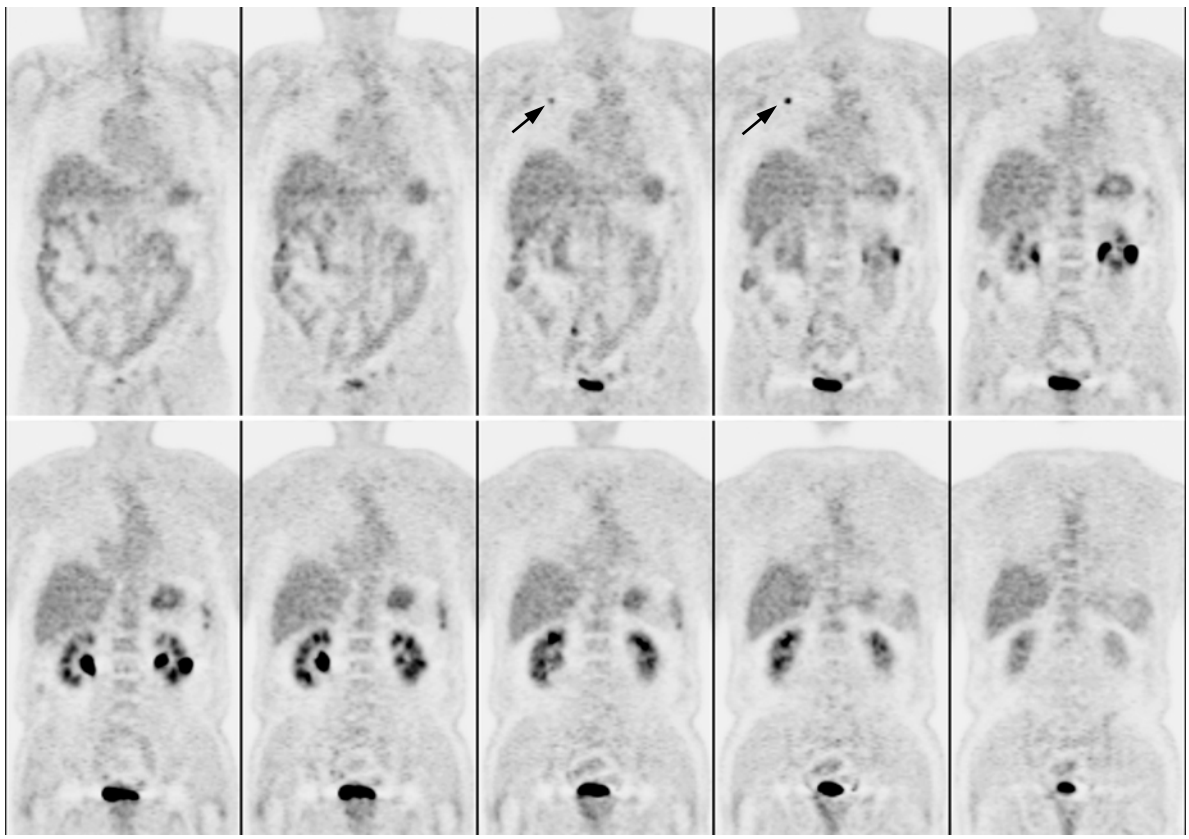

Fig. 18.8. A 68-year-old man with thyroid cancer and elevated blood levels of thyroglobulin. The WBI-131 scan was negative. FDG-PET showed a focal area of abnormal uptake in the right upper lobe of the lung. The diagnosis was confirmed with surgery and histology

showed a sensitivity and specificity of 80 % and 83 %, respectively, thus confirming that FDG-PET is suitable for the preoperative evaluation of such patients.

FDG uptake in metastases from differentiated thyroid cancer is correlated with poor differentiation and may therefore be indicative of a poor prognosis. FDG-PET may have a role also in anaplastic thyroid cancer, which usually does not accumulate radioiodine. Patients over 45 years of age with distant metastases who show FDG uptake at FDG-PET should be considered at high risk: multivariate analysis has demonstrated that the volume of FDG-avid disease is the single strongest predictor of survival (Lind et al. 2000; Wang et al. 2000). Also the relationship between TSH stimulation and FDG uptake has been recently studied. Most locally recurrent and metastatic follicular and papillary thyroid carcinomas exhibited a significant increase in FDG uptake on TSH stimulation, and this could result in detection of new lesions or classification of the FDG uptake pattern as typical for malignancy (Moog et al. 2000).

The integrated PET-CT systems can have a role in the evaluation of thyroid nodules, because a high negative value for malignancy has been shown, making this a potentially useful tool in the evaluation of thyroid nodules with indeterminate fine-needle aspiration (Mitchell et al. 2005). Combined PET-CT fusion scanning was most useful in the detection and management of recurrent papillary thyroid cancer in patients who had elevated thyroglobulin levels and no longer had concentrated radioactive iodine. In 100 % of cases in which PET-CT localized a region suspicious for malignancy, histopathological findings confirmed the results (Nahas et al. 2005).

18.13 Conclusions

The technology of nuclear medicine makes it possible to trace the biochemical processes wherever they occur throughout the human body. PET has provided an exciting way to define diseases in term of abnormalities of biological mechanism in cells, tissues and organs. In oncology one of the most important measurements is the rate of utilization of glucose, which can be measured with ^{18}F-FDG. Other changes in neoplastic cells occur and they can be detected by means of other molecules labeled with positron emitting radioisotopes. These radiopharmaceuticals depict amino acid transport, protein synthesis, DNA replication, blood flow, membrane precursor incorporation, receptor expression, gene expression, etc. Using coincidence detection to localize the origin of pairs of positrons, commercial PET scanners achieve about 4 – 5 mm resolution, somewhat better than that of SPECT scanners. The increasing impact of PET in medicine has given it a primary role in oncology. The advantages offered by this high-level technology are demonstrated by the impressive increase in FDG-PET studies in oncology all over the world. This progressive trend is based on the fact that there is clear evidence that many treatment strategies are often decided, changed and planned on the basis of PET findings.

In the past 5 years the hybrid PET-CT system, introduced in 2001, has increased the diagnostic power of PET. Images acquired with the two modalities are combined to provide metabolic information from PET and detailed anatomic information from CT on a single set of images. PET gives information that is very different from that obtainable with other image modalities. However, the paucity of anatomic landmarks on PET images makes this hybrid system extremely useful: metabolic data are integrated with cross-sectional data and this addition improves primarily the specificity, but also the sensitivity, in tumor imaging (Fig. 18.9). Thus PET-CT is a more accurate test than either of its components. This added value is a result of the fact that the attenuation correction needed for PET can be derived from CT, and PET-CT examinations are 30 % faster than PET alone with standard attenuation correction. The hybrid PET-CT systems have therefore seen a very rapid uptake. In Europe at present the number of scanner installations is approximately 230 PET and 150 PET-CT scanners, out of a total of 380 PET scanners. Since the parallel development of new radiopharmaceuticals has enhanced the possibility of better studying and characterizing tumors, the number of cyclotrons installed with radiochemistry facilities is also impressive and today accounts for 120 units. The facilities available for PET imaging have shown a steady increase over the years. As far as the distribution of PET facilities is concerned, at present there are more than over 2.5 PET scanners per 1,000,000 inhabitants in the US and nearly 1.5 per 1,000,000 inhabitants in Europe.

All these considerations permit the conclusion that the present state of PET in oncology is good and its future is bright, also because the understanding and perception of the clinical value of PET is continuously growing among oncologists. PET as a diagnostic modality has been shown to be cost-effective, sparing further unnecessary diagnostic tests and saving the cost of several non-appropriate medical and surgical strategies. Besides, some indications of PET and PET-CT are maturing, such as monitoring response to cancer therapy and radiation therapy planning. PET has become a more and more important technique for the assessment of therapeutic response, and this will likely increase the proportion of studies that are performed to determine ongoing treatment strategies. The regulators and the pharmaceutical industry are developing proposals to incorporate PET into drug development. The conventional imaging modality for radiation therapy planning

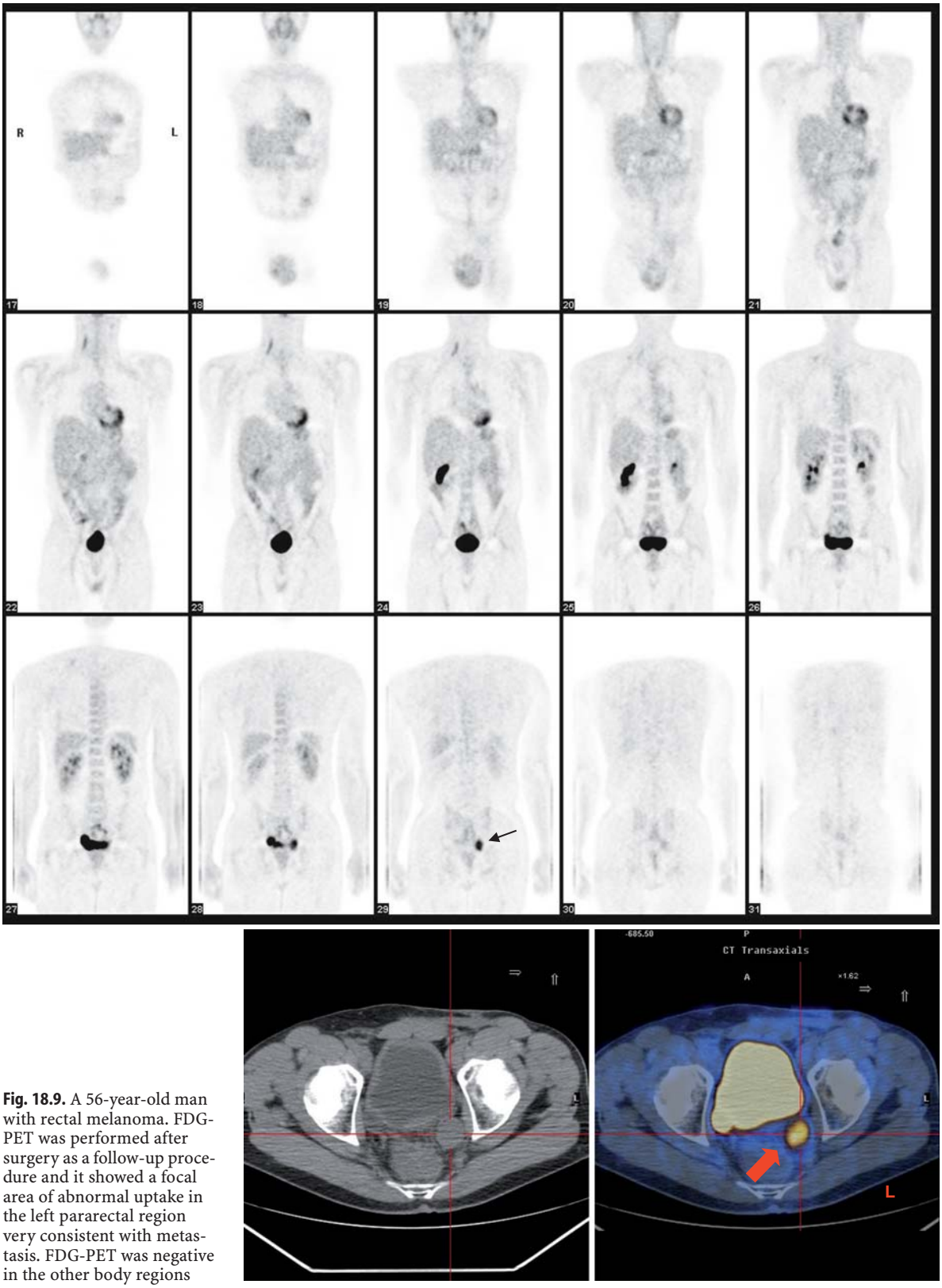

Fig. 18.9. A 56-year-old man with rectal melanoma. FDG-PET was performed after surgery as a follow-up procedure and it showed a focal area of abnormal uptake in the left pararectal region very consistent with metastasis. FDG-PET was negative in the other body regions

is still CT; however, the ability of PET to provide lesion identification voxel-by-voxel, to depict unsuspected metastases and to monitor treatment response, has made PET-CT a successful tool also to be adopted in this area. Many studies have demonstrated that PET-CT is very effective both in defining the target volumes for radiation therapy and in characterizing the distribution of the biological resistance to radiation therapy (hypoxic target volume). This multi-imaging modality generates different information that should be handled with radiation therapy systems in order to increase the delivered dose to the lesions, while minimizing the dose to the normal tissues.

The story of PET and recent advances demonstrate that over the years the technology of PET has continued to improve (hardware, software, detectors, electronics, etc.). In the forseeable future PET images will become better in quality, as has been shown by the results obtained with the experimental use of PET scanners in animal models. These instruments are able to operate at a resolution of 2 mm or less, and probably the resolution of the next generation of PET scanners will be around 1 mm. Of course a higher resolution means a better lesion detectability, and it is well known that cancer is more curable when it is detected at an early stage. The intensive research in the field of radiochemistry and the clinical use of new radiopharmaceuticals will contribute to the investigation of cancer biology, making available to the field of oncology more specific tracers for different tumor types and for particular indications.

It is obvious that all these technologies are very expensive, and the developments described above require large investments and great resources in manpower and money. However, on the basis of the evolution of PET over the last decade and the current position occupied by PET in clinical oncology, there is no doubt that oncologists today cannot ignore the results being obtained with this instrumentation.

Acknowledgements. The authors thank Dr. Federica Elisei, School of Specialization of Nuclear Medicine, University of Milan, for her help with the bibliographic research. The authors are also grateful to Miss Annaluisa De Simone Sorrentino for her participation in the editorial work.

References

Adams S, Baum RP, Rink T, Schumm-Drager PM, Usadel KH, Hoh G (1998a) Limited value of fluorine-18 fluorodeoxyglucose positron emission tomography for the imaging of neuroendocrine tumours. Eur J Nucl Med 25:79 – 83

Adams S, Baum RP, Stuckensen T, Bitter K, Hor G (1998b) Prospective comparison of 18F-FDG PET with conventional imaging modalities (CT, MRI, US) in lymph node staging of head and neck cancer. Eur J Nucl Med 25:1255 – 1260

Adler LP, Bakale G (2001) Positron emission tomography imaging. In: Khalkhali I, Maublant JC, Goldsmith SJ (eds) Nuclear oncology. Diagnosis and therapy. Lippincott, Williams & Wilkins, Philadelphia, pp 289 – 295

Adler LP, Faulhaber PF, Schnur KC, Al-Kasi NL, Shenk RR (1997) Axillary lymph node metastases: screening with (F-18)2-deoxy-2-fluoro-D-glucose (FDG) PET. Radiology 203: 323 – 327

Ahlstrom H, Eriksson B, Bergstrom M, Bjurling P, Langstrom B, Oberg K (1995) Pancreatic neuroendocrine tumors: Diagnosis with PET. Radiology 195:333 – 337

Ahmad A, Barrington S, Maisey M, Rubens RD (1999) Use of positron emission tomography in evaluation of brachial plexopathy in breast cancer patients. Br J Cancer 79:478 – 482

Ak I, Stokkel MP, Pauwels EK (2000) Positron emission tomography with 2-(18F)fluoro-2-deoxy-D-glucose in oncology. Part II. The clinical value in detecting and staging primary tumours. J Cancer Res 126:560 – 574

Anderson CJ, Dehdashti F, Cutler PD, Scharz SW, Laforest Bass LA, Lewis JS, McCarthy DW (2001) 64Cu-TETA-octreotide as a PET imaging agent for patients with neuroendocrine tumors. J Nucl Med 42:213 – 221

Arbab AS, Koizumi K, Toyama K, Araki T (1996) Uptake of technetium-99m-tetrofosmin, technetium-99m-MIBI and thallium-201 in tumor cell lines. J Nucl Med 37:1551 – 1556

Arulampalam THA, Costa DC, Loizidou M, Visvikis D, Ell PJ, Taylor I (2001) Positron emission tomography in colorectal cancer. Br J Surg 88:176 – 89

Arulampalam THA, Francis DL, Visvikis D, Taylor I, Ell PJ (2004) FDG-PET for the pre-operative staging of colorectal liver metastases. Eur J Surg Oncol 30:286 – 91

Ashamalla H, Rafla S, Parikh K, Mokhtar B, Goswami G, Kambam S, Abdel-Dayem H, Guirguis A, Ross P, Evola A (2005) The contribution of integrated PET/CT to the evolving definition of treatment volumes in radiation treatment planning in lung cancer. Int J Radiat Oncol Biol Phys 63(4):1016 – 23

Avril N, Menzel M, Dose J, Schelling M, Weber W, Janicke F, Nathrath W, Schwaiger M (2001) Glucose metabolism of breast cancer assessed by 18F-FDG PET: histological and immunohistochemical tissue analysis. J Nucl Med 42:9 – 16

Avril N, Sassen S, Schmalfeldt B, Naehrig J, Rutke S, Weber WA, Werner M, Graeff H, Schwaiger M, Kuhn W (2005) Prediction of response to neoadjuvant chemotherapy by sequential F-18-fluorodeoxyglucose positron emission tomography in patients with advanced-stage ovarian cancer. J Clin Oncol 23(30):7445 – 53. Erratum in: J Clin Oncol 2005 23(36):9445

Bar-Shalom R, Guralnik L, Tsalic M, Leiderman M, Frenkel A, Gaitini D, Ben-Nun A, Keidar Z, Israel O (2005) The additional value of PET/CT over PET in FDG imaging of oesophageal cancer. Eur J Nucl Med Mol Imaging 32(8):918 – 24

Bartold SP, Donohoe KJ, Fletcher JW, Haynie TP, Henkin RE, Silberstein EB, Royal HD, Van den Abbeele A (1997) Procedure guide-line for gallium scintigraphy in the evaluation of malignant disease. J Nucl Med 38:990

Baum RP, Presselt N, Bonnet R (1999) Pulmonary nodules and non-small-cell bronchial carcinoma. In: Ruhlmann J, Oehr P, Biersack HJ (eds) PET in oncology: basics and clinical applications. Springer, Berlin Heidelberg New York, pp 102 – 119

Bellon JR, Mankoff DA, Eubank WB (2000) Evaluation of the international mammary (IM) lymph node (LN) chain by PET in locally advanced breast cancer (LABC). J Nucl Med 41:145P

Bender H, Kirst J, Palmedo H, Schomburg A, Wagner U, Ruhlmann J, Biersack HJ (1997) Value of 18fluoro-deoxyglucose positron emission tomography in the staging of recurrent breast carcinoma. Anticancer Res 17:1687 – 1692

Bender H, Palmedo H, Biersack HJ (1998) Breast imaging with

positron emission tomography. In: Taillefer R, Khalkhali I, Waxman AD, Biersack HJ (eds) Radionuclide imaging of the breast. M Dekker, New York, pp 147 – 175
Blackstock AW, Farmer MR, Lovato J, Mishra G, Melin SA, Oaks T, Aklilu M, Clark PB, Levine EA (2006) A prospective evaluation of the impact of 18-F-fluoro-deoxy-D-glucose positron emission tomography staging on survival for patients with locally advanced esophageal cancer. Int J Radiat Oncol Biol Phys 64(2):455 – 60
Bohdiewicz PJ (1998) Indium-111 satumomab pendetide: the first FDA-approved monoclonal antibody for tumor imaging. J Nucl Med 26:155 – 163
Bokemeyer C, Kollmannsberger C, Oechsle K, Dohmen BM, Pfannenberg A, Claussen CD, Bares R, Kanz L (2002) Early prediction of treatment response to high-dose salvage chemotherapy in patients with relapsed germ cell cancer using [(18)F]FDG PET. Br J Cancer 86(4):506 – 11
Bombardieri E, Crippa F, Maffioli L, Greco M (1997a) Nuclear medicine techniques for the study of breast cancer. Eur J Nucl Med 24:809 – 824
Bombardieri E, Crippa F, Rossetti C, Fazio F (1997b) The need of cost-effectiveness evaluation when using high-cost equipment in national health services. Tumori 83:544 – 546
Bombardieri E, Crippa F, Maffioli L, Draisma A, Chiti A, Agresti R, Greco M (1998) Nuclear medicine approaches for detection of axillary lymph node metastases. Q J Nucl Med 42:54 – 65
Bombardieri E, Carriò I, Gonzalez P, Serafini A, Turner HJ, Virgolini I, Maffioli L (1999) Main diagnostic application of nuclear medicine in oncology. Eur J Nucl Med 26:21 – 27
Bombardieri E, Aliberti G, De Graaf C, Pauwels EKJ, Crippa F (2001) Positron emission tomography (PET) and the nuclear medicine modalities in staging gastrointestinal cancer. Semin Surg Oncol 20:134 – 146
Bombardieri E, Aktolun C, Baum RP, Bishof-Delaloye A, Buscombe J, Chatal FJ, Maffioli L, Moncayo R, Mortelmans L, Reske SN (2003) FDG-PET: procedure guidelines for tumor imaging. J Nucl Med Mol Imaging 30:115 – 124
Bombardieri E, Seregni E, Villano C, Chiti A, Bajetta E (2004) Position of nuclear medicine techniques in the diagnostic work-up of neuroendocrine tumors. Q J Nucl Med Mol Imaging 48(2):150 – 63
Brady MS, Akhurst T, Spanknebel K, Hilton S, Gonen M, Patel A, Larson S (2006) Utility of preoperative [(18)]F fluorodeoxyglucose-positron emission tomography scanning in high-risk melanoma patients. Ann Surg Oncol 15 (in press)
Bristow RE, Giuntoli RL 2nd, Pannu HK, Schulick RD, Fishman EK, Wahl RL (2005) Combined PET/CT for detecting recurrent ovarian cancer limited to retroperitoneal lymph nodes. Gynecol Oncol 99(2):294 – 300. Epub 2005 Jul 26
Burton C, Ell PJ, Linch D (2004) The role of PET imaging in lymphoma. Br J Haematol 126:772 – 84
Cheson BD, Horning SJ, Coiffier B, Shipp MA, Fisher RI, Connors JM, Lister TA, Vose J, Grillo-Lopez A, Hagenbeek A, Cabanillas F, Klippensten D, Hiddemann W, Castellino R, Harris NL, Armitage JO, Carter W, Hoppe R, Canellos GP (1999) Report of an international workshop to standardise response criteria for non-Hodgkin's lymphomas. J Clin Oncol 17:1244
Chiti A, Schreiner FAG, Crippa F, Pauwels EKJ, Bombardieri E (1999) Nuclear medicine procedures in lung cancer. Eur J Nucl Med 26:533 – 555
Chu E, Devita VT (2001) Principles of cancer management: chemotherapy. In: Cancer: principles and practice of oncology. Lippincott Williams & Wilkins. Philadelphia
Coleman R, DeGrado TR, Wang S, Baldwin S, Orr MD, Reiman R, Prince DT (2000) Preliminary evaluation of F-18 fluorocholine (FCH) as a PET tumor imaging agent. Clin Positron Imaging 3:147
Corstens F (2001) Nuclear medicine techniques for the diagnosis and therapy of prostate carcinoma. Eur Urol 40:294 – 299
Crippa F, Bombardieri E, Seregni E, Castellani MR, Gasparini M, Maffioli L, Pizzichetta M, Buraggi GL (1992) Single determination of CA 15.3 and bone scintigraphy in the diagnosis of skeletal metastases of breast cancer. J Nucl Med 36:52 – 55
Crippa F, Seregni E, Agresti R, Chiesa C, Pascali C, Bogni A, Decise D, De Sanctis V, Greco M, Daidone MG, Bombardieri E (1998) Association between (18F)fluorodeoxyglucose uptake and postoperative histopathology, hormone receptor status, thymidine labelling index and p53 in primary breast cancer: a preliminary observation. Eur J Nucl Med 25: 1429 – 1434
Crippa F, Leutner M, Belli F, Gallino F, Greco M, Pilotti S, Cascinelli N, Bombardieri E (2000) Which kinds of lymph node metastases can FDG PET detect? A clinical study in melanoma. J Nucl Med 41:1491 – 1494
De Witte O, Levivier M, Violon P, Salmon I, Damhaut P, Wikler D, Jr, Hildebrand J, Brotchi J, Goldman S (1996) Prognostic value positron emission tomography with 18F-fluoro-2-deoxy-D-glucose in the low-grade glioma. Neurosurgery 39: 470 – 476
Delbeke D (1999) Oncological applications of FDG-PET imaging. J Nucl Med 40:1706 – 1715
Delbeke D, Valk P (2001) Positron emission tomography imaging: diagnosis and management. In: Khalkhali I, Maublant JC, Goldsmith SJ (eds) Nuclear oncology. Lippincott, Williams & Wilkins, Philadelphia, pp 351 – 360
Delbeke D, Vitola JV, Sandler MP, Arildsen RC, Powers TA, Wright JK, Chapman WC, Pinson CW (1997) Staging recurrent metastatic colorectal carcinoma with PET. J Nucl Med 38:1196 – 1201
Delcambre C, Reman O, Henry-Amar M, Peny AM, Macro M, Cheze S, Genot JY, Tanguy A, Switsers O, Van HL, Coutte J, Leporrier M, Bardet S (2000) Clinical relevance of gallium-67 scintigraphy in lymphoma before and after therapy. Eur J Nucl Med 27:176 – 184
Derlon JM, Petit-Taboue MC, Chapon F, Beaudouin V, Noel MH, Creveuil C, Courtheoux P, Houtteville JP (1997) The in vivo metabolic pattern of low-grade brain gliomas: a positron emission tomographic study using 18F fluorodeoxyglucose and 11C-L-methylmethionine. Neurosurgery 40:276 – 287
Derlon JM, Chapon F, Noel MH, Khouri S, Benali K, Petit-Taboue MC, Houtteville JP, Chajari MH, Bouvard G (2000) Non-invasive grading of oligodendrogliomas: correlations between in vivo metabolic pattern and histopathology. Eur J Nucl Med 27:778 – 787
Diederichs CG, Staib L, Glatting G, Beger HG, Reske SN (1998) FDG PET: elevated plasma glucose reduces both uptake and detection rate of pancreatic malignancies. J Nucl Med 39:1030 – 1033
Diederichs CG, Staib L, Vogel J, Glasbrenner B, Glatting G, Brambs HJ, Beger HG, Reske SN (2000) Values and limitations of 18F-fluorodeoxyglucose positron emission tomography with preoperative evaluation of patients with pancreatic masses. Pancreas 20:109 – 116
Dietl B, Marienhagen J (2005) The therapeutic impact of (18)F-FDG whole body PET. A radiooncologist's view. Nuklearmedizin 44(1):8 – 14
Dietlein M, Weber W, Schwaiger M, Schicha H (2003) 18F-Fluorodeoxyglucose positron emission tomography in restaging of colorectal cancer. Nuklearmedizin 42:145 – 56
Dimitrakopoulou-Strauss A, Strauss LG (2003) PET imaging of prostate cancer with 11C-acetate. J Nucl Med 44(4):556 – 8
Dimitrakopoulou-Strauss A, Strauss LG, Burger C (2001) Quantitative PET studies in pretreated melanoma patients: a comparison of 6 – 18F-fluoro-L-dopa with 18F-FDG and

15O-water using compartment and noncompartment analysis. J Nucl Med 42:248 – 256
Dobos N, Rubesin SE (2002) Radiologic imaging modalities in the diagnosis and management of colorectal cancer. Hematol Oncol Clin North Am 16(4):875 – 95
Draisma A, Maffioli L, Gasparini M, Savelli G, Pauwels E, Bombardieri E (1998) Gallium-67 as a tumor-seeking agent in lymphomas – a review. Tumori 84:434 – 441
Ell PJ (2006) The contribution of PET/CT to improved patient management. Br J Radiol 79:32 – 36
Engel H, Steinert H, Buck A, Berthold T, Huch Boni RA, von Schulthess GK (1996) Whole-body PET: physicologic and artifactual fluorodeoxyglucose accumulations. J Nucl Med 37:441 – 446
Eriksson B, Orlefors H, Sundin A, Skogseid B, Langstrom B, Bergstrom M, Oberg K (1999) Positron emission tomography in neuroendocrine tumours. Ital J Gastroenterol Hepatol 2:S167 – 171
Erturk SM, Ichikawa T, Fujii H, Yasuda S, Ros PR (2006) PET imaging for evaluation of metastatic colorectal cancer of the liver. Eur J Radiol 31
Eschmann SM, Paulsen F, Reimold M, Dittmann H, Welz S, Reischl G, Machulla HJ, Bares R (2005) Prognostic impact of hypoxia imaging with 18F-misonidazole PET in non-small cell lung cancer and head and neck cancer before radiotherapy. J Nucl Med 46(2):253 – 60
Freeny PC (2001) Pancreatic carcinoma: imaging update. Dig Dis 19:37 – 46
Friedman KP, Wahl RL (2004) Clinical use of positron emission tomography in the management of cutaneous melanoma. Semin Nucl Med 34(4):242 – 53
Froehlich A, Diederichs CG, Staib L, Vogel J, Beger HG, Reske SN (1999) Detection of liver metastases from pancreatic cancer using FDG PET. J Nucl Med 40:250 – 255
Fueger BJ, Weber WA, Quon A, Crawford TL, Allen-Auerbach MS, Halpern BS, Ratib O, Phelps ME, Czernin J (2005) Performance of 2-deoxy-2-[F-18]fluoro-D-glucose positron emission tomography and integrated PET/CT in restaged breast cancer patients. Mol Imaging Biol 7(5):369 – 76
Gambhir SS, Shepherd JE, Shah BD, Hart E, Hoh CK, Valk PE, Emi T, Phelps ME (1998) Analytical decision model for the cost-effective management of solitary pulmonary nodules. J Clin Oncol 16:2113 – 2125
Gambhir SS, Czernin J, Shimmer J, Silverman DHS, Coleman E, Phelps ME (2001) A tabulated summary of the FDG PET literature. J Nucl Med 42:1S–93S
Gasparini M, Bombardieri E, Castellani M, Tondini C, Maffioli L, Devizzi L, Gerundini P (1998) Gallium-67 scintigraphy evaluation of therapy in non-Hodgkin's lymphoma. J Nucl Med 39:1586 – 1590
Gimenez M, Crespo-Jara AA, Villar L, Calvo R, Abizu J, Cabrera A (1999) Preoperative and intraoperative uptake of 18FDG-PET in axillary metastases of breast cancer. A pathological correlation. J Nucl Med 40:138P
Goh BK, Tan YM, Chung YF (2005) Utility of fusion CT-PET in the diagnosis of small pancreatic carcinoma. World J Gastroenterol 11(24):3800 – 2
Greco M, Crippa F, Agresti R, Seregni E, Gerali A, Giovanazzi R, Micheli A, Asero S, Ferraris C, Gennaro M, Bombardieri E, Cascinelli N (2001) Axillary lymph node staging in breast cancer by 2-fluoro-2-deoxy-D-glucose-positron emission tomography: clinical evaluation and alternative management. J Natl Cancer Inst 93:630 – 635
Greven KM, Williams DW 3rd, McGuirt WF Sr, Harkness BA, D'Agostino RB Jr, Keyes JW Jr, Watson NE Jr (2001) Serial positron emission tomography scans following radiation therapy of patients with head and neck cancer. Head Neck 23(11):942 – 6
Grunwald F, Kalicke T, Feine U, Lietzenmayer R, Scheidhauer K, Dietlein M, Schober O, Lerch H, Brandt-Mainz K, Burchert W, Hiltermann G, Cremerius U, Biersack HJ (1999) Fluorine-18 fluorodeoxyglucose positron emission tomography in thyroid cancer: results of a multicentre study. Eur J Nucl Med 26:1547 – 1552
Gupta NC, Nicholson P, Bloomfield SM (1999) FDG-PET in the staging work-up of patients with suspected intracranial metastatic tumors. Ann Surg 230:202 – 206
Hafner J, Schmid MH, Kempf W, Burg G, Kunzi W, Meuli-Simmen C, Neff P, Meyer V, Mihic D, Garzoli E, Jungius KP, Seifert B, Dummer R, Steinert H (2004) Baseline staging in cutaneous malignant melanoma. Br J Dermatol 150(4):677 – 86
Hanson MW, Glantz MJ, Hoffman JM, Friedman AH, Burger PC, Schold SC, Coleman RE (1991) FDG-PET in the selection of brain lesions for biopsy. J Comp Assist Tomogr 15:796 – 801
Hart DP, Avivi I, Thomson KJ, Peggs KS, Morris EC, Goldstone AH, et al. (2005) Use of 18F-FDG positron emission tomography following allogeneic transplantation to guide adoptive immunotherapy with donor lymphocyte infusions. Br J Haematol 128:824 – 9
Hartman TE (2005) Radiologic evaluation of the solitary pulmonary nodule. Radiol Clin North Am 43(3):459 – 65, vii
Haseman MK, Rosenthal SA, Polascik TJ (2000) Capromab pendetide imaging of prostate cancer. Cancer Biother Radiopharm 15:131 – 140
Hathaway PB, Mankoff DA, Maravilla KR, Austin-Seymour MM, Ellis GK, Gralow JR, Cortese AA, Hayes CE, Moe RE (1999) Value of combined FDG PET and MR imaging in the evaluation suspected recurrent local-regional breast cancer: preliminary experience. Radiology 210:807 – 814
Haugen BR, Lin EC (2001) Isotope imaging for metastatic thyroid cancer. Endocrinol Metab Clin North Am 30:469 – 492
Hauth EA, Antoch G, Stattaus J, Kuehl H, Veit P, Bockisch A, Kimmig R, Forsting M (2005) Evaluation of integrated whole-body PET/CT in the detection of recurrent ovarian cancer. Eur J Radiol 56(2):263 – 8
Hayashi N, Tamaki N, Yonekura Y (1998) Imaging of the hepatocellular carcinoma using dynamic positron emission tomography with nitrogen-13-ammonia. J Nucl Med 26:254 – 257
Heald AE, Hoffman JM, Barlett JA, Waskin HA (1996) Differentiation of central nervous system lesions in AIDS patients using positron emission tomography (PET). Int J STD AIDS 7:337
Heicappell R, Muller-Mattheis V, Reinhardt M, Vosberg H, Gerharz CD, Muller-Gartner H, Ackermann R (1999) Staging of pelvic lymph nodes in neoplasms of the bladder and prostate by positron emission tomography with 2-18F-2-deoxy-D-glucose. Eur Urol 36:582 – 587
Heinrich S, Goerres GW, Schafer M, Sagmeister M, Bauerfeind P, Pestalozzi BC, Hany TF, von Schulthess GK, Clavien PA (2005) Positron emission tomography/computed tomography influences on the management of resectable pancreatic cancer and its cost-effectiveness. Ann Surg 242(2):235 – 43
Helal BO, Merlet P, Toubert ME, Franc B, Schwartz C, Gauthier-Koelesnikov H, Pringent A, Syrota A (2001) Clinical impact of 18F-FDG PET in thyroid carcinoma patients with elevated thyroglobulin levels and negative 131I scanning results after therapy. J Nucl Med 42:1464 – 1469
Herbert ME, Lowe VJ, Hoffman JM, Patz EF Jr, Anscher MS (1996) Positron emission tomography in the pretreatment evaluation and follow-up of non-small cell lung cancer patients treated with radiotherapy: preliminary findings. Am J Clin Oncol 19:416 – 421
Hicks RJ, MacManus MP, Seymour JF (2005a) Initial staging of lymphoma with positron emission tomography and computed tomography. Semin Nucl Med 35(3):165 – 75

Hicks RJ, Rischin D, Fisher R, Binns D, Scott AM, Peters LJ (2005b) Utility of FMISO PET in advanced head and neck cancer treated with chemoradiation incorporating a hypoxia-targeting chemotherapy agent. Eur J Nucl Med Mol Imaging 32(12):1384 – 91

Hillner BE, Tunuguntla R, Fratkin M (2004) Clinical decisions associated with positron emission tomography in a prospective cohort of patients with suspected or known cancer at one United States center. J Clin Oncol 22:4147 – 56

Hoch CK, Schiepers C, Seltzer MA, Gambhir SS, Silverman DH, Czernin J, Maddahi J, Phelps ME (1997) PET in oncology: will it replace the other modalities? Semin Nucl Med 27: 94 – 106

Hoegerle S, Schneider B, Kraft A, Moser E, Nitzsche EU (1999) Imaging of a metastatic gastrointestinal carcinoid by F-18-DOPA positron emission tomography. Nuklearmedizin 38:127 – 130

Hoegerle S, Altehoefer C, Ghanem N, Koehler G, Waller CF, Scheruebl H, Moser E, Nitzsche E (2001) Whole-body 18F dopa PET for detection of gastrointestinal carcinoid tumors. Radiology 22:373 – 380

Hoh CK (1999) Positron emission tomography imaging. In: Khalkhali I, Maublant JC, Goldsmith SJ (eds) Nuclear oncology. Lippincott Williams & Wilkins, Philadelphia, pp 343 – 349

Hooft L, Hoekstra OS, Deville W, Lips P, Teule GJ, Boers M, van Tulder MW (2001) Diagnostic accuracy of 18F-fluorodeoxyglucose positron emission tomography in the follow-up of papillary or follicular thyroid cancer. J Clin Endocrinol Metab 86:3779 – 3786

Houvinen R, Leskinen-Kallio S, Nagren K, Lehikoinen P, Ruotsalainen U, Teras M (1993) Carbon-11-methionine and PET in evaluation of treatment response of breast cancer. Br J Cancer 67:787 – 791

Huebner RH, Park KC, Shepherd JE, Schwimmer J, Czernin J, Phelps ME, et al. (2000) A meta-analysis of the literature for whole-body FDG PET detection of recurrent colorectal cancer. J Nucl Med 41:1177 – 89

Hughes SJ, Prvulovich EM, Witherow H, Kalavrezos N, Ell PJ (2004) A comparison of FDG PET/CT and MRI versus histology for staging of primary head and neck cancers and detection of recurrent disease. J Nucl Med 45:80

Hutchings M, Loft A, Hansen M, Pedersen LM, Buhl T, Jurlander J, Buus S, Keiding S, D'Amore F, Boesen AM, Berthelsen AK, Specht L (2006) FDG-PET after two cycles of chemotherapy predicts treatment failure and progression-free survival in Hodgkin lymphoma. Blood 107(1):52 – 9

Institute for Clinical PET (1994) ICP Breast Cancer: assessing axillary lymph node involvement. Can it provide a comprehensive and less invasive alternative to dissection? In: Clinical application and economic implication of PET in the assessment of axillary lymph node involvement in breast cancer: a retrospective study. Abstract from the 1994 ICP Meeting, pp 2 – 8

Imdahl A, Nitzsche E, Krautmann F, Hogerle S, Boos S, Einert A, Sontheimer J, Farthmann EH (1999) Evaluation of positron emission tomography with 2-[^{18}F]fluoro-2-deoxy-D-glucose for the differentiation of chronic pancreatitis and pancreatic cancer. Br J Surg 86:194 – 199

Isasi CR, Moadel RM, Blaufox MD (2005) A meta-analysis of FDG-PET for the evaluation of breast cancer recurrence and metastases. Breast Cancer Res Treat 90(2):105 – 12

Ishikawa M, Kikuchi H, Miyatake S, Oda Y, Yonekura Y, Nishizawa S (1993) Glucose consumption in recurrent gliomas. Neurosurgery 33:28 – 33

Ishimori T, Saga T, Nagata Y, Nakamoto Y, Higashi T, Mamede M, Mukai T, Negoro Y, Aoki T, Hiraoka M, Konishi J (2004) 18F-FDG and 11C-methionine PET for evaluation of treatment response of lung cancer after stereotactic radiotherapy. Ann Nucl Med 18(8):669 – 74

Ishimori T, Patel PV, Wahl RL (2005) Detection of unexpected additional primary malignancies with PET/CT. J Nucl Med 46(5):752 – 7

Jadvar H, Fischman AJ (2001) Evaluation of pancreatic carcinoma with FDG PET. Abdom Imaging 26:254 – 259

Jerusalem G, Beguin Y, Fassotte MF, Najjar F, Paulus P, Rigo P, Fillet G (1999) Whole-body positron emission tomography using F-18-fluorodeoxyglucose for post-treatment evaluation in Hodgkin's disease and non-Hodgkin's lymphoma has a higher diagnostic and prognostic value than classical computed tomography scan imaging. Blood 94:429 – 433

Jungehulsing M, Scheidhauer K, Damm M, Pietrzyk U, Eckel H, Schicha H, Stennert E (2000) 2F-fluoro-2-deoxy-D-glucose positron emission tomography is a sensitive tool for the detection of occult primary cancer (carcinoma of unknown primary syndrome) with head and neck lymph node manifestation. Otolaryngol Head Neck Surg 123:294 – 301

Kanyari Z, Orosz L, Juhasz B, Tanyi M, Nemeth E, Tron L, Damjanovich L, Lukacs G, Kalvin B (2005) The role of positron emission tomography (PET) in the detection of local recurrence and metastases of colorectal cancer. Magy Seb J 58(3):179 – 83

Kaschten B, Stevenaert A, Sadzot B, Deprez M, Degueldre C, Del Fiore G, Luxen A, Reznik M (1998) Preoperative evaluation of 54 gliomas by PET with fluorine-18-fluorodeoxyglucose and/or carbon-11-methionine. J Nucl Med 39:778 – 785

Kau RJ, Alexiou C, Laubenbacher C, Werner M, Schwaiger M, Arnold W (1999) Lymph node detection of head and neck squamous cell carcinoma by positron emission tomography with fluorodeoxyglucose F18 in a routine clinical setting. Arch Otolaryngol Head Neck Surg 125:1322 – 1328

Keidar Z, Haim N, Guralnik L, et al. (2005) PET/CT using 18-FDG in suspected lung cancer recurrence: diagnostic value and impact on patient management. J Nucl Med 45:1640 – 6

Khan N, Oriuchi N, Higuchi T, Zhang H, Endo K (2003) PET in the follow-up of differentiated thyroid cancer. Br J Radiol 76(910):690 – 5

Kieninger AN, Welsh R, Bendick PJ, Zelenock G, Chmielewski GW (2006) Positron-emission tomography as a prognostic tool for early-stage lung cancer. Am J Surg 191(3):433 – 6

Kim EE, Chung SK, Haynie TP, Kim CG, Cho BJ, Podoloff DA, Tilbury RS, Yang DJ, Yung WK, Moser RP Jr (1992) Differentiation of residual or recurrent tumors from post-treatment changes with F-18 FDG PET. Radiographics 12:269 – 279

Klein M, Freedman N, Lotem M, Marciano R, Moshe S, Gimon Chisin R (2000) Contribution of whole body F-18 FDG-PET and lymphoscintigraphy to the assessment of regional and distant metastases in cutaneous malignant melanoma. A pilot study. Nuklearmedizin 39:56 – 61

Klose T, Leidl R, Buchmann I, Brambs HJ, Reske SN (2000) Primary staging of lymphomas: Cost-effectiveness of FDG-PET versus computed tomography. Eur J Nucl Med 27:1457 – 1464

Kobori O, Kirihara Y, Kosaka N, Hara T (1999) Positron emission tomography of esophageal carcinoma using (11)C-choline and (18)F-fluorodeoxyglucose: a novel method of preoperative lymph node staging. Cancer 86:1638 – 1648

Kole AC, Nieweg OE, Pruim J, Paans AM, Plukker JT, Hoekstra HJ, Schraffordt Koops H, Vaalburg W (1997) Standardized uptake value and quantification of metabolism for breast cancer imaging with FDG and L-(1 – 11C)tyrosine PET. J Nucl Med 38:692 – 696

Koshy M, Paulino AC, Howell R, Schuster D, Halkar R, Davis LW (2005) F-18 FDG PET-CT fusion in radiotherapy treatment planning for head and neck cancer. Head Neck 27(6):494 – 502

Kostakoglu L, Leonard JP, Coleman M, Goldsmith SJ (2004) The role of FDG-PET imaging in the management of lymphoma. Clin Adv Hematol Oncol 2(2):115 – 21

Kotzerke J, Volkmer BG, Neumaier B, Gschwend JE, Hautmann RE, Reske SN (2002) Carbon-11 acetate positron emission tomography can detect local recurrence of prostate cancer. Eur J Nucl Med Mol Imaging 29(10):1380 – 4

Koukouraki S, Strauss LG, Georgoulias V, Schuhmacher J, Haberkorn U, Karkavitsas N, Dimitrakopoulou-Strauss A (2006) Evaluation of the pharmacokinetics of (68)-Ga-DOTATOC in patients with metastatic neuroendocrine tumours scheduled for (90)Y-DOTATOC therapy. Eur J Nucl Med Mol Imaging 17:1 – 7

Krohn KA (2001) Evaluation of alternative approaches for imaging cellular growth. Q J Nucl Med 45:174 – 178

Ksperk RK, Riesener KP, Wilms K, Schumpelick V (2001) Limited value of positron emission tomography in treatment of pancreatic cancer: surgeon's view. World J Surg 25:1134 – 1139

Kumar R, Zhuang H, Alavi A (2004) PET in the management of urologic malignancies. Radiol Clin North Am 42(6):1141 – 53

Kumar R, Mavi A, Bural G, Alavi A (2005) Fluorodeoxyglucose-PET in the management of malignant melanoma. Radiol Clin North Am 43(1):23 – 33

Kumar R, Zhuang H, Schnall M, Conant E, Damia S, Weinstein S, Chandra P, Czerniecki B, Alavi A (2006) FDG PET positive lymph nodes are highly predictive of metastasis in breast cancer. Nucl Med Commun 27(3):231 – 6

Kwee SA, Coel MN, Lim J, Ko JP (2005) Prostate cancer localization with 18fluorine fluorocholine positron emission tomography. J Urol 173(1):252 – 5

Lammertsma AA, Wise RJ, Cox TCS, Thomas DGT, Jones T (1985) Measurement of blood flow, oxygen utilization, oxygen extraction ratio and functional blood volume in human brain tumors and surrounding oedematous tissues. Br J Radiol 58:725 – 734

Lamy PJ, Comte F, Eberle MC (2005) Combined role of tumor markers and 18fluoro-deoxyglucose-positron emission tomography (18FDG-PET) in follow-up of cancer patients. Bull Cancer 92(10):858 – 64

Landheer ML, Steffens MG, Klinkenbijl JH, Westenberg AH, Oyen WJ (2005) Value of fluorodeoxyglucose positron emission tomography in women with breast cancer. Br J Surg 92(11):1363 – 7

Lapela M, Eigtved A, Jyrkkio S, Grenman R, Kurki T, Lindholm P, Nuutinen J, Sutinen E, Solin O, Bjornskov I, Bretlau P, Friberg L, Holm S, Jensen M, Sand Hansen H, Minn H (2000) Experience in qualitative and quantitative FDG PET in follow-up of patients with suspected recurrence from head and neck cancer. Eur J Cancer 36:858 – 867

Lardinois D, Weder W, Hany TF, Kamel EM, Korom S, Seifert B, et al. (2003) Staging of non-small-cell lung cancer with integrated positron-emission tomography and computed tomography. N Engl J Med 348:2500 – 7

Lassen U, Daugaard G, Eigtved A, Hojgaard L, Damgaard K, Rorth M (2003) Whole-body FDG-PET in patients with stage I non-seminomatous germ cell tumours. Eur J Nucl Med Mol Imaging 30(3):396 – 402

Laverman P, Boerman OC, Corsten FH, Oyen WJ (2002) Fluorinated amino acids for tumour imaging with positron emission tomography. Eur J Nucl Med Mol Imaging 29:681 – 690

Lenzo NP, Moschilla G, Patrikeos A (2004) Diffuse splenic metastases from seminoma visualized on FDG PET. AJR Am J Roentgenol 183(2):525 – 7

Lewis JS, Welth MJ (2001) PET imaging of hypoxia. J Nucl Med 45:183 – 188

Liberale G, Van Laethem JL, Gay F, Goldman S, Nagy N, Coppens E, Gelin M, Nakadi IE (2004) The role of PET scan in the preoperative management of oesophageal cancer. Eur J Surg Oncol 30(9):942 – 7

Lind P, Kumming G, Matschnig S, Heinisch M, Gallowitsch HJ, Mikosch P, Kresnik E, Gomez I, Unterweger O (2000) The role of F18-FDG PET in thyroid cancer. Acta Med Austriaca 27:38 – 41

Liu IJ, Zafar MB, Lai YH, Segall GM, Terris MK (2001) Fluorodeoxyglucose positron emission tomography studies in diagnosis and staging of clinically organ confined prostate cancer. Urology 57:108 – 111

Lonneux M (2005) PET-scan in colorectal cancer. Acta Chir Belg 105(4):333 – 7

Lonneux M, Lawson G, Ide C, Bausart R, Remacle M, Pauwels S (2000) Positron emission tomography with fluorodeoxyglucose for suspected head and neck tumor recurrence in the symptomatic patient. Laryngoscope 110:1493 – 1497

Lowe VJ, Duhaylongsod FG, Patz EF, Delong DM, Hoffman J, Wolfe WG, Coleman RE (1997) FDG-PET and lung malignancy: a retrospective study of pulmonary and PET analysis. Radiology 202:435 – 439

MacManus MP, Hicks RJ, Matthews JP, Wirth A, Rischin D, Ball DL (2005) Metabolic (FDG-PET) response after radical radiotherapy/chemoradiotherapy for non-small cell lung cancer correlates with patterns of failure. Lung Cancer 49(1):95 – 108

Maffioli L, Gasparini M, Chiti A, Gramaglia A, Mongioj V, Pozzi A, Bombardieri E (1996) Clinical role of technetium-99m sestamibi single-photon emission tomography in evaluating pretreated patients with brain tumours. Eur J Nucl Med 23:308 – 311

Magnani P, Carretta A, Rizzo G, Fazio F, Vanzulli A, Lucignani G, Zannini P, Messa C, Landoni C, Gilardi MC, Del Maschio A (1999) FDG-PET and spiral CT image fusion for mediastinal lymph node assessment of non-small cell lung cancer patients. J Cardiovasc Surg 40:741 – 748

Maisey NR, Webb A, Flux GD, Padhani A, Cunningham DC, Ot RJ, Norman A (2000) FDG-PET in the prediction of survival of patients with cancer of the pancreas: a pilot study. Br J Cancer 83:287 – 293

Marom EM, McAdams HP, Erasmus JJ, Goodman PC, Culhuan DK, Coleman RE, Herndon JE, Patz EF Jr (1999) Staging non-small cell lung cancer with whole-body PET. Radiology 212:803 – 809

Mason NS, Mathis CA (2003) Radiohalogens for PET imaging in positron emission tomography: basic science and clinical practice. Springer, Berlin Heidelberg New York

McQuade P, McCarthy DW, Welch MJ (2003) Metal radionuclides for PET imaging in positron emission tomography: basic science and clinical practice. Springer, Berlin Heidelberg New York

Meignan M, Haioun C, Itti E, Rahmouni A, Reyes F (2006) Value of [18F]fluorodeoxyglucose-positron emission tomography in managing patients with aggressive non-Hodgkin's lymphoma. Clin Lymphoma Myelom 6(4):306 – 13

Messa C, Bettinardi V, Picchio M, Pelosi E, Landoni C, Gianolli L, Gilardi MC, Fazio F (2004) PET/CT in diagnostic oncology. Q J Nucl Med Mol Imaging 48:66 – 75

Messa C, Ceresoli GL, Rizzo G, Artioli D, Cattaneo M, Castellone P, Gregorc V, Picchio M, Landoni C, Fazio F (2005) Feasibility of [18F]FDG-PET and coregistered CT on clinical target volume definition of advanced non-small cell lung cancer. Q J Nucl Med Mol Imaging 49(3):259 – 66

Mijnhout GS, Hoekstra OS, van Tulder MW, Teule GJ, Deville WL (2001) Systematic review of the diagnostic accuracy of 18F-fluorodeoxyglucose positron emission tomography in melanoma patients. Cancer 91:1530 – 1542

Mikhaeel NG, Hutchings M, Fields PA, O'Doherty MJ, Timothy AR (2005) FDG-PET after two to three cycles of chemothera-

py predicts progression-free and overall survival in high-grade non-Hodgkin lymphoma. Ann Oncol 16(9):1514 – 23
Mineura K, Shioya H, Kowada M, Uemura K (1997) Tumor extent of slowly progressive oligodendroglioma determined by 18F-fluorophenylalanine positron emission tomography. Eur J Radiol 25:30 – 35
Mitchell JC, Grant F, Evenson AR, Parker JA, Hasselgren PO, Parangi S (2005) Preoperative evaluation of thyroid nodules with 18FDG-PET/CT. Surgery 138(6):1166 – 74
Moog F, Linke R, Manthey N, Tiling R, Knesewitsch P, Tatsch K, Hahn K (2000) Influence of thyroid-stimulating hormone levels on uptake of FDG in recurrent and metastatic differentiated thyroid carcinoma. J Nucl Med 41:1989 – 1995
Morris MJ, Akhurst T, Larson SM, Ditullio M, Chu E, Siedlecki K, Verbel D, Heller G, Kelly WK, Slovin S, Schwartz L, Scher HI (2005) Fluorodeoxyglucose positron emission tomography as an outcome measure for castrate metastatic prostate cancer treated with antimicrotubule chemotherapy. Clin Cancer Res 11(9):3210 – 6
Moureau-Zabotto L, Touboul E, Lerouge D, Deniaud-Alexandre E, Grahek D, Foulquier JN, Petegnief Y, Gres B, El Balaa H, Kerrou K, Montravers F, Keraudy K, Tiret E, Gendre JP, Grange JD, Houry S, Talbot JN (2005) Impact of CT and 18F-deoxyglucose positron emission tomography image fusion for conformal radiotherapy in esophageal carcinoma. Int J Radiat Oncol Biol Phys 63(2):340 – 5
Murakami M, Miyamoto T, Iida T, Tsukada H, Watanabe M, Shida M, Maeda H, Nasu S, Yasuda S, Yasuda M, Ide M (2006) Whole-body positron emission tomography and tumor marker CA125 for detection of recurrence in epithelial ovarian cancer. Int J Gynecol Cancer 16 Suppl 1:99 – 107
Myers LL, Wax MK, Nabi H, Simpson GT, Lamonica D (1998) Positron emission tomography in the evaluation of the N0 neck. Laryngoscope 108:232 – 6
Nahas Z, Goldenberg D, Fakhry C, Ewertz M, Zeiger M, Ladenson PW, Wahl R, Tufano RP (2005) The role of positron emission tomography/computed tomography in the management of recurrent papillary thyroid carcinoma. Laryngoscope 115(2):237 – 43
Nair N, Ali A, Dowlatshahi K, Fan M, Lamonica G (2000) Positron emission tomography with fluorine-18 fluorodeoxyglucose to evaluate response of early breast carcinoma treated with stereotaxic interstitial laser therapy. Clin Nucl Med 25:505 – 507
Nakamoto Y, Saga T, Ishimori T, Mamede M, Togashi K, Higuchi T, Mandai M, Fujii S, Sakahara H, Konishi J (2001) Clinical value of positron emission tomography with FDG for recurrent ovarian cancer. AJR Am J Roentgenol 176:1449 – 1454
Nakata B, Nishimura S, Ishikawa T, Ohira M, Nishino H, Kawa J, Ochi H, Hirakawa K (2001) Prognostic predictive value of 18F-fluorodeoxyglucose positron emission tomography for patients with pancreatic cancer. Int J Oncol 19:53 – 58
Nishiyama Y, Yamamoto Y, Yokoe K, Monden T, Sasakawa Y, Tsutsui K, Satoh K, Ohkawa M (2005) Contribution of whole body FDG-PET to the detection of distant metastasis in pancreatic cancer. Ann Nucl Med 19(6):491 – 7
Nuutinen J, Sonninen P, Lehikoinen P, Sutinen E, Valavaara R, Eronen E, Norrgård S, Kulmala J, Teras M, Minn H (2000) Radiotherapy treatment planning and long-term follow-up with (11C)-methionine PET in patients with low-grade astrocytoma. Int J Rad Oncol Biol Phys 48:43 – 52
Oyama N, Akino H, Suzuki Y, Kanamaru H, Ishida H, Tanase K, Sadato N, Yonekura Y, Okada K (2001) FDG PET for evaluating the change of glucose metabolism in prostate cancer after androgen ablation. Nucl Med Commun 22:963 – 969
Oyama N, Miller TR, Dehdashti F, Siegel BA, Fischer KC, Michalski JM, Kibel AS, Andriole GL, Picus J, Welch MJ (2003) 11C-acetate PET imaging of prostate cancer: detection of recurrent disease at PSA relapse. J Nucl Med 44(4):549 – 55
Pakos EE, Fotopoulos AD, Ioannidis JP (2005) 18F-FDG PET for evaluation of bone marrow infiltration in staging of lymphoma: a meta-analysis. J Nucl Med 46(6):958 – 63
Pandit-Taskar N (2005) Oncologic imaging in gynecologic malignancies. J Nucl Med 46(11):1842 – 50
Pasquali C, Rubello D, Sperti C, Gasparoni P, Liessi G, Chierichetti F, Ferlin G, Pedrazzoli S (1998) Neuroendocrine tumor imaging: can FDG PET detect tumors with poor prognosis and aggressive behaviour? World J Surg 22:588 – 592
Pauleit D, Stoffels G, Schaden W, Hamacher K, Bauer D, Tellmann L, Herzog H, Broer S, Coenen HH, Langen KJ (2005) PET with O-(2 – 18F-fluoroethyl)-L-tyrosine in peripheral tumors: first clinical results. J Nucl Med 46(3):411 – 6
Paulus P, Benoit TH, Bury TH (1995) Positron emission tomography with 18F-fluorodeoxyglucose in the assessment of solitary pulmonary nodules. Eur J Nucl Med 22:775
Picchio M, Messa C, Landoni C, Gianolli L, Sironi S, Brioschi M, Matarrese M, Matei DV, De Cobelli F, Del Maschio A, Rocco F, Rigatti P, Fazio F (2003) Value of [11C]choline-positron emission tomography for re-staging prostate cancer: a comparison with [18F]fluorodeoxyglucose-positron emission tomography. J Urol 169(4):1337 – 40
Pinkas L, Robins PD, Forstrom LA, Mahoney DW, Mullan BP (1999) Clinical experience with radiolabelled monoclonal antibodies in the detection of colorectal and ovarian carcinoma recurrence and review of the literature. Nucl Med Commun 20:689 – 696
Pirotte B, Goldman S, Massager N, David P, Wikler D, Vandesteene A, Salmon I, Brotchi J, Levivier M (2004) Comparison of 18F-FDG and 11C-methionine for PET-guided stereotactic brain biopsy of gliomas. J Nucl Med 45(8):1293 – 8
Pramesh CS, Mistry RC (2005) Role of PET scan in management of oesophageal cancer. Eur J Surg Oncol 31(4):449
Rampin L, Nanni C, Fanti S, Rubello D (2005) Value of PET-CT fusion imaging in avoiding potential pitfalls in the interpretation of 18F-FDG accumulation in the distal oesophagus. Eur J Nucl Med Mol Imaging 32(8):990 – 2
Rasmussen I, Sorensen J, Langstrom B, Haglund U (2004) Is positron emission tomography using 18F-fluorodeoxyglucose and 11C-acetate valuable in diagnosing indeterminate pancreatic masses? Scand J Surg 93(3):191 – 7
Reinhardt MJ, Matthies A, Biersack HJ (2002) PET-imaging in tumors of the reproductive tract. Q J Nucl Med 46(2):105 – 12
Reinhardt MJ, Joe AY, Jaeger U, Huber A, Matthies A, Bucerius J, Roedel R, Strunk H, Bieber T, Biersack HJ, Tuting T (2006) Diagnostic performance of whole body dual modality 18F-FDG PET/CT imaging for N- and M-staging of malignant melanoma: experience with 250 consecutive patients. J Clin Oncol 24(7):1178 – 87
Reske SN, Buchmann I (2001) Positron emission tomography imaging: hemapoietic tumors. In: Khalkali I, Maublant J, Goldsmith SJ (eds) Nuclear oncology: diagnosis and therapy. Lippincott, Williams & Wilkins, Philadelphia, pp 487 – 492
Richard S, Swanson MD (2001) Is an FDG-PET scan the new imaging standard for colon cancer? Ann Surg Oncol 8:752 – 753
Rigacci L, Castagnoli A, Dini C, Carpaneto A, Matteini M, Alterini R, Carrai V, Nassi L, Bernardi F, Pieroni C, Bosi A (2005) 18FDG-positron emission tomography in post treatment evaluation of residual mass in Hodgkin's lymphoma: long-term results. Oncol Rep 14(5):1209 – 14
Rizk N, Downey RJ, Akhurst T, Gonen M, Bains MS, Larson S, Rusch V (2006) Preoperative 18[F]-fluorodeoxyglucose positron emission tomography standardized uptake values predict survival after esophageal adenocarcinoma resection. Ann Thorac Surg 81(3):1076 – 81

Römer W, Hanauske AR, Ziegler S, Thodtmann R, Weber W, Fuchs C, Enne W, Herz M, Nerl C, Garbrecht M, Schwaiger M (1998) Positron emission tomography in non-Hodgkin's lymphoma: assessment of chemotherapy with fluorodeoxyglucose. Blood 91:4464 – 4471

Rose PG, Faulhaber P, Miraldi F, Abdul-Karim FW (2001) Positive emission tomography for evaluating a complete clinical response in patients with ovarian or peritoneal carcinoma: correlation with secondlook laparotomy. Gyneocl Oncol 82:17 – 21

Ruhlmann J, Oehr P (1999) Colorectal cancer. In: Ruhlmann J, Oehr P, Biersack HJ (eds) PET in oncology. Springer-Verlag, Berlin, pp 135 – 144

Schelling M, Avril N, Nahrig J, Kuhn W, Romer W, Sattler D, Werner M, Dose J, Janicke F, Graeff H, Schwaiger M (2000) Positron emission tomography using (18F)fluorodeoxyglucose for monitoring primary chemotherapy in breast cancer. J Clin Oncol 18:1689 – 1695

Schluter B, Bohuslavizki KH, Beyer W, Plotkin M, Buchert R, Clausen M (2001) Impact of FDG-PET on patients with differentiated thyroid cancer who present with elevated thyroglobulin and negative 131I scan. J Nucl Med 42:71 – 76

Schmid DT, John H, Zweifel R, Cservenyak T, Westera G, Goerres GW, von Schulthess GK, Hany TF (2005) Fluorocholine PET/CT in patients with prostate cancer: initial experience. Radiology 235(2):623 – 8

Schoder H, Yeung HW, Larson SM (2004) PET/CT in oncology: integration into clinical management of lymphoma, melanoma, and gastrointestinal malignancies. J Nucl Med 45 Suppl 1:72S–81S

Schwartz DL, Ford EC, Rajendran J, Yueh B, Coltrera MD, Virgin J, Anzai Y, Haynor D, Lewellen B, Mattes D, Kinahan P, Meyer J, Phillips M, Leblanc M, Krohn K, Eary J, Laramore GE (2005) FDG-PET/CT-guided intensity modulated head and neck radiotherapy: a pilot investigation. Head Neck 27(6):478 – 87

Scott WJ, Shepherd J, Gambhir SS (1998) Cost-effectiveness of FDG-PET for staging non-small cell lung cancer: a decision analysis. Ann Thoracic Surg 66:1876 – 1883

Segall GM, Johnson DL (2001) Positron emission tomography imaging. In: Khalkhali I, Maublant J, Goldsmith SJ (eds) Nuclear oncology diagnosis and therapy. Lippincott, Williams & Wilkins, Philadelphia, pp 557 – 562

Sendler A, Avril N, Helmberger H, Stollfuss J, Weber W, Beng F, Schwaiger M, Roder JD, Siewert JR (2000) Preoperative evaluation of pancreatic masses with positron emission tomography using 18F-fluorodeoxyglucose: diagnostic limitations. World J Surg 24:1121 – 1129

Seregni E, Bombardieri E (1999) Tumor markers in oncology. In: Aktolun C, Tauxe WN (eds) Nuclear oncology. Springer-Verlag, Berlin Heidelberg New York, pp 415 – 432

Shiga T, Tsukamoto E, Nakada K, Morita K, Kato T, Mabuchi M, Yoshinaga K, Katoh C, Kuge Y, Tamaki N (2001) Comparison of 18F-FDG, 131I-Na, and 201Tl in diagnosis of recurrent or metastatic thyroid carcinoma. J Nucl Med 42:414 – 419

Shinoura N, Nishijima M, Hara T, Haisa T, Yamamoto H, Fujii K, Mitsui I, Kosaka N, Kondo T, Hara T (1997) Brain tumors: detection with C-11 choline PET. Radiology 202:497 – 503

Sloka JS, Hollett PD, Mathews M (2005) Cost-effectiveness of positron emission tomography in breast cancer. Mol Imaging Biol 7(5):351 – 60

Soper JT (2001) Radiographic imaging in gynecologic oncology. Clin Obstet Gynecol 44:485 – 494

Steinert HC, Hauser M, Allemann F, Engel H, Berthold T, von Schulthess GK, Weder W (1997) Non-small cell lung cancer: nodal staging with FDG PET versus CT, with correlative lymph node mapping and sampling. Radiology 202:441 – 446

Strauss LG (2000) Sensitivity and specificity of positron emission tomography (PET) for the diagnosis of lymph node metastases. Recent Results Cancer Res 157:12 – 19

Strunk H, Bucerius J, Jaeger U, Joe A, Flacke S, Reinhardt M, Hortling N, Palmedo H (2005) Combined FDG PET/CT imaging for restaging of colorectal cancer patients: impact of image fusion on staging accuracy. Rofo 177(9):1235 – 41

Stumpe KD, Dazzi H, Schaffner A, von Schulthess GK (2000) Infection imaging using whole-body FDG-PET. Eur J Nucl Med 27:822 – 832

Sundin A, Eriksson B, Bergstrom M, Bjurling P, Lindner KJ, Oberg K, Langstrom B (2000) Demonstration of (11C) 5-hydroxy-L-tryptophan uptake and decarboxylation in carcinoid tumors by specific positioning labeling in positron emission tomography. Nucl Med Biol 27:33 – 41

Sung J, Espiritu JI, Segall GM, Terris MK (2003) Fluorodeoxyglucose positron emission tomography studies in the diagnosis and staging of clinically advanced prostate cancer. BJU Int 92(1):24 – 7

Swetter S, Carroll L, Johnson D, Segall G (2000) Positron emission tomography (PET) is superior to computerized tomography (CT) for metastatic staging in melanoma patients. Clin Positron Imaging 3:154

Takekuma M, Maeda M, Ozawa T, Yasumi K, Torizuka T (2005) Positron emission tomography with 18F-fluoro-2-deoxyglucose for the detection of recurrent ovarian cancer. Int J Clin Oncol 10(3):177 – 81

Taki S, Kakuda K, Kakuma K, Kobayashi K, Ohashi M, Ito S, Yokoyama M, Annen Y, Tonami N (1999) 201Tl SPECT in the differential diagnosis of brain tumours. Nucl Med Comm 20:637 – 645

Talbot JN, Haioun C, Rain JD, Meignan M, Wioland M, Misset JL, Grahek D, Kerrou K, Montravers F (2001) 18F–FDG positron imaging in clinical management of lymphoma patients. Crit Rev Oncol Hematol 38:193 – 221

Tatsumi M, Cohade C, Mourtzikos KA, Fishman EK, Wahl RL (2005) Initial experience with FDG-PET/CT in the evaluation of breast cancer. Eur J Nucl Med Mol Imaging 33(3):254 – 62

Tewson TJ, Krohon KA (1998) PET radiopharmaceuticals: state-of-the-art and future prospects. Semin Nucl Med 28:221 – 234

Toth G, Lengyel Z, Balkay L, Salah MA, Tron L, Toth C (2005) Detection of prostate cancer with 11C-methionine positron emission tomography. J Urol 173(1):66 – 9

Townsend DW, Beyer T (2003) Integrated structure/function imaging with X-ray CT and PET in positron emission tomography basic science and clinical practice. Springer, Berlin Heidelberg New York

Trampal C, Maldonado A, Sancho Cuesta F, Morales S, Senor de Uria C, Panades G, Ortega F (2000) Role of the positron emission tomography (PET) in suspected tumor recurrence when there is increased serum tumor markers. Rev Esp Med Nucl 19:279 – 287

Tyler JL, Diksic M, Villemure JG, Evans AC, Meyer E, Yamamoto YL, Feindel W (1987) Metabolic and hemodynamic evaluation of gliomas using positron emission tomography. J Nucl Med 28:1123 – 1133

Valk PE, Abella-Columna E, Haseman MK, Pounds TR, Tesar RD, Myers RW, Greiss HB, Hofer GA (1999) Whole-body PET imaging with F-18-fluorodeoxyglucose in management of recurrent colorectal cancer. Arch Surg 21:517 – 522

Valliappan S, Joyce JM, Myers DT (1999) Possible false-positive metastatic prostate cancer on In-111 capromab pendetide scan as a result of a pelvic kidney. Clin Nucl Med 24:984 – 985

van Westreenen HL, Heeren PA, van Dullemen HM, van der Jagt EJ, Jager PL, Groen H, Plukker JT (2005a) Positron emission tomography with F-18-fluorodeoxyglucose in a combined staging strategy of esophageal cancer prevents unnecessary surgical explorations. J Gastrointest Surg 9(1):54 – 61

van Westreenen HL, Plukker JT, Cobben DC, Verhoogt CJ, Groen H, Jager PL (2005b) Prognostic value of the standardized uptake value in esophageal cancer. AJR Am J Roentgenol 185(2):436 – 40

Vansteenkiste JF, Stroobants SG, De Leyn PR, Dupont PJ, Verschakelen JA, Nackaerts KL, Mortelmans LA, and the Leuven Lung Cancer Study Group (1997) Mediastinal lymph node staging with FDG-PET scan in patient with potentially operable non-small-cell lung cancer. A prospective analysis of 50 cases. Chest 112:1480 – 1486

Varandolo L, Stokkel MP, Mazzi U, Pauwels EKJ (2000) 18F-labeled radiopharmaceuticals for PET in oncology excluding FDG. Nucl Med Biol 27:103 – 112

Verboom P, van Tinteren H, Hoekstra OS, Smit EF, van den Bergh HAM, Schreurs AJM, et al., and the PLUS Study Group (2003) Cost-effectiveness of FDG-PET in staging non-small cell lung cancer: the PLUS study. Eur J Nucl Med Mol Imaging 30:1444 – 9

Vitola JV, Delbeke D, Meranze SG, Mazer MJ, Pinson CW (1996) Positron emission tomography with F-18-fluorodeoxyglucose to evaluate the results of hepatic chemoembolization. Cancer 78:2216 – 2222

von Rahden BH, Sarbia M, Stein HJ (2006) Medical image. Combined FDG-PET/CT and CT-guided biopsy in diagnosing oesophageal cancer recurrence. N Z Med J 119(1228): U1810

Vrieze O, Haustermans K, De Wever W, Lerut T, Van Cutsem E, Ectors N, Hiele M, Flamen P (2004) Is there a role for FGD-PET in radiotherapy planning in esophageal carcinoma? Radiother Oncol 73(3):269 – 75

Wagner JD, Schauwecker D, Hutchins G, Coleman JJ 3rd (1997) Initial assessment of positron emission tomography for detection of nonpalpable regional lymphatic metastases in melanoma. J Surg Oncol 64:181 – 189

Wagner JD, Schauwecker DS, Davidson D, Wenck S, Jung SH, Hutchins G (2001) FDG-PET sensitivity for melanoma lymph node metastases is dependent on tumor volume. J Surg Oncol 77:237 – 242

Wahl RL (1998) Overview of the current status of PET in breast cancer imaging. Q J Nucl Med 42:1 – 7

Wahl RL, Hutchins GD, Buchsbaum DJ, Liebert M, Grossman HB, Fisher S (1991) 18F-2-deoxy-2-fluoro-D-glucose uptake into human tumor xenografts. Feasibility studies for cancer imaging with positron-emission tomography. Cancer 67: 1544 – 1550

Wang W, Larson SM, Fazzari M, Tickoo SK, Kolbert K, Sgouros G, Yeung H, Macapinlac H, Rosai J, Robbins RJ (2000) Prognostic value of 18F-fluorodeoxyglucose positron emission tomographic scanning in patients with thyroid. J Clin Endocrinol Metab 85:1107 – 1113

Weber WA, Schwaiger M, Avril N (2000) Quantitative assessment of tumor metabolism using FDG-PET imaging. Nucl Med Biol 27:683 – 687

Wechalekar K, Sharma B, Cook G (2005) PET/CT in oncology – a major advance. Clin Radiol 60:1143 – 1155

Weir L, Worsley D, Bernstein V (2005) The value of FDG positron emission tomography in the management of patients with breast cancer. Breast J 11(3):204 – 9

Wester HJ, Herz M, Weber W, Heiss P, Senekowitsch-Schmidtke R, Schwaiger M, Stocklin G (1999) Synthesis and radiopharmacology of O(2-(18F)fluoroethyl)-L-tyrosine for tumor imaging. J Nucl Med 40:205 – 212

Wieder HA, Beer AJ, Lordick F, Ott K, Fischer M, Rummeny EJ, Ziegler S, Siewer JR, Schwaiger M, Weber WA (2005) Comparison of changes in tumor metabolic activity and tumor size during chemotherapy of adenocarcinomas of the esophagogastric junction. J Nucl Med 46(12):2029 – 34

Wiering B, Krabbe PF, Jager GJ, Oyen WJ, Ruers TJ (2005) The impact of fluor-18-deoxyglucose-positron emission tomography in the management of colorectal liver metastases. Cancer 104(12):2658 – 70

Yap CS, Czernin J, Fishbein MC, Cameron RB, Schiepers C, Phelps ME, Weber WA (2006) Evaluation of thoracic tumors with 18F-fluorothymidine and 18F-fluorodeoxyglucose-positron emission tomography. Chest 129(2):393 – 401

Yoshika T, Fukuda H, Fujiwara T, Iwata R, Ido T, Murakawa Y, Gamo M, Ishioka C, Kanamaru R (1999) FDG PET evaluation of residual masses and regrowth abdominal lymph node metastases form colon cancer compared with CT during chemotherapy. Clin Nucl Med 24:261 – 263

Yoshida S, Nakagomi K, Goto S, Futatsubashi M, Torizuka T (2005) 11C-choline positron emission tomography in prostate cancer: primary staging and recurrent site staging. Urol Int 74(3):214 – 20

Yutani K, Tatsumi M, Shiba E, Kusuoka H, Nishimura T (1999) Comparison of dual-head coincidence gamma camera FDG imaging with FDG PET in detection of breast cancer and axillary lymph node metastasis. J Nucl Med 40:1003 – 1008

Zimny M, Bares R, Fass J, Adam G, Cremerius U, Dohmen B, Klever P, Sabri O, Schumpelick V, Buell U (1997) Fluorine-18 fluorodeoxyglucose positron emission tomography in the differential diagnosis of pancreatic carcinoma: a report of 106 cases. Eur J Nucl Med 24:678 – 682

Zinzani PL, Martelli M, Magagnoli M, Pescarmona E, Scaramucci L, Palombi F, Bendandi M, Martelli MP, Ascani S, Orcioni GF, Pileri SA, Mandelli F, Tura S (1999) Treatment and clinical management of primary mediastinal large B-cell lymphoma with sclerosis: MACOP-B regimen and mediastinal radiotherapy monitored by 67 Ga scan in 50 patients. Blood 94:3289

19 Miscellaneous

L. Pávics

19.1 Lacrimal Dacryoscintigraphy

Several methods are available to examine the function and morphology of the lacrimal drainage system under physiological conditions. Radionuclide scintigraphy is a sensitive method which is not cumbersome for the patient. Dacryoscintigraphy was first introduced by Rossomondo et al. in 1972. Since then the method has been modified by several groups and its significance supported by numerous studies. Indications of dacryoscintigraphy are obstructive disorders of the lacrimal drainage system. The method is helpful in the diagnosis of tear flow disturbances and in the follow-up for the detection of therapy response (von Denffer et al. 1984; Brockmann et al. 2005).

The lacrimal drainage system begins with the puncta. One punctum is present at the medial end of both the superior and inferior eye lids. The puncta are situated on slight elevations called the lacrimal papillae. Malposition or stenosis of the puncta may cause epiphora. Through the puncta the lacrima flows into the superior and inferior vertical canaliculus, which is about 2 mm long and joins in the 8-mm-long horizontal canaliculus at a right angle called the ampulla. These usually join and form the common canaliculus, which immediately enters the (naso)lacrimal sac through the valve of Rosenmüller (a flap of mucosa to prevent reflux). The (naso)lacrimal sac is about 10 mm long and funnels into the 12-mm-long nasolacrimal duct. It opens into the inferior nasal meatus. The valve of Hasner closes the opening. Within the nasolacrimal duct other valves are also present. The number of these valves differs between individuals.

Capillarity ensures that 70 % of the tears enter the inferior canaliculus and 30 % through the superior canaliculus. On blinking, the attachment of the preseptal orbicular muscle helps create positive and negative pressure in the lacrimal sac, which sucks the tears into it (the tear pump). Gravity then helps to keep the sac empty.

Obstruction or stenosis of the lacrimal drainage system is related predominantly to inflammation or trauma.

^{99m}Tc-pertechnetate in physiologic saline solution has been established as the most useful tracer for dacryoscintigraphy. The dose should be 2 – 4 MBq in about 10 µl volume. The investigation can be performed with the patient in the lying or sitting position, and the patient's head should be held firmly during the investigation so that the use of a headholder or slit-lamp headrest is recommended. The drop of radiopharmaceutical should be carefully applied to the conjunctiva preferably simultaneously on both sides in front of the gamma camera. The overflowing tracer is wiped away. The camera is equipped with a low energy high-resolution (LEHR) collimator, zoom × 1.6, matrix e.g. 64 × 64 or even higher. The dynamic data acquisition is started immediately with a 10-s/image frequency up to 2 min, followed by static images after 5, 10, 15 and 20 min. If available the use of a pinhole collimator (aperture 1 – 2 mm) is of advantage for static imaging. After finishing the acquisition the eye is flashed with physiologic saline to reduce the absorbed dose in the eye. The dynamic study is evaluated by the ROI technique. The generation of time activity curves from the different regions (conjunctival sac, nasolacrimal sac, nasolacrimal duct and nose) is recommended.

The normal dynamics of tear flow vary over a wide range (comparison to the contralateral symptom free side is helpful). As a rule, the tracer flows through the canaliculi in a few seconds (~10 s), and the tracer should appear within 10 min in the cavity of the nose.

Several investigations have shown that dacryoscintigraphy is a highly sensitive method. A normal finding excludes with a high probability disturbance of the tear flow. With abnormal results further morphological investigations are needed for the exact definition of the abnormality. In the follow-up because of its high sensitivity and lower radiation exposure, radionuclide dacryoscintigraphy is recommended.

The advantage of the method is its high sensitivity; the limitation of the technique is related to its spatial resolution.

The radiation exposure of the lens in normal lacrimal drainage is 0.14 – 0.21 mGy, and under pathological conditions it is about 4 times higher, but these values are well below the absorbed dose of a skull X-ray (30 mGy) (Brizel et al. 1975; Robertson et al. 1979).

19.2 Radionuclide Hysterosalpingography

Radionuclide hysterosalpingography, or hysterosalpingo-radionuclide scintigraphy, was designed to evaluate the migration of a particulate radiopharmaceutical from the vagina to the peritoneal cavity and ovaries as well as to image and functionally outline the pathways between these two extremities of the female reproductive system.

The female reproductive system comprises the ovaries, fallopian tubes, uterus, vagina accessory glands, and external genital organs. The two fallopian tubes extend outwards from the uterus to embrace the ovaries. The end of the tube near the ovary expands to form a funnel-shaped infundibulum, which is surrounded by fingerlike extensions called fimbriae. The oocyte enters the peritoneal cavity before it enters the fallopian tube. At the time of ovulation the fimbriae increase their activity and create currents in the peritoneal fluid in the direction of the tube. Inside the fallopian tube the oocyte is moved along by the rhythmic beating of cilia and by peristaltic action of the muscle of the tube. Successful fertilization requires coordinated migration of sperm from the vagina (deposited near the external os of the cervix) and an ovum from the ovarium. The fertilization usually occurs in the ampullary portion (next to the infundibulum) of the fallopian tube.

Obstruction of the fallopian tubes is a common cause of infertility.

Radionuclide hysterosalpingography is used as a method to investigate fallopian tube patency under physiological conditions, and was first described by Iturralde et al. in 1981. The original method was modified and the activity used has been decreased to 18 MBq of ^{99m}Tc-human serum albumin macroaggregate (HSA MAA), which should be placed in less than 1 ml in the posterior cervical fornix. Data acquisition starts promptly using a gamma camera equipped with a predominantly parallel collimator and continues for 2 h or until bilateral spillage in the peritoneum. When necessary, oblique images can help to separate the anatomic structures (Becker et al. 1988). Other groups recommend the use of ^{99m}Tc-hexamethylene-propyleneamine-oxime (HMPAO) labeled spermatozoa as a radiopharmaceutical (an intrauterine device, IUD, inhibits the migration of sperm only), but in other conditions ^{99m}Tc-pertechnetate has also been used successfully.

Under physiological conditions patency is indicated by prompt flow of activity through the uterus and fallopian tubes with hot spots at the sites of the ovaries or spillage into the peritoneum. On the dominant side radiopharmaceutical transport is accelerated.

In the case of obstructed transport, the failure of visualization from the cornu of the uterine cavity to the fallopian tube ("cornu cut off sign") is diagnostic. Misinterpretation of the images is possible by the overlap of vaginal or uterine activity with intraperitoneal accumulation or by confusing the activity remaining in the vagina with the uterus.

Radionuclide hysterosalpingography is helpful in patients with unexplained infertility also when X-ray contrast salpingography is normal, in the follow-up after reanastomosis surgery or when there is suspected tubal ligation, and beneficial in aiding selection of the method of artificial insemination.

The advantage of the method is that it makes possible to investigate tubal patency under physiological conditions in quite a sensitive way. But we should take into account that spermatic transport is menstrual cycle dependent; therefore the timing of the investigation plays a role in the correct interpretation. Radionuclide hysterosalpingography purports the spermatic transport function, but does not demonstrate the capability of the oviduct to transport ova or embryos in the reverse direction.

The radiation exposure of the ovaria during radionuclide hysterosalpingography is 0.6 – 1.5 mGy/MBq (Yang et al. 1992).

19.3 Scrotal Scintigraphy

Scrotal scintigraphy was introduced for the differentiation from other conditions of acute torsion of the testicle – which needs urgent surgical intervention – and inflammation or appendicular torsion, for which treatments are conservative. The method was first described by Nadel et al. in 1973.

The scrotum comprises a thin layer of dartos muscle continuous with the superficial fascia of the groin and peritoneum covered by skin. The medial extension of the dartos muscle separates the scrotum into left and right compartments. Each hemiscrotum contains a testicle (size range 14 – 35 cm^3) covered by a dense capsule, the tunica albuginea. The testicle descends down the retroperitoneum, bringing with it the spermatic cord, and its vascular lymphatic and neural lifeline. On top of the testis is the epididymis, the distal tail of which leads to the vas deferens, ascends the spermatic cord and ends in the ejaculatory duct. The testis and epididymis are covered by a double layer of the tunica vaginalis, which is a contiguous extension of the peritoneum. The lower pole of the testis is loosely attached to the floor of the scrotum by the gubernaculum.

Four other vestigial structures are also of importance because these structures can twist themselves, mimicking testicular torsion. These are: the appendix testis (remnant of the müllerian tube), the appendix epididymis, the paradidymis, and the vas aberrans (these are mesonephric remnants). The testicular artery (the principal arterial supply of the testicle) origi-

nates from the abdominal aorta, inferior to the renal artery. Branches of the deferential artery originating from the internal iliac artery and cremasteric branches of the inferior epigastric artery also run within the spermatic cord and anastomose with the testicular artery. The scrotum is supplied by the internal superficial and deep pudendal vessels, which have no anastomoses with the testicle supplying vessels. Testicular veins drain into the plexus pampiniformis, which as an anastomosing venous complex surrounds the spermatic cord and leads to the testicular and cremasteric veins. Valves within the testicular veins prevent the retrograde reflux of the blood.

Two types of testicular torsion have been described, intravaginal torsion in children and adults and extravaginal torsion in neonates. The exact cause of intravaginal torsion is unknown. Patients generally complain of acute onset of testicular pain. Nausea and vomiting might also be present. Within 6 – 12 h perfusion should be restored otherwise irreversible damage of spermatogenetic function develops. Extravaginal torsion usually occurs during the testicular descent. The scrotum is generally swollen at birth, blue red discoloration is present and testicular necrosis is almost uniform.

Nowadays scrotal scintigraphy is performed with ^{99m}Tc-pertechnetate or for lowering the radiation exposure with ^{99m}Tc-DTPA. In adults the dose is 550 – 750 MBq, and the minimal dose in children is 100 MBq. The patient is positioned supine under the gamma camera or stands in front of it. The penis is taped upwards to the abdominal wall and a thin layer of lead plate is placed under the scrotum to diminish soft tissue activity. At the time of injection a dynamic study is started with an image frequency of 1 – 3 s/frame with a duration of 1 min. Two and 10 min after injection static images are obtained from the anterior view with about 0.5 – 1 million counts. Markers can help to clear the correct anatomical positions of the testicles. For better visualization of the structures, zoomed images are helpful (Bockisch et al. 1989).

In normal cases the flow in the testicular artery is poorly visualized and significant intrascrotal activity is not present because of the low perfusion normally present. On static images the scrotum appears with symmetrical and homogeneous distribution of activity.

Extravaginal torsion in neonates is clinically obvious; therefore scintigraphy is not needed. In the early phase (5 – 7 h after symptoms onset) of intravaginal testicular torsion the perfusion is decreased but it is not always discernible on the dynamic images of the investigation because of the low baseline flow. On static blood pool images a unilateral decrease of activity is observed on the affected side. In the case of spontaneous detorsion a normal distribution or diffuse hyperemia of the involved side may be present. Later (until 24 h after onset) perfusion is absent and due to the increasing inflammation a hyperemic rim with progressively increasing activity surrounds the photopenic testicle ("bull's-eye," "halo" or "rim" sign). As time elapses after the symptom onset, the rim becomes pronounced but it is difficult to completely exclude testicular viability according to the result of the scintigraphy. In epididymo-orchitis, static images demonstrate diffusely increased activity and increased blood flow. The radionuclide appearance is normal or mild hyperemia with focal or diffuse photopenic defects is visible in torsion of the testicular appendices. Other conditions such as abscess, hydrocele, hematoma, or hernia can simulate acute or missed torsion on scintigraphy; therefore a comprehensive examination of the patient and clinical data is necessary for the correct image interpretation.

The sensitivity of the examination is high (96 %). The positive predictive value of cold lesion is about 63 %, but most of the "false positive" cases require surgery as well. The procedure is also highly acceptable in the evaluation of the effects of surgical interventions during the follow-up (Bockisch et al. 1989; Lutzker and Zuckier 1990).

Scrotal scintigraphy frequently contributes to patient management and minimizes unnecessary interventions.

References

Becker W, Steck T, Albert P, Borner W (1988) Hysterosalpingoscintigraphy: a simple and accurate method of evaluating fallopian tube patency. Nuklearmedizin 27(6):252 – 7

Bockisch A, van Ahlen H, Makarewitsch J, Ruhlmann J, Hotze A, Biersack HJ (1989) The significance of testicular scintigraphy for the differential diagnosis of the acute scrotum. Nuklearmedizin 28(3):84 – 7

Brizel HE, Sheils WC, Brown M (1975) The effects of radiotherapy on the nasolacrimal system as evaluated by dacryoscintigraphy. Radiology 116(2):373 – 81

Brockmann H, Wilhelm K, Joe A, Palmedo H, Biersack HJ (2005) Nasolacrimal drainage obstruction after radioiodine therapy: case report and a review of the literature. Clin Nucl Med 30(8):543 – 5

Iturralde M, Venter PF (1981) Hysterosalpingo-radionuclide scintigraphy (HERS). Semin Nucl Med 11(4):301 – 14

Lutzker LG, Zuckier LS (1990) Testicular scanning and other applications of radionuclide imaging of the genital tract. Semin Nucl Med 20(2):159 – 88

Nadel NS, Gitter MH, Hahn LC, Vernon AR (1973) Preoperative diagnosis of testicular torsion. Urology 1(5):478 – 9

Robertson JS, Brown ML, Colvard DM (1979) Radiation absorbed dose to the lens in dacryoscintigraphy with $^{99m}TcO_4^-$. Radiology 133(3):747 – 50

Rossomondo RM, Carlton WH, Trueblood JH, Thomas RP (1972) A new method of evaluating lacrimal drainage. Arch Ophthalmol 88(5):523 – 5

von Denffer H, Dressler J, Pabst HW (1984) Lacrimal dacryoscintigraphy. Semin Nucl Med 14(1):8 – 15

Yang KT, Chiang JH, Chen BS, Liang CH, Lee SF, Liao SC (1992) Radionuclide hysterosalpingography with technetium-99m-pertechnetate: application and radiation dose to the ovaries. J Nucl Med 33(2):282 – 6

Practical Considerations in the Radionuclide Imaging of Children

20

D.S. Levine, H.R. Nadel

20.1 Introduction

Although many types of diagnostic nuclear medicine studies are common to both adult and paediatric practice, certain studies are performed much more commonly for children. These include examinations of the urinary, hepatobiliary, gastrointestinal, cardiovascular and endocrine systems, together with those utilized in tumour imaging. The radiotracer biodistributions, common clinical indications, recommended imaging protocols and typical effective radiation doses are described for this range of procedures.

Minimum and maximum dose activities are quoted in the text; the paediatric dose is administered according to body weight as a proportion of the maximum adult dose. In situations where the calculated paediatric dose falls below the minimum dose, the latter is administered. The effective radiation doses listed are for a 20-kg 5-year-old child except where indicated.

20.2 Central Nervous System

20.2.1 Cerebral Perfusion Scan

Tracer: ^{99m}Tc-Hexamethylpropyleneamine oxime (HMPAO): 370–740 MBq IV
Effective dose: 6 mSv (Stabin and Gelfand 1998)
Critical organ: Lacrimal glands (Kowalsky and Falen 2004)

The two most common indications for this study are localization of an epileptogenic focus and the assessment of brain death; there are no contraindications. 3.5–7% of the injected dose of this lipophilic tracer localizes in neurones in proportion to regional cerebral blood flow within 2 min of injection, becoming converted to a hydrophilic derivative and trapped intracellularly. The majority of this trapped tracer remains in the brain for 8 h with no redistribution (Kowalsky and Falen 2004). Extracerebral uptake may be seen in lacrimal glands, thycoid, myocardium, lungs, liver, spleen, kidneys, urinary bladder, intestinal tract, subcutaneous fat and skeletal muscle. Tracer is eliminated via the gastrointestinal tract and urine. For epileptogenic focus localization, both interictal and ictal studies are required for comparison. Laser guides may be useful in positioning the patient's head. Video electroencephalographic (EEG) monitoring confirms the patient's ictal or interictal status prior to tracer injection, which should occur, for interictal studies, with the patient relaxed and at rest in quiet, dimly lit surroundings. Imaging is performed at 90–120 min post-injection. SPECT is essential and the use of an ultra-high resolution collimator is preferred. Epileptogenic foci classically show reduced perfusion interictally and increased perfusion ictally (Fig. 20.1a). For brain death assessment, imaging is performed 20 min following injection and planar images are obtained without the need for SPECT. In order to be consistent with brain death, dynamic flow images must demonstrate absence of flow in anterior, middle and posterior cerebral arteries with absence of cerebral tracer activity on the delayed planar images (Fig. 20.1b). Scalp flow from external carotid artery may be present and must not be confused with cerebral perfusion.

20.2.2 Ventriculoperitoneal Shunt Study

This study is performed to assess ventriculoperitoneal shunt patency; there are no contraindications.

Tracer: ^{99m}Tc-Diethylenetriaminepentaacetic acid (DTPA): 37 MBq introduced via shunt reservoir
Effective dose: <0.5 mSv (Stabin and Gelfand 1998)

A fresh batch of tracer is obtained and is checked for apyrogenicity and radiochemical purity (required to be $>90\%$). With aseptic technique, tracer is carefully injected into the shunt reservoir with sterile technique; a small volume (typically 2–3 ml) is used to minimize fluid displacement due to the injection itself. Dynam-

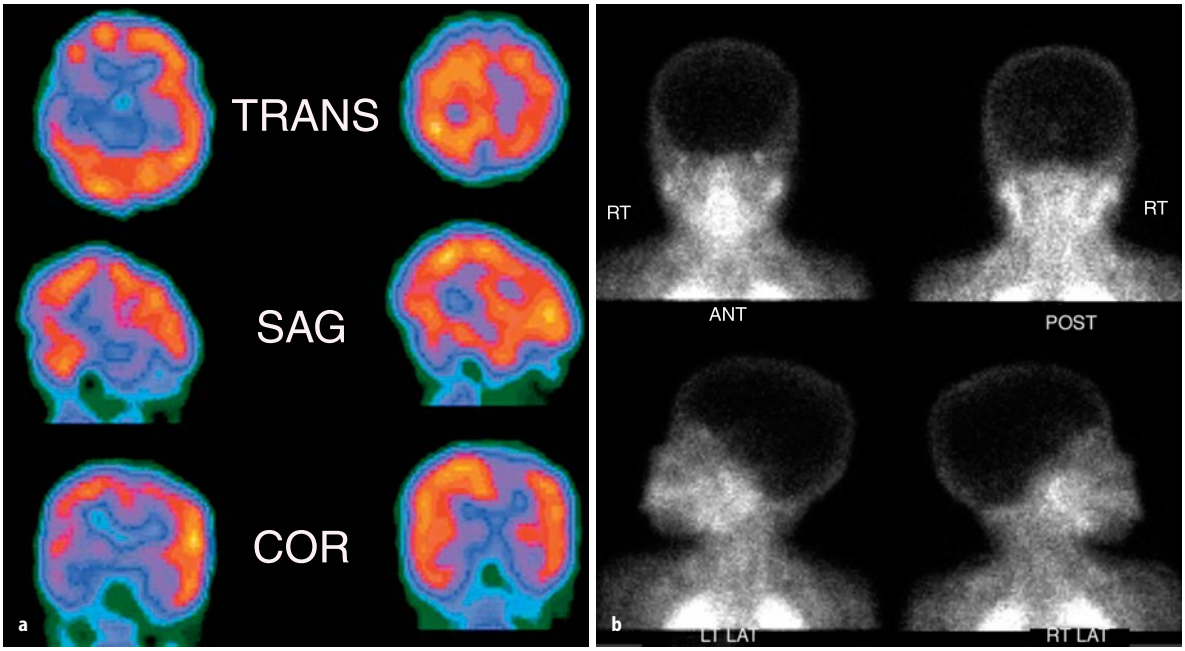

Fig. 20.1. a Epileptogenic focus – selected SPECT images: interictal images *on the left*; ictal images *on the right*. A focus of decreased perfusion is present within the right frontotemporal region on the interictal images which shows hyperperfusion on the ictal images. **b** Brain death – delayed planar images show absent cerebral tracer activity

ic images encompass the whole of the length of the shunt tubing. Decubitus views of the abdomen should be obtained to exclude loculation of tracer at shunt tip. Tracer should flow through the shunt and be dispersed within the peritoneal cavity rapidly and without delay.

20.3 Thyroid

20.3.1 Neonatal Thyroid Scan

This test is indicated for neonates with elevated serum thyroid stimulating hormone (TSH) detected on routine screening; there are no contraindications.

Tracer:	^{99m}Tc-Pertechnetate: 37 – 185 MBq. Typical injected activity for newborn: 37 MBq IV
Effective dose:	For newborn: 0.9 mSv (Stabin and Gelfand 1998)
Critical organ:	Colon (Kowalsky and Falen 2004)

One to 2 % of the injected dose is trapped but not organified by thyroid epithelial cells (Kowalsky and Falen 2004). Activity is seen within choroid plexus, salivary glands, thyroid gland, and gastric mucosa; the tracer undergoes urinary and intestinal excretion. Since tracer is secreted into saliva, early imaging following intravenous injection is required, typically at 20 min, to avoid confusion between salivary pooling and ectopic thyroid tissue. The lower head, neck and thorax are imaged with a parallel high resolution collimator. Anterior and oblique views are obtained if activity appears in a normal suprasternal location (Fig. 20.2a). The examination is modified if the activity appears ectopic in location: anterior images are obtained, with and without markers at the suprasternal notch (Fig. 20.2b); a lateral view with a chin marker is also obtained. Subsequently, higher quality images may be obtained with a pinhole collimator but without the use of markers – these images cannot be obtained with markers for risk of distortion. The role of markers is to permit differentiation of anatomic versus ectopic functioning thyroid tissue when present; the latter often produces a hypothyroid state due to insufficient hormone production. Tracer activity in a normally located gland associated with elevated TSH indicates dyshormonogenesis. Absent thyroid activity is very likely to reflect an absent gland, although maternal autoimmune hypothyroidism may produce a similar picture in the infant due to transplacental antibody passage.

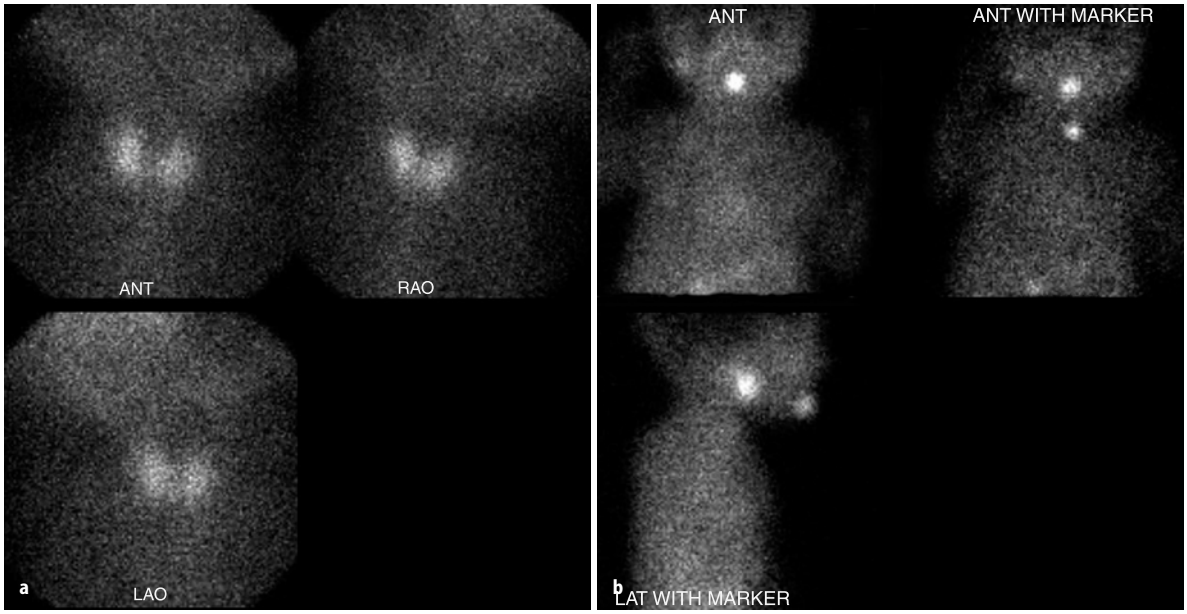

Fig. 20.2. a Normal thyroid – anterior and oblique show normal neonatal morphology and position. **b** Lingual thyroid – images with and without chin marker show midline tracer activity in the region of root of tongue

20.4 Heart

20.4.1 First Pass Study

The commonest indication for this study is the diagnosis and assessment of left to right shunts, for example, atrial and ventricular septal defects.

Tracer: ^{99m}Tc-Sodium pertechnetate: 74 – 740 MBq IV
Effective dose: 1.2 mSv (Stabin and Gelfand 1998)
Critical organ: Colon (Kowalsky and Falen 2004)

The patient is positioned supine and tracer is injected via antecubital fossa vein rapidly followed by normal saline flush. A large bore cannula and a fast-release tourniquet are used to maximize the compactness of the tracer bolus. Immediate dynamic imaging is obtained with a high sensitivity parallel-hole collimator positioned over the anterior thorax. The patient must be at rest and not crying or straining during study. A region of interest (ROI) is placed over the superior vena cava and a time-activity curve is generated. If a single tracer bolus peak of less than 3 s duration is present then the injection is considered acceptably compact and a second time-activity curve is generated from an ROI placed over the mid-section of either lung. A normal pulmonary time-activity curve generated by gamma-variate fit characteristically shows a rapid rise to a single peak, descent to a trough just above baseline followed by a second rise to a single peak, which is broader and shows a lower amplitude than the first. The first peak reflects initial passage of tracer through the lungs and the second peak represents the portion of the initial bolus returning to the lungs after passage through the systemic circulation. Similarly, dynamic images normally show sequential tracer passage through the SVC, right atrium, right ventricle, lungs, left atrium, left ventricle and aorta; the latter are visualized with minimal pulmonary activity. Persistent pulmonary tracer activity and poor visualization of the left heart indicate left to right shunting, which may be quantified by the ratio of pulmonary to systemic blood flow (Qp:Qs); a ratio of up to 1.2:1 is considered normal (Treves 1995). By convention, the largest shunt reported is 3:1.

20.5 Kidneys

20.5.1 Cortical Scintigraphy

The commonest indications for this study are the diagnosis of acute pyelonephritis, the assessment of renal scarring, relative renal function or of a solitary, ectopic or duplicated kidney. There are no contraindications.

Tracer: ^{99m}Tc-Dimercaptosuccinic acid (DMSA): 11 – 111 MBq
Effective dose: 0.8 mSv (Stabin and Gelfand 1998)
Critical organ: Kidney (Kowalsky and Falen 2004)

Approximately 40 – 65 % of the injected dose of ^{99m}Tc-DMSA binds to proximal convoluted tubule cells by

2 – 3 h following intravenous injection (Kowalsky and Falen 2004). Hepatobiliary elimination only becomes significant in renal failure. Static imaging is performed at 3 h post-injection, and for patients under 6 months of age, posterior and posterior oblique pinhole planar images of the kidneys are obtained utilizing a high resolution collimator. For children over this age, posterior and posterior oblique planar images of the kidneys are obtained and are supplemented by SPECT. ROIs drawn around each kidney on the posterior image are used to calculate the divided renal function. DMSA is not seen within the renal medulla or collecting system, although in neonates and young infants, some tracer excretion may be seen within the urinary bladder. A differential function of the left kidney in the range 45 – 57 % is considered normal (Pusuwan et al. 1999). Acute pyelonephritic defects are usually geographic, single or multiple focal photopenic regions without associated volume loss (Fig. 20.3a); alternatively, a generalized reduction in tracer activity may also be seen (Majd and Rushton 1992; De Sadeleer et al. 2000). Such defects typically take 6 – 12 months to resolve (Fig. 20.3b). Persisting wedge-shaped, ovoid or flattened photopenic defects with associated volume loss imply cortical scarring. Co-existing acute pyelonephritis and scarring may only be reliably distinguished with follow-up studies. In the context of acute infection, a negative DMSA scan excludes kidneys that are at risk of scarring.

20.5.2 Dynamic Renography

As a means of assessing renal clearance and excretion, dynamic radionuclide renography is commonly performed in the paediatric setting and, in general, the techniques are similar to those utilized in adult practice. The investigation remains mired in controversy, however, with regards to the exact technique used and the means of interpretation; a detailed discussion is beyond the scope of this chapter. Nonetheless, some general observations can be made with regards to paediatric applications. Common indications in children include the evaluation of renal tract dilatation, assessment of the efficacy of surgical intervention in cases of renal tract obstruction, assessment of a complex duplex kidney, and evaluation of the kidneys in cases of renal trauma and renal transplantation. There are no contraindications.

Tracers:	^{99m}Tc-Mercaptoacetyltriglycine (MAG3): 18 – 185 MBq or ^{99m}Tc-diethylenetriaminepentaacetic acid (DTPA): 37 – 370 MBq
Effective dose:	0.6 mSv (MAG3); 0.4 mSv (DTPA) (Stabin and Gelfand 1998)
Critical organ:	Urinary bladder (Kowalsky and Falen 2004)

Renal clearance is tracer-dependent: ^{99m}Tc-DTPA is filtered at the glomerulus whereas ^{99m}Tc-MAG3 undergoes tubular secretion. The latter achieves greater renal clearance, resulting in a more favourable background to kidney activity ratio, and for this reason is the preferred tracer, especially in infants of less than 1 year of age, in whom glomerular filtration has not yet reached adult rates (Treves 1995; Gordon et al. 2000).

The child must be well hydrated before the examination is started. Babies and infants may be given an extra feed; older children should be encouraged to drink at least 300 cc of fluid; an alternative means of hydration is an intravenous infusion of normal saline, continued through the examination. Having voided, the child is positioned supine on the imaging table with the collimator directly beneath and is immobilized by the means described within the bone scan section (vide infra). Since both supine positioning and the presence of a full bladder can affect renal drainage, data collection must continue at the end of the study until after the child has voided so that renal drainage may be assessed when the bladder has emptied. Similarly, a change of posture following diuretic administration is essential

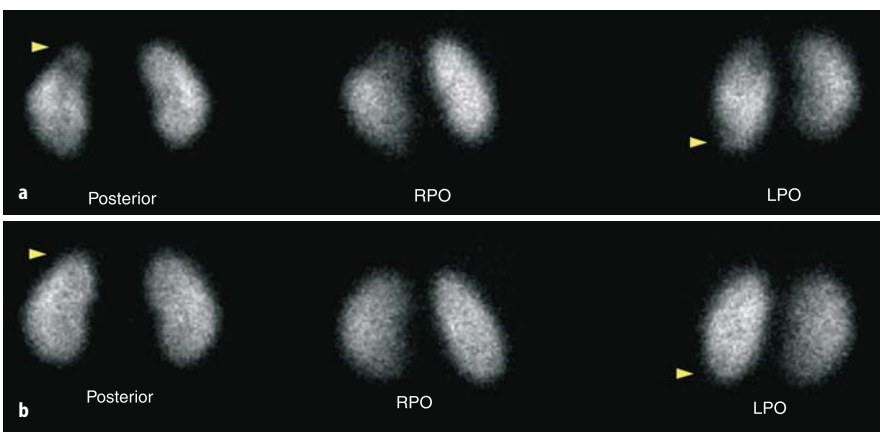

Fig. 20.3. Acute pyelonephritis – geographic photopenic defects in the upper and lower poles of the left kidney (indicated by *yellow arrows* in **a**), which show complete interval resolution on follow-up imaging 6 months later (**b**)

to preclude apparent impairment of drainage due simply to supine positioning.

With regards to the commonest indication for renography, the assessment of renal tract dilatation, irrespective of the technique employed for performing the examination and interpreting the results, the studies can usually be divided into those which are normal, those which show marked impairment of drainage and those which are intermediate. The first group requires no intervention and most authorities would agree that the second group requires either further immediate evaluation or therapy. It is the children falling into the intermediate group that have posed difficulty with regards to management. Current practice at our institution is for these children to undergo serial follow-up with pain or a significant deterioration in the perfusion and/or differential function of the affected kidney prompting intervention.

20.6 Urinary Bladder

20.6.1 Direct Radionuclide Cystography

This study may be performed for the assessment of vesicoureteric reflux (VUR), either as an initial or as a follow-up investigation in females. The study may also be performed for males but only in follow-up circumstances, where the initial diagnosis of VUR has been made with fluoroscopic voiding cystourethrography, an examination which permits the exclusion of a posterior urethral valve – an important consideration in males. The presence of a low-lying or ectopic kidney poses a relative contraindication for direct radionuclide cystography due to the inherent unreliability of detecting VUR in these cases, secondary to renal proximity to the bladder (Treves 1995).

Tracer:	^{99m}Tc-Diethylenetriaminepentaacetic acid (DTPA): 10 – 40 MBq instilled via urinary catheter
Effective dose:	< 0.05 mSv (Stabin and Gelfand 1998)
Critical organ:	Urinary bladder (Kowalsky and Falen 2004)

There is no systemic tracer activity since absorption of ^{99m}Tc-DTPA from the urinary bladder is negligible. Antibiotic prophylaxis should be considered in all children undergoing urinary bladder catheterization – local practices vary in this regard. Following catheterization under aseptic technique, the radiotracer dose is injected into the catheter tubing followed by an infusion of sterile normal saline under hydrostatic pressure. The infusion is terminated when either the calculated age-dependent maximum volume is reached or the child appears uncomfortable – whichever occurs first. Following voiding, the bladder may be re-filled and the procedure repeated up to three times to increase the sensitivity of VUR detection. Dynamic imaging with a general purpose collimator commences with bladder filling and terminates with the final micturition. During data processing, ROIs may be drawn over the urinary bladder and kidneys to permit the generation of time-activity curves useful in study interpretation. An increase in tracer activity within the renal pelvis occurring during bladder filling and/or emptying, and preferably shown on dynamic images as well as on time-activity curves derived from renal pelvic ROIs, implies VUR. VUR should be described by the anatomic level to which it reaches, for example, ureter, renal pelvis or parenchyma. An alternative technique is indirect radionuclide cystography (IRC) – a potential adjunct to dynamic diuretic renography, having the advantages over DRC of permitting a more physiologic assessment of VUR without the need for bladder catheterization. More easily performed in children who are toilet-trained, this technique has reduced sensitivity since only VUR occurring during voiding can be identified.

20.7 Gut and Liver

20.7.1 Gastric Emptying Study

The evaluation of children with chronic aspiration or gastro-oesophageal reflux constitutes a common indication for this examination, which is also performed in children with suspected or established motility disturbances, for example secondary to cystic fibrosis. There are no contraindications.

Tracer:	^{99m}Tc-Sulphur colloid: 20 MBq orally
Effective dose:	1.5 mSv (Stabin and Gelfand 1998)
Critical organ:	Proximal colon (Kowalsky and Falen 2004)

There is negligible systemic tracer absorption – only gastrointestinal tract activity should be seen. Age-dependent fasting is instituted prior to the examination. Radiotracer is added to a small aliquot of infant formula, which is then fed to the child, followed by a volume of unlabelled formula equal to that which the child normally takes. In older children who have already had dietary exposure to eggs, the tracer may be added to one egg prior to cooking, which the child will then eat as part of an egg meal. Radiolabelled feed or meal must be ingested as soon as possible after preparation, generally within 10 min; the time for ingestion should be recorded as well as whether or not the whole of the prepared feed or meal was ingested. Infants whose radiolabelled feed is to be given via a feeding tube must have radiographic confirmation that the tube tip lies in the

stomach (and not more distally) prior to feed administration. For children with a gastrostomy tube, in order to prevent "dumping", a small volume (typically 20 ml) of unlabelled feed is initially introduced followed by the tracer dose in a small aliquot of feed and then an unlabelled volume of feed equal to that which the patient normally takes. Anterior and posterior planar images with a field of view to include the distal oesophagus, stomach and small bowel are obtained immediately and at 15-min intervals up to 90 min – infants are held upright between images; older children are encouraged to walk. The patient is imaged in a supine position, carefully checked to ensure consistency. An ROI drawn around the stomach on both the anterior and posterior views allows a time-activity curve to be generated from the geometric mean of the counts. A follow-up study must always be performed in the same way as prior studies to permit a valid comparison of results. Patients may be re-tested on prokinetic medications, such as domperidone, in order to assess treatment efficacy. Our practice is to consider normal those studies where 50 % or more of the gastric contents empties by 90 min post-ingestion, with a gastric emptying half time of up to 90 min. Conversely, stomach activity residual of greater than 50 % at 90 min or an emptying half time greater than 90 min is considered evidence of delayed emptying.

20.7.2 Gastro-oesophageal Reflux Study

Common indications include regurgitation and failure to thrive, suspected oesophagitis and chronic respiratory symptoms; there are no contraindications.

Tracer:	^{99m}Tc-Sulphur colloid: 20 MBq orally
Effective dose:	1.5 mSv (Stabin and Gelfand 1998)
Critical organ:	Proximal colon (Kowalsky and Falen 2004)

There is negligible systemic tracer absorption with only gastrointestinal tract activity being seen. The tracer is administered in the same way as for a gastric emptying study (vide infra). Note that tracer administration in water or juice is avoided, to reduce the risk of tracer "sticking" within the oesophagus. The patient is positioned supine on the gamma camera, so that both the stomach and thorax are within the field of view and the patient is then fed with imaging starting immediately. Dynamic imaging is obtained for 60 min and is followed by static anterior and posterior images of the thorax. Sternal markers allow localization of abnormal activity. An ROI placed over the oesophagus allows the generation of a time-activity curve with reflux being demonstrated as one or more sharp spikes; care must be taken to ensure that patient movement does not generate spurious spikes. Reflux may be categorized by the number of episodes occurring during 1 h of imaging, for example, mild (< 10 episodes), moderate (10 – 20 episodes) or severe (> 20 episodes). Aspiration appears as tracheal or lung activity on the 1 and 4 h static thorax views. Care must be taken since contamination from vomit or regurgitation can mimic these appearances.

The clinical question of whether or not children with neurologic disorders aspirate can be answered with the salivagram. With the child placed supine and the camera positioned to include both the oropharynx and chest, a small volume (typically 0.1 ml) of ^{99m}Tc-sulphur colloid is placed on the tongue and allowed to mix with oral secretions. If too large a volume of tracer is used, the child is likely to swallow immediately, emptying the mouth of tracer. Immediate dynamic imaging is acquired for 30 min after which anterior and posterior static images are supplemented by an anterior image with a marker; additional lateral views may be acquired as necessary. When present, tracer activity within the tracheobronchial tree is usually clearly identifiable and confirms aspiration.

20.7.3 Ectopic Gastric Mucosa Scan (Meckel's Scan)

This study is performed to localize ectopic gastric mucosa within a Meckel diverticulum as a source of unexplained painless bleeding. Patients who have undergone either a radiolabelled red blood cell scan within the preceding 24 h or a recent gastrointestinal contrast study with barium still within the bowel are contraindicated from undergoing a Meckel's scan.

Tracer:	^{99m}Tc-Sodium pertechnetate: 37 – 370 MBq IV
Effective dose:	1.5 mSv (Stabin and Gelfand 1998)
Critical organ:	Proximal colon (Kowalsky and Falen 2004)

Twenty-five percent of the injected tracer accumulates in functioning gastric mucosa. Activity is also seen within the choroid plexus, salivary and thyroid glands; the tracer undergoes urinary and intestinal excretion (Kowalsky and Falen 2004). The patient is positioned supine with an empty bladder. Pretreatment with a histamine H_2 blocker is recommended to reduce gastric mucosal secretions, for example, ranitidine 1 mg/kg IV (up to a maximum of 50 mg) administered over 20 min. Tracer is subsequently injected simultaneously to the start of imaging. One full minute of anterior dynamic imaging, including the whole abdomen from top of diaphragm to inferior extent of urinary bladder, is followed by further continuous anterior imaging for at least 15 min. In children less than 2 years of age, static images of the thorax are also obtained to exclude ectopic gastric mucosa in a bronchopulmonary foregut malformation.

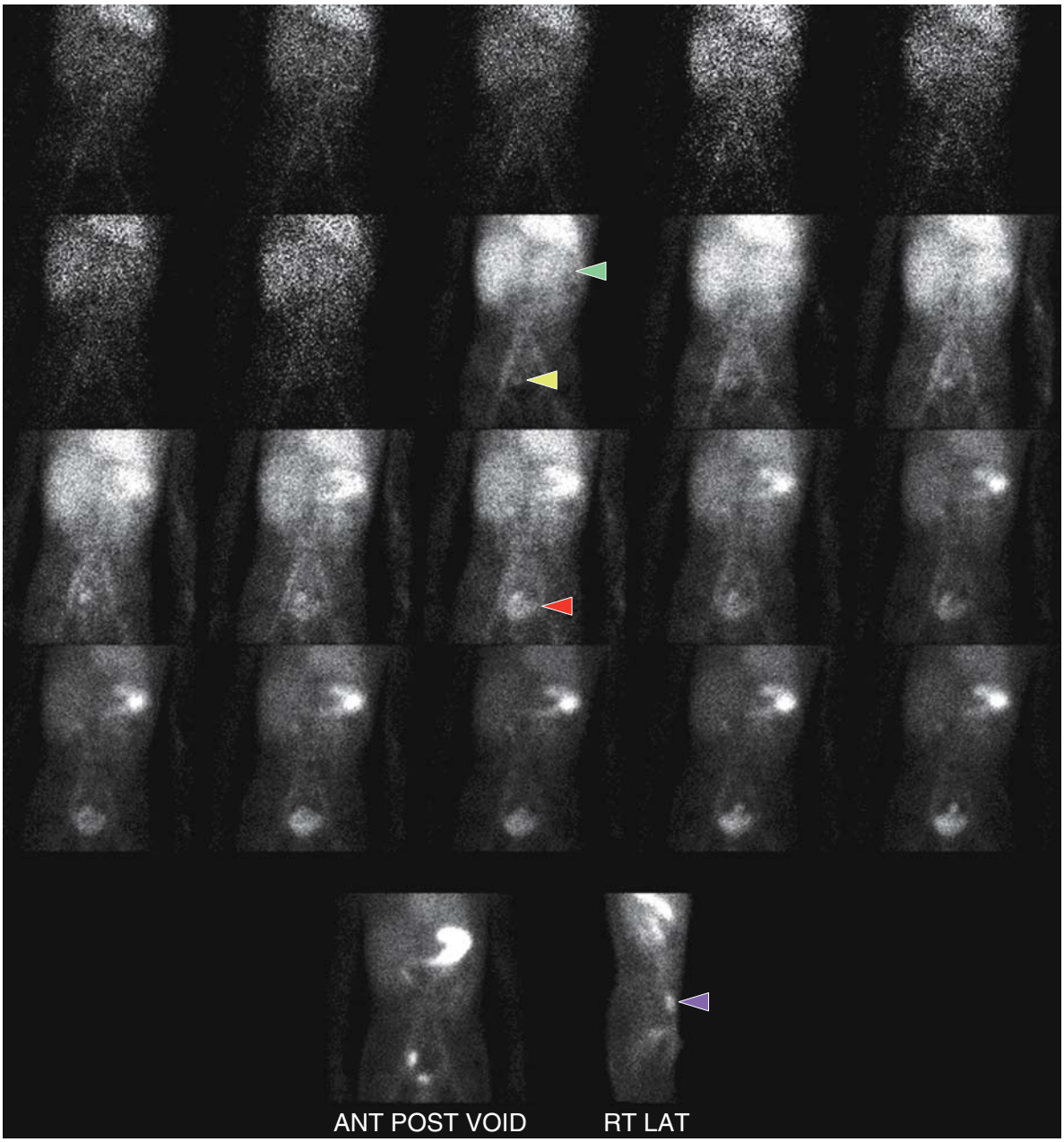

Fig. 20.4. Meckel diverticulum – anterior dynamic images show a focus of tracer activity (*yellow arrow*) appearing synchronously with the stomach activity (*green arrow*), and lying adjacent to the urinary bladder (*red arrow*). A lateral post-void image shows this focus of tracer activity (*mauve arrow*) to lie superoanterior to the urinary bladder

Ectopic gastric mucosa activity should appear at the same time as normal gastric mucosa and may occur anywhere in the abdomen, although the right lower quadrant is the commonest location (Fig. 20.4). Ureteric or bladder activity may be confused for ectopic gastric mucosa but the latter should show activity first. With time, normal tracer activity will transit from the stomach lumen into the small bowel lumen but can be distinguished from ectopic gastric mucosa by its delayed appearance and lack of focality, tending to be more of an ill-defined mildly increased region of tracer activity. Lateral, oblique, upright and post-void views, as well as SPECT, may be of use in localizing tracer activity. Giving the patient a drink of water will often flush ureteric tracer activity into the bladder when there is doubt regarding the nature of a right lower quadrant focus of activity. False negative results are most commonly due to poor technique but, in the presence of active bleeding, may be due to necrosis of an ulcerated focus of ectopic gastric mucosa. False positive

results may reflect any inflammatory process, for example appendicitis, or a lesion containing ectopic gastric mucosa, such as a duplication cyst.

20.7.4 Hepatobiliary Scintigraphy

The exclusion of biliary atresia, evaluation of a suspected choledochal cyst or post-surgical biliary leak are the commonest indications for this examination; there are no contraindications.

Tracer: ^{99m}Tc-Dimethylphenylcarbamoylmethyliminodiacetic acid (HIDA) or similar iminodiacetic acid derivative: 11 – 111 MBq IV
Effective dose: For newborn: 1 – 2 mSv (Stabin and Gelfand 1998)
Critical organ: Colon (Kowalsky and Falen 2004)

The tracer undergoes the same hepatocyte uptake, transport and excretion pathway as bilirubin (Kowalsky and Falen 2004). In the evaluation of neonatal jaundice, activation of hepatic excretory enzymes with phenobarbital pretreatment (5 mg/kg/day for the 5 days prior to imaging) is necessary to permit attempted differentiation of neonatal hepatitis from biliary atresia. Supine whole abdomen imaging is obtained with the dome of the liver at the top of the field of view following an age-appropriate period of fasting: neonates have one feed withheld and are usually fed after the 2 h image is complete. For 1 h following tracer injection, a dynamic sequence is obtained with subsequent static images obtained at regular intervals, for example at 2, 4, 6 h and so on until tracer is confidently seen within the bowel or 24 h have elapsed, whichever occurs first. Additional oblique and lateral views as well as SPECT may be helpful. If gallbladder filling is visualized, the patient is fed formula or a milk drink whilst an additional dynamic sequence is obtained.

A normal neonatal study demonstrates tracer clearance from the blood pool by 5 min; the end point of the study is visualization of bowel activity, usually within 1 h. The gallbladder and biliary tree are not typically visualized in the neonate. In a patient with biliary atresia, rapid tracer clearance from the blood pool is usually seen with lack of bowel activity by 24 h (Fig. 20.5). Delayed tracer clearance from the blood pool with delayed hepatic excretion into bowel implies neonatal

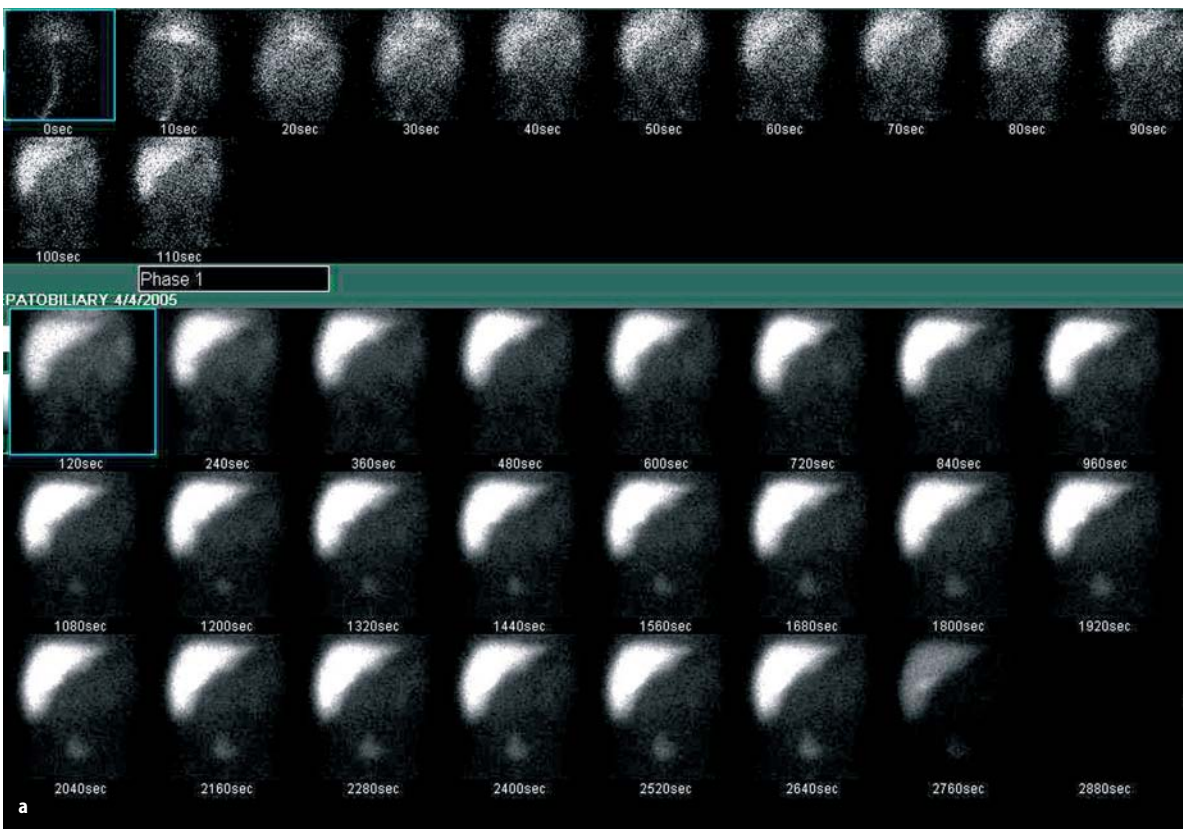

Fig. 20.5. Biliary atresia – dynamic images (**a**) show normal tracer clearance from the blood pool but failure of subsequent excretion into bowel, confirmed on the delayed planar images (**b**). Note faint renal tracer activity reflecting secondary excretion pathway

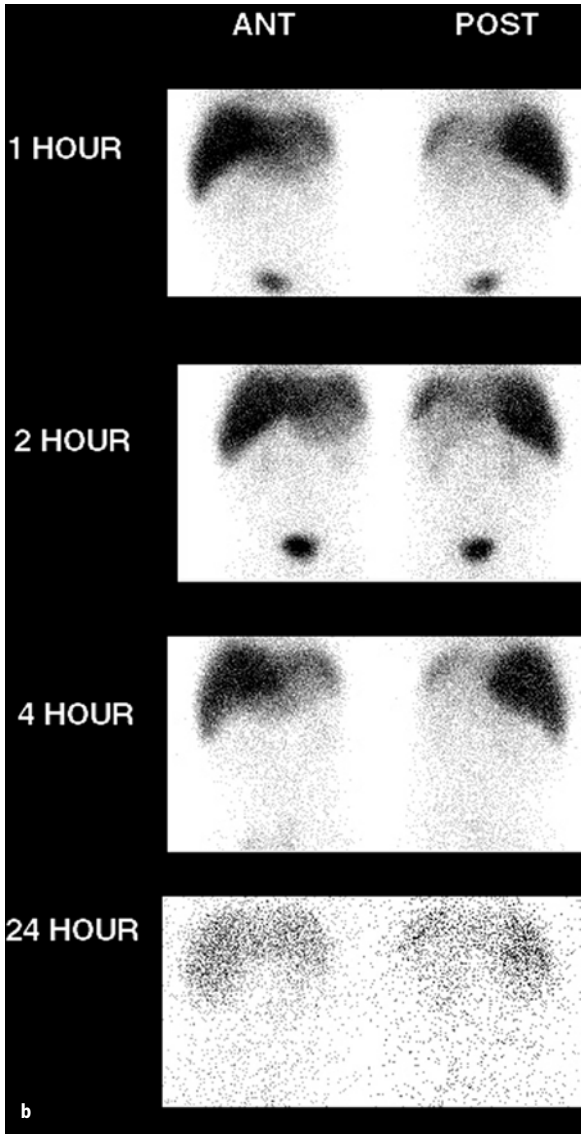

Fig. 20.5. (*Cont.*)

hepatitis. In practice, however, bowel activity may be so delayed that it is effectively not visualized and in such cases biliary atresia cannot be excluded with certainty. Therefore, the value of hepatobiliary scintigraphy lies in the exclusion of biliary atresia in cases where bowel activity is demonstrated, since in all other cases, the possibility of this diagnosis cannot be excluded.

Non-obstructing choledochal cysts usually manifest as prolonged tracer retention at the site of a pericholecystic cystic structure demonstrated by anatomic imaging. In cases of post-surgical biliary leak, progressive accumulation of either perihepatic or free abdominal tracer activity may be seen.

20.8 Tumour Imaging

20.8.1 Thallium Scan

This study is typically performed in cases of osteosarcoma, Ewing's sarcoma and rhabdomyosarcoma for determination of the extent of the primary tumour, as a baseline for future treatment response evaluation, and for evaluation of recurrence. There are no contraindications.

Tracer: ^{201}Thallous chloride: 111 – 142 MBq IV
Effective dose: 55 mSv (Stabin and Gelfand 1998)
Critical organ: Kidneys (Kowalsky and Falen 2004)

Thallium-201 localizes to choroid plexus, eyes, salivary glands, thyroid, heart, liver, stomach, large bowel, kidneys, testes and skeletal muscle (Fig. 20.6a). The tracer has a disappearance half time from the blood of less than 1 min, giving a high tumour/blood ratio shortly after injection. The mechanism of ^{201}Tl concentration in tumours is multifactorial and thought to relate to increased blood flow, capillary permeability and membrane expression of the Na-K ATPase pump. Urinary excretion is the principal route but is slow (biologic $T_{1/2}$ of 10 days), which, in combination with the long physical $T_{1/2}$ of 73 h, produces a high radiation burden (Kowalsky and Falen 2004). Approximately 5 min after injection, static views of the heart and tumour site are obtained, followed by whole body planar images with SPECT of the tumour site. Additional planar images of the heart and tumour site are obtained at 1 and 4 h. Although up to 100 % sensitivity for bone and soft tissue sarcomas has been reported, a baseline study is essential to confirm tumour ^{201}Tl avidity. Tracer uptake usually decreases significantly in post-chemotherapy pre-definitive surgery patients whose tumours have shown histological response and this effect can be quantified with lesion to background activity ratios (Fig. 20.6b) (Nadel 1993).

20.8.2 MIBG Scan

Common indications comprise the confirmation, staging and post-treatment assessment of neuroectodermally derived tumours such as neuroblastoma, phaeochromocytoma and ganglioneuroma. The study is contraindicated for children medicated with certain agents, as described below.

Tracer: ^{123}I-Metaiodobenzylguanidine (MIBG): 80 – 400 MBq IV
Effective dose: 3.7 mSv (Stabin and Gelfand 1998)
Critical organ: Urinary bladder (Kowalsky and Falen 2004)

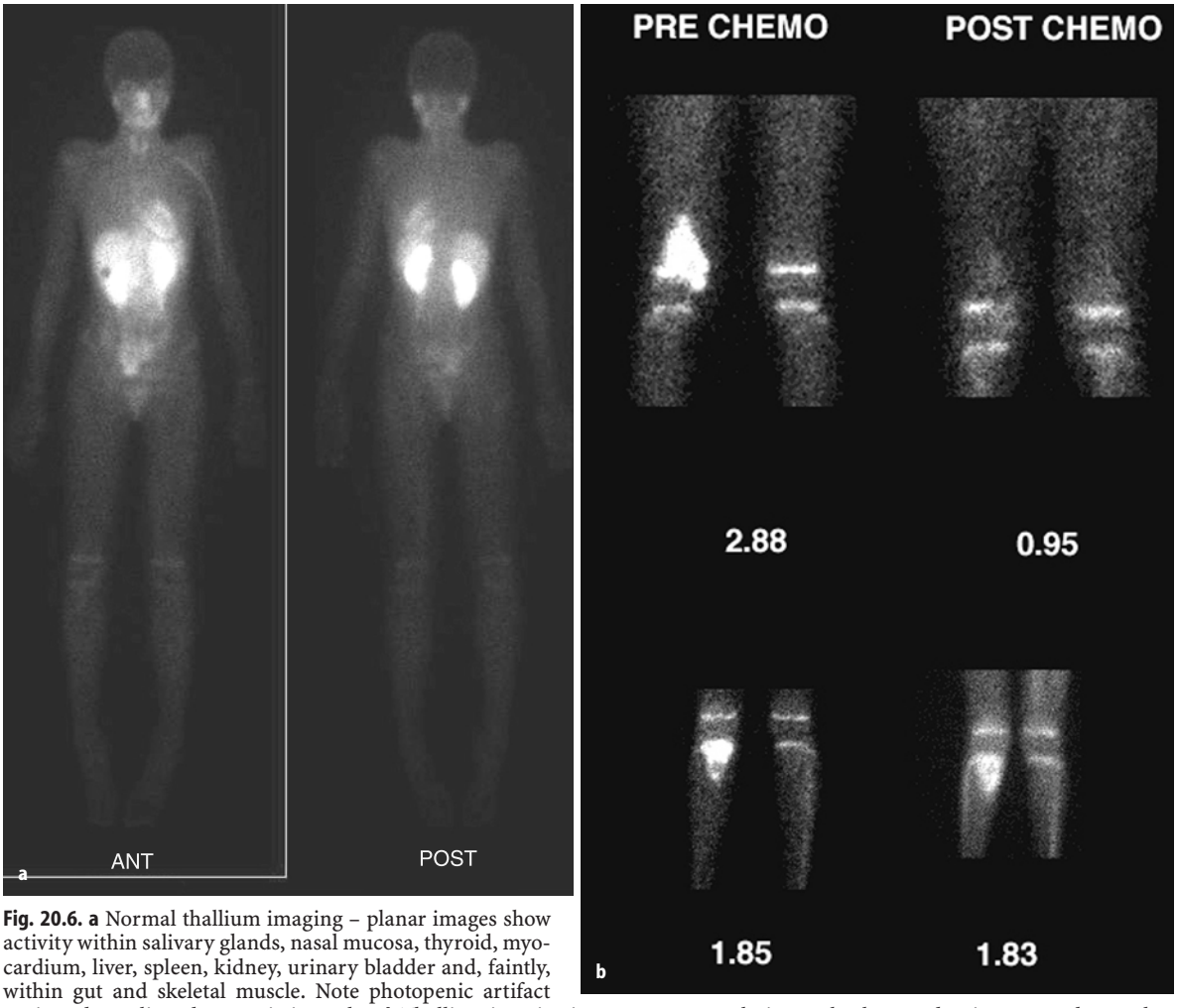

Fig. 20.6. a Normal thallium imaging – planar images show activity within salivary glands, nasal mucosa, thyroid, myocardium, liver, spleen, kidney, urinary bladder and, faintly, within gut and skeletal muscle. Note photopenic artifact projected over liver due to coin in pocket. **b** Thallium imaging in osteosarcoma – lesion-to-background ratios pre- and post-chemotherapy in good (*upper image*) and poorly responding (*lower image*) patients. Good response on thallium imaging correlates with good histological response to therapy

MIBG is an analogue of noradrenaline with a specific active uptake mechanism believed to be responsible for uptake by tissues with sympathetic innervation including liver, spleen, myocardium, salivary glands, adrenal glands, and certain neuroendocrine tumours (Fig. 20.7a). Skeletal muscles, nasal mucosa, lungs, urinary tract, colon, gallbladder and thyroid may also demonstrate accumulation of tracer of variable intensity. No skeletal uptake should be seen. Extremities show only slight muscular activity and in these cases the bone may appear as a photon deficient area (Kowalsky and Falen 2004; Olivier et al. 2002).

Prior to tracer injection, the patient's current treatment regime must be checked to exclude agents known to interfere with MIBG imaging. The most common are sympathomimetics such as salbutamol and pseudoephedrine (the latter commonly found in non-prescription cold remedies). Many cardiac drugs such as calcium channel blockers, angiotensin-converting enzyme inhibitors and adrenergic receptor blockers also interfere with MIBG biodistribution, although such drugs are rarely found in a paediatric population. Beginning on the day before tracer injection until the day after injection, children should receive a daily age-dependent dose of oral potassium iodide to reduce tracer uptake by the thyroid gland; rapid blockade by perchlorate given once immediately prior to tracer injection is an alternative (Nadel 1996). Tracer is given by slow injection over 5 min, preferably into a peripheral vein rather than a central venous access device since tracer persistence within certain of these devices may occasionally confound image interpretation. When possible, patients should be encouraged to drink copious fluids and to void frequently following tracer injection. Imaging starts at 24 h with whole body planar images ideally supplemented by spot views of skull and torso.

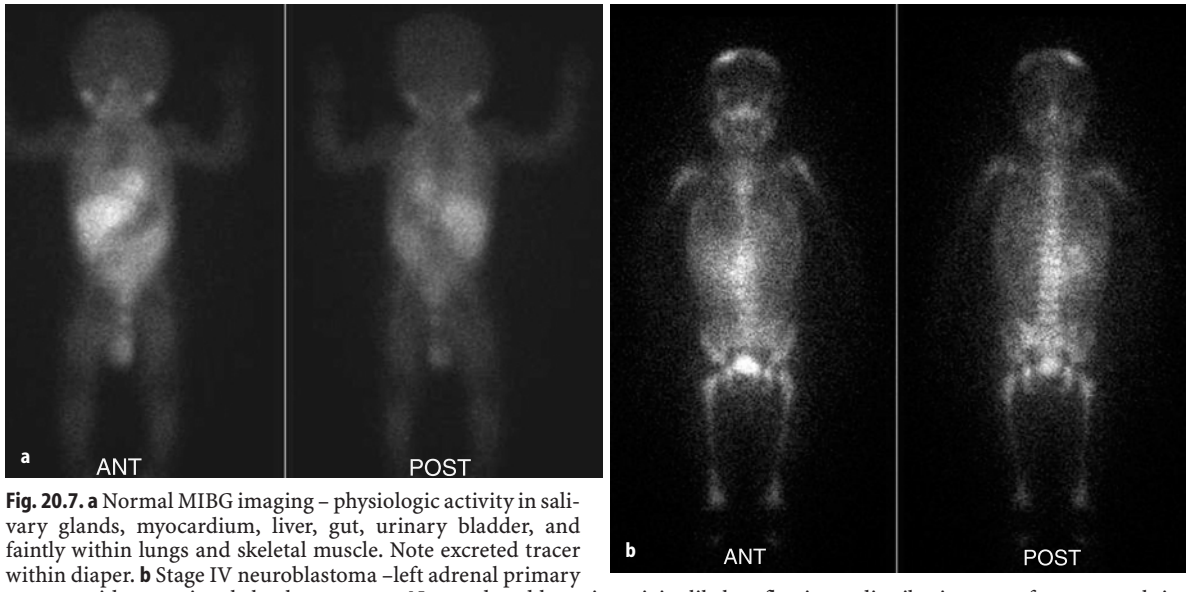

Fig. 20.7. a Normal MIBG imaging – physiologic activity in salivary glands, myocardium, liver, gut, urinary bladder, and faintly within lungs and skeletal muscle. Note excreted tracer within diaper. **b** Stage IV neuroblastoma –left adrenal primary tumour with extensive skeletal metastases. Note reduced hepatic activity likely reflecting redistribution away from normal tissues to tumour

SPECT of the torso is recommended and additional 48 h planar whole body images may also be obtained.

Primary tumour and metastases show MIBG uptake; degree of uptake may be similar in benign and malignant tumours and maturation of neuroblastoma to ganglioneuroma may occur with no change in uptake intensity. Skeletal MIBG uptake may be localized or diffuse with tracer uptake being due either to cortical bone metastases or bone marrow infiltration or both (Fig. 20.7b). False negative scans may occur in cases where lesions are smaller than the spatial resolution of the imaging system or where metastatic lesions are too close to the primary tumour or to a site of physiologic tracer uptake to be differentiated. A small proportion (<6%) of neuroblastoma tumours are not MIBG-avid (Nadel 1996).

20.8.3 ^{18}FDG-PET/CT

Tracer:	^{18}F-fluorodeoxyglucose (^{18}FDG: 37–370 MBq IV
Effective dose:	5 mSv for ^{18}FDG PET alone; ~13–23 mSv for ^{18}FDG PET/CT (Anonymous 1998, Chapple, Willis and Frame 2002)
Critical organ:	Urinary bladder (Kowalsky and Falen 2004)

The combined acquisition of ^{18}fluorodeoxyglucose positron emission tomography and computed tomography (^{18}FDG-PET/CT) is proving to be a powerful tool for the paediatric imaging specialist. After being taken up into cells by the glucose transporter and undergoing initial phosphorylation, ^{18}FDG cannot continue along the usual pathways for glucose metabolism, and instead becomes trapped, accumulating intracellularly. The distribution of tracer therefore allows mapping of metabolically active tissues. Most tissues show physiologic tracer accumulation to some degree; brain, tonsillar and adenoidal lymphoid tissue, larynx, thymus, heart, liver, spleen, gut, kidneys and urinary bladder tend to show the greatest accumulation in normal subjects. Potential pitfalls include tracer accumulation localizing to brown adipose tissue, typically in a symmetric distribution within the neck, paraspinal and perinephric regions; recognizing normal bone marrow accumulation may be difficult as appearances vary with age. In certain situations, distinguishing accumulation due to thymic rebound from that due to anterior mediastinal lymphoma recurrence may be problematic (Fig. 20.8). Current clinical indications include the staging, response assessment and re-staging of malignancy and, to date, most paediatric clinical experience has been accumulated with lymphoma (including Hodgkin, non-Hodgkin and Burkitt sub-types) (Fig. 20.9), osteogenic and Ewing's sarcoma and rhabdomyosarcoma. With respect to cerebral tumours, ^{18}FDG-PET/CT has a role in establishing sites for biopsy, assessing tumour response and differentiating radiation necrosis from recurrence, although other, more specific tracers may be more useful in this anatomic region.

Full-body rather than "eyes-to-thighs" imaging is advocated in children due to the relatively increased incidence of distal limb metastases with tumours such as rhabdomyosarcoma and lymphoma. Issues remaining to be clarified include the extent to which PET/CT can

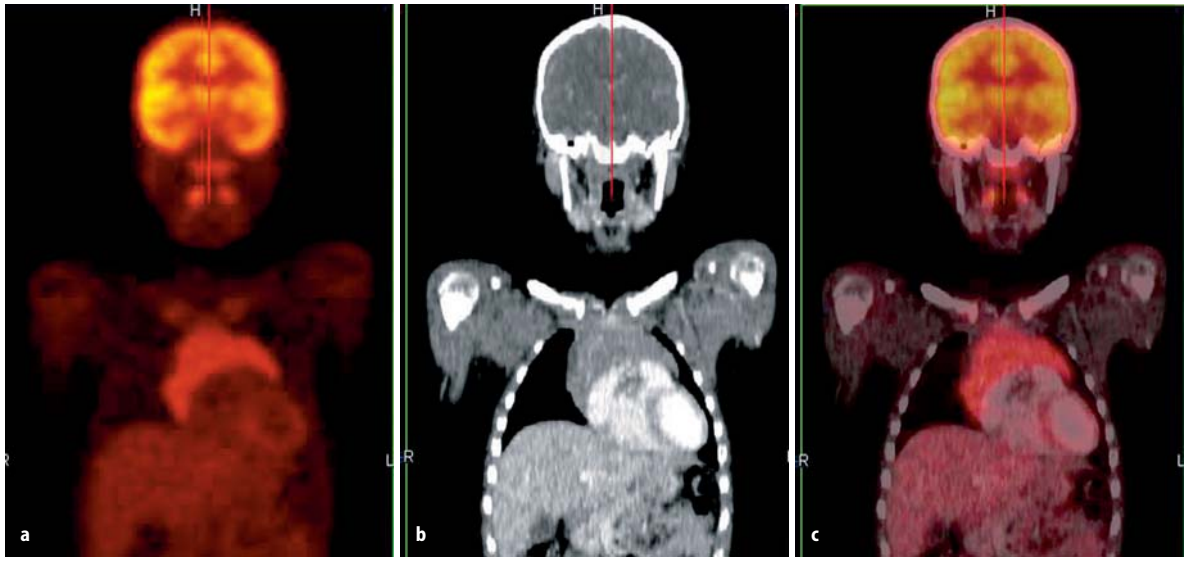

Fig. 20.8. ^{18}FDG PET/CT – cropped coronal PET (**a**), CT (**b**) and PET/CT (**c**) images show exuberant thymic rebound in a 7-year male 3 months after completion of treatment for Hodgkin lymphoma of the neck

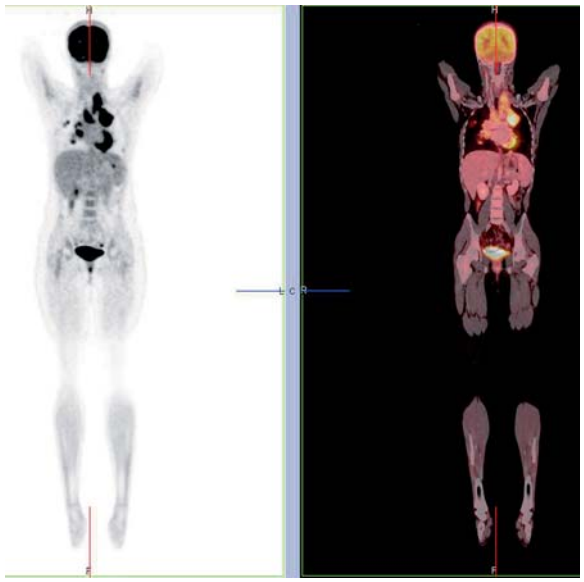

Fig. 20.9. Whole-body staging ^{18}FDG PET/CT examination in a 14-year-old female with Hodgkin lymphoma. Coronal PET (*left image*) and fused PET/CT (*right image*) images show left cervical, anterior mediastinal, paratracheal, hilar and lung parenchymal tracer accumulation co-registering to abnormal soft tissue masses. Focal tracer accumulation within spleen reflects additional visceral involvement

replace the conventional CT component of tumour protocols, the value of intravenous and oral CT contrast materials, the use of low-dose versus standard-dose CT exposure parameters and the most appropriate length of the ^{18}FDG uptake period. These, and other issues, will be resolved as further experience is gained with the combined modality.

20.9 Bone

20.9.1 Bone Scan

Common indications include imaging for suspected bone infection, inflammation and trauma, the evaluation of benign bone tumours and tumour-like conditions, the staging of primary bone malignancy and the evaluation of metastatic disease. Special uses include whole-body surveying in suspected non-accidental injury and bone dysplasia, the evaluation of suspected aseptic necrosis of the femoral head, and reflex sympathetic dystrophy. Finally, the bone scan has a valuable whole-body survey role in the case of the child who limps or refuses to weight bear, when the cause is not apparent on plain radiography – in these cases, a negative bone scan excludes significant pathology with a very high degree of confidence. There are no contraindications to the bone scan.

Tracer:	^{99m}Tc-Methylenediphosphonate (MDP): 185 – 925 MBq
Effective dose:	2.7 mSv (Stabin and Gelfand 1998)
Critical organ:	Urinary bladder (Kowalsky and Falen 2004)

^{99m}Tc-MDP appears to localize within bone by binding to calcium ions in bone crystals, a process known as chemisorption. The tracer's affinity is greatest for amorphous calcium phosphate, more prevalent in new bone, than for the crystalline hydroxyapatite, which is more prevalent in mature bone. This is thought to be the mechanism whereby the tracer shows greatest activity in regions of osteogenic activity, where the amor-

phous calcium phosphate of new bone predominates (Kowalsky and Falen 2004).

Significant abnormalities on paediatric bone scintigraphy often have a subtle appearance and consistently good technique is essential for the production of high quality diagnostic imaging. Sedation is almost never required – babies and infants may be "bundled" and wrapped to a holding device; older children may be suitably immobilized by the use of sandbags. In addition, many modern gamma cameras have the option of a built-in video player with a viewing screen positioned in the child's line of sight – in our experience, a great aid to immobilization. The value of experienced paediatric technologists cannot be overstated in making the child feel comfortable and secure.

Recent bone or joint intervention will affect tracer distribution and confound interpretation and for this reason bone scanning following procedures such as joint aspiration and bone biopsy is to be avoided.

In general, the child should always be positioned supine, as close as possible to the gamma camera. Meticulous attention to patient positioning is required in order to optimize image quality and permit proper assessment of, for example, long bone metaphyses and the small bones of the hands and feet. Positioning of the legs in the radiographic neutral position, with the feet turned in, permits optimal visualization of the lower limb long bones and may be supplemented by lateral views where appropriate. Lateral views of the feet are acquired routinely and may be supplemented by dorsal and plantar views as necessary. Imaging of the hands and feet of larger children may be obtained in the sitting position, with the forearms or feet on the collimator. Pinhole or magnified views of small parts, such as hips, are often helpful. Irrespective of the clinical indication, whole body views are mandatory, to exclude multifocal pathology even when not considered likely. The use of side markers is also mandatory.

Tracer is injected into a peripheral vein, preferably remote from the site of clinical concern. From the time of tracer injection onwards, children should be encouraged to drink plentiful fluids and to void frequently, especially prior to the delayed images, when a full bladder precludes full visualization of the pelvis. In cases of malignancy and focal bone disease, a three-phase bone scan may be acquired. This comprises blood flow (or radionuclide angiography), blood pool (or immediate) and delayed phases. The blood flow phase is acquired dynamically for 120 s immediately following rapid tracer injection. The extent of the patient imaged during this phase depends on the size of the child and the indication for the scan. Usually, the primary region of interest will be imaged during this phase, for example, the pelvis in a child with hip pain. The blood or immediate phase is acquired next; this comprises a static image or set of images, covering the wider primary region of interest and is obtained for 1 min between approximately the 2nd and 3rd minutes following injection. In cases where the pathology is suspected to be widespread, for example bone metastatic disease, whole body blood pool images may be acquired.

Delayed images are obtained between 2 and 4 h following injection. Foci of abnormal tracer activity must be demonstrated in two planes. We have found the routine use of SPECT acquisitions to be helpful, often clarifying questionable abnormalities on the planar images. SPECT is especially useful when spinal pathology is suspected. The use of a small patient table allowing a small scan radius is recommended. Finally, the acquisition of 24 h delayed images may be useful in certain cases, for example, where the distinction between cellulitis and osteomyelitis cannot be confidently made on the basis of the standard imaging protocol. It should be noted that, although the background to lesion activity ratio is advantageous at 24 h, the absolute count rate is low and image acquisition time needs to be extended accordingly (Treves 1995).

In general, many of the principles of interpretation of the adult bone scan can be applied to paediatric practice but with certain caveats. Firstly, knowledge of the normal appearances of the growing skeleton at different ages and the normal variants are important in preventing errors of interpretation. Secondly, not uncommonly the only bone scan evidence of systemic malignancy such as leukaemia, lymphoma and neuroblastoma may be subtly increased or decreased metaphyseal tracer activity or loss of the clear definition of the physis – abnormalities that are easily missed by the unwary. Thirdly, in babies and small children especially, early osteomyelitis may appear normal on the bone scan; decreased tracer activity in the affected region may also be seen (Rosovsky et al. 1994). Usually, by 24 h after the onset of symptoms, bone scan abnormality will be evident and for this reason, the temptation to image these children too early in the course of their illness should be avoided. Finally, in children, the affected limb in the majority of cases of reflex sympathetic dystrophy, also known as chronic regional pain syndrome shows decreased tracer activity, rather than increased, as is more commonly seen in the adult population. As in adult practice, the bone scan must be interpreted within the context of the other imaging investigations that have been obtained.

References

Anonymous (1998) Radiation dose to patients from radiopharmaceuticals – ICRP Publication 80 (addendum 2 to ICRP publication 53). Annals of the ICRP 28:1 – 126

Chapple CL, Willis S, Frame J (2002) Effective dose in paediatric computed tomography. Phys Med Biol 47:107 – 115

De Sadeleer C, Piepsz A, Ham HR (2000) Atlas on acute pyelonephritis in children. Clin Nucl Med 25(7):541 – 545

Gordon I, Colarinha P, Fettich J, et al. (2000) Guidelines for standard and diuretic renography in children. On-line guidelines issued under the auspices of the Paediatric Committee of the European Association of Nuclear Medicine, 2000

Kowalsky RJ, Falen SW (2004) Radiopharmaceuticals in nuclear pharmacy and nuclear medicine, 2nd edn. American Pharmacists Association, Washington DC

Majd M, Rushton HG (1992) Renal cortical scintigraphy in the diagnosis of acute pyelonephritis. Semin Nucl Med 2:98 –111

Nadel HR (1993) Thallium-201 for oncological imaging in children. Semin Nucl Med 3:243 – 254

Nadel HR (1996) Nuclear oncology in children. In: Freeman LM (ed) Nuclear medicine annual. Raven Press, New York

Olivier P, Colarinha P, Fettich J, et al. (2002) Guidelines for radioiodinated MIBG scintigraphy in children. On-line guidelines issued under the auspices of the Paediatric Committee of the European Association of Nuclear Medicine, 2002

Pusuwan P, Reyes L, Gordon I (1999) Normal appearances of technetium-99m dimercaptosuccinic acid in children on planar imaging. Eur J Nucl Med 26:483 – 488

Rosovsky M, Goldfarb CR, Finestone H, et al. (1994) Cold spots in pediatric bone imaging. Semin Nucl Med 2:184 – 186

Smith T, Gordon I (1998) An update of radiopharmaceutical schedules in children. Nucl Med Commun 19(11):1023 – 36

Stabin MG, Gelfand MJ (1998) Dosimetry of pediatric nuclear medicine procedures. Q J Nucl Med 42:93 – 112

Treves ST (1995) Pediatric nuclear medicine, 2nd edn. Springer-Verlag, New York

Radioiodine Therapy for Benign Thyroid Disease 21

S.E.M. Clarke

21.1 Introduction

21.1.1 Historical Perspective

Diseases of the thyroid constitute the most common form of endocrine disorders and, over the past 60 years, nuclear medicine has contributed significantly to the management of thyroid patients, both in terms of diagnosis and treatment (Williams et al. 1949). Radionuclide therapy for both benign disease (thyrotoxicosis and goitre) and thyroid cancer has served as a model for the development of other radionuclide therapies in recent years.

The presence of iodine in the thyroid gland was reported in 1895 by Baumann. The first reports of radionuclide therapy for thyrotoxicosis used iodine-130, and iodine-131 rapidly became the favoured radionuclide with β- and γ-ray emissions and a half-life suitable for therapy (Varma et al. 1970).

Although there have been many years of clinical experience in the use of ^{131}I radioiodine for the treatment of benign thyroid disease, there are few prospective studies published comparing the efficacy of ^{131}I radioiodine and other treatment modalities such as antithyroid drugs or surgery. The development of guidelines (Meier et al. 2002; Lazarus et al. 1995) for the management of thyrotoxicosis and the use of ^{131}I radioiodine has resulted in some harmonisation of practice although there are still significant differences in the protocols used in Europe compared with the USA.

In this chapter, the theory of radioiodine therapy will be explained, the clinical role explored and the practical aspects of treatment of benign thyroid disease considered. The new developments in clinical practice will also be outlined.

21.1.2 Synthesis of Thyroid Hormones

Thyroxine and triiodothyronine are synthesized in the thyroid follicular cells by the iodination of tyrosine. Iodine is taken up in the follicular cells by an active ATP-dependent transport mechanism through the stimulation of thyroid-stimulating hormone (TSH). In recent years, the thyroid sodium iodide symporter (NIS) has been cloned (Dai et al. 1996) and in vitro and in vivo studies have given new insights into iodide transport mechanisms and their defects (Filetti et al. 1999; Dadachova and Carrasco 2004). The iodine pump increases in the presence of iodine deficiency. Peroxidase and hydrogen peroxidase enzymes oxidize the iodine, which is then linked to the tyrosine molecules in the tyrosine-rich thyroglobulin. The iodothyronines are produced, which couple to form triiodothyronine (T3) or tetra-iodothyronine (T4). The process of iodination is inhibited by the presence of excess iodine. The thyroglobulin is then hydrolysed, liberating T3 and T4, which are secreted into the circulation where they are bound to thyroid-binding globulin, thyroid-binding pre-albumin and albumin. This process of iodination is blocked by perchlorate and by the presence of excess iodine.

The residence time of iodine within the thyroid is known to be increased by the administration of lithium (Turner et al. 1976).

21.1.3 Control of Thyroid Hormone Production

The production of TSH occurs in the anterior part of the pituitary. This production is in turn regulated by suppressants and stimulators. Thyroxine, T3, somatostatin and dobutamine all act as suppressors of TSH, and T4 is also believed to have a direct TSH-suppressing action.

The production of TSH is stimulated by thyrotropin-releasing hormone, which is found in various parts of the body including the hypothalamus. The release of TRH is inhibited by T4 and T3. TSH stimulates thyroid hormone production by stimulating cyclic AMP and by activating the incorporation of thyroglobulin in the thyroid follicular cells by a process of endocytosis.

This negative feedback system has implications for the treatment of patients with solitary autonomous nodules. If patients are treated when the TSH level is maximally suppressed, the radiation dose to the normal thyroid is minimised and post ^{131}I radioiodine hypothyroidism is avoided in many patients.

21.1.4 Pathology of the Thyroid Gland

Like all endocrine organs, the thyroid gland may over- or underproduce hormones or be subject to malignant change. ^{131}I may be used to treat the various forms of thyroid hormone overproduction and also, more recently, its use in non-toxic goitre has been explored.

21.1.5 Thyrotoxicosis

The clinical symptoms of thyrotoxicosis are classically those of weight loss, heat intolerance, tremor and palpitations, increased bowel frequency and increased anxiety. The signs include tachycardia and tremor of the outstretched hands. There may be a bruit audible over the thyroid gland, and a systolic flow murmur may be audible over the precordium. In some patients, particularly those with severe disease or a prolonged period before diagnosis, evidence of proximal muscle wasting may be present.

There are two main pathological processes resulting in thyrotoxicosis. The first is a diffuse process affecting the whole gland; the second is a focal process affecting one or several areas of the gland. It is important to differentiate between these two main causes of thyrotoxicosis as the management of these pathologies differs.

21.1.5.1 Toxic Diffuse Goitre (Graves' Disease, Basedow's Disease)

Toxic diffuse goitre is an autoimmune process caused by the production of a stimulating antibody to the TSH receptor. The disease may be familial, although the pattern of inheritance is unclear. Various factors have been implicated in the development of Graves' disease and these include pregnancy and stress (Safran et al. 1987). The autoimmune process not only affects the thyroid gland but may also affect the eyes in 50 % of cases and, more rarely, can be associated with the development of pretibial myxoedema and thyroid acropachy. The causative antibody, variously known as thyroid-stimulating immunoglobulin or TSH-receptor antibody, may be assayed and can be demonstrated in 90 % of patients with the clinical syndrome of Graves' disease. Although the level of antibody tends to correlate with the severity of clinical symptoms, this is not invariable. The link between TSH-receptor antibody and dysthyroid eye disease remains unclear. It would appear from various studies that the TSH-receptor antibody itself is not the causative factor in dysthyroid eye disease, and recent papers have implicated a 64 – 67 kDa protein present in the serum of patients with dysthyroid eye disease which reacts with pig eye muscle (Boucher et al. 1992).

21.1.5.2 Toxic Nodular Goitre (Plummer's Disease)

In patients with multinodular goitres, there is an increased likelihood of the development of multiple focal areas of thyroid autonomy resulting in elevations of free T4 and free T3 levels. This form of toxic nodular goitre is particularly common in geographical areas where endemic goitre is prevalent. Germany, Austria and Switzerland are countries with a previous history of dietary iodine deficiency, and there is a higher prevalence of multinodular goitre in these countries compared with the UK (European Thyroid Association 1985).

Patients may also develop a single nodule, which on isotope imaging is demonstrated to show increased uptake with suppression of the remainder of the gland. Uninodular toxic goitre is diagnosed using conventional biochemical tests and radionuclide imaging with technetium-99m (^{99m}Tc) or iodine-123 (^{123}I) (Fig. 21.1).

The presenting symptoms of uninodular or multinodular toxic goitre are similar to those of Graves' disease, but with the absence of eye signs, thyroid acropachy or pretibial myxoedema. This tends to be a disease of old people and, in the elderly, the clinical presentation may be non-classical with minimal signs and symptoms apart from tachycardia that may progress to atrial fibrillation and heart failure.

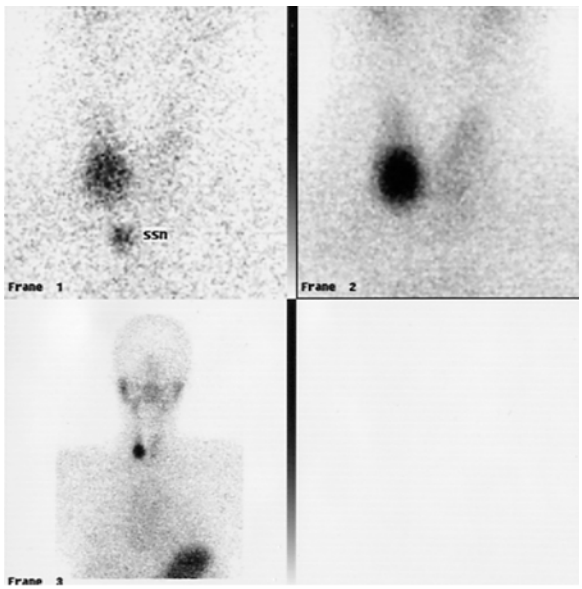

Fig. 21.1. ^{99m}Tc Thyroid scan in a patient with biochemical evidence of thyrotoxicosis. *Upper right zoomed image* demonstrates a toxic nodule in the lower pole of the right lobe of thyroid with suppression of the remainder of the gland

21.1.6
Diagnosis of Thyrotoxicosis

The diagnosis of thyrotoxicosis is made on the basis of history, clinical examination and investigations. The investigations include free T4, free T3 which will be elevated and ultra-sensitive TSH measurements which will be low. A ^{99m}Tc or an ^{123}I thyroid scan will differentiate toxic diffuse goitre from toxic nodular goitre. Thyroid-stimulating immunoglobulin measurement, if raised, will strongly support a diagnosis of toxic diffuse goitre, as does the presence of dysthyroid eye disease.

21.2
Radiopharmaceutical

21.2.1
Iodine-131

Iodine-131 has a physical half-life of 8.04 days, which is well suited to the biological half-life of iodine in patients with differentiated thyroid cancer but is long compared with the biological half-life of iodine in the thyrotoxic patient. The medium energy beta-particle emission (E_{max} = 0.61 MeV), with a path length of about 0.8 mm in tissue, ensures an intracellular radiation dose following the cellular internalization of ^{131}I. The gamma emissions of ^{131}I (principal gamma energy 364 KeV) have both benefits and disadvantages. Gamma-ray emissions facilitate gamma-camera imaging, which enables tracer doses of ^{131}I to be used for dosimetry calculations.

The high-energy gamma emissions, however, contribute to the unwanted whole-body radiation burden associated with radionuclide therapy and also to the radiation protection problems for the staff and the patients' relatives.

21.3
Clinical Indications

21.3.1
Toxic Diffuse Goitre

The management of toxic diffuse goitre (Graves' disease) in Europe is generally that of a prolonged course of anti-thyroid medication (carbimazole, methimazole or propylthiouracil). Data show that the continuance of treatment for 12 – 18 months results in an approximately 50 % cure rate on discontinuing anti-thyroid medication (Allanic et al. 1990). Second-line treatment following failure of anti-thyroid medication, non-compliance or in patients who are not responding to anti-thyroid treatment is either ^{131}I or, alternatively, surgery.

In the USA, there is a current trend to early ^{131}I treatment with little or no pre-treatment with anti-thyroid medication (Klein et al. 1994). The value of pretreatment with anti-thyroid medication, however, is the potential cure rate in half the patients treated, and the rapid control of symptoms that cannot be achieved with ^{131}I, particularly in those patients who are markedly symptomatic (Lazarus et al. 1995). Santos et al. have demonstrated in a small series that propylthiouracil reduces the efficacy of radioiodine treatment, however, when compared with no pretreatment or treatment with methimazole (Santos et al. 2004).

As toxic diffuse goitre frequently affects young and middle-aged women, the issue of using ^{131}I in women of childbearing years has been a subject for discussion. A survey of practice in Europe, Japan and the USA found that one-third of doctors in the USA believed ^{131}I to be an appropriate treatment for women of age 19. Only 4 % of European doctors thought that ^{131}I was appropriate in such a case, although this does not reflect current European practice (Wartofsky et al. 1991).

In the previous decades, such women were not selected for ^{131}I therapy because of the potential risk to the offspring. However, to date, no evidence has been presented to suggest damage to the offspring of patients treated with ^{131}I despite large patient population studies (Hayek et al. 1970; Sarkar et al. 1976).

The use of ^{131}I in young patients remains controversial. In the USA, treatment of patients under the age of 18 with ^{131}I is now taking place routinely. In Europe, however, the concerns about radioiodine treatment in young patients with radiosensitive tissues has led to a general limitation of ^{131}I use to adults. It is important to recognize and consider the risks of thyroid surgery in children. It has been estimated that 16 – 35 % of children treated with sub-total thyroidectomy experience acute complications with permanent complications occurring in up to 8 % of children (Bacon and Laury 1965; Ching et al. 1977).

The marked variation in the use of ^{131}I throughout the world, both in terms of the patients who are selected for treatment and the protocols for treatment, is now recognized and surveys of practice undertaken in Europe, Japan, India and the USA confirm this variation (Turner et al. 1976; Schicha and Scheidhauer 1993; Kusakabe and Maki 1993; Mithal et al. 1993).

Surgery as a second-line treatment is less commonly used, although in certain parts of the world it remains the second-line treatment of choice for women of childbearing years. Kuma et al. (1991) have shown clearly that there is an increased morbidity associated with surgery compared with ^{131}I therapy. There is also the risk of subsequent recurrence in the residual thyroid if a total thyroidectomy is not performed. Hypothyroidism is also a post-operative complication of surgery (Sarkar et al. 1976).

21.3.2 Toxic Nodular Goitre

Patients with toxic nodular goitre are generally considered to be ideally suited for ^{131}I therapy. A short period of treatment using anti-thyroid medication is recommended in patients who are extremely symptomatic, and in the elderly. It is essential to ensure that the normal thyroid tissue is suppressed at the time of ^{131}I therapy, and this will require an adequate period of discontinuation of anti-thyroid medication before radioiodine treatment. In patients with mild to moderate elevations of thyroid hormone levels and who are relatively asymptomatic, direct treatment with radioiodine may be considered.

In addition to treating the thyrotoxicosis in toxic nodular goitre, a reduction in nodule size is achieved (Erdogan et al. 2004). In patients with large goitres, several doses of radioiodine may be required to render the patient euthyroid (Fig. 21.2).

21.3.3 Non-Toxic Nodular Goitre

In recent years, the use of radioiodine in the treatment of non-toxic multinodular goitre has been explored (Wesche et al. 1995; Huysmanns et al. 1994). Radioiodine is particularly useful in elderly patients and those with medical contraindications to surgery. Goitre shrinkage is well documented, but multiple doses of radioiodine are frequently required.

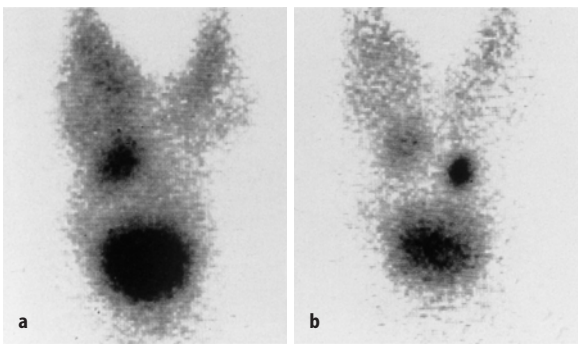

Fig. 21.2. ^{99m}Tc Thyroid scan (**a**) in a patient with a toxic multinodular goitre and retrosternal extension. Patient received an 800 MBq dose of ^{131}I iodine. After 6 months the patient's thyroid function tests were still marginally elevated. A repeat ^{99m}Tc thyroid scan (**b**) confirmed partial treatment with reduced uptake in the right sided toxic nodule but persisting uptake in the retrosternal midline nodule. A further toxic nodule is now visualized in the left lobe. After a further treatment with radioiodine, the patient became euthyroid

21.4 Methodology of Radioiodine Therapy for Thyrotoxicosis

21.4.1 Practical Aspects of Therapy

Patients who have been selected for ^{131}I radioiodine treatment should have the implications of therapy explained clearly. It is generally considered good practice to render the patient euthyroid before treatment, as ^{131}I radioiodine administration will cause a transient elevation in free T4 and free T3 levels approximately 7 days following administration. In the symptomatically well-controlled patient this will have little effect, but in symptomatically toxic patients, this further elevation of thyroid hormone may trigger palpitations, atrial fibrillation and heart failure. This is a particular problem in the elderly. Symptomatic control may be achieved using beta blockade. Since carbimazole blocks the organification of iodine within the thyroid, carbimazole therapy should be discontinued at least 48 h before therapy is undertaken to ensure adequate residence time of ^{131}I within the follicular cells.

There has been controversy as to whether pretreatment with carbimazole, methimazole or propylthiouracil reduces the subsequent efficacy of radioiodine. Santos et al. have found that pretreatment with propylthiouracil reduces the effectiveness of radioiodine treatment in patients with Graves' disease. The same effect was not observed with methimazole pretreatment (Santos et al. 2004).

The requirement to admit patients varies considerably across the world. In many countries in Europe, admission is required for doses of 185 MBq and above. In the USA, doses up to 1,000 MBq may be given with the patient as an outpatient. Admission should be considered for the elderly with a risk of heart failure.

Before therapy, patients should be asked to sign a consent form and should be informed of restrictions on working, contact with children and pregnancy before doing so, both verbally and in writing (Safran et al. 1987; Singer et al. 1995). The length of time for which restrictions should be observed varies by country, but time should be taken with the patient before treatment to ensure that appropriate restrictions are understood and will be adhered to.

Pregnancy and breast-feeding are absolute contraindications to radioiodine therapy, and it is recommended that a pregnancy test should be undertaken in women of childbearing years who are about to receive radioiodine therapy and in whom pregnancy may be an issue.

The restrictions on work and contact with small children will also depend on national dose limits, and these should be discussed with each patient individually (Safran et al. 1987; Bacon and Laury 1965). Studies

are now being undertaken following radioiodine therapy, and these data confirm that with adequate precautions, the dose to family members is minimal (Thompson and Harding 1991).

In patients in whom thyrotoxicosis is not well controlled before radioiodine therapy, it may be necessary to re-commence anti-thyroid medication for a short interval following treatment. All patients should be given written instructions about the precautions to be observed. In addition, the need to avoid pregnancy for 4 months following radioiodine treatment should be emphasized to female patients.

Iodine-131 may be administered in liquid form or as a capsule. The advantages of the capsule are those of radiation protection for staff administering the radioiodine; the disadvantages are those of expense and loss of flexibility in dose. Unusually, ^{131}I radioiodine may be given intravenously in patients in whom vomiting is a problem. ^{131}I should be administered in a designated area by trained staff in accordance with the national regulations.

Patients should be encouraged to drink large volumes of fluid for a 24-h period following radioiodine therapy to lower the radiation dose to the bladder.

21.4.2 Dose Considerations

The determination of the activity of radioiodine to be administered in patients with thyrotoxicosis remains a topic of controversy. The controversy centres around whether it is possible to avoid hypothyroidism and successfully treat hyperthyroidism by using careful dosimetry calculations. Although much has been written on this subject, there appears to be no consensus as to the optimal protocol for deciding the dose. Current practice therefore ranges from the use of careful dose calculation to a fixed-dose protocol.

21.4.2.1 Dosimetry Calculation

Various formulae have been generated which may be used to estimate the administered activity required to deliver an effective radiation dose to the gland to render the patient euthyroid and avoid unnecessary radiation being administered (Shapiro 1993). Most formulae require information on ^{131}I uptake and clearance of radioiodine by the gland, and the weight or volume of the gland. The percentage uptake and clearance of radioiodine may be estimated using tracer doses of radioiodine (Bockisch et al. 1994). It is unclear, however, whether tracer doses may have the mild stunning effect on the thyroid follicular cells, thereby altering the uptake and clearance of subsequent therapy doses. In addition, variations in iodine intake in the diet between the tracer study and the therapy may affect the reproducibility of radioiodine uptake and clearance as has clearly been shown by van Isselt et al. (Tjerk et al. 2001).

The volume of the gland may be estimated using ultrasound measurements (Tsuruta et al. 1993), but in patients with toxic nodular disease or in patients with toxic diffuse disease in a multinodular goitre, the measured volume of the gland does not necessarily correspond to the functioning volume. It is therefore likely that ultrasound estimates of volumes are most accurate in patients with toxic diffuse goitre and least accurate in patients with multiple toxic nodules in multinodular disease. ^{124}I-PET studies have been used by Flower et al. (1994) to determine more accurately the functioning volume of the thyroid gland.

Results of studies published using these volume estimates to calculate administered dose, however, show that there continues to be an incidence of hypothyroidism and persisting hyperthyroidism in patients treated using these calculations. Other factors such as the duration and effect of pre-treatment with anti-thyroid medication and the issue of varying radiosensitivity may well explain why careful dosimetric measurements fail to predict reliably the dose that will render the patient euthyroid without subsequent hypothyroidism. It is noted, for example, that patients of Afro-Caribbean and African origin appear to be more resistant to treatment with both antithyroid drugs and radioiodine compared with Caucasian patient groups (personal observation).

Low calculated dose protocols aim to deliver 80 Gy to the thyroid, whereas high calculated dose protocols aim to deliver 300 Gy. Willemsen et al. (1993) have shown that the administered dose required to deliver a delivered dose of 300 Gy ranged from 240 to 3,120 MBq. As might be predicted, Reinhardt et al. demonstrated that the frequency of hypothyroidism increased from 27 % after 150 Gy to 68 % after 300 Gy but that persistent hyperthyroidism decreased from 27 % after 150 Gy to 8 % after 300 Gy (Reinhardt et al. 2002).

21.4.2.2 Fixed-Dose Protocol

Fixed-dose protocols range from those that take account of the size of the gland, usually determined clinically by giving smaller doses to small glands on palpation and larger doses to clinically larger glands, and those protocols that attempt electively to ablate the thyroid gland.

As might be predicted, low-dose protocols result in a lower instance of hypothyroidism in the first year, but the long-term outcome shows a significant incidence of hypothyroidism at 15 years (35 – 40 %) compared with 50 – 70 % incidence using high-dose regimes (Kinser et al. 1989; Hardisty et al. 1990; Johnson 1993).

The administered dose used in an attempt to ablate the thyroid gland varies world-wide, and is usually limited by the maximum permissible dose to be administered to an outpatient. In the USA, 1,000 MBq may therefore be administered, whereas in the UK, 800 MBq is the standard upper limit for outpatient administration. Results in the UK published by Kendall-Taylor et al. (1984) using a 500 MBq fixed-dose show that ablation was achieved in only 64% of patients with a small percentage of patients still remaining hyperthyroid following treatment.

The disadvantage of electively rendering a patient hypothyroid is that, in effect, one pathology is exchanged for another. There is a need to ensure that patients who have been rendered hypothyroid remain on adequate replacement doses of thyroxine for life. The study by Kendall-Taylor et al. (1984) demonstrated that 2% of patients who had been rendered hypothyroid and started on thyroxine were not taking treatment and a further 3% of patients had been recognized by their physicians to be non-compliant.

Hardisty et al. (1990) explored the efficacy and cost-effectiveness of varying dose protocols, and concluded that both hypothyroidism and persisting hyperthyroidism were unavoidable whichever dose protocols were used. In addition, they noted that when cost to both the patients and the Health Service was considered, the use of high fixed-dose attempting to ablate the thyroid gland appeared more cost-effective (Hardisty et al. 1990).

21.4.3 Side Effects and Complications

The major complication of radioiodine therapy is hypothyroidism. This may occur in the early post-treatment period, particularly if higher administered activities are given. Alternatively, it may develop gradually in the years following treatment (Huysmanns et al. 1994). The later-onset hypothyroidism occurs at a rate of approximately 4% per year, and therefore it has been estimated that on follow-up after 25 years 100% of patients treated with radioiodine will be hypothyroid. It has been postulated that this long-term hypothyroidism relates in part to the natural outcome of Graves' disease (Kendall-Taylor et al. 1984). The incidence of post-radioiodine hypothyroidism, however, is markedly lower in patients treated for a solitary toxic nodule compared with those with Graves' disease (Wesche et al. 1995; Ng Tang Fui and Maisey 1979). This is undoubtedly due to the protection of the suppressed area of the gland at the time of treatment and emphasizes the need to ensure that patients have adequate time off anti-thyroid treatment before radioiodine therapy to ensure adequate suppression of the normal areas of the gland.

Careful follow-up of patients following radioiodine therapy is therefore mandatory, and should be coordinated by a trained thyroid practitioner. In the early post-therapy period, it is recommended that this follow-up is undertaken within a hospital environment. Subsequently, follow-up may be undertaken in conjunction with a community physician (Safran et al. 1987). The management of these patients is greatly facilitated by computer-assisted follow-up programming.

Patients whose hypothyroidism develops rapidly following radioiodine treatment are frequently extremely symptomatic, whereas patients with delayed onset hypothyroidism may not present with classical hypothyroid symptoms. Weight gain and tiredness are key clinical symptoms in diagnosing post-therapy hypothyroidism.

Other side effects and complications of radioiodine therapy are remarkably few. Patients with large goitres may notice transient swelling of the goitre approximately 1 week following therapy and some discomfort may be associated with this swelling. As has been previously stated, there may be a transient rise in fT4 and fT3 levels 7–10 days following radioiodine treatment, and in patients who have been poorly controlled before radioiodine therapy there may be an exacerbation of palpitations and heart failure. Slight discomfort of the salivary glands may be noted, but this is unusual with the doses used for thyrotoxicosis therapy. Iodine allergy is not a contraindication to radioiodine therapy.

In patients with large goitres in whom tracheal compression is present before therapy, a worsening of pressure symptoms in the immediate post-therapy period may be noticed. This complication is, in fact, rare. Patients with severe tracheal narrowing should be admitted for therapy with surgical cover. Surgery should be considered as an alternative to radioiodine therapy in this particular group.

21.4.4 Dysthyroid Eye Disease

There has been much discussion as to the effect of radioiodine therapy on dysthyroid eye disease. Reports in the literature yield conflicting information (Catz and Tsao 1965; Hamilton et al. 1967).

Catz and Tsao (1965) have demonstrated that an improvement in ophthalmopathy can be obtained following ^{131}I radioiodine ablation of the thyroid, which they believe to be due to the destruction of the antigenic stimulus to antibody formation. Peqqequat et al. (1967), using non-ablative doses, showed a varying response following therapy with some of the patients improving and a few patients deteriorating. Jones et al. (1969) observed that while lid retraction improved following ^{131}I treatment in patients with Graves' ophthalmopathy, exophthalmos remained unchanged or dete-

riorated, and in 50 % of the patients periorbital oedema was observed following treatment. Bartalena in a large prospective study demonstrated that dysthyroid eye disease was exacerbated in 15 % of patients after radioiodine and the exacerbation persisted in 8 % (Bartalena et al. 1988). It is therefore recommended that patients with severe dysthyroid eye disease should not be treated during an acute exacerbation. A course of high-dose steroids may be considered as a prelude to radioiodine therapy in this small percentage of patients. Bartalena's prospective study also showed that a course of prednisolone given with the radioiodine prevented the exacerbation. Tallstedt et al. (1994) have studied the effects of thyroxine administered in the early post-radioiodine period, and they conclude that the early administration of thyroxine after radioiodine reduces the occurrence of Graves' ophthalmopathy. Pretreatment with methimazole prior to radioiodine treatment has been shown in a prospective, randomised study to reduce the rise in TSH receptor antibodies post radioiodine (Andrade et al. 2004). Although the study was not designed to assess exacerbations of dysthyroid eye disease, the role of pre-treatment with antithyroid drugs to reduce the levels of TSH receptor antibodies before radioiodine treatment warrants further evaluation.

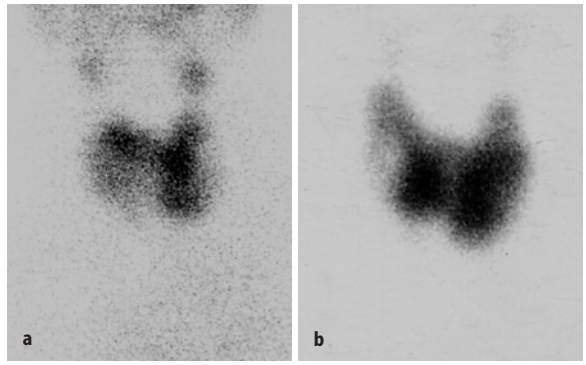

Fig. 21.3. a ^{99m}Tc Thyroid scan in a patient with a non-toxic multinodular goitre and pressure symptoms. Twenty minutes uptake of 2.50 % was within the normal range (0.4 – 4.0 %). An 800 MBq dose of ^{131}I iodine was given. **b** Three months after radioiodine treatment, the patient developed symptoms of thyrotoxicosis. ^{99m}Tc scan now shows a diffusely increased pattern of uptake on the background on multinodularity. The 20 min uptake has risen to 11.8 %, confirming the development of toxic diffuse goitre (Graves' disease)

21.4.5 Radioiodine Therapy of Non-Toxic Goitre

The role of radioiodine in the treatment of non-toxic goitre and the optimal protocol are still subjects for research and discussion.

Varying dose regimes have been described on the basis of dosimetry calculation. High administered doses are required in view of the relatively low overall uptake compared with a toxic goitre. Recently, however, recombinant TSH has been used to increase the uptake of radioiodine in non-toxic goitres by increasing the homogeneity of uptake. The therapeutic dose of radioiodine may be reduced by 50 – 60 % without loss of thyroid volume reduction (Nieuwlats et al. 2004). Although, historically, patients with evidence of tracheal compression were not deemed suitable for radioiodine therapy, it is now apparent that the theoretical risk of increasing tracheal compression in the immediate post-treatment period does not in fact occur (Reinhardt et al. 2002). Nevertheless, in patients with significant stridor, admission for observation is recommended.

Following radioiodine therapy, thyroid function tests should be performed at regular intervals. While hypothyroidism appears an uncommon complication, the development of hyperthyroidism with a picture suggestive of Graves' disease has been reported (Nygaards et al. 1993) (Fig. 21.3). The mechanism for this is unclear, but it is presumed that the release of thyroid antigen may be the trigger for the development of autoimmune thyrotoxicosis. As these patients are frequently elderly and may have cardiovascular disease, careful follow-up is essential as hyperthyroidism may well exacerbate cardiac symptoms in this population.

References

Allanic H, Fauchet R, Orgiazzi A (1990) Antithyroid drugs and Graves' disease: a prospective randomised evaluation of the efficacy of treatment duration. J Clin Endocrinol Metab 70:675 – 9

Andrade VA, Gross JL, Mata AL (2004) Serum thyrotropin receptor autoantibodies level after 131I therapy in Graves' patients: effect of pre-treatment with methimazole evaluated by a prospective randomized study. Eur J Endocrinol 151:467 – 474

Bacon GE, Laury GH (1965) Experience with surgical treatment of thyrotoxicosis in children. J Pediatr 67:1 – 5

Bartalena L, Marocci C, Bogazzi F, Manetti L, Tanda ML, Dell'Unto E, BrunoBossio G, Nardi M (1988) Relation between therapy for hyperthyroidism and the course of Graves' ophthalmopathy. N Engl J Med 338:73 – 78

Baumann E (1895) Uber das normale Vorkommen von Jod im Tierkorper. Z Physiol Chem 21:319

Becker DR (1982) Radioactive iodine in the treatment of hyperthyroidism. In: Beckers C (ed) Thyroid disease. Pergamon Press, Paris, pp 145 – 8

Bockisch A, Jamitzy T, Derwantz R, Biersack HJ (1994) Optimized dose planning of radioiodine therapy of benign thyroidal diseases. J Nucl Med 34:1632 – 8

Boucher CA, Bemard BF, Zhang ZG, Salvin M, Rodien P, Triller H, Wall JR (1992) Nature and significance of orbital autoantigens and their autoantibodies in thyroid associated ophthalmopathy. Autoimmunity 13:89 – 93

Catz B, Tsao J (1965) Total 131-I thyroid remnant ablation for pretibial myxoedema. Clin Res 13:130 – 2

Ching T, Warden MJ, Hefferman RA (1977) Thyroid surgery in children and teenagers. Arch Otolaryngol 103:544 – 6

Dadachova E, Carrasco N (2004) The Na^+/I symporter: Imaging and therapeutic applications. Semin Nucl Med 34:23 – 31
Dai G, Levy O, Carrasco N (1996) Cloning and characterization of the thyroid iodide transporter. Nature 379:458 – 460
Erdogan MF, Kucuk NO, Anil C, et al. (2004) Effect of radioiodine therapy on thyroid nodule size and function in patients with toxic adenomas. Nucl Med Comm 25:1083 – 1087
European Thyroid Association (1985) Goitre and iodine deficiency in Europe. Report of the Sub-Committee for the Study of Endemic Goitre and Iodine Deficiency of the European Thyroid Association (ETA). Lancet i:1289 – 1292
Filetti S, Bidart J-M, Arturi F, Caillou B, Russo D, Schlumberger M (1999) Sodium/iodide symporter: a key transport system in thyroid cancer cell metabolism. Eur J Endocrinol 141: 443 – 457
Flower MA, al-Saadi D, Harmer CL, McCready VR, Ott RJ (1994) Dose response study on thyrotoxic patients undergoing positron emission tomography and radioiodine therapy. Eur J Nucl Med 21:531 – 6
Hamilton R, Mayberry W, McConahey W, Hanson K (1967) Ophthalmopathy of Graves' disease: a comparison between patients treated surgically and patients treated with radioiodine. Mayo Clin Proc 42:812 – 18
Hardisty CA, Jones SJ, Hedley AJ, Munro DS, Bewsher PD, Weir RD (1990) Clinical outcome and costs of care in radioiodine treatment of hyperthyroidism. J R Coll Physicians 24:36 – 42
Hayek A, Chapman EM, Crawford JD (1970) Long term results of treatment of thyrotoxicosis in children and adolescents with radioactive iodine. N Engl J Med 283:949 – 53
Huysmanns DA, Hermus AR, Corstens FH, Barentsz JO, Kloppenborg PW (1994) Large compressive goiters treated with radioiodine. Ann Intern Med 121:757 – 62
Johnson JK (1993) Outcome of treating thyrotoxic patients with a standard dose of radioactive iodine. Scottish Med J 38:142 – 4
Jones D, Munro D, Wilson G (1969) Observations on the cause of exophthalmos after 131-iodine therapy. Proc R Soc Med 52:15 – 18
Kendall-Taylor P, Keir M, Ross WM (1984) Ablative radioiodine therapy for hyperthyroidism: long term follow up study. Br Med J 289:361 – 3
Kinser JA, Roesler H, Furrer T, Grutter D, Zimmerman H (1989) Nonimmunogenic hyperthyroidism: incidence after radioiodine and surgical treatment. J Nucl Med 30:1960 – 5
Klein I, Becker DV, Levey GS (1994) Treatment of thyroid disease. Ann Intern Med 121:281 – 8
Kuma K, Matsuzuka F, Kobayashi A, Hirai K, Fukata S, Tamai H, Miyauci A, Sugawara M (1991) Natural course of Graves' disease after subtotal thyroidectomy and management of patients with postoperative thyroid dysfunction. Am J Med Sci 302:8 – 12
Kusakabe K, Maki M (1993) Radionuclide therapy of thyroid disease radioactive iodine therapy. Jpn J Nucl Med 30: 813 – 19
Lazarus JH, Clarke SEM, Franklyn JA, Harding LK (1995) Guidelines – the use of radioiodine in the management of hyperthyroidism. The radioiodine audit subcommittee of the Royal College of Physicians Committee on Diabetes and Endocrinology and the Research Unit of the Royal College of Physicians. Chameleon Press, London
Lazarus JH, Clarke SEM, Franklyn JA, Harding LK (1995) Guidelines – the use of radioiodine in the management of hyperthyroidism. The radioiodine audit subcommittee of the Royal College of Physicians Committee on Diabetes and Endocrinology and the Research Unit of the Royal College of Physicians. Chameleon Press, London
Meier DA, Brill DR, Becker DV, Clarke SEM, et al. (2002) Procedure guidelines for therapy of thyroid diseases with iodine-131. J Nucl Med 43:856 – 861
Mithal A, Shah A, Kumar S (1993) The management of Graves' disease by Indian thyroidologists. Nat Med J India 6:163 – 6
Ng Tang Fui SC, Maisey MN (1979) Standard dose of 131-iodine therapy for hyperthyroidism caused by autonomously functioning thyroid nodules. Clin Endocrinol 10:69 – 77
Nieuwlats WA, Hermus AR, Ross HA, Buijs WC, Edelbroek MA, Bus JW, Corstens FH, Huysmans DA (2004) Dosimetry of radioiodine therapy in patients with nodular goiter after pretreatment with a single low dose of recombinant human thyroid stimulating hormone. J Nucl Med 45:626 – 633
Nygaards B, Hegedus L, Gervil M, Hjalgrim H, Soe-Jensen P, Hansen JM (1993) Radioiodine treatment of multinodular nontoxic goitre. Br Med J 307:828 – 32
Peqquequat E, Mayberry W, McConahey W, Wyse E (1967) Large doses of radioiodine in Graves' disease: effect on ophthalmopathy and long acting thyroid stimulator. Mayo Clin Proc 42:802 – 11
Reinhardt MJ, Brink I, Alexius Y, von Mallek D, Ezziddin S, Palmedo H, Krause TM (2002) Radioiodine therapy in Graves' disease based on the tissue absorbed dose calculations: effect of pretreatment thyroid volume on clinical outcome. Eur J Nucl Med 29:1118 – 1124
Safran M, Paul TL, Roti E, Braverman LE (1987) Environmental factors affecting autoimmune thyroid disease. Endocrinol Metab Clin North Am 16:327 – 42
Santos R, Romaldini JH, Ward LS (2004) Propylthiouracil reduces the effectiveness of radioiodine treatment in hyperthyroid patients with Graves' disease. Thyroid 14:525 – 530
Santos RB, Romaldini JH, Ward LS (2004) Propylthiouracil reduces the effectiveness of radioiodine treatment in hyperthyroid patients with Graves' disease. Thyroid 14:525 – 530
Sarkar SD, Beierwaltes WH, Gill SP, Contey BJ (1976) Subsequent fertility and birth histories of children and adolescents treated with 131iodine for thyroid cancer. J Nucl Med 17:460 – 4
Schicha H, Scheidhauer K (1993) Radioiodine therapy in Europe – a survey. Nuklearmedizin 32:321 – 4
Shapiro B (1993) Optimization of radioiodine therapy: what have we learnt after 50 years. J Nucl Med 34:1638 – 41
Singer PA, Cooper DS, Levy EG, Ladenson PW, Braverman LE, Daniels G, Greenspan FS, McDougall IR, Nikolai TF (1995) Treatment guidelines for patients with hyperthyroidism and hypothyroidism. Standards of care committee. American Thyroid Association. JAMA 273:808 – 12
Tallstedt L, Lundell G, Blomgren H, Bring J (1994) Does early administration of thyroxine reduce the development of Graves' ophthalmopathy after radioiodine treatment. Eur J Nucl Med 130:494 – 7
Thompson WH, Harding LK (1991) Radiation protection issues associated with nuclear medicine outpatients. Nucl Med Commun 16:879 – 92
Tjerk WA, de Bruin, Carine DL, de Klerk JMH, van Isselt JW (2001) Standardized radioiodine therapy in Graves' disease: the persistent effect of thyroid weight and radioiodine uptake on outcome in: Dosage assessment for radioiodine therapy for benign thyroid disease. H van Isselt ISBN 90 393 2583 9
Tsuruta M, Nagayama Y, Izumi M, Nagataki S (1993) Long term follow-up studies on iodine-131 treatment of hyperthyroid Graves' disease based on the measurement of thyroid volume by ultrasonography. Ann Intern Med 7:193 – 7
Turner JG, Brownie BEW, Rogers TGH (1976) Lithium as an adjunct to radioiodine therapy for thyrotoxicosis. Lancet 1:614 – 615
Varma VM, Beierwaltes WH, Notal M, Nishiyama R, Copp JE (1970) Treatment of thyroid cancer. JAMA 214:1437 – 42

Wartofsky L, Glinoer D, Solomon B, Nagataki S, Lagasse R, Nagayama Y, Izumi M (1991) Differences and similarities in the diagnosis and treatment of Graves' disease in Europe, Japan and the United States. Thyroid 1:129 – 35

Wesche MF, Tie-v-Buul MM, Smits NJ, Wiersinga WM (1995) Reduction in goiter size by 131I therapy in patients with non-toxic multinodular goitre. Eur J Endocrinol 132:86 – 7

Willemsen UF, Knesewitsch P, Kreisig T, Pickardt CR, Kirsch CM (1993) Functional results of radioiodine therapy with a 300 Gy absorbed dose in Graves' disease. Eur J Nucl Med 20:1050 – 5

Williams RH, Tovery BT, Jaffe H (1949) Radiotherapies. Am J Med 7:702 – 4

22 Radioiodine Therapy: Malignant Thyroid Disease

P. Lind, I. Igerc, S. Kohlfürst

22.1 Historical Perspective and Introduction

It was more than 60 years ago in 1943 that thyroid cancer was treated for the first time. The story of radioiodine started in 1935 at the Massachusetts Institute of Technology in cooperation with the Thyroid Unit of the Massachussetts General Hospital (Stanbury 1991). Diagnostic thyroid studies were performed for the first time in 1937 using iodine-128. In 1938, not more than 1 year later, I-130 and I-131 were discovered, followed by the first treatment of benign thyroid disease in 1941. In 1946 the Oak Ridge National Laboratory produced I-131 for routine use and from this time on I-131 treatment was increasingly performed not only in benign thyroid diseases but also in differentiated thyroid cancer (DTC). It was as early as 1949 that a patient with metastasizing thyroid cancer was treated for the first time in Europe. With 1 – 2 % of all malignancies, thyroid cancer is counted among the rare neoplastic diseases (Langsteger et al. 1993). The incidence of thyroid cancer is variable in different regions but is increasing worldwide. The figures range from 1.1 in the UK up to 15.4/100,000/year in Hawaii. In our own department the age standardized ratio per 100,000 inhabitants (ASR) of thyroid cancer changed from 5.0/1.43 between 1984 and 1989 to 12.67/5.33 between 1996 and 2001 in females and males respectively (Gomez Segovia et al. 2004). In contrast to iodine deficiency, ionizing radiation to the neck, especially if received during childhood, is an important pathogenetic factor for the development of DTC. The reasons for the increase are still controversial. Interestingly, however, apart from a better diagnostic armamentarium using ultrasonography and US-guided fine needle aspiration biopsy for the detection of small cancers, also pT4 tumors (pT3b according TNM classification 2003 suppl) have increased fivefold and overall incidence has increased especially in the population of under 30 years. Thus the radioactive fallout due to the Chernobyl nuclear reactor accident should be considered as a possible pathogenic factor. It also has to be mentioned that in former iodine deficient countries, that now belong to iodine sufficient areas, mainly due to salt iodination, the incidence of DTC is increasing and histopathology has changed from follicular to papillary DTC (Lind et al. 2002). Today in countries with sufficient iodine supply or only moderate iodine deficiency, papillary thyroid cancer accounts for more than 70 – 80 % of DTC. The female to male ratio is reported to be 3:1 for papillary and 2:1 for follicular DTC (Franceschi and La Vecchia 1994). Depending on the age structure of a population, peak incidence of papillary DTC and follicular thyroid cancer ranges between 30 and 40 years and 30 and 50 years respectively (Hundahl et al. 1998). In general the prognosis of DTC is very good. However, it is worse in males than in females and mortality due to DTC is significantly higher in iodine deficient regions than in areas with adequate iodine supply. Besides appropriate surgery, meaning total or near total thyroidectomy with staging lymphadenectomy, there is evidence that the additional use of radioiodine for remnant ablation reduces recurrent and metastatic disease (Table 22.1) (Mazzaferri 2000). On the other hand, repeated high dose radioiodine therapy (RIT) is of benefit for patients with iodine positive recurrence or metastases (Robbins and Schlumberger 2005; Woodrum and Gauger 2005; Klain et al. 2002). However, one has to bear in mind that one-third of recurrences and metastases do not take up iodine or become iodine negative within the course of the disease. Therefore diagnostic modalities such as F-18-FDG PET or PET/CT should be performed in the follow-up of DTC to detect iodine negative metastases at an early stage.

Table 22.1. Recurrence and metastasis rate in patients with surgery, radioiodine therapy (RIT) and thyroid hormone treatment (THT) (A), surgery and THT (B), and surgery only (C) according to Mazzaferri (1997)

	A (%)	B (%)	C (%)	*p* value
Recurrence	7	22	35	0.001
Papillary cancer	8	23	35	0.001
Follicular cancer	7	17	33	0.03
Metastases	0	3	8	0.002

22.2 Therapeutic Approaches in DTC Before RIT

With the exception of papillary thyroid cancer pT1a (according TNM classification 2003 suppl), which is treated only by surgery, the therapy of DTC includes total thyroidectomy, radioiodine remnant ablation and TSH suppressive thyroid hormone treatment. Adjuvant external radiation therapy is still controversial. In our department it is performed in patients with a TNM classification of pT3bN1M0 and R1.

In general, the goal of thyroid surgery in DTC is the radical removal of the primary tumor and lymph node metastases in the neck. There is still, however, an ongoing discussion of how this goal can be achieved. Despite some differences between the USA and Europe, there are several arguments for performing total thyroidectomy in all tumor stages except papillary thyroid cancer pT1a: thyroid cancer is often multifocal; residual small tumors may dedifferentiate, increasing the rate of (maybe iodine negative) local recurrence and distant metastases; thyroglobulin and diagnostic I-131 whole-body scintigraphy (d-I-131 WBS) is much more difficult to interpret, if remnants persist. As it is known that multifocal DTC occurs in up to 80 % of cases, total or at least near total thyroidectomy is certainly better suited for achieving the therapeutic goal than unilateral procedures, when DTC has been proven. Papillary pT1a DTC (< 1 cm diameter), especially in younger patients, does not need a second intervention. All other tumors should be reoperated on when thyroid remnants are proven and postoperative I-131 uptake is > 10 %.

22.3 Iodine Metabolism and the Radionuclide Iodine-131

Iodine is taken up selectively by thyrocytes via the so-called sodium/iodine symporter – NIS (iodization). This mechanism allows iodine to be concentrated within the thyroid gland. Promoted by thyroid peroxidase, iodine is then bound to thyroglobulin (iodination), and stored within the colloid of the follicles. The uptake mechanism of radioactive iodine (I-123 or I-131) does not differ from nutritional iodine uptake in the normal gland. Iodine metabolism in thyroid cancer, however, is altered compared to normal tissue, mostly related to decreased expression of NIS (Klain et al. 2002). This means that iodine uptake in thyroid cancer tissue is decreased; in one-third of patients it is completely absent (iodine negative recurrence and metastases). In most patients with thyroid cancer there is also a defect of iodination, which leads to shortening of the biological half-life and a defect in hormone synthesis. In contrast to a decreased expression of NIS, thyroid stimulating hormone (TSH) receptors are found in most thyroid cancer tissues. Therefore not only the iodine uptake is stimulated by TSH but also the growth of cancer cells. TSH also increases thyroglobulin (Tg) production and release, even in tissue unable to store iodine. I-131, used for RIT, is a gamma and beta emitter and most of the radiation is delivered by beta particles with a maximum energy of 0.61 MeV, a physical half-life of 8.02 days and a medium path length in tissue of about 0.4 mm (for properties of I-131 see Table 22.2). The additional gamma-ray emission has more advantages than disadvantages. Gamma emission, with an energy of 364 MeV (81 %), allows gamma camera imaging, which enables dosimetric calculations as well as post-therapeutic whole body scintigraphy (pt-I-131 WBS) after RIT. Disadvantages include additional unwanted whole body radiation to the patient and radiation protection problems for the staff. Whereas the biological half-life in normal thyroid tissue is about 8 days, it decreases to 3 – 5 days in hyperthyroidism and is sometimes lower than 3 days in thyroid cancer.

Table 22.2. Properties of I-131

Radio-nuclide	Half-life (days)	Emax beta (MeV)	Mean range (mm)	y-energy (KeV)
Iodine-131	8.1	0.61	0.4	364 (81 %)

22.4 Clinical Indications for RIT

22.4.1 Patient Preparation

According to the national radiation protection law for high dose radioiodine therapy, a special treatment ward for open radionuclides with a special waste deposit area must be available in most countries (Figs. 22.1 – 22.3).

The patient is informed about the treatment procedure and special requirements and precautions during the time he or she is isolated in the therapy ward. A written consent form is signed by the patient and pregnancy has to be excluded in younger females before treatment. At the time of RIT the patient should be well hydrated orally and the radiation of the salivary glands should be reduced by administration of vitamin C containing drops or chewing gum. For gastric protection H_2-blockers or proton pump inhibitors, and in the case of larger remnants also corticosteroids, are administered. According to the activity administered and the national radiation regulations, the patient remains in the therapy ward for 3 – 7 days. Since recombinant human TSH (rhTSH) has been available for several years but has not been used routinely and has not been registered for each treatment indication, there are differ-

Fig. 22.1. Therapy ward at the Department of Nuclear Medicine and Endocrinology, PET/CT Center Klagenfurt

Fig. 22.2. Waste disposal area at the Department of Nuclear Medicine and Endocrinology, PET/CT Center Klagenfurt

Fig. 22.3. Waste disposal area at the Department of Nuclear Medicine and Endocrinology, PET/CT Center Klagenfurt

ences in the patient preparation. After total or near total thyroidectomy the patient should be without thyroid hormone medication for at least 4–6 weeks. During this time and especially for the last week before RIT, a low iodine diet should be prescribed. Before administration of radioiodine it is necessary that bTSH exceeds 50 mU/l and urinary iodine excretion is below 150 µg/l. Up to the late 1990s, for diagnosis and treatment of recurrent and metastatic disease, thyroid hormone had to be withdrawn for 4–6 weeks to reach elevated bTSH leading to hypothyroidism with all its side effects. For several years rhTSH has been available for the measurement of rhTSH stimulated Tg and the diagnostic I-131 WBS (Ladenson et al. 1997; Haugen et al. 1999). Recently rhTSH has also been used to simulate radioiodine uptake before treatment of recurrent and metastatic disease (Robbins et al. 2002; Lippi et al. 2001; Kohlfürst and Lind 2005). One possible schedule of rhTSH aided RIT is the following: withdrawal of thyroid hormone for 5–7 days, not leading to hypothyroidism, but lowering the iodine content of the body; intramuscular injection of 0.9 mg rhTSH on day 1 and 2; measurement of bTSH and urinary iodine excretion on day 3; administration of the therapeutic dose in the case of bTSH >50 mU/l and an iodine excretion below 150 µg/l; and post-therapeutic I-131 WBS at day 7.

22.4.2 RIT in Remnant Ablation

In most European countries, with the exception of papillary thyroid cancer pT1aN0 (TNM classification 2003 suppl) or pT1(<1 cm)N0 (TNM 2003), radioiodine remnant ablation is performed in all patients operated on for differentiated papillary and follicular thyroid cancer. One reason for this strategy is the fact that thyroid cancer may be multifocal, thus leading to an elevated risk of recurrent and metastatic disease. Mazzaferri demonstrated that after radioiodine remnant ablation at 16% the recurrence rate was significantly lower compared to 38% without RIT (Mazzaferri 2000). Also the cancer related death rate was significantly lower after RIT (2%) compared to patients who did not receive radioiodine (8%). The second reason for performing radioiodine remnant ablation is the more difficult interpretation of I-131 WBS and Tg in the case of remnant tissue. In most thyroid centers after surgery no thyroid hormone is given for 4–6 weeks. After this time the bTSH should exceed 50 mU/l in the case of total or near total thyroidectomy. A pre-therapeutic radioiodine test is performed for dose calculation or in the case of insufficient surgical treatment. Large rem-

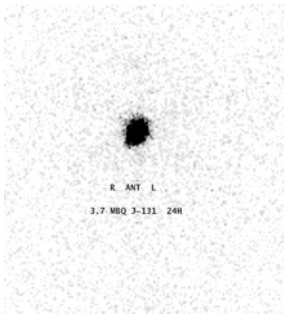

Fig. 22.4. Thyroid remnant on the left side after lobectomy on the right side and subtotal thyroidectomy on the left side: I-131 24 h uptake: 12 %. Consequence: completion thyroidectomy

nants with a 24 h radioiodine uptake above 10 % should be reoperated on (Fig. 22.4). The use of rhTSH for remnant ablation is now registered. Robbins et al. compared the outcome of radioiodine remnant ablation after withdrawal of thyroid hormone and after rhTSH (Robbins et al. 2001, 2002). Using comparable activities, remnant ablation was complete in 84 % after rhTSH and in 81 % after thyroid hormone withdrawal.

In the case of dose calculation an absorbed dose of 300 – 500 Gy should be sufficient to ablate remnants after appropriate surgery. For the fixed dose concepts there are two strategies currently in use. Most thyroid cancer centers administer activities between 2,960 and 3,700 MBq I-131 for remnant ablation. There is also evidence that activities as low as 1,100 MBq are sufficient to ablate small thyroid remnants (Van Wyngaarden and McDougall 1996; Johannsen et al. 1991). In a study by Johannsen et al. there was no difference in the postoperative ablation rate between an administered activity of 3,700 and one of 1,073 MBq I-131. Bal et al. randomized 565 thyroid cancer patients in eight groups starting with an activity of 555 MBq for ablation, increasing the activity in 185 MBq steps up to 1,850 MBq (Bal et al. 2004). The successful ablation rate was statistically significantly different in patients receiving less than 925 MBq (61.8 %) compared to those receiving more than 925 MBq (81.6 %). However, if the result after remnant ablation treatment were a thyroid bed uptake below 1 % and a TSH stimulated Tg below 0.5 ng/ml, the success rate of low activity remnant ablation might be questionable. In a comparative study between low, intermediate and high activities for remnant ablation by Comptois et al., the ablation rate was much higher for 3,700 MBq (60 – 100 %) compared to low dose activities (7 – 83 %) (Comptois et al. 1993). A further argument for higher activities is the fact that occult metastases not detectable by radioiodine scanning may be treated during the first course of RIT. There is still controversy over calculated or fixed activity and over the activity given in the case of a standard concept for fixed activities. However, one has to bear in mind that for an optimal follow-up with the highest specificity for Tg a complete remnant ablation is necessary (Fig. 22.5a, b).

22.4.3 Diagnostic I-131 WBS and Thyroid Stunning

With the exception of remnant ablation where a low activity of I-131 uptake is administered to measure the 24 h I-131 uptake within the thyroid bed, in all other situations with increasing serum Tg and the intention of high dose RIT the question of whether diagnostic I-131 WBS should be performed to localize recurrent or metastatic disease arises. However, it is known that low dose d-I-131 WBS has a low sensitivity and higher doses may lead to thyroid stunning (Coakly 1998). Leger et al. demonstrated that an activity of 185 MBq, the most frequently used activity for d-I-131 WBS, leads to thyroid stunning (Leger et al. 1998). Muratet et al. compared the post-treatment outcome using a diagnostic activity of 37 MBq and 111 MBq I-131 before treatment with 3,700 MBq I-131 (Muratet et al. 1998). Successful outcome of RIT was more frequent after a diagnostic activity of 37 MBq (76 %) than after 111 MBq (50 %). The authors recommended not to administer more than 37 MBq I-131 for diagnostic purposes. These low activities, however, are known to have a low sensitivity for detecting recurrence, lymph node or distant metastases. Therefore the question of the usefulness of a diagnostic I-131 WBS in the case of increasing serum Tg remains (Lind 1999).

22.4.4 RIT in Local Recurrent Disease

In the case of recurrent disease RIT may be the treatment of choice. If there is a larger recurrence or radioiodine uptake is faint, indicating additional iodine negative parts of the tumor, additional surgery should be performed. There is also evidence that probe-guided surgery may be of advantage in difficult cases (Fig. 22.6) (Travagli et al. 1998). It also has to be mentioned that after several courses of RIT for recurrent disease iodine negative metastases may develop. These recurrences, detectable by ultrasonography, Tc-99m-labeled cationic complexes (Tc-99m-tetrofosmin/sestamibi) and/or F-18-FDG PET, should be re-evaluated for a surgical approach (Fig. 22.7) (Lind et al. 1997, 1999, 2003). Most thyroid cancer centers use a fixed activity of 5,550 MBq I-131 for (repeated) treatment of recurrent disease followed by post-therapeutic I-131 WBS 5 days after treatment. Four to 6 months after RIT the situation should be re-evaluated by rhTSH aided serum Tg measurement. In the case of still measurable Tg (> 3 ng/ml), a repeated dose of radioiodine is administered. If there are increasing Tg levels after repeated RIT, development of iodine negative tumor cells is suspected. This development can be imaged by F-18-FDG PET or PET/CT (Fig. 22.8) and followed by surgery if technically possible.

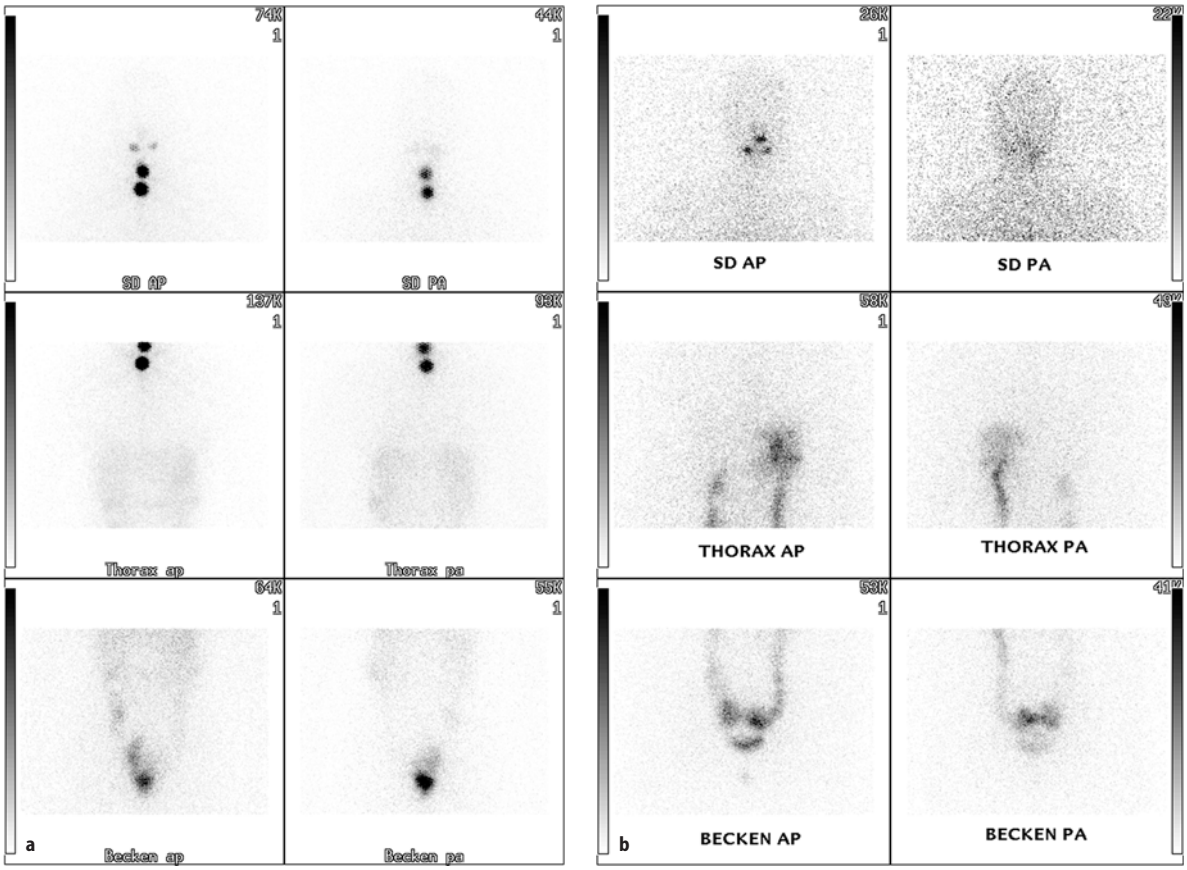

Fig. 22.5. Post-therapy I-131 WBS after 2,960 MBq: small remnant on the right side and lobus pyramidalis after near total thyroidectomy due to papillary thyroid cancer, pT2N0Mx (**a**). Four months after RIT the diagnostic I-131 WBS (185 MBq) demonstrated no iodine accumulation in the thyroid and serum Tg was negative: <0.5 ng/ml (R102) (**b**)

Fig. 22.6. Localization and preoperative marking of an iodine positive recurrence to be reoperated on. Intraoperative use of a gamma probe for exact recurrence detection

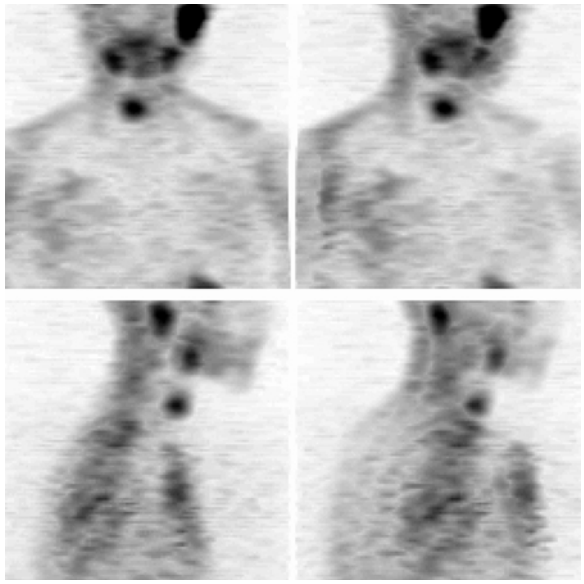

Fig. 22.7. Tc-99m-Tetrofosmin positive recurrence after 3 years after thyroidectomy and RIT. The serum Tg level increased under TSH stimulation up to 4.6 ng/ml (R99)

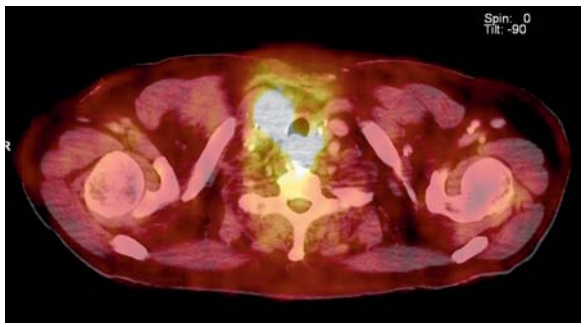

Fig. 22.8. Positive FDG PET/CT in an I-131 negative recurrence on the right side and retrotracheal

22.4.5 RIT in Lymph Node Metastases

The treatment of choice for persisting or newly developing lymph node metastases is a combination of surgery and RIT (Samann et al. 1992). Larger lymph node metastases need extensive surgery followed by RIT, whereas for small lymph node metastases (micrometastases) RIT alone can be sufficient. However, cancer cells have been found in lymph node metastases after several courses of RIT, even when Tg becomes negative. A cure of lymph node metastases after repeated courses of RIT alone, especially in larger nodes, is therefore unlikely (Fig. 22.9). Salvatori et al. treated ten patients with lymph node metastases after thyroidectomy and at least two ineffective RITs by radio-guided surgery (Salvatori et al. 2003). All patients had positive I-131 uptake in the lymph node metastases in the presurgical 3.7 GBq pt-I-131 WBS. Seven out of ten patients were negative in the subsequent pt-I-131 WBS. After radio-guided surgery the mean decrease in the absolute counts and the lesion to background count ratios were 77.6% (52.7% minimum and 94.6% maximum) and 77.4% (52.3% minimum, 94.8% maximum), respectively. After lymph node dissection, with or without probe guided assistance, an additional treatment with 5,550 MBq radioiodine is administered until TSH stimulated serum Tg levels and at least one post-therapeutic I-131 WBS are negative.

22.4.6 RIT in Distant Metastases

Distant metastases, especially from follicular thyroid cancer, develop mostly in lung, bone, brain and very rarely in the liver (Figs. 22.10, 22.11). With the exception of disseminated lung metastases, a cure by repeated RIT is unlikely. For bone, brain and liver metastases additional surgery and/or external radiotherapy can be

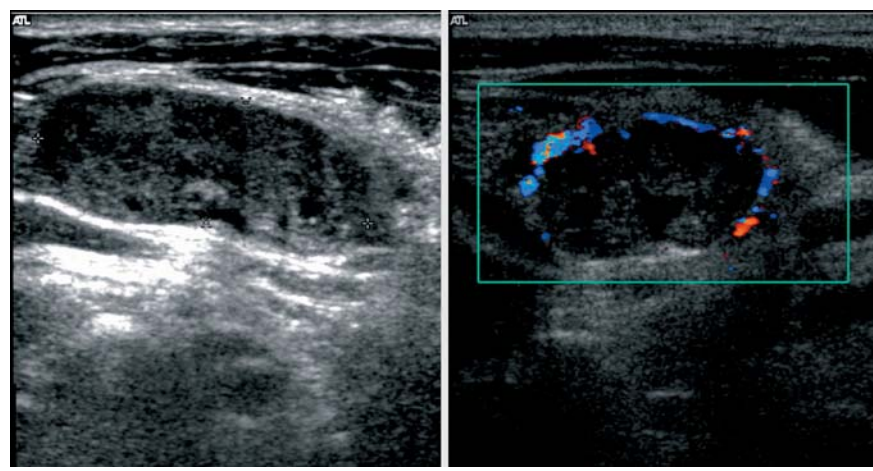

Fig. 22.9. Large sonographically hypoechogenic lymph node metastases on the right side scheduled for surgery

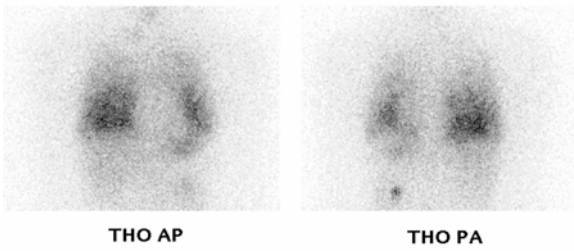

Fig. 22.10. Post-therapy I-131 WBS 5 days after 7,400 MBq I-131: diffuse I-131 uptake in both lungs

beneficial for the patient. In general, favorable prognostic factors for response to RIT in distant metastases are early detection with limited disease, younger age, relevant I-131 uptake and lack of F-18-FDG uptake. Usually activities of about 7,400 MBq are administered in patients with distant metastases. RIT can be repeated several times with 4 – 6 month intervals up to a cumulative dosis of 37, in some cases 74 GBq. For the follow-up of these patients the value of a diagnostic I-131 WBS is controversial. In our opinion it is useless, because a diagnostic I-131 WBS performed after activities of below 74 MBq has a low sensitivity and higher activities may lead to thyroid stunning, thus reducing the I-131 uptake of the following treatment (Leger et al. 1998; Muratet et al. 1998; Lind 1999). The reduction of I-131 uptake in the follow-up post-therapeutic I-131 WBS has to be correlated with a decrease of serum Tg. Decreasing I-131 uptake but increasing serum Tg in the course of repeated RIT is an indicator of cell dedifferentiation and progressive disease (Fig. 22.12a, b). In this case further courses of RIT are not indicated. Haq et al. as-

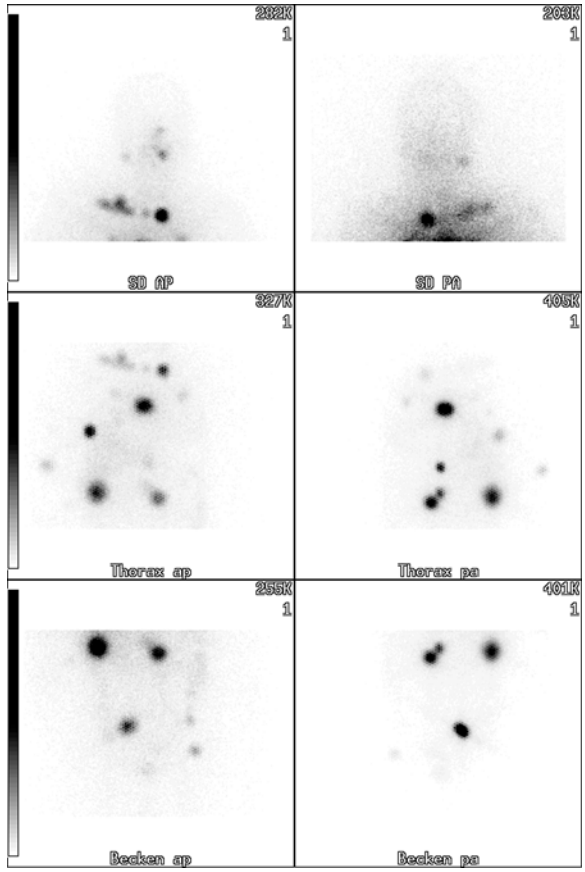

Fig. 22.11. Post-therapy I-131 WBS 5 days after 7,400 MBq I-131: multiple I-131 positive bone metastases from follicular thyroid cancer

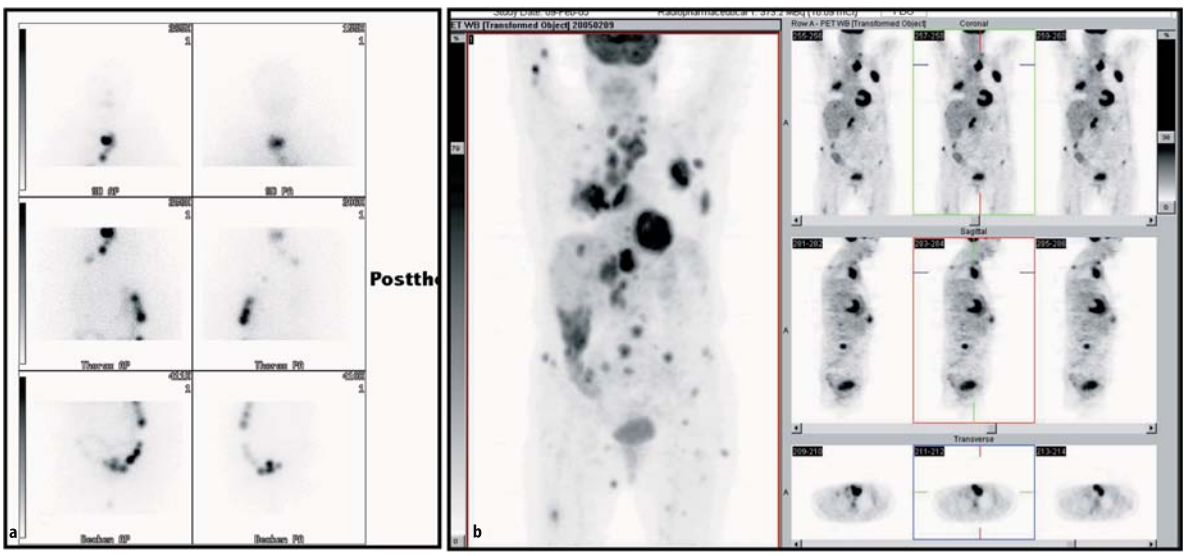

Fig. 22.12. Post-therapy I-131 WBS (**a**) with I-131 positive local recurrence. Increasing serum Tg despite three times high dose RIT: FDG PET demonstrates the extent of the disease with multiple lung bone and soft tissue metastases (**b**)

sessed the efficacy and morbidity of repeated high dose RIT in advanced thyroid cancer (Haq et al. 2004). In the 38 treated patients the cumulative activities ranged from 11.8 to 84.5 GBq (mean 29.4 GBq per patient). The mean duration of follow-up was 83 months. A complete response was observed in 18.4%, stable disease in 10.5% and progressive disease in 71.1%. The authors conclude that repeated RIT in advanced thyroid cancer appears to be of no apparent benefit and may lead to late morbidity. With the early use of F-18-FDG PET or PET/CT, additional iodine negative metastases are easily detectable. In the case of mixed iodine positive and negative metastases or only iodine negative, FDG positive metastases, further RIT is of no benefit to the patient. However, the treatment of I-131 negative, FDG PET positive metastases remains difficult. There are data for an effect of redifferentiation using retinoic acid followed by high dose RIT in about 40% of patients (Grünwald et al. 1998; Simon et al. 2002). Also the effect of somatostatin receptor analogues in this situation is still controversial (Robbins et al. 2000).

In rare cases metastases from differentiated thyroid cancer may produce hyperthyroidism (Fig. 22.13). In these cases anti-thyroid drug premedication can be necessary. The amount of activity given to these patients needs dosimetric data acquired over 4 days, which is, however, not easy to obtain (Sisson and Carey 2001).

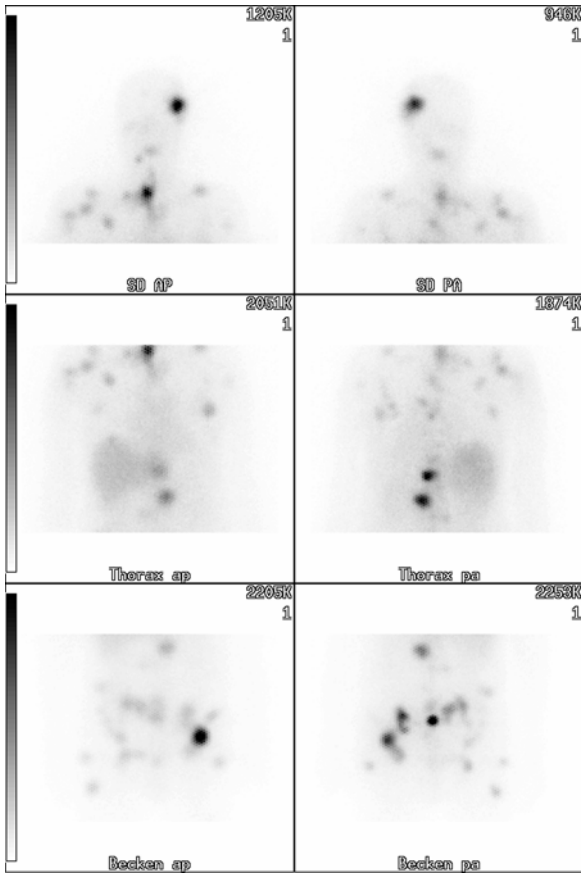

Fig. 22.13. Post-therapy I-131 WBS 5 days after 3,700 MBq I-131: multiple I-131 positive bone metastases producing overt hyperthyroidism

22.4.7 Lung Metastases

In a study by Schlumberger, complete remission occurred in 83% of patients with disseminated lung metastases (normal X-ray) but only in 53% with micronodular and 15% with macronodular lung metastases (Schlumberger 1998). In the case of disseminated lung metastases, repeated RIT can cure the patient (Fig. 22.14). In the case of nodular lung metastases, RIT must be considered as palliative treatment. Ilgan et al. reported on the treatment response and value of high

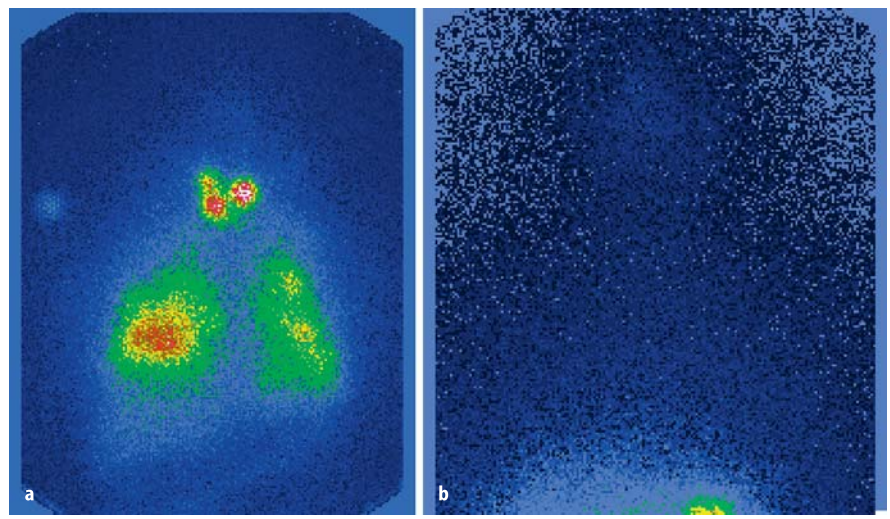

Fig. 22.14. Post-therapy I-131 WBS 5 days after 7,400 MBq I-131: Remnant and disseminated I-131 positive lung metastases after the first treatment (**a**) and negative I-131 WBS after 6 times RIT with a cumulative dose of 44 GBq (Tg 1.2 ng/ml, R89) (**b**)

resolution CT in patients with lung metastases (Ilgan et al. 2004). A total of 42 out of 1,023 patients with thyroid cancer (4%) had lung metastases, 30 at the time of diagnosis and 12 during the follow-up period. Applied single and total activity were 1.8–10.4 GBq and 5.5–43.7 GBq respectively. Twelve patients with advanced metastatic disease died of thyroid cancer, one due to second malignancy. Ten patients were completely free of disease, and 7 were stable at the time of the study. Despite negative chest X-ray in 14 patients, high resolution CT detected metastases in 10 out of them.

22.4.8 Bone Metastases

Like lung metastases bone metastases are also frequent in thyroid cancer patients (Fig. 22.15). Sometimes in advanced stages follicular thyroid cancer is diagnosed via pain due to bone metastases. Several authors gave the recommendation that, if possible, in case of bone metastases surgical resection to debulk the tumor mass should be performed followed by high dose RIT (Mazzaferri 2000; Sweeney and Jonston 1995). Additional external radiation therapy is also an adjuvant treatment option in case of bone metastases (Schlumberger et al. 1996; Tubiana 1981). RIT alone is hardly able to cure patients from bone metastases, but has a palliative effect. However, Petrich et al. conclude in their study on the effectiveness of RIT in bone metastases that in patients younger than 45 years and small numbers of metastases patients can be treated with curative intention (Petrich et al. 2001a). Eight out of 107 patients with bone metastases due to thyroid cancer were younger, 99 older, than 45 years in this retrospective study. Total or partial remission was more frequent in the younger group (62.5%) compared to the group aged over 45 (49.5%).

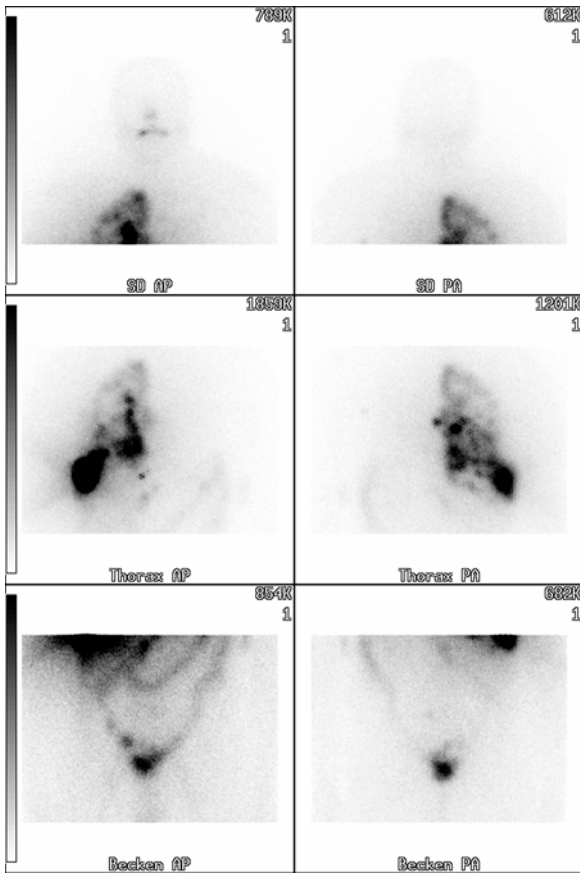

Fig. 22.15. Post-therapy I-131 WBS 5 days after 7,400 MBq I-131: Pleural and lung metatstases on the right side. There is an additional huge bone metastasis in the right thorax (ribs) which was additionally treated by external radiotherapy

22.4.9 Brain Metastases

With a frequency <1% brain metastases are rare in DTC. If diagnosed, neurosurgery should be performed followed by RIT in the case of iodine accumulation (Fig. 22.16). RIT, however, has to be performed under the administration of corticosteroids. Although patients with brain metastases have a poor prognosis, there is some evidence that RIT may prolong survival (Chiu et al. 1997). In a review by McWilliams et al. on 16 patients with brain metastases from thyroid cancer, surgical resection was associated with a trend towards longer survival (20.8 months vs. 2.7 months) (McWilliams et al. 2003). Of 12 patients with brain metastases (five anaplastic, six differentiated, one medullary thyroid cancer) reported by Salvati et al., none of them demonstrated I-131 uptake (Salvati et al. 2001). All metastases were surgically removed and all patients were treated with external radiotherapy (45 Gy). The value of RIT in brain metastases is, however, not proven.

22.4.10 Side Effects of RIT

Compared to the benefits of RIT, the side effects are not serious, especially in uncomplicated cases when the patient is cured after one ablative dose of radioiodine. If surgery was not appropriate and a larger remnant has to be treated by radioiodine, thyroiditis is a common side effect. Administration of corticosteroids, however, can reduce local pain during the treatment period. Corticosteroids must also be administered for the treatment of brain metastases and bone metastases in the case of neural compression. In about 30% of cases acute swelling of the salivary gland can occur. Although lemon candy or vitamin C containing drops are generally recommended, there is evidence from a recent study that lemon candy should not be given until 24 h after RIT. An early administration may induce a signifi-

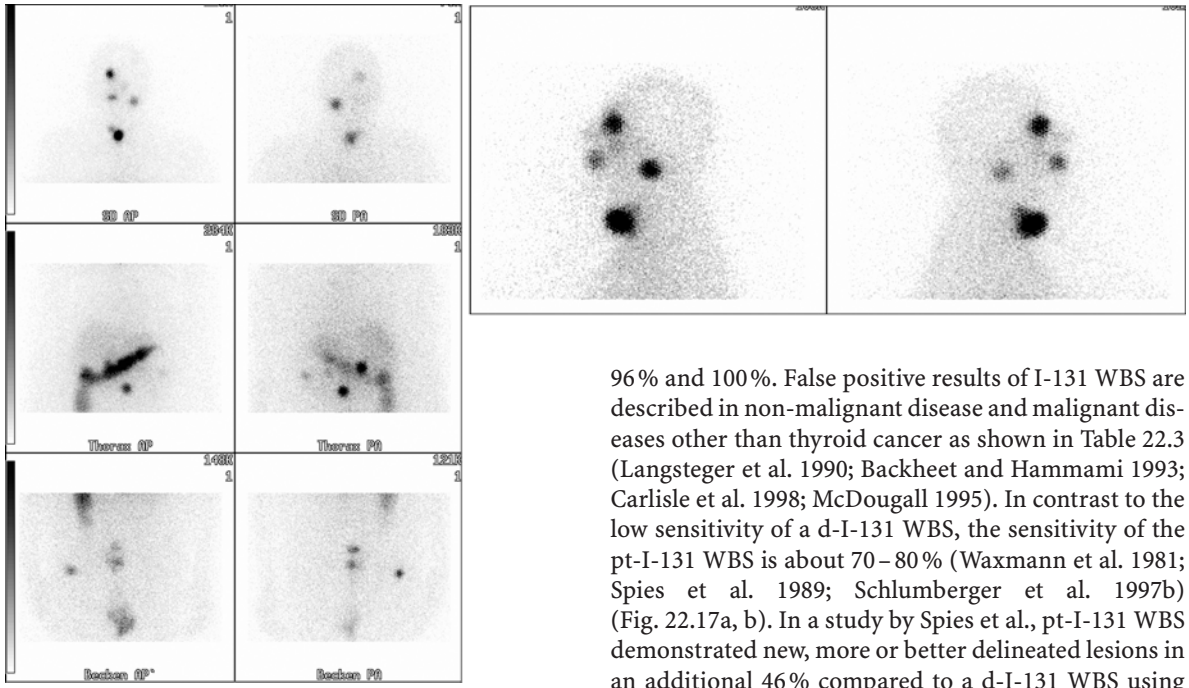

Fig. 22.16. Post-therapy I-131 WBS 5 days after 7,400 MBq I-131: Two residual I-131 positive brain metastases after neurosurgery in the right frontal and left cerebellar regions; additional local recurrence and bone metastases

cant increase in salivary gland damage (Nakada et al. 2005). After several courses of RIT a dry mouth may remain as a late complication. There is also evidence that after repeated RIT an impairment of the lacrimal glands may occur (Zettinig et al. 2002). In about 5% of patients thrombocytopenia and leukopenia develop depending on the cumulative dose administered. In the case of disseminated lung metastases and repeated RIT, fibrosis of the lung may occur. Miscarriages are very rare and occur only in the first year after RIT. Also gonadal dysfunction in men is observed only in single cases (Schlumberger et al. 1997a; Winters and Berga 1997).

22.5 Post-therapy I-131 Whole Body Scintigraphy and Non-Specific Tracers to Detect I-131 Negative Metastases

Five to 7 days after RIT using high activities of I-131, a post-therapeutic I-131 WBS (pt-I-131 WBS) is acquired to localize I-131 uptake. The acquisition should be performed as spot imaging in anterior and posterior projections from the head and neck, thorax, abdomen and pelvis using a gamma camera with a high energy all purpose collimator. The specificity of a pt-I-131 WBS does not differ from a d-I-131 WBS and ranges between 96% and 100%. False positive results of I-131 WBS are described in non-malignant disease and malignant diseases other than thyroid cancer as shown in Table 22.3 (Langsteger et al. 1990; Backheet and Hammami 1993; Carlisle et al. 1998; McDougall 1995). In contrast to the low sensitivity of a d-I-131 WBS, the sensitivity of the pt-I-131 WBS is about 70–80% (Waxmann et al. 1981; Spies et al. 1989; Schlumberger et al. 1997b) (Fig. 22.17a, b). In a study by Spies et al., pt-I-131 WBS demonstrated new, more or better delineated lesions in an additional 46% compared to a d-I-131 WBS using 185 MBq (Spies et al. 1989). Pacini et al. demonstrated that out of 17 patients with elevated serum Tg but negative d-I-131 WBS (185 MBq), 16 showed an I-131 positive lesion after high dose RIT (Pacini et al. 1987). Similar results were found by Pineda et al. (1995). However, the topic is still controversial (Lind 2003; Biermann and Schober 2003). In the case of only faint uptake in the pt-I-131 WBS, SPECT may be of advantage. The resolution of an I-131 WBS is limited and the possibility of localizing the lesions is often difficult. A combination of SPECT/CT will bring an improvement in lesion localization. In a study by Ruf et al. the combination of SPECT/CT changed the interpretation of I-131 scans in 38% on a lesions basis and in 25% on a patients basis. In addition fused images were able to rule out most of the artifacts (Ruf et al. 2004). However, the extent of I-131 positive lesions must be correlated with the serum Tg level. One-third of metastases are less differentiated, and in addition in the course of several radioiodine therapies a dedifferentiation of metastases may occur. Although the prognosis of differentiated thyroid cancer

Table 22.3. False positive I-131 retention in non-tumorous diseases and other malignancies (from Lind 1999)

Non-tumors	Tumors
Sinusitis	Salivary adenocarcinoma
Dental disease	Meningeoma
Tracheostoma	Lung cancer
Gallbladder	Thymus (lymphoma)
Zenker's diverticulum	Ovarian cancer
Plaque of psoriasis	Teratoma
Rheumatoid arthritis	Neurilemoma
Hiatal hernia, achalasia	Gastric adenocarcinoma

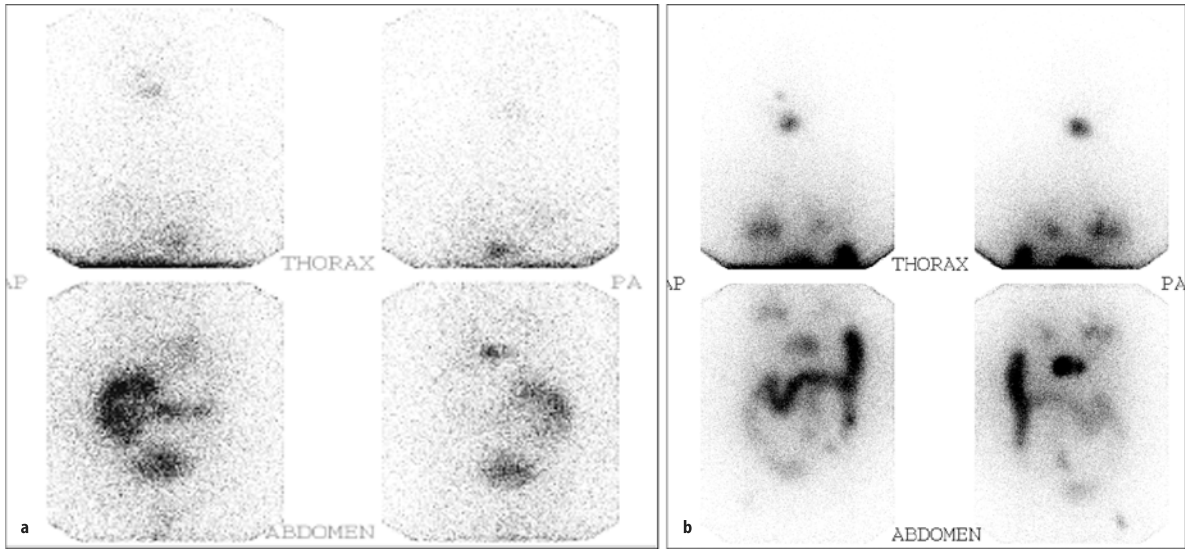

Fig. 22.17. a Diagnostic I-131 WBS demonstrating a bone metastasis in vertebra X. **b** Post-therapy I-131 WBS after 7,400 MBq is much more sensitive, giving a better delineation of the bone metastasis and showing additional lung metastases

is excellent, with a 10 year survival of 96 % for papillary and 80 % for follicular thyroid cancer, the presence or development of I-131 negative metastases is associated with a clear decrease in survival. In addition to I-131 WBS, which detects iodine positive recurrences and metastases, there is a need for non-specific tracers, which accumulate in iodine negative lesions. Tl-201 and newer agents such as Tc-99m-sestamibi or Tc-99m-tetrofosmin are able to detect most of the I-131 positive as well as I-131 negative metastases (Lind et al. 1999). However, the resolution of a single photon emitter is limited and about 20 – 25 % of less differentiated metastases are not detectable using conventional radionuclides and tracers. To overcome this problem FDG positron emission tomography (PET) was introduced in the follow-up of thyroid cancer patients (Feine et al. 1996). According to the recent German consensus conference in 2000, the follow-up of thyroid cancer in patients with elevated serum Tg but negative I-131 WBS belongs to a 1a indication for F-18-FDG PET (Reske and Kotzerke 2001). The first investigations using FDG PET in the follow-up of differentiated thyroid cancer have already demonstrated that F-18-FDG uptake represents less differentiated thyroid cancer cells or dedifferentiation of cells. Feine and coworkers investigated 41 patients, comparing F-18-FDG PET and I-131 WBS in the follow-up of differentiated thyroid cancer (Feine et al. 1996). Combined imaging resulted in a sensitivity of about 95 % in detecting recurrences and metastases. Alternating uptake (I-131 negative but F-18-FDG positive or I-131 positive and F-18-FDG negative) was found in 90 % of patients. The authors conclude that beside an increase of sensitivity using I-131 WBS and F-18-FDG PET, uptake of F-18-FDG seems to be an indicator for poor differentiation. In a multicenter trial, Grünwald et al. compared the sensitivity and specificity of F-18-FDG PET, I-131 WBS and Tc-99m-sestamibi/Tl-201 WBS (Grünwald et al. 1999). The sensitivity of F-18-FDG PET, I-131 WBS and Tc-99m-sestamibi/Tl-201 was 75 %, 50 % and 53 % and specificity 90 %, 99 % and 92 % respectively. The sensitivity of F-18 FDG PET increased to 85 % in a subgroup of patients with I-131 negative WBS. In an older study with a smaller group of patients, Grünwald et al. demonstrated that F-18-FDG uptake is better correlated to Tc-99m-sestamibi than to I-131 scintigraphy (Grünwald et al. 1997). Similar results were obtained by our group comparing F-18-FDG PET, Tc-99m-tetrofosmin WBS and post-therapeutic I-131 WBS in the follow-up of thyroid cancer in 35 patients (Lind et al. 2000). According to the German consensus conference in 2000, sensitivity and specificity of F-18-FDG PET in detecting I-131 negative metastases in the case of elevated thyroglobulin were 85 – 94 % and 90 – 95 %, respectively (Reske and Kotzerke 2001). In a study by Schlütter and coworkers, a total of 118 F-18-FDG PET studies in 64 patients with elevated thyroglobulin but negative I-131 WBS with respect to change of therapy due to outcome of F-18-FDG PET were performed (Schluetter et al. 2001). Forty-four patients had positive F-18-FDG PET (34 true positive, 7 false positive, 2 with secondary malignancy, 1 non-evaluable), and 20 patients had negative PET scans (5 true negative, 15 false negative). According to these results, the positive predictive value (PPV) was 83 %, the negative predictive value (NPV) only 25 %. Treatment strategy was changed in 19 of 34 patients with true positive PET scans. It has to be mentioned that the sensitivity of F-18-FDG PET is higher under endogenous or exogenous

TSH stimulation. Moog and coworkers investigated ten thyroid cancer patients under TSH suppressive L-thyroxine therapy and after withdrawal of L-thyroxine (TSH >22 mU/l). They demonstrated that the tumor-to-background ratio increased after TSH stimulation from 3.85 to 5.84 ($p<0.001$) (Moog et al. 2000). Similar preliminary results with an increase of the standardized uptake value from 1.3 to 4.4 are reported by Petrich et al. using recombinant TSH before F-18-FDG PET (Petrich et al. 2001b).

22.6 Future Expectations

22.6.1 Recombinant TSH

One of the big issues for thyroid cancer patients in recent years has been the introduction of recombinant TSH for the follow-up of differentiated thyroid cancer (Mazzaferri and Kloos 2000). The advantage for the patients is the lack of hypothyroid symptoms after several weeks withdrawal of thyroid hormone for performing a d-I-131 WBS and measuring TSH stimulated serum Tg. Based on a European expert group on thyroid cancer, for low risk patients, with negative d-131 WBS and TSH stimulated Tg 1 year after surgery and radioiodine remnant ablation, rhTSH stimulated serum Tg and sonography are sufficient for the subsequent follow-up of patients (Schlumberger et al. 2004). Much more important than the use of rhTSH for diagnostic purposes is the short term elevation of TSH for RIT by rhTSH. Because most of the recurrent and metastatic thyroid cancer cells express TSH receptors, a long term TSH elevation, as it is produced by withdrawal of thyroid hormones for several weeks for radioiodine administration, may lead to growth of tumor cells that exceed the effect of RIT. In contrast to remnant ablation, which may also be an indication for rhTSH, the most important impact for rhTSH is the treatment of metastatic disease with radioiodine (Robbins et al. 2002; Lippi et al. 2001; Barbaro et al. 2004; Pacini et al. 2002). De Keizer et al. performed dosimetric calculations after rhTSH aided RIT. Although they found a variable tumor radiation of between 1.3 and 36.8 Gy (mean: 26.3 Gy), treatment led to disease stabilization in 45% of cases (deKeizer et al. 2003). There is an increasing number of thyroid cancer centers that treat patients under rhTSH. In our center rhTSH has been administered routinely to all thyroid cancer patients for follow-up since 2001 and many of the patients with recurrent or metastatic disease have been treated under rhTSH since that time with good results (Kohlfürst and Lind 2005). In single cases when comparing the pt-I-131 WBS after withdrawal of thyroid hormones and rhTSH, the uptake seems sometimes a little lower with rhTSH. However, rhTSH aided RIT is one of the significant advances in thyroid oncology and an enormous advantage for the patients.

22.6.2 Combined SPECT/CT and PET/CT

The direction of imaging in the future is toward a better anatomical localization of metabolic active tumor lesions using different radionuclides and tracers such as somatostatin receptor analogues. Post-therapeutic I-131 WBS combined with SPECT/CT will be the imaging modality of choice after RIT. In combination with F-18 FDG PET/CT, the complete extent of the disease with exact anatomical localization of iodine positive and iodine negative lesions will be available (Lind and Igerc 2004). This is not only important for exact staging and restaging of metastasizing thyroid cancer but also for an individual based multimodality treatment of these patients, including RIT, surgery, external radiotherapy, retinoic acid and somatostatin receptor therapy (Figs. 22.18 – 22.20).

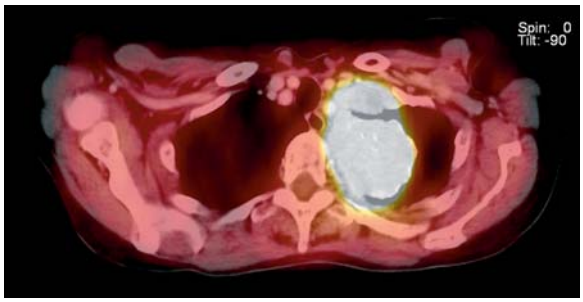

Fig. 22.18. FDG PET/CT in a patient with lung metastasis infiltrating the pleura

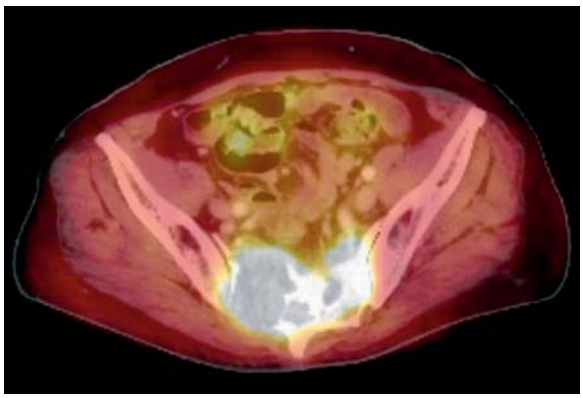

Fig. 22.19. Sixty-three-year-old male after thyroidectomy and four times RIT due to follicular thyroid cancer, pT4NxM1R1; bone metastases in the sacrum; PET/CT changed the radiation field also including the left part of the sacrum

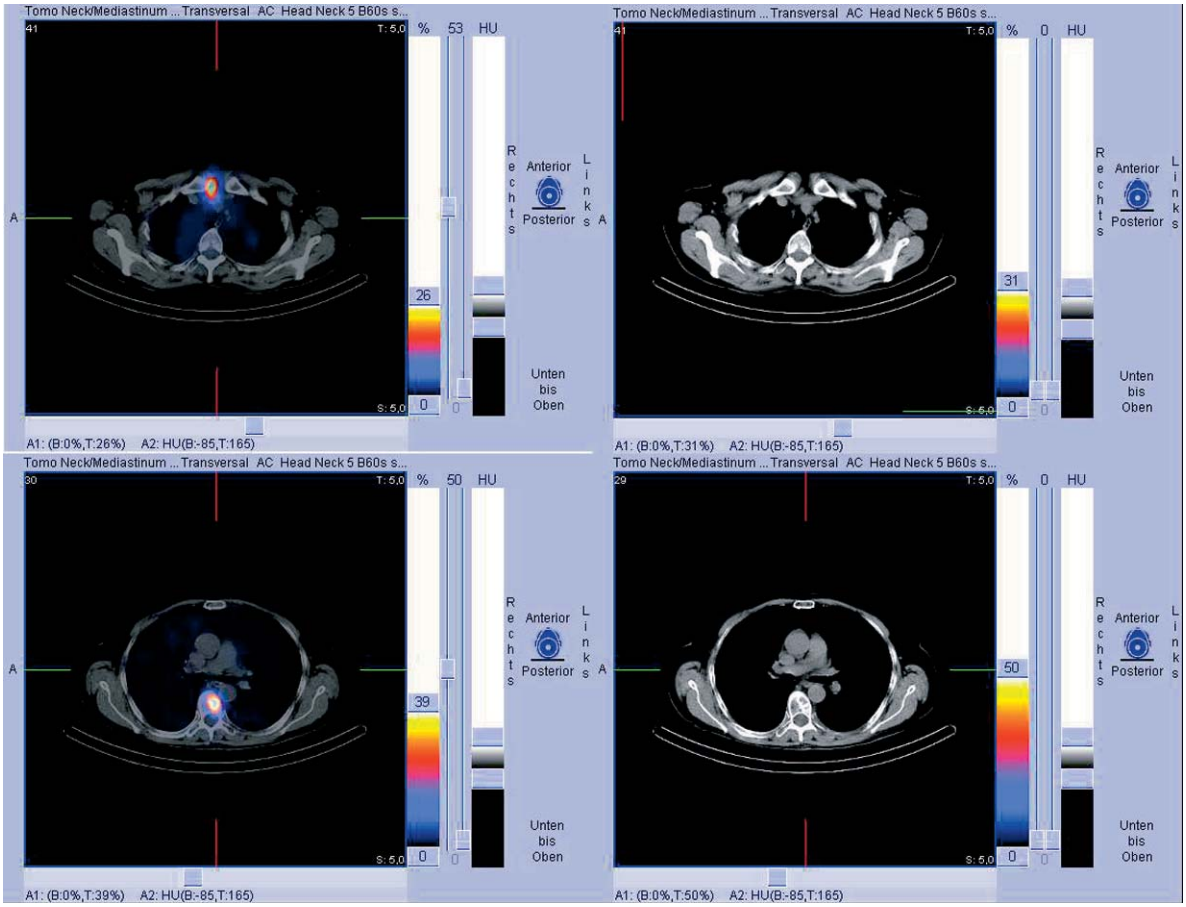

Fig. 22.20. 58 year old female after 2 times thyroidectomy and 5 times radioiodine therapy due to metastasing follicular thyroid cancer. Planar post-therapy I-131 WBS demonstrated two areas with focal midline uptake in the mediastinum without possibility to differentiate between local recurrence, lymph node metastases and bone metastases. Spect/CT demonstrated clear localisation in a local recurrence of the upper active area (*upper row*) and a bone metastasis of the lower active area (*lower row*). The consequence was additional external radiotherapy of the bone metastasis and surgery of the local recurrence

22.6.3 Dosimetry Using I-124 PET

As dosimetry is very cumbersome for RIT, especially in metastatic disease, new ways to adapt the administered activity to the individual patient's need are desirable. One possibility is the use of I-124 PET in combination with a three-dimensional-internal dosimetry software. Sgouros et al. performed three to four I-124 PET imaging studies over a period of 7 days to calculate the individual dose for patients with metastatic thyroid cancer (Sgouros et al. 2004). Mean absorbed dose values and absorbed dose for individual tumors ranged from 1.2 to 540 Gy and from 0.3 to 4,000 Gy, respectively. In the future I-124 PET may play an important role in the individual dosimetry of patients with metastatic thyroid cancer.

References

Backheet S, Hammami MM (1993) False positive thyroid cancer metastases on whole-body radioiodine scanning due to retained radioactivity in the oesophagus. Eur J Nucl Med 20:415

Bal CS, Kumar A, Pant GS (2004) Radioiodine dose for remnant ablation in differentiated thyroid carcinoma: a randomized clinical trial in 509 patients. J Endocrinol Metab 89:1666–1673

Barbaro D, Boni G, Meucci G, et al. (2004) Radioiodine treatment with 30 mCi after recombinant human thyrotropin stimulation in thyroid cancer: effectiveness for postsurgical remnant ablation and possible role of iodine content in L-thyroxine in the outcome of ablation. J Endocrinol Metab 88:4110–4115

Biermann M, Schober O (2003) Should high hTg levels in the absence of iodine uptake be treated? Eur J Nucl Med 30:160–163

Carlisle M, Cortes A, McDougall IR (1998) Uptake of I-131 in the bilary tract: a potential cause of false positive result of scintiscan. Clin Nucl Med 23:524–527

Chiu AC, Delpassand ES, Sherman SI (1997) Prognosis and treatment of brain metastases in thyroid carcinoma. J Clin Endocrinol Metab 82:3637 – 3642
Coakly AJ (1998) Thyroid stunning. Eur J Nucl Med 25:203 – 204
Comptois R, Theriault C, Del Vecchio P (1993) Assessment of efficacy of iodine-131 for thyroid ablation. J Nucl Med 34: 1727 – 1730
deKeizer B, Brans B, Hoekstra A, et al. (2003) Tumor dosimetry and response in patients with metastatic differentiated thyroid cancer using recombinant human thyrotropin before radioiodine therapy. Eur J Nucl Med Mol Imaging 30:367 – 373
Feine U, Lizenmayer R, Hanke JP, et al. (1996) Fluorine-18 FDG and iodine-131 uptake in thyroid cancer. J Nucl Med 37: 1468 – 1472
Franceschi S, La Vecchia C (1994) Thyroid cancer. Cancer Survey 19 – 20:393 – 422
Gomez Segovia I, Gallowitsch HJ, Kresnik E, et al. (2004) Descriptive epidemiology of thyroid carcinoma in Carinthia, Austria: 1984 – 2001. Histological features and tumor classification of 734 cases under elevated general iodination of table salt since 1990: population based age stratified analysis on thyroid carcinoma incidence. Thyroid 14:277 – 286
Grünwald F, Menzel C, Bender H, et al. (1997) Comparison of 18FDG-PET with 131-iodine and 99mTc-sestamibi scintigraphy in differentiated thyroid cancer. Thyroid 7:327 – 335
Grünwald F, Menzel C, Bender H, et al. (1998) Redifferentiation therapy-induced radioiodine uptake in thyroid cancer. J Nucl Med 39:1903 – 1906
Grünwald F, Kalicke T, Feine U, et al. (1999) Fluorine-18-fluorodeoxyglucose positron emission tomography in thyroid cancer: results of a multicenter study. Eur J Nucl Med 26:1547 – 1552
Haq MS, McCready RV, Harmer CL (2004) Treatment of advanced differentiated thyroid carcinoma with high activity radioiodine therapy. Nucl Med Commun 25:799 – 805
Haugen BR, Pacini F, Reiners C, et al. (1999) A comparison of recombinant human thyrotropin and thyroid hormone withdrawal for the detection of remnant or cancer. J Endocrinol Metab 84:3877 – 3885
Hundahl SA, Fleming ID, Fremgen AM, Menk HR (1998) A national cancer data base report on 53,856 cases of thyroid carcinoma treated in the U.S. 1985 – 1995. Cancer 82:2638 – 2648
Ilgan S, Karacalioglu AO, Pabuscu Y, et al. (2004) I-131 treatment and high resolution CT: results in patients with lung metastases from differentiated thyroid carcinoma. Eur J Nucl Med Mol Imaging 31:825 – 830
Johannsen K, Woodhouse NJ, Odugbesan O (1991) Comparison of 1073 MBq and 3700 MBq iodine-131 in postoperative ablation of residual thyroid tissue in patients with differentiated thyroid cancer. J Nucl Med 32:1640 – 1641
Klain M, Ricard M, Leboulleux S, et al. (2002) Radioiodine therapy for papillary and follicular thyroid carcinoma. Eur J Nucl Med 29:S479–S485
Kohlfürst S, Lind P (2005) Recombinant human thyrotropin (rhTSH) is helpful in the follow up and I-131 therapy of patients with thyroid cancer. A report of the results and benefits using rhTSH in clinical routine. Thyroid (in press)
Ladenson PW, Braverman LE, Mazzferri EL, et al. (1997) Comparison of administration of recombinant human thyrotropin with withdrawal of thyroid hormone for radioactive iodine scanning in patients with thyroid carcinoma. N Engl J Med 337:888 – 896
Langsteger W, Lind P, Költringer P, et al. (1990) Misinterpretation of iodine uptake in papillary thyroid carcinoma and primary lung adenocarcinoma. J Cancer Res Clin Oncol 116:8 – 12
Langsteger W, Költringer P, Wolf G, et al. (1993) The impact of geographical, clinical, dietary and radiation-induced features in epidemiology of thyroid cancer. Eur J Cancer 11:1547 – 1553
Leger FA, Izembart M, Dagousset F, et al. (1998) Decreased uptake of therapeutic doses of iodine-131 after 185 MBq iodine-131 diagnostic imaging for thyroid remnants in differentiated thyroid carcinoma. Eur J Nucl Med 25:242 – 246
Lind P (1999) I-131 whole-body scintigraphy in thyroid cancer patients. Q J Nucl Med 43:188 – 194
Lind P (2003) Should high hTg levels in the absence of iodine uptake be treated? Eur J Nucl Med 30:157 – 160
Lind P, Igerc I (2004) PET and PET/CT in the following up of thyroid cancer patients in thyroid cancer. In: Langsteger W, Sungler P, Lind P, Niederle B (eds) KOOP, Vienna. CD Rom
Lind P, Gallowitsch HJ, Langsteger W, et al. (1997) Tc-99m tetrofosmin whole body scintigraphy in the follow up of differentiated thyroid carcinoma. J Nucl Med 38:348 – 352
Lind P, Gallowitsch HJ, Mikosch P, Kresnik E, et al. (1999) Comparison of different tracers in the follow up of differentiated thyroid carcinoma. AMA 26:115 – 118
Lind P, Kumnig G, Matschnig S, et al. (2000) The role of F-18-FDG PET in thyroid cancer. AMA 27:38 – 41
Lind P, Kumnig G, Heinisch M, et al. (2002) Iodine supplementation in Austria: methods and results. Thyroid 12:903 – 907
Lind P, Kresnik E, Kumnig G, et al. (2003) F-18-FDG PET in the follow up of thyroid cancer. AMA 30:17 – 21
Lippi F, Cappezone M, Angelini F, et al. (2001) Radioiodine treatment of metastatic differentiated thyroid cancer in patients on L-thyroxine, using recombinant human TSH. Eur J Endocrinol 144:5 – 11
Mazzaferri EL (1997) Thyroid remnant I131 ablation for papillary and follicular thyroid carcinoma. Thyroid 7:265 – 271
Mazzaferri EL (2000) Carcinoma of follicular epithelium: radioiodine and other treatment outcomes. In: Braverman LE, Utiger RD (eds) The thyroid: a fundamental and clinical text, 8th edn. Lippincott-Raven, Philadelphia, pp 922 – 945
Mazzaferri E, Kloos R (2000) Recombinant human TSH in the management of well-differentiated thyroid cancer: Current strategies and future directions. Thyroid 10:767 – 778
McDougall IR (1995) Whole body scintigraphy with radioiodine-131. A comprehensive list of false positives with some examples. Clin Nucl Med 20:869 – 875
McWilliams RR, Giannini G, Hay ID, et al. (2003) Management of brain metastases from thyroid carcinoma: a study of 16 pathologically confirmed cases over 25 years. Cancer 98:356 – 362
Moog F, Linke R, Manthey N, et al. (2000) Influence of thyroid-stimulating hormone levels on uptake of FDG in recurrent and metastatic differentiated thyroid carcinoma. J Nucl Med 41:1989 – 1995
Muratet JP, Daver A, Minier JF, Larra F (1998) Influence of scanning doses of iodine-131 on subsequent first ablative treatment outcome in patients operated on for differentiated thyroid carcinoma. J Nucl Med 39:1546 – 1550
Nakada K, Ishibashi T, Takei T, et al. (2005) Does lemon candy decrease salivary gland damage after radioiodine therapy for thyroid cancer? J Nucl Med 46:261 – 266
Pacini F, Lippi F, Formica N, et al. (1987) Therapeutic doses of I-131 reveal undiagnosed metastases in thyroid cancer patients with detectable serum thyroglobulin levels. J Nucl Med 38:1888 – 1891
Pacini F, Molinaro E, Castagna MG, et al. (2002) Ablation of thyroid residues with 30 mCi I-131: a comparison in thyroid cancer patients with recombinant TSH or thyroid hormone withdrawal. J Clin Endocrinol Metab 87:4059 – 4062
Petrich T, Widjaja A, Musholt TJ, et al. (2001a) Outcome of radioiodine therapy in 107 patients with differentiated thyroid

carcinoma and initial bone metastases: side effects and influence of age. Eur J Nucl Med 203 – 208
Petrich T, Börner AR, Weckesser E, et al. (2001b) Follow up of thyroid cancer patients using rhTSH – preliminary results. Nucl Med 40:7 – 14
Pineda JD, Lee T, Ain K, et al. (1995) I-131 therapy for thyroid cancer patients with elevated thyroglobulin and negative diagnostic scan. J Endocrinol Metab 80:1488 – 1492
Reske SN, Kotzerke J (2001) FDG PET for clinical use. Results of the 3rd German Interdisciplinary Consensus Conference, "Onko PET III", 21st July and 19th September 2000. Eur J Nucl Med 28:1707 – 1723
Robbins RJ, Schlumberger MJ (2005) The evolving role of I-131 for the treatment of differentiated thyroid carcinoma. J Nucl Med 46:28S–37S
Robbins JR, Hill RH, Wang W, et al. (2000) Inhibition of metabolic activity in papillary thyroid carcinoma by a somatostatin analogue. Thyroid 10:177 – 183
Robbins RJ, Tuttle RM, Sonenberg M, et al. (2001) Radioiodine ablation of thyroid remnants after preparation with recombinant human thyrotropin. Thyroid 11:865 – 869
Robbins RJ, Larson SM, Sinha N, et al. (2002) A retrospective review of the effectiveness of recombinant human TSH as a preparation for radioiodine thyroid remnant ablation. J Nucl Med 43:1482 – 1488
Ruf J, Lehmkuhl L, Bertram H, et al. (2004) Impact of SPECT and integrated low dose CT after radioiodine therapy on the management of patients with thyroid carcinoma. Nucl Med Commun 1177 – 1182
Salvati M, Frati A, Rocchi G, et al. (2001) Single brain metastases from thyroid cancer: report of twelve cases and review of literature. J Neurooncol 51:33 – 40
Salvatori M, Rufini V, Reale F, et al. (2003) Radio-guided surgery for lymph node recurrences of differentiated thyroid cancer. World J Surg 27:770 – 775
Samann NA, Schultz PN, Hickey RC, Goepfert H, Haynie TP, Jonston DA, Ordonez NG (1992) The results of various modalities of treatment of well differentiated thyroid carcinomas: a retrospective review of 1599 patients. J Clin Endocrinol Metab 75:714 – 720
Schluetter B, Bohuslavizki KH, Beyer W, et al. (2001) Impact of FDG PET on patients with well differentiated thyroid cancer who present with elevated thyroglobulin and negative I-131 scan. J Nucl Med 42:71 – 76
Schlumberger M (1998) Papillary and follicular thyroid carcinoma (review). N Engl J Med 338:297 – 306
Schlumberger M, Challeton C, De Vathaire F, et al. (1996) Radioactive iodine treatment and external radiotherapy in 394 patients with lung and bone metastases from thyroid carcinoma. J Nucl Med 37:598 – 605
Schlumberger M, de Vatheire F, Ceccarelli F, et al. (1997a) Exposure to radioactive I-131 for scintigraphy or therapy does not preclude pregnancy in thyroid cancer patients. J Nucl Med 37:606 – 612
Schlumberger M, Mancusi F, Baudin E, Pacini F (1997b) I-131 therapy for elevated thyroglobulin levels. Thyroid 7:273 – 276
Schlumberger M, Berg G, Cohen O, et al. (2004) Follow up of low risk patients with differentiated thyroid carcinoma: a European perspective. Eur J Endocrinol 150:105 – 112
Sgouros G, Kolbert KS, Sheik A, et al. (2004) Patient-specific dosimetry for I-131 thyroid cancer therapy using I-124 PET and 3-dimensional-internal dosimetry (3D-ID) software. J Nucl Med 45:1366 – 1372
Simon D, Korber C, Krausch, et al. (2002) Clinical impact of retinoids in redifferentiation therapy of advanced thyroid cancer: final results of a pilot study. Eur J Nucl Med Mol Imaging 29:775 – 782
Sisson JC, Carey JE (2001) Thyroid carcinoma with high levels of function: treatment with I-131. J Nucl Med 42:975 – 983
Spies WG, Wojtowitz CH, Spies SM, et al. (1989) Value of post-therapy whole-body I-131 imaging in the evaluation of patients with thyroid carcinoma having undergone high dose I-131 therapy. Clin Nucl Med 14:793 – 780
Stanbury JB (1991) A constant ferment (a history of the thyroid clinic and laboratory at the Massachusetts General Hospital: 1913 – 1990). The Ipswich Press, Ipswich, MA
Sweeney DC, Jonston DS (1995) Radioiodine therapy for thyroid cancer. Endocrinol Metab Clin North Am 24:803 – 839
Travagli JP, Cailleux AF, Ricard M, et al. (1998) Combination of radio-iodine (I-131) and probe guided surgery for persistent or recurrent thyroid carcinoma. J Endocrinol Metab 83: 2675 – 2680
Tubiana M (1981) External radiotherapy and radioiodine in the treatment of thyroid cancer. World J Surg 5:75 – 82
Van Wyngaarden M, McDougall IR (1996) What is the role of 1100 MBq (30 mCi) radioiodine 131I in the treatment of patients with differentiated thyroid cancer? Nucl Med Commun 17:199 – 207
Waxmann A, Ramanna L, Chapman N, et al. (1981) The significance of I-131 scan dose in patients with thyroid cancer: determination of ablation: Concise communication. J Nucl Med 22:861 – 865
Winters S, Berga S (1997) Gonadal dysfunctions in patients with thyroid disorders. Endocrinologist 7:167 – 173
Woodrum DT, Gauger PG (2005) Role of I-131 in the treatment of differentiated thyroid cancer. J Surg Oncol 89:114 – 121
Zettinig G, Hanselmayer G, Füger B, et al. (2002) Long term impairment of the lacrimal glands after radioiodine therapy: a cross sectional study. Eur J Nucl Med Mol Imaging 29:1428 – 1432

Radionuclide Therapy of Bone Metastases 23

H. Palmedo

23.1 Introduction

Radionuclide therapy of bone metastases represents a systemic therapy with intravenous administration of open radioactive agents. It is the aim of each radiation therapy to apply a maximal dose to the target – in this case bone metastases – and a minimal dose to the rest of the body. The dose to the rest of the body determines the frequency and intensity of side effects and limits treatment efficacy.

Bone metastases are frequent and will occur with every physician treating oncologic patients (Cserhati 1987). Many solid tumors generate bone metastases. Typically, patients with breast, prostate and lung cancer are concerned. Over 60% of all breast cancer patients develop osseous metastases of the osteolytic or combined osteolytic/osteoblastic type during the course of the disease (Paterson 1987). Half of prostate cancer and a third of lung cancer patients will develop metastatic bone disease. In prostate cancer, bone metastases are predominantly osteoblastic (Jacobs 1983).

Once bone metastases are diagnosed, the disease must be classified as incurable (Eisenberger et al. 1985). At this stage, quality of life and prolongation of survival are the important parameters that form the basis for further medical decision making.

Although bone metastases are rarely the cause of cancer-related death, they lead to serious complications (Nielsen et al. 1991): (1) 30–60% of patients develop pain symptoms of varying intensity; (2) predominantly the osteolytic type has the tendency to develop fractures resulting in considerable morbidity; (3) a hypercalcemic syndrome due to increased bone resorption of osteolytic metastases can occur, and this can also appear as a paraneoplastic syndrome; and (4) if there is extensive metastatic disease the bone marrow can be destroyed and clinically relevant alterations of the blood counts can be observed.

Chronic pain syndrome is the most important complication of bone metastases and has a negative impact on quality of life and the social environment of the patient. These patients represent the main indication for radionuclide therapy. Up to one-half of patients do not receive adequate pain treatment (Strumpf 1993). About two-thirds of pain patients complain about break-through pain, meaning a simultaneous appearance of strong pain in spite of the intake of analgesics. It is therapeutically relevant that, in most of these patients with break-through pain, optimization of pain therapy is possible (Strumpf 1993).

From a pathophysiologic point of view, it is difficult to differentiate nociceptor pain from neuropathic pain (nerval pain). Nociceptor pain is mediated by free sensoric nerve endings of the nociceptor cells that can be found throughout the body (Zimmermann 1984). A large amount of nociceptors are located in the skin, the skeletal musculature, the tendons, the joints and the intestine (Besson and Chaouch 1987). Depending on their location, we differentiate between somatic and visceral or superficially and deeply located nociceptor pain. Visceral excitations are frequently projected to special skin regions, the so-called dermatoma. While the nociceptor pain is generally described by the patient as being of a stinging, gnawing or dull character, neuropathic pain is described as burning and appearing suddenly (e.g., in the case of nerve plexus infiltration) (Willis 1985). Therefore, interrogation of the patient will lead to a differentiation between the two pain entities at an early stage. This is extremely important because radionuclide therapy is useful in nociceptor pain patients but not for neuropathy pain.

Physiologically, the nociceptor is not activated unless strong mechanical or thermal influences are present (Resch 1991). This makes sense as, e.g., a warm object should not cause painful sensations. However, the nociceptor can be sensitized by the production of endogene, algetic agents: an arthritis patient will suffer from pain even if the smallest movements and the slightest pressure are applied to an affected joint. In these cases, substances like prostaglandin E, bradykinin, histamine, and interleukin act as pain mediators changing the microcirculation and permeability of vessels and leading to a decrease of the excitation level (Mense 1981; Schmidt 1991). Lymphocytes and macrophages assist in this process. The simultaneous excretion of different pain mediators can lead to an exponential increase in their effect. This principle is known in the

field of pharmacological pain treatment, and therefore agents inhibiting the production of, e.g., prostaglandin E are successfully administered in pain patients.

The nociceptor cell can also regulate its excitation level itself. By secretion of the so-called substance P, a vasodilatation and consequently an invasion of inflammatory cells and an enhanced secretion of pain mediators will occur. This process is often called a neurogene inflammation (Mense 1981).

Bone metastases can generate pain either by a strong mechanical impact to the nociceptor or by an osteoblastic – and osteoclastic induced – excretion of pain mediators that result in the described sensitization of the nociceptor (Mundy and Martin 1989).

23.2 Radiopharmaceuticals

Radionuclide therapy of bone metastases was started decades ago with the administration of phosphorus-32 (Kaplan et al. 1960). P-32 is incorporated into the DNA of rapidly proliferating cells of the bone marrow as well as in the trabecular and cortical structures of the bone. The ratio of normal bone to metastatic tissue was calculated at 1:2, and therefore is relatively low (Lewington 1993). This inappropriate ratio and the frequently observed strong myelosuppression were the reasons for abandoning phosphorus-32.

Since that time a variety of β-emitters have been investigated for therapy of bone metastases (Table 23.1). The maximal β-energy lies between 0.8 and 2.3 MeV, the average β-energy between 0.27 and 0.8 MeV. The electrons deposit their radiation energy in a field of a few millimeters around the place of decay. The physical half-lives of the mentioned nuclides differ considerably from each other (from 2 to 52 days). Therefore, the energy per time unit transferred to the tissue varies from nuclide to nuclide, although the total amount of radiation energy may be the same for two radionuclides. Principally, the radiation dose can be applied over a very short period, necessitating a high dose rate, or over a longer time period administering a radionuclide with a low dose rate. Since the aspect of killing tumor cells has gained more and more importance, new treatment schemes that use repeated radionuclide applications and that administer radionuclides combined with low dose chemotherapy are increasingly being favored.

The two calcium analogs strontium-89 chloride and yttrium-90 are taken up by the bone depending on the intensity of the osseous metabolism (Poner and Mertens 1991; Kutzner et al. 1981; Blake et al. 1989). Strontium-89 is excreted renally to 70 – 90 % and is eliminated from the vascular compartment within the first few hours (Blake et al. 1987). Except for the bone uptake and the excretion via the urinary system, there is no accumulation in any organ system. Depending on the extension of metastatic disease, the tracer uptake in the skeletal system ranges between 12 % and 90 % of the administered activity. The more extensive the bone metastases the quicker is the blood clearance into the skeleton. The accumulation of strontium-89 chloride in metastatic lesions is 5 – 20 times as high as the accumulation in normal bone tissue. Ninety days after the administration, 20 – 88 % of the injected strontium-89 activity was found in metastatic bone lesions (Blake et al. 1986). The effective half-life was calculated to be over 50 days and thus strontium-89 chloride delivers a low dose rate radiation.

A different radiopharmaceutical option is to label radionuclides to phosphonates that are known to have a high osteoaffinity. In the diagnostic field, this principle was achieved by introducing bone scintigraphy into the clinical routine and transferring to therapy after developing radiopharmaceuticals such as samarium-153 ethylenediaminetetramethylenephosphonate (Sm-153 EDTMP) and rhenium-186 hydroxyethylidenediphosphonate (Re-186 HEDP) (Holmes 1992; Ketring 1987). Also these agents are excreted mainly by the kidneys and they disappear rapidly from the vascular compartment (Singh et al. 1989; de Klerk et al. 1992). Twelve hours after the administration, 50 % of the administered activity of Re-186 HEDP and Sm-153 EDTMP has been eliminated renally. The uptake in the skeleton ranges between 20 – 30 % and 30 – 50 % of the injected dose for Re-186 HEDP and Sm-153 EDTMP, respectively. Depending on the intensity of bone metabolism, the radiolabeled phosphonates are accumulated via adhesion to bone and bone metastases. The accumulation in the metastatic lesions is between 3 and 20 times as high as normal bone. The effective half-life of Re-186 HEDP and Sm-153 EDTMP lies in the range of 2 – 3 days.

Nuclide	Sr-89	Sm-153	Re-186	Re-188	P-32	Y-90	Sn-117
Half-life (days)	52	2.1	3.8	0.7	14	2.7	13.6
βmax energy (MeV)	1.4	0.8	1.1	2.1	1.7	2.27	CE
Max. range (mm) (Soft tissue)	6.6	3.7	4.6	10.0	8.1	10.9	0.9

Table 23.1. Physical properties of radionuclides used for treatment of bone metastases

23.3 Methodology

23.3.1 Dosimetry

None of the commercially available radiopharmaceuticals for bone palliation (Sr-89 chloride, Re-186 HEDP and Sm-153 EDTMP) accumulate in the tumor cell itself but they are deposited in close vicinity to the bone, emitting the radiation to tumor and pain mediator cells. The higher the β-energy of the radionuclide the longer is the range of the electrons into the tissue. Since bone is characterized by high energy absorption, the range of therapeutic electrons emitted by osteotropic radionuclides does not reach more than a few millimeters at a maximum.

The creation of bone tissue takes place around conglomerations of tumor cells in primitive tumor bone or osteoid (Gerson et al. 1972). If osteolytic metastases are present, a broad resorption line in lacunes is found at a distance of 80 – 100 μm to the tumor borders (Baud and Boivin 1980). In the case of osteoblastic metastases, resorption lacunes are rarely found. Typically, the trabecula are covered by freshly produced bone tissue and the agent is integrated deeply into the bone structure. Therefore, the accumulation of radiopharmaceuticals is much higher in osteoblastic than in osteolytic metastases, with ratios of 1:15 and 1:3, respectively. The uptake of the radionuclide determines the therapeutic dose in the bone metastases and, thus, the predictive value of bone scintigraphy previous to treatment is indispensable even if osseous metastases have already been diagnosed by other imaging modalities.

To calculate the radiation dose to apply to tumor tissue and organs, different methods are used (Blake et al. 1988; Eary et al. 1993; Maxon et al 1981), showing a deviation of the calculated to the real dose of up to 50 %. Generally, a time-activity curve is generated over the region of interest, e.g., a reference metastasis, by ROI analysis of multiple whole-body scintigrams. The area under the curve represents the accumulated activity that has to be normalized to the target volume and must be multiplied by the S-value. The S-value contains nuclide and tissue specific parameters such as the average energy per decay and the radiation sensitivity of the concerned tissue.

Using different models of dosimetry, the dose to bone metastases was calculated for strontium-89 chloride and rhenium-186 HEDP to be 60 – 600 mGy and 11 – 108 mGy per MBq administered activity, respectively (see Table 23.1; Blake et al. 1988; Eary 1990; Maxon et al. 1988). Taking standard doses of 4 mCi Sr-89 chloride, 70 mCi Sm-153 EDTMP and 35 mCi Re-186 HEDP, the radiation dose to bone metastases lies between 8 and 90 Gy, 10 and 70 Gy and 14 and 140 Gy, respectively (see Table 23.2). Normal bone tissue receives a dose between 1 and 2.5 Gy that is significantly below that of metastatic lesions. The variation in radiation dose in osseous metastases can be explained by the different intensity of radionuclide accumulation in the metastases. This stresses the importance of pretherapeutic scintigraphy to perform at least a visual estimation of the tumor uptake and to predict therapy response.

Table 23.2. Nuclides and carriers of the radiopharmaceutical

Nuclide	Carrier
Strontium-89	Chloride
Samarium-153	EDTMP
Rhenium-186/188	HEDP
Yttrium-90	Citrate
Phosphorus-32	Orthophosphate

The organ doses are also listed in Table 23.2, demonstrating that kidneys and bladder receive uncritical doses. Obviously, the critical organ is the bone marrow, which is exposed to doses between 1 and 1.5 Gy. At this level, the first alterations of blood counts can be expected (Blake et al. 1988; Eary 1990; Maxon 1988).

23.3.2 Pain Documentation

Documentation of pain is difficult because large inter- and intraindividual variations exist for the parameter "pain." Chronic pain results in important alterations of the patient's behavior concerning all fields of life. It is recommended to use standardized questionnaires for pain documentation to evaluate the success of the treatment. Pain questionnaires should not be preserved for scientific purposes. Moreover, the clinician should increasingly perform patient interrogations using standardized pain questionnaires and use these as a basis for decisions about further treatment. For the daily routine, such a questionnaire must be short but comprehensive enough to include the fields "pain," "activity of patient" and "consumption of analgesics." There are a variety of different pain scores and questionnaires that supply these items of information adequately (Foley and Arbit 1989). The reader's attention is drawn to the well evaluated and widely used visual analog scale (VAS) and the scoring of analgesic consumption using Foley's score. Additionally, we would recommend adding some well chosen questions for the patient's daily activities that have to be scored (e.g., Health Assessment Questionnaire = HAQ). However, an internally developed system of pain assessment may also serve for the evaluation of pain therapy.

23.4 Clinical Indications

23.4.1 Pain Palliation

The application of radionuclides for treatment of painful bone metastases has been investigated for several decades. Beginning in the 1960s, the first nuclide administered for pain therapy of multiple osseous metastases was phosphorus-32 (Kaplan et al. 1960). Since that time many different radiopharmaceuticals such as strontium-89 chloride, yttrium-90 citrate, rhenium-186 HEDP, samarium-153 EDTMP, tin-177m DTPA, and rhenium-188 HEDP have been investigated. This list is not complete and therefore this chapter can only concern itself with the most important agents.

Firstly, strontium-89 chloride (Sr-89) must be mentioned, since it is the nuclide with which the nuclear medicine community has obtained the largest experience. Laing et al. (1991) treated 119 prostate cancer patients with painful metastatic bone disease, who did not respond to conventional therapy, by application of Sr-89. A total of 75% of the patients demonstrated a marked improvement of the pain status and every fifth patient was almost completely painfree. The effect of Sr-89 treatment began 10–20 days postinjection and reached a maximum after 6 weeks. Pain improvement lasted for 6 months on average with a variation between 4 and 15 months. This group evaluated efficiency of treatment by pain intensity, change of pain medication, the patient's mobility and a score for the general patient's condition. The authors could not find a significant advantage of a dosage of 3.0 MBq/kg body weight over that of 1.5 or 2.2 MBq/kg, resulting in a recommended dose of 150 MBq or 4 mCi of Sr-89. This dose has been considered the standard dosage since that time. Lewington et al. (1991) performed a randomized, placebo-controlled, double-blinded study in prostate cancer patients who were refractory to hormonal treatment and external radiation therapy. The patients treated with Sr-89 showed a significantly better pain reduction than the patients in the placebo group. Also in this study, the evaluation of efficacy comprised all the above-mentioned parameters of Laing's study. Considering that these patients were end-stage patients who had failed all conventional therapy, the effect of Sr-89 treatment is impressive. Further studies confirmed the beneficial effect of Sr-89 for pain treatment in prostate cancer patients. Quilty et al. (1993) demonstrated in 284 prostate cancer patients that one injection of Sr-89 was as efficient as a hemibody irradiation frequently showing intolerable side effects.

In the group of new radiopharmaceuticals, samarium-153 EDTMP (Sm-153) and rhenium-186 HEDP (Re-186) are the best studied and also commercially available agents. In a double blind and placebo-controlled study, Serafini et al. (1998) investigated the effect of Sm-153 in 80 prostate cancer patients. Four weeks after the injection of a single dose of 1.0 mCi/kg body weight, an improvement of the pain situation was observed in 72% of the patients. In 31% of patients, an almost complete pain reduction could be found. Four months after the treatment, 43% of the patients showed a continuing improvement of pain symptoms. In this study, the visual analog scale for different regions of the body, the consumption of analgesics and a pain scoring system performed by the physician served as criteria for treatment response. The response rate of the Sm-153 group was significantly better than that of the placebo group, which showed response rates of 40% and 2% after 4 weeks and 4 months, respectively. Furthermore, the study delivered evidence that a dose of 1.0 mCi/kg body weight results more frequently and for a longer period in pain reduction than a dose of 0.5 mCi/kg body weight. However, Tian et al. (1999) were not able to confirm in their multicenter trial that the two different dose groups of Sm-153 have a different effect on pain palliation. Collins et al. (1993) report that the beginning of pain alleviation can be expected after 7–14 days. Also for Re-186, Maxon et al. (1988) demonstrated in a group of 20 patients that a significant improvement of pain can be achieved in 80% of the cases after a single injection. The investigated parameters were a special pain and analgesic index. Maxon et al. used a standard dose of 30–35 mCi per patient. Our own experience in 30 patients with osseous metastases due to different tumor types revealed a response rate of 70% and an average time of 4 weeks for pain relief beginning 1 week after injection of Re-186 (Palmedo 1996). The main criterion of treatment response was the visual analog scale. Also the follow-up study published by Schoeneich et al. (1997) in 44 patients confirmed these results. In all cited studies, treatment consisted of a single injection of 35 mCi Re-186. Quirijnen et al. (1996) performed a dose escalation study in 43 prostate cancer patients investigating the effect of Re-186 in dosage groups of 35 mCi, 50/65 mCi and 80/95 mCi. The authors used a multimodality score to determine the pain situation consisting of the parameters pain intensity, analgesic consumption and general activity of patients. The single parameters scored were then accordingly transferred to a total overall score using a special algorithm. Referring to these very strict criteria, the activity groups of 35 mCi, 50/65 mCi and 80/95 mCi showed response rates of 33%, 78% and 70%, respectively. Although the correlation of response rate and dosage was not statistically significant, there was a clear tendency to favor the dose of 50–65 mCi. Unfortunately, the commercially available standard dose of 35 mCi (1.3 GBq) Re-186 was not increased to 65 mCi (2.4 GBq). Han et al. (1999) conducted a double-blind, placebo-controlled, randomized trial testing Re-

186 in hormone-resistant prostate cancer patients with painful bone metastases (Placorhen study). They included 111 patients and assessed pain relief using an electronic pain diary containing questions reflecting the multidimensional character of chronic pain. The total response of patients treated with Re-186 was statistically significantly better than that of the placebo group. Also the rate of patients requesting additional radiotherapy was lower in the Re-186 group at 44% than in the placebo group at 67%. Amazingly, the overall response rate of Re-186 was only 30% on average. One reason for this might be the mentioned low dose activity of Re-186 that was also used in the Placorhen trial. In summary, there is sufficient evidence-based data that confirm the benefit of radionuclide therapy as an effective treatment modality of painful osseous metastases in hormone-refractory prostate cancer patients.

These radiopharmaceuticals were not exclusively used to treat prostate cancer patients but also other tumors such as breast cancer and lung cancer. The tumor most frequently studied after prostate cancer is carcinoma of the breast. Robinson (1993) reported a response rate of 81% in breast cancer patients with multiple bone metastases investigating 500 patients with different tumors retrospectively after injection of Sr-89 at a standard dose. Baziotis et al. (1998) treated 64 breast cancer patients by a single injection with 2 MBq/kg body weight of Sr-89. They found an improvement of the pain situation in 80% of the cases including 35% of patients demonstrating almost complete pain relief. The average time of response was 3 months.

For the radiopharmaceutical Sm-153 EDTMP, the already mentioned studies by Serafini et al. and Tian et al. also investigated breast cancer patients. They reported effective pain therapy in 72–85% of metastatic bone disease with a mean duration of 1–2 months. After 4 months, the response rate was still at the level of 43%. Hauswirth et al. (1998) prospectively investigated 17 breast cancer patients receiving 35 mCi Re-186 and found a response rate of 60% and a mean duration of response of 5 weeks. Our follow-up study in 30 patients confirmed these data and showed that repetition of treatment could prolong the duration of pain relief (Palmedo et al. 1999). Han et al. (1999) investigated 24 breast cancer patients in a dose-escalation study administering doses between 35 mCi and 80 mCi and assessed therapeutic effect by a multimodality pain evaluation scoring system. They also found a response rate of 60% and a mean duration of 1 month. In summary, also in breast cancer patients, there is evidence that radionuclide therapy is effective in palliating painful bone metastases.

23.4.2 Progression Free Interval and Survival

In a randomized, placebo-controlled phase-III study, Porter et al. (1993) investigated the efficacy of Sr-89 treatment for hormone-refractory prostate cancer patients as an adjunct to radiation therapy. They irradiated 126 patients with multiple osseous metastases, progressive disease and a significant pain syndrome by external beam therapy and additional administration of either placebo or Sr-89. Besides the pain documentation, the authors recorded the frequency of newly appearing painful bone metastases and also the overall survival. Three months after radiation therapy, the rates of new osseous metastases were 66% and 41% in the placebo group and the Sr-89 group, respectively. This difference was statistically significant. Also the time interval between Sr-89 or placebo injection and a second external beam irradiation due to recurrent pain symptoms was significantly longer for the Sr-89 group at 35 weeks than for the placebo group at 20 weeks. This tumoricidal effect was confirmed by laboratory testing of PSA and alkaline phosphatase. More patients in the Sr-89 group demonstrated a reduction over 50% within the first 4 months after treatment. These results were confirmed by a different study performed by Quilty et al. (1993) in 284 prostate cancer patients with bone metastases. In this study, one patient group received either local radiation therapy or hemibody irradiation depending on the site and extension of metastases. The other patient group underwent a single injection treatment with Sr-89. Comparing both groups it was observed that pain reduction was equivalent; however, new pain foci were significantly less frequent in the Sr-89 group, even when compared to hemibody irradiation. The necessity of a new radiation therapy due to these new ain sites was also less frequent in the Sr-89 group when compared to local radiation therapy but not when compared to hemibody irradiation.

Both studies cited give evidence that radionuclide therapy with Sr-89 is more than pure pain palliation and certainly has a tumoricidal effect. This favors an earlier than late stage administration of Sr-89 in prostate cancer patients ideally combined with external radiotherapy. In the cited studies, no prolongation of overall survival could be proven for Sr-89. To enhance survival it seems that an additional antitumor effect is necessary (see "New Treatment Strategies" below).

23.4.3 Side Effects

Looking at the dosimetric data (Table 23.3), it becomes quite clear that the organ limiting therapeutic dosage is the blood cell generating system. No other organs are affected by side effects. It is known that blood cell

Table 23.3. Organ and whole body doses for commercially available radiopharmaceuticals using standard amounts of applied radioactivity

Organ	Radiation doses in grays/sieverts		
	Sr-89 chloride (4 mCi)	Sm-153 EDTMP (70 mCi)	Re-186 HEDP (35 mCi)
Kidneys	0.9	0.8	1.4
Bladder	0.2	0.6	0.63
Bone	2.5	1.5	1.05
Bone marrow	1.6	1.2	0.97
Metastases	8 – 90	10 – 70	14 – 140
Whole body	0.43	0.23	0.105

counts can change if a dose of 1 Gy or more is applied. Therefore, the most relevant side effect of radionuclide therapy of bone metastases is a thrombo- and leukopenia. If the mentioned standard doses are applied for the different radionuclides and if pre-treatment blood counts are normal, changes in blood counts are moderate. However, for patients who have received chemotherapy, it may be necessary to take into account that bone marrow reserve is limited. In these cases, blood counts must be considered more critical and a certain time interval (generally the time to the expected nadir of thrombo- or leukopenia) must be accepted before a new myelosuppressive treatment can be started. Also it may be necessary to reduce the dosage of the radionuclide for treatment.

In the British multicenter study, Quilty et al. (1993) describe that leuko- and thrombocyte counts demonstrate an average decrease of 30 – 40 % compared to baseline values after the injection of 200 MBq (5.4 mCi). The average interval of the maximal decrease (nadir) of thrombo- and leukocytes was 6 weeks (4 – 8 weeks). In the follow-up, blood counts increased again, but at week 12 after injection baseline levels still had not been reached. Significant toxicity (WHO grade III and IV) of blood counts was observed in only 7 % of patients. In the cited study, only one patient needed thrombocyte concentrate due to treatment related toxicity. The erythrocyte count and hemoglobin levels were not altered by radionuclide therapy. In comparison to Sr-89 therapy, hemibody irradiation necessitated twice as many blood transfusions. Also nausea, vomiting and diarrhea were observed four times more frequently after hemibody irradiation. Laing et al. (1991) confirmed in their study that the main side effect was a thrombocytopenia with an average decrease of 25 % and a nadir at week 6. No patient showed a toxicity of more than grade II.

Also Sm-153 EDTMP and Re-186 HEDP lead to a mild hematotoxicity if a dose of 1.0 mCi/kg body weight and of 35 mCi are administered, respectively. The nadir of the 20 – 30 % decrease of thrombo- and leukocytes was found to be at week 4 – 5. In contrast to Sr-89, after injection of these newer radionuclides, baseline levels will be reached at week 8 postinjection. Erythrocyte counts and hemoglobin do not change and toxicity is maximally grade II. If higher doses of Sm-153 EDTMP (> 2.0 mCi/kg BW) and Re-186 HEDP (> 70 mCi) are used, grade III or higher toxicity can occur.

The patient must be informed that pain syndromes might be aggravating for some days (flare-effect) and go back to the initial level afterwards. Rarely is it necessary to increase the pain medication in this situation. In the authors' experience, the flare phenomenon is less frequent than described (up to 30 % of cases).

There are some case reports in the literature describing temporary paresis and paresthesia for Re-186 HEDP in patients with extensive metastatic disease of the skull base and of the vertebral column. However, this might also be caused by progressive bone metastases. After more than 400 treatments with rhenium-HEDP, we were unable to observe any patient who had developed temporary paresis and paresthesia due to radionuclide therapy. Conversely, one patient with pretherapeutic, unilateral hypoglossus paresis showed significant improvement of tongue movement after Re-188 HEDP treatment. Eight weeks after radionuclide therapy, paresis had completely disappeared.

23.4.4 New Treatment Strategies

To enhance the effect of radionuclide therapy on the cancer cells, the following new strategies have been recently investigated: combined radionuclide and chemotherapy, high dose radionuclide therapy, and repeated radionuclide therapy.

It is known that special cytotoxic agents like cisplatin work as a radiosensitizer (Geldof et al. 1999). This means that the addition of chemotherapy and radiation therapy not only has an accumulative effect on tumor cells, but this should result in an exponentially increased cell killing. If both treatment modalities are applied simultaneously, the side effects will also increase. Therefore, the administration of a reduced-dosage protocol for chemotherapy would mean that side effects could be kept at a stable level but efficiency would increase due to a higher tumoricidal effect of combination therapy.

However, in 1992 Mertens et al. investigated 18 hormone-refractory prostate cancer patients who received a combination of 4 mCi Sr-89 and a low-dose cisplatin infusion (35 mg/m^2). They observed good pain palliation and an improvement in hemoglobin, tumor markers and bone scans in some patients. Sciuto et al. (2002) randomized 70 patients with painful bone metastases either to a group A receiving 148 MBq Sr-89 and 50 mg/m^2 cisplatin or to a group B receiving 148 MBq Sr-89 plus placebo. The follow-up was until death to evaluate

outcome. Overall pain relief occurred in 91% of patients in arm A and 63% of patients in arm B, with a median duration of 120 days in arm A and 60 days in arm B. New painful sites on previously asymptomatic bone metastases appeared in 14% of patients in arm A and in 30% of patients in arm B. The median survival without new painful sites was 4 months in arm A and 2 months in arm B. Sciuto et al. observed a progression of bone disease in 27% and 64% of patients in group A and B, respectively. This shows quite clearly that the progression of bone metastases is slowed down by combined therapy and, therefore, that new painful sites are significantly less frequent. Importantly, this improves quality of remaining life, especially because hematologic toxicity is moderate. Between both arms of the cited study, there was no significant difference with regard to side effects. Median global survival was better at 9 months for combined therapy (only 6 months for Sr-89 alone) but the difference was not statistically significant. That also overall survival can be improved by combined chemo- and radionuclide therapy was demonstrated by a study of Tu et al. (2001). They investigated 103 patients with advanced, hormone-refractory prostate cancer and performed induction chemotherapy consisting of ketoconazole (400 mg orally thrice daily for 7 days) and doxorubicin (20 mg/m^2 weeks 1, 3 and 5) alternating with estramustine (140 mg orally thrice daily for 7 days) and vinblastine (4 mg/m^2 intravenously on the first day of every week). After two or three cycles of induction chemotherapy, 72 patients who were clinically stable or responders were randomized to one group receiving chemotherapy with doxorubicin and Sr-89 or to a second group receiving chemotherapy alone. Chemotherapy with doxorubicin was administered weekly for 6 weeks and Sr-89 was given at week 1 at a dose of 2.035 MBq/kg body weight (approximately 4 mCi for a 70 kg person). A substantial (more than 80% from baseline) and continued (for at least 8 weeks) decrease of PSA values was observed in 72% and 36% of the combined (doxorubicin plus Sr-89) and of the doxorubicin-alone treatment groups, respectively. The median time to progression was significantly longer after combined therapy at 13.9 months in contrast to 7.0 months after pure chemotherapy. The median survival of patients also increased from 16.8 months (chemotherapy alone) to 27.7 months after additional injection of Sr-89. Moreover, 52% of patients with bone pain showed a complete resolution of pain. The authors hypothesize that Sr-89 is not only responsible for an additional tumoricidal effect but also has an impact on the microenvironment of the bone (e.g., paracrine growth factors), leading to an increasing resistance against metastatic tumor cells.

Akerley et al. (2002) performed a multicenter study in hormone-refractory prostate cancer patients using estramustine (600 mg/m^2 daily in weeks 1 – 4 and 7 – 10) and vinblastine (4 mg/m^2 intravenously each week for weeks 1 – 4 and 7 – 10) combined with Sr-89 2.2 MBq/kg body weight (equaling 4 mCi for a 70 kg individual). Courses were repeated every 12 weeks, meaning that repeated doses of SR-89 were applied. The authors assessed treatment response based on a change in the serum prostate specific antigen level. A greater than or equal to 50% decline of PSA for at least 6 weeks was observed in 21 of 44 patients (48%) with a mean duration of response of 23 weeks. Hematologic toxicity was within the expected range. This study is interesting because it shows that the addition of Sr-89 to chemotherapy and its repeated administration is safe and effective. Furthermore, this study also confirms that there is a tumoricidal effect on the prostate cancer cells. Repeated injections of radionuclides seem to enhance the treatment efficacy. However, clinicians are often concerned about hematological toxicity when radionuclide therapy is repeated or administered simultaneously with chemotherapy. Tu and colleagues (2005) investigated in a subgroup analysis 34 prostate cancer patients who had undergone combined chemotherapy with doxorubicin and a single Sr-89 injection. Subsequently, they assessed hematotoxicity in terms of bone marrow failure and the ability to tolerate additional treatments during a median of 25 months follow-up after Sr-89 administration. Within the 6 months after receiving Sr-89, no patient developed bone marrow failure. Five of 34 patients developed bone marrow failure at a median of 23 months after the Sr-89 treatment. Bone marrow biopsy performed in two of these five patients showed complete replacement of the marrow by tumor cells. In the remaining 3 (9%) patients, a differentiation could not be made between tumor cell invasion and bone marrow aplasia originating from beta irradiation. However, these data show that bone marrow failure, even after simultaneously applied chemotherapy and radionuclide treatment, is rather unlikely, and if suspected also aplasia induced by diffuse bone marrow infiltration must be considered. This has to be kept in mind when clinicians blame radionuclide therapy predominantly for bone marrow failure. This does not seem to be justified. Furthermore, it is evident that a therapeutic regimen applying chemotherapy and radionuclide therapy separated by a time interval of 4 – 8 weeks or more is substantially less toxic for the bone marrow than a treatment simultaneously affecting the hematopoietic system. In the therapy tolerance study of Tu et al., 91% of patients received subsequent cytotoxic treatments at a median of 11 months after Sr-89 injection. In their analysis, the authors state that a single dose of Sr-89 combined with chemotherapy did not affect the delivery of subsequent courses of chemotherapy in a selected patient group.

As a further cytotoxic agent, gemcitabine has been investigated in combination with Sr-89 in patients with

androgen independent prostate carcinoma and bone metastases. Pagliaro et al. (2003) performed a phase I/II study applying gemcitabine at a dosage of 600 mg or 800 mg/m^2 on days 1, 8, 15, 43, 50 and 57 and a single dose of Sr-89 (55 μCi/kg equaling almost 4 mCi for 70 kg body weight) on day 8. The authors treated 15 patients but there was no response measured by prostate specific antigen concentration. However, six patients had stable disease. The authors conclude that 800 mg/m^2 gemcitabine is the maximally tolerated dose for the combination and that a response rate of over 10 % cannot be expected. Therefore, further studies with gemcitabine at the indicated dosage and schedule are not warranted.

Another new approach to enhancing efficacy of radionuclide therapy is to repeat the injection, aiming at a higher radiation dose. Rhenium-188 hydroxyethylidene diphosphonate (Re-188 HEDP) is a new radiopharmaceutical that we have previously investigated for pain palliation of bone metastases (Palmedo et al. 2000). We have shown that application of Re-188 HEDP in humans is safe and that pain palliation can be achieved in about 70 % of patients. A major advantage is that rhenium-188 is inexpensively available on demand from a W-188/Re-188 generator and a kit is available for easy radiolabeling of the bone seeking hydroxyethylidene diphosphonate (HEDP) (Knapp 1998). The most important physical characteristics of Re-188 are its emission of high energy beta particles with a maximal energy of 2.1 MeV and a relatively short physical half-life of 17 h. Re-188 is readily available and due to its high dose constant it offers the possibility of repeated therapy without additional costs compared to those of a single injection. We performed a prospective phase II trial in 64 hormone-refractory prostate carcinoma patients who were randomly assigned to one of two groups (Palmedo et al. 2003). One group (group A) received a single injection of Re-188 HEDP, and patients of group B received two injections (interval 8 weeks). After therapy, patients were followed up by assessment of pain palliation and clinical outcome until death. In both groups, toxicity was low with moderate thrombo- and leukopenia (max. CTC Grade II). The effectiveness of Re-188 HEDP for pain palliation for repeated treatment (Group B) was significantly better with a response rate and time of response of 92 % and 5.66 months, respectively. In this group, 11 (39 %) of 28 patients had a PSA decrease of more than 50 % for at least 8 weeks in comparison to 2 (7 %) of 30 patients in the single-injection group (Group A). The median times to progression of group A and group B were 2.3 and 7.0 months, respectively, and the median overall survivals of group A and group B were 7.0 months and 12.7 months, respectively. These differences were statistically different. Our data confirm that bone-targeted therapy with high-energy rhenium-188 HEDP has an antitumor effect in prostate cancer patients, resulting in a better clinical outcome. One advantage of a short-living radionuclide like rhenium-188 HEDP is that it can deliver a high dose rate, meaning a high radiation dose within a relatively short time interval. Moreover, we think that the high-electron energy (2.1 MeV) of rhenium-188 HEDP is an important factor. This results in electrons ranging from approximately 3 to 5 mm in osseous tissue. We suppose that the high-energy radiation of rhenium-188 HEDP reaches the tumor tissue, which is surrounded by bone trabecula. This would lead to cytotoxic effects in the outer layers of the tumor. By repeating treatment with rhenium-188 HEDP within an interval short enough to avoid new tumor growth, the following tumor layer could be eradicated (onion peeling). We believe that a time interval even shorter than 6 – 8 weeks would be more effective and that therapy might be repeated several times to enhance the cytostatic effect. This seems to be possible because toxicity, which was limited to the bone marrow, was very moderate after repeated treatment with rhenium-188 HEDP. Recently, we have been evaluating our experience in patients treated with up to six cycles of radionuclide therapy. In our experience, it seems that patients can significantly benefit from multiple injections of Re-188 HEDP without increasing the rate of bone marrow failure and without inhibiting further chemotherapy.

A third new approach is the application of high dose radionuclide therapy necessitating bone marrow support. Anderson et al. (2002) administered different doses of Sm-153 EDTMP (1, 3, 4.5, 6, 12, 19 and 30 mCi/kg body weight; the standard dose of Sm-153 EDTMP for pain palliation is 1.0 mCi/kg BW) in 30 patients with locally recurrent or metastatic osteosarcoma or skeletal metastases. Patients received peripheral-blood progenitor cell (PBPC) or bone marrow support. The authors found that marrow radiation doses were linear with the injected amount of Sm-153 EDTMP. Also the grade of cytopenia was dose-related. After PBPC or marrow infusion on day 14 after Sm-153 EDTMP injection, recovery of hematopoiesis was problematic in two patients who had received 30 mCi/kg BW and were infused with less than 2 × 106 CD34/kg. However, in the remaining patients, no complications were observed. Reduction or elimination of opiates for pain was seen in all patients, and there was no adverse change in appetite or performance status. The authors conclude that high-dose irradiation (39 – 241 Gy) by bone-targeted therapy with Sm-153 EDTMP is feasible and that non-hematologic side effects are minimal.

References

Akerley W, Butera J, Wehbe T, Noto R, Stein B, Safran H, Cummings F, Sambandam S, Maynard J, Di Rienzo G, Leone L (2002) A multiinstitutional, concurrent chemoradiation trial of strontium-89, estramustine, and vinblastine for hormone refractory prostate carcinoma involving bone. Cancer 94(6):1654 – 60

Anderson PM, Wiseman GA, Dispenzieri A, Arndt CA, Hartmann LC, Smithson WA, Mullan BP, Bruland OS (2002) High-dose samarium-153 ethylene diamine tetramethylene phosphonate: low toxicity of skeletal irradiation in patients with osteosarcoma and bone metastases. J Clin Oncol 20(1):189 – 96

Baud C-A, Boivin G (1980) Periosteocytic remodelling in the vicinity of bone metastases. In: Donath A, Courvoisier B (eds) Bone and tumours. Hans Huber, Bern, pp 280 – 298

Baziotis N, Yakoumakis E, Zissimopoulos A, et al. (1998) Sr-89 chloride in the treatment of bone metastases from breast cancer. Oncology 55:377 – 81

Besson JM, Chaouch A (1987) Peripheral and spinal mechanisms of nociception. Physiol Rev 67:67 – 186

Bishayee A, Rao D, Srivastava S, et al. (2000) Marrow-sparing effects of Sn-117m DTPA for radionuclide therapy of bone cancer. J Nucl Med 41:2043 – 2050

Blake GM, Zivanovic MA, McEwan AJ, Ackery DM (1986) Sr-89 therapy: strontium kinetics in disseminated carcinoma of the prostate. Eur J Nucl Med 12:447 – 454

Blake GM, Zivanovic MA, McEwan AJ, Batty VB, Ackery DM (1987) 89Sr radionuclide therapy: dosimetry and haematological toxicity in two patients with metastasising prostatic carcinoma. Eur J Nucl Med 13:41 – 46

Blake GM, Zivanovic MA, Blaquiere RM, Fine DR, McEwan AJ, Ackery DM (1988) Strontium-89 therapy: measurement of absorbed dose to skeletal metastases. J Nucl Med 29:549 – 557

Blake GM, Wood JF, Wood PJ, Zivanovic MA, Lewington VJ (1989a) 89Sr therapy: strontium plasma clearance in disseminated prostatic carcinoma. Eur J Nucl Med 15:49 – 54

Blake GM, Zivanovic MA, Lewington VJ (1989b) Measurements of the strontium plasma clearance rate in patients receiving Sr89 radionuclide therapy. Eur J Nucl Med 15:780 – 783

Collins C, Eary JF, Donaldson G, et al. (1993) Samarium-153-EDTMP in bone metastases of hormone refractory prostate carcinoma: a phase I/II trial. J Nucl Med 34:1839 – 1844

Cserhati P (1987) Metastatic disease in breast cancer. J Clin Oncol 21:1235 – 41

de Klerk JMH, van Dijk A, van het Schip AD, Zonnenberg BA, van Rijk PP (1992) Pharmacokinetics of rhenium-186 after administration of rhenium-186-HEDP to patients with bone metastases. J Nucl Med 33:646 – 651

Eary JF, Collins C, Stabin M, et al. (1993) Samarium-153-EDTMP biodistribution and dosimetry estimation. J Nucl Med 34:1031 – 1036

Eisenberger MA, Simon R, O'Dwyer PJ, Wittes RE, Friedman MA (1985) A reevaluation of nonhormonal cytotoxic chemotherapy in the treatment of prostatic carcinoma. J Clin Oncol 3:827 – 841

Foley KM, Arbit E (1989) The management of cancer pain. In: DeVita VT, Hellman S, Rosenberg SA (eds) Cancer: principles and practice of oncology, 3rd edn. Lippincott, Philadelphia, pp 2064 – 2087

Geldof AA, de Rooij L, Versteegh RT, Newling DW, Teule GJ (1999) Combination 186Re-HEDP and cisplatin supra-additive treatment effects in prostate cancer cells. J Nucl Med 40(4):667 – 71

Gerson BD, Dorfman HD, Norman A, Mantius HJ (1972) Patterns of localization in osteosarcoma. J Bone Joint Surg 54:817 – 827

Han S, Zonnenberg B, De Klerk J, et al. (1999) Re-186 HEDP in breast cancer patients with metastatic bone pain. J Nucl Med 40:639 – 642

Hauswirth AE, Palmedo H, Dierke-Dzierzon C, et al. (1998) Pain therapy in multiple bone metastases in breast carcinoma. Zentralbl Gynäkol 120:83 – 86

Hillner BE, et al. (2000) American Society of Clinical Oncology guideline on the role of bisphosphonates in breast cancer. J Clin Oncol 18:1378 – 91

Holmes RA (1992) [153Sm] EDTMP: a potential therapy for bone cancer pain. Semin Nucl Med 22:41 – 45

Jacobs SC (1983) Spread of prostatic cancer to bone. Urology 21:337 – 344

Kaplan E, Fels IG, Kotlowski BR (1960) Therapy of carcinoma of the prostate metastatic to bone with P-32 labeled condensed phosphate. J Nucl Med 1:1 – 13

Ketring AR (1987) 153Sm-EDTMP and 186Re-HEDP as bone therapeutic radiopharmaceuticals. Nucl Med Biol 14:223 – 232

Kutzner J, Dähnert W, Schreyer T, Grimm W, Brod KH, Becker M (1981) Yttrium-90 zur Schmerztherapie von Knochenmetastasen. Nuklearmedizin 20:229

Laing AH, Ackery DM, Bayly RJ, et al. (1991) Strontium-89 chloride for pain palliation in prostatic skeletal malignancy. Br J Rad 64:816 – 822

Lewington VJ (1993) Targeted radionuclide therapy for bone metastases. Eur J Nucl Med 20:66 – 74

Lewington VJ, McEwan AJ, Ackery DM, et al. (1991) A prospective, randomised double-blind crossover study to examine the efficacy of strontium-89 in pain palliation in patients with advanced prostate cancer metastatic to bone. Eur J Cancer 27:954 – 958

Maxon HR, Deutsch EA, Thomas SR (1988) Re-186 (Sn)HEDP for treatment of multiple metastatic foci in bone: human biodistribution and dosimetric studies. Radiology 166:501 – 507

McEwan AJB, Amyotte GA, McGowan DG, MacGillivray JA, Porter AT (1994) Retrospective analysis of the cost effectiveness of treatment with Metastron (Strontium-89 chloride) in patients with prostate cancer metastatic to bone. Nucl Med Commun 15:567 – 71

Mense S (1981) Sensitization of group IV muscle receptors to bradykinin by 5-hydroxytryptamine and prostaglandin E2. Brain Res 225:95 – 105

Mertens WC, Porter AT, Reid RH, Powe JE (1992) Strontium-89 and low-dose infusion cisplatin for patients with hormone refractory prostate carcinoma metastatic to bone: a preliminary report. J Nucl Med 33(8):1437 – 43

Mundy GR, Martin TJ (1989) Pathophysiology of skeletal complications of cancer. In: Mundy GR, Martin TJ (eds) Physiology and pharmacology of Bone. Springer-Verlag, Berlin Heidelberg New York, pp 641 – 44

Nielsen OS, Munro AJ, Tannock IF (1991) Bone metastases: pathophysiology and management policy. J Clin Oncol 9(3):509 – 524

Pagliaro LC, Delpassand ES, Williams D, Millikan RE, Tu SM, Logothetis CJ (2003) A phase I/II study of strontium-89 combined with gemcitabine in the treatment of patients with androgen independent prostate carcinoma and bone metastases. Cancer 97(12):2988 – 94

Palmedo H, Bender H, Schomburg A, Grünwald F, Schoeneich G, Zamora P, Reichmann K, Dierke-Dzierzon C, Mallmann P, Biersack HJ (1996) Schmerztherapie mit Rhenium-186 HEDP bei multiplen Knochenmetastasen. Nuklearmedizin 35:63 – 67

Palmedo H, Grünwald F, Wagner U, et al. (1998) Remission of

bone metastases after combined chemotherapy and radionuclide therapy with Re-186 HEDP. Clin Nucl Med 23:501 – 4
Palmedo H, Bender H, Dierke-Dzierzon C, Carl UM, Krebs D, Risse J, Biersack HJ (1999) Pain palliation with rhenium-186 HEDP in breast cancer patients with disseminated bone metastases. Clin Nucl Med 24:643 – 648
Palmedo H, Guhlke S, Bender H, Sartor J, Schoeneich G, Risse J, Grünwald F, Knapp FF, Biersack HJ (2000) Dose escalation study with rhenium-188 HEDP in prostate cancer patients with osseous metastases. Eur J Nucl Med 27:123 – 130
Palmedo H, Manka-Waluch A, Albers P, Schmidt-Wolf IG, Reinhardt M, Ezziddin S, Joe A, Roedel R, Fimmers R, Knapp FF Jr, Guhlke S, Biersack HJ (2003) Repeated bone-targeted therapy for hormone-refractory prostate carcinoma: randomized phase II trial with the new, high-energy radiopharmaceutical rhenium-188 hydroxyethylidenediphosphonate. J Clin Oncol 21(15):2869 – 75
Palmedo H, Rockstroh JK, Bangard M, et al. (2006) Therapy with rhenium-186 HEDP in medication-refractory patients with painful multifocal arthritis: initial results of a prospective study. Radiology (accepted for publication)
Paterson AHG (1987) Bone metastases in breast cancer, prostate cancer and myeloma. Bone 8 (Suppl 1):17 – 22
Poner A, Mertens W (1991) Strontium 89 in the treatment of metastatic prostate cancer. Can J Oncol 1:11 – 18
Porter AT, McEwan AJB, Powe JE, et al. (1993) Results of a randomized phase-III trial to evaluate the efficacy of strontium-89 adjuvant to local field external beam irradiation in the management of endocrine resistant metastatic prostate cancer. Int J Radiat Oncol Biol Phys 25:805 – 813
Quilty PM, Kirk D, Bolger JJ, et al. (1993) A comparison of the palliative effect of strontium 89 and external beam radiotherapy in metastatic prostate cancer. Radiother Oncol 31: 33 – 40
Quirijnen JMSP, Han SH, Zonnenberg BA, et al. (1996) Efficacy of rhenium-186-HEDP in prostate cancer patients with metastatic bone pain. J Nucl Med 37:1511 – 1515
Resch K (1991) Der entzündliche Gelenkschmerz. In: Zimmermann M, Zeidler H, Ehlers H (eds) Rheuma und Schmerz. Der Schmerz 5(Suppl 1):3 – 12
Robinson RG (1993) Strontium-89 precursor targeted therapy for pain relief of blastic metastatic disease. Cancer 72: 3433 – 5
Schmidt RF (1991) Physiologie und Pathophysiologie der Schmerzentstehung und Schmerzverarbeitung im Bewegungssystem. In: Zimmermann M, Zeidler H, Ehlers H (eds) Rheuma und Schmerz. Der Schmerz 5(Suppl 1):13 – 28
Schoeneich G, Palmedo H, Dierke-Dzierzon C, Müller SC, Biersack HJ (1997) Palliative radionuclide therapy of painful bone metastases. Scand J Urol Nephrol 31:445 – 448
Sciuto R, Festa A, Rea S, Pasqualoni R, Bergomi S, Petrilli G, Maini CL (2002) Effects of low-dose cisplatin on 89Sr therapy for painful bone metastases from prostate cancer: a randomized clinical trial. J Nucl Med 43(1):79 – 86
Serafini AN, Houston SJ, Resche I, et al. (1998) Palliation of pain associated with metastatic bone cancer using samarium-153 lexidronam: a double blind placebo-controlled trial. J Clin Oncol 16:1574 – 1581
Singh A, Holmes RA, Farhangi M (1989) Human pharmacokinetics of samarium-153 EDTMP in metastatic cancer. J Nucl Med 30:1814 – 1818
Strumpf M (1993) Krebbsschmerz. In: Zenz J, Jurna I (eds) Lehrbuch der Schmerztherapie. Wissenschaftliche Verlagsgesellschaft, Stuttgart, pp 427 – 436
Tian J, Zhang J, Hou Q, et al. (1999) Multicentre trial on the efficacy and toxicity of single dose samarium-153 EDTMP as a palliative treatment for painful skeletal metastases in China. Eur J Nucl Med 26:2 – 7
Tu S, Millikan RE, Mengistu B, et al. (2001) Bone targeted therapy for advanced androgen-independent carcinoma of the prostate: a randomised phase II trial. Lancet 357:336 – 41
Tu SM, Kim J, Pagliaro LC, Vakar-Lopez F, Wong FC, Wen S, General R, Podoloff DA, Lin SH, Logothetis CJ (2005) Therapy tolerance in selected patients with androgen-independent prostate cancer following strontium-89 combined with chemotherapy. J Clin Oncol 23(31):7904 – 10
Willis WD (1985) The pain system. Karger-Verlag, Basel, pp 341 – 388
Zimmermann M (1984) Physiologie von Nozizeption und Schmerz. In: Zimmermann M, Handwerker HO (eds) Schmerz – Konzepte und ärztliches Handeln. Springer-Verlag, Berlin, pp 1 – 43

Peptide Receptor Radionuclide Therapy 24

J.J.M. Teunissen, D.J. Kwekkeboom, M. de Jong, J.-P. Esser, R. Valkema, E.P. Krenning

This chapter is based on an earlier article with the same title and by the same authors which appeared in *Best Practice & Research: Clinical Gastroenterology,* August 2005.

24.1 Brief Introduction and Historical Perspective

Somatostatin receptor scintigraphy, which was developed in the late 1980s, has become an important imaging modality in patients with somatostatin receptor-positive tumors (Krenning et al. 1993; Kwekkeboom et al. 2000). This is not only because of its high sensitivity in the visualization of somatostatin receptor-positive tumors and thereby the ability to localize otherwise undetectable disease, but also because of its ability to select known metastatic disease for peptide receptor radionuclide therapy (PRRT) with radiolabeled somatostatin analogs. Especially in patients with inoperable or metastatic gastroenteropancreatic (GEP) tumors (i.e., gastrointestinal carcinoids, functioning and non-functioning pancreatic endocrine tumors), this new modality of targeted therapy is very promising.

24.2 Radiopharmaceuticals Employed

Currently, several radiolabeled somatostatin analogs are used to treat patients with somatostatin receptor-positive metastasized GEP tumors. These conjugates all consist of a somatostatin analog, such as octreotide or octreotate, a complexing moiety (or chelator), and a radionuclide. The chelator, which is attached to the somatostatin analog, enables a stable connection between the analog and radionuclide. The basic principle of tumor targeting after systemic administration of the conjugate involves binding to somatostatin receptors, which are expressed on the cell surface of the tumor cell, followed by effective internalization of the radionuclide-peptide complex (Andersson et al. 1996; de Jong et al. 1998; Hofland et al. 1995). The emitted radiation can damage the DNA which, subsequently, may lead to the induction of cell death. In clinical practice different combinations of radionuclides and somatostatin analogs are used to target the somatostatin receptor-positive tumor. These analogs differ from each other in their affinity for the various somatostatin receptor subtypes (SSTR). This variable affinity is important because it can have great influence on the clinical effectiveness of the radiolabeled somatostatin analog. The available radionuclides and somatostatin analogs used will be discussed.

24.2.1 Radionuclides

Indium (^{111}In), yttrium (^{90}Y) and lutetium (^{177}Lu) have been the most frequently used radionuclides for targeted radiotherapy in the various clinical trials during the past decade. Differences in physical properties of these radionuclides, which are important for the effectiveness of therapy, include emitted particles, particle energy and tissue penetration range (Table 24.1). ^{111}In, coupled via the chelator diethylenetriaminopentoacetic acid (DTPA) to D-Phe^{1}-octreotide ([^{111}In-DTPA^{0}]octreotide; ^{111}In-octreotide), was used in the first clinical trials in which patients with metastasized GEP tumors were treated with radiolabeled somatostatin analogs (Krenning et al. 1994; McCarthy et al. 2000; Valkema et al. 2002a). Besides gamma (γ)-radiation, which makes ^{111}In a suitable radionuclide for imaging, it emits both Auger and conversion electrons with a medium-to-short tissue penetration range (0.02–10 and 200–500 μm, respectively). In vitro PRRT studies with [^{111}In-DTPA^{0}]octreotide showed that the therapeutic effect was dependent on internalization, which enables the Auger electrons to reach the nucleus (Capello et al. 2003). These results indicate that the Auger electrons and not the conversion electrons can be held responsible for the reported tumor responses with ^{111}In labeled somatostatin analogs. In an attempt to increase the efficacy of PRRT, clinical trials that followed used β-emitting radionuclides, such as ^{90}Y or ^{177}Lu. Radionuclides emitting β-radiation have greater therapeutic potential since the emitted particle range exceeds the cell diameter (Krenning et al. 1999; O'Donoghue et al. 1995; Smith

et al. 2000). Furthermore, the ability to irradiate neighboring cells is an advantage in tumors, such as breast carcinomas, which are characterized by a heterogeneous somatostatin receptor tissue distribution, with regions of high density next to regions which lack expression of the receptor (Reubi et al. 1990). As expected, the clinical and pre-clinical studies in which ^{90}Y or ^{177}Lu coupled somatostatin analogs were used demonstrated more effectiveness in terms of tumor shrinkage than somatostatin analogs coupled to ^{111}In (de Jong et al. 2002; Kwekkeboom et al. 2003a; Virgolini et al. 2002; Waldherr et al. 2002a). O'Donoghue et al., who used a mathematical model to examine the tumor curability and its relationship to tumor size for 22 β-emitting radionuclides, calculated optimal tumor diameters for cure of 34 mm and 2 mm, for ^{90}Y and ^{177}Lu, respectively (O'Donoghue et al. 1995). With respect to these calculations, the pre-clinical studies by de Jong et al. (2001b, 2002) in which Lewis rats bearing somatostatin receptor-positive pancreatic CA20948 tumors of different sizes (0.1 – 15 cm^2) were treated with [^{177}Lu-DOTA^0,Tyr^3]octreotate (^{177}Lu-DOTATATE) and [^{90}Y-DOTA^0,Tyr^3]octreotide (^{90}Y-DOTATOC) are of special interest. After treatment with ^{177}Lu-DOTATATE (total cumulative dose of 555 MBq; maximum estimated tumor dose of 60 Gy), a higher cure rate was observed in the group of rats bearing small tumors (≤ 1 cm^2) than in the rats bearing larger tumors (≥ 1 cm^2; mean ~5 cm^2). In contrast, treatment with a single dose of 370 MBq ^{90}Y-DOTATOC, leading up to a maximum of 60 Gy in the medium-sized (3 – 9 cm^2) tumors, showed less cure within the group of rats bearing small (≤ 1 cm^2) tumors compared with rats bearing medium-sized tumors (Fig. 24.1) (de Jong et al. 2001a). These results indicated that treatment with the combination of ^{90}Y and ^{177}Lu labeled somatostatin analogs can be more effective in the treatment of multiple tumors which differ in size than one of the analogs separately. Recently, de Jong et al. reported the results of such a combination versus single analog therapy (de Jong et al. 2005). In rats bearing both a small (< 0.5 cm^2) and a large tumor (7 – 9 cm^2), significantly better survival was observed after PRRT with the combination of 185 MBq (half dose) ^{90}Y-DOTATOC and 278 MBq (half dose) ^{177}Lu-DOTATATE, than with a single full dose of 370 MBq ^{90}Y-DOTATOC or 555 MBq ^{177}Lu-DOTATATE. To translate these results to the clinical setting with patients with GEP tumors, ^{90}Y-labeled somatostatin analogs may be more effective in larger tumors, whereas ^{177}Lu-labeled somatostatin analogs may be more effective in smaller tumors, with the combination of both radionuclides as the most suitable therapy for the clinical situation in which most patients have tumor metastases varying in size. Unfortunately, randomized controlled clinical studies comparing therapeutic efficacy of ^{90}Y and ^{177}Lu somatostatin analogs or combinational based regimens are still lacking.

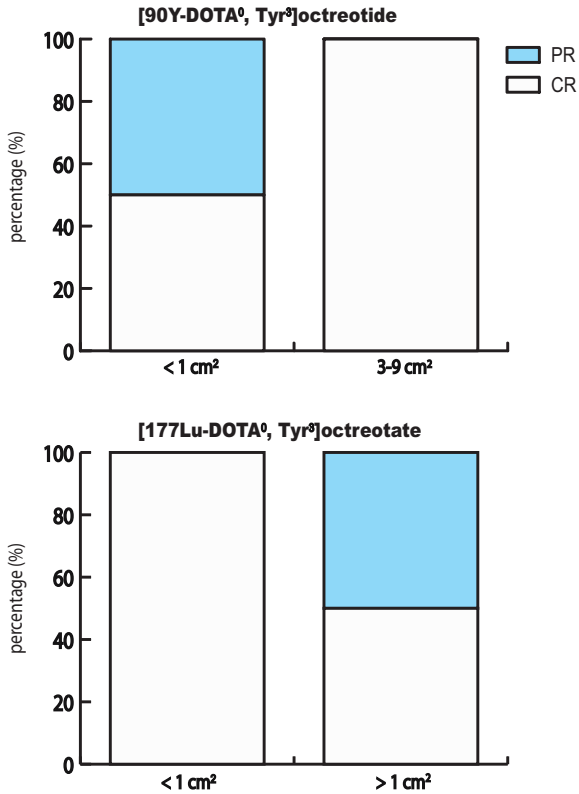

Fig. 24.1. Cure rate (expressed as percentage of cured rats) found in groups of rats bearing CA20948 tumors of different indicated sizes after treatment with 370 MBq [^{90}Y-DOTA^0, Tyr^3]octreotide or 555 MBq [^{177}Lu-DOTA^0, Tyr^3]octreotate (maximum estimated tumor dose of 60 Gy for both treatments). *PR* partial response, *CR* complete response (data used after de Jong et al. 2002)

Radionuclide	Emitted particle	Particle energy (mean keV)	Maximum tissue penetration range (~ number of cells[a])	Half-life (days)
Indium (^{111}In)	Auger electrons γ-radiation	3 and 19 keV 171 and 245 keV	10 μm (< 1)	2.8
Yttrium (^{90}Y)	β-radiation	935 keV	12 mm (~600)	2.7
Lutetium (^{177}Lu)	β-radiation γ-radiation	130 keV	2 mm (~100)	6.7

Table 24.1. Physical characteristics of the radionuclides used in peptide receptor radionuclide therapy

[a] Number of cells based on an average tumor cell size of 20 μm

24.2.2 Somatostatin Analogs

The various ^{111}In, ^{90}Y or ^{177}Lu labeled somatostatin analogs differ in their affinity for the expressed somatostatin receptors. Five human somatostatin receptor subtypes (SSTR1–SSTR5) that bind native human somatostatin (SS14) and its high affinity 28-amino-acid precursor (SS-28) have been cloned (Panetta et al. 1994; Rohrer et al. 1993; Yamada et al. 1992). However, their affinity for synthetic somatostatin analogs differs considerably. The "cold" analog octreotide, which is frequently used to control symptoms related to hormone overproduction by the GEP tumor, binds with high affinity to SSTR2 and with low affinity to SSTR3 and SSTR5, whereas it does not bind to SSTR1 and SSTR4 (Bruno and Berelowitz 1993; Yamada et al. 1993). Furthermore, autoradiography studies by Reubi et al. (2000) demonstrated that after labeling of octreotide, via DTPA, with^{111}In, the affinities to SSTR2 and SSTR5 are diminished (Table 24.2). However, despite the change in affinities, SSTR2 remains the receptor subtype to which [^{111}In-DTPA^0]octreotide has the highest affinity. Hofland et al. (2003) demonstrated that the uptake of [^{111}In-DTPA^0]octreotide in somatostatin receptor-positive organs of mice is predominantly determined by SSTR2. Moreover, John et al. (1996) demonstrated that a positive [^{111}In-DTPA^0]octreotide scintigram in patients with neuroendocrine tumors is mainly due to SSTR2 expression, whereas SSTR1, SSTR3, SSTR4, and probably SSTR5 are less important. Radiolabeled somatostatin analogs which had a higher affinity for the SSTR2 than ^{111}In-octreotide and, therefore, were potentially more effective for therapy, then became available. Small structural changes in the radioligand molecule, like different radionuclides, chelators or peptides, revealed distinct differences in the binding properties of the analog for the various SSTR subtypes (Table 24.2) (Reubi et al. 2000). In animal experiments, several ^{111}In-labeled somatostatin analogs showed higher specific uptake in somatostatin receptor-positive organs than ^{111}In-labeled [DTPA^0]octreotide (de Jong et al. 1998). Furthermore, the analog [DOTA^0, Tyr^3]octreotate has a ninefold higher affinity for the SSTR2 compared to [DOTA^0, Tyr^3]octreotide, whereas the affinities to SSTR3 and SSTR5 were found to be lower (Reubi et al. 2000). In line with the higher affinity for the SSTR2, biodistribution studies on ^{111}In-octreotide and ^{177}Lu-DOTATATE scintigraphy showed a three- to fourfold higher tumor uptake in four out of five patients with somatostatin positive tumors, of which three were GEP tumors (Kwekkeboom et al. 2001). As most GEP tumors are known to predominantly express the SSTR2, all clinical studies selected a radiolabeled somatostatin analog for PRRT with at least a high affinity for the SSTR2.

24.3 Clinical Studies

Several phase I and phase II PRRT studies in which different radiolabeled somatostatin analogs were used have been published and are discussed. With the accumulating increased experience, it has become clear that the bone marrow and kidneys are the most important dose limiting organs in this type of therapy.

24.3.1 [^{111}In-DTPA^0]octreotide

The first radiolabeled somatostatin analog therapy in GEP patients with advanced stage disease was based on the administration of high dosages of ^{111}In-octreotide, which at that time was available for diagnostic purposes (Table 24.3) (Anthony et al. 2002; Buscombe et al. 2003; McCarthy et al. 2000; Valkema et al. 2002a). The total cumulative dose varied from 3.1 GBq up to

Table 24.2. Affinity profiles (IC_{50}) for human SSTR1–SSTR5 (hSSTR1–5) of a series of somatostatin analogs. [a]All values are $IC_{50} \pm$ SEM in nM. The number of experiments is in parenthesis. (Data after Reubi et al. 2000)

Peptide	hSSTR1	hSSTR2	hSSTR3	hSSTR4	hSSTR5
SS-28	5.2 ± 0.3 (19)	2.7 ± 0.3 (19)	7.7 ± 0.9 (19)	5.6 ± 0.4 (19)	4.0 ± 0.3 (19)
Octreotide	> 10,000 (5)	2.0 ± 0.7 (5)	187 ± 55 (3)	> 1,000 (4)	22 ± 6 (5)
DTPA-octreotide	> 10,000 (6)	12 ± 2 (5)	376 ± 84 (5)	> 1,000 (5)	299 ± 50 (6)
^{111}In-octreotide	> 10,000 (5)	22 ± 3.6 (5)	182 ± 13 (5)	> 1,000 (5)	237 ± 52 (5)
DOTATOC	> 10,000 (7)	14 ± 2.6 (6)	880 ± 324 (4)	> 1,000 (6)	393 ± 84 (6)
^{90}Y-DOTATOC	> 10,000 (4)	11 ± 1.7 (6)	389 ± 135 (5)	> 10,000 (5)	114 ± 29 (5)
DOTALAN	> 10,000 (7)	26 ± 3.4 (6)	771 ± 229 (6)	> 10,000 (4)	73 ± 12 (6)
^{90}Y-DOTALAN	> 10,000 (3)	23 ± 5 (4)	290 ± 105 (4)	> 10,000 (4)	16 ± 3.4 (4)
DOTA-OC	> 10,000 (3)	14 ± 3 (4)	27 ± 9 (4)	> 1,000 (4)	103 ± 39 (3)
^{90}Y-DOTA-OC	> 10,000 (5)	20 ± 2 (5)	27 ± 8 (5)	> 10,000 (4)	57 ± 22 (4)
DTPA-Tyr^3-octreotate	> 10,000 (4)	3.9 ± 1 (4)	> 10,000 (4)	> 1,000 (4)	> 1,000 (4)
^{111}In-DTPA-Tyr^3-octreotate	> 10,000 (3)	1.3 ± 0.2 (3)	> 10,000 (3)	433 ± 16 (3)	> 1,000 (3)
DOTA-Tyr^3-octreotate	> 10,000 (3)	1.5 ± 0.4 (3)	> 1,000 (3)	453 ± 176 (3)	547 ± 160 (3)
^{90}Y-DOTA-Tyr^3-octreotate	> 10,000 (3)	1.6 ± 0.4 (3)	> 1,000 (3)	523 ± 239 (3)	187 ± 50 (3)

Table 24.3. Peptide receptor radionuclide therapy with ^{111}In-octreotide in patients with GEP tumors

Authors	No. of patients	PD before therapy	Cum. dose (GBq)	Response[a] PR	MR[b]	SD	PD
Valkema et al. (2002a)	26	92 % (clinical and/or imaging based)	4.7 – 160.0	–	2 (8 %)	15 (58 %)	9 (35 %)
Anthony et al. (2002)	26	100 % (clinical and/or imaging based)	6.7 – 46.6	2 (8 %)	N/I	21 (81 %)	3 (11 %)
Buscombe et al. (2003)	12	100 % (biochemical or imaging based)	3.1 – 36.6	2 (17 %)	N/I	7 (58 %)	3 (25 %)

Cum. dose, cumulative dose of ^{111}In-octreotide; N/I, not indicated

[a] Criteria of tumor response: PR (partial remission), > 50 % reduction of tumor size; MR (minor remission), 25 – 50 % reduction of tumor size; SD (stable disease), ± 25 % reduction or increase of tumor size; PD (progressive disease), > 25 % increase of tumor size

[b] Modification of SWOG criteria, including MR (minor remission), between 25 % and 50 % reduction in tumor size

160.0 GBq. In a report by Valkema et al. (2002a), in which the outcome of ^{111}In-octreotide treatment in 50 patients with somatostatin receptor-positive tumors was reviewed, 15 out of the 26 (58 %) GEP patients had stabilization of their metastatic disease and 2/26 (8 %) had minor remission (MR). MR was defined as a reduction in tumor size between 25 % and 50 %. Patients with stable disease (SD) and MR (17/26; 65 %) were considered to have had a beneficial therapeutic effect as all patients had documented progressive disease at study entry. In another report by Anthony et al. (2002), 2/26 (8 %) patients had partial remission (PR), whereas 21/26 (81 %) had SD. Buscombe et al. (2003) reported the outcome of ^{111}In-octreotide therapy in 12 GEP patients treated with cumulative activities as high as 36.6 GBq. Seven out of 12 (58 %) patients had SD 6 months after the last therapy, 2/12 (17 %) had PR and 3/12 (25 %) had progressive disease despite treatment.

All the clinical PRRT studies reported encouraging and promising results, especially in terms of clinical benefit and biochemical responses. However, reported cases of objective tumor shrinkage were few. These outcomes suggested that the antitumor effect of ^{111}In-octreotide is not ideal for peptide receptor radionuclide therapy (PRRT), at least for visible GEP tumors. However, experimental data in rats have shown that high doses of ^{111}In-octreotide can inhibit the growth of liver metastases after injection of SST2 receptor-positive tumor cells in the portal vein (Slooter et al. 1999). These results indicate that PRRT with ^{111}In-labeled analogs might be effective in the treatment of micro-metastases or metastatic spread during initial surgery. However, clinical studies that could confirm these observations are lacking.

24.3.2 [^{90}Y-DOTA^0, Tyr^3]octreotide, [^{90}Y-DOTA]lanreotide and [^{90}Y-DOTA^0,Tyr^3]octreotate

In the clinical trials that followed the PRRT with ^{111}In-labeled analogs, ^{90}Y-labeled analogs were used. A summary of these studies is shown in Table 24.4. In 1998, Otte et al. (1998) reported the first results of ten patients with somatostatin receptor-positive tumors treated with ^{90}Y-DOTATOC. Two out of ten patients had PR, six had SD and in two patients ^{18}F-deoxyglucose-positron emission tomography (^{18}F-FDG-PET), after administration as a single dose of ^{90}Y-DOTATOC, showed a substantial reduction of FDG uptake in the tumor. In the studies that followed, response rates (complete remission, CR, and PR) in patients with GEP tumors, who were either treated with 6.0 GBq/m^2 or 7.4 GBq/m^2, were 10/37 (27 %) and 8/37 (22 %), respectively (Waldherr et al. 2001, 2002a). To determine whether a decrease in the number of treatments, but at the same time maintaining the maximum cumulative dose of 7.4 GBq/m^2 due to an increase of dosage per treatment, could increase the objective response, another study was performed (Waldherr et al. 2002b). Twelve out of 35 patients (34 %) had CR or PR, which indicated a higher percentage of tumor regression. No increase in side effects was reported. Although these results suggested that an increase of dose and, as a consequence, a decrease in number of therapeutic injections, could be more beneficial, it must be stressed that this was not a randomized controlled trial and the number of treated patients was low. Nonetheless, the variation in protocol characteristics, like the number of treatments, doses per treatment or the length of treatment interval, is of great interest and may play an important role in the reported outcome of PRRT studies. Randomized studies on the effects of these variables are therefore needed.

Table 24.4. Peptide receptor radionuclide therapy with ^{90}Y and ^{177}Lu-labeled somatostatin analogs in patients with neuroendocrine GEP tumors

Authors (year of publication)	No. of patients	PD before therapy	Cum. dose (GBq)	Response[a] CR	PR	MR[b]	SD	PD	CR + PR
[^{90}Y-DOTA^0, Tyr^3]octreotide									
Otte et al. (1999)	16	N/I		0	1 (6%)	N/I	14 (88%)	1 (6%)	1/16 (6%)
Waldherr et al. (2001)	37	34/37 (84%)		1 (3%)	9 (24%)	N/I	23 (62%)	4 (11%)	10/37 (27%)
Waldherr et al. (2002a)	37	37/37 (100%)		1 (3%)	7 (19%)	N/I	6 (70%)	3 (8%)	8/37 (22%)
Waldherr et al. (2002b)	35	35/35 (100%)		2 (6%)	10 (29%)	N/I	19 (54%)	4 (11%)	12/35 (34%)
Bodei et al. (2003)	21	N/I		0	6 (29%)	N/I	11 (52%)	4 (19%)	6/21 (29%)
Valkema et al. (2003a)	54	41/54[c] (76%)		0	4 (7%)	7 (13%)	33 (61%)	10 (19%)	4/54 (7%)
[^{90}Y-DOTA]lanreotide									
Virgolini et al. (2002)	39	39/39 (100%)		0	0	8 (20%)	17 (44%)	14 (36%)	0/39 (0%)
[^{90}Y-DOTA^0,Tyr^3] octreotate									
Baum et al. (2004a, 2004b)	75	67/75 (89%)		0	28 (37%)	N/I	39 (52%)	8 (11%)	28/75 (37%)
[^{177}Lu-DOTA^0,Tyr^3] octreotate									
Kwekkeboom et al. (2005)	131	55/131 (42%)		3 (2%)	32 (26%)	24 (19%)	44 (35%)	22 (18%)	35/125[d] (28%)

[a] Criteria of tumor response (SWOG): CR (complete remission), no evidence of disease; PR (partial remission), > 50% reduction of tumor size; SD (stable disease), ± 25% reduction or increase of tumor size; PD (progressive disease), > 25% increase of tumor size
[b] Modification of SWOG criteria including MR (minor remission), between 25% and 50% reduction of tumor size; N/I, not indicated
[c] R. Valkema, personal communication (2004)
[d] In 125 out of 131 patients tumor size was evaluable

Clinical studies performed in Milan also used ^{90}Y-DOTATOC to treat various somatostatin receptor-positive tumors (Bodei et al. 2003, 2004; Chinol et al. 2002; Paganelli et al. 2001, 2002). Recently, Bodei et al. (2004) reported their experience with ^{90}Y-DOTATOC, in which a total of 141 patients with various, somatostatin positive tumors were treated. An objective response (CR and PR) of 26% was observed. More precisely, 23% of patients who had progressive disease before therapy (113/141; 80%) had CR or PR, whereas in the group with stable disease (28/141; 20%) 32% had CR or PR. Unfortunately, specified treatment outcome according to tumor type was not given. However, it was reported that most of the patients who had a favorable outcome had neuroendocrine GEP tumors. In a more detailed study from Milan, the outcome of therapy in 40 patients with somatostatin receptor-positive tumors was reported (Bodei et al. 2003). The cumulative dose, which was given in two cycles, ranged from 5.9 to 11.1 GBq of ^{90}Y-DOTATOC. In the group of GEP tumors, this therapy regimen resulted in PR in 6 out of 21 patients (29%), whereas 11/21 (52%) had SD and 4/21 (19%) had progressive disease (PD). Valkema et al. (2003a) reported the preliminary results of a multicenter phase I study which was performed in Rotterdam, Brussels and Tampa. The objective was to define the maximum tolerated single and four-cycle doses of ^{90}Y-DOTATOC (de Jong et al. 2002; Smith et al. 2000; Valkema et al. 2002b). Escalating doses up to 14.8 GBq/m^2 in four doses or up to 9.3 GBq/m^2 in a single dose were administered to a total of 60 patients. Four out of the 54 (7%) patients who were treated with their maximum allowed dose had PR, 7/54 (13%) had MR and 33/54 (61%) had stabilization of disease. Anti-tumor effect in terms of improvement of response, according to the SWOG (Southwest Oncology Group) tumor response criteria, including stable disease and minor remission in patients with progressive disease at the start of therapy, was reported as 65% (Valkema et al. 2003). The median time to progression of that same group had not been reached at 26 months (Valkema et al. 2003).

In a multicenter European study (MAURITIUS), another ^{90}Y-labeled somatostatin analog, ^{90}Y-DOTA-lanreotide, was used to treat 39 GEP patients. The total cumulative dose ranged from 1.9 GBq to 8.6 GBq (50–232 mCi) of ^{90}Y-DOTA-lanreotide (Virgolini et al. 2002). Eight out of 39 (20%) patients had MR, 17/39 (44%) had SD. The first results of the therapeutic efficacy in patients with somatostatin receptor-positive tumors with the somatostatin analog [^{90}Y-DOTA^0,Tyr^3]octreotate (^{90}Y-DOTATATE) were recently reported by Baum et al. (2004a, b). Twenty-eight out of 75

(37 %) of patients had PR and 39/75 (52 %) had SD after therapy. Therefore, ^{90}Y-DOTATATE might also be a promising ^{90}Y labeled somatostatin analog. Despite the differences in somatostatin analogs and protocols used in the various ^{90}Y based PRRT studies, the reported results of therapy in terms of complete and partial remission percentages ranging up to 37 % (Table 24.4) indicated an improvement of therapeutic effectiveness compared with the studies with ^{111}In labeled octreotide.

24.3.3 [^{177}Lu-DOTA^0,Tyr^3]octreotate

The first encouraging results of [^{177}Lu-DOTA^0,Tyr^3]octreotate (^{177}Lu-DOTATATE) therapy were described in a study of 35 patients with neuroendocrine GEP tumors, who had a follow-up of 3 – 6 months after receiving their final dose (Kwekkeboom et al. 2003a). Patients were treated with escalating dosages from 100 to 150, and a maximum of 200 mCi (3.7, 5.6, or 7.4 GBq, respectively) ^{177}Lu-DOTATATE, up to a final cumulative dose of 600 – 800 mCi (22.2 – 29.6 GBq), with treatment intervals of 6 – 9 weeks. The effects of the therapy on tumor size were evaluable in 34 patients. Three months after the final administration a CR was found in one patient (3 %), PR in 12 (35 %), SD in 14 (41 %), and PD in 7 (21 %), including three patients who died during the treatment period. In an update of this treatment in 131 patients, of which 125 were evaluable for tumor size, CR was found in three patients (2 %), PR in 32 (26 %), MR in 24 (19 %), SD in 44 (35 %), and PD in 22 patients (18 %). The effect of ^{177}Lu-DOTATATE therapy on tumor size, uptake on post-therapy scintigraphy, liver enzymes and the tumor marker chromogranin A in a patient who had partial remission is shown in Fig. 24.2. Median time to progression was not reached at 36 months from therapy start (Kwekkeboom et al.

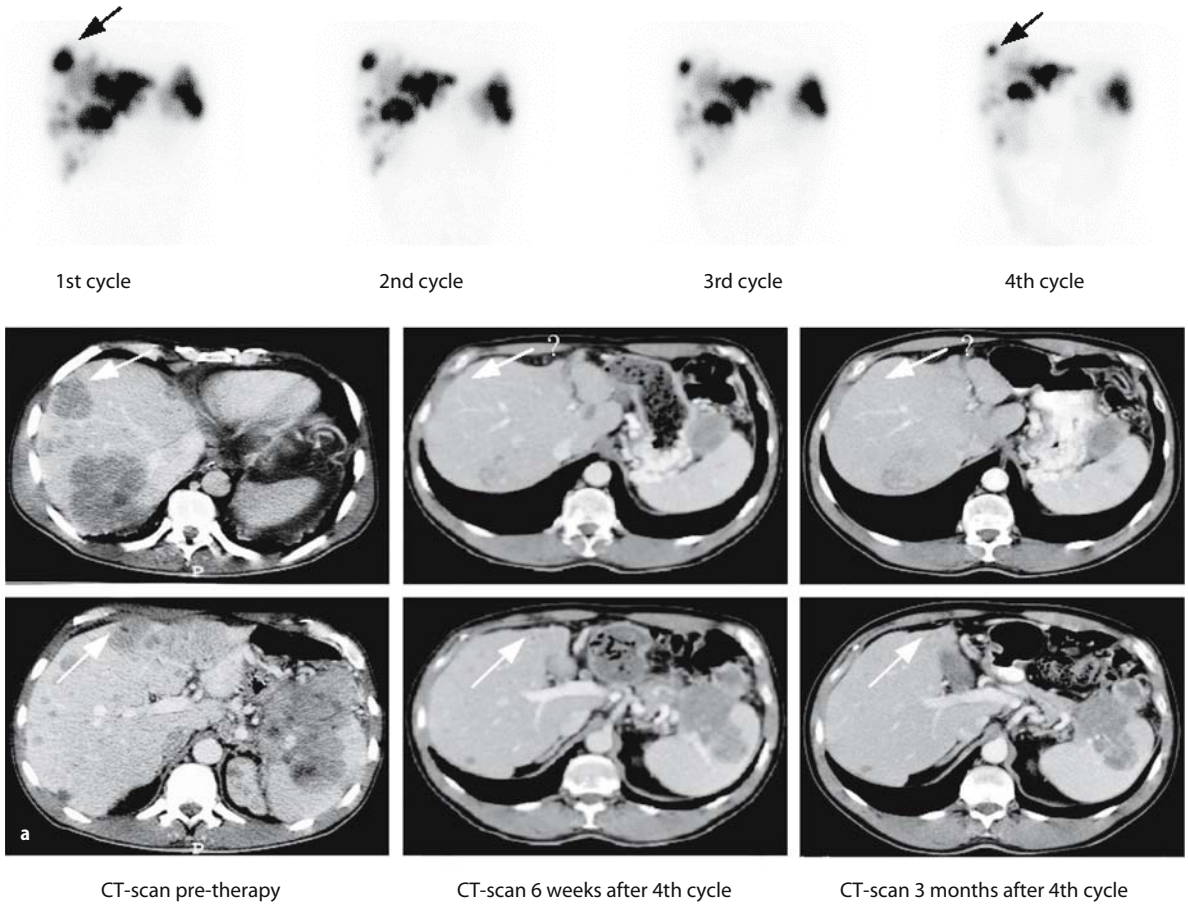

Fig. 24.2a, b. Baseline and follow-up data of a patient with carcinoid with liver metastases. *Top* Post-therapy scintigraphy after each cycle is shown. Note the decrease in uptake of [^{177}Lu-DOTA^0, Tyr^3]octreotate on the last scintigraphy in comparison with the first (*black arrows* indicate index lesion). *Middle* Three and 6 months after four cycles of therapy the patient had a partial remission (> 50 % decrease of tumor volume on CT; *white arrows* indicate index lesion). **b** Regression of tumor mass was accompanied by a decrease of the serum concentration of alkaline phosphatase (reference range 0 – 119 U/l), gamma-GT (reference range 0 – 49 U/l) and the tumor marker chromogranin A (reference range 10 – 100 ng/ml)

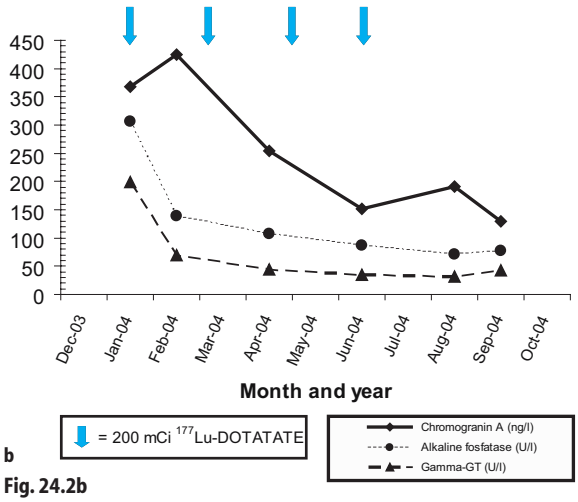

b

Fig. 24.2b

2005). Logistic regression analyses demonstrated that higher remission rates correlated positively with high uptake during pretherapy [^{111}In-DTPA^0]octreotide scintigraphy and a limited number of liver metastases, whereas PD was significantly more frequent in patients with a low KPS and extensive disease. Furthermore, it was observed that in patients who eventually had tumor regression less uptake was seen on the third or fourth post-therapy scintigraphy compared with the first post-therapy scintigraphy. Therefore, it was concluded that, considering the time of progression, ^{177}Lu-DOTATATE performed considerably better than chemotherapy.

24.3.4 Comparison of the Different Treatments

Treatment with ^{90}Y and ^{177}Lu labeled somatostatin analogs is very encouraging in terms of tumor shrinkage. However, a direct comparison to evaluate the optimal treatment remains difficult. Differences in treatment protocol, such as administered doses, dosing schemes and the tumor response criteria used, can be responsible for the observed differences in treatment outcome. Therefore, randomized controlled trials are necessary to define the optimal PRRT and treatment scheme.

24.4 Side Effects and Radiation Toxicity

Adverse reactions observed after PRRT can be divided into direct side effects and more delayed effects of radiotoxicity. Direct effects commonly mentioned after and during therapy are nausea, vomiting and abdominal pain (Anthony et al. 2002; Kwekkeboom et al. 2003a; Waldherr et al. 2001). In general, these side effects occur in a minority of patients and are easily treated with anti-emetics or pain medication. Mild hair loss was observed in patients treated with ^{177}Lu-DOTATATE, but hair growth had normalized at follow-up 3–6 months after the last administration (Kwekkeboom et al. 2003a). Beside these mild side effects, more serious toxicity may occur, especially to the bone marrow, kidneys and liver. The reported percentages of these side effects or toxicities are shown in Table 24.5.

24.4.1 Hematologic Toxicity

Hematologic toxicities grade 3–4 for hemoglobin (HGB), white blood cells (WBC) and platelets (PLT) were reported up to a maximum of 15% (Anthony et al. 2002; Bodei et al. 2003; Kwekkeboom et al. 2003b; Otte et al. 1999; Valkema et al. 2002a; Valkema et al. 2003a; Waldherr et al. 2002a). In general, the decrease in blood cell count was transient, and only occasionally was transfusion needed. More serious side effects were reported in a clinical trial in which 50 patients were treated with ^{111}In-octreotide (Valkema et al. 2002a). Leuke-

Table 24.5. Side effects in patients with somatostatin receptor-positive (GEP and non-GEP) tumors treated with different radiolabeled somatostatin analogs

Authors (year of publication)	Radioligand	No. of patients	Grade 3–4 hematologic toxicity[a]			Other toxicity
			Platelets	HGB	WBC	
Valkema et al. (2002a)	[^{111}In-DTPA^0]octreotide	50	10%	15%	2%	3 AML/MDS
Anthony et al. (2002)	[^{111}In-DTPA^0]octreotide	27	7%	11%	7%	3 Liver, 1 renal
Bodei et al. (2003)	[^{90}Y-DOTA^0,Tyr^3]octreotide	40	7%	3%	7%	
Otte et al. (1999)	[^{90}Y-DOTA^0,Tyr^3]octreotide	29	3%	7%	0%	4 Renal[b]
Waldherr et al. (2002a)	[^{90}Y-DOTA^0,Tyr^3]octreotide	39	0%	3%	0%	1 Renal
Valkema et al. (2003a)	[^{90}Y-DOTA^0,Tyr^3]octreotide	60	12%	8%	13%	1 MDS, 1 liver, 1 renal
Kwekkeboom et al. (2003b)	[^{177}Lu-DOTA^0,Tyr^3]octreotate	201	3%	1%	2%	1 MDS, 2 liver[c], 1 renal

Percentages are based on patient numbers. *AML*, acute myeloid leukemia; *MDS*, myelodysplastic syndrome

[a] Most of the mentioned hematologic toxicities were transient. See ref. for more detailed information

[b] No amino acid infusion in half of the patients

[c] D.J. Kwekkeboom, personal communication (2004)

mia and myelodysplastic syndrome (MDS) were reported in three patients who had been treated with total cumulative doses of > 2.7 Ci (> 100 GBq) and an estimated cumulative bone marrow radiation dose of about 3 Gy. One patient, who developed acute myeloid leukemia 17 months after the first dose of ^{111}In-octreotide, had had chemotherapy and treatment with interferon before PRRT. The other two patients who had had no previous cytotoxic therapy developed MDS after more than 3 years. None of the 44 patients who were treated with a cumulative dose lower than 100 GBq developed MDS or leukemia. In a phase I trial with ^{90}Y-DOTATOC (Novartis; Basel, Switzerland) in which the objective was to define the maximal tolerated single and four-cycle doses, one patient had MDS 2 years after the start of PRRT; this patient also had previous chemotherapy (Valkema et al. 2003a). In the report by Kwekkeboom et al. (2003b), who studied the patients treated with ^{177}Lu-DOTATATE as PRRT, one patient in the whole group of patients who had been treated, or were being treated up to that moment (201 patients; 637 administration), developed MDS. Also, this patient had had chemotherapy in the past. In summary, hematologic toxicity in PRRT is in general mild and reversible and the risk of developing MDS or leukemia is low if certain dosing limits are being respected.

24.4.2 Renal Toxicity

Chelated somatostatin analogs are predominantly cleared by the kidneys. Accumulation and retention of these analogs within the kidney occurs, but is not somatostatin receptor mediated (Bakker et al. 1991). Because of the rapid clearance, [^{111}In-DTPA^0]octreotide can be safely applied for diagnostic use without any damage to the kidneys (Krenning et al. 1992, 1993). However, for therapeutic use, the renal accumulation and the relatively long renal effective half-life of the radiopharmaceutical can be dose-limiting. In external beam radiation therapy, renal absorbed doses of 23 Gy (fractions of 2 Gy) may cause nephropathy in 5 % of patients in 5 years, whereas 28 Gy leads to a 50 % risk in the same period (Emami et al. 1991). However, since PRRT is applied as a continuous low-dose radiation with intracellular accumulation, a maximum cumulative dose limit of 23 Gy may not be applicable. The first reports on acute (6 – 12 months after radiation exposure) and late (1 – 5 years after exposure) renal side effects appeared after the use of ^{90}Y-DOTATOC in various clinical trials (Cybulla et al. 2001; Moll et al. 2001; Otte et al. 1998; Stoffel et al. 2001). The results suggested that a cumulative dose of ^{90}Y-DOTATOC of more than 7.4 GBq/m^2 might be a risk factor for renal insufficiency (Otte et al. 1998). However, some years later, a case report of a patient who developed late-onset renal insufficiency with a total cumulative dose < 7.4 GBq/m^2 indicated that even less radiation can cause renal damage at a later time point (Cybulla et al. 2001). In contrast, no renal toxicity in patients treated with [^{111}In-DTPA^0]octreotide was found (Valkema et al. 2002a). The difference between ^{111}In and ^{90}Y with regard to induction of radiation nephropathy may be explained by the difference in emitted particle range (~10 µm vs. ~12 mm, respectively). The Auger electrons emitted by ^{111}In within the tubulus cells do not reach the radiosensitive glomeruli. This particle range advantage might also be the reason why only one patient of a group of 200 patients treated with ^{177}Lu-DOTATATE developed renal failure (Kwekkeboom et al. 2003b). Although the number of reported patients with radiation nephropathy was relatively low and the potential benefit for the patients outweighs the risk of occurrence of this severe complication, it became clear that PRRT induced radiation nephropathy is difficult to predict with the currently applied maximum cumulative dose limits. Two recent studies in which patients were treated with ^{90}Y-DOTATOC provided more insight into individual kidney dosimetry and the importance of it in PRRT (Barone et al. 2005; Valkema et al. 2005). These studies indicated that apart from the total renal radiation dose, the dose volume, fractionation rate and the clinical parameters hypertension, diabetes and age are relevant risk factors for the development of renal function loss.

Obviously, kidney protection methods to prevent the kidney from a high absorbed dose with each administration are of importance. The most important method currently used to reduce renal uptake of radioactivity in PRRT is the use of amino acid solutions which can be easily co-administered during therapy. Pre-clinical studies showed that infusion of positively charged amino acids, mainly L-lysine and L-arginine, are able to reduce the tubular reabsorption of radiolabeled somatostatin analogs in rats (de Jong et al. 1996). Clinical studies proved that co-infusion with a combination of the amino acids L-lysine and L-arginine or a mixed amino acid solution on the day of therapy led to a reduction of renal uptake of between 20 % and 47 % (Bodei et al. 2003; Jamar et al. 2003; Kwekkeboom et al. 2001; Rolleman et al. 2003). Higher doses of amino acids are more effective but have the disadvantage of the induction of a higher incidence of side effects, such as nausea, vomiting and, especially with higher doses of L-lysine, hyperkalemia (Barone et al. 2004; Rolleman et al. 2003).

24.4.3 Liver Toxicity

Most patients treated with PRRT in the clinical trials studied had liver metastases. The extent of liver involvement ranged from a single lesion to diffuse liver

involvement with pronounced hepatomegaly. It is therefore not unlikely that PRRT can induce hepatocellular radiation injury. However, in clinical practice it may be difficult to distinguish an increase of liver function parameters induced by radiation from subtle progression of liver metastases. Anthony et al. (2002) reported three patients (out of a total of 27), treated with ^{111}In-octreotide, in whom a temporary increase of liver function parameters (grade IV liver toxicity; WHO toxicity grading) was observed. All three patients had tumor replacement of more than 75 % of their hepatic parenchyma and treatment-associated necrosis on the CT scans. In patients with less extensive liver disease, changes in liver function parameters did not occur. A significant increase of liver function parameters after administration of ^{90}Y-DOTATOC was reported in two studies (Bushnell et al. 2003a; Valkema et al. 2003a). Valkema et al. (2003) reported one transient grade 3 toxicity in a group of 60 patients treated with ^{90}Y-DOTATOC (Phase I study). In another study, 15 patients with proven liver metastases (of whom 12 had extensive liver involvement defined as 25 % or more) from neuroendocrine tumors were treated with three cycles of 120 mCi each (4.4 GBq) (Bushnell et al. 2003a). In only four of these 15 patients, one or more of the three liver enzymes that were measured – serum aspartate aminotransferase, alanine aminotransferase and alkaline phosphatase – increased at least one grade, according to the World Health Organization common toxicity criteria, from baseline to final follow-up measurement (4 – 6 weeks post cycle 3). It was concluded that patients with diffuse somatostatin receptor-positive hepatic metastases can be treated with cumulative administered activity of 360 mCi (13.2 GBq) of ^{90}Y-DOTATOC with only a small chance of developing mild acute or subacute hepatic injury. In the group of patients treated with ^{177}Lu-DOTATATE, significantly increased liver function parameters (grade IV liver toxicity) were evident in two patients after the first cycle of treatment (Kwekkeboom, personal communication). One patient, who suffered from a rapidly growing neuroendocrine tumor with extensive liver involvement, clinically progressed to liver failure within 3 weeks and died shortly thereafter. Whether the aggressive nature of the tumor or PRRT induced toxicity led to this fatal condition remains unclear. The other patient, who after the first therapy developed dyspnea, acute abdominal pain and an increase of liver function parameters, was hospitalized for several weeks. Gradually, liver function parameters and hyperbilirubinemia returned to pretherapy levels. Treatment with ^{177}Lu-DOTATATE was continued 6 months after the first therapy with a reduced dose of 1.9 GBq followed by a third administration of 4.1 GBq without any acute side effects.

24.5 Clinical Practice and Indications

In patients with metastasized GEP tumors, for whom surgery is no longer an option, PRRT can be an effective alternative therapeutic modality with limited side effects. The results, in terms of tumor volume reduction as shown in the different clinical trials, are very encouraging and seem to compare favorably with chemotherapy. However, no randomized controlled study has been performed to confirm this.

Although proven effective in a substantial percentage of patients, PRRT has not been recognized widely as alternative systemic therapy. Instead, the "wait-and-see" approach often remains the mainstay of initial management in patients with unresectable disease. The rationale for this approach is found in the natural history of well-differentiated GEP tumors without treatment, in which tumors can be indolent for many years, and the well-being of patients, even with metastasized tumors, can be unchanged for many years. However, the reported studies on PRRT clearly indicate that patients with documented progressive disease or a substantial increase in symptoms can benefit from this therapy. The recognition of the possible benefit of PRRT for patients with GEP tumors is increasing, but its implementation within the whole therapeutic array is rather poor. Factors that contribute to this include the fact that PRRT is a relatively novel therapeutic modality, the lack of approved radiopharmaceuticals, which is in part related to the increase in governmental demands, and therapy-related costs.

24.5.1 Indications for PRRT

Candidates for PRRT are those patients with inoperable GEP tumors who have progressive disease or symptomatology which is difficult to manage with medication alone. If it is agreed that the malignancy is inoperable, the tumor has to be somatostatin receptor-positive, based on tumor uptake on ^{111}In-octreotide scintigraphy. Furthermore, the amount of tumor uptake has to be equal to or higher than in normal liver tissue (according to criteria previously described by Krenning et al. 1999). High uptake during ^{111}In-octreotide scintigraphy has been shown to be correlated with tumor regression after PRRT (Kwekkeboom et al. 2003a). Additionally, because of the radiation to the bone marrow and the risk of temporary bone-marrow suppression, patients need to fulfil certain minimal hematologic criteria. Kidney function has to be determined before therapy to exclude patients with signs of impending renal failure (glomerular filtration rate < 40 ml/min). The presence of bone metastases, which are present in a minority of patients, is no exclusion criterion. As a rule, if

Table 24.6. Recommended selection criteria for peptide receptor radionuclide therapy in patients with neuroendocrine GEP tumors

Inclusion
Sufficient tumor uptake on ^{111}In-octreotide scintigrams
Hematology
Hemoglobin ≥ 5.0 mmol/l
White blood cell count ≥ $2-3.5\times10^9$/l
Platelet count ≥ $75-100\times10^9$/l
Kidney function
Creatinine (serum) ≥ 150 µmol/l or creatinine clearance ≥ 40 ml/min
Karnofsky Performance Status ≥ 50
Life expectancy > 6 months
Exclusion
Chemotherapy within 6 weeks prior to treatment start
Pregnancy/lactation

a tumor response occurs, all tumor sites decrease in size. However, cystic and bone lesions seem to respond in a more protracted way than the more common solid liver metastases. Up to now, no systematic study has been performed to address the issue of a possible differential response of metastases based on their location. Full patient selection criteria are summarized in Table 24.6.

24.5.2 Timing of Therapy

Currently, there is no consensus about when to start PRRT in patients with GEP tumors. The stage of disease at which the diagnosis is made is highly variable and ranges from localized non-metastatic primary tumor to more advanced or end-stage disease with hepatomegaly and ascites. In a recent report in which the relationships between delay of diagnosis, extent of disease, and survival in 115 patients with carcinoid were studied, a mean delay in the diagnosis of 66 months was found (Toth-Fejel and Pommier 2004). It was concluded that the diagnosis of carcinoid is difficult and, therefore, a delay of diagnosis by physicians common. Strikingly, the delay of the diagnosis did not correlate with the extent of the disease. However, the extent of the disease did correlate with survival. Patients with primary tumors and lymph node metastases were less likely to die of carcinoid disease than patients with hepatic metastases, carcinomatosis or extra-abdominal metastases. Unfortunately, reports on PRRT with explicit survival data are few. In the multicenter trial with ^{111}In-octreotide (Valkema et al. 2002a), it was reported that PRRT in end-stage patients with higher tumor burden was less likely to have a favorable outcome than in patients with lower tumor burden or in better general condition. Survival data in a group of 27 patients treated with ^{111}In-octreotide presented by Anthony et al. (2002) suggested a survival benefit in patients treated with ^{111}In-octreotide. However, the number of patients studied was low and the survival data of the treated group was compared with data of a historical control group. In the clinical studies with ^{177}Lu-DOTATATE, it was suggested that because of the high success rate of the therapy, the low incidence of side effects and the high median time to progression (> 36 months), its use can be advocated in patients with metastasized, unresectable GEP tumors without waiting for tumor progression (de Jong et al. 2003; Kwekkeboom et al. 2003a). Another argument in favor of early treatment is that neuroendocrine tumors can dedifferentiate in the course of the disease and thereby lose the expression of somatostatin receptors. Treatment with radiolabeled somatostatin analogs will then be impossible (Kwekkeboom et al. 2003a). However, whether early treatment would benefit patients with metastasized, unresectable GEP tumors in terms of longer survival remains to be studied and should imply randomization into a group with and without PRRT. At this moment, when there seems to be proof that PRRT is an effective therapy, such a survival study seems unethical. Another issue, regarding the question of whether we should treat patients with PRRT at an early stage of the disease or wait for further disease progression, is the benefit in terms of clinical response and quality of life. Only a limited number of studies address this issue. There is, however, a growing awareness of its importance in clinical oncology trials, especially in therapies for which cure is not the primary goal and survival gains are low or unknown (Sanders et al. 1998). As a consequence the more recent PRRT reports have included data on clini-

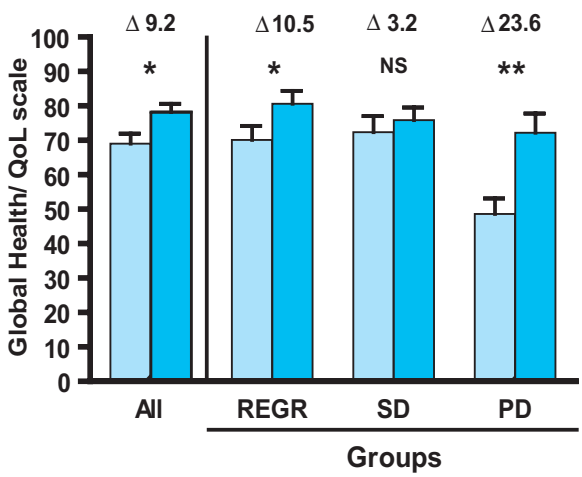

Fig. 24.3. Global health/quality of life scale scores of all the patients ($n = 50$) and the different outcome groups according to tumor evaluation before (*bars light blue*) and 3 months after (*darker blue*) ^{177}lutetium-octreotate therapy. *REGR* regression (CR, PR and MR), *SD* stable disease, *PD* progressive disease, *NS* not significant. Standard errors to the mean (SEM) are shown; $^*p < 0.05$, $^{**}p < 0.01$, *NS* not significant (ANOVA, two-sided; $p < 0.05$ was considered significant). (Data used from Teunissen et al. 2004)

cal effectiveness of therapy. Two studies with ^{90}Y-DOTATOC provided evidence for a favorable clinical response in 60–70% of the patients (Bushnell et al. 2003b; Valkema et al. 2002b). In patients treated with ^{177}Lu-DOTATATE, quality of life (QoL) assessment showed significant improvement of the global health/QoL score (Δ score of +9.2; scale range 0–100; $p < 0.01$), especially in those patients with proven tumor regression (Δ score of +10.5; $p < 0.05$) (Teunissen et al. 2004) (Fig. 24.3). Although the assessment methods for identifying clinical changes differ in these studies, the combined results indicate that patients may experience clinical benefit from PRRT.

24.6 Future Developments

A direction of future research to improve the current PRRT in GEP tumors includes the development of new stable somatostatin analogs with high affinity for the different somatostatin receptor subtypes. The new analog [DOTA^0-1-naphthyl^3]octreotide (DOTANOC), for example, is an analog that has high affinity for SSTR2, SSTR3 and SSTR5 (Wild et al. 2003). Therefore, it might be a promising analog to be used for treatment of patients with tumors that not only bear SSTR2, but also express SSTR3 and/or SSTR5. Furthermore, combined treatment with different radiolabeled somatostatin analogs, in analogy with the favorable response with combinational chemotherapy in solid tumors, compared to single agent therapy, is of great interest. Of course, this approach will be limited by the combined toxicity of the radiolabeled peptides. Preclinical PRRT studies with ^{90}Y-DOTATOC and ^{177}Lu-DOTATATE indicate that there is an optimal tumor size in terms of tumor reduction efficacy for each radionuclide. As most patients have metastatic disease with tumors of different size, combination PRRT could achieve higher cure rates compared with single agent therapy.

Higher cure rates are possible when the density of expressed somatostatin receptors is enhanced. In vitro and in vivo studies show that irradiation of neuroendocrine AR42J (rat pancreatic tumor) cells can upregulate the expression of SSTR2 and gastrin receptors (Béhé et al. 2003). PRRT after upregulated expression of SSTR2 may lead to higher uptake of the radiolabeled peptide and consequently higher therapeutic efficacy.

Most research in PRRT is focussed on the different subtypes of the somatostatin receptor. However, neuroendocrine tumors may express other tumor specific peptides, such as vasoactive intestinal peptide, cholecystokinin, bombesin and glucagon-like peptide-1 receptors (Reubi and Waser 2003). The concomitant expression of these receptors could be used in the future in a multi-receptor PRRT to target more efficiently GEP tumors in each patient individually. Especially in tumors with a heterogeneous or even reciprocal receptor distribution, this approach could be very favorable in terms of achieving a more homogenous distribution of the absorbed radiation dose within the tumor mass. Furthermore, two or more radioligands administered concomitantly could considerably increase the therapeutic dose to the tumor (Reubi et al. 2005).

The combination of PRRT with surgery and/or chemotherapy as a multimodality treatment strategy is of interest and requires the start of randomized trials to prove whether current results may be improved. Studies that can also be considered are the use of PRRT combined with surgery in an adjuvant setting to irradiate occult metastases. Furthermore, the use of PRRT in a neo-adjuvant setting, debulking the tumor mass followed by surgery in patients with initially locally advanced inoperable disease, has been described (Van Eijck 2005).

External beam radiotherapy in combination with chemotherapy such as gemcitabine, which is a known potent radiation sensitizer, has been shown to have favorable effects in patients with non-small cell lung cancer (van Putten et al. 2003). Although the patients were treated with external radiotherapy, gemcitabine or other radiosensitizing agents with concurrent PRRT might prove effective in the future.

References

Andersson P, et al. (1996) Internalization of indium-111 into human neuroendocrine tumor cells after incubation with indium-111-DTPA-D-Phe1-octreotide. J Nucl Med 37(12): 2002–2006

Anthony LB, et al. (2002) Indium-111-pentetreotide prolongs survival in gastroenteropancreatic malignancies. Semin Nucl Med 32(2):123–132

Bakker WH, et al. (1991) In vivo application of [111In-DTPA-D-Phe1]-octreotide for detection of somatostatin receptor-positive tumors in rats. Life Sci 49(22):1593–1601

Barone R, et al. (2004) Metabolic effects of amino acid solutions infused for renal protection during therapy with radiolabelled somatostatin analogues. Nephrol Dial Transplant 19(9):2275–2281

Barone R, et al. (2005) Patient-specific dosimetry in predicting renal toxicity with 90Y-DOTATOC: Relevance of kidney volume and dose rate in finding a dose-effect relationship. J Nucl Med 46 (1 Suppl):99–106

Baum RP, et al. (2004a) Intravenous and intra-arterial peptide receptor radionuclide therapy (PRRT) using Y-90-DOTA-Tyr3-octreotate (Y-90-DOTA-TATE) in patients with metastatic neuroendocrine tumors. Eur J Nucl Med 31 (Suppl 2):S238 (abstract)

Baum RP, et al. (2004b) Peptidrezeptorvermittelte Radiotherapie (PRRT) neuroendokriner tumoren klinischen Indikationen und Erfahrung mit 90Yttrium-markierten Somatostatinanaloga. Der Onkologe 10(10):1098–1110

Béhé M, et al. (2003) Upregulation of gastrin and somatostatin receptor after irradiation. Eur J Nucl Med 44 (Suppl2):S218 (abstract)

Bodei L, et al. (2003) Receptor-mediated radionuclide therapy

with 90Y-DOTATOC in association with amino acid infusion: A phase I study. Eur J Nucl Med Mol Imaging 30(2): 207 – 216
Bodei L, et al. (2004) Receptor radionuclide therapy with (90)Y-[DOTA](0)-Tyr(3)-octreotide ((90)Y-DOTATOC) in neuroendocrine tumours. Eur J Nucl Med Mol Imaging 31(7):1038 – 1046
Bruno JF, Berelowitz M (1993) Somatostatin receptors: Orphan that found family and function. Mol Cell Neurosci 4(4): 307 – 309
Buscombe JR, et al. (2003) Long-term efficacy of high-activity 111In-pentetreotide therapy in patients with disseminated neuroendocrine tumors. J Nucl Med 44(1):1 – 6
Bushnell D, et al. (2003a) Assessment of hepatic toxicity from treatment with 90Y-SMT 487 (OctreoTher(TM)) in patients with diffuse somatostatin receptor positive liver metastases. Cancer Biother Radiopharm 18(4):581 – 588
Bushnell D, et al. (2003b) Evaluating the clinical effectiveness of 90Y-SMT 487 in patients with neuroendocrine tumors. J Nucl Med 44(10):1556 – 1560
Capello A, et al. (2003) Peptide receptor radionuclide therapy in vitro using [111In-DTPA0]octreotide. J Nucl Med 44(1): 98 – 104
Chinol M, et al. (2002) Receptor-mediated radiotherapy with Y-DOTA-D-Phe-Tyr-octreotide: The experience of the European Institute of Oncology group. Semin Nucl Med 32(2): 141 – 147
Cybulla M, et al. (2001) End-stage renal disease after treatment with 90Y-DOTATOC. Eur J Nucl Med 28(10):1552 – 1554
de Jong M, et al. (1996) Inhibition of renal uptake of indium-111-DTPA-octreotide in vivo. J Nucl Med 37(8):1388 – 1392
de Jong M, et al. (1998) Comparison of (111)In-labeled somatostatin analogues for tumor scintigraphy and radionuclide therapy. Cancer Res 58(3):437 – 441
de Jong M, et al. (2001a) Tumor response after [(90)Y-DOTA(0),Tyr(3)]octreotide radionuclide therapy in a transplantable rat tumor model is dependent on tumor size. J Nucl Med 42(12):1841 – 1846
de Jong M, et al. (2001b) Receptor-targeted radionuclide therapy using radiolabelled somatostatin analogues: Tumour size versus curability. J Nucl Med 28(8):1026 (abstract)
de Jong M, et al. (2002) Somatostatin receptor-targeted radionuclide therapy of tumors: Preclinical and clinical findings. Semin Nucl Med 32(2):133 – 140
de Jong M, et al. (2003) Radiolabelled peptides for tumour therapy: Current status and future directions. Plenary lecture at the EANM 2002. Eur J Nucl Med Mol Imaging 30(3):463 – 469
de Jong M, et al. (2005) Combination radionuclide therapy using 177Lu- and 90Y-labeled somatostatin analogs. J Nucl Med 46 (1 Suppl):13 – 17
Emami B, et al. (1991) Tolerance of normal tissue to therapeutic irradiation. Int J Radiat Oncol Biol Phys 21(1):109 – 122
Hofland LJ, et al. (1995) Internalization of the radioiodinated somatostatin analog [125I-Tyr3]octreotide by mouse and human pituitary tumor cells: Increase by unlabeled octreotide. Endocrinology 136(9):3698 – 3706
Hofland LJ, et al. (2003) Crucial role for somatostatin receptor subtype 2 in determining the uptake of [111In-DTPA-D-Phe1]octreotide in somatostatin receptor-positive organs. J Nucl Med 44(8):1315 – 1321
Jamar F, et al. (2003) 86Y-DOTA(0)-D-Phe1-Tyr3-octreotide (SMT487) – a phase 1 clinical study: Pharmacokinetics, biodistribution and renal protective effect of different regimens of amino acid co-infusion. Eur J Nucl Med Mol Imaging 30(4):510 – 518
John M, et al. (1996) Positive somatostatin receptor scintigraphy correlates with the presence of somatostatin receptor subtype 2. Gut 38(1):33 – 39
Krenning EP, et al. (1992) Somatostatin receptor scintigraphy with indium-111-DTPA-d-phe-1-octreotide in man: Metabolism, dosimetry and comparison with iodine-123-Tyr-3-octreotide. J Nucl Med 33(5):652 – 658
Krenning EP, et al. (1993) Somatostatin receptor scintigraphy with [111In-DTPA-D-Phe1]- and [123I-Tyr3]-octreotide: The Rotterdam experience with more than 1000 patients. Eur J Nucl Med 20(8):716 – 731
Krenning EP, et al. (1994) Radiotherapy with a radiolabeled somatostatin analogue, [111in-DTPA-D-Phe1]-octreotide. A case history. Ann N Y Acad Sci 733:496 – 506
Krenning EP, et al. (1999) Radiolabelled somatostatin analogue(s) for peptide receptor scintigraphy and radionuclide therapy. Ann Oncol 10 (Suppl 2):S23 – 29
Kwekkeboom D, et al. (2000) Peptide receptor imaging and therapy. J Nucl Med 41(10):1704 – 1713
Kwekkeboom DJ, et al. (2001) [177Lu-DOTA0,Tyr3]octreotate: Comparison with [111In-DTPA0]octreotide in patients. Eur J Nucl Med 28(9):1319 – 1325
Kwekkeboom DJ, et al. (2003a) Treatment of patients with gastro-entero-pancreatic (GEP) tumours with the novel radiolabelled somatostatin analogue [(177)Lu-DOTA(0),Tyr(3)]octreotate. Eur J Nucl Med Mol Imaging 30(3):417 – 422
Kwekkeboom DJ, et al. (2003b) Treatment with Lu-177-DOTA-Tyr3-octreotate in patients with neuroendocrine tumors: Interim results. Eur J Nucl Med Mol Imaging 30 (Suppl 2) (Suppl 2):S231 (abstract)
Kwekkeboom DJ, et al. (2005) Radiolabeled somatostatin analog [177Lu-DOTA0,Tyr3]octreotate in patients with endocrine gastroenteropancreatic tumors. J Clin Oncol 23(12): 2754 – 2762
McCarthy KE, et al. (2000) In situ radiotherapy with 111In-pentetreotide. State of the art and perspectives. Q J Nucl Med 44(1):88 – 95
Moll S, et al. (2001) A new cause of renal thrombotic microangiopathy: Yttrium 90-DOTATOC internal radiotherapy. Am J Kidney Dis 37(4):847 – 851
O'Donoghue JA, et al. (1995) Relationships between tumor size and curability for uniformly targeted therapy with beta-emitting radionuclides. J Nucl Med 36(10):1902 – 1909
Otte A, et al. (1998) Yttrium-90-labelled somatostatin-analogue for cancer treatment. Lancet 351(9100):417 – 418
Otte A, et al. (1999) Yttrium-90 DOTATOC: First clinical results. Eur J Nucl Med 26(11):1439 – 1447
Paganelli G, et al. (2001) Receptor-mediated radiotherapy with 90Y-DOTA-D Phe1-Tyr3-octreotide. Eur J Nucl Med 28(4): 426 – 434
Paganelli G, et al. (2002) 90Y-DOTA-D-Phe1-Tyr3-octreotide in therapy of neuroendocrine malignancies. Biopolymers 66(6):393 – 398
Panetta R, et al. (1994) Molecular cloning, functional characterization, and chromosomal localization of a human somatostatin receptor (somatostatin receptor type 5) with preferential affinity for somatostatin-28. Mol Pharmacol 45(3):417 – 427
Reubi JC, Waser B (2003) Concomitant expression of several peptide receptors in neuroendocrine tumours: Molecular basis for in vivo multireceptor tumour targeting. Eur J Nucl Med Mol Imaging 30(5):781 – 793
Reubi JC, et al. (1990) Somatostatin receptor incidence and distribution in breast cancer using receptor autoradiography: Relationship to EGF receptors. Int J Cancer 46(3):416 – 420
Reubi JC, et al. (2000) Affinity profiles for human somatostatin receptor subtypes SST1–SST5 of somatostatin radiotracers selected for scintigraphic and radiotherapeutic use. Eur J Nucl Med 27(3):273 – 282
Reubi JC, et al. (2005) Candidates for peptide receptor radiotherapy today and in the future. J Nucl Med 46 Suppl 1:67S–75S

Rohrer L, et al. (1993) Cloning and characterization of a fourth human somatostatin receptor. Proc Natl Acad Sci U S A 90(9):4196 – 4200
Rolleman EJ, et al. (2003) Safe and effective inhibition of renal uptake of radiolabelled octreotide by a combination of lysine and arginine. Eur J Nucl Med Mol Imaging 30(1):9 – 15
Sanders C, et al. (1998) Reporting on quality of life in randomised controlled trials: Bibliographic study. BMJ (Clinical Research ed.)317 (7167):1191 – 1194
Slooter GD, et al. (1999) Anti-proliferative effect of radiolabelled octreotide in a metastases model in rat liver. Int J Cancer 81(5):767 – 771
Smith MC, et al. (2000) OctreoTher: Ongoing early clinical development of a somatostatin-receptor-targeted radionuclide antineoplastic therapy. Digestion 62 (Suppl 1):69 – 72
Stoffel MP, et al. (2001) Radiation nephropathy after radiotherapy in metastatic medullary thyroid carcinoma. Nephrol Dial Transplant 16(5):1082 – 1083
Teunissen JJ, et al. (2004) Quality of life in patients with gastroenteropancreatic tumors treated with [177Lu-DOTA0, Tyr3]octreotate. J Clin Oncol 22(13):2724 – 2729
Toth-Fejel S, Pommier RF (2004) Relationships among delay of diagnosis, extent of disease, and survival in patients with abdominal carcinoid tumors. Am J Surg 187(5):575 – 579
Valkema R, et al. (2002a) Phase I study of peptide receptor radionuclide therapy with [In-DTPA]octreotide: The Rotterdam experience. Semin Nucl Med 32(2):110 – 122
Valkema R, et al. (2002b) Phase 1 study of therapy with 90Y-SMT487 (OctreoTher) in patients with somatostatin receptor (SS-R) positive tumors. J Nucl Med 43 (Suppl):33P (abstract)
Valkema R, et al. (2003a) Long-term follow-up of a phase 1 study of peptide receptor radionuclide therapy (PRRT) with (90Y-DOTA0,Tyr3)octreotide in patients with somatostatin receptor positive tumours. Eur J Nucl Med 30 (Suppl 2):S232 (abstract)
Valkema R, et al. (2003b) Survival in patients with neuroendocrine tumors after treatment with [90Y-DOTA,Tyr) in a phase-1 study. J Nucl Med 44 (Suppl 2):136P
Valkema R, et al. (2005) Long-term follow-up of renal function after peptide receptor radiation therapy with 90Y-DOTA0,Tyr3-octreotide and 177Lu-DOTA0, Tyr3-octreotate. J Nucl Med 46 (1 Suppl):83 – 91
Van Eijck CH (2005) Treatment of advanced endocrine gastroenteropancreatic tumours using radiolabelled somatostatin analogues. Br J Surg 92(11):1333 – 1334
van Putten JWG, et al. (2003) A phase I study of gemcitabine with concurrent radiotherapy in stage III, locally advanced non-small cell lung cancer. Clin Cancer Res 9(7):2472 – 2477
Virgolini I, et al. (2002) In- and Y-DOTA-lanreotide: Results and implications of the Mauritius trial. Semin Nucl Med 32(2):148 – 155
Waldherr C, et al. (2001) The clinical value of [90Y-DOTA]-d-phe1-Tyr3-octreotide (90Y-DOTATOC) in the treatment of neuroendocrine tumours: A clinical phase II study. Ann Oncol 12(7):941 – 945
Waldherr C, et al. (2002a) Tumor response and clinical benefit in neuroendocrine tumors after 7.4 GBq (90)Y-DOTATOC. J Nucl Med 43(5):610 – 616
Waldherr C, et al. (2002b) Does tumor response depend on the number of treatment sessions at constant injected dose using 90yttrium-DOTATOC in neuroendocrine tumors? Eur J Nucl Med 29:S100 (abstract)
Wild D, et al. (2003) DOTA-NOC, a high-affinity ligand of somatostatin receptor subtypes 2, 3 and 5 for labelling with various radiometals. Eur J Nucl Med Mol Imaging 30(10): 1338 – 1347
Yamada Y, et al. (1992) Cloning and functional characterization of a family of human and mouse somatostatin receptors expressed in brain, gastrointestinal tract, and kidney. Proc Natl Acad Sci U S A 89(1):251 – 255
Yamada Y, et al. (1993) Cloning, functional expression and pharmacological characterization of a fourth (hSSTR4) and a fifth (hSSTR5) human somatostatin receptor subtype. Biochem Biophys Res Commun 195(2):844 – 852

25 Neuroendocrine Tumors (MIBG)

M. Welsch, F. Grünwald

25.1 Introduction

Uptake of radiopharmaceuticals in the adrenal medulla was first demonstrated in 1967, using C-14-labeled epinephrine and precursors (Morales et al. 1967). In subsequent years this tracer was shown to depict neuroblastomas and pheochromocytomas (Lieberman et al. 1969; Anderson et al. 1973). In 1976 an iodinated compound of dopamine and a year later a radioiodinated bretylium analog were introduced (Ice et al. 1975; Korn et al. 1977). In 1980 the concentration of I-131-iodobenzylguanidine in the adrenal medulla was reported (Wieland et al. 1980).

25.2 Radiopharmaceuticals

Metaiodobenzylguanidine (MIBG) consists of a combination of the benzyl portion of bretylium and the guanidine group of guanethidine, and is radioiodinated in position 3 of the aromatic ring (Wieland et al. 1980). It shows a similar molecular structure to the adrenergic neurotransmitter norepinephrine (NE). NE, which is synthesized and stored in adrenergic granules, is then secreted and to some extent reassumed by the adrenergic cells. Through this uptake mechanism MIBG is transported into the chromaffin storage granules in adrenergic tissue as a false transmitter (Beierwaltes 1991). A sodium-dependent uptake mechanism has been reported, which can be inhibited by selective neuronal uptake-one inhibitors, as well as a sodium-independent uptake mechanism, which is a passive diffusion process (Tobes et al. 1985).

After intravenous injection, MIBG is cleared from the vascular compartment within 1 h. Physiologic distribution is found in the salivary glands, spleen, liver and urinary bladder (Wafelman et al. 1994). Portrayal of the salivary gland and spleen is due to the sympathic innervation, whereas the liver shows up because of its large volume (Nakajo et al. 1983). MIBG is excreted predominantly via the urine; less than 2% has been detected in the feces. Between 60% and 92% of iodinated MIBG is excreted unaltered; metabolites found in the urine are metaiodohippuric acid, radioiodide, and occasionally parahydroxymetaiodobenzylguanidine and metaiodobenzoic acid (Wafelman et al. 1994).

Radioactive labeling can be performed using I-123, I-125 or I-131. I-123-MIBG is considered the superior agent for diagnostic purposes. It shows an ideal gamma ray energy for imaging, has a lower radiation burden due to a shorter half-life and presents a limited particulate emission caused by the decay by electron capture (Shapiro and Gross 1987; Nakatani et al. 2002). I-131-MIBG is applied mainly for therapeutic purposes, using the beta ray energy and longer half-life for optimal efficacy (Castellani et al. 2000).

No-carrier added radioiodinated MIBG has been shown to achieve higher levels of specifically incorporated radioactivity than carrier-added MIBG (Franceschini et al. 1995). In an attempt to further improve the specific uptake characteristics, new MIBG derivates have been developed recently. One compound containing the non-polar methyl group at the 4-position of the aromatic ring, 3-[I-131]iodo-4-methyl-benzylguanidine (MeIBG), showed a higher cellular retention in animal and in vitro studies, compared to I-125-MIBG (Vaidyanathan et al. 2004).

25.3 Methodology

25.3.1 Patient Preparation

Thyroid blocking is essential before administration of MIBG in order to prevent thyroid irradiation caused by the uptake of free I-131 which emerges from chemical instability and biologic decomposition of MIBG. For diagnostic applications of I-123-MIBG, 100 mg of potassium iodide (van Santen et al. 2002) or 23 mg/kg body weight of sodium perchlorate is given orally 20 min before up to 4 days after tracer injection. For MIBG therapy the thyroid should be blocked with 100 mg potassium iodide starting 1 day before tracer application and continued for at least 14 days. A potassium iodide medication of 14 days showed that after

Table 25.1. Drugs interfering with MIBG uptake and storage

Mechanism of interaction	Medication	Suggested withdrawal
1. Inhibition of uptake-one	Tricyclic antidepressants	7 – 21 days
	Cocaine	7 – 14 days
	Labetalol	14 days
	α-Antagonists	7 – 14 days
	Antipsychotics	21 – 28 days
2. Inhibition of granular uptake	Reserpine, tetrabenazine	14 days
3. Competition for granular uptake	Sympathomimetics	7 – 14 days
4. Depletion of content from storage granules	Reserpine, tetrabenzaine	14 days
	Labetalol	14 days
	Guanethidine	14 days
5. Calcium mediated	Calcium antagonist	14 days
6. Others	β-Adrenergic antagonists	7 – 14 days

3.5 years follow-up 64 % of patients suffered from a thyrotropin elevation (van Santen et al. 2002). Another study administering potassium iodide over 4 weeks after therapy measured thyroidal absorbed radioiodide doses of up to 30 Gy (Brans et al. 2002). In 2003 a concept to improve thyroid protection was investigated (van Santen et al. 2003). A combined therapy of 100 µg/m^2 thyroxine, 0.5 mg/kg body weight methimazole and 90 mg potassium iodide were given. The follow-up after a median of 19 months showed elevated thyrotropin levels in only 17.4 % of patients.

Some medications have been shown to interfere with MIBG kinetics. There are various mechanisms of interaction with uptake or storage in the granules (Wafelman et al. 1994; Khafagi et al. 1989; Babich et al. 1997). Table 25.1 gives an overview of the different drugs. A reduced uptake in salivary glands has been proposed as an indicator of drug interference (Britton 1997; Zaplatnikov et al. 2004).

25.3.2 Radionuclide Dosage and Administration

According to the EANM procedure guidelines (Bombardieri et al. 2003), 40 – 80 MBq (1.2 – 2.2 mCi) I-131-MIBG or 400 MBq (10.8 mCi) I-123-MIBG should be used for adults for diagnostic imaging. The appropriate dosage for children is weight adapted and can be calculated using the schedule of the Pediatric Task Group of the EANM (Piepsz et al. 1990). A minimum dose of 80 MBq I-123-MIBG or 35 MBq I-131 is required and the maximal administered activity should not exceed 400 MBq (10.8 mCi) I-123-MIBG or 80 MBq (2.16 mCi) I-131-MIBG.

For therapeutic use reported doses vary. For the treatment of carcinoid tumors median doses of 6.75 GBq (182 mCi) (Sywak et al. 2004) and 14.8 GBq (400 mCi) (Safford et al. 2002) have been described. In a report on the treatment of malignant pheochromocytoma the median single dose was as high as 29.6 GBq (800 mCi). For the treatment of neuroblastoma 3.7 – 7.4 GBq (100 – 200 mCi) is used for adults (Castellani et al. 2000) and the administered doses for children range from 2.5 to 5.5 GBq (from 68 to 149 mCi) (Castellani et al. 2000; Garaventa et al. 1999).

A slow intravenous administration is essential to prevent release of norepinephrine from storage granules due to MIBG, which could result in a hypertensive crisis.

After injection vital signs should be monitored (McEwan et al. 1985). Additionally, an α-receptor blocker should be available.

25.3.3 Image Acquisition

Images are acquired with a large field gamma camera. For examinations with I-131-MIBG, a high energy, parallel hole collimator is needed and an energy window of 20 % centered at 364 keV. For imaging with I-123-MIBG, a low energy, high resolution collimator is used with the energy window of 20 % centered at 159 keV (EANM guidelines: Bombardieri et al. 2003).

Most tumors are visible after 24 h. Due to a decline in liver activity over time, a better contrast may be achieved 48 or even 72 h after injection (McEwan et al. 1985). Therefore, whole body images are recommended 24 and 48 h after injection, and an additional scan after 72 h may be helpful in some cases where I-131-MIBG is used. Anterior and posterior views are acquired with a scan speed of 4 cm/min for I-131-MIBG and a speed of 5 cm/min for I-123-MIBG (EANM guidelines: Bombardieri et al. 2003). In addition, SPECT images should be performed. SPECT has been reported to increase the number of detected lesions (Rufini et al. 1996). In another investigation the number of lesions detected remained unaltered, but the certainty of interpretation was improved by SPECT imaging (Gelfand et al. 1994).

25.3.4 Dosimetry

Dosimetric considerations are important, especially when children are examined or the radiopharmaceutical is used for therapy. The relative equivalent dose for I-131-MIBG is 140 µSv/MBq (µSv/0.03 mCi), which leads to an effective equivalent dose of 5.6 – 11.2 mSv for the use of 40 – 80 MBq (1.2 – 2.2 mCi) I-131-MIBG. For I-123-MIBG the relative equivalent dose is 14 µSv/MBq (µSv/0.03 mCi), equalling an effective equivalent dose of 5.6 mSv for the use of 400 MBq (10.8 mCi) I-123-MIBG.

For therapeutic use different dosimetric concepts are reported. One approach was reported by Monsieurs et al. The whole body absorbed dose can be used as a representation of bone marrow toxicity. To calculate the absorbed dose, I-131-MIBG or I-123-MIBG images can be acquired. Calculation with I-131 labeling has the advantage of allowing measurement of the bi-exponential pattern of whole body clearance. Monsieurs et al. used a combination of pretherapeutic I-123-MIBG scans and post-therapeutic I-131-MIBG images (Monsieurs et al. 2002). Flux et al. (2003) described a determination of absorbed dose ratios from 3D dose distributions. The most precise method seems to be the one proposed by Flower et al. An activity of 75 MBq (2 mCi) I-131-MIBG is administered and a series of planar whole body images acquired starting on day 3 up to 4 weeks. Whole body retention and organ uptake can be measured using the ROI technique. For decay correction a point source with a defined activity of I-131 is placed in the field of view for each acquired image (Flower and Fielding 1996). A less time consuming protocol suggests whole body images from day 3 through day 7 for post-therapeutic treatment (Matthay et al. 2001). The most useful regimen, however, seems to be the performing images starting immediately after injection of 100 MBq (2.7 mCi) I-131-MIBG with a dynamic acquisition of the kidneys in order to calculate renal toxicity. Whole body planar images in anterior and posterior views are carried out 30 min, 24, 48 and 72 h after injection. From this data the absorbed dose ratios for the whole body, organs and tumor sites can be calculated and the necessary therapeutic activity extrapolated (Kranert et al., unpublished data). It is important not to exceed the maximum allowable bone marrow absorbed dose of 2 Gy for adults and 2.5 Gy for children. The maximal doses for administration can be taken from the tables of the International Commission of Radiological Protection (ICRP). In cases where stem cell rescue is possible, higher bone marrow doses are possible.

25.3.5 Adverse Effects

For diagnosis with radioiodinated MIBG adverse effects are very rare. They are due to a release of catecholamines from storage granules and may occur after too rapid injection. Symptoms include tachycardia, hypertension, pallor, vomiting and abdominal pain (Bombardieri et al. 2003).

For the therapeutic use of I-131-MIBG possible hematological side effects are predominant, especially if the bone marrow is affected by the tumor. This risk increases after chemotherapy (Hoefnagel 1999).

25.4 Clinical Indications

25.4.1 Neuroblastoma

Neuroblastoma is the most frequent extracranial solid tumor in childhood. The tumor arises from the sympathic nervous system and is localized mainly in the adrenal gland but also in the cervical, thoracic and abdominal sympathetic chain ganglia as well as the para-sympathetic nervous system. MIBG scintigraphy has been shown to be very useful in the diagnosis and follow-up of neuroblastoma (Klingebiel et al. 1992; Kohnert et al. 1997). The indications for the use of MIBG in neuroblastoma have been summarized by Shulkin et al. For initial diagnosis MIBG is able to distinguish neuroblastomas from other small round cell tumors in childhood. An important quality of MIBG in staging is the detection of lesions that are otherwise not depicted, especially those localized in the thoracolumbar spine. Therapy response can also be monitored, since positive MIBG uptake can be considered as evidence of viable tumor (Shulkin and Shapiro 1998) (Figs. 25.1, 25.2). Sensitivity is described as between 84 % and 93.7 % (Claudiani et al. 1995; Rufini et al. 1996; Zagar et al. 1995). FDG-PET has also been reported to show good results for monitoring neuroblastoma (Kushner et al. 2001).

I-131-MIBG plays an important role in the therapy of neuroblastoma. Today, it is used mainly for recurrent

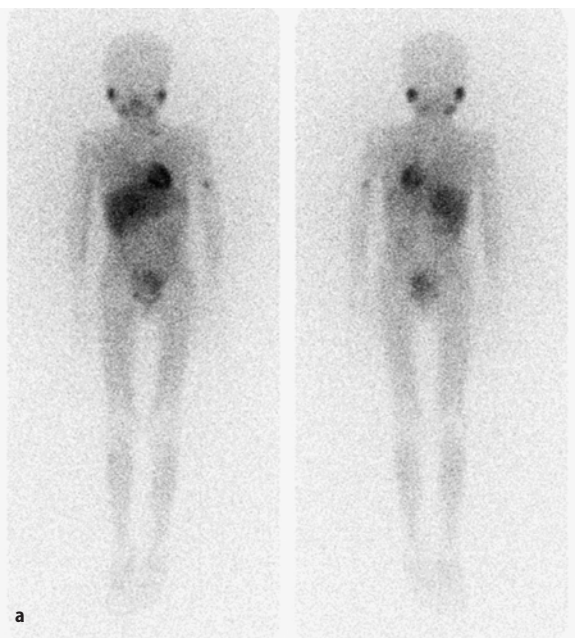

Fig. 25.1. Nine-year-old patient with neuroblastoma stage 4. The patient underwent chemotherapy, operation, high-dose chemotherapy and antibody therapy. Whole body MIBG scintigraphy (**a**) shows a metastasis in the left humerus and an inhomogeneous distribution in the left supraclavicular region

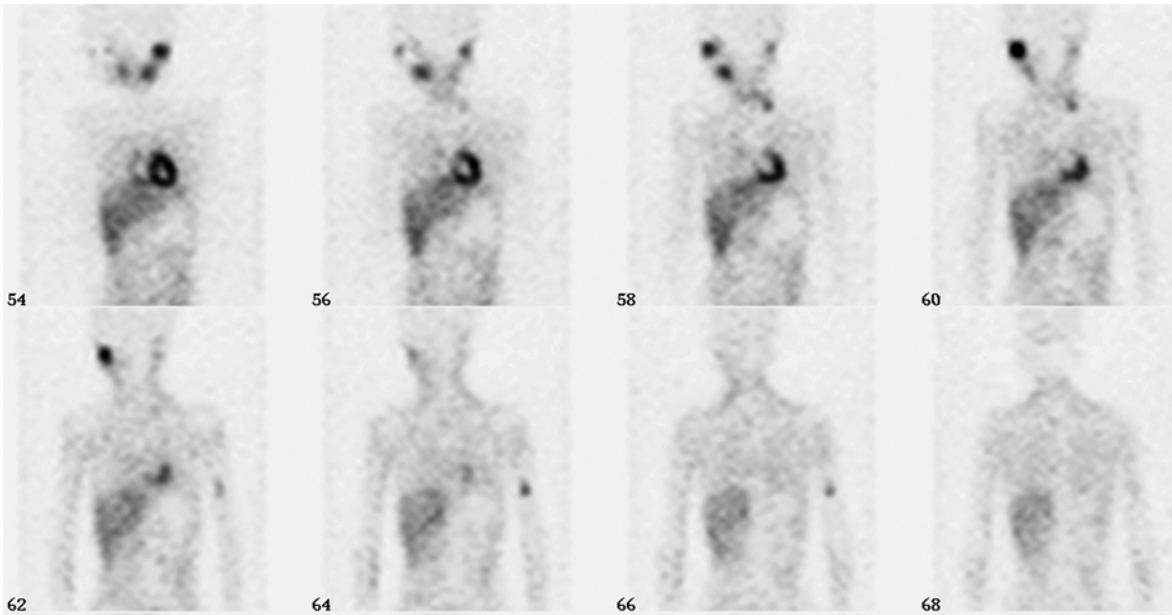

Fig. 25.1. b SPECT images reveal the left supraclavicular lymph node metastasis

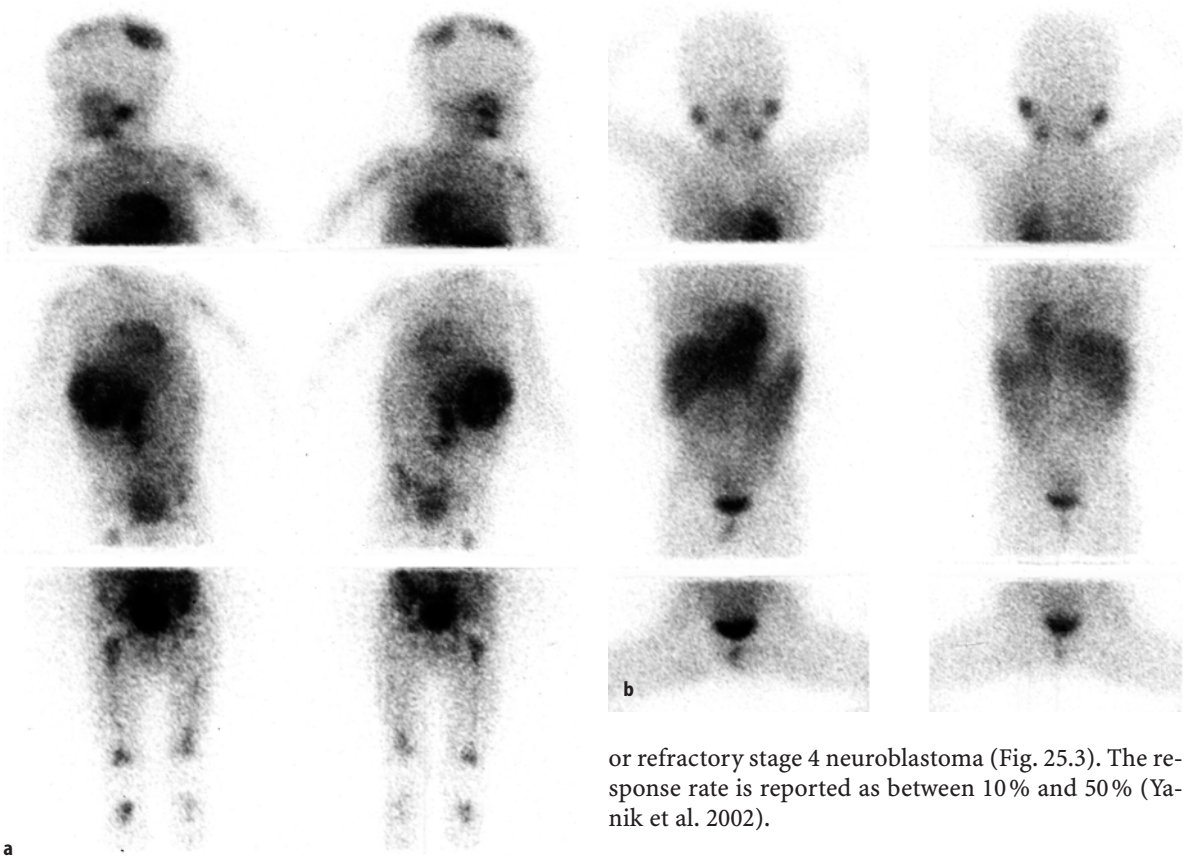

Fig. 25.2. Four-year-old patient with neuroblastoma stage 4. Whole body MIBG scintigraphy shows the images at diagnosis (**a**) with the abdominal primary tumor, hepatic metastases and skeletal infiltration in the skull, and the upper and lower limbs. The follow-up examination (**b**) reveals a complete response after chemotherapy and operation

or refractory stage 4 neuroblastoma (Fig. 25.3). The response rate is reported as between 10 % and 50 % (Yanik et al. 2002).

25.4.2 Pheochromocytoma and Paraganglioma

Pheochromocytomas and paragangliomas arise from the paraganglion system. While pheochromocytomas

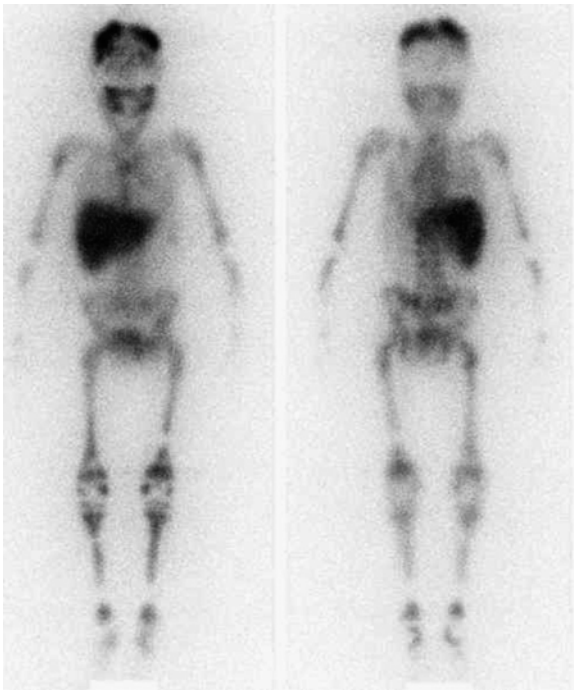

◁ **Fig. 25.3.** Eight-year-old patient with multiple metastases of a neuroblastoma stage 4. Post-therapeutic whole body scintigraphy shows extensive skeletal/bone marrow infiltration

are located in the adrenal medulla, paragangliomas can be found in the sympathetic chain ganglia and the para-sympathetic nervous system. MIBG scintigraphy is recommended as the initial localization technique, especially in extra-adrenal disease and recurrence (Velchik et al. 1989). It has been described as the most sensitive imaging procedure for pheochromocytoma (Mozley et al. 1994). Sensitivity is reported to be up to 100 % in pheochromocytoma (Brink et al. 2005; Maurea et al. 2002; Warren et al. 1989; Zagar et al. 1995). For paragangliomas the reported sensitivity is about 90 % (Brink et al. 2005). FDG-PET is positive in most pheochromocytomas (Shulkin et al. 1999), and has proven valuable for monitoring the efficacy of MIBG therapy (Menzel et al. 2003).

MIBG also plays a role in therapeutic use in pheochromocytoma and paraganglioma (Fig. 25.4). It can

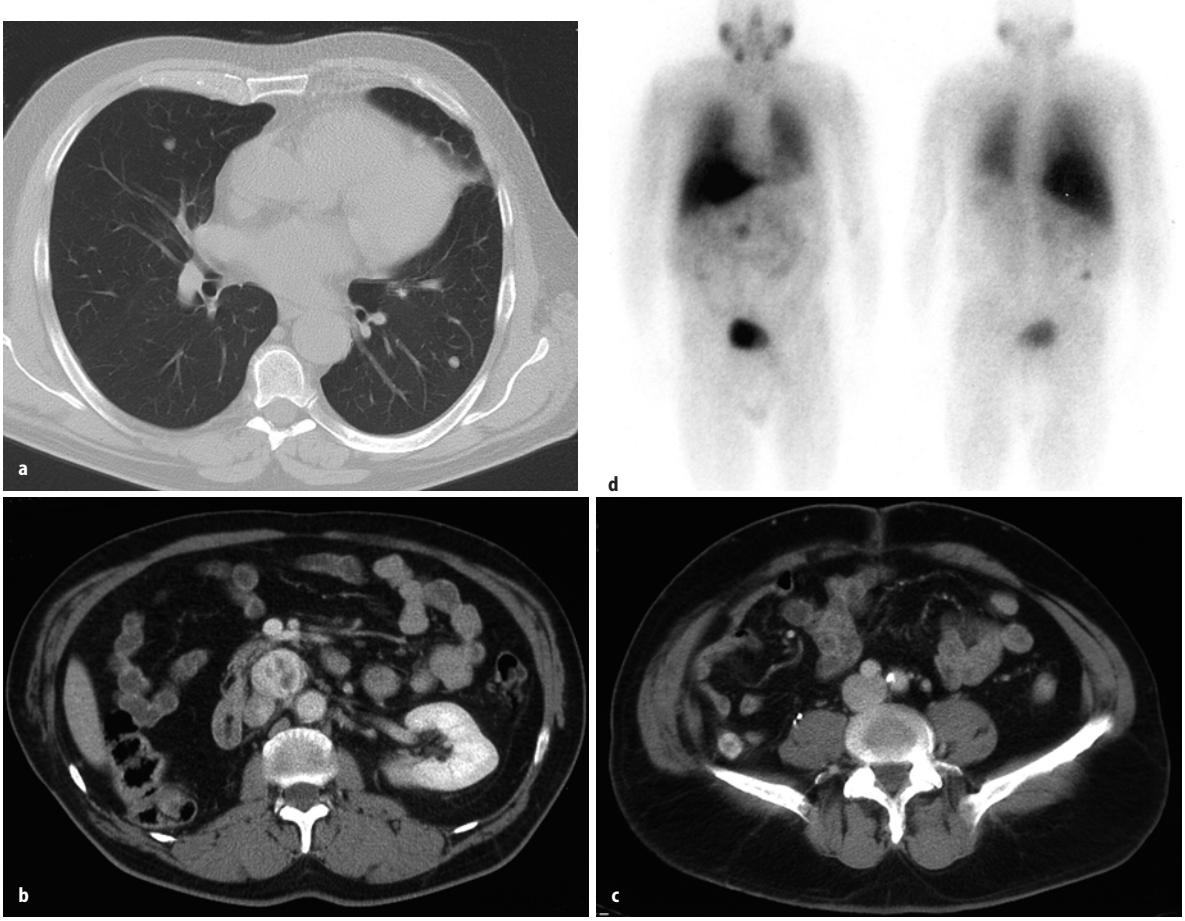

Fig. 25.4. Sixty-three-year-old patient with a metastatic pheochromocytoma. The CT shows a lesion in the right ventral lung (**a**), an abdominal lesion (**b**) and a pelvic focus on the right side (**c**), and an additional hepatic metastasis is described (not shown). The abdominal and pelvic lesions can easily be visualized by MIBG, whereas the pulmonary metastasis is hard to distinguish (**d**). FDG-PET revealed the hepatic metastasis as well as other lesions in the lower abdomen (**e**)

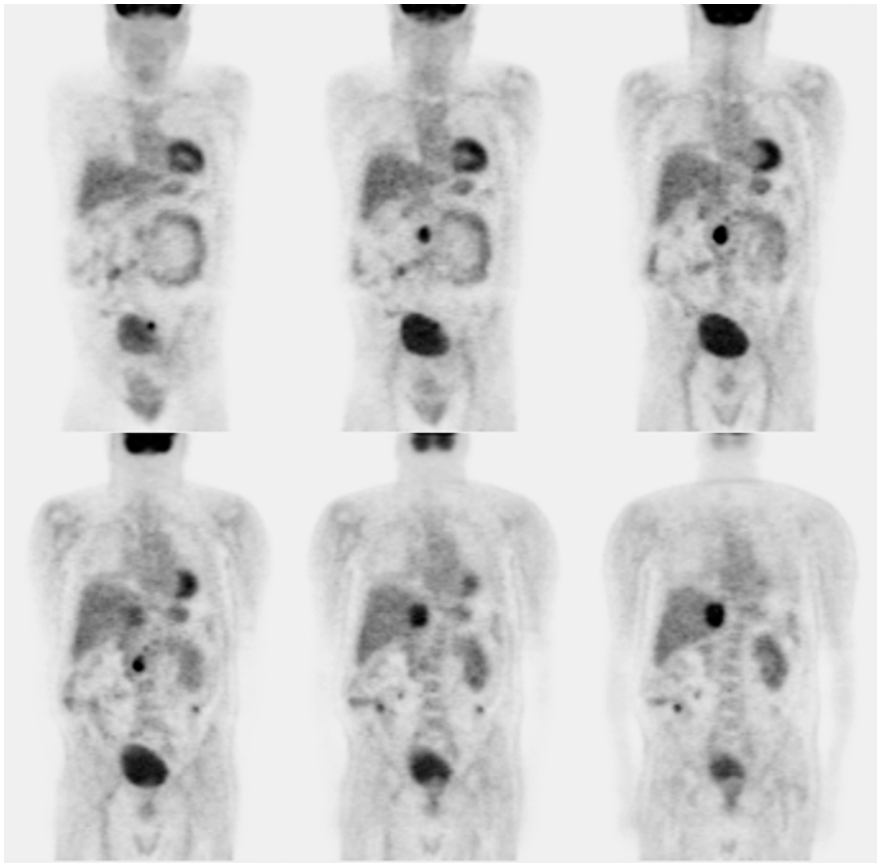

Fig. 25.4e

be used for symptomatic therapy to reduce hormonal activity and to control hypertension as well as relieve the pain of metastases (Hoefnagel et al. 1991). Also a curative use has been proposed (Rose et al. 2003).

25.4.3 Medullary Thyroid Carcinoma

Medullary thyroid carcinoma (MTC) is a malignancy originating from the parafollicular C-cells of the thyroid, with an incidence of 3 in 100,000 inhabitants per year. Other imaging techniques such as MRI, CT and FDG-PET play the main role in the diagnosis of MTC (Diehl et al. 2001). FDG-PET has shown a sensitivity of 78 % and a specificity of 79 % for the detection of metastases or recurrence of MTC and was superior to somatostatin receptor scintigraphy, DMSA scintigraphy, MIBI scintigraphy and CT. Only MRI showed comparable results with a sensitivity of 82 % but a specificity of only 67 %.

MIBG scintigraphy can also be useful in the staging and restaging of MTC. The sensitivity given in the literature ranges from 11 % to 50 % (Clarke et al. 1988; Verga et al. 1989; Troncone et al. 1989). MIBG scintigraphy can be used for staging of primary and recurrent MTC and is especially useful to determine therapeutic options with I-131-MIBG (Fig. 25.5).

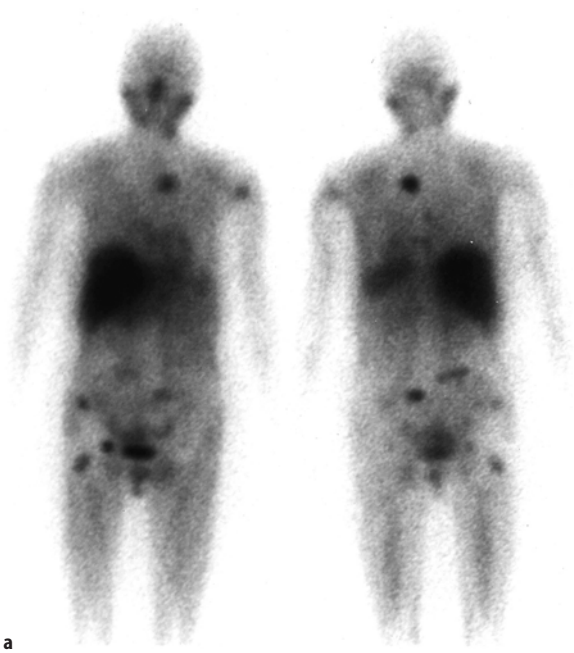

a

Fig. 25.5. Fifty-three-year-old patient with metastatic MTC. Whole body MIBG scintigraphy shows multiple skeletal metastases in a costovertebral joint of the upper thoracic spine, in the left proximal humerus, in the right proximal femur and multiple lesions in the pelvic bones (**a**)

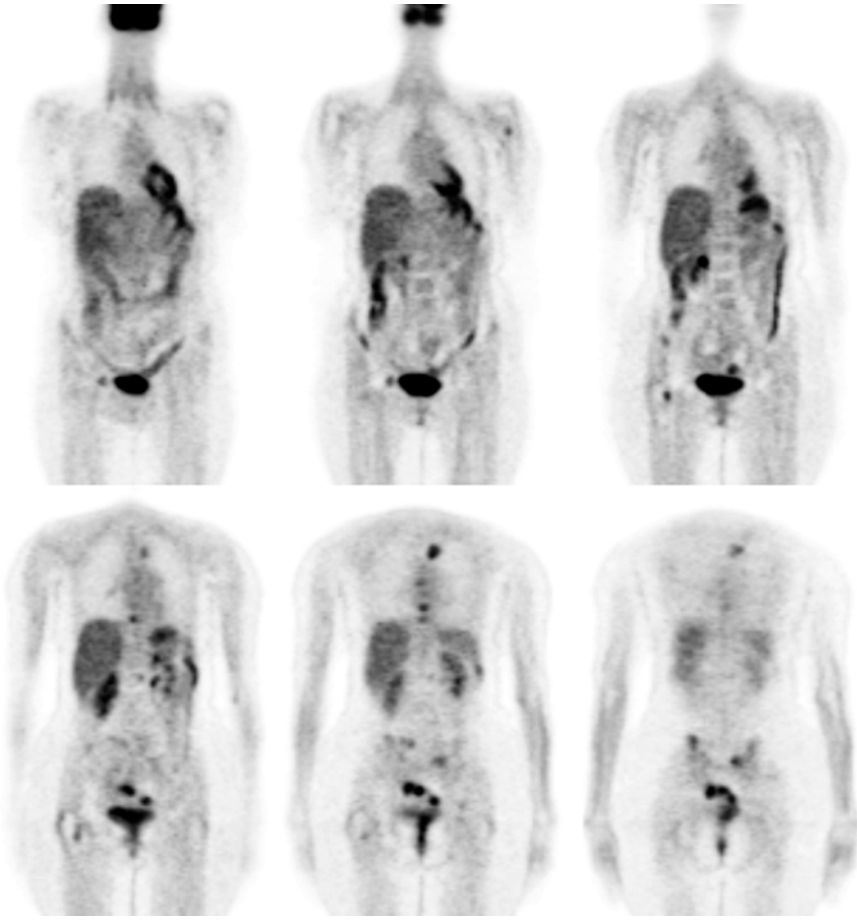

Fig. 25.5. b FDG-PET is also positive for these metastases and visualizes multiple foci in the thoracic spine, in addition

25.4.4 Carcinoid Tumors

Carcinoids are epithelial tumors originating from the enterochromaffin cells of the APUD system with an incidence of 16/100,000 per year. MIBG scintigraphy is useful if tumors cannot be detected by other imaging methods. In addition, MIBG scintigraphy is needed when treatment with I-131-MIBG is desired (Oberg and Eriksson 2005). In one study a sensitivity of 64 % was reported (Nocaudie-Calzada et al. 1996). Midgut carcinoids, localized in the ileum and cecum, were reported to take up MIBG better than foregut tumors, found in the pancreas, stomach and bronchus (Feldman et al. 1986). As another non-invasive method, PET with C-11 – 5-hydroxytryptophan has been reported to show positive tracer accumulation in 95 % of patients (Oberg and Eriksson 2005).

25.4.5 Others

Positive MIBG uptake has also been described in ganglioneuromas, ganglioneuroblastomas and Merkel cell tumors. Ganglioneuromas are rare, benign tumors of the peripheral nervous system occurring in about 1 in 100,000 children. Ganglioneuroblastomas are even less frequent with an incidence of less than 5 per million children. The degree of differentiation determines the likelihood of growing and metastasizing. MIBG scintigraphy has been reported to be positive by some authors, with a detection rate of up to 57 % (Clerico et al. 1991; Tosaka et al. 1999; Geoerger et al. 2001).

Merkel cell carcinomas are neuroendocrine tumors of the skin. Some reports describe positive MIBG uptake in these tumors (Watanabe et al. 1998; Castagnoli et al. 1992).

25.4.6 Pitfalls

In children under the age of 6 months an intense myocardial MIBG uptake may be visualized leading to a heterogeneous display of the right mediastinal region due to tracer accumulation in the right heart. Furthermore a bilateral symmetrical uptake occurs frequently in the upper thoracic region and may be misinterpreted as representing retro- or supraclavicular lymph nodes. Finally, the physiologically high liver uptake can hamper

the diagnosis of liver metastases, since they can hardly be distinguished from the background liver activity (Bonnin et al. 1994).

25.5 Future Developments

Combination therapies have already been performed with MIBG and different chemotherapies such as cisplatin, vincristine, VP16, iphosphamide, carboplatin, epirubicin, cyclophosphamide and topotecan for the treatment of neuroblastoma (Mastrangelo et al. 1995; Sari et al. 2001; Gaze et al. 2005). In these treatment concepts an additional combination with hyperbaric oxygen (HBO) may be auspicious. Combined HBO and MIBG therapy showed promising results in 1995 (Voûte et al. 1995). According to the Frankfurt protocol, patients are administered a weight adapted dose of between 2.96 and 7.4 GBq (80 and 200 mCi) I-131-MIBG. On the subsequent 4 days an HBO session is performed. Pressure is increased slowly over 15 min to a total of 2.4 bar. An intermittent oxygen supply of 100 % is given for 20 min periods with pauses of 5 min for a total of 95 min. Decompression is then performed slowly over another 15 min (Diehl et al. 2004) (Fig. 25.6). The effect of this combination therapy is based on three mechanisms: (1) MIBG itself has a discrete antiproliferative effect, independent of the iodide isotope, by inhibition of complex I of the respiratory chain. This leads to a discharge of paired electrons, resulting in an increased production of superoxide radicals. Neuroblastoma cells are more vulnerable to these radicals, since they show a decreased activity of enzymes responsible for the metabolism of radicals to water and oxygen. (2) The radiation of iodide-131 shows effects on a cellular basis. (3) Under HBO the oxygen accumulation within the tumor increases, depending on the partial pressure, which further increases the production of radicals.

Finally, further development of antibody therapy is desirable. Therapy with unlabeled antiGD2 antibodies ch 14.18. has already been implemented in routine therapy (Klingebiel et al. 1998). Radiolabeled antibodies have also been used for diagnostic purposes (Carrel et al. 1997). A therapy with radiolabeled antibodies will hopefully be available in the future.

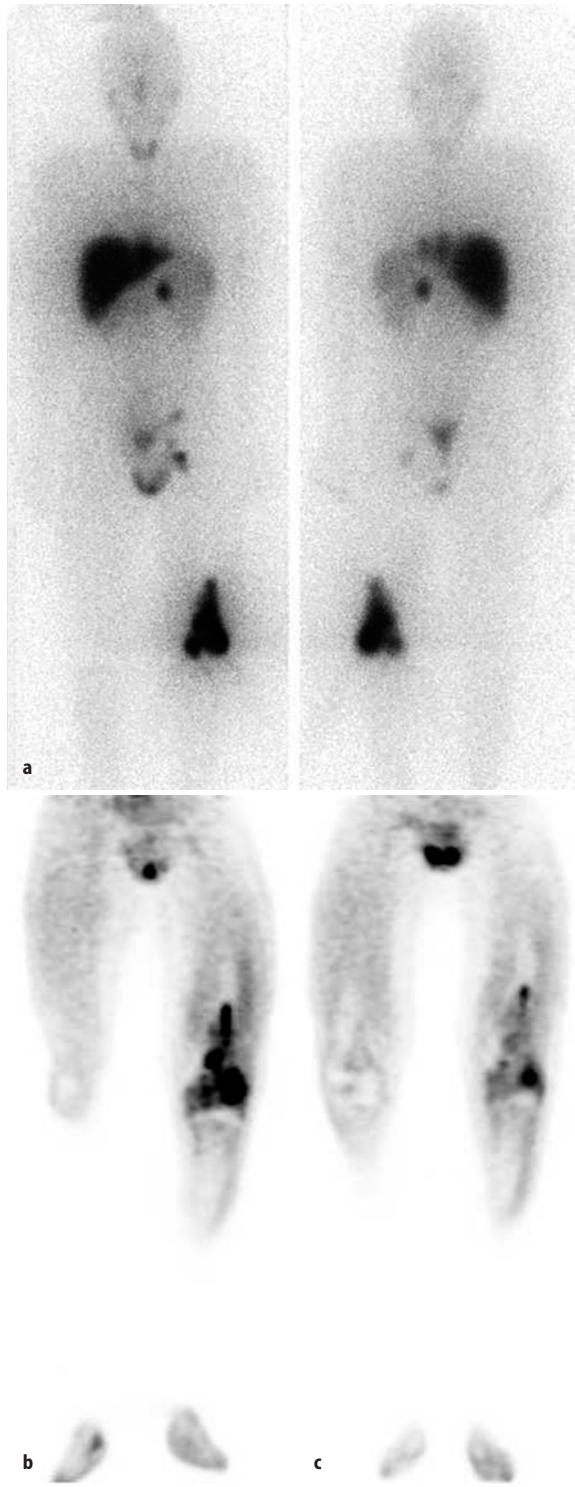

Fig. 25.6. Seventeen-year-old patient with metastatic neuroblastoma stage 4. Whole body MIBG scintigraphy shows a skeletal metastasis in the left distal femur and inguinal lymph node metastases on the left side (**a**). FDG-PET images of the lower limbs reveal an intense glucose consumption in the femoral metastasis (**b**) with a significant reduction of metabolic activity 2 weeks after combined MIBG and HBO therapy (max. SUV before therapy: 3.8.; max. SUV after therapy: 2.7) (**c**)

References

Anderson BG, Beierwaltes WH, Harrison TS, Ansari AN, Buswink AA, Ice RD (1973) Labeled dopamine concentration in pheochromocytomas. J Nucl Med 14:781 – 784

Babich JW, Graham W, Fischman AJ (1997) Effect of adrenergic receptor ligands on metaiodobenzylguanidine uptake and storage in neuroblastoma cells. Eur J Nucl Med 24:538 – 543

Beierwaltes WH (1991) Endocrine imaging: parathyroid, adrenal cortex and medulla, and other endocrine tumors. Part II. J Nucl Med 32:1627 – 1639

Bombardieri E, Aktolun C, Baum RP, Bishof-Delaloye A, Buscombe J, Chatal JF, Maffioli L, Moncayo R, Mortelmans L, Reske SN (2003) 131I/123I-metaiodobenzylguanidine (MIBG) scintigraphy: procedure guidelines for tumour imaging. Eur J Nucl Med Mol Imaging 30:132 – 139

Bonnin F, Lumbroso J, Tenenbaum F, Hartmann O, Parmentier C (1994) Refining interpretation of MIBG scans in children. J Nucl Med 35:803 – 810

Brans B, Monsieurs M, Laureys G, Kaufman JM, Thierens H, Dierckx RA (2002) Thyroidal uptake and radiation dose after repetitive I-131-MIBG treatments: influence of potassium iodide for thyroid blocking. Med Pediatr Oncol 38: 41 – 46

Brink I, Hoegerle S, Klisch J, Bley TA (2005) Imaging of pheochromocytoma and paraganglioma. Fam Cancer 4:61 – 68

Britton KE (1997) Positive MIBG scanning at the time of relapse in neuroblastoma which was MIBG negative at diagnosis. Br J Radiol 70:969. Comment in: Schwarz et al. (1997) Br J Radiol 70:90 – 92

Carrel F, Amstutz H, Novak-Hofer I, Schubiger PA (1997) Evaluation of radioiodinated and radiocopper labeled monovalent fragments of monoclonal antibody chCE7 for targeting of neuroblastoma. Nucl Med Biol 24:539 – 546

Castagnoli A, Biti G, De Cristofaro MT, Ferri P, Magrini SM, Papi MG, Bianchi S (1992) Merkel cell carcinoma and iodine-131 metaiodobenzylguanidine scan. Eur J Nucl Med 19:913 – 916

Castellani MR, Chiti A, Seregni E, Bombardieri E (2000) Role of 131I-metaiodobenzylguanidine (MIBG) in the treatment of neuroendocrine tumours. Experience of the National Cancer Institute of Milan. Q J Nucl Med 44:77 – 87

Clarke SE, Lazarus CR, Wraight P, Sampson C, Maisey MN (1988) Pentavalent [99mTc]DMSA, [131I]MIBG, and [99mTc]MDP – an evaluation of three imaging techniques in patients with medullary carcinoma of the thyroid. J Nucl Med 29:33 – 38

Claudiani F, Stimamigliio P, Bertolazzi L, Cabria M, Conte M, Villavecchia GP, Garaventa A, Lanino E, De Bernardi B, Scopinaro G (1995) Radioiodinated meta-iodobenzylguanidine in the diagnosis of childhood neuroblastoma. Q J Nucl Med 39:21 – 24

Clerico A, Jenkner A, Castello MA, Ciofetta G, Lucarelli C, Codini M (1991) Functionally active ganglioneuroma with increased plasma and urinary catecholamines and positive iodine 131-meta-iodobenzylguanidine scintigraphy. Med Pediatr Oncol 19:329 – 333

Diehl M, Risse JH, Brandt-Mainz K, Dietlein M, Bohuslavizki KH, Matheja P, Lange H, Bredow J, Körber C, Grünwald F (2001) Fluorine-18 fluorodeoxyglucose positron emission tomography in medullary thyroid cancer: results of a multicentre study. Eur J Nucl Med 28:1671 – 1676

Diehl M, Fußhoeller G, Menzel C, Kranert WT, Graichen S, Klingebiel Th, Grünwald F (2004) Hyperbarer Sauerstoff zur Intensivierung der 131I-MIBG-Therapie beim therapierefraktären Neuroblastom Stadium 4 (case repeort). Nuklearmedizin 43:N77–N80

Feldman JM, Blinder RA, Lucas KJ, Coleman RE (1986) Iodine-131 metaiodobenzylguanidine scintigraphy of carcinoid tumors. J Nucl Med 27:1691 – 1696

Flower MA, Fielding SL (1996) Radiation dosimetry for 131I-mIBG therapy of neuroblastoma. Phys Med Biol 41:1933 – 1940

Flux GD, Guy MJ, Papavasileiou P, South C, Chittenden SJ, Flower MA, Meller ST (2003) Absorbed dose ratios for repeated therapy of neuroblastoma with I-131 mIBG. Cancer Biother Radiopharm 18:81 – 87

Franceschini R, Pecorale A, Chinol M, Calcagni ML, Servidei T, Riccardi R, Troncone L (1995) In vitro and in vivo studies with no-carrier added radioiodinated MIBG. Q J Nucl Med 39:72 – 77

Garaventa A, Bellagamba O, Lo Piccolo MS, Milanaccio C, Lanino E, Bertolazzi L, Villavecchia GP, Cabria M, Scopinaro G, Claudiano F, De Bernardi B (1999) I-131-metaiodobenzylgunaidine (I-1313-MIBG) therapy for residual neuroblastoma: a mono-institutional experience with 43 patients. Br J Cancer 81:1378 – 1384

Gaze MN, Chang YC, Flux GD, Mairs RJ, Saran FH, Meller ST (2005) Feasibility of dosimetry-based high-dose 131I-metaiodobenzylguanidine with topotecan as a radiosensitizer in children with metastatic neuroblastoma. Cancer Biother Radiopharm 20:195 – 199

Gelfand MJ, Elgazzar AH, Kriss VM, Masters PR, Golsch GJ (1994) Iodine-123-MIBG SPECT versus planar imaging in children with neural crest tumors. J Nucl Med 35:1753 – 1757

Geoerger B, Hero B, Harms D, Grebe J, Scheidhauer K, Berthold F (2001) Metabolic activity and clinical features of primary ganglioneuromas. Cancer 91:1905 – 1913

Hoefnagel CA (1999) Nuclear medicine therapy of neuroblastoma. Q J Nucl Med 43:336 – 343

Hoefnagel CA, Schornagel J, Valdes Olmos RA (1991) [131I]metaiodobenzylguanidine therapy for malignant phaeochromocytoma: interference of medication. J Nucl Biol Med 35:308 – 312

Ice RD, Wieland DM, Beirwaltes WH, Lawton RG, Redmond MJ (1975) Concentration of dopamine analogs in the adrenal medulla. J Nucl Med 16:1147 – 1151

Khafagi FA, Shapiro B, Fig LM, Mallette S, Sisson JC (1989) Labetalol reduces iodine-131 MIBG uptake by pheochromocytoma and normal tissues. J Nucl Med 30:481 – 489

Klingebiel T, Reuland P, Feine U, Niethammer D (1992) Verlaufsbeurteilung des metastasierten Neuroblastoms mittels hochdosiertem [^{131}J-meta]Jodobenzylguanidin. Nuklearmedizin 31:209 – 212

Klingebiel T, Bader P, Bares R, Beck J, Jürgens H, Lang P, Niethammer D, Rath B, Handgretinger R (1998) Treatment of neuroblastoma stage 4 with ^{131}I-meta-iodo-benzylguanidine, high-dose chemotherapy and immunotherapy. A pilot study. Eur J Cancer 34:1398 – 1402

Kohnert K, Lerch H, Thelen M, Jürgens H, Schober O (1997) Recurrence of a stage IV neuroblastoma. Nuklearmedizin 36:32 – 35

Korn N, Buswink A, Yu T, Carr EA Jr, Carroll M, Counsell RE (1977) A radioiodinated bretylium analog as a potential agent for scanning the adrenal medulla. J Nucl Med 18: 87 – 89

Kushner BH, Yeung HW, Larson SM, Kramer K, Cheung NK (2001) Extending positron emission tomography scan utility to high-risk neuroblastoma: fluorine-18 fluorodeoxyglucose positron emission tomography as sole imaging modality in follow-up of patients. J Clin Oncol 19:3397 – 3405

Lieberman LM, Beierwaltes WH, Varma VM, Weinhold P, Ling R (1969) Labeled dopamine concentration in human adrenal medulla and in neuroblastoma. J Nucl Med 10:93 – 97

Mastrangelo R, Tornesello A, Riccardi R, Lasorella A, Mastrangelo S, Mancini A, Rufini V, Troncone L (1995) A new ap-

proach in the treatment of stage IV neuroblastoma using a combination of [131I]meta-iodobenzylguanidine (MIBG) and cisplatin. Eur J Cancer 31A:606 – 611
Matthay KK, Panina C, Huberty J, Price D, Glidden DV, Tang HR, Hawkins RA, Veatch J, Hasegawa B (2001) Correlation of tumor and whole-body dosimetry with tumor response and toxicity in refractory neuroblastoma treated with (131)I-MIBG. J Nucl Med 42:1713 – 1721
Maurea S, Klain M, Caraco C, Ziviello M, Salvatore M (2002) Diagnostic accuracy of radionuclide imaging using 131I nor-cholesterol or meta-iodobenzylguanidine in patients with hypersecreting or non-hypersecreting adrenal tumours. Nucl Med Commun 23:951 – 960
McEwan AJ, Shapiro B, Sisson JC, Beierwaltes WH, Ackery DM (1985) Radio-iodobenzylguanidine for the scintigraphic location and therapy of adrenergic tumors. Semin Nucl Med 15:132 – 153
Menzel C, Graichen S, Berner U, Risse JH, Diehl M, Dobert N, Hamscho N, Grunwald F (2003) Monitoring the efficacy of iodine-131-MIBG therapy using fluorine-18-FDG-PET. Acta Med Austriaca 30:37 – 40
Monsieurs M, Brans B, Bacher K, Dierckx R, Thierens H (2002) Patient dosimetry for 131I-MIBG therapy for neuroendocrine tumours based on 123I-MIBG scans. Eur J Nucl Med Mol Imaging 29:1581 – 1587
Morales JO, Beierwaltes WH, Counsell RE, Meier DH (1967) The concentration of radioactivity from labeled epinephrine and its precursors in the dog adrenal medulla. J Nucl Med 8:800 – 809
Mozley PD, Kim CK, Mohsin J, Jatlow A, Gosfield E 3rd, Alavi A (1994) The efficacy of iodine-123-MIBG as a screening test for pheochromocytoma. J Nucl Med 35:1138 – 1144
Nakajo M, Shapiro B, Copp J, Kalff V, Gross MD, Sisson JC, Beierwaltes WH (1983) The normal and abnormal distribution of the adrenomedullary imaging agent m-[I-131]iodobenzylguanidine (I-131 MIBG) in man: evaluation by scintigraphy. J Nucl Med 24:672 – 682
Nakatani T, Hayama T, Uchida J, Nakamura K, Takemoto Y, Sugimura K (2002) Diagnostic localization of extra-adrenal pheochromocytoma: comparison of (123)I-MIBG imaging and (131)I-MIBG imaging. Oncol Rep 9:1225 – 1227
Nocaudie-Calzada M, Huglo D, Carnaille B, Proye C, Marchandise X (1996) Comparison of somatostatin analogue and metaiodobenzylguanidine scintigraphy for the detection of carcinoid tumours. Eur J Nucl Med 23:1448 – 1454
Oberg K, Eriksson B (2005) Nuclear medicine in the detection, staging and treatment of gastrointestinal carcinoid tumours. Best Pract Res Clin Endocrinol Metab 19:265 – 276
Piepsz A, Hahn K, Roca I, Ciofetta G, Toth G, Gordon I, Kolinska J, Gwidlet J (1990) A radiopharmaceutical schedule for imaging in paediatrics. Paediatric Task Group European Association Nuclear Medicine. Eur J Nucl Med 17:127 – 129
Rose B, Matthay KK, Price D, Huberty J, Klencke B, Norton JA, Fitzgerald PA (2003) High-dose I-131-metaiodobenzylguanidine therapy for 12 patients with malignant phaeochromocytoma. Am Cancer Soc 98:239 – 248
Rufini V, Fisher GA, Shulkin BL, Sisson JC, Shapiro B (1996) Iodine-123-MIBG imaging of neuroblastoma: utility of SPECT and delayed imaging. J Nucl Med 37:1464 – 1468
Safford SD, Coleman RE, Gockerman JP, Moore J, Feldman J, Onaitis MW, Tyler DS, Olson JA Jr (2002) Iodine-131 metaiodobenzylguanidine treatment for metastatic carcinoid. Results in 98 patients. Cancer 101:1987 – 1993
Sari O, Ugur O, Emir S, Akyuz C (2001) Combined use of chemotherapy and 131I-metaiodobenzylguanidine in the treatment of advanced-stage neuroblastoma. Turk J Pediatr 43:29 – 33
Shapiro B, Gross MD (1987) Radiochemistry, biochemistry, and kinetics of 131I-metaiodobenzylguanidine (MIBG) and 123I-MIBG: clinical implications of the use of 123I-MIBG. Med Pediatr Oncol 15:170 – 177
Shulkin BL, Thompson NW, Shapiro B, Francis IR, Sisson JC (1999) Pheochromocytomas: imaging with 2-[fluorine-18]fluoro-2-deoxy-D-glucose PET Radiology 212:35 – 41
Sywak MS, Pasieka JL, McEwan A, Kline G, Rorstad O (2004) 131I-meta-iodobenzylguanidine in the management of metastatic midgut carcinoid. Tumors World J Surg 28:1157 – 1162
Tobes MC, Jaques S Jr, Wieland DM, Sisson JC (1985) Effect of uptake-one inhibitors on the uptake of norepinephrine and metaiodobenzylguanidine. J Nucl Med 26:897 – 907
Tosaka A, Ando M, Arisawa C, Okano T (1999) Endocrinologically active retroperitoneal ganglioneuroma with positive iodine-131-metaiodobenzylguanidine scintigraphy. Int J Urol 6:471 – 474
Troncone L, Rufini V, De Rosa G, Testa A (1989) Diagnostic and therapeutic potential of new radiopharmaceutical agents in medullary thyroid carcinoma. Henry Ford Hosp Med J 37:178 – 184
Vaidyanathan G, Welsh PC, Vitorello KC, Snyder S, Friedman HS, Zalutsky MR (2004) A 4-methyl-substituted meta-iodobenzylguanidine analogue with prolonged retention in human neuroblastoma cells. Eur J Nucl Med Mol Imaging 31:1362 – 1370
van Santen HM, de Kraker J, van Eck BL, de Vijlder JJ, Vulsma T (2002) High incidence of thyroid dysfunction despite prophylaxis with potassium iodide during (131)I-meta-iodobenzylguanidine treatment in children with neuroblastoma. Cancer 94:2081 – 2089
van Santen HM, de Kraker J, van Eck BL, de Vijlder JJ, Vulsma T (2003) Improved radiation protection of the thyroid gland with thyroxine, methimazole, and potassium iodide during diagnostic and therapeutic use of radiolabeled metaiodobenzylguanidine in children with neuroblastoma. Cancer 98:389 – 396
Velchik MG, Alavi A, Kressel HY, Engelman K (1989) Localization of pheochromocytoma: MIBG [correction of MIGB], CT, and MRI correlation. J Nucl Med 30:328 – 336
Verga U, Muratori F, Di Sacco G, Banfi F, Libroia A (1989) The role of radiopharmaceuticals MIBG and (V) DMSA in the diagnosis of medullary thyroid carcinoma. Henry Ford Hosp Med J 37:175 – 177
Voûte PA, van der Kleij AJ, De Kraker J, Hoefnagel CA, Thiel-van Buul MMC, Van Gennip H (1995) Clinical experience with radiation enhancement by hyperbaric oxygen in children with recurrent neuroblastoma stage IV. Eur J Cancer 31:596 – 600
Wafelman AR, Hoefnagel CA, Maes RA, Beijnen JH (1994) Radioiodinated metaiodobenzylguanidine: a review of its biodistribution and pharmacokinetics, drug interactions, cytotoxicity and dosimetry. Eur J Nucl Med 21:545 – 559
Warren MJ, Shepstone BJ, Soper N (1989) Iodine-131 meta-iodobenzylguanidine (131I-MIBG) for the localization of suspected phaeochromocytoma. Nucl Med Commun 10:467 – 475
Watanabe N, Shimizu M, Kageyama M, Kitagawa K, Hayasaka S, Seto H (1998) 123I-MIBG SPECT of Merkel cell carcinoma. Br J Radiol 71:886 – 887
Wieland DM, Wu J, Brown LE, Mangner TJ, Swanson DP, Beierwaltes WH (1980) Radiolabeled adrenergic neuron-blocking agents: adrenomedullary imaging with [131I]iodobenzylguanidine. J Nucl Med 21:349 – 353
Yanik GA, Levine JE, Matthay KK, Sisson JC, Shulkin BL, Shapiro B, Hubers D, Spalding S, Braun T, Ferrara JL, Hutchinson RJ (2002) Pilot study of iodine-131-metaiodobenzylguanidine in combination with myeloablative chemotherapy

and autologous stem-cell support for the treatment of neuroblastoma. J Clin Oncol 20:2142 – 2149
Zagar I, Han R, Mitrovic S (1995) Meta-[131I]iodobenzylguanidine in the scintigraphic evaluation of neural crest tumors. Q J Nucl Med 39:13 – 16
Zaplatnikov K, Menzel C, Dobert N, Hamscho N, Kranert WT, Gotthard M, Behr TM, Grünwald F (2004) Case report: drug interference with MIBG uptake in a patient with metastatic paraganglioma. Br J Radiol 77:525 – 527

Radioimmunotherapy

26

R.P. Baum, V. Prasad, J.P. Oliva

26.1 Introduction

Since Paul Ehrlich proposed the hypothesis (*Seitenkettentheorie*) more than a century ago that bacteria can be killed by selective usage of certain compounds having specific affinity to the bacteria and thus acting as a "magic bullet," antibodies have captured the imagination of scientists dealing with diseases. Cancer was and still remains among the most intriguing and challenging of diseases for which the exact cure for its many forms is not available to date. Parallel to the development of certain compounds such as sulfur and nitrogen mustard, with the capacity to modify the DNA and thus retard and kill the growth of cancer cells (Sausville and Longo 2005), Pressman and colleagues showed that radiolabeled antibodies had the potential to localize tumors in rabbits (Pressman and Keighley 1948; Pressman und Korngold 1953; Pressman et al. 1957). This was soon followed by first attempts by Beierwaltes and his colleagues at curing cancer in patients using radiolabeled polyclonal antibodies. An inability to find a way to purify the antitumor globulin from other globulins in order to increase the specificity was the major limitation of the study (Bale and Spar 1957; Pressman and Korngold 1953). The development of monoclonal antibodies (mAbs) using the hybridoma technique was a major breakthrough because mAbs generated by this technique had a very high specificity for antigens (Kohler and Milstein 1975). Initial studies for localization of tumor using radioimmunoimaging in humans showed encouraging results in renal cell carcinomas and gliomas (Belitsky et al. 1978; Day et al. 1965). However, the use of mAbs for the treatment of cancer was not very successful in the preliminary studies. Their immunogenicity, due to the murine origin of these mAbs, and their poor ability to generate an effective immune response against the cancer cells, marred the promising role of antibody mediated cancer therapy (Badger et al. 1987; Khazaeli et al. 1994; Lee et al. 1998). It was possible to circumvent the problem of antigenicity of murine mAbs by the development of chimeric, humanized and fully human mAbs (Feldhaus and Siegel 2004; Hoogenboom and Chames 2000; Irving et al. 2001; Lipovsek and Pluckthun 2004). These unconjugated mAbs were envisaged to have a high potential for cancer therapy; however, because of certain inherent limitations, even they have failed to live up to their potential. Slow extravasation from the blood, poor tumor vascularization, poor lymphatic drainage, antigen heterogeneity and interactions between mAbs and their receptors have been thought to be responsible for this lack of prolonged and efficient intratumoral unconjugated mAb uptake (Green et al. 1994; Jain 1990; Lonberg et al. 1994; Ruiz-Cabello et al. 2002; Saga et al. 1995). The other contributing factor which has led to the limited therapeutic efficacy is the extent to which ADCC (antibody dependent cell-mediated cytotoxicity), induction of direct signaling events or complement-dependent cytotoxicity leads to the cancer cell death (Wu and Senter 2005). These failures of unconjugated mAbs lead to the concept of arming these highly specific molecules with compounds which have additional cell killing properties like drugs, toxins and radionuclides. Radioimmunotherapy (RIT) has the added advantage over the mAbs labeled with drugs or toxins because (1) radionuclides are not sensitive to multidrug resistance, (2) even those cancer cells which do not express targeted antigen can be sterilized because of the phenomenon of "cross-fire" (Dixon 2003), and (3) simultaneous localization of the tumor is possible through radioimmunoscintigraphy (Baum et al. 1987; Perkins and Baum 1988). In 1950, Beierwaltes conducted the first clinical trial to investigate the therapeutic potential of ^{131}I-labeled rabbit antibodies in 14 patients having metastatic melanoma and documented the pathologically confirmed complete remission in one patient (Beierwaltes 1974). Since then numerous studies have been conducted; however, radioimmunotherapy had its major breakthrough with the approval of ibritumomab tiuxetan (Zevalin; murine CD20 mAb conjugated to ^{90}Y) by the FDA in February 2002 (Borghaei and Schilder 2004). This was immediately followed by the approval of another radioimmunoconjugate, ^{131}I-tositumomab (Bexxar), in the year 2003 (Wahl 2005). The road to this success was not easy because of several challenges including the possible decay of radionuclide conjugated mAbs before being delivered to the target site, the pos-

sible perturbation of mAb antigen binding site by the conjugates and the possible suboptimal pharmacokinetics and biodistribution of the mAb carriers (Wu and Senter 2005). Even now most of the success that radioimmunotherapy has achieved is mainly in the low volume tumors like hematological malignancies. Medical scientists are still working on expanding the field of RIT into solid tumors.

In order to understand the rationale used and the complexities associated with the use of these radiopharmaceuticals in radioimmunotherapy for the treatment of some of the indolent carcinomas, it is essential to understand the key steps for the development and manufacture of monoclonal antibodies, the methods and mechanism of action of radionuclides used for conjugation with mAbs, and their pharmacokinetics and normal tissue uptake.

26.2 Radiopharmaceuticals for Radioimmunotherapy

26.2.1 Development and Manufacture of mAbs

The targeting antibodies used for RIT should ideally have the following properties: (1) low immunogenicity for repeated administration, (2) optimal antigen binding, (3) good tumor penetration, (4) good rate of clearance from normal tissues (essential for efficient and specific tumor targeting and thus decreasing the radiation exposure to normal tissues), (5) optimal tumor residence time for delivering therapeutic radiation dose and (6) optimal tumor accretion. The initial studies of radioimmunoimaging and radioimmunotherapy were performed mostly with animal derived polyclonal antibodies which lacked in specificity (Goldenberg et al. 1978; Order et al. 1985, 1989, 1991; Primus and Goldenberg 1980; Vriesendorp et al. 1999). The development of the hybridoma technique made the mAbs target specific but still suffered because of three major factors: (1) immunogenicity of murine origin of the mAbs limiting the administration to one or two cycles, (2) no significant improvement in tumor uptake because of the limited number of tumor binding sites and (3) the poor pharmacokinetics for effective usage in RIT (Goldenberg 2002). The strategy developed to improve the pharmacokinetics for effective RIT was the development of smaller molecules for faster clearance and better tumor penetration. Radiolabeled antibody fragments and subfragments have been found to have good therapeutic effects in animal models with rapid clearance and good tumor penetration. Bivalent F (ab')$_2$ and monovalent F ab' fragments belong to this class of molecule (Baum 1999; Behr et al. 2000; Behr and Goldenberg 1996; Buchegger et al. 1989, 1990, 1996, 2000; Juweid et al. 1996; Larson et al. 1983, 1985; Milenic 2000). Various diabodies (M_r 55,000) and minibodies having molecular weights above the range for rapid renal clearance have been constructed with the aim of binding to more than two antigen molecules while retaining the property of rapid clearance from the body (Milenic 2000) (Table 26.2). However, this improvement in tumor to non-tumor uptake was achieved at the cost of lower affinity and decreased tumor residence time leading to lowered absolute tumor uptake as compared to the intact immunoglobulins (IgG). As of now, these small molecular constructs are being considered for use in pretargeting strategies which deal with separation of tumor targeting from the delivery of therapeutic radionuclides and are discussed in detail later on. These diabodies and minibodies have also found significant usage in the evaluation of biokinetics of certain drugs and tracers using PET and radioimmunoimaging of certain forms of cancer using a gamma camera (SPECT). ^{68}Ga-radiolabeled F ab' fragments of trastuzumab monitoring Her2 expression (Smith-Jones et al. 2004) and the use of ^{123}I-labeled scFv dimer with specific affinity for the fibronectin extradomain B, which is expressed in tumor neovasculature, are two expamles (Santimaria et al. 2003). Whether these fragments and subfragments of antibodies will have any role in RIT is still a matter of debate as is shown by several animal studies (Behr et al. 2000; Buchegger et al. 1989, 1990, 1996; Larson et al. 1983, 1985). Various antibodies and antibody fragments used

Properties	IgG	Fab'	F(ab')$_2$	scFv	Diabody
Biological					
Capability to induce immune response	Present	Absent	Absent	Absent	Absent
$T_{1/2}$ in blood	2–3 days	4 h	1–2 days	1 h	<4 h
Target organ	Liver	Kidney	Liver	Kidney	Kidney
Physical					
Molecular weight	150 K	50 K	100 K	40 K	20 K
Tumor binding					
Optimal accretion time	Days	Hours	Day	Hour	Hours
Duration	++++	+++	++	+	+++
Uptake	++++	+++	++	+	+++

Table 26.1. Salient properties of commonly used monoclonal antibodies/antibody fragments. (Modified from Goldenberg 2002)

++++ indicates maximum and + indicates minimum, with the rest (++ and +++) being intermediate between these two

Table 26.2. Monoclonal antibodies approved by the FDA for use in oncology. (Modified from Adams and Weiner 2005)

Trade name	FDA approval	Source	Format and isotype	Target	Indication
Immunoconjugates					
^{90}Y-Ibritumomab tiuxetan (Zevalin) with rituximab	2002	Murine	^{90}Y-IgG1	CD20	Lymphoma
Tositumomab and ^{131}I-tositumomab	2003	Murine	^{131}I-IgG2a	CD20	Lymphoma
Gemtuzumab (Myelotarg)	2000	Human mAb, drug derived from streptomyces	hIgG4-calicheamicin	CD33	Acute myelogenous leukemia
Unconjugated mAbs					
Rituximab (Rituxan)	1997	Murine-human chimeric	hIgG1	CD20	Lymphoma
Trastuzumab (Herceptin)	1998	Humanized	hIgG1	HER2/neu	Breast cancer
Alemtuzumab (Campath-1H)	2001	Humanized	hIgG1	CD52	Chronic lymphocytic leukemia
Cetuximab (Erbitux)	2004	Murine-human chimeric	hIgG1	EGF receptor	Colorectal cancer
Bevacizumab (Avastin)	2004	Murine-human chimeric	hIgG1	VEGF	Colorectal, lung cancer

in immunotherapy/radioimmunotherapy and their salient properties are shown in Table 26.1.

The problem of antigenicity after repeated administration of the initial mAbs was overcome by the development of chimerized, humanized and fully human antibodies. In gradual steps of development, murine mAbs were first converted into murine/human chimeras which subsequently were made into murine CDR-grafted human antibodies and ultimately into fully human antibodies. Most of the clinical experience has been exclusively with chimeric and CDR-grafted antibodies. The results have documented less antigenicity as compared to the previous generation mAbs (Goldenberg 2002; McQuarrie et al. 1994). Future studies are being directed towards resolving the issue of superiority between these three congeners. Chimeric antibodies have been shown to generate immune response (Meredith et al. 1993). It is also expected that fully human antibodies may generate T-cell dependent or anti-idiotype immune response (Goldenberg 2002).

One of the most important considerations and constraints in the development and research usage of these mAbs is the implementation of the GMP (Good Manufacture Practice) law in most parts of the developed world. The legislation requires pre-clinical testing and management of clinical trials, which will greatly increase the cost of running and reduce the number of such research programs. This law has necessitated the development and awareness of ways and means to use the limited resources for designing manufacture protocols of mAbs. Table 26.2 lists the mAbs (conjugated and unconjugated) which are presently approved for use in oncology.

26.2.2 Radioimmunoconjugation for RIT

The following factors have to be taken into consideration for the radionuclides used for conjugation with mAbs for effective RIT: (1) physical and chemical properties, (2) nature of radiation emitted, (3) fate of the radionuclide after the metabolism of antibody in vivo and (4) the need for a simple, efficient and reproducible commercial method for radioimmunoconjugation. Some of the clinically relevant properties of radionuclides used at present in RIT are listed in Table 26.3. In order to deliver the effective killing dose to the cancerous cells, a choice has to be made between alpha particles, beta particles and Auger electrons. One has to bear in mind that the efficacy of RIT depends not only on the properties of the radionuclides and mAbs but is also very sensitive to the type of tumor, its location, size, physiology, morphology and radiosensitivity to radionuclides. There has to be an adequate balance between the dose delivered to the normal tissues and the tumor so that there is reduced radiation toxicity with effective radiation killing dose.

Table 26.3. Radionuclides presently used in RIT

Radionuclide	$t_{1/2}$ (h)	Emission used in therapy	Emax (keV)	Maximum pathlength (mm)
^{131}I	193	β	610	2.0
^{90}Y	64	β	2,280	12.0
^{177}Lu	161	β	496	1.5
^{186}Re	91	β	1,080	5.0
^{188}Re	17	β	2,120	11.0
^{67}Cu	62	β	577	1.8
^{211}At	7.2	α	7,450	0.08
^{212}Bi	1	α	8,780	0.09
^{213}Bi	0.77	α	>6,000	<0.1
^{125}I	1,442.4	Low energy electrons	350	0.02
^{67}Ga	79.2	Low energy electrons	180	0.02

The two most commonly used radionuclides in RIT are the β-emitters ^{90}Y and ^{131}I. Other β-particle-emitting radionuclides that are being used clinically for RIT are ^{177}Lu,^{67}Cu, ^{186}Re and ^{188}Re (Alvarez et al. 1997; De-

Nardo et al. 1999; Hughes et al. 2000; Jacobs et al. 1993; Meredith et al. 1996; Seitz et al. 1999). β-particles are available in a wide range of half-lives and emissions and have longer path lengths than α-particles. History suggests that ^{131}I has been used most commonly for radiotherapy because it is readily available, is inexpensive, is capable of being imaged using gamma cameras (thus making it possible to perform dosimetry), has a half-life of only 8 days and is conjugated with proteins with relative ease. Considering the physical properties of ^{131}I, the Nuclear Regulatory Commission of the United States has approved the RIT of patients using ^{131}I on an outpatient basis (Siegel 1998). In spite of these advantages, the use of ^{131}I in RIT suffers from certain drawbacks like rapid degradation of radioimmunoconjugates resulting in reduced overall tumor dose and tumor residence time (Goldenberg 2002). Compared to ^{131}I, ^{90}Y is a pure β-emitter and the β-particle emitted has a higher energy and path length (2 mm for ^{131}I vs 12 mm for ^{90}Y), making it suitable for irradiation of tumors having larger dimension. The other favorable property of ^{90}Y is its longer residence time because it is a residualizing label. Radiolabeling of ^{90}Y with mAbs is very effective with high yield and good stability. The most common chelator which is being used for achieving these encouraging results is 1,4,7,10-tetraazacyclododecane-*N,N',N'',N'''*-tetraacetic acid (DOTA). Antibody conjugation is achieved by the activation with *N*-hydroxysulfosuccinimide (Govindan et al. 1998).

The use of α-particles for RIT is relatively new but has shown promising results. The development of ^{234}Ra and ^{225}Ac generators, which produce high yields of α-particle-emitting ^{212}Bi and ^{213}Bi, respectively, has opened up the possibility of conjugation with mAbs (McDevitt et al. 1998; Sgouros et al. 1999). The other α-particle-emitting radionuclide, ^{211}At, which is a cyclotron product, has also been used in RIT (Aurlien et al. 2000; Zalutsky and Vaidyanathan 2000). These α-particle emitting radionuclides have a high LET (~100 keV μm) and a very short path length (< 0.1 mm). The possibility of delivering high LET radiation from a very short range on DNA, resulting in strand breaks, has been the major cause for this renewed interest. One of the prerequisites for these α-particle-emitting radionuclides being used in RIT is the availability of fast mAb conjugation methods because of the very short life of these particles. Most of the conjugation methods used these days take less than 2 h, which is still not sufficient. These radionuclides find their best usage in the treatment of micrometastases or circulating tumor cells. The radionuclides,^{125}I emitting low energy electrons, are also being increasingly used for RIT.

26.3 Different Strategies for RIT

26.3.1 Factors to Be Considered for Developing an Effective RIT Strategy

As is true for most of the therapy regimes used in cancer, a RIT regime takes into consideration the amount of radioactivity administered and the number of cycles used for achieving an optimal therapeutic effect with minimal toxicity/side effects. Radioimmunotherapy, although it appears simple in principle, becomes complex in achieving the desired effect as it is dependent upon three separate but interdependent variables, i.e., the radionuclide, the antibody, and the characteristics of the tumor and host. In order to achieve a therapeutic effect, minute details concerning these factors have to be taken into consideration, of which of paramount importance is the development of a strategy to deliver an adequate dose of radioactivity for killing the cancer cells without affecting the normal tissues. The potential for high absorbed dose of the bone marrow due to circulating or bone tumour bound antibody, the fear of developing bone marrow toxicity prevents the delivery of an adequate amount of radiation dose to the tumor cells. The data from external beam radiotherapy suggests that a minimum cumulative tumor dose of 5,000 cGy should be delivered to provide an adequate therapeutic response. However, even at an accretion as high as 0.01 % of the injected dose/g of tumor, radiolabeled antibodies deliver a cumulative tumor dose of less than 1,500 cGy (Goldenberg 2002).

The response of the tumor depends upon the type of cells it is composed of, its vascularity and volume of the tumor. Most of the damaging effects of radiation occur in the presence of an adequate oxygen concentration. This makes the vascularity of the tumor a very important factor in determining the outcome of RIT. Delivery of the radioimmunoconjugates to the tumor also depends on the vascularity. The normal physiologic distribution of the tumor antigens against which the antibodies are prepared also has an important role to play. The toxicity due to RIT may rise if the antibody is not tumor specific. Taking all these factors together, the strategies which have been developed for RIT differ according to whether the tumor is solid and bulky or has a small volume. It has been observed that whereas RIT has gained sufficient therapeutic potential in hematopoietic malignancies, and minimal or micrometastatic disease, it has failed to deliver an adequate radiation dose in solid tumors.

26.3.2 Pretargeting Strategies

The aim of pretargeting strategies (i.e., the use of cold, nonradiolabeled molecules prior to the administration

of radioimmunoconjugates) is to increase the amount of radioactivity administered without having serious detrimental side effects on the normal tissues. Almost all the pretargeting strategies use modified mAbs (Goldenberg et al. 2006). It is possible to create, chemically or through genetic engineering, from monovalent antibody fragments, other antibody fragments (bispecific monoclonal antibody, bsmAb) which not only bind to the specific antigen but also have the capacity to bind to another hapten chelate. Radiolabeled chelates are prepared that have higher clearance, diffusion rates and permeation. These radiolabeled chelates are injected after the administration of bsmAbs, which leads to the rapid and highly selective tumor uptake (Boerman et al. 2003; Chang et al. 2002; Goodwin and Meares 2001). In order to achieve the ideal condition of almost zero background activity and maximal tumor concentration, scientists have added a third step in this concept of pretargeting by the incorporation of another molecule, rightly called the scavenger molecule or chaser, which leads to the removal of tumor targeted macromolecule from the circulation. Indeed, the use of pretargeting strategies in RIT and radioimmunoimaging has been very successful in delivering a higher amount of radiation to the tumor as compared to those achieved using radiolabeled IgG directly as is documented by several studies (Axworthy et al. 2000; Boerman et al. 2003; Chang et al. 2002; Sharkey et al. 2003).

In order to simplify the concept of pretargeting strategies, they can be divided into two broad groups: (1) the two step method and (2) the three step method. In the two step method, bsmAb is constructed, which has one hapten binding site (radiochelate binding site) and one to two target binding sites (tumor antigen detecting site) (Le Doussal et al. 1989). The bsmAbs used for RIT are very small sized molecules equivalent to F $(ab')_2$. The small size of the bsmAbs enables them to penetrate deep into the tumor tissue, making it possible for the radiolabeled components to deliver a uniform radiation dose to the tumor. A sufficient time gap (several days) is given between step 1 (injection of bsmAbs) and step 2 (injection of radiolabeled component) for adequate clearance of the bsmAbs, otherwise there will be an increase in the nontumor-tumor ratio because of complex formation between the two components in the circulation.

The three step methods currently being employed in pretargeting strategies for RIT are: (1) streptavidin (StAv) or avidin conjugated mAb and radiolabeled biotin (Axworthy et al. 1994; Moro et al. 1997; Waldmann 2003), (2) avidin-biotin (Casadevall 1998; Chinol et al. 2003; Paganelli et al. 1990, 1991; Saga et al. 1994; Yao et al. 1995) and (3) antibody conjugated DNA and complementary nucleotide sequence (He et al. 2004). The high affinity of avidin for biotin and availability of four binding sites has been instrumental in bringing forward this concept of using streptavidin or avidin and biotin in pretargeting strategies (Hnatowich et al. 1987). In the first method, StAv conjugated to mAb is injected first, followed by administration of a clearing agent for removal of StAv-mAb complex from the circulation, and subsequently, in the third step, radiolabeled biotin (^{90}Y-biotin) is injected. However, rapid trafficking of mAb-StAv conjugate into the liver and kidneys makes its biodistribution unfavorable for RIT, leading to the use of modification of the technique. In the second method, radiolabeled biotin is also used. However, instead of using Stav-mAb complex, mAb-biotin complex is used first. In the second step, avidin is injected to remove the biotinylated IgG from the circulation and then StAv is added, which penetrates deep into the tumor and binds to the mAb-biotin complex. The use of avidin prior to the administration of StAv for the clearance of biotinylated IgG from the system is based upon the rationale that avidin is cleared faster from the circulation compared to StAv (because avidin is glycosylated and StAv is nonglycosylated). Most of the biotinylated conjugates are made to withstand the effect of biotinidase, lest there be free radionuclide in the serum due to the breakdown of biotin-radionuclide complex (Chauhan and Dakshinamurti 1986; Goodwin et al. 1998; Karacay et al. 1997; Sabatino et al. 2003). In the third method, target specific mAb conjugated with oligonucleotides is injected first followed by the administration of complementary oligonucleotide for the clearance of mAb-oligonucleotide complex. In the final step, radiolabeled oligonucleotides are injected. Different clinical conditions in which these strategies have been employed until now will be discussed in the section dealing with clinical studies in this chapter (Barbet et al. 1998; Bardies et al. 1996; Breitz et al. 1998, 1999; Chetanneau et al. 1994; Cremonesi et al. 1999; Gruaz-Guyon et al. 2001; Kalofonos et al. 1990; Knox et al. 2000; Kraeber-Bodere et al. 1999; Le Doussal et al. 1993; Magnani et al. 1996; Paganelli et al. 1999; Shen et al. 2005; Stickney et al. 1991; Vuillez et al. 1997, 1999).

While the uses of bsmAbs and StAv have their own merits and demerits in pretargeting strategies, results have suggested that StAv is immunogenic even after the first exposure (Breitz et al. 2000; Paganelli et al. 1999). The same is true for the use of murine bsmAbs, prompting scientists to shift to more humanized and fully humanized bsmAbs for pretargeting (Kraeber-Bodere et al. 2003; Le Doussal et al. 1993).

26.3.3 Combination Therapy

The aim of multimodality therapy in the treatment of cancer is to increase the therapeutic efficacy while decreasing the adverse effects. To date there have been few clinical studies which have documented the improved

efficacy of RIT if combined with chemotherapy (Press et al. 2003; Vose et al. 2005; Winter 2004; Wong et al. 2003). These studies will be discussed briefly in the section concerning clinical studies in this chapter. Another concept which has been in vogue for a few years is the use of radionuclides with different radiation properties for the treatment of both bulky disease and micrometastases (O'Donoghue et al. 1995). The concept of combining external beam radiation therapy with radionuclide therapy is also being developed, named exclusively by R.P. Baum as COMBIERT (combined internal external radiation therapy). Whether these concepts will remain true to their potential is yet to be seen.

26.3.4 Dosimetry for RIT

The dosimetry approaches for the calculation of tumor, total body and normal organ radiation absorbed doses in RIT are similar to those for other radiopharmaceuticals. The reader is referred to the section on dosimetry in this book (Chapters 1, 2).

26.3.5 Nonmyeloablative vs Myeloablative RIT

In general for the delivery of cytocidal radioactivity to the tumor cells, two different approaches of RIT are in vogue: the low dose or nonmyeloablative approach and the high dose or myeloablative approach (DeNardo et al. 2001; Juweid et al. 1999a). In the low dose approach the dose of radionuclide given does not result in myeloablation. The only significant and dose limiting toxicity (DLT) of this approach is myelosuppression, which usually occurs 2 – 3 weeks post-therapy. The nadir of the toxicity is reached at 4 – 8 weeks, with the full recovery usually happening by 12 weeks. Nonhematological toxicity is minimal with this approach (Cheson 2001; DeNardo et al. 1987, 1994, 1998; Gelman et al. 1990; Juweid et al. 1995, 1999b; Kaminski et al. 1992, 1996, 2000; O'Donnell et al. 2000; Scheinberg et al. 1990; Vose et al. 2000a, 2000b; Weiden et al. 2000; Wiseman et al. 1999, 2002; Witzig et al. 1999, 2002a, 2002b). In the high dose myeloablative RIT approach, the higher amount of radioactivity administered results in a higher probability (sometimes almost certain) of having a bone marrow ablation (Juweid et al. 2000; Liu et al. 1998; Press et al. 1989, 1993, 1995). Therefore, this approach usually requires a hematopoietic, generally autologous, stem-cell transplant (HSCT) with peripheral blood stem cells or bone marrow. Apart from this severe toxicity, the myeloablative approach also results in significant nonhematological toxicity to other organs, which usually appears within 1 – 2 months after therapy, with full recovery usually completed within a few weeks. The DLT for this approach is gastrointestinal and cardiopulmonary toxicity. Hepatic toxicity is also observed.

26.3.6 Dosing Methods for RIT

There are two different methods for prescribing the amount of radioactivity to be administered in the myeloablative or nonmyeloablative approaches of RIT. The first method is dosimetry based, in which the amount of radioactivity to be given is derived from the radiation dose to the critical dose-limiting organ. As already described in the previous section, the maximum tolerated dose (MTD) depends on the critical organs, which are red marrow/total body (as a surrogate to marrow) in the nonmyeloablative regime of RIT (Juweid et al. 1999b; Kaminski et al. 1992, 1993, 1996; Vose et al. 2000b) or the second organ, e.g., lungs, heart, gastrointestinal tract, in the myeloablative regime (Juweid et al. 2000; Press et al. 1989, 1993, 1995). Pretherapy tracer imaging is used for calculating the radioactivity to be administered taking into account the anticipated radiation dose to the critical organ/MBq of administered activity. This method of calculation of radioactivity to be administered for RIT is patient specific as the mAb pharmacokinetics varies significantly from one individual to another.

The second method is based on the fixed amounts of radioactivity or body weight/body surface corrected radiation dose (DeNardo et al. 1987, 1994, 1998; Juweid et al. 1995; O'Donnell et al. 2000; Parker et al. 1990; Scheinberg et al. 1990; Vose et al. 2000a; Wiseman et al. 1999; Witzig et al. 1999). It is the simpler of the two methods and does not require a pretherapy tracer study but is not patient specific.

26.3.7 Immuno-PET

The concept of immuno-PET is on the horizon and it is postulated that through serial quantitative PET or PET/CT hybrid cameras, it will be possible to ascertain the labeled mAb concentration in the tumor and thereby facilitate the dosing of the mAb for RIT. It will also be possible to perform individualized dosimetry with far more accuracy, which will limit the toxicity and thereby increase the therapeutic index and effectiveness of RIT. Zirconium-89-labeled chimeric monoclonal antibody U36 is one such radiopharmaceutical which can be used for the purpose (Borjesson et al. 2006; Zalutsky 2006).

26.3.8 RIT vs Immunotherapy

There are certain distinct advantages of RIT over immunotherapy either using unconjugated antibodies or

toxin conjugated antibodies. In RIT, specifically in the case of B-cell NHL, the cytocidal effect is more pronounced than immunotherapy as both biologic and immunologic mechanisms of the antitumor effects of mAbs, e.g., apoptosis and ADCC, come into play along with the radiation induced damage to the tumor cells. The "cross fire" or the "bystander" effect of radiation in RIT, which results in damage to the neighboring nontargeted cells and thus obviates the need to target every cell in the tumor, is a definite advantage over immunotherapy, in which the antitumor effect on a tumor cell is apparent only if it is targeted with the mAb (Juweid 2002).

26.4 Clinical Studies

This section will deal with the most common disease conditions in which the utility of RIT has been conducted most often and in which there is a clear-cut advantage of the implementation of RIT for improved prognosis/quality of life of patients. Broadly, the clinical conditions in which RIT has been implemented and studied can be classified into hematological malignancies and solid tumor. This classification is justified because of the different parameters which have to be taken into consideration when using RIT for these conditions.

26.4.1 Hematopoietic Tumors

26.4.1.1 B-Cell Non-Hodgkin's Lymphoma

B-cell non-Hodgkin's lymphoma (NHL) is the most frequently diagnosed cancer of the immune system. In the year 2004, more than 54,000 new cases of NHL were diagnosed. There are numerous histologic variants of NHL, which are best classified using the WHO criteria (Armitage et al. 2001). Approximately 80 % of lymphomas are of B-cell origin, which are further classified traditionally into low grade, intermediate grade and high grade lymphomas. The Ann-Arbor system is used for staging of the patients (stage I–IV) (Armitage et al. 2001). To define the prognosis of a patient, the following parameters are taken into account: age, stage, lactate dehydrogenase level, WHO performance status and amount of extranodal involvement. Although low grade or indolent NHLs respond initially to many therapies, they ultimately relapse and then become refractory to therapy, leading to an average survival of 5 – 15 years. In contrast, more than 50 % of intermediate grade and high grade NHLs, cumulatively called aggressive lymphomas, show a durable response to multiagent anthracycline based chemotherapy (Armitage et al. 2001). Nevertheless, nearly 40 % of patients with aggressive B-cell NHL are not cured by standard or high dose conventional therapy. Administration of rituximab induced transient partial response is seen in only 30 % of these patients (Coiffier et al. 1998).

Stage I and II indolent NHLs can be treated with radiotherapy. Stage III and IV NHLs are treated with numerous chemotherapeutic and immunotherapeutic regimes and have an initial response rate of 50 – 70 %, with the mean duration of response being 12 – 24 months (Armitage et al. 2001). The maximum response rate is achieved with CHOP (cyclophosphamide, doxorubicin, vincristine and prednisone) and rituximab, reaching as high as 70 – 100 % (Czuczman et al. 1999). These responses are temporary, with nearly all the patients relapsing for the first time within 18 – 50 months (Armitage et al. 2001). There is progressive decline in response rates leading to shorter response duration with each additional therapy. Many of the indolent lymphomas eventually transform into an aggressive variant with a completely different and difficult clinical course resulting in failure of many of the chemotherapy regimens (Armitage et al. 2001).

B-cell NHL patients not responding to chemotherapy and immunotherapy or who relapse after these therapies are the ideal candidates for the institution of RIT.

The potential role of RIT in B-cell NHL was first described by DeNardo et al. in a patient treated with ^{131}I-labeled anti-B-cell lymphoma mAb (called Lym-1). Since then, numerous trials have been conducted, with the majority showing significant improvement in the patient's disease status after treatment with these radioimmunoconjugates. Among various other reasons, the tumor biology of B-cell NHL makes it an ideal candidate for RIT. NHL is radiosensitive and expresses numerous target specific antigens, making it easier for scientists to create specific mAb against these antigens. The numerous antigens which have been targeted until now for RIT are listed in Table 26.4. However, only ibritumomab tiuxetan (Zevalin; murine mAb against CD20 antigen conjugated to ^{90}Y) and tositumomab (Bexxar; murine mAb against CD20 antigen conjugated to ^{131}I) has been approved by the FDA so far.

^{90}Y-Ibritumomab Tiuxetan (Zevalin)

Zevalin prepared by IDEC pharmaceuticals, San Diego, CA, was the first radioimmunoconjugate to be approved by the FDA for clinical use in February 2002. It consists of ^{90}Y labeled murine antibody to CD20. Based upon the International Workshop response criteria, Zevalin has been found to produce a response rate of 74 – 83 % in patients with relapsed/refractory low grade, follicular, or CD20+ transformed NHL (Knox et al. 1996; Witzig et al. 2000a, 2000b). It has also been documented based upon the same response criteria

Table 26.4. Radioimmunoconjugates currently used in oncology

Clinical indications	Radiolabeled antibodies
Hematological malignancies	
NHL	^{90}Y-ibritumomab tiuxetan[a]
	^{131}I-tositumomab[a]
	^{90}Y-epratuzumab anti-CD22 IgG
Leukemia	^{131}I-BCB anti-CD45 IgG
	^{90}Y- or ^{188}Re-anti-CD66 IgG
	^{213}Bi-HuM195 anti-CD33 IgG
NHL, Hodgkin's lymphoma and T-cell lymphoma	^{90}Y-anti-Tac IgG
Solid malignancies	
Colorectal cancer	^{90}Y-T84.66 anti-CEA IgG
	^{131}I- and ^{90}Y-iabetuzumab (anti-CEA IgG)
	^{131}I-CC49-ΔCH2
	^{125}I/^{131}I-A33 IgG
	^{90}Y-biotin pretargeted with CC49 StAv fusion protein
Prostate cancer	^{177}Lu-J591IgG
	^{131}I-murine CC49 mAb
	^{90}Y-CYT-356 capromab pendetide
Ovarian cancer	^{90}Y/^{177}Lu-CC49
	^{90}Y-Hu3S193
	^{131}I-anti-CEA IgG
	^{90}Y-biotin pretargeted by biotinylated mAb cocktail
Glioma	^{90}Y-BC-2 and BC4 anti-tenascin
	^{125}I-425 IgG
	^{131}I labeled antitenascin
Pancreatic cancer	^{90}Y-PAM4 IgG
Lung cancer	^{131}I-ch TNT
Breast cancer	^{90}Y-Br-E3
	^{211}At-81C6
	^{131}I-81C6
	^{90}Y-170H.82
	^{131}I-CC49
Renal cancer	^{131}I-cG250 IgG
Medullary thyroid cancer	^{131}I-Hapten pretargeted by anti-CEA bsmAb
CNS or leptomeningeal cancer	^{131}I-BH9 IgG
Medulloblastoma	^{131}I-3F8 IgG
Head and neck cancer	^{186}Re-bivatuzumab
Hepatocellular carcinoma	^{131}I-Hepama IgG
	^{90}Y-hAFP IgG

[a] Approved by FDA for RIT of NHL

that Zevalin has the response rate of 83% in patients who failed to respond to rituximab.

Dosimetry and Dosing. The results of dosimetry and dosing of ^{90}Y-ibritumomab tiuxetan in several studies have come to the following conclusions (Wagner et al. 2002):

1. ^{90}Y-ibritumomab tiuxetan can be administered safely without significant toxicity if the dose is based upon a patient's body weight and the pretreatment platelet counts. If the pretreatment platelet count is 150×10^9/L, then a dose of 14.8 MBq/kg can be administered and if pretreatment platelet count is 100×10^9/L, then a dose of 11.1 MBq/kg is recommended.
2. Dosimetry was not required if the patients have the desired pre-treatment platelet count and $< 25\%$ bone marrow involvement (as determined by bone marrow biopsy).
3. Dosimetry should ideally be performed if the indication for use of ^{90}Y-ibritumomab tiuxetan is different from the one defined in the registration trials in patients with low grade NHL.
4. Almost the whole of radioactivity administered in the therapeutic dose of ^{90}Y-ibritumomab is retained in the body, with only $7.3 \pm 3.25\%$ being excreted through the kidneys (primary pathway of clearance).
5. As an additional safety measure, ^{111}In-ibritumomab tiuxetan scintigraphy can be performed to confirm the expected biodistribution of ^{90}Y-ibritumomab (in the US the In-111 study must be done).

Preparation and Administration. The procedure for radiolabeling of ^{90}Y-ibritumomab tiuxetan begins with 1,480 MBq. The patient dose ranges between 777 and 1,110 MBq, with the maximum administered activity of 1,184 MBq. Zevalin is commercially available in solution form, containing 3.2 mg of the immunoconjugate in 2 ml of saline solution. A quantity of 1,480 MBq of ^{90}Y can be incorporated in 1.3 ml of the solution, resulting in a relatively low dose of mAb being administered (Wagner et al. 2002).

The radiochemical purity of the preparation is checked prior to its administration to the patient. If it is 95%, then the preparation can be used for injection into the patient. For radiation safety measures the drug is kept in plastic or acrylic shields and the syringe should also be shielded accordingly. The drug can be prepared at a regional radiopharmacy center and distributed to the user centers.

Prior to the administration of Zevalin, 450 mg of rituximab is injected over 4–6 h. This step is essential to improve tumor targeting by blocking easily accessible CD20 sites in the peripheral blood and preventing indiscriminate uptake of the radioimmunoconjugate in the reticuloendothelial system (Zelenetz 1999). ^{90}Y-ibritumomab tiuxetan administration should begin within 4 h of completion of rituximab dose (Wiseman et al. 2000). A slow intravenous push over 10 min rather than a rapid intravenous bolus is the preferred mode of injection. The patients can be injected on an outpatient basis.

Adverse Effects and Toxicity. The most common nonhematologic adverse effects of ^{90}Y-ibritumomab tiuxetan therapy are as follows: asthenia, nausea, infec-

tion, fever, chills and abdominal pain (Wagner et al. 2002). Because of the murine mAb component of Zevalin, anaphylaxis, a potentially serious adverse effect, may develop.

Development of human antimouse antibody (HAMA) response to murine antibodies (Konig et al. 2002) is common but the intensity of the reaction is not very high in NHL patients who have already received chemotherapy. The most deleterious effect of this reaction to the murine antibody is limitation of the number of therapy cycles which can be instituted in patients already documented to have had HAMA response (Goldenberg 2002). Keeping these anaphylactic reactions in mind, it is obligatory to make sure that epinephrine, antihistamines and corticosteroids are readily available during the administration of Zevalin as well as rituximab.

Radiation Safety Measures. As mentioned already, ^{90}Y-ibritumomab tiuxetan can be administered on an outpatient basis. The treatment with Zevalin results in the emission of β-particles and bremsstrahlung radiation. Since there is no emission of penetrating γ-radiation, the risk of radiation exposure to healthcare workers, patients, family members or other close contacts is minimal. In accordance with US guidelines (*Criteria for the Release of Individuals Administered Radioactive Material.* Nuclear Regulatory Commission, Washington, DC, US, 1997. Title 10 CFR parts 20 and 35:62 FR 4120; and *Release of Patients Administered Radioactive Materials*. Nuclear Regulatory Commission, Washington, DC, US, 1997. Regulatory Guide 8.39), patients can be released immediately after therapy. Minimal risks associated with the use of ^{90}Y labeled monoclonal antibodies preclude the need for determining activity limits or dose limits for the patients. The recommended instructions to be given to patients who have been treated with ^{90}Y-ibritumomab tiuxetan are as follows (Wagner et al. 2002):

1. Up to 3 days post-therapy: (a) proper care to be taken during micturition to prevent spilling of urine. Spilled urine should be cleaned up. (b) Good hand washing after using the toilet. (c) Disposal of any body fluid contaminated material, e.g. in a toilet or in a plastic bag in the household trash.
2. Up to 1 week after therapy: use of condoms for sexual intercourse.

Some patients may be required to be treated as inpatients for medical reasons. These patients should be handled like every other patient and no precautions other than the universal precautions are needed (Wagner et al. 2002).

^{131}I-Tositumomab (Bexxar)

^{131}I-tositumomab was approved by the FDA for the treatment of relapsed and refractory B-cell NHL patients in June 2003. It is now manufactured commercially by GlaxoSmithKline under the tradename Bexxar. It consists of IgG2a murine mAb against CD20.

Dosimetry and Dosing. Unlike Zevalin, individualized dosimetry is essential prior to the administration of Bexxar. For dosimetry (Davies 2004), 450 mg of unlabeled tositumomab is given intravenously over 1 h followed by infusion of 35 mg of (185 MBq) iodine (^{131}I) tositumomab over 20 min. Whole body images are acquired under the gamma camera at 1 h post-injection and then on the 2nd, 3rd, 4th, 6th and 7th days. A best-fit line derived from a time activity curve of the percentage of residual injected radioactivity is used to calculate the total body residence time. The MTD calculated for ^{131}I-tositumomab is 75 cGy. This value is taken into consideration when calculating the total dose of ^{131}I-tositumomab to be administered to the patient. The rationale for using individualized dosimetry is to increase the *therapeutic index*, which is defined as the ratio of the radiation absorbed dose delivered to cancerous cells and the dose delivered to normal tissues.

Preparation and Administration. Bexxar is supplied by a centralized radiopharmacy and is not prepared in-house or in regional centers. For the end users, it comes in two different forms depending on its use. For the purpose of dosimetry, it is supplied at radioactivity (^{131}I) and protein (tositumomab) concentrations of 0.61 mCi/ml and 0.1 mg/ml, respectively. The therapeutic dosage form consists of 5.6 mCi/ml and 1.1 mg/ml of radioactivity (^{131}I) and protein (tositumomab) respectively. Free radio-iodine and other reactants are removed at the manufacturer's end by chromatographic purification steps. The potential of thyroid damage from Bexxar is high because of ^{131}I (Goldenberg 2002). Therefore thyroid blockage is recommended 1 day prior to, to continue up to 14 days after, the administration of ^{131}I-tositumomab. It is essential to monitor the platelet count before prescribing the dose for ^{131}I-tositumomab. Cold, nonradioactive tositumomab (450 mg) is administered intravenously over 1 h followed by a patient specific whole body dose of ^{131}I-tositumomab over 20 min. The radioactivity to be administered is calculated with the aim of delivering 75 cGy, provided the patient's platelet count is 150×10^9/L. Patients having relative thrombocytopenia ($100 - 149 \times 10^9$/L) should be given a radioactivity amount equivalent to the delivery of a total body dose of 65 cGy, because of grade IV hematological toxicity, which is observed with high frequency in these patients (Davies 2004). If the bone marrow reserve is >25 %, then the Bexxar regimen should

not be administered. It is recommended that the therapeutic dose of ^{131}I-tositumomab should be delivered within 8 – 14 days of the initiation of dosimetric steps.

Adverse Effects and Toxicity. *Immediate:* As compared to Zevalin, infusional adverse reaction is minimal with Bexxar. Nonhematological toxicity is also minimal (Goldenberg 2002). Sometimes a serious hypersensitivity reaction, including anaphylaxis, is observed with ^{131}I-tositumomab. In patients who have not received chemotherapy previously, the incidence of HAMA after Bexxar is as high as approximately 60 % (Wahl et al. 2000). This is a potential drawback of the regime as the development of HAMA precludes the administration of the second cycle of the regime. It is essential to keep medications to combat these hypersensitivity reactions ready prior to the administration of ^{131}I-tositumomab.

Long Term Adverse Effects: Because of the usually high release of ^{131}I from Bexxar, the chances of developing hypothyroidism are high even with thyroid blockage (Gregory et al. 2004). The majority of patients treated with Bexxar develop grade III/IV hematological toxicities across the full range of administered doses (Davies 2004). Severe thrombocytopenia and neutropenia are the most common hematological adverse reactions. These hematological adverse effects reach a nadir at 4 – 6 weeks after therapy and recover to grade II by the 9th week (Davies 2004). Some patients treated with Bexxar have also shown myelodysplasia on long-term follow-up. But these patients were heavily pretreated with chemotherapy, which might have been a separate contributory factor (Goldenberg 2002). ^{131}I released from Bexxar is cleared from the kidneys, thereby precluding its usage in hydronephrosis or renal dysfunction of another etiology.

Radiation Safety Measures. According to the new Nuclear Regulatory Commission regulations for the administration of ^{131}I for therapy, Bexxar can be given to most (but not all) patients on an outpatient basis in the US (Siegel 1998). The essential prerequisite for the new regulation is that the total effective dose equivalent to another individual from exposure to a patient treated with ^{131}I containing radiopharmaceutical should be > 500 mrem. *However, in the UK and many other European countries including Germany, the administration is still done on an inpatient basis*. Renal clearance of ^{131}I released from Bexxar makes it mandatory to explain about hygiene and toilet habits to the patients. Healthcare workers should handle the urine or patient's body fluid contaminated materials in accordance with the set guidelines for handling of ^{131}I.

Clinical Experience of Radioimmunotherapy in B-Cell NHL

To date there have been numerous studies and trials done to evaluate the efficacy of RIT in the treatment of B-cell NHL in various clinical settings. It is beyond the scope of this book to elaborate upon all of these studies. The results of some of the studies in various clinical settings of NHL are summarized in Table 26.5.

A brief outline of some of these studies along with their conclusions is mentioned in the following paragraphs.

RIT in Relapsed /Refractory B-Cell NHL or Transformed Lymphoma. In a prospective randomized trial of Zevalin in 143 patients with refractory/relapsed low grade follicular lymphoma or transformed NHL, Zevalin was found to have an overall objective response rate (ORR) and a completion rate (CR) of 80 % and 30 % respectively as compared to 56 % and 16 % in the group that received unlabeled rituximab (Witzig et al. 2000c). This study also showed that Zevalin when given at a nonmyeloablative dose of 15 MBq/kg delivered acceptable radiation absorbed doses to normal organs without performing pre-therapy dosimetry with ^{111}In-labeled Zevalin. In a similar study, in patients with relapsed or refractory NHL, Bexxar was found to have an overall ORR and CR of 55 % and 33 % respectively as against 19 % (ORR) and 8 % (CR) in patients treated with unconjugated tositumomab (Davis et al. 2003). The median duration of response was not reached in the patient group treated with Bexxar as compared to 28.1 months for those treated with tositumomab. In a phase II study in patients with indolent (the majority follicular) or transformed indolent lymphoma at the time of 1st or 2nd recurrence, 76 % of the patients were found to respond to Bexxar, with 49 % achieving a CR (Davies et al. 2004). The response rate was highest in patients with follicular lymphoma (OR 79 %). In the results of a phase I/II study in patients with relapsed or refractory B-cell NHL treated with Zevalin published by Witzig et al. (1999) and Wiseman et al. (1999), it was observed that Zevalin was able to achieve an ORR of 67 %, with low-grade lymphoma showing the maximum ORR of 82 % as compared to 43 % for intermediate grade lymphoma. Time to disease progression and the duration of response as estimated by Kaplan-Meier estimates were found to be 12.7 months and 11.6 months respectively. In patients with transformed indolent lymphoma, Bexxar has been reported to have an ORR and a CR of 39 % and 25 % respectively (Zelenetz et al. 2002). The majority of the patients enrolled in this study had a poor prognosis. The median duration of response of patients achieving CR was 36 months.

Table 26.5. RIT in NHL: representative studies

References	No. of patients	Radioimmunoconjugate	Target	Isotype of mAb	Myeloablative RIT	Dosing schedule	Responses
Behr et al. (1999c, 2002a)	3	^{131}I-hLL2	CD22	Humanized IgG2a	1/3	Single	1CR, 1PR, 1PD
	5	^{131}I-C2B8	CD20	Chimeric IgG1	5/5	RID/RIT	3CR, 1PR, 1NA
	7	^{131}I-C2B8	CD20	Chimeric IgG1	7/7	RID/RIT	6CR, 1PR
Czuczman et al. (1993)	18	^{131}I-OKB7	CD21	Murine IgG2b	Not given	Quadruple	1PR, 12SD, 5NA
DeNardo et al. (1990, 1998*)	18	^{131}I-Lym-1	HLA-DR10	Murine IgG2a	Not given	Multiple	2CR, 8PR, 3SD, 1PD
	21	^{131}I-Lym-1	HLA-DR10	Murine IgG2a	Not given	RID/RIT at 1 – 4 weeks	7CR, 4PR, 9SD, 1PD
Davis et al. (2001)	42	^{131}I-anti-B1	CD20	Murine IgG2a	Not given	RID/RIT	14CR, 9PR
Goldenberg et al. (1991)	7	^{131}I-LL2	CD22	Murine IgG2a	Not given	Double	2PR, 3SD
Juweid et al. (1995, 1999b)	7	^{131}I-LL2	CD22	Murine IgG2a	Not given	Multiple	1CR, 1PR, 5 unk
	13	^{131}I-LL2 F(ab)$_2$	CD22	Murine F(ab)$_2$	Not given	Multiple	1CR, 1PR, 11 unk
	1	^{131}I-cLL2	CD22	Chimeric IgG2a	Not given	Multiple	1 unk
	3	^{131}I-LL2	CD22	Murine IgG2a	3/3	Multiple	2PR, 1NE
	13	^{131}I-hLL2	CD22	Humanized IgG2a	Not given	RID/RIT	1CR, 1PR, 5SD, 6PD
	7	^{90}Y-hLL2	CD22	Humanized IgG2a	Not given	RID/RIT	2PR, 5PD
Kaminski et al. (2005**)	76	^{131}I-anti-B1	CD20	Murine IgG2a	Not given	RID/RIT	57CR, 15PR
Linden et al. (1999)	8	^{131}I-LL2	CD22	Murine IgG22a	Not given	RID/RIT at 1 – 3 weeks	3PR, 1SD, 4PD
O'Donnell et al. (1999)	12	^{67}Cu-Lym-1	HLA-DR10	Murine IgG2a	Not given	Multiple	1CR, 6PR
Press et al. (1993)	6	^{131}I-MB-1	CD37	Murine IgG1	3/6	RID/RIT	6CR
	1	^{131}I-1F5	CD20	Murine IgG2a	1/1	RID/RIT	1PR
	12	^{131}I-anti-B1	CD20	Murine IgG2a	11/12	RID/RIT	10CR, 1PD, 1SD
Postema et al. (2003***)	15	^{186}Re-hLL2	CD22	Humanized IgG2a	Not given	RID/RIT	1CR, 4PR, 4SD, 6PD
Scheidhauer et al. (2003)	26	^{131}I-C2B8	CD22	Chimeric IgG1	Not given	RID/RIT	9CR, 5PR
	25	^{131}I-C2B8	CD22	Chimeric IgG1	25/25	RID/RIT	12CR, 7PR
Witzig et al. (2002b, 2002c)	143	^{90}Y-ibritumomab tiuxetan	CD20	Murine IgG2a	Not given	RID/RIT	80 %ORR, 30 %CR
	54	^{90}Y-ibritumomab tiuxetan	CD20	Murine IgG2a	Not given	Multiple, RID/RIT	74 %ORR, 15 %CR, 59 %PR
Wiseman and Witzig (2005)	211	^{90}Y-ibritumomab tiuxetan	CD20	Murine IgG2a	–	Multiple	TTP 29.3 months. Median TTP was 53.9 months in patients with ongoing response

CR complete remission, *PR* partial remission, *SD* stable disease, *PD* progressive disease, *unk* unknown, *TTP* time to progression, *ORR* overall response rate, *RIT* radioimmunotherapy, *NA* not available, *RID* radioimmunodosimetry

* DeNardo GL, DeNardo SJ, Goldstein DS, Kroger LA, Lamborn KR, Levy NB, McGahan JP, Salako Q, Shen S, Lewis JP Maximum-tolerated dose, toxicity, and efficacy of (131)I-Lym-1 antibody for fractionated radioimmunotherapy of non-Hodgkin's lymphoma J Clin Oncol. 1998 Oct; 16(10):3246 – 56

** Kaminski MS, Tuck M, Estes J, et al. I-131 tositumomab therapy as initial treatment for fullicular lymphoma. N Engl J Med. 2005; 352:496 – 498

***Postema EJ, Raemaekers JM, Oyen WJ, Boerman OC, Mandigers CM, Goldenberg DM, van Dongen GA, Corstens FH Final results of a phase I radioimmunotherapy trial using (186)Re-epratuzumab for the treatment of patients with non-Hodgkin's lymphoma Clin Cancer Res. 2003 Sep 1; 9(10 Pt 2)3995S – 4002S

RIT Following Failure of Rituximab. The initial results of a phase II multi-center study in patients who failed to respond to rituximab and were later treated with Bexxar showed that 68 % of patients with follicular lymphoma responded, with 30 % achieving CR (Horning et al. 2002). In this subgroup of NHL patients, in a separate study, Zevalin was found to have an ORR of 74 %, with 15 % achieving CR in accordance with the Cheson criteria (Cheson et al. 1999; Witzig et al. 2000c), or an ORR of 59 % and a CR of 4 % by the IDEC criteria. Duration of response was also significantly longer (7.7 months vs 4 months) in patients receiving Zevalin after rituximab failure. The Kaplan-Meier estimated time to progression of disease was found to be 6.8 months for all patients and 8.7 patients for responders.

First Line Therapy. In order to evaluate the efficacy of RIT in patients of B-cell NHL who were not treated previously with chemotherapy or immunotherapy, Wahl et al. conducted a phase II study in patients in stage III or stage IV of low grade or transformed NHL (Wahl et al. 2000). These patients were treated with dosimetry-based radioactivity doses of Bexxar reaching 75 cGy to the total body. It was found that 97 % of the patients showed a PR or CR, 63 % achieved CR, and the median duration of response was not reached until 38 months of follow-up, with median duration of follow-up being 16.2 %. However, the potential drawback to the use of Bexxar as the first line therapy is the high incidence of HAMA response observed due to the murine origin of tositumomab. The use of humanized chimeric or hyperchimeric mAb regimens containing very small amounts of murine mAb is being contemplated.

Summary of Results of Phase II and Phase III Studies with Nonmyeloablative Doses of ^{131}I-Tositumomab and ^{90}Y-Ibritumomab Tiuxetan. The reported studies have clearly demonstrated that both of these radionuclide conjugated mAbs are quite effective in the treatment of relapsed/refractory low-grade and transformed NHL with an ORR and CR of 60 – 80 % and 20 – 30 % respectively (Juweid 2002). The median duration of response observed with both these radioimmunoconjugates is 1 year. In aggressive NHL, phase I/II studies in a limited number of patients have shown that RIT causes ORR and CR in 30 – 40 % and 10 – 30 % of patients respectively (Kaminski et al. 1996, 2000; Witzig et al. 1999).

Results of Phase II Myeloablative Dose of RIT. Most of the limited number of studies evaluating the myeloablative dose regime of RIT have been performed with Bexxar (Liu et al. 1998; Press et al. 1995). The limited experience has suggested that this treatment approach results in higher CR and longer duration of response compared with nonmyeloablative RIT in patients with relapsed/refractory low-grade B-cell NHL. However, there are numerous merits and demerits of these studies and conclusions about the efficacy of a myeloablative dose regime of RIT can only be ascertained with future studies.

RIT Combined with Chemotherapy. In an effort to improve the outcome of patients, studies have been conducted to evaluate the efficacy of combining chemotherapy with RIT. Two approaches have been used: (1) a nonmyeloablative approach (low dose RIT combined with standard or low dose chemotherapy) and (2) a myeloablative approach (high dose RIT combined with either standard or high dose chemotherapy, HDC). The second approach usually requires HSCT to control myelotoxicity. Leonard et al. (1999) demonstrated in their study that sequential standard dose chemotherapy (fludarabarine), when combined with low dose ^{131}I-tositumomab in patients with previously untreated low-grade, transformed or follicular NHL, results in increased efficacy with acceptable toxicity level as compared to fludarabarine alone. None of the patients in this study showed a HAMA response, probably due to the prior administration of fludarabarine, which suppresses the immune response. Future studies are being designed to evaluate the efficacy of concurrent administration of RIT and chemotherapy to exploit the potential radiosensitizing effect of chemotherapy.

The myeloablative approach was evaluated by Press et al. (2000). It was observed that sequential high-dose RIT (up to 2,500 cGy of 2.5 mg/kg ^{131}I-tositumomab) and HDC (60 mg/kg etoposide and 100 mg/kg cyclophosphamide) when administered in relapsed/refractory cases of B-cell NHL results in progression free survival and overall survival in 73 % and 85 % of patients followed up to 2 years. The mortality rate in this group was 8 %, which was due to opportunistic infections and nonhematological toxicities; the data is similar to that observed with combination of HDC and total body irradiation (TBI). By this approach, it was possible to deliver a median tumor dose of 38 Gy with RIT as compared to only 12 Gy with TBI (this data was arrived at on the assumption that the median tumor to lung radiation absorbed dose ratio was 1.5) (Juweid 2002).

Summary of RIT in B-Cell NHL

The following conclusions can be drawn from various trials on the use of RIT in NHL (Goldenberg 2002):

1. RIT can achieve a significant and durable response in patients who relapse after chemotherapy/have bulky disease.
2. Even a low radiation dose can achieve an objective tumor response.
3. As compared to the nonmyeloablative dose, a myeloablative dose combined with autologous bone

marrow or peripheral stem cell transplantation can result in overall response rates with significant longer duration of response.
4. Patients having low tumor burden with low bone marrow involvement and without splenomegaly are better responders.
5. The combined approach of using RIT and chemotherapy may be more effective than any single modality.
6. RIT appears superior to unconjugated mAb in the therapy of patients with relapsed B-cell NHL.
7. Hypothyroidism, myelodysplasia and possible secondary neoplasms are the expected long term adverse effects of RIT.
8. Unconjugated antibodies may improve the biodistribution of radioimmunoconjugates.
9. The tumor dosimetry of mAbs conjugated with ^{90}Y appears superior to ^{131}I conjugated mAbs.

RIT in Other Hematological Malignancies

Efficacy of RIT in other hematological malignancies like cutaneous T-cell lymphoma, chronic lymphocytic leukemia (CLL), acute leukemia and multiple myeloma have been documented in a few studies (Goldenberg 2002). The most promising results have been documented in acute leukemia, in which RIT was shown to improve the outcome of bone marrow grafting by decreasing the relapse rate (Corcoran et al. 1996; Matthews et al. 1999). In the study, ^{131}I-labeled anti-CD45 murine antibody (BC8) for RIT was combined with cyclophosphamide and 12 Gy total-body irradiation as a bone marrow conditioning regimen. The disease free survival significantly improved in AML/myelodysplastic syndrome or acute lymphoblastic leukemia (Matthews et al. 1999). Mention should be made of the use of ^{213}Bi, an α-emitter with an LET of 8 MeV and a half-life of 45.6 min which was conjugated with humanized anti-CD33 antibody and used for treatment of leukemia (Sgouros et al. 1999). The results, although in a very small group of patients, showed that α-particle radioimmunoconjugates can deliver a several fold higher amount of radiation dose to liver, spleen and marrow as compared to β-particle radioimmunoconjugates.

26.4.2 RIT in Solid Tumors

The popularity achieved by RIT in the successful treatment of B-cell NHL encouraged clinical scientists to venture into and expand the field of RIT in solid tumors. However, the inherent radioresistant property of these tumors as well as the immunogenicity of murine proteins and relatively slow clearance of humanized intact immunoglobulins has meant that scientists have not had a major success as was achieved with NHL (Goldenberg 2002; Jhanwar and Divgi 2005). At the same time, a better understanding of the methodology essential for delivering significant amounts of radioactivity to tumor has opened up new avenues for expanding the role of RIT in solid tumors (Divgi 2006). The main tumor antigens against which the target antibodies (either chimeric or humanized form) have been used are CEA, TAG-72, MUC1, tenascin, and prostate specific membrane antigen (PSMA). Along with the other factors which govern the outcome of treatment with radioimmunoconjugates, the main concern in RIT of solid tumor is to develop a radioimmunoconjugate which matches the heterogeneity of antigen expression of these tumors and also has a high penetration (Jhanwar and Divgi 2005). The following sections will briefly cover some of the solid tumors for which RIT has achieved some sort of success in phase I/II dose-escalation studies in which suboptimal doses were used. One of the major limitations in coming to a definite conclusion from these studies is that the majority of the studies were conducted on patients having advanced stage disease in which the prognosis was poor in any case (Goldenberg 2002).

26.4.2.1 Colon Cancer

Colon cancer has been most commonly used as a model for use of RIT in solid tumors (Table 26.6). Carcinoembryonic antigen (CEA), which is expressed in a number of cancers, has been used for the localization of tumors using immunoscintigraphy (Baum et al. 1989). RIT with ^{131}I-labeled murine and humanized anti-CEA antibodies in colorectal and other cancers has been performed (Fig. 26.1). A phase II study using humanized ^{131}I-labeled anti-CEA mAb (hMN-14) in patients with small volume metastasis refractory to treatment and patients who have had curative surgical resection of metachronous liver metastases, has shown an overall response rate of 58% with a mean duration of response of 9 months in both groups (Behr et al. 2002b). The study, although meant to evaluate the efficacy of RIT in solid tumor, again proves that the present methodology of RIT is suitable for small volume disease rather than bulky disease. Another phase 1 study (Wong et al. 2003) conducted in patients with metastatic CEA producing malignancies for evaluating the efficacy of ^{90}Y-anti-CEA chimeric T84.66 antibodies demonstrated that there was no response in these patients and that the toxicity of radioimmunoconjugate was radionuclide dependent. This observation has given an edge to the unconjugated antibodies as a separate treatment modality rather than the conjugated ones. However, contrary to this study, several earlier studies using ^{131}I-labeled CEA have documented a modest response (Behr et al. 1997a, 1997b; Juweid et al. 1996).

Table 26.6. RIT in colorectal cancer: representative phase I/II studies

Reference studies	No. of patients	Radioimmunoconjugate	Target	Isotype of mAb	Responses	Comments
Behr et al. (1997a, 1999b, 2002b)	12	^{131}I-MN-14	CEA	Humanized IgG1	2PR, 4 mixed/minimum response/SD, CEA reduction in 9	
	30	^{131}I-MN-14	CEA	Humanized IgG1	3PR, 8 mixed response	Adjuvant RIT in 9 patients after surgical removal of metastases
	57	^{131}I-NP4 (IMMU-4)	CEA	Murine F(ab')$_2$	1PR, 4 mixed/minor response and 7 stabilization disease after previously progressive disease	
Divgi et al. (1995*)	24	^{131}I-CC-49	TAG72	Murine IgG1	No response	
Juweid et al. (1996)	13	^{131}I-NP4 (IMMU-4)	CEA	Murine F(ab')$_2$	7SD	
Meredith et al. (1992, 1995, 1996)	12	^{131}I-B72.3	TAG72	Chimeric IgG4	3SD, 1 minimum response	
	14	^{131}I-COL-1 + ^{131}I-CC49	CEA/ TAG72	Murine IgG1	4SD	Dual antibody combined with IFNa-2b
	28	^{125}I-17 – 1A	Ep-CAM	Chimeric IgG2a	10SD	
Mittal et al. (1996)	9	^{131}I-IMMU-4	CEA	Murine IgG1	1PR	Hyperthermia used
Welt et al. (1994, 1996)	21	^{125}I-A33	A33	Murine IgG2a	1 mixed response, 12SD	
	23	^{131}I-A33	A33	Murine IgG2a	3 mixed response	
Wong et al. (2003)	21	^{90}Y-T84.66	CEA	Chimeric IgG1	11SD, 1 mixed response	
Ychou et al. (1998)	10	^{131}I-F6	CEA	Murine F(ab')$_2$	1PR, 2SD, 6PD	

* Divgi CR, Scott AM, Dantis L, Capitelli P, Siler K, Hilton S, Finn RD, Kemeny N, Kelsen D, Kostakoglu L, et al. Phase I radioimmunotherapy trial with iodine-131-CC49 in metastatic colon carcinoma. J Nucl Med. 1995 Apr; 36(4):586 – 92

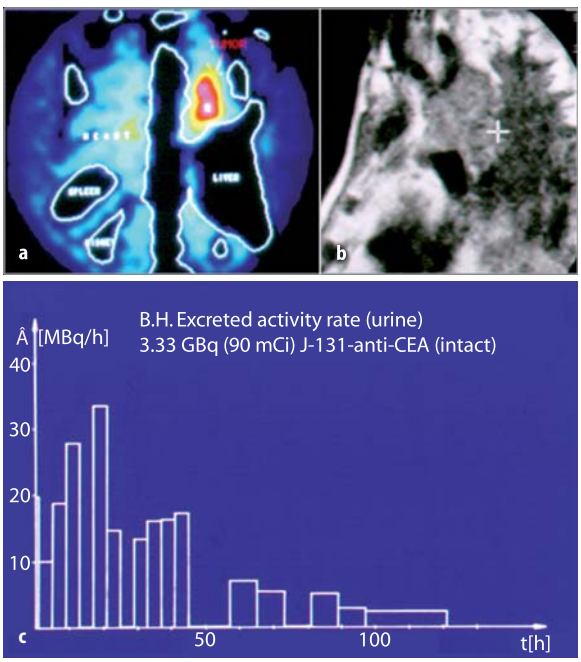

Other radioimmunoconjugates like ^{131}I-anti-CEA/19-9 (Fig. 26.2), ^{131}I-anti-CA125 (Fig. 26.3), ^{131}I-CC49, ^{90}Y-CC49 and ^{131}I-A33 have been targeted without any objective response (Table 26.6). Intra-arterial administration of radiolabeled antibodies (Fig. 26.4) was tried, but did not result in much greater success. Pretargeting strategies using streptavidin conjugates of the NR-LU-10 pancarcinoma antibody and ^{90}Y-biotin have shown only a modest response of 8 % along with diarrhea as the grade IV nonhematological toxicity, the results being much inferior as to what was suggested by preclinical studies (Knox et al. 2000).

◁

Fig. 26.1. Radioimmunotherapy using an intact anti-CEA antibody, labeled with I-131 (3.33 GBq, 90 mCi) in a patient with recurrent, irresectable squamous cell carcinoma of the lung. Serum CEA was strongly elevated (679 ng/ml). Posterior image of the thorax (**a**) using a double tracer isocontour technique (DTICT) after subtraction of a Tc-99m colloid scan from the I-131 scan for outlining the anatomical structures (early image fusion technique); **b** MRI scan of the thorax outlining the infiltrating tumor; **c** excreted activity in urine (in MBq/h) over 4 days after therapy

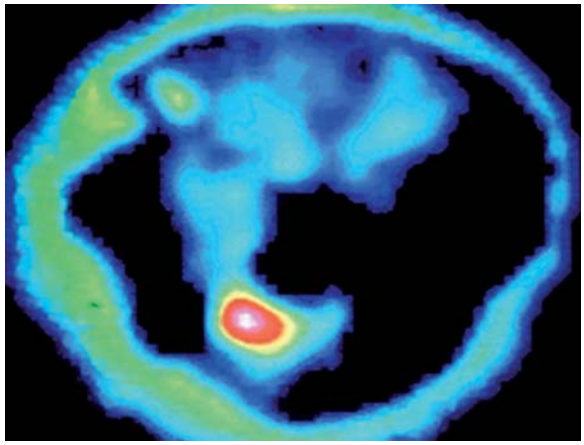

Fig. 26.2. First radioimmunotherapy using a cocktail of I-131 labeled anti-CEA/CA19-9 $F(ab')_2$ antibodies (2.33 GBq, 63 mCi) in a 13-year-old girl with recurrent sigmoid carcinoma and peritoneal carcinosis (University Medical Center, Frankfurt/Main, Germany, July 1985). Transversal SPECT slice (DTICT) showing high uptake in an abdominal lesion. Tumor dosimetry/half-life: whole-body 0.46 Gy/2.2 days; liver 2.9 Gy/2.2 days; tumor abdomen 14 Gy/2.3 days

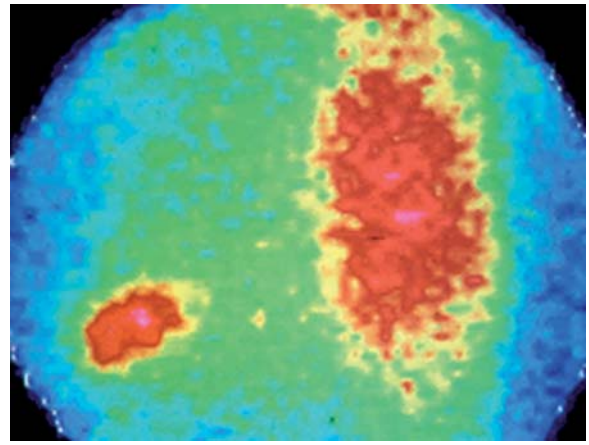

Fig. 26.3. Radioimmunotherapy using I-131-OC 125 $F(ab')_2$ antibodies for treatment of a diffuse, infiltrating mucinous adenocarcinoma with lymphangiosis carcinomatosa of both lungs expressing the CA125 antigen (as shown by immunohistochemistry, serum CA125 800 U/ml) in a 39-year-old male. Planar posterior image of thorax/abdomen revealing significant uptake in the right hemithorax as well as uptake in the spleen (antibody complexation due to HAMA formation after the diagnostic study)

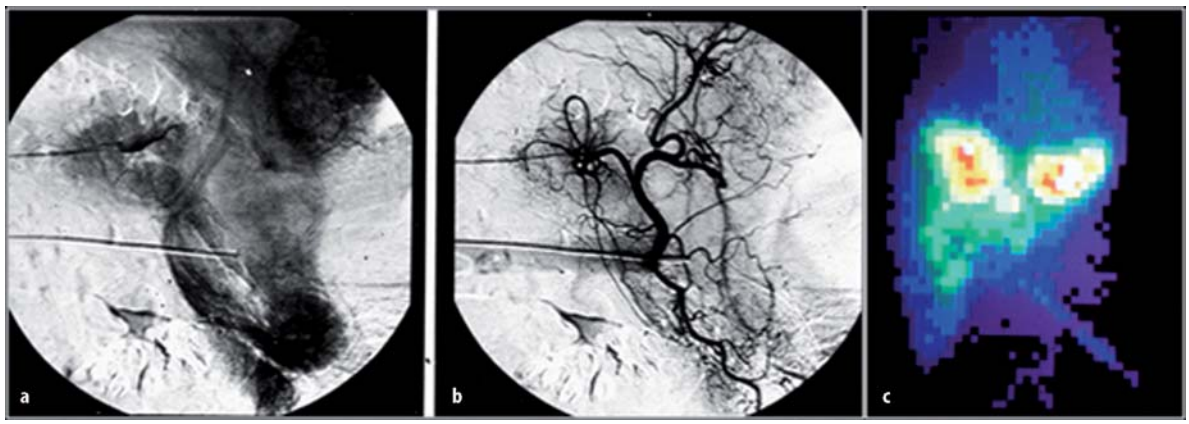

Fig. 26.4. Intra-arterial radioimmunotherapy (intact anti-CEA antibody injected together with DSM particles to slow down the blood flow) via the hepatic artery in a patient with colorectal liver metastases. Arterial (**a**) and late (**b**) phase of digital subtraction angiography (DSA) shows hyperperfused lesions in the right hepatic lobe; dynamic immunoscintigraphy (**c**) reveals high uptake in the CEA-positive metastases 2 min after starting the intra-arterial infusion

26.4.2.2 Prostate Cancer

The success of diagnostic markers in prostate cancer prompted scientists to target them for RIT. However, most of the radioimmunoconjugates like ^{131}I-murine CC49 mAb and ^{90}Y-CYT-356 capromab pendetide antibody have not shown any objective response (Dillman 1996; Knox et al. 1996; Meredith et al. 1994, 1999). PSMA, which is not a secreted antigen, has also been targeted for RIT of prostate cancer. ^{90}Y labeled PSMA mAb 7E11/CY356 has demonstrated no therapeutic efficacy. The possible explanation for this failure is the targeting of the internal epitope of PSMA by this agent (McDevitt et al. 2001). Phase I studies using ^{90}Y and ^{177}Lu labeled-mAb J591, which targets the external domain of PSMA, are being conducted (Nanus et al. 2003).

26.4.2.3 Ovarian Cancer

The success story of RIT in ovarian cancer has been a bit different from that in other solid tumors. It has been documented that ^{90}Y-labeled MUC1 antibody when given intraperitoneally in patients with ovarian cancer stage IC–IV without any evidence of disease after debulking and platinum based chemotherapy, results in significant prolongation of duration of disease free survival (80 % 5 year survival rate as compared to 55 % for nonrandomized chemotherapy controls without RIT)

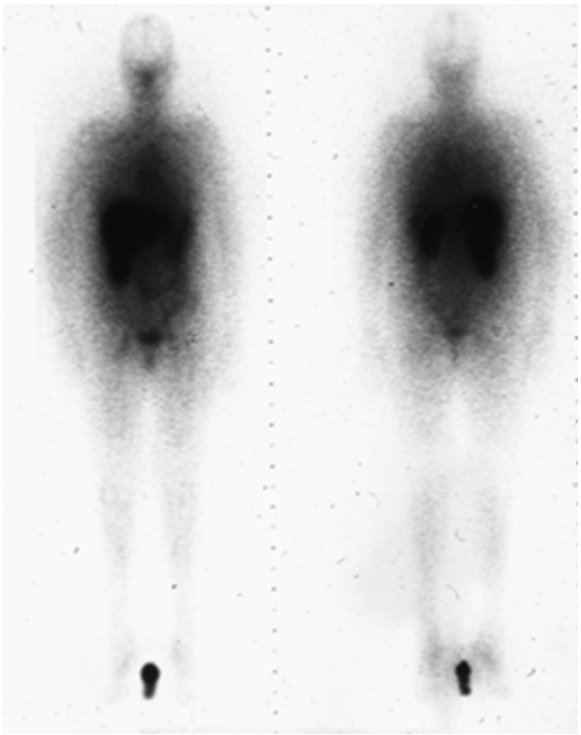

Fig. 26.5. First radioimmunotherapy (September 1997) using a Re-188 labeled anti-CA125 antibody for treatment of a patient with recurrent ovarian cancer [whole body scan 24 h after therapy with 3.7 GBq (100 mCi) B43.13 antibody]

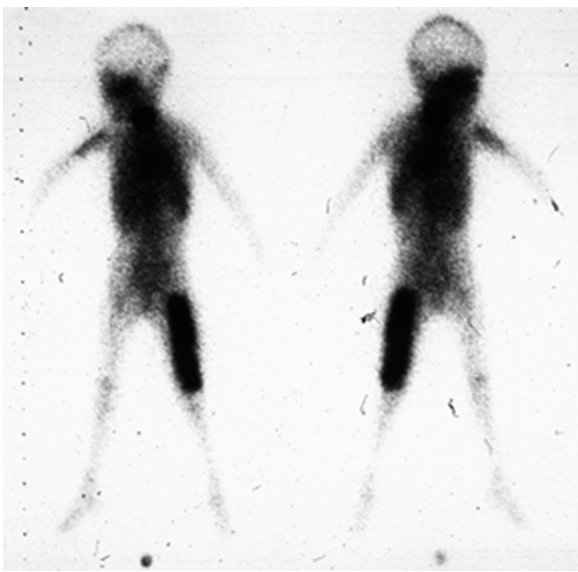

Fig. 26.6. First radioimmunotherapy (March 1994) of a 4-year-old child with metastatic neuroblastoma using 12 mg of the I-131 labeled (2.26 GBq, 61 mCi) chimeric anti-NCAM antibody ch14.18 antibody showing strong uptake in bone metastases in the left femur (whole-body anterior/posterior scan 8 days after therapy)

(Nicholson et al. 1998). The same group has also demonstrated that this therapy is more effective when used in patients with tumor nodules less than 2 cm and no response is observed when the tumors are larger (Epenetos et al. 1987). The success of ^{186}Re-NR-LU-10 and ^{177}Lu-CC49 given intraperitoneally in patients having tumor nodules > 5 mm or micrometastatic disease supports the previous notion that RIT is mainly useful in non-bulky tumors (Jacobs et al. 1993; Meredith et al. 1996). However, preliminary studies by Baum et al. (unpublished) using ^{188}Re-B43.13 antibody in patients with small volume recurrences of ovarian cancer (Fig. 26.5) did not show a significant improvement as compared to conventional chemotherapy. Although the development of HAMA is a potential limitation for RIT in ovarian carcinomas (Oltrogge et al. 1997), in some of the studies (Mobus et al. 2003; Noujaim et al. 2001; Schultes et al. 1998), it has been documented that development of immune response to murine monoclonal antibody-B43.13 correlates well with the survival of patients with recurrent ovarian cancer; patients developing immune response had significantly prolonged survival compared to the ones not showing any immune response.

26.4.2.4 Brain and Other CNS Tumors

The tumors of brain and other CNS tumors have been treated successfully using locoregional RIT. ^{90}Y and ^{131}I labeled antitenascin antibodies have been used for this purpose (Riva et al. 2000). These radioimmunoconjugates have been shown to significantly prolong the median survival for patients with glioblastoma when injected directly into the tumor bed after surgery. Among the two radionuclides, ^{90}Y has been shown to have better results in bulky disease with fewer radioprotection problems (Goldenberg 2002).

Intra-arterial RIT using ^{131}I and ^{125}I-labeled antibodies has been used with evidence of objective response in patients with brain tumor (Brady et al. 1990; Kalofonos et al. 1989). ^{125}I-antiepidermal growth factor receptor antibody 425 has been used effectively both intravenously and intra-arterially for treatment of patients with glioblastoma multiforme with similar results (Brady et al. 1990; Zalutsky et al. 1990). Some other tumors which have been treated using locoregional injections are medulloblastoma and neuroblastoma (Kemshead et al. 1992).

Other solid tumors for which RIT is being employed are neuroblastoma (Fig. 26.6), renal cell carcinoma, breast cancer, urinary bladder carcinoma and medullary thyroid cancer. A recent study has shown the efficacy of pretargeted RIT with bsmAb and ^{131}I-labeled bivalent hapten in patients with advanced, progressive MTC (Goldenberg et al. 2006). The patients treated

with RIT had a longer survival than patients without RIT, with the main toxicity being hematological. Preliminary results using ^{90}Y labeled with chimeric anti-CEA antibody (cT84.66) along with stem cell reinfusion have shown promising evidence of antitumor activity in patients with breast cancer (Wong et al. 1999).

26.5 Conclusions

In the recent past there has been immense interest generated in RIT because of the wide success of "magic bullets" targeted with radionuclides. This upward trend in the curve of success of RIT, specifically in low volume tumors, has been greatly helped by the development of genetic engineering. No longer is the science limited to using monoclonal antibodies of foreign origin, but the prospect of having fully humanized monoclonal antibodies has greatly enthused workers across the globe into finding appropriate and ideal radioimmunoconjugates for RIT. The success of Zevalin and Bexxar speaks volumes for the efforts being put in. The search for newer target antigens like Cuban monoclonal antibody (MoA) anti-egf-egf-ior-r3 (Oliva et al. 2004), IOR-C5 (Oliva et al. 2001), and 174H.64 (Baum et al. 1993) have generated new interest. Much still needs to be done in expanding the usage of RIT in solid tumors. The success of locoregional therapy along with other therapeutic modalities in solid tumor has widened horizons, and the future appears bright for radioimmunotherapy in our efforts to fight cancer.

References

Adams GP, Weiner LM (2005) Monoclonal antibody therapy of cancer. Nature Biotechnol 23:1147 – 57

Alvarez RD, Partridge EE, Khazaeli MB, Plott G, Austin M, Kilgore L, Russell CD, Liu T, Grizzle WE, Schlom J, LoBuglio AF, Meredith RF (1997) Intraperitoneal radioimmunotherapy of ovarian cancer with 177Lu-CC49: a phase I/II study. Gynecol Oncol 65:94 – 101

Armitage JO, Mauch PM, Harris NL, Bierman P (2001) Non-Hodgkins lymphoma. Lippincott, Williams & Wilkins, Philadelphia

Aurlien E, Larsen RH, Kvalheim G, Bruland OS (2000) Demonstration of highly specific toxicity of the alpha-emitting radioimmunoconjugate(211)At-rituximab against non-Hodgkin's lymphoma cells. Br J Cancer 83:1375 – 9

Axworthy DB, Fritzberg AR, Hylarides MD, et.al. (1994) Preclinical evaluation of anti-tumor monoclonal antibody/streptavidin conjugate for pretargeted 90Y radioimmunotherapy in a mouse xenograft model. J Immunother 16:158

Axworthy DB, Reno JM, Hylarides MD, Mallett RW, Theodore LJ, Gustavson LM, Su F, Hobson LJ, Beaumier PL, Fritzberg AR (2000) Cure of human carcinoma xenografts by a single dose of pretargeted yttrium-90 with negligible toxicity. Proc Natl Acad Sci U S A 97:1802 – 7

Badger CC, Anasetti C, Davis J, Bernstein ID (1987) Treatment of malignancy with unmodified antibody. Pathol Immunopathol Res 6:419 – 34

Bale WF, Spar IL (1957) Studies directed towards use of antibodies as carriers of radioactivity for therapy. Adv Biol Med Phys 5:285 – 356

Barbet J, Peltier P, Bardet S, Vuillez JP, Bachelot I, Denet S, Olivier P, Leccia F, Corcuff B, Huglo D, Proye C, Rouvier E, Meyer P, Chatal JF (1998) Radioimmunodetection of medullary thyroid carcinoma using indium-111 bivalent hapten and anti-CEA x anti-DTPA-indium bispecific antibody. J Nucl Med 39:1172 – 8

Bardies M, Bardet S, Faivre-Chauvet A, Peltier P, Douillard JY, Mahe M, Fiche M, Lisbona A, Giacalone F, Meyer P, Gautherot E, Rouvier E, Barbet J, Chatal JF (1996) Bispecific antibody and iodine-131-labeled bivalent hapten dosimetry in patients with medullary thyroid or small-cell lung cancer. J Nucl Med 37:1853 – 9

Baum RP (1999) At the crossroads: from cancer imaging and therapy using radiolabeled monoclonal antibodies to metabolic tumour imaging with positron emission tomography (PET). Ind J Nucl Med:51 – 66

Baum RP, Lorenz M, Senekowitsch R, Albrecht M, Hor G (1987) [Clinical results of immunoscintigraphy and radioimmunotherapy]. Nuklearmedizin 26:68 – 78

Baum RP, Hertel A, Lorenz M, Schwarz A, Encke A, Hor G (1989) ^{99m}Tc-labelled anti-CEA monoclonal antibody for tumour immunoscintigraphy: first clinical results. Nucl Med Commun 10:345 – 52

Baum RP, Adams S, Kiefer J, Niesen A, Knecht R, Howaldt HP, Hertel A, Adamietz IA, Sykes T, Boniface GR, et al. (1993) A novel technetium-99m labeled monoclonal antibody (174H.64) for staging head and neck cancer by immuno-SPECT. Acta Oncol 32:747 – 51

Behr TM, Goldenberg DM (1996) Improved prospects for cancer therapy with radiolabeled antibody fragments and peptides? J Nucl Med 37:834 – 6

Behr TM, Sharkey RM, Juweid ME, Dunn RM, Vagg RC, Ying Z, Zhang CH, Swayne LC, Vardi Y, Siegel JA, Goldenberg DM (1997a) Phase I/II clinical radioimmunotherapy with an iodine-131-labeled anti-carcinoembryonic antigen murine monoclonal antibody IgG. J Nucl Med 38:858 – 70

Behr TM, Sharkey RM, Juweid ME, Dunn RM, Ying Z, Zhang CH, Siegel JA, Goldenberg DM (1997b) Variables influencing tumor dosimetry in radioimmunotherapy of CEA-expressing cancers with anti-CEA and antimucin monoclonal antibodies. J Nucl Med 38:409 – 18

Behr TM, Memtsoudis S, Vougioukas V, Liersch T, Gratz S, Schmidt F, Lorf T, Post S, Wormann B, Hiddemann W, Ringe B, Becker W (1999a) Radioimmunotherapy of colorectal cancer in small volume disease and in an adjuvant setting: preclinical evaluation in comparison to equitoxic chemotherapy and initial results of an ongoing phase-I/II clinical trial. Anticancer Res 19:2427 – 32

Behr TM, Salib AL, Liersch T, Behe M, Angerstein C, Blumenthal RD, Fayyazi A, Sharkey RM, Ringe B, Becker H, Wormann B, Hiddemann W, Goldenberg DM, Becker W (1999b) Radioimmunotherapy of small volume disease of colorectal cancer metastatic to the liver: preclinical evaluation in comparison to standard chemotherapy and initial results of a phase I clinical study. Clin Cancer Res 5:3232s–3242s

Behr TM, Wormann B, Gramatzki M, Riggert J, Gratz S, Behe M, Griesinger F, Sharkey RM, Kolb HJ, Hiddemann W, Goldenberg DM, Becker W (1999c) Low- versus high-dose radioimmunotherapy with humanized anti-CD22 or chimeric anti-CD20 antibodies in a broad spectrum of B cell-associated malignancies. Clin Cancer Res 5:3304s–3314s

Behr TM, Blumenthal RD, Memtsoudis S, Sharkey RM, Gratz S, Becker W, Goldenberg DM (2000) Cure of metastatic human

colonic cancer in mice with radiolabeled monoclonal antibody fragments. Clin Cancer Res 6:4900 – 7
Behr TM, Griesinger F, Riggert J, Gratz S, Behe M, Kaufmann CC, Wormann B, Brittinger G, Becker W (2002a) High-dose myeloablative radioimmunotherapy of mantle cell non-Hodgkin lymphoma with the iodine-131-labeled chimeric anti-CD20 antibody C2B8 and autologous stem cell support. Results of a pilot study. Cancer 94:1363 – 72
Behr TM, Liersch T, Greiner-Bechert L, Griesinger F, Behe M, Markus PM, Gratz S, Angerstein C, Brittinger G, Becker H, Goldenberg DM, Becker W (2002b) Radioimmunotherapy of small-volume disease of metastatic colorectal cancer. Cancer 94:1373 – 81
Beierwaltes WH (1974) Radioiodine-labelled compounds previously or currently used for tumour localisation. In: Proceedings of an Advisory Group Meeting on Tumour Localisation with Radioactive Agents. Panel Proceedings Series. International Atomic Energy Agency Vienna, Austria, pp 47 – 56
Belitsky P, Ghose T, Aquino J, Norvell ST, Blair AH (1978) Radionuclide imaging of primary renal-cell carcinoma by I-131-labeled antitumor antibody. J Nucl Med 19:427 – 30
Boerman OC, van Schaijk FG, Oyen WJ, Corstens FH (2003) Pretargeted radioimmunotherapy of cancer: progress step by step. J Nucl Med 44:400 – 11
Borghaei H, Schilder RJ (2004) Safety and efficacy of radioimmunotherapy with yttrium 90 ibritumomab tiuxetan (Zevalin). Semin Nucl Med 34:4 – 9
Borjesson PK, Jauw YW, Boellaard R, de Bree R, Comans EF, Roos JC, Castelijns JA, Vosjan MJ, Kummer JA, Leemans CR, Lammertsma AA, van Dongen GA (2006) Performance of immuno-positron emission tomography with zirconium-89-labeled chimeric monoclonal antibody U36 in the detection of lymph node metastases in head and neck cancer patients. Clin Cancer Res 12:2133 – 40
Brady LW, Markoe AM, Woo DV, Rackover MA, Koprowski H, Steplewski Z, Peyster RG (1990) Iodine125 labeled anti-epidermal growth factor receptor-425 in the treatment of malignant astrocytomas. A pilot study. J Neurosurg Sci 34: 243 – 9
Breitz HB, Fisher DR, Wessels BW (1998) Marrow toxicity and radiation absorbed dose estimates from rhenium-186-labeled monoclonal antibody. J Nucl Med 39:1746 – 51
Breitz HB, Fisher DR, Goris ML, Knox S, Ratliff B, Murtha AD, Weiden PL (1999) Radiation absorbed dose estimation for 90Y-DOTA-biotin with pretargeted NR-LU-10/streptavidin. Cancer Biother Radiopharm 14:381 – 95
Breitz HB, Weiden PL, Beaumier PL, Axworthy DB, Seiler C, Su F, M, Graves S, Bryan K, Reno JM (2000) Clinical optimization of pretargeted radioimmunotherapy with antibody-streptavidin conjugate and 90Y-DOTA-biotin. J Nucl Med 41:131 – 40
Buchegger F, Pfister C, Fournier K, Prevel F, Schreyer M, Carrel S, Mach JP (1989) Ablation of human colon carcinoma in nude mice by 131I-labeled monoclonal anti-carcinoembryonic antigen antibody F(ab')2 fragments. J Clin Invest 83:1449 – 56
Buchegger F, Pelegrin A, Delaloye B, Bischof-Delaloye A, Mach JP (1990) Iodine-131-labeled MAb F(ab')2 fragments are more efficient and less toxic than intact anti-CEA antibodies in radioimmunotherapy of large human colon carcinoma grafted in nude mice. J Nucl Med 31:1035 – 44
Buchegger F, Mach JP, Folli S, Delaloye B, Bischof-Delaloye A, Pelegrin A (1996) Higher efficiency of 131I-labeled anti-carcinoembryonic antigen-monoclonal antibody F(ab')2 as compared to intact antibodies in radioimmunotherapy of established human colon carcinoma grafted in nude mice. Recent Res Cancer Res 141:19 – 35
Buchegger F, Allal AS, Roth A, Papazyan JP, Dupertuis Y, Mirimanoff RO, Gillet M, Pelegrin A, Mach JP, Slosman DO (2000) Combined radioimmunotherapy and radiotherapy of liver metastases from colorectal cancer: a feasibility study. Anticancer Res 20:1889 – 96
Casadevall A (1998) Antibody-based therapies as anti-infective agents. Expert Opin Investig Drugs 7:307 – 21
Chang CH, Sharkey RM, Rossi EA, Karacay H, McBride W, Hansen HJ, Chatal JF, Barbet J, Goldenberg DM (2002) Molecular advances in pretargeting radioimmunotherapy with bispecific antibodies. Mol Cancer Ther 1:553 – 63
Chauhan J, Dakshinamurti K (1986) Purification and characterization of human serum biotinidase. J Biol Chem 261: 4268 – 75
Cheson BD (2001) Some like it hot! J Clin Oncol 19:3908 – 11
Cheson BD, Horning SJ, Coiffier B, Shipp MA, Fisher RI, Connors JM, Lister TA, Vose J, Grillo-Lopez A, Hagenbeek A, Cabanillas F, Klippensten D, Hiddemann W, Castellino R, Harris NL, Armitage JO, Carter W, Hoppe R, Canellos GP (1999) Report of an international workshop to standardize response criteria for non-Hodgkin's lymphomas. NCI Sponsored International Working Group. J Clin Oncol 17:1244
Chetanneau A, Barbet J, Peltier P, Le Doussal JM, Gruaz-Guyon A, Bernard AM, Resche I, Rouvier E, Bourguet P, Delaage M, et al. (1994) Pretargeted imaging of colorectal cancer recurrences using an 111In-labelled bivalent hapten and a bispecific antibody conjugate. Nucl Med Commun 15:972 – 80
Chinol M, De Cobelli O, Trifiro G, Scardino E, Bartolomei M, Verweij F, Papi S, Matei DV, Paganelli G (2003) Localization of avidin in superficial bladder cancer: a potentially new approach for radionuclide therapy. Eur Urol 44:556 – 9
Coiffier B, Haioun C, Ketterer N, Engert A, Tilly H, Ma D, Johnson, P, Lister A, Feuring-Buske M, Radford JA, Capdeville R, Diehl V, Reyes F (1998) Rituximab (anti-CD20 monoclonal antibody) for the treatment of patients with relapsing or refractory aggressive lymphoma: a multicenter phase II study. Blood 92:1927 – 32
Corcoran MC, Press OW, Matthews DC, Appelbaum FR, Bernstein ID (1996) The role of radioimmunotherapy in bone marrow transplantation. Curr Opin Hematol 3:438 – 45
Cremonesi M, Ferrari M, Chinol M, Stabin MG, Grana C, Prisco G, Robertson C, Tosi G, Paganelli G (1999) Three-step radioimmunotherapy with yttrium-90 biotin: dosimetry and pharmacokinetics in cancer patients. Eur J Nucl Med 26:110 – 20
Czuczman MS, Straus DJ, Divgi CR, Graham M, Garin-Chesa P, Finn R, Myers J, Old LJ, Larson SM, Scheinberg DA (1993) Phase I dose-escalation trial of iodine 131-labeled monoclonal antibody OKB7 in patients with non-Hodgkin's lymphoma. J Clin Oncol 11:2021 – 9
Czuczman MS, Grillo-Lopez AJ, White CA, Saleh M, Gordon L, LoBuglio AF, Jonas C, Klippenstein D, Dallaire B, Varns C (1999) Treatment of patients with low-grade B-cell lymphoma with the combination of chimeric anti-CD20 monoclonal antibody and CHOP chemotherapy. J Clin Oncol 17:268 – 76
Davies AJ (2004) Tositumomab and iodine [131I] tositumomab in the management of follicular lymphoma. An oncologist's view. Q J Nucl Med Mol Imaging 48:305 – 16
Davis T, Kaminski MS, Leonard JP, Hsu FJ, Wilkinson M, Wahl RL (2003) Long-term results of a randomised trial comparing tositumomab and iodine I131-tositumomab (BEXXAR) with tositumomab alone in patients with relapsed or refractory low-grade (lg) or transformed low grade (t-lg) non-Hodgkin's lymphoma (NHL). Blood 102:405a
Davies AJ, Rohatiner AZ, Howell S, Britton KE, Owens SE, Micallef IN, Deakin DP, Carrington BM, Lawrance JA, Vinnicombe S, Mather SJ, Clayton J, Foley R, Jan H, Kroll S, Harris M, Amess J, Norton AJ, Lister TA, Radford JA (2004) Tositu-

momab and iodine I 131 tositumomab for recurrent indolent and transformed B-cell non-Hodgkin's lymphoma. J Clin Oncol 22:1469 – 79

Davis TA, Kaminski MS, Leonard JP, Gregory SA, Wahl RL, Hsu FJ, Wilkinson M, Frankel SR, Serafini A, Zelenetz AD, Kroll S, Coleman M, Levy R, Knox SJ (2001) Results of a randomized study of Bexxar (tositumomab or iodine I-131 tositumomab) versus unlabeled tositumomab in patients with relapsed or refractory low-grade or transformed non-Hodgkin's lymphoma (NHL). In: Proc Am Soc Hematology, pp 3503

Day ED, Lassiter S, Woodhall B, Mahaley JL, Mahaley MS, Jr (1965) The localization of radioantibodies in human brain tumors. I. Preliminary exploration. Cancer Res 25:773 – 8

DeNardo SJ, DeNardo GL, O'Grady LF, Macey DJ, Mills SL, Epstein AL, Peng JS, McGahan JP (1987) Treatment of a patient with B cell lymphoma by I-131 LYM-1 monoclonal antibodies. Int J Biol Markers 2:49 – 53

DeNardo GL, DeNardo SJ, O'Grady LF, Levy NB, Adams GP, Mills SL (1990) Fractionated radioimmunotherapy of B-cell malignancies with 131I-Lym-1. Cancer Res 50:1014s–1016s

DeNardo GL, Lewis JP, DeNardo SJ, O'Grady LF (1994) Effect of Lym-1 radioimmunoconjugate on refractory chronic lymphocytic leukemia. Cancer 73:1425 – 32

DeNardo GL, DeNardo SJ, Goldstein DS, Kroger LA, Lamborn KR, Levy NB, McGahan JP, Salako Q, Shen S, Lewis JP (1998) Maximum-tolerated dose, toxicity, and efficacy of (131)I-Lym-1 antibody for fractionated radioimmunotherapy of non-Hodgkin's lymphoma. J Clin Oncol 16:3246 – 56

DeNardo GL, Kukis DL, Shen S, DeNardo DA, Meares CF, DeNardo SJ (1999) 67Cu-versus 131I-labeled Lym-1 antibody: comparative pharmacokinetics and dosimetry in patients with non-Hodgkin's lymphoma. Clin Cancer Res 5:533 – 41

DeNardo GL, Juweid ME, White CA, Wiseman GA, DeNardo SJ (2001) Role of radiation dosimetry in radioimmunotherapy planning and treatment dosing. Crit Rev Oncol Hematol 39:203 – 18

Dillman RO (1996) Why event-free survival is better than tumor response or other measures of survival as an endpoint in cancer trials. Cancer Biother Radiopharm 11:99 – 104

Divgi C (2006) Editorial: what ails solid tumor radioimmunotherapy? Cancer Biother Radiopharm 21:81 – 4

Divgi CR, Scott AM, Dantis L, Capitelli P, Siler K, Hilton S, Finn RD, Kemeny N, Kelsen D, Kostakoglu L, et al. (1995) Phase I radioimmunotherapy trial with iodine-131-CC49 in metastatic colon carcinoma. J Nucl Med 36:586 – 92

Dixon KL (2003) The radiation biology of radioimmunotherapy. Nucl Med Commun 24:951 – 7

Epenetos AA, Munro AJ, Stewart S, Rampling R, Lambert HE, McKenzie CG, Soutter P, Rahemtulla A, Hooker G, Sivolapenko GB, et al. (1987) Antibody-guided irradiation of advanced ovarian cancer with intraperitoneally administered radiolabeled monoclonal antibodies. J Clin Oncol 5:1890 – 9

Feldhaus MJ, Siegel RW (2004) Yeast display of antibody fragments: a discovery and characterization platform. J Immunol Methods 290:69 – 80

Gelman R, Gelber R, Henderson IC, Coleman CN, Harris JR (1990) Improved methodology for analyzing local and distant recurrence. J Clin Oncol 8:548 – 55

Goldenberg DM (2002) Targeted therapy of cancer with radiolabeled antibodies. J Nucl Med 43:693 – 713

Goldenberg DM, DeLand F, Kim E, Bennett S, Primus FJ, van Nagell JR, Jr, Estes N, DeSimone P, Rayburn P (1978) Use of radiolabeled antibodies to carcinoembryonic antigen for the detection and localization of diverse cancers by external photoscanning. N Engl J Med 298:1384 – 6

Goldenberg DM, Horowitz JA, Sharkey RM, Hall TC, Murthy S, Goldenberg H, Lee RE, Stein R, Siegel JA, Izon DO, et al. (1991) Targeting, dosimetry, and radioimmunotherapy of B-cell lymphomas with iodine-131-labeled LL2 monoclonal antibody. J Clin Oncol 9:548 – 64

Goldenberg DM, Sharkey RM, Paganelli G, Barbet J, Chatal JF (2006) Antibody pretargeting advances cancer radioimmunodetection and radioimmunotherapy. J Clin Oncol 24:823 – 834

Goodwin DA, Meares CF (2001) Advances in pretargeting biotechnology. Biotechnol Adv 19:435 – 50

Goodwin DA, Meares CF, Osen M (1998) Biological properties of biotin-chelate conjugates for pretargeted diagnosis and therapy with the avidin/biotin system. J Nucl Med 39:1813 – 1818

Govindan SV, Shih LB, Goldenberg DM, Sharkey RM, Karacay H, Donnelly JE, Losman MJ, Hansen HJ, Griffiths GL (1998) 90Yttrium-labeled complementarity-determining-region-grafted monoclonal antibodies for radioimmunotherapy: radiolabeling and animal biodistribution studies. Bioconjug Chem 9:773 – 82

Green LL, Hardy MC, Maynard-Currie CE, Tsuda H, Louie DM, Mendez MJ, Abderrahim H, Noguchi M, Smith DH, Zeng Y, et al. (1994) Antigen-specific human monoclonal antibodies from mice engineered with human Ig heavy and light chain YACs. Nat Genet 7:13 – 21

Gregory SA, Leonard JP, Knox SJ, Zelenetz AD, Armitage JO, Kaminski MS (2004) The iodine I131 tositumomab therapeutic regimen: Summary of safety in 995 patients with relapsed/refractory low grade (LG) and transformed LG non-Hodgkin's lymphoma (NHL). American Society of Clinical Oncology, Annual Meeting Proceedings (post-meeting edition). J Clin Oncol 22(14S):6732

Gruaz-Guyon A, Janevik-Ivanovska E, Raguin O, De Labriolle-Vaylet C, Barbet J (2001) Radiolabeled bivalent haptens for tumor immunodetection and radioimmunotherapy. Q J Nucl Med 45:201 – 6

He J, Liu G, Gupta S, Zhang Y, Rusckowski M, Hnatowich DJ (2004) Amplification targeting: a modified pretargeting approach with potential for signal amplification – proof of a concept. J Nucl Med 45:1087 – 95

Hnatowich DJ, Virzi F, Rusckowski M (1987) Investigations of avidin and biotin for imaging applications. J Nucl Med 28:1294 – 302

Hoogenboom HR, Chames P (2000) Natural and designer binding sites made by phage display technology. Immunol Today 21:371 – 8

Horning SJ, Younes A, Lucas J, Podoloff D, Jain V (2002) Rituximab treatment failures: tositumomab and iodine (131I) tositumomab (Bexxar) can produce meaningful durable responses. Blood 100:357a

Hughes OD, Bishop MC, Perkins AC, Wastie ML, Denton G, Price MR, Frier M, Denley H, Rutherford R, Schubiger PA (2000) Targeting superficial bladder cancer by the intravesical administration of copper-67-labeled anti-MUC1 mucin monoclonal antibody C595. J Clin Oncol 18:363 – 70

Irving RA, Coia G, Roberts A, Nuttall SD, Hudson PJ (2001) Ribosome display and affinity maturation: from antibodies to single V-domains and steps towards cancer therapeutics. J Immunol Methods 248:31 – 45

Jacobs AJ, Fer M, Su FM, Breitz H, Thompson J, Goodgold H, Cain J, Heaps J, Weiden P (1993) A phase I trial of a rhenium 186-labeled monoclonal antibody administered intraperitoneally in ovarian carcinoma: toxicity and clinical response. Obstet Gynecol 82:586 – 93

Jain RK (1990) Tumor physiology and antibody delivery. Front Radiat Ther Oncol 24:32 – 46; discussion 64 – 8

Jhanwar YS, Divgi C (2005) Current status of therapy of solid tumors. J Nucl Med 46 Suppl 1:141S–150S

Juweid ME (2002) Radioimmunotherapy of B-cell non-Hod-

gkin's lymphoma: from clinical trials to clinical practice. J Nucl Med 43:1507 – 29
Juweid M, Sharkey RM, Markowitz A, Behr T, Swayne LC, Dunn R, Hansen HJ, Shevitz J, Leung SO, Rubin AD, et al. (1995) Treatment of non-Hodgkin's lymphoma with radiolabeled murine, chimeric, or humanized LL2, an anti-CD22 monoclonal antibody. Cancer Res 55:5899s–5907s
Juweid ME, Sharkey RM, Behr T, Swayne LC, Dunn R, Siegel J, Goldenberg DM (1996) Radioimmunotherapy of patients with small-volume tumors using iodine-131-labeled anti-CEA monoclonal antibody NP-4 F(ab')2. J Nucl Med 37: 1504 – 10
Juweid M, Sharkey RM, Goldenberg DM (1999a) Radioimmunotherapy of non-Hodgkins lymphoma with non-myeloablative doses of radiolabeled monoclonal antibodies. Harwood Academic, Philadelphia
Juweid ME, Stadtmauer E, Hajjar G, Sharkey RM, Suleiman S, Luger S, Swayne LC, Alavi A, Goldenberg DM (1999b) Pharmacokinetics, dosimetry, and initial therapeutic results with 131I- and (111)In-/90Y-labeled humanized LL2 anti-CD22 monoclonal antibody in patients with relapsed, refractory non-Hodgkin's lymphoma. Clin Cancer Res 5: 3292s–3303s
Juweid ME, Hajjar G, Stein R, Sharkey RM, Herskovic T, Swayne LC, Suleiman S, Pereira M, Rubin AD, Goldenberg DM (2000) Initial experience with high-dose radioimmunotherapy of metastatic medullary thyroid cancer using 131I-MN-14 F(ab)2 anti-carcinoembryonic antigen MAb and AHSCR. J Nucl Med 41:93 – 103
Kalofonos HP, Pawlikowska TR, Hemingway A, Courtenay-Luck N, Dhokia B, Snook D, Sivolapenko GB, Hooker GR, McKenzie CG, Lavender PJ, et al. (1989) Antibody guided diagnosis and therapy of brain gliomas using radiolabeled monoclonal antibodies against epidermal growth factor receptor and placental alkaline phosphatase. J Nucl Med 30:1636 – 45
Kalofonos HP, Rusckowski M, Siebecker DA, Sivolapenko GB, Snook D, Lavender JP, Epenetos AA, Hnatowich DJ (1990) Imaging of tumor in patients with indium-111-labeled biotin and streptavidin-conjugated antibodies: preliminary communication. J Nucl Med 31:1791 – 6
Kaminski MS, Fig LM, Zasadny KR, Koral KF, DelRosario RB, Francis IR, Hanson CA, Normolle DP, Mudgett E, Liu CP, et al. (1992) Imaging, dosimetry, and radioimmunotherapy with iodine 131-labeled anti-CD37 antibody in B-cell lymphoma. J Clin Oncol 10:1696 – 711
Kaminski MS, Zasadny KR, Francis IR, Milik AW, Ross CW, Moon SD, Crawford SM, Burgess JM, Petry NA, Butchko GM, et al. (1993) Radioimmunotherapy of B-cell lymphoma with [131I]anti-B1 (anti-CD20) antibody. N Engl J Med 329:459 – 65
Kaminski MS, Zasadny KR, Francis IR, Fenner MC, Ross CW, Milik AW, Estes J, Tuck M, Regan D, Fisher S, Glenn SD, Wahl RL (1996) Iodine-131-anti-B1 radioimmunotherapy for B-cell lymphoma. J Clin Oncol 14:1974 – 81
Kaminski MS, Estes J, Zasadny KR, Francis IR, Ross CW, Tuck M, Regan D, Fisher S, Gutierrez J, Kroll S, Stagg R, Tidmarsh G, Wahl RL (2000) Radioimmunotherapy with iodine (131)I tositumomab for relapsed or refractory B-cell non-Hodgkin lymphoma: updated results and long-term follow-up of the University of Michigan experience. Blood 96:1259 – 66
Karacay H, Sharkey RM, Govindan SV, McBride WJ, Goldenberg DM, Hansen HJ, Griffiths GL (1997) Development of a streptavidin-anti-carcinoembryonic antigen antibody, radiolabeled biotin pretargeting method for radioimmunotherapy of colorectal cancer. Reagent development. Bioconjug Chem 8:585 – 94
Kemshead JT, Papanastassiou V, Coakham HB, Pizer BL (1992) Monoclonal antibodies in the treatment of central nervous system malignancies. Eur J Cancer 28:511 – 3
Khazaeli MB, Conry RM, LoBuglio AF (1994) Human immune response to monoclonal antibodies. J Immunother 15:42 – 52
Knox SJ, Goris ML, Trisler K, Negrin R, Davis T, Liles TM, Grillo-Lopez A, Chinn P, Varns C, Ning SC, Fowler S, Deb N, Becker M, Marquez C, Levy R (1996) Yttrium-90-labeled anti-CD20 monoclonal antibody therapy of recurrent B-cell lymphoma. Clin Cancer Res 2:457 – 70
Knox SJ, Goris ML, Tempero M, Weiden PL, Gentner L, Breitz H, Adams GP, Axworthy D, Gaffigan S, Bryan K, Fisher DR, Colcher D, Horak ID, Weiner LM (2000) Phase II trial of yttrium-90-DOTA-biotin pretargeted by NR-LU-10 antibody/streptavidin in patients with metastatic colon cancer. Clin Cancer Res 6:406 – 14
Kohler G, Milstein C (1975) Continuous cultures of fused cells secreting antibody of predefined specificity. Nature 256: 495 – 7
Konig T, Baum RP, Radtke M, Franke D (2002) HAMA-ELISA medac: a new assay for the quantitation of human anti-mouse antibodies. Clin Lab 48:207 – 10
Kraeber-Bodere F, Bardet S, Hoefnagel CA, Vieira MR, Vuillez JP, Murat A, Ferreira TC, Bardies M, Ferrer L, Resche I, Gautherot E, Rouvier E, Barbet J, Chatal JF (1999) Radioimmunotherapy in medullary thyroid cancer using bispecific antibody and iodine 131-labeled bivalent hapten: preliminary results of a phase I/II clinical trial. Clin Cancer Res 5:3190s–3198s
Kraeber-Bodere F, Faivre-Chauvet A, Ferrer L, Vuillez JP, Brard PY, Rousseau C, Resche I, Devillers A, Laffont S, Bardies M, Chang K, Sharkey RM, Goldenberg DM, Chatal JF, Barbet J (2003) Pharmacokinetics and dosimetry studies for optimization of anti-carcinoembryonic antigen x anti-hapten bispecific antibody-mediated pretargeting of iodine-131-labeled hapten in a phase I radioimmunotherapy trial. Clin Cancer Res 9:3973S–81S
Larson SM, Carrasquillo JA, Krohn KA, Brown JP, McGuffin RW, Ferens JM, Graham MM, Hill LD, Beaumier PL, Hellstrom KE, et al. (1983) Localization of 131I-labeled p97-specific Fab fragments in human melanoma as a basis for radiotherapy. J Clin Invest 72:2101 – 14
Larson SM, Carrasquillo JA, McGuffin RW, Krohn KA, Ferens JM, Hill LD, Beaumier PL, Reynolds JC, Hellstrom KE, Hellstrom I (1985) Use of I-131 labeled, murine Fab against a high molecular weight antigen of human melanoma: preliminary experience. Radiology 155:487 – 92
Le Doussal JM, Martin M, Gautherot E, Delaage M, Barbet J (1989) In vitro and in vivo targeting of radiolabeled monovalent and divalent haptens with dual specificity monoclonal antibody conjugates: enhanced divalent hapten affinity for cell-bound antibody conjugate. J Nucl Med 30:1358 – 66
Le Doussal JM, Chetanneau A, Gruaz-Guyon A, Martin M, Gautherot E, Lehur PA, Chatal JF, Delaage M, Barbet J (1993) Bispecific monoclonal antibody-mediated targeting of an indium-111-labeled DTPA dimer to primary colorectal tumors: pharmacokinetics, biodistribution, scintigraphy and immune response. J Nucl Med 34:1662 – 71
Lee J, Fenton BM, Koch CJ, Frelinger JG, Lord EM (1998) Interleukin 2 expression by tumor cells alters both the immune response and the tumor microenvironment. Cancer Res 58:1478 – 85
Leonard JP, Coleman CN, Kostakoglu K, et al. (1999). Fludarabine monophosphate followed by iodine 131I tositumomab for untreated low grade and follicular non-Hodgkin's lymphoma (NHL). Blood 94(Suppl):90a
Linden O, Tennvall J, Cavallin-Stahl E, Darte L, Garkavij M, Lindner KJ, Ljungberg M, Ohlsson T, Sjogreen K, Wingardh K, Strand SE (1999) Radioimmunotherapy using 131I-la-

beled anti-CD22 monoclonal antibody (LL2) in patients with previously treated B-cell lymphomas. Clin Cancer Res 5:3287s–3291s
Lipovsek D, Pluckthun A (2004) In-vitro protein evolution by ribosome display and mRNA display. J Immunol Methods 290:51 – 67
Liu SY, Eary JF, Petersdorf SH, Martin PJ, Maloney DG, Appelbaum FR, Matthews DC, Bush SA, Durack LD, Fisher DR, Gooley TA, Bernstein ID, Press OW (1998) Follow-up of relapsed B-cell lymphoma patients treated with iodine-131-labeled anti-CD20 antibody and autologous stem-cell rescue. J Clin Oncol 16:3270 – 8
Lonberg N, Taylor LD, Harding FA, Trounstine M, Higgins KM, Schramm SR, Kuo CC, Mashayekh R, Wymore K, McCabe JG, et al. (1994) Antigen-specific human antibodies from mice comprising four distinct genetic modifications. Nature 368:856 – 9
Magnani P, Paganelli G, Modorati G, Zito F, Songini C, Sudati F, Koch P, Maecke HR, Brancato R, Siccardi AG, Fazio F (1996) Quantitative comparison of direct antibody labeling and tumor pretargeting in uveal melanoma. J Nucl Med 37:967 – 71
Matthews DC, Appelbaum FR, Eary JF, Fisher DR, Durack LD, Hui TE, Martin PJ, Mitchell D, Press OW, Storb R, Bernstein ID (1999) Phase I study of (131)I-anti-CD45 antibody plus cyclophosphamide and total body irradiation for advanced acute leukemia and myelodysplastic syndrome. Blood 94:1237 – 47
McDevitt MR, Sgouros G, Finn RD, Humm JL, Jurcic JG, Larson SM, Scheinberg DA (1998) Radioimmunotherapy with alpha-emitting nuclides. Eur J Nucl Med 25:1341 – 51
McDevitt MR, Ma D, Lai LT, Simon J, Borchardt P, Frank RK, Wu K, Pellegrini V, Curcio MJ, Miederer M, Bander NH, Scheinberg DA (2001) Tumor therapy with targeted atomic nanogenerators. Science 294:1537 – 40
McQuarrie SA, Baum RP, Golberg L, Niesen A, Golberg K, Noujaim AA, McEwan AJ (1994) A pharmacokinetic comparison of murine and chimeric forms of the 99mTc-labelled 174H.64 monoclonal antibody. J Nucl Biol Med 38:140 – 4
Meredith RF, Khazaeli MB, Liu T, Plott G, Wheeler RH, Russell C, Colcher D, Schlom J, Shochat D, LoBuglio AF (1992) Dose fractionation of radiolabeled antibodies in patients with metastatic colon cancer. J Nucl Med 33:1648 – 53
Meredith RF, Khazaeli MB, Plott WE, et al. (1993) Effect of human immune response on repeat course of 131I-chimeric b72.3 antibody therapy. Antibody Immunoconj Radiopharm 6:39 – 46
Meredith RF, Bueschen AJ, Khazaeli MB, Plott WE, Grizzle WE, Wheeler RH, Schlom J, Russell CD, Liu T, LoBuglio AF (1994) Treatment of metastatic prostate carcinoma with radiolabeled antibody CC49. J Nucl Med 35:1017 – 22
Meredith RF, Khazaeli MB, Plott WE, Spencer SA, Wheeler RH, Brady LW, Woo DV, LoBuglio AF (1995) Initial clinical evaluation of iodine-125-labeled chimeric 17 – 1A for metastatic colon cancer. J Nucl Med 36:2229 – 33
Meredith RF, Partridge EE, Alvarez RD, Khazaeli MB, Plott G, Russell CD, Wheeler RH, Liu T, Grizzle WE, Schlom J, LoBuglio AF (1996) Intraperitoneal radioimmunotherapy of ovarian cancer with lutetium-177-CC49. J Nucl Med 37: 1491 – 6
Meredith RF, Khazaeli MB, Macey DJ, Grizzle WE, Mayo M, Schlom J, Russell CD, LoBuglio AF (1999) Phase II study of interferon-enhanced 131I-labeled high affinity CC49 monoclonal antibody therapy in patients with metastatic prostate cancer. Clin Cancer Res 5:3254s–3258s
Milenic DE (2000) Radioimmunotherapy: designer molecules to potentiate effective therapy. Semin Radiat Oncol 10: 139 – 55
Mittal BB, Zimmer MA, Sathiaseelan V, Benson AB, 3rd, Mittal RR, Dutta S, Rosen ST, Spies SM, Mettler JM, Groch MW (1996) Phase I/II trial of combined 131I anti-CEA monoclonal antibody and hyperthermia in patients with advanced colorectal adenocarcinoma. Cancer 78:1861 – 70
Mobus VJ, Baum RP, Bolle M, Kreienberg R, Noujaim AA, Schultes BC, Nicodemus CF (2003) Immune responses to murine monoclonal antibody-B43.13 correlate with prolonged survival of women with recurrent ovarian cancer. Am J Obstet Gynecol 189:28 – 36
Moro M, Pelagi M, Fulci G, Paganelli G, Dellabona P, Casorati G, Siccardi AG, Corti A (1997) Tumor cell targeting with antibody-avidin complexes and biotinylated tumor necrosis factor alpha. Cancer Res 57:1922 – 8
Nanus DM, Milowsky MI, Kostakoglu L, Smith-Jones PM, Vallabahajosula S, Goldsmith SJ, Bander NH (2003) Clinical use of monoclonal antibody HuJ591 therapy: targeting prostate specific membrane antigen. J Urol 170:S84 – 8; discussion S88 – 9
Nicholson S, Gooden CS, Hird V, Maraveyas A, Mason P, Lambert HE, Meares CF, Epenetos AA (1998) Radioimmunotherapy after chemotherapy compared to chemotherapy alone in the treatment of advanced ovarian cancer: a matched analysis. Oncol Rep 5:223 – 6
Noujaim AA, Schultes BC, Baum RP, Madiyalakan R (2001) Induction of CA125-specific B and T cell responses in patients injected with MAb-B43.13 – evidence for antibody-mediated antigen-processing and presentation of CA125 in vivo. Cancer Biother Radiopharm 16:187 – 203
O'Donnell RT, DeNardo GL, Kukis DL, Lamborn KR, Shen S, Yuan A, Goldstein DS, Mirick GR, DeNardo SJ (1999) 67Copper-2-iminothiolane-6-[p-(bromoacetamido)benzyl-TETA-Lym-1 for radioimmunotherapy of non-Hodgkin's lymphoma. Clin Cancer Res 5:3330s–3336s
O'Donnell RT, Shen S, Denardo SJ, Wun T, Kukis DL, Goldstein DS, Denardo GL (2000) A phase I study of 90Y-2IT-BAD-Lym-1 in patients with non-Hodgkin's lymphoma. Anticancer Res 20:3647 – 55
O'Donoghue JA, Bardies M, Wheldon TE (1995) Relationships between tumor size and curability for uniformly targeted therapy with beta-emitting radionuclides. J Nucl Med 36: 1902 – 9
Oliva JP, Pimentel G, Borron M, Peralta R, Ortiz R, Oliver B, Diaz N, Sanchez I, Vazquez AM, Baum RP (2001) [Pilot study with the monoclonal antibody IOR-C5 as a potential agent of radioimmunoscintigraphy in colorectal cancer]. Rev Esp Med Nucl 20:282 – 8
Oliva JP, Cruz T, Pimentel G, Quesada W, Ortiz R, Abreu M, Sanchez I, Diaz N, Baum RP (2004) [Radioimmunolocalization of head and neck tumors with a new monoclonal antibody against the EGF receptor. Preliminary results]. Rev Esp Med Nucl 23:273 – 8
Oltrogge JB, Baum RP, Lema KN, Donnerstag B, Hor G (1997) How to overcome the disturbing effects of human anti-mouse antibodies (HAMA) on in vitro assays. Int J Biol Markers 12:15 – 7
Order SE, Stillwagon GB, Klein JL, Leichner PK, Siegelman SS, Fishman EK, Ettinger DS, Haulk T, Kopher K, Finney K, et al. (1985) Iodine 131 antiferritin, a new treatment modality in hepatoma: a Radiation Therapy Oncology Group study. J Clin Oncol 3:1573 – 82
Order SE, Sleeper AM, Stillwagon GB, Klein JL, Leichner PK (1989) Current status of radioimmunoglobulins in the treatment of human malignancy. Oncology (Williston Park) 3:115 – 20; discussion 122, 129 – 30
Order S, Pajak T, Leibel S, Asbell S, Leichner P, Ettinger D, Stillwagon G, Herpst J, Haulk T, Kopher K, et al. (1991) A randomized prospective trial comparing full dose chemotherapy to 131I antiferritin: an RTOG study. Int J Radiat Oncol Biol Phys 20:953 – 63

Paganelli G, Pervez S, Siccardi AG, Rowlinson G, Deleide G, Chiolerio F, Malcovati M, Scassellati GA, Epenetos AA (1990) Intraperitoneal radio-localization of tumors pre-targeted by biotinylated monoclonal antibodies. Int J Cancer 45:1184 – 9

Paganelli G, Magnani P, Zito F, Villa E, Sudati F, Lopalco L, Rossetti C, Malcovati M, Chiolerio F, Seccamani E, et al. (1991) Three-step monoclonal antibody tumor targeting in carcinoembryonic antigen-positive patients. Cancer Res 51: 5960 – 6

Paganelli G, Grana C, Chinol M, Cremonesi M, De Cicco C, De Braud F, Robertson C, Zurrida S, Casadio C, Zoboli S, Siccardi AG, Veronesi U (1999) Antibody-guided three-step therapy for high grade glioma with yttrium-90 biotin. Eur J Nucl Med 26:348 – 57

Parker BA, Vassos AB, Halpern SE, Miller RA, Hupf H, Amox DG, Simoni JL, Starr RJ, Green MR, Royston I (1990) Radioimmunotherapy of human B-cell lymphoma with 90Y-conjugated antiidiotype monoclonal antibody. Cancer Res 50:1022s–1028s

Perkins AC, Baum RP (1988) Immunoscintigraphy and immunotherapy 1988. Report of the 3rd IRIST Meeting, Frankfurt/Main, March 1988. Int J Biol Markers 3:265 – 72

Press OW, Eary JF, Badger CC, Martin PJ, Appelbaum FR, Levy R, Miller R, Brown S, Nelp WB, Krohn KA, et al. (1989) Treatment of refractory non-Hodgkin's lymphoma with radiolabeled MB-1 (anti-CD37) antibody. J Clin Oncol 7:1027 – 38

Press OW, Eary JF, Appelbaum FR, Martin PJ, Badger CC, Nelp WB, Glenn S, Butchko G, Fisher D, Porter B, et al. (1993) Radiolabeled-antibody therapy of B-cell lymphoma with autologous bone marrow support. N Engl J Med 329:1219 – 24

Press OW, Eary JF, Appelbaum FR, Martin PJ, Nelp WB, Glenn S, Fisher DR, Porter B, Matthews DC, Gooley T, et al. (1995) Phase II trial of 131I-B1 (anti-CD20) antibody therapy with autologous stem cell transplantation for relapsed B cell lymphomas. Lancet 346:336 – 40

Press OW, Eary JF, Gooley T, Gopal AK, Liu S, Rajendran JG, Maloney DG, Petersdorf S, Bush SA, Durack LD, Martin PJ, Fisher DR, Wood B, Borrow JW, Porter B, Smith JP, Matthews DC, Appelbaum FR, Bernstein ID (2000) A phase I/II trial of iodine-131-tositumomab (anti-CD20), etoposide, cyclophosphamide, and autologous stem cell transplantation for relapsed B-cell lymphomas. Blood 96:2934 – 42

Press OW, Unger JM, Braziel RM, Maloney DG, Miller TP, LeBlanc M, Gaynor ER, Rivkin SE, Fisher RI (2003) A phase 2 trial of CHOP chemotherapy followed by tositumomab/iodine I 131 tositumomab for previously untreated follicular non-Hodgkin lymphoma: Southwest Oncology Group Protocol S9911. Blood 102:1606 – 12

Pressman D, Keighley G (1948) The zone of activities of antibodies as determined by the use of radioactive tracers; the zone of activity of nephrotoxic antikidney serum. J Immunol 59:141 – 146

Pressman D, Korngold L (1953) The in vivo localisation of anti-Wagner-osteogenic-sarcoma antibodies. Cancer 6:619 – 623

Pressman D, Day ED, Blau M (1957) The use of paired labeling in the determination of tumor-localizing antibodies. Cancer Res 17:845 – 850

Primus FJ, Goldenberg DM (1980) Immunological considerations in the use of goat antibodies to carcinoembryonic antigen for the radioimmunodetection of cancer. Cancer Res 40:2979 – 83

Riva P, Franceschi G, Riva N, Casi M, Santimaria M, Adamo M (2000) Role of nuclear medicine in the treatment of malignant gliomas: the locoregional radioimmunotherapy approach. Eur J Nucl Med 27:601 – 9

Ruiz-Cabello F, Cabrera T, Lopez-Nevot MA, Garrido F (2002) Impaired surface antigen presentation in tumors: implications for T cell-based immunotherapy. Semin Cancer Biol 12:15 – 24

Sabatino G, Chinol M, Paganelli G, Papi S, Chelli M, Leone G, Papini AM, De Luca A, Ginanneschi M (2003) A new biotin derivative-DOTA conjugate as a candidate for pretargeted diagnosis and therapy of tumors. J Med Chem 46:3170 – 3

Saga T, Weinstein JN, Jeong JM, Heya T, Lee JT, Le N, Paik CH, Sung C, Neumann RD (1994) Two-step targeting of experimental lung metastases with biotinylated antibody and radiolabeled streptavidin. Cancer Res 54:2160 – 5

Saga T, Neumann RD, Heya T, Sato J, Kinuya S, Le N, Paik CH, Weinstein JN (1995) Targeting cancer micrometastases with monoclonal antibodies: a binding-site barrier. Proc Natl Acad Sci U S A 92:8999 – 9003

Santimaria M, Moscatelli G, Viale GL, Giovannoni L, Neri G, Viti F, Leprini A, Borsi L, Castellani P, Zardi L, Neri D, Riva P (2003) Immunoscintigraphic detection of the ED-B domain of fibronectin, a marker of angiogenesis, in patients with cancer. Clin Cancer Res 9:571 – 9

Sausville EA, Longo DL (2005) Principles of cancer treatment: surgery, chemotherapy, and biologic therapy. In: Kasper DL, Braunwald E, Fauci AS, Hauser SL, Longo DL, Jameson JL (eds) Harrison's principles of internal medicine, 16th edn. McGraw Hill, New York, pp 464 – 482

Scheidhauer K, Schwarz K, von Schilling C, Schmidt B, Wolf I, Peschel C, Schwaiger M (2003) Pradiktion von Remission und ereignisfereim Uberleben nach Radioimmunotherapie (RIT) von Non-Hodgkin's-Lymphomen. In: "41 Jahrestagung DGN", p V152 (abstract)

Scheinberg DA, Straus DJ, Yeh SD, Divgi C, Garin-Chesa P, Graham M, Pentlow K, Coit D, Oettgen HF, Old LJ (1990) A phase I toxicity, pharmacology, and dosimetry trial of monoclonal antibody OKB7 in patients with non-Hodgkin's lymphoma: effects of tumor burden and antigen expression. J Clin Oncol 8:792 – 803

Schultes BC, Baum RP, Niesen A, Noujaim AA, Madiyalakan R (1998) Anti-idiotype induction therapy: anti-CA125 antibodies (Ab3) mediated tumor killing in patients treated with Ovarex mAb B43.13 (Ab1). Cancer Immunol Immunother 46:201 – 12

Seitz U, Neumaier B, Glatting G, Kotzerke J, Bunjes D, Reske SN (1999) Preparation and evaluation of the rhenium-188-labelled anti-NCA antigen monoclonal antibody BW 250/183 for radioimmunotherapy of leukaemia. Eur J Nucl Med 26:1265 – 73

Sgouros G, Ballangrud AM, Jurcic JG, McDevitt MR, Humm JL, Erdi YE, Mehta BM, Finn RD, Larson SM, Scheinberg DA (1999) Pharmacokinetics and dosimetry of an alpha-particle emitter labeled antibody: 213Bi-HuM195 (anti-CD33) in patients with leukemia. J Nucl Med 40:1935 – 46

Sharkey RM, Karacay H, Richel H, McBride WJ, Rossi EA, Chang K, Yeldell D, Griffiths GL, Hansen HJ, Goldenberg DM (2003) Optimizing bispecific antibody pretargeting for use in radioimmunotherapy. Clin Cancer Res 9:3897S–913S

Shen S, Forero A, LoBuglio AF, Breitz H, Khazaeli MB, Fisher DR, Wang W, Meredith RF (2005) Patient-specific dosimetry of pretargeted radioimmunotherapy using CC49 fusion protein in patients with gastrointestinal malignancies. J Nucl Med 46:642 – 51

Siegel JA (1998) Revised Nuclear Regulatory Commission regulations for release of patients administered radioactive materials: outpatient iodine-131 anti-B1 therapy. J Nucl Med 39:28S–33S

Smith-Jones PM, Solit DB, Akhurst T, Afroze F, Rosen N, Larson SM (2004) Imaging the pharmacodynamics of HER2 degradation in response to Hsp90 inhibitors. Nat Biotechnol 22:701 – 6

Stickney DR, Anderson LD, Slater JB, Ahlem CN, Kirk GA,

Schweighardt SA, Frincke JM (1991) Bifunctional antibody: a binary radiopharmaceutical delivery system for imaging colorectal carcinoma. Cancer Res 51:6650 – 5

Vose JM, Colcher D, Gobar L, Bierman PJ, Augustine S, Tempero M, Leichner P, Lynch JC, Goldenberg D, Armitage JO (2000a) Phase I/II trial of multiple dose 131Iodine-MAb LL2 (CD22) in patients with recurrent non-Hodgkin's lymphoma. Leuk Lymphoma 38:91 – 101

Vose JM, Wahl RL, Saleh M, Rohatiner AZ, Knox SJ, Radford JA, Zelenetz AD, Tidmarsh GF, Stagg RJ, Kaminski MS (2000b) Multicenter phase II study of iodine-131 tositumomab for chemotherapy-relapsed/refractory low-grade and transformed low-grade B-cell non-Hodgkin's lymphomas. J Clin Oncol 18:1316 – 23

Vose JM, Bierman PJ, Enke C, Hankins J, Bociek G, Lynch JC, Armitage JO (2005) Phase I trial of iodine-131 tositumomab with high-dose chemotherapy and autologous stem-cell transplantation for relapsed non-Hodgkin's lymphoma. J Clin Oncol 23:461 – 7

Vriesendorp HM, Quadri SM, Wyllie CT, Lai J, Borchardt PE, Harris L, Wucher R, Askew E, Schweichler L (1999) Fractionated radiolabeled antiferritin therapy for patients with recurrent Hodgkin's disease. Clin Cancer Res 5:3324s–3329s

Vuillez JP, Moro D, Brichon PY, Rouvier E, Brambilla E, Barbet J, Peltier P, Meyer P, Sarrazin R, Brambilla C (1997) Two-step immunoscintigraphy for non-small-cell lung cancer staging using a bispecific anti-CEA/anti-indium-DTPA antibody and an indium-111-labeled DTPA dimer. J Nucl Med 38:507 – 11

Vuillez JP, Kraeber-Bodere F, Moro D, Bardies M, Douillard JY, Gautherot E, Rouvier E, Barbet J, Garban F, Moreau P, Chatal JF (1999) Radioimmunotherapy of small cell lung carcinoma with the two-step method using a bispecific anti-carcinoembryonic antigen/anti-diethylenetriaminepentaacetic acid (DTPA) antibody and iodine-131 Di-DTPA hapten: results of a phase I/II trial. Clin Cancer Res 5:3259s–3267s

Wagner HN, Jr, Wiseman GA, Marcus CS, Nabi HA, Nagle CE, Fink-Bennett DM, Lamonica DM, Conti PS (2002) Administration guidelines for radioimmunotherapy of non-Hodgkin's lymphoma with (90)Y-labeled anti-CD20 monoclonal antibody. J Nucl Med 43:267 – 72

Wahl RL (2005) Tositumomab and (131) therapy in non-Hodgkins lymphoma. J Nucl Med 46(Suppl):128s–140s

Wahl RL, Zasadny KR, Estes J, et al., (2000) Single center experience with iodine 131I tositumomab radioimmunotherapy for previously untreated follicular lymphoma (FL). J Nucl Med 41(Suppl):79

Waldmann TA (2003) Immunotherapy: past, present and future. Nat Med 9:269 – 77

Weiden PL, Breitz HB, Press O, Appelbaum JW, Bryan JK, Gaffigan S, Stone D, Axworthy D, Fisher D, Reno J (2000) Pretargeted radioimmunotherapy (PRIT) for treatment of non-Hodgkin's lymphoma (NHL): initial phase I/II study results. Cancer Biother Radiopharm 15:15 – 29

Welt S, Divgi CR, Kemeny N, Finn RD, Scott AM, Graham M, Germain JS, Richards EC, Larson SM, Oettgen HF, et al. (1994) Phase I/II study of iodine 131-labeled monoclonal antibody A33 in patients with advanced colon cancer. J Clin Oncol 12:1561 – 71

Welt S, Scott AM, Divgi CR, Kemeny NE, Finn RD, Daghighian F, Germain JS, Richards EC, Larson SM, Old LJ (1996) Phase I/II study of iodine 125-labeled monoclonal antibody A33 in patients with advanced colon cancer. J Clin Oncol 14:1787 – 1797

Winter JN (2004) Combining yttrium 90-labeled ibritumomab tiuxetan with high-dose chemotherapy and stem cell support in patients with relapsed non-Hodgkin's lymphoma. Clin Lymphoma 5 Suppl 1:S22 – 6

Wiseman GA, Witzig TE (2005) Yttrium-90 (90Y) ibritumomab tiuxetan (Zevalin) induces long-term durable responses in patients with relapsed or refractory B-cell non-Hodgkin's lymphoma. Cancer Biother Radiopharm 20:185 – 188

Wiseman GA, White CA, Witzig TE, Gordon LI, Emmanouilides C, Raubitschek A, Janakiraman N, Gutheil J, Schilder RJ, Spies S, Silverman DH, Grillo-Lopez AJ (1999) Radioimmunotherapy of relapsed non-Hodgkin's lymphoma with zevalin, a 90Y-labeled anti-CD20 monoclonal antibody. Clin Cancer Res 5:3281s–3286s

Wiseman G, Gordon L, Leigh BR, et al. (2000) Safety and efficacy of the Zevalin radioimmunotherapy regimen are not diminished by extending the time interval between rituximab infusion and zevalin injection. Blood 96:251b

Wiseman GA, Gordon LI, Multani PS, Witzig TE, Spies S, Bartlett NL, Schilder RJ, Murray JL, Saleh M, Allen RS, Grillo-Lopez AJ, White CA (2002) Ibritumomab tiuxetan radioimmunotherapy for patients with relapsed or refractory non-Hodgkin lymphoma and mild thrombocytopenia: a phase II multicenter trial. Blood 99:4336 – 42

Witzig TE, White CA, Wiseman GA, Gordon LI, Emmanouilides C, Raubitschek A, Janakiraman N, Gutheil J, Schilder RJ, Spies S, Silverman DH, Parker E, Grillo-Lopez AJ (1999) Phase I/II trial of IDEC-Y2B8 radioimmunotherapy for treatment of relapsed or refractory CD20(+) B-cell non-Hodgkin's lymphoma. J Clin Oncol 17:3793 – 803

Witzig TE, Gordon LI, Wiseman GA, et al. (2000a) Reduced dose Zevalin is safe and effective in patients with relapsed or refractory, low grade, follicular or CD20+ transformed B cell non-Hodgkin's lymphoma (L/F/T NHL) and mild thrombocytopenia. Blood 96:728a

Witzig TE, White CA, Flinn IW, et al. (2000b) Zevalin radioimmunotherapy of rituximab refractory follicular non-Hodgkin's lymphoma. Blood 96:507a

Witzig TE, White CA, Gordon LI, et al. (2000c) Final results of a randomized controlled study of the Zevalin radioimmunotherapy regimen versus a standard course of rituximab immunotherapy for B-cell NHL. Blood 96(abstract):3591

Witzig TE, Flinn IW, Gordon LI, Emmanouilides C, Czuczman MS, Saleh MN, Cripe L, Wiseman G, Olejnik T, Multani PS, White CA (2002a) Treatment with ibritumomab tiuxetan radioimmunotherapy in patients with rituximab-refractory follicular non-Hodgkin's lymphoma. J Clin Oncol 20:3262 –9

Witzig TE, Gordon LI, Cabanillas F, Czuczman MS, Emmanouilides C, Joyce R, Pohlman BL, Bartlett NL, Wiseman GA, Padre N, Grillo-Lopez AJ, Multani P, White CA (2002b) Randomized controlled trial of yttrium-90-labeled ibritumomab tiuxetan radioimmunotherapy versus rituximab immunotherapy for patients with relapsed or refractory low-grade, follicular, or transformed B-cell non-Hodgkin's lymphoma. J Clin Oncol 20:2453 – 63

Wong JY, Shibata S, Williams LE, Kwok CS, Liu A, Chu DZ, Yamauchi DM, Wilczynski S, Ikle DN, Wu AM, Yazaki PJ, Shively JE, Doroshow JH, Raubitschek AA (2003) A Phase I trial of 90Y-anti-carcinoembryonic antigen chimeric T84.66 radioimmunotherapy with 5-fluorouracil in patients with metastatic colorectal cancer. Clin Cancer Res 9:5842 – 52

Wong JY, Somlo G, Odom-Maryon T, Williams LE, Liu A, Yamauchi D, Wu AM, Yazaki P, Wilczynski S, Shively JE, Forman S, Doroshow JH, Raubitschek AA (1999) Initial clinical experience evaluating Yttrium-90-chimeric T84.66 anticarcinoembryonic antigen antibody and autologous hematopoietic stem cell support in patients with carcinoembryonic antigen-producing metastatic breast cancer. Clin Cancer Res 5:3224s–3231s

Wu AM, Senter PD (2005) Arming antibodies: prospects and challenges for immunoconjugates. Nat Biotechnol 23:1137 – 1146

Yao Z, Zhang M, Kobayashi H, Sakahara H, Nakada H, Yamashina I, Konishi J (1995) Improved targeting of radiolabeled streptavidin in tumors pretargeted with biotinylated monoclonal antibodies through an avidin chase. J Nucl Med 36:837 – 41

Ychou M, Pelegrin A, Faurous P, Robert B, Saccavini JC, Guerreau D, Rossi JF, Fabbro M, Buchegger F, Mach JP, Artus JC (1998) Phase-I/II radio-immunotherapy study with iodine-131-labeled anti-CEA monoclonal antibody F6 F(ab')2 in patients with non-resectable liver metastases from colorectal cancer. Int J Cancer 75:615 – 9

Zalutsky MR (2006) Potential of immuno-positron emission tomography for tumor imaging and immunotherapy planning. Clin Cancer Res 12:1958 – 60

Zalutsky MR, Vaidyanathan G (2000) Astatine-211-labeled radiotherapeutics: an emerging approach to targeted alpha-particle radiotherapy. Curr Pharm Des 6:1433 – 55

Zalutsky MR, Moseley RP, Benjamin JC, Colapinto EV, Fuller GN, Coakham HP, Bigner DD (1990) Monoclonal antibody and F(ab')2 fragment delivery to tumor in patients with glioma: comparison of intracarotid and intravenous administration. Cancer Res 50:4105 – 10

Zelenetz AD (1999) Radioimmunotherapy for lymphoma. Curr Opin Oncol 11:375 – 80

Zelenetz AD, Saleh M, Vose J, Younes A, Kaminski MS (2002) Patients with transformed low grade follicular lymphoma attain durable responses following outpatient radioimmunotherapy with tositumomab and iodine (131I) tositumomab (Bexxar). Blood 100:357a

Intra-arterial Therapy of Liver Tumours 27

E. Garin, P. Bourguet

27.1 Introduction

Hepatocellular carcinoma (HCC) is one of the most frequent cancers worldwide; in fact, it is ranked fifth in importance with approximately 437,000 new cases per annum (Bosch et al. 1999). Its incidence is increasing in many countries (Trinchet and Beaugrand 1999; Taylor-Robinson et al. 1997; Deuffic and Poynard 1998; El-Serag and Mason 1999). The first recognized risk factor is the presence of a cirrhosis that may be associated with various possible aetiologies (B and C viral infections, alcohol, haemochromatosis). This increased incidence is related to the better health care of patients suffering from cirrhosis, but also to a strong increase in chronic hepatitis C (Trinchet and Beaugrand 1999; Taylor-Robinson et al. 1997; Deuffic and Poynard 1998; Okuda 2000). Indeed, in France, approximately 500,000 people would appear to be infected by the hepatitis C virus (Trinchet and Beaugrand 1999). It is estimated that about 66 % present with chronic hepatitis and that 20 % will develop cirrhosis in 10 – 20 years in the absence of treatment. In France, it is estimated that the mortality linked to HCC occurring with hepatitis C virus cirrhosis will increase by 150 % in men and 200 % in women from now until 2020 (Deuffic et al. 1999). We may thus consider that, in the years to come, HCC will pose a problem for public health.

In the absence of cirrhosis, some histological evidence is necessary to establish the diagnosis of HCC. On the other hand, during the conference of EASL-Barcelona 2000 (European Association for the Study of the Liver), it was established that, when there is an underlying cirrhosis, the diagnosis of HCC could be done in the absence of histological evidence provided the following criteria are combined: description by two different imagery techniques of a focused lesion larger than 2 cm exhibiting an arterial hypervascularization or description of a focused lesion larger than 2 cm with an arterial hypervascularization (only one imagery technique) associated with a rise in AFP (Bruix et al. 2001).

The assessment of extension usually carried out is summarized by an ultrasound scan or an abdominal CT (Bruix et al. 2001), the risk of remote metastases being regarded as relatively low. At the time of the initial diagnosis, between 6 % and 19 % of the patients risk being faced with a metastatic form (Llovet et al. 1999; Chlebowski et al. 1984; Calvet et al. 1990). On the other hand, there is a higher risk of seeing the development of metastases during later evolution, involving 12 – 33 % of patients according to the reported series (Llovet et al. 1999; Arii et al. 2001; Andrews et al. 1994; Badvie 2000). The metastatic sites most frequently found, in order of decreasing frequency, are the lungs, the lymph nodes, the peritoneum and the bones (Arii et al. 2001; Badvie 2000).

Even for cases of complete spontaneous regression which have been described (Kaczynski et al. 1998), prognosis for this cancer is extremely poor. Indeed, a curative treatment (liver transplantation, surgical resection, ethanol injection or radiofrequency tissue ablation) can only be carried out in less than 25 % of cases, either because of operational contraindications (advanced cirrhosis in particular), the presence of locally advanced forms (multifocal lesions, invasion of the portal vein) or, more rarely, metastatic dissemination (Badvie 2000). Taking all patients together, the rates of spontaneous survival at 1, 2 and 3 years were 54 %, 40 % and 28 %, respectively, in the study of Llovet et al. (1999). The respective survival rates were 80 %, 65 % and 50 % for patients who did not present with any poor prognostic factors and 29 %, 16 % and 8 % for the patients who had poor prognostic factors (Llovet et al. 1999). Median rates of survival of only 4 – 12 weeks are even described in forms with the worst prognosis (The CLIP Investigators 1998; Levi et al. 2002).

The only really effective treatments are local surgery (resection, transplantation) and ablative techniques (alcoholization, cryotherapy, radiofrequency). However, such approaches can only be proposed for a small number of patients (15 – 25 %) (Badvie 2000; De Sanctis et al. 1998) even if the proportion tends to rise because of a rigorous monitoring of the population at risk and the tracking of earlier forms (Arii et al. 2001; Lau 2002). The rates of survival with these three therapeutic methods (resection, transplantation, local ablative tech-

nique) are similar at 30 – 50 % survival at 5 years (Bruix et al. 2001; Badvie 2000; Lau 2002; Otto et al. 1998). In the forms having a better prognosis, survival at 5 years can even reach 70 – 80 % (Bruix et al. 2001; Arii et al. 2001).

For patients who are not candidates for a radical treatment and who do not present with an excessively advanced form, a palliative treatment can be proposed mainly consisting of chemoembolization or intra-arterial metabolic radiotherapy. Indeed, external radiotherapy is of little use because of the high risk of hepatic toxicity. Classically, systemic chemotherapy leads only to a low level of response without any improvement in survival (Bruix et al. 2001; Badvie 2000; Lau 2002; Leung 2001). Even if recent protocols of polychemotherapy are able to obtain a high rate of response of 26 %, this is at the expense of a major haematological toxicity (Leung 1999). Moreover, intra-arterial chemotherapy has not proved to be reliable (Leung 2001). Other therapeutic approaches are beginning to be evaluated. The use of anti-hormonal agents (tamoxifen) has yielded contradictory results (Lau 2002; Leung 2001), as well as the use of octreotide (Kouroumalis et al. 1998; Yuen et al. 2002). At present, the two most used therapeutic approaches remain arterial chemoembolization with lipiodol and metabolic radiation therapy using arterial administration. This concept is based on the occurrence of a double vascularization of the liver (hepatic artery and portal vein) and on the fact that HCC vascularization arises mainly from the hepatic artery, whereas 80 % of the vascularization of the non-tumoral liver takes place via the portal vein.

However, the effectiveness of chemoembolization remains a matter of debate: various non-randomized retrospective studies appear to have demonstrated a benefit in terms of survival when using chemoembolization with lipiodol (Bronowiki et al. 1994; Stefanini et al. 1995). Three controlled randomized studies aimed at showing the effectiveness of chemoembolization with lipiodol versus therapeutic abstention have appeared to yield negative results (Pelletier et al. 1990; Groupe d'étude et de traitement du carcinome hépatocellulaire 1995; Madden et al. 1993). In the study by Pelletier on 42 patients, the rates of survival at 6 months and 1 year were, respectively, 33 % and 24 % for the patients treated by chemoembolization, against 52 % and 31 % in the control group (Pelletier et al. 1990). In a second study relating to 96 patients (Groupe d'étude et de traitement du carcinome hépatocellulaire 1995) there was no significant difference in survival between the chemoembolization group ($n = 50$) and the control group ($n = 46$). On the other hand, chemoembolization was responsible for a significant number of episodes of hepatocellular insufficiency (47 episodes among 30 patients). In a third study that included 50 patients (Madden et al. 1993) the median survival was 48 days in the treated group ($n = 50$) as against 51 days in the untreated group ($n = 50$). Finally, two recent randomized studies on chemoembolization yielded positive results, but at the expense of a considerable toxicity (Llovet et al. 2002; Lo et al. 2002). In the study of Llovet, where 112 patients were randomized between simple embolization ($n = 37$), chemoembolization ($n = 40$) or monitoring ($n = 30$), the probabilities of survival at 1 and 2 years were, respectively, 75 % and 50 % (embolization), 83 % and 63 % (chemoembolization) and 63 % and 27 % (monitoring), $p = 0.009$ (Llovet et al. 2002). We should nevertheless point out that, in the chemoembolization group with the better prognosis, the patients had a significantly less elevated level of bilirubinaemia (a good prognosis factor found in the classification of Okuda and Clip) than in the control group (Llovet et al. 2002). In addition, there were major complications related to the chemoembolization: 1 death and some severe complications for 11 patients (2 cases of cholecystitis, 2 cases of leucopenia, 1 hepatic infarction, 1 peritonitis, 1 bacteraemia, 1 alopecia, 1 allergic dermatitis, 1 septic shock, 1 ischaemic cholecystitis) (Llovet et al. 2002). In the study of Lo et al., the rates of survival at 1, 2 and 3 years were 57 %, 31 % and 26 %, respectively, for the chemoembolization group ($n = 40$) versus 32 %, 11 % and 3 % for the monitored group ($n = 40$), $p = 0.002$ (Lo et al. 2002). Comparing the treatments in the chemoembolization group and the control group, the complications leading to death were as follows: hepatocellular insufficiency, 5 versus 1; digestive haemorrhage, 4 versus 0; tumoral rupture, 2 versus 0; sepsis, 0 versus 2 (Lo et al. 2002).

The effective absence of a treatment that is well tolerated for patients having an inoperable HCC has led to the development of arterial metabolic radiotherapy.

Thus, the intra-arterial injection of certain therapeutic agents makes it possible to obtain a high "tumour to non-tumoral liver" ratio. This allows the delivery of a high dose to the tumour, while preserving the healthy liver to a maximum extent.

The most commonly used radioactive agent is iodine-131 labelled lipiodol. Other agents are in course of evaluation or development, including microspheres labelled with yttrium-90, certain radiolabelled antibodies and, finally, lipiodol labelled with rhenium-188.

27.2 Iodine-131 Labelled Lipiodol

27.2.1 Composition and Fixation Mechanism

Ethiodol or lipiodol (Lipiodol, Guerbet, France) is a secondarily iodized oil (38% by weight) extracted from poppy seeds. It is made up of the polyunsaturated mono, di- and tri-iodized esters of linoleic acid (73%), oleic acid (14%), palmitic acid (9%) and stearic acid (3%), and was used initially in the diagnosis of HCC (Nakakuma et al. 1985, Yumoto et al. 1985). In fact, by administering lipiodol as a contrast agent by selective catheterization of the hepatic artery followed by scintiscanning, it is possible to detect HCC or satellite tumours of known HCC that cannot be located by conventional examinations (arteriography, scanner, ultrasound) (Yumoto et al. 1985).

Iodine-131 is a radioelement that possesses some interesting properties for therapeutic use: its β emission (maximum at 606 keV) and γ emission (main peak at 365 keV) allows us to carry out an external detection. The γ-ray emission is a disadvantage since it leads to irradiation of the surrounding personnel. The 8 days half-life of this radioelement is also a drawback. These two properties impose a hospitalization of patients treated by ^{131}I-lipiodol in a shielded area for at least 8 days. The labelling of the lipiodol by iodine-131 is carried out by a simple isotopic exchange reaction.

^{131}I-lipiodol is marketed under the tradename of Lipiocis (Schering CIS Biointernational, Berlin, Germany).

Certain factors have been reported to explain the tumoral retention of the lipiodol: accumulation of lipiodol in the peritumoral sinusoids by a mechanism of embolization (Miller et al. 1987; Kan 1996; Kan et al. 1989; Nakakuma et al. 1983), possible modification of the membrane potential of the tumoral vessels (Kobayashi et al. 1987), fixation of the cancerous cells onto the membrane (Park et al. 1990; Chou et al. 1995), penetration into the cancerous cells (Park et al. 1990; Chou et al. 1994, 1995; Iwai et al. 1984) and, finally, a slower elimination of the lipiodol from the tumours compared with healthy hepatic tissues due to a weakly developed tumoral lymphatic system (Kan 1996; Iwai et al. 1984). The idea of using this agent as a therapeutic vector arose from the observation of a prolonged retention of lipiodol on the HCC several months after intra-arterial injection via the hepatic artery (Konno et al. 1984).

27.2.2 Biodistribution of ^{131}I-Lipiodol (Lipiocis)

The biodistribution of ^{131}I-lipiodol was studied on several series of patients (Raoul et al. 1986, 1988, 1993; Nakajo et al. 1988; Hind et al. 1992) using low doses of radiolabelled lipiodol (2–70 MBq), the largest series comprising 47 and 52 subjects (Raoul et al. 1988, 1993).

Injected by intra-arterial administration, after arteriography, ^{131}I-lipiodol is fixed preferentially at the level of the liver, the tumours, and the lungs (cf. Fig. 27.1a–f).

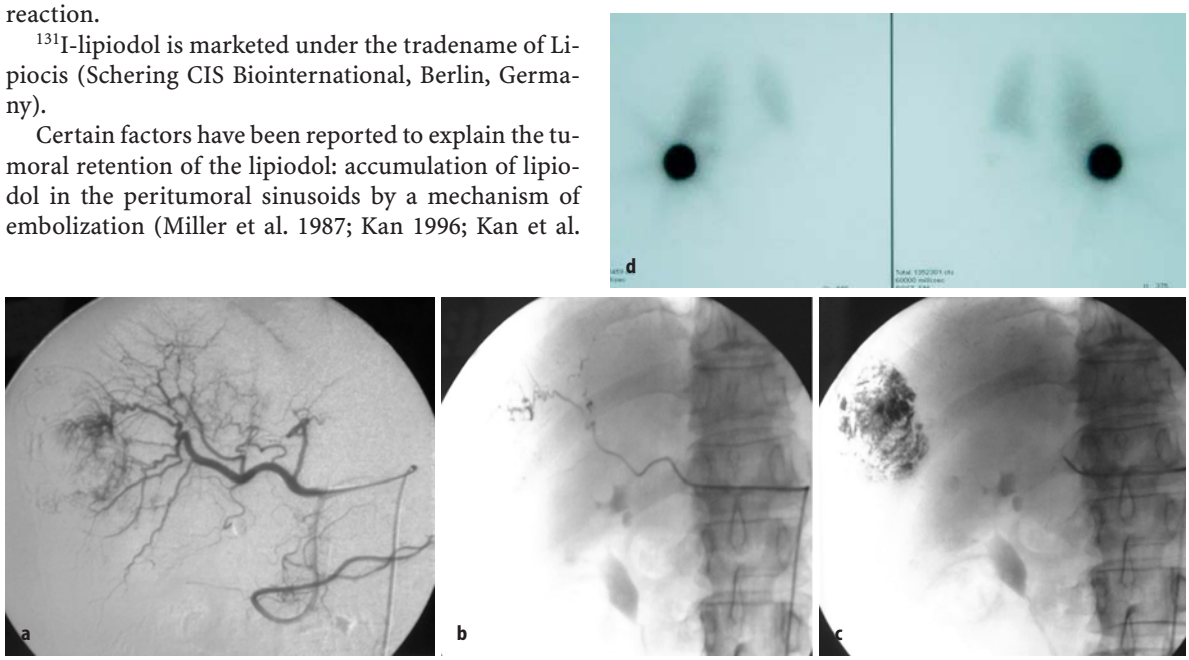

Fig. 27.1. Sixty-five-year-old patient presenting with a bifocal HCC, showing a 54×42 mm nodule at the junction of segments V and VI, and a 31×30 mm nodule in segment IV. **a** Arteriography carried out before the first injection of ^{131}I-lipiodol: intense hypervascularization of the nodule at the junction of segments V and VI. Note the presence of a reflux in the gastroduodenal artery during the injection of contrast product as a bolus. **b** Injection of ^{131}I-lipiodol via the common hepatic artery by controlling the speed of injection to avoid reflux in the gastroduodenal artery. **c** At the end of the injection of ^{131}I-lipiodol: strong retention in the nodule at the junction of segments V and VI

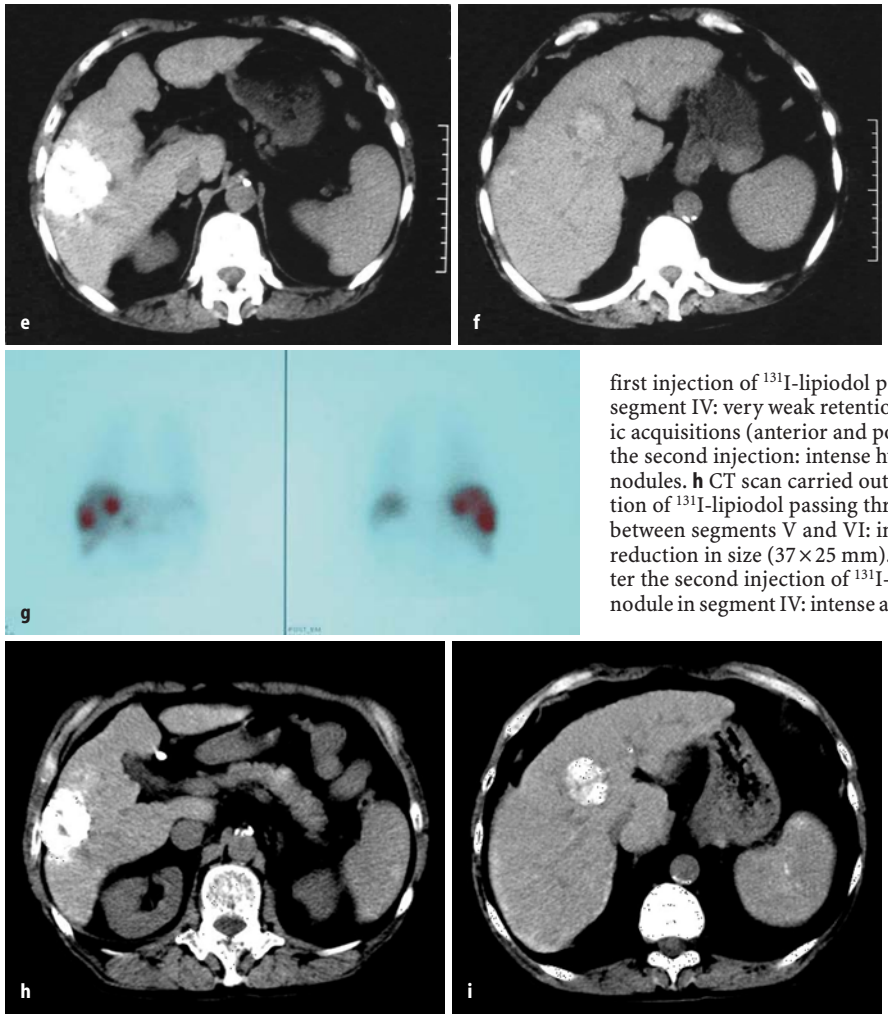

Fig. 27.1. d Scintigraphic acquisitions (anterior and posterior views) carried out 8 days after the first injection: intense hyperfixation in the nodule at the junction of segments V and VI. **e** CT scan carried out 8 days after the first injection of ^{131}I-lipiodol, passing through the nodule at the junction of segments V and VI: intense and homogeneous retention of ^{131}I-lipiodol. **f** CT scan carried out 8 days after the first injection of ^{131}I-lipiodol passing through the nodule in segment IV: very weak retention of ^{131}I-lipiodol. **g** Scintigraphic acquisitions (anterior and posterior) carried out 8 days after the second injection: intense hyperfixation at the level of both nodules. **h** CT scan carried out 8 days after the second injection of ^{131}I-lipiodol passing through the nodule at the junction between segments V and VI: intense retention of ^{131}I-lipiodol, reduction in size (37 × 25 mm). **i** CT scan carried out 8 days after the second injection of ^{131}I-lipiodol passing through the nodule in segment IV: intense and heterogenous retention of ^{131}I-lipiodol, with size unchanged. Comments: During the first treatment, vascular flow is deviated towards the larger tumour, and the smaller tumour of segment IV appears to accumulate very little ^{131}I-lipiodol. During the second treatment, the partial response of the larger tumour leads to a redistribution of the vascularization towards the smaller tumour, which thus becomes accessible to the treatment (marked accumulation of ^{131}I-lipiodol)

The "tumour to non-tumoral liver" ratio is high when measured on planar imaging, yielding values of 4.3 ± 2.6 and 4.2 ± 2.3 (Raoul et al. 1988, 1993), and can reach very high values, 15 – 20, when it is measured in SPECT mode (Yoo et al. 1994; Park et al. 1987). This ratio increases with time (Raoul et al. 1988; Nakajo et al. 1988; Hind et al. 1992; Yoo et al. 1994; Madsen et al. 1988; Yumoto et al. 1992). The retention of ^{131}I-lipiodol, which can be assessed by tomodensitometric examination, depends on the size of the tumour and decreases with increasing size. Indeed, 88 % of the HCCs smaller than 5 cm exhibit a high retention (of type 3 or 4 according to the criteria of Maki et al. 1985), whereas 74 % of the HCCs larger than 10 cm exhibit a weak retention of less than 50 % (of type 1 or 2 according to the criteria of Maki) (Raoul et al. 1993). This point has been confirmed by other studies (Brans et al. 2003).

The percentage of the activity of ^{131}I-lipiodol present in the liver varies between 70 % and 90 % (Raoul et al. 1986; Hind et al. 1992; Madsen et al. 1988) and decreases with time (Raoul et al. 1986; Nakajo et al. 1986) [44, 46]. In parallel, pulmonary uptake increases, testifying to a secondary release of the lipiodol from the liver towards the lungs (Raoul et al. 1986; Nakajo et al. 1986), most probably linked to a fragmentation of the lipidic droplets (Kan 1996; Kan et al. 1989; Kobayashi et al. 1987). The activity of ^{131}I-lipiodol that can be located in the lungs ranges between 10 % and 43 % (Raoul et al. 1988) and increases with time (Roul et al. 1986; Nakajo et al. 1986; Yumoto et al. 1992).

Otherwise, there is a significant uptake in the thyroid, particularly with the administration of therapeutic doses (Risse et al. 2000; Toubeau et al. 2001; Bacher et al. 2002; Monsieur et al. 2003). No significant fixation of ^{131}I-lipiodol has been detected at the level of other organs.

^{131}I-lipiodol is eliminated mainly through the urinary tract, amounting to 30 – 50 % of the injected activity at day 8, but also to a small extent (< 3 %) by way of the faeces at day 5 (Raoul et al. 1988). The effective half-life of ^{131}I-lipiodol found in these various studies is around 4 – 6 days (Raoul et al. 1988, 1993; Nakajo et al.

1988) for the whole body. In one study, the half-life is 5.2 days for the whole body, 4.3 days for the liver, 5.8 days for the tumour, 4.5 days for the lungs and 6 days for the thyroid (Monsieur et al. 2003).

27.2.3 Therapeutic Use of ^{131}I-Labelled Lipiodol: Feasibility Studies

Many feasibility studies have been carried out, mainly within the framework of the treatment of inoperable HCC (Bacher et al. 2002; Bhattacharya et al. 1995; Brans et al. 2001, 2003; Bretagne et al. 1988; De Baere et al. 1999; Kajiya et al. 1993; Kobayashi et al. 1986; Leung et al. 1994; Lui et al. 1990; Madsen et al. 1998; Maini et al. 1996; Monsieur et al. 2003; Park et al. 1987; Partenski et al. 2000; Raoul et al. 1992; Rindani et al. 2002; Risse et al. 2000; Toubeau et al. 2001; Yoo et al. 1989, 1991, 1994; Yumoto et al. 1992). A certain number of points have thus been raised.

27.2.3.1 Route of Administration

Two types of administration can be carried out: selective injection into the hepatic artery itself, downstream from the start of the gastroduodenal artery (Bretagne et al. 1988; De Baere et al. 1999; Leung et al. 1994; Raoul et al. 1992; Risse et al. 2000), or hyperselective injection at the level of the hepatic artery (right- or left-hand side), at a segmental or even a sub-segmental artery (Brans et al. 2001; Kajiya et al. 1993; Kobayashi et al. 1986; Maini et al. 1996; Yoo et al. 1989, 1991, 1994; Yumoto et al. 1992).

For a given injected activity, hyperselective administration allows an increase in the dose of ^{131}I-lipiodol delivered to the tumour, thus increasing the dose delivered to the tumour (Maini et al. 1996; Yoo et al. 1994; Yumoto et al. 1992) while reducing the dose delivered to the non-tumoral liver and the lungs (Yoo et al. 1994). However, this assumption was contradicted in a recent study that compared the activity found in the tumours (expressed as a percentage activity injected per millilitre of tumour) among 14 patients having a selective injection and 10 patients having a hyperselective injection (Brans et al. 2003). This study did not reveal any significant difference between the "hyperselective injection" group (0.72 ± 0.65 %/ml) and the "selective injection" group (0.43 ± 0.51 %/ml). Nevertheless, we should consider these results with extreme prudence because tumoral volume is much higher in the "hyperselective injection" group (on average, 46.5 ml as against 6.52 ml for the "selective injection" group), while it appears established that the tumoral uptake of lipiodol becomes weaker as tumoral volume increases (Raoul et al. 1993). In addition, the non-irradiation of the presumably healthy hepatic parenchyma involves some major disadvantages. On the one hand, it deprives the patient of prophylactic irradiation that has proven effective in reducing the risk of recurrence (Lau et al. 1999), while, on the other hand, this type of injection can lead to a dramatic acceleration of the tumoral progression for a non-irradiated pre-existing lesion. This phenomenon was initially described in one reported case (Raoul et al. 1996), and was found in another study in one patient of a group of ten with hyperselective injection (Brans et al. 2003).

27.2.3.2 Dosimetry

The activity to be injected into a patient with the aim of performing metabolic radiotherapy (as any type of radiotherapy) must take account of two factors: (1) the dose needed to be delivered to the tumour in order to obtain a therapeutic effect and (2) the dose not to be exceeded at the level of the critical organs. The generally accepted tumoricidal dose for HCC is 120 Gy. The two critical organs concerned in the use of ^{131}I-lipiodol are the liver and the lungs. In the case of external radiotherapy, the limiting doses not to be exceeded for these organs are known and depend on fractionation. These doses correspond to 30 Gy for a total irradiation of the liver (Ingold et al. 1965) and 7 – 25 Gy for the lungs as a function of fractionation (Margolis and Phillips 1969). In the case of metabolic radiotherapy, the critical doses for these two organs are not known with precision but would appear to be much higher than with external radiotherapy. With the use of metabolic radiotherapy, the critical doses for these two organs are not known with precision but seem much higher than with external radiotherapy, i.e., 80 – 150 Gy for the liver (Andrews et al. 1994; Gray et al. 1990) and 30 – 50 Gy for the lungs (Leung et al. 1995).

The activity of ^{131}I-lipiodol administered by injection is very variable from one study to another and can reach 4.44 GBq (Park et al. 1987). Indeed, according to different studies, the activity injected is calculated according to the dosimetry hoped for at the level of the tumour (Yoo et al. 1991, 1994), by setting a dose not to be exceeded for the critical organs (Kajiya et al. 1993; Preketes et al. 1996; Raoul et al. 1992), or even, in certain cases, by using standard doses of 2.22 GBq (Raoul et al. 1997, 2003).

27.2.3.3 Therapeutic Results from ^{131}I-Lipiodol

According to different studies, the rates of survival at 6 months, 1 year and 2 years after treatment vary, respectively, from 33 % to 60 % (Raoul et al. 1992; De Baere et al. 1999), 6 % to 53 % (De Baere et al. 1999; Rindani et al. 2002) and 0 % to 53 % (Raoul et al. 1992; Rindani et al. 2002).

A partial or incomplete response rate (defined by a reduction of more than 50% in the tumour size or amount of alpha-fetoproteins) of 12–71% is found according to the different studies (Kobayashi et al. 1986; Yoo et al. 1991). Taking into account the whole set of studies carried out, the average partial response rate is probably around 30–40%. Some histologically documented cases of complete response have been described (Kobayashi et al. 1986; Bretagne et al. 1988). A study targeted on ^{131}I-lipiodol used as neoadjuvant treatment before transplantation or resection found a high rate of complete histological responses: 8 cases out of 34 patients (Raoul et al. 2003).

The response rates depend on the morphological type of the HCC (nodular, multinodular or infiltrating) as well as its size. It is highest for the nodular forms and lowest for the infiltrating forms (Park et al. 1987; Yoo et al. 1989). Yoo et al. estimated the response rate at 73.7% for nodular forms, 44.4% for multinodular forms and 13% for infiltrating forms (Yoo et al. 1989). The response rate increases if the size of the HCC decreases: in one study, it is estimated at 80% for a size equal to 5 cm or less, 60% for a size ranging between 5 and 8 cm, 50% for a size ranging between 8 and 10 cm and 21.9% for a size of 10 cm or more (Yoo et al. 1989).

For certain patients (in particular, patients with large or multiple tumours), several injections may be necessary to obtain an effective response, either for achieving a satisfactory cumulative dose in a nodule or for treating initially poorly vascularized lesions. In fact, in multinodular forms an initial vascular robbery by a large hypervascularized lesion that becomes hypovascularized as it is responding to the treatment may occur (cf Fig. 27.1G–I).

In addition, several studies have reported a major antalgic effect of ^{131}I-lipiodol for patients presenting with pains related to their HCC (Battacharya et al. 1995; Raoul et al. 1992; Rindani et al. 2002).

27.2.3.4 Side Effects

Rare side effects can occur that are potentially serious: major asthenia, prolonged fever, digestive haemorrhage and severe hepatic insufficiency (4 deaths in a study comprising 26; Battacharya et al. 1995). Finally, pneumopathy has also been mentioned, whose immunoallergic origin (Raoul et al. 1992, 1994) or post-radiation origin (Preketes et al. 1996) remains a matter of debate. The frequency of these pneumopathies is difficult to evaluate because, out of the 500 treatments published, pulmonary complications were reported in 11 patients (Brans et al. 2003; Preketes et al. 1996; Raoul et al. 1992; Rindani et al. 2002), including 8 in the same series (Preketes et al. 1996). Moreover, other types of pulmonary pathology can occur in this category of patient (carcinomatous lymphangitis and infectious pneumopathies) (Maublant et al. 2001). These pneumopathies occur very gradually several weeks after the injection and lead to death in approximately 50% of cases in spite of a treatment associating antibiotherapy with corticoids. There is currently no predictive factor able to determine in principle if a patient is likely to develop a pneumopathy after an injection of ^{131}I-lipiodol.

Minor and frequently encountered side effects include asthenia, anorexia, a rise in temperature and fugitive hepatalgies. A transitory disturbance of the hepatic balance and a moderate and reversible leucopenia can also be found.

27.2.4 Indication of Treatment by ^{131}I-Lipiodol

The three most classic indications are the palliative treatment of HCC with portal thrombosis, palliative treatment of HCC without portal thrombosis and adjuvant treatment after surgery.

The first indication validated by a randomized study was the treatment of HCC with portal thrombosis (Raoul et al. 1994). In this study 27 patients with HCC and portal thrombosis were randomized between treatment by ^{131}I-lipiodol, using an activity of 2.2 GBq ($n=14$) and medical supportive therapy (control group, $n=13$). The intra-arterial injection of ^{131}I-lipiodol was repeated if possible at 2, 5, 8, and 12 months. The effectiveness was evaluated on rate of survival, evolution of the AFP level and angiography. This study indicated an important and significant improvement of survival ($p<0.01$) for the patients treated by ^{131}I-lipiodol, the survival rate (IC 95%) at 3, 6, and 9 months being 71% (48–95%), 48% (12–55%), 7% (1–31%) for the group treated versus 10% (1–33%), 0% and 0% for the group control group. Median survival was 28 weeks for the patients treated by ^{131}I-lipiodol and 8 weeks for the reference group, respectively.

The second possible indication is inoperable HCC, which is the most frequent clinical situation. The majority of feasibility studies have related to this indication. A randomized study has compared ^{131}I-lipiodol and chemoembolization in this indication (Raoul et al. 1997). This study showed the two therapeutic methods have the same effectiveness, but there is a better tolerance for the treatment with ^{131}I-lipiodol. The patients presenting with unresectable and non-transplantable HCC were randomized between groups treated by ^{131}I-lipiodol (2.2 GBq, $n=73$) or by chemoembolization (70 mg cisplatin; $n=69$). The treatments were repeated if possible at 2, 5, 8, 12 and 18 months. The tumoral response was evaluated on tumour size, the AFP assay and the survival rate, the latter parameter being the principal criterion of judgement. A total of 129 patients (including 65 in the ^{131}I-lipiodol group and 64 in the

chemoembolization group) could be evaluated, but 13 patients were excluded, mainly due to the presence of a portal thrombosis. No evidence was found for any significant difference in the survival rate. Indeed, the survival rates of the ^{131}I-lipiodol versus the chemoembolization groups were, respectively, 69 % versus 66 % at 6 months, 38 % versus 42 % at 1 year, 22 % versus 22 % at 2 years, 14 % versus 3 % at 3 years, and finally 10 % versus 0 % at 4 years. Moreover, this study failed to reveal any significant difference in the response rates (there were 1 and 0 complete responses compared with 15 and 16 partial responses in the ^{131}I-lipiodol and chemoembolization groups, respectively). The tolerance was significantly better for the ^{131}I-lipiodol group than for the chemo-embolization group. In fact, there were 5 severe side effects observed in the ^{131}I-lipiodol group (1 pneumopathy, 1 hepatic insufficiency, 1 extreme asthenia, 1 high and prolonged temperature rise, 1 psychiatric decompensation) and 0 deaths ascribable to the treatment. By comparison, the chemo-embolization group showed 29 severe side effects (7 cases of intense pain, 9 digestive haemorrhages, 9 hepatic insufficiencies, 2 haemoperitoneums, 1 ischaemic cholecystitis, 1 bronchospasm) and 6 deaths ascribable to the treatment.

In this indication, which corresponds to the palliative treatment of inoperable HCC, this treatment should be reserved for nodular or multinodular HCC that are not excessively large (size of the nodules smaller than 6 – 8 cm, with less than 50 % of the volume of the liver affected).

The third possible indication is concerned with ^{131}I-lipiodol as an adjuvant treatment after surgery (Boucher et al. 2003; Lau et al. 1999; Partanski et al. 2000). This indication was initially validated by a randomized study (Lau et al. 1999). Forty-three patients initially treated by surgery were randomized between adjuvant treatment by ^{131}I-lipiodol (1,850 MBq, $n=21$) and a control group without adjuvant treatment ($n=22$). Over an average follow-up of 34.6 months (range: 14.1 – 69.7 months), there were 6 relapses (28.5 %) in the group treated by ^{131}I-lipiodol versus 21 (59 %) in the control group ($p=0.04$). The average survival without recurrence in the treatment and control groups was 57.2 months (0.4 – 69.7) and 13.6 months (2.1 – 68.3), respectively ($p=0.037$). The survival rate at 3 years in the treatment and control groups was 86.4 % and 43.6 %, respectively ($p=0.039$). Taking into account the benefit in terms of survival related to the use of ^{131}I-lipiodol, the study was stopped before its completion for ethical reasons. However, the results of this study have been criticized (Pocock and White 1999). Indeed, some authors have argued that this study was stopped too early, and that it is preferable to apply a significance threshold of 0.001 % for such trials. For this reason, a new study has been started that plans to cover 300 patients (Tan et al. 2002).

However, two other non-randomized studies have reported similar results in terms of rate of recurrence and survival at 3 years (Boucher et al. 2003; Partanski et al. 2000). In the first study comprising 28 patients, the survival rate at 3 years was 86 % (Partanski et al. 2000). The second study (Boucher et al. 2003) concerned 76 patients (38 without adjuvant treatment and 38 with ^{131}I-lipiodol as adjuvant), showing a significant difference in the percentage of survival without recurrence at 3 years (68.4 ± 9.7 % for the adjuvant treatment group versus 41.5 ± 10.5 % for the control group, $p<0.02$). There was also a significant difference in the percentage of survival at 3 years (91.7 ± 4.6 % for the adjuvant treatment group versus 49.9 ± 10 % for the control group, $p<0.02$) (Boucher et al. 2003).

A treatment with ^{131}I-lipiodol could also be proposed in other indications:

- Antalgic treatment for refractory hyperalgic HCC using conventional analgesics or in patients not supporting analgesics or in the presence of contraindications.
- Curative treatment for HCC of small size inaccessible to local treatment (surgery, radiofrequency) on criteria other than extension of the HCC (evolved cirrhosis, operational contraindications of a general order, site of the lesion).
- Neo-adjuvant treatment before hepatic transplantation, aimed at reducing the risk of recurrence on graft. Two preliminary feasibility studies have been published (Brans et al. 2001; Veilhan et al. 2000) but the long-term results on the recurrence rate are not yet available. A study has just been published on the long-term results of the administration of ^{131}I-lipiodol before resection ($n=20$) or transplantation ($n=14$) (Raoul et al. 2003). Survival at 5 years is 69 % after transplantation and 36 % after resection.
- Neoadjuvant treatment before a possible hepatic resection, for certain HCCs that are too large to be operated on at the outset, with the aim of reducing tumoral weight so that a subsequent operation can be envisaged. Although there has been no targeted study on this indication, success with such a therapeutic approach has already been reported (Bretagne et al. 1988; Raoul 2001).

27.2.5 Contraindications

Different contraindications have been identified for a treatment with ^{131}I-lipiodol:

- Pregnant women or women of childbearing age, in the absence of effective contraception for a duration of at least 1 year after the last injection.

- Presence of distant metastasis.
- Locally very advanced HCC (Okuda III) or patients presenting with evolved cirrhosis.
- Severe respiratory or renal insufficiency.
- Severe leucopenia (< 1.5 Giga/L), severe thrombopenia (< 50 Giga/L)
- History of iodine allergy.
- Severe pathology of the aorta or femoral arteries, contraindicating hepatic arteriography.
- Finally, any mental or physical condition not allowing a period of isolation.

27.2.6 Factors Improving the Effectiveness of ^{131}I-Lipiodol Treatment

Various means could be used to attempt to increase the therapeutic effectiveness of ^{131}I-lipiodol, but, as pointed out above, the response rate is only 30 – 40 % and this treatment does not seem any more effective than chemoembolization.

A certain number of approaches can lead to an improvement in tumoral targeting or a reduction in the tumoral clearance of ^{131}I-lipiodol.

The administration of ^{131}I-lipiodol in the most selective way possible leads to an increase in the dosimetry by enhancing the activity delivered to the tumour. This assumption has recently been called into question by the study of Brans et al., but their results would nevertheless appear debatable because of the large difference in tumoral size between the group treated by selective injection and the group treated by hyperselective injection (Brans et al. 2003).

Angiotensin II would also make it possible to increase the flow of radiolabelled microspheres towards the tumour, due to vasoconstriction acting mainly on the normal vessel and not on the tumoral vessels (Burton et al. 1985, 1988; Sasaki et al. 1985). In this way, the tumour to non-tumoral liver ratio can be increased by a factor of 1.5 – 3.3 (Burton et al. 1988; Sasaki et al. 1985).

A vasodilatation of the tumoral vessels following an external irradiation of 6 – 9 Gy can lead to an increase in the tumour to non-tumoral liver ratio (Order et al. 1986; Leichner et al. 1988). In the first study, the dose rate at the level of the tumour was multiplied by 1.7 after external radiotherapy (Order et al. 1986). In the second study, after an external radiotherapy of 6 – 9 Gy, fixation in the tumour was multiplied by an average factor of 2.8 in eight patients (Leichner et al. 1988).

Two interesting studies have shown that, by increasing the viscosity of the lipiodol, it is possible to improve the tumoral targeting, probably by reducing the tumoral clearance of the lipiodol (De Baere et al. 1996; Hamuro et al. 1999).

In the first study, the "viscosity effect" was tested in vivo on a tumoral model of hepatic rabbit tumour by investigating the influence of various formulations of ^{131}I-lipiodol (pure, oil-in-water or water-in-oil emulsions with droplets of various sizes) (De Baere et al. 1996). This study showed that use of ^{131}I-lipiodol as an emulsion in water with large droplets (> 70 % in the range 70 – 100 μm) led to an enhancement of the "tumour to non-tumoral liver" ratio by a factor of 2 or 3. It was also found that use of this type of emulsion could reduce pulmonary fixation by a factor of 3. These observations are particularly interesting, but the routine use of ^{131}I-lipiodol in an emulsion is difficult to set up because of radiation protection constraints (due to their instability, emulsions need to be prepared at the patient's bedside). One study showed it was possible to prepare stabilized emulsions (Yi et al. 1998) that could be useful in the formulation of emulsified ^{131}I-lipiodol, while another study indicated that this type of stabilized emulsion produced an opposite effect, i.e. a fall in tumoral uptake because of the stabilizing agent used (Garin et al. 2005).

The second study was carried out on cold lipiodol, whose viscosity was modified by the addition of triolein (Hamuro et al. 1999). The author reported that the use of hyperviscous lipiodol (i.e. 0.0318 Pa S instead of 0.023 Pa S, the normal viscosity of the lipiodol used in this study) led to a sustainable threefold increase in the amount of lipiodol present in the tumour (effect persisting 14 days after the injection). On the other hand, this author did not study the influence of viscosity on pulmonary uptake.

Another approach for enhancing the effectiveness of ^{131}I-lipiodol would be the use of therapeutic combinations.

Various arguments plead in favour of a combination with chemotherapy. An in vitro study on HepG2 cell cultures indicated that the combination of radiotherapy and chemotherapy (^{131}I + doxorubicin or cisplatin) was significantly more toxic than a treatment by radiotherapy alone or chemotherapy alone (Chenoufi et al. 1998). Two recent studies give preliminary results for the combination ^{131}I-lipiodol + cisplatin at low doses (Brans et al. 2002; Raoul et al. 2002). In the first study, comprising 20 patients treated with ^{131}I-lipiodol + cisplatin ($n = 10$) or ^{131}I-lipiodol alone ($n = 10$), the rate of stabilization or response was 90 % in the group receiving cisplatin as against 40 % in the group treated by ^{131}I-lipiodol alone (Brans et al. 2002). In the second series, comprising 37 patients all treated with ^{131}I-lipiodol + cisplatin, the objective response rate was 46 % (non-comparative study) (Raoul et al. 2002). These results were obtained without any major increase of toxicity (Brans et al. 2002; Raoul et al. 2002).

The use of lipiodol labelled with different types of emitter could also represent an interesting therapeutic combination. Indeed, it has been established that the sensitivity of a lesion to a given radioelement depends

directly on the size of the lesion (Amin et al. 1993; O'Donogue et al. 1995; Weldon et al. 1991). Radioelements emitting high-energy β-particles, which therefore have a long range, are especially effective on relatively large lesions. In fact, for lesions of small size compared to the mean path, the dose delivered at these lesions will be reduced and a large part of the dose will be delivered into the neighbouring tissues. Thus, for iodine-131, the lesion size corresponding to a probability of optimal effectiveness ranges between 0.5 and 12 mm according to Amin et al. (1993) and between 2.5 and 5 mm according to O' Donoghue et al. (1995), while lesions smaller than 2.5 mm are not very sensitive to this radioelement (Amin et al. 1993; O'Donogue et al. 1995; Weldon et al. 1991). Otherwise, certain radioelements, such as those emitting Auger electrons (i.e. iodine-125), have an extremely short mean path (< 1 mm) and are only effective on lesions of very small size (Humm 1986). Thus, the idea arose of combining two types of radioelement, one with a short range and the other with a longer range, in order to obtain optimal effectiveness (O'Donogue et al. 1995; Weldon et al. 1991). This hypothesis has just been confirmed in vitro by concomitant use of lipiodol labelled with iodine-131 and iodine-125 on a strain of hepatocarcinoma (Towu et al. 2001).

Finally, a combination of ^{131}I-lipiodol with external radiotherapy could also be envisaged in order to provide an overdosage on the tumour as evoked for other tumours (Mazeron et al. 1991; Saito et al. 2000).

27.3 Use of Lipiodol Labelled with Another Radioelement

27.3.1 Lipiodol Labelled with Yttrium-90 (^{90}Y-Lipiodol)

A few studies have been concerned with the labelling of lipiodol by yttrium-90 (Wang et al. 1995, 1996). The purpose of these two studies was to analyse the biodistribution of ^{90}Y-lipiodol in healthy animals (Wang et al. 1995) and in those with an HCC (Wang et al. 1996). These studies showed that ^{90}Y-lipiodol injected intra-arterially had a similar behaviour to ^{131}I-lipiodol, with a preferential distribution in the liver and then in the lungs. For the animal with HCC, ^{90}Y-lipiodol was concentrated in the tumour with a "tumour to healthy liver" ratio of 3.03 at 1 h increasing to 6.45 at 72 h (Wang et al. 1996). However, these studies revealed an initially weak medullar fixation that increased by a factor of 2 – 4 in 24 h, probably related to a release of ^{90}Y into the systemic circulation (Wang et al. 1995, 1996). For this reason, the labelling of lipiodol by yttrium-90 was abandoned.

A recent original study described an indirect labelling of lipiodol with yttrium-90 by means of a lipophilic oxine complex (^{90}Y-oxine lipiodol) (Yu et al. 2002). The procedure is similar to those used for the indirect labelling of lipiodol with rhenium-188 (solubilization in the lipiodol of a radiolabelled lipophilic complex). This study reported a high labelling yield (97.6 ± 1.1 %), with a stability of 87.8 % at 7 days. While this approach appears interesting, it did not provide a rigorous study of biodistribution, and medullary uptake in particular was not evaluated. Such a study appears necessary in the animal before planning to test this new approach in humans.

27.3.2 Lipiodol Marked with Rhenium-188

Rhenium-188 is a radioelement with interesting properties for therapeutic use: intense β-emission (max. 2.118 MeV), a relatively short half-life of 16.9 h, and weak γ-emission (155 keV, 14 %), allowing external detection and thus a simple dosimetric approach. Its relatively short half-life of 16.9 h is an advantage in terms of radiation protection. The production of ^{188}Re from a tungsten-188/rhenium-188 generator enables a relatively easy use of this radioelement on the spot (satisfactory availability because of the 69-day half-life of tungsten-188 and its reduced cost) (Knapp et al. 1994). In addition, because of the short half-life and the type of emission, the radiation protection constraints are less stringent than with the use of iodine-131. Indeed, the duration of hospitalization could be reduced to 24 – 48 h in a normal room, as compared with 7 days in a shielded room when using iodine-131. These aspects should enable us to make this tpe of treatment accessible to a greater number of patients.

Research is currently active on the development of ^{188}Re lipiodol labelling (Boschi et al. 2004; Garin et al. 2004a, b; Jeong et al. 2001; Lambert et al. 2005; Lee et al. 2002; Lepareur et al. 2004; Luo et al. 2004; Paeng et al. 2003; Sundram et al. 2001, 2002, 2003; Wang et al. 1996; Wang et al. 1996; Wang et al. 2004). Studies of biodistribution carried out on animals have yielded satisfactory results (Garin et al. 2004a, b; Jeong et al. 2001; Wang et al. 1996; Wang et al. 1996). Indeed, the labelling of the lipiodol thus carried out is stable in vitro for at least 24 h (Wang et al. 1996; Wang et al. 1996) and even for 48 h (Garin et al. 2004; Jeong et al. 2001). The intra-arterial injection of ^{188}Re-lipiodol exhibits a behaviour similar to ^{131}I-lipiodol, with a preferential distribution at the level of the liver and then on the lungs (Garin et al. 2004a, b; Jeong et al. 2001; Wang et al. 1996; Wang et al. 1996). On an animal with HCC, the ^{188}Re-lipiodol is concentrated at the level of the tumour, yielding a high "tumour to healthy liver" ratio (Garin et al. 2004; Jeong et al. 2001; Wang et al. 1996) that increases with time from 5 to 10 between 1 and 48 h (Wang et al. 1996). The first case of administration on a human was described

in 2001 (Sundram et al. 2001). The results of two studies of phase III have also just been published (Sundram et al. 2002, 2003; Lambert et al. 2005).

Two approaches have been described for labelling lipiodol.

The first approach is based on a direct labelling (with covalent bonding) of the lipiodol using a chelating agent that is secondarily tagged with ^{188}Re (Wang et al. 1996; Wang et al. 1996). Although this labelling method gives satisfactory biodistribution results, it poses some problems of reproducibility and has thus been abandoned.

The second approach depends on labelling a lipophilic chelating agent with ^{188}Re, which is then put into solution secondarily with the lipiodol. In this case, there is no covalent bond between the chelate and the lipiodol (Boschi et al. 2004; Garin et al. 2004a, b; Jeong et al. 2001; Lambert et al. 2005; Lee et al. 2002; Lepareur et al. 2004; Luo et al. 2004; Paeng et al. 2003; Sundram et al. 2001; Sundram et al. 2002, 2003). Five types of complex are currently described in the literature.

The first two complexes to be described were TDD (2, 2, 9-tetramethyl-4, 7-diaza-1, 10-decaneditiol) (Jeong et al. 2001; Sundram et al. 2001) and HDD (4-hexadecyl 1 – 2, 9, 9-tetramethyl-4, 7-diaza-1, 10-decanethiol) (Lambert et al. 2005; Lee et al. 2002; Paeng et al. 2003; Sundram et al. 2002, 2003). The second of these methods seems more promising (Lambert et al. 2005; Lee et al. 2002; Paeng et al. 2003; Sundram et al. 2002, 2003), in particular because of the prolonged intratumoral retention of ^{188}Re-HDD lipiodol (Paeng et al. 2003), even if the labelling yield is not optimal (Lee et al. 2002; Sundram et al. 2002). In fact, the labelling yield ranges between only 50 % and 70 % (Lee et al. 2002), which can pose problems for the synthesis of therapeutic doses of high activity. In a phase-I clinical study on 16 patients, it was not always possible to produce the activity necessary to attain the therapeutic doses (Sundram et al. 2002). Nevertheless, in this study, the patients appear to have been treated with doses of ^{188}Re-TDD lipiodol, ranging between 1.8 and 7.5 GBq. The scintiscans carried out towards the end of the treatments confirmed that this type of radiolabelling appears stable in vivo since the ^{188}Re-TDD lipiodol was detected mainly at the level of the liver as well as the tumours, and to a lesser extent in the lungs and, finally, in the digestive tract. A partial response was observed in one case and, above all, a stabilization of the lesion in 13 cases. The results of a study of phase I, II (taking up again the previous phase I) have recently been published (Sundram et al. 2003). Out of 70 patients treated by ^{188}Re-HDD lipiodol, there were 4 partial responses, 43 stabilizations and 23 progressions. However, these results should be qualified by the presence of a strong urinary elimination of ^{188}Re-HDD lipiodol (41.1 % of the injected activity remaining after 76 h), reflecting the poor stability of labelling in vivo (Lambert et al. 2005).

The third labelling method is based on the ^{188}Re-SSS complex (Garin et al. 2004a, b; Lepareur et al. 2004). The studies carried out with this complex showed that the labelling yield was very high (97.3 ± 2.1 %) (Garin et al. 2004), with the labelling of the lipiodol remaining stable in vitro and in vivo for at least 48 h (RCP of 91 ± 4 % at 48 h) (Garin et al. 2004). This latter study also highlighted a very weak urinary and digestive elimination of ^{188}Re-SSS lipiodol (2.3 ± 0.5 % and 4.8 ± 1.9 %, respectively, to 48 h) (Garin et al. 2004), which represents a clear advantage compared with previously described complexes. Moreover, the study of biodistribution in rats with HCC confirmed the presence of a satisfactory tumoral targeting (Garin et al. 2004). The greater stability is probably explained by the fact that the ^{188}Re is in oxidation state III in complex ^{188}Re-SSS, whereas it is of the level of oxidation state V in the other complexes described. However, there is currently no available data on the use of ^{188}Re-SSS lipiodol in humans.

The fourth labelling method described is ^{188}ReN-DEDC lipiodol, which is obtained with an RCP of 97 ± 2 % and a yield of 96 ± 3 % (Boschi et al. 2004). This labelling is stable at low activity (PRC of 93.2 % at 48 h), but is degraded with time with strong activity under the effect of radiolysis. In fact, with radiolabelling doses ranging from 7.7 to 12 GBq, the RCP at 4 hours is 88.3 ± 0.14 % and falls to only 50.2 % at 12 hours. ^{188}ReN-DEDC lipiodol with activities of 2.5 – 6 GBq was injected into 12 patients having an inoperable HCC (Boschi et al. 2004). This treatment was indeed tolerated (except in one patient who presented with a myelosuppression), and led to one partial response and six stabilizations. However, urinary collection was not carried out to study the stability of labelling in vivo.

The fifth type of indirect labelling described makes use of ^{188}Re-ECD lipiodol (Luo et al. 3004). It is obtained with a yield of 79.77 ± 3 % and an RCP higher than 94 % for labelling with low activity. On the other hand, the study of biodistribution in the rat with HCC is disappointing since, firstly, the "tumour to non-tumoral liver" ratio decreases with time (average values of 13.21 at 1 h and 6.84 at 48 h) and, secondly, there is a significant thyroid, gastric and urinary activity indicating a poor stability of this labelling in vivo.

Lastly, a recent study has described a direct labelling of lipiodol by rhenium-188, without the use of a complex (Wang et al. 2003). With this type of labelling, the yield seems excellent at 1 and 24 h (> 99 %). However, certain points remain unclear: (1) for the calculation of radiochemical purity (RCP), the retention factor (RF) for ^{188}Re-lipiodol is spread out between 0.3 and 0.6; (2) it is not known if the labellings were carried out with weak or high activity and, especially, (3) the study of

biodistribution carried out on the rat with HCC highlights a large fall in the tumoral activity between the 24th and the 48th hours (13 ± 5 % and 7 ± 3 %, respectively, of the activity injected per gram of tumour), reflecting a poor stability of this product in vivo.

27.4 ^{90}Y-Labelled Microspheres

In several preliminary studies, relating mainly to the treatment of hepatic metastases, resin or ceramic microspheres have been used with encouraging response rates (Ho et al. 1998). However, some important side effects were observed: secondary medullary toxicity with a release of yttrium-90 from the microspheres, post-radiation-induced pulmonary fibrosis and digestive haemorrhages following on from pulmonary and gastrointestinal shunts.

This therapeutic approach can be used more safely owing to the development of new microspheres composed of resin or glass containing yttrium-90 in a stable form (i.e. without systematic release of the radioelement incorporated into the matrix of the microspheres), along with the application of a dosimetric model (Ho et al. 1996, 1997). The dosimetric model is based on carrying out hepatic scintiscanning after injection into the hepatic artery of macro-aggregates of human albumin serum labelled with ^{99m}Tc (^{99m}Tc-MAA). The methodology implemented makes it possible to locate and quantify a possible pulmonary shunt, whose frequency is estimated at 7.6 % for patients presenting with an HCC (as against 4.7 % for those with metastases) and whose intensity is highly variable, from 1 % to 75 % (Ho et al. 1997). It also makes it possible to look for a gastrointestinal shunt as well as estimate the dose to the tumour, healthy liver and lungs.

Two products are marketed: resin microspheres of approximately 35 μm diameter, SIR-Spheres (Medical Sirtec Ltd., Australia), and glass microspheres of from 20 to 30 μm, TeraSperes (MDS Nordion, Ottawa, Canada).

Twelve feasibility studies (none of them randomized) have been published following these two technological advances (Cao et al. 1999; Dancey et al. 2000; Goin et al. 2005; Ho et al. 2001; Houle et al. 1989; Lau et al. 1994, 1998; Liu et al. 2004; Salem et al. 2004; Shepherd et al. 1992; Tian et al. 1996; Yan et al. 1993), including just over 300 patients presenting with inoperable HCC. There were no observed cases of medullar toxicity. The search for a pulmonary shunt and the dosimetric approach at the level of the lungs allows us to identify and exclude reliably those patients at risk of radiation-induced pneumopathy. Indeed, in these studies, only two patients presented with a radiation-induced pneumopathy (Dancey et al. 2000; Goin et al. 2005). In spite of the exclusion of the patients having a gastrointestinal shunt identified by scintiscanning with ^{99m}Tc-MAA, several cases occurred of severe digestive haemorrhage (some even fatal): 1 patient out of 10 treated in the study of Shepherd et al. (1992), 4 patients out of 18 treated by Yan et al. (1993) and 3 patients out of 22 treated by Dancey et al. (2000). Various factors allow us to explain the occurrence of these digestive haemorrhages: difficulty of recognizing a gastrointestinal shunt from hepatic activity based on scintiscanning with ^{99m}Tc-MAA (Dancey et al. 2000), increase of portal hypertension related to an irradiation of the portal system (Yan et al. 1993), reflux of radiolabelled microspheres towards the digestive tract (Ho et al. 2001), and, finally, irradiation of the digestive tract by a neighbouring hepatic lesion.

The observed response rates vary between 0 % and 72 % according to the size (reduction in size > 50 %), and between 30 % and 100 % according to the level of alpha-fetoprotein (reduction > 50 %) (Lau et al. 1994, 1998; Shepherd et al.1992; Yan et al. 1993; Dancey et al. 2000). The response rate (as a function of size) is correlated with the estimated dose at the level of the tumour: in the study of Lau et al., 7/8 of the patients (87.5 %) who had received more than 120 Gy on their tumour showed a partial response as against 1/8 of the patients (12.5 %) who had received less than 120 Gy. Two cases have been described of complete histological response (Lau et al. 1998).

One study showed a considerable improvement in median survival for patients at low risk compared with those at high risk (466 as against 108, respectively), thus providing an incentive for the rigorous selection of patients for whom treatment by microspheres could be beneficial (Goin et al. 2005).

Finally, one study is noteworthy from the mode of injection used (Tian et al. 1996). In this study, 33 patients, including 27 with HCC and 6 with metastases, were treated by direct intra-tumoral administration of 74 – 92.5 MBq in the form of microspheres labelled with yttrium-90 under ultrasound guidance. According to the size of the lesions, several injections were necessary per session and several sessions were carried out (without exceeding a total activity of 1,110 MBq). The response rate (reduction in size measured by ultrasound) was 90 %, with a size reduction of more than 50 % in 37 % of the lesions that could be evaluated. The treatment was well tolerated in all cases, despite the presence of a moderate pulmonary activity identifiable in six patients on post-therapeutic scintiscanning.

27.5 Radioimmunotherapy

The principle of radioimmunotherapy is based on the specific recognition of a tumoral antigen by a radiolabelled antibody. In theory, this makes it possible to deliver selective irradiation to the tumour.

Different types of antibody have been tested for the treatment of inoperable HCCs: anti-CEA antibodies (Leichner et al. 1984), anti-AFP (Leichner et al. 1984), anti-ferritin (Abrams et al. 1998; Fan et al. 1992; Liu et al. 1989; Order et al. 1985, 1986; Tang et al. 1990) and, finally, anti-monoclonal HCC (hepama-1) (Chen et al. 2004; Zeng et al. 1993, 1994, 1998). Some encouraging results have been obtained, with response rates varying between 23 % and 65 % (Order et al. 1985; Tang et al. 1990). In particular, radioimmunotherapy made it possible to obtain a tumoral reduction, with 25 – 48 % of the patients treated being reconsidered as operable (Fan et al. 1992; Liu et al. 1989; Tang et al. 1990; Zeng et al. 1993, 1998). Nevertheless, these results should be considered with prudence since (1) the criteria of response (% reduction in tumoral weight) are not always specified (Liu et al. 1989; Tang et al. 1990), (2) the radioimmunotherapy is always associated with another therapeutic method (external radiotherapy, chemotherapy or arterial fixation) and (3) a selection bias exists in certain studies for patients generally presenting with HCC of a massive type (under-representation of the more advanced multinodular forms) (Zeng et al. 1998). Moreover, studies comparing radioimmunotherapy with other therapeutic methods (chemotherapy) yield discordant results: two randomized prospective studies failed to show any benefit in terms of survival with the use of radiolabelled antibodies (Abrams et al. 1998; Order et al. 1991), whereas two non-randomized studies revealed an improvement of survival in patients treated by radioimmunotherapy (Fan et al. 1992; Zeng et al. 1998).

This therapeutic approach also runs up against various obstacles. The intratumoral availability of the antibodies is generally low, with a "tumour to non-tumoral liver" fixation ratio varying, on average, from 1.7 to 2.1 (Fan et al. 1992; Liu et al. 1989; Order et al. 1986). A reaction against the host can frequently develop (34 – 82 % of cases) (Chen et al. 2004; Fan et al. 1992; Zeng et al. 1993, 1994, 1998), which contraindicates an additional administration. Medullar toxicity can occur, particularly after intravenous administration, and can be important, especially in cases of combination with chemotherapy (Abrams et al. 1998; Fan et al. 1992).

Although iodine-131 was used in the majority of cases, antibody labelling could also have been performed with yttrium-90 (Klein et al. 1989; Order et al. 1986) since this radioelement exhibits properties that are more advantageous.

27.6 Hepatic Metastases

There are many effective therapeutic approaches in the treatment of hepatic metastases. Internal radiotherapy has little to offer in this indication, if only in the event of resistance to conventional treatments, chemotherapy in particular. However, under such conditions, we are faced with advanced forms that probably do not represent a good indication for internal radiotherapy.

27.6.1 Hepatic Metastases and ^{131}I-Lipiodol

The few studies carried out in this field are disappointing (Bretagne et al. 1988; Hind et al. 1992; Perring et al. 1994; Raoul et al. 1988). Biodistribution studies show that the "metastasis/non-tumoral liver" fixation ratios are not as high as for HCC (Hind et al. 1992; Perring et al. 1994; Raoul et al. 1988), probably due to a preferential fixing of ^{131}I-lipiodol at the periphery of the metastases (Perring et al. 1994). In addition, Bretagne et al. (1988) report that, among 8 patients presenting with hepatic metastases treated by ^{131}I-lipiodol, no objective response was observed even if a clear and sustained antalgic effect was found in 3 patients with pain.

27.6.2 Use of Microspheres Labelled with ^{90}Y in the Treatment of Hepatic Metastases

Several preliminary studies from the 1980s and 1990s showed that microspheres labelled with ^{90}Y could be of interest in the treatment of hepatic metastases (Ariel and Padula 1978; Grady 1979; Gray et al. 1989, 1992; Mantravadi et al. 1982). Indeed, Grady obtained an objective response rate of 68 % on a series of 25 patients, but the injection of microspheres was accompanied by adrenaline perfusion (with the aim of redistributing arterial flow towards the tumours) (Grady 1979). Ariel and Padula obtained a 40 % response on a series of 65 patients, but chemotherapy was combined with the microspheres (Ariel and Padula 1978). From a series of 12 patients, Mantravadi et al. obtained a partial response in 25 % of the cases (Mantravadi et al. 1982). On a series of 29 patients, Gray et al. obtained a morphological response rate of 48 % and a lowering of CEA levels in 88 % of the cases (Gray et al. 1992). However, in this latter study, metabolic radiotherapy was combined with intra-arterial chemotherapy using 5FU. In addition, the technique for administering the microspheres was extremely constraining (Gray et al. 1989, 1992): they were injected surgically after clamping the arteries vascularizing the healthy hepatic segments (in order to limit irradiation) and ligaturing the arteries derived from the hepatic artery vascularizing the stom-

ach and duodenum (in order to avoid the passage of microspheres into this region). Although the injected microspheres contained a high amount of activity (0.72 – 4.22 GBq in a single administration, in the study of Gray et al. 1992), these various studies provide no information on the level of exposure of the personnel. Lastly, this treatment was accompanied by a certain number of side effects: myelo-suppression related to a release of ^{90}Y, and a risk of post-radiation induced pneumopathies related to the passage of microspheres into the lungs.

More recent studies (in the 1990s) also produced some interesting results, by using microspheres of greater stability and a different injection technique (injection by catheterization according to the technique of Seldinger, after scintiscanning on hepatic and pulmonary perfusion of ^{99m}Tc-MAA) (Andrews et al. 1994; Gray et al. 2000; Herba et al. 1988). Indeed, in studying a series of 24 patients including 23 with hepatic metastases (and 1 HCC), Andrews et al. obtained a partial response rate of 21 % and a stabilization rate of 29 % (for patients not referred to chemotherapy) (Andrews et al. 1994). In 71 patients with colorectal cancer metastases, Gray et al. found a morphological response rate of 75 % (reduction in size of more than 30 %) after injection of microspheres with 2 – 3 GBq, the treatment being combined with an angiotensin II perfusion and intra-arterial chemotherapy (Gray et al. 2000).

Finally, two recent studies are particularly interesting (Gray et al. 2001; Stubb et al. 2001).

In the first study (Gray et al. 2001), 70 patients were randomized between intra-arterial chemotherapy alone ($n = 34$) or treatment by SIR-Spères + angiotensin II + scintiscanning with ^{99m}Tc-MAA (injected after a surgical operation to insert a hepatic catheter and ligature any additional hepatic arteries, $n = 36$). The response rate was significantly higher in the group that received SIR-Spères (44 % versus 17.6 %, $p = 0.01$), and survival without recurrence was significantly longer in the group treated by SIR-Spères (15.9 versus 9.7 months, $p = 0.001$). Finally, overall survival among patients surviving more than 15 months was higher in the group treated by SIR-Spères. These results were obtained with a similar toxicity in both groups: 23 cases with toxicity of rank 3 or 4 (anaemia; rise in levels of bilirubin, alkaline phosphatases or transaminases; nausea; diarrhoea). In the second study, which was non-randomized and comprised 38 patients, Stubbs et al. obtained a response rate of 90 % by combining the treatment by microspheres with the use of angiotensin II as well as intra-arterial chemotherapy, associated with a moderate toxicity (three duodenal ulcers, including one causing a digestive haemorrhage requiring a surgical operation) (Stubbs et al. 2001).

With the use of microspheres, we should nevertheless point out the need to carry out scanning with ^{99m}Tc-MAA before the injection. This is performed in order to look for the presence of a shunt contraindicating the treatment or, as in the study of Gray et al. (2001), the need for a surgical operation. These points are important to stress since they add considerably to the difficulty of this therapeutic approach.

27.6.3 Radioimmunotherapy and Treatment of Hepatic Metastases

Few studies have led to a clinical use of this approach. They depend on the use of antibodies or fragments of anti-CEA antibody.

The most interesting results were obtained with the humanized anti-CEA antibody (MAb) hMN-14 labelled with iodine-131 in a phase I study, and secondarily in a targeted phase II study among patients with small-sized metastases (< 3 cm) resistant to chemotherapy (Behr et al. 1999, 2002).

The study of phase I included 12 patients and indicated a medullary toxicity with a dose not to be exceeded of 2.22 GBq (Behr et al. 1999). Out of the 12 treated patients, 18 % partial and 45 % minor responses were observed.

These results were confirmed in the phase II study, which included 30 patients treated by a single dose of 2.22 GBq. In this study, 19 patients had lesions that could be evaluated, a partial response was observed in 16 % of the cases and a minor response in 42 % of the cases, with an average response duration of 9 months (Behr et al. 2002). Only one toxicity of rank 4 was found (thrombopenia). The treatment could be repeated in five cases, without any increase in toxicity.

These results are interesting because they concern patients who are resistant to chemotherapy, but, on the other hand, they were obtained on small-sized tumours. Less convincing results were published with large tumours (3 % of partial response, 31 % of minor responses or stabilization) (Behr et al. 1997).

Otherwise, some encouraging results have been obtained in animals within the framework of combined radioimmunotherapy and antiangiogenic therapies (Kinuya et al. 2004; Li et al. 2002). In these two cited studies, the therapeutic combination was significantly more effective than either of the two treatments used in isolation.

27.7 Conclusions

Hepatocellular carcinoma is one of the most frequent cancers worldwide. For patients who are not concerned by a radical treatment and who do not present with distant metastases, two therapeutic approaches can be

proposed: chemoembolization or metabolic radiotherapy by arterial administration, in particular internal radiotherapy by means of lipiodol labelled with iodine-131 (^{131}I-lipiodol).

The effectiveness of ^{131}I-lipiodol treatment is proven both in the treatment of hepatocellular carcinomas (HCC) with portal thrombosis and also as an adjuvant to surgery in operated HCCs. This treatment is at least as effective as chemoembolization, but is tolerated much better. However, it leads to partial responses in approximately only 40 % of cases. For reasons of radiation protection, the patients must be hospitalized and isolated in a shielded room for a duration of 8 days, which represents an important handicap with the use of this technique.

Microspheres labelled with yttrium-90 provide a potentially effective therapeutic approach, but there is a risk of severe digestive haemorrhage and radiation-induced pneumopathy. This imposes the need to carry out scintiscanning on ^{99m}Tc-MAA after intra-arterial injection in order to evaluate the risk. In addition, the recession with this technique is much less important than with ^{131}I-lipiodol.

Radioimmunotherapy is another therapeutic method that can be considered. Nevertheless, its development is limited by various factors such as medullary toxicity and the frequent occurrence of reactions against the host.

This approach is less effective with regard to hepatic metastases, in particular with the use of ^{131}I-lipiodol and radioimmunotherapy. On the other hand, two recent studies have shown interesting results for yttrium-90-labelled microspheres used in combination with chemotherapy.

The future prospects for this approach, involving metabolic radiotherapy by arterial administration, will probably hinge on the development of methods for labelling lipiodol with rhenium-188, as well as the use of procedures leading to improvements in the tumoral targeting and/or combinations with other therapies (chemotherapy, antiangiogenic therapy, external radiotherapy, etc.).

References

Abrams RA, et al. (1998) Survival results among patients with alpha-fetoprotein-positive, unresectable hepatocellular carcinoma: analysis of three sequential treatments of the RTOG and Johns Hopkins Oncology Center. Cancer J Sci Am 4(3):178 – 184

Amin AE, et al. (1993) Radiobiological modeling of combined targeted 131I therapy and total body irradiation for treatment of disseminated tumors of differing radiosensitivity. Int J Radiat Oncol Biol Phys 27:323 – 330

Andrews JC, et al. (1994) Hepatic radioembolisation with yttrium-90 containing glass microspheres: preliminary results and clinical follow-up. J Nucl Med 35:1637 – 1644

Ariel IM, Padula G (1978) Treatment of symptomatic metastatic cancer to the liver from primary colon and rectal cancer by the intra-arterial administration of chemotherapy and radioactive isotopes. J Surg Oncol 10:327 – 336

Arii S, et al. (2001) Characteristics of recurrent hepatocellular carcinoma in Japan and our surgical experience. J Hepatobiliary Pancreat Surg 8:397 – 403

Bacher K, et al. (2002) Thyroid uptake and radiation dose after 131I-lipiodol treatment: is thyroid blocking by potassium iodide necessary? Eur J Nucl Med 29:1311 – 1316

Badvie S (2000) Hepatocellular carcinoma. Postgrad Med J 76:4 – 11

Behr TM, et al. (1997) Phase I/II clinical radioimmunotherapy with an iodine-131-labeled anti-carcinoembryonic antigen murine monoclonal antibody IgG. J Nucl Med 38(6):858 – 70

Behr TM, et al. (1999) Radioimmunotherapy of small volume disease of colorectal cancer metastatic to the liver: preclinical evaluation in comparison to standard chemotherapy and initial results of a phase I clinical study. Clin Cancer Res 5(10 Suppl):3232s–3242s

Behr TM, et al. (2002) Radioimmunotherapy of small-volume disease of metastatic colorectal cancer. Cancer 94(4 Suppl):1373 – 81

Bhattacharya S, et al. (1995) Epirubicin-Lipiodol chemotherapy versus ^{131}iodine-lipiodol radiotherapy in the treatment of unresectable hepatocellular carcinoma. Cancer 76:2202 – 2210

Bosch FX, et al. (1999) Epidemiology of primary liver cancer. Semin Liver Dis 19(3):271 – 285

Boschi A, et al. (2004) A kit formulation for the preparation of 188Re-lipiodol: preclinical studies and preliminary therapeutic evaluation in patients with unresectable hepatocellular carcinoma. Nucl Med Comm 25(7):691 – 699

Boucher E, et al. (2003) Adjuvant intra-arterial injection of iodine-131-labelled lipiodol after resection of hepatocellular carcinoma. Hepatology 38:1237 – 1241

Brans B, et al. (2001) The anti-tumoral activity of neoadjuvant intra-arterial 131I-Lipiodol treatment for hepatocellular carcinoma: a pilot study. Cancer Biother Radiopharm 4:333 – 338

Brans B, et al. (2002) Combined iodine-131 lipiodol therapy with low-dose cisplatin as radiosensitiser: preliminary study results in hepatocellular carcinoma. Eur J Nucl Med 29:928 – 932

Brans B, et al. (2003) Intra-arterial radionuclide therapy for liver tumours: effect of selectivity of catheterization and 131I-lipiodol delivery on tumor uptake and response. Nucl Med Comm 24:391 – 396

Bretagne JF, et al. (1988) Hepatic artery injection of I-131-labeled Lipiodol. Radiology 168:547 – 550

Bronowiki JP, et al. (1994) Transcatheter oily chemoembolization for hepatocellular carcinoma. A 4-year study of 127 French patients. Cancer 74:16 – 24

Bruix J, et al. (2001) Clinical management of hepatocellular carcinoma. Conclusions of the Barcelona-2000 EASL conference. J Hepatol 35:421 – 430

Burton MA, et al. (1985) Manipulation of experimental rat and rabbit liver tumor blood flow with angiotensin II. Cancer Res 45:5390 – 5393

Burton MA, et al. (1988) Effect of angiotensin II on blood flow in the transplanted sheep squamous cell carcinoma. Eur J Cancer Clin Oncol 24:1373 – 1376

Calvet X, et al. (1990) Prognostic factors of hepatocellular carcinoma in the west: a multivariate analysis in 206 patients. Hepatology 12:753 – 760

Cao X, et al. (1999) Hepatic radioembolisation with yttrium-90 glass microspheres for treatment of primary liver cancer. Chinese Med J 112(5):430 – 432

Chen S, et al. (2004) Phase I clinical trial of targeted therapy us-

ing 131I-Hepama-1 mAb in patients with hepatocellular carcinoma. Cancer Biother Radiopharm 19(5):589 – 600
Chenoufi N, et al. (1998) In vitro demonstration of synergy between radionuclide and chemotherapy. J Nucl Med 39:900 – 903
Chlebowski RT, et al. (1984) Hepatocellular carcinoma, diagnostic and prognostic features in North American patients. Cancer 53:2701 – 2706
Chou FI, et al. (1994) I-131-lipiodol cytotoxicity in hepatoma cells. Proc Natl Sci Council ROC 18:154 – 160
Chou FI, et al. (1995) Lipiodol uptake and retention by human hepatoma cells. Nucl Med Biol 22(3):379 – 386
Dancey JE, et al. (2000) Treatment of non resectable hepatocellular carcinoma with intrahepatic ^{90}yttrium microspheres. J Nucl Med 41:1673 – 1681
De Baere T, et al. (1996) Quantification of tumor uptake of iodized oils and emulsions of iodized oils: experimental study. Radiology 201:731 – 735
De Baere, et al. (1999) Hepatic intraarterial ^{131}I iodized oil for treatment of hepatocellular carcinoma in patient with impeded portal venous flow. Radiology 212:665 – 668
De Sanctis JT, et al. (1998) Percutaneous treatment of hepatic neoplasms: a review of the current techniques. Cardiovasc Intervent Radiol 21:273 – 296
Deuffic S, Poynard T (1998) Trends in primary liver cancer. Lancet 351:214 – 215
Deuffic S, et al. (1999) Modelling the hepatitis C virus epidemic in France. Hepatology 29:1596 – 1601
El-Serag HB, Mason AC (1999) Rising incidence of hepatocellular carcinoma in the United States. N Engl J Med 340:745 – 750
Fan Z, et al. (1992) Radioiodinated anti-hepatocellular carcinoma (HCC) ferritin. Targeting therapy, tumor imaging and anti-antibody response in patients with hepatic arterial infusion. J Cancer Res Clin Oncol 118:371 – 376
Garin E, et al. (2003) Safe radiation exposure of medical personnel using simple radioprotection means while administering ^{131}I-lipiodol therapy for hepatocellular carcinoma. Nucl Med Comm 24:671 – 678
Garin E, et al. (2004a) ^{188}Re-SSS lipiodol: radiolabelling and biodistribution following injection into the hepatic artery of rats bearing hepatoma. Nucl Med Comm 25:1007 – 1013
Garin E, et al. (2004b) Development and biodistribution of ^{188}Re-SSS lipiodol following injection into hepatic artery of healthy pig. Eur J Nucl Med Mol Imaging 31:542 – 546
Garin E, et al. (2005) Effect of stabilized lipiodol emulsion on experimentally induced hepatocellular carcinoma in rats. J Vasc Intervent Radiol 16(6):849 – 856
Goin JE, et al. (2005) Treatment of unresectable hepatocellular carcinoma with intrahepatic yttrium 90 microspheres: a risk-stratification analysis. J Vasc Interv Radiol 16(2):195 – 203
Grady ED (1979) Internal radiation therapy of hepatic cancer. Dis Col Rect 22(6):371 – 375
Gray BN, et al. (1989) Selective internal radiation (SIR) therapy for treatment of liver metastases: measurement of response rate. J Surg Oncol 42:192 – 196
Gray BN, et al. (1990) Tolerance of the liver to the effects of yttrium-90 radiation. Int J Radiat Oncol Biol Phys 18:619 – 623
Gray BN, et al. (1992) Regression of liver metastases following treatment with yttrium-90 microspheres. Austr N Z J Surg 62:105 – 110
Gray BN, et al. (2000) Treatment of colorectal liver metastases with SIR-spheres plus chemotherapy. GI Cancer 3(4):249 – 257
Gray BN, et al. (2001) Randomized trial of SIR-spheres® plus chemotherapy vs. chemotherapy alone for treating patients with liver metastases from primary large bowel cancer. Ann Oncol 12:1711 – 1720
Groupe d'étude et de traitement du carcinome hépatocellulaire (1995) A comparison of lipiodol chemoembolization and conservative treatment for unresectable hepatocellular carcinoma. N Engl J Med 332:1256 – 1261
Hamuro M, et al. (1999) New oily agents for targeting chemoembolisation for hepatocellular carcinoma. Cardiovasc Int Radiol 22:130 – 134
Herba MJ, et al. (1988) Hepatic malignancies: improved treatment with intraarterial Y-90. Radiology 169:311 – 314
Hind RE, et al. (1992) Biodistribution of Lipiodol following hepatic arterial injection. Br J Surg 79:952 – 954
Ho S, et al. (1996) Partition model for estimating radiation doses from yttrium-90 microspheres in treating hepatic tumours. Eur J Nucl Med 23:947 – 952
Ho S, et al. (1997a) Arteriovenous shunts in patients with hepatic tumors. J Nucl Med 38:1201 – 1205
Ho S, et al. (1997b) Clinical evaluation of the partition model for estimating radiation doses from yttrium-90 microspheres in the treatment of hepatic cancers. Eur J Nucl Med 24:293 – 298
Ho S, et al. (1998) Internal radiation therapy for patients with primary or metastatic hepatic cancer. Cancer 83:1894 – 1907
Ho S, et al. (2001) Intrahepatic ^{90}Y-microspheres for hepatocellular carcinoma. Eur J Nucl Med 42:1587 – 1589
Houle, et al. (1989) Hepatocellular carcinoma: a pilot trial of treatment with Y-90 microspheres. Radiology 172:857 – 860
Humm JL (1986) Dosimetric aspects of radiolabeled antibodies for tumor therapy. J Nucl Med 27:1490 – 1497
Ingold JA, et al. (1965) Radiation hepatitis. Am J Roentgen Radium Ther Nucl Med 93:200 – 208.
Iwai K, et al. (1984) Use of oily contrast medium for selective drug targeting to tumor: enhanced therapeutic effect and X-ray image. Cancer Res 44:2115 – 2121
Jeong JM, et al. (2001) Lipiodol solution of a lipophilic agent, ^{188}Re-TDD, for the treatment of liver cancer. Nucl Med Biol 28:197 – 204
Kaczynski, et al. (1998) Spontaneous regression of HCC. Histopathology 32:147 – 150
Kajiya Y, et al. (1993) Transarterial internal radiation therapy with I-131 lipiodol for multifocal hepatocellular carcinoma: intermediate and long term results. Cardiovasc Intervent Radiol 16:150 – 157
Kan Z (1996) Dynamic study of iodized oil in the liver and blood supply to hepatic tumors. An experimental investigation in several animal species. Acta Radiol 37(Suppl):6 – 25
Kan Z, et al. (1989) In vivo microscopy of the liver after injection of lipiodol into the hepatic artery and portal vein in the rat. Acta Radiol 30:419 – 425
Kinuya S, et al. (2004) Improved survival of mice bearing liver metastases of colon cancer cells treated with a combination of radioimmunotherapy and antiangiogenic therapy. Eur J Nucl Med Mol Imaging 31(7):981 – 5
Klein JL, et al. (1989) Yttrium 90 and iodine 131 radioimmunoglobulin therapy of an experimental human hepatoma. Cancer Res 49:6383 – 6389
Knapp FF, Jr, et al. (1994) Processing of reactor-produced ^{188}W for fabrication of clinical scale alumina-based ^{188}W/^{188}Re generators. Appl Radiat Isot 45:1123 – 1128
Kobayashi H, et al. (1986) Treatment of hepatocellular carcinoma by transarterial injection of anticancer agents in iodized oil suspension or of radioactive iodized oil solution. Acta Radiol Diag 27:139 – 147
Kobayashi H, et al. (1987) Intra-arterial injection of adriamycin/mitomicin C Lipiodol suspension in liver metastases. Acta Radiologica 28:275 – 280
Konno T, et al. (1984) Selective targeting of anticancer drug and simultaneous image enhancement in solid tumors by arterially administered lipid contrast medium. Cancer 54:2367 – 2374

Kouroumalis E, et al. (1998) Treatment of hepatocellular carcinoma with octreotide: a randomised controlled study. Gut 42:442 – 447
Lambert B, et al. (2005) 188Re-HDD/lipiodol therapy for hepatocellular carcinoma: a phase I clinical trial. J Nucl Med 46(1):60 – 6
Lau WY (2002) Management of hepatocellular carcinoma. J R Coll Surg Edinb 47:389 – 399
Lau WY, et al. (1994) Treatment of inoperable hepatocellular carcinoma with intrahepatic arterial yttrium-90 microspheres: a phase I and II study. Br J Cancer 70:994 – 999
Lau WY, et al. (1998) Selective internal radiation therapy for nonresectable hepatocellular carcinoma with intraarterial infusion of ^{90}yttrium microspheres. Int J Radiat Oncol Biol Phys 40(3):583 – 592
Lau WY, et al. (1999) Adjuvant intra-arterial iodine-131-labelled Lipiodol for respectable hepatocellular carcinoma: a prospective randomized trial. Lancet 353:797 – 801
Lee YS, et al. (2002) Synthesis of ^{188}Re-labelled long chain alkyl diaminedithiol for therapy of liver cancer. Nucl Med Comm 23:237 – 242
Leichner PK, et al. (1984) Comparative tumor dose from ^{131}I-labeled polyclonal anti-ferritin, anti AFP, and anti-CEA in primary liver cancers. Cancer Drug Delivery 1(4):321 – 328
Leichner PK, et al. (1988) Dosimetry and treatment planning for ^{90}Y-labeled antiferritin in hepatoma. Int J Radiat Oncol Biol Phys 14:1033 – 1042
Lepareur N, et al. (2004) A kit formulation for the labelling of Lipiodol with generator-produced ^{188}Re. J Label Compounds Radiopharm 47:857 – 867
Leung TWT, et al. (1994) Selective internal radiation therapy with intra-arterial iodine-131-Lipiodol in inoperable hepatocellular carcinoma. J Nucl Med 35:1313 – 1318
Leung TWT, et al. (1995) Radiation pneumonitis after selective internal radiation treatment with intraarterial 90yttrium-microspheres for inoperable hepatic tumors. Int J Radiat Oncol Biol Phys 33:19 – 24
Leung TWT, et al. (1999) Complete pathological remission is possible with systemic combination chemotherapy for inoperable hepatocellular carcinoma. Clin Cancer Res 5:1676 – 1681
Leung TWT, Johnson PJ (2001) Systemic therapy for hepatocellular carcinoma. Semin Oncol 28:514 – 520
Levy I, Sherman M (2002) Staging of hepatocellular carcinoma: assessment of the Clip, Okuda and Child-Pugh staging systems in a cohort of 257 patients in Toronto. Gut 50:881 – 885
Li XF, et al. (2002) Benefits of combined radioimmunotherapy and anti-angiogenic therapy in a liver metastasis model of human colon cancer cells. Eur J Nucl Med Mol Imaging 29(12):1669 – 74
Liu KD, et al. (1989) Radioimmunotherapy for hepatocellular carcinoma (HCC) using ^{131}I-anti HCC isoferritin IgG: preliminary results of experimental and clinical studies. Int J Radiat Oncol Biol Phys 16:319 – 323
Liu MD, et al. (2004) Use of yttrium-90 TheraSphere for the treatment of unresectable hepatocellular carcinoma. Am Surg 70(11):947 – 53
Llovet JM, et al. (1999) Natural history of untreated non surgical hepatocellular carcinoma: rationale for the design and evaluation of therapeutic trials. Hepatology 29:62 – 67
Llovet JM, et al. (2002) Arterial embolisation or chemoembolisation versus symptomatic treatment in patients with unresectable hepatocellular carcinoma: a randomised controlled trial. Lancet 359:1734 – 1739
Lo CM, et al. (2002) Randomized controlled trial of transarterial lipiodol chemoembolization for unresectable hepatocellular carcinoma. Hepatology 35:1164 – 1171
Lui WY, et al. (1990) Report of a pilot study of intra-arterial injection of I-131 Lipiodol for the treatment of hepatoma. Chin Med J (Taipei) 46:125 – 133
Luo TY, et al. (2004) Preparation and biodistribution of rhenium-188 ECD/lipiodol in rats following hepatic arterial injection. Nucl Med Biol 31:671 – 677
Madden MV, et al. (1993) Randomised trial of targeted chemotherapy with lipiodol and epidoxorubicin compared with symptomatic treatment hepatoma. Gut 34:1598 – 1600
Madsen MT, et al. (1988) Dosimetry of iodine 131 ethiodol in the treatment of hepatoma. J Nucl Med 29:1038 – 1044
Maini CL, et al. (1996) Superselective intra-arterial radiometabolic therapy with I-131 Lipiodol in hepatocellular carcinoma. Clin Nucl Med 21:221 – 226
Maki S, et al. (1985) Image enhancement in computerized tomography for sensitive diagnosis of liver cancer and semiquantitation of tumor selective drug targeting with oily contrast medium. Cancer 56(4):751 – 757
Mantravadi RVP, et al. (1982) Intraarterial yttrium 90 in the treatment of hepatic malignancy. Radiology 142:783 – 786
Margolis LW, Phillips TL (1969) Whole lung irradiation for metastatic tumor. Radiology 93:1173 – 1179
Maublant J, et al. (2001) Médecine nucléaire en oncologie: nouvelles modalités diagnostiques et thérapeutiques. Bull Cancer 88:35 – 44
Mazeron JJ, et al. (1991) Influence of dose rate on local control of breast carcinoma treated by external beam irradiation plus iridium 192 implant. Int J Radiat Oncol Biol Phys 21:1173 – 1177
Miller DL, et al. (1987) Distribution of iodized oil within the liver after hepatic arterial injection. Radiology 162:849 – 852
Monsieur MA, et al. (2003) Patient dosimetry for ^{131}I-lipiodol therapy. Eur J Nucl Med 30:554 – 561
Nakajo M, et al. (1988) Biodistribution and in vivo kinetics of iodine 131 Lipiodol infused via the hepatic artery of patients with hepatic cancer. J Nucl Med 29:1066 – 1077
Nakakuma K, et al. (1983) Studies on anticancer treatment with an oily anticancer drug injected into the ligated feeding hepatic artery for liver cancer. Cancer 52:2193 – 2200
Nakakuma K, et al. (1985) Hepatocellular carcinoma and metastatic cancer detected by iodized oil. Radiology 154:15 – 17
O'Donoghue JA, et al. (1995) Relationship between tumor size and curability for uniformly targeted therapy with beta-emitting radionuclides. J Nucl Med 36:1902 – 1909
Okuda K (2000) Hepatocellular carcinoma. J Hepatol 32 (Suppl 1):225 – 237
Order SE, et al. (1985) Iodine 131 antiferritin, a new treatment modality in hepatoma: a radiation therapy oncology group study. J Clin Oncol 3:1573 – 1582
Order SE, et al. (1986) ^{90}yttrium antiferritin – a new therapeutic radiolabeled antibody. Int J Radiat Oncol Biol Phys 12:277 – 281
Order SE, et al. (1991) A randomized prospective trial comparing full dose chemotherapy to 131I antiferritin: an RTOG study. Int J Radiat Oncol Biol Phys 20:953 – 963
Otto G, et al. (1998) Survival and recurrence after liver transplantation versus liver resection for hepatocellular carcinoma, a retrospective analysis. Ann Surg 227:424 – 432
Paeng JC, et al. (2003) Lipiodol solution of ^{188}Re-HDD as a new therapeutic agent for transhepatic arterial embolisation in liver cancer: preclinical study in a rabbit liver cancer model. J Nucl Med 44:2033 – 2038
Park CH, et al. (1987) Treatment of hepatocellular carcinoma (HCC) with radiolabelled Lipiodol: a preliminary report. Nucl Med Comm 8:1075 – 1087
Park CH, et al. (1990) Distribution of Lipiodol in hepatocellular carcinoma. Liver 10:72 – 78
Partensky C, et al. (2000) Intra-arterial iodine 131-labeled Lipiodol as adjuvant therapy after curative liver resection for hepatocellular carcinoma. Arch Surg 135:1298 – 1300

Pelletier G, et al. (1990) A randomized trial of hepatic arterial chemoembolization in patients with unresectable hepatocellular carcinoma. J Hepatol 11:181 – 184
Perring S, et al. (1994) Dosimetric assessment of radiolabelled lipiodol as a potential therapeutic agent in colorectal liver metastases using combined CT and SPECT. Nucl Med Comm 15:34 – 38
Pocock S, White I (1999) Trials stopped early: too good to be true. Lancet 353:943 – 944
Preketes AP, et al. (1996) Pulmonary toxicity following Lipiodol I-131 treatment for liver tumours. Reg Cancer Treat 9:21 – 26
Raoul JL (2001) Lipiocis et carcinome hepatocellulaire. Médecine Nucléaire – imagerie fonctionnelle et métabolique 25:671 – 674
Raoul JL, et al. (1986) L'angiographie lipiodolée au cours des carcinomes hépatocellulaires. Apport du Lipiodol marqué à l'iode 131. J Radiol 67:797 – 801
Raoul JL, et al. (1988) Hepatic artery injection of I-131-labeled Lipiodol. Part 1. Biodistribution study results in patients with hepatocellular carcinoma and liver metastases. Radiology 168:541 – 545
Raoul JL, et al. (1992) Internal radiation therapy for hepatocellular carcinoma. Results of a French multicenter phase II trial of transarterial injection of iodine 131-labeled Lipiodol. Cancer 69:346 – 352
Raoul JL, et al. (1993) Usefulness of hepatic artery injection of iodized oil and I-131-labeled iodized oil before the therapeutic decision in hepatocellular carcinoma. J Scan Gastroenterol 28:217 – 223
Raoul JL, et al. (1994) Randomized controlled trial for hepatocellular carcinoma with portal vein thrombosis: intra-arterial iodine-131-iodized oil versus medical support. J Nucl Med 35:1782 – 1787
Raoul JL, et al. (1996) Limitations of hyperselective intraarterial injections for the treatment of hepatocellular carcinoma. Invest Radiol 31:305 – 307
Raoul JL, et al. (1997) Prospective randomized trial of chemoembolization versus intra-arterial injection of ^{131}I-labeled iodized oil in the treatment of hepatocellular carcinoma. Hepatology 26:1156 – 1161
Raoul JL, et al. (2002) Association of CDDP and intra-arterial injection of 131I-lipiodol (lip 131I) in the treatment of hepatocellular carcinoma (HCC): results of a phase II trial. J Clin Oncol 21:563
Raoul JL, et al. (2003) Preoperative treatment of hepatocellular carcinoma with intra-arterial injection of 131I-labelled lipiodol. Br J Surg 90:1379 – 1383
Rindani R, et al. (2002) 131I-lipiodol therapy for unresectable hepatocellular carcinoma. ANZ J Surg 72:210 – 214
Risse JH, et al. (2000) Intraarterial HCC therapy with I-131-Lipiodol. Cancer Biother Radiopharm 15:65 – 71
Saito M, et al. (2000) Treatment of roentgenographically occult endobronchial carcinoma with external beam radiotherapy and intraluminal low-dose-rate brachytherapy: second report. Int J Radiat Oncol Biol Phys 47:673 – 680
Salem R, et al. (2004) Use of yttrium-90 glass microspheres (TheraSphere) for the treatment of unresectable hepatocellular carcinoma in patients with portal vein thrombosis. J Vasc Interv Radiol 15(4):335 – 45
Sasaki Y, et al. (1985) Changes in distribution of hepatic blood flow induced by intraarterial infusion of angiotensin II in human hepatic cancer. Cancer 55:311 – 316
Shepherd FA, et al. (1992) A phase I dose escalation trial of yttrium-90 microspheres in the treatment of primary hepatocellular carcinoma. Cancer 70:2250 – 2254
Stefanini GF, et al. (1995) Efficacy of transarterial targeted treatments on survival of patients with hepatocellular carcinoma. An Italian experience. Cancer 75:2427 – 2434
Stubbs RS, et al. (2001) Selective internal radiation therapy (SIRT) with ^{90}Yttrium microspheres for extensive colorectal liver metastases. Hepatogastroenterology 48:333 – 337
Sundram FX, et al. (2001) ^{188}Rhenium-TDD-lipiodol in treatment of inoperable primary hepatocellular carcinoma – A case report. Ann Acad Med Singapore 30:542 – 545
Sundram FX, et al. (2002) Trans-arterial rhenium-188 lipiodol in the treatment of inoperable hepatocellular carcinoma. An IAEA sponsored multi-centre phase 1 study. World J Nucl Med 1:5 – 11
Sundram F, et al. (2003) Preliminary results of transarterial rhenium-188 HDD lipiodol in the treatment of inoperable primary hepatocellular carcinoma. Eur J Nucl Med Mol Imaging 31:250 – 257
Tan SB, et al. (2002) Following a trial that stopped early: what next for adjuvant hepatic intra-arterial iodine-131 lipiodol in resectable hepatocellular carcinoma. J Clin Oncol 20:1709
Tang ZY, et al. (1990) Radioimmunotherapy in the multimodality treatment of hepatocellular carcinoma with reference to second look resection. Cancer 65:211 – 215
Taylor-Robinson SD, et al. (1997) Increase in primary liver cancer in the UK, 1974 – 94. Lancet 350:1142 – 1143
The CLIP Investigators (1998) A new prognostic system for hepatocellular carcinoma: a retrospective study on 435 patients. Hepatology 28:751 – 755
Tian JH, et al. (1996) Ultrasound-guided internal radiotherapy using yttrium-90-glass microspheres for liver malignancies. J Nucl Med 37:958 – 963
Toubeau M, et al. (2001) ^{131}I thyroid uptake in patients treated with ^{131}I-Lipiodol for hepatocellular carcinoma. Eur J Nucl Med 28:669 – 670
Towu E, et al. (2001) In-vitro uptake of radioactive lipiodol I-131 and I-125 by hepatoblastoma: implications for targeted radiotherapy. Pediatr Surg Int 17:609 – 613
Trinchet JC, Beaugrand M (1999) Augmentation de l'incidence du carcinome hépatocellulaire dans les pays occidentaux. Gastroenterol Clin Biol 23:1286 – 1288
Veilhan LA, et al. (2000) Prevention of recurrence of hepatocellular carcinoma after orthotopic liver transplantation by neoadjuvant intraarterial injections of iodine-131-labelled Lipiodol. Results of a pilot study. Eur J Nucl Med 27:941
Wang SJ, et al. (1995) Preparation and biodistribution of yttrium-90 lipiodol in rats following hepatic arterial injection. Eur J Nucl Med 22:233 – 236
Wang SJ, et al. (1996a) Biodistribution of rhenium-188 lipiodol infused via the hepatic artery of rats with hepatic tumours. Eur J Nucl Med 23:13 – 17
Wang SJ, et al. (1996b) Hepatic artery injection of yttrium-90-lipiodol: biodistribution in rats with hepatome. J Nucl Med 37:332 – 335
Wang SJ, et al. (1996c) Radiolabelling of lipiodol with generator produced ^{188}Re for hepatic tumor therapy. Appl Radiat Isot 47:267 – 271
Wang SJ, et al. (2004) A new technique for labeling lipiodol with ^{188}Re in the treatment of hepatic tumor. J Radioanal Nucl Chem 261:189 – 193
Wheldon TE, et al. (1991) The curability of tumours of differing size by targeted radiotherapy using 131I or 90Y. Radiother Oncol 21:91 – 99
Yan ZP, et al. (1993) An experimental study and clinical pilot trials on yttrium-90 glass microspheres through the hepatic artery for treatment of primary liver cancer. Cancer 72:3210 – 3215
Yi SW, et al. (1998) Stable lipiodolized emulsions for hepatoma targeting and treatment by transcatheter arterial chemoembolisation. J Control Release 50:135 – 143
Yoo HS, et al. (1989) Radioiodinated fatty acid esters in the management of hepatocellular carcinoma: preliminary findings. Cancer Chemother Pharmacol 23 (Suppl):S54–S58

Yoo HS, et al. (1991) Nodular hepatocellular carcinoma. Treatment with subsegmental intraarterial injection of iodine 131-labeled iodized oil. Cancer 68:1878 – 1884

Yoo HS, et al. (1994) Small hepatocellular carcinoma: high dose internal radiation therapy with super selective intra-arterial injection of I-131-labeled Lipiodol. Cancer Chemother Pharmacol 33 (Suppl):S128–S133

Yu J, et al. (2002) ^{90}Y-oxine-ethiodol, a potential radiopharmaceutical for the treatment of liver cancer. Appl Radiat Isot 58:567 – 573

Yuen MF, et al. (2002) A randomized placebo-controlled study of long acting octreotide for treatment of hepatocellular carcinoma. Hepatology 36(3):687 – 691

Yumoto Y, et al. (1985) Hepatocellular carcinoma detected by iodized oil. Radiology 154:19 – 24

Yumoto Y, et al. (1992) Treatment of hepatocellular carcinoma by transcatheter hepatic arterial injection of radioactive iodized oil solution. Cancer Chemother Pharmacol 31 (Suppl):S128–S136

Zeng ZC, et al. (1993) Radioimmunotherapy for unresectable hepatocellular carcinoma using ^{131}I-hepama-1 mAb: preliminary results. J Cancer Res Clin Oncol 119:257 – 259

Zeng ZC, et al. (1994) Human anti-(murine Ig) antibody responses in patients with hepatocellular carcinoma receiving intrahepatic arterial ^{131}I-labeled hepama-1 mAb. Preliminary results and discussion. Cancer Immunol Immunother 39:332 – 336

Zeng ZC, et al. (1998) Improved long term survival for hepatocellular carcinoma (HCC) with a combination of surgery and hepatic intraarterial infusion of ^{131}I-anti-HCC mAb. Phase I/II clinical trials. J Cancer Res Clin Oncol 124: 275 – 280

Radioisotope Therapy of Malignant Pleural and Peritoneal Effusions

28

J. Bucerius, H.-J. Biersack

Treatment of malignant pleural or peritoneal effusions is one of the "oldest" therapies using radioactive isotopes and was first described by J.H. Müller more than 50 years ago (Müller 1945).

For the first therapeutic experiments, radioactive zinc (zinc-63) was used as zinc sulfide which was dissolved in pectin solution. Beginning in 1949, Müller administered gold colloid (gold-198) in patients suffering from malignant pleural and peritoneal effusions (Müller 1950). The main benefit as compared to zinc was a simplified production of a greater amount of the radioisotope, which made its wider distribution possible. Beginning in the mid 1950s, therapy with phosphorus-32 as colloidal chromic-phosphate, or yttrium-90 as fluoride, chloride or silicate, became more and more popular for the treatment of malignant pleural and peritoneal effusions (Kent and Moses 1951; Root et al. 1954; Jaffe 1955). A few years later, the administration of lutetium-177 chloride for these diseases was described (Kyker et al. 1954; Yamashita et al. 1960).

28.1 Indications and Contraindications for Intracavitary Therapies with Radioisotopes

Intracavitary treatment with radioisotopes, as a palliative procedure, can be basically applied for all malignant pleural and peritoneal effusions. However, there has to be no doubt that the effusion is related to the carcinomatosis of the visceral cavity in question.

For effusions related to cardiovascular, metabolic or rheumatic diseases, treatment with radioisotopes is not indicated. Furthermore, closed effusions are a contraindication for the treatment with radioisotopes due to the missing distribution of the radioisotope and, therefore, the high risk of radiation induced necroses.

28.2 Application of Intracavitary Therapy with Radioisotopes

Before administration of the therapy isotope, an effusion chamber has to be excluded. For this purpose, a chest X-ray during standing and lying down should be performed. Furthermore, the free distribution of a diagnostic isotope in the pleura or the peritoneum should be documented. The latter can be performed after intrapleural or peritoneal administration of approximately 185 MBq ^{99m}Tc-sulfur or tin colloid using a gamma camera for imaging (Tally et al. 1974). In cases of free distribution of the effusion both in a horizontal and a vertical direction, a chamber formation of the effusion can be excluded satisfactorily. Afterwards, the intrapleural or peritoneal administration of the therapy radioisotope can be safely performed.

For puncture of the pleura, a commercially available puncture set can be used. Firstly, the pleural effusion should be released as much as possible, while a residual volume of the effusion of approximately 250 – 500 ml should remain in situ. This volume should be documented with a chest X-ray or an ultrasound examination of the pleura. The residual volume of the effusion is mandatory for a homogenous distribution of the therapy radioisotope in the pleura or the peritoneum. Subsequently, the treatment radioisotope [approximately 50 mCi (1,850 MBq) ^{90}Y-silicate for pleura and 100 mCi (3,700 MBq) for peritoneum] can be injected. After the injection and sterile covering of the site of puncture, the patient should change his or her body position every 15 min during the first 6 – 8 h in order to achieve a homogenous distribution of the radioisotope over the whole serosa. This should be carried out under the supervision of an experienced physician. After 24 h approximately 90 % of the administered activity is fixed in the pleura or peritoneum (zum Winkel et al. 1979).

28.3 Side Effects of Radioisotope Therapy

Basically, radiation of the bone marrow, with a reduction in leukocytes and/or thrombocytes, cannot be excluded. However, these side effects are rather rare (Lang and Riccabona 1974). Additionally, adhesions or necroses are uncommon.

28.4 Radiation Protection

No special radiation protection procedures are required for pure β-radiation since yttrium (^{90}Y) or phosphorus (^{32}P) does not reach the environment. According to the German law on radiation protection, patients must stay for at least 48 h in the ward after each therapy session with radioisotopes. As radiocolloids are reabsorbed only to a very small extent, no special protection procedures are necessary with regard to possible radioactivity in the urine or feces.

28.5 Results of Intracavitary Therapy with Radioisotopes

The comparability of the results obtained with the different protocols for the treatment of malignant pleural or peritoneal effusions is limited as patient characteristics, study designs, and study end points are mostly very different. However, several studies have indicated a temporary cessation of the effusion reflow in 50 – 70 % of treated patients (Jaffe 1955; Lang and Riccabona 1974; Chang et al. 1957; Kligerman and Habif 1995). The best results have been achieved in patients suffering from ovarian or breast cancer.

Lang and Riccabona reported an extension of the time interval between two indicated punctures from 10 to 68 days after intracavitary treatment (Lang and Riccabona 1974). An improvement of the general condition of the patients could be observed in up to 55 % of patients. Austgen and associates reported the administration of ^{90}Y-silicate for intracavitary treatment (Augsten et al. 1984). They found a cessation of effusion reflow in 9 of 20 treated patients for an average of 3.5 months.

Kramer and associates reported a single case of the development of a malignant pleural mesothelioma as a late complication of radiotherapy for Hodgkin's disease. After primary treatment and to relieve symptoms of dyspnea secondary to pleural effusion, a thoracic drain was installed, followed by intracavitary administration of yttrium-90 (Kramer et al. 2000). The patients remained in good clinical condition for at least 6 years after diagnosis. The authors concluded that considering the few therapeutic options the use of ^{90}Y-silicate intrapleural installation could be propagated as a safe and effective antitumor treatment for a selected group of patients with malignant pleural mesothelioma.

During the last few decades the number of intracavitary treatments with radioisotopes has strongly declined, being used mainly in cases of pleural carcinomatosis with effusion. This is mainly due to the promising results obtained with the thoracoscopically intrapleural administration of magnesium silicate (talcum) in patients suffering from persistent malignant pleura effusions. This palliative therapy can be applied during general anesthesia and is associated with a success rate of approximately 90 % (Daniel et al. 1990). However, together with further therapy alternatives (e.g., intrapleural administration of 5-fluorouracil, bleomycin, Novantrone, etc.), treatment with radioactive isotopes may play a particular role in refractory effusions after the described administration of talcum, especially in patients with severely impaired general conditions or contraindications for general anesthesia due to concomitant diseases.

In contrast to malignant pleural effusions, a different situation arises in patients suffering from malignant effusions due to peritoneal carcinomatosis. Usually no surgical options (with the exception of "tumor debulking") are present in these patients, who are mainly in the higher grades of tumor growth. This is mainly relevant for the palliative treatment of peritoneal carcinomatosis of ovarian cancer. Primarily for this type of cancer, a growing interest in treatment with radioisotopes has been observed in recent years. In a prospective study, Young and associates reported an identical 5-year survival rate of patients with ovarian cancer (tumor stage FIGO II, i.e., tumor restricted to the pelvis) and treatment with intraperitoneal administration of ^{32}P as compared to the standard chemotherapy with melphalan (Young et al. 1990). Therefore, curative treatment for this kind of cancer seems possible.

However, the effect of radiation administration is not solely restricted to tumor cells, necessarily limiting the antineoplastic effect of the treatment with radioisotopes. As such, much effort is being made to evaluate concepts for a more effective distribution of the ionizing radiation. During the last few years, research has focused primarily on the administration of radioactive labeled antibodies. In 1986, Pectasides and associates reported an antibody-guided irradiation of malignant pleural and pericardial effusions (Pectasides et al. 1986). The tumor-associated antibodies were radiolabelled with iodine-131 and subsequently administered intrapleurally and pericardially in patients suffering from malignant effusions. Ten out of 13 effusions (3 pericardial and 7 pleural) responded completely with no fluid reflow between 3 and 18 months. Furthermore,

they found no clinical or hematological toxicity. In a report of three cases, iodine-131 radiolabeled tumor-associated monoclonal antibodies were given to a patient with malignant pleural effusion, intrapericardially to a patient with pericardial effusion and a tumor mass invading the pericardium, and intraperitoneally to a patient with stage III ovarian cancer resistant to chemotherapy (Hammersmith Oncology Group 1984). Cytological examination after antibody-guided therapy showed no neoplastic cells in the residual fluid from patient 1 or peritoneal washings from patient 3. In patient 2, computed tomography of the pericardium showed that the tumor mass had diminished and the pericardial effusion had resolved. Once again, no clinical or other toxicity was observed.

In a previous study, Epenetos and associates reported a long-term evaluation of patients with ovarian cancer and intraperitoneal administration of ^{90}Y-labeled monoclonal antibodies (Epenetos et al. 2000). The preliminary results of this study suggest that a substantial proportion of patients who achieve complete remission with conventional therapy can achieve a long-term benefit when treated with intraperitoneal radioimmunotherapy with ^{90}Y-labeled antibodies.

References

Austgen M, Schlimmer P, Wilhelm H, Trendelenburg F (1984) Palliative therapy of tumor-induced pleural effusions with 90Yttrium-silicate. Eur J Respir Dis 65:64

Chang CA, Janzen AH, Shorneck AB, Rosenbaum PJ (1957) Treatment of malignant effusions by intracavitary injection of radioactive colloidal gold. Am J Roentgenol 77:486

Daniel TM, Tribble CG, Rodgers BM (1990) Thoracoscopy and talc poudrage for pneumothoraces and effusions. Ann Thorac Surg 50:186

Epenetos AA, Hird V, Lambert H, Mason P, Coulter C (2000) Long-term survival of patients with advanced ovarian cancer treated with intraperitoneal radioimmunotherapy. Int J Gynecol Cancer 10:44 (S1)

Hammersmith Oncology Group and the Imperial Cancer Research Fund (1984) Antibody-guided irradiation of malignant lesions: three cases illustrating a new method of treatment. A report from the Hammersmith Oncology Group and the Imperial Cancer Research Fund. Lancet 30:1441

Jaffe HL (1955) Treatment of malignant serous effusions with radioactive colloidal chromic phosphate. Am J Roentgenol 74:657

Kent EM, Moses C (1951) Radioactive isotopes in the palliative management of carcinomatosis of the pleura. J Thorac Surg 22:503

Kligerman MM, Habif DV (1995) The use of radioactive gold in the treatment of effusion due to carcinomatosis of the pleura and the peritoneum. Am J Roentgenol 75:651

Kramer G, Gans S, Rijnders A, Leer J (2000) Long term survival of a patient with malignant pleural mesothelioma as a late complication of radiotherapy for Hodgkin's disease treated with 90yttrium-silicate. Lung Cancer 27:205

Kyker GC, Cress EA, Gleason GL (1954) Distribution of yttrium administered by various routes. Fed Proc 13:245 (cited by Lang and Riccabona)

Lang T, Riccabona G (1974) Langzeitergebnisse der intrakavitären Isotopentherapie maligner Ergüsse. Nuklearmediziner 12:245

Müller JH (1945) Über die Verwendung von künstlich radioaktiven Isotopen zur Erzielung von lokalisierten Strahlenwirkungen. Experientia 1:199

Müller JH (1950) Weitere Entwicklung der Therapie von Peritonealkarzinosen bei Ovarialkarzinom mit künstlicher Radioaktivität (Au-198). Gynaecologica 129:298

Pectasides D, Stewart S, Courtenay-Luck N, et al. (1986) Antibody-guided irradiation of malignant pleural and pericardial effusions. Br J Cancer 53:727

Root SW, Tyror MP, Andrews GA, Kniseley RM (1954) Distribution of colloidal radioactive chromic phosphate after intracavitary administration. Radiology 63:251

Tally TE, Goldberg ME, Loken MK (1974) The use of 99mTc sulphur colloid to assess the distribution of 32P chromic phosphate. J Nucl Med 15:190

Yamashita HS, Igari S, Lino Y (1960) Fundamental studies and clinical experience on the Lutetium (Lu-177) therapy. Int J Appl Radiat 8:113

Young RC, Walton LA, Ellenberg SS, et al. (1990) Adjuvant therapy in stage I and stage II epithelial ovarian cancer. N Engl J Med 322:1021

zum Winkel K, Chone B, Hermann HJ, Schenk P (1979) Möglichkeiten und Grenzen der Therapie mit offenen radioaktiven Substanzen. Dtsch Ärztebl 76:619

29 Radiosynoviorthesis (Radiation Synovectomy)

G. Mödder

29.1 Introduction

Radiosynoviorthesis (RSO) is a proven important instrument for local treatment of chronic inflammatory joint diseases in the context of medical and orthopaedic efforts. The term radiosynoviorthesis was created by Delbarre et al. 1968, meaning the restoration (*orthesis*) of the *synov*ium by means of *radio*nuclides. By local administration of radioactive agents an attempt is made to influence the synovial process favourably as an alternative to surgical synovectomy. In the Anglo-American literature the term "radiosynovectomy" or "radiation synovectomy" came into use.

The first descriptions of the method go back to Ishido (1923) and Fellinger and Schmid (1952).

In Germany, RSO nowadays is performed in about 63,000 joints per year, as much as radioiodine therapy in thyroid diseases.

29.2 Indications

Basically RSO is indicated for the local treatment of almost all kinds of chronic synovitis (Mödder 2001a, b; Kampen et al. 2001). The *main indications* for radiosynoviorthesis are (modified according to German and European guidelines: Farahati et al. 1999; Clunie and Fischer 2003):

- Rheumatoid arthritis
- Seronegative spondyloarthropathy (i.e., reactive arthritis, psoriatic arthritis)
- Haemarthrosis in haemophiliacs
- Recurrent joint effusions (i.e., after arthroscopy)
- Pigmented villonodular synovitis (PVNS)
- Osteoarthritis (activated arthrosis)
- After joint prosthesis: persistent effusions, polyethylene disease
- Undifferentiated arthritis (where the arthritis is characterized by synovitis, synovial thickening or effusion)

Absolute contraindications:

- Pregnancy
- Breast feeding
- Local skin infection
- Acute rupture of popliteal cyst (Baker's cyst)

Relative contraindications:

- RSO should only be used in children and young patients (< 20 years) if the benefit of treatment is likely to outweigh the potential hazards. But it is routinely applied in haemophilic children.
- Extensive joint instability with bone destruction

29.3 Radiopharmaceuticals

The most common and approved radiopharmaceuticals used for RSO are:

- [^{90}Y]yttrium citrate or silicate ([^{90}Y]colloid), only used for RSO of knee joints
- [^{186}Re]rhenium sulphide ([^{186}Re]colloid), used for RSO of middle sized joints
- [^{169}Er]erbium citrate ([^{169}Er]colloid), used for RSO of small joints

Table 29.1. Proven dosages for the most frequently treated joints

Joint	Radioisotope	Dose (MBq)
Knee joint	Yttrium-90	185 – 222
Glenohumeral joint	Rhenium-186	74
Elbow joint	Rhenium-186	74
Wrist joint	Rhenium-186	55 – 74
Hip joint	Rhenium-186	111 – 185
Ankle joint	Rhenium-186	74
Talonavicular/subtalar joint	Rhenium-186	55
Metacarpophalangeal joint (MCP)	Erbium-169	20 – 40
Proximal interphalangeal joint (PIP)	Erbium-169	10 – 20
Distal interphalangeal joint (DIP)	Erbium-169	10 – 15
Metatarsophalangeal joint (MTP)	Erbium-169	30 – 40
Thumb base	Erbium-169	30

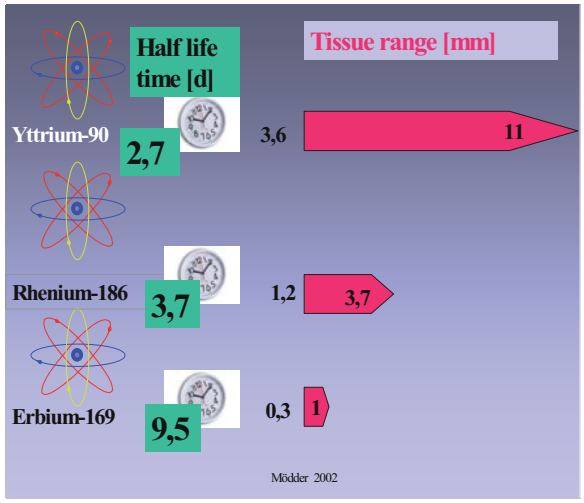

Fig. 29.1. Radioisotopes for radiosynoviorthesis

The physical characteristics of these radioisotopes are shown in Fig. 29.1. Proven dosages are listed in Table 29.1. These radiopharmaceuticals are β-emitters in colloidal suspensions.

Other radiopharmaceuticals rarely used for RSO are dysprosium-165 ferric hydroxide, holmium-166 hydroxyapatite and samarium-153 hydroxyapatite.

29.4 Mechanism of Action

"Synovitis is the villain of the drama" (Mannerfeldt), in rheumatic diseases causing brutal destruction of cartilage, bone, tendons and ligaments correlated with pain, swelling and loss of function. After intra-articular administration the radioactive particles in colloidal form are taken up by phagocytosis in synovial macrophages. A particle size of about 5 ± 10 nm is essential to avoid leakage and provide homogenous distribution on the surface of the synovium. β-radiation leads to coagulation necrosis, sclerosis and fibrosis of the synovial tissue including vessels and pain receptors, resulting in reducing effusion, swelling and pain of the joint. Due to the fact that cartilage has no ability to phagocytose, this tissue is not a target for the radiation effects (Ishido 1923).

The remark "synovitis is the villain of the drama" is not only valid for rheumatic diseases but also for osteoarthritis (activated arthrosis). Arthrosis with typical joint space narrowing as a result of cartilage defects is not associated with pain because cartilage has no nerves and vessels. Only after detritus leads to synovitis does simple arthrosis escalate to inflammation (activated arthrosis = osteoarthritis) with pain, swelling and effusions (Otte 2002; Mödder 2001a; Mödder 2006). The rather good effects of RSO in osteoarthritis (i.e., knee joint) will be lacking if mechanical problems such as severe instability and axe deviation predominate.

Simultaneous intra-articular injection of corticosteroids (i.e., triamcinolone hexacetonide or triamcinolone acetonide) is recommended because this might reduce local inflammation due to radionuclide instillation and prolong residence time of the radiopharmaceutical agent in the joint (11). An additional reason is the reduction of the often superposed layer of oedema on the synovium so that the thin film of radioisotopes gets closer to the destructing pannus – resulting in improvement of the effect of RSO.

29.5 Side Effects

Early: Temporarily increased synovitis (rapid relief by local application of ice)
Late: Local radionecrosis (rare)

29.6 Methodology

29.6.1 Patient Selection

Rheumatic patients need systemic treatment with antirheumatoid drugs because rheumatism is a systemic disease. If after at least 6 months a few joints do not show adequate improvement even after corticosteroid injections into the affected joints, these joints are selected for RSO, thus avoiding escalation of systemic therapy with its possible side effects. In monarthritis or oligoarthritis RSO could be the therapy of first choice, after failure of locally administered corticosteroids (Mödder 2001b; Fischer and Mödder 2005).

Orthopaedic patients should be selected after failure of local corticoid injection and/or ineffective conservative treatment. But also after plenty of surgical interventions RSO might improve the complaints of the patient, i.e., after total knee replacement (Mödder and Mödder-Reese 2001) or effusions after arthroscopy. Some authors recommend RSO after arthroscopy as a routine method to improve results (Kerschbaumer and Herresthal 1996; Thabe 1997). The time interval between arthroscopy or joint surgery (i.e., villonodular synovitis) and RSO should be planned as (4–)6 weeks.

29.6.2 Diagnostic Studies Prior to RSO

- Medical history, clinical inspection, examination of joint function.
- *X-ray images* provide basic information about the joint.
- *Ultrasound study* evaluates joint space, synovial structure and thickness and extent of effusion, and assesses tenosynovialitis or rotator cuff tear (shoulder). Ultrasound is obligatory prior to performing RSO to rule out a Baker's cyst (Fig. 29.2).
- *Multiphase scintigraphy* with ^{99m}Tc-MDP (or similar radiopharmaceuticals) is the best diagnostic tool for detecting and demonstrating inflammation of the synovium, thus – including findings of the clinical examination – selecting joints for RSO. In the first step (10 min p.i.) *soft tissue scintigraphy* detects the degree of active inflammation of synovium. In the second step (3 h p.i.) *bone scintigraphy* assesses the bone involvement in the painful process. The study reveals nearly indispensable information in activated arthrosis (osteoarthritis) and gives the best overview over multiple joint involvement especially in (also seronegative) polyarthritis (Mödder 2001a) (Figs. 29.3, 29.4).
- Magnetic resonance imaging might be suitable for additional information in a few patients (i.e., bone oedema, femur head necrosis).

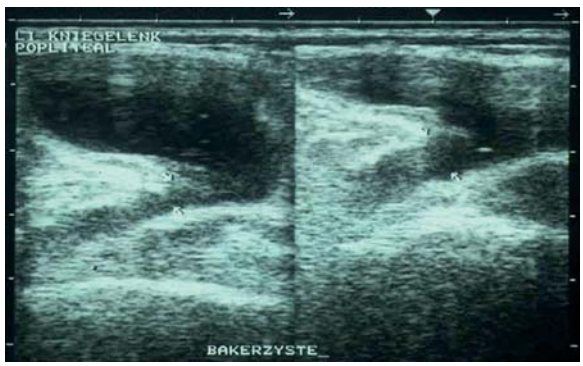

Fig. 29.2. Ultrasound of a Baker's cyst (transverse). Check for valve mechanism. *Left* The connecting duct between the knee joint (*below*) and Baker's cyst is seen. *Right* By soundhead pressure the cyst is decreased in size and the duct dilates. There is no valve mechanism

Fig. 29.3. The hands as the "visiting card" of the rheumatic patient. Soft tissue scintigram with ^{99m}Tc-MDP shows a typical pattern in psoriatic arthritis

29.6.3 Performance of RSO

29.6.3.1 Joint Puncture

A suitable room and strict asepsis are necessary. A good puncture technique is essential (for details see Mödder 2001a). The best puncture technique for the knee joint is shown in Fig. 29.5.

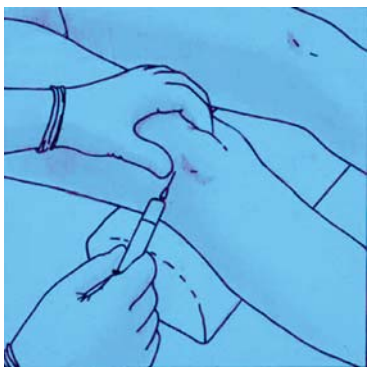

Fig. 29.5. Injection technique for the knee joint. Beware of injecting beside the ligamentum patellae with the patient in the sitting position, because then there is the danger of injecting yttrium-90 into the crucial ligaments or into Hoffa's fat body

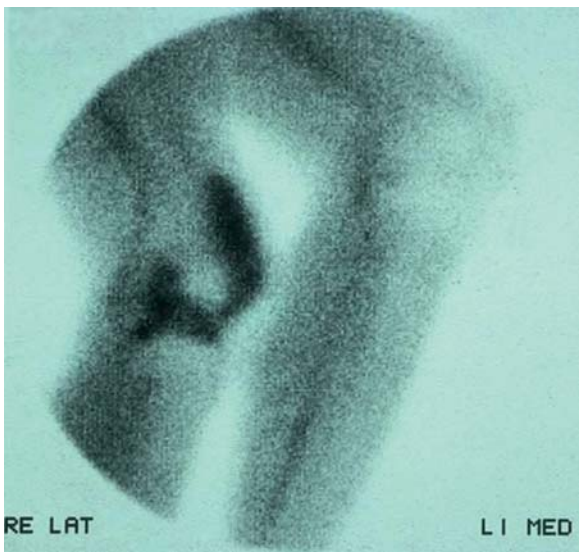

Fig. 29.4. Non-specific but highly sensitive synovitis – typical increased accumulation above the right knee joint in a patient with knee osteoarthritis. In rheumatoid arthritis the scintigram would look identical

29.6.3.2 Fluoroscopy

Apart from the knee, all joints have to be punctured for RSO by fluoroscopy and often by arthrography. Dye distribution predicts the distribution of radionuclide which is injected immediately afterwards. Using this procedure perfect needle position in the cavity of the joint is ensured (Fig. 29.6a, b).

Examples of the importance of fluoroscopic control for an absolutely exact injection technique are given in Figs. 29.7 and 29.8.

Figure 29.9 illustrates (a) a soft tissue scintigram, (b) an arthrogram and (c) a distribution scintigram as a proof for a perfect performance.

29.6.3.3 Radiation Safety Considerations

For the patient: Very late radiation induced stochastic hazards have not been observed (Vuorela et al. 2003). The effective dose to the whole body is estimated to be 30 times lower than in iodine-131 therapy of benign thyroid diseases (Manil et al. 2001).

For the personnel: To avoid high radiation exposure for the fingers during preparation and administration of yttrium-90 radiation, protection has to be provided by use of acrylic syringe protectors, nitrile or vinyl gloves, β-fingerdosimeters, etc. (Brenner 2006) (Fig. 29.10).

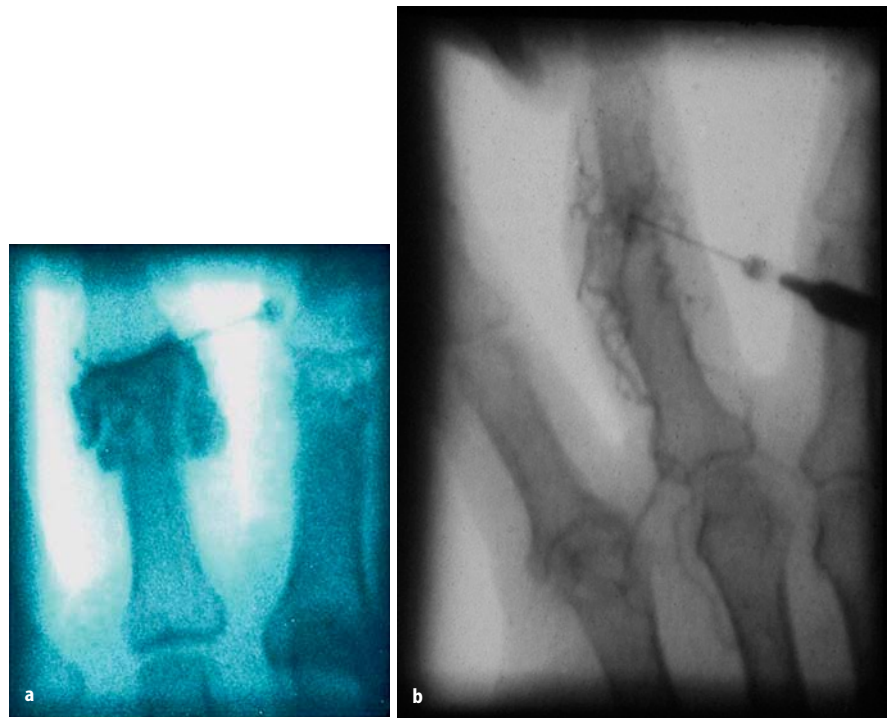

Fig. 29.6. a Arthrogram after perfect injection into a proximal interphalangeal joint (PIP) joint. **b** Arthrogram of a PIP joint. Intra-articular position of the needle, but *not in the cavity*. The contrast medium is injected into a villus with transportation by vessels. If this occurred with injection of erbium-169, it would be followed by side effects

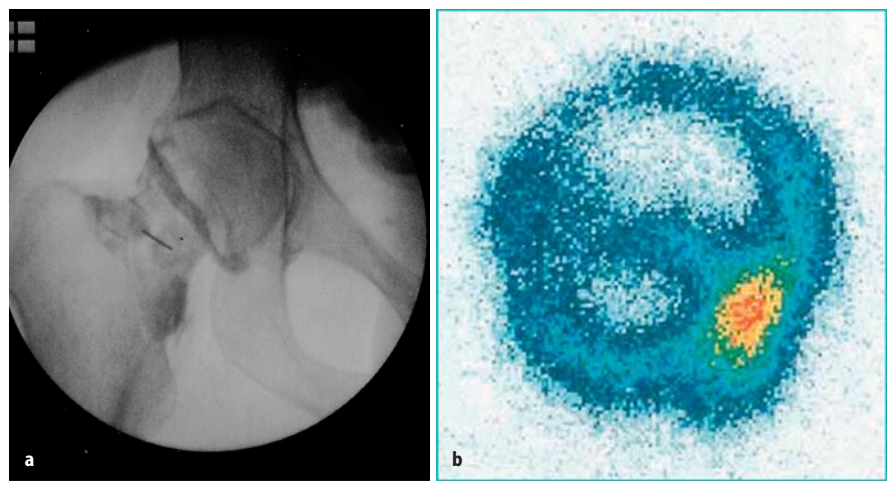

Fig. 29.7. a Arthrogram of a hip joint. The image shows the perfect and safe needle position. Beware of injecting into the joint space as usually recommended! You would risk destroying the ligamentum capitis femoris and thus cause femur head necrosis. **b** Distribution scintigram after injection of rhenium-186 colloid into the hip joint

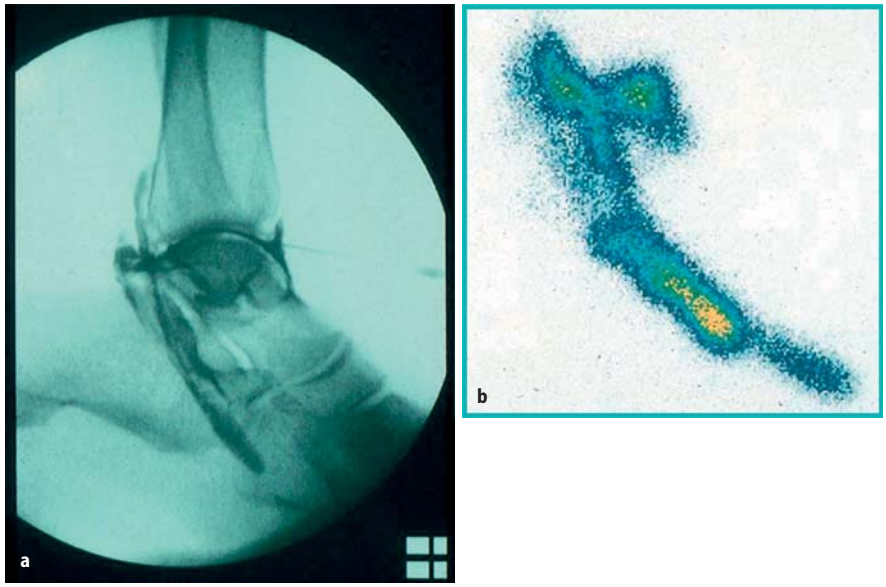

Fig. 29.8. a Arthrogram during RSO of ankle joint. Also a peroneal tenosynovialitis is involved in the psoriatic process. **b** The distribution scintigram demonstrates distribution of rhenium-186 within the ankle joint and within the peroneal sheet, indicating a good RSO effect for both structures

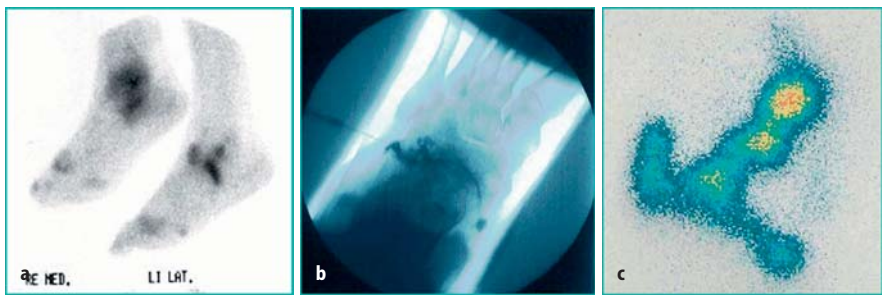

Fig. 29.9. Patient with rheumatoid arthritis was submitted for RSO of the left ankle. **a** Soft tissue scintigram detected no inflammatory involvement in the ankle but in the talonavicular, subtalar and calcaneocuboid joint. **b** Arthrogram after injection in the calcaneocuboid joint. **c** Distribution scintigram demonstrating perfect distribution in all joints marked in the diagnostic scintigram (**a**)

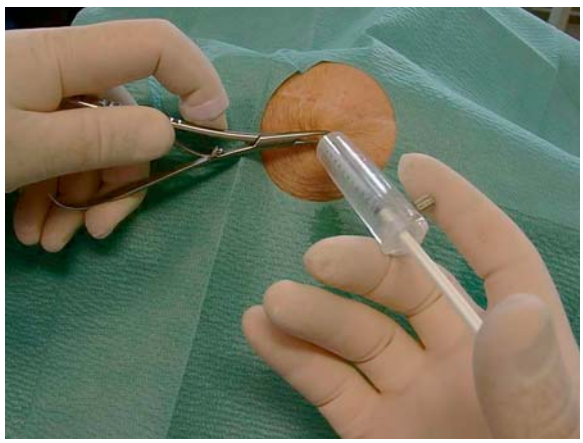

Fig. 29.10. Radiation protection for the RSO performing doctor: sterile gloves, forceps, and finger ring dosimeter (see text)

29.6.4 After RSO/Follow-up

- *A distribution scintigram* confirms the appropriate intra-articular distribution of the radiopharmaceutical. Scintigraphy is enabled after use of yttrium-90 by its *Röntgenbremsstrahlung*, after use of rhenium-186 by its gamma portion (140 keV). After the use of erbium-169 no scintigram is available.
- The joint has to be immobilized to avoid necrosis of injection channel or skin caused by reflux and to avoid transport of radioactive particles through the lymphatic vessels (leakage). A splint is required for 48 h. After removal of the splint the joint should be treated with care for 1 week, but then the patient should go into training of the joint and muscles.
- In our experience, the first *follow-up* is recommended about 6 months after RSO, or of course earlier when problems (reactive inflammation, suspected infection, swelling of Baker's cyst) occur. Clinical evaluation, possibly ultrasound scans of the joints and also checking that sufficient active joint training has been done, belong to the basic control steps.

Sometimes an effusion fluid or a Baker's cyst has to be punctured before the development of the definitive effect of RSO. Clinical examination and ultrasound scans, sometimes control of scintigraphy, should take place 12 months after treatment.

29.7 Repetition of Radiosynoviorthesis

Radiosynoviorthesis should be performed at an early stage of the disease, when cartilage damage is minimal. Reasons for non-satisfactory results of RSO might be, e.g., rapidly recurrent effusions, strongly developed thickness of synovial villus, enlargement of the joint cavity by additional cavities (Baker's cyst, bursa subdeltoidea), unfavourable Larsen stage, etc. Then a repetition of RSO (Re-RSO) may be indicated, normally not earlier than 6 months after the previous procedure (Mödder 2001a). Re-RSO of the wrist will not only treat the proximal wrist joint but will additionally reach the intercarpal compartments. And after total knee replacement the deeper layers of polyethylene disease can be attacked by Re-RSO. A new fraction is more effective than a primarily enhanced dose (Pinkert 2006) (Fig. 29.11a, b).

29.8 Results

Response rates reported in an abundant literature range from about < 60 % to > 80 % for all joints, often with greater success for rheumatoid diseases than for osteoarthritis. Most of the studies relating to RSO in the last 40 years do not fulfil the criteria of modern evidence based medicine, but recently a number of well designed trials have been carried out in order to evaluate the efficacy of RSO. In a multicentre prospective study an improvement of 78 % without a significant difference in rheumatoid arthritis or osteoarthritis was found (Farahati et al. 1999). In a prospective study on rheumatoid arthritis, Göbel et al. (1997) found a significant improvement in terms of pain and swelling after 3 years and a reduced progression of radiological destruction compared to triamcinolone. More recently two prospective multicentre studies carried out under strict evidence based medicine criteria demonstrated a significant improvement (pain, swelling, joint mobility) for erbium-169 versus placebo (Kahan et al. 2004) and after 2 years for rhenium-186 versus high dose corticosteroid (Tebib et al. 2004).

In a recent study, Jahangier et al. (2005) drew unfavourable conclusions about the performance of RSO with yttrium-90. But it could be demonstrated that their conclusions were wrong because the results in fact provided evidence for the efficacy of RSO with yttrium-90 (Kampen and Czech 2006; Mödder and Langer 2006).

Kresnik et al. (2002) investigated the clinical outcome of radiosynoviorthesis in a meta-analysis including 2,190 treated joints. They found an overall response rate of 72.5 ± 17 %. In rheumatoid arthritis RSO was successful in 66.7 ± 15.4 %. There was a difference according to the Steinbrocker stages (Steinbrocker I: 72.8 ± 12.3 %; Steinbrocker II: 64 ± 17.3 %; Steinbrocker III and IV: 52.4 ± 23.6 %). The response rate in osteoarthritis was 56 ± 11 %, with better results in the case of

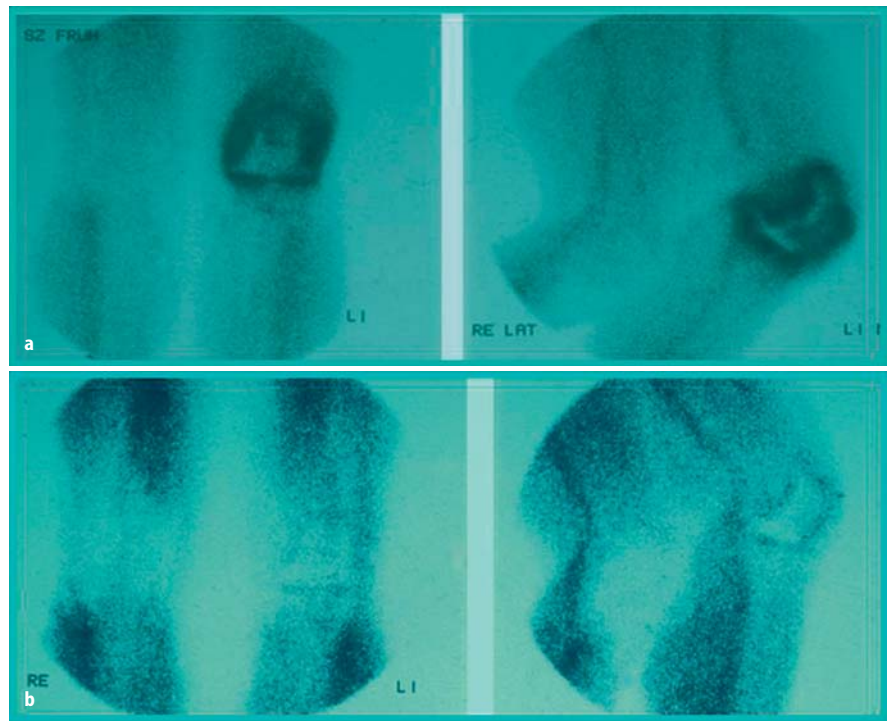

Fig. 29.11. a Prior to RSO: left knee joint with polyethylene disease, pain and recurrent effusions. **b** After RSO: improvement with regard to symptoms and scintigraphic findings

minimal radiological changes. Improvement in haemophilia and Willebrand's disease was 91 ± 4.3 %, and in pigmented villonodular synovitis it was 77.3 ± 25.3 %.

The conclusion of this study was that radiosynoviorthesis provides better results in rheumatoid arthritis than in osteoarthritis. Minimal or moderate changes according to Steinbrocker stages I and II respond better to radionuclide therapy than do stages III and IV. Deformed or unstable joints might fail treatment and therefore surgical interventions should be considered. Close cooperation with orthopaedists and rheumatologists is necessary in the consideration of RSO for each patient to ensure optimal medical care.

References

Brenner W (2006) Grundlagen und Technik der Radiosynoviorthese. Der Nuklearmediziner 29:5 – 14

Clunie G, Fischer M (2003) EANM procedure guidelines for radiosynovectomy. Eur J Nucl Med 30:BP12–BP16

Delbarre F, Cayla J, Menkes CJ, Aignan J, Roucayrol JC, Ingrand J (1968) La synoviorthèse par les radioisotopes. Presse Med 76:1045 – 1050

Farahati J, Kenn W, Körber C, et al. (1999a) Zeit bis zur Remission nach Radiosynovektomie (RSV). Nuklearmedizin 38:254 – 255

Farahati J, Reiners Chr, Fischer M, Mödder G, Franke C, Mahlstedt J, Sörensen H (1999b) Leitlinie für die Radiosynoviorthese. Nuklearmedizin 38:254 – 255

Fellinger K, Schmid J (1952) Die lokale Behandlung der rheumatischen Erkrankungen. Wiener Z Inn Med 33:351 – 363

Fischer M, Mödder G (2002) Radionuclide therapy of inflammatory diseases. Nucl Med Commun 23:829 – 831

Göbel D, Gratz S, von Rothkirch T, Becker W (1997) Chronische Polyarthritis und Radiosynoviorthese: Eine prospektive, kontrollierte Studie der Injektionstherapie mit Erbium-169 und Rhenium-186. Z Rheumatol 56:207 – 213

Ishido C (1923) Über die Wirkung des Radiothoriums auf die Gelenke. Strahlentherapie 15:537 – 544

Jahangier ZN, Jacobs JWG, Lafeber FPJG, Moolenburgh JD, Swen WAA, Bruyn GAW, Griep EN, ter Borg E-J, Bijlsma JWJ (2005) Is radiation synovectomy for arthritis of the knee more effective than intraarticular treatment with glucocorticoids? Arthritis Rheumatism 52(11):3391 – 3402

Kahan A, Mödder G, Menkes CJ, et al. (2004) 169-Erbium-citrate synoviorthesis after failure of local corticosteroid injection to treat rheumatoid arthritis-affected finger joints. Clin Exp Rheumatol 22:722 – 726

Kampen WU, Czech N (2006) Is radiation synovectomy of the knee more effective than intraarticular treatment with glucocorticoids? A comment on the article of Jahangier et al. Arthr Rheum 56:385

Kampen WU, Brenner W, Kroeger S, Sawula JA, Bohuslavizki KH, Henze E (2001) Long-term results of radiation synovectomy: a clinical follow-up study. Nucl Med Commun 22:239 – 246

Kerschbaumer F, Herresthal J (1996) Arthroskopische Synovektomie und Radiosynoviorthese. Z Rheumatol 55:388 – 393

Kresnik E, Mikosch P, Gallowitsch HJ, Jesenko R, Just H, Kogler D, Gasser J, Heinisch M, Unterweger O, Kumnig G, Gomez I, Lind P (2002) Clinical outcome of radiosynoviorthesis: a meta-analysis including 2190 treated joints. Nucl Med Commun 23(7):683 – 688

Lengsfeld P, Pinkert J, Voth M, Yanch J (2005) Comprehensive Rationale for Doses of Y-90, Re-186, and Er-169 for Radiosynoviorthesis (RSO) 43. Gemeinsame Jahrestagung der Deutschen, Österreichischen und Schweizerischen Gesellschaften für Nuklearmedizin, Basel, Nuklearmedizin 44:A84

Manil L, Voisin P, Aubert B, Guerreau D, Verrier P, Lebegue L, Wargnies JP, Di Paola M, Barbier Y, Chossat F, Menkes CJ, Tebib J, Devaux JY, Kahan A (2001) Physical and biological dosimetry in patients undergoing radiosynoviorthesis with erbium-169 and rhenium-186. Nucl Med Commun 22:405 – 416

Mödder G (2001a) Radiosynoviorthesis. Involvement of nuclear medicine in rheumatology and orthopaedics. Warlich, Meckenheim

Mödder G (2001b) Radiosynoviorthese, ^{224}Radiumtherapie und Röntgenstrahlentherapie. In: Zeidler H, Zacher J, Hiepe F (eds) Interdisziplinäre klinische Rheumatologie. Springer, Berlin Heidelberg New York, pp 361 – 377

Mödder G (2006) Radiosynoviorthese bei aktivierter Fingerpolyarthrose. Der Nuklearmediziner 29:21 – 27

Mödder G, Langer H-E (2006) Evidence of the efficacy of radiation synovectomy with yttrium-90: comment on the article by Jahangier et al. Arthritis Rheum 56:386

Mödder G, Mödder-Reese R (2001) Radiosynoviorthese nach Knieendoprothesen: Effektive Therapie bei "Polyethylene disease" Der Nuklearmediziner 2(24):97 – 103

Otte P (2000) Der Arthrose-Prozeß. Gelenkerhaltung – Gefährdung – Destruktion, Teil 1: Osteochondrale Strukturen. Rheumatologie Orthopädie 11. Novartis Pharma Verlag, Nürnberg

Tebib JG, Manil LM, Mödder G, Verrier P, et al. (2004) Better results with rhenium-186 radiosynoviorthesis than with cortivazol in rheumatoid arthritis (RA): a two-year follow-up randomized controlled multicenter study. Clin Exp Rheumatol 22:609 – 616

Thabe H (1997) Operative Behandlungskonzepte, Kapitel 5.3. In: Thabe H (ed) Praktische Rheumatherapie. Chapman & Hall, Weinheim

Vuorela J, Sokka T, Pukkala E, Hannonen P (2003) Does yttrium radiosynovectomy increase the risk of cancer in patients with rheumatoid arthritis? Ann Rheum Dis 62:251 – 253

Miscellaneous

30

J. Kropp

30.1 Polycythemia Vera

30.1.1 Introduction and Historical Perspective

Polycythemia vera (Vaquez-Osler disease) – PCV – was first described in the year 1892 by Vaquez. Today the understanding is that PCV is a clonal neoplastic disease with the proliferation of erythrocytes. Together with chronic myelocytic leukemia, osteomyelofibrosis (OMF) and thrombocythemia, it is included in the group of myeloproliferative diseases (MPD). All the bone marrow elements (erythrocytes, megacaryocytes, granulocytes, and fibroblasts) are involved in the hyperplasia but erythropoiesis is the dominant factor. Also extramedullary hematopoiesis is possible. Hypervolemia, increased cardiac output, hyperviscosity and the resultant impaired blood flow are the reasons for most clinical manifestations.

Polycythemia vera is a rare disease with an incidence of 2 out of 10^5 per year, and at the onset of the disease most patients are about 60 years of age. After the proliferative phase of PCV a stable level of the disease develops in which even normal hematocrit levels are possible without specific treatment. The reduced erythropoietic activity often combined with the still enhanced thrombo- and granulopoiesis is addressed as the "spent phase." Finally the myeloproliferative disease changes into a myelofibrosis which is almost indistinguishable from a primary osteomyelofibrosis. In the final stage of PCV as well as in all other MPDs, a blastic transformation may occur which is similar to the blastic boost of a chronic myelocytic leukemia (CML).

The cause of the disease has not yet been discovered but there are hints of a mutation in the domain of the erythropoietin receptor. For several years it has been known that in PCV erythroid progenitor cells present with an abnormal sensitivity against several cytokines such as the insulin-like growth factor (Roberts and Smith 1997), interleukin-3, granulocyte-macrophage colony-stimulating factor (GM-CSF) and stem cell factor (Dai et al. 1994). Moliterno described a diminished expression of the thrombopoietin receptor (Moliterno et al. 1998). Also an increased expression of Bcl-X – an inhibitor of apoptosis – was demonstrated in patients with PCV (Silva et al. 1998).

The first clinical use of phosphorus-32 in the chemical form of sodium-hydrogen-phosphate (sodium orthophosphate, $Na_2H^{32}P0_4$) was performed over 60 years ago by Lawrence at Berkeley, California. The radiopharmaceutical was used in this work to treat leukemia (Lawrence 1940). On the first occasion it was used in 1939, patients with PCV were treated with P-32. Until that date therapy of PCV consisted of blood-letting, administration of acetylphenylhydrazine, Fowler's solution or external beam radiation of the long tubular bones and the spleen (Berlin 2000).

Today radioactive phosphorus-32 is used for the treatment of patients with PCV (Osgood 1968), for pain palliation in patients with bone metastases (McEwan 2000; Silberstein 1993) as well for other former indications which no longer play a role today.

30.1.2 Radiopharmaceuticals Employed

30.1.2.1 Physical Chemistry

Phosphorus-32 is a pure β-emitter with a half-life of 14.3 days. The average energy of the emitted β-particles at 0.695 is relatively low, the maximum energy is 1.71 MeV and the average range in tissue is about 3 mm, with a maximum of 8 mm (Harbert 1987; Silberstein 1979).

Radiophosphorus for the therapy of PCV is used in the chemical form of sodium-hydrogen-phosphate (sodium orthophosphate, $Na_2H^{32}P0_4\ 2 \times H_2O$).

30.1.2.2 Radiopharmacokinetics and Dosimetry

Ionic P-32 enriches in the form of orthophosphate in tissues with increased turnover of phosphorus (proliferative and protein synthesizing cells) and is taken up in the nucleoproteins of the nucleus of blood stem cells. Autoradiography has revealed that the uptake of radiophosphorus is proportional to the intensity of cell division.

Therefore there is a preferential uptake in the bone marrow, lymph nodes and spleen as well as in the case of increased proliferation of early stages of the red cell line. The biologic effect of P-32 is based on the direct action of the radiation (DNA strand breaks), DNA incorporation as well as on the biochemical effect of the released stable sulfur, which is not normally contained in nucleic acids (Silberstein 1979).

According to Nilsson, a predominant suppression of the hyperproliferating cells occurs and to a lesser extent a destruction of cells (Murray and Ell 1994). The uptake in the DNA diminishes cell proliferation but can also induce neoplastic disease (Sostre 1995). Six weeks after administration of 240 MBq P-32 in patients with PCV, Blomgren et al. found a decrease of peripheral lymphocytes of 20%; mainly B cells and natural killer cells were involved followed by HNK-1 cells and T cells. The authors concluded that the lymphocytes which are mature in the bone marrow are preferentially involved in the P-32 therapy (Blomgren et al. 1990). Two hours after i.v. injection an equilibrium is reached between intra- and extravascular space. P-32 shows a biexponential elimination from the blood. The fast component has a biological half-life of 1.7 ± 0.7 days followed by a slow component with a half-life of 22.5 ± 5.9 days for blood and 0.8 ± 0.5 and 20.0 ± 5.1 days for plasma. Whole body excretion is monoexponential with a half-life of 39.2 ± 4.5 days. For the biological half-life in the bone marrow, values of 7 – 9 days are reported (Murray and Ell 1994), whereas the half-life in the bone of the pelvis is about 9 days and in the sternum 7 days. Six to 24 h after injection the radioactivity in the bone increases four- to sixfold compared to muscle or fat tissue as well as the skin. This quotient further increases to six- to tenfold after 3 days. This also holds for the liver and spleen. About 70% of the administered activity disintegrates within the body (Sostre 1995). Five to 10% of the activity is eliminated by the kidneys within 24 h; the cumulative urinary excretion is 20 – 50% (Büll et al. 1999). The average bone marrow dose is reported to be 24 rad/mCi (0.54 – 1.35 cGy/MBq), corresponding to an effective equivalent dose of 2.2 mSv/MBq (Bareford 1991). From a total radiation dose of the bone of 24 rad/mCi (6.48 mGy/MBq), about 10 rad/mCi (2.7 mGy/MBq) is to the trabecular bone, 13 rad/mCi (3.51 mGy/MBq) to the bone marrow and about 1 rad/mCi (0.27 mGy/MBq) to the cortical bone (Silberstein 1979). According to Sostre, beyond a dose to the bone marrow of 1 Gy, increasing numbers of neoplastic diseases may occur (Sostre 1995). A blood-letting before the administration of P-32 of 400 – 700 ml should serve as a stimulation to cell regeneration and to increase the amount and speed of the uptake of P-32 into the precursor blood cells.

30.1.3 Clinical Indications

Most patients are older than 60 years at first diagnosis (4th to 7th decades) and males are more often involved than females. Patients are striking by their rubeosis facies (Osler 1903) often combined with a cyanosis of the lips as well as the extremities. Vertigo, headache, tinnitus and pruritus are often reported. Spleno- and hepatomegaly are prominent symptoms after a longer course of the disease. Berlin reported that more than 75% of patients present with splenomegaly and about 40% with hepatomegaly (Berlin 1975). An increased tendency for bleeding may occur into the GI tract, the uterus, within the brain and the conjunctiva.

Frequent thrombosis and ulcers of the stomach have also been observed (Table 30.1).

Often an extension of the bone marrow in the leg and arms can be noticed, e.g., in bone marrow scintigraphy (Fig. 30.1a, b).

Incidents of thromboembolism are frequent, in particular cerebrovascular (40%) or hemorrhagic (6%) events, which are the most severe complications and the most frequent cause of death (Berk et al. 1986; Chievitz and Thiede 1962; Edwards and Cooley 1970). Thomas et al., using Xe-133 measurements of the cerebral blood flow (CBF) in patients with PCV and hematocrit (HCT) levels of between 53% and 62%, found a severe reduction in CBF which was reversible after normalization of the hematocrit level (Thomas et al. 1977). In other studies of the global and regional CBF also with Xe-133 at rest and under stimulation with acetazolamide, in nine out of ten cases regional disturbances of the CBF were found (Franke et al. 1993). Also an increased risk of hemorrhagic events, epistaxis, ecchymosis and menorrhagia were more frequently found and surgical and dentistry interventions showed an excessive morbidity and mortality. Most of the complications consisted of uncontrollable bleedings or thromboses and there is a connection between the frequency of complications and the HCT value, where an HCT > 52% is associated with a sevenfold increased risk of experiencing such an incident. In addition, the

Table 30.1. Percentage abundance of clinical symptoms in PCV

Headache	48
Fatigue	47
Pruritus	43
Vertigo	43
Sweating	33
Visual disturbance	31
Loss of body weight	29
Paresthesia	29
Dyspnea	26
Joint symptoms	26
Upper abdominal pain	24

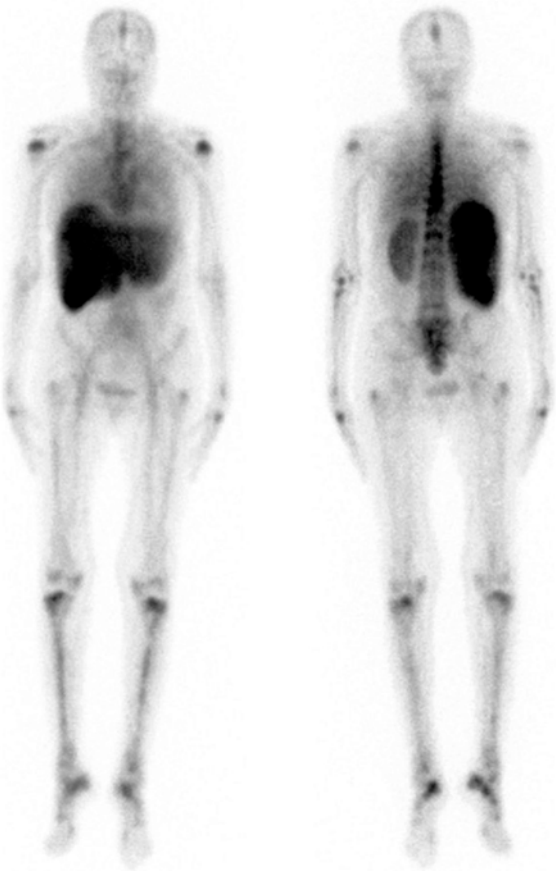

a

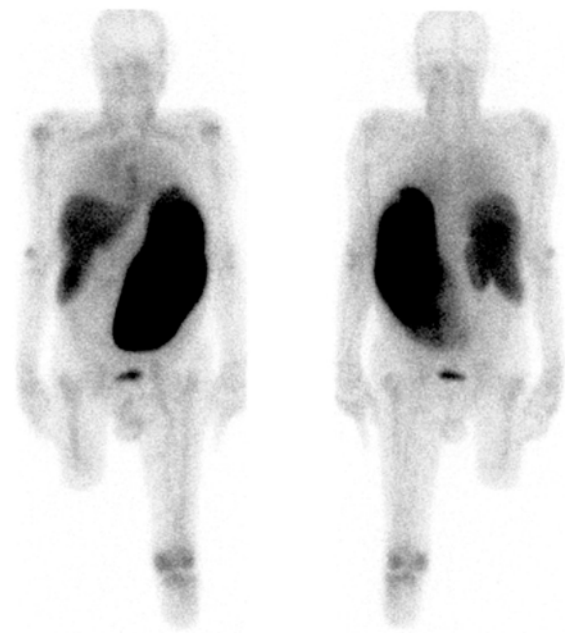

b

Fig. 30.1. a Seventy-year-old patient with PCV. Whole body scintigraphy with a Tc-99m-labeled antigranulocyte antibody (BW 250/183) in the ventral (*left*) and dorsal (*right*) view. Hepatomegaly, decrease of the mass of the bone marrow with extension in the extremities as a sign of enhanced erythropoiesis. **b** Seventy-three-year-old patient with PCV in the end stage with OMF. Whole body scintigraphy with a Tc-99m-labeled antigranulocyte antibody (BW 250/183) in the ventral (*left*) and dorsal (*right*) view. High grade spleno- and hepatomegaly, and complete destruction of the bone marrow with subsequent blood formation in the spleen and liver

time period between the preoperative normalization of the hematocrit level is of importance where the risk of experiencing a complication is almost comparable to that in healthy normal subjects if this period is more than 4 months. In a small cohort of patients gout may occur whereas an isolated hyperuricemia is often symptomless. Elevated levels of uric acid can be found in about 70% of patients (Hoffman and Wasserman 1979). Pruritus can be found frequently, which might be treated in severe cases with antihistamine (Weick et al. 1982).

30.1.4 Diagnosis of PCV

30.1.4.1 Laboratory Values

An increased hematocrit level can usually be found in PCV patients. Erythrocyte and thrombocyte counts are severely increased, whereas leukocytes are increased only moderately. If an increased hematocrit level is found, the next and leading diagnostic step is evaluation of the total mass or volume of the erythrocytes, perhaps by radioactive labeled erythrocytes and/or albumin. In patients with severe PCV large blood volumes are distributed in dilated veins so that equilibrium is reached only very slowly and blood samples drawn even after 1 h may underestimate the dilution which is noticed in studies to determine the volume of erythrocytes. If the hematocrit level is over 60% in male and >57% in female patients, an increase in the volume of erythrocytes is obvious and a measurement of this volume can be skipped. The normal values for the total volume of erythrocytes (not to be confused with the mean volume of erythrocytes, MCV) are about 30±2.5 ml/kg BW for female, 25±2.5 ml/kg BW for male patients, and 40 ml/kg BW for newborns, or they can be calculated using height (H) and weight (W) of the patients with $8.6 \times H + 18.6 \times W - 830$ (ml) for male and $7.49 \times H + 14.32 \times W) - 603$ (ml) for female patients (Geigy Scientific Tables).

In the differential white blood count there are signs indicating an increased regeneration of erythrocytes (polychromasia and poikilocytosis), anisocytosis, left-

ward shift of the granulopoiesis and an increased number of eosinophilic and basophilic granulocytes. The reticulocyte counts are frequently increased. Also pathologic increased values of the index of the alkaline leukocytic phosphatase are found frequently in patients with PCV (about 70 % of the patients), increased vitamin B_{12} (about 40 %), if the disease is untreated increased binding capacity for B_{12} (70 %), and increased uric acid. The oxygen saturation is increased beyond 92 % in contrast to hypoxia related polyglobuly.

The estimation of the arterial blood gases therefore should be performed in the frame of the diagnostic work-up.

30.1.4.2 Differential Diagnoses

A relative polycythemia (spurious polycythemia, polycythemia rubra hypertonica, stress induced erythrocytosis, i.e., Gaisböck's disease) is present if a normal volume of the erythrocytes is combined with a reduction of the plasma volume which might be due to dehydration (often associated with smoking and abuse of alcohol). Relative erythrocytoses are found on combustion, erythropoietin abuse (doping), diarrhea and under diuretic medication. Polyglobuly (formerly named secondary polycythemia), which is connected with an increase in the volume of erythrocytes, is mainly due to an increased formation of erythropoietin. Erythropoietin is enhanced in polyglobuly and decreased in PCV so that the verification of an increased serum level of erythropoietin definitively excludes a PCV. Hypoxia due to lung or cardiovascular diseases such as intracardiac shunts, abnormal hemoglobulin conditions such as carboxy hemoglobulinemia, an abnormal affinity of hemoglobulin to oxygen, residence at altitude and hypoventilation syndromes are stimuli of an increased formation of erythropoietin as well as several kidney and tumor diseases (Berlin 1975). Therefore in cases with polyglobuly a morphologic investigation of the kidneys should be performed.

But also a PCV in the case of a normal hematocrit level is possible; this is the case if there is simultaneously an increased mass of the erythrocytes as well as an increased plasma volume. Therefore, particularly if other suspicious findings are present, e.g., clarification of a thrombosis in the presence of a leukocytosis, one should take into consideration a masked PCV (inapparent PCV) (Lamy et al. 1997). Possible causes of an increased hematocrit level are metabolic and hormonal diseases, e.g., Cushing's syndrome as well as tumor diseases, e.g., hepatocellular carcinoma and hemangioblastoma of the cerebellum.

For the diagnosis of chronic myeloproliferative diseases (CMD), the recommendations of the "Polycythemia Vera Study Group" (PVSG) are used. Besides the delineation against reactive erythrocytoses a differentiation of PCV within the group of CMD is very important, which is often very difficult because borderline cases are frequent. The diagnostic criteria of the PVSG are presented in Table 30.2 and the so-called Rotterdam criteria in Table 30.3.

A PCV is assumed if criteria A1–3 or A1+A2 and two criteria of category B are present. Although the criteria of the PVSG are more widely used, the criteria of the European Working Group are also shown because in a single case they allow a more precise delineation of reactive thrombocythemias (Table 30.3). If only criteria A1–A3 are fulfilled, a PVC in an early stage can be assumed (idiopathic erythrocytosis). A1+A2+A3 and any B criteria prove a PCV.

Table 30.2. Criteria of the PVSG for diagnosis of a PVC. *ALP* alkaline leukocyte phosphatase

A1 Increased mass of erythrocytes Male ≥ 36 ml/kg BW Female ≥ 32 ml/kg BW	**B1** Thrombocytosis > 400,000/L
A2 Normal oxygen saturation > 92 %	**B2** Leukocytosis > 12,000/L No fever, no infection
A3 Splenomegaly	**B3** ALP score > 100 *Or* Vitamin B_{12} > 900 ng/L *Or* Increased B_{12} binding capacity > 2,200 ng/L

Table 30.3. Criteria of the European Working Group for diagnosis of a PVC

A1 Increased mass of erythrocytes Male ≥ 36 ml/kg BW Female ≥ 32 ml/kg BW	**B1** Thrombocytosis > 400,000/L
A2 No sign of secondary polycythemia	**B2** Granulocytosis > 10,000/L
A3 Histology of the bone marrow with increase of: a) Mature and large megakaryocytes arranged in nests b) Fibers of reticulin c) And/or cellularity	**B3** ALP score > 100 without explaining reactive causes
	B4 Splenomegaly
	B5 BFU-E without erythropoietin detectable

30.1.5 Therapy of PVC

30.1.5.1 Antiproliferative Therapy with Phosphorus-32

The first therapies with radiophosphorus were performed in patients with leukemia in the late 1930s, whereas our own experience has been gained since 1960. According to several reports, the number of therapies in patients with PCV increased during the 1970s but decreased during the 1980s after several papers in which an increased rate of leukemia after P-32 therapy was reported. But today this form of therapy is more and more of interest especially in elderly patients according to some publications in which an obvious advantage and a greater significance of P-32 therapy in comparison to chemotherapy has been reported (McDougall 2000; Najean and Rain 1997a; Tesselaar et al. 1996). The following reasons are emphasized for this conclusion: P-32 is easy to administer (simple i.v. injection), there are no problems with compliance, no side effects, fewer blood counts required compared to chemotherapy, a very high success rate, and life expectancy is not influenced today by side effects.

30.1.5.2 Administration of $Na_2H^{32}PO_4$

Wassermann recommended the following procedure for the therapy of PCV with P-32 (Sostre 1995):

- Preceding the radiophosphorus therapy blood-letting should be performed to achieve a hematocrit level of 42 – 47 %.
- An initial radioactivity of 74 – 111 MBq (2 – 3 mCi/m^2 body surface) should be injected intravenously but the total radioactivity should not go beyond 185 MBq because then a bone marrow dose of > 1 Gy is attained.
- Determination of blood counts every 3 – 4 weeks after the administration.
- If again a hematocrit level of over 47 % is reached and the leukocyte and thrombocyte counts are not reduced by more than 25 % after 12 weeks, one should perform another blood-letting and a second therapy with radiophosphorus.
- The total activity should be 25 % higher than for the first one.
- These therapy cycles are reiterated until an adequate therapeutic effect is obvious, but the individual activity should not exceed 260 MBq (7 mCi).
- In this time period, frequent blood-lettings should be performed if needed to achieve a hematocrit level of below 47 % even if a blood-letting of about 500 ml every 2nd to 3rd day is required.

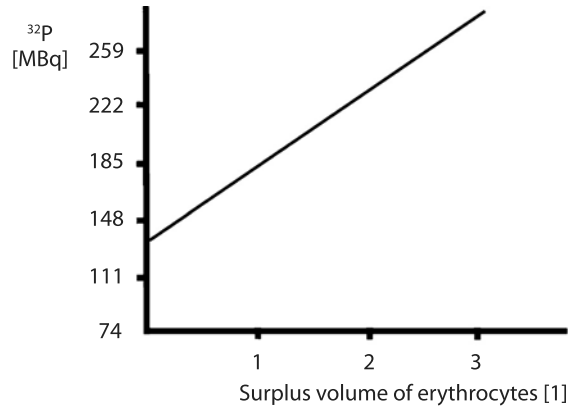

Fig. 30.2. Nomogram to read the dose of P-32 needed for the therapy of PCV adapted to the surplus volume of erythrocytes

- No further therapies should be performed despite a hematocrit level of above 47 % if the thrombocyte count is below 100×10^3/L or the leukocyte count is below 3×10^3/L (Roberts and Smith 1997; Silberstein 1979).
- In the case of remission, blood count controls should be performed every 2 – 3 months where remissions may last months through years.
- In the case of a failure of the radiophosphorus therapy, another therapy modality must be chosen.

The administration of the radioactivity must be strictly intravenous with thorough flushing of all lines. Also an oral administration is possible with a 1.3-fold higher activity compared to i.v. administration but a radiation dose to the GI tract should be considered.

The therapy activity can be administered as a single dose of 185 MBq or adapted to the surplus volume of erythrocytes because it can be assumed that the reduction of the number of erythrocytes is proportional to the applied activity. The required activity can be read in this case from a nomogram (Hume et al. 1966) as shown in Fig. 30.2.

In most cases of P-32 therapy, a previous blood-letting of 400 – 700 ml is performed. To avoid hypovolemic complications it might be combined with an infusion of a volume compensation fluid. Also infusion of plasma might be considered to avoid protein loss.

In a study initiated by the PVSG, 431 patients were enrolled in a randomized way into three arms: (1) blood-letting alone, (2) P-32 therapy, and (3) chemotherapy with chlorambucil.

The chemotherapy turned out to be the worst of the three (Berk et al. 1981), and was ceased particularly due to the high rates of secondary leukemias.

30.1.5.3 Therapy by Blood-Letting

The effect of a blood-letting consists of the induction of a chronic depletion of iron, which blocks the erythropoiesis. This therapy might be performed in adaption to the hematocrit level by repeating a blood withdrawal of 500 ml in each session to achieve a value below 47 %. If erythrocytes are separated during the withdrawal and the plasma reinjected, the volume may be increased up to 1,500 ml. The advantage of this therapy is the fast and initial effect and then the low frequency of repetition of the intervention. However, there are several reasons why a thrombocytosis might develop, which might worsen under this therapy modality.

30.1.5.4 Hydroxyurea

The drugs of choice in the inhibition of cell proliferation are hydroxyurea derivatives, which are non-alkylation substrates that selectively inhibit cells in the S-phase of the cell cycle, but according to recent publications they are associated with a higher incidence of leukemia (Tefferi and Silverstein 1998). With hydroxyurea (HU), the hematocrit level can be very effectively lowered, the number of leuko- and thrombocytes diminished and the splenomegaly and pruritus positively influenced (Donovan et al. 1984). HU shows a rapid effect at an initial dose of about 20 mg/kg BW, but frequent checks are necessary especially due to the possible leukopenia. The number of blood cells normalizes in about 80 % of patients within 12 weeks, but unfortunately there is no durable remission so that the therapy must follow an individual scheme. Frequently side effects are GI tract complaints and skin reactions, whereas stomatitis, and neuro- and liver toxicity, are rarely observed. Due to the leukemic risk, the indication must be very strict so that early cases of PCV should not be treated in this way.

One study enrolled 106 patients, of whom 53 were treated only with HU and the others by other modalities; in both groups an adequate control of the hematocrit level and number of thrombocytes within 12 weeks was achieved in 80 – 90 % of the patients (Berk et al. 1986).

Other drugs such as pipobroman (1,4-bis[3-bromopropionyl]piperazine), which has been used since the 1960s for the therapy of PCV (Najean and Rain 1997), are seldomly used, and the success and rate of side effects have been comparable to those in a group of patients treated with HU. Busulfan is another drug used and one study has reported a longer time period of remission, a slightly but significantly longer survival but more severe side effects (Zittoun 1986). Anagrelide is a new drug which has an unknown inhibitory effect on the poiesis of megakaryocytes and after 1 week a decrease in the number of thrombocytes. Because it has a vasodilatory effect, one side effect is a decrease in the blood pressure, and one must be careful in patients with heart failure. Also interferon (INF) is used in the therapy of PCV, but to date no sufficient data are present to evaluate its usefulness. A recently published review (Lengfelder et al. 2000) of a meta-analysis including 279 patients reported that in 82 % of the patients the frequency of blood-letting could be reduced, in 50 % a stable hematocrit value was achieved, in 45 % without an accompanying phlebothrombosis, in 77 % a decrease of splenomegaly, and in 81 % a disappearance of pruritus was achieved. It is assumed that there are no secondary neoplastic diseases connected with this therapy, which is a major advantage, although partly offset by severe side effects (25 % breaking off the therapy) and high costs. The long-term survival cannot as yet be specified.

30.1.5.5 Time Course, Aim of Therapy and Prognosis

The main aim of all therapy modalities is the immediate and long lasting reduction of the risk of vascular complications by decreasing the hematocrit values. Due to the relatively good prognosis of this neoplastic disease, also long lasting complications as well as the induction of secondary malignancies and myelofibrosis are of major importance. Average survival after the diagnosis depends on the therapeutic regimen. Patients with untreated PCV show only a short survival of about 1.5 years (Murray and Ell 1994), whereas with chemotherapy or P-32 therapy the average survival is 10 – 15 years. A therapy only by blood-lettings over some years is possible only in very few patients. Despite the numerous studies to date, a final and conclusive comparison of the several therapeutic regimens regarding the prognosis is not possible, which is mostly immanent to these studies and to discuss which would be beyond the scope of this chapter, already having been discussed elsewhere (Bredow et al. 2001).

In a recent publication (Najean and Rain 1997), the higher risk of leukemia, myelodysplastic syndromes or lymphomas was emphasized; in patients treated with P-32 this is about 10 % in the 10th year after diagnosis, with an increase of 30 % in the 20th year. The risk was not dose dependent. The risk of developing other tumors was 15 % 10 years after P-32 administration. Tumors of the gastrointestinal tract were not observed, but patients receiving P-32 and HU had a significantly higher risk of 19 %. In contrast, in a more recent paper (Balan and Critchley 1997) describing treatments of patients with PCV with P-32 over a therapeutic period of 15 years, a low incidence of leukemia was reported. Within a period of 2 – 12 years (median 6 years), 13 pa-

tients (5.5%) developed a myelofibrosis after a single therapy with P-32 and 18 patients (7.6%) developed acute leukemia after 2–11 years and one to five therapies. Other tumors were detected in 19 (8%) patients. These authors also recommend P-32 therapy especially in elderly patients as an easy to apply and cost-effective modality. Unfortunately there is no large randomized study available to date in which the therapies with P-32 and HU have been compared. Therefore neither the survival rates nor the incidence of complications and secondary malignancies can be compared.

30.1.5.6 Anticoagulation

The prophylactic administration of anticoagulative drugs before therapy with P-32 like acetylsalicylic acid with severely enhanced numbers of thrombocytes is ineffective (Berk et al. 1986). It was not possible to reduce the thromboembolic complications. Just the reverse effect was recorded because a significant increase in hemorrhagia of the gastrointestinal tract was noticed which might be due to the dose of acetylsalicylic acid, which was chosen too high. An ongoing study (ECLAP, European Collaboration on Low dose Aspirin in Polycythemia vera) might clarify this question.

30.1.5.7 Allogenic Bone Marrow Transplantation

Few experiences have been reported with this method and due to the high therapy related mortality it is preserved only for very special cases although some successful treatments have been published (Anderson et al. 1997).

30.1.6 Discussion

A significant improvement of survival in patients with PCV after therapy with P-32 was reported over 30 years ago (Osgood 1968). The Polycythemia Vera Study Group (PVSG) and the European Organization for Research and Treatment of Cancer (EORTC) performed larger studies to compare several therapy regimens in which despite the rarity of the disease over 1,000 patients were enrolled within 15 different protocols (Berk et al. 1986). But due to the different study protocols, termination of the different study arms at different time points, the very inhomogeneous groups and therapy modalities which changed over time, a direct comparison of the different arms especially in terms of long-term comparability has not been possible (Najean and Rain 1997b). Also the French groups emphasized repeatedly that in their studies disease control by phlebotomy is possible only over a limited period. Due to sideropenia very severe impairments are possible in single cases, so that for these cases the term "polycythemic cripple" was introduced.

Side effects, e.g., thromboembolic complications, were predominantly present in the group of patients treated only with blood-letting especially within the first 4 years of the disease, whereas in P-32 treated patients within a time period of 10 years malignancies especially acute leukemias were frequently observed. Also non-hematologic diseases like tumors of the GI tract and skin tumors were present in an increased percentage. Due to the lack of direct more recent comparisons between alkylating substrates and P-32, the incidence of secondary malignancies is difficult to calculate.

Since the early 1970s there has been controversy over the value of the competing therapy modalities (phlebotomy, chemotherapy, P-32) (Wagner et al. 1995). Against this background the indications for therapy with P-32 in the literature are as follows (Sostre 1995):

- No or only minor effect of hydroxyurea
- Age over 70 years and minor risk of secondary malignancies
- Chemotherapy refused by the patient
- Unwillingness to undergo frequent blood count checks as is mandatory under chemotherapy

Athens (1993) also recommended to use P-32 only in patients who do not respond to hydroxyurea. The combined use of P-32 with alkylating substrates or hydroxyurea is associated with a higher risk of secondary malignancies.

After P-32 therapy a primary therapy response can be expected in 60–85% of patients. Reports on the duration of the remission are in the range of 3–4 years (Meuret et al. 1975). Our own experience has documented a duration of a complete remission of about 24 months as an average (4 months to 10 years) after the first therapy. The average survival was 7 years, which was significantly longer compared to patients treated only with blood-letting. A relationship to distinct symptoms of the disease like the number of erythrocytes and splenomegaly could not be substantiated. Three months after therapy an impressive decrease of blood cell counts, mass of erythrocytes and hemoglobulin up to normal values was substantiated. Correlated to these findings a marked improvement of the clinical symptoms and complications could be stated. The full therapeutic effect is established after the first administration in most of the patients and in our own experience only 10 out of 117 patients needed a second or third therapy and only one patient a fifth treatment. No patient showed resistance to this treatment. Chronic myelocytic courses or OMF were substantiated in only 7% of patients independently of the total cumulative dose. The latter finding indicates that these complica-

tions are more the final stadium of the disease than treatment related effects.

In a later study Najean and Rain evaluated 114 patients treated with P-32 and reported a mean survival of 13.5 years, which is only less than the result of 15.2 years reported by the French Statistical Institute (Najean and Rain 1997b). In a retrospective study of 52 patients who were treated with P-32, Meuret et al. found a median survival of 12.5 years (Meuret et al. 1975). Most of the patients died due to thromboembolic or hemorrhagic complications and the incidence of acute leukemias was reported to be 4%.

In addition, the earlier recommendations of the PVSG may be taken into account (Berk et al. 1986):

1. Due to the increasing risk with age of developing thromboembolic complications, patients older than 70 years are most effectively treated with P-32 combined with a blood-letting.
2. Patients below 50 years of age, especially women of child bearing age, should be treated only with blood-lettings if no risk of thromboembolic complications is obvious. A myelosuppressive therapy may be performed if a high frequency of blood-letting is needed or thromboembolic complications are anamnestically known.
3. The greatest uncertainty exists concerning the role of a myelodepressive therapy in the age group of 50 through 70 years. In these younger patients therapy by blood-letting should be performed if no signs of thromboembolic complications are obvious. In other cases a myelosuppressive therapy with hydroxyurea is recommended.
4. A high grade splenomegaly with local symptoms, bone pain, marked pruritus or a difficult situation with the patient's veins may also be reasons to initiate an additional myelosuppressive therapy as well. Although the available data do not prove a statistically significant correlation between an increased thrombocyte count and an increased risk of thromboembolic complications, many clinicians believe that a marked thrombocytosis makes a myelosuppression necessary.

Because acute side effects are very rare and the application by the i.v. route is very easy to perform in the treatment by P-32, this procedure seems especially valuable and practical in older patients. The expenditure for nursing in comparison to the chemotherapy is markedly reduced, and therefore McDougall (2000) also recommended this therapy regimen for older patients.

30.1.7 Conclusions

Many authors agree that for therapy of polycythemia vera no single therapy regimen exists which is optimally effective for every age of patient [6, 34, 41] (Berlin 2000; Donovan et al. 1984; Osgood 1968). Sole blood-letting as a permanent therapy is not feasible, the compliance of the patients is low, and the incidence of vascular complications high. For differential indications outside clinical studies for the therapy of patients with a high risk of developing a thrombosis and/or high thrombocyte counts, therapy with hydroxyurea (HU) and interferon-α (IFN) are in the first line. Younger patients with a higher life expectancy are preferably treated with IFN to avoid the risk of secondary leukemia whereas older people should be preferably treated with HU because it is the therapy with fewer side effects. For patients in the higher age groups (above 65 years) with limited life expectancy, P-32 therapy is still a very reasonable treatment option because the effort required for monitoring is lowest compared to other regimens and a very good quality of life is guaranteed.

30.2 Intracoronary Radiation Therapy (IRT)

30.2.1 Introduction and Historical Perspective

In-stent restenosis results from neointimal hyperplasia. Until the advent of drug eluting stents, pharmacological approaches for the suppression of this neointimal response, repeat balloon angioplasty, atheroablative techniques and repeat stenting have all been disappointing. As early as 1993 the initial reports were published on the use of intracoronary radiation for the prevention of neointimal hyperplasia using the antiproliferative effect of radiation (Kunkel et al. 1993). The first more systemic study was published in 1997 (Condado et al. 1997), and meanwhile in many randomized, placebo-controlled, double-blind studies, intracoronary radiation therapy using various isotopes proved to be highly effective, reducing the rate of repeat in-stent restenosis also with the γ-emitter iridium-192 or with the β-emitters phosphorus-32 and strontium-90/yttrium (Waksman et al. 2000, 2002a; Leon et al. 2001; Popma et al. 2002).

30.2.2 Radiopharmaceuticals Employed

Consideration in this chapter will be limited to nuclear medicine methods, i.e., the liquid filled balloon with open radioisotopes, but data for these systems are scarce. These systems are easy to handle and self-centering, and filling is performed with several radiopharmaceuticals labeled with the β-emitter rhenium-188. Due to its physical characteristics, this radionuclide does not require additional shielding in the catheterization laboratory and it has been shown to provide homogeneous dose distribution in the vessel wall (Mak-

kar et al. 2000). The rhenium-188 solution is produced on the day of intervention by eluting a $^{188}W/^{188}Re$ generator. The effluent is concentrated (to approximately 7.5 GBq/ml; range: 4–9 GBq/ml), checked in the dose calibrator and loaded into the application device. The preparation of the rhenium solution has also been described in detail in a recent paper (Reynen et al. 2004).

30.2.2.1 Radiation Protection

Measurements of the radiation exposure at various distances and positions reveal an extra exposure by the intracoronary irradiation by the ^{188}Re liquid-filled balloon of 2.5 μSv compared to 150 μSv if fluoroscopy is switched on. To exclude radioactive contamination of the patient, 2 ml blood may be drawn immediately before and shortly after the procedure and monitored for radioactivity. Immediately prior to the procedure, perchlorate (60 drops) should be administered to prevent absorption of the radionuclide by the thyroid gland or gastric mucosa in case of balloon rupture. To increase excretion of the radiopharmaceutical in case of a balloon rupture, other groups labeled the ^{188}Re to MAG_3 (Hang et al. 2003) or DTPA [55], molecules that are rapidly excreted by the kidneys.

30.2.3 Methodology

In principle the therapy procedure is as follows: immediately after successful repeat PTCA (defined as residual stenosis of less than 30% in diameter by visual estimation with TIMI grade III flow on angiography) of an in-stent restenosis by balloon dilatation with high pressure (≥14 atm), a second balloon is directed into the redilated coronary segment. This second balloon is then filled with the solution containing ^{188}Re or saline in the sham procedure in the DRAIN trial by a special application device. This device, which is surrounded by a 1-cm-thick acrylic shield, consists of a two-sided syringe with two separate chambers: one contains the isotope and is coupled with a conventional PTCA balloon by redundant self-sealing connectors; the other chamber contains saline solution and is connected to the PTCA inflation device. Pressurizing the inflation device hydraulically pushes ^{188}Re fluid from the hot chamber into the balloon placed in the target lesion. The special, semi-professional application device used in our study is shown in Fig. 30.3a, b.

The set-up in the catheter room (CR) of our study is shown in Fig. 30.4.

After irradiation, the whole system is removed – the PTCA balloon is not disconnected from the ISAT – and brought to the Clinic for Nuclear Medicine for decay. In other studies different applicators were used, which is a drawback of this therapy method because there is no standard and approved device worldwide.

Low inflation pressures (3 atm.) in the therapy balloon are used to avoid balloon rupture with certainty. The radiation balloon should be 0.5 mm bigger in diameter than the dilatation balloon to achieve accurate contact to the vessel wall and, whenever possible, the length of the balloon should be chosen such that the ra-

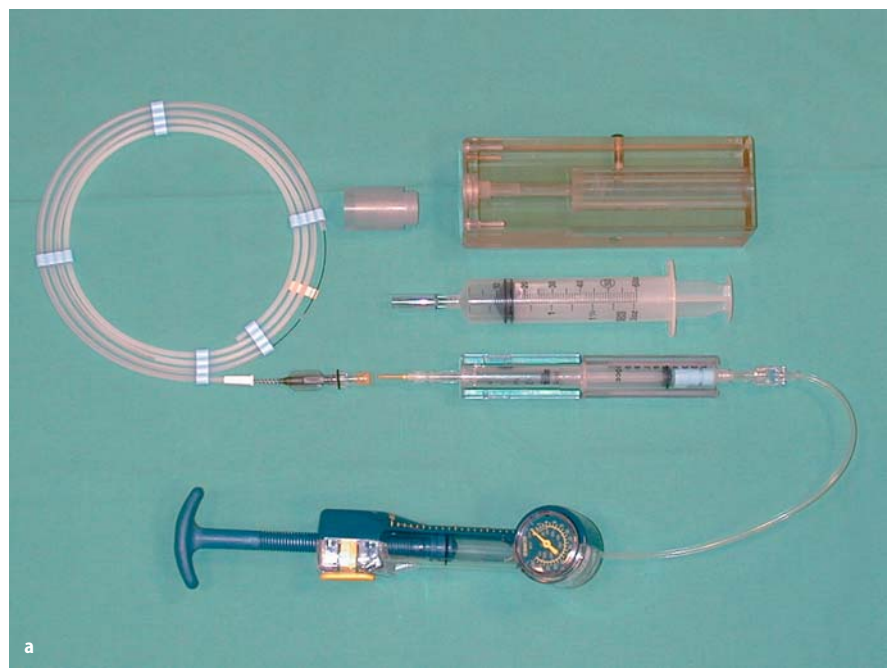

Fig. 30.3. a Isotope storage and transfer unit (ISAT) for the administration of the radiation to the coronary artery with a standard PTCA balloon. Single parts of the system are shown, with the PTCA inflation device at the bottom already connected (during a therapy session it is done in the CR) to the two-sided sealed syringe (TSS) with two separate chambers. Above this is a 50 cc syringe, which is used in the CL to render a vacuum in the PTCA balloon through the self-sealing septum, which is already attached to the inflation lumen of the balloon and the Lucite shielding above, which is simultaneously the holder for the TSS. In front is the special adapter for connecting the radioisotope chamber with the PTCA balloon through the self-sealing septum.

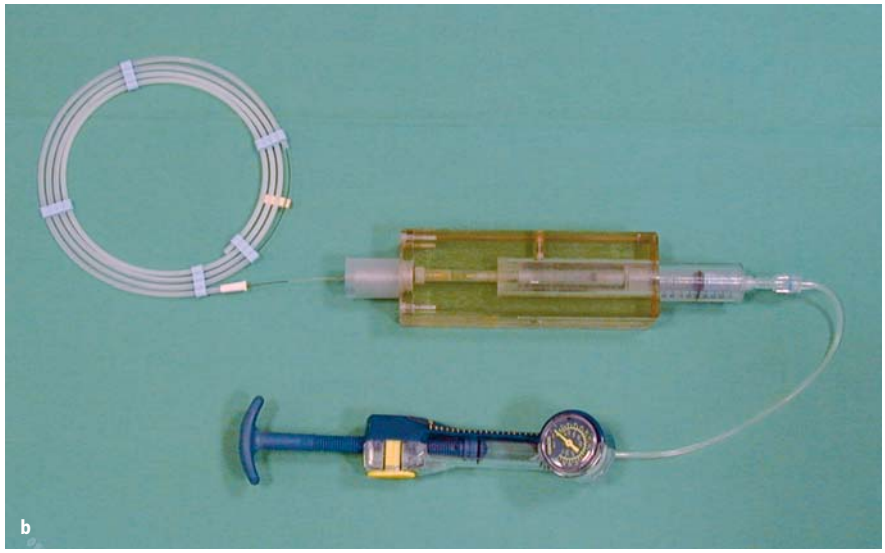

Fig. 30.3. b Isotope storage and transfer unit (ISAT) for the administration of the radiation to the coronary artery with a standard PTCA balloon. All parts of **a** are mounted ready for the therapy

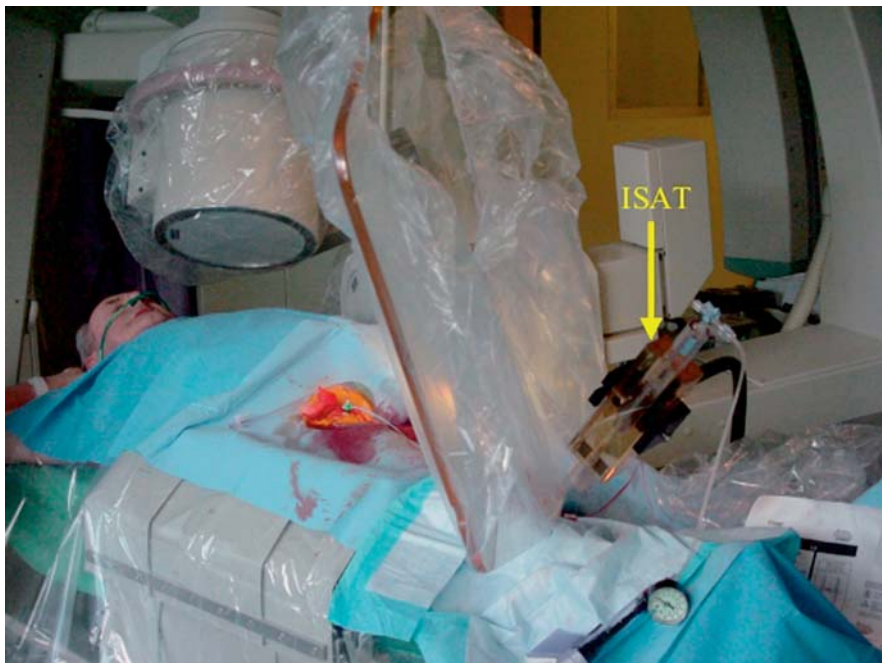

Fig. 30.4. Situation in the catheter room for administering radiation or placebo to the patient's coronary artery. The ISAT (Fig. 30.3, *arrow*), which is loaded in the hot laboratory of the Nuclear Medicine Department, is already connected by the special adapter to the standard PTCA balloon and held by a table-mounted articulated arm

diation balloon exceeds the target lesion by about 5 mm proximally and distally to avoid the so called geographical miss (GM), which means that there are injured vessel segments by PTCA but not irradiated by the second balloon. It has to been shown that these segments have a high potential of developing restenosis, called the "edge phenomenon."

Depending on the concentration of the radioactivity, the time of elution, and the diameter of the target vessel and of the balloon, respectively, the radiation time varies to reach 30–35 Gy at 0.5 mm depth of the vessel wall since animal models with this device have demonstrated about 30 Gy at 0.5 mm in the vessel wall to be the optimal dose to suppress intimal hyperplasia (Makkar et al. 2000). Based on these constraints, radiation time can be calculated and documented by simple software tools even on-site.

Patients should be pretreated with acetylsalicylic acid (300 mg daily) and clopidogrel (75 mg daily) for at least 3 days and postintervention patients are given acetylsalicylic acid and clopidogrel daily for 6 months; thereafter, only acetylsalicylic acid is given in a reduced dosage (100 mg daily) combined with clopidogrel for another 6 months to avoid early and late thrombosis of the irradiated segment.

30.2.4 Clinical Indications

There are reports (Hang et al. 2003; Koo et al. 2004; Fox et al. 2001; Park et al. 2001; Reynen et al. 2004) which have evaluated balloon-based systems using several radionuclides showing that this approach is feasible, safe and effective in reducing the rate of restenosis. Our own experience is based on a randomized, double-blind, placebo-controlled and prospective study in patients with in-stent restenosis which is unique to my knowledge because all other studies are case controlled.

Patients with stented coronary arteries who suffer from angina or have signs of ischemia on stress testing may be selected for repeated percutaneous coronary intervention (PCI) and if in-stent restenosis is obvious treated with this method. But patients with unsuccessful repeat PTCA (residual stenosis more than 30 %, myocardial infarction with increase of creatine kinase more than double the normal value – normally < 80 U/L) or repeat PTCA with stent implantation prior to brachytherapy should be excluded since the results of our pilot study (Reynen et al. 2004) revealed a significantly worse clinical as well as angiographic outcome in patients with newly implanted stents. The same result was also found in former studies (Reynen et al. 2004; Serruys et al. 2002; Leon et al. 2001; Waksman et al. 2002b; Costa et al. 1999; Kim et al. 2004). In some other clinical settings, such as a stenosis length of more than 40 mm, a reference vessel diameter of less than 2.0 mm or more than 4.0 mm, unprotected left main coronary artery stenosis, bifurcation lesions, right ostial lesions, angiographic signs of thrombus, left ventricular ejection fraction less than 30 %, myocardial infarction within the preceding 72 h, severe bleeding within the prior 6 months, contraindication to antiplatelet therapy, or pregnancy, an intracoronary radiation therapy seems less suitable. This also applies to patients with poor renal function (serum creatinine more than 3.0 mg/dl), since in the case of balloon rupture, it is impossible to eliminate the radionuclide ^{188}Re with forced diuresis.

Repeat coronary angiography should be performed in cases of new angina, or in cases where the stress test leads one to suspect new ischemia, or routinely at 6 months after the intervention, respectively. According to Mehran et al. (1999), in-stent lesions are classified as focal (less than 10 mm in length – class I) or diffuse lesions or occlusions (class IV); diffuse lesions (more than 10 mm in length) are either limited within the stent (class II) or exceed the stent (class III). For 1-year clinical follow-up, patients may be seen as outpatients or interviewed by phone. The questionnaire should include the following questions: clinical status and major cardiac events including death, non-fatal myocardial infarction, and repeat revascularization.

30.2.5 Results of Intracoronary Radiation Therapy Using the ^{188}Re Liquid-Filled Balloon

There are at least two sufficiently large studies investigating the treatment of de-novo or in-stent restenoses with long-term follow-up of at least 1 year: the Seoul National University Post-Angioplasty RhEnium irradiation (SPARE) study (Cho et al. 2004) and the Dresden prospective, RAndomized, placebo-controlled, double-blind, IN-stent restenosis trial (DRAIN) (Reynen et al. 2006). In both studies the easy to handle, self-centering rhenium-188 liquid-filled standard PTCA balloon was used. The chemical pattern of the ^{188}Re was either perrhenate (DRAIN) or labeled to DTPA (SPARE).

In DRAIN a total of 218 patients were treated (41 in a pilot study, 177 in the randomized part) and 201 in SPARE, which was considered sufficient for a liable statistical analysis (Machin and Campbell 1987); in both studies the rate of repeat angiography was up to 95 %, supporting the reliability of the results.

In DRAIN, even in six patients in-stent reocclusions were first reopened and dilated and then IRT was carried out. In most other randomized brachytherapy trials, this high-risk patient population was excluded, which makes our results even more reliable.

Radiation time in both studies was about 500 ± 200 s, and during the balloon inflation almost all patients suffered from angina and in some but not many patients the radiation time had to be fractionated, which is easily to perform with both systems used. The inflation times in the sham procedures in the DRAIN study did not differ significantly from those in the irradiated group. No major complications had been noted during the procedures in both studies.

During follow-up some patients developed late subacute thrombosis at the intervention site and most of the events occurred after discontinuation of the clopidogrel medication. Therefore intensive consent information of the patients is needed to continue the antiplatelet medication for at least 12 months. An angiographic example is demonstrated in Fig. 30.5.

Minimal lumen diameters before and immediately postintervention as well as at 6 months are shown in Fig. 30.6 for the irradiated and sham procedure treated patients, respectively, of the DRAIN study and the other angiographic endpoints in Table 30.4.

The data of MACE are shown in Table 30.5 and Fig. 30.7.

It is obvious that in all clinical parameters the irradiated group has a better outcome compared to the placebo treated patients. The same holds for the

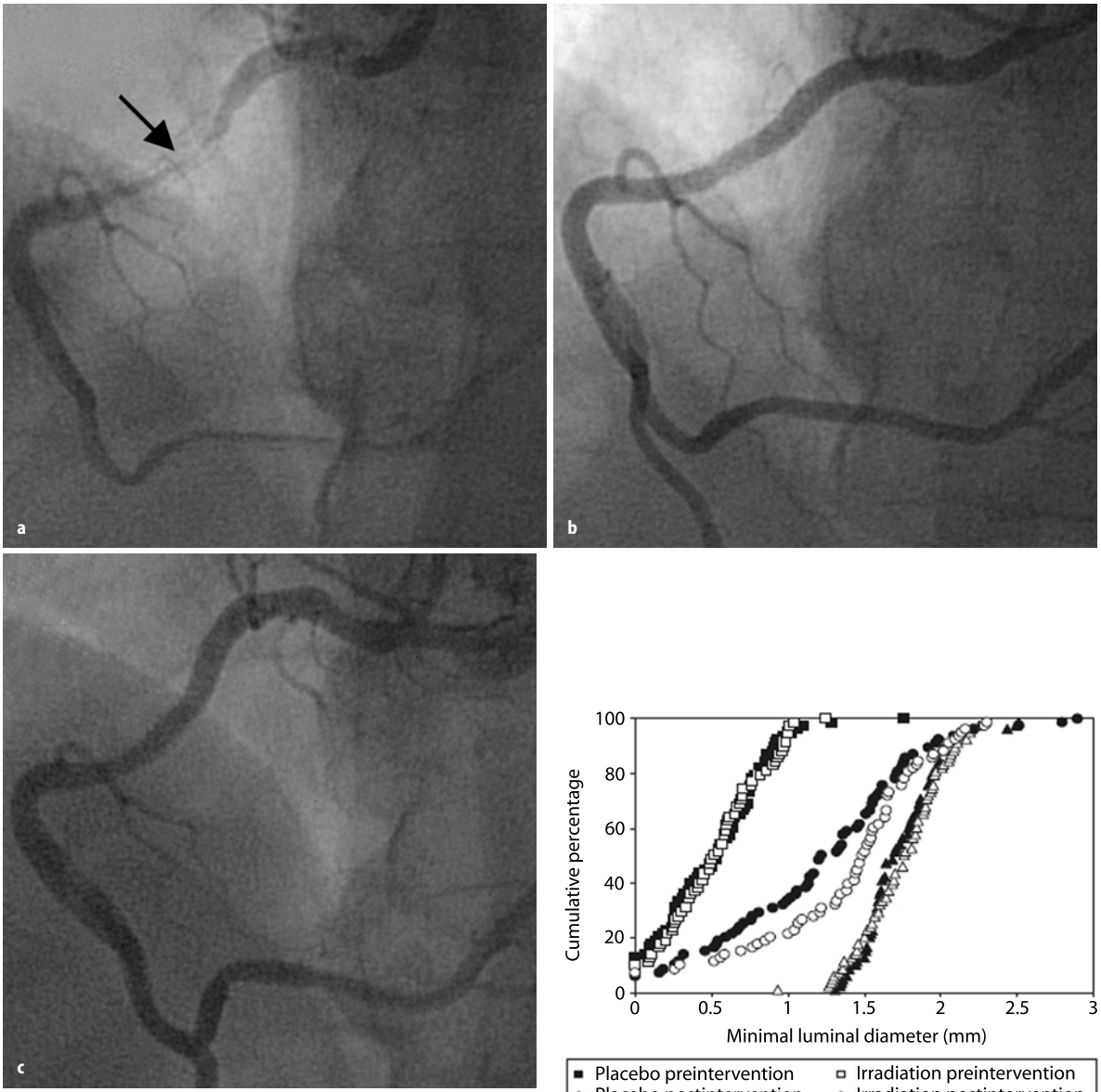

Fig. 30.5. a High-grade in-stent restenosis of the proximal right coronary artery (*arrow*). Before repeat PTCA. **b** Right coronary artery after repeat PTCA and intracoronary radiotherapy. Good result of restoration of flow. **c** Right coronary artery at follow-up angiography after 6 months with excellent long-term result of restoration of flow

Fig. 30.6. Minimal lumen diameters before and immediately after repeat PTCA followed by brachytherapy as well as after 6 months

Table 30.4. Angiographic endpoints in the DRAIN study

	Irradiation ($n=78$)	Sham procedure ($n=78$)	P*
Mean diameter stenosis (%)			
Before reintervention	78 ± 12	78 ± 14	–
After reintervention	26 ± 8	24 ± 7	–
At 6 months	44 ± 21	52 ± 22	0.02
Restenosis rate at 6 months (%)	20	40	0.01
Late loss index	0.29 ± 0.48	0.44 ± 0.44	0.04

* P indicated when less than 0.25

Table 30.5. Major cardiac events in the first year following intracoronary radiation therapy

	Irradiation ($n=82$)	Sham procedure ($n=82$)	P*
Death	0	0	–
Myocardial infarction			
Non-Q-wave	1	1	–
Q-wave	0	0	–
TVR	11	21	0.05
Repeat PTCA	11	18	–
Bypass surgery	0	3	–

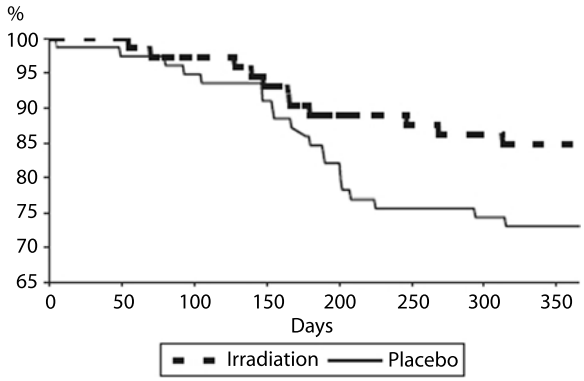

Fig. 30.7. Event-free survival in the patients irradiated and those with sham procedure

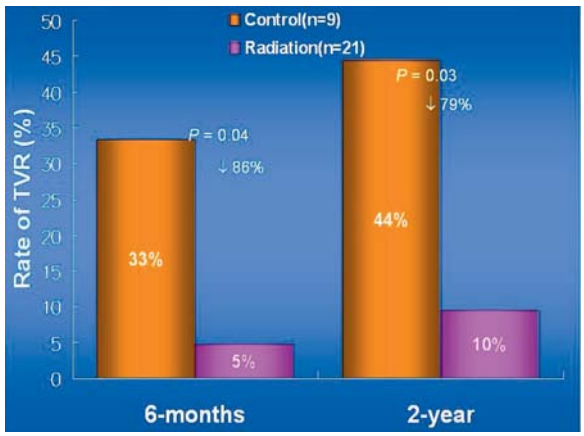

Fig. 30.8. Clinical outcome of the in-stent restenosis subgroup in the SPARE trial

SPARE trial, which is shown for one parameter in Fig. 30.8.

In DRAIN the subgroup with diabetes could be evaluated, revealing that more patients undergoing irradiation than patients undergoing sham procedure suffered from this disease. The interesting evaluation in this subgroup revealed that restenosis rate amounted to 18 % in the irradiated and 41 % in the sham procedure group ($p = 0.04$), suggesting that intracoronary radiation therapy compared to sham procedure was in particular effective in diabetics as was also shown in an earlier trial (Moses et al. 2002).

Angiographically "edge phenomenon" due to GM was observed only in one patient in the DRAIN study, but in 24 cases in the SPARE trial, which might indicate that exact placement of the radiation balloon is more difficult in de-novo lesions because most of the patients in SPARE were of this type.

30.2.6 Discussion

Our study and others demonstrated that intracoronary radiation therapy in patients with in-stent restenosis having undergone successful reintervention using a self-centering angioplasty balloon-based system filled with the liquid β-emitter ^{188}Re is safe and effective in reducing the rate of repeat restenosis and has a favorable clinical outcome. Feasibility and safety of this and comparable irradiation systems using the identical isotope but in different radiopharmaceuticals (Hang et al. 2003; Koo et al. 2004; Fox et al. 2001; Park et al. 2001; Reynen et al. 2004) have already been documented. Furthermore, in de-novo lesions, other groups showed that IRT has no benefit regarding the clinical outcome (Serruys et al. 2002; Kim et al. 2004; Raizner et al. 2000).

In patients with in-stent restenosis, as with other γ- or β-radiation emitting systems, there has been until now no randomized, *placebo-controlled*, double-blind study with the ^{188}Re liquid-filled balloon system except for a small randomized but not placebo-controlled trial with 21 patients (Schühlen et al. 2001). The balloon-based irradiation system using liquid and open radiation sources is user friendly and easy to handle compared to other devices for brachytherapy. It is comparatively cheap (additional costs per procedure are only about $350), and provides homogeneous dose distribution to the vessel wall since it is self-centering (Makkar et al. 2000). All lesions which are amenable to balloon dilatation are able to be irradiated with these systems. The additional procedural time consumption is only about 15 min, which seems reasonable. But only patients with in-stent restenosis after successful repeat angioplasty seem to have a clinical benefit in terms of target vessel revascularization (TVR), mean luminal diameter (MLD), late lumen loss (LLD), late loss index (LLI) and major cardiac events (MACE), which is most important because it has been shown previously that this patient group has a high risk of developing re-restenosis after repeat intervention (Bauters et al. 1998). All studies showed that with this balloon-based system, repeat diameter reduction of the lesion at 6 months and restenosis rate were lowered significantly. Late stent thrombosis is rare in the irradiated patients if the antiplatelet medication is continued for at least 1 year and patients should be very carefully informed.

Since stent implantation is a tremendous predisposing factor for subacute and late stent thrombosis (Teirstein et al. 1997; Waksman et al. 2000; Waksman et al. 2002a, c; Popma et al. 2002), stent implantation should be avoided whenever possible; intracoronary brachytherapy was not even performed in two patients (DRAIN) in whom stent implantation was inevitable

during repeat coronary angioplasty. Follow-up of the patients in trials dealing with IRT has shown promise (Kim et al. 2004), and also in DRAIN and SPARE the follow-up after 1 and even after 3 years showed a significant benefit of irradiation and it may be stated that during the 1st year of follow-up, the number of serious cardiac events such as death or myocardial infarction was very low in the irradiated patients.

In case of the soluble ^{188}Re there is some risk to the patient in the case of a balloon rupture but it is limited since the half-life of the radionuclide is comparatively short and it may be eliminated by forced diuresis, which may even be enhanced if the isotope is labeled to a molecule which is rapidly excreted by the kidneys. The ^{188}W/^{188}Re is not an approved radiopharmaceutical so it may be used in studies only, but there are some companies on the way to getting this approved.

30.2.7 Conclusions

Intracoronary radiation therapy with a balloon-based system using the liquid β-emitting radionuclide ^{188}Ren is an easy to handle, safe, comparatively cheap and effective therapeutic option in cases of in-stent restenosis, providing a significantly reduced rate of repeat restenosis, target vessel revascularization and clinical outcome. Additional stenting should be avoided and antiplatelet medication must be maintained for at least 1 year after the procedure. A randomized comparison with drug-eluting stents might be of value.

30.3 Treatment in Ankylosing Spondylitis

30.3.1 Introduction and Historical Perspective

The first parenteral "Thorium X" administration was performed as early as 1922 by the Frenchman Léri, but the first report about the possibility of treatment with "Thorium X" was noted in the *Berliner Klinische Wochenschrift* in 1913 by Bickel. Treatment for ankylosing spondylitis (AS) with ^{224}Ra has been used in Germany from 1948 through 1985 with good results, e.g., Koch reported on 940 patients treated with impressive long-term control of pain. His patients had subjective but also objective improvement of their behavior. He did not notice radiation induced malignancies (Koch 1978). Production was then discontinued for economic reasons and due to criticism (Spiess 1957), which was not justified. ^{224}Ra has again been available since 1999 and treatment has been in a low-dose scheme, i.e., intravenous administration of 1 MBq ^{224}Ra weekly for 10 weeks, which has been unchanged since 1954. It has to be emphasized that ankylosing spondylitis is the second most common of the rheumatoid diseases and is therefore connected with high morbidity and costs. Recently the responsible governmental institutions withdrew approval for ^{224}Ra due to the availability of non-radioactive drugs like TNF-α receptor inhibitors which show the same effectiveness in the control of the disease symptoms but are not very cost effective. It is therefore expected that this therapy method will again receive less interest worldwide.

30.3.2 Radiopharmaceuticals Employed

The isotope ^{224}Ra is an α-emitter with a physical half-life of 3.6 days and a radiation energy of 5.7 MeV. The effective half-life is 1.7 days in the human body. It behaves like a homologue of calcium with preferential accumulation in zones of calcification and ossification. The pharmacological effects in ankylosing spondylitis are antiosteoblastic and anti-inflammatory with subsequent relief of pain, improvement of mobility, and reduced spinal ossification.

30.3.3 Clinical Indications

Therapy with ^{224}Ra was considered to be indicated with radiologically proven early ankylosing of one or two parts of the spine with ongoing inflammation diagnosed by a value of the C-reactive protein (CRP) above 10 mg/l, clinical progression failing to respond to non-steroidal anti-inflammatory drugs (NSAIDs), and/or if analgesic/anti-inflammatory drugs are contraindicated. Contraindications for this therapy were considered to be diseases of the blood formation system, recent fractures, severe liver damage, pregnancy and lactation, age of patient less than 21 years, and acute infection.

Our own experience is based on 16 patients in whom AS was diagnosed 18 years previously as an average and who had a follow-up after 3 months of the last injection. In Fig. 30.9 an example of a two phase whole body bone scan is shown with positive signs for AS. During the treatment we performed weekly measurements of full blood count, liver enzymes, CRP and ESR (erythrocyte sedimentation rate).

For the evaluation of the response to therapy, pain evaluation can be done by oral interview; the function mainly of the spinal column can be evaluated by the standardized Bath Ankylosing Spondylitis Functional Index (BASFI) questionnaire, which is a rheumatological index for the measurement of movement restrictions in everyday situations; the course of the medication should be questioned by oral interview; and the acute phase-reactants can be measured by CRP/ESR evaluation.

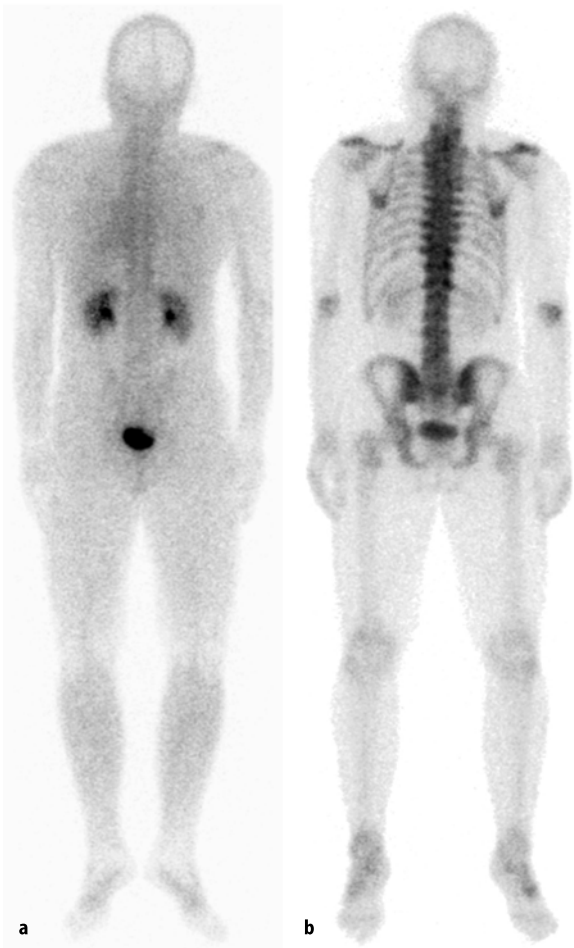

Fig. 30.9. Two-phase whole body bone scintigraphy in the posterior view of a patient with ankylosing spondylitis. **a** Early soft tissue phase with typical paravertebral accumulation of the radiopharmaceutical. **b** Late bone phase with typical hot spots in the small vertebral joints

Complications of this therapy are a drop of the leukocyte count by 27 %, platelets by 21 % with unchanged hemoglobulin value and liver enzymes. The changes in the blood count are not severe enough in either case to discontinue the ^{224}Ra therapy.

30.3.4 Results of ^{224}Ra Therapy

Nineteen percent of our patients were free of pain after the therapy and were free of restriction of movement, and 63 % reported a marked pain reduction and/or improved spinal mobility. Only three patients communicated an unchanged situation. The change of medication was impressive because six out of ten patients were able to discontinue NSAIDs, three of out three patients discontinued and/or reduced methotrexate, two out of five reported the same with steroids and one out of two with sulfasalazine. In total, 80 % of the patients experienced a reduction of pain, a reduction of analgesic medication and in 9 out of the 16 patients a improvement of mobility could be objectively evaluated by a 20 % reduction in BASFI, which is shown in Fig. 30.10.

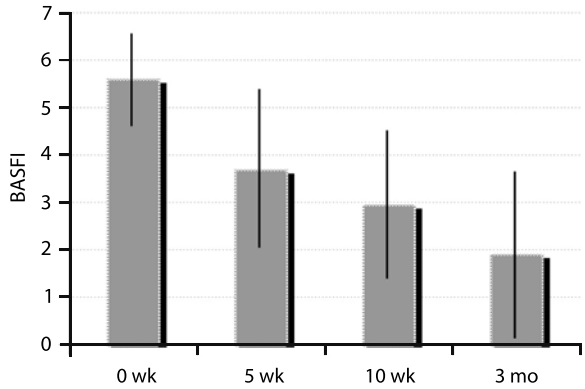

Fig. 30.10. Improvement of mobility in 19 patients with ankylosing spondylitis based on a 20 % reduction of BASFI (Bath Ankylosing Spondylitis Functional Index)

30.3.5 Conclusions

The treatment of ankylosing spondylitis by ^{224}Ra is very effective with only minor side effects, and based on the results of older studies (Koch 1978) a long-term therapeutic effect can be expected. In terms of cost this therapy is favorable to other treatment methods developed more recently like TNF-α inhibitors but which are not very well evaluated to date. Therefore ^{224}Ra may be considered as the only established baseline treatment.

Acknowledgements. I would like to thank my colleague Jan Bredow, MD, for his support in writing the polycythemia vera part of this chapter and in discussing his experience and data on these patients. I especially thank Klaus Reynen, MD, with whom I conducted the DRAIN study over several years, which became one of the largest placebo controlled trials worldwide in the field of intracoronary radiation therapy in patients with in-stent stenoses. In particular I would like to thank my colleague and friend Furn F. (Russ) Knapp for his support and help in using and handling the ^{188}W/^{188}Re generator and his valuable discussions about our clinical studies.

References

Anderson JE, Sale G, Appelbaum FR, Chauncey TR, Storb R (1997) Allogeneic marrow transplantation for primary myelofibrosis and myelofibrosis secondary to polycythaemia vera or essential thrombocytosis. Br J Haematol 98:1010 – 1016

Athens JW (1993) Polycythemia vera. In: Lee GR, Bithell TC, Foerster J, Athens JW, Lukens JN (eds) Wintrobe's clinical hematology, 9th edn. Lea & Febiger, Philadelphia, pp 398 – 452

Balan KK, Critchley M (1997) Outcome of 259 patients with primary proliferative polycythaemia (PPP) and idiopathic thrombocythaemia (IT) treated in a regional nuclear medicine department with phosphorus-32 – A 15 year review. Br J Radiol 70:1169 – 1173

Bareford D (1991) The role of 32P in the management of haematological disorders. Nucl Med Commun 12:751 – 753

Bauters C, Banos JL, Van Belle E, McFadden EP, Lablanche JM, Bertrand ME (1998) Six-month angiographic outcome after successful repeat percutaneous intervention for in-stent restenosis. Circulation 97:318 – 321

Berk PD, Goldberg JD, Silverstein MN, et al. (1981) Increased incidence of acute leukemia in polycythemia vera associated with chlorambucil therapy. N Engl J Med 304:441 – 447

Berk PD, Goldberg JD, Donovan PB, et al. (1986) Therapeutic recommendations in polycythemia vera based on Polycythemia Vera Study Group protocols. Semin Hematol 23: 132 – 143

Berlin NI (1975) Diagnosis and classification of the polycythemias. Semin Hematol 12:339 – 351

Berlin NI (2000) Treatment of the myeloproliferative disorders with 32P. Eur J Haematol 65:1 – 7

Blomgren H, Petrini B, Wasserman J, von Stedingk LV, Svedmyr E (1990) Changes of the blood lymphocyte population following 32P treatment for polycythemia vera. Eur J Haematol 44:302 – 306

Bredow J, Schuler U, Pinkert J, Franke WG (2001) Polycythaemia vera: Diagnostik, Differenzialtherapie und Stellenwert der ^{32}P-Behandlung heute. Der Nuklearmediziner 2:85 – 96

Büll U, Schicha H, Biersack HJ, et al. (1999) Nuklearmedizin, 3rd edn. Georg Thieme Verlag, Stuttgart

Chievitz E, Thiede T (1962) Complications and causes of death in polycythaemia vera. Acta Med Scand 172:513 – 523

Cho YS, Kim MA, Hwang KK, Koo BK, Oh S, Chae IH, Kim HS, Lee DS, Oh BH, Lee MM, Park YB, Choi YS (2004) Two-year clinical follow-up results of intracoronary radiation therapy with rhenium-188-diethylene triamine penta-acetic acid-filled balloon. Catheter Cardiovasc Interv 63:274 – 281

Condado JA, Waksman R, Gurdiel O, Espinosa R, Gonzalez J, Burger B, Villoria G, Acquatella H, Crocker IR, Seung KB, Liprie SF (1997) Long-term angiographic and clinical outcome after percutaneous transluminal coronary angioplasty and intracoronary radiation therapy in humans. Circulation 96:727 – 732

Costa MA, Sabaté M, van der Giessen WJ, Kay P, Cervinka P, Ligthart JMR, Serrano P, Coen VLMA, Levendag PC, Serruys PW (1999) Late coronary occlusion after intracoronary brachytherapy. Circulation 100:789 – 792

Dai CH, Krantz SB, Koury ST, Kollar K (1994) Polycythaemia vera. IV. Specific binding of stem cell factor to normal and polycythaemia vera highly purified erythroid progenitor cells. Br J Haematol 88:497 – 505

Donovan PB, Kaplan ME, Goldberg JD, et al. (1984) Treatment of polycythemia vera with hydroxyurea. Am J Hematol 17:329 – 334

Edwards EA, Cooley MH (1970) Peripheral vascular symptoms as the initial manifestation of polycythemia vera. JAMA 214:1463 – 1467

Fox RA, Barker P, Guy D, Smart G, Henson PW, Mews GC, Gibbons F (2001) The use of ^{188}Re to treat in-stent re-stenosis of coronary arteries. Australas Phys Eng Sci Med 24:160 – 165

Franke WG, Unger L, Müller J (1993) Untersuchungen des zerebralen Blutflusses bei Polycythaemia vera rubra mit nuklearmedizinischen Methoden. Der Nuklearmediziner 2:125 – 133

Geigy Scientific Tables (1985) Hematology and human genetics. Ciba Geigy, Basel, p 66

Hang C-L, Fu M, Hsieh B-T, Leung SW, Wu C-J, Yip H-K, Ting G (2003) Intracoronary β-irradiation with liquid Rhenium-188. Results of the Taiwan radiation in prevention of post-pure balloon angioplasty restenosis study. Chest 124:1284 – 1293

Harbert JC (1987) Phosphorus-32 therapy in the myeloproliferative diseases. In: Harbert JC (ed) Nuclear medicine therapy. Georg Thieme Verlag, Stuttgart

Hoffman R, Wasserman LR (1979) Natural history and management of polycythemia vera. Adv Intern Med 24:255 – 285

Hume R, Cowell MA, Goldberg A (1966) Prediction of the dose of radioactive phosphorus in the treatment of polycythaemia vera. Clin Radiol 17:295 – 298

Kim KI, Bae J, Kang HJ, Koo BK, Youn TJ, Kim SH, Chae IH, Kim HS, Sohn DW, Oh BH, Lee MM, Park YB, Choi YS, Lee DS (2004) Three-year clinical follow-up results of intracoronary radiation therapy using a rhenium-188-diethylene-triamine-penta-acetic-acid-filled balloon system. Circ J 68:532 – 537

Koch W (1978) Indikationsstellung und Ergebnisse einer Radium-224 (Thorium-X)-Therapie der Spondylitis ankylopoietica (Sp.a.). Z Orthop 116:608 – 616

Koo B-K, Lee M-M, Oh S, Chae I-H, Kim H-S, Sohn D-W, Oh B-H, Park Y-B, Choi Y-S, Lee DS (2004) Effects of β-radiation with a ^{188}rhenium-filled balloon catheter system on non-stented adjacent coronary artery segments. Int J Cardiol 96:73 – 77

Kunkel B, Müller R, Müller W, Weikl A, Dunst J, Bachmann K (1993) Lokale intrakoronare Iridiumbestrahlung zur Reduktion der Restenoserate nach PTCA. Z Kardiol 82 Suppl 3:50 (abstract)

Lamy T, Devillers A, Bernard M, et al. (1997) Inapparent polycythemia vera: An unrecognized diagnosis. Am J Med 102:14 – 20

Lawrence JH (1940) Nuclear physics and therapy: Preliminary report on a new method for the treatment of leukemia and polycythemia. Radiology 52:51 – 60

Lengfelder E, Berger U, Hehlmann R (2000) Interferon alpha in the treatment of polycythemia vera. Ann Hematol 79:103 – 109

Leon MB, Teirstein PS, Moses JW, Tripuraneni P, Lansky AJ, Jani S, Wong C, Fish D, Ellis S, Holmes DR, Kerieakes D, Kuntz RE (2001) Localized intracoronary gamma-radiation therapy to inhibit the recurrence of restenosis after stenting. N Engl J Med 344:250 – 256

Machin D, Campbell MJ (1987) Statistical tables for the design of clinical trials. Blackwell Scientific Publications, Oxford

Makkar R, Whiting J, Li A, Honda H, Fishbein MC, Knapp FF, Hausleiter J, Litvack F, Eigler NL (2000) Effects of β^--emitting ^{188}Re balloon in stented porcine coronary arteries. An angiographic, intravascular ultrasound, and histomorphometric study. Circulation 102:3117 – 3123

McDougall IR (2000) Systemic radiation therapy with unsealed radionuclides. Semin Radiat Oncol 10:94 – 102

McEwan AJ (2000) Use of radionuclides for the palliation of bone metastases. Semin Radiat Oncol 10:103 – 114

Mehran R, Dangas G, Abizaid AS, Mintz GS, Lansky AJ, Satler LF, Pichard AD, Kent KM, Stone GW, Leon MB (1999) Angiographic patterns of in-stent restenosis: classification and implications for long-term outcome. Circulation 100:1872 – 1878

Meuret G, Hoffman G, Gmelin R (1975) Experience with radioactive phosphorus therapy in cases of polycythemia vera. Strahlentherapie 149:49 – 54
Moliterno AR, Hankins WD, Spivak JL (1998) Impaired expression of the thrombopoietin receptor by platelets from patients with polycythemia vera. N Engl J Med 338:572 – 580
Moses JW, Moussa I, Leon MB, Teirstein PS, Fish RD, Ellis SG, Nawas D, Kluck B, Giorgianni JA, Donohoe D, Kuntz RE (2002) Effect of catheter-based iridium-192 gamma brachytherapy on the added risk of restenosis from diabetes mellitus after intervention for in-stent restenosis (subanalysis of the gamma I randomized trial). Am J Cardiol 90:243 – 247
Murray IPC, Ell PJ (1994) Nuclear medicine in clinical diagnosis and treatment. Churchill Livingstone, Edinburgh
Najean Y, Rain JD (1997) Treatment of polycythemia vera: The use of hydroxyurea and pipobroman in 292 patients under the age of 65 years. Blood 90:3370 – 3377
Najean Y, Rain JD (1997a) Treatment of polycythemia vera: Use of 32P alone or in combination with maintenance therapy using hydroxyurea in 461 patients greater than 65 years of age. The French Polycythemia Study Group. Blood 89:2319 – 2327
Najean Y, Rain JD (1997b) The very long-term evolution of polycythemia vera: An analysis of 318 patients initially treated by phlebotomy or 32P between 1969 and 1981. Semin Hematol 34:6 – 16
Osgood EE (1968) The case for 32P in treatment of polycythemia vera. Blood 32:492 – 499
Osler W (1903) Chronic cyanosis with polycythemia and enlarged spleen: a new clinical entity. Am J Med Sci 126:187 – 192
Park S-W, Hong M-K, Moon DH, Oh SJ, Lee CW, Kim J-J, Park S-J (2001) Treatment of diffuse in-stent restenosis with rotational atherectomy followed by radiation therapy with rhenium-188-mercaptoacetyltriglycine-filled balloon. J Am Coll Cardiol 38:631 – 637
Popma JJ, Suntharalingam M, Lansky AJ, Heuser RR, Speiser B, Teirstein PS, Massullo V, Bass T, Henderson R, Silber S, von Rottkay P, Bonan R, Ho KKL, Osattin A, Kuntz RE, for the Stents and Radiation Therapy (START) Investigators (2002) Randomized trial of $^{90}Sr/^{90}Y$ γ-radiation versus placebo control for treatment of in-stent restenosis. Circulation 106: 1090 – 1096
Raizner AE, Oesterle SN, Waksman R, Serruys PW, Colombo A, Lim Y-L, Yeung AC, van der Giessen WJ, Vandertie L, Chiu JK, White LR, Fitzgerald PJ, Kaluza GL, Ali NM (2000) Inhibition of restenosis with β-emitting radiotherapy. Report of the proliferation reduction with vascular energy trial (PREVENT). Circulation 102:951 – 958
Reynen K, Köckeritz U, Kropp J, Wunderlich G, Knapp FF, Schmeißer A, Strasser RH (2004) Intracoronary radiotherapy with a ^{188}Rhenium liquid-filled PTCA balloon system in in-stent restenosis: acute and long-term angiographic results, as well as 1-year clinical follow-up. Int J Cardiol 95: 29 – 34
Reynen K, Kropp J, Köckeritz U, Wunderlich G, Knapp FF, Schmeisser A, Strasser RH (2006) Intracoronary radiotherapy with a ^{188}Rhenium liquid-filled PTCA balloon system in in-stent restenosis: a single-center, prospective, randomized, placebo-controlled, double-blind evaluation. Coron Artery Dis 17:371 – 377
Roberts BE, Smith AH (1997) Use of radioactive phosphorus in haematology. Blood Rev 11:146 – 153
Schühlen H, Eigler N, Whiting JS, Haubner R, Hausleiter J, Dirschinger J, Kastrati A, Schwaiger M, Schömig A (2001) Usefulness of intracoronary brachytherapy for in-stent restenosis with a ^{188}Re liquid-filled balloon. Am J Cardiol 87:463 – 466
Serruys PW, Sianos G, van der Giessen W, Bonnier HJRM, Urban P, Wijns W, Benit E, Vandormael M, Dörr R, Disco C, Debbas N, Silber S on behalf of the BRIE Study Group (2002) Intracoronary β-radiation to reduce restenosis after balloon angioplasty and stenting. The Beta Radiation in Europe (BRIE) study. Eur Heart J 23:1351 – 1359
Silberstein EB (1979) Radionuclide therapy of hematologic disorders. Semin Nucl Med 9:100 – 107
Silberstein EB (1993) The treatment of painful osseous metastases with phosphorus-32-labeled phosphates. Semin Oncol 20:1 – 21
Silva M, Richard C, Benito A, et al. (1998) Expression of Bcl-X in erythroid precursors from patients with polycythemia vera. N Engl J Med 338:564 – 571
Sostre S (1995) Treatment of polycythemia vera. In: Wagner HNJ (ed) Principles of nuclear medicine, 2nd edn. WB Saunders, Philadelphia
Spiess H (1957) Exostotische Dysplasie durch Strahlenwirkung? Dt Med Wochenschr 82:1483 – 1484
Tefferi A, Silverstein MN (1998) Treatment of polycythaemia vera and essential thrombocythaemia. Baillieres Clin Haematol 11:769 – 785
Teirstein PS, Massullo V, Jani S, Popma JJ, Mintz GS, Russo RJ, Schatz RA, Guarneri EM, Steuterman S, Morris NB, Leon MB, Tripuraneni P (1997) Catheter-based radiotherapy to inhibit restenosis after coronary stenting. N Engl J Med 336:1697 – 1703
Tesselaar ME, Wijermans PW, Metsaars JA, Gerrits WB, Haak HL (1996) Radioactive phosphorus (32P); an old but not bad treatment for polycythemia vera. Ned Tijdschr Geneeskd 140:1900 – 1902
Thomas DJ, du Boulay BG, Marshall J, et al. (1977) Cerebral blood-flow in polycythaemia. Lancet 2:161 – 163
Wagner HN, Szabo Z, Buchmann JW (1995) Principles of nuclear medicine, 2nd edn. WB Saunders, Philadelphia
Waksman R, White RL, Chan RC, Bass BG, Geirlach L, Mintz GS, Satler LF, Mehran R, Serruys PW, Lansky AJ, Fitzgerald P, Bhargava B, Kent KM, Pichard AD, Leon MB, for the Washington Radiation for In-Stent Restenosis Trial (WRIST) Investigators (2000) Intracoronary γ-radiation therapy after angioplasty inhibits recurrence in patients with in-stent restenosis. Circulation 101:2165 – 2171
Waksman R, Raizner AE, Yeung AC, Lansky AJ, Vandertie L, on behalf of the INHIBIT Investigators (2002a) Use of localized intracoronary γ-radiation in treatment of in-stent restenosis: the INHIBIT randomised controlled trial. Lancet 359:551 – 557
Waksman R, Ajani AE, Pinnow E, Cheneau E, Leborgne L, Dieble R, Bui AB, Satler LF, Pichard AD, Kent KK, Lindsay J (2002b) Twelve versus six months of clopidogrel to reduce major cardiac events in patients undergoing radiation therapy for in-stent restenosis. Washington Radiation for In-Stent Restenosis Trial (WRIST) 12 versus WRIST PLUS. Circulation 106:776 – 778
Waksman R, Ajani AE, White RL, Chan RC, Satler LF, Kent KM, Pichard AD, Pinnow EE, Bui AB, Ramee S, Teirstein P, Lindsay J (2002c) Intravascular gamma radiation for in-stent restenosis in saphenous-vein bypass grafts. N Engl J Med 346:1194 – 1199
Weick JK, Donovan PB, Najean Y, et al. (1982) The use of cimetidine for the treatment of pruritus in polycythemia vera. Arch Intern Med 142:241 – 242
Zittoun R (1986) Busulfan versus 32P in polycythaemia vera. Drugs Exp Clin Res 12:283 – 285

Subject Index